

MOLECULES INTO MATERIALS

Case Studies in Materials Chemistry —
Mixed Valency, Magnetism and Superconductivity

PETER DAY

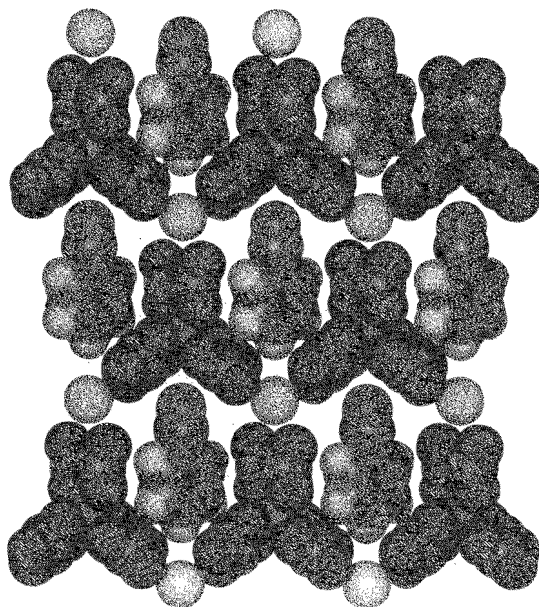
MOLECULES INTO MATERIALS

Case Studies in Materials Chemistry —
Mixed Valency, Magnetism and Superconductivity

This page intentionally left blank

MOLECULES INTO MATERIALS

Case Studies in Materials Chemistry —
Mixed Valency, Magnetism and Superconductivity



PETER DAY

The Royal Institution of Great Britain, UK

 World Scientific

NEW JERSEY • LONDON • SINGAPORE • BEIJING • SHANGHAI • HONG KONG • TAIPEI • CHENNAI

Published by

World Scientific Publishing Co. Pte. Ltd.

5 Toh Tuck Link, Singapore 596224

USA office: 27 Warren Street, Suite 401-402, Hackensack, NJ 07601

UK office: 57 Shelton Street, Covent Garden, London WC2H 9HE

British Library Cataloguing-in-Publication Data

A catalogue record for this book is available from the British Library.

MOLECULES INTO MATERIALS

Case Studies in Materials Chemistry — Mixed Valency, Magnetism and Superconductivity

Copyright © 2007 by World Scientific Publishing Co. Pte. Ltd.

All rights reserved. This book, or parts thereof, may not be reproduced in any form or by any means, electronic or mechanical, including photocopying, recording or any information storage and retrieval system now known or to be invented, without written permission from the Publisher.

For photocopying of material in this volume, please pay a copying fee through the Copyright Clearance Center, Inc., 222 Rosewood Drive, Danvers, MA 01923, USA. In this case permission to photocopy is not required from the publisher.

ISBN-13 978-981-270-038-4

ISBN-10 981-270-038-2

Dedication

The articles collected together in this book represent the accumulated efforts of a very large number of people over the years such as final year undergraduate project students, graduate students, postdoctoral research assistants, Research Fellows, exchange visitors from many countries, and colleagues from many University Departments and Research Institutes. I hope I can bring them all together under the common heading '*friends*'. The results described in these pages are largely due to their skills and insights. Unfortunately, there are too many to name individually and to single out names would be invidious. So this book is warmly dedicated collectively to my *co-workers*.

This page intentionally left blank

Why this book?

Science, as much as politics, is concerned with issues. At each moment, as the clock moves forward, communities with common interests and enthusiasts for particular doctrines or approaches (activists, in political parlance) turn their searchlights on to matters that appear to be of importance at that instant. However, there is a profound difference between science and politics in this regard. In politics, the big issues (personal freedom, collective action) keep recurring in different forms; in science, each field, once ploughed, never reverts entirely to scrub; the understanding gained is added to the pile, often to be deployed later in different circumstances. It is in that spirit that the present book is conceived. It collects first (or very early) thoughts on several topics that have since gained wider prominence and interest. Science being an experimental business, many of the articles reproduced here contain data or procedures that may have been superseded in the following years or decades; even the compounds themselves are often only the simplest prototypes, known as 'proofs of principle' by the patent attorneys. Nevertheless, it is hoped that their interest is not just historical or even archaeological, but that it will offer some sense of science in formation.

The core matter of this body of work can be subsumed under the label 'materials chemistry', a phrase that was entirely unknown at the time this work began. It is certainly Chemistry since it deals with the way that atoms are brought together to form molecules or more extended arrays, and the properties that flow from that. The properties, however, are largely physical ones and may be classed as electronic, i.e. spectroscopic, magnetic, electron transport and the like. Not only electronic, but collective (i.e. belonging to the ensemble as a whole rather than one individual constituent unit) and this is what constituted the traditional boundary between chemistry and condensed matter physics at least in the 1960s and 1970s. That was the era when physicists began to realise that there were many fascinating collective phenomena to be observed in solids that contained many more than two atoms in a unit-cell and chemists to appreciate that there was a wide world of possibility beyond the individual molecule. It was a privilege for me to play some part in bringing about this evolution, but in summing up the transformation that has taken place in solid state science over the past 40 years, let me defer to the words of a theoretical physicist. Great excitement accompanied the discovery of the first organic molecular superconductor in 1980 [1], but at a gathering of chemists and physicists

discussing the new horizons being opened up even in advance of that date, Bill Little (exponent of excitonic superconductivity — still yet to be observed) made the following prophetic remarks:

... The quest for a truly organic superconductor remains a major goal of many research efforts. In a very real sense this is what keeps much of our research afloat. A fortunate by-product has been the large amount of exciting physics and chemistry which has resulted from these endeavours. This has more than justified the effort to date. But perhaps the most valuable consequence and one which will have greatest long term impact has been the emergence of research groups where true interdisciplinary work is done, where physicists and chemists have learned to talk and work with one another in close effective collaboration. The impact of this on materials science can be expected to be great [2].

His words were now proven right.

For an inorganic chemist, the journey from molecules to materials starts with coordination chemistry, one of the ways in which metal ions, that have so many fascinating properties like magnetism or optical spectra, enter into the molecular state. My story begins from a desire to rationalise the optical spectra of molecular transition metal complexes involving the transfer of electronic charge from one part of the molecule to another. That triggers a host of phenomena (first remarked a century ago because they were visually spectacular) which arise from the way the molecular coordination complexes interact with one another when placed side by side in a crystal. These range from shifts in absorption bands that arise from intramolecular excitations to the ones where an electron is transferred from molecule to molecule. In the latter case (mixed valence), it proved possible to rationalise properties of such compounds across the Periodic Table through a simple model that has stood the test of time for 40 years.

Finally, we come to extended interactions across the entire crystal lattice, well known in continuous lattice compounds such as oxides, but much less appreciated in molecular inorganic compounds. Here, not only magnetism but also extreme quantum mechanical effects like superconductivity come into play. For example, the interplay between magnetism and superconductivity becomes an arena for molecular chemists, and at the same time gives rise to complications such as structural chirality.

None of this complexity was dreamt of either by physicists or chemists in the 1970s. This collection of reprints endeavours to chart at least one trajectory of progress through the ensuing jungle. It could never have been accomplished without the enthusiastic and talented support of many students and collaborators (for that word read 'friends'), whose names appear among the publications' co-authors. To them, my gratitude is immeasurable and hence as a small token of thanks, I dedicated this collection to them.

References

- [1] D. Jerome, A. Mazaud, M. Ribaud and K. Bechgaard, *J Physique (Lett.)* **41**, L95 (1980).
- [2] W. A. Little, in *Chemistry and Physics of One-Dimensional Metals*, ed. H. J. Keller, New York, Plenum Press, 1977, pp. 257.

This page intentionally left blank

Contents

Dedication	v
Why this book?	vii
Chapter 1	1
Inorganic Charge Transfer Spectra	3
Reprint 1.1 Charge-Transfer Spectra of Some Inorganic Complexes in Solution	6
J.C. Barnes and P. Day <i>J Chem Soc</i> 3886 (1964).	
Reprint 1.2 Analysis of the Charge-Transfer Spectra of Some First- Transition-Series Tetrahalide Complexes	13
B.D. Bird and P. Day <i>J Chem Phys</i> 49 , 392 (1968).	
Reprint 1.3 Electronic Spectra of Some Post-Transition-Metal Halide Complexes	25
P. Day and R.H. Seal <i>J Chem Soc Dal Trans</i> 2054 (1972).	
Reprint 1.4 Ultraviolet Spectra of Some First Transition Series Pseudohalide Complexes	30
P. Day <i>Inorg Chem</i> 5 , 1619 (1966).	
Reprint 1.5 The Spectra of Complexes of Conjugated Ligands. Part 1. Charge-Transfer in Phenanthroline Complexes: Energy Shifts on Substitution	33
P. Day and N. Sanders <i>J Chem Soc A</i> 1530 (1967).	
Reprint 1.6 The Spectra of Complexes of Conjugated Ligands. Part II. Charge-Transfer in Substituted Phenanthroline Complexes: Intensities	40
P. Day and N. Sanders <i>J Chem Soc A</i> 1536 (1967).	

Chapter 2		47
Metal Complexes in Solids: Optical Effects and Low-Dimensionality		49
Reprint 2.1	Cooperative Effects in the Electronic Spectra of Inorganic Solids P. Day <i>Inorg Chim Acta Rev</i> 3 , 81 (1969).	51
Reprint 2.2	Local and Collective States in Single and Mixed Valency Chain Compounds P. Day <i>Am Chem Soc Symp Ser</i> 5 , 234 (1974).	68
Reprint 2.3	Excitons in One-Dimensional Tetracyanoplatinite Salts P. Day <i>J Am Chem Soc</i> 97 , 1588 (1975).	88
Reprint 2.4	Why is Silver Chromate Red? The 4.2 K Polarized Electronic Spectrum of Chromate in Silver Sulphate D.J. Robbins and P. Day <i>Mol Phys</i> 34 , 893 (1977).	90
Reprint 2.5	Chemical Classification of Structures and Properties of Low-Dimensional Inorganic Compounds P. Day <i>Ann NY Acad Sci</i> 313 , 9 (1978).	96
Chapter 3		113
Mixed Valence Compounds		115
Reprint 3.1	Spectra and Constitution of Antimony(III), Antimony(V) Hexahalide Salts and Related Compounds P. Day <i>Inorg Chem</i> 2 , 452 (1963).	120
Reprint 3.2	Anion Ordering in Mixed-Valence Cs ₂ SbCl ₆ and Related Salts K. Prassides and P. Day <i>J Am Chem Soc</i> 105 , 3366 (1983).	125

Reprint 3.3	Charge Transfer in Mixed-Valence Solids. Part IV. Electronic Spectra of Hexachloroantimonates(III, V) L. Atkinson and P. Day <i>J Chem Soc A</i> 2423 (1969).	128
Reprint 3.4	Charge Transfer in Mixed-Valence Solids. Part V. Semiconductivity of Hexachloroantimonates(III, V) L. Atkinson and P. Day <i>J Chem Soc A</i> 2432 (1969).	137
Reprint 3.5	Mixed Valence Chemistry — A Survey and Classification M.B. Robin and P. Day <i>Adv Inorg Chem and Radiochem</i> 10 , 248 (1967).	142
Reprint 3.6	Trapping of Valence States in a Ruthenium(II, III) — Pyrazine Complex B. Mayoh and P. Day <i>J Am Chem Soc</i> 94 , 2885 (1972).	318
Reprint 3.7	Charge Transfer in Mixed-Valence Solids. Part VIII. Contribution of Valence Delocalisation to the Ferromagnetism of Prussian Blue B. Mayoh and P. Day <i>J Chem Soc Dal Trans</i> 1483 (1976).	320
Reprint 3.8	Valence Delocalization in Prussian Blue $\text{Fe}_4^{\text{III}}[\text{Fe}^{\text{II}}(\text{CN})_6]_3 \cdot x\text{D}_2\text{O}$, by Polarized Neutron Diffraction P. Day, F. Herren, A. Ludi, H. U. Güdel, F. Hulliger and D. Givord <i>Helv Chim Acta</i> 63 , 148 (1980).	325
Reprint 3.9	Mixed Valency Chemistry: A Survey of 10 Years Progress P. Day <i>Int Rev Phys Chem</i> 1 , 149 (1981).	331
Reprint 3.10	Vibronic Coupling Model for Mixed-Valence Compounds. Extension to Two-Site Two-Electron Systems K. Prassides, P.N. Schatz, K.Y. Wong and P. Day <i>J Phys Chem</i> 90 , 5588 (1986).	376
Reprint 3.11	Charge Transfer in Mixed-Valence Solids. Part I. Crystal Spectra of Chlorocuprates(I, II) P. Day and D.W. Smith <i>J Chem Soc A</i> 1045 (1967).	386

Reprint 3.12	Temperature Variation of the Intervalence Absorption Band of Hexachloroantimonate(III, V) Ions in a Crystal Lattice	389
	K. Prassides and P. Day <i>J Chem Soc Faraday Trans 2</i> 80 , 85 (1984).	
	Chapter 4	401
	Transparent Ferromagnets: Structures and Optical Properties	403
Reprint 4.1	New Transparent Ferromagnets	408
	P. Day <i>Acc Chem Res</i> 12 , 236 (1979).	
Reprint 4.2	Magnetic Susceptibility and Optical Spectra of the Organic-intercalated Two-Dimensional Ferromagnets Bis(monomethylammonium)- and Bis(monoethylammonium) Tetrachlorochromate(II)	416
	C. Bellitto and P. Day <i>J Chem Soc Dal Trans</i> 1207 (1978).	
Reprint 4.3	Correlation of Magnetic and Optical Properties in the Organic-Intercalated Two-Dimensional Ionic Ferromagnet Bis(Monomethylammonium) Tetrachlorochromate (II)	422
	C. Bellitto and P. Day <i>J Chem Soc Chem Commun</i> 511 (1978).	
Reprint 4.4	Organic-Intercalated Halogenochromates(II): Low-Dimensional Magnets	424
	C. Bellitto and P. Day <i>J Mater Chem</i> 2 , 265 (1992).	
Reprint 4.5	Temperature Variation of Exciton — Magnon Absorption Bands in Metamagnetic Transition-Metal Dihalides	431
	D.J. Robbins and P. Day <i>J Phys C: Solid State Phys</i> 9 , 867 (1976).	
Reprint 4.6	Nickel Dibromide: A Magnetic Detective Story	447
	P. Day <i>Acc Chem Res</i> 21 , 250 (1988).	
Reprint 4.7	Optical Properties of Ferromagnetic K_2CrCl_4	452
	P. Day, A.K. Gregson and D.H. Leech <i>Phys Rev Letts</i> 30 , 19 (1973).	

Reprint 4.8	Magnetic Susceptibility and Magnetization of the Ionic Ferromagnets Dipotassium, Dirubidium, and Dicaesium Tetrachlorochromate(II) A.K. Gregson, P. Day, D.H. Leech and M.J. Fair <i>J Chem Soc Dal Trans</i> 1306 (1975).	456
Chapter 5		463
Molecule-Based Magnets		465
Reprint 5.1	Ferrimagnetic Mixed-Valency and Mixed-Metal Tris(oxalato)Iron(III) Compounds: Synthesis, Structure, and Magnetism C. Mathonière, C.J. Nuttall, S.G. Carling and P. Day <i>Inorg Chem</i> 35 , 1201 (1996).	469
Reprint 5.2	The Magnetic Structures of the Layer Ferri-Magnets $P(C_6D_5)_4M^{II}Fe(C_2O_4)_3(M^{II}=Mn, Fe)$ C.J. Nuttall and P. Day <i>Inorg Chem</i> 37 , 3885 (1998).	475
Reprint 5.3	Magnetization of the Layer Compounds $AFe^{II}Fe^{III}(C_2O_4)_3$ (A=Organic Cation), in Low and High Magnetic Fields: Manifestation of Néel N and Q Type Ferrimagnetism in a Molecular Lattice C.J. Nuttall and P. Day <i>Chem Mater</i> 10 , 3050 (1998).	479
Reprint 5.4	Polarized Neutron Diffraction and Mössbauer Spectral Study of Short-Range Magnetic Correlations in the Ferrimagnetic Layered Compounds $(PPh_4)[Fe^{II}Fe^{III}(ox)_3]$ and $(NBU_4)[Fe^{II}Fe^{III}(ox)_3]$ S.G. Carling <i>et al.</i> <i>Phys Rev B</i> 66 , 104407 (2002).	487
Reprint 5.5	Ion-Radical Salts: A New Type of Molecular Ferrimagnet S.S. Turner and P. Day <i>J Mater Chem</i> 15 , 23 (2005).	499
Reprint 5.6	TTF Based Charge Transfer Salts of $[M(NCS)_4(C_9H_7N)_2]^-$ where M=Cr, Fe and C_9H_7N =Isoquinoline; Observation of Bulk Ferrimagnetic Order	502

S.S. Turner, C. Michaut, S. Durot, P. Day,
T. Gelbrich and M.B. Hursthouse
J Chem Soc Dal Trans 905 (2000).

	Chapter 6	507
	Molecular Metals and Superconductors	509
Reprint 6.1	Structure and Properties of Tris[Bis(Ethylenedithio)-Tetrathiafulvalenium]Tetrachloro-Copper(II) Hydrate, (BEDT-TTF) ₃ CuCl ₄ ·H ₂ O: First Evidence for Coexistence of Localized and Conduction Electrons in a Metallic Charge-Transfer Salt	515
	P. Day, M. Kurmoo, T. Mallah, I.R. Marsden, R.H. Friend, F.L. Pratt, W. Hayes, D. Chasseau, J. Gaultier and L. Ducasse <i>J Am Chem Soc</i> 114 , 10722 (1992).	
Reprint 6.2	Crystal and Electronic Structures and Electrical, Magnetic, and Optical Properties of Two Copper Tetrahalide Salts of Bis(Ethylenedithio)-Tetrathiafulvalene	523
	I.R. Marsden, M.L. Allan, R.H. Friend, M. Kurmoo, D. Kanazawa, P. Day, G. Bravic, D. Chasseau, L. Ducasse and W. Hayes <i>Phys Rev B</i> 50 , 2118 (1994).	
Reprint 6.3	Crystal Structure and Magnetism of (BEDT-TTF) ₂ MCl ₄ (BEDT-TTF=Bis(Ethylenedithio)Tetrathiafulvalene; M=Ga, Fe).	533
	M. Kurmoo, P. Day, P. Guionneau, G. Bravic, D. Chasseau, L. Ducasse, M.L. Allan, I.D. Marsden and R.H. Friend <i>Inorg Chem</i> 35 , 4719 (1996).	
Reprint 6.4	Superconducting and Semiconducting Magnetic Charge Transfer Salts: (BEDT-TTF) ₄ AFe(C ₂ O ₄) ₃ ·C ₆ H ₅ CN(A=H ₂ O, K, NH ₄)	541
	M. Kurmoo, A.W. Graham, P. Day, S.J. Coles, M.B. Hursthouse, J.L. Caulfield, J. Singleton, F.L. Pratt, W. Hayes, L. Ducasse and P. Guionneau <i>J Am Chem Soc</i> 117 , 12209 (1995).	

- Reprint 6.5 Crystal Chemistry and Physical Properties of Superconducting and Semiconducting Charge Transfer Salts of the Type $(\text{BEDT-TTF})_4[\text{A}^{\text{I}}\text{M}^{\text{III}}(\text{C}_2\text{O}_4)_3]\cdot\text{PhCN}(\text{A}^{\text{I}}=\text{H}_3\text{O}, \text{NH}_4, \text{K}; \text{M}^{\text{III}}=\text{Cr}, \text{Fe}, \text{Co}, \text{Al}; \text{BEDT-TTF}=\text{Bis}(\text{Ethylenedithio})\text{Tetrathiafulvalene})$ 550
L. Martin, S.S. Turner, P. Day, P. Guionneau, J.A.K. Howard, D.E. Hibbs, M.E. Light, M.B. Hursthouse, M. Uruichi and K. Yakushi
Inorg Chem **40**, 1363 (2001).
- Reprint 6.6 New Superconducting Charge-Transfer Salts $(\text{BEDT-TTF})_4[\text{A}\cdot\text{M}(\text{C}_2\text{O}_4)_3]\cdot\text{C}_6\text{H}_5\text{NO}_2$ ($\text{A}=\text{H}_3\text{O}$ or NH_4 , $\text{M}=\text{Cr}$ or Fe , $\text{BEDT-TTF}=\text{Bis}(\text{Ethylenedithio})\text{Tetrathiafulvalene}$) 559
S. Rashid, S.S. Turner, P. Day, J.A.K. Howard, P. Guionneau, E.J.L. McInnes, F.E. Mabbs, R.J.H. Clark, S. Firth and T. Biggs
J Mater Chem **11**, 2095 (2001).
- Reprint 6.7 The First Proton-Conducting Metallic Ion-Radical Salts 566
A. Akutsu-Sato, H. Akutsu, S.S. Turner, P. Day, M.R. Probert, J.A.K. Howard, T. Akutagawa, S. Takeda, T. Nakamura and T. Mori
Angew Chem Int Ed **44**, 292 (2005).
- Reprint 6.8 Magnetic Molecular Semiconductors and Superconductors: BEDT-TTF Tris-Oxalato-Metallate(III) Salts 570
P. Day and M. Kurmoo
Syn Metals **85**, 1445 (1997).
- Reprint 6.9 Determining the Charge Distribution in BEDT-TTF Salts 576
P. Guionneau, C.J. Kepert, G. Bravic, D. Chasseau, M.R. Truter, M. Kurmoo and P. Day
Syn Metals **86**, 1973 (1997).
- Reprint 6.10 Crystal Structures and Physical Properties of Bis(Ethylenedithio)-Tetrathiafulvalene Charge-Transfer Salts with FeX_4^- ($\text{X}=\text{Cl}$ or Br) Anions 578

T. Mallah, C. Hollis, S. Bott, M. Kurmoo, P. Day,
M. Allan and R.H. Friend
J Chem Soc Dal Trans 859 (1990).

Epilogue

585

CHAPTER 1

This page intentionally left blank

Inorganic Charge Transfer Spectra

The foundation for understanding collective electronic behavior of crystals must lie in the electronic structures of their constituent atoms and molecules, as exemplified by the frontier molecular orbitals. In the case of transition-metal compounds which are relatively ionic, such as oxides or molecular coordination complexes, these frontier orbitals originate from the highest filled levels of the anion or ligand, the partly occupied nd -shell and the empty, predominantly ns and np orbitals of the metal. Some knowledge of the spatial and energy distribution of these orbitals is therefore essential to understanding bulk physical properties. Nevertheless, from 1950s to 1970s, a paradoxical situation arose whereby inorganic chemists interested in the structure and bonding of transition-metal complexes, derived considerable information about the electronic ground-states by measuring the properties of excited states. Since the properties of such complexes are strongly influenced by the presence of partly-filled d -orbitals, the prevailing model for their chemical bonding was a symmetry-based perturbation approach known successively as crystal field theory and ligand field theory, which enabled the relative energies and occupancies of the d -orbitals to be estimated, at least qualitatively. The beautiful colours often associated with many transition-metal complexes (although far from exclusively, as we shall see later) originate from transitions between states arising from these d -orbital configurations. Measuring and interpreting so-called ligand field spectra thus became a notable cottage industry.

Whilst much valuable information was gained by these endeavours, from a spectroscopic point of view, they rested on yet another paradox: by their nature, the purely intra-configurational transitions are electric-dipole-forbidden, a feature that explains why the colours are often rather pale, e.g. copper(II) sulphate or in the case of pale pink manganese(II) sulphate, spin-forbidden as well. The paradox deepened further as it became clear that, although it plays a significant role in influencing the stereochemistry, magnetism and of course the colour, the partly-filled d -shell is only peripherally involved in binding the metal and ligands together. The overlap is significantly larger between the metal s - and p -orbitals and those of the ligand. Consequently, probing the energy distribution and atomic orbital composition of those molecular orbital levels lying above and below the d -shell appeared as an important step towards understanding how such levels (known as HOMO and LUMO by the organic chemists) might be modified when the molecular metal complex is

placed inside a crystal lattice. Moreover, since the transitions between these levels are electric-dipole-allowed, they contribute significantly (and sometimes dominantly) to the observed colours.

Yet, why is the epithet ‘charge transfer’ applied to these spectra? This is because the highest energy completely filled orbitals below those of mainly d-character are substantially localised on the ligands, and likewise, the lowest completely empty orbitals. Depending on the location of the d-orbitals on the energy scale between these filled and empty levels, the lowest energy allowed transitions are either from the filled to the d- or from the d- to the empty orbitals. In both instances, passing from the ground to the excited state profoundly modifies the charge distribution, either in the direction ligand-to-metal or *vice versa*. The earliest identification of this class of spectra with charge transfer came from empirical correlations with thermodynamic data such as oxidation-reduction potentials [1] and the first paper in this section describes such correlations, embracing 4f and 5f examples in addition to 3d [2]. Here, the metal complexes are simple 1:1 ion-pairs in solution, but what is more challenging is the situation when the metal is surrounded by several ligand atoms.

Early studies of charge transfer spectra quickly came up against the problem that no readily parametrisable semi-empirical model existed for the frontier orbitals comparable to the perturbation model of ligand field theory. A first priority was therefore to extract definitive assignments of observed spectra to specific excited configurations. In this respect, regular octahedral and tetrahedral MX_4 and MX_6 species are excellent testbeds because the spectra are well-resolved and the excited configurations, together with the states arising from them, can be defined in terms of symmetry-adapted wavefunctions. This means that vector-coupling can be applied in a fashion somewhat analogous to the ligand field approach. In this way, the charge transfer spectra of tetrahalogeno-3d complexes were analysed [3] using Griffith’s irreducible tensor method [4]. In the rather simpler circumstances of post-transition-metal complexes, where the d-shell is completely filled, the same method was used to assign the tetra- and hexahalide spectra [5].

Moving away from mono-atomic ligands such as oxide and halide to the more complicated situation presented by polyatomic ones, empirical correlations with the definitively assigned spectra of the corresponding monoatomic ligand species provide a valuable toehold. Among the simplest polyatomic ligands are the so-called pseudohalides NCX^- ($\text{X} = \text{O}, \text{S}, \text{Se}$), which also form four- and six-coordinate complexes with a wide range of metals. Correlations with the corresponding halide complexes clearly demonstrate that the lowest energy allowed transitions are likewise of charge transfer type [6].

Instances where the lowest unoccupied orbitals of the ligand lie close in energy to the d-orbitals occur where the ligands are conjugated aromatic bases such as

N-heterocycles. These include biological ligands such as porphyrin, but one of the most famous examples is 1,10-phenanthroline, much used as a colorimetric reagent for Fe(II) and Cu(I), by reason of the intense visible colours it generates. Such ligands have numerous potential substitution sites where electron-donating or withdrawing groups can be inserted to perturb the empty π^* molecular orbitals, and because it once played an important role as a colorimetric reagent, analytical chemists had already made many variants of it. Taking advantage of the opportunity of a statistical approach, the energies and intensities of the metal-to-ligand charge transfer were analysed using only one single substituent, methyl [7,8]. This shows that changes in the energy of both the metal and ligand levels has to be taken into account, proving possible with very simple models such as the Huckel theory.

References

- [1] F. S. Dainton, *J Chem Soc*, 1533 (1952); R. J. P. Williams, *J Chem Soc*, 137 (1953).
- [2] J. C. Barnes and P. Day, *J Chem Soc*, 3886 (1964). (**Reprint 1.1**)
- [3] B. D. Bird and P. Day, *J Chem Phys* **49**: 392 (1968). (**Reprint 1.2**)
- [4] J. S. Griffith, *The Irreducible Tensor Method for Molecular Symmetry Groups*, Prentice-Hall, Englewood Cliffs, 1962.
- [5] P. Day and R. H. Seal, *J. C. S. Dalton Trans*, 2054 (1972). (**Reprint 1.3**)
- [6] P. Day, *Inorg Chem* **5**: 1619 (1966). (**Reprint 1.4**)
- [7] P. Day and N. Sanders, *J Chem Soc (A)*, 1530 (1967). (**Reprint 1.5**)
- [8] *idem ibid*, 1536 (1967). (**Reprint 1.6**)

Preprinted from the Journal of the Chemical Society,
October 1964, (740), pages 3886—3892.

740. Charge-transfer Spectra of Some Inorganic Complexes in Solution.

By J. C. BARNES and P. DAY.

The wavenumbers of charge-transfer bands in 1 : 1 complexes between an oxidizing metal and a series of reducing ligands are plotted against those for other metals with the same ligands. The resulting straight line plots are used to discuss the stereochemistry of copper, redox potentials, the spectra of thiocyanate complexes, and solvent effects.

SOLUTIONS of reducible metal ions and oxidizable anions frequently exhibit absorption bands in the visible and near ultraviolet regions which are commonly assigned to electron transfer from the anion to the metal. The absorption energy is also related to the electron-donating and -withdrawing power of the ions as measured by other parameters such as redox potentials and electronegativities. For example, Jørgensen¹ compared the energies of corresponding bands in the spectra of many hexahalides of second- and third-row transition metals. He found that the energy gaps between chloride and bromide, and bromide and iodide, remained constant throughout and that they were proportional to the Pauling electronegativity differences between the pairs of halogens. By considering the bands of different metals with the same halogen he was also able to obtain a set of "optical" electronegativities for the metals on the assumption that the observed electron-transfer energy was proportional to the difference between two energy terms, one characteristic of the metal and the other of the halogen.

Hexahalide complexes containing low-energy electron-transfer bands are not, however, available outside the second and third transition series, though Jørgensen has used tetrahalides and halogenopentammines in an attempt to set up a corresponding series of optical electronegativities for the first transition series.²

To calculate additive "optical" electronegativities the observed charge-transfer-energies must be corrected for the spin-pairing energy in the metal ion. The Racah inter electronic repulsion parameters B and E_3 and the ligand field splitting Δ which are needed to derive this energy are often difficult to estimate with sufficient accuracy. Frequently the spin-pairing energy term is large compared with the observed wavenumber and the uncertainty introduced limits the sensitivity of the optical electronegativity.

A major difficulty in extending this type of correlation to other parts of the Periodic Table is that the association constants for halide complexes are not large and decrease sharply with decreasing halogen electronegativity. That is to say, the lanthanides, actinides and first transition series belong to the Chatt-Ahrland A group. Thus, we cannot obtain spectra of aqueous solutions of species where the inner co-ordination shell is occupied entirely by halogen atoms and if we are to extend this type of correlation we must find another system

One possibility is to use non-aqueous solvents of low dielectric constant. Thus, bands have been observed for bromide complexes of the reducible lanthanides in ethanol, though such complexes are never observed in dilute aqueous solution.³ An alternative is to consider species $M(H_2O)_{n-1}X$ where n is the favoured co-ordination in aqueous solutions, choosing anions X which give sufficiently stable complexes of this stoichiometry in aqueous solution.

Elsewhere we have reported formation constants and spectra of some complexes with the reducible trivalent lanthanides.⁴ These show that in dilute solution the only species that need be postulated is $M(H_2O)_{n-1}X$ if X is a weakly complexing ligand, such as thiocyanate or sulphate. The choice is limited to relatively highly reducing or extremely colourless

anions since the bands appear well into the u.v. region and are of quite low intensity (ϵ 50—100).

The band positions (in kK) obtained for the suspected electron-transfer bands in the lanthanide complexes can be compared with data for analogous transition metal and actinide complexes. Some data exist for the well characterized species $\text{Cu}^{\text{II}}(\text{H}_2\text{O})_5\text{X}$, $\text{Fe}^{\text{III}}(\text{H}_2\text{O})_5\text{X}$, and $\text{UO}_2^{2+}(\text{H}_2\text{O})_{n-1}\text{X}$, but the best example of the formula type MY_{n-1}X is the set of complexes $\text{Co}^{\text{III}}(\text{NH}_3)_5\text{X}$. Because of the high electronegativity of ammonia relative to X, the lowest energy intense u.v. bands have been repeatedly assigned to charge transfer from X to the cobalt atom. These cobalt pentammine bands are therefore a suitable background against which to study the dependence on X of the $\text{M}(\text{H}_2\text{O})_{n-1}\text{X}$ spectra. To avoid the uncertainty of the optical electronegativity method we have chosen to plot observed band energies without assuming any theoretical model.

Fig. 1 shows the positions of the first intense bands in $\text{Eu}(\text{H}_2\text{O})_{n-1}\text{X}$, $\text{Yb}(\text{H}_2\text{O})_{n-1}\text{X}$, $\text{Cu}(\text{H}_2\text{O})_5\text{X}$, $\text{Fe}(\text{H}_2\text{O})_5\text{X}$, and $\text{UO}_2(\text{H}_2\text{O})_{n-1}\text{X}$ plotted against the charge-transfer energies in $\text{Co}(\text{NH}_3)_5\text{X}$ for a series of ligands X. All spectra were measured in water except for the lanthanide halides which refer to uncharacterized species in ethanol (see below). The near 1 : 1 correlation observed in all the plots justifies our assumption that in the two

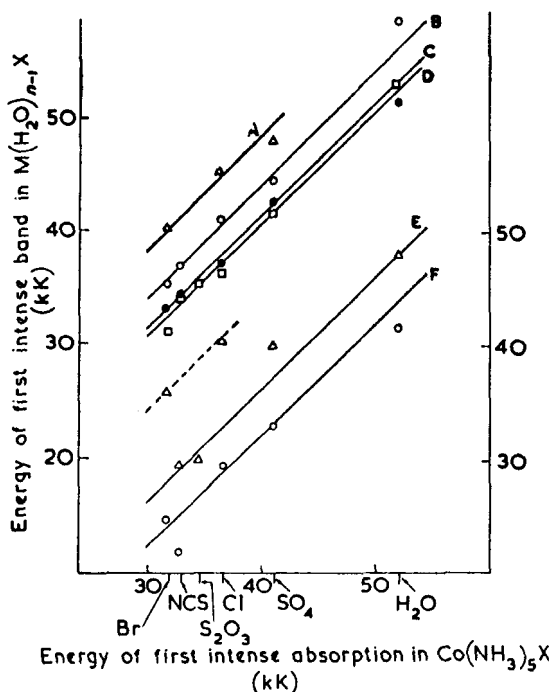


FIG. 1. The sources of the data are: FeNCS^{2+} , Perrin, *J. Amer. Chem. Soc.*, 1958, **80**, 3852; FeBr^{2+} , Lister and Rivington, *Canad. J. Chem.*, 1955, **33**, 1603; FeCl^{2+} and $\text{Fe}(\text{H}_2\text{O})_6^{3+}$, Gamlen and Jordon, *J.*, 1953, 1437; FeSO_4^+ , Whiteker and Davidson, *J. Amer. Chem. Soc.*, 1953, **75**, 3081; CuCl^+ , McConnell and Davidson, *ibid.*, 1950, **72**, 3164; CuBr^+ , Farrington, *ibid.*, 1952, **74**, 966; UO_2SO_4 , Morgans, Ph.D. Thesis, Univ. of Wales, 1959. Cobalt pentammine spectra are from von Kiss and Czegledy, *Z. anorg. Chem.*, 1938, **235**, 407. All the lanthanide data are from the preceding paper. Other points not referenced were measured during this study. A, Sm^{3+} ; B, Yb^{3+} ; C, UO_2^{2+} ; D, Eu^{3+} ; E, Cu^{2+} ; F, Fe^{3+} . [Right hand scale refers to Cu^{2+} and Fe^{3+} .]

transition metals, three lanthanides and one actinide studied, the lowest energy-allowed bands result from charge-transfer from the single group X to the metal. The unit slope of the plots in Fig. 1 also ensures that there is a reciprocal correlation between the bands

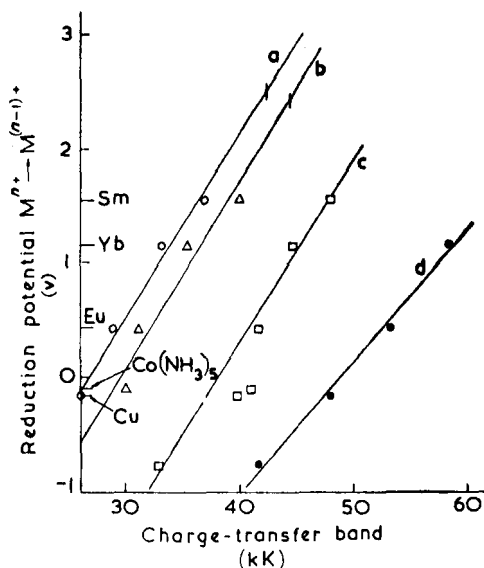
of pairs of anions with a series of metals. The points scatter surprisingly little about the line of unit slope, the major exceptions being those for $X = \text{H}_2\text{O}$. These occur at such a high energy that they are difficult to measure accurately.

DISCUSSION

Plots of the same type as Fig. 1 can be used in discussing a number of chemical problems. In the following sections they are applied to the study of stereochemistry, redox potentials, solvent effects, and band assignments.

Copper(II) Spectra.—The deviation of the two cupric monohalide points cannot be ascribed to experimental error because the spectra contained very well defined bands and the species are definitely characterized. A line joining the two points is approximately parallel to the line through the other cupric points but about 7 kK higher. One explanation for the difference between the halogens and the other complexes might be that they occupy a different type of site. Now it is well known that the cupric ion has a distorted environment in many solid compounds owing to the Jahn–Teller effect. Most frequently there are four ligands close to the metal and two further away, forming an elongated octahedron. Thus formally it is possible for a ligand to occupy one of two distinguishable sites. Where the co-ordination sphere contains two dissimilar ligands it has been suggested⁵ that the group producing the higher ligand field occupies the sites closer to the metal. Thus in both forms of $\text{Cu}(\text{NH}_3)_2\text{Br}_2$ where two ammonia molecules and four bromide ions are attached to the copper,⁶ the ammonia ligands are along a short axis. One form has two

FIG. 2. Reduction potentials and charge-transfer bands. a, Thiocyanate (ethanol); b, Bromide (ethanol); c, Sulphate (aqueous); d, Water.



bromide atoms completing the equatorial plane and the remaining bromides axial, whereas in the other the four bromide atoms complete a flattened octahedron. No X-ray structure has revealed a group producing a higher ligand field lying at substantially greater distance than one of lower field. The halogens have a markedly weaker ligand field strength than oxygen donors and thiocyanate, and so in solution the halogen donors are much more likely to remain on the long axis. A comparison of the spectra of $[\text{Co}(\text{NH}_3)_5\text{Br}]^{2+}$ and $[\text{Co}(\text{NH}_3)_6]^{3+}\text{Br}^-$ shows that the longer the internuclear distance the higher the energy of the charge transfer transition. The band observed in the hexa-aquocupric ion must represent electron transfer from the closest water, and since the other oxygen donors and thiocyanate give a good 1 : 1 slope through this point in Fig. 1 we can assume that the

lowest energy band represents charge transfer from the ligand X when the Cu-X distance is at its shortest. This explains the unusually high energies of the copper halide bands.

Correlation with Redox Potentials.—Dainton⁷ studied the charge-transfer spectra and redox potentials of a series of first-row transition metals. He found a good linear correlation between the edge of the intense absorption of the divalent metal perchlorates in aqueous solution and the M^{3+}/M^{2+} standard potentials. These spectra result from charge transfer from M^{2+} to the solvent. The use of the edge rather than the band maximum is probably justified since the band half widths are not likely to change greatly from one element to another. In Fig. 2 we plot data for some of the species already discussed against the one electron reduction potentials for the metal ions.⁸ The plots, which are approximately linear, have slopes near to that observed by Dainton, but of course with the opposite sign. We find that 1 volt (redox) corresponds to 8 ± 1 kK, that is roughly to 1 eV.

One use of this correlation is to predict inaccessible reduction potentials where charge-transfer energies are known. For example, we know the position of the bands in $TmCNS^{2+}$ and $TmBr^{2+}$ in ethanol and by inserting these values in plots for other thiocyanates and bromides in ethanol (Fig. 2) we obtain two estimates of $E_0(Tm^{3+}/Tm^{2+})$, both in the region of 2.5 v. No experimental value for this potential has ever been reported but it is known to be well above that of Sm^{3+} , 1.55 v.

Ultraviolet Spectra of Thiocyanate Complexes.—We have already noted that when the charge-transfer energies of a series of metals with a given anion are plotted against the energies for the same metals with a second anion, straight lines of nearly unit slope are obtained. With other anions, similar plots may be used to test assignments by investigating the correlation with sets of bands known to originate from charge transfer.

Aqueous potassium thiocyanate has its first absorption maximum well above 50 kK (55 kK in the solid), but a number of thiocyanate complexes have an intense band in the near-ultraviolet region whose position is nearly independent of the oxidizing character of the metal ion. This band has been ascribed to a strongly perturbed ligand transition.⁹ In contrast, the intense visible absorption of $Fe(NCS)(H_2O)_5^{2+}$ is usually described as a charge-transfer absorption. Elsewhere we have assigned the monosulphate frequencies in Fig. 1 to charge transfer,⁴ and Fig. 3 shows that there is a good 1 : 1 correlation with the corresponding thiocyanate frequencies. Furthermore, non-reducible ions such as La^{3+} , Gd^{3+} , and Zn^{2+} produce no such bands. There is little doubt, therefore, that the u.v. bands in the thiocyanates of all the reducible metals in Fig. 3 result from charge transfer to the metal.

Most of the data supporting the hypothesis of a perturbed ligand transition refer to Group VIII complexes where the ligand is bound to the metal through sulphur,¹⁰ and in contrast to the thiocyanates in Fig. 3 the metal-to-thiocyanate ratio is either four or six. In Fig. 4 we plot these band maxima against the lowest energy charge transfer bands of the chloride and bromide complexes of the appropriate stoichiometry. It can be seen that some small dependence on the metal remains.

The energy levels of linear triatomic molecules, including SCN^- , have been classified by Mulliken¹¹ and discussed at greater length by Walsh.¹² They agree that the highest occupied level, 2π in Mulliken's notation, has very little charge on the carbon atom (none in an A-B-A molecule) and consists mainly (entirely in A-B-A) of two pairs of out-of-phase $p\pi$ orbitals on the end atoms. In the lowest vacant molecular orbital charge is more evenly distributed between the three $p\pi(x)$ and $p\pi(y)$ orbitals, adjacent pairs of atomic orbitals being out of phase. In 2π , most of the charge will be placed on the nitrogen because of its greater electronegativity, so the lowest-energy absorption results in a net transfer of charge from nitrogen to carbon. Let us examine the effect on this absorption of attaching a reducible metal to either end of the ligand.

At the nitrogen end, an electron-attracting metal is expected to hinder the transfer of charge from nitrogen to carbon, raising the energy of the ligand transition. A metal atom

at the sulphur end, however, will have the opposite effect, and stabilize the ligand excited state by withdrawing charge from the nitrogen. Thus we have an explanation for the metal dependence shown in Fig. 4. The small shifts compared with the halide ligand-to-metal charge-transfer spectra are accounted for if the thiocyanate transitions are localized on the ligand. Oxidizable metals bound to the nitrogen end of thiocyanate would be expected to have the same effect on the ligand transition as reducible metals bound to sulphur. The only reported spectra of such species, $\text{Co}(\text{NCS})_4^{2-}$ and $\text{Mo}(\text{NCS})_6^{3-}$, have their first intense bands at 32.8 and 31.0 kK, respectively.^{9,13} We cannot compare these

FIG. 3. Ultraviolet spectra of thiocyanate, chloride, and sulphate complexes.

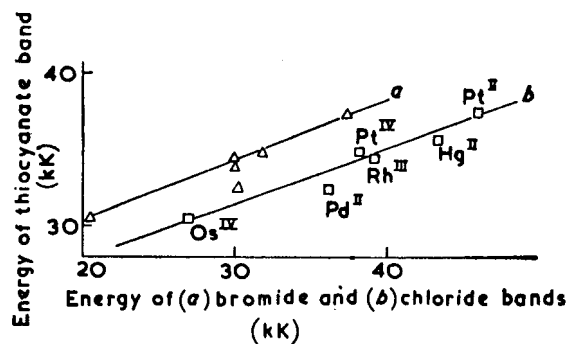
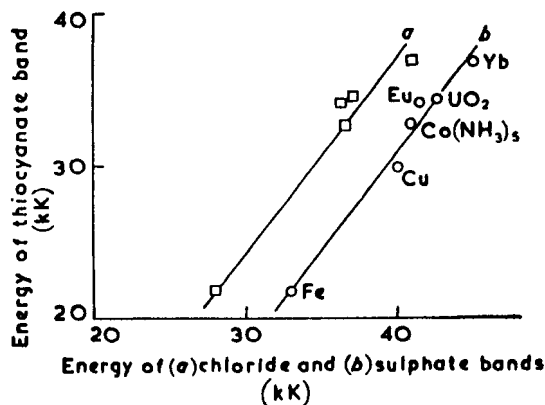


FIG. 4. Ultraviolet spectra of chloride, bromide, and thiocyanate complexes.

with CoCl_4^{2-} and MoCl_6^{3-} spectra because the latter result from charge transfer to the metal. Referring to $\text{Co}(\text{NCS})(\text{H}_2\text{O})_5^+$, the band at 36.7 kK is not a ligand-to-metal charge transfer because Fig. 3 would then predict a cobalt monosulphate band at about 44 kK, whereas solutions containing this species have no absorption below that of sulphate itself. The band in $\text{Co}(\text{NCS})(\text{H}_2\text{O})_5^+$, and probably also the one in $\text{Co}(\text{NCS})_4^{2-}$, is therefore the same perturbed ligand transition as in the Group VIII complexes. We have no clear data on the one remaining class of thiocyanate complex, that of an oxidizable metal bound through sulphur. One might expect that platinum(II) would act as a donor to thiocyanate rather than an acceptor, but Gray and Ballhausen¹⁴ have assigned the tetrahalide bands as ligand-to-metal charge transfer and these, when plotted with the thiocyanate values (Fig. 4), give points on the line.

Our conclusion then is that the lowest-energy-allowed transitions of reducible metal thiocyanates bound through nitrogen should be of charge-transfer type, whilst reducible metal thiocyanates bound through sulphur, and oxidizable metal thiocyanates bound through nitrogen exhibit only the perturbed ligand band.

Spectra in Ethanol.—The difficulty in discussing spectra of complexes in non-aqueous solvents is that few studies have related them to stoichiometries and formation constants. We know that the charge-transfer spectra are a very sensitive function of the metal-to-

ligand ratio. For example, CuBr^+ in aqueous solution has a single band at 36.0 kK, but as more bromide is added it splits into two, and further bands appear in the visible region as species up to CuBr_4^{2-} are formed. The energy of the first band observed as bromide is added to cupric perchlorate solutions decreases when ethanol replaces water in the solvent.¹⁵ We have to decide whether this is due to the formation of higher species or simply to the replacement of water by ethanol round the central atom. Both in water^{15a} and 90% ethanol,^{15c} the band has been proved to represent only CuBr^+ though the formation constant rises from 2 to 10 in the medium of lower dielectric constant. When excess of bromide is added the band shape changes in the same way in 100% ethanol as in water or 90% ethanol so the first species in ethanol is also CuBr^+ . We can therefore say quite definitely that the shift shown for CuBr^+ in Table 1 does represent the effect of solvation changes and not the formation of higher species.

This movement of ion-pair charge-transfer bands to lower energy as we change from water to ethanol is quite general. In Table 1 we present the band positions for copper(II) and uranyl halides and pseudohalides in the two solvents. The shifts are all very similar. Table 2 shows that for EuNCS^{2+} the change is not linear with percentage composition of solvent, most of the movement occurring between 90 and 100% ethanol. The much smaller shifts in ligand-field spectra show the same solvent dependence. To study the shifts with solvent we have used plots of the same type as Fig. 1. When the charge-transfer band positions of one ligand are plotted against those of another in the same solvent they form a straight line of almost unit slope, e.g., in water, thiocyanate against sulphate, and in ethanol, thiocyanate against bromide. However, when we plot the ethanolic data for thiocyanate, chloride, and bromide against that for aqueous sulphate we get a set of parallel straight lines but their slope is no longer close to unity (data in Table 3, ref. 4).

We can seek an explanation for these observations in Jørgensen's concept of optical electronegativity.^{2,3} He holds that the energy of the charge-transfer band represents the difference in energy between ligand donor and metal acceptor orbitals. As we have already mentioned, the latter must be corrected for the energy required to change the spin multiplicity of the metal, and for the energy difference between the unsplit d -shell of the free ion and the orbital to which the electron is transferred in the complex. The latter is a function of the ligand field splitting parameter Δ . Thus the energy of the charge transfer band is given by

$$\delta = E_L - E_M - (\text{spin-pairing correction}) + \Delta$$

The ligand and metal energies E_L , E_M are atomic parameters and independent of solvent. For the copper compounds the spin-pairing correction is zero, so on Jørgensen's theory the shift would be entirely attributable to a change in Δ . The shifts shown in Table 1 are

TABLE 1.
Charge-transfer bands of 1 : 1 complexes (kK).

	Cu^{2+}			UO_2^{2+}		
	Water	Ethanol	Diff.	Water	Ethanol	Diff.
Cl	40.4	36.0	4.4	37.0	33.9	3.1
Br	36.0	32.3	3.7	33.3	30.0	3.3
NCS	29.4	26.0	3.4	34.5	29.4	5.1
CN				32.3	29.0	3.3

TABLE 2.

Solvent dependence of the europium monothiocyanate charge-transfer band.

% Ethanol	0	20	40	60	80	90	95	100
max. (kK)	34.5	34.5	34.5	33.9	33.3	32.8	32.5	29.4

over 3 kK for copper but the ligand-field band shift is only 0.14 kK so this cannot be the complete explanation. The spin-pairing correction for UO_2^{2+} is also zero ($5f^0 \rightarrow 5f^1$), but in the same way, we do not expect Δ to change by 3 kK between water and ethanol.

A more probable explanation for the shifts is that solvents of lower dielectric constant will stabilize the less dipolar excited state, so that in going from water to ethanol the band moves to lower energy. The absorption bands of organic charge transfer complexes have a comparable solvent dependence, though since the excited state is usually more dipolar than the ground state, the bands move to lower energy¹⁶ in solvents of higher dielectric constant. The potential-energy difference between a 2.5 Å dipole in water (ϵ 80) and ethanol (ϵ 30) is roughly equivalent to 1 kK, so that coulomb stabilization of the ground state by the solvent provides a major contribution to the observed shift.

Besides the additive correction of Table 2, the fact that the plots do not have unit slope suggests that a multiplicative correction is also necessary. That such a correction applies only to the cation can be seen at once from the constancy of the shifts for different ligands with the same metal in Table 1, but Jørgensen's optical electronegativity theory only provides for additive corrections to the energy levels of the metal. Deviations from unit slope are well known in organic donor-acceptor complexes, when the band maxima for a given donor with a set of acceptors are plotted against the maxima in the complexes of another donor having, for example, the additional possibility of forming hydrogen bonds.¹⁷ Perhaps a similar explanation could be given for our own observations, but Mulliken¹⁸ has pointed out that the linear relationships frequently found between bands in organic donor-acceptor complexes are not obvious from theoretical arguments.

We thank Drs. C. K. Jørgensen and R. J. P. Williams for discussions, N.A.T.O. for a Fellowship (to J. C. B.), and the D.S.I.R. for a Studentship (to P. D.).

INORGANIC CHEMISTRY LABORATORY,
SOUTH PARKS ROAD, OXFORD.

[Received, October 1st, 1963.]

- ¹ Jørgensen, *Mol. Phys.*, 1959, **2**, 309.
- ² Jørgensen, *Mol. Phys.*, 1963, **6**, 43.
- ³ Jørgensen, *Mol. Phys.*, 1962, **5**, 271.
- ⁴ Barnes, preceding Paper.
- ⁵ Wells, "Structural Inorganic Chemistry," Oxford University Press, Oxford, 3rd edn., p. 89.
- ⁶ Hanic, *Acta Cryst.*, 1959, **12**, 739; Hanic and Cakajdova, *ibid.*, **11**, 610.
- ⁷ Dainton, *J.*, 1952, 1533.
- ⁸ Latimer, "Oxidation Potentials," Prentice-Hall, N.J., 2nd edn., 1952.
- ⁹ Jørgensen, "Absorption Spectra and Chemical Bonding in Complexes," Pergamon, Oxford, 1962, p. 196.
- ¹⁰ *E.g.*, Mitchell and Williams, *J.*, 1960, 1912.
- ¹¹ Mulliken, *J. Chem. Phys.*, 1935, **3**, 720; *Rev. Mod. Phys.*, 1942, **14**, 204.
- ¹² Walsh, *J.*, 1953, 2260.
- ¹³ Lewis, Nyholm, and Smith, *J.*, 1961, 4597.
- ¹⁴ Gray and Ballhausen, *J. Amer. Chem. Soc.*, 1963, **85**, 260.
- ¹⁵ (a) Farrington, *J. Amer. Chem. Soc.*, 1952, **74**, 966; (b) Matsuo, *J. Chem. Soc. Japan*, 1961, **82**, 1330; (c) Barnes and Hume, *J. Phys. Chem.*, 1963, **67**, 526.
- ¹⁶ Foster and Hammick, *J.*, 1954, 2685.
- ¹⁷ Foster, *Trans. Faraday Soc.*, 1963, **59**, 1059.
- ¹⁸ Reid and Mulliken, *J. Amer. Chem. Soc.*, 1954, **76**, 3869.

Reprinted from THE JOURNAL OF CHEMICAL PHYSICS, Vol. 49, No. 1, 392-403, 1 July 1968
 Printed in U. S. A.

Analysis of the Charge-Transfer Spectra of Some First-Transition-Series Tetrahalide Complexes

B. D. BIRD AND P. DAY

University of Oxford, Inorganic Chemistry Laboratory, Oxford, England

(Received 27 November 1967)

The charge-transfer spectra of 10 tetrahalide complexes of the first transition series have been measured at 77°K in the form of evaporated films or rigid glassy solutions. To assign the spectra in detail, theoretical expressions are developed, using vector coupling methods, to describe the first-order effect of spin-orbit coupling at both the metal and the ligand nucleus on the terms arising from each of the excited charge-transfer configurations. Theoretical expressions for the intensities of charge-transfer transitions are also derived by the same method and tested by substituting approximate LCAO eigenvectors. The assignments established by these arguments lead to the conclusion that the highest occupied orbitals of mainly ligand character occur throughout in the order $1e < 3t_2 < 4t_1$ with a total energy spread of about 15 kK.

In proportion to the experimental and theoretical ingenuity devoted to measuring and analyzing electric-dipole forbidden transitions of metal complexes in the last 20 years,^{1,2} the electric-dipole-allowed bands have been rather neglected. Apart from the pioneering work of Jørgensen on hexalides,³ and a long-standing⁴ and continuing⁵ interest in the spectrum of MnO_4^- , there is little detailed work to which one can refer. Neither is there any commonly accepted theoretical scheme for analyzing such spectra and extracting theoretical parameters from them in the way which has become commonplace in ligand-field spectroscopy. This is curious, since in many respects electric-dipole-allowed transitions should be capable of much simpler theoretical treatment than those which are forbidden by symmetry or spin selection rules, as has been found in the study of organic molecular spectra.⁶ Yet it is probably true to say that at the present moment, there is not a single charge-transfer spectrum of any metal complex whose detailed assignment, band by band, is universally agreed upon. For this there are a number of reasons, both experimental and theoretical: the bands are nearly always intense, and quite frequently rather broad; they sometimes occur far enough into the ultraviolet to become entangled with intraligand transitions and absorption by the solvent. Theoretical analyses encounter the difficulty that one can no longer use a perturbation approach based on the assumption that both ground and excited orbitals are largely localized on the same atomic center. However, there can be no doubt that if correctly analyzed, these spectra contain a wealth of information in some ways more relevant to chemists than that furnished by intrasubshell transi-

tions because it concerns orbitals of both metal and ligand character, some of which are deeply engaged in molecular binding. Before such information can be extracted, detailed unambiguous spectral assignments must be established. Molecules of high symmetry and low molecular complexity are obvious candidates for such a program, of which Jørgensen's hexahalide work³ is a good example. Tetrahedral oxyanions other than permanganate have also received some attention,⁷ but we believe that as a starting point for the simple analysis of charge-transfer spectra they have the disadvantage of a high degree of covalency. It may be helpful in making preliminary assignments to be able to say that the orbital from which an electron comes is predominantly ligand in character while that to which it goes is almost entirely metal. From this point of view the tetrahalide complexes of the first transition metals with oxidation states 2+ and 3+ commend themselves. A further reason for preferring to begin by studying 3d complexes is that the spin-orbit coupling constants of these metals are relatively low.⁸

The room-temperature charge-transfer spectra of many of the 3d tetrahalides, with some tentative assignments, have been given in a previous paper.⁹ To obtain better resolution of the many overlapping bands, measurements have now been made at low temperatures and, in a number of cases, to considerably higher energies.

EXPERIMENTAL

Crystalline samples of the tetrahalogeno anions were prepared as tetramethylammonium and tetraethylammonium salts by well-established methods,¹⁰ and satisfactory analyses were obtained.

Since the absorption bands to be measured have molar extinction coefficients of 3000 and upwards, measurements must be made either on dilute solutions or with very short path lengths. Of the solvents which

¹ C. K. Jørgensen, *Absorption Spectra and Chemical Bonding in Complexes* (Pergamon Press, Ltd., Oxford, England, 1962).

² C. J. Ballhausen, *Introduction to Ligand Field Theory* (McGraw-Hill Book Co., New York, 1963).

³ C. K. Jørgensen, *Mol. Phys.* **2**, 309 (1959).

⁴ M. Wolfsberg and L. Helmholz, *J. Chem. Phys.* **20**, 837 (1952).

⁵ S. L. Holt and C. J. Ballhausen, *Theoret. Chim. Acta* **7**, 313 (1967).

⁶ J. N. Murrell, *The Theory of the Electronic Spectra of Organic Molecules* (Methuen and Co., Ltd., London, 1963).

⁷ A. Carrington and D. S. Schonland, *Mol. Phys.* **3**, 331 (1960).

⁸ T. M. Dunn, *Trans. Faraday Soc.* **57**, 1441 (1961).

⁹ P. Day and C. K. Jørgensen, *J. Chem. Soc.* **1964**, 6226.

¹⁰ N. S. Gill and R. S. Nyholm, *J. Chem. Soc.* **1959**, 3997.

form clear rigid glasses at 77°K,¹¹ only ethanol sufficiently dissolved both the compounds and an excess of tetra-alkylammonium halide, required to suppress solvolysis. For each compound, spectra were measured at room temperature in ethanolic solution containing various concentrations of excess halide ion to discover the lowest concentration at which solvolysis was completely suppressed.

Spectra were measured at 77°K in a VLT-2 cryostat containing a FM-01 cell, both made by Research and Industrial Instruments Company. The spectrophotometer used was a Unicam SP700.

Two major disadvantages of working with glassy solutions are, first, that the glass quite often cracks, imparting a slope to the baseline of the spectrum and, second, that the large concentration of excess halide ion present obscures the farther ultraviolet. A much more convenient technique, using samples in the form of evaporated films, was therefore devised.¹²

When attempting to prepare crystalline samples of tetrahalogeno complexes using tetra-*n*-butylammonium as cation, it was noticed that evaporation of ethanolic solutions of the salt left, not crystals, but a gum, and that crystallization only took place after a matter of days. Evaporation of a few drops of such a solution on the window of the low-temperature cell gave a thin amorphous film, entirely homogeneous under the microscope, whose transmission spectrum corresponded precisely, both as to the positions and relative intensities of the bands, with that of a solution in dichloromethane containing excess halide ion. The spectra of all the cobalt(II) and nickel(II) tetrahalides in Figs. 4 and 5 were measured in this way, and the absence of solvent and excess halide ion permitted spectra to be recorded up to much higher energies than previously.⁹ The next series of absorption bands beyond those shown in Figs. 2-5 are approximately 10 times more intense and, from their relatively small energy variation from one complex to another, have been characterized as basically internal halide-ion transitions.

Evaporated films containing FeCl_4^- and FeBr_4^- could not be prepared using tetra-*n*-butylammonium halides, as crystallization occurred much more readily. Figure 3 therefore presents the low-temperature spectra of these anions in ethanolic glasses.

THEORY

The charge-transfer spectra of metal-halide complexes result from excitation of electrons from σ - and π -bonding orbitals of predominantly ligand character or from nonbonding ligand orbitals into vacancies in the σ - and π -antibonding orbitals, which are mainly localized on the metal.³ In tetrahedral complexes, we

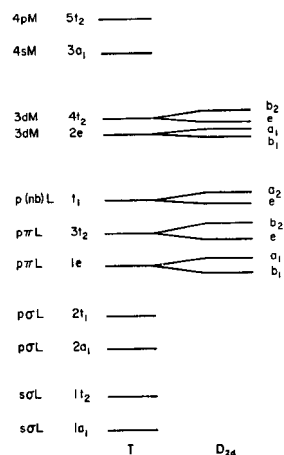


FIG. 1. Qualitative molecular-orbital scheme for a tetrahedral (T_d) or flattened tetrahedral (D_{3d}) molecule MX_4^{n-} , using a basis set consisting of $3d$, $4s$, $4p$ of M and ns and np of L. The left-hand column lists the atomic orbital expected to make the largest contribution to each molecular orbital.

are concerned with the one-electron molecular orbitals $1e$, $2e$, t_1 , $3t_2$, and $4t_2$, using the conventional numbering scheme (Refs. 13, 14, and Fig. 1), and hence with excited-electron configurations such as $(t_1)^6(2e)^3(4t_2)^3(\text{FeX}_4^-)$. In general, these configurations each give rise to a number of spectroscopic terms (Table I), but we only consider those which are accessible by electric-dipole-allowed transitions from the ground state. The first problem is to assign the observed absorption bands to these terms.

Each band is characterized experimentally by its energy and intensity. The energy depends both on the difference in one-electron orbital energy between, say, t_1 and $2e$, and on the change in interelectron repulsion accompanying the transition. An assessment of the latter good enough to be of any use in assignment would require the full rigour of an SCF-MO calculation, but even in the few cases in which this has been seriously attempted,^{15,16} a good deal of uncertainty still remained. Our aim is rather to use assignment of the spectra to extract empirical information which could then be used to parametrize theoretical calculations. Though absolute calculations of transition energies are therefore out of the question at the moment, assessment of the contributions of smaller perturbation terms in the molecular hamiltonian looks a more promising line of attack. A feature at once apparent from Figs. 2-5 is the increasing complexity of the spectra going from chloride to iodide. This is unlikely to be the result of increasingly resolved vibrational fine structure since metal-halogen vibrational frequencies

¹³ C. J. Ballhausen and H. B. Gray, *Molecular Orbital Theory* (Benjamin Press, Inc., New York, 1964), pp. 108-109.

¹⁴ P. Ros and C. G. A. Schuit, *Theoret. Chim. Acta* **4**, 1 (1966).

¹⁵ S. Sugano and R. S. Shulman, *Phys. Rev.* **130**, 517 (1963).

¹⁶ J. P. Dahl and C. J. Ballhausen, *Advan. Quantum Chem.* **4**, 170 (1967).

¹¹ For a useful list, see F. J. Smith, J. K. Smith, and S. P. McGlynn, *Rev. Sci. Instr.* **33**, 1367 (1962).

¹² B. D. Bird and P. Day, *Chem. Commun.* **1967**, 741.

decrease in that order. Following Jørgensen, we therefore connect the appearance of fine structure with the increasing spin-orbit coupling constant of the halogen. Thus we derive expressions for the diagonal matrix elements of spin-orbit coupling for the various charge-transfer states and compare them with the experimental fine structure in Figs. 2-5. Information of potential value in assigning the electric-dipole-allowed transitions is also contained in the observed intensities of the bands. To extract it, as well as to calculate the matrix elements of spin-orbit coupling, requires the construction of ground- and excited-state wavefunctions which span the appropriate representations of the orbital (or, in the case of spin-orbit coupling, spinor) group. For states of high degeneracy, this procedure is rather laborious and we therefore make use of the tensor-operator method, which was first developed by Racah¹⁷ and Wigner¹⁸ for treating problems in spherical symmetry. Tanabe and Kamimura¹⁹ applied the method to lower symmetries, when calculating matrix elements of spin-orbit coupling for octahedral crystal-field states, but for the present purpose the most convenient formulation is that of Griffith.²⁰

Griffith defined vector coupling coefficients, V coefficients, such that the basis functions $|c\gamma\rangle$ of a direct-product representation c are related to the components of the basis functions $|\alpha\alpha\rangle$, $|\beta\beta\rangle$ of the constituent representations ($a \times b = c$) by

$$|c\gamma\rangle = [\lambda(c)]^{1/2} \sum_{\alpha} \sum_{\beta} V \begin{pmatrix} a & b & c \\ \alpha & \beta & \gamma \end{pmatrix} |\alpha\alpha\rangle |\beta\beta\rangle,$$

where $\lambda(c)$ is the degeneracy of c and α, β , and γ denote components of the basis functions. These coefficients enable us to express the matrix elements of a tensor operator g^e spanning the irreducible representation c

$$\begin{aligned} \langle a^{m-1}(\frac{1}{2}a)b^n(S'h')Sh || \sum_{\mathbf{r}} \mathbf{r} || a^m(1A_1)b^{n-1}(Sh'')Sh'' \rangle \\ = (-1)^{3S+S'+3/2}(n(2S'+1)\lambda(h)\lambda(h')/2S+1)^{1/2} \langle b, b^{n-1}(Sh'') || b^n(S'h') \rangle \\ \times W \begin{pmatrix} a & b & T_2 \\ h' & h & h' \end{pmatrix} \langle b || \mathbf{r} || a \rangle, \quad (4) \end{aligned}$$

where the terms corresponding to the subshell configurations have degeneracies λ and the coefficients of fractional parentage for the T_d group are available.²⁰ Calculations of the intensities to be expected of charge-transfer transitions such as $(t_1)^6(2e)^4(4t_2)^3(4A_2)$

¹⁷ G. Racah, Phys. Rev. **62**, 438 (1942).

¹⁸ E. Wigner, *Group Theory and its Application to the Quantum Mechanics of Atomic Spectra* (Academic Press Inc., New York, 1959).

¹⁹ Y. Tanabe and H. Kamimura, J. Phys. Soc. Japan **13**, 880 (1958).

²⁰ J. S. Griffith, *The Irreducible Tensor Method for Molecular Symmetry Groups* (Prentice-Hall, Inc., Englewood Cliffs, N.J., 1962).

thus:

$$\langle \alpha\alpha | g_r^e | \beta\beta \rangle = \langle a || g^e || b \rangle V \begin{pmatrix} a & b & c \\ \alpha & \beta & \gamma \end{pmatrix}, \quad (1)$$

where the reduced matrix element $\langle a || g^e || b \rangle$ is simply a constant independent of the components of a , b , and g^e . Thus we can relate matrix elements differing only in the components of the functions they contain. Eq. (1) is an extension of the Wigner-Eckart theorem.²¹ Our interest is in the matrix elements of n -electron molecular systems, for example in the term $2S+1h$ of the configuration a^n , so we begin by reducing the matrix elements of a one-electron spin-independent operator U^f for n electrons over the n -electron wavefunctions to those of an operator for one electron, first by reducing it,

$$\begin{aligned} \langle a^n ShM\theta | U_{\phi}^f | a^n S'h'M'\theta' \rangle \\ = \delta_{SS'}\delta_{MM'}\langle a^n ShM || U^f || a^n S'h'M' \rangle V \begin{pmatrix} h & h' & f \\ \theta & \theta' & \phi \end{pmatrix}, \quad (2) \end{aligned}$$

and then by a further reduction to a matrix element of the space function of a alone. Griffith²⁰ has shown that

$$\langle a^n ShM || U^f || a^n S'h'M' \rangle = \langle a || U^f || a \rangle g_{hh'}(a, f), \quad (3)$$

where the $g_{hh'}(a, f)$, which are available²⁰ as a tabulation, are functions of the coefficients of fractional parentage²² between a^{n-1} and a wavefunctions and also of sums of products of V coefficients, called by Griffith W coefficients. Expressions can also be derived for matrix elements between configurations such as $a^{m-1}b^n$ and $a^m b^{n-1}$. The spin-independent operator of relevance to the present study is the electric-dipole-moment operator, and it is also worth noting that we are throughout concerned with ground-state configurations in which one of the subshells is completely filled. A development of Eq. (3) is then

$(t_1)^5(2e)^4(4t_2)^4(4T_1)$ in CoX_4^{2-} therefore reduce to the evaluation of Eq. (4) and the estimation of $\langle b || \mathbf{r} || a \rangle$ from suitable wavefunctions, if available.

The quantity to be calculated is the dipole strength $D = [1/\lambda(a)]$

$$\times \sum_{ij} | \langle \Psi(\text{ground state}) | \mathbf{r} | \Psi(\text{excited state}) \rangle |^2, \quad (5)$$

²¹ B. R. Judd, *Operator Techniques in Atomic Spectroscopy* (McGraw-Hill Book Co., New York, 1963).

²² J. S. Griffith, *The Theory of Transition Metal Ions* (Cambridge University Press, London, 1960).

TABLE I. Charge-transfer excited states of tetrahalide complexes in the absence of spin-orbit coupling. Terms to which transitions are forbidden are in parentheses.

Ground state:	6A_1	4A_2	3T_1
Allowed excited terms:	6T_2	4T_1	${}^3A_2, {}^3E, {}^3T_1, {}^3T_2$
One-electron transitions:			
$t_1 \rightarrow 2e$	$({}^6T_1) {}^6T_2$	2e full	2e full
$t_1 \rightarrow 4t_2$	$({}^6A_2) ({}^6E) ({}^6T_1) {}^6T_2$	$({}^4A_1) ({}^4E) {}^4T_1 ({}^4T_2)$	${}^3A_2, {}^3E, {}^3T_1, {}^3T_2$
$3t_2 \rightarrow 2e$	$({}^6T_1) {}^6T_2$	2e full	2e full
$3t_2 \rightarrow 4t_2$	$({}^6A_1) ({}^6E) ({}^6T_1) {}^6T_2$	$({}^4A_2) ({}^4E) {}^4T_1 ({}^4T_2)$	$({}^3A_1) {}^3E, {}^3T_1, {}^3T_2$
$1e \rightarrow 2e$	$({}^4A_1) ({}^6A_2) ({}^6E)$	2e full	2e full
$1e \rightarrow 4t_2$	$({}^6T_1) {}^6T_2$	${}^4T_1 ({}^4T_2)$	${}^3T_1, {}^3T_2$

where the summation is over all the components of the excited state and $\lambda(a)$ is the degeneracy of the ground state. Using the transition $A_2 \rightarrow T_1$ as an example, Eq. (1) enables us to put

$$\langle A_2 \parallel \sum_i r_i \parallel T_1 \rangle = \sqrt{3} \langle A_2 \mid x \mid T_1(x) \rangle,$$

so that

$$D = \langle A_2 \parallel \sum_i r_i \parallel T_1 \rangle^2. \quad (6a)$$

Similarly, for the other dipole-allowed transitions of interest,

$$T_1 \rightarrow A_2: D = \frac{1}{3} \langle T_1 \parallel \sum r \parallel A_2 \rangle^2, \quad (6b)$$

$$T_1 \rightarrow E: D = \frac{1}{3} \langle T_1 \parallel \sum r \parallel E \rangle^2, \quad (6c)$$

$$T_1 \rightarrow T_1: D = \frac{1}{3} \langle T_1 \parallel \sum r \parallel T_1 \rangle^2, \quad (6d)$$

$$T_1 \rightarrow T_2: D = \frac{1}{3} \langle T_1 \parallel \sum r \parallel T_2 \rangle^2. \quad (6e)$$

Equation (4) enables these reduced matrix elements of state wavefunctions to be further reduced to one-electron reduced matrix elements and hence, by a final application of Eq. (1), to ordinary one-electron matrix elements. The relations between the reduced and ordinary one-electron matrix elements thus derived are

$$\langle e \parallel r \parallel t_1 \rangle = \sqrt{3} \langle e(\varepsilon) \mid z \mid t_1(z) \rangle, \quad (7a)$$

$$\langle t_2 \parallel r \parallel t_1 \rangle = 6^{1/2} \langle t_2(x) \mid y \mid t_1(z) \rangle, \quad (7b)$$

$$\langle t_2 \parallel r \parallel e \rangle = -\sqrt{3} \langle t_2(z) \mid z \mid e(\theta) \rangle, \quad (7c)$$

$$\langle 3'2 \parallel r \parallel 4t_2 \rangle = -6^{1/2} \langle 3t_2(z) \mid y \mid 4t_2(x) \rangle. \quad (7d)$$

We now wish to derive relationships between the ordinary one-electron matrix elements and the analytic form of the molecular orbitals, but the type of approximation to be employed requires some preliminary

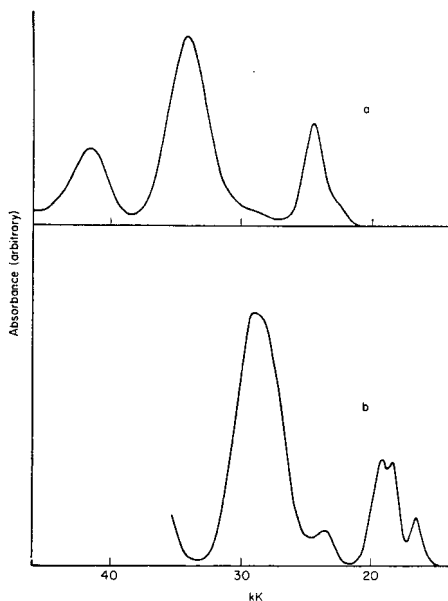


FIG. 2. The charge-transfer spectra of (a) CuCl_4^{2-} (evaporated film) and (b) CuBr_4^{2-} (glassy solution) at 77°K.

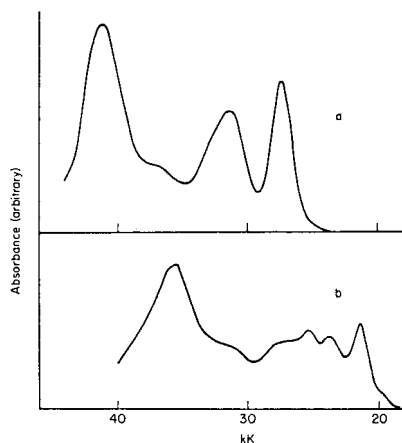


FIG. 3. The charge-transfer spectra of (a) FeCl_4^- and (b) FeBr_4^- , measured at 77°K in ethanolic glasses.

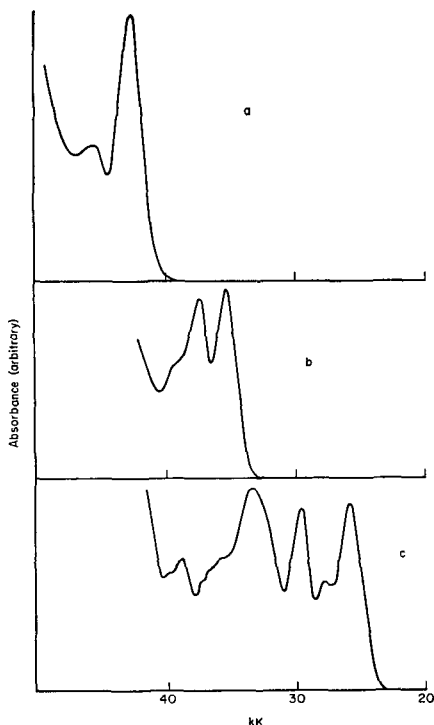


FIG. 4. The charge-transfer spectra of (a) CoCl_4^{2-} , (b) CoBr_4^{2-} , and (c) CoI_4^{2-} at 77°K . (a) and (c) are evaporated films and (b) an ethanolic glass.

discussion. Wolfsberg and Helmholz,⁴ who were the first to calculate transition-moment integrals for tetrahedral metal complexes, neglected all two-center integrals in the expansion of the molecular orbitals, thus arriving at a simple expression involving only the projection of the metal-ligand bonds on to the x axis and the molecular-orbital mixing coefficients. Likewise Carrington and Schonland⁷ neglected "charge-transfer" integrals when calculating molecular-orbital coefficients for MnO_4^- from spectral intensities, an approximation whose validity was recently demonstrated by an exact calculation²³ of the oscillator strengths for CuCl_4^{2-} . If the molecular orbitals of the complex are written

$$\phi = C_M \chi_M + C_L \chi_L, \quad (8)$$

where χ_M and χ_L are symmetry-adapted metal and ligand orbital combinations, the calculation of Avoird and Ross²³ showed that the only appreciable contribution to $\langle \phi | \mathbf{r} | \phi \rangle$ was $C_L C_L' \langle \chi_L | \mathbf{r} | \chi_L' \rangle$. Their conclusion has been further confirmed by Weirs and Reynolds²⁴ for a wide range of C_L . If integrals involving

²³ A. van der Avoird and P. Ros, *Theoret. Chim. Acta* **4**, 13 (1966).

²⁴ B. H. Wiers and W. L. Reynolds, *Inorg. Chem.* **5**, 2016 (1966).

atomic orbitals on different ligands are also neglected,

$$\langle \psi_{ir} | q | \psi_{js} \rangle = \pm \delta_{rs} \delta_{ij} R / \sqrt{3}, \quad (9)$$

where ψ_{ir} and ψ_{js} are ligand orbitals r and s on centers i and j , q is x , y , or z , and $\pm R/\sqrt{3}$ is the projection of R , the metal-ligand distance, on the q axis. The one-electron transition dipole matrix elements required to calculate the intensities of transitions from $1e$, $3t_2$, and t_1 to $2e$ and $4t_2$ are thus found to be

$$\langle e(\epsilon) | z | t_1(z) \rangle = -C_2 R / \sqrt{3}, \quad (10a)$$

$$\langle t_2(x) | y | t_1(z) \rangle = \frac{1}{2} C_7 R, \quad (10b)$$

$$\langle t_2(z) | z | e(\theta) \rangle = -C_2 C_7 R / \sqrt{3}, \quad (10c)$$

$$\langle 3t_2(z) | y | 4t_2(x) \rangle = (C_6 C_6' + C_6 C_6' - \frac{1}{2} C_7 C_7') R / \sqrt{3}. \quad (10d)$$

The labeling of metal and ligand axes and the symmetry-adapted combinations of ligand orbitals used in this work are those of Ballhausen and Gray.¹² Molecular-orbital mixing coefficients are defined in Table II.

We discuss some estimates of the magnitudes of the C_i and their application to the assignment of the charge-transfer bands of particular complexes later. It is of interest to notice at this point, however, that the ratios of the dipole strengths of different bands in the same

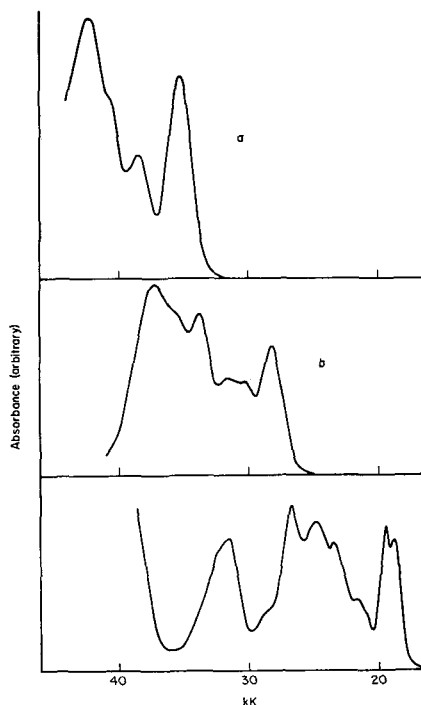


FIG. 5. The charge-transfer spectra of (a) NiCl_4^{2-} , (b) NiBr_4^{2-} , and (c) NiI_4^{2-} at 77°K (all evaporated films).

spectrum can yield direct estimates of molecular-orbital coefficients, within the approximations just discussed. For instance, $D(3t_2 \rightarrow 2e)/D(t_1 \rightarrow 2e)$ is equal to C_7' , the π -bonding coefficient in $3t_2$, and similarly $D(1e \rightarrow 4t_2)/D(t_1 \rightarrow 4t_2)$ equals $\frac{2}{3}C_2'^2$, where C_2' is the ligand π coefficient in the $1e$ molecular orbital.

The expressions for electric-dipole transition moments [Eqs. (4) and (6)] have been derived under the assumption that we are dealing with good Russell-Saunders states. Should this not be so, two major consequences may follow:

(a) breakdown of selection rules and appearance of spin-forbidden Russell-Saunders states;

(b) splitting of the allowed states.

The qualitative evolution of the spectra (Figs. 2-5) from chloride to iodide does not suggest that (a) is of great importance because while the number of bands increases, there is no noticeable trend of increasing intensity among any of the emerging components. One has, rather, the impression that bands which in the chlorides are single become increasingly separated into components of comparable intensities in the heavier halides. We therefore calculate the first-order effect of spin-orbit coupling only on those excited states which were accessible from the ground state in the absence of spin-orbit coupling.

Following Tanabe and Kamimura,¹⁹ Griffith²⁰ has again given procedures for simplifying matrix elements of spin-orbit coupling $\mathbf{s} \cdot \mathbf{u}$ for molecular spinor states down to reduced one-electron matrix elements of \mathbf{u} , the molecular-angular-momentum operator

$$\mathbf{u} = \sum_i \zeta_i(\mathbf{r}) \mathbf{l}_i, \quad (11)$$

where the summation is over all nuclei. The LCAO approximation then allows the expansion of such molecular matrix elements into spin-orbit matrix elements of the free atoms if many-center terms are neglected, a reasonable approximation since the spin-orbit coupling constant is roughly proportional to r^{-3} . Only in the case of the metal $4p$ orbitals might one anticipate any difficulty with this approximation, and fortunately they make a rather small contribution to the molecular orbitals of interest here.

To calculate the matrix elements of spin-orbit coupling we make use of spinor-group wavefunctions, that is kets such as $|ShJt\rangle$, where t is a spinor irreducible representation and J is a number to distinguish the t 's if there is more than one in the ^{2S+1}h term. The reduced matrix elements of the n -electron spin-orbit coupling operator

$$\mathcal{H}C_s = \sum_{k=1}^n \mathbf{s}(k) \cdot \mathbf{u}(k), \quad (12)$$

which is diagonal in t and τ , are then defined by

$$\begin{aligned} \langle a^n ShJt\tau | \mathcal{H}C_s | a^n S'h'J'\tau' \rangle \\ = \langle a^n Sh | \sum_{k=1}^n s(k) u(k) | a^n S'h' \rangle \Omega_{J,J'} \begin{pmatrix} S & S' & T_1 \\ h' & h & t \end{pmatrix}. \end{aligned} \quad (13)$$

For definitions and tabulations of Ω coefficients, the reader is referred once again to Griffith's book.²⁰ In a manner quite analogous to that described above for the reduction of the (spin-independent) electric-dipole-moment matrix elements, the reduced n -electron spin-orbit matrix elements are further reduced to one-electron matrix elements

$$\begin{aligned} \langle a^n Sh | \sum_{k=1}^n s(k) u(k) | a^n S'h' \rangle \\ = \langle \frac{1}{2}a | su | \frac{1}{2}a \rangle G_n(Sh, S'h'), \end{aligned} \quad (14)$$

values of G_n being available.²⁰ Thus, by means of the final relationship²⁰

$$\langle \frac{1}{2}a | su | \frac{1}{2}a \rangle = \frac{1}{2}(i6^{1/2}) \langle a | u | a \rangle, \quad (15)$$

the first-order splitting of the state ^{2S+1}h by spin-orbit coupling is resolved into a calculation of the reduced one-electron matrix element of the molecular-angular-momentum operator $\langle a | u | a \rangle$.

The diagonal spin-orbit matrix element of configurations containing two open shells, $a^m b^n$, is given by a somewhat more complicated expression, which we quote here without further comment, so that it can be used later:

$$\begin{aligned} \langle a^m(S_1 h_1) b^n(S_2 h_2) Sh | \sum_{k=1}^n s(k) u(k) | a^m(S_1' h_1') b^n(S_2' h_2') S'h' \rangle \\ = (-1)^{S_1+S_2+h_1+h_2'} [(2S+1)(2S'+1)\lambda(h)\lambda(h')]^{1/2} [(-1)^{S'+h'} \delta_{S_2 S_2'} \delta_{h_2 h_2'} \bar{W} \begin{pmatrix} S_1' & S_1 & 1 \\ S & S' & S_2 \end{pmatrix} \\ \times \bar{W} \begin{pmatrix} h_1' & h_1 & T_1 \\ h & h' & h_2 \end{pmatrix} G_m(S_1 h_1, S_1' h_1') \langle \frac{1}{2}a | su | \frac{1}{2}a \rangle + (-1)^{S+h} \delta_{S_1 S_1'} \delta_{h_1 h_1'} \\ \times \bar{W} \begin{pmatrix} S_2' & S_2 & 1 \\ S & S' & S_1 \end{pmatrix} \bar{W} \begin{pmatrix} h_2' & h_2 & T_1 \\ h & h' & h_1 \end{pmatrix} G_n(S_2 h_2, S_2' h_2') \langle \frac{1}{2}b | su | \frac{1}{2}b \rangle]. \end{aligned} \quad (16)$$

TABLE II. Numbering of LCAO eigenvectors for tetrahalide complexes. Ligand orbital combinations are those of Ballhausen and Gray (Ref. 12).

Metal		Ligand			
4 <i>p</i>	3 <i>d</i>	<i>pσ</i>	<i>pπ</i>	<i>s</i>	
<i>e</i>	...	<i>c</i> ₁	...	<i>c</i> ₂	...
<i>t</i> ₂	<i>c</i> ₃	<i>c</i> ₄	<i>c</i> ₅	<i>c</i> ₇	<i>c</i> ₆

We now calculate the reduced matrix elements of u in the LCAO approximation, noting first that from Eq. (1),

$$\langle t_2(\alpha) | u(\gamma) | t_2(\beta) \rangle = \langle t_2 || u || t_2 \rangle V \begin{pmatrix} T_2 & T_2 & T_1 \\ \alpha & \beta & \gamma \end{pmatrix}, \quad (17)$$

where α, β , and γ are the components x, y , or z of the representation t_2 . The V coefficient equals $-(6)^{-1/2} \epsilon_{\alpha\beta\gamma}$, where $\epsilon_{\alpha\beta\gamma}$ is zero if any pair of α, β, γ are equal and ± 1 , depending on the order of x, y, z in α, β, γ . Still using the coordinate system and numbering scheme of Ballhausen and Gray,¹²

$$\begin{aligned} \langle t_2(y) | u_z | t_2(x) \rangle &= c_3^2 \langle p_y | u_z | p_x \rangle + c_4^2 \langle d_{xz} | u_z | d_{yz} \rangle \\ &\quad - (\sqrt{3}/8) c_6 c_7 (z_1 + z_2 - z_3 - z_4 | u_z | y_1 + y_2 - y_3 - y_4) \\ &\quad + (\sqrt{3}/8) c_6 c_7 (y_1 - y_2 + y_3 - y_4 | u_z | z_1 - z_2 + z_3 - z_4) \\ &\quad - (\sqrt{3}/16) c_7^2 (x_1 - x_2 + x_3 - x_4 | u_z | y_1 + y_2 - y_3 - y_4) \\ &\quad + (\sqrt{3}/16) c_7^2 (y_1 - y_2 + y_3 - y_4 | u_z | x_1 + x_2 - x_3 - x_4). \end{aligned} \quad (18)$$

Next, we expand u_z according to Eq. (11) and transform l_z on the ligands into the components of l within the ligand coordinate system. For example,

$$l_z(1) = (1/\sqrt{3}) l(z_1) + (\sqrt{2}/\sqrt{3}) l(x_1). \quad (19)$$

We are then left with matrix elements of l between atomic orbitals, which are expressible in terms of reduced matrix elements as follows:

$$\langle p || l || p \rangle = i6^{1/2} \hbar; \quad \langle d(t_2) || l || d(t_2) \rangle = -i6^{1/2} \hbar. \quad (20)$$

Finally, we find

$$\langle t_2 || u || t_2 \rangle = 6^{1/2} i [c_3^2 \zeta_{4p} - c_4^2 \zeta_{3d} - (\sqrt{2} c_6 c_7 - \frac{1}{2} c_7^2) \zeta_{pl}] \hbar, \quad (21a)$$

$$\langle t_1 || u || t_1 \rangle = \frac{1}{2} (6^{1/2} i) \zeta_{pl} \hbar, \quad (21b)$$

where ζ_{4p} and ζ_{3d} are the spin-orbit coupling constants⁹ of the metal for its effective oxidation state in the complex and ζ_{pl} is the spin-orbit coupling constant of the ligand.

Equation (21a) is of some interest in relation to the work of Ballhausen and Liehr²⁵ on the effect of spin-orbit coupling on the $d-d$ spectra of octahedral and

tetrahedral complexes. Working within the crystal-field framework, they ascribed spin-orbit coupling to the metal alone and scaled down ζ_{3d} to account for ligand orbital mixing. Such an approach would not be open to us here, as even in complexes such as CoBr_4^{2-} the major spin-orbit contribution is from the ligand, but it might be worthwhile to recast the earlier work into a molecular-orbital framework. Apart from Jørgensen's analysis⁹ of the hexahalide charge-transfer spectra already referred to, the only work on metal complexes to date which has explicitly considered spin-orbit coupling at ligand nuclei appears to be that of Missetich and Buch,²⁶ who found it essential to a discussion of the g values even in a compound as ionic as KNiF_3 .

DISCUSSION

Armed with the general theoretical results of the previous section, we now consider assignments of the spectra in Figs. 2-5, by estimating the relative intensities and spin-orbit splittings of the excited states for each compound.

Tetrahalogenocuprates(II)

The room-temperature charge-transfer spectra of CuCl_4^{2-} and CuBr_4^{2-} have been reported, both in solution and in single crystals, by numerous authors.^{9,27-28} If the complexes were undistorted tetrahedra, it would be expected that assignment would be quite straightforward, since a single excited state 2T arises from the transfer of an electron of each of the filled ligand orbitals to the unique hole in $4t_2$. However, the molecular symmetry is in fact D_{2d} rather than T_d , so $4t_2$ is split into e and b_2 with the unpaired electron in the latter. The orbitals $1e, 3t_2$, and t_1 are likewise split into $b_1 + a_1, b_2 + e$, and $a_2 + e$, respectively, so that if only spin-allowed transitions are considered, we might expect to observe pairs of transitions ${}^2B_1 + {}^2A_1, {}^2B_2 + {}^2E$, and ${}^2A_2 + {}^2E$. Inclusion of spin-orbit coupling would further split 2E . Since only E and A_1 excited states are accessible from a B_2 ground state, the pairs of transitions $(b_2 + e) \rightarrow b_2$ and $(a_2 + e) \rightarrow b_2$ might each consist of a weak and an intense component. Examination of the spectra (Fig. 2) shows that this is indeed the case. The major bands of CuCl_4^{2-} at 24.4 and 34.05 kK are each preceded by shoulders (22.5 and 29.2 kK), while in the tetrabromide, cooling to 77°K brings about resolution of what, at room temperature, are shoulders, into separate weak bands. Polarized spectroscopy of single crystals²⁹ has demonstrated conclusively that the excited states of CuCl_4^{2-} at 24.4 and 34.05 kK are of E type and that the next, at 41.5, is A_1 . Ferguson²⁸ also considered that the first shoulder (22.5 kK) was A_2 , but both he and Sharnoff²⁹ assign the second shoulder to E . There are difficulties in

²⁶ A. A. Missetich and T. Buch, J. Chem. Phys. **41**, 2524 (1964).
²⁷ C. Furlani and G. Morpurgo, Theoret. Chim. Acta **1**, 103 (1963).

²⁸ J. Ferguson, J. Chem. Phys. **39**, 116 (1963).

²⁵ C. J. Ballhausen and A. D. Liehr, Ann. Phys. N.Y. **6**, 134 (1959).

interpreting the crystal spectra of CuCl_4^{2-} both because the weak shoulders of interest are not very well resolved and because it is difficult to make crystals of Cs_2ZnCl_4 homogeneously doped with the flattened CuCl_4^{2-} ion. Identification of the weak absorptions at 29.2 and 23.5 kK in CuCl_4^{2-} and CuBr_4^{2-} as ${}^2B_2({}^2T_2$ in T_d) is substantiated by a number of arguments. First, the result of Jahn-Teller distortion would then be to split 2T_2 by 5.2 and 5.7 kK in the chloride and bromide, respectively, compared with 1.7 and 2.15 kK for 2T_1 . The splitting of orbital $3t_2$ is thus more dependent on molecular geometry than t_1 , a conclusion quite consistent with the former's bonding character. Furthermore, the splitting is larger in the tetrabromide, the geometry of which is further removed from tetrahedral than that of the tetrachloride. The most powerful piece of evidence, however, comes from the magnetic circular dichroism (Faraday effect) spectrum³⁰ of CuBr_4^{2-} . The Faraday effect is a powerful means for assessing the degeneracies of electronic transitions since the so-called A terms, which have characteristic line shapes, are only seen when either the ground or excited state is orbitally degenerate. Since the ground state of CuBr_4^{2-} is 2B_2 , the presence of an A term diagnoses a 2E excited state. Both bands at 18.3 and 29.2 kK have substantial A terms in the room-temperature Faraday-effect spectrum, but neither the two weaker bands at 16.5 and 23.5 nor the stronger one at 37.2 kK show any sign of such absorption, only B terms being present. It can therefore be stated with some confidence that the band at 23.5 kK, which is analogous to the one at 29.2 in CuCl_4^{2-} , does not arise from 2E .

In the spectrum measured at 77°K [Fig. 2(b)], pronounced splittings of both 18.5- and 29.2-kK bands are visible in CuBr_4^{2-} , though no such effect occurs in CuCl_4^{2-} . This may be ascribed to the separation of 2E states into E' and E'' by spin-orbit coupling at the halogen. If the direction of Jahn-Teller distortion of CuX_4^{2-} is taken as the z axis, the atomic-orbital combinations spanning the irreducible representation e in D_{2d} are the same as $t_1(x)$ and $t_1(y)$ in T_d . From first-order perturbation theory of degenerate states, the spin-orbit splitting of ${}^2E({}^2T_1)$ is then $\frac{1}{2}\zeta_{4p}$, or 1.24 kK if we take ζ_{4p} to be the spin-orbit coupling constant of a free bromine atom. The observed splitting of the 19.0-kK band is about 0.70 kK. The preferred assignment of all the bands in the low-temperature spectra of the tetrahalogenocuprates(II) are then as shown in Table III.

Tetrahalogenoferrates(III)

After the cupric halides, those of iron(III) are expected to present the fewest problems of assignment, because from the 6A_1 ground state only one term

(6T_2) of each excited configuration is accessible in the absence of spin-orbit effects. To use Eq. (10) to estimate the relative intensities of the various transitions it becomes necessary to make some assumptions about the approximate magnitudes of the c_i . Zaslow and Rundle³¹ reported a Wolfsberg-Helmholz molecular-orbital calculation for FeCl_4^- , but we do not believe this to be suitable for the present purpose because such calculations are known to overemphasize the degree of metal-ligand mixing and also because "exchange" terms were entirely neglected in this calculation. The theoretically most realistic calculation on a tetrahalogeno anion to date appears to be that of Ros and Schuit³² on CuCl_4^{2-} , since as few empirical parameters as possible were introduced and the diagonal elements of the Hamiltonian were calculated from the wavefunctions of the free ions, instead of being estimated from atomic ionization potentials. In this and the following sections, wherever rough estimates of molecular-orbital coefficients for tetrachloro anions are required, we have therefore chosen to employ those of Ros and Schuit. Quite evidently these are not expected to be accurate for other ions than CuCl_4^{2-} and are, indeed, of unknown accuracy even for that ion, but if used judiciously they may help us to gain some preliminary orientation among the spectra by suggesting which transitions may be particularly weak or intense.

Adopting this procedure, together with Richard and Gregory's³² value of 2.196 Å for the Fe-Cl bond length, Eqs. (4)-(7), and (10) then indicate the following dipole strengths for the lowest-energy ${}^6A_1 \rightarrow {}^6T_2$ transitions of FeCl_4^- :

$t_1 \rightarrow 2e$	$t_1 \rightarrow 4t_2$	$3t_2 \rightarrow 2e$	$3t_2 \rightarrow 4t_2$
1.77	1.11	0.09	1.38

Since, as we pointed out above, the ratio $D(3t_2 \rightarrow 2e)/D(t_1 \rightarrow 2e)$ is equal to the square of the π -bonding coefficient in $3t_2$, the transition $3t_2 \rightarrow 2e$ is expected to be somewhat weaker than the others.

The spectrum of FeCl_4^- [Fig. 3(a)] contains four bands, one of which is much less prominent than the others, so a straightforward identification becomes possible if the observed band energies are combined with the calculated transition moments above to give a set of oscillator strengths which can be compared with those observed experimentally:

	λ	$f(\text{calculated})$	$f(\text{observed})$
27.48 kK:	$t_1 \rightarrow 2e$	0.51	0.11
31.52 kK:	$t_1 \rightarrow 4t_2$	0.39	0.16
37.0 kK:	$3t_2 \rightarrow 2e$	0.03	0.07
41.25 kK:	$3t_2 \rightarrow 4t_2$	0.63	0.28

²⁹ M. Sharnoff and C. W. Reimann, J. Chem. Phys. **46**, 2634 (1967).

³⁰ A. J. McCaffery and P. N. Schatz (private communication, 1967).

³¹ B. Zaslow and R. E. Rundle, J. Phys. Chem. **61**, 490 (1957).

³² R. R. Richards and N. W. Gregory, J. Phys. Chem. **69**, 239 (1965).

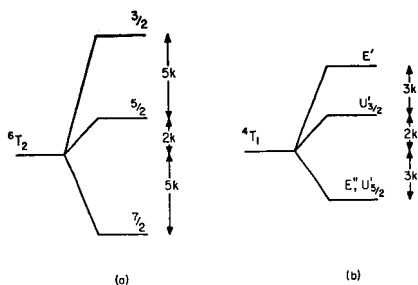


FIG. 6. First-order spin-orbit splitting of charge-transfer excited states: (a) ${}^6T_2(\text{FeX}_4^-)$, (b) ${}^4T_1(\text{CoX}_4^{2-})$. The unit of splitting is defined in the text.

The observed oscillator strengths are derived from a Gaussian analysis of the 77°K spectrum which took account of the evident asymmetry of the 31.5-kK band. Additional evidence on the assignment of the first two bands comes from the observed half-widths. The greater breadth of the 31.52-kK band (5.4 kK

compared with 2 kK for the 27.48-kK band) suggests that the latter transition is to the more antibonding $4t_2$ orbital. It may also be of some significance that the energy differences between the first and second bands (4.04 kK) and between the third and fourth bands (4.25 kK) are both close to the value of Δ estimated from the ligand-field spectrum.

Despite the broad similarity with FeCl_4^- , in discussing the assignment of FeBr_4^- [Fig. 3(b)], spin-orbit interactions at the bromine atoms must be taken into account. 6T_2 States are split into three states, as shown in Fig. 6 (a), where the unit of splitting, k , is $[1/6(35)^{1/2}] \langle {}^6T_2 || \sum su || {}^6T_2 \rangle$. From the $J = \frac{5}{2}$ ground state, transitions are possible to $J = \frac{3}{2}, \frac{5}{2}, \frac{7}{2}$; hence, each band which appears single in FeCl_4^- ($\zeta_{\text{Cl}} 0.59$ kK) is expected to split in FeBr_4^- ($\zeta_{\text{Br}} 2.46$ kK) into three. The unit of splitting k must be evaluated for the 6T_2 state arising from each of the lowest excited configurations, and by a further generalization of Eq. (16), taking account of three open shells in the excited states, we find for $t_1 \rightarrow 2e$

$$\langle t_1^5({}^2T_1) 2e^3({}^2E) 4t_2^3({}^4A_2) {}^6T_2 || \sum su || t_1^5({}^2T_1) 2e^3({}^2E) 4t_2^3({}^4A_2) {}^6T_2 \rangle = [7^{1/2}/2(5)^{1/2}] \langle \frac{1}{2}t_1 || su || \frac{1}{2}t_1 \rangle. \quad (22)$$

By substituting Eqs. (16) and (21b) the total energy spread of the three spin-orbit states is $(3/10)\zeta_{4p}$, or approximately 0.75 kK, independent of any estimates of eigenvectors. Similarly, for $t_1 \rightarrow 4t_2$,

$$\langle t_1^5({}^2T_1) 2e^2({}^3A_2) 4t_2^4({}^3T_1) {}^6T_2 || \sum su || t_1^5({}^2T_1) 2e^2({}^3A_2) 4t_2^4({}^3T_1) {}^6T_2 \rangle \\ = -[7^{1/2}/2(5)^{1/2}] [\langle \frac{1}{2}t_1 || su || \frac{1}{2}t_1 \rangle + \langle \frac{1}{2}4t_2 || su || \frac{1}{2}4t_2 \rangle], \quad (23)$$

and the same substitutions indicate a total spread of 1.4 kK. The assignment of the bands at 31.0 and 35.6 kK proceeds by a clear empirical analogy with FeCl_4^- , but the origin of the extra peaks in the 25-kK region requires further discussion. Nevertheless, simply looking at the spectrum of FeBr_4^- one has the impression that the three bands at 23.65, 25.4, and 27.2 kK correlate with the broad and somewhat asymmetric band of FeCl_4^- at 31.52 kK, the separations of the three peaks being near the ratio required by Fig. 6(a).

The lowest-energy band does not seem to be split either in FeCl_4^- or FeBr_4^- , so from the approximate values of the spin-orbit matrix elements above, the most plausible assignment of the FeBr_4^- spectrum is as follows: the 21.35-kK band contains all the spin-orbit components of ${}^6T_2(t_1 \rightarrow 2e)$ and the group of three bands to higher energy comes from ${}^6T_2(t_1 \rightarrow 4t_2)$. That the total energy spread of this group exceeds our prediction by a factor of 2 need not invalidate the assignment, since errors in estimating the splitting are expected both from the use of approximate eigenvectors and from our neglect of second-order effects. Spectra measured at higher resolution on single crystals at lower temperatures are evidently required before we can say more. Mention may also briefly be made of the spectrum of

FeI_4^- , recently prepared by Ryan.³³ A band at 14.3 and 21.3-kK bands of FeCl_4^- and FeBr_4^- , is followed by a group of three bands (17.2, 18.5, and 21.3 kK) of comparable intensity and another much more intense band (27.0 kK). The total energy spread of all these bands parallels the other tetrahalogenoferrates(III), and broadly similar assignments must therefore be made. The spectral energy differences cannot be compared quantitatively with the other data in Table III, since only the room-temperature FeI_4^- spectrum is available. Comparison with the spectra of FeCl_4^- and FeBr_4^- , previously measured⁹ at room temperature, indicates an increasing separation of the components of the second excited state from chloride to iodide, in agreement with our detailed conclusions derived from the low-temperature spectra.

Tetrahalogenocobaltates(II)

Again, as with the Fe(III) tetrahalides, each excited configuration $\gamma^{n-1}2e^44t_2^4$ contains only one term, 4T_1 , accessible by a dipole-allowed transition from the

³³ J. L. Ryan (unpublished work), quoted by C. K. Jørgensen, in *Chemical Applications of Spectroscopy*, B. G. Wybourne, Ed. (Interscience Publishers, Inc., New York, to be published).

401

SPECTRA OF TETRAHALIDE COMPLEXES

TABLE III. Charge-transfer spectra of 3d tetrahalide complexes at 77°K (10³ cm⁻¹). Assignments are given as terms arising from one-electron transitions, with spin-orbit components (Griffith's nomenclature) in parentheses.

	Cl	Br	I
Cu(II)	$a_2 \rightarrow 4b_2$	22.5 3A_2	16.5 3A_2
(D_{2d})	$4e \rightarrow 4b_2$	24.4 1E	18.3 ${}^1E(E')$ 19.0 ${}^1E(E'')$
	$3b_2 \rightarrow 4b_2$	29.2 3B_2	23.5 3B_2
	$3e \rightarrow 4b_2$	34.05 2E	(28.8) ${}^2E(E')$ 29.4 ${}^2E(E'')$
	$3a_1 \rightarrow 4b_2$	41.48 3A_1	37.2 3A_1
Fe(III)	$t_1 \rightarrow 2e$	27.48 1T_2	21.35 ${}^1T_2 (J = \frac{3}{2}, \frac{3}{2}, \frac{3}{2})$ 23.65 ${}^2E_2(\frac{3}{2})$
	$t_1 \rightarrow 4t_2$	31.52 2E_2	25.4 ${}^2E_2(\frac{3}{2})$ (27.2) ${}^2E_2(\frac{3}{2})$
	$3t_2 \rightarrow 2e$	(36.8) 3T_2	(31.0) ${}^3T_2(\frac{3}{2}, \frac{3}{2}, \frac{3}{2})$
	$3t_2 \rightarrow 4t_2$	41.25 4T_2	45.4 ${}^4T_2(\frac{3}{2}, \frac{3}{2})$ (46.0) ${}^4T_2(\frac{3}{2})$
Co(II)	$t_1 \rightarrow 4t_2$	12.6 1T_1	35.4 ${}^1T_1(E', U_{3/2}')$
		45.5 ?	37.45 ${}^1T_1(U_{3/2}')$ 38.9 ${}^1T_1(E')$
	$3t_2 \rightarrow 4t_2$		25.8 ${}^1T_1(U_{3/2}')$ 27.8 ${}^1T_1(E'')$ 29.75 ${}^1T_1(U_{3/2}')$
	$1e \rightarrow 4t_2$		33.5 2T_1 (35.75) ? (36.5) ? (36.5) ? 38.65 3T_1 (39.9) ?
Ni(II)	$t_1 \rightarrow 4t_2$	35.27 ${}^3A_2(T_2) + {}^1E(T_2)$	28.3 ${}^3A_2(T_2) + {}^1E(T_2)$
		38.25 ${}^1T_1(T_2) + {}^1T_2(T_2)$	30.05 ${}^1T_1(T_2)$ or ${}^1T_2(T_2)$ 31.2 ${}^1T_2(T_2)$ or ${}^1T_1(T_2)$
	$3t_2 \rightarrow 4t_2$	(40.4) ${}^2T_1(T_2) + {}^2T_2(T_2)$	33.7 ${}^2T_1(T_2)$ or ${}^2T_2(T_2)$ (35.5) ${}^2T_2(T_2)$ or ${}^2T_1(T_2)$
		42.35 ${}^2E(T_2)$	37.1 ${}^2E(T_2)$
	$1e \rightarrow 4t_2$		18.85 ${}^3A_2(T_2)$ 19.55 ${}^1E(T_2)$ (21.0) 1T_1 or ${}^1T_2(T_2)$ 21.67 1T_2 or ${}^1T_1(T_2)$ 23.45 ${}^2T_1(T_2)$ or ${}^2T_2(T_2)$ 24.75 ${}^2T_2(T_2)$ or ${}^2T_1(T_2)$ 26.85 ${}^2E(T_2)$ (29.0) ? 31.7 ${}^3T_1(T_2)$ (32.8) ${}^3T_2(T_2)$

^a FeI₄⁻ spectrum (room temperature) from Ref. 33.

4A_2 ground state in the absence of spin-orbit coupling. Unlike FeX₄⁻, the 2e subshell is now filled, so the interpretation of the spectra may be more straightforward, though the higher-energy transitions are not accessible because they are overlaid by internal halide-ion transitions.¹⁴

Intensity calculations do not contribute any information of great value in this case, except to suggest that, as for the Cu(II) and Fe(III) halides, $3t_2 \rightarrow 4t_2$ is considerably more intense than $t_1 \rightarrow 4t_2$ while $1e \rightarrow 4t_2$ is rather weaker. On the other hand, spin-orbit effects are very valuable.

The ground states of CoX₄²⁻ are not split under spin-orbit perturbation (4A_2 becomes U'), but 4T_1 excited states are split as shown in Fig. 6(b) (see Table IV for the other excited states). E'' and $U_{3/2}'$ are accidentally degenerate and the units of splitting are, for $t_1 \rightarrow 4t_2$,

$$k = (1/36) (\langle \frac{1}{2}t_1 || su || \frac{1}{2}t_1 \rangle + \langle \frac{1}{2}4t_2 || su || \frac{1}{2}4t_2 \rangle), \quad (24)$$

and, for $3t_2 \rightarrow 4t_2$,

$$k = -(1/36) (\langle \frac{1}{2}3t_2 || su || \frac{1}{2}3t_2 \rangle + \langle \frac{1}{2}4t_2 || su || \frac{1}{2}4t_2 \rangle), \quad (25)$$

i.e., the splitting of the latter is inverted. Inserting Ros and Schuit's¹⁴ eigenvectors for $3t_2$ and $4t_2$ and the free-atom halogen spin-orbit coupling constants, we find that the total energy spreads of the spin-orbit states arising from the various 4T_1 are as follows:

	$t_1 \rightarrow 4t_2$	$3t_2 \rightarrow 4t_2$	$1e \rightarrow 4t_2$
CoBr ₄ ²⁻	1.55	0.93	0.46
CoI ₄ ²⁻	3.33	2.42	1.11

According to Fig. 6(b) the three spin-orbit components of each 4T_1 should occur with energy separations in the ratio 5:3. In CoCl₄²⁻, ξ_{3p} is too small for anything to be seen, but in CoBr₄²⁻ [Fig. 4(b)] there are indeed three closely spaced components of the first charge-transfer transition, with a total spread of 3.5 kK, separated in the approximate ratio 4:3. By an extension of the theory given earlier it is possible to calculate the transition-dipole matrix elements for the individual spin-orbit components,

$$D = \sum_{\tau} | \langle {}^4A_2U' | m_z | {}^4T_1\tau \rangle |^2, \quad (26)$$

TABLE IV. Spinor-group excited states of CoX_4^{2-} and NiX_4^{2-} . Forbidden states are in parentheses.

Orbital transition	CoX_4^{2-}	NiX_4^{2-}
$t_1 \rightarrow 4t_2$	4A_1 U'	3A_2 T_2
	4E $E' + E'' + U'$	3E $(T_1), T_2$
	4T_1 $E' + E'' + 2U'$	3T_1 $(A_1), (E), (T_1),$ T_2
	4T_2 $E' + E'' + 2U'$	3T_2 $(A_2), (E), (T_1),$ T_2
$3t_2 \rightarrow 4t_2$	4A_2 U'	3A_1 (T_1)
	4E $E' + E'' + U'$	3E $(T_1), T_2$
	4T_1 $E' + E'' + 2U'$	3T_1 $(A_1), (E), (T_1),$ T_2
	4T_2 $E' + E'' + 2U'$	3T_2 $(A_2), (E), (T_1),$ T_2
$1e \rightarrow 4t_2$	4T_1 $E' + E'' + 2U'$	3T_1 $(A_1), (E), (T_1),$ T_2
	4T_2 $E' + E'' + 2U'$	3T_2 $(A_2), (E), (T_1),$ T_2

in terms of the reduced matrix element $m = \langle {}^4A_2 || r || {}^4T_1 \rangle$. Using coefficients analogous to the W coefficients but involving double-group representations, we find that the transitions to E' and E'' both have transition dipoles of $(2/9) m^2$, and to $U_{3/2}'$ and $U_{5/2}'$, $(4/9) m^2$. Because E'' and $U_{5/2}'$ are accidentally degenerate, the transition dipoles of the three bands in order of increasing energy should be $0.667 (E'' + U_{5/2}')$, $0.444 (U_{3/2}')$, and $0.222 (E')$, all in units of m^2 . Agreement with the relative intensities as well as the energies of the three observed bands is extremely satisfactory, and we therefore have no hesitation in assigning them as the spin-orbit components of ${}^4T_1 (t_1 \rightarrow 4t_2)$. Unfortunately, the higher-energy bands are completely obscured by the internal bromide-ion transition, which has its maximum at 47.4 kK.¹⁴

The successful interpretation of the lowest-energy bands of CoBr_4^{2-} suggests that the first bands of CoI_4^{2-} may have a similar origin. In particular, the major bands at 25.80 and 29.75 kK appear analogous to those at 35.40 and 37.45 kK in CoBr_4^{2-} , since the spin-orbit coupling constant of iodine is approximately twice that of bromine. However, the band at 33.5 kK is too intense to be the third component of $t_1 \rightarrow 4t_2$ and must belong to $3t_2 \rightarrow 4t_2$. If second-order effects are important, the small band at 27.8 kK has the appropriate relative intensity to be E'' , separated from $U_{5/2}'$, with which it is degenerate in CoBr_4^{2-} . Otherwise, it may be one of the many possible spin-forbidden transitions. The lower intensity of the next group of bands, in the 38–40-kK region, implies that they come from $1e \rightarrow 4t_2$ excited states provided, once again, that they are not spin-forbidden transitions.

Tetrahalogenonickelates (II)

From the 3T_1 ground states of NiX_4^{2-} , transitions to four excited terms (3A_2 , 3E , 3T_1 , and 3T_2) are electric dipole allowed. As each excited configuration

$\gamma^n - 12e^4 t_1^5$ gives rise to more than one of these terms (see Table I), we anticipate some difficulty in assigning the spectra, though countering this pessimistic prediction we note that spin-orbit coupling will not complicate matters any further, because only one spinor state of each term is allowed (see Table IV). No estimates of the splitting of charge-transfer-excited configurations by electron repulsion have ever been made, so once again we examine the spectra from a purely empirical point of view, using the symmetry arguments embodied in the tensor method.

From Eq. (4) the ratios of intensities for the terms arising from the $t_1 \rightarrow 4t_2$ transition (A_2 , E , T_1 , T_2) are discovered to be 4:2:3:3, while for $3t_2 \rightarrow 4t_2$, $E:T_1:T_2$ is 2:1:1, and for $1e \rightarrow 4t_2$, $T_1:T_2$ is 3:1. Again employing Ros and Schuit's¹³ eigenvectors and the observed bond length³⁴ of NiCl_4^{2-} , the total dipole strengths of all the terms of each excited configuration are $0.804 (t_1 \rightarrow 4t_2)$, $0.984 (3t_2 \rightarrow 4t_2)$, and $0.342 (1e \rightarrow 4t_2)$.

Liehr and Ballhausen²⁵ estimated the ground-state splitting of NiX_4^{2-} by spin-orbit interactions, using a crystal-field model, and demonstrated that A_1 lay lowest of the four spinor states (A_1 , E , T_1 , T_2) of 3T_1 . Our estimate of the first-order splitting, by means of the tensor method, is rather smaller than the crystal-field result, which included second-order effects. Nevertheless, at 77°K, the population of the other spinor states above A_1 should not be very great.

Of the allowed terms arising from the transition $t_1 \rightarrow 4t_2$ in NiX_4^{2-} , 3A_2 and 3E are not affected by spin-orbit interaction because they have no orbital angular momentum, but the T_2 spinor states of both 3T_1 and 3T_2 suffer identical first-order displacements, equal to

$$-\frac{1}{\sqrt{2}} (\langle \frac{1}{2} t_1 || su || \frac{3}{2} t_1 \rangle + \langle \frac{3}{2} 4t_2 || su || \frac{1}{2} 4t_2 \rangle). \quad (27)$$

Similarly, the states $T_2 ({}^3T_1)$ and $T_2 ({}^3T_2)$ of the $3t_2 \rightarrow 4t_2$ transition are together displaced in the opposite direction by

$$\frac{1}{\sqrt{2}} (\langle \frac{3}{2} 3t_2 || su || \frac{1}{2} 3t_2 \rangle + \langle \frac{3}{2} 4t_2 || su || \frac{1}{2} 4t_2 \rangle). \quad (28)$$

Finally, the two T_2 states of the $1e \rightarrow 4t_2$ transitions are displaced in opposite directions by $\frac{1}{\sqrt{2}} (\langle \frac{1}{2} 4t_2 || su || \frac{3}{2} 4t_2 \rangle)$. We cannot use the spin-orbit splittings alone, as we did with CoBr_4^{2-} , to assign the NiX_4^{2-} spectra in Figs. 5(a)–(c) because the band positions of the latter are also determined, to an unknown extent, by interelectronic repulsion. But by studying the relative intensities of the bands and the evolution of the spectra with changing halogen, a set of plausible assignments may be arrived at.

The spectrum of NiI_4^{2-} [Fig. 5(c)] contains nine major bands in three groups, the highest in energy of which is obscured in the chloride and bromide by internal halide-ion transitions. The central group of bands is slightly more intense than those on either side of it, though not by such a margin as in, for example,

³⁴ P. Pauling, *Inorg. Chem.* **5**, 1498 (1966).

the Cu(II) halides. Further, the total energy spread of all the bands of NiI_4^{2-} is comparable with, though slightly smaller than, that of CuX_4^{2-} . As the starting point for our assignment we therefore propose that the asymmetric envelope at 31.7 kK contains the T_1 and T_2 spinor components of $1e \rightarrow 4t_2$, that the band group between 24 and 29 kK contains the components of $3t_2 \rightarrow 4t_2$, and that the lowest energy group comes from $t_1 \rightarrow 4t_2$. T_1 of $1e \rightarrow 4t_2$ is calculated to be three times more intense than T_2 , so the peak at 31.7 kK is assigned to the former, and the shoulder to higher energy (approximately 32.8 kK) to the latter. As the most intense member of the second group, the band at 26.85 kK must be the E component of $3t_2 \rightarrow 4t_2$, while the most likely candidates for the weaker T_1 and T_2 are the bands to lower energy at 24.85 and 23.45 kK. The corresponding bands of NiBr_4^{2-} lie at 37.1 (E), 35.5; and 33.7 kK (T_1 and T_2). We have, of course, no means at present of discovering which band is T_1 and which T_2 . The most intense member of the lowest-energy band group in NiI_4^{2-} at 19.55 kK, must be assigned as the A_2 component of $t_1 \rightarrow 4t_2$, but the locations of the remaining three (E , T_1 , T_2) are more problematic. A plausible scheme would put E at 18.85 kK, with T_1 and T_2 to higher energy, one as the band at 21.67 kK and the other either as the rather ill-defined shoulder at 21.0 kK or underneath the $3t_2 \rightarrow 4t_2$ group. In NiBr_4^{2-} , T_1 , and T_2 , which should have similar intensities, would then be represented by the twin bands at 30.05 and 31.20 kK.

GENERAL CONCLUSIONS

Table III collects the detailed assignments of all those bands among the first-transition-series tetrahalide complexes which can be considered to have been positively identified by the arguments set out in the previous section. Our first conclusion must be that the irreducible tensor method has proved an invaluable tool for calculating matrix elements of states derived from electron configurations with as many as three open shells. While we have used theoretical estimates of LCAO eigenvectors to calculate rough values for some of the reduced matrix elements which act as scaling parameters in the tensor method, this procedure has only been used to obtain a preliminary orientation

among the spectra and a feeling for some of the orders of magnitude involved. There can be no doubt that in the future, when data on the charge-transfer spectra have been obtained at higher resolutions, from doped crystals at lower temperatures, for example, these matrix elements will be obtained unambiguously and precisely from observation alone. Direct empirical estimates of LCAO eigenvectors will then be available for comparison with those which fit other empirical data (e.g., Faraday effect and paramagnetic resonance)—and theories.

For the present, with the proviso that only first-order effects have been considered, we note the following general conclusions:

(1) The order of the highest occupied orbitals, mainly localized on the ligands, remains constant throughout the series: $1e < 3t_2 < t_1$.

(2) The effect of interelectronic repulsion in separating terms of charge-transfer configurations is small.

(3) The effect of spin-orbit coupling at the halogen is rather larger, and becomes decisive to any interpretation of the bromide and iodide spectra. The most noticeable consequence of spin-orbit coupling is to separate the spinor states of those terms which are allowed in its absence. No bands have definitely been detected which would have been forbidden in the absence of spin-orbit coupling.

(4) If the baricenters of the groups of spinor states are compared, the three orbitals $1e$, $3t_2$, and t_1 cover an energy range of roughly 15 kK, biggest (18 kK) in CuBr_4^{2-} and smallest (11 kK) in NiI_4^{2-} .

(5) The separation between t_1 and both $2e$ and $4t_2$ becomes smaller along the sequence $\text{Co(II)} > \text{Ni(II)} > \text{Fe(III)} > \text{Cu(II)}$ for a given halogen. It may be significant that there have been reports³³ of the preparation of FeI_4^- , but not yet of CuI_4^{2-} .

(6) Approximate though realistic LCAO eigenvectors yield estimates of band intensities which appear to be in reasonable agreement with observation when used with the dipole length operator, despite the recent assertion that the dipole velocity operator may be more suitable for intensity calculations with approximate wavefunctions.³⁵

³⁵ A. Hansen, *Theoret. Chim. Acta* (to be published).

Electronic Spectra of Some Post-transition-metal Halide Complexes

By P. Day* and R. H. Seal, University of Oxford, Inorganic Chemistry Laboratory, South Parks Road, Oxford OX1 3QR

The electronic absorption spectra of tetrahalide complexes of Zn^{II} , Cd^{II} , Hg^{II} , and Tl^{III} have been measured either in solution or as thin films. The effects of second-order spin-orbit coupling account satisfactorily for the observed band intensities and splittings. The one-electron transitions responsible for the lowest-energy groups of absorption bands are all of the type $t_2 \rightarrow a_1$. There is no evidence for transitions from the non-bonding t_1 or e molecular orbitals, and an explanation is advanced for their non-appearance.

WHILST the charge-transfer spectra of transition-metal compounds have begun to receive much attention, very little work has been reported on the spectra of non-transition-metal complexes in spite of the fact that, lacking the complexities of a partly filled d -shell, they should in principle be easier to interpret. As with transitional-metal charge-transfer spectra, such interpretation is expected to provide quantitative information on bonding. Unambiguous assignments are, of course, a necessary pre-requisite to extracting information from the spectra, and for this purpose molecules of high symmetry and low complexity are not appropriate.^{1,2} We have therefore examined the absorption spectra of a series of tetrahedral halide complexes of the post-transition metals Zn, Cd, Hg, and Tl. Evidence for the geometry of these complex ions comes mainly from measurements of far-i.r. and Raman spectra.^{3,4} While a number of these electronic spectra have been reported,⁵⁻⁹ it has not always been the custom to ensure that the complex ions do not dissociate in the solutions studied. For example the equilibrium constants of Eillendt and Cruse¹⁰ for the $Hg^{II}-X^-$ systems in acetonitrile (the solvent used for our measurements) show that dilute solutions of $(Et_4N)_2HgX_4$ require a considerable quantity of added halide ion to ensure complete formation of HgX_4^{2-} . Even in the case of those complex halides for which reliable data have appeared^{8,9} we consider it worthwhile to determine the spectra again to obtain accurate band shapes, which could then be subjected to Gaussian analysis to yield reliable measures of transition intensity.

EXPERIMENTAL

Samples of the compounds $(Et_4N)_2MX_4$ ($M = Cd, Hg$; $X = Cl, Br, I$) were prepared by a method similar to that used by Gill and Nyholm¹¹ for the corresponding complex halides of zinc and a variety of transition metals. The compounds precipitate on mixing ethanolic solutions of the component halides, Et_4NX and MX_2 . In the case of the mercury complexes, it is known¹² that reaction between Et_4NX and HgX_2 can lead to products of the type Et_4NHgX_3 and $Et_4NHg_2X_5$, in addition to $(Et_4N)_2HgX_4$. The precaution was taken of employing about twice the amount of Et_4NX required for complete formation of

$(Et_4N)_2MX_4$ in each case. The mercury complexes were recrystallised from acetonitrile; the bromo-complex required additional recrystallisation from nitromethane. The cadmium complexes were adequately pure without recrystallisation, which in any case appears to cause some dissociation. Analyses are in Table 1.

TABLE I
Analyses (%)

Compound	C		H		N	
	Found	Calc.	Found	Calc.	Found	Calc.
$(Et_4N)_2HgCl_4$	32.2	31.9	6.6	6.6	4.7	4.65
$(Et_4N)_2HgBr_4$	24.5	24.6	5.0	5.2	3.35	3.6
$(Et_4N)_2HgI_4$	19.4	19.8	4.3	4.2	2.8	2.9
$(Et_4N)_2CdCl_4$	37.6	37.3	8.15	7.8	5.7	5.4
$(Et_4N)_2CdBr_4$	27.5	27.75	6.0	5.8	4.1	4.0
$(Et_4N)_2CdI_4$	21.9	21.9	5.15	4.6	3.0	3.2

The zinc complexes $(Bu_4N)ZnX_4$ used were examined as thin films⁸ prepared by the evaporation of ethanolic solutions of Bu_4NX and ZnX_2 in 2:1 mole ratio on a piece of silica. Samples of the compounds Et_4NTlX_4 were kindly made available by Dr. R. A. Walton.

Absorption spectra of the compounds $(Et_4N)_2HgX_4$ in acetonitrile solution were obtained with a pathlength of 1 mm. In the absence of free halide ion, Beer's law was not obeyed, owing to extensive dissociation.¹⁰ The minimum of X^- required for essentially complete formation of HgX_4^{2-} , used in obtaining the spectra of Figure 1, was ca. 10 times the amount of $(Et_4N)_2HgX_4$ for the chloro- and bromo-complexes, and 20 times for the iodo-compound. Satisfactory Beer's law plots were obtained under these conditions.

The tetrahalogenothallates were also examined in acetonitrile solution: in this case there is no appreciable dissociation, and addition of halide is not required. (Added halide causes changes in the spectra of Et_4NTlCl_4 and Et_4NTlBr_4 which are attributable to associations leading to five- and six-co-ordinated species; in contrast, the iodo-complex shows no such change. This is consistent with the known existence of such higher co-ordinated complexes with Cl^- and Br^- , and the lack of evidence for any similar complex with I^- .¹³) Figure 2 shows the spectra of the ions TlX_4^- .

Solution spectra of the tetrahalogenocadmates cannot

* G. B. Deacon and B. O. West, *J. Chem. Soc.*, 1961, 3929.

⁸ B. D. Bird and P. Day, *Chem. Comm.*, 1967, 741.

⁹ R. A. Walton, *Co-ordination Chem. Rev.*, 1971, 6, 1.

¹⁰ G. Eillendt and K. Cruse, *Z. phys. Chem. (Leipzig)*, 1952, 201, 130.

¹¹ R. S. Gill and R. S. Nyholm, *J. Chem. Soc.*, 1959, 3997.

¹² Gmelin's *Handbuch der Anorganischen Chemie*, Hg, Part B1, Verlag Chemie, Weinheim, 1965.

¹³ 'Stability Constants of Metal-ion Complexes; Part II: Inorganic Ligands,' eds. J. Bjerrum, G. Schwarzenbach and L. G. Sillen, Chemical Society, London, 1964.

¹ C. K. Jorgensen, *Mol. Phys.*, 1959, 2, 309.
² B. D. Bird and P. Day, *J. Chem. Phys.*, 1968, 49, 392.
³ J. G. Spiro, *Inorg. Chem.*, 1967, 6, 569.
⁴ A. Sabatini and L. Sacconi, *J. Amer. Chem. Soc.*, 1964, 86, 17.
⁵ H. Fromherz, *Z. Elektrochem.*, 1931, 37, 553.
⁶ C. Merritt, jun., H. M. Hershenson, and L. B. Rogers, *Analyt. Chem.*, 1953, 25, 572.

1972

2055

be obtained in the presence of excess of halide ion as the absorptions of CdX_4^{2-} and X^- in acetonitrile lie in the same spectral region. The spectra of these compounds

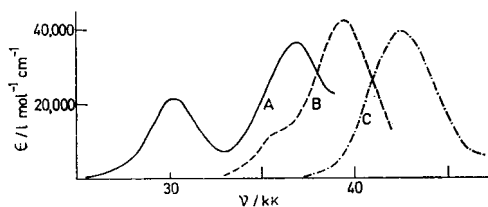


FIGURE 1 Spectra of the ions HgX_4^{2-} in acetonitrile solution: A, HgI_4^{2-} ; B, HgBr_4^{2-} ; and C, HgCl_4^{2-} .

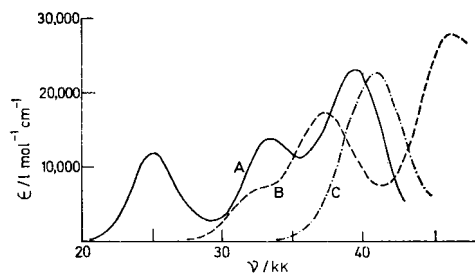


FIGURE 2 Spectra of the ions TiX_4^- in acetonitrile solution: A, TiI_4^- ; B, TiBr_4^- ; and C, TiCl_4^- .

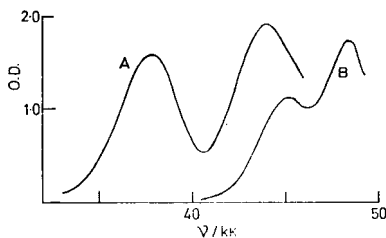


FIGURE 3 Spectra of the ions A, CdI_4^{2-} ; B, CdBr_4^{2-} as doped polymer films

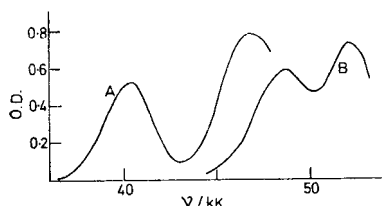


FIGURE 4 Spectra of the ions A, ZnI_4^{2-} ; and B, ZnBr_4^{2-} as evaporated films of the tetrabutylammonium salts

were therefore obtained by doping samples into polymer films, a method successfully employed by Briat and Rivoal.¹⁴

¹⁴ B. Briat and J. C. Rivoal, *Compt. rend.*, 1970, **271**, 1166.

¹⁵ C. E. Moore, 'Atomic Energy Levels,' National Bureau of Standards, Circular 467, vols. II and III, Washington, 1958.

Polyvinyl chloride of molecular weight *ca.* 100,000 gave a film with good transmission up to about 48 kK when a solution in dichloromethane was evaporated. Doped films were prepared by adding solutions of the cadmium complex halides in this solvent to the polyvinyl chloride solution before evaporation. Both the bromo- and iodo-complexes gave satisfactory absorption spectra (Figure 3). The chloro-complex showed no appreciable absorption up to 50 kK.

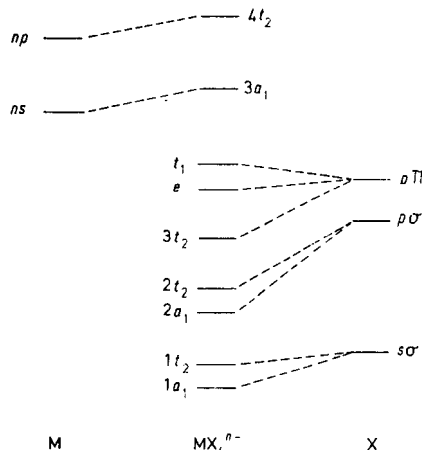


FIGURE 5 Molecular orbital scheme for tetrahedral complex ions MX_4^{n-} : broken lines indicate the atomic orbital expected to make the largest contribution to each molecular orbital

In the case of the tetrahalogenozincates, the high energy of the transitions again prevents the measurement of solution spectra, and we employed thin evaporated films, as in our earlier study of the far-u.v. spectra of transition-metal halide complexes. The tetrachlorozincate complex has no absorption maximum within the range of our spectrophotometer (185 nm). The spectra of the other two complexes are shown in Figure 4.

All absorption spectra were obtained with a Cary 14 spectrophotometer, where necessary with nitrogen purging, and were measured at room temperature.

DISCUSSION

Theory and Interpretation.—Figure 5 shows a qualitative molecular orbital scheme for a post-transition-metal tetrahalide complex. It is similar to that used for first transition series tetrahalide complexes,² but excluding the metal $(n-1)d$ orbitals, which in the post-transition metals become a part of the core (as indicated by atomic energy levels¹⁵). Thus in the post-transition-metal complexes, the e molecular orbital, which is bonding in transition-series complexes, becomes non-bonding like t_1 . The relative positions of t_1 and e orbitals in Group IVB tetrahalides have been discussed by Green *et al.*,¹⁶ who concluded both from

¹⁶ J. C. Green, M. L. H. Green, P. J. Joachim, A. F. Orchard, and D. W. Turner, *Phil. Trans. Roy. Soc.*, 1970, **A**, **268**, 111.

2056

J.C.S. Dalton

the experimental evidence of photoelectron spectroscopy and from calculations of the interactions within the X_4 tetrahedron that the t_1 orbital lies above the e orbital. We adopt the same ordering in Figure 5 though it is not essential to our treatment. In the ground state all orbitals up to and including the non-bonding levels are filled, giving a $1A_1$ term.

In what follows we employ the co-ordinate system and symmetry-adapted combinations of ligand orbitals of Ballhausen and Gray.¹⁷ Molecular orbital mixing coefficients for t_2 orbitals are defined in Table 2 to be consistent with those used previously.² Electronic

TABLE 2

Metal	Ligand		
np	$p\sigma$	$p\pi$	s
c_3	c_5	c_7	c_6

transitions are allowed from the $1A_1$ ground term to $1T_2$ excited terms, which can result from the one-electron transitions $nt_2 \rightarrow 3a_1$ ($n = 1, 2, \text{ or } 3$). No doubt the transition $1t_2 \rightarrow 3a_1$, and in some cases $2t_2 \rightarrow 3a_1$ also, occur at energies outside the range of our measurements, and we similarly discount the possibility of transitions to the $4t_2$ orbital in view of the high energy¹⁵ of the np metal orbitals. Under the influence of spin-orbit coupling one may expect to see transitions to the T_2 spinor states arising from excited terms $3T_2$, $3E$, and

TABLE 3

Band parameters from Gaussian analysis of absorption spectra: for thin films the values of the extinction coefficient, E , and dipole strength, D , are relative to those of band 1

Complex	Band	ν_{\max}/kk	$\frac{\epsilon}{\text{l mol}^{-1} \text{cm}^{-1}}$	D/D^2
HgCl ₄ ²⁻	1	42.6	39,200	38.0
	1	35.5	8760	6.25
HgBr ₄ ²⁻	2	39.5	41,400	40.0
	1	30.3	20,600	21.9
HgI ₄ ²⁻	2	36.9	35,400	40.9
	1	41.0	22,200	27.5
TlCl ₄ ⁻	1	32.0	5150	5.97
	2	37.3	17,000	23.8
TlI ₄ ⁻	3	46.7	27,600	36.1
	1	25.2	11,600	18.0
	2	33.5	13,200	18.3
CdBr ₄ ²⁻	3	39.5	22,900	27.4
	1	45.0	1	1
	2	48.5	1.52	1.10
CdI ₄ ²⁻	1	37.7	1	1
	2	44.2	1.24	1.17
ZnBr ₄ ²⁻	1	48.6	1	1
	2	52.4	1.22	0.864
ZnI ₄ ²⁻	1	40.3	1	1
	2	47.0	1.53	1.73

$3T_1$ as well as $1T_2$: the last two terms, resulting from one-electron transitions $e \rightarrow 3a_1$ and $t_1 \rightarrow 3a_1$ respectively, may be expected to lie lower in energy than $3T_2$ and $1T_2$.

¹⁷ C. J. Ballhausen and H. B. Gray, 'Molecular Orbital Theory,' Benjamin, New York, 1964.

¹⁸ C. K. Jorgensen, 'Orbitals in Atoms and Molecules,' Academic Press, London, 1962.

According to the experimental evidence, the development of the spectra of the Group IIB tetrahalide anions from the chloro- to the iodo-complex suggests the emergence of a spin-forbidden band.

To obtain more precise transition energies and intensities from the overlapping bands, we have carried out a Gaussian analysis of each of the spectra in Figures 1-4, giving the parameters of Table 3. The separation of the two bands in the bromo- and iodo-complexes of the Group IIB metals is then seen to be rather greater than the halogen spin-orbit coupling constant (Table 4).¹⁸

TABLE 4

Spin-orbit coupling constants/kk, from Jørgensen's tabulation¹⁸ or calculated by us from atomic spectral data¹⁵

Atom	ζ_M	Atom	ζ_X
Zn	0.39	Cl	0.59
Cd	1.14	Br	2.46
Hg	4.27	I	5.07
Tl	5.20		

In view of our remarks above it is reasonable to assume that the lowest-energy group of bands in these spectra arises from the transition $3t_2 \rightarrow 3a_1$. The two Russell-Saunders terms $1T_2$ and $3T_2$, of the configuration $3t_2^3 3a_1^1$ could then be mixed *via* second-order spin-orbit coupling, so that the transition to the latter becomes partially allowed. We now test this hypothesis, using the vector coupling method in Griffith's¹⁹ formulation (1) for calculation of matrix elements of the spin-orbit coupling Hamiltonian,²⁰ where κ indexes the electrons and \mathbf{u} is given by equation (2), the summation being

$$\mathcal{H}_{so} = \sum_{\kappa=1}^n \mathbf{s}(\kappa) \mathbf{u}(\kappa) \quad (1)$$

$$\mathbf{u} = \sum_i \zeta_i(\tau) \mathbf{l}_i \quad (2)$$

over all nuclei. Writing spinor group wavefunctions as kets such as $|ShJt\tau\rangle$, where τ is a component of a spinor irreducible representation t arising from a term $2^s + 1h$, and J is a number to distinguish the t 's if more than one occurs in the term, one may reduce matrix elements of \mathcal{H}_{so} (which is diagonal in t and τ) according to (3) where

$$\langle ShJt\tau | \mathcal{H}_{so} | S'h'J't\tau \rangle = \langle Sh || \mathcal{H}_{so} || S'h' \rangle \Omega_{JJ'} \begin{pmatrix} SS'T_1 \\ h'h't \end{pmatrix} \quad (3)$$

the Ω -coefficients have been tabulated (ref. 20, Table E1). Further reduction to one-electron reduced matrix elements can be achieved for particular types of electron configuration, *e.g.*, if the terms $2^s + 1h$ and $2^{s'} + 1h'$ both arise from a configuration $a^m b^n$ having two open shells one may use equation (10.14) of ref. 20 to give a sum of contributions from $\langle \frac{1}{2}a || su || \frac{1}{2}a \rangle$ and $\langle \frac{1}{2}b || su || \frac{1}{2}b \rangle$, the reduced matrix elements of one-electron wavefunctions.

In our case we have, by applying equation (3),

¹⁹ J. S. Griffith, 'The Irreducible Tensor Method for Molecular Symmetry Group,' Prentice-Hall, Englewood Cliffs, N. J., 1962.

²⁰ A. A. Misetich and J. Buch, *J. Chem. Phys.*, 1964, **41**, 2524.

1972

2057

equations (4) and (5). Further, we have equation (6), and finally equations (7)–(9).

$$\langle {}^1T_2T_2 | \mathcal{H}_{so} | {}^1T_2T_2 \rangle = 0 \quad (4)$$

$$\langle {}^3T_2T_2 | \mathcal{H}_{so} | {}^3T_2T_2 \rangle = \frac{1}{6} \langle {}^3T_2 | \mathcal{H}_{so} | {}^3T_2 \rangle \quad (5)$$

$$\begin{aligned} \langle {}^3T_2 | \mathcal{H}_{so} | {}^3T_2 \rangle = \\ \langle t_2^5 ({}^2T_2) a_1 ({}^2A_1) {}^3T_2 | \mathcal{H}_{so} | t_2^5 ({}^2T_2) a_1 ({}^2A_1) {}^3T_2 \rangle \\ = - \langle \frac{1}{2} t_2 | su | \frac{1}{2} t_2 \rangle \end{aligned} \quad (6)$$

$$\langle {}^3T_2T_2 | \mathcal{H}_{so} | {}^1T_2T_2 \rangle = \langle {}^1T_2T_2 | \mathcal{H}_{so} | {}^3T_2T_2 \rangle \quad (7)$$

$$= \frac{1}{3} \langle {}^3T_2 | \mathcal{H}_{so} | {}^1T_2 \rangle \quad (8)$$

$$\langle {}^3T_2 | \mathcal{H}_{so} | {}^1T_2 \rangle = - \frac{1}{\sqrt{2}} \langle \frac{1}{2} t_2 | su | \frac{1}{2} t_2 \rangle \quad (9)$$

We define S by equation (10) and construct the

$$S = \langle \frac{1}{2} t_2 | su | \frac{1}{2} t_2 \rangle \quad (10)$$

secular determinant (11) for the interaction of $| {}^1T_2T_2 \rangle$

$$\begin{vmatrix} -\frac{1}{3}S - K - E & -\frac{1}{3\sqrt{2}}S \\ -\frac{1}{3\sqrt{2}}S & -E \end{vmatrix} = 0 \quad (11)$$

and $| {}^3T_2T_2 \rangle$, where K is the interelectron repulsion separating the terms 3T_2 and 1T_2 . The wavefunctions after interaction are the linear combinations (12) and (13). Solution of the secular determinant gives the

$$\psi = b_1 | {}^3T_2T_2 \rangle + b_2 | {}^1T_2T_2 \rangle \quad (12)$$

$$\psi' = b'_1 | {}^3T_2T_2 \rangle + b'_2 | {}^1T_2T_2 \rangle \quad (13)$$

energies (14) and hence the separation of the two bands

$$\begin{aligned} E = -S/12 - K/2 \pm [(S/4 \pm K/2)^2 - SK/6]^{1/2} \\ = -S/12 - K/2 \pm X \end{aligned} \quad (14)$$

will be given by (15). Solution of the secular equations for b_2 and b'_2 gives the relation (16) where the positive

$$d = 2X \quad (15)$$

$$b_2, b'_2 = \left| 1 + \frac{S^2}{18(S/12 \pm K/2 \pm X)^2} \right|^{-1/2} \quad (16)$$

sign refers to b_2 and the negative to b'_2 , and ψ is taken to be the higher-energy wavefunction. The ratio, R , of intensities of high and low energy transitions can now be obtained from equation (16), and is shown by equations (17) and (18). We now have two relations

$$R = \frac{|\langle {}^1A_1 | r | \psi \rangle|^2}{|\langle {}^1A_1 | r | \psi' \rangle|^2} = \frac{b_2^2}{b_2'^2} \quad (17)$$

$$= \frac{X + S/12 + K/2}{X - S/12 - K/2} \quad (18)$$

ships [equations (15) and (18)] involving the observables, d and R , and the parameters of the theory, S and K . Writing the latter explicitly in terms of the former, however, we find that the sign of S is indeterminate. However, the limiting value of R as $K/S \rightarrow 0$ depends

on the sign of S , being $\frac{1}{2}$ if $S < 0$ and 2 if $S > 0$. In nearly every case the experimental ratio of intensities is less than 2, suggesting that S is negative in these systems. This agrees with the photoelectron spectroscopy results of Green *et al.*,¹⁶ who find that the highest occupied t_2 molecular orbital in the Group IVB tetrahalides has a value of S which is negative, and close to its maximum possible value. To determine this maximum we recall that one-electron reduced matrix elements of the type $\langle \frac{1}{2} t_2 | su | \frac{1}{2} t_2 \rangle$ can be expressed^{2,21} in terms of molecular orbital coefficients and atomic spin-orbit coupling constants. Neglecting many-centre integrals, we have equation (19) where ζ_M and ζ_X are the

$$\langle \frac{1}{2} t_2 | su | \frac{1}{2} t_2 \rangle = -3[c_6^2 \zeta_M - (\sqrt{2}c_7 - \frac{1}{2}c_7^2)\zeta_X] \quad (19)$$

spin-orbit coupling constants of metal and halogen respectively in the p valence shell. Green *et al.*¹⁶ pointed out that when ζ_M is small, S has its negative maximum of $-3\zeta_X$ for $c_6 = -\sqrt{\frac{1}{3}}$, $c_7 = +\sqrt{\frac{2}{3}}$, $c_3 = c_6 = 0$ and that the Group IVB tetrabromides exhibited values of S in the region of $-3\zeta_{Br}$.

In our case, assuming S to be negative, we obtain the values of S and K for the Group IIB complexes given in Table 5. S approaches the limit of $-3\zeta_X$ fairly closely

TABLE 5

The parameters S and K , derived from experimental results. See text for explanation of assignments (i) and (ii) of TlX_4^-

Complex	S/kk	K/kk
ZnBr ₄ ²⁻	-8.1	1.1
ZnI ₄ ²⁻	-13.7	4.1
CdBr ₄ ²⁻	-7.4	1.4
CdI ₄ ²⁻	-13.8	2.8
HgBr ₄ ²⁻	-5.7	3.8
HgI ₄ ²⁻	-13.4	4.3
TlBr ₄ ⁻ (i)	-9.1	4.7
TlBr ₄ ⁻ (ii)	-19.4	5.2
TlI ₄ ⁻ (i)	-17.5	3.0
TlI ₄ ⁻ (ii)	-12.5	3.3

in most cases (only once does S exceed this limiting value, and then by a small amount). For the lighter metals Zn and Cd, which have quite small ζ_M (Table 4), our results therefore indicate that in the $3t_2$ level there is little metal participation and the mixing of halogen $p\sigma$ - and $p\pi$ -orbitals is considerable. The value of ζ_{Hg} is not small compared with ζ_X , so that one cannot draw reliable conclusions about the LCAO coefficients in the mercury complexes.

We now investigate the tetrahalogenothallate spectra in the light of the preceding discussion. The third band seen in the spectra of the bromo- and iodo-complexes could reasonably originate in one of two ways: it might be an orbitally-forbidden transition from t_1 or e to $3a_1$ at low energy, the other two bands corresponding to those of the Group IIB complexes; alternatively it may be that the latter are paralleled in the two lowest-energy bands of the TlX_4^- spectra, the highest-energy

²¹ B. D. Bird, D.Phil. Thesis, Oxford, 1969.

2058

J.C.S. Dalton

band resulting from a more deeply lying molecular orbital.

Transition energies alone suggest that the latter interpretation is the correct one. The first absorption peak of TlCl_4^- , which is not split by spin-orbit coupling, lies at lower energy than HgCl_4^{2-} in agreement with our expectation that Tl^{III} is the more oxidising metal ion. One might expect then that the behaviour of the other halogen-complexes would parallel that of the chlorides. Table 3 and the spectra themselves show that this is consistent with the assignment of bands 1 and 2, but not 2 and 3, to the excited configuration $3t_2^5 3a_1$.

Band splittings and intensities support the same assignment, for TlBr_4^- at least, when the method used above is applied to pairs of adjacent bands in each spectrum to obtain values of S and K (Table 3). Assignment (i) assumes that bands 1 and 2 come from the configuration $3t_2^5 3a_1$, while assignment (ii) assumes that bands 2 and 3 come from this configuration. In the case of TlBr_4^- , (ii) gives a value of S which is numerically far too large to be credible; (i) also gives $S < -3\zeta_{\text{Br}}$, but since ζ_{Tl} is more than twice as large as ζ_{Br} , a small amount of metal participation in the $3t_2$ molecular orbital leads to a value of the magnitude observed. The situation is less clear for TlI_4^- ; (ii) leads to a value of S closer to those found in the Group IIB complexes, but this does not preclude (i). A fairly small contribution from the metal, if slightly positively charged, could result in the larger value (we calculate ζ for Tl^+ from atomic spectral data¹⁵ to be 8.18 kK). Considerable metal participation in the bonding molecular orbitals is to be expected in this complex of a trivalent metal ion with iodide, the most polarisable of the halides, particularly as the spectrum of TlBr_4^- suggests that c_3 is not negligible in the $3t_2$ molecular orbital of this complex.

On balance the first of the possible assignments seems more reasonable for both complexes but it is surprising that no trace of the orbitally-forbidden excited states can be found in the absorption spectra. We therefore pursue the spin-orbit analysis further to find an explanation why they do not appear. The large number of parameters involved in a full perturbation treatment of the mixing of 1T_2 , 3T_2 , 3T_1 , and 3E terms prevents a useful comparison with experimental results since one would have to include the three separations between the terms and several matrix elements of \mathcal{H}_{so} . It turns out, however, that the spin-orbit matrix alone is informative.

Matrix elements governing the mixing of 1T_2 into the 3T_1 and 3E terms involve three open shells, $3t_2$, $3a_1$, and t_1 or e . Although Griffith¹⁹ has not extended the irreducible tensor method to three open shells, Bird²¹ has given the necessary reduction formula. We find

equation (20) by equation (3). Reducing the right

$$\langle {}^3T_1 T_2 | \mathcal{H}_{\text{so}} | {}^1T_2 T_2 \rangle = -\frac{1}{3} \langle {}^3T_1 | \mathcal{H}_{\text{so}} | {}^1T_2 \rangle \quad (20)$$

hand side further we obtain equations (21) and (22).

$$\begin{aligned} \langle {}^3T_1 | \mathcal{H}_{\text{so}} | {}^1T_2 \rangle &= \\ \langle t_2^6 ({}^1A_1) t_1^5 ({}^2T_1) a_1 ({}^2A_1) {}^3T_1 | \mathcal{H}_{\text{so}} | t_2^5 ({}^2T_2) t_1^6 ({}^1A_1) a_1 ({}^2A_1) {}^1T_2 \rangle &= \\ &= -\frac{1}{\sqrt{2}} \langle \frac{1}{2} t_2 | \text{su} | \frac{1}{2} t_1 \rangle \quad (21) \end{aligned}$$

$$\begin{aligned} \langle {}^3E T_2 | \mathcal{H}_{\text{so}} | {}^1T_2 T_2 \rangle &= \frac{1}{3} \langle {}^3E | \mathcal{H}_{\text{so}} | {}^1T_2 \rangle \\ &= \frac{1}{3\sqrt{2}} \langle \frac{1}{2} t_2 | \text{su} | \frac{1}{2} e \rangle \quad (22) \end{aligned}$$

The one-electron reduced matrix elements have been evaluated²¹ as in equation (23) and (24).

$$\langle \frac{1}{2} t_2 | \text{su} | \frac{1}{2} t_1 \rangle = \frac{\sqrt{3}}{2} (\sqrt{2} c_5 + c_7) \zeta_X \quad (23)$$

$$\langle \frac{1}{2} t_2 | \text{su} | \frac{1}{2} e \rangle = \frac{\sqrt{3}}{2} (\sqrt{2} c_5 + c_7) \zeta_Y \quad (24)$$

We have already noted that the values of S derived from the absorption spectra imply a halogen contribution close to the maximum permitted, which in turn implies a ratio of c_5/c_7 of ca. $-1/\sqrt{2}$. Such a ratio makes the reduced matrix elements of equations (8) and (9) vanish, so the absence of the orbitally-forbidden transitions is explained.

CONCLUSION

We have obtained a satisfactory interpretation of these absorption spectra in terms of the one-electron transition $3t_2 \rightarrow 3a_1$, the highest-energy band in the cases of TlBr_4^- and TlI_4^- probably being due to $2t_2 \rightarrow 3a_1$.

Our analysis has taken no account of the halogen $(n+1)s$ orbitals, which may contribute significantly to the $3a_1$ molecular orbital.⁸ Such an admixture will not affect the discussion of spin-orbit effects, and our conclusions about the composition of the $3t_2$ molecular orbital remain valid. Increasing effective nuclear charge of the halogen, resulting from greater covalence in the M-X bond, will cause an increase in the energy of a ligand-localised transition of the type $n\bar{p} \rightarrow (n+1)s$.⁸ In ZnX_4^{2-} the transitions observed are rather close to those of halide in ionic salts such as Bu_4NX , but in descending Group IIB the bands move to lower energy though the bonding is likely to become more covalent. Only for ZnX_4^{2-} is the participation of halogen $(n+1)s$ in the $3a_1$ molecular orbital likely to be important.

We are grateful to Dr. B. D. Bird who carried out some of the initial theoretical work on these complexes and to the S.R.C. for an equipment grant.

[2/1064 Received, 11th May, 1972]

[Reprinted from the *Inorganic Chemistry*, **5**, 1619 (1966).]
Copyright 1966 by the American Chemical Society and reprinted by permission of the copyright owner.

CONTRIBUTION FROM THE INORGANIC CHEMISTRY
LABORATORY, UNIVERSITY OF OXFORD, OXFORD, ENGLAND

Ultraviolet Spectra of Some First Transition Series Pseudohalide Complexes

By P. DAY

Received May 2, 1966

The $\pi-\pi^*$ transitions of many conjugated ligands are very little modified by complex formation, but the spectra of thiocyanate complexes usually contain intense absorption bands at much lower energies than the free anion. In certain cases (*e.g.*, iron(III)) these are

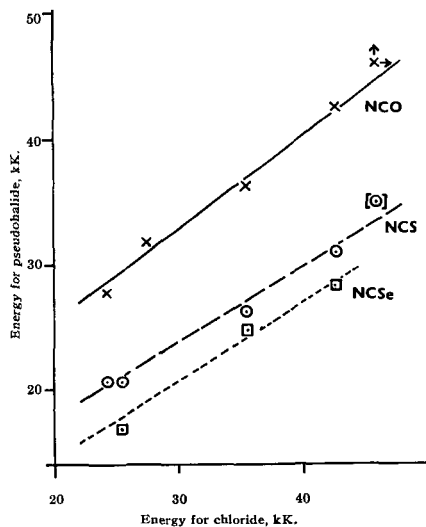


Figure 1.—The lowest energy allowed transitions in chloride and pseudohalide complexes.

clearly charge-transfer bands, though in others (e.g., platinum(II) and -(IV)) the rather weak dependence of band energy on the oxidizing or reducing power of the metal suggests that they may be intraligand $\pi-\pi^*$ transitions. In an earlier investigation,¹ the energies of the first intense bands in two series of thiocyanate complexes $M(NCS)(H_2O)_n^{m+}$ and $M(SCN)_p^{q-}$ were plotted against the energies of the first intense bands in the corresponding halide complexes $MX(H_2O)_n^{m+}$ and MX_p^{q-} on the assumption that the halide bands resulted from ligand-to-metal charge transfer. In the former series, straight lines of almost unit slope were obtained, but in the latter the slopes were much less than unity. This suggested that, when the thiocyanate ion is bonded to the metal through nitrogen, the first intense band is due to ligand-to-metal charge transfer but that, when it is bonded through sulfur, the band is primarily intraligand $\pi-\pi^*$ in origin.

Forster and Goodgame recently reported the preparations and ligand field and vibrational spectra of a number of first transition series pseudohalide complexes.² Though the solids in a number of cases had octahedral coordination, when dissolved in dipolar, weakly coordinating solvents, most of the divalent metals gave complexes $M(NCX)_4^{2-}$, and far-infrared spectra showed that coordination was always through nitrogen. Since the charge-transfer spectra of all of the tetrahedral complexes of manganese(II) to copper(II) have recently been reported,³ a comparison of the type described above should help in assigning the pseudohalide spectra.

Table I shows the energies and extinction coefficients of the available tetrahedral pseudohalide com-

TABLE I
SPECTRA OF PSEUDOHALIDE COMPLEXES (kK) WITH
EXTINCTION COEFFICIENTS IN PARENTHESES

Mn(II)	NCO	>46
	NCS	~35 ^a
Fe(III)	NCO ^c	27.8 (5120); 31.8 (14,400); 34 (13,980); 40 (6220)
	NCS ^b	20.70 (>17,000); 32; 34.2 (5000); 40.5 (>20,000)
	NCS ^{a,c,b}	~17
Co(II)	NCO	42.50 (9320)
	NCS	31.00 (12,170); 39.5 (2500); >44 (>30,000)
	NCSe	28.30 (6850); 43.2 (32,000)
Ni(II)	NCO	36.30 (5890); 39.5 (3500); >44
	NCS	26.30 (5000); ~34 (~800); ~39 (~1600)
	NCS ^{a,c,b}	~25
Cu(II)	NCO	27.80 (4160); 32.30 (2503)
	NCS	20.65 (2490); 39 (3560); 42.75 (40,500)
Zn(II)	NCO	>46
	NCS	>44
	NCSe	41 (10,000)

^a Powder reflectance. ^b Octahedral. ^c In acetonitrile solution.

plexes. The manganese(II) and zinc(II) complexes have no intense absorption bands at appreciably lower energies than those of the uncomplexed pseudohalide ions. In contrast, Figure 1 shows the energies of the first intense bands in the other isocyanates and isothiocyanates plotted against those in the chlorides with corresponding formulas. An excellent correlation is seen, the slopes of the plots being approximately 0.7, compared with 1.0 for lanthanide and other thiocyanate ion pairs plotted against chloride ion pairs, and about 0.3 when sulfur-bonded thiocyanates are plotted against chlorides. Thus, the bands are clearly of predominantly charge-transfer character, though in a description of the complexes according to a self-consistent field (e.g., Pariser-Parr-Pople) formalism, the classification of excited states as charge transfer, $\pi-\pi^*$, etc., might not be possible.

Several other points of interest about the pseudohalide ultraviolet spectra are worth mentioning. First, the extinction coefficients are generally similar to those in the corresponding tetrahalides, but the half-widths are often much greater, e.g., $Cu(NCS)_4^{2-}$, 4.1 kK, and $CuCl_4^{2-}$, 1.5 kK. Second, where the first intense band is at a low energy, there is frequently no further intense absorption over an energy range up to 20 kK. Thus, for example, after the bands at 31.00 kK in $Co(NCS)_4^{2-}$, 28.30 kK in $Co(NCSe)_4^{2-}$, and 20.65 kK in $Cu(NCS)_4^{2-}$, the next absorption maximum does not occur until well above 40 kK. Indeed, it is most likely that the very intense bands then occurring are related to the internal absorption bands of free pseudohalide anions rather than charge-transfer transitions. This is in marked contrast to the tetrahalides, where a complicated succession of closely spaced bands is frequently observed.³ The higher energy transitions in tetrahalides may be due either to $t_2\sigma \rightarrow t_2\sigma^*$ or to $e\pi \rightarrow t_2\sigma^*$, though there is the further possibility that some of the fine structure results from intermediate

(1) J. C. Barnes and P. Day, *J. Chem. Soc.*, 3886 (1964).

(2) D. Forster and D. M. L. Goodgame, *ibid.*, 2790 (1964); 262, 268 (1965); *Inorg. Chem.*, **4**, 715, 823, 1712 (1965).

(3) P. Day and C. K. Jørgensen, *J. Chem. Soc.*, 6226 (1964).

coupling in the halogen, an effect which would not be expected in the pseudohalides bound to the metal through the light donor nitrogen.

A third interesting question concerns the inductive effect of the nonbonded group VI atom on the energy of charge transfer from the nitrogen of the pseudohalide to the metal. As expected, this energy falls in the sequence NCO, NCS, NCSe, but the magnitude of the effect is quite surprising. The average difference between isocyanate and isothiocyanate bands of the same metal is 10 kK, which is greater than the difference between chloride and bromide or bromide and iodide.³ Where it can be estimated, the difference between isothiocyanate and isoselenocyanate is much smaller, about 2-3 kK.

The present work, therefore, confirms the previous generalization¹ that the lowest energy allowed transi-

tions of metal thiocyanates bound through nitrogen are primarily ligand-to-metal charge-transfer type and also extends the generalization to isocyanates and isoselenocyanates.

Experimental Section

The tetra- and hexapseudohalide complexes were prepared as tetramethyl-, tetraethyl-, or tetra-*n*-butylammonium salts by the methods described by Forster and Goodgame.¹ Satisfactory analyses were obtained.

Spectra were measured in dichloromethane solution on a Unicam SP700. No excess ligand was added since tetraalkylammonium pseudohalides are rather insoluble in this very weakly coordinating solvent. However, it is to be expected that solvolysis of nitrogen-bonded pseudohalide complexes will be less pronounced than that of the corresponding halides.

Acknowledgment.—Thanks are due to Drs. D. Forster and D. M. L. Goodgame for discussions and the gift of a number of compounds.

The Spectra of Complexes of Conjugated Ligands. Part I. Charge-transfer in Phenanthroline Complexes: Energy Shifts on Substitution

By P. Day and N. Sanders, Inorganic Chemistry Laboratory, University of Oxford, South Parks Road, Oxford

A theoretical treatment is given of the charge-transfer bands of ferrous, ferric, and cuprous phenanthroline complexes. Methyl substituents are shown to cause additive shifts in the band frequency. The best values of the shifts associated with substitution are extracted statistically and interpreted by Hückel molecular orbital theory. It is necessary to assume that the methyl groups perturb the molecule both by changing the energy of the π -molecular orbital involved in charge-transfer, and by changing the energy of the d -orbitals. The latter effect can be accounted for as a purely inductive (σ) effect, produced by the change in the σ -donor power of the ligands, which can be assessed theoretically or experimentally. This treatment provides an assignment of the molecular orbital involved in charge-transfer. Furthermore, it is shown that the methyl group acts both inductively and hyperconjugatively; appropriate parameters are obtained from the data and compared with results from other sources. Finally, the relations between d -orbital energy and ligand σ -donor power are discussed.

ELECTRONIC spectra of complexes can, to a zero-order approximation, be divided into internal transitions of the ligand, internal transitions of the metal, and charge-transfer (CT) transitions.¹ The last of these types has a unique advantage, namely, that it offers the possibility of investigating changes in the levels of individual orbitals; in so far as the transition involves the migration of an electron from a donor to an acceptor orbital, we may hope to perturb the two orbitals independently. Complexes of conjugated ligands have been chosen for study because at least the theoretical treatment of the ligands is relatively well understood. The approximation of σ - π separation is known to give good results in a wide variety of aromatic compounds. Furthermore, it is particularly easy to find closely related series of ligands in this field.

In this Paper, in which we try to discover which are the important factors governing CT spectra, one-electron Hückel molecular orbitals (HMO's) will be used throughout. We shall also ignore metal-ligand π -bonding, thus assuming that our transitions are of purely CT character. This assumption has been very successful in interpreting the CT spectra of aromatic π -complexes.²

One of the best ways of characterising the orbitals involved in electronic transitions is to apply perturbations by means of substituents.³ In this Paper, and the one following, we discuss the spectra of methyl-substituted phenanthroline (phen) complexes, extract substituent parameters statistically and interpret them to obtain assignments and properties of the orbitals involved.

The ferrous and ferric tris-phen complexes are low-spin and have D_3 symmetry (forming three-bladed propellers). It is possible to substitute methyl groups in the 3(8), 4(7) and 5(6) positions (see Figure 1), but methyl groups in the 2 or 9 positions hinder formation of the tris-complexes.⁴ The complex $\text{Cu}(\text{phen})_2^+$ has D_{2d}

symmetry, the cuprous ion having an irregular tetrahedral environment. In this case it is possible to place substituents in the 2 and 9 positions.

The assignment of the visible absorption bands of these complexes to CT was made on the usual grounds.⁵ First, they are peculiar to the complexes; they are not ligand transitions and they are too intense to be internal d - d transitions of the metal. Secondly, such bands only

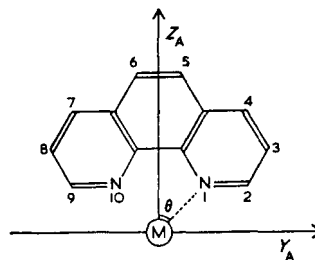


FIGURE 1 Numbering scheme for phen and axes for phen and its mono-complexes

occur in complexes of reducing or oxidising metal ions. Third, the effects of powerful substituents were considered. Our results below confirm the assignment as metal to ligand CT in the cuprous and ferrous complexes, and ligand to metal CT in the ferric complexes.

The spectrum of the ferrous complex is shown in Figure 2. The ligand transitions are only slightly modified on complex formation, and are affected to practically the same extent by all divalent central ions.⁶

Smith and his co-workers^{7,8} pointed out that substitution in a given position produces a definite change in the CT energy. Several other linear relationships have been noted among measurements of other properties of substituted phen and related complexes,^{5,9} such as

⁵ R. J. P. Williams, *J. Chem. Soc.*, 1953, 137.

⁶ P. Krumholtz, *J. Amer. Chem. Soc.*, 1955, 77, 777.

⁷ W. W. Brandt and G. F. Smith, *Analyt. Chem.*, 1949, 21, 1313.

⁸ W. H. McCurdy and G. F. Smith, *Analyt.*, 1952, 77, 846.

⁹ R. V. G. Ewens, *Nature*, 1945, 155, 398; G. F. Smith and F. P. Richter, *Ind. Eng. Chem. Analyt.*, 1944, 16, 580; W. W. Brandt and D. K. Gullstrom, *J. Amer. Chem. Soc.*, 1952, 74, 3532; G. F. Smith and W. M. Banick, *Talanta*, 1959, 2, 348; B. R. James, D.Phil. Thesis, Oxford, 1960; G. F. Smith and D. H. Wilkins, *Analyt. Chim. Acta*, 1959, 10, 139.

¹ C. K. Jorgensen, "Absorption Spectra and Chemical Bonding in Complexes," Pergamon, Oxford, 1962.

² (a) M. J. S. Dewar and A. R. Lepley, *J. Amer. Chem. Soc.*, 1961, 83, 4560; (b) M. J. S. Dewar and H. Rogers, *J. Amer. Chem. Soc.*, 1962, 84, 395; (c) A. R. Lepley, *J. Amer. Chem. Soc.*, 1962, 84, 3577; (d) A. R. Lepley, *J. Amer. Chem. Soc.*, 1964, 86, 2545; (e) A. R. Lepley, personal communication.

³ E.g., J. R. Platt, *J. Opt. Soc. Amer.*, 1953, 43, 252.

⁴ W. W. Brandt, F. P. Dwyer, and E. C. Gyarfás, *Chem. Rev.*, 1954, 54, 954.

TABLE I

Data on methyl-substituted phen.: CT frequencies and extinction coefficients in ferrous, ferric, and cuprous complexes, ligand pK_a 's and redox potentials of the ferrous-ferric couples

Substitution positions	Ferrous ^a		Ferric ^a		Cuprous ^b		Ligand ^c (Δ) pK_a	(Δ)Fe ^c Redox (v)
	(Δ) ν kK	$10^{-3} \times (\Delta)\epsilon$	(Δ) ν kK	$10^{-1} \times (\Delta)\epsilon$	(Δ) ν kK	$10^{-3} \times (\Delta)\epsilon$		
3	19.61	111	16.89	78	22.99	70.4	4.86	1.10
4	+0.31	+4	-1.26	+21	+0.10	+5.3	+0.14	-0.03
5	-0.04	-24	+0.38		-0.05	+8.5		
	-0.19	+11	-0.08		-0.26	+4.2		-0.04
2,4							+1.10	
2,9					-1.01	+8.5	+1.31	
3,4	+0.19	+26			-0.03	+8.1	+0.76	-0.13
3,5	+0.15	+14	-1.51	+2	-0.19	+7.4		
3,6	+0.15	+11	-1.62	+15	-0.21	+11.0		
3,7	+0.31	+15	-0.94	+29	+0.05	+13.0	+0.71	
3,8	+0.55	+4	-2.40	+10	+0.18	+9.5	+0.37	-0.07
4,5	-0.23	+16	+0.50	+17	-0.13	+9.7		-0.15
4,6	-0.23	+16	+0.35	+32	-0.29	+12.8	+0.85	-0.15
4,7	-0.08	+29	+0.97	+72	-0.14	+19.4		-0.22
5,6	-0.38	+15			-0.52	+11.8		-0.10
3,4,6	0.00	+13	-1.39	+26	-0.24	+20.8	+1.07	-0.18
3,4,7	+0.23	+29	-0.89	+38	-0.05	+21.3	+1.13	-0.22
3,4,8	+0.51	+19	-2.10		+0.10	+10.1		
3,5,6	-0.08	+7	-1.51	0	-0.42	+9.5	+0.48	
3,5,7	+0.09	+14	-1.02	+18	-0.24	+15.4	+1.04	-0.17
3,5,8	+0.39	+8	-2.29	+70	-0.11	+10.9	+0.41	-0.11
3,6,7	0.00	+25			-0.26	+16.4		
4,5,7	-0.27	+34	+0.97	+30	-0.35	+20.8		
2,4,7,9					-0.82	+18.2	+1.64	
3,4,6,7	0.00	+29	-0.68	+19 _s	-0.29	+23.3	+1.59	-0.26
3,4,6,8	+0.23	+5	-2.05		-0.08	+19.0	+1.21	-0.21
3,4,7,8	+0.39	+27	-1.62	+37	+0.10	+25.2	+1.45	-0.25
3,5,6,8	+0.23	+5	-2.40		-0.29	+16.0	+0.68	-0.17

^a From ref. 7, except unsubstituted ferric (ref. 11). ^b From ref. 8. ^c From ref. 9.

pK_a 's and redox potentials, but these have not previously been examined quantitatively.

Assignments.—The data to be used^{7,8,10,11} are listed in Table I. In each column, the first figure gives the

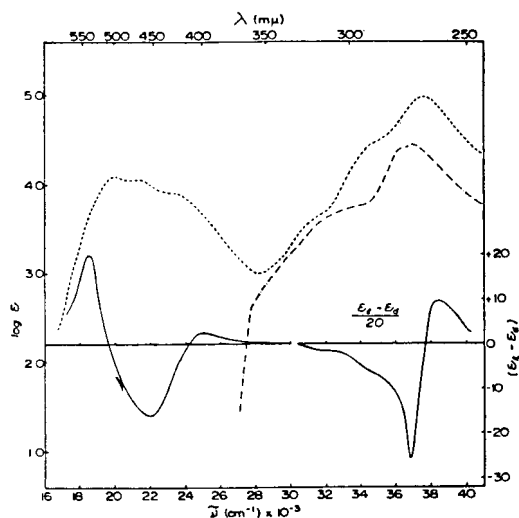


FIGURE 2 (+)₂₈₉-[Fe(phen)₂](ClO₄)₂: CD curve (—), absorption curve (---); absorption curve of phen in N-hydrochloric acid (- · - · -). Reproduced, with permission, from J. Hidaka and B. E. Douglas, *Inorg. Chem.*, 1964, **3**, 1180. (Copyright, The American Chemical Society)

value of the quantity for unsubstituted phen. Subsequent rows are expressed as differences from this first figure. While this means that the unsubstituted value has been overweighted in the presentation of the Table, this criticism does not apply to the subsequent treatment of the data.

We shall use a one-ligand approximation, in which the hypothetical mono-complexes (with the spin states of the fully formed complexes) have C_{2v} symmetry.

Symmetry limitations upon the transitions. Using the axes of Figure 1, the " t_{2g} " orbitals of the approximately octahedral symmetry are derived from $d_{x^2-y^2}$, d_{z^2} , and d_{yz} , and the " t_2 " of the tetrahedron from d_{yz} , d_{zx} , and d_{xy} . The ligand π -MO's form bases for representations A_2 and B_1 of C_{2v} , with and without nodes in the plane of symmetry perpendicular to the molecular plane. Following Orgel,¹² we shall designate MO's of symmetry A_2 by χ and those of symmetry B_1 by ψ . The selection rules for CT are given explicitly in the following Paper;¹³ it is sufficient to state here that CT from the " t_2 " subshell is formally allowed to ligand MO's of either type, with polarisation along either the long or the short axis of the ligand, or perpendicular to its plane.

Evaluation of the effects associated with each methyl group. We wish to fit the observed values, y , of the

¹⁰ A. A. Schilt and G. F. Smith, *J. Phys. Chem.*, 1956, **60**, 1546.

¹¹ J. C. Tomkinson, unpublished results.

¹² L. E. Orgel, *J. Chem. Soc.*, 1961, 3633.

¹³ P. Day and N. Sanders, following Paper.

1532

J. Chem. Soc. (A), 1967

various properties such as pK_a and CT energy to equations of the form,

$$y = y_0 + \sum_r \Delta_r y \cdot n_r \quad (1)$$

n_r is the number of methyl groups in the position r or its mirror image in the phen molecule, so it may take the value 0, 1, or 2, and $\Delta_r y$ is the effect of a methyl group in position r on the property y . The values of y_0 and the $\Delta_r y$ (regression coefficients) are determined in accordance with the principle of least squares.

The regression coefficients, and parameters measuring the quality of the fit, are given in Table 2 for each of the

TABLE 2

Results of regressions to determine the effects ($\Delta_r y$) of substitution with methyl groups in various positions (r) upon properties (y) of phen [see equation (1)] (The column headed S.E. gives the standard error of an estimate from the regression equation, and V.R. is the variance ratio of the regression; ν , ferrous = frequency of the CT band in the ferrous complex, etc., Fe redox = ferrous/ferric redox potential)

Meaning of y	y_0	$\Delta_2 y$	$\Delta_3 y$	Ref.
ν , ferrous, kK	19.64		$+0.268 \pm 0.011$	1
ν , ferric, kK ...	16.85		-1.23 ± 0.06	2
ν , cuprous, kK	22.95	-0.420 ± 0.020	$+0.097 \pm 0.031$	3
Phen pK_a 's ...	4.96	$+0.44 \pm 0.08$	$+0.14 \pm 0.07$	4
Fe redox (ν) ...	1.10		-0.030 ± 0.003	5

Ref.	$\Delta_1 y$	$\Delta_3 y$	S.E.	V.R.
1	-0.063 ± 0.012	-0.190 ± 0.013	0.04	279
2	$+0.39 \pm 0.06$	-0.05 ± 0.08	0.22	168
3	-0.031 ± 0.013	-0.239 ± 0.016	0.05	185
4	$+0.05 \pm 0.06$	$+0.19 \pm 0.07$	0.17	29
5	-0.096 ± 0.003	-0.048 ± 0.004	0.01	335

properties examined. A value of the variance ratio greater than about 5 is highly significant (1% level) of correlation. The quality of the fit is also illustrated graphically for the CT band in the ferrous complex (Figure 3), by plotting observed energy against that calculated from the best equation of the form (1).

The ferrous and cuprous CT energies and the redox potentials of the iron complexes are accounted for within experimental error. In the ferric case, there is a standard error of 0.22 kK but the bands concerned are very broad, and insertion of cross terms in the regression equation did not give any significant improvement in fit, so we have obtained no evidence for deviation from additivity in this case either.

The pK_a 's show appreciable departures from the linear equation (standard error 0.17), but the only two bases which depart far from the line (maximum 0.35) are 2,9-disubstituted compounds, in which special steric or electronic effects might be involved. The other points all lie within 0.15 pK_a units of the line (the range of variation in the series is 1.6 pK_a units). The assumption that the two nitrogen atoms act independently predicts

¹⁴ I. R. Beattie and M. Webster, *J. Phys. Chem.*, 1962, **66**, 115; M. J. Fahsel and C. V. Banks, *J. Amer. Chem. Soc.*, 1966, **88**, 878.

¹⁵ A. Streitwieser, jun., "Molecular Orbital Theory for Organic Chemists," Wiley, New York, 1961.

a different (non-additive) effect of substitution on base strength which fails completely to give agreement with experiment. This is further evidence that the proton is symmetrically placed between the two nitrogen atoms, presumably on a bridging water molecule.¹⁴

HMO theory. The one-electron π -MO's of phen were calculated using the Hückel approximations,¹⁵ by means of a computer programme written for the Ferranti

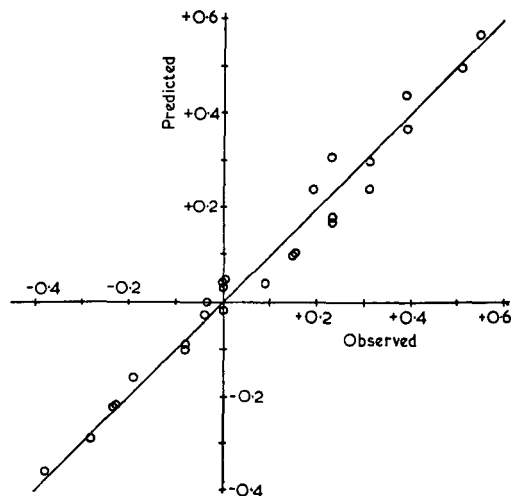


FIGURE 3 Additivity of the effects of successive methyl substitution on the energy of ferrous to phen CT: predictions from the regression equation plotted against observed energies (as shifts measured from 19.61 kK)

Mercury by M. D. Poole.¹⁶ The MO's are taken in the form:

$$\Phi_i = \sum_r c_{ri} \phi_r \quad (2)$$

where the ϕ_r are atomic orbitals. Coulomb integrals, $\langle \phi_r | H | \phi_r \rangle \equiv \alpha_r$, and resonance integrals, $\langle \phi_r | H | \phi_s \rangle \equiv \beta_{rs}$, are expressed as:

$$\alpha_r = \alpha + h_r \beta; \quad \beta_{rs} = h_{rs} \beta \quad (3)$$

where α and β are the standard values for carbon. Orbital energies are then obtained in the form,

$$E_i = \alpha - x_i \beta \quad (4)$$

h was taken as unity for all the bonds within the aromatic rings; h was taken as zero for all the carbon atoms, and 0.5 for the nitrogen atoms, the value suggested by the SCF calculations of Mataga.¹⁷

There are two low-lying empty orbitals, numbers 8 (type χ) and 9 (type ψ), and two high-energy filled orbitals, numbers 6 (type χ) and 7 (type ψ).

Where possible, we shall now use a perturbation

¹⁶ Wave Mechanics Group, Mathematical Institute, University of Oxford, *Progress Report*, 1961–1962, **8**, 39.

¹⁷ N. Mataga and K. Nishimoto, *Z. phys. Chem. (Frankfurt)*, 1957, *N.F.* **13**, 140.

method to deal with the substituents. The three types of model currently widely used for the methyl group, the inductive, hyperconjugative and heteroatom models and the particular values of the parameters used for them are reviewed by Streitwieser.¹⁵

The first-order effect of an inductive substituent at carbon atom r upon the energy of orbital Φ_i of the parent molecule is given by,¹⁸

$$\Delta E_i = c_{ri}^2 \Delta \alpha_r \quad (5)$$

which will be additive on multiple substitution. The corresponding formula for a mesomeric perturbation is,¹⁹

$$\Delta E_i = \frac{c_{ri}^2 c_{sj}^2}{E_i - E_j} \beta_{rs}^2 \quad (6)$$

where s and j refer to substituent orbitals.

The hyperconjugative model supplies two substituent MO's, the heteroatom, one. There is no first-order term due to a conjugative perturbation and, to a first approximation, we may add the effects of induction and mesomerism and the effects of polysubstitution.

Thus an inductive perturbation raises the energies of all the MO's of the parent molecule by an amount proportional to c_{ri}^2 . A heteroatom perturbation raises the energies of all orbitals lying above the heteroatom orbital, which includes all those with which we are concerned, but its effect is less upon orbitals of higher energy because of the denominator $E_i - E_j$. The pure hyperconjugative model predicts a compression of the energies of the orbitals which concern us. However, for a given orbital, and a given type of substituent, the energy shifts produced by substitution at the various positions r are always proportional to c_{ri}^2 so we shall write,

$$\Delta E_i = -\lambda_i c_{ri}^2 \beta \quad (7)$$

using β (the standard C-C value) as a convenient energy unit.

It will also be necessary to calculate the effects of methyl groups upon the π -electron charges on the nitrogen atoms, q_N ($= 2 \sum_{i=1}^m c_{Ni}^2$, where the lowest m orbitals are doubly occupied). The effect of an inductive perturbation upon q_N is readily obtained¹⁸ from the atom-atom polarisabilities, $\pi_{r,s}$, which are printed by the computer programme:

$$\Delta q_r = \pi_{r,s} \Delta \alpha_s \quad (8)$$

To calculate the effects of conjugative substitution by a perturbation method is considerably more difficult, and so they were obtained by complete HMO solutions for the substituted molecules. Using Streitwieser's parameters in the case of phen, the heteroatom model predicts a change in q_N approximately equivalent to that produced by an inductive effect of $\Delta \alpha = -0.22\beta$ at the same position, while the pure hyperconjugative

effect is equivalent to $\Delta \alpha = -0.041\beta$. It is not obvious why the values of Δq_N predicted by the different models should run parallel, but it is important to investigate the range over which this relationship is valid, from the point of view of extension of this approach to other substituents.

Interpretation of the statistically derived parameters. We may now hope to interpret the effects of methyl groups in various positions on CT energy in terms of the perturbation of the ligand π -MO involved, which is proportional, for a given orbital, to c_{ri}^2 [equation (7)]. Thus all positions of substitution should produce effects of the same sign. This is not observed, (Tables 1 and 2) and so it is not adequate to assume that there is no interaction between ligand and metal ion. The approximation of pure CT may be retained, however, by making the next simplest assumption, namely that the interaction is a purely inductive one (*i.e.*, a σ effect). The energy of the d -orbital involved in CT must be related to the effective charge on the metal, and hence to the charge on the attached ligand atom. Over a small enough range, the relation between the d -orbital energy and charge on the ligand nitrogen atoms may be taken as linear. Thus we avoid explicitly dealing with the orbitals of the metal ion by using a parameter relating to the ligand.

The observed shifts are thus fitted to a combination of a term proportional to c_{ri}^2 , representing the perturbation of a ligand orbital Φ_i , and a term proportional to $\pi_{N,r}$, representing the perturbation of the metal d -orbital (actually the sum of $\pi_{N,r}$ for the two nitrogen atoms in the ligand, say $\Delta_r \sigma = \pi_{1,r} + \pi_{10,r}$).

$$\Delta_r \nu = l + m_1 c_{ri}^2 + m_2 \Delta_r \sigma \quad (9)$$

where $\Delta_r \nu$ is one of the coefficients in equation (1) determined above. The equations (9) include one for each type of substitution position, r , and one for the unsubstituted case, so there are two sets of four equations for the ferrous and ferric complexes, and one set of five for the cuprous. Methyl groups destabilise π -orbitals in the energy range which concerns us, and decrease the electron density on the carbon atom adjacent to them, which in most cases increases the negative charge on the nitrogen atoms. Thus m_1 in equation (9) should be positive and m_2 negative for CT from metal to ligand, while the signs should be reversed for ligand to metal CT.

It is also of interest to use empirical measures of the σ -donor power of the ligand for $\Delta_r \sigma$ in (9). The pK_a is such a parameter, since π -bonding with the proton may be neglected. The redox potentials have also been considered as a measure of d -orbital energy.

The various quantities to be inserted in equation (9) are shown graphically in Figure 4. The success of our explanation of the shifts may now be assessed both by observing the quality of the fits obtained to the sets of

¹⁸ C. A. Coulson and H. C. Longuet-Higgins, *Proc. Roy. Soc.*, 1947, *A*, **191**, 39.

¹⁹ H. C. Longuet-Higgins and R. G. Sowden, *J. Chem. Soc.*, 1952, 1404.

1534

J. Chem. Soc. (A), 1967

equations (9), and by inspecting the signs of the regression coefficients. Table 3 lists these coefficients, the variance ratio, and the percentage of the variation explained. In all cases, both the above criteria agree in their assignment of which ligand MO is involved in the transition; CT from the cuprous or ferrous ion goes to orbital 9 of the HMO calculation (the next to lowest empty, type ψ), while an electron is transferred to the ferric ion from MO 6 (the next to highest filled, type χ).

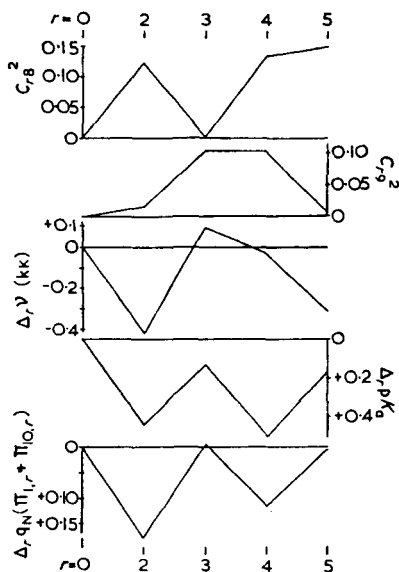


FIGURE 4 Shifts in the energy ($\Delta\nu$) of cuprous to phen CT associated with substitution in various positions (r), and factors relevant to their explanation. The latter are plotted in the sense in which they are expected to influence the CT energy (hypsochromic shifts upwards). Unsubstituted values are plotted as $r = 0$, vertical scales at alternate sides for clarity only

The most probable value for the variance ratio, if there is no correlation, is unity; higher values are indicative of a successful fit. Formal statistical significance for a single one of the fits (explaining four or five observed quantities with three adjustables) requires a very high value but if the three fits are taken together, the results are highly significant.

Having decided which π -MO's are involved in CT, we turn to the interpretation of the values of the regression coefficients.

Further Conclusions.—Models for the methyl group. To a first order, a methyl group attached to carbon atom r affects the energy of MO Φ , according to equation (7), so

²⁰ A. Streitwieser, jun., *J. Phys. Chem.*, 1962, **66**, 368; *J. Amer. Chem. Soc.*, 1960, **82**, 4123.

²¹ E. S. Pysh and N. C. Yang, *J. Amer. Chem. Soc.*, 1963, **85**, 2124.

²² W. C. Neikam and M. M. Desmond, *J. Amer. Chem. Soc.*, 1964, **86**, 4811.

the evaluation of m_1 in equations (9) gives values for λ_8 and λ_9 . Taking 6.7 and 3.9 kK as the most probable values for m_1 for orbitals 6 and 9, respectively, and using $\beta = -25$ kK = -3.1 eV:

$$\lambda_8 = 0.27 \text{ and } \lambda_9 = 0.16 \quad (10)$$

so that the low-lying orbital is destabilised more than the higher one. These values for λ_i are compared in Figure 5 with the predictions of various recommended models for the methyl group, and with other results of methods for investigating the energies of individual orbitals.²⁰⁻²⁴

The predictions plotted are those of the three models recommended by Streitwieser,¹⁵ and a pure hyperconjugative model.²⁵ Curves have also been drawn

TABLE 3

Results of regressions to explain the effects on CT energies of substitution in the various positions [No. = number of the HMO used in the fit, σ = parameter used to measure σ -donor power, l , m_1 , and m_2 are the coefficients of equation (9), the column headed % lists the percentage of variation explained, and V.R. is the variance ratio]

Metal	No.	σ	l	m_1	m_2	%	V.R.
Ferrous	8	q_N	+0.136	-2.19	+0.80	67	1.0
	8	pK_A	+0.097	-2.86	+0.53	75	1.9
	9	q_N	-0.094	+3.43	-2.86	79	2.5
	9	pK_A	-0.015	+4.08	-0.94	99.4	90
Cuprous	8	q_N	+0.05	-1.33	-0.96	57	1.3
	8	pK_A	+0.03	-2.14	+0.10	48	0.9
	9	q_N	-0.13	+2.46	-1.73	81	4.2
	9	pK_A	-0.08	+3.41	-0.76	87	6.9
Ferric	6	q_N	+0.02	-6.63	+55.0	99.9	747
	6	pK_A	-0.07	-7.29	+1.38	99	39
	7	q_N	-0.06	+2.55	+6.86	50	0.5
	7	pK_A	-0.06	+2.40	+1.08	29	0.2

through our points. Two points are sufficient to determine the heteroatom parameters completely ($h_X = 3.0$, $k_{CX} = 0.75$); we have chosen to redetermine h_{CX} and k_{CY} out of the five parameters given by Streitwieser (obtaining: $h_{CX} = -0.16$, $k_{CY} = 0.77$). These two curves illustrate how closely the heteroatom model may be tailored to fit a combination of hyperconjugation and induction.

The following conclusions may be drawn from Figure 5. (a) The ionisation potential measurements give high values for $-\lambda$; the other, solution, measurements give a rather large scatter, but there are no obvious systematic differences between measurements in different solvents; our two points lie well within the belt of other results.

The value of $-\lambda$ obtained from CT in methyl-benzene complexes with tetracyanoethylene is taken from Lepley,²¹ who assumed that CT comes from that one of the degenerate pair of benzene orbitals which is the more

²³ A. Streitwieser, jun., and I. Schwager, *J. Phys. Chem.*, 1962, **66**, 2316.

²⁴ E. L. Mackor, G. Dallinga, J. H. Kruizinga, and A. Hofstra, *Rec. Trav. chim.*, 1956, **75**, 838; E. L. Mackor, A. Hofstra, and J. H. van der Waals, *Trans. Faraday Soc.*, 1958, **54**, 186.

²⁵ C. A. Coulson and V. A. Crawford, *J. Chem. Soc.*, 1953, 2052.

org. Phys. Theor.

1535

destabilised by the substituents. Assuming instead that the measurements gives the mean of the two CT energies, the value obtained for $-\lambda$ increases from 0.21 to 0.25, in very good agreement with our results.

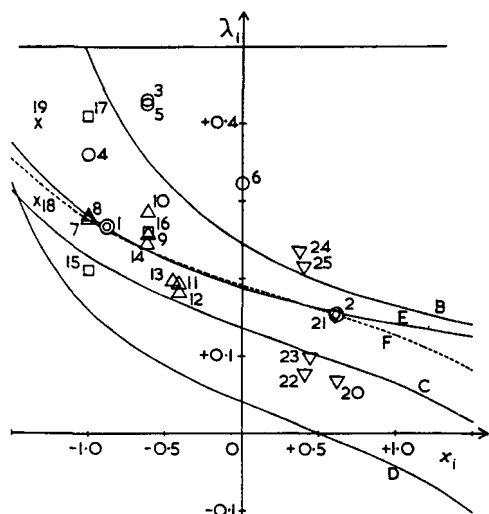


FIGURE 5 Theoretical and experimental effects of methyl groups on MO energies [measured by λ_i of equation (7)], as a function of the unperturbed energies [$\alpha - x_i\beta$, equation (4)]. Theoretical: A, inductive, B, heteroatom, and C, hyperconjugative plus inductive, from Streitwieser; D, Coulson and Crawford's hyperconjugative model; E, heteroatom, and F, hyperconjugative plus inductive, constructed to fit our experimental points, 1 and 2

Experimental: \odot our points; \circ ionisation potentials^{20, 21}; Δ polarographic oxidation^{21, 22}; \square CT to tetracyanoethylene^{24, 25}; \times basicities²⁴; ∇ polarographic reduction²²

In detail (number of substitution positions in parentheses): 1, CT from phen MO 6 (3); 2, CT to phen MO 9 (4); 3, butadiene (2); 4, benzene (4); 5, naphthalene (2); 6, allyl (2); 7, 8, benzene (5, 11) (different workers); 9, 10, naphthalene (2); 11, 12, anthracene (1); 13, 1,2-benzanthracene (12); 14, butadiene (1); 15, benzene (11); 16, naphthalene, 1st band (2); 17, naphthalene, 2nd band (2); 18, "a number of aromatics"; 19, "benzene homologues"; 20, naphthalene (2); 21, phenanthrene (3); 22, anthracene (2); 23, pyrene (3); 24, fluoranthene (3); 25, azulene (5)

(b) Methyl groups raise the energies of low-lying orbitals more than those of high ones. However, an inductive contribution is necessary in the use of the hyperconjugative model, and it seems safest to regard the heteroatom model as providing an empirical fit to the true curve.

(c) In the case of naphthalene, for which the necessary data is available, it appears that, where we have assumed that two measurements refer to essentially similar processes, this assumption is more accurate than the postulate that HMO theory will explain the observed shifts. This is illustrated in Table 4, where it is seen that empirically, the highest occupied orbital appears to have about equal coefficients on atoms 1 and 2, instead of the predicted 1 : 2 ratio in c^2 . The figures for

polarographic reduction are surprising; the relative effects of 1- and 2-substituents are more consistent with involvement of the next to lowest empty orbital (this assumption also gives a more reasonable value for λ).

(d) We have no evidence in any of the above results but our own for an electron leaving any but the highest occupied orbital in an ionisation-type process.

TABLE 4

Effects of methyl substitution at position r on the energies of the MO's of naphthalene [$\Delta_r E_{\text{occ}}(\Delta_r E_{\text{emp}})$ = the energy change of an occupied (empty) orbital on substitution at position r , in eV]

r	1	2
$c_{1r}^2 = c_{2r}^2$, from HMO theory	0.181	0.069
$c_{1r}^2 = c_{2r}^2$, from HMO theory	0	0.167
$\Delta_r E_{\text{occ}}$, from polarographic oxidation	+0.11	+0.11
$\Delta_r E_{\text{occ}}$, from CT to tetracyanoethylene	+0.11	+0.09
$\Delta_r E_{\text{occ}}$, from photoionisation	+0.16	+0.17
$\Delta_r E_{\text{occ}}$, 2nd CT to tetracyanoethylene	+0.04	+0.17
$\Delta_r E_{\text{emp}}$, from polarographic reduction	+0.015	+0.045
Change in p -band energy, eV	-0.087	-0.016
Approximate empirical prediction	-0.09	-0.05
Our model for methyl predicts:		
$\Delta_r E_4$	0	+0.145
$\Delta_r E_5$	+0.135	+0.051
$\Delta_r E_6$	+0.084	+0.032
$\Delta_r E_7$	0	+0.065
Change in p -band energy, eV	-0.050	-0.019

Sensitivity of metal d -orbital energy to charge on the ligands. The coefficients m_2 of (9) give a measure of the sensitivity of the d -orbitals of the metal ion to the σ -donor power of the ligand. The ratio of the values from the different complexes is approximately, cuprous : ferrous : ferric = 0.8 : 1.0 : 1.8. In both ferrous and ferric the configuration change is $d^5 \leftrightarrow d^8$ in the CT approximation. Though the net charges on the ligands differ, the resulting difference in q_N is not of a greater order of magnitude than changes produced by substitution, suggesting that the ratio 1.8 : 1 arises from the different metal-ligand distances in the two complexes.

Relations between different measures of σ -donor power. The patterns of the effects of methyl substitution upon pK_a and upon the HMO charge, q_N , are shown in Figure 4. They differ in that the sharply alternating predictions of HMO theory are blurred, and that substitution at distant positions has a greater effect on pK_a than on calculated charge.

pK_a Changes are expected to follow charge changes in a series of bases if it is assumed that the part of the total free energy of protonation most sensitive to substitution is the change in total π -energy (ref. 26). The proportionality constant obtained by fitting pK_a to q_N is consistent with that obtained for bases with a single heterocyclic nitrogen atom²⁷ and the suggestion that the proton is symmetrically placed with respect

²⁶ O. Chalvet, R. Daudel, and F. Peradejordi, "Molecular Orbitals in Chemistry, Physics, and Biology," ed. P.-O. Lowdin and B. Pullman, Academic Press, New York, 1964, p. 475.

²⁷ H. C. Longuet-Higgins, *J. Chem. Phys.*, 1950, 18, 275.

1536

J. Chem. Soc. (A), 1967

to the two nitrogen atoms of phen. The fit of the pK_a can be considerably improved by using an "auxiliary inductive parameter" (cf. ref. 28).

Changes in ferrous-ferric redox potentials on substitution run very closely parallel to those of ligand pK_a 's. This may be interpreted in terms of the stability constants of the two sets of complexes; it suggests that changes in these constants are determined by changes in σ -bonding (the proportionality constant has the expected sign.). Alternatively, the change in redox

potential may be regarded as giving another estimate for the sensitivity to pK_a of the energy of the $d^0 \rightarrow d^5$ process. This "adiabatic" figure can be compared with the "vertical" ones obtained from CT energies. The three values are entirely consistent.

We have not yet considered the origin of the intensities of the CT bands; this is the main subject of the following paper.

[6/1527 Received, December 5th, 1966]

* J. J. Elliott and S. F. Mason, *J. Chem. Soc.*, 1959, 2352.

The Spectra of Complexes of Conjugated Ligands.¹ Part II. Charge-transfer in Substituted Phenanthroline Complexes: Intensities

By P. Day and N. Sanders, Inorganic Chemistry Laboratory, University of Oxford, South Parks Road, Oxford

Measurement of the charge-transfer band of tris(phenanthroline)iron(II) at low temperature provides support for the suggestion that its fine structure arises from a vibrational progression in the excited state.

A one-electron theory of charge-transfer is applied to the charge-transfer bands of ferrous, ferric, and cuprous phenanthroline complexes. The energies of the *d*-orbitals are calculated, and possible reasons for the involvement of unexpected ligand molecular orbitals are discussed. The origin of the intensities is then considered, and it is suggested that the main source of intensity is the transition moment resulting from the transfer of charge itself, though borrowing from internal ferrous and cuprous (not ferric) transitions, and borrowing from internal ligand transitions may be appreciable. Metal-ligand resonance and overlap integrals are estimated from the data.

The effects of substitution on extinction coefficients are additive for cuprous complexes. The effects of substitution in each position are extracted statistically; the results are not in perfect agreement with the predictions derived from any of the sources of intensity considered, but do not contradict the assignment mentioned above.

PART I of this Series¹ was concerned with the effects of substitution with methyl groups upon the energy of charge-transfer (CT) bands in phenanthroline (phen) complexes. The shifts produced by successive substitution were shown to be additive, and the energy changes associated with methyl groups in the different positions of the phen molecule were extracted statistically. These values were then interpreted on a one-electron, one-ligand model; it proved necessary to allow for an inductive effect of the ligand upon the energies of the orbitals of the metal, but it was unnecessary to depart from the assumption of "pure CT," that is, the neglect of mixing between the donor and acceptor orbitals. Here, we shall continue to speak almost entirely in one-electron terms, but will abandon the other restrictions mentioned.

The interpretation of energy shifts given in the previous Paper provided three types of information. First, it was possible to assign the molecular orbital (MO) involved in CT; the ferrous and cuprous ions transfer an electron to MO 9 of the Hückel Molecular Orbital (HMO) calculation, rather than orbital 8 as might be expected, and CT occurs from HMO number 6 to the ferric ion. Second, a model of the methyl group was derived, which involves both an inductive and a hyperconjugative effect. Finally, some information was obtained about the magnitude of the changes in metal *d*-orbital energy produced by changing the σ -donor power of the ligand.

¹ P. Day and N. Sanders, preceding Paper.

² P. Krumholtz, *J. Amer. Chem. Soc.*, 1953, **75**, 2163.

We now discuss the intensity of these CT bands. Those of the cuprous and ferrous complexes show some structure, and we must first decide whether this is the result of several electronic components.

The spectrum of the air-stable ferrous complex was measured in an ethanol glass at liquid nitrogen temperature; the result is compared with the room temperature spectrum in Figure 1.

Krumholtz, who discovered a very close resemblance between the visible spectra of various ferrous tris-complexes of ligands containing the group N=C-C=N both in energy² and structure,³ suggests³ that the structure is the result of vibrational coupling.

Our low temperature spectrum shows two quite well resolved peaks and a very clear shoulder. The two separations are equal to within experimental error (of the order of 100 cm.⁻¹), good evidence that the structure is a vibrational progression. The infrared spectra of unsubstituted phen complexes with different metals are very similar, bands shifting by up to about 30 cm.⁻¹ among the ligand and the various complexes.⁴ The bands in the 1400 to 1650 region were assigned to ring deformations. Their energies show rough linear correlations with the field produced by the metal ion (regarded as a point charge) at the nitrogen atoms.

³ P. Krumholtz, "Theory and Structure of Complex Compounds, Papers presented at the Symposium held in Wrocław, Poland, 1962," ed. B. Jezowska-Trzebiatowska, Pergamon, Oxford, 1964, p. 217.

⁴ A. A. Schilt and R. C. Taylor, *J. Inorg. Nuclear Chem.*, 1959, **9**, 211.

The HMO model of the excited state suggests that the observed CT peak separations (1500 cm^{-1}) should not differ by more than about 20 cm^{-1} from a band in the

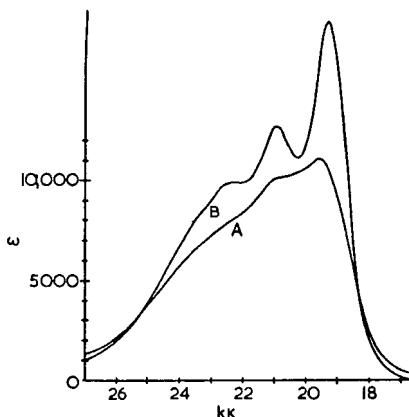


FIGURE 1 Visible absorption spectrum of ferrous tris-phen, (A) at room temperature and (B) at liquid nitrogen temperature. Curve (B) is drawn to an arbitrary vertical scale

infrared spectrum of the ferrous or ferric complex. There is indeed a strong band in the phen spectrum at 1505 , which moves to higher energies (1512 – 1527) in the complexes. It is one of the most sensitive to the charge on the central ion.

Intensity in the Unsubstituted Complexes.—Experimental parameters relating to dipole strengths in phen complexes are given in Table 1. Axes are as given in

	Ferric*	Ferrous ^b
Area ($\text{cm}^{-1} \times \epsilon$ units)	3.73×10^6	60.5×10^6
ν (kK), Mean frequency	16.9	20.6
Oscillator strength	0.0161	0.261
Dipole strength	2.02×10^{-34}	2.70×10^{-33}
$ Q $, transition moment	1.42×10^{-18}	5.19×10^{-18}
r (Å), Effective dipole length ..	0.296	1.080
per ligand	0.171	0.624

* J. C. Tomkinson, unpublished results. Our measurements.

Figure 1 of the preceding Paper, and Figure 2. Figure 2a follows Orgel.⁵ It is also convenient to use the group-theoretical axes for D_3 , labelled X, Y, Z in which the Z axis is taken as the threefold axis (positive in the direction of positive x, y, z), and the X and Y axes form a right-handed system with it, such that the positive X axis passes through the twofold axis of ligand A.

Symmetry Requirements.—The cuprous and ferrous ground states have closed shells and are therefore totally symmetric; their excited states have symmetries which are products of the symmetries of the hole and the ligand MO involved; the ferric ground state has the symmetry of the hole in its d -shell, its excited state has

⁵ L. E. Orgel, *J. Chem. Soc.*, 1961, 3683.

the symmetry of the ligand MO providing the electron in CT.

All relevant products of the symmetries of one d -orbital and one ligand MO, together with the associated polarisation of CT absorption, are given in Table 2.

TABLE 2
Product of ground and excited state symmetries and allowed polarisation directions for relevant combinations of metal d - and ligand π -orbitals

2a Mono-complexes, symmetry C_{3v}	
d -Orbital	Ligand MO type
$d_{xy} (a_2)$	$\psi (b_1)$ $\chi (a_2)$
$d_{xz} (b_1)$	b_2, y_A a_1, z_A
$d_{yz} (b_2)$	a_1, z_A b_2, y_A
$d_{xy}, d_{yz} (b_2)$	$a_2, -$ b_1, x_A
$d_{xz}, d_{yz}, d_{xy} (a_1)$	b_1, x_A $a_2, -$

2b Tris-complexes, symmetry D_3 (d = irreducible representation of d -orbital; $\psi_{a_i} = a_i$ combination of ψ -type MO's, etc.)	
Ligand MO:	
d ψ_{a_1} ψ_e χ_{a_1} χ_e	
a_1 a_2, Z e, X, Y $a_1, -$ e, X, Y	
e e, X, Y $a_1 + a_2 + e$ e, X, Y $a_1 + a_2 + e$	
	X, Y, Z X, Y, Z

2c Bis-complexes, symmetry D_{3d}	
d -Orbital	Ligand MO (ψ_i)
d_{xy}, b_2	e, X, Y
d_{xz}, rz, e	$a_1 + a_2 + b_1 + b_2, Z$

We continue to use the notation introduced in the preceding Paper (taken from ref. 6), in which a ligand MO of symmetry b_2 in the C_{2v} point group of the isolated

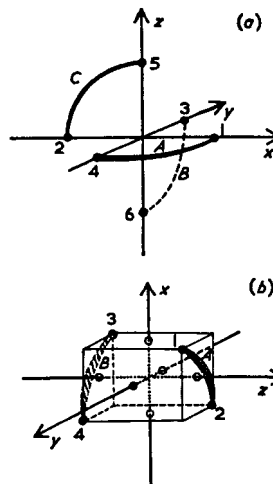


FIGURE 2 Axes, numbering of nitrogen atoms, and labelling of ligands. 2(a) Tris-complexes (D_3), "octahedral" axes. 2(b) Bis-complexes (D_{3d})

ligand is referred to as "type ψ " (no central nodal plane) and one of a_1 symmetry as "type χ ". It was shown empirically in the preceding Paper that we are

* R. A. Palmer and T. S. Piper, *Inorg. Chem.*, 1966, 5, 864.

concerned with MO 9 (type ψ) in the cuprous and ferrous complexes, and MO 6 (χ) in the ferric. We form linear combinations of these in the complexes.

Relations between Intensities in Mono-, Bis-, and Tris-complexes.—Table 2a lists allowed CT transitions polarised in the x_A , y_A , and z_A directions in the hypothetical mono-complexes, regardless of whether χ or ψ orbitals are involved. It may be shown by explicit consideration of the MO's in the complexes that the total dipole strength in the tris complexes is three times, and that in the bis-complex twice, that of a mono-complex. The redistribution of intensity among the allowed transitions of Tables 2b and c is, in general, more complicated than that predicted by a simple coupled-oscillator model (described in ref. 7, applied to β bands in ref. 8).

CT Theory.—There is considerable doubt as to the precise origin of the intensity of CT bands in general (e.g., ref. 9), but the intensities of our bands indicates that they are allowed by the multiplicity and symmetry selection rules.

Following the approach of Murrell,⁹ let the one-electron transition be $\phi^0 \rightarrow \phi^1$; then, to a zero order, $\phi^0 = \phi_d$ is a wave function of the donor in the charge-transferred state (D^+ , say), and $\phi^1 = \phi_a$ is a wave function of the acceptor (A). The corresponding transition moment is $\langle \phi_d | Q | \phi_a \rangle$ ($Q = er$), which is zero in the absence of overlap between ϕ_d and ϕ_a . It may then be shown that the energy of CT is given by

$$E_{CT} = I_d - E_a + C \quad (1)$$

where I_d is the ionisation potential of the donor, E_a the electron affinity of the acceptor, and C a Coulomb term.

A resonance integral between ϕ_d and ϕ_a , $H_{da} = \langle \phi_d | H | \phi_a \rangle = \beta_{da}$, mixes the two orbitals, producing

$$\phi^0 = \phi_d + \lambda_{da}\phi_a; \quad \phi^1 = \phi_a - \lambda_{da}\phi_d \quad (2)$$

within the HMO approximation. Perturbation theory gives the mixing coefficient as

$$\lambda_{da} = \frac{H_{da}}{H_{dd} - H_{aa}} = \frac{-\beta_{da}}{I_d - E_a + C} = -\frac{\beta_{da}}{E_{CT}} \quad (3)$$

This contradicts the formula given by Murrell,⁹ in that the denominator is the observed CT energy, whereas Murrell gives $I_d - E_a$, but is, in fact, obtained by substituting Murrell's expressions for H_{dd} and H_{aa} .

The transition moment is now:

$$\begin{aligned} \langle \phi^0 | Q | \phi^1 \rangle &= \langle \phi_d | Q | \phi_a \rangle + \\ &\quad \lambda_{da} (\langle \phi_d | Q | \phi_a \rangle - \langle \phi_d | Q | \phi_d \rangle) \quad (4) \\ &= Q_{da} + \lambda_{da}(Q_{aa} - Q_{dd}), \text{ say.} \end{aligned}$$

Q_{da} . The "contact" CT term, is unlikely to be very important (an estimate of it will be made later); it is also more consistent with HMO theory to set it equal to zero. The second term is the product of a mixing coefficient and the dipole moment of the transferred charge, and will be referred to as the "transfer" term.

⁷ J. N. Murrell, "The Theory of the Electronic Spectra of Organic Molecules," Methuen, London, 1963, ch. 7.

Table 2a shows that, in the hypothetical mono-complexes, only the transitions $d_{x_A y_A} \leftrightarrow \psi_A$ and $d_{z_A y_A} \leftrightarrow \chi_A$ will derive intensity from "transfer" terms, since only in these cases are there non-zero resonance integrals between ϕ_d and ϕ_a . Both of these transitions are short-axis polarised, an illustration of the general rule that "transfer" intensity must always be polarised in the direction of CT. This rule is preserved in the bis- and tris-complexes; thus, transfer intensity can only be X, Y -polarised in D_3 .

Mixing of the orbitals of D^+ and A other than those actually involved in CT will lead to other sources of intensity. If ϕ_{d^*} represents an empty donor orbital, ϕ_a a full acceptor orbital, and ϕ_{a^*} an empty acceptor orbital other than ϕ_a , we may expect to cover the other major sources of intensity as follows:

$$\begin{aligned} \phi^0 &= \phi_d + \lambda_{da}\phi_a + \Sigma \lambda_{da}\phi_a + \Sigma \lambda_{da}\phi_{a^*} \quad (5) \\ \phi^1 &= \phi_a - \lambda_{da}\phi_d + \Sigma \lambda_{da^*}\phi_{a^*} \end{aligned}$$

Then:

$$\begin{aligned} \langle \phi^0 | Q | \phi^1 \rangle &= Q_C + Q_T + \Sigma \lambda_{da} \langle \phi_d | Q | \phi_a \rangle + \\ &\quad \Sigma \lambda_{da} \langle \phi_{a^*} | Q | \phi_a \rangle + \Sigma \lambda_{da} \langle \phi_d | Q | \phi_{a^*} \rangle \quad (6) \\ &= Q_C + Q_T + Q_A + Q_{A^*} + Q_D, \text{ say.} \end{aligned}$$

Q_C and Q_T are the contact and transfer terms already considered, Q_A is the moment borrowed from internal transitions of the acceptor, Q_{A^*} is borrowed from transition moments between empty acceptor orbitals, and Q_D from internal donor transitions. Terms involving squares of mixing coefficients and higher order perturbations have been ignored.

We now consider the numerical implications of the above formulae.

Numerical Calculations on the Unsubstituted Complexes.—We first evaluate the energies of the one-electron metal d -orbitals in the form $\alpha_C + \beta_{CC}$. α_C and β_{CC} replace α and β of the preceding Paper to avoid confusion; α_C must remain in the expression for the d -orbital energies since they will be determined relative to those of the HMO's; β_{CC} will be taken as 25 kK and used simply as a convenient energy unit. In equation (1), E_a (ferrous and cuprous) or I_d (ferric) is already known in the form $\alpha_C + x\beta_{CC}$ from the HMO calculation with $h_N = 0.5$; the CT energies are known, so it only remains to calculate the values of C . In the ferrous and cuprous cases, C is approximately the Coulomb attraction between the metal ion D^+ , regarded as a point charge, and an electron in HMO 9, regarded as a series of point charges of magnitude $c_r e^2$ on the various atoms r . In the ferric case, C is the repulsion between the hole in a ligand MO and a ferrous ion. The resulting values of C are +70, -120, and -80 kK for ferric, ferrous, and cuprous complexes, giving d -orbital energies $\alpha_C + 3.0\beta_{CC}$, $\alpha_C + 5.0\beta_{CC}$, and $\alpha_C + 3.5\beta_{CC}$. As expected, the ferric orbital is less stable than the ferrous; in both cases, we are concerned with $d^5 \leftrightarrow d^6$ changes (i.e., I_d for ferrous

⁸ A. J. McCaffery and S. F. Mason, *Proc. Chem. Soc.*, 1963, 211.

⁹ J. N. Murrell, *Quart. Rev.*, 1961, 15, 191.

Inorg. Phys. Theor.

1539

and E_a for ferric), and the closer proximity of the ligands to the ferric ion should destabilise the d -orbitals as discussed in the preceding Paper.

In what follows, it will be necessary to give a value to α_C . Values used are usually very close to the first ionisation potential of carbon (11.265 eV); we shall take $\alpha_C = 90 \text{ kK} \cong 11.2 \text{ eV} \cong 3.6\beta_{CC}$.

It is also convenient to discuss at this point why ligand orbitals 6 and 9 are involved in CT rather than 7 and 8. A calculation of the Coulomb term for CT to MO 8 suggests that this should occur at higher energy than CT to MO 9. Furthermore, our value of $h_N = 0.5$ cannot be very realistic when the nitrogen atom is attached to a metal; increasing this value will also lower the energy of CT to MO 9 relative to MO 8. In the ferric case, however, both these factors tend to make CT from orbital 7 even lower in energy compared with orbital 6. Furthermore, no explanation in terms of d - p π -bonding is available. Thus we cannot explain the use of MO 6 within our one-electron treatment.

Finally, it should be mentioned while discussing electrostatic calculations that there is a very large attraction energy between the central metal ion and the HMO-calculated ligand charges.

We now investigate the intensities, first assuming that they are derived from the transfer term, and then making an estimate of the magnitude of the other terms using the value of the metal-ligand resonance integral deduced.

In the ferrous case, the total transfer intensity expected is $\sqrt{2.3}(\sqrt{2c_{N9}}\beta_{ML}/E_{CT})^2Q_\psi^2$. The first $\sqrt{2}$ arises from the fact that either of the two electrons in an occupied orbital may be excited; there is no such factor in the ferric case. Q_ψ is $|(Q_{aa} - Q_{dd})|$ of equation (4) for MO 9 in a mono-complex; its calculated value is $e \times 2.49 \text{ \AA}$. ($\sqrt{2c_{N9}}\beta_{ML}/E_{CT}$) is the mixing coefficient for a mono-complex; β_{ML} is the resonance integral between a d -orbital and an ideally oriented $2p$ -orbital of a ligand nitrogen atom⁵ (e.g., d_{zz} and $2p_z$ of N_1 in Figure 2a). It is not certain whether all this intensity is contained in the observed band (HMO theory suggests that it is divided into two closely spaced equal parts); furthermore, HMO theory usually predicts values about three times too high for the intensities of $\pi \rightarrow \pi^*$ transitions. In view of all this uncertainty, we will tentatively equate the above expression for intensity to three times the observed; this gives $\beta_{ML} = 11 \text{ kK}$.

In the ferric case, if the transition is $d_e \rightarrow \chi_e$, the situation is analogous to the ferrous one, leading to $\beta_{ML} = 8.5 \text{ kK}$. If, on the other hand, the transition is $d_{a_1} \rightarrow \chi_e$, β_{ML} becomes 6 kK.

Now, according to the one-electron theory, the β_{da} 's, proportional to β_{ML} 's, are matrix elements of the Hamiltonian of D^*A ; thus the values from the ferrous and ferric CT bands both involve the ferric ion, and should be similar. This makes the $d_{a_1} \rightarrow \chi_e$ assign-

ment less plausible than $d_e \rightarrow \chi_e$, and we shall assume $\beta_{ML} = 8.5 \text{ kK}$.

We can now estimate the metal-ligand overlap integrals, and the contact CT intensities. According to the Wolfsberg-Helmholtz approximation,¹⁰ a resonance integral in a π -bond may be approximated by, $H_{ij} = 2S_{ij}(H_{ii} + H_{jj})/2$. Application of this expression to our two values of β_{ML} gives $S = 0.03$ for both ferrous and ferric cases. This value is undoubtedly of the correct order of magnitude; the d -orbital size in these complexes should not be too different from that in the neutral iron atom (cf. Orgel's remarks¹¹ on hydrated Mn(II) and the gaseous atom), and Brown and Fitzpatrick¹² have derived a value of about 0.06 for overlap with a carbon $2p$ - π orbital, using the best available self-consistent-field (SCF) wave functions for neutral iron.

Using $S \cong 0.03$, and reasonable assumptions for orbital sizes, it seems that $|Q_e|$ of equation (6) is unlikely to be greater than about $e \times 0.02 \text{ \AA}$ per ligand in the ferrous complexes, compared with the total of 0.62 \AA per ligand to be explained.

The obvious sources of intensity from internal metal transitions are $d \leftrightarrow p$ transitions; $3d \rightarrow 4p$ contributions will appear in the ferrous moment by mixing of $4p$ with ψ_p ; in the ferric case, a Q_A -type moment might appear by mixing of χ_6 with $3p$, and a Q_{A^*} contribution by the mixing of χ_6 with $4p$. In fact, χ -type orbitals will not mix with central-atom orbitals, so we need only consider the ferrous and cuprous complexes. Considering the maximum overlap between, and the radii of, a $3d$ and $4p$ orbital, we estimate that the absolute maximum dipole length which can be borrowed from such a transition as $d_{xy} \rightarrow p_x$ is 0.25 \AA .

Summing over the d and p orbitals, it seems that, in the ferrous complexes, an absolute maximum of 0.35 \AA dipole length per ligand is available from this source; the total to be explained per ligand is 0.62 \AA . We conclude that internal metal transitions may contribute quite appreciably to the intensity of the ferrous CT band but are almost certainly not the largest source of intensity.

We finally consider the possibility of borrowing from internal ligand transitions. A number of disturbing features arise in the actual calculation of Q_A and Q_{A^*} . First, though the denominators of the relevant mixing coefficients can be formally calculated, they involve the difference between two very large Coulomb terms (one is implicit in our evaluation of I_d), so little faith can be placed in them. Second, the HMO calculated $\pi \rightarrow \pi^*$ transition energies and moments agree poorly with experiment; it is not possible to explain the fact that the strongest, β , band is polarised along the ligand short axis. However, from calculations possible at this stage, we conclude once again that, while this may be an appreciable source of intensity, it is probably not the major one. The ferric case is even more difficult to deal with, so it has not been considered.

¹⁰ C. J. Ballhausen and H. B. Gray, "Molecular Orbital Theory," Benjamin, New York, 1964, p. 118.

¹¹ L. E. Orgel, *J. Chem. Phys.*, 1955, **23**, 1824.

¹² D. A. Brown and N. J. Fitzpatrick, *J. Chem. Soc. (A)*, 1966, 941.

1540

J. Chem. Soc. (A), 1967

Our assignment of intensity implies that the ferrous to phen CT will have mixed polarisation, but that the short-axis component will be the more intense. This is exactly what is observed in the ferrous to $\alpha\alpha'$ -dipyridyl CT in the tris-complex of this ligand.⁶

Substituent Effects on Intensities.—*Additivity of effects of successive substitution.* We now discuss the extinction coefficients summarised in Table 1 of the preceding Paper. Smith and his co-workers^{13,14} conclude that, unlike the frequency shifts, the changes in extinction coefficients of the CT bands on substitution are not accurately additive. To test this conclusion more quantitatively, multiple regressions have been carried out, with the results recorded in Table 3.

TABLE 3

Regressions to determine the effects ($\Delta_r\epsilon$) of substitution with methyl groups in various positions (r) upon extinction coefficients of CT bands (ϵ_0 = regression constant, $\Delta_r\epsilon$ = regression coefficients, S.E. = standard error of estimate from the regression equation, V.R. = variance ratio)

Complex	$10^{-3}\epsilon_0$	$10^{-3}\Delta_5\epsilon$	$10^{-3}\Delta_6\epsilon$	$10^{-3}\Delta_7\epsilon$
Cuprous ...	71.7	$+2.2 \pm 1.0$	$+3.1 \pm 0.5$	$+7.6 \pm 0.4$
Ferrous ...	120		-2.1 ± 1.9	$+10.6 \pm 2.2$
Ferric.....	9.27		$+0.5 \pm 5.5$	$+1.1 \pm 3.7$
Complex	$10^{-3}\Delta_r\epsilon$	S.E.	V.R.	Ref.
Cuprous ...	$+4.0 \pm 0.6$	2.5	35.4	1
Ferrous ...	$+0.7 \pm 2.7$	5.1	21.1	2
Ferric.....	-0.5 ± 7.1	2.0	1.5	3

In the ferric complexes, the assumption of additivity is a complete failure (the variance ratio is 1.55, while 3.41 is required for significant correlation). However, these compounds are very unstable, so we place little weight on this observation.

On the other hand, variation in the cuprous intensities is explained to within probable experimental error by the best linear equation.

In the ferrous case, the variance ratio is highly significant of correlation, but closer inspection shows that this only means that the intensity changes are dominated by substituents in the 4 and 7 positions. The errors in the prediction from the regression equation range up to 10%. We have redetermined the extinction coefficients for the few ligands still available, and obtain percentage increments on substitution roughly proportional to those of the corresponding cuprous complexes (see Table 4).

We shall therefore only consider the cuprous complexes. It will be assumed that the extinction coefficient is proportional to the integrated band area.

Interpretation of the changes in extinction coefficients on substitution. In the treatment of the effects of substitution on intensities, much more attention has so far been paid to forbidden than to allowed bands (e.g.,

¹³ W. W. Brandt and G. F. Smith, *Analyt. Chem.*, 1949, **21**, 1313.

¹⁴ W. H. McCurdy and G. F. Smith, *Analyst*, 1952, **77**, 846.

¹⁵ J. R. Platt, "Systematics of the Electronic Spectra of Conjugated Molecules," Wiley, New York, 1964.

TABLE 4

Percentage changes in extinction coefficients of metal to phen CT bands on substitution

Substitution positions	Ferrous			Cuprous
	This work	Smith ¹³	Smith ¹⁴	
5	+3	+10	+4	+4
4,7	+24	+26		+25
5,6	+11	+14	+12	+14
3,4,7,8	+23	+24		+33
3,5,6,8	+14	+5		+20

Platt¹⁵). However, Platt has pointed out¹⁶ that, for symmetry-allowed transitions in a centrosymmetric molecule, the effects of substitution on intensity should be additive within the range of applicability of first-order perturbation theory. Petruska¹⁷ has given a detailed proof of this. The restriction to centrosymmetric molecules seems unnecessary; either Platt's or Petruska's arguments may be extended. The only source of non-additivity with small perturbations would seem to arise with degenerate ground states (such as probably occur in the ferric complexes); if unsymmetrical substitution lifts the degeneracy of the ground state sufficiently for the populations of the two levels to be appreciably different, non-additivity may be observed. The pattern of substituent effects should help to determine the source of CT intensity. Thus, if it is all derived from the transfer term:

$$\epsilon \propto E_{CT}(c_{N9}\beta_{LM}Q_{\psi}/E_{CT})^2 \quad (7)$$

Taking logarithms and differentiating:

$$\Delta\epsilon/\epsilon = 2\Delta c_{N9}/c_{N9} - \Delta E_{CT}/E_{CT} + 2\Delta Q_{\psi}^2/Q_{\psi}^2 + 2\Delta\beta_{ML}/\beta_{ML} \quad (8)$$

The second term on the right hand side of equation (8) is experimentally known, while the first and third are calculable from HMO theory; subtraction of these from $\Delta\epsilon/\epsilon$ should leave $2\Delta\beta_{ML}/\beta_{ML}$, which, to be consistent with our discussion so far, should be proportional to the change in σ -donor power of the ligand. As may be seen from Table 5, this prediction is only roughly borne out. We may deduce that $\Delta\beta_{ML}/\beta_{ML}$ is about 0.1 per unit change in ligand pK_a . Table 5 also lists the quantities which should run parallel to pK_a if other sources are responsible for the intensity (changes in the unknown denominators of mixing coefficients have been ignored). It will be seen that the predictions for borrowing from internal metal transitions or contact terms fit the pK_a quite well, while no one of the internal ligand transitions provides a reasonable fit.

At this stage, it appears that our previous conclusion that the main source of intensity is the transfer term is not grossly in disagreement with the observed substituent effects on intensity; the error in our predictions may lie in the theory or in the assumption that extinction coefficient is proportional to band area.

This concludes our treatment of the phen complexes at

¹⁶ J. R. Platt, *J. Chem. Phys.*, 1951, **19**, 1418; *J. Amer. Chem. Soc.*, 1952, **74**, 276.

¹⁷ J. Petruska, *J. Chem. Phys.*, 1961, **34**, 1111.

TABLE 5

Percentage changes in extinction coefficients of cuprous complexes on substitution ($\Delta_r \epsilon/\epsilon$), and factors relevant to their explanation. Five possible explanations of the intensity predict that the last five rows (respectively) should run parallel to $\Delta_r K_a$

Position (r)	2	3	4	5
$\Delta_r \epsilon/\epsilon$ (%), observed	+3.0	+4.3	+10.5	+5.5
$\Delta_r \nu/\nu$ (%), observed	-1.8	+0.4	-0.1	-1.0
$\Delta_r \epsilon/\epsilon - \Delta_r \nu/\nu$ (%)	+4.8	+3.8	+10.6	+6.6
$2\Delta_r Q\psi/Q\psi$ (%)	+1.3	-3.2	+3.6	+0.2
$2\Delta_r c_{N\psi}/c_{N\psi}$ (%)	-2.8	+3.1	-2.9	+0.2
$\Delta_r pK_a$	+0.44	+0.14	+0.50	+0.19
"Transfer" prediction, $2\Delta\beta_{ML}/\beta_{ML}$ (%) from equation (8)	+2.7	+4.8	+9.7	+4.1
Internal metal/contact prediction	+7.7	+0.8	+13.5	+6.4
Internal ligand prediction, transition:				
MO 6 \rightarrow MO 9	+17.4	+7.9	-6.1	+8.5
MO 7 \rightarrow MO 9	-6.8	+11.6	-15.7	+20.8
MO 8 \rightarrow MO 9	+7.9	-0.7	+22.9	-1.9

the HMO level. There are three very obvious defects in the treatment given so far. First, the metal ion and the ligands are given very different treatment; for the ligands, we use a fixed basis set of one $2p\pi$ atomic orbital per atom, while for the metal ions, we talk in terms of changing effective nuclear charge and orbital size. Further, there are the deficiencies inherent in the HMO framework, the lack of any sort of charge self-consistency,

and the lack of any explicit account of inter-electron repulsion. Future work on these complexes will attempt to overcome these defects.

EXPERIMENTAL

The low-temperature spectrum was measured in an ethanol glass, with 1 mm.-path length. A Research and Industrial Instruments Co. cell (VLT 2) fitted with silica windows was used in a Unicam SP 700 spectrophotometer.

Percentage changes in extinction coefficients of the ferrous to phen CT band on substitution were determined by adding a little of each solid ligand to standard aqueous ferrous ion at a pH of about 4. The results are given in Table 4, where they are compared with values from Table 1 of the preceding Paper (*i.e.*, from ref. 13). This Table also gives some values quoted more recently by Smith¹⁸ (the two sources agree on the extinction coefficient of the unsubstituted complex). Finally, the percentage increments in extinction coefficients of the cuprous complexes are given; the only difference between the extinction coefficients of refs. 14 and 18 lies in the value for the unsubstituted complex, for which we have 7040,¹⁴ 7250,¹⁸ and 7170 (best regression, Table 3). We have assumed a value of 7200 in preparing Table 4.

The substituted ligands were obtained from the G. Frederick Smith Chemical Co., and the unsubstituted one from The British Drug Houses, Ltd.

[6/1526 Received, December 5th, 1966]

¹⁸ G. Frederick Smith Chemical Co., Price List, Columbus, Ohio, 1958.

This page intentionally left blank

CHAPTER 2

This page intentionally left blank

Metal Complexes in Solids: Optical Effects and Low-Dimensionality

Given the great success of ligand field theory in explaining the energies and intensities of optical absorption and emission in both molecular transition-metal complexes and solids, it came to dominate chemists' thinking regarding the electronic structures of such compounds, despite the fact that other energy levels and types of transition sometimes play an important part, as we have already seen in the previous chapter. Even the charge transfer excitations of Chap. 1 are localised to nearest neighbour atoms or molecules — from halide ion to metal or metal to conjugated ligand. Thus, the intense purple colour of the permanganate ion $[\text{MnO}_4]^-$ due to excitation from the highest filled t_1 level localised on the O to the empty e level of the Mn, is not greatly modified upon passing from dilute solution either to a solid solution such as $\text{K}(\text{Mn},\text{Cl})\text{O}_4$ or even to the pure solid KMnO_4 . It was this simple fact (equally applicable to most ligand field spectra) that led Jorgensen to coin the expressive phrase 'additivity of ionic colours' [1]. He meant that in general, the properties of a solid could be thought of as the sum of its constituents. For example, NiO , with a rocksalt structure, is more or less the same green colour as $[\text{Ni}(\text{H}_2\text{O})_6]\text{Cl}_2$, but because the Ni^{2+} in both is surrounded by an octahedron of O atoms. Even in binary solids, be they molecular-like $[\text{Cr}(\text{NH}_3)_6][\text{FeCl}_6]$ or continuous lattice-like MnCr_2O_4 , the lowest energy excited states are remarkably close to being a superposition of those of the constituent metal ions taken separately. The effect can even be seen with the naked eye, i.e. when blue $[\text{Cu}(\text{H}_2\text{O})_6]^{2+}$ forms a salt with yellow $[\text{CuCl}_4]^{2-}$, resulting in a green crystal.

The additivity of ionic colours indicates that there is no significant interaction between the constituents when they are brought together. Being of a contrarian disposition, in the 1960s I therefore started to look for cases where it broke down because they would signify that such interactions were indeed present, although of a type that was yet to be determined [2]. Some examples can be traced to essentially trivial explanations. For example, when Cr^{3+} is substitutionally doped into Al_2O_3 (known as corundum), the result is ruby red, but pure Cr_2O_3 , which also has the corundum structure, is green. Here, it is simply a matter of the differing ionic radii of Cr^{3+} and Al^{3+} : in dilute solid solution in Al_2O_3 , Cr^{3+} is 'squeezed', shifting the ligand field transitions responsible for the colour to higher frequency. However, this simple explanation masks a smaller and more subtle effect. Early development work on ruby lasers found that their efficiency decreased markedly at higher Cr^{3+}

concentrations. As in a liquid solution, ideality in a solid solution is a thermodynamic fiction. The energy levels of a near-neighbour pair of Cr^{3+} are not the same as those of two Cr^{3+} when widely separated because of an antiferromagnetic exchange interaction mediated by the bridging O.

Some of the most spectacular departures from additivity of ionic colours had been noticed nearly a century ago, because no advanced spectroscopy was needed to discern them. In fact, examples of coordination complexes first made in the 19th century (and even earlier, in the case of Prussian Blue) had been given their trivial names for that reason: Magnus' Green Salt, $[\text{Pt}(\text{NH}_3)_4][\text{PtCl}_4]$ is composed of a cation which is colourless in isolation and an anion that is red [3]; likewise, Wolfram's Red Salt, $[\text{Pt}^{\text{II}}(\text{C}_2\text{H}_5\text{NH}_2)_4][\text{Pt}^{\text{IV}}(\text{C}_2\text{H}_5\text{NH}_2)_4\text{Cl}_2]\text{Cl}_4$, has two constituents which are colourless when separated. Such effects are rendered even more noticeable by the fact that they are often extremely anisotropic because the coordination complexes composing them (and in particular their central metal ions) are organised into layers or chains in the crystalline state [4,5].

The reasons for cooperative optical effects in the solid state are many and various. They range from magnetic exchange interactions on an energy scale of $10\text{--}50\text{ cm}^{-1}$, causing marked intensity changes but only small energy shifts, to the interaction between transition dipoles where the parent transitions are electric dipole-allowed. In the latter, the formation of excitons can lead to shifts of many thousands of cm^{-1} , completely transforming the colour of the crystal compared with its constituent ions [6]. Dipolar interactions are also involved, seen from the remarkable shift of the absorption with inter-molecular spacing [6]. None of those examples involve electron transfer between the constituent molecules, but where more than one oxidation state of an element is present in the lattice, then such transfer can take place both optically and adiabatically, yielding another fruitful source of solid state phenomena. That issue is taken up in the next chapter.

References

- [1] C. K. Jorgensen, *Absorption Spectra and Chemical Bonding in Complexes*, Oxford, Pergamon Press, 1963.
- [2] P. Day, *Inorg Chim Acta Rev* **3**: 81–97 (1969). (**Reprint 2.1**)
- [3] P. Day, A. F. Orchard, A. J. Thomson and R. J. P. Williams, *J Chem Phys* **42**: 1973–1981 (1965); *idem ibid* **43**: 3763–3764 (1965).
- [4] P. Day, *Amer Chem Soc Symp Series* **5**: 234–253 (1974). (**Reprint 2.2**)
- [5] P. Day, *Ann N Y Acad Sci* **313**: 9–24 (1978). (**Reprint 2.4**)
- [6] P. Day, *J Amer Chem Soc* **97**: 1588–1589 (1975). (**Reprint 2.3**)

COOPERATIVE EFFECTS IN THE ELECTRONIC SPECTRA
OF INORGANIC SOLIDS

P. Day

*University of Oxford, Inorganic Chemistry Laboratory,
South Parks Road, Oxford, United Kingdom*

CONTENTS

I.	Introduction	81
II.	Ligand Field Spectra	82
	A. Exchange Interactions in Magnetically Ordered Crystals; Transition Metal Fluorides	82
	B. Environmental Effects; Magnus' Green Salt	84
III.	Charge Transfer Spectra	86
	A. Intramolecular transitions	86
	1. Magnus' Green Salt	86
	2. Nickel(II) Dimethylglyoximate	87
	3. Cyanopalladites and -platinites	90
	4. Oxalatoplatinites	91
	B. Intermolecular transitions	92
	1. Hexahalides and Tetroxo-anion Salts	92
	2. Hexacyanides	92
	3. Mixed valence Salts	93
IV.	Conclusion	96
V.	References	97

I. INTRODUCTION

One consequence of the remarkable success of ligand field theory in rationalizing the electronic structures of transition metal-containing molecules has been to focus the attention of spectroscopists on the properties of single ions or small clusters of ions. Because the visible spectrum of Ni^{II} in aqueous solution is so similar to that of NiO or of Ni^{II} dissolved in MgO , theoretical treatments of the spectrum of NiO rightly take as their starting point a single Ni^{2+} surrounded by six oxide ions and view the optical properties of the solid lattice as a degenerate superposition of the 10^{23} single ion excited states. This is clearly a sensible approach to electronic transitions, such as d-d transitions, which to a good approximation take place entirely within a single Heitler-London ionic configuration $\text{Ni}^{2+}\text{O}^{2-}\text{Ni}^{2+}\text{O}^{2-}$, but it is not so obvious that it provides a good starting point for describing electron transfer transitions, in which many degenerate or near-degenerate and interacting configurations such as $\text{Ni}^{2+}\text{O}^{-}\text{Ni}^{+}\text{O}^{2-}$, $\text{Ni}^{2+}\text{O}^{2-}\text{Ni}^{+}\text{O}^{-}$ etc. have to be considered. Still, even here this principle, which has been called¹ colloquially the additivity of ionic colors, seems to be reasonably well obeyed. For example, although no spectra of the concentrated solid have been reported (apart from powder reflectance²), it is quite clear from their colors that the spectra of solid KMnO_4 and MnO_4^{-} in solution must be very similar. Similarly, Jørgensen¹ has shown that only minor band shifts accompany the incorporation of IrCl_6^{2-} in various antiferroite lattices. Thus, for transition metal spectroscopists studying solids, it has usually been a matter for surprise and special

explanation when features are found in the spectra of solids which seem to have no analogies in the spectra of the single ions or isolated clusters of which the solid is composed.

Sometimes, in the early days of solid state transition metal spectroscopy, such concern was based on a misunderstanding of the absorption mechanisms available to a metal containing molecule. For example Yamada³ found that the lowest energy intense transition in nickel(II) dimethylglyoxime crystals occurred at much lower energy than in solution, and was polarised perpendicular to the plane of the complex, an unusual situation by comparison with any planar aromatic molecule. But his conclusion that this was an immediate consequence of metal-metal « bonding » (or even « interaction ») within the stacks of molecules in the crystal cannot be sustained when we notice that the first intense band in the nickel(II) N-methyl-salicylaldehyde crystal,⁴ where there are no such stacks, has a similar polarisation. In both molecules, there are several purely intramolecular transitions, such as $3d \rightarrow 4p$ or $3d_{z^2} \rightarrow \pi^*$ (ligand), whose transition dipoles would be directed perpendicular to the molecular plane, and which would hence be plausible candidates for the observed bands. Still, the fact remains that in nickel dimethylglyoxime this band does occur at lower energy and with greater intensity in the crystal than in solution, and it is thus the shift and intensification, not merely the existence of the band, which requires the explanation.

Phenomena such as Yamada found in nickel dimethylglyoxime will be named « cooperative effects » in this review, and we shall use this phrase to denote spectroscopic features peculiar to a system in its

aggregated state. The phrase is intended to cover particularly marked shifts or changes of intensity by transitions whose antecedents can be traced in the spectra of isolated molecules, or alternatively, the appearance of entirely new transitions for which no such parentage can be found. Intermolecular or interionic charge transfer transitions are frequently the source of the latter type of absorption band, but recent experiments on the ligand field transitions of antiferromagnetic crystals have shown that magnetic interactions can also lead to new absorption bands not found in magnetically dilute materials, or even in the concentrated crystals in their paramagnetic state. We shall dismiss as trivial in the present context those effects which merely result from gross changes of ligand field from one lattice to another. For example, the remarkable color difference between Cr_2O_3 (green) and ruby ($\text{Cr}^{3+}/\text{Al}_2\text{O}_3$ red) is largely attributable to the difference in lattice dimensions between the two materials, and hence to a change in Δ . On the other hand, absorption bands which have been traced to transitions among pairs of Cr^{3+} ions in ruby,⁵ certainly fall within the compass of this review. However, apart from examples like the last one, we shall concentrate on pure undiluted materials. Hence, spectral changes brought about by vibrational perturbations around point defects in otherwise perfect lattices will not concern us, though a great deal of useful information can be extracted from them.

The plan of the review is to consider cooperative perturbations first on ligand field, and then on charge transfer states. In both cases I will describe a number of selected examples in some detail, instead of attempting to make a few comments about each of the multitude of available examples. In adopting this approach I am aware of having left out a great deal of important and interesting material, but it is to be hoped that the examples chosen are at least illustrative of the range of phenomena covered by the title.

II. LIGAND FIELD SPECTRA

A. EXCHANGE INTERACTIONS IN MAGNETICALLY ORDERED CRYSTALS; TRANSITION METAL FLUORIDES

Perhaps the area of solid state ligand field spectroscopy which has seen the greatest activity in the last few years is that concerned with the fine structure observed in sharp line transitions of magnetically ordered materials.

Exchange interactions between pairs of magnetic ions doped into diamagnetic host lattices were first observed by Owen *et al.*⁶ using paramagnetic resonance. The system that they studied, IrCl_6^{2-} doped in alkali metal hexachlorostannate(IV) salts, does not permit very strong antiferromagnetic interactions since the distance between nearest neighbour iridium atoms is about 7 Å. By working with solids in which superexchange is much stronger, for example the complex perovskite $\text{A}^1\text{B}^1\text{F}_3$, it has recently become possible to observe optical effects associated with

the magnetic ordering. Nevertheless, the effects are small, and can only be seen by working at rather high resolution on sharp bands at low temperatures. One impetus to these studies has been the interest in laser activity in transition metal doped crystals, and the first clear observation of cooperative magnetic effects on ligand field excited states came from emission studies on ruby.⁵

The ${}^2\text{E} \rightarrow {}^4\text{A}_2$ emission of octahedrally coordinated Cr^{3+} is split into two components by the trigonal distortion of the sites in Al_2O_3 , and close examination showed that these were also accompanied by other weak lines. These so-called « sidebands » were extremely unusual in having intensities relative to the main bands which were roughly proportional to the Cr^{3+} ion concentration. Such bands must be attributed to new states originating in randomly distributed near neighbour pairs of Cr^{3+} . At very low Cr^{3+} concentrations (below 0.5 Atomic %) the intensity dependence was accurately linear, but became steeper at higher concentrations, possibly because the pairs were stealing excitation from single ion transitions. The extent to which the sideband emission of the pairs is separated from the single ion emission evidently depends on the size of the pairwise exchange interaction, and often has the order of magnitude 50 cm^{-1} . Corresponding effects in the absorption spectrum of highly doped ruby were also observed. Linz and Newnham⁷ found that the intensity of the band system near 3400 Å varied as $[\text{Cr}^{3+}]^2$ but the one near 4770 Å as $[\text{Cr}^{3+}]$. However, they did not attempt any quantitative explanation of their results. In fact the corundum structure allows the possibility of several types of near neighbour pairs, each of which might be expected to produce a slightly different sideband spectrum. Temperature and uniaxial stress dependence experiments have helped to sort out a lot of these lines, but we shall not go into details, referring the interested reader to accounts in various symposia on quantum electronics.⁸ McClure⁹ also examined the spectrum of pure Cr_2O_3 , finding evidence for exchange coupling from the temperature dependence of the ${}^4\text{A}_2 \rightarrow {}^2\text{E}$ fine structure, but he too did not analyse the data quantitatively.

Similar effects to those observed when pairs of magnetic ions are coupled in a diamagnetic host

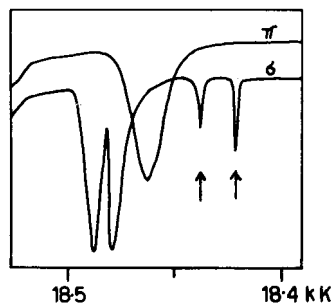


Figure 1. The spectrum¹¹ of crystalline MnF_2 under high resolution in the region of ${}^4\text{A}_g(\text{S}) \rightarrow {}^6\text{T}_g(\text{G})$. The pure magnetic-dipole transitions are indicated by arrows.

are of course to be expected in pure lattices of magnetic ions in the antiferromagnetic state, i.e. below the Neel temperature. A few years after the ruby sidebands had been detected, it was noticed¹⁰ that the spin-forbidden electric-dipole forbidden ${}^6A_{1g} \rightarrow {}^4T_{1g}$ absorption band in the 4°K spectrum of MnF_2 had a much greater intensity than would have been anticipated. The zero-phonon line, which would be only magnetic-dipole allowed, would be expected to be extremely weak, though of course accompanied by vibronic sidebands of the usual type. These, on the basis of experience with other systems will be about 300 cm^{-1} distant from the electronic origin, i.e. one quantum of an asymmetric stretch within the local MnF_6^{4-} octahedron. In fact, at 4°K the ${}^6A_{1g}({}^6S) \rightarrow {}^4T_{1g}({}^4G)$ transition of MnF_2 consists¹¹ of two sharp weak magnetic-dipole lines (Figure 1), identified as such by their polarisations, but the bulk of the intensity is in three broad electric-dipole lines about 50 cm^{-1} to higher energy. Apart from their small separation from the pure magnetic-dipole lines, the electric-dipole lines do not have the temperature dependence of intensity which would be associated with phonon-assisted transitions. They are therefore apparently electric-dipole allowed, and their intensity derives from magnetic coupling between the ions in the lattice. Pictorially one would say that while one ion makes the electronic transition a neighbouring ion undergoes a spin-flip which keeps the total spin-projection on a given axis constant. In the case of a pure antiferromagnetic lattice, ligand field excited states on individual ions are sufficiently weakly coupled to their neighbours to be considered to a good approximation as Frenkel excitons, and likewise the accompanying magnetic excitation in the electronic ground states of the neighbouring ions couple weakly with each other to produce spin-waves, called magnons. Just as in the Davydov theory¹² of weakly coupled electronically excited states, the number of magnons, and hence of magnon sidebands, is determined by the number of inequivalent ions in the unit-cell.

Another striking illustration of the effect of magnetic ordering on ligand field transitions comes from the work of McClure¹³ on Mn doped ZnS. Apart from the 4700 Å and 5080 Å lines, there is practically no resemblance between the spectra of 1% and 5% crystals, the absorption of the latter being entirely dominated by pairs. In fact, from the integrated band areas it was found that pairs of Mn^{2+} absorb at least fourteen times as intensely as single ions. The sharpness of the ${}^6A_{1g} \rightarrow {}^4E_g$, ${}^4A_{1g}({}^4G)$ bands in Mn^{2+} systems make them an attractive probe for examining magnetic interactions. At low concentration and low temperature, for example, McClure detected just two sharp lines near 4700 Å in (Zn, Mn)S and assigned them to the magnetic-dipole transitions ${}^6A_{1g} \rightarrow {}^4E_g$ (21270 cm^{-1}) and ${}^6A_{1g} \rightarrow {}^4A_{1g}$ (21555 cm^{-1}). As temperature and concentration are raised, however, no less than nine bands can be resolved in this spectral region. Only one definitely corresponds to a single ion transition; two of the concentration dependent lines only appear above 15°K, while the other six remained clearly visible down to

4°K. The intensities of the two temperature dependent lines follow a Boltzman law, indicating an exchange interaction between pairs of Mn^{2+} in their ground states equivalent to about 30 cm^{-1} .

A particularly useful way of detecting magnon sidebands, first described by Russell, McClure and Stout,¹⁴ is to study their Zeeman splitting. The pure magnetic-dipole transitions, localized on one cation sublattice, undergo Zeeman splitting

$$E = \pm \beta H(g, m_l - g_0 m_0) \quad (1)$$

where g and m are the g -factor and spin-projection quantum number of the ground and excited states, e.g. for $Mn^{2+} -5/2 \rightarrow -3/2$, $g = 2$ and $\Delta E = 4\beta H$. On the other hand in the sidebands a pair of ions change spin and there is no, or very small, Zeeman effect:

$$\Delta E = \pm \beta H(g, m_l - g_0 m_0) \pm \beta H(g_0 m_0' - g_0 m_0) \quad (2)$$

With all the g 's approximately equal to 2, $\Delta E \sim 0$. This expectation was verified for the sidebands of the MnF_2 ${}^6A_{1g} \rightarrow {}^4T_{1g}$ transition using pulsed field measurements up to 170 kG.

Detailed theory for the enhancement of electric-dipole intensity by exchange coupling has been given by Tanabe, Moriya and Sugano.¹⁵ The essential feature is that the system consisting of a pair of magnetic ions, together with the anion(s) separating them, $M-X-M$, should not have a centre of symmetry; it is then of no consequence whether single M lie at centres of inversion.

Although MnF_2 is the example which has been most closely studied to date, magnon sideband structure has also been observed in FeF_2 ,¹⁶ CoF_2 , NiF_2 ¹⁷ and several anhydrous transition metal carbonates.¹⁸ In very weakly antiferromagnetic materials of course, the exciton and magnon lines will be extremely close and difficult to resolve. Related work on cooperative magnetic effects on the spectra of pairs of Mn^{2+} and Ni^{2+} in $KZnF_3$ was reported in a series of elegant papers by Ferguson, Guggenheim and Tanabe.¹⁹⁻²² The intensities of the pair spectra were found to be an order of magnitude higher than those of isolated ions, so that even in crystals containing as little as 1 atomic % Mn, absorption by pairs dominated the spectrum. A qualitative example of this effect can be given: the bands at 4000 and 3300 Å in $KMnF_3$ are sixteen times as intense as the corresponding bands in the spectrum of $Mn(H_2O)_6^{2+}$, though the other bands (4300, 3600, 3000 Å) are only twice as intense.

As in the case of the ${}^6A_{1g} \rightarrow {}^4T_{1g}$ transition of MnF_2 , it was shown that the transitions ${}^6A_{1g} \rightarrow {}^4E_g({}^4G)$ in $KMnF_3$ were electric-dipole in character and had temperature independent oscillator strengths. The particularly sharp ${}^4A_{1g}({}^4G)$ component at 4000 Å under high resolution consisted of four bands, whose relative intensities were temperature dependent in the manner shown in Figure 2, taken from Ref. 21. A pairwise exchange Hamiltonian $J.S_a.S_b$ leads to the energy levels

$$(1/2)[S(S+1) - S_a(S_a+1) - S_b(S_b+1)] \quad (3)$$

so that the energy separations between the four components should be 2K, 5K, 9K, in terms of an apparent coupling constant. The actual separations were found to be 4.7, 6.5 and 10.7 cm^{-1} . All except the lowest energy line are hot bands, and disappear at 4°K.

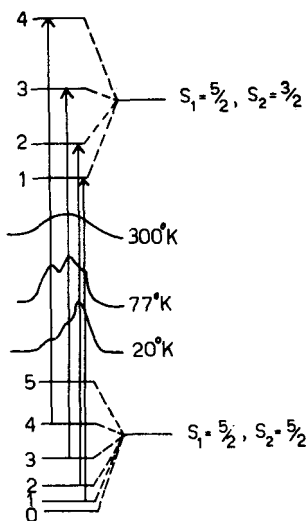


Figure 2. The energy levels of pairs of Mn^{2+} and the temperature dependence of ${}^6\text{A}_{1g} \rightarrow {}^4\text{A}_{1g}$ in moderately concentrated $\text{Mn}^{2+}/\text{KZnF}_3$.²¹

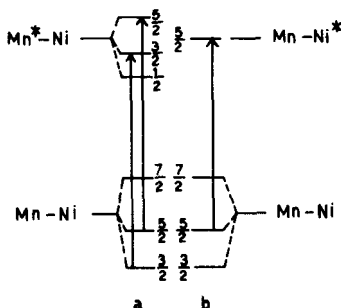


Figure 3. The energy levels of exchange-coupled $\text{Mn}^{2+}-\text{Ni}^{2+}$ pairs in KZnF_3 .²² (a) supposes that Mn^{2+} is excited, and (b) Ni^{2+} .

Crystals of KZnF_3 containing small amounts of both Mn^{2+} and Ni^{2+} (1-2 atomic %) show fine structure²² in the ligand field spectra of each ion resulting from Mn_2 and Ni_2 pairs but, even more interesting, a further structure due to NiMn pairs. The two possibilities, corresponding to electronic excitation of either metal ion, are shown in Figure 3. The ${}^3\text{A}_2 \rightarrow {}^1\text{E}$ band of Ni^{2+} is not split by interaction with neighbouring Mn^{2+} , but the two expected components of ${}^6\text{A}_{1g} \rightarrow {}^4\text{E}_g({}^4\text{G})$ in the Mn^{2+} spectrum were detected (25054 and 25029 cm^{-1}). The latter, which disappeared at low temperature, was assigned to the $5/2 \rightarrow 3/2$ transition, and a Boltzman analysis of its

temperature dependent intensity enabled the $5/2 \rightarrow 3/2$ splitting of the ground state to be determined. A value of $J = 18 \text{ cm}^{-1}$ for the exchange integral between Ni^{2+} and Mn^{2+} was thus obtained. It is particularly interesting to notice that in a series of mixed crystals $\text{KMn}_x\text{Ni}_{1-x}\text{F}_3$ the oscillator strength of the ${}^6\text{A}_{1g} \rightarrow {}^4\text{E}_g({}^4\text{G})\text{Mn}^{2+}$ transition is actually a linear function of x , interaction with the Ni^{2+} producing a very pronounced increase in intensity.

Although the ${}^3\text{A}_2 \rightarrow {}^1\text{E}$ Ni^{2+} transition cannot be split by interaction either with Mn^{2+} or other Ni^{2+} , because the excited state is non-degenerate, it should nevertheless be shifted. Adopting a molecular field model for the exchange interaction, that is, considering each ion as exposed to an effective magnetic field derived from contributions by all the other ions, one would predict that the ground state would be split by

$$g\beta H_{\text{eff}} = 3kT_N/(S+1) \quad (4)$$

at 0°K. The Neel temperature T_N of KNiF_3 is 275°K, and the ground state splitting therefore about 330 cm^{-1} . At low temperature the ${}^3\text{A}_2 \rightarrow {}^1\text{E}$ band should hence be shifted by this amount, but estimates²³ based on the data from KNiF_3 and $\text{K}(\text{Ni}, \text{Zn})\text{F}_3$ suggest that the shift is only about half as big. It may therefore be that a pairwise interaction model, such as we described above for $\text{K}(\text{Mn}, \text{Zn})\text{F}_3$, is a better starting point for a description of these systems.

B. ENVIRONMENTAL EFFECTS; MAGNUS GREEN SALT

The magnetic effects on ligand field spectra that we have just described are rather small, and one requires high resolution methods to observe them. Other effects of crystalline environment can sometimes have a much more noticeable influence on the appearance of ligand field transitions. The simplest kind of crystal field effect, merely a change of internuclear distance, as when an ion is substituted for one of larger or smaller ionic radius, is scarcely worth considering, but there are a number of examples of complex ions whose ligand field spectra are altered almost out of recognition by placing them in an environment where specific interactions with other neighbouring ions can take place. One of the best known of these is the PtCl_4^{2-} ion in the lattice of Magnus' Green Salt.

In aqueous solution and in solid K_2PtCl_4 , the PtCl_4^{2-} ion is red; the solution²⁴ and polarised crystal spectra,^{25,26} with the assignments that now seem to be universally agreed, are set out in Table I. Apart from a small, nearly uniform, red shift by all the bands going from solution into the solid state, the two spectra are very similar, even the relative intensities of the bands being broadly comparable. This is to be expected since K_2PtCl_4 has a simple tetragonal structure in which the anions are stacked on top of each other in eclipsed arrays. Thus the anion site symmetry in the lattice is to a good approximation the same (D_{4h}) as the point symmetry of a single anion, and because there is only one molecule per unit cell no Davydov splittings¹² should occur.

Table I. The spectrum of PtCl_4^{2-} in solution and in various crystalline environments,^{24-26,32} (Energies in kK, extinction coefficients in brackets)

		$3A_{2g}$	$3E_g$	$3B_{1g}$	$1A_{2g}$	$1E_g$	$1B_{1g}$
PtCl_4^{2-} (2M HCl solution)		17.7 (2.6)	21.0 (15)	—	25.5 (59)	30.2 (64)	(37.9)
K_2PtCl_6	xy	17.3 (5)	20.4 (17.5)	(23.8 (30)	26.0 (45)	28.5 (57)	(36.5)
	z	—	20.2 (20)	(23.8 (10)	—	29.3 (70)	—
$\text{Pt}(\text{C}_2\text{H}_5\text{NH}_2)_2\text{PtCl}_4$	xy	—	19.0 (45)	—	24.8 (135)	26.6 (140)	(33.5)
	z	—	18.8 (70)	—	—	27.2 (190)	—
$\text{Pt}(\text{CH}_3\text{NH}_2)_2\text{PtCl}_4$	xy	—	17.3 (35)	—	—	25.2 (190)	(30)
	z	—	17.3 (100)	(23) (120)	—	25.3 (340)	—
$\text{Pt}(\text{NH}_3)_2\text{PtCl}_4$	xy	—	16.5 (20)	—	—	24.9 (170)	(30)
	z	—	16.5 (150)	(23) (190)	—	24.9 (305)	—

On the other hand Magnus' Green Salt, $\text{Pt}(\text{NH}_3)_4\text{PtCl}_4$, as the name implies, is dark green, a very peculiar circumstance when it is recalled that $\text{Pt}(\text{NH}_3)_4^{2+}$, both in aqueous solution and in the form of solid salts like $\text{Pt}(\text{NH}_3)_4\text{Cl}_2$ is colourless; its lowest energy absorption band lies at 34.7 kK. Like K_2PtCl_6 , MGS has a crystal structure consisting of stacks of planar ions.²⁷ Anions and cations alternate, and the distance between adjacent platinum atoms is only 3.25 Å, compared with 4.10 Å in K_2PtCl_6 . The earliest polarised crystal spectrum of Magnus' Green Salt²⁸ gave an indication that the first absorption band (16.5 kK) was very largely polarised perpendicular to the planes of both anions and cations, i.e. parallel to the chains of metal atoms, although the absorption appeared to be so intense that little structure could be resolved beyond the absorption edge. Because nickel(II) dimethylglyoxime, with a rather similar crystal structure,²⁹ also had its lowest energy absorption band polarised perpendicular to the molecular plane³ (and hence parallel to the stack of metal atoms) it was assumed that this was somehow connected with a bonding interaction between the metal ions.

What might be called the «metal-metal bonding» approach to the spectrum of MGS was pursued a stage further by Miller.³⁰ By examining the colours and crystal structures of a variety of compounds with the general formula Pt_nPtX_4 , where A was an alkylamine and X either Cl^- or Br^- , he came to the conclusion that only those salts in which the anions and cations formed stacks with closely spaced metal atoms were green, all others being the expected pink. Miller³¹ also worked out a quantitative description of the bonding in such a chain of metal ions, taking into account the different energies of the basis orbitals on the platinum atoms of the anion and cation. The assumption was that the filled $5d_{z^2}$ orbitals of the square planar d^8 complexes overlapped to form a one-dimensional band which, if there were a large number of atoms N in the chain, would have eigenvalues

$$E_n = (\alpha_c + \alpha_a)/2 \pm (1/2)[(\alpha_c - \alpha_a)^2 \pm 16\beta^2 \cdot \cos^2(n\pi/(N+1))]^{1/2} \quad (5)$$

α_c and α_a are the orbital energies of cation and anion $5d_{z^2}$ and β is the resonance integral $\langle 5d_{z^2}(\text{A}) | \text{H} | 5d_{z^2}(\text{C}) \rangle$ between nearest neighbours. Formation of a band in this way would have two observable consequences on the electronic spectrum. First, ligand

field transitions within either PtA_4^{2+} or PtX_4^{2-} which involved d would be broadened and second, there might exist new excited states resulting from transitions between anion and cation states.

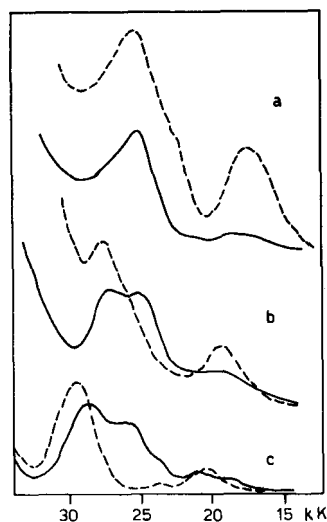


Figure 4. Polarised transmission spectra of Magnus' Green Salt analogues.³² (a) $\text{Pt}(\text{CH}_3\text{NH}_2)_2\text{PtCl}_4$; (b) $\text{Pt}(\text{C}_2\text{H}_5\text{NH}_2)_2\text{PtCl}_4$; (c) K_2PtCl_6 . Spectra indicated by dotted lines were measured with the electric vector perpendicular to the planes of the molecules and the full lines with this vector parallel.

Yamada²⁸ originally thought that the entire visible spectrum of MGS came from transitions of band-to-band type, but more recent measurements of the polarised crystal spectra of a series of Pt_nPtCl_4 compounds^{26,32} have shown that this is not the case. The three spectra illustrated in Figure 4 show very clearly that the three major absorption bands below 30 kK in the methylamine analogue of MGS (which has a similar structure and identical metal-metal spacing) are all related in parentage to bands in the spectrum of K_2PtCl_6 . The intermediate example, ethylamine MGS, has a metal-metal spacing rather bigger than MGS (3.40 Å), but much smaller than K_2PtCl_6 . We can therefore include both these compounds in Table I, and propose assignments analogous to those suggested for PtCl_4^{2-} in solution and in its potassium salt.

Our conclusion that the visible spectra of the PtA_4PtX_4 compounds arise from d-d transitions of the PtX_4^{2-} groups, perturbed by the neighbouring cations is further strengthened by comparing the diffuse reflectance spectra of a great many other compounds containing palladium as well as platinum.²⁶ For example, the reflectance spectra of $\text{PdA}_4\text{PdCl}_4$ and $\text{PtA}_4\text{PdCl}_4$ are very similar to that of K_2PdCl_4 , though shifted a little to lower frequencies. The red shift of the anion absorption, relative to the potassium salt, is more noticeable in PdA_4PtX_4 on the other hand, and most pronounced of all in PtA_4PtX_4 where, in addition, one finds a definite correlation with metal-metal distance.

According to the assignments in Table I the $\text{PtCl}_4^{2-} \ ^1\text{A}_{1g} \rightarrow \ ^1\text{A}_{1g}$ and $\ ^1\text{A}_{1g} \rightarrow \ ^1\text{B}_{1g}$ transitions are shifted about 5 kK to the red in MGS. Both transitions involve orbitals with a z-component (d_{xz}, d_{yz} in the former and d_{z^2} in the latter), which are susceptible to perturbation by cation d_{z^2} electrons. By contrast $\ ^1\text{A}_{1g} \rightarrow \ ^1\text{A}_{2g}$, which is polarised entirely within the anion plane, is scarcely affected by the change of cation. It therefore seems that there are no transitions left in the visible which could be assigned to transitions delocalized along the metal atom chains. In fact, the only remaining band in the entire spectrum of MGS which might have received such an assignment was one found²⁶ in the infrared at about 6 kK, and for which no analogy could be found in the spectrum of K_2PtCl_4 . Miller, who mentions it³¹ as being apparently rather intense in the diffuse reflectance spectrum, thought it was an intermolecular charge transfer transition, but diffuse reflectance spectra are notoriously deceptive in the way that they accentuate weak bands and a single crystal transmission spectrum²⁶ showed that the band had a molar extinction coefficient a good deal less than 20 L./mole cm. Another measurement³² reduced this figure still further, to an upper limit of 1.75 L./mole cm., and finally Kondo³³ demonstrated that it was actually an N-H overtone vibration of the cation. So in the end, the entire spectrum of MGS was assigned without the need to take into account any delocalization of electrons between the anions and cations, either in the ground or in any of the lower excited states. The ligand field spectrum of PtCl_4^{2-} is nevertheless highly perturbed in the MGS lattice, but to discover the reasons for that, we must consider the ultraviolet spectrum in more detail.

III. CHARGE TRANSFER SPECTRA

A. INTRAMOLECULAR TRANSITIONS

1. *Magnus' Green Salt.* In the previous section we described how the color changes in the series of Magnus' Green Salts, thought at first to arise from transitions to delocalized conduction bands in the column of metal atoms, can in fact be traced to variations in the ligand field spectrum of the PtX_4^{2-} ($\text{X} = \text{Cl}$ or Br), perturbed to differing degrees by the various $\text{Pt}(\text{amine})_2^{2+}$. The variations consist of (1) a shift of the main bands to lower energy and (2)

an overall intensification of the bands which, however, is particularly noticeable in those polarised in the z-direction. Since these ligand field bands gain their intensity by vibronic mixing with allowed transitions (almost certainly of the charge transfer type) the effects observed on going from K_2PtCl_4 to $\text{Pt}(\text{NH}_3)_2\text{PtCl}_4$ are expected to be traceable to changes in the intense bands in the ultraviolet.

The absorption in all the crystals above 30 kK is too intense for single crystal transmission spectra to be measured, even using the microscopic technique,²⁶ but diffuse reflectance spectra of powders diluted homogeneously in KCl or LiF yield useful qualitative information. Thus it was found²⁶ that the lowest intense absorption band of K_2PtCl_4 occurs at 42.5 kK, whilst PtCl_4^{2-} in aqueous solution has its first intense band at 46.4 kK ($\epsilon = 11800$).²⁴ These presumably represent the same transition. Alternative assignments of this transition have previously been given; either as a $3d \rightarrow 4p$ transition²⁴ localized on the platinum, or a ligand-to-metal charge transfer³⁴ $\pi(\text{Cl}) \rightarrow 3d_{xz-yz}$. The latter allows two possibilities, $\ ^1\text{A}_{2u}(\pi(b_{2u})) \rightarrow 3d_{xz-yz}$, z-polarised or $\ ^1\text{E}_u(\pi(e_u)) \rightarrow 3d_{xz-yz}$, xy-polarised). The charge transfer assignment now seems preferable, and from arguments about the ordering of the π -ligand levels, Gray and Ballhausen³⁴ preferred the $\ ^1\text{A}_{2u}$ assignment.

In contrast with the rather small difference between the spectra of PtCl_4^{2-} in solution and in K_2PtCl_4 , the diffuse reflectance spectra²⁶ show that the first intense band in Magnus' Green Salt already occurs at 34.5 kK. The cation $\text{Pt}(\text{NH}_3)_2^{2+}$ has no intense absorption in this region, since the first intense maximum in the solution spectrum of $\text{Pt}(\text{NH}_3)_4\text{Cl}_2$ is not found until 51.2 kK ($\epsilon = 8830$).³⁵ Hence it was suggested that the first intense band of PtCl_4^{2-} in the Green Salts had been shifted by the crystal field of the cations. The smaller size of the energy denominator in the vibronic mixing expression

$$\psi = \psi_0 - \frac{Q(\psi_0 | \psi \partial v / \partial Q)_0 | \psi_0}{E_0 - E_u} \cdot \psi_u$$

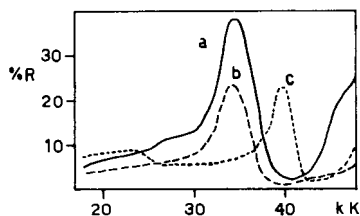
would then account for the increased intensity of the PtCl_4^{2-} ligand field bands in the Green Salts. Furthermore, if the lowest PtCl_4^{2-} charge transfer band were indeed $\ ^1\text{A}_{2u}$, the increased z-polarised intensity of the ligand field bands would also be accounted for. Of course, as we have just noticed, the energies of the first charge transfer bands of PtCl_4^{2-} and $\text{Pt}(\text{NH}_3)_2^{2+}$ are not very different in solution, so perhaps it might be equally plausible to say that it was the $\text{Pt}(\text{NH}_3)_2^{2+}$ band whose energy had been so decreased in the Green Salts, though in that case there is no obvious reason why the PtCl_4^{2-} ligand field bands should have been so intensified.

Experiments to determine the polarisations of the ultraviolet bands in the Green Salts were recently performed by Anex,³⁵ using the specular reflection method. One of his spectra is shown in Figure 5 and the numerical results for the three compounds studied in Table II. By the Kramers-Kronig transform method, Anex derived absorption constants

Table II. The ultraviolet specular reflection spectra of Magnus' Green Salt analogues.³⁵

	Energy (kK)	Derived extinction coefficient	Transition moment (Å)
Pt(NH ₃) ₂ PtCl ₄	34.5	58000	0.95
Pt(CH ₃ NH ₂) ₂ PtCl ₄	34.4	49000	0.82
Pt(C ₂ H ₅ NH ₂) ₂ PtCl ₄	39.9	70000	0.79

from his reflection data. We see that the first intense band is indeed z-polarised, and that its energy in the various compounds agrees very well with the diffuse reflectance peaks. No single crystal reflection spectra were reported for K₂PtCl₄, but the most plausible interpretation of the set of data available is that the band which shifts downwards along the series of Green Salts is the ¹A_{2g} charge transfer band of PtCl₄²⁻. Anex found some more supporting evidence for this assignment by calculating the intensification expected in the z-polarised ligand field bands, assuming that all the z-polarised intensity in the visible comes from vibronic mixing with the ultraviolet transitions. In that case, the z-polarised intensity of a given ligand field transition should be proportional to the oscillator strength of the charge transfer band and inversely proportional to the energy separation between the allowed and forbidden bands. To obtain a direct comparison between the extinction coefficients derived from the reflection spectra and the value quoted above for PtCl₄²⁻ in solution though, it should be noted that the latter refers to randomly oriented molecules. If the 46.6 kK band in solution is the ¹A_{1g}→¹A_{2g} transition, its extinction coefficient must be multiplied by 3 for comparison with Table II. Nevertheless, the Green Salt ultraviolet bands all have higher intensities than PtCl₄²⁻ in solution, though it is worth noting that the energies and transition dipole lengths are by no means linearly related: the dipole length of the MGS band is greater than that of methylamine MGS, though their energies are almost the same, while the energies in the methylamine and ethylamine compounds are very different though their dipole lengths are the same.

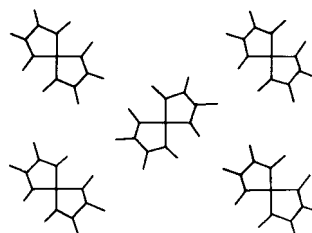
**Figure 5.** Polarised ultraviolet reflection spectra of Magnus' Green Salt analogues.³⁵ (a) Pt(NH₃)₂PtCl₄; (b) Pt(CH₃NH₂)₂PtCl₄; (c) Pt(C₂H₅NH₂)₂PtCl₄.

Using the observed position of the lowest energy visible band in the polarised transmission spectra, and its peak extinction coefficient in the z-polarisation

as a measure of intensity, Anex obtained good agreement for the ratio of ligand field band intensities between MGS and its ethylamine analogue (calculated 0.52, observed approximately 0.5). Thus there can be no doubt that the cooperative effect requiring explanation concerns the ultraviolet transitions, and that the spectral changes which produce the startling color change from pink to green in these materials are merely a consequence of the changes in the higher energy allowed bands.

The best way of describing the shifts in these ¹A_{2g} charge transfer bands would be by way of electrostatic interaction between transition dipoles on neighbouring molecules. Since these molecules are unlike (Pt(NH₃)₂²⁺ and PtCl₄²⁻) the Davydov interaction would be of the second-order type,¹² reliable estimates of which would require a summation over all the lower excited states of both molecules. Undoubtedly a major contribution from each molecule would come from 5d_{z²}→6p_z atomic transitions on the platinum atoms, but since these have never been conclusively identified in the molecular spectra, there is little more that can be said. The following example, on the other hand, is a good example of a first order Davydov effect in a stack of like atoms.

2. *Nickel(II) dimethylglyoximate* (NiDMG). The chain of events in the story of this material has a good deal in common with that of Magnus' Green Salt. NiDMG has an orthorhombic structure,²⁹ space group D_{2h}²⁶, with 4 molecules in the unit cell. The molecules, which have point symmetry D_{2h} (though this is not required by the space group) are all aligned with their planes exactly parallel to (001). They hence form sets of stacks, within which the nickel atoms of adjacent molecules approach to 3.245 Å. Since the methyl groups are the «thickest» parts of the molecules, alternate members of each stack are rotated by 90°, as shown in Figure 6. Platinum(II) dimethylglyoximate has the same structure,³⁶ and doubtless the palladium(II) compound too.

**Figure 6.** Schematic view of the crystal structure of nickel(II) dimethylglyoximate,²⁹ projected along the c-axis.

NiDMG forms dark red needle shaped crystals, but it seems that no comment had been made about the difference between the colors of the crystals and solutions of this substance until after the structure had been shown to be unusual. In their paper on the crystal structure Godycki and Rundle²⁹ remarked that the crystals were only slightly pleochroic, but

this must have been due to the thickness of the specimens they were examining, because shortly afterwards Yamada³ published a crystal spectrum showing that the lowest frequency absorption was much more intense when the incident electric vector was parallel to the needle axis than when it was perpendicular. Yamada contrasted NiDMG with copper(II) DMG, in which he found the first absorption band polarised substantially within the molecular plane, and concluded that the difference between the two substances resulted from their different crystal structures: in copper(II) DMG there are no columns of closely spaced metal atoms. Unfortunately, as Anex³⁷ has already pointed out, Yamada's spectrum is not capable of detailed interpretation because the maximum optical density that the records appears to depend more on the stray light level of his instrument than on the peak absorption of the crystal. Nevertheless, with the instrumentation available in 1953, these spectra represent a considerable achievement.

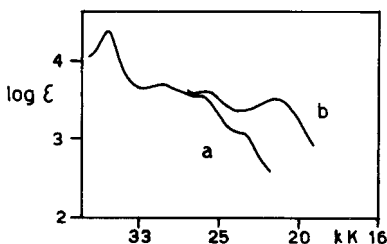


Figure 7. Absorption spectra of (a) a chloroform solution and (b) a colloidal suspension of nickel (II) dimethylglyoximates.³⁸

The first clear demonstration that the spectrum of NiDMG in the solid state was substantially different from that in solution came from Banks and Barnum³⁸ who, realizing that the optical density of the solid was so great that direct measurements of crystal transmission spectra would be hazardous, determined the spectra of samples in the form of colloidal suspensions. The suspensions were made by precipitating the complex aqueous solution at the correct pH in the presence of a protective colloid such as gelatin. One of these spectra, with the spectrum of a chloroform solution of NiDMG, is shown in Figure 7. We see that the band at 18.05 kK in the suspension, which is the one whose dichroism Yamada measured in the crystalline state, has no obvious analogue in the solution spectrum. For convenience, among the many possible names for this new absorption (color band, interaction band) we shall call it simply the green band. By the same method, Banks and Barnum also measured the spectra of several other nickel(II) α -dioxime complexes which have crystal structures closely related to NiDMG, and found a definite relationship between the frequency of the new low energy band which appeared in all the spectra and the Ni-Ni spacing in the crystal. However, they state that the absorption bands measured in such colloidal suspensions shift

with solvent and digestion time, so it is difficult to know how much weight to place on their observations. The same workers also attempted to measure some crystal transmission spectra, but apart from the expected shift in the absorption edge with changing polarisation, their spectra reveal no further information about the solid-state cooperative effect.

One kind of experiment which could be extremely significant was first performed by Banks and Barnum,³⁸ and later repeated by Basu, Cook, and Bedford.³⁹ This involved measuring the spectra of mixed solids containing nickel(II) and either palladium(II) or platinum(II) DMG in various proportions. Banks and Barnum prepared their mixtures as colloids by adding DMG solution to a mixed solution of the two cations, and comparing the transmission spectra with colloidal solutions containing pure NiDMG and Pd or PtDMG which had been prepared separately and then mixed. Basu *et al.*³⁹ measured transmission spectra of powders dispersed in NaCl discs. The two sets of data agree quite well as to the wavelengths of the bands in both homogeneously and heterogeneously mixed solids, thus demonstrating that both methods yield reliable information about the spectra of solids or, less plausibly, that they are both affected to the same degree by stray light. On the other hand, the two groups of authors differ widely in their interpretations of the data.

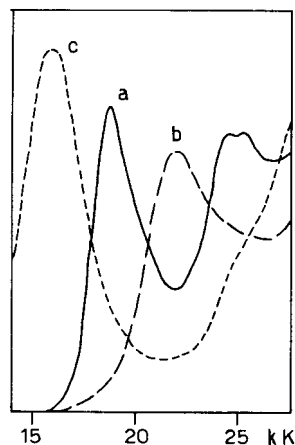
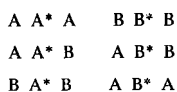


Figure 8. The spectra of (a) nickel (II); (b) palladium (II) and (c) platinum (II) dimethylglyoximates dispersed in KCl pellets.³⁹

Like NiDMG, PdDMG and PtDMG both have absorption bands at low energy in the solid state which cannot easily be identified with any bands in the solution spectra. The three spectra, taken from Basu *et al.*'s paper, are shown in Figure 8. Mechanical mixtures of solid PdDMG and PtDMG simply have absorption bands at the same positions as the pure materials but samples containing roughly equal amounts of the two salts homogeneously mixed by co-precipitation have a single rather broad peak about midway bet-

ween those of the pure substances. Banks and Bar-num took this as evidence that the excited state in the mixed crystals, and hence by implication also in the pure ones, was delocalized among a large number of molecules. Rundle⁴⁰ proposed in outline, and Miller³¹ later in detail, schemes by which Bloch energy bands extending along the chain of metal atoms could be constructed in principle in a number of different ways, using the filled $3d_{z^2}$ and empty $4p_z$ as basis functions, and which would have served to describe this type of excitation. However, Basu *et al.*³⁹ put forward quite a different explanation for the appearance of the mixed crystal absorption bands. From Figure 8 we see that the Pd and Pt compounds have the greatest separation between their peaks, and when a small fraction of PdDMG is doped into the Pt compound, or vice versa, the effect is to shift the Pt band to higher energy in the former case, and the Pd band to lower energy in the latter. Thus Basu *et al.*³⁹ tried out the hypothesis that when placed together in the crystal, any molecule *i* would shift the frequency of absorption of its two immediate neighbours from their solution values by an amount ν_i , irrespective of the identity of the neighbours. A binary mixed crystal would then have six absorption bands, corresponding to excitation of the two components, surrounded by the three possible combinations of neighbours:



If the components were randomly distributed along the stacks, the relative intensities of the bands can be worked out quite straightforwardly, and the shifts observed in all the binary combinations could be satisfactorily accounted for using three ν_i . Such an explanation, of course, does not require that the transition has any intermolecular character at all. We shall see below how this simple hypothesis can be incorporated into a general picture of exciton processes in this type of crystal.

Just as in the two previous investigations, Basu *et al.*³⁹ recorded polarised transmission spectra of single crystals of NiDMG, this time as a function of temperature, but the results were no more satisfactory than before. Once again the intensity of the first absorption band defeated the experimenters, who found very low dichroic ratios, maximum optical densities corresponding to a molar extinction coefficient of 300, and extremely broad absorption bands in contrast to the sharpness of the ones measured in the NaCl pellets. However, they misinterpreted the reason for the lack of structure in their crystal transmission spectra, compared with the NaCl pellet spectra, and actually placed greater weight on the former, remarking that the sharp peaks in the pellet spectra may result from scattering or reflection by the small dispersed particles. It was Anex⁴¹ who recently showed that this conclusion was the precise opposite of the truth by recording for the first time a well resolved polarised transmission spectrum of NiDMG. To obtain samples thin enough for absorption studies, Anex used a film sublimed on to

a quartz plate. Parts of the film consisted of oriented crystals, and allowed him to measure the spectrum shown in Figure 9. By this means he found that the molar extinction coefficient of the green band was in fact as high as 5000 and that it was entirely polarised along the *c*-axis. The excellent agreement between Anex's crystal spectrum and Basu *et al.*'s pellet spectra emerges clearly from Figures 8 and 9.

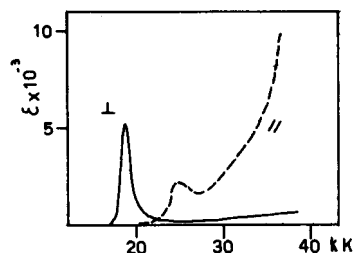


Figure 9. Polarised transmission spectrum of an oriented film of nickel(II) dimethylglyoximate.⁴¹

The need to resort to a crystalline sublimed film of NiDMG, and the poor resolution achieved by previous attempts to measure transmission spectra using thick crystals, is a good illustration of how difficult it can be to obtain reliable absorption spectra of highly absorbing solids. In such circumstances reflection spectroscopy comes into its own. Anex measured the polarised reflection spectrum of a thick NiDMG crystal, confirmed that the green band was entirely out-of-plane polarised and by carrying out a Kramers-Kronig transform derived an absorption spectrum whose peak positions and even bandwidths corresponded very closely to those of the sublimed film. Also, a point of some importance for the assignment of the green band, by comparison with the spectrum of NiDMG in CHCl_3 solution he was also able to show that the appearance of this band on crystallization was accompanied by a loss of intensity in the higher energy part of the spectrum.

Unlike NiDMG, nickel(II) ethylmethylglyoxime (NiEMG) can be crystallized in two modifications, orthorhombic, with a structure closely resembling NiDMG, and monoclinic,⁴² in which the molecules are not stacked plane-to-plane, and in which the closest Ni-Ni approach is 4.75 Å. Comparisons between the polarised transmission spectra of these materials are very revealing. In orthorhombic NiEMG, as in NiDMG, the only absorption below 38 kK polarised along the columns of metal atoms is the green band, but in the monoclinic modification there is no trace of this absorption. The crystal structure of monoclinic NiEMG is such that the polarised spectrum can be approximately resolved into components parallel and perpendicular to the molecular plane and the lowest energy absorption band with predominantly out-of-plane polarisation occurs at 22.8 kK. The next bands, which are polarised in the molecular plane, are at 26.2 and 30.9 kK, approximately corresponding to a pair of similarly polarised bands in orthorhombic NiEMG. Anex's proposal, reinforced by spectral data on several other related com-

pounds with different Ni-Ni separations, is that the 22.8 kK band, intensified and shifted to lower energy, is the origin of the green band. Since the polarised crystal spectrum of monoclinic NiDMG, when averaged over all directions in space, closely resembles the spectrum of a chloroform solution, the oriented gas model applies to the crystal and the 22.8 kK transition is to a locally excited state.

Possible intramolecular transitions which would be polarised perpendicular to the molecular plane are metal-to-ligand charge transfer or, much less plausibly, 3d to 4p localized on the metal. Ligand $\pi \rightarrow \pi^*$ transitions will be polarised in the plane of the molecule and in any case are confined to the region above 35 kK, if the spectrum of the free ligand is a reliable guide. There are no ligand-to-metal charge transfer states with the correct polarisation, bearing in mind that the metal acceptor orbital is $3d_{x^2-y^2}$; but the low energy absorption bands in diamagnetic iron(II) dimethylglyoximate and other α -diimines have long,⁴³ and for good reason, been attributed to metal-to-ligand charge transfer. A low-spin d^8 complex belonging to the point group D_{2h} has two such transitions which are electric-dipole allowed: from $3d_z \rightarrow \pi^* b_{1u}$ and $3d_{xy} \rightarrow \pi^* b_{2u}$. The latter would be forbidden in D_{4h} and may therefore be expected to have a rather low intensity. A purely atomic $3d \rightarrow 4p$ transition would be highly allowed, though at a very high energy: Anex suggests that a small amount of $3d \rightarrow 4p$ character, mixed into the $3d_z \rightarrow \pi^* b_{1u}$ charge transfer state by the crystal field in the orthorhombic compounds, is the mechanism for intensifying the z-polarised band found at 22.8 kK in the spectra of solutions and of the monoclinic crystal. The language of Davydov theory¹² is the most convenient for describing this mixing and also enables us to see an even more straightforward explanation for the behaviour of the green band.

Because alternate molecules within the stacks in the NiDMG crystal are rotated through 90° we can consider the «unit-cell» of each stack as consisting of two of these molecules. If we suppose that the electrostatic interaction between transition dipoles is much stronger within than between stacks, an out-of-plane polarised molecular transition, with a transition moment M , leads to two crystal excited states, split apart by the interaction of transition dipoles along the stacks. With a z-polarised molecular transition, the transition dipoles of the entire stack are parallel, so the Davydov interaction is at a maximum. Then one of the crystal excited states has a transition moment $2M$ and the other zero. As usual we need only consider dipole-dipole terms in calculating the energy separation between these two states, which is given by the sum of a series representing the separations of translationally inequivalent molecules within the stack:

$$4e^2(M)^2 \left\{ \frac{1}{R^3} + \frac{1}{(3R)^3} + \frac{1}{(5R)^3} + \dots \right\} \quad (5)$$

Here R is the metal-metal separation between neighbouring molecules. Obviously this sum is overwhelmingly dominated by the nearest neighbours, and it is also most important to observe that the sign of the total interaction is such that it is the intense Davydov

component which lies at lower energy. If the z-polarised molecular transition had a dipole length of 1 Å, not an unreasonable intensity for a charge transfer transition, the Davydov splitting would be about 14 kK! A band shift from the isolated molecule to the crystal of about 4 kK in the case of NiDMG thus appears quite reasonable, especially when it is borne in mind that second-order mixing with nickel atom $3d_z \rightarrow 4p_z$ transitions could also contribute. The proposed mechanism also explains the fact that the energy of the green band increases as the molecular spacing increases. Indeed, if the rather extensive data of Banks and Barnum is used to plot the band energy against $1/R^3$, a satisfactory correlation is obtained which extrapolates to about 24-25 kK when $R \rightarrow \infty$.

Thus it appears that the «abnormal» dichroism and low energy absorption in these materials is a result of electrostatic crystal field interaction between neighbouring intramolecular transition dipoles, and that no metal-metal bond, or band, formation need be invoked to rationalize these phenomena.

3. *Cyanopalladites and -platinites.* Another series of square planar d^8 ions in which the crystal dichroism has been said to be «abnormal» is the alkaline earth pallado- and platinocyanides. The crystal structures are not known in any detail; the only available X-ray data date from the '30's⁴⁴⁻⁴⁶ and the reliability factors are so large in a number of cases that it may be doubted whether the proposed structure has any significance at all. In all cases the cyanide group was assumed to scatter as a single atom and the water molecules which occur in all the structures were not conclusively located. Another complicating feature is that different members of the series contain different, and even perhaps variable, amounts of crystal water. Nevertheless, in spite of these problems there can be no doubt that in outline the lattices all contain stacks of square planar $M(CN)_4^{2-}$ ions with closely approaching metal ions, as in MGS and NiDMG. In some of the compounds the planes of the anions make a small angle to the direction of the stack.

The earliest polarised absorption spectra were measured by Yamada.⁴⁷ In the platinocyanides he found very marked dichroism, with much more intense absorption when the electric vector was polarised perpendicular to the planes of the complexes. As in the cases of MGS and NiDMG his apparatus was not sensitive enough to determine the shape and extinction coefficient of the band but it is certain that no intense transitions of the isolated ions are found at this energy. With the electric vector parallel to the complex planes a single sharp absorption can be seen in the 18-22 kK region, but in view of the extreme intensity of out-of-plane absorption in this region, and the fact that Yamada was using condensing optics (and hence convergent incident light), this apparently in-plane absorption may actually be part of the out-of-plane band. The same in-plane polarised bands were seen by Moncuit⁴⁸ using a similar kind of apparatus, but apparently with much lower intensity. If the band is genuine, its intensity must be borrowed vibronically from the out-of-plane band, as Moncuit suggests.

Cooperative Effects in Inorganic Spectra

91

Table III. The spectra of pallado- and platinumocyanide crystals.^{49,50}

Pd-Pd distance (Å)				Pt-Pt distance			
CaPd(CN) ₄ · 5H ₂ O	3.32	xy	31.7(1.1·10 ⁻³)	CaPt(CN) ₄ · 5H ₂ O	3.33	xy	23.0(2.5·10 ⁻³)
		z	29.0(v. large)			z	23.9(1.1)
SrPd(CN) ₄ · 5H ₂ O	3.63	xy	35.7(2.6·10 ⁻³)	SrPt(CN) ₄ · 5H ₂ O	—	xy	27.0(5.10 ⁻³)
		z	32.0(v. large)			z	28.3(0.76)
BaPd(CN) ₄ · 4H ₂ O	3.37	xy	30.3(0.6·10 ⁻³)	BaPt(CN) ₄ · 5H ₂ O	3.27	xy	—
		z	28.5(v. large)			z	22.7(1.0)

Although Yamada⁴⁷ could not follow the energy variation of the out-of-plane absorption he found that the weaker in-plane band shifted noticeably from one compound to another (Table III). Changing the alkaline earth cation most likely affects the Pt(CN)₄²⁻ spectrum through an alteration in the Pt—Pt distance; as the interplanar spacing becomes smaller the band moves to lower frequency. This is not just the effect of increasing the atomic number of the cation because neither the band frequency nor Pt—Pt distance vary monotonically with cation Z.

Moncuit⁴⁹ has also found a similar variation among the alkaline earth palladocyanides. These crystals are colourless since the intense out-of-plane absorption does not occur until approximately 32 kK. Data on the bands polarised in the complex planes are included in Table III for comparison with the platinumocyanides.

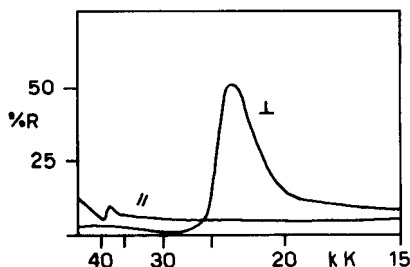


Figure 10. Polarised reflection spectrum of barium tetracyanoplatinite (II).⁵⁰

Because the out-of-plane absorption of all these crystals is so intense, reflection spectroscopy is again the most reliable method of obtaining absorption data. Moncuit and Poulet⁵⁰ have measured the polarised reflection spectra of all the alkaline earth platinumocyanides at room temperature and calculated oscillator strengths for the transitions from Drude's theory. A representative example of their spectra is shown in Figure 10. They find that in all the crystals there are two major bands. The lowest in energy is quite sharp, just as Yamada⁴⁷ and also Moncuit⁴⁹ found for the in-plane polarised component in transmission. It is overwhelmingly out-of-plane polarised and, according to the calculation, enormously intense ($f \sim 1.0$). The other band, near 38 kK, is predominantly in-plane polarised and considerably less intense. Poulet and Moncuit assign the lower band to $5d_{z^2} \rightarrow 6p_z(\text{Pt})$ and the higher to a charge transfer $5d_{z^2}(\text{Pt}) \rightarrow \pi^* e_u(\text{CN}^-)$. Certainly

there is no band in the solution spectrum of Pt(CN)₄²⁻ anywhere in the visible or near ultraviolet with anything like the intensity of the lowest energy band in the crystal, though Moncuit⁴⁹ has found a band of Pt(CN)₄²⁻ in aqueous solution at 46.3 kK with an oscillator strength of 0.3. Thus the experimental results for the platinumocyanides seem quite comparable to those we have described already for the MGS salts and NiDMG. The explanations commonly given for the « abnormal » absorption are also the same; both Yamada⁴⁷ and later Moncuit⁵⁰ advocate a $d_{z^2} \rightarrow p_z$ assignment for the intense low energy crystal band. It has not yet been made clear, however, why, apart from the formation of d_{z^2} or p_z bands along the stacks, this transition should be found at such a low energy in the crystal. Unfortunately there is no other evidence for the existence of such energy bands. In the opinion of the reviewer an explanation of the observed effects based on Davydov coupling of intramolecular transitions, either a first-order interaction of $d_{z^2} \rightarrow p_z$ or a first-order interaction of metal-to-ligand charge transfer transitions, together with a second-order interaction of these with $d_{z^2} \rightarrow p_{xz}$, would adequately explain these observations without any need to invoke electron exchange in the ground state.

4. *Oxalato-platinites.* Strong « abnormal » dichroism has been found in a number of oxalato-platinite salts, but the results may possibly be complicated by the existence of non-stoichiometric mixed valence materials. The PtOX₂²⁻ ion in solution is yellow, because of the tail of an intense absorption band which peaks at 35 kK. Most of the work on solid derivatives has been done by Krogmann. He has determined⁵¹ the structure of K₂PtOX₂ · 2H₂O, which is the same yellow colour as PtOX₂²⁻ in solution. Here the square planar anions are completely isolated from each other and no stacks of anions can be distinguished. On the other hand there exist partially oxidized materials like K_{1.6}PtOX₂ · 2H₂O, which apparently do have such stacks,⁵² with very close metal-metal spacing (2.81 Å). Mg_{0.82}PtOX₂ · 5.3H₂O is another example.⁵³ These compounds have a copper-lustre, so there is certainly some new absorption in the visible. It is also reported that the crystals are strongly dichroic, the colour being most intense when the electric vector is parallel to the needle axes, i.e. along the direction of the stacks. It would be plausible to dismiss this simply as mixed-valence absorption,⁵⁴ like that found in Pt(NH₃)₂Cl₂ · Pt(NH₃)₂Cl₄ for example,⁵⁵ if it were not for the fact that Krogmann has recently prepared⁵⁶ a stoichiometric single-valence material which has the same proper-

ties. He found that when calcium oxalato-platinite is crystallized above 50°C, red needle shaped crystals which analyse as $\text{CaPtOX}_2 \cdot 3.5\text{H}_2\text{O}$, result. Below 50°C, yellow crystals with the formula $\text{CaPtOX}_2 \cdot 8\text{H}_2\text{O}$ are formed. The structure of the red needles has been determined: stacks of PtOX_2^{2-} ions are aligned along the needle axis with a Pt—Pt spacing of 3.18 Å, and furthermore, the first absorption band is polarised along the needle axis. No detailed spectra of any of these crystals have been published yet, but it seems likely that they will provide us with yet another example of the phenomenon that we are now reviewing.

B. INTERMOLECULAR TRANSITIONS

1. *Hexahalides and Tetroxo-anions.* Apart from shifts, intensification or splitting of transitions which are predominantly intramolecular or intra-ionic in character, another important class of phenomena which could be called « cooperative effects » concerns the appearance of new transitions in the solid state spectrum which cannot be traced to parent transitions of the components. On an « independent systems » approach to the solid state, such as we applied to intramolecular transitions in Section III A, these must be described as intermolecular or interionic charge transfer states. By analogy with molecular crystals they could equally be called ionized exciton states,⁵⁷ though with the proviso that the electron and the hole are constrained each to a different set of sites occupied by one of the components. A particularly simple example, much studied by solid state physicists,⁵⁸ would be NaCl, excited states of which might be formed either from atomic $3p \rightarrow 4s$ excitations of the Cl^- or alternatively $3p(\text{Cl}^-) \rightarrow 4s(\text{Na}^+)$ charge transfer. Of course, ionized exciton states may be formed in which the electron and hole are widely separated in the crystal (Wannier⁵⁹ excitons) and in such cases one could consider the electron-hole interaction on a simple point-charge basis, deriving a set of « Rydberg » levels converging towards the bottom of the conduction band. Sequences of lines of this type are well known in many inorganic solids such as Cu_2O ,⁶⁰ GaSe etc., but they will not be described here. Rather, we will mention some less familiar examples in which the acceptor orbital is not atomic, as in NaCl, but the lowest empty MO of a metal complex. The internal transitions of the metal complex (usually ligand-to-metal charge transfer) are not as heavily mixed with each other by the crystal potential as the Cl^- transitions in NaCl, for instance. (As we remarked at the very beginning the absorption spectrum of solid KMnO_4 is not very different to that of the MnO_4^- ion in liquid solution in water or in solid solution in KClO_4). Thus the effects we wish to observe may be more clearly differentiated in this type of system.

A typical example of such an intermolecular charge transfer band occurs in Tl_2IrCl_6 , as Jørgensen⁶¹ first noticed. Alkali metal hexachloroiridates(IV) are dark red, but both the thallium and silver salts, first prepared by Delepine,⁶² are dark blue. In the powder

reflection spectra of these materials, in addition to absorption bands of the anions, there is a new band, very broad and intense, in the region 7500–5500 Å. A more detailed study,⁶³ diluting hexachloroiridate into hexachloroplatinate lattices, revealed that in alkali metal salts the intramolecular ligand-to-metal charge transfer bands of IrCl_6^{2-} shift to lower energy as the size of the cation decreases. On the other hand $\text{Tl}_2\text{Ir}_{0.05}\text{Pt}_{0.95}\text{Cl}_6$ had a completely different spectrum; the intramolecular charge transfer bands were almost entirely smeared out and a new band appeared at 6250 Å. A similar phenomenon occurred in the silver salt, and additional low energy bands could likewise be seen in the silver and thallium salts of hexachlorosmate(IV) and hexachlororhenate(IV). Thus, for example, ReCl_6^{2-} in solution and in its alkali metal salts is green, but Ag_2ReCl_6 is orange. Jørgensen's^{61,63} results on these solids are collected in Table IV, from which it can be seen that the new absorption band always occurs between 5 and 10 kK below the first intense intramolecular charge transfer band. That the latter is also broadened and shifted argues some degree of configuration interaction between the local and ionized exciton states. Another way of stating the same thing is that if the electron were to come from a purely atomic 4d or 6s orbital on Ag or Tl and were donated to a pure 4d or 5d orbital on the hexahalide, the energy of the intermolecular transition should be independent of the halogen. Preliminary indications are that this is not the case.

Table IV. Energies of interionic charge transfer transitions in hexahalide salts and the first halogen-to-metal charge transfer band.⁶³

	Ag_2MCl_6	Tl_2MCl_6	MCl_6^{2-}
M = Re(IV)	24.0	25.0	35.6
Os(IV)	17.0	18.0	27.0
Ir(IV)	15.0	16.0	20.5

Another class of electron-accepting molecules are the tetroxo-anions, and the salts of these with electron-donating cations similarly show intermolecular charge transfer bands. K_2CrO_4 is yellow, for example, but Ag_2CrO_4 and Tl_2CrO_4 are deep red in colour. Symons and Trevalion⁶⁴ reported the diffuse reflectance spectrum of AgMnO_4 , noting simply a red shift of the MnO_4^- bands, but it is clear from Jørgensen's⁶³ spectrum of a solid solution of AgMnO_4 in AgClO_4 that there is a new absorption band centred at 7000 Å, i.e. about 5000 cm^{-1} below the first band of MnO_4^- . In contrast to the IrCl_6^{2-} bands in Tl_2IrCl_6 , the MnO_4^- bands in $\text{Ag}(\text{Mn}, \text{Cl})\text{O}_4$ remain well defined.

2. *Hexacyanides.* A further example which has been studied in some detail by several physical methods,⁶⁵ $\text{Tl}_3\text{Fe}(\text{CN})_6$, is of particular interest in the present context as polarised single crystal spectra were measured. Compared with $\text{K}_3\text{Fe}(\text{CN})_6$ this substance has a new absorption band at 21.2 kK with

a molar extinction coefficient in the solid state of approximately 1000. The appearance of this band in a sample homogeneously diluted in $K_3Fe(CN)_6$ is shown in Figure 11. There is also an increase both in the intensity and the bandwidth of the lowest energy internal charge transfer band of $Fe(CN)_6^{3-}$, which lies at 24.0 kK in solution and 22.5 kK in the thallium(I) salt. In $K_3Fe(CN)_6$ its maximum extinction coefficient is around 600, but in $Tl_3Fe(CN)_6$ around 1300. The most interesting feature of the spectrum, however, is that the 21.2 kK band is polarised perpendicular to the c-axis of the crystal. The monoclinic unit cell of $K_3Fe(CN)_6$,⁶⁶ isomorphous with $Tl_3Fe(CN)_6$, contains two $Fe(CN)_6^{3-}$, both of which have two-fold axes parallel to the c-axis, and six potassium atoms, which fall into two sets. One set is surrounded by an irregular octahedron of nitrogen atoms, two at 2.87 Å, two at 3.02 Å and two at 3.14 Å, while the other has roughly a trigonal prismatic coordination, with two nitrogens at 2.57 Å and four at 2.77 Å. It is the latter set which, together with the iron atoms of the $Fe(CN)_6^{3-}$, define a plane perpendicular to the c-axis and hence from this set of more closely coordinated thallium atoms that the electron migrates to the $Fe(CN)_6^{3-}$ during the intermolecular charge transfer process. $Tl_3Fe(CN)_6$ was also shown⁶⁵ to behave as a semiconductor, and it would be extremely interesting to know whether the bulk charge migration shows the same anisotropy as the light absorption.

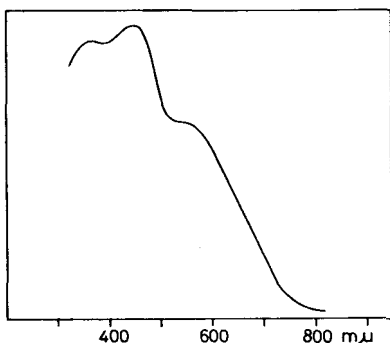


Figure 11. Diffuse reflectance spectrum of $K_3Fe(CN)_6$ doped with Tl^+ .

Following the work on the thallium salt, Braterman⁶⁷ investigated a much more extensive series of ferro-, ferri- and cobalticyanide salts of divalent transition metal cations. These materials are extremely insoluble and thus could not be grown into crystals large enough for direct spectroscopic study. However, by precipitating the compounds rapidly as very fine powders, it proved possible to make colloidal suspensions suitable for transmission spectroscopy, a technique employed by Robin⁶⁸ in earlier work on Prussian blue. In addition to ligand field transitions of the divalent ions, which confirmed that the ligand field strength of the nitrogen end of coordinated cyanide is close to water in the spec-

trochemical series, Braterman found a number of other bands at lower energies than the anion ligand field transitions. The latter he assigned to interionic charge transfer, from cation metal to anion metal in ferri- and cobalticyanides and in the opposite direction in the ferrocyanides. Where more than one interionic charge transfer band was seen, the separations between the transitions were ascribed to differences in the term structures of the donor or acceptor ions in the excited state. For example, cobalt(II) ferrocyanide has two iron-to-cobalt charge transfer bands, at 27 and 35 kK (Figure 12). In the excited state, the configuration of the iron atom is t_{2g}^5 , i.e. ${}^2T_{2g}$, but the electron may have been added to the initial $t_{2g}^5 e_g^2 ({}^4T_1)$ cobalt(II) in three different ways, i.e.

$$t_{2g}^5 ({}^1A_{1g})e_g^2 ({}^1A_{2g}){}^1A_{2g}$$

$$t_{2g}^5 ({}^2T_{2g})e_g^2 ({}^2E_g)T_{2g}$$

$$t_{2g}^5 ({}^2T_{2g})e_g^2 ({}^2E_g)T_{1g}$$

The relative energies of these three terms are, respectively, 0, Δ and $\Delta + 12B$ so the 27 kK band was assigned to $t_{2g}^5 ({}^2T_{2g})Fe^{III} \cdot t_{2g}^5 e_g^2 ({}^1A_{2g})Co^I$ and the 35 kK band to $t_{2g}^5 ({}^2T_{2g})Fe^{III} \cdot t_{2g}^5 e_g^2 ({}^2T_{2g})Co^I$ or, in shorter form, $t_{2g}(Fe) \rightarrow t_{2g}(Co)$ and $t_{2g}(Fe) \rightarrow e_g(Co)$. It is interesting that conforming to the local symmetry of the lattice, the lower energy $t_{2g} \rightarrow t_{2g}$ transition is a good deal more intense than $t_{2g} \rightarrow e_g$.

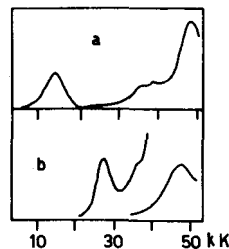


Figure 12. Spectra of colloidal suspensions of (a) ferric ferrocyanide (Prussian blue); (b) cobalt(II) ferrocyanide.⁶⁷

Of course, the transition metal ferrocyanide which has interionic charge transfer bands at the lowest energy of all is the ferric salt, otherwise known as Prussian blue. Robin⁶⁸ assigned the spectrum of this material by assuming that charge transfer occurred from low spin iron(II) to high spin iron(III), forming excited states $t_{2g}^5 ({}^2T_{2g})Fe^{III} \cdot t_{2g}^5 e_g^2 ({}^5T_{2g})Fe^{II}$ and $t_{2g}^5 ({}^2T_{2g})Fe^{III} \cdot t_{2g}^5 e_g^2 ({}^3E_g)Fe^{II}$. As in the cobalt(II) ferrocyanide just discussed, the $t_{2g} \rightarrow t_{2g}$ band, which appears as low as 14.2 kK in Prussian blue, is considerably more intense than $t_{2g} \rightarrow e_g$, seen at 25 kK (Figure 12(a)).

3. *Mixed valence salts.* Mixed valence compounds, that is, compounds containing the same element in two differing valency states in the same lattice, are a source of some of the most spectacular cooperative electronic effects to be found in inorganic solids. Some of these have been the subject of recent reviews,^{54,69} so we shall not go into very much detail

here. It is worth remarking, however, that after surveying the very extensive experimental information available about this type of material, Robin and the present author⁵⁴ concluded that three classes of electronic behaviour could be distinguished among them.

If the ligand fields about the two metal ion sites are extremely dissimilar (for example, one four and one eight coordinate, as in GaCl_2)⁷⁰ any interionic charge transfer states must occur at very high energies and no cooperative electronic effects are likely to be found. This uninteresting type of material was called class I. At the opposite extreme, if all cations occupy sites of identical symmetry and field strength (*i.e.* bond length), there will be a genuinely non-integral number of electrons associated with each. Thus if interaction between the cations is sufficiently strong to permit a description of the bonding in terms of Bloch bands, such bands will be only partially occupied and hence the material will behave as a metal. An example of this situation (called class III) is the series of tungsten bronzes, Na_xWO_3 .⁷¹ The optical properties of class III mixed valence solids are entirely « cooperative » in character, in the sense that no trace of single ion excitations is to be found, band-to-band transitions alone being responsible for the light absorption. The study of these materials then lies properly in the realm of solid state physics. Of much greater interest in the context of the present review are those substances which come between the two extremes of class I and III behaviour. If the ligand fields around the two cation sites are similar, but still distinguishable (class II) the valences will be quite firmly trapped in the ground state, and even perhaps in some of the excited states, so that single ion excitations may be observed. Other excited states, however, will be of interionic charge transfer type, like those described in the previous section.

Many examples of class II mixed valence behaviour are cited in the review articles referred to, but very few have been investigated closely enough to delineate with any precision the factors which determine the energy, intensity and shape of the resulting interionic charge transfer bands. By reference to one example which has been studied in the author's laboratory, however, some general features can be pointed out.

The salt caesium hexachloroantimonate(III, V), Cs_2SbCl_6 , first investigated by Wells⁷² in 1901, has a crystal structure⁷³ which approximates to the cubic antiferroite type, containing discrete SbCl_6 octahedra. In striking contrast to CsSbCl_6 and Cs_3SbCl_6 , which are both colourless, Cs_2SbCl_6 is deep blue. The crystal structure of the related deep red-brown compound $(\text{NH}_4)_2\text{SbBr}_6$, recently determined by Lawton and Jacobson,⁷⁴ reveals a superlattice ordering of SbBr_6^- and SbBr_6^{3-} octahedra, distinguishable by their different antimony-chlorine bond lengths. In the far infrared and laser-excited Raman spectra⁷⁵ of the mixed valence salts, the vibrational frequencies of the component ions are only shifted by one or two wavenumbers from their values in the corresponding single valency salts. Furthermore, the ul-

traviolet spectra, measured by diffuse reflectance,⁷⁶ contain bands which are easily identified as single ion excitations of the components. For example, to the characteristically sharp $5s^2(^1S_0) \rightarrow 5s5p(^3P_1)$ transitions found in $\text{Co}(\text{NH}_3)_6\text{SbCl}_6$ and Cs_3SbCl_6 at 29.0 and 28.0 kK corresponds a band at 29.3 kK in Cs_2SbCl_6 , and to the chlorine-to-antimony charge transfer band at 34.0 kK in CsSbCl_6 a band at 36.0 kK in the same compound. The weight of evidence therefore points to a very small interaction between Sb^{III} and Sb^{V} in the ground state.

If we call the two types of antimony site in the lattice A and B, the interionic charge transfer transition which is responsible for the new absorption band appearing in the visible may be written to a good approximation as $\text{Sb}_A^{\text{III}}(5s^2)\text{Sb}_B^{\text{V}}(5s^0) \rightarrow \text{Sb}_A^{\text{IV}}(5s^1)\text{Sb}_B^{\text{IV}}(5s^1)$. The fact that the mixed valence absorption band does not shift very much (about 1 kK) in the series of isomorphous salts $\text{Cs}_2\text{Sb}_x\text{Sb}_{1-x}\text{Cl}_6$ when x changes from about 0.1 to 1.0⁷⁷ signifies that only pairwise interaction between Sb^{III} and Sb^{V} need be considered. Then we are considering an excitation from an orbital $(\sqrt{1-\alpha^2} \cdot \Phi_A + \alpha \Phi_B)$ to $(\beta \Phi_A - \sqrt{1-\beta^2} \cdot \Phi_B)$. If Φ_A and Φ_B were pure 5s orbitals the energy of the mixed valence transition would be independent of whether the antimony was surrounded by an octahedron of chloride or bromide ions. In fact this is not the case; the lowest energy band in Cs_2SbCl_6 is at 17 kK while in $(\text{NH}_4)_2\text{SbBr}_6$ it is at 9 kK.⁷⁸ Further, there is a single report⁷⁹ of the preparation of K_2SbF_6 which indicates that it is colourless, *i.e.* no absorption bands lower than about 25 kK. Clearly, in each compound, the 5s shell in both the three and five valent constituent ions has some covalent interaction with the halide ligands which alters its electron affinity (in SbX_6^-) or ionization potential (in SbX_6^{3-}). Independent evidence for such covalency comes from the red shift of $ns^2 \rightarrow nsnp$ transitions with increasing halogen atomic number. Little information is available about this trend in Sb(III) halide complexes, but $^1P_1(6s6p)$ in Bi(III) decreases from 114.6 kK in the gaseous ion to 45.0, 38.5 and 29.8 in the hexacoordinated chloride, bromide and iodide, respectively.⁸⁰ At present there is little that one can say quantitatively about the absolute energies of the mixed valence absorption bands,

except that in the expression $I(A) - E(B) - \int \frac{1}{r} \Phi_A^2 d\tau_1 \Phi_B^2 d\tau_2$, where $I(A)$ is the ionization energy at site A and $E(B)$ the electron affinity at site B, the third term, representing coulomb interaction between the electron and hole after charge transfer, is probably small since the electron is being transferred over a distance of about 7 Å. The coulomb term could be estimated roughly from the known lattice dimensions, but to estimate $I(5s)$ in SbX_6^{3-} and $E(5s)$ in SbX_6^- molecular orbital calculations would be needed.

A good deal of useful information can be derived, on the other hand, by examining the intensities of mixed valence absorption bands. Again considering the simple pairwise interaction between a predominantly 5s orbital on SbX_6^{3-} and a similar orbital on SbX_6^- , it is clear that in expanding the transition

moment integral⁵⁴

$$\mu = \int [(1-\alpha^2)^n \Phi_a + \alpha \Phi_b] r [\beta \Phi_a - (1-\beta^2)^n \Phi_b] d\tau \quad (6)$$

only one-centre terms need be taken into account, because overlap between the charge densities Φ_a^2 and Φ_b^2 is presumed negligible. Then, neglecting α^2 and β^2 as small quantities

$$\mu \sim 1/2(\alpha + \beta)R \quad (7)$$

where R is the distance between the two antimony atoms. Quantitative information about the intensity of the visible absorption bands in antimony(III, V) hexachloride salts has recently become available from a study of the single crystal transmission spectra of Sb(III, V) doped hexachlorostannate(IV) salts.⁷⁷ The colourless salts Cs_2SnCl_6 and $(\text{NH}_4)_2\text{SnCl}_6$ cannot be used conveniently as host lattices because they crystallize in the form of octahedra, but $(\text{CH}_3\text{NH}_3)_2\text{SnCl}_6$, whose structure was determined many years ago by Wyckoff,⁸¹ crystallizes as thin hexagonal plates very suitable for transmission spectroscopy. By measuring the spectra of a number of crystals of this compound, doped with varying amounts of antimony, it was found first, that the intensity of the visible absorption band was indeed proportional to the square of the antimony concentration, as required by the assignment to an interionic charge transfer state and second, that the extinction coefficient of the band was quite low. Very few absolute intensity measurements have been reported for mixed valence absorption bands, but a widespread impression has existed that the presence of ions of the same element in two valency states is accompanied by intense colours. In one of the few reports of this phenomenon, Robin⁸⁸ found that the extinction coefficient per mole of Prussian blue was 8500. In this compound the iron atoms are 5.1 Å apart, and are bridged by the cyanide groups, but when no bridging groups exist between the two ions involved in the electron transfer, extinction coefficients can be much lower. For example, in the salts $\text{Co}(\text{NH}_3)_6(\text{Cu}^{\text{I}}\text{Cl}_4)_x(\text{Cu}^{\text{II}}\text{Cl}_5)_{1-x}$ it is lower than that of the first hexamminecobalt(III) ligand field band.⁸²

In a crystal with the formula $(\text{CH}_3\text{NH}_3)_2\text{Sb}_{0.1}\text{Sn}_{0.9}\text{Cl}_6$, the linear absorption constant at the maximum of the

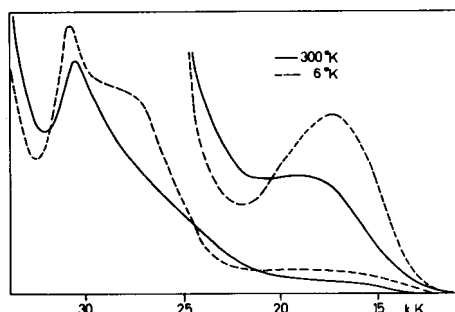


Figure 13. Transmission spectra of a crystal of $(\text{CH}_3\text{NH}_3)_2(\text{Sn,Sb})\text{Cl}_6$ at room temperature and at 6°K.⁷⁷

18 kK band (Figure 13) was 100 cm^{-1} at room temperature, equivalent to a molar extinction coefficient per pair of antimony atoms of 300 l/mole/cm . Combining this with the halfwidth (3 kK at room temperature) and assuming that the band is approximately gaussian, we find that μ is about 0.12 \AA . Since R is in the region of 7 \AA , the average of α and β in equation 7 is less than 0.02, so the extent of delocalization is extremely small.

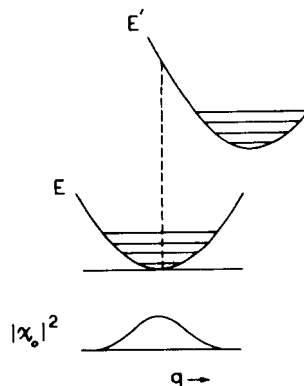


Figure 14. Potential energy surfaces for the ground and excited states of a transition accompanied by a large change in dimension.

Figure 13 shows that as the temperature is lowered, the mixed valence absorption band becomes narrower but that, even at the lowest temperatures, no vibronic structure is resolved. This fact suggests that in the excited state following a Franck-Condon transition, the chromophore is very strongly displaced from its equilibrium configuration, and hence that many excited state vibrational quanta have been excited. A comparable situation, which has received a great deal of experimental and theoretical attention during the last ten years, is found in the spectra of F-centres in alkali halide crystals,⁸³ where the optical electron has been assumed to couple with the entire spectrum of lattice phonons. By examining the variation of the optical band-width with temperature, it has proved possible to estimate the characteristic vibrational frequency active in broadening the optical absorption line.⁸⁴ The alkali halide situation is complicated by the fact that both local modes around the defect, and lattice modes delocalized across the entire crystal, may contribute to the line broadening. In the present example, however, it is clear from the similarity between the far infrared and Raman spectra of the hexahalo-antimonate ions in solution and in the solid state that in the latter the local modes, involving antimony-halogen bond stretching, remain well defined.

The analysis is very much simplified by assuming that the ground and excited state vibrational frequencies are equal. The shape function of the band is given by a sum over all the vibrational levels of both ground and excited state weighted, for temperatures

above absolute zero, by a Boltzmann factor relating to the population of the ground state levels:⁸⁵

$$G(v) = \sum_{\nu} P(\nu) |\langle \chi' | \chi \rangle|^2 \cdot \delta \{ \nu - (E'_{\nu} - E_{\nu}) / h \} \quad (8)$$

In this equation ν , ν' , E_{ν} and E'_{ν} are vibrational quantum numbers and energies of the ground and excited states and $P(\nu)$ is the ground state Boltzmann factor $e^{-\nu\beta} / (1 - e^{-\beta})$, where $\beta = \hbar\omega / kT$. The χ 's are the vibrational wave functions, assumed harmonic, and hence the associated energies are

$$E_{\nu} = E_0(g) + \hbar\omega(\nu + 1/2) \quad \text{and} \quad E'_{\nu} = E_0(u) + \hbar\omega(\nu' + 1/2) \quad (9)$$

The situation is shown schematically in Figure 14. Evaluation of the sum in equation 8 leads to the following expression relating the halfwidth of the band, H , to the temperature:

$$H^2 = 8(\ln 2) \hbar^2 \omega^2 S \cdot \coth(\hbar\omega / 2kT) \quad (10)$$

ω is the effective vibrational frequency and S , the so-called « Huang-Rhys factor », is the ratio between the vibrational energy excited in the upper electronic state after the transition to the energy of a single vibrational quantum, *i.e.* $(\frac{1}{2}\omega^2\Delta q^2) / (\hbar\omega)$. Equation 10 can be tested by plotting $\coth^{-1}(H/H_0)^2$, where H_0 is the halfwidth of the band at absolute zero (in practice at 4°K), against $1/T$. In the case of the hexachloroantimonate(III, V) crystal spectra, such a plot yields a straight line with a slope corresponding to $\omega = 210 \text{ cm}^{-1}$, and the level of agreement between the data and equation 10 may be judged from Figure 15. Clearly, 210 cm^{-1} is an average over the frequencies of all the vibrational modes of SbCl_6^- and SbCl_5^{2-} in their ground states, and over all the modes of SbCl_6^{2-} , which we presume to have been

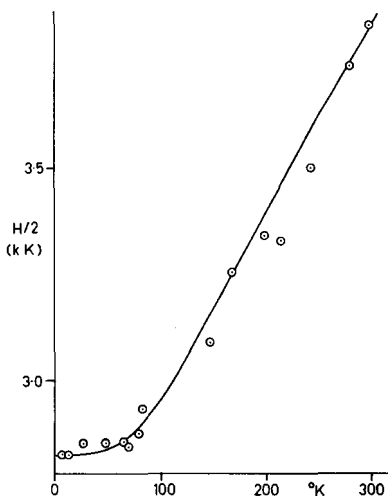


Figure 15. The relation between halfwidth and temperature of the mixed valence transition (17 kK) illustrated in Figure 13. The line is drawn according to equation (10), with $\omega = 210 \text{ cm}^{-1}$.

formed in the excited state. The ground state frequencies of the tri- and pentavalent ions are, of course, known, though we do not know what weight to attribute to each when forming an average. Nevertheless, it is certainly significant that if we take an average over the frequencies in Table V, weighting them only with respect to degeneracy, the resulting « average vibrational frequencies » (163 cm^{-1} for SbCl_6^{3-} and 249 cm^{-1}) fall equally on both sides of the observed figure of 210 cm^{-1} . It therefore seems certain that it is the change in dimension of the two ions after an electron has been transferred between them that provides the major source of broadening of the mixed valence absorption band.

Table V. Vibrational frequencies of hexachloroantimonates (cm^{-1}).²⁵

	$a_{ig}(\text{R})$	$e_g(\text{R})$	$t_{u}(\text{IR})$	$t_{u}(\text{IR})$	$t_{g}(\text{R})$
SbCl_6^{3-}	267	214	178	(130?)	(111)
SbCl_6^-	329	280	348	182	170

More detailed comparative studies of line broadening in other mixed valence materials will help to pin down with even greater precision the geometries and charge distributions in these unusual excited states.

IV. CONCLUSIONS

In this brief review we have made no attempt at a comprehensive survey of all work which has been done on cooperative phenomena in inorganic spectra. Rather, by selecting a number of particularly interesting and, we hope, representative examples from both ligand field and charge transfer spectra our aim has been to illustrate the extraordinary range and variety of such phenomena available for study. Low temperature and high resolution spectroscopic techniques have obviously been essential to the work on the magnetic fine structure of ligand field bands, just as techniques for measuring polarised transmission and reflection spectra of microscopic crystals have been to the work on charge transfer spectra. But it is not only through new methods that advances have come. Recognition of theoretical analogies, for example between the exciton approach to excited states of molecular crystals and the coupling of intramolecular charge transfer states in inorganic solids, have also been important. Thus it is to be hoped that, by drawing together some of these disparate topics, we have demonstrated that the electronic spectra of metal complexes in the solid state offer a great deal more information than merely the symmetry of a ligand field, or the configuration of a partly filled d-shell.

Acknowledgment. It is a pleasure to acknowledge the hospitality of the Cyanamid European Research Institute, Geneva, and particularly that of Dr. C. K. Jørgensen during the Summer of 1968, when most of this review was written.

Cooperative Effects in Inorganic Spectra

97

V. REFERENCES

- (1) C. K. Jørgensen, Absorption Spectra, and Chemical Bonding in Complexes, Pergamon Press, Oxford, 1962.
- (2) G. Kortüm and H. Schöttler, *Z. Electrochem.* 57, 353 (1953).
- (3) S. Yamada and R. Tsuchida, *J. Am. Chem. Soc.* 75, 6351 (1953).
- (4) J. Ferguson, *J. Chem. Phys.* 34, 611 (1961).
- (5) A. L. Schawlow, D. L. Wood, and A. M. Clogston, *Phys. Rev. Letters* 3, 271 (1959).
- (6) J. H. E. Griffiths, J. Owen, J. G. Park, and M. F. Partridge, *Phys. Rev.* 108, 1345 (1957).
- (7) A. Linz and R. E. Newnham, *Phys. Rev.* 123, 500 (1961).
- (8) Quantum Electronics (ed. C. H. Townes) Columbia 1960; see also Proceedings of conferences on the same subject ed. by J. R. Singer, 1961; P. Grivet and N. Bloembergen, *Dunod*, 1964; P. L. Kelley, B. Lax, and P. E. Tannenwald, McGraw Hill, 1966.
- (9) D. S. McClure, *J. Chem. Phys.* 38, 2289 (1963).
- (10) J. W. Stout, *J. Chem. Phys.* 31, 709 (1959).
- (11) R. L. Greene, D. D. Sell, W. M. Yen, A. L. Schawlow, and R. M. White, *Phys. Rev. Letters* 15, 656 (1965).
- (12) D. P. Craig and P. C. Hobbins, *J. Chem. Soc.* 539 (1955); D. P. Craig, *ibid.*, 2302 (1955).
- (13) D. S. McClure, *J. Chem. Phys.* 39, 2850 (1963).
- (14) P. G. Russel, D. S. McClure, and J. W. Stout, *Phys. Rev. Letters* 16, 176 (1966).
- (15) J. Tanabe, J. Moriya, and S. Sugano, *Phys. Rev. Letters* 15, 1023 (1965).
- (16) J. W. Halley and I. Silvera, *Phys. Rev. Letters* 15, 654 (1965).
- (17) M. Balkumski, P. Moch, and R. G. Shulman, *J. Chem. Phys.* 40, 1897 (1964).
- (18) D. S. McClure, in «Spectra of Ions in Crystals», ed. H. M. Crosswhite and H. Moos, New York, Interscience, 1966.
- (19) J. Ferguson, H. J. Guggenheim, and Y. Tanabe, *Phys. Rev. Letters* 14, 537 (1965).
- (20) J. Ferguson, H. J. Guggenheim, and Y. Tanabe, *J. Appl. Phys.* 36, 1045 (1965).
- (21) J. Ferguson, H. J. Guggenheim, and Y. Tanabe, *J. Phys. Soc. Japan* 21, 692 (1966).
- (22) J. Ferguson, H. J. Guggenheim, and Y. Tanabe, *J. Chem. Phys.* 45, 1134 (1966).
- (23) J. Ferguson and H. J. Guggenheim, *J. Chem. Phys.* 44, 1095 (1966).
- (24) J. Chatt, G. A. Gamlen, and L. E. Orgel, *J. Chem. Soc.* 486 (1958).
- (25) D. S. Martin and C. A. Lenhardt, *Inorg. Chem.* 3, 1368 (1964).
- (26) P. Day, A. F. Orchard, A. J. Thomson, and R. J. P. Williams, *J. Chem. Phys.* 42, 1973 (1965).
- (27) M. Atoji, J. W. Richardson, and R. E. Rundle, *J. Am. Chem. Soc.* 79, 3017 (1957).
- (28) S. Yamada, *J. Am. Chem. Soc.* 73, 1579 (1951).
- (29) L. E. Godyekt and R. E. Rundle, *Acta Cryst.* 6, 487 (1953).
- (30) J. R. Miller, *J. Chem. Soc.* 4452 (1961).
- (31) J. R. Miller, *J. Chem. Soc.* 713 (1965).
- (32) P. Day, A. F. Orchard, A. J. Thomson, and R. J. P. Williams, *J. Chem. Phys.* 43, 3763 (1965).
- (33) Y. Kondo and C. K. Jørgensen, Proc. 11th Int. Conf. on Coord. Chem., Kyoto, Japan, 1967.
- (34) H. B. Gray and C. J. Ballhausen, *J. Am. Chem. Soc.* 85, 260 (1963).
- (35) B. G. Anex, M. E. Ross, and M. W. Hedgecock, *J. Chem. Phys.* 46, 1090 (1967).
- (36) E. Frasson, C. Panattoni, and R. Zannetti, *Acta Cryst.* 12, 1027 (1959).
- (37) B. G. Anex, *Mol. Cryst.* 1, 1 (1966).
- (38) C. V. Banks and D. W. Barnum, *J. Am. Chem. Soc.* 80, 4767 (1958).
- (39) G. Basu, G. M. Cook, and R. L. Belford, *Inorg. Chem.* 3, 1361 (1964).
- (40) R. E. Rundle, *J. Phys. Chem.* 61, 45 (1957).
- (41) B. G. Anex and F. K. Krist, *J. Am. Chem. Soc.* 89, 6114 (1967).
- (42) E. Frasson and C. Panattoni, *Acta Cryst.* 13, 893 (1960).
- (43) R. J. P. Williams, *J. Chem. Soc.* 137 (1955).
- (44) R. M. Bozorth and L. Pauling, *Phys. Rev.* 39, 538 (1932).
- (45) H. Brasseur, *Z. Krist.* 88, 210, 221 (1934).
- (46) H. Brasseur, *Bull. Soc. Roy. Sci. Liège*, 4, 24 (1935).
- (47) S. Yamada, *Bull. Chem. Soc. Japan* 24, 125 (1951).
- (48) C. Moncuit, *J. Phys. Rad.* 25, 833 (1964).
- (49) A. Macadre and C. Moncint, *Compt. rend.* 261, 2339 (1965).
- (50) C. Moncuit and H. Poulet, *J. Phys. Rad.* 23, 353 (1962).
- (51) R. Mattes and K. Krogmann, *Z. anorg. Chem.* 332, 247 (1964).
- (52) K. Krogmann, *Ber.* 99, 3402 (1966).
- (53) K. Krogmann, *Z. anorg. Chem.* 383, 97 (1968).
- (54) M. B. Robin and P. Day, *Adv. Inorg. Chem. and Radiochem.* 10, 248 (1967).
- (55) S. Yamada and R. Tsuchida, *Bull. Chem. Soc. Japan* 29, 421 (1956).
- (56) K. Krogmann, *Z. Naturforsch.* 23b, 1012 (1968).
- (57) L. E. Lyons, *J. Chem. Soc.* 5001 (1957).
- (58) N. F. Mott and R. W. Gurney, Electronic Processes in Ionic Crystals, Clarendon Press, Oxford, 1940.
- (59) G. H. Wannier, *Phys. Rev.* 52, 191 (1957).
- (60) S. Nikitine, *Helv. Phys. Acta* 28, 307 (1955).
- (61) C. K. Jørgensen, *Mol. Phys.* 4, 235 (1961).
- (62) M. Delepine, *Ann. Chim.* 7, 277 (1917).
- (63) C. K. Jørgensen, *Acta Chem. Scand.* 17, 1034 (1963).
- (64) M. C. R. Symons and P. A. Trevalion, *J. Chem. Soc.* 3503 (1962).
- (65) D. Herbison-Evans, P. B. P. Phipps and R. J. P. Williams, *J. Chem. Soc.* 6170 (1965).
- (66) V. Barkhatov and H. Zhdanov, *Acta Physicochem. URSS* 16, 123 (1942); N. A. Curry and W. A. Runciman, *Acta Cryst.* 12, 674 (1959).
- (67) P. S. Braterman, *J. Chem. Soc. (A)* 1471 (1966).
- (68) M. B. Robin, *Inorg. Chem.* 1, 377 (1962).
- (69) G. C. Allen and N. S. Hush, *Prog. Inorg. Chem.* 8, (1967).
- (70) G. Garton and H. M. Powell, *J. Inorg. Nucl. Chem.* 4, 84 (1957).
- (71) L. Killborg, *Adv. Chem. Ser.* 39, 37 (1963).
- (72) H. L. Wells and F. J. Metzger, *Am. Chem. J.* 26, 268 (1901).
- (73) K. A. Jensen, *Z. anorg. Chem.* 232, 192 (1937).
- (74) S. L. Lawton and R. A. Jacobson, *Inorg. Chem.* 5, 743 (1966).
- (75) T. Barrowcliffe, I. R. Beattie, P. Day, and K. Livingston, *J. Chem. Soc. (A)* 1810 (1967).
- (76) P. Day, D. Phil. Thesis, Oxford, 1965.
- (77) L. Atkinson and P. Day, *J. Chem. Soc. (A)*, in press.
- (78) P. Day, *Inorg. Chem.* 2, 452 (1963).
- (79) Proc. 2nd Int. Conf. on Coord. Chem., Copenhagen, 1953.
- (80) R. A. Walton, R. W. Matthews, and C. K. Jørgensen, *Inorg. Chim. Acta*, 1, 355 (1967).
- (81) R. W. G. Wyckoff, *Am. J. Sci.* 14, 349 (1928).
- (82) P. Day and D. W. Smith, *J. Chem. Soc. (A)* 1045 (1967).
- (83) J. J. Markham, F-Centres in Alkali Halides, Solid Physics Supplement No. 8, Academic Press, New York, 1966.
- (84) J. J. Markham, *Rev. Mod. Phys.* 31, 956 (1959).

Local and Collective States in Single and Mixed Valency Chain Compounds

P. DAY

University of Oxford, South Parks Rd., Oxford OX1 3QR, England

Abstract

Compounds containing chains of metal atoms are found with four distinct classes of structure, each of which, as a result of the widely varying strength of the metal-metal interaction, has associated with it its own characteristic pattern of physical properties. Thus one may have either single or mixed valency phases with near neighbor contact between metal ions formed either directly or through anion bridges. The optical, X-ray photo electron, magnetic and transport properties of examples of each class are surveyed, with particular emphasis on work carried out at Oxford, to highlight the relative importance of single center and collective excited states in each category, in relation to their structures and the magnitude of the metal-metal interaction. It is pointed out that a collective description may be appropriate for magnetic and electronic excitations even without electron delocalization.

1. Introduction

Only in the last few years have inorganic chemists interested in the electronic structures of metal complexes paid much attention to the consequences of the interactions which can take place between molecules and ions placed next to each other in the solid state. At their weakest such interactions may manifest themselves only in relatively subtle shifts and splittings of electronic absorption bands, and in magnetic ordering at low temperatures. On the other hand, strong intermolecular interactions lead to spectacular color changes or the appearance of new absorption bands not found in the spectra of the isolated

molecules or ions. Finally, in extreme cases the entire range of physical properties of the crystal may be profoundly different from those expected of ordinary ionic or molecular solids. Of the latter situation, the most famous instance is certainly the one-dimensional metallic conducting behavior of the partially oxidized platinum compounds such as $K_2Pt(CN)_4Br_{0.3} \cdot 3H_2O$. The exceptional properties of this material have served to focus attention on metal atom chain compounds in general.

For a number of years we ourselves have been interested in both magnetic and charge transfer interaction effects in inorganic crystals. The purpose of the present paper is to bring together some of these observations, primarily concentrating on one-dimensional examples, to exemplify how the optical, magnetic and electron transport properties are influenced by the strength of the metal-metal interaction. Metal atom chain compounds are found with a great variety of structures and are formed by a large number of different elements. It may be useful therefore to attempt some general classification of the pattern of physical behavior characteristic of each structure type, and of the strength of the metal-metal interaction. One reason why this class of materials is so interesting is that they span the entire range from localized to collective behavior and thus should be a good testing ground for theoretical models of the solid state.

2. Localized and Collective States

Before discussing the various classes of metal chain compound, a general point which needs to be touched on concerns the meaning of the words 'localized' and 'collective' as used in this context. Unlike solid state physicists, inorganic chemists are not usually accustomed to constructing wavefunctions which are invariant to the operations of translation within a periodic lattice. Nevertheless, if a crystal such as $K_2Pt(CN)_4$ absorbs a photon of such an energy that one of the constituent complex anions undergoes a ligand field transition, it is an inescapable fact that we do not know which of the 10^{23} anions in the crystal has been excited, and that as a result, the excited state wavefunction must allow an equal probability of each ion being excited: in other words the wavefunction is a Bloch function. In one sense the state which it describes is 'collective,' since the excitation belongs to the whole lattice. How far and how fast it can move in practice, however, depends on the magnitude of inter-ionic coupling or transfer integrals compared with either intra-ionic electron correlation or repulsion effects on the one hand, or electronic-vibrational interactions on the other. Crudely, if the excitation is capable of being transferred from molecule to molecule faster than each molecule can accommodate its geometry to the excitation, then the excitation, or 'exciton,' 'belongs' to the whole lattice.

Otherwise, its range of travel is limited to a few adjacent molecules (or finally, only to one), and it is localized.

Delocalization of excitation, however, is far from implying delocalization of electrons, or the occurrence of electronic conductivity. Exciton migration over hundreds of angstroms is familiar in aromatic molecular crystals, for example, yet in their ground states they are excellent insulators. For conductivity it is obvious that we need to form crystal states in which the electron occupancy at different sites has been altered, e.g., creating $\text{Pt}(\text{CN})_4^{3-}$ and $\text{Pt}(\text{CN})_4^-$ in $\text{K}_2\text{Pt}(\text{CN})_4$. In ordinary ionic and molecular crystals such processes require a large energy input, and it is therefore inappropriate to talk of collective electron states in these materials. Interionic electron transfer states are only formed readily in solids containing an integral number of electrons per atom when the electron concentration is high enough to screen an excited electron from the positive hole left on the ion from which it originated. In contrast, if different sites in the crystal are already occupied by different numbers of electrons when the lattice is formed, much less energy is needed to form states in which these sites are merely interchanged. It may then be possible to form conducting states at lower electron concentrations, or with smaller overlap between ions, than one would need to generate energy bands of finite width in stoichiometric single valence solids. This is the significance of mixed valency, as we shall see in the survey of metal ion chain compounds which follows:

3. Types of Transition Metal Chain Compound

Transition metal compounds in which each cation has only two nearest neighbors are formed both in single and mixed valency situations. In turn, each of these may be formed either with or without anion bridges between the neighboring cations. Some examples of each type of compound are given in Table 1. The principal class of anion bridges single valence chains is that of the hexagonal perovskites ABX_3 . When X is a halide ion and A a univalent ion the lattice can be thought of as made up of a close packed array of A and X, if they are of comparable size, e.g., Cs^+ and Cl^- . Now in a close packed assembly of ions the number of octahedral holes equals the number of close packed atoms, but in the system AX_3 only one quarter of the octahedral holes are surrounded exclusively by X^- ions and are hence available for occupation by the B^{2+} cations. The ABX_3 stoichiometry would then be generated by filling all the holes of this type. If the lattice of $(\text{A}+3\text{X})$ is cubic close packed we have the cubic perovskite structure formed by many oxides and fluorides. However another possibility is hexagonal close packing of $(\text{A}+3\text{X})$. In that case the octahedral BX_6 groups are stacked in columns sharing pairs of opposite faces so that the

Table 1. Examples of Transition Metal Chain Compounds

	<u>Single Valence</u>	<u>Mixed Valence</u>
<u>Anion Bridged</u>	Hexagonal perovskites, $ABX_3:3d^n$ $AMCl_3$ (A = alkali metal or NR_4^+ , M = V, Cr, Mn, Fe, Co, Ni) $CsMCl_3 \cdot 2H_2O$ (M = Mn, Fe, Co)	$d^8:d^6$ square planar/octahedral halides $PtCl_3$ Wolframs red salt $d^{10}:d^8$ linear/square planar halides $CsAuCl_3$
<u>Direct</u>	Square planar $3d^8$, $4d^8$, $5d^8$ $M(DMG)_2$ (M = Ni, Pd, Pt) K_2PtCl_4 , $PtCl_2$ $Pt(NH_3)_4PtCl_4$ $APt(CN)_4$ $Ir(CO)_2acac$	Square planar $5d^{8-n}$ $A_2Pt(CN)_4X_n$ $A_{2-n}Pt(CN)_4$ $A_{2-n}Pt(C_2O_4)_2$

B to B separation is much smaller parallel to the c-axis of the hexagonal unit cell than perpendicular to it. If the BX_6 octahedra were undistorted, and if the ionic radius of A^+ were equal to that of X^- the ratio of the nearest neighbor B-B distance along the stacks to the distance between stacks would be 2.449. In many examples, however, the ratio is larger since one can use cations such as $N(CH_3)_4^+$ which are bigger than X^- . On the other hand, with undistorted BX_6 the nearest neighbor B-B distance is $2/\sqrt{3}$ times the B-X bond length. It is clear therefore that the anions will play an important role in any exchange processes between the B ions. Whatever the pathway of the B-B interaction though. A convincing demonstration of its one-dimensionality is provided by the ratio of intra-chain and inter-chain exchange integrals in a compound such as $N(CH_3)_4MnCl_3$, which has been determined as 10^3 (2).

The other class of single valence chain compounds in which anion bridging plays a role are the hydrated ternary transition metal halides. Here the coordination of each bivalent metal ion is again octahedral, consisting of four halide ions and two cis-water molecules (3). The octahedra are joined into chains through approximately 180° bridges involving the trans halide ions.

Halide bridges between cations of differing oxidation state are mainly confined to situations in which one of the cations has a low spin d^8 configuration, and hence basically square planar coordination. The vacant sites perpendicular to the plane containing the ligands may then be occupied by halide ions which are themselves coordinated to another cation. In the most common examples of this type, the second cation has a low spin d^6 configuration and thus octahedral coordination. The halide bridges may also be the terminal groups of linearly coordinated d^{10} cations such as Au^I . In fact, a famous example of the latter is the black compound known as Wells' salt, which has the empirical formula $CsAuCl_3$. The structure, determined many years ago by Elliot and Pauling (4) contains chains of alternating linear $AuCl_2$ and square planar $AuCl_4$. However, each $AuCl_2$ also has four chloride ions from four $AuCl_4$ coordinated at right angles to its principal axis, so in toto, the lattice could be viewed as a distorted version of the cubic close packed perovskite.

To achieve a close enough approach between metal ions for direct interaction between them to outweigh interactions through bridging ligand groups, the most favorable situation is clearly to have complexes which are coordinatively unsaturated, so that another metal ion, or complex, can act, as it were, as a ligand. The most familiar examples of coordinative unsaturation are square planar complexes, so it is among low spin d^8 compounds that some of the most spectacular intermetallic interaction effects are found, both in single and mixed valency compounds. Also, because it is the trans sites in such a geometry, which

are available for coordination, polymerization is bound to give linear systems. Single valence examples are found with $3d^8$, $4d^8$ and $5d^8$ configurations, both where the units are neutral molecules like $PtCl_2$, anions like $Pd(CN)_4^{2-}$ or alternating anions and cations, as in Magnus' Green Salt. In all of these, important intermetallic interaction effects are observed, as we shall indicate later. At the present time examples of direct metal-metal interactions in mixed valence chains are only known for systems based on partial oxidation of square planar complexes in the third transition series. We and others have made repeated efforts to prepare Ni and Pd analogues of the partially oxidized Pt chain compounds, but with no success. Even attempts to dope $K_2Pt(CN)_4Br_0.30.3H_2O$ with $Pd(CN)_4^{2-}$ or $Ni(CN)_4^{2-}$ by co-crystallizing it in the presence of large excesses of these two ions do not lead to any detectable incorporation of $3d^8$ or $4d^8$ complex. Whether this is because the greater radial extension of the $5d$ orbital is needed to obtain sufficient overlap between the cations to stabilize the band structure, or whether it is connected with the smaller $nd-(n+1)p$ separation in the third transition series we cannot say.

Following this brief and generalized survey of the main structure types of the metal chain compounds, some account can now be given of the physical properties associated with each type. In order to avoid this having too much of the character of a review, reference will mainly be made to work on chain compounds which has been carried out in Oxford in the last few years.

4. Single Valence Metal Chain Compounds

(a) Anion Bridged Compounds. An outline of the properties of single valence metal chain compounds is given in Table 2, which highlights the differences found between compounds containing anion bridges rather than directly interacting metal ions. The key observation is that none of the anion bridged compounds have any low energy excited states of metal-to-metal charge transfer type. Since, as we have noted, it is mixing of this kind of state into the ground state which leads to collective electronic behavior, it is no surprise that all known examples are insulating, with localized ground states. Ligand-to-metal charge transfer states exist in the ultraviolet, however, and insofar as these involve the bridging ligands, their mixing into the ground state provides a mechanism for superexchange, leading to magnetic ordering at low temperatures. At lot has been written about one-dimensional magnetic ordering, but a single representative example will illustrate some of the characteristics of this kind of system.

Unlike $CsCuCl_3$, which distorts from the hexagonal perovskite structure so as to provide each Cu atom with four short and two long bonds, the other first transition series ion which

Table 2. Properties of Single Valence Transition Metal Chains

	<u>Anion Bridged</u>	<u>Direct Interaction</u>
<u>Optical</u>		
(a) Locally excited (ligand field)	Weakly perturbed by exciton-magnon interaction (unusual temperature dependence of intensity)	Vibronic transitions strongly perturbed by UV charge transfer states
(b) Collective (d→p or charge transfer)	None at low energy Usual halide → metal transitions only	Large Davydov shifts when E chain
<u>Magnetic</u>	Ferromagnetic or antiferromagnetic at low temperatures Weak superexchange	Diamagnetic (anisotropic?)
<u>Transport</u>	Insulator	Semiconductor (probably extrinsic)

customarily shows strong Jahn-Teller distortion, Cr^{II} , forms a compound CsCrCl_3 which, at least above 172 K, has an undistorted hexagonal perovskite structure (5). That one-dimensional spin correlations are important in this compound follows at once from the temperature variation of the magnetic susceptibility which has a broad maximum near 170 K, then decreases with the onset of antiferromagnetism. In fact though, three dimensional magnetic ordering does not take place until the Neel temperature of 16 K is passed, so between 170 and 16 K only antiferromagnetic interactions within the chains are of any importance. An even more direct measure of the one-dimensionality of the spin correlations is the dispersion of the spin-wave excitations parallel and perpendicular to the chain (6). Just as we have to write the electronic excited state wavefunctions of a crystal as Bloch functions, so as to allow the excitation an equal probability of residing on any of the constituent ions, so, in the same way, must a magnetic excitation (that is, the deviation of a spin from the direction it would have in the totally ordered lattice) be delocalized. Spin waves of differing wavelengths (or wave vectors) have different energies, which can be determined by inelastic neutron scattering, thus building up a picture of the dispersion curve experimentally. The experimental spin-wave dispersion of CsCrCl_3 near 4 K parallel and perpendicular to the chains is shown in Figure 1. Although the results do not cover the entire Brillouin zone, because of the small size of the crystal available to us, they do show very clearly that the dispersion perpendicular to the c -axis is essentially zero. The exchange integral between neighboring Cr ions in the basal plane is therefore negligibly small whilst within the chains curve fitting to the experimental points on the dispersion curve gives $J_1 \sim 26.7 \text{ cm}^{-1}$.

Since customarily there are no charge transfer states in the visible or near ultraviolet in this class of compound, the lowest energy excited states are ligand field in type, and can therefore be described as Frenkel, or tight-binding, excitons. Many ligand-field excited states have spin projections different from the ground state and transitions to them should consequently be electric dipole forbidden. It has been known for a number of years, however, that such transitions can be rendered allowed in antiferromagnetic compounds by using the exchange interaction to couple an exciton formed with decrease of spin (e.g., sextet to quartet) with a spin deviation among the rest of the ions in the lattice, which remain in their ground states. The most famous examples of such 'exciton-magnon' combination bands are found in manganese salts (7), so it is interesting to see how the effect manifests itself in Mn^{II} salts of the hexagonal perovskite type, which contain chains of antiferromagnetically coupled ions like that found above in CsCrCl_3 .

In overall appearance the ligand field spectra of Mn^{II} chain compounds are much like those of other six-coordinate Mn^{II}

complexes, confirming again that the metal-metal interactions in anion bridged single valence chains are weak. Two features stand out, however. First, the oscillator strengths of the transitions are greater than in non-bridged ('outer-sphere') salts where magnetic interactions are negligible. Second, the temperature dependences of the oscillator strengths follow a rather curious pattern, quite unlike that of the usual 'coth' plot for a simple vibronically induced transition. Some experimental examples are shown in Figure 2(a) (8). In all cases the oscillator strength increases rapidly at first when the temperature is raised above 4.2 K, then passes through a broad maximum at a temperature which varies from one compound to another, but appears to be the same for all the bands in each compound. Then after dropping slightly it finally increases slowly and monotonically towards room temperature. This variation has some general resemblance to the curve of susceptibility vs. temperature for these materials (9). In fact, the results in Figure 2(a) stimulated Tanabe and Ebara to calculate the intensity, frequency and linewidth variation of the magnon sidebands in linear antiferromagnets, with the result shown in Figure 2(b) (10). It can be seen that the overall form of the variation is nicely reproduced. Tanabe's theory requires that the temperature at which the broad maximum occurs in the intensity is approximately $|J/k|S(S+1)$. For the three compounds we investigated, the values of J/k derived from the spectra are listed in Table 3, which also shows that for the two compounds for which we have susceptibility data (9,11), the level of agreement between the latter and the optically derived value of J/k is very satisfactory.

(b) Directly Interacting Metal Ions. When metal ions are brought close enough together in a chain to interact directly, without the intermediary of a bridging ligand, the effect of the neighboring ions on the electronic states of each metal ion is naturally increased. Unfortunately no examples of such chains are known in which the constituent ions have unpaired spins because, as we noted already, they are all based on square planar d^8 complexes. The single exception known to us is $\text{Pt}(\text{NH}_3)_4\text{CuCl}_4$ which, however, contains chains of alternating $\text{Pt}(\text{NH}_3)_4^{2+}$ and CuCl_4^{2-} and so has a diamagnetic ion between each pair of d^9 ions. Consequently it has a Neel temperature of only 0.5°K , from which near neighbor exchange integral of about 0.25 cm^{-1} can be estimated (12).

Turning to optical properties, one finds two different types of situations in the single valence chains with directly interacting metal ions, depending on whether the lowest energy excited states of the constituent complexes are forbidden or allowed. The former are most likely to be ligand field states, which are parity forbidden from the ground state in centrosymmetric complexes like PtCl_4^{2-} and may in addition be

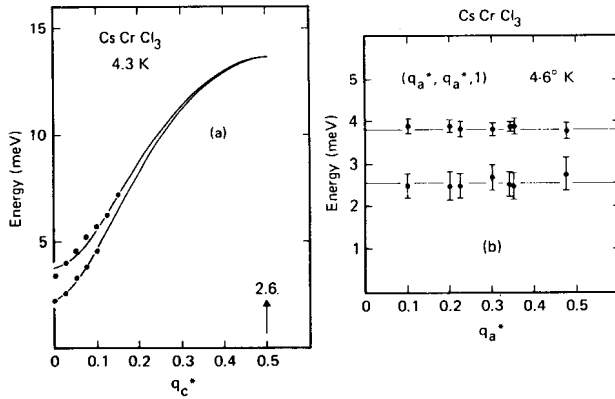


Figure 1. Dispersion of spin waves propagating (a) parallel and (b) perpendicular to the Cr chains in the linear antiferromagnet CsCrCl₃

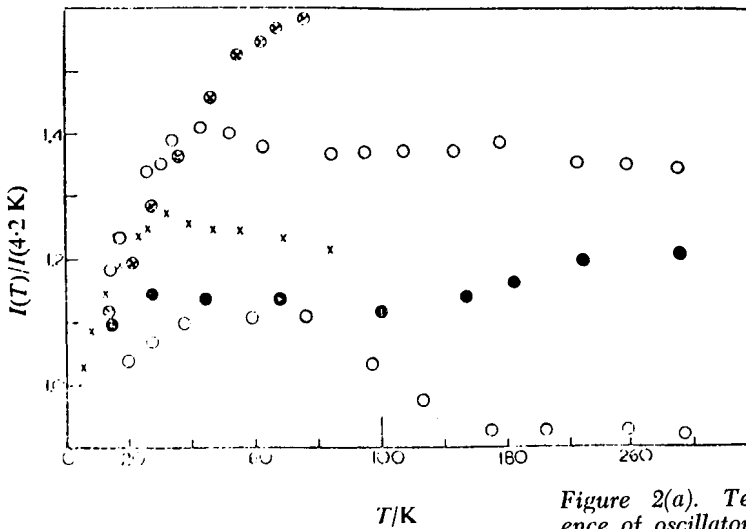


Figure 2(a). Temperature dependence of oscillator strengths of ligand field transitions in linear antiferromagnets $N(CH_3)_2 MnCl_3$ and $CsMnX_3 \cdot 2H_2O$ ($X = Cl, Br$) (8)

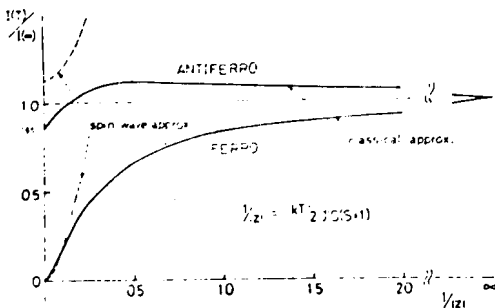


Figure 2(b). Calculated temperature variation of oscillator strengths of exciton-magnon transitions in linear antiferromagnets and ferromagnets (10)

spin-forbidden. The latter may be either 'atomic' (e.g., $5d \rightarrow 6p$ in Pt^{II} complexes) or charge transfer.

Cases where the lowest excited states are of ligand field type are the salts K_2PtCl_4 , $\text{Pt}(\text{NH}_3)_4\text{PtCl}_4$, $\text{Pt}(\text{NH}_3)_4\text{PtCl}_4$, Magnus' Green Salt (MGS), although some of the earlier workers thought that the unusual color of the last example pointed to 'metal-metal bonding,' and the existence of new excited states which could not be traced back in parentage to any intramolecular transitions of the constituent anion or cation (13). At first sight it does seem peculiar that MGS should be green, since $\text{Pt}(\text{NH}_3)_4^{2+}$ is colorless, both in solution and in $\text{Pt}(\text{NH}_3)_4\text{Cl}_2$, while PtCl_4^{2-} is pink in solution and in K_2PtCl_4 . Nevertheless, by looking at the way the polarized crystal spectra vary along a series of MGS analogues $\text{Pt}(\text{RNH}_2)_4\text{PtCl}_4$ as the R group is made more bulky, we showed some years ago (14) that the visible bands in MGS are all traceable to ligand field transitions appearing in the spectrum of PtCl_4^{2-} in K_2PtCl_4 , albeit with red shifts up to 4000 cm^{-1} . Examples of these are shown in Figure 3. They are also considerably intensified compared to K_2PtCl_4 , most dramatically when the incident electric vector is parallel to the metal stack (15). The reason for the intensification is assumed to lie in the fact that the transitions borrow their intensity vibronically from allowed transitions out in the ultraviolet which are themselves strongly red-shifted by the intermolecular interaction.

Intense absorption when the incident electric vector is parallel to the metal chains has often been taken as evidence for metal-metal bonding, but as we first pointed out (16), this conclusion may be based on a false interpretation of the available absorption mechanisms. It is undoubtedly true, of nickel dimethylglyoximate for example, that the crystal, which contains metal chains, has an intense absorption band in the visible, polarized parallel to the chains, which does not appear in the solution spectrum. It is equally true, however, that the first intense band of nickel N-methyl-salicyaldimine, which does not form chains in the crystal, is also polarized perpendicular to the molecular planes. In both cases the transition is most probably a $d_{z^2} \rightarrow \pi^*$ charge transfer, but the feature distinguishing them is that when the molecules are stacked plane to plane the transition dipoles are all parallel, so interactions between them are maximized and very large Davydov shifts occur. No intermolecular electron exchange need be invoked in either case. In fact, we believe that in general, when the lowest energy excited states of the molecular units are polarized perpendicular to their planes, the lowest excited states of the stacks of molecules in the crystal are always neutral Frenkel excitons rather than ionic excitons. This prejudice is based on the magnitude of the Davydov splitting to which the neutral excitons will be subject (a 'back of an envelope' calculation suggests around $14,000 \text{ cm}^{-1}$ for transition

Table 3. Temperature Dependence of Intensity of Magnon Sidebands in Linear Antiferromagnets

	T_{\max} (exp.)	J/k	J/k (susceptibility)
$\text{CsMnCl}_3 \cdot 2\text{H}_2\text{O}$	20-40 K	3.3 K	3.0 K
$\text{CsMnBr}_3 \cdot 2\text{H}_2\text{O}$	30-60	4.5	-
$(\text{NMe}_4)\text{MnCl}_3$	50-80	6.7	6.3

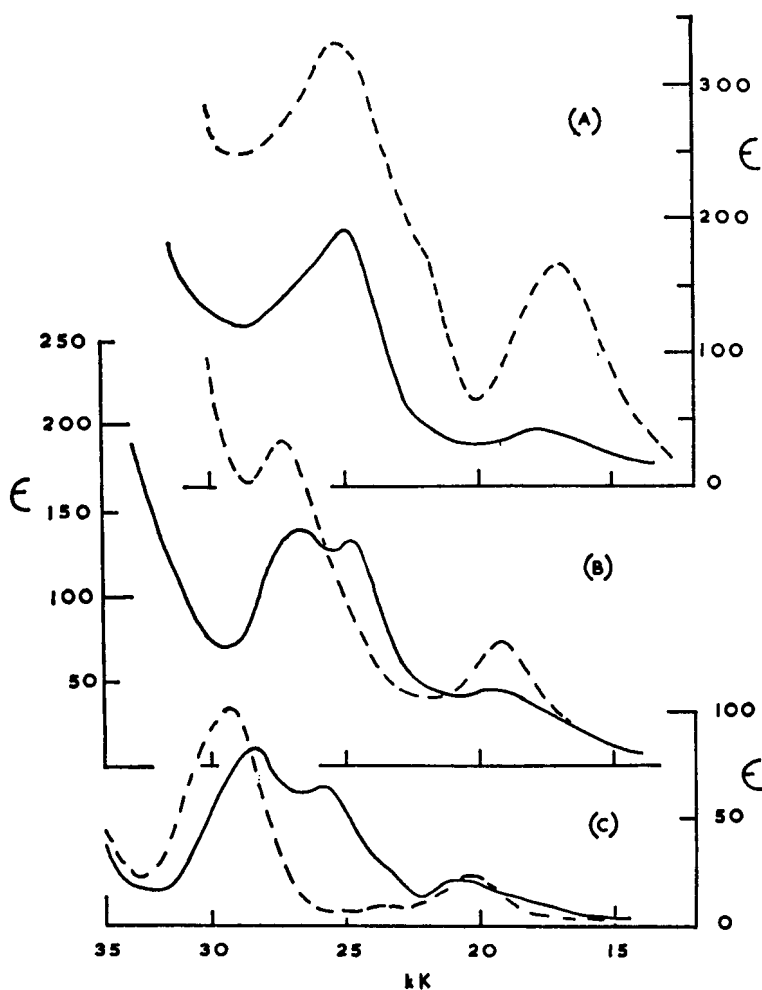


Figure 3. Polarized absorption spectra of (a) $\text{Pt}(\text{CH}_3\text{NH}_2)_3\text{PtCl}_3$, (b) $\text{Pt}(\text{C}_2\text{H}_5\text{NH}_2)_3\text{PtCl}_3$, and (c) K_2PtCl_6 . Dotted lines are $E c$, full lines $E c(15)$.

dipole length of 1\AA in a stack of molecules separated by 3.25\AA). On the other hand, if the parent transition is polarized within the molecular planes, Davydov splitting of its neutral excitons in the crystal is smaller (actually one half of the other in the point dipole approximation) and ionic excitons may become observable. An example here is the work of Martin and his colleagues on PtX_2 (17,18).

One way of verifying that 'new' electronic transitions appearing in chain compounds with polarizations parallel to the stacks are actually Davydov components of transitions which take place in the ultraviolet in the isolated units is to determine how their energy varies as one changes the intermolecular spacing in the stacks. In the point dipole approximation the separation between the Davydov components is proportional to $|M|^2/R^3$, where M is the transition dipole moment and R the distance between the centers of the molecules (19). A particularly favorable set of molecules to exemplify this expression is that of the tetracyano-platinites. Many salts of this anion contain stacks of $\text{Pt}(\text{CN})_4^{2-}$ with their planes parallel, though with changing cation the Pt-Pt spacing can be varied from 3.13\AA (Mg) to 3.69\AA (Rb) (20). Although the lowest excited state of $\text{Pt}(\text{CN})_4^{2-}$ in solution lies at $35,600\text{ cm}^{-1}$, in all such salts there is an extremely intense absorption band in the visible or near ultraviolet, polarized entirely along the direction of the stacks. With increasing Pt-Pt separation the band moves to higher energy, and in Figure 4 we plot its energy against $1/R^3$. Both for the tetracyano-platinites and the isomorphous tetracyanopalladites, which are included on the same plot, there is a very satisfactory correlation between these two quantities. Furthermore, extrapolating the two straight lines of Figure 4 to $R = \infty$, i.e., to the isolated molecule, we find energies of $44,800\text{ cm}^{-1}$ ($\text{Pt}(\text{CN})_4^{2-}$) and $52,900\text{ cm}^{-1}$ ($\text{Pt}(\text{CN})_4^{2-}$) which, bearing in mind that the aqueous solution spectra of the ions do not strictly represent those of the isolated molecules, is well within the energy range of the z-polarized allowed transitions assigned by Mason and Gray (21).

5. Mixed Valence Metal Chain Compounds

About forty elements form compounds in which, to satisfy the observed stoichiometry, one has to assign different oxidation numbers to different metal ions of the same element in the same lattice. These so-called 'mixed valence' compounds often have properties far from a simple superposition of those we would predict for each of the oxidation states taken separately. In particular, if the sites occupied by the metal ions of differing valency have similar coordination numbers and ligand environments, the energy needed to transfer an electron from one to the other, i.e., to interchange the valencies, may be very low. Indeed, if the metal ion sites in the lattice of our

Table 4. Properties of Mixed Valence Transition Metal Chains

	<u>Anion Bridged</u>	<u>Direct Interaction</u>
<u>Optical</u>		
(a) Locally excited (ligand field)	Only weakly perturbed when E_{\perp} chain	No ligand field states seen Weak allowed transitions when E_{\perp} chains
(b) Collective (charge transfer or metallic)	Metal \rightarrow metal charge transfer for E_{\parallel} chains	Opaque at all frequencies for E_{\parallel} chains Plasma edge in visible
<u>Magnetic</u>	Diamagnetic	Diamagnetic
<u>Transport</u>	Semiconductor (probably intrinsic)	Metallic at 300K Insulator at 4K
<u>Mixed Valence Class</u>	II	IIIB (Incipiently II??)
(ESCA, Mossbauer etc.)	(Valences trapped)	(Metal atoms equivalent)

mixed valence compound all turn out to be crystallographically identical, then one may have a non-integral number of electrons at each site, even in the ground state. Searching out the known mixed valence compounds from all corners of the Periodic Table, and correlating their properties with the observed structures, we find that they can be divided into three broad classes (22). If the ligand fields around the ions of differing valence are very different, ionized excitons, or in chemists' language metal-to-metal charge transfer states, lie a long way above the ground state whose properties, along with those of many lower excited states, are very close to being just a superposition of the properties of the constituent ions. This category, called class I, is of little interest here. At the opposite extreme, a truly non-integral number of electrons at each metal ion site, which would be required if they are all crystallographically identical, can only be achieved in a metal if the lattice is continuous. This category we call class III. Between classes I and III lies a continuous spectrum of cases (class II) in which two types of metal ion sites can be distinguished by crystallography, but in which ionized excitons lie close enough to the ground state that they contribute to the optical spectrum in the visible or even the near infrared. Some of the ionized excitons may even have the correct symmetry to mix with the ground state, partly smudging out the formal oxidation numbers defined by counting electrons at the two metal ion sites. We will now examine the properties of the known mixed valence metal chain compounds in the light of this simple classification. Just as in the single valence chains, we distinguish the two cases of anion bridging and directly interacting metal ions.

(a) Anion Bridged Compounds. All the anion bridged Pt and Au compounds have two sets of crystallographically distinct metal ion sites, and may therefore be characterized as containing trapped valences in their ground states, (II,IV) in the former and (I,III) in the latter. X-ray photoelectron (XPS) spectroscopy should be a powerful tool for deciding whether different partial charges must be assigned to the ions or each type of site, because we might hope to see core ionizations from each type. If we do not (assuming that the reason is not simply the poor resolution of the technique), then the partial charges are equal or, said another way, the electrons are exchanging between the sites more rapidly than the time taken for the core electron to be ejected. Figure 5 shows some XPS spectra of Pt chain compounds in the 4f region (23), including the mixed valence $\text{Pt}^{\text{II}}\text{enCl}_3$ (en: ethylenediamine). Crystallographically, the latter can be thought of as made up of alternating square planar $\text{Pt}^{\text{II}}\text{enCl}_2$ and octahedral $\text{Pt}^{\text{IV}}\text{enCl}_4$ molecules. Comparison between the spectra of $\text{Pt}^{\text{II}}\text{enCl}_3$ and its separated constituent molecules is made more difficult by the ease with which $\text{Pt}^{\text{II}}\text{enCl}_4$ and $\text{Pt}^{\text{IV}}\text{enCl}_3$ reduce in the X-ray beam. However, by carefully

Figure 4. Variation in energy of the lowest intense transition in solid palladocyanides and platinumocyanide salts with intermetallic spacing

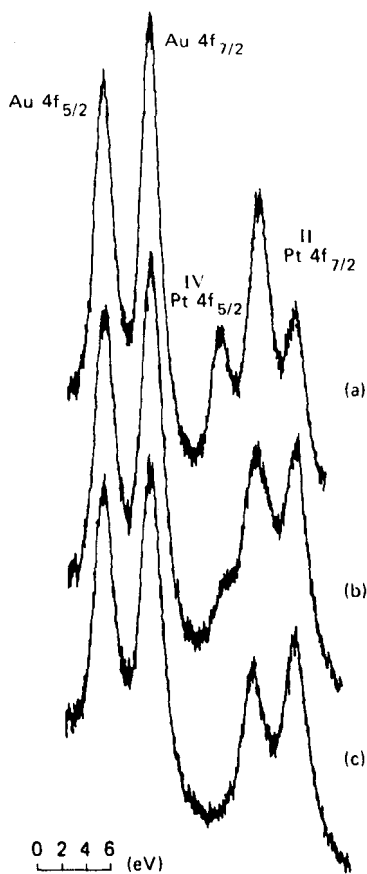
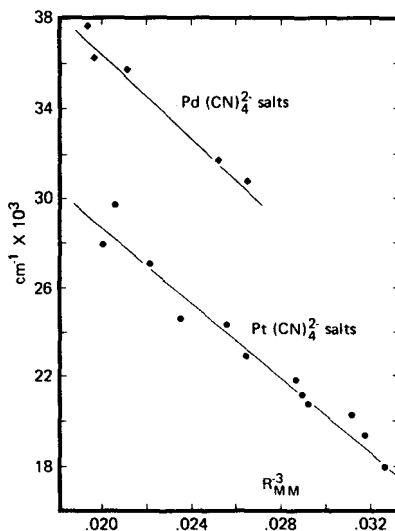


Figure 5. XPS spectra of Pt chain compounds in the Pt 4f region, (a) $PtCl_4$, (b) $PtCl_3$, (c) $PtCl_2$

following the spectra of these two compounds as a function of irradiation time one finds that the PtCl_3 spectrum is indeed close to a superposition of those of PtCl_2 and PtCl_4 (Figure 6).

However, the same cannot be said of the optical properties, for in addition to weak absorption bands, polarized perpendicular to the chains, which do identify closely with locally excited ligand from transitions of the constituents, PtCl_3 and other similar salts all have intense absorption across most of the visible, polarized entirely parallel to the chains (24). This we assign as due to metal to metal charge transfer, i.e., to ionized exciton states, and the compounds belong to class II defined above. Because the valences in the ground state are trapped, though, the crystals are semiconducting rather than metallic.

(b) Directly Interacting Metal Ions. In the single valence chains when the metal ions were brought close enough together to interact directly, instead of through a bridging group, large Davydov shifts of the neutral exciton states showed that the metal-metal interaction was very much increased. A comparable effect on the ionized exciton states of a mixed valence chain might bring them close enough to the ground state for the system to find itself on the other side of a Mott transition, and to have a conducting ground state in which the electron states were truly collective. This is the background to the recent interest in compounds like $\text{K}_2\text{Pt}(\text{CN})_4\text{Br}_{0.30}\cdot 3\text{H}_2\text{O}(\text{KCP})$ (25). At first sight it has all the characteristics expected of a class III mixed valency compound: despite the non-integral oxidation number, all the Pt atoms appear to occupy crystallographically equivalent sites; with the incident electric vector parallel to the chains it is opaque throughout the visible and infrared down to very low frequencies, and has a plasma edge in the reflectivity in the visible; at room temperature it is a metallic conductor. Unfortunately, if more interestingly, however, there are some features which complicate such a simple view. At low temperature, the compound is not metallic, but semiconducting. There is also evidence of a tendency for the Pt atoms to become inequivalent as a result of long wavelength acoustic phonon instabilities. If such an instability, which showed up by inelastic neutron scattering as a Kohn anomaly in the acoustic phonon dispersion became locked in as a static distortion, it would provide enough reason for the energy gap at low temperature. A crucial experiment would therefore be to examine the crystal structure at liquid helium temperature.

We recently collected X-ray diffraction data from a single crystal of KCP at room temperature, 77° and 4.2°K (26). The arrangement of the diffractometer and cryostat required one to concentrate on one crystal axis at a time, and we chose the $(0,0,l)$. Within that limitation we found no sign of Bragg peaks

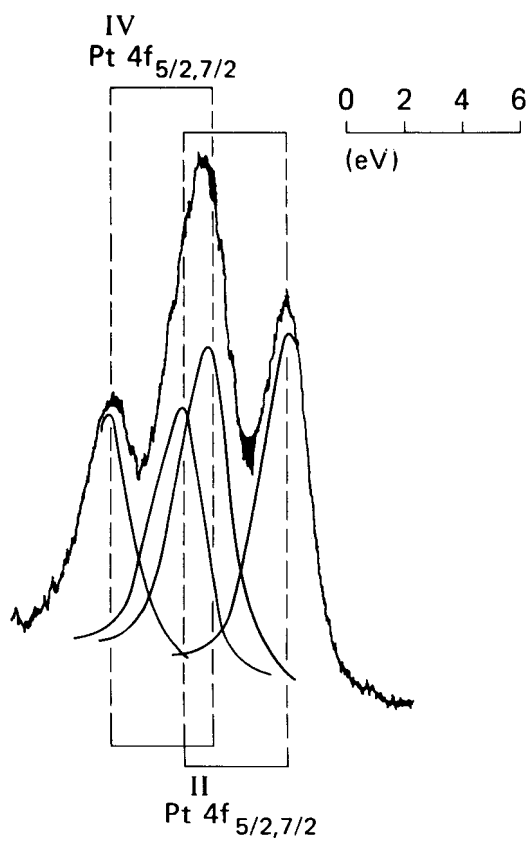


Figure 6. XPS spectrum of PtCl₃ in the Pt 4f region after surface cleaning

corresponding to 'locking in' a Peierls distortion at the repeat distance (6.67 times the Pt-Pt spacing) suggested by the neutron scattering results. What we did find, however, is a set of seven peaks indexing as $(0,0,\epsilon)$, where $\epsilon = n/\zeta$. The peaks with n odd are weaker than those with n even, and a least squares fit to the Bragg angles of those with $n = 1,2,3,4,6,8,10$ yields a value for ζ of 8.97. A key observation is that the peaks are present at room temperature as well as at 4.2°K, and that they do not vary in any discontinuous way as the temperature is lowered. They must therefore result from some superlattice ordering which has not previously been detected. Our present view is that the superlattice is probably connected with ordering among the bromide ions, supposed in the original crystal structure determination to be randomly distributed on three fifths of the available sites within channels between the stacks of $\text{Pt}(\text{CN})_4$ groups. From analogies with other 'tunnel' compounds, such as the hexagonal tungsten bronzes, we believe a random distribution of anions is a priori unlikely, a view reinforced by the very narrow composition range which KCP exhibits. Since it has become such an important model compound for one-dimensional metallic behavior the subtler details of its structure obviously deserve the closest attention.

Literature Cited

1. Wells, A. F., "Structural Inorganic Chemistry," 3rd ed., p. 375, Oxford University Press, Oxford, 1962.
2. Hutchings, M. T., Shirane, G., Birgeneau, R. J. and Holt, S. L., Phys. Rev. (1972), B5, 1999.
3. Jensen, S. J., Andersen, P. and Rasmussen, S. E., Acta Chem. Scand. (1962), 16, 1890.
4. Elliot, N. and Pauling, L., J. Amer. Chem. Soc. (1938), 60, 1846.
5. McPherson, A. L., Kistenmacher, T. J., Folkers, J. B. and Stucky, G. D., J. Chem. Phys. (1972), 57, 3771.
6. Hutchings, M. T., Day, P., Gregson, A. K., Leech, D. H. and Rainford, B. D., Physical Society Meeting, Manchester, England, January 1974.
7. Sell, D. D., Greene, R. L. and White, R. M., Phys. Rev. (1967), 158, 489.
8. Day, P. and Dubicki, L., J.C.S. Faraday II (1973), 69, 363.

17. DAY *Chain Compounds* 253
9. Dingle, R., Lines, M. E. and Holt, S. L., *Phys. Rev.* (1969), 187, 643.
10. Ebara, K. and Tanabe, Y., *J. Phys. Soc. Japan* (1974), 36, 93.
11. Smith, T. and Friedberg, S. A., *Phys. Rev.* (1968), 176, 660.
12. Soos, Z. G., Huang, T. Z., Valentine, J. S. and Hughes, R. C., *Phys. Rev.* (1973), B8, 993.
13. Yamada, S. *J. Amer. Chem. Soc.* (1951), 73, 1579.
14. Day, P., Orchard, A. F., Thomson, A. J. and Williams, R. J. P., *J. Chem. Phys.* (1965), 42, 1973.
15. *idem.*, *ibid.* (1965), 43, 3763.
16. Day, P., *Inorg. Chim. Acta Rev.* (1969), 3, 81.
17. Martin, D. S., Hunter, L. D., Kroening, R. F. and Coley, R. F., *J. Amer. Chem. Soc.* (1971), 93, 5433.
18. Kroening, R. F., Hunter, L. D., Rush, R. M., Clardy, J. C. and Martin, D. S., *J. Phys. Chem.* (1973), 77, 3077.
19. Craig, D. P. and Walmsley, S. H., "Exitons in Molecular Crystals," W. A. Benjamin Inc., New York, 1968.
20. Moreau-Colin, M. L., *Structure and Bonding* (1972), 10, 167.
21. Mason, W. R. and Gray, H. B., *J. Amer. Chem. Soc.* (1968), 90, 5721.
22. Robin, M. B. and Day, P., *Adv. Inorg. Chem. and Radiochem.* (1967), 10, 247.
23. McGilp, J. *Chemistry, Part II Thesis*, Oxford, 1973.
24. Yamada, S. and Tsuchida, R., *Bull. Chem. Soc. Japan* (1956), 29, 894.
25. See papers by K. Krogman and H. R. Zeller in this symposium.
26. Griffiths, D., Day, P. and Wedgwood, F. A., unpublished.

Excitons in One-Dimensional Tetracyanoplatinite Salts

Sir:

Although the recent flurry of activity¹ on the electronic properties of metal chain compounds has been mainly concerned with the so-called "partly oxidized" (i.e., mixed valence²) platinum salts, in the solid state quite a lot of ordinary divalent square planar platinum salts form stacks in which the metal atoms are also brought into reasonably close proximity. These compounds are of course insulators, not metals, but they do have extremely unusual optical properties which are clearly the result of the one-dimensional character of their crystal lattices. The purpose of this note is to draw attention to a strikingly simple correlation between the structural and optical parameters in one set of Pt(II) salts, the tetracyanoplatinites, which strongly suggests that the lowest excited states of one-dimensional single valence platinum compounds can be described as neutral Frenkel excitons, propagating along the stacks.

Briefly stated, the unusual optical properties of the tetracyanoplatinites are the following: in dilute aqueous solution the isolated $\text{Pt}(\text{CN})_4^{2-}$ ion has major absorption bands at 35,800 ($\epsilon = 1480$), 39,200 ($\epsilon = 10700$), and 46,100 cm^{-1} ($\epsilon = 22100$).³ It does not appear to have any further absorption bands, even weak ones, at lower energies. Nevertheless, many tetracyanoplatinite salts, particularly those of group 1A and 2A cations are intensely colored and, moreover, exhibit strong visible luminescence. Polarized single-crystal reflection spectra⁴ of Mg, Ca, Sr, and Ba tetracyanoplatinites demonstrate that at room temperature the visible absorption consists of a single broad band, polarized almost entirely parallel to the metal atom chains, whose oscillator strength in that direction has the order of magnitude of unity. The frequency of the band varies very markedly from one salt to another; it lies lowest in $\text{MgPt}(\text{CN})_4 \cdot 7\text{H}_2\text{O}$, which also has the shortest Pt-Pt spacing (3.13 Å⁵). That the frequency in fact varies monotonically with Pt-Pt spac-

ing is demonstrated by the extensive set of structural and optical data collected by Moreau-Colin.⁶

Since the tetracyanoplatinites are insulating crystals in which the molecular units remain clearly distinguishable, it seems a priori probable that the lowest crystal excited states should be neutral Frenkel excitons formed from simple molecular transitions, coupled by the intermolecular interaction potential. The simplest approximation to the latter is the point multipole expansion. Because the intense low energy crystal absorption band is polarized parallel to the Pt chains, its origin must lie in an allowed transition polarized perpendicular to the planes of the units, i.e., A_{2u} in the double group D_{4h}^* , which could arise either from a metal-to-ligand charge transfer ($d_{z^2} \rightarrow a_{2u}\pi^*$) or a $d_{z^2} \rightarrow p_z$ transition of the metal or, perhaps more likely, some admixture of the two. The molecular transition dipole vectors within each stack then being parallel to one another, the resulting crystal transition should suffer a Davydov shift to lower energy which in the point dipole approximation,⁷ and assuming only interactions between nearest neighbors in the stack, would be $2e^2|M|^2/R^3$, where M is the transition dipole moment in the free ion and R is the Pt-Pt spacing within the stack. This possibility was mooted some years ago⁸ but without definitive evidence.

An obvious means of testing whether the observed bands are indeed still Davydov components would thus be to plot their energies against R^{-3} . This we have done in Figure 1, for both tetracyanoplatinites and tetracyanopalladites, using the data of Moreau-Colin.⁶ The result is such an excellent linear correlation that there can be no doubt of the essential correctness of the original hypothesis. Furthermore the extrapolated frequencies of the transitions at $R = \infty$ (i.e., for the free ions) are 44,800 and 52,900 cm^{-1} for $\text{Pt}(\text{CN})_4^{2-}$ and $\text{Pd}(\text{CN})_4^{2-}$, respectively, well within the range of energy of the intense transitions of both ions in solution.

Yet more confirmation comes from the assignments of the relevant states in the free ions. A spin-orbit calculation³

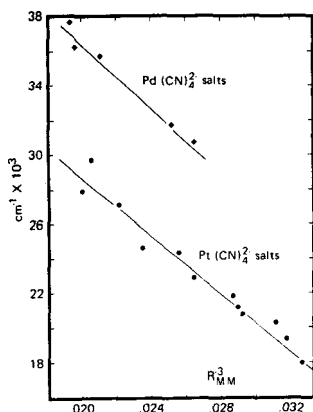


Figure 1. Absorption energies and nearest neighbor metal-metal distances in tetracyanoplatinates and tetracyanopalladates.

carried out to assign the solution magnetic circular dichroism spectrum of $\text{Pt}(\text{CN})_4^{2-}$ placed the A_{2u} state with predominant $^1A_{2u}$ parentage beneath the band envelope at $46,100 \text{ cm}^{-1}$, while a transition state calculation⁹ of the $5a_{1g} \rightarrow 3a_{2u}$ ($^1A_{2u}$) excitation in the same ion by the $X\alpha$ scattered wave method predicted it at $50,600 \text{ cm}^{-1}$. Bearing in mind that the reference point of the Davydov calculation is the free ion in the gas phase, the agreement of these numbers with the extrapolated free ion excitation energy is satisfactory. Turning to the intensity in the simple point dipole approximation, the slope of the line in Figure 1 would be just $-2e^2|M|^2$; experimentally it is approximately

$-0.008e^2A^2$, equivalent to a transition dipole length of about 1.9 \AA . An estimate based on the area of the $46,100\text{-cm}^{-1}$ absorption band of $\text{Pt}(\text{CN})_4^{2-}$ in solution was just under 0.8 \AA . This discrepancy between the observed and predicted free ion dipole lengths is no doubt a measure of the approximation we have made by assuming only a point dipole-dipole interaction and not carrying out a summation over the whole lattice. Nevertheless, the discrepancy is not too great.

The success of this extremely simple approach to the tetracyanoplatinite crystal spectra leads us to suggest that the unusual optical properties of other crystals containing one-dimensional arrays of square planar d^8 complexes, such as the dimethylglyoximates,¹⁰ might be capable of a similar explanation, as we already tentatively suggested earlier.¹¹

References and Notes

- (1) Some recent reviews and collections of papers are (a) H. R. Zeller, *Festkoerperprobleme*, **13**, 31 (1973); (b) "Extended Interactions between Transition Metal Ions", *Am. Chem. Soc. Symp. Ser.*, in press; (c) H. J. Keller, Ed., "One Dimensional Electronic Properties", Plenum Press, New York, N.Y., in press.
- (2) M. B. Robin and P. Day, *Adv. Inorg. Chem. Radiochem.*, **10**, 247 (1967).
- (3) S. B. Piepho, P. N. Schatz, and A. J. McCaffery, *J. Am. Chem. Soc.*, **91**, 5994 (1969).
- (4) C. Monclut and H. Poulet, *J. Phys. (Paris)*, **23**, 353 (1962).
- (5) R. M. Bozorth and L. Pauling, *Phys. Rev.*, **39**, 537 (1932).
- (6) M. L. Moreau-Colin, *Struct. Bonding (Berlin)*, **10**, 167 (1972).
- (7) D. P. Craig and P. C. Hobbins, *J. Chem. Soc.*, 539 (1955); D. Fox and O. Schnepf, *J. Chem. Phys.*, **23**, 767 (1955).
- (8) C. Monclut, *J. Phys. (Paris)*, **24**, 833 (1964).
- (9) L. V. Interrante and R. P. Messmer, in ref 1b.
- (10) B. G. Anex and F. K. Krist, *J. Am. Chem. Soc.*, **89**, 6114 (1967).
- (11) P. Day, *Inorg. Chim. Acta Rev.*, **3**, 81 (1969).

P. Day
 St. John's College
 Oxford OX1 3JP, England
 Received December 14, 1974

Why is silver chromate red? The 4.2 K polarized electronic spectrum of chromate in silver sulphate

by DAVID J. ROBBINS† and PETER DAY

Oxford University, Inorganic Chemistry Laboratory,
South Parks Road, Oxford, OX1 3QR

(Received 6 April 1977)

1. INTRODUCTION

It is a fact well known to schoolboys doing qualitative analysis that silver chromate is brick-red, though potassium chromate, in common with most other chromate salts, is yellow. The reason for this obvious difference in colour however is not very clear. When diluted in K_2SO_4 the CrO_4^{2-} ion shows an intense absorption band beginning near $26\,300\text{ cm}^{-1}$, which at 20 K [1] or 4.2 K [2] is resolved into a series of vibrational progressions in the $\nu_1(a_1)$ mode, with average frequencies about 780 cm^{-1} . From the site-group splitting of the zero-phonon band in the orthorhombic K_2SO_4 host lattice [2], as well as from the sign and magnitude of the magnetic circular dichroism associated with the same band system in the solution spectrum [3], it is clear that the chromate ion absorption between $26\,000$ and $33\,000\text{ cm}^{-1}$ is to be assigned as ${}^1A_1(t_1^6 e^0) \rightarrow {}^1T_2(t_1^5 e^1)$, i.e. to the transfer of an electron from the highest filled molecular orbital localized on the oxygens, to the lowest empty molecular orbital mainly localized on the chromium. This assignment is precisely analogous to that of the first intense band system in the isoelectronic permanganate ion. The next higher absorption band stretches from about $35\,000$ to $42\,000\text{ cm}^{-1}$, peaking at $38\,000\text{ cm}^{-1}$. In the 20 K spectrum of chromate in K_2SO_4 , Teltow [1] also found a very weak band system commencing at $22\,480\text{ cm}^{-1}$, whose presence in pure K_2CrO_4 was confirmed more recently by Butowicz [4]. Most probably, the latter band is ${}^1A_1(t_1^6 e^0) \rightarrow {}^1T_1(t_1^5 e^1)$, again by analogy with the corresponding band system of permanganate [5]. In general, it seems that the spectrum of the chromate ion is only modestly affected on passing from the ion in dilute aqueous solution to a solid solution in K_2SO_4 to pure K_2CrO_4 and that its yellow colour primarily results from the tail of the $26\,000\text{ cm}^{-1}$ band stretching down into the visible. On the other hand, it has been stated [6] that the red colour of Ag_2CrO_4 originates from a strong band near 450 nm ($22\,200\text{ cm}^{-1}$) for which there is no obvious analogy in the other spectra we have referred to. Jørgensen [6] assigned the new absorption band to charge transfer from $Ag^+(4d)$ to the empty e-shell of the chromate ion, pointing out that other silver, and also thallium salts of tetroxo and hexahalogeno-anions appeared to have similar bands. Jørgensen's [6] spectrum of Ag_2CrO_4 , like those also measured by Symons and Trevalion [7], was obtained by diffuse reflectance from a powder at room temperature. As part of a programme of experiments designed to obtain precise assignments of the

† Present address : Royal Radar and Signals Establishment, Great Malvern, Worcs.

charge-transfer transitions of tetroxo-ions in crystals [5, 8, 9] we have therefore obtained the polarized spectrum of the chromate ion at 4.2 K, doped in a crystal of Ag_2SO_4 .

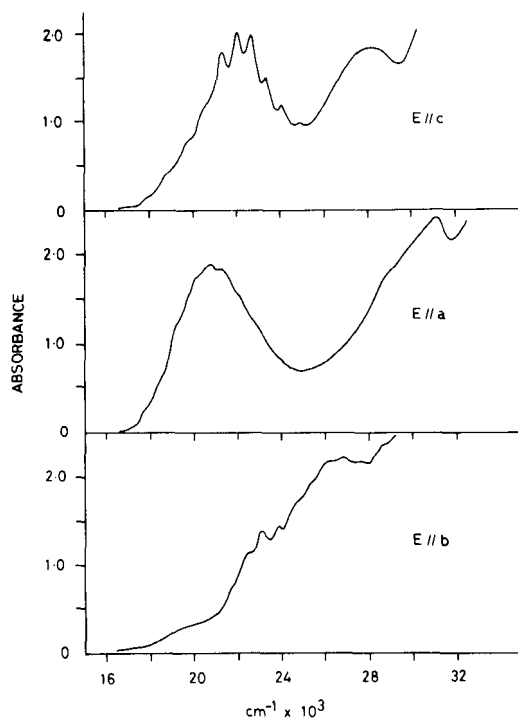
2. EXPERIMENTAL

Silver sulphate crystals, lightly doped with chromate ions, were grown in U-tubes by the gel-diffusion method [10]. The bottom of a U-tube was filled with sodium silicate gel, and after it had set one side-arm was filled with silver nitrate solution and the other with potassium sulphate solution containing a little potassium chromate. Over a period of 1–2 weeks crystals then grew inside the gel.

Silver sulphate is orthorhombic (V_h^{24} ; Fddd) [11] and so three independent linearly polarized spectra should be obtained. Crystals were polished to expose (100) and (010) faces and oriented by Weissenberg photography. The spectra were measured at 4.2 K between 16 000 and 30 000 cm^{-1} by a Cary 14R spectrophotometer equipped with an Oxford Instruments CF 100 continuous-flow cryostat. The incident light was polarized by a calcite Glan prism.

3. RESULTS AND DISCUSSION

The three spectra measured with the electric vector incident parallel to the a , b and c -axes of the crystal are shown in the figure and the energies of the



Electronic spectrum of chromate in silver sulphate. Absorption maxima/ cm^{-1} .

Research notes

895

The 4.2 K polarized absorption spectrum of chromate ions doped in silver sulphate.

$E a$	$E b$	$E c$
(17800)		(18000)
(18600)		(18900)
(19400)	(190)	(19800)
(20200)	(20450)	(20650)
20780	(21700)	21350
21300	22550	22100
22050	23150	22720
22850	23920	23400
		24130
	(24850)	24950
	(25500)	
	26250	
	26880	
	27650	
(29500)	28700	28200
31100		

various peaks are listed in the table. Major peaks, each exhibiting vibrational fine structure, occur in the b and c spectra with their most intense vibronic components at 23 200 and 22 100 cm^{-1} respectively, the former being much weaker than the latter. The corresponding band in the a spectrum peaks at lower energy (20 800 cm^{-1}) and does not have such well-resolved fine structure as the other two. In each spectrum there is also at least one other band at higher energy before we encounter the fundamental absorption edge of the host lattice: in the b and c spectra it lies at 26 880 and 28 200 cm^{-1} respectively, whilst in the a spectrum it is blue-shifted to 31 100 cm^{-1} . Although not so well resolved as in the spectrum of the chromate ion doped in potassium sulphate, in every case where it can be disentangled in the present spectrum the vibrational fine structure is assignable to a progression in a frequency of about 750 cm^{-1} . Such a frequency has also been found [1, 2] in the chromate ion spectrum in potassium sulphate, where it is said to correspond to the $\nu_1(a_1)$ totally symmetric Cr-O stretching mode. Progressions in the same mode are found in the charge-transfer spectra of other tetroxo-ions such as permanganate [9, 12] and manganate [8]. In view of the similarity between the vibrational frequency intervals within the first intense band of chromate in both the potassium and silver sulphate host lattices, as well as the similarity between the overall band shapes and Franck-Condon factors, there seems little doubt that they should be assigned to similar excited states. If this conclusion is accepted, there is no longer any need to invoke Jørgensen's [6] hypothesis of an 'extra' transition of $\text{Ag}^+(4d) \rightarrow \text{Cr}(e)$ type to explain why silver chromate is a different colour from potassium chromate. Rather, it is the result of a substantial red-shift in the ${}^1A_1(t_1^6 e^0) \rightarrow {}^1T_2(t_1^5 e^1)$ transition of the chromate ion itself on passing from the potassium to the silver salt.

Other spectral changes also accompany the red-shift, and are no doubt due to differences in the site perturbations experienced by the chromate ion in the two lattices, quite apart from any differences in the nature of the interactions between the cations and the chromate ion. The crystal structure of silver sulphate, though also orthorhombic, is quite different from that of potassium sulphate. Some controversy surrounded the original structure determination [13, 14] but it seems that it is isomorphous with the phase called Na_2SO_4 (V). Unfortunately, no-one has re-examined the structure since 1932 and inspection of the atomic coordinates reveals that, probably because of the small number of reflections whose intensities could be measured at that time, the sulphate ions were constrained to be regular tetrahedra. Consequently we cannot use the structure of the host lattice as a guide to the magnitude of the site-group perturbation on the chromate ion. Nevertheless, there are a number of striking differences between the structure of potassium sulphate (and chromate) and silver sulphate which help to explain the differences in the spectra of the chromate ion when doped in them. First the coordination around the cation is quite different in the two lattices: in the potassium salt the potassium ion has a very irregular environment of oxygen atoms, giving a coordination number of 9–10, whilst in silver sulphate the silver ions have only five oxygen neighbours [11]. It is worth noticing that silver chromate itself does not have quite the same structure as silver sulphate, but has two crystallographically independent silver ion sites, one roughly a tetragonal bipyramid, the other a distorted tetrahedron [15]. However, the difference between the silver sulphate and potassium sulphate lattices lies in the arrangement of the cations with respect to each other. Whereas the potassium ions in potassium sulphate are separated by oxygen atoms of the sulphate groups, in silver sulphate the silver ions are confined to channels so that they form zig-zag chains parallel to the a -axis. Within these chains the separation of neighbouring silver ions is no more than 3.3 Å. The most strongly perturbed spectrum is the one with the electric vector parallel to a , i.e. to the silver atom chains. Thus the presence of the chains is in some way affecting what must predominantly be an intramolecular charge transfer transition of the tetroxo-anion. The most straightforward explanation would be simply that the anion was being subjected to a particularly large site perturbation, decomposing the 1T_2 tetrahedral parent state into one ${}^1A'$ and two ${}^1A''$ states, in the same way as in the potassium sulphate host. However, in the latter the total energy spread of the three C_s site components is only about 3000 cm^{-1} [2], more or less the same as that of the 2T_2 charge-transfer state of the manganate ion in the same lattice [8, 16]. In the present case, if we assign the three lowest energy absorption bands to low symmetry components of the same tetrahedral parent state, their zero-phonon lines are spread over some 1800 cm^{-1} . A very big distortion of the sulphate groups, and hence of the substituted chromate, would be needed to explain such a big splitting. Whilst this is not out of the question, we would like to suggest an alternative possibility, which might also serve to explain why all three components suffer a substantial red-shift from their positions in the potassium sulphate host. As Jørgensen pointed out [6, 17], the difference between silver(I) and thallium(I) salts as host lattices, compared with alkali metal salts, is that they have readily excitable electrons of their own. This is manifested not only in the fact that they can be oxidized, and so form excited states in which they have transferred an electron to a neighbouring ion, but also

that they have their own intra-ionic excited states, $4d \rightarrow 5s$, $5p$ in the former and $6s \rightarrow 6p$ in the latter. If we are right in assigning the lowest energy bands of chromate in silver sulphate to intramolecular charge transfer of the chromate rather than metal-to-metal charge transfer, both the intermolecular charge transfer and the local transitions of the cations must occur somewhere higher up in the spectrum. In organic molecular crystals one is familiar with Davydov effects, a convenient portmanteau word for shifts and splittings of intramolecular transitions brought about by the crystalline potential and usually described as an interaction between the transition electric dipoles of the molecules [18]. Such an effect has also been suggested recently as an explanation for the large structure dependent red-shifts in the spectra of tetracyanoplatinite crystals [19]. Normally one thinks of first-order Davydov splittings, when a molecular electronic transition splits in a crystal into the same number of components as translationally inequivalent molecules in the unit cell. A further possibility, however, is a second-order Davydov effect, that is, mixing between two non-degenerate intramolecular transitions through the crystal potential, lowering the energy of one and raising that of the other. In the present instance the higher energy transition would be the intra-ionic excitation on the silver ion and the lower the intramolecular charge-transfer excitation of the chromate. The excited states localized on the silver ions would also themselves form an exciton band whose dispersion, because of the chain structure in the silver sulphate crystals, would be extremely anisotropic and so in consequence would be the second-order Davydov shift of any other transition mixed with it. Thus we have a plausible explanation for the greater red-shift of the chromate absorption band in the $E||a$ spectrum. Since the assignments of the higher energy absorption bands of chromate are not clear, even in host lattices such as potassium sulphate, we make no comment here on the higher bands of the ion in the silver sulphate lattice, except that the interval between the first two major bands, at least in the $E||a$ spectrum, is of the same magnitude as in potassium sulphate.

4. CONCLUSIONS

The major conclusion from our study of the 4 K polarized crystal spectrum of the chromate ion doped into silver sulphate is that the first intense band system, between $18\ 000$ and $24\ 000\ \text{cm}^{-1}$ has many of the characteristics of the ${}^1A_1(t_1^6 e^0) \rightarrow {}^1T_2(t_1^5 e^1)$ intramolecular charge-transfer transition whose Franck-Condon maximum is found at about $28\ 000\ \text{cm}^{-1}$ when chromate is doped into potassium sulphate. There is no low-lying transitions which can be assigned as inter-ionic charge transfer from silver $4d$ to the chromate ion. Most probably, therefore, the reason for the red colour of silver chromate is that the first electric-dipole-allowed chromate transition shifts about $5000\ \text{cm}^{-1}$ to lower energy compared with the yellow potassium salt.

We are grateful to the Science Research Council for an equipment grant and a research Fellowship (to D.J.R.).

REFERENCES

- [1] TELTOW, J., 1939, *Z. phys. Chem. B*, **43**, 198.
- [2] DUINCKER, J. C., and BALLHAUSEN, C. J., 1968, *Theor. chim. Acta*, **12**, 325.

- [3] SCHATZ, P. N., McCAFFERY, A. J., SENTAKA, W., HENNING, G. N., RITCHIE, A. B., and STEPHENS, P. J., 1966, *J. chem. Phys.*, **45**, 722.
- [4] BUTOWIEZ, B., 1970, *J. Phys., Paris*, **31**, 477.
- [5] COLLINGWOOD, J. C., DAY, P., DENNING, R. G., ROBBINS, D. J., DiSIPIO, L., and OLEARI, L., 1972, *Chem. Phys. Lett.*, **13**, 567.
- [6] JØRGENSEN, C. K., 1963, *Acta chem. scand.*, **17**, 1034.
- [7] SYMONS, M. C. R., and TREVALION, P. A., 1962, *J. chem. Soc.*, p. 3503.
- [8] DAY, P., DiSIPIO, L., INGLETTO, G., and OLEARI, L., 1973, *J. chem. Soc., Dalton Trans.*, p. 2595.
- [9] COX, P. A., ROBBINS, D. J., and DAY, P., 1975, *Molec. Phys.*, **30**, 405.
- [10] HENISCH, H. K., 1965, *Crystal Growth from Gels* (University of Pennsylvania Press).
- [11] WYCKOFF, R. G., 1968, *Crystal Structures*, Vol. 3, 2nd edition (John Wiley & Co.), p. 109.
- [12] HOLT, S. L., and BALLHAUSEN, C. J., *Theor. chim. Acta*, **7**, 313.
- [13] HERREMAN, K., and ILGE, W., 1931, *Z. Kristallogr.*, **80**, 402.
- [14] ZACHARIASEN, W. H., 1932, *Z. Kristallogr.*, **82**, 161.
- [15] HACKERT, M. L., and JACOBSON, R. A., 1971, *J. Solid-st. Chem.*, **3**, 364.
- [16] DiSIPIO, L., OLEARI, L., and DAY, P., 1972, *J. Chem. Soc., Faraday Trans. II*, **68**, 1032.
- [17] JØRGENSEN, C. K., 1961, *Molec. Phys.*, **4**, 235.
- [18] CRAIG, D. P., and WALMSLEY, S. H., 1968, *Excitons in Molecular Crystals* (Benjamin).
- [19] DAY, P., 1975, *J. Am. chem. Soc.*, **97**, 1588.

Reprinted from
ANNALS OF THE NEW YORK ACADEMY OF SCIENCES
Volume 313 Pages 9 – 24
September 29, 1978 26214

PART I. GENERAL PAPERS

**CHEMICAL CLASSIFICATION OF STRUCTURES AND
PROPERTIES OF LOW-DIMENSIONAL
INORGANIC COMPOUNDS***

P. Day

Oxford University
Inorganic Chemistry Laboratory
Oxford OX1 3QR, England

Efforts to find relationships between the crystal and electronic structures of compounds and their physical properties form the lifeblood of physical inorganic chemistry and much of solid-state physics. Ground rules for describing the electronic structures of simple molecules and solids have been available for just about fifty years now, in the form of the Heitler-London (or valence bond) model and the molecular orbital (or band) model. However, the immense variety of structures and compound types available to the chemist, as well as increasingly ingenious efforts in the field of synthesis, constantly challenge our understanding and force us to renew and refine criteria for physical behavior that previously seemed adequate to describe the paradigm cases known to the physicist. The materials whose properties form the subject matter of the conference on which this annal is based present us with many illustrations of this proposition. It may be appropriate to begin by mentioning just one of them.

In 1949 Mott¹ pointed out that quite different physical properties would be expected from compounds whose ground states were best described by a Heitler-London wavefunction from those which one would expect of a compound whose ground state was described by a molecular orbital or band wavefunction. The simplest example is that of a chain of atoms, each carrying a single valence electron. The Heitler-London wavefunction describes a ground state that is insulating, with exactly one electron localized on each atom, and with a considerable activation energy needed to create the charge fluctuations required for conductivity. The molecular orbital model, by contrast, would give us an exactly half-filled band, which permits charge fluctuations, or in other words, ionic states, and hence describes a conductor. Clearly there has to be some crossover from the realm of validity of one model to the other as a function, for example, of orbital overlap, interatomic spacing, electronic density, or some other comparable variable. Much effort over the last twenty years has gone into a search for inorganic compounds lying sufficiently close to this boundary on either side that applying some external variable such as pressure or temperature would transform the ground state from insulating to conducting. Much interesting structural chemistry and solid-state physics, mainly of oxides,² has come out of this activity, but the point I wish to make here is that it now appears that there exists at least one whole class of substance to which Mott's idea, at any rate in its simplest form, does not apply. According to the Mott-Hubbard model, if there is an integral number of electrons per

*Manuscript received August 31, 1977.

site we either have a metal or else an insulator in which each site carries the same number of localized valence electrons. Consider, however, the many metal atom chain compounds of which Wolfram's Red Salt, $[\text{Pt}(\text{EtNH}_2)_4][\text{Pt}(\text{EtNH}_2)_4\text{Cl}_2]\cdot\text{Cl}_4\cdot 4\text{H}_2\text{O}$, could be thought of as a prototype. These compounds are insulators (at least at ambient pressure,³ and when not deliberately doped with impurities), and the average Pt oxidation state is +3. Yet there are many reasons⁴ for believing that in fact the oxidation states of the Pt atoms alternate between +2 and +4. Instead of having one electron in each $5d_{z^2}$ orbital on every Pt atom we have alternately two and none. Why?

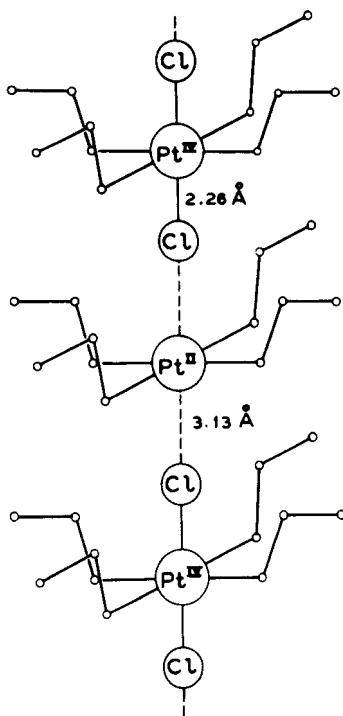


FIGURE 1. The chain structure of Wolfram's Red Salt.

The answer is that if we introduce into our chain of atoms, each carrying one valence electron, a closed-shell atom or molecule bridging every pair of adjacent atoms, then in addition to the intrasite electron correlation U and the intersite transfer integral t (which a chemist would call the electron repulsion parameter and resonance integral), we have a third variable, namely, an electron-phonon coupling constant. Inclusion of the latter can apparently make it energetically favorable for the valence electrons to pair up on alternate centers, displacements of the bridging groups providing the extra variable in the structure that leads to the new kind of ground state.

I mention this example at the outset because it illustrates how even one of the simplest structures one could envisage, the diatomic chain . . . ABABA . . . , contains features that require us to reappraise some of the most fundamental hypotheses of solid-state theory. Yet although we can write the "operative" part of the chain in a straightforward way, the formula of Wolfram's Red Salt given above and shown in FIGURE 1 exemplifies how relatively complicated molecular architecture is often needed before the requirements for physical behavior approximating to one- or two-dimensional can be realized. There can be no doubt, however, that the incursion into solid-state physics of a whole new range of chemical substances containing layers or chains of interacting atoms has been a strongly revitalizing intellectual influence in the last few years, bringing in its wake both new physical phenomena such as Peierls distortions and charge-density waves, and also a new kind of partnership between chemists and physicists. The object of this paper is to introduce, from a chemist's point of view, some of the compounds whose physical properties are going to be dealt with in detail by later authors, but at the same time to attempt at the broadest level some kind of synthesis between structure and properties in the low-dimensional field. Mere categorization in itself is of little value unless based on a proper appreciation of the magnitudes of the electronic factors that bring about the observed patterns of behavior.

Let us return for a moment to the Hamiltonian describing a chain of atoms, using the form introduced by Hubbard.⁵ For hydrogen-like atoms it would be written in its simplest form as

$$\mathcal{H} = \sum_{\sigma} \sum_{ij} C_{i\sigma}^{\dagger} C_{j\sigma} t_{ij} + U \sum_i n_{i\sigma} n_{i-\sigma}$$

where the summation is taken over all nearest neighbor ions i, j , on which the electron may have a spin of $\pm\sigma$. The spin direction, of course, is conserved when the electron hops from site to site, but two electrons with opposed spins on the same site repel one another to an extent determined by U . Confining our attention to compounds between metallic elements and ones with rather higher electronegativity, such as C , N , and O (though possibly also P and S), the electrons whose behavior determines the collective properties of the solid are the valence-shell electrons on the metal atoms. The transfer integral t_{ij} is therefore going to be a strong function of the metal-metal separation, which, in turn, is going to depend on the size and nature of any bridging groups or anions. If the only pathway between the metal ions lies through such bridges, transfer between the metal ion orbitals could only take place to the extent that there is a set of orbitals on the bridging group nonorthogonal to both sets of metal orbitals, and in proportion to the resulting metal-ligand covalency. Mixing between metal and ligand orbitals is of course governed by the usual symmetry considerations, which also underlie the simple rules relating the dominant sign of the magnetic exchange between localized electrons in partly filled subshells, and interacting through intervening anions, as set out originally by Kanamori⁷ and Goodenough.⁸ These rules have their basis in a perturbation approach⁹ to electron delocalization between metal and ligand orbitals which attempts to estimate metal-ligand electron transfer by supposing mixing between two Heitler-London configurations containing different

numbers of electrons on the two centers, for example $M^{2+}A^-$ and M^+A^0 . Electronic transitions between configurations of this kind are, quite simply, charge-transfer transitions. In favorable cases it may even be possible to locate the excited state in question in the optical spectrum and hence, by estimating metal-ligand resonance integrals by appropriate overlap integrals, to calculate how much electrons occupying (for example) d-orbitals are delocalized from one metal ion to another through an intervening ligand. In the context of some of the metal-organic substances to be discussed in this volume it is important to realize that, although

TABLE I
SOME SINGLE-VALENCE LOW-DIMENSIONAL INORGANIC COMPOUNDS

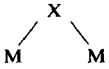
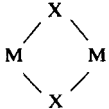
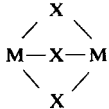
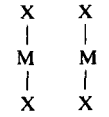
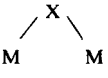
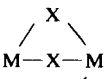
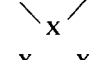
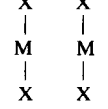
Geometry of Bridging Groups	Chains	Layers
$M-X-M$	Silicates (pyroxenes, amphiboles) $Sr(PbF_5)F$ $NbOCl_3$ $FeF_3 \cdot 3H_2O$	Silicates (micas and clays, e.g. montmorillonite) K_2NiF_4 and related compounds (Rb_2MnF_4 , Cs_2CrCl_4 , etc.) Organic intercalated structures related to $K_2NiF_4((RNH_3)_2MX_4)$ High-oxidation state ternary oxides (e.g. Ca_2MnO_4)
	Nonmetal oxides (SeO_2 , Sb_2O_3) Polymers of non-metals (e.g. SN_x) CrO_3	
	4-coordinate (a) tetrahedral ($BeCl_2$, SiS_2 , $KFeS_2$) (b) planar ($PdCl_2$, PtS) 6-coordinate with terminal groups $MX_2 \cdot 2Y$ (X = halogen, Y = H_2O , pyridine, $\frac{1}{2}$ phenanthroline etc.)	MX_2 (a) halides of 3d elements ($FeCl_2$ etc.) (b) chalcogenides of 4d and 5d elements (TaS etc.) Oxyhalides ($FeOCl$)
	Hexagonal perovskites (a) halides AMX_3 (A = group IA or organic cation; M = V, Cr, Mn, Fe, Co, Ni, Ca) (b) oxides (e.g. $BaNiO_3$)	—
	Planar d^8 complexes (a) anions: $A_2[Pt(CN)_4]$ (b) neutral molecules: $Nidmg_2$, $Ptbipy_2Cl_2$ (c) salts: $[Pt(NH_3)_4][PtCl_4]$	metal-rich phases: $GdCl$

TABLE 2
SOME MIXED-VALENCE LOW-DIMENSIONAL INORGANIC COMPOUNDS

Geometry of Bridging Groups	Chains (1D)	Layers (2D)
M—X—M	Pt(NH ₃) ₂ Cl ₃ , Wolfram's Red Salt, etc. Magnetic phases Mo _n O _{3n-1}	Ca _{2-x} Y _x MnO ₄
	B-subgroup oxides: Pb ₃ O ₄ , Sb ₂ O ₄ TIS	KCu ₄ S ₃
	—	—
	K ₂ Pt(CN) ₄ Br _{0.30} · 3H ₂ O(KCP) K _{0.60} Ir(CO) ₂ Cl ₂ · O · 5H ₂ O Gd ₂ Cl ₃	GaS metal-rich phases: Ag ₂ F, Hf ₂ S
		

the kind of strategy we have just described has been applied conventionally to monoatomic bridging anions like oxide¹⁰ or halides, there is no reason at all why we should not use it to calculate electron delocalization through polyatomic ligands that bind simultaneously to two metal ions. The formalism can be applied in a particularly neat fashion when the ligands have conjugated systems of π -orbitals, since one can then use a simple Hückel calculation as a guide to the molecular orbital coefficients in the frontier orbitals (organic chemist's nomenclature for the highest occupied and lowest unoccupied) and even to their energies. We ourselves demonstrated this point a few years ago by calculating "valence delocalization coefficients" for mixed valency Fe(II,III) and Ru(II,III) dimers and polymers in which the metal ions are bridged either by the monoatomic oxide ion, diatomic cyanide,¹¹ or the aromatic molecule pyrazine.¹²

In TABLES 1 and 2 are set out a series of representative examples of metal atom layer and chain compounds, categorized according to the number, and hence the geometrical arrangement, of the groups bridging the metal atoms. Clearly we cannot include every one of the enormous number of layer and chain compounds now known, but an attempt has been made to include at least one member of each of the major types. Several generalizations can be made immediately on inspecting these lists. First, there is a straightforward distinction between continuous and molecular lattices; that is, between solids in which the strongest low-dimensional interactions are carried between the metallic centers through bonds and those made up from discrete molecular units having an independent chemical existence—for example, in solution or in the gas phase. The latter comprise only chain examples because they appear to be formed exclusively by flat molecules. In that connection it is worth noticing in passing that even the most electronically innocuous aromatic hydrocarbon molecules form distinctly chain-like stacks in

crystals for this very simple reason, although the details of the structures themselves are determined by repulsions between nonbonded hydrogens on neighboring molecules. A second point is that although a few examples of compounds containing only nonmetallic elements have been included, the overwhelming proportion of the examples in TABLES 1 and 2 are compounds of metals. Polymers of nonmetals exist in large numbers, of course (e.g. silicones, phosphonitrilics, and even hydrocarbons!), but few have electronic properties that would make them interesting to a meeting of this kind.

Apart from those molecular solids consisting of essentially planar units, for which packing efficiency alone might justify columnar structures, it is an interesting and not very easy question why three-dimensional lattices should order themselves in such a way as to produce columns or layers of closely spaced atoms. In nonmetallic elements simple operation of the (8-N)-rule based on the attainment of a closed-shell valence-bond configuration is a sufficient explanation. For instance, sulphur atoms in Group VI bind two neighbors and so give chains, whereas the three near neighbors bond in pyramidal configuration around phosphorus define the infinite puckered sheets found in black phosphorus. Among some classes of compound, too, empirical regularities become clear. In the perovskites, ABX_3 , there exists a very large body of lore¹³ about the conditions needed to produce the hexagonal arrangement, in which chains of octahedral BX_6 groups share opposite faces, rather than the cubic type, with BX_6 groups sharing only apices. According to Stucky and his colleagues,¹⁴ the hexagonal arrangement is favored by increasing ligand field stabilization energy, larger X groups and, up to a point, larger A groups, though beyond a certain point large organic cations may favor the formation of discrete molecular anions such as $NiCl_4^{2-}$.

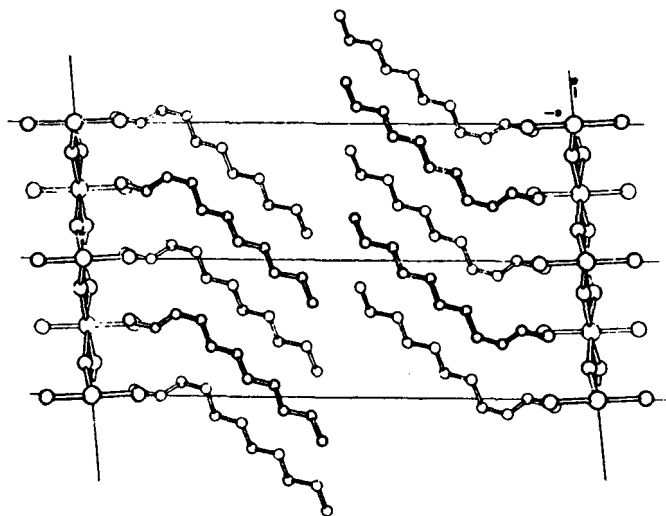


FIGURE 2. The alternating layers of organic and inorganic material in $(C_{10}H_{21}NH_3)_2MnCl_4$.¹⁵

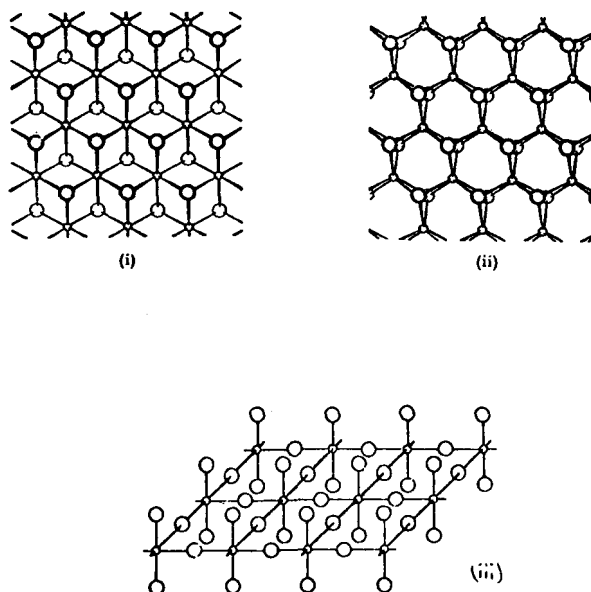


FIGURE 3. MX_2 layers. (i) CdCl_2 and CdI_2 , (ii) MoS_2 , (iii) K_2NiF_4 .

Similar correlations with ionic sizes, and consequently preferred coordination numbers, can be found among the compounds with a stoichiometry A_2BX_4 , where X is a halogen and A a unipositive cation. Larger X favor smaller coordination numbers around B and so produce lattices containing discrete tetrahedral molecular anions like NiI_4^{2-} . Similarly, bulky A ions lead to discrete molecular anions. On the other hand, small A, such as the lighter Group IA cations, combined with small X (F^-), form compounds with 6-coordination around B, and hence infinite layer anions of the type found in the K_2NiF_4 structure. Shape, as well as total volume, of an organic A-group is also an important influence on the type of lattice formed by the B and X groups with which it is combined. For example, tetra-alkylammonium cations, being bulky but also roughly spherical (or at any rate crab-shaped), yield compounds containing tetrahedral BX_4 anions packed in a three-dimensional array, but monoalkylammonium cations, being roughly cylindrical with the positive charge located at one end, give A_2BX_4 compounds in which the organic and inorganic constituents are segregated from one another, as in FIGURE 2.¹⁵ Willett discusses the magnetic properties of some of these unusual sheet compounds in this volume.

In simple binary compounds MX_2 electronic considerations are as important as mere size in determining whether a three-dimensionally infinite lattice or a layer lattice is formed. For example, many transition metal oxides with the stoichiometry MO_2 have lattices based on the rutile structure, i.e., essentially three-dimensional, while the corresponding sulphides, selenides, and tellurides have layer structures, either of the CdX_2 type, as shown in FIGURE 3(i), or like MoS_2 (FIGURE 3(ii)),

containing metal ions coordinated by trigonal prisms of chalcogenide atoms. In describing the factors influencing the choice between octahedral metal atom coordination, as in the layers of TiS_2 , with trigonal prismatic as in MoS_2 and WS_2 , it may be relevant to recall that among the very small number of discrete molecular coordination complexes with trigonal prismatic coordination, 5d elements in Groups VI and VII and sulphur ligands such as dithiolates figure strongly.¹⁶ Among halides, too, we find a similar general correlation between ligand electronegativity and propensity for forming layer lattices. Thus the difluorides of the 3d elements have mostly rutile structures but the heavier halides have either CdCl_2 or CdI_2 structures, although all have octahedral coordination around the metal atoms.¹⁷

A further category of materials containing layers or chains of closely spaced atoms, which have begun to assume greater importance in the last few years, are what one might call the "metal-rich" phases. Usually halides or chalcogenides, these are commonly made by reacting a "normal" compound such as GdCl_3 with excess metal. In the Gd case, which is quite typical, one finds compounds Gd_2Cl_3 , containing chains of Gd_6 octahedra,¹⁸ and eventually GdCl , in which these octahedra have become linked together to form sheets.¹⁹ The structural systematics of this transformation, based on the idea of progressively condensing M_6X_8 groups, have been neatly illustrated by Simon²⁰ (FIGURE 4), who has also reviewed the entire field. Mixed valency metal-rich layer halides like Ag_2F , with the anti- CdI_2 structure, have been known for many years,²¹ but have more recently been joined by the chalcogenides Hf_2S ,²² Nb_2Se ,²³ and so on. In all examples of this type the concentration of metal atoms is sufficiently high for one to be able to talk of metallic lattices, in one or two dimensions, separated by nonmetal atoms.

Contrasting with the kind of metallic chains in metal-rich compounds, in

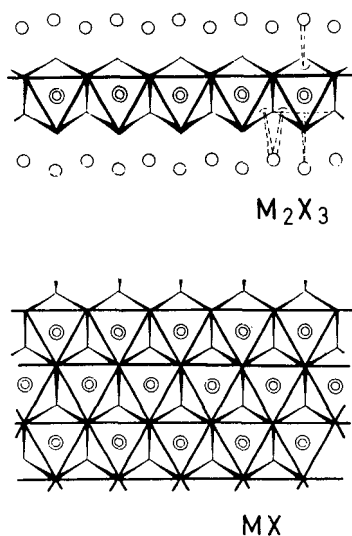


FIGURE 4. Derivation of metal-rich chain and layer structures by condensing M_6X_8 units.²⁰

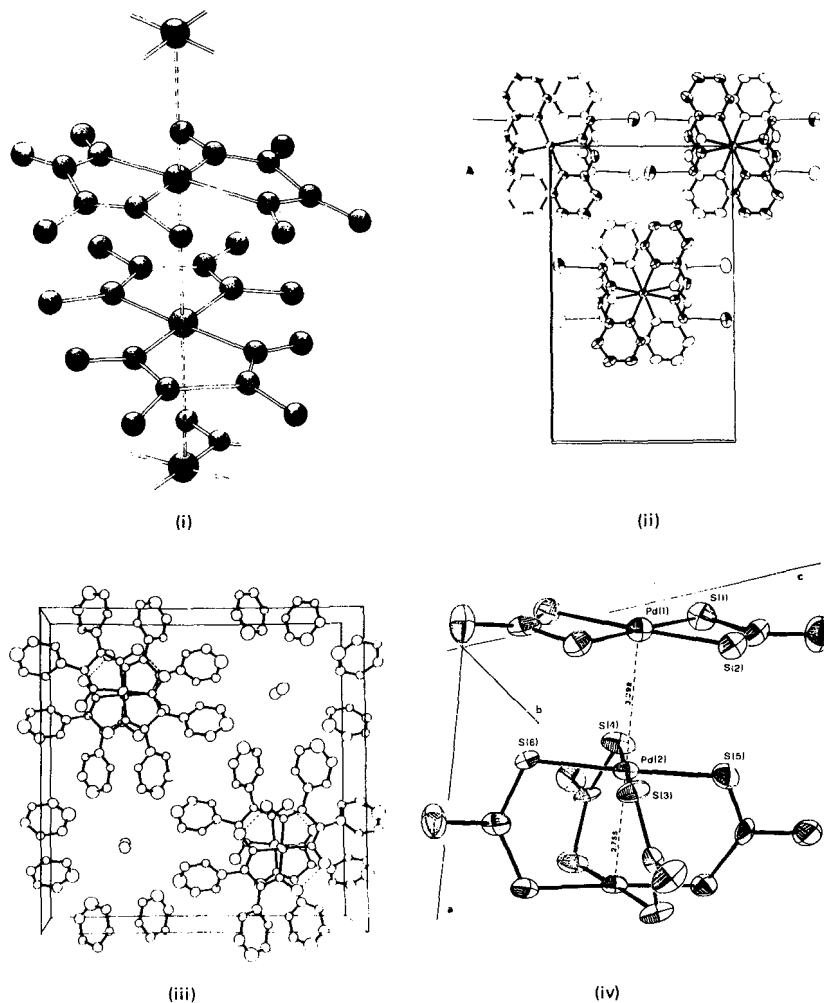


FIGURE 5. Examples of metal chain compounds. (i) Bis(dimethylglyoximate)Ni(II),²⁴ (ii) Bis(N-ethylpyridinecarboxaldimate)Pt(II),²⁹ (iii) Bis(diphenylglyoximate)Ni(II) iodide,²⁵ (iv) Bis(dithioacetato)Pd(II).³¹

which the repeat unit is itself a metal cluster, metal atom chain compounds formed by square planar complexes containing more elaborate ligands and chelating agents are characterized by strings of singly connected metal atoms. Whether the average oxidation state of the metal atoms is integral or not, simple strings of metal atoms then form the dominant structural feature. How much electrons, excitons, magnons, or phonons propagating on one stack are influenced by what is

happening on neighboring stacks depends on such factors as the size of the ligands around the metal ions and hence the distance between the stacks, the extent to which electrons in the valence orbitals of the metal ions are delocalized on to the ligands through conjugation, or connections between ligands on neighboring chains through hydrogen-bonding. Some examples will illustrate the rich variety of chemical variation possible. FIGURE 5 shows four instances of stacked planar metal complexes containing oxygen, nitrogen or sulphur-donor ligands. Bis-(dimethylglyoximato)Ni(II)²⁴ (i) was one of the first such complexes whose structure was determined, and it illustrates how closer metal-metal spacings are achieved by rotating successive molecules in the stack through 90° so that Van der Waals repulsions between the filled orbitals of the conjugated ligands are minimized. Similar packing is found in bis(diphenylglyoximato)Ni^{II} iodide²⁵ (iii), where the methyl groups of (i) have been replaced by phenyls, with the result that the stacks are now much further apart. One result of this bigger separation is that the structure contains channels which, in (iii) are filled by iodine, proved by resonance Raman experiments to be in the form of I₃⁻. A common structural feature of such "tunnel" compounds is variable composition (compare, for example, the hexagonal tungsten bronzes), and compounds related to (iii) depart substantially from the formal Ni:I stoichiometry of 1:1.²⁶ Note, though, that even if the Ni:I ratio were 1:1 the metal atom chain would still be mixed valency, since the iodine is present as I₃⁻. As we shall see later, mixed valency is a fundamental requirement for high conduction in this class of compound. In fact, the compound (iii) has a specific conductivity at least 10⁵ greater than that of the parent unoxidized material. Another recently discovered series of compounds, no doubt related in structure to (iii), are the transition-metal phthalocyanine polyiodides,²⁷ which have very low activation energies and room-temperature conductivities as high as 1 ohm⁻¹cm⁻¹, although one has to be cautious about attributing the electron transport to d-band overlap, since the metal-free derivative also has a high conductivity. The contributions of Keller and Marks to this annal deal with this type of compound. A different mode of overlap between planar conjugated organic ligands is shown in FIGURE 5(ii), where projecting methyl group substituents also separate the stacked molecules.²⁸ It is a good illustration of the way in which substituents can modify metal-metal overlap, because in the corresponding unsubstituted complex, which also forms stacks,²⁹ the Pt-Pt spacing is 3.245 Å, compared with 3.363 Å in the methyl compound. Clearly, the closer one can bring the metal atoms together in these stacks, the stronger the interaction between them will be. Particularly close intermetallic spacings can sometimes be achieved in complexes of sulphur-donor ligands such as the dithiolates, though in bis(ethylenedithiolate) Pd(II) and -Pt(II) this results in formation of discrete dimers, which are not themselves stacked together.³⁰ Another fascinating possibility (FIGURE 5(iv)) is to join the planar units together by means of bridging ligands, in this case simply dithioacetate, but while the really close contact (2.755 Å) takes place within a discrete dimer, one crystal modification of bis(dithioacetate)Pd(II) contains stacks of dimers, and another contains stacks consisting of alternating dimers and monomers.³¹

It seems to be a reasonable generalization that for really substantial intermetallic interactions in stacked planar Group VIII metal complexes, sufficient, for

example, to yield a high conductivity, the metal-metal spacing should be less than about 3.1 Å. Thus the Schiff base complex of FIGURE 5 (ii) is rather a good insulator. This requirement creates a fundamental difficulty when the ligands bound to the metal ions contain π -electrons, because the metal ions are required to be closer together than the normal Van der Waals approach distance between conjugated organic molecules. In cases where the four groups bound in a square plane around the metal ion have a rod-like shape, for instance, cyanides, the steric problem can be solved by rotating alternate metal complex molecules in the stack so that the ligands avoid one another. Williams and his colleagues³² have pointed out that in a series of tetracyanoplatinite salts, with both single and mixed valency, there appears to be a rough correlation between Pt-Pt spacing and the torsion angle between adjacent $\text{Pt}(\text{CN})_4$ units, varying from a completely eclipsed arrangement

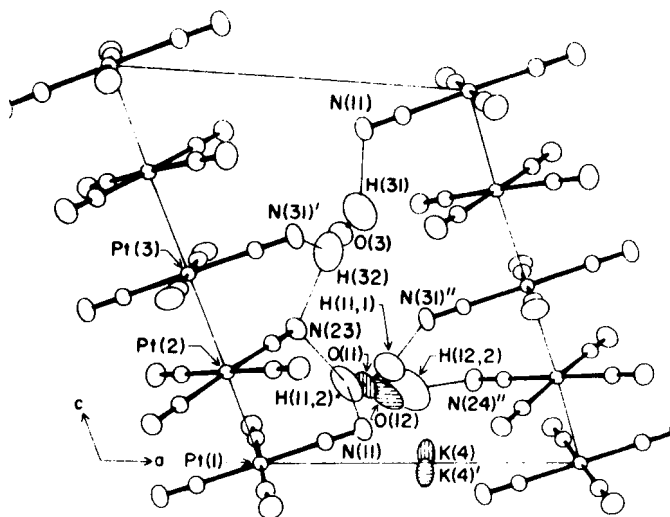


FIGURE 6. Interchain hydrogen bonding in $\text{K}_{1.75}\text{Pt}(\text{CN})_4 \cdot 1.5\text{H}_2\text{O}$.^{32,34}

in $\text{Na}_2\text{Pt}(\text{CN})_4 \cdot 3\text{H}_2\text{O}$ (Pt-Pt spacings 3.65 and 3.75 Å) to completely staggered in $\text{K}_2\text{Pt}(\text{CN})_4\text{Br}_{0.30}3\text{H}_2\text{O}$ (Pt-Pt spacing 2.89 Å). The point is developed further in Williams' contribution to this volume. On the other hand, Van der Waals repulsion between the cyanides cannot be the only factor determining the torsion angle because in $\text{Rb}_2\text{Pt}(\text{CN})_4 \cdot 1.5\text{H}_2\text{O}$, with a Pt-Pt spacing of 3.48 Å the torsion angles vary from 29.2 to 35.2°, but in $\text{Rb}_2\text{Pd}(\text{CN})_4 \cdot \text{H}_2\text{O}$ (Pd-Pd spacing 3.72 Å) the torsion angles are only 15.7–16.8°. Since this class of compound invariably contains water molecules separating the stacks along with the alkali metal cations, the other important influence on the arrangement of the cyanide groups is hydrogen-bonding to the nitrogen atoms. A particularly clear illustration of this phenomenon is $\text{K}_{1.75}\text{Pt}(\text{CN})_4 \cdot 1.5\text{H}_2\text{O}$ ^{32,34} (FIGURE 6).

Among the low-dimensional compounds we have been describing are examples of metals, insulators, semiconductors, superconductors, ferromagnets, antiferromagnets, and so on; i.e., just about every kind of solid-state physical behavior that could possibly be found. One might perhaps just be tempted to say, therefore, that the electronic factors that determine this behavior are only a trivial extension of the well-known principles at work in simple three-dimensional lattices, like the transition metal oxides. In general terms this is, of course, true. The symmetry requirements of orbitals involved in direct or indirect magnetic exchange pathways and the balance of on-site or intersite electron repulsion and transfer integrals, for example, are all "local" factors dependent on near-neighbor pairwise interactions and thus independent of dimensionality as such. Nevertheless, restricting the dominant intermetallic interactions to one or two dimensions by the kind of structural constraints we have been describing has two important consequences. First of all, the correlation of structure and properties is greatly simplified, because of the smaller number of interaction pathways that have to be taken into account. Second (and from the point of view of physical theory, very intriguingly and productively) is the appearance of a whole new realm of phenomena confined specifically to low-dimensional materials. The latter, for example, charge-density waves and Peierls distortions, are the subject of several other contributions to this conference.³⁵ On the other hand, the question of a broader chemical correlation between structure and property in low-dimensional materials has not been very widely examined.

After surveying the properties of many different kinds of metal atom chain compounds, it was argued in Reference 4 that four broad groupings of physical behavior could be distinguished, and that these were correlated, on the one hand, with whether the most important near neighbor metal-metal interaction was by direct overlap or *via* a bridging ligand, and on the other hand, with whether the compound was of single or mixed valence. These ideas have been developed at greater length in Reference 36, but we conclude this introductory paper by summarizing them here.

Briefly, our thesis is that each of the four categories just mentioned is characterized by a quite distinct pattern of physical behavior, with only a very small number of exceptions. Thus, among single-valence metal chain compounds in which the intermetallic interaction is carried by bridging anions, for example the hexagonal perovskites, there are no metallic conductors, and the overwhelming proportion are magnetic insulators. Single-valence metal chains having direct metal-metal contact are likewise insulating, unless doped with mixed-valence impurities, but in the best-known examples, such as the tetracyanoplatinates or Magnus' Green Salt, the intermetallic interaction is strong enough to have quite a marked effect on their optical properties, as described by Yersin (this volume). Nevertheless, because they are not photoconductors,³⁷ one has to conclude that even in the excited state electrons and holes do not become uncoupled. Indeed, in the tetracyanoplatinates the way in which the energies of the excited states vary with intermetallic distance strongly supports the view that they should be described to a first approximation as neutral Frenkel excitons propagating along the stacks of molecules.^{38,39}

Mixed valency, defined either as fluctuating or nonintegral electron occu-

pancy of each metal atom site, is a potent factor leading to higher conduction in chain compounds because much less energy is needed to move a charge fluctuation already built into the chain than to create an electron-hole pair in a chain in which each metal atom carries the same integral charge. It is interesting to note that an explanation along these lines has also been put forward⁴⁰ for the high conductivity of the organic charge-transfer salts such as TTF-TCNQ which contain segregated stacks of donor and acceptor molecules. Nevertheless, not all mixed valence metal chain compounds conduct; the example we began with—Wolfram's Red Salt—is a good insulator. This is because chains containing anions or molecules bridging between the metal atoms have, as we showed above in the case of Wolfram's Red Salt, a very simple mechanism of electron-phonon interaction that pins the phase of the charge fluctuation along the chain. The result is a simple superlattice of metal oxidation states (... II, IV, II, IV... in Wolfram's Red Salt) which places the system in class II of our old classification of mixed-valence compounds⁴¹ and consequently leads to an insulating ground state. Still, in mixed-valence anion-bridged metal chains the lowest optically accessible excited state is no longer a neutral Frenkel exciton but an ionic exciton arising from an intervalence charge-transfer transition. The Franck-Condon transition energy of this kind of state is usually of the order of 1–2 eV³⁶ (the origin of the red color of Wolfram's Salt), but the relaxed excited state must be much lower. How far is the bridging anion displaced when an electron is transferred from Pt(II) to Pt(IV) in Wolfram's Salt? An elegant means of answering this question is resonance Raman spectroscopy, as shown in this volume by Clark. It is precisely the axial stretching mode between the metal and the bridging anion that is selectively enhanced in intensity when one excites the Raman spectrum of this type of compound by irradiating within the Franck-Condon envelope of the intervalence absorption band. The relative intensities of successive overtones of this fundamental enable one to estimate how far along the vibrational coordinate the oscillator is displaced in the relaxed electronic excited state. A calculation⁴² based on Mingardi and Siebrand's⁴³ theory of the resonance Raman effect suggests that at the minimum in the potential energy surface of the Pt(II) → Pt(IV) charge-transfer excited state, the bridging halide ion indeed is nearly equidistant from the two Pt ions, as expected if the Heitler-London configuration of the state is close to Pt(III), Pt(III).

All this implies very strongly that mixed-valence metal chain compounds with bridging groups are unlikely to be good conductors. Removing the bridging groups and bringing the metal atoms into direct contact has two consequences which are expected to increase the chances of finding high conductivity. First, the transfer integral is enhanced but equally important, if charge-compensating anions, necessarily present in simple stoichiometric ratios, are removed from the metal chain itself and placed in sidegroups or channels between the metal chains; one then has an opportunity of varying the average oxidation state, or electron occupancy of the metal atoms' valence shells, away from simple ratios 1:1, 1:2, and so on. This is important if one is to stabilize a conducting ground state, partly because electron-phonon interactions that may trap the desired charge mobility are thereby weakened, but also because the active phonons might have wave-vectors incommensurate with the underlying lattice. Should that be the case the resulting charge-density wave might still be able to carry a current. By contrast, in Wolf-

TABLE 3
 PROPERTIES OF METAL-CHAIN COMPOUNDS WITH EXAMPLES FROM THIS VOLUME

	Properties			Examples
	Optical	Magnetic	Electron Transport	(This Volume)
Single Valence Bridged	discrete weak ligand field transitions	weak ferro- or antiferromagnetic superexchange	insulators	Willett
Direct	ligand field bands strongly perturbed. Allowed bands strongly shifted by dipolar coupling.	diamagnetic	insulators conducting under pressure	Williams, Yersin Gordon <i>et al.</i> , Geoffroy, <i>et al.</i>
Mixed Valence Bridged (Robin-Day class II)	lowest transition is ionic exciton ($M \rightarrow M$ charge transfer)	diamagnetic	semiconductors metallic under high pressure	El Sharif <i>et al.</i> , Meyer Taube
Direct (Robin-Day class III)	plasma edge in visible reflectivity		metals at 300°K become semiconducting at low temperature (Peierls distortion)	Williams, Underhill, Reis, Chartier <i>et al.</i> , Metgert <i>et al.</i> , Stucky <i>et al.</i> , Balch, Keller, Marks, Endres

ram's Red Salt one might regard the superlattice of trapped oxidation states as a consequence of a strong Peierls distortion, producing a static charge-density wave with a wave-vector of 0.5 in the Brillouin zone of the original undistorted diatomic chain. It is in fact among the mixed-valence directly interacting metal chains that the one-dimensional metallic conductors are found, for instance KCP ($\text{K}_2\text{Pt}(\text{CN})_4\text{Br}_{0.30} \cdot 3\text{H}_2\text{O}$) and its cation-deficient analog in FIGURE 6. Much more is written about them later in this volume. In TABLE 3 we simply summarize the behavior of the four categories of metal chain. Although much of the recent excitement about low-dimensional compounds has resulted from the fact that one could even synthesize such things as "molecular metals" (a conjunction of adjective and noun that would have sounded totally paradoxical five years ago), I believe that as chemists and physicists we should not lose sight of the sheer variety of other types of physical behavior accessible to us through this very broad class of substances. Potentially most exciting of all, though, is the opportunity it presents for chemists to devise quite new kinds of material showing phenomena unpredictable by the physical theories designed in earlier days to rationalize the behavior of much simpler substances. It is to be hoped that the introductory survey presented here has succeeded both in showing some of this variety and setting out some chemical guidelines by which crystal and electronic structure may be related to properties in this fascinating group of substances.

NOTES AND REFERENCES

1. MOTT, N. F. 1949. *Proc. Phys. Soc. (London)* **A62**: 416.
2. ADLER, D., for example. 1968. *Rev. Mod. Phys.* **40**: 729.
3. INTERRANTE, L. V. & F. BUNDY. 1974. *Inorg. Chem.* **13**: 1158.
4. DAY, P. 1974. *In Extended Interactions between Transition Metal Ions*. L. Interrante, Ed.: 234. Amer. Chem. Soc. Washington, D.C.
5. HUBBARD, J. 1963. *Proc. Roy. Soc.* **A276**: 238.
6. GRAY, H. B. & C. J. BALLHAUSEN. 1962. *Molecular Orbital Theory*. Benjamin. New York, N.Y.
7. KANAMORI, J. 1959. *J. Phys. Chem. Solids* **10**: 87.
8. GOODENOUGH, J. B. 1960. *Phys. Rev.* **117**: 1442.
9. ANDERSON, P. W. 1950. *Phys. Rev.* **79**: 350.
10. NESBET, R. K. 1960. *Phys. Rev.* **119**: 658.
11. MAYOH, B. & P. DAY. 1973. *J. Chem. Soc., Dalton Trans.*: 846.
12. MAYOH, B. & P. DAY. 1974. *Inorg. Chem.* **13**: 2223.
13. GOODENOUGH, J. B. & J. M. LONGO. 1970. *In Landolt-Bornstein Tabellen. New Series, Group III. Vol. 4*.
14. SEKUTOWSKI, D., R. JUNGST & G. D. STUCKY. 1974. *In Extended Interactions between Transition Metal Ions*. L. Interrante, Ed.: 142. Amer. Chem. Soc. Washington, D.C.
15. CIAJOLO, R. M., P. CORRADINI & V. PAVONE. 1976. *Gazz. Chim. Ital.* **106**: 807.
16. EISENBERG, R. & J. A. IBERS. 1965. *J. Amer. Chem. Soc.* **87**: 3776.
17. WELLS, A. F. 1962. *Structural Inorganic Chemistry*. 3rd edit.: 334. Clarendon Press. Oxford, England.
18. LOKKEN, D. A. & J. D. CORBETT. 1973. *Inorg. Chem.* **12**: 556.
19. SIMON, A., H. MATTAUSCH & N. HOLZER. 1977. *In press*.
20. SIMON, A. 1976. *Chem. Unserer Zeit.* **10**: 1.
21. OTT, H. & H. SEYFARTH. 1928. *Z. Krist.* **67**: 430.
22. FRANZEN, H. F. & J. GRAHAM. 1966. *Z. Krist.* **123**: 133.
23. COWARD, B. R., L. R. NORRBY & H. F. FRANZEN. 1969. *Acta Cryst.* **B25**: 1729.
24. FRASSON, E., C. PANATTONI & R. ZANNETTI. 1959. *Acta Cryst.* **12**: 1027.

25. GLEIZES, A., T. J. MARKS & J. A. IBERS. 1975. *J. Amer. Chem. Soc.* **97**: 3545.
26. MILLER, J. S. & C. H. GRIFFITHS. 1977. *J. Amer. Chem. Soc.* **99**: 749.
27. PETERSEN, J. L., C. R. SCHRAMM, D. R. STOJAKOVIC, B. M. HOFFMAN & T. J. MARKS. 1977. *J. Amer. Chem. Soc.* **99**: 287.
28. PHELPS, D. W., W. F. LITTLE & D. J. HODGSON. 1976. *Inorg. Chem.* **15**: 2263.
29. NORDQUIST, K. W., D. W. PHELPS, W. F. LITTLE & D. J. HODGSON. 1976. *J. Amer. Chem. Soc.* **98**: 1104.
30. BROWALL, K. W., T. BURSH, L. V. INTERRANTE & J. S. KASPER. 1972. *Inorg. Chem.* **11**: 1800.
31. PIOVESANA, O., L. SESTILI, C. BELLITTO, A. FLAMINI, M. TOMASSINI, P. F. ZANAZZI & A. R. ZANZARI. 1977. *J. Amer. Chem. Soc.* In press.
32. WILLIAMS, J. M., K. D. KEEFER, D. M. WASHECHECK & W. P. ENRIGHT. 1976. *Inorg. Chem.* **15**: 2446.
33. KOCH, T. R., P. L. JOHNSON & J. M. WILLIAMS. 1977. *Inorg. Chem.* **16**: 640.
34. REIS, A. H., S. W. PETERSON, D. M. WASHECHECK & J. S. MILLER. 1976. *Inorg. Chem.* **15**: 2455.
35. See, for example, CHAIKIN, P., A. J. HEEGER & W. A. LITTLE. This Annal.
36. DAY, P. 1977. *In Chemistry and Physics of One-dimensional Metals*. H. J. Keller, Ed.: 197. Plenum Publishing Corp. New York, N.Y.
37. PAINE, J. & P. DAY. 1976. Unpublished work.
38. DAY, P. 1969. *Inorg. Chem. Acta Rev.* **3**: 81.
39. DAY, P. 1975. *J. Amer. Chem. Soc.* **97**: 1588.
40. TORRANCE, J. B. *In Chemistry and Physics of One-dimensional Metals*. H. J. Keller, Ed. Plenum Publishing Corp. New York, N.Y., and this volume.
41. ROBIN, M. B. & P. DAY. 1967. *Adv. Inorg. Chem. Radiochem.* **10**: 247.
42. DAY, P. 1977. Unpublished work.
43. MINGARDI, M. & W. SIEBRAND. 1975. *J. Chem. Phys.* **62**: 1074.

DISCUSSION

J. TORRANCE: There are many effects in organic materials that are strongly analogous to the effects you have described for inorganic materials. In particular, mixed valence is important in both the TTF halides and (TTF)(TCNQ). In addition, the difference you pointed out between integral and subintegral number of electrons per molecule is the difference between insulators and metals in the case of the organic systems.

DAY: The significant feature in all the highly conducting organic and inorganic systems is indeed a nonintegral average number of valence electrons per molecule. On the other hand, at least in the inorganic systems, one has to be aware that the reverse of the preceding statement is *not* always true: a nonintegral number of electrons per molecule is necessary, but not a sufficient condition because charge fluctuations may become very deeply pinned as a result of the different geometrical coordination preferences of different metal-oxidation states.

This page intentionally left blank

CHAPTER 3

This page intentionally left blank

Mixed Valence Compounds

Valency is a word that is not heard very often on the lips of chemists at the beginning of the 21st century, although it was once used very commonly to denote the bonds formed between atoms (e.g. Pauling's now quite defunct valence bond model [1]). To describe the effective number of electrons associated with a given atom when found inside a molecule or solid (in particular d-electrons in transition metal compounds), the phrase 'oxidation state' has largely supplanted it [2]. However, it does continue in everyday usage as part of the phrase 'mixed valency' or mixed valence in American English. 'Mixed oxidation state' gives a clearer idea of what the latter phrase signifies, namely, the situation where the number of electrons assigned to each atom is not an integer: for instance, Fe_3O_4 . The word 'mixed' also opens up a number of questions: to what extent are the oxidation states of the different atoms mixed; could they not just be integers but different from one atom of the same element to another? and if they are integral but different, can they exchange? It is significant that one of the earliest phrases attached to the phenomenon that we now call 'mixed valence', nearly a hundred years ago, was 'oscillating valency' [3]. Finally, it is worth noting that it takes at least two atoms of the same element in one molecule or lattice before their valencies (or oxidation states) can mix. Thus, we find ourselves at once leaving the cosy world of mono-nuclear transition metal complexes so beloved of the protagonists of ligand field theory for the wider horizons of poly-nuclear complexes and aggregates.

Two situations, both immediately evident from the stoichiometric chemical formula derived from elemental analysis, serve to point out the existence of mixed valence in a compound. On one hand, an empirical formula based on the assumption that the anions are closed-shell, leads to a non-integral mean cation oxidation state ($\text{AFe}_2(\text{C}_2\text{O}_4)_3$, where A is an organic cation such as $[\text{P}(\text{C}_6\text{H}_5)_4]^+$ [4]). On the other hand, the mean metal oxidation state may be integral but highly unusual, even implausible, for the element in question. An example of the latter would be $\text{Pd}(\text{NH}_3)_2\text{Cl}_3$ [5], since the 'normal' states of Pd are 0, +2 and +4. The first group of mixed valence compounds that I looked into in detail [6] were of that type since they appeared to contain Sb in the +4 oxidation state when the more usual oxidation states for that element are +3 and +5. Clearly, a 1:1 ratio of the latter would lead to the stoichiometry observed in Cs_2SbCl_6 .

As already mentioned in Chap. 2, intense colour often but not always accompanies mixed valency, and Cs_2SbCl_6 is dark blue, a highly unusual colour for a post-transition metal compound. Indeed, it was because of their colours that mixed valence compounds came to the notice of chemists long before the paler and more subtle colours of many other transition metal compounds were remarked on. First noticed in the 18th century, Prussian Blue is a prime example and Cs_2SbCl_6 was first reported more than a hundred years ago [7]. The crystal structure of Cs_2SbCl_6 approximates that of Cs_2SnCl_6 and one of the compound's attractions as a test-bed for learning about mixed valence arises from the fact that crystalline solid solutions $\text{Cs}_2\text{Sb}_{1-x}\text{Sn}_x\text{Cl}_6$ can easily be made with colours ranging from blue-black through to green and yellow to colourless, as x goes from 0–1. This fact does not imply that the Sb is in the +4 oxidation state since a set of compounds $\text{Cs}_2\text{M}^{\text{III}}_{0.5}\text{Sb}^{\text{V}}_{0.5}\text{Cl}_6$ with $\text{M}^{\text{III}} = \text{In}, \text{Tl}, \text{Bi}, \text{Fe}, \text{Rh}$ also have the same structure. Furthermore, Cs_2SbCl_6 is diamagnetic while Sb^{IV} would have an electron configuration $5s^1$. It was first proven by Raman and infrared spectroscopy [8] that it contained individually identifiable $[\text{Sb}^{\text{III}}\text{Cl}_6]^{3-}$ and $[\text{Sb}^{\text{V}}\text{Cl}_6]^-$. However, direct observation of the superlattice of the two octahedral species differing only in Sb-Cl bond length had to wait a further 20 years for high resolution powder neutron diffraction [9].

The fact that $\text{Sb}^{\text{III/V}}$ can be doped into a Sn^{IV} lattice and Sb^{III} into In^{III} , makes it possible to measure the bulk physical properties of electronic spectroscopy and electrical conductivity quantitatively as a function of composition [10, 11]. As expected, the specific conductivity is a linear function of Sb^{III} concentration and a quadratic one of the total Sb content. The blue colour turns out to be due to a single very broad absorption band near 19000 cm^{-1} , which shifts to lower frequency with dilution. This band, similar to those found in many other mixed valency solids, arises from a transition in which an electron is transferred from the highest occupied orbital of the lower oxidation state ion ($5s^2$ in Sb^{III}) to the lowest unoccupied orbital in the higher oxidation state ion ($5s^0$ in Sb^{V}). By measuring its intensity quantitatively, one can therefore estimate the overlap between the donor and acceptor levels. Since the bands are quite intense, this can be done only by recording the transmission through a diluted single crystal.

The prototype $\text{Sb}^{\text{III/V}}$ system gives a glimpse into some of the features of mixed valency, but looking across the whole Periodic Table, it is evident that there is huge variety in their properties. Some are metals while others are insulators; some are black, others are colourless and so forth. Given that some two-thirds of all elements form such compounds, it is not very surprising whether there are in fact any unifying principles that could possibly apply across the whole gamut. Having collated (for the first time) all the evidence available up till then, Mel Robin, then at Bell Laboratories, and I made such a proposal in 1967 [12]. The framework we adopted led to a scheme for classifying mixed valence compounds, following the similarity

or difference between the sites of differing oxidation state. The concept is an extremely simple one taken from the Heitler–London model, namely that if a metal M can appear in two different oxidation states (say P and Q) and there are two identifiable sites in the crystal (A and B), then the degree of mixing between the alternative Heitler–London configurations $M^P_A M^Q_B$ and $M^Q_A M^P_B$ will depend on the energy difference between them, and hence on how distinguishable they are crystallographically. If the sites are very different (e.g. octahedral and tetrahedral with very different bond lengths), then there will be little or no ‘contamination’ of one configuration by the other; the valences will be completely trapped and there will be no electron transfer, optical or thermal. Conversely, if A and B are indistinguishable, the oxidation states are genuinely non-integral and we have a metal if the compound has a continuous lattice. Between these two extremes named classes I and III, lie many intermediate cases (class II) where the two configurations are not of equal energy, but are also not very different. The optical inter-valence excitation energy then lies in the visible, hence dark colours and semi-conduction is also anticipated.

What has become known as the Robin–Day model was essentially static, but as is so often the case in science, a few years later, a new compound was synthesised which could not be fitted into this framework, thus providing the trigger to extend it. The dimeric Creutz–Taube ion $[(\text{NH}_3)_5\text{Ru}^{\text{II}}(\text{pyrazine})\text{Ru}^{\text{III}}(\text{NH}_3)_5]^{5+}$ [13] appears to contradict the R–D model because each Ru has the same ligand environment, while different physical methods indicate that they may be distinguishable or not, depending on the time-window probed. This paradox is circumvented if the R–D model is extended into the dynamic regime [14]. Then, the question of whether the two zero-order configurations $\text{Ru}^{\text{II}}_A \text{Ru}^{\text{III}}_B$ and $\text{Ru}^{\text{III}}_A \text{Ru}^{\text{II}}_B$ contribute equally (class III) or unequally (class II) to the ground-state depends on the relative magnitudes of adiabatic charge transfer energy and the inter-ionic resonance integral (E_{ad} and H_{res} in Ref. [14]). However, even that model fails to tackle the problem in its full subtlety because it still invokes the Born–Oppenheimer approximation by assuming that the total wave-function can be factorised into electronic and vibrational components. Casting aside that approximation, Piepho, Krausz and Schatz [15] analysed the full vibronic problem; their work is summarised in Ref. [16].

Returning to the original prototype of Cs_2SbCl_6 and the compounds related to Wolfram’s Red Salt, a further issue comes to the fore. In these examples, the oxidation states P and Q differ by two electrons and not one, so in principle, there are three configurations to consider, each with its own potential energy surface. In the $\text{Sb}^{\text{III/V}}$ example, they are $\text{Sb}^{\text{III}}_A \text{Sb}^{\text{V}}_B$, $\text{Sb}^{\text{V}}_A \text{Sb}^{\text{III}}_B$ and $\text{Sb}^{\text{IV}}_A \text{Sb}^{\text{IV}}_B$. There is an interesting analogy here with the phenomenon known to solid state physicists as ‘negative U ’ [17]. Why should a configuration $5s^2_A 5s^0_B$ ever be more stable than $5s^1_A 5s^1_B$, given that electrons repel one another? It is as if the two electrons are attracted to each other. The solution to this dilemma is that we are not concerned

with atoms but molecules in which the environment of A and B are different, so lattice polarisation has to be taken into account [18]. Nevertheless, the vibronic analysis can be extended to this three-level situation [19], which allows the optical intervalence transition to be explained quantitatively, both for $\text{Sb}^{\text{III/V}}$ and $\text{Pt}^{\text{II/IV}}$ [16]. In light of the crucial role played by Cooper pairs in superconductivity, and the subsequent discovery of high temperature superconductors such as $\text{La}_{2-x}\text{Sr}_x\text{CuO}_4$ that are mixed valency in type, this phenomenon takes on a heightened significance.

Before leaving the topic of mixed valence compounds, a final aspect worth considering is their magnetic behaviour. If oxidation states P and Q are essentially localised to sites A and B, the magnetic moments of the sites will just be those of P and Q taken separately, e.g. in Prussian Blue, high spin Fe^{III} and low spin Fe^{II} . However, if the resonance integral between the two sites is not zero, the moments interact, and if the compound has an infinitely extended lattice, it results in long-range magnetic order. Prussian Blue is a specially fascinating example because low spin Fe^{II} has no unpaired electrons, and in the cubic lattice, the high spin Fe^{III} are separated by more than 10 Å and five intervening closed shell atoms: $\text{Fe}^{\text{III}}\text{-NC-Fe}^{\text{II}}\text{-CN-Fe}^{\text{III}}$. Remarkably, Prussian Blue does become magnetically ordered, and even more remarkably, it is a ferromagnet. Using the R-D model and a perturbation approach to the intervening atoms, it proved possible to demonstrate how this comes about through the mixing of the excited $\text{Fe}^{\text{II}} \rightarrow \text{Fe}^{\text{III}}$ intervalence configuration into the ground state [20]. The first ever use of neutron polarisation analysis to a molecular-based magnetic material [21] also helped to estimate the degree of mixing experimentally. This presages much of the later work on molecular magnets, some of which is described in Chap. 5.

References

- [1] L. Pauling, *The Nature of the Chemical Bond*, Prentice-Hall, Englewood Cliffs.
- [2] C. K. Jorgensen, *Oxidation Numbers and Oxidation States*, Springer-Verlag, Berlin.
- [3] K. A. Hofmann and K. Hoeschele, *Ber Deut Chem Ges* **48**: 20 (1915).
- [4] C. Mathoniere, C. J. Nuttall, S. G. Carling and P. Day, *Inorg Chem* **35**: 41–48 (1996).
- [5] H. Sainte-Claire Deville and H. Debray, *Compt Rend* **86**: 927 (1878).
- [6] P. Day, *Inorg Chem* **2**: 452–456 (1963). (**Reprint 3.1**)
- [7] C. Setterberg, *Oefversigt K Vetensk Akad Forhandl* **6**: 23 (1882).
- [8] T. Barrowcliffe, I. R. Beattie, P. Day and K. Livingston, *J Chem Soc A*, 1810–1812 (1967).
- [9] K. Prassides, A. K. Cheetham and P. Day, *J Amer Chem Soc* **105**: 3366–3368 (1983). (**Reprint 3.2**)
- [10] L. Atkinson and P. Day, *J Chem Soc A*, 2423–2431 (1969). (**Reprint 3.3**)
- [11] *idem ibid*, 2432–2436 (1969). (**Reprint 3.4**)
- [12] M. B. Robin and P. Day, *Adv Inorg Chem Radiochem* **10**: 248–422 (1967). (**Reprint 3.5**)

-
- [13] C. Creutz and H. Taube, *J Amer Chem Soc* **91**: 3988 (1969).
- [14] B. Mayoh and P. Day, *J Amer Chem Soc* **94**: 2885–2886 (1972). (**Reprint 3.6**)
- [15] S. B. Piepho, E. R. Krausz and P. N. Schatz, *J Amer Chem Soc* **100**: 2996 (1978).
- [16] P. Day, *Int Rev Phys Chem* **1**: 149 (1981). (**Reprint 3.9**)
- [17] P. W. Anderson, *Phys Rev Lett* **34**: 953 (1975).
- [18] K. Prassides and P. Day, *Inorg Chem* **24**: 1109 (1985).
- [19] K. Prassides and P. Day, *J Chem Soc Faraday Trans* **2**: **80**, 85–95 (1984).
- [20] B. Mayoh and P. Day, *J Chem Soc Dalton Trans*, 1483 (1976). (**Reprint 3.7**)
- [21] F. Herren, A. Ludi, H. U. Guedel, D. Givord and P. Day, *Helv Chim Acta* **63**: 148 (1980). (**Reprint 3.8**)

CONTRIBUTION FROM CYANAMID EUROPEAN RESEARCH INSTITUTE,
 COLOGNY, GENEVA, SWITZERLAND

Spectra and Constitution of Antimony(III), Antimony(V) Hexahalide Salts and Related Compounds

By PETER DAY¹

Received October 22, 1962

Reflection spectra of Sb(III), Sb(V); Bi(III), Sb(V); In(III), Sb(V); and Tl(III), Sb(V) hexahalide complexes diluted in hexahalostannate(IV) crystals are reported for a number of cations. The pure compounds $\text{Cs}_2\text{Bi}_{0.5}\text{Sb}_{0.5}\text{Cl}_6$, $\text{Cs}_2\text{In}_{0.5}\text{Sb}_{0.5}\text{Cl}_6$, and $\text{Cs}_2\text{Tl}_{0.5}\text{Sb}_{0.5}\text{Cl}_6$ also have been prepared and characterized from their X-ray powder photographs. The Bi and In compounds show evidence of superlattice formation which is assumed to exist, undetected, in the Sb(III), Sb(V) compounds. On this evidence the solid spectra have been assigned to electron transfer transitions from the n_s^2 or $(n+1)s^2$ shell of the trivalent ion to the n_s^0 shell of the pentavalent ion. The abnormally deep colors of the In and Tl compounds also are discussed.

The "interaction color" of Sb(III), Sb(V) in HCl solution was studied some time ago,² but the spectra of the corresponding solids have not been reported, although the appearance of the crystals suggests that they must be quite different. The cesium salt Cs_2SbCl_6 was first prepared by Wells,³ who showed that it was isomorphous with Cs_2PbCl_6 , and the ammonium compound also forms mixed crystals with $(\text{NH}_4)_2\text{SnCl}_6$ and $(\text{NH}_4)_2\text{PtCl}_6$.⁴ Early authors thought that these compounds were derivatives of SbCl_4 , but Elliot showed that $(\text{NH}_4)_2\text{SbBr}_6$ was diamagnetic,^{5a} and therefore presumably contained equal amounts of Sb(III) and Sb(V). Sb(IV) remains a possibility if the compounds were antiferromagnetic, with a very high Néel temperature. There is a simple theory^{5b} for antiferromagnetism in the isostructural K_2IrCl_6 which invokes electron transfer from chlorine to iridium, but when it is applied to the antimony case, one finds that the maximum amount of charge transfer could not give a Néel temperature above 50°K., so the compounds would be strongly paramagnetic at room temperature. This is further strong evidence against Sb(IV).

However, the X-ray powder diagrams⁶ can be indexed quite accurately in terms of a pure K_2PtCl_6 lattice, *i.e.*, the Sb(III)Cl₆ and Sb(V)Cl₆ units are either indistinguishable or randomly distributed. Since these units carry different charges if there really are two different valences present, a random distribution is per-

haps not likely. The X-ray scattering powers of Sb(III) and Sb(V) must be so similar that a superlattice could not be detected.

The intense colors of mixed valence solids make it very difficult to measure their transmission spectra, and only a few are recorded in the literature.⁷ Their diffuse reflection spectra also are broadened and distorted. Because the antimony(III),(V) solids can be homogeneously diluted with Sn(IV), this problem is avoided. Only diffuse reflection spectra are reported here, but we hope later to obtain oscillator strengths as a function of concentration from single crystal spectra using a microscope.

If this class of compounds contains Sb(III) and Sb(V), we would expect analogous Bi(III), Sb(V) salts, and the cesium compound has been prepared. In an effort to discover whether there is a superlattice of trivalent and pentavalent ions, we also prepared In(III), Sb(V), and Tl(III), Sb(V), salts.

Experimental

Preparations.—All the preparations were carried out in 12 M HCl solution. For the Sb(III), Sb(V) compounds Weinland and Schmidt's method⁴ is convenient. A solution of Sb_2O_3 is divided into two equal portions, one of which is saturated with chlorine, and then warmed to remove the excess. Recombining the two solutions produces the characteristic yellow "interaction color." When anhydrous SnCl_4 is added, followed by an alkali metal halide solution, mixed Sb(III), Sb(V), Sn(IV) compounds crystallize on cooling.

For equal ratios of Sb to Sn, more concentrated solutions deposit chlorostannate crystals containing more Sb (*i.e.*, darker color). Thus, because the chlorostannates become more soluble in 12 M HCl with decreasing size of the alkali metal cation,

(1) University of Oxford, Inorganic Chemistry Laboratory, South Parks Road, Oxford, England.

(2) J. E. Whitney and N. Davidson, *J. Am. Chem. Soc.*, **71**, 3809 (1949).

(3) H. L. Wells and F. J. Metzger, *Am. Chem. J.*, **26**, 268 (1901).

(4) R. F. Weinland and H. Schmidt, *Ber.*, **38**, 1080 (1905).

(5) (a) N. Elliot, *J. Chem. Phys.*, **3**, 298 (1934); (b) J. H. E. Griffiths, J. Owen, J. G. Park, and M. F. Partridge, *Proc. Roy. Soc. (London)*, **A260**, 84 (1959).

(6) K. A. Jensen, *Z. anorg. allgem. Chem.*, **232**, 193 (1937).

(7) S. Yamada and R. Tsuchida, *Ann. Rept. Sci. Works, Fac. Sci. Osaka Univ.*, **4**, 79 (1956).

Vol. 2, No. 3, June, 1963

ANTIMONY(III), ANTIMONY(V) HEXAHALIDE SALTS 453

and the chlorides less soluble, potassium chlorostannate will not incorporate a high proportion of Sb. Sodium chlorostannate is in any case hydrated, and has a different structure.

Sb(III), Sb(V) hexabromides and their hexabromostannate-(IV) dilutions were made according to Ephraim and Weinberg.^{8a}

$\text{Cs}_2\text{Bi}_{0.5}\text{Sb}_{0.5}\text{Cl}_6$.— Sb_2O_3 (0.12 g.) in 8 ml. of 12 M HCl is oxidized with chlorine; the solution is warmed to 60° and added to a solution if 0.23 g. of Bi_2O_3 in 4 ml. of HCl at the same temperature. This mixture is added to a 60° solution of 0.75 g. of CsCl in 8 ml. of HCl and the immediate dark red precipitate is quickly filtered. In this way the product showed no signs of contaminating CsSbCl_6 crystals under the microscope. Washing with cold 12 M HCl caused some decomposition, so the crystalline precipitate was sucked dry and pressed between filter paper.

$\text{Cs}_2\text{In}_{0.5}\text{Sb}_{0.5}\text{Cl}_6$ and $\text{Cs}_2\text{Tl}_{0.5}\text{Sb}_{0.5}\text{Cl}_6$.— Sb_2O_3 (0.14 g.) and 0.22 g. of InCl_3 in 10 ml. of 12 M HCl are oxidized with chlorine and added to a solution of 0.67 g. of CsCl in 10 ml. of HCl, to give a finely divided pale yellow precipitate. The Ti(III)Sb(V) salt was prepared in the same way using a Ti(III) solution prepared by passing chlorine through a suspension of 0.25 g. of Ti_2SO_4 in 20 ml. of HCl until it had all dissolved. Both mixed salts precipitate at room temperature at concentrations for which neither In(III) , Ti(III) , nor Sb(V) will give a solid with CsCl, even on strong cooling. In(III)Sb(V) and Ti(III)Sb(V) compounds already have been reported briefly,^{8b} but without details of preparation or analysis.

Analyses.⁹—Calcd. for $\text{Cs}_2\text{Bi}_{0.5}\text{Sb}_{0.5}\text{Cl}_6$: Cs, 41.3; Bi, 16.3; Sb, 9.5. Found: Cs, 41.0; Bi, 15.5; Sb, 9.0. Calcd. for $\text{Cs}_2\text{In}_{0.5}\text{Sb}_{0.5}\text{Cl}_6$: Cs, 44.5; In, 9.6; Sb, 10.2. Found: Cs, 44.0; In, 9.6; Sb, 10.7. Calcd. for $\text{Cs}_2\text{Tl}_{0.5}\text{Sb}_{0.5}\text{Cl}_6$: Cs, 41.4; Tl, 15.9; Sb, 9.5. Found: Cs, 41.8; Tl, 15.3; Sb, 9.6.

X-Ray Powder Photographs.—A Siemens counter diffractometer was used with Ni filtered $\text{CuK}\alpha$ radiation. Each μ -parameter in Table IV is the mean of the values giving the best agreement with the calculated intensity for each (hkl). Intensities were measured by making several photostat copies of each trace and then cutting the peaks out and weighing them. Tables I, II, and III contain the observed and calculated spacings and intensities.

Visible Spectra.—In powder reflection spectra, intense absorption bands often are flattened and distorted because small amounts of stray light become dominating, and the Rayleigh scattering powers of sample and standard are not the same. A Beckman DU spectrophotometer with a diffuse reflection attachment therefore was used to measure the spectra as the difference between two samples homogeneously diluted with different amounts of Sn(IV), but prepared at the same concentration. The particle sizes were further matched by grinding each sample for the same length of time in the same agate mortar. Figure 1 gives the Sb(III), Sb(V) difference spectra, and all the absorption maxima are in Table V.

Results and Discussion

The X-ray powder diagrams of $\text{Cs}_2\text{Bi}_{0.5}\text{Sb}_{0.5}\text{Cl}_6$, $\text{Cs}_2\text{In}_{0.5}\text{Sb}_{0.5}\text{Cl}_6$, and $\text{Cs}_2\text{Tl}_{0.5}\text{Sb}_{0.5}\text{Cl}_6$ all can be indexed as O_h^5 (Fm 3m), isomorphous with K_2PtCl_6 . In the Bi and In compounds, however, there are several very weak reflections not allowed by that space group (mixed even and odd indices). They are quite close to the noise level of the counter so that their spacings cannot be observed very accurately, but they are reproducible in different samples and at different instrument noise levels. They do not appear to be impurity lines, because the powder diagrams of likely impurities such as

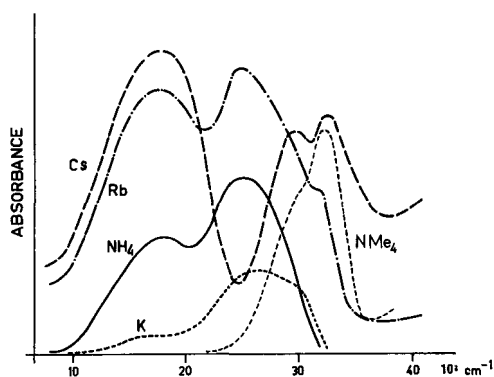


Fig. 1.—Difference spectra of $\text{A}_2[\text{Sb(III)}_{0.5}\text{Sb(V)}_{0.5}]_n\text{Sn(IV)}_{1-n}\text{Cl}_6$.

TABLE I
X-RAY POWDER DATA FOR $\text{Cs}_2\text{Bi}_{0.5}\text{Sb}_{0.5}\text{Cl}_6$

hkl	$10^4 Q_{\text{obs}}^a$	$10^4 Q_{\text{calcd}}$	I_{hkl}/I_{220}^b	$ F_{hkl} ^2 L_p \cdot p^{cc}$
111	272	272	0.51	0.53
200	0.00	.002
211	592	...	vw	...
220	726	725
300/221	834	816	vw	...
311	1007	997	.28	.25
222	1097	1089	.60	.30
320	1186	1179	vw	...
400	1456	1451	.52	.63
331	1737	1723	.13	.09
420	...	1814	.00	.007
422	2186	2176	.43	.68
511	2445	2440	.15	.12
33301
440	2897	2901	.46	.43
531	3166	3174	.12	.12
600	...	3265	.00	.00
442002
620	3618	3625	.14	.22
533	3905	3899	.03	.03
622	3983	3990	.06	.11
444	4351	4350	.22	.15
711	4620	4622	.07	.02
55105
640	...	4718	.00	.001
642	5074	5080	.14	.25
731	5348	5349	.06	.03
55303
800	5808	5803	vw	...
733	6092	6078	vw	...
822	6530	6532	vw	...
660
751	6810	6800	vw	...
555
840	7252	7252	vw	...

^a $Q_{\text{obs}} = 1/d^2$. ^b Intensity tabulated relative to (220). ^c L_p = Lorentz and polarization factors, p^c = multiplicity factor.

CsSbCl_6 , $\text{CsInCl}_6 \cdot \text{H}_2\text{O}$, etc., do not have strong reflections at the appropriate spacings, and their more intense reflections do not appear. In any case, with the accuracy attainable, the Q_{hkl} values of the weak lines agree with the unit cell dimensions calculated from stronger reflections. It appears, then, that we have evidence for a doubled unit cell, *i.e.*, a superlattice.

(8) (a) F. Ephraim and S. Weinberg, *Ber.*, **42**, 4450 (1909); (b) A. Tovberg-Jensen and S. E. Rasmussen, *Acta Chem. Scand.*, **9**, 708 (1955).

(9) Analyses by Analix S.A., Geneva.

TABLE II

X-RAY POWDER DATA FOR $\text{Cs}_2\text{In}_{0.5}\text{Sb}_{0.5}\text{Cl}_6$				
<i>hkl</i>	$10^4 Q_{\text{obsd}}$	$10^4 Q_{\text{calcd}}$	I_{hkl}/I_{220}	$ F_{hkl} ^2 Lp \cdot p^*$
111	280	278
200	...	370	0.00	0.13
300/221	840	834	vw	...
220	741	740
310	919	926	vw	...
311	1021	1018	.26	.17
222	1114	1111	.61	.49
320	1212	1213	vw	...
400	1480	1480	.66	.68
331	...	1759	.05	.04
420	...	1851	.00	.04
422	2225	2221	.37	.44
510/431	2414	2408	vw	...
511	2500	2499	.12	.11
333007
440	2960	2961	.55	.46
531	3238	3238	.09	.10
600	...	3330	.00	.000
44202
620	3710	3704	.08	.23
533	3982	3982	.04	.02
622	4071	4072	.10	.17
444	4422	4441	.10	.15
711	4708	4721	.06	.01
55105
640	...	4816007
642	5181	5181	.14	.25
731	5430	5462	.03	.009
55303
800	5935	5922	.05	.07
822	6665	6663	vw	...
660
751	6944	6941	vw	...
555
662	7041	7039	vw	...
840	7404	7408	vw	...
911	7682	7682	vw	...

Atoji and Watanabe¹⁰ also found extra lines in the powder diagram of the mixed valence compound $\text{Co}(\text{NH}_3)_6\text{PbCl}_6$. This compound, of a deep purple color, and evidently containing Pb(II) and Pb(IV), is otherwise isomorphous with $\text{Co}(\text{NH}_3)_6\text{TiCl}_6$ and $\text{Co}(\text{NH}_3)_6\text{BiCl}_6$. PbCl_6^{4-} is known to form a regular octahedron,¹¹ and PbCl_6^{2-} is also octahedral, so that superlattice formation in the mixed compound will only be detectable through the changed metal-halogen distance. The group VB hexachloride units have not been closely studied crystallographically, but we know from the cobalt(III) hexaammine salts above that BiCl_6^{3-} is a regular octahedron, and the powder diagram of the rather unstable Cs_3SbCl_6 also can be indexed as O_h^5 (anti- BiF_6), so it seems that SbCl_6^{3-} is not greatly distorted by its $5s^2$ electrons. The ns^0 systems, SbCl_6^- , TiCl_6^{3-} , and InCl_6^{3-} , all should be undistorted octahedra. No structures containing SbCl_6^- or InCl_6^{3-} are available, but TiCl_6^{3-} has been determined in potassium¹² and cobalt(III) hexaammine salts.¹³

In the absence of information about Sb(V)-Cl and

TABLE III

X-RAY POWDER DATA FOR $\text{Cs}_2\text{Tl}_{0.5}\text{Sb}_{0.5}\text{Cl}_6$				
<i>hkl</i>	$10^4 Q_{\text{obsd}}$	$10^4 Q_{\text{calcd}}$	I_{hkl}/I_{220}	$ F_{hkl} ^2 Lp \cdot p^*$
111	277	277
200	370	369	0.02	0.002
220	746	738
311	1019	1014	.19	.25
222	1114	1107	>1.2	.31
400	1474	1476	.42	.63
331	1756	1753	.11	.08
420	...	1845	.00	.007
422	2210	2214	.39	.45
511	2489	2491	.13	.10
33301
440	2954	2954	.37	.42
531	3239	3229	.10	.12
600	...	3321	.00	.00
442002
620	3689	3689	.05	.22
533	3955	3965	.02	.03
622	4055	4060	.04	.10
444	4445	4430	.31	.14
711	4728	4705	.06	.02
55105
640	...	4800	.00	.001
642	5177	5168	.15	.18
731	5431	5446	.06	.03
55303
800	5935	5903	vw	...
733	...	6182	vw	...
822	6630	6642	vw	...
660
751	6935	6920	vw	...
555

TABLE IV

SUMMARY OF UNIT CELL DIMENSIONS AND PARAMETERS		
	<i>a</i> /2, Å	<i>u</i>
$\text{Cs}_2\text{Bi}_{0.5}\text{Sb}_{0.5}\text{Cl}_6$	10.50	0.239 ± 0.015
$\text{Cs}_2\text{In}_{0.5}\text{Sb}_{0.5}\text{Cl}_6$	10.39	0.232 ± 0.025
$\text{Cs}_2\text{Tl}_{0.5}\text{Sb}_{0.5}\text{Cl}_6$	10.41	0.238 ± 0.015

TABLE V

	DIFFERENCE SPECTRA OF Sb(III), Sb(V) HEXAHALIDES (10^3 cm^{-1})			
	Chlorides		Bromides	
K	18.5	27.0	...	8-9 19.0
NH_4	18.2	26.5	...	9.5 18.8
Rb	18.05	25.4	27-29	31-32 8-9 16.7
Cs	17.9	...	29.3	32.3 ~9 17.6
$\text{N}(\text{CH}_3)_4$	27-29	32.3 ... 18.9
$\text{N}(\text{C}_2\text{H}_5)_4$	~33 ... 20.5

In(III)-Cl distances the unit cell dimensions and chlorine atom parameters recorded in Table IV cannot be interpreted conclusively, but determinations of suitable indium and antimony compounds are being planned. In any case, single crystal measurements will be necessary to improve the accuracy of the parameters in the mixed compounds because many of the F_{hkl} are not very steep functions of *u* in the region of interest.

The colors of the Sb(III), Sb(V) solids are quite different from the solutions that they precipitate from. This is caused by the broad new band at about 18,000 cm^{-1} . Dilute (less than 5%) solids are yellow like the solutions, but deep blue Rb_2SbCl_6 is only about 8.5 *M* from its density, while in Whitney and David-

(10) M. Atoji and T. Watanabe, *J. Chem. Phys.*, **20**, 1045 (1952).(11) Chr. Kn. Müller, *Kgl. Danske Videnskab Selskab, Mat. Fys. Medd.*, **32**, No. 3 (1960).(12) J. L. Hoard and L. Goldstein, *J. Chem. Phys.*, **3**, 645 (1935).(13) T. Watanabe, M. Atoji, and C. Okazaki, *Acta Cryst.*, **3**, 405 (1950).

Vol. 2, No. 3, June, 1963

ANTIMONY(III), ANTIMONY(V) HEXAHALIDE SALTS 455

son's 1.5 *M* solution spectrum² there is no trace of a shoulder between 15,000 and 20,000 cm^{-1} . One possible reason for this striking change is that the Sb(III) species in solution is much more likely to be SbCl_4^- than SbCl_6^{3-} as in the solid. The positions of mixed-valence interaction bands in solution certainly change with chloride concentration, because McConnell and Davidson's^{14a} Cu(I), Cu(II) spectrum in 0.3 *M* Cl⁻ has its peak at 400 $\text{m}\mu$; at 6.0 *M* it has shifted to 490 $\text{m}\mu$, and in some early measurements in 10 *M* chloride^{14b} the peak has moved still further, to 550 $\text{m}\mu$, which is also the wave length obtained from the difference spectrum of Mori's¹⁵ solid cobalt(III) hexaammine chlorocuprates(I), (II). However, the yellow rather than pale blue color of diluted Sb(III), Sb(V) salts suggests that even in the solid, the long wave length band is much weaker than the ultraviolet band.

From Fig. 1 and Table V we see that there are several remarkable changes in the Sb(III), Sb(V) chloride and bromide spectra as the cation is changed. With increasing ionic radius from K to Cs, the long wave length band moves slightly to lower energy. In K and NH_4 salts the second band is single, but partly in Rb, and wholly in Cs, it has moved to higher energy and split into two components. Increasing the cation size still further produces a dramatic alteration. The $\text{N}(\text{CH}_3)_4$ and $\text{N}(\text{C}_2\text{H}_5)_4$ salts are no longer blue or dark brown but pale yellow, owing to the complete disappearance of the long wave length absorption. The former still shows the split higher energy band but in the latter this too has nearly disappeared. It may be that the solution in HCl is behaving in the same way as the large cation solids, with the electron transferring group separated by a cation such as $(\text{H}_3\text{O}^+)(\text{H}_2\text{O})_3$.

We made a rough comparison of intensities of the long wave length bands in the NH_4 and Rb salts, by taking the reflection spectra of two pairs of solids containing similar proportions of Sb to Sn, and found that there was no significant difference, so this effect apparently is confined to the larger cations. Exactly the same phenomenon occurs in the bromides, though the whole spectrum has shifted to lower energy, with the first band now in the infrared. Also the second band is no longer split by the larger cations. Bi(III), Sb(V) hexachlorides are dark red, by an increase of 6000 cm^{-1} in the energy of the first band. Absorption by the component ions obscures the higher bands.

The simplest explanation for the strong colors of the Sb(III), Sb(V) and Bi(III), Sb(V) compounds is that we have an electron transfer from the $5s^2$ or $6s^2$ shell of the trivalent ion to the $5s$ shell of Sb(V). A convenient simple model for the interaction color of an isolated pair would be a transition from $\text{H}^- + \text{H}^+$ to $2\text{H}\cdot$ at about 7 Å. separation, which actually has a high negative energy. The reason why the ground state in the Sb system is Sb(III) + Sb(V) and not Sb(IV) therefore must be sought in the extra variable not

present in the model, namely, the Sb-Cl separation. However, we can see at once that such a transition, whatever its energy, would have two components, a triplet and a singlet. To account for the number of bands in the solid spectrum it will be necessary to consider the increased number of nearest neighbors possible in the A_2MX_6 lattice.

Transfer to $5p$ of Sb(V) also may occur, but if we assume that the $5s$ level in Sb(III) has lower energy than in Sb(V), because it has trapped the "extra" two electrons, then the $5s [\text{Sb(III)}] \rightarrow 5p [\text{Sb(V)}]$ transition must have a higher energy than $5s [\text{Sb(III)}] \rightarrow 5p [\text{Sb(III)}]$, the triplet and singlet components of which are already far in the ultraviolet at 35,000 and 43,000 cm^{-1} . We now have to try to account for the number of bands observed.

There are two ways of introducing a superlattice in a face-centered cubic lattice such as that of the MX_6 compounds in the antiferro structure. One can have successive layers either in the (110) or in the (111) plane. However, the former probably would involve tetragonal distortion of the lattice, and only double the unit cell in one direction. Since this is not observed in the X-ray data we will assume the latter. This gives an octahedron of $\text{M}'\text{X}_6$ units surrounding every MX_6 . The hole state of MX_6 after transferring an electron to the M' atoms is $5s^1$, *i.e.*, A_{1g} in O_h , and the excited electron, which can be on any of the six M' atoms, is also A_{1g} ($5s^1$), giving $6 \times 4 = 24$ possible excited states. The factor of four arises from the four possible spin states of the electron-hole pair.¹⁶ Irreducible representations of the total wave functions for the 24 exciton states are given by the direct products of the representations of the hole and electron states, including the spin representations, as

$$\text{singlet: } \text{A}_{1g} \times (\text{A}_{1g} + \text{E}_g + \text{T}_{1u}) \times \text{A}_{1g} = \text{A}_{1g} + \text{E}_g + \text{T}_{1u}$$

$$\text{triplet: } \text{A}_{1g} \times (\text{A}_{1g} + \text{E}_g + \text{T}_{1u}) \times \text{T}_{1g} = \\ \text{A}_{1u} + \text{E}_u + 2\text{T}_{1g} + \text{T}_{1u} + \text{T}_{2g} + \text{T}_{2u}$$

Only those states can be reached by dipole-allowed transitions which have a total symmetry of T_{1u} , so we have one singlet and one triplet only.

If we consider the possibility that the structure is random, and take the full cuboctahedron¹⁷ of surrounding units, by the same procedure we have

$$\text{singlet: } \text{A}_{1g} \times (\text{A}_{1g} + \text{E}_g + \text{T}_{1u} + \text{T}_{2g} + \text{T}_{2u}) \times \text{A}_{1g} = \\ \text{A}_{1g} + \text{E}_g + \text{T}_{1u} + \text{T}_{2g} + \text{T}_{2u}$$

$$\text{triplet: } \text{A}_{1g} \times (\text{A}_{1g} + \text{E}_g + \text{T}_{1u} + \text{T}_{2g} + \text{T}_{2u}) \times \text{T}_{1g} = \\ \text{A}_{1u} + \text{A}_{2g} + \text{A}_{2u} + \text{E}_g + \\ 2\text{E}_u + 3\text{T}_{1g} + 2\text{T}_{1u} + 2\text{T}_{2g} + 2\text{T}_{2u}$$

i.e., there are now two dipole-allowed triplets and one singlet.

If the superlattice ordering is in the (111) direction it is possible to introduce a trigonal distortion in the surrounding octahedron of MX_6 without producing any trigonal distortion in the lattice as a whole, but only an

(14) (a) H. M. McConnell and N. Davidson, *J. Am. Chem. Soc.*, **73**, 3168 (1950); (b) E. Doelmann and H. Fromherz, *Z. physik. Chem.*, **171b**, 371 (1934).

(15) M. Mori, *Bull. Chem. Soc. Japan*, **33**, 985 (1960).

(16) A. W. Overhauser, *Phys. Rev.*, **101**, 1702 (1956).

(17) J. R. Canon and G. H. Duffey, *J. Chem. Phys.*, **35**, 1657 (1961).

isotropic expansion. We then would have to consider D_{3d} , with the direct product representations

$$\text{singlet: } A_{1g} \times (A_{1g} + A_{2u} + E_g + E_u) \times A_{1g} = \\ A_{1g} + A_{2u} + E_g + E_u$$

$$\text{triplet: } A_{1g} \times (A_{1g} + A_{2u} + A_{2u} + E_g + E_u) \times T_{1g} = \\ A_{1u} + A_{2g} + E_g + E_u$$

The state with the total symmetry A_{2u} is polarized along the z -direction, and E_u in the xy plane, so there are two singlets and one triplet allowed.

Assuming that the ordering in the Sb(III), Sb(V) hexachlorides and hexabromides is the same as that postulated for the Bi(III), Sb(V) and In(III), Sb(V) hexachlorides, the two bands in the K and NH_4 salts are easily assigned to the one singlet and one triplet allowed by an octahedral environment. It is not likely that we have the two triplets and one singlet required of the full cuboctahedral situation for, as we already have remarked, the lower energy band undoubtedly is less intense than the higher, perhaps by a factor of five or ten. It certainly is significant that only in the large light cations does the lowest band disappear, while in the large heavy Cs it is as intense as in K. Perhaps from K to Cs, increasing size and decreasing overlap roughly cancel with increasing Z . In the Rb and Cs salts, on the other hand, the splitting of the ultraviolet band might easily be accounted for by a small trigonal distortion to D_{3d} . We do not know, of course, how large a physical distortion would be needed to give the observed splitting, but it is worth noting the lack of splitting in the large hexabromo ion with even the largest cations.

Our assumption that charge transfer is occurring between the $5s$ states of Sb(III) and Sb(V), together with the hypothesis of superlattice formation, therefore leads to a correct prediction of the number and intensity ratio of the new absorption bands. However, the fact that dilute Sb(III), Sb(V) compounds are pale yellow rather than pale blue, and the complete disappearance of the long wave length band in the tetramethylammonium salt, might be taken to suggest that the two bands do not have the same concentration dependence. Single crystal spectra must be undertaken to settle this point.

The colors of the In(III), Sb(V) and Tl(III), Sb(V) compounds are altogether more difficult to rationalize. Their ease of formation, which must be related to the

favorable energetics of the antiferroite $A_2\text{MX}_6$ lattice, compared with $A_2\text{MX}_6$ and AMX_6 , also is surprising. Both compounds absorb at longer wave lengths than either component ion and, by making Sn(IV) dilutions, we find one new band in each Cs salt, at $30,800\text{ cm}^{-1}$ for In and $29,600\text{ cm}^{-1}$ for Tl. The In salt is pale yellow, and the Tl deep lemon yellow, though In(III) in HCl does not absorb until much further into the ultraviolet than CsSbCl_6 , itself quite white. Watanabe, *et al.*,¹³ noticed that their cobalt(III) hexaammine hexachlorothallate had a rather deeper color than expected from the cation alone, and correlated it with the abnormally short Tl-Cl bond length they found (2.48 Å. compared with 2.55 Å. for $\text{K}_3\text{TlCl}_6 \cdot 2\text{H}_2\text{O}$ ¹² and an average of 2.54 Å. for $\text{Cs}_2\text{TlCl}_6\text{H}_2\text{O}$ ¹⁸). They also discovered that on cooling in liquid air it became almost colorless, and on heating, deep orange. Cesium Tl(III), Sb(V) hexachloride behaves in exactly the same way.

Two possible explanations are that a chlorine to thallium charge transfer band is being shifted by compression, or that the hexachlorothallate group is transferring an electron to cobalt(III) hexaammine or SbCl_6^- . Neither alternative is very satisfactory. If the band has been shifted to the red by pressure, it ought not to be shifted back to the blue again by lowering the temperature, and though anions are known (*e.g.*, I^-)¹⁹ which give charge transfer bands with $\text{Co}(\text{NH}_3)_6^{3+}$, TlCl_6^{3-} does not seem a likely candidate. On the other hand, a formal consideration of the ionization potentials shows that the energy liberated when an electron is added to Sb^{5+} is greater than the energy needed to form Tl^{4+} from Tl^{3+} by 5.7 e.v. The corresponding figures for Sb(III), Bi(III), and In(III) are 11.5, 10.7, and -2.2 e.v. One could test the compression hypothesis by making the corresponding rhodium(III) hexaammine salt, which probably has the same structure, and whose first cation absorption bands lie much further into the ultraviolet.

Acknowledgments.—The author wishes to thank the American Cyanamid Company for a Visiting Fellowship to their European Research Institute, and particularly Dr. C. K. Jørgensen of the Institute for very many interesting conversations.

(18) H. P. Klug, E. Kummer, and I. Alexander, *J. Am. Chem. Soc.*, **70**, 3064 (1948).

(19) M. Linhard, *Z. Elektrochem.*, **50**, 224 (1944).

Anion Ordering in Mixed-Valence Cs_2SbCl_6 and Related Salts

Kosmas Prassides and Peter Day*

*Inorganic Chemistry Laboratory
 Oxford University, Oxford OX1 3QR, United Kingdom*

Anthony K. Cheetham

*Chemical Crystallography Laboratory
 Oxford University, Oxford OX1 3QR, United Kingdom*

Received January 21, 1983

Cs_2SbCl_6 , first prepared in 1901,¹ was originally described as an Sb^{V} salt. However, a great deal of spectroscopic evidence (e.g., Mössbauer,² far infrared,³ Raman,⁴ ultraviolet,⁵ and photoelectron spectra⁶) points to the existence of distinguishable $\text{Sb}^{\text{III}}\text{Cl}_6^{3-}$ and $\text{Sb}^{\text{V}}\text{Cl}_6^-$ in the structure, and its semiconductivity⁷ and visible absorption^{5,8} show that Cs_2SbCl_6 is a classical Robin-Day⁹ class II mixed-valency compound. Additional recent measurements¹⁰ of the far infrared and Raman spectra have also been interpreted in terms of increased localization of the Sb oxidation states at low temperature. Nevertheless, there remains a puzzle about its crystal structure. Wells⁴ showed that Cs_2SbCl_6 forms mixed crystals with salts like Cs_2SnCl_6 and Cs_2PtCl_6 , and early X-ray powder diffraction patterns^{11,12} were indexed by using the space group $Fm\bar{3}m$.

X-ray powder photographs of mixed-metal compounds $\text{Cs}_2\text{M}^{\text{III}}_{0.5}\text{Sb}_{0.5}\text{Cl}_6$ ⁸ were also indexed as $Fm\bar{3}m$, implying that the MCl_6^{3-} and SbCl_6^- groups were randomly distributed. Given the difference in charge between the two anions, this seems inherently unlikely, and given that the X-ray scattering is dominated by the Cs and Sb, we have recorded neutron powder diffraction profiles of Cs_2SbCl_6 itself and a number of mixed-metal analogues. We find that there is indeed a superlattice ordering of Sb^{III} (and other M^{III}) and Sb^{V} at low temperature in several salts of this type, while others remain disordered. The presence or absence

- (1) Wells, H. L.; Metzger, F. J. *Am. Chem. J.* **1901**, 26, 268.
- (2) Birchall, T.; Valle, B. D.; Martineau, E.; Milne, J. B. *J. Chem. Soc. A* **1971**, 1855. Donaldson, J. D.; Tricker, M. J.; Dale, B. W. *J. Chem. Soc., Dalton Trans.* **1972**, 893. Longworth, G.; Day, P. *Inorg. Nucl. Chem. Lett.* **1976**, 12, 451.
- (3) Barrowcliffe, T.; Beattie, I. R.; Day, P.; Livingstone, K. *J. Chem. Soc. A* **1967**, 1810. Clark, H. W.; Swanson, B. I. *J. Am. Chem. Soc.* **1981**, 103, 2928.
- (4) Clark, R. J. H.; Trumble, W. R. *J. Chem. Soc., Dalton Trans.* **1976**, 1145.
- (5) Atkinson, L.; Day, P. *J. Chem. Soc. A* **1968**, 2423.
- (6) Tricker, M. J.; Adams, I.; Thomas, J. M. *Inorg. Nucl. Chem. Lett.* **1972**, 8, 633. Burroughs, P.; Hamnett, A.; Orchard, A. F. *J. Chem. Soc., Dalton Trans.* **1974**, 565.
- (7) Atkinson, L.; Day, P. *J. Chem. Soc. A* **1968**, 2432.
- (8) Day, P. *Inorg. Chem.* **1963**, 2, 452.
- (9) Robin, M. B.; Day, P. *Adv. Inorg. Chem. Radiochem.* **1967**, 10, 247.
- (10) Clark, H. W.; Swanson, B. I. *J. Am. Chem. Soc.* **1981**, 103, 2928.
- (11) Jensen, K. A. Z. *Anorg. Allg. Chem.* **1937**, 232, 193.
- (12) Tovborg-Jensen, A.; Rasmussen, S. E. *Acta Chem. Scand.* **1955**, 9, 708.

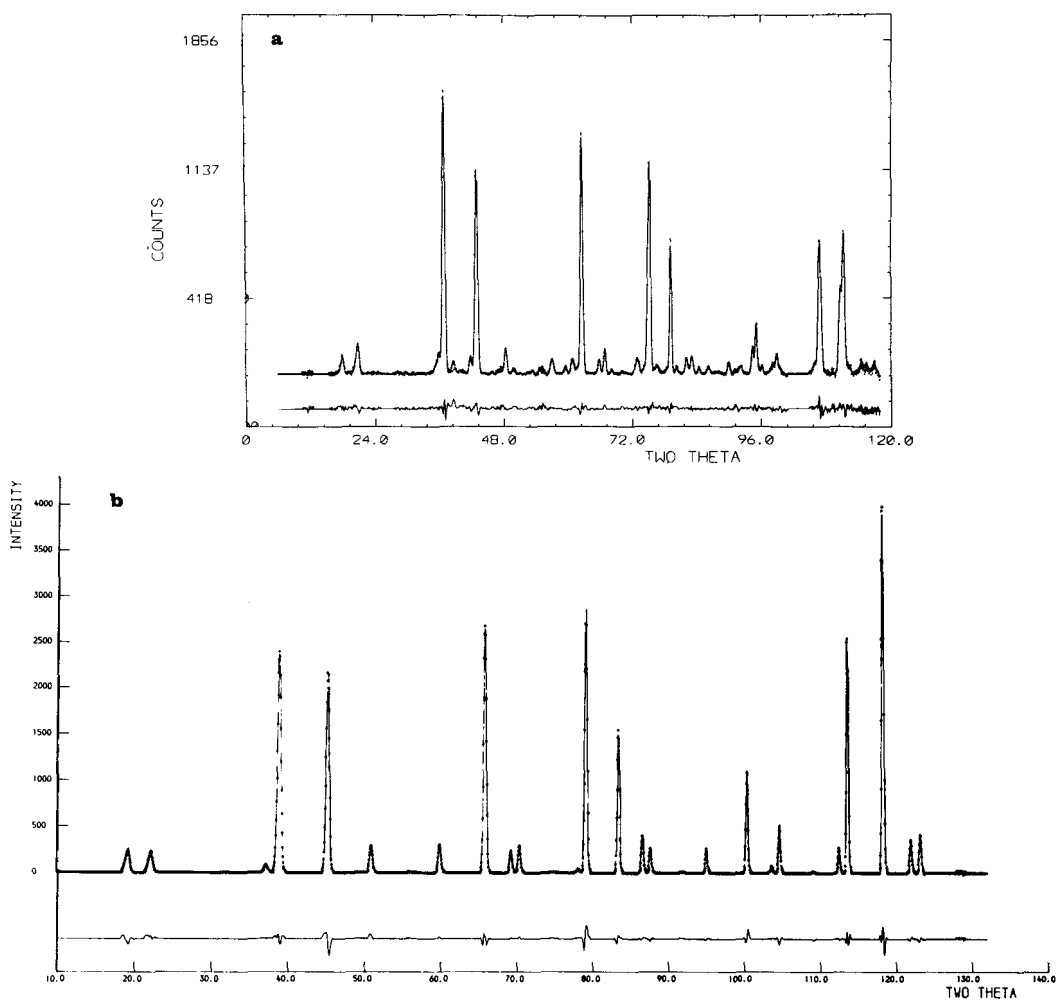


Figure 1. Powder neutron diffraction profiles of (a) $\text{Cs}_2\text{Sb}_{0.5}^{\text{III}}\text{Sb}_{0.5}^{\text{V}}\text{Cl}_6$ and (b) $\text{Rb}_2\text{Fe}_{0.5}^{\text{III}}\text{Sb}_{0.5}^{\text{V}}\text{Cl}_6$.

Table I. Unit Cell Parameters and Bond Lengths for $\text{A}_2\text{M}_{0.5}^{\text{III}}\text{Cl}_6$ (Å)

A	M^{III}	a_0	c_0	av $\text{M}^{\text{III}}\text{-Cl}$	av $\text{Sb}^{\text{V}}\text{-Cl}$	$\text{M}^{\text{III,V}}\text{-Cl}$	$R_{\text{wpr}} \%$ ^a
Cs	Bi	10.3558 (2)	20.8415 (6)	2.683	2.398	2.541	9.15
	Sb	10.3092 (3)	20.7288 (7)	2.646	2.384	2.515	9.20 ^b
	Tl	10.2994 (4)	20.6114 (15)	2.554	2.389	2.472	11.40
	In	10.2788 (2)				2.438	11.78
Rb	Fe	10.2044 (1)				2.386	8.29
	Tl	10.0613 (1)				2.448	9.26
	In	10.0307 (1)				2.426	7.33
	Fe	9.9437 (1)				2.379	8.40
	Rh	9.9093 (1)				2.361	8.66

^a R defined in ref 16. ^b Biphasic refinement.¹⁵

of superlattice ordering correlates with the average $\text{M}^{\text{III,V}}\text{-Cl}$ bond length.

The powder neutron diffraction profiles were recorded at 4.7 K on the D1A diffractometer at the Institut Laue-Langevin, Grenoble. The samples were contained in vanadium cans held in a helium cryostat, and the mean neutron wavelength was 1.909 Å. All the compounds were prepared by standard methods^{1,8} and had been carefully checked by X-ray powder diffraction to ensure

that they were free of trace impurities of starting materials. A small amount of $\alpha\text{-Cs}_2\text{Sb}_2\text{Cl}_6$ was identified as an impurity in Cs_2SbCl_6 (see below). Typical scans of Cs and Rb salts are shown in Figure 1. The background has been subtracted. It is clear at once that, in addition to the major reflections common to both compounds, the Cs salt (Figure 1a) has numerous weaker reflections indicative of superlattice ordering. All the reflections observed in $\text{Rb}_2\text{Fe}_{0.5}\text{Sb}_{0.5}\text{Cl}_6$ (Figure 1b) are accounted for by the

3368

space group $Fm\bar{3}m$ with $a_0 = 9.944$ Å, and all the "extra" reflections in the Cs profile (Figure 1a) are described by the tetragonal space group $I4_1/amd$ with $a_0 = 10.309$ Å and $c_0 = 20.729$ Å. Refinement of each profile by the Rietveld technique¹³ using the POWDER system¹⁴ on the SERC Interactive Computing Facility leads to the fits shown in Figure 1 and the unit cell parameters and bond lengths listed in Table I. In refining the Cs_2SbCl_6 profile, account was taken of the $Cs_2Sb_2Cl_9$ impurity by using a multiphase fitting procedure.¹⁵ An absorption correction was applied to all the powder diffraction profiles by Hewat's method.¹⁶

The proposed ordering of $M^{III}Cl_6^{3-}$ and $Sb^VCl_6^-$ in the tetragonal salts is similar to that postulated in a single-crystal X-ray diffraction study of $(NH_4)_2SbBr_6$.¹⁷ Each $M^{III}Cl_6^{3-}$ is surrounded by eight $SbCl_6^-$ and four $M^{III}Cl_6^{3-}$, the latter at the corners of a tetrahedron. The $Fm\bar{3}m$ unit cell (that of the K_2PtCl_6 structure) is doubled along one axis. In contrast to $(NH_4)_2SbBr_6$ we find less than 0.5° angular distortion of the $SbCl_6^-$ but a small (2.5°) D_{2d} distortion of $SbCl_6^{3-}$ and $BiCl_6^{3-}$, to be compared with $TiCl_6^{3-}$, which showed an angular distortion of 1.5° . In the cubic salts the space group constrains all anions to be octahedral. An important parameter in theories of electron transfer in mixed-valency compounds is the difference in bond lengths around the ions of different oxidation state. In the present case we find $Sb^{III}-Cl$ is 2.646 and Sb^V-Cl 2.384 Å compared with 2.63 and 2.35 Å in $(C_2H_7NH_3)_4Sb_0.5^{III}Sb_0.5^VCl_6(Cl)_2$,¹⁶ which has a rather different structure. Of the nine salts $A_2M_0.5^{III}Sb_0.5^VCl_6$ investigated, three were found to have superlattice ordering of $M^{III}Cl_6^{3-}$ and $Sb^VCl_6^-$, the rest being disordered. All the Rb salts were disordered, and among the Cs salts ordering was found in both salts in which M^{III} had an ns^2 electron configuration and one where M^{III} was an ns^0 ion (Tl^{III}). To identify the reasons for this result, we note that the average $(M^{III}, Sb^V)-Cl$ bond lengths span a range from 2.541 to 2.361 Å (Table I). The change from order to disorder occurs between 2.472 ($Cs_2Tl_{0.5}Sb_{0.5}Cl_6$) and 2.448 Å ($Rb_2Tl_{0.5}Sb_{0.5}Cl_6$). Salts with an average $(M^{III}, Sb^V)-Cl$ bond length greater than 2.472 Å are ordered while all those where it is less than 2.448

Å are disordered. Thus the difference in size between MCl_6^{3-} and $SbCl_6^-$ appears to be the dominant factor. Unfortunately $Rb_2Sb_{0.5}^{III}Sb_{0.5}^VCl_6$ is very unstable and transforms easily to the monoclinic salt $Rb_{2.6}SbCl_6$, but we are continuing powder neutron diffraction work on the hexabromoantimonates(III,V) and related mixed-metal salts to clarify the structural principles governing this class of compound.

Acknowledgment. We are grateful to the Institut Laue-Langevin for providing neutron beam time and to S. Heathman for help with the experiments. We have also received financial assistance from the Science and Engineering Research Council. K.P. thanks Christ Church, Oxford, for a Senior Scholarship.

Registry No. $Cs_2Bi^{III}Sb_{0.5}^VCl_6$, 12441-33-7; $Cs_2Sb^{III}Sb_{0.5}^VCl_6$, 17805-64-0; $Cs_2Tl^{III}Sb_{0.5}^VCl_6$, 41875-61-0; $Cs_2In^{III}Sb_{0.5}^VCl_6$, 41875-60-9; $Cs_2Fe^{III}Sb_{0.5}^VCl_6$, 61269-02-1; $Rb_2Tl^{III}Sb_{0.5}^VCl_6$, 12432-76-7; $Rb_2In^{III}Sb_{0.5}^VCl_6$, 85370-04-3; $Rb_2Fe^{III}Sb_{0.5}^VCl_6$, 61269-01-0; $Rb_2Rh^{III}Sb_{0.5}^VCl_6$, 85370-05-4.

Supplementary Material Available: Table of positional and thermal parameters (4 pages). Ordering information is given on any current masthead page.

(13) Rietveld, H. M. Reactor Centrum Nederland Research Report RCN 104, 1969, unpublished. Rietveldt, H. M. *J. Appl. Crystallogr.* **1969**, *2*, 65.

(14) Rae-Smith, A. R.; Cheetham, A. K.; Skarnulis, A. J. *J. Appl. Crystallogr.* **1979**, *12*, 485.

(15) Thomas, M. W.; Bendall, P. J. *Acta Crystallogr., Sect. A* **1978**, *A34*, S351. Fitch, A. N.; Wright, A. F.; Fender, B. E. F. *Acta Crystallogr., Sect. B* **1982**, *B38*, 2546.

(16) Hewat, A. W. *Acta Crystallogr., Sect. A* **1979**, *A35*, 248.

(17) Lawton, S. L.; Jacobson, R. A. *Inorg. Chem.* **1966**, *5*, 743.

(18) Birke, G.; Latscha, H. P.; Pritzkow, H. *Z. Naturforsch., B* **1976**, *31B*, 1285.

Charge Transfer in Mixed-valence Solids. Part IV.¹ Electronic Spectra of Hexachloroantimonates(III,V)

By L. Atkinson and P. Day,* Inorganic Chemistry Laboratory, South Parks Road, Oxford

Four series of hexachloroantimonate(III,V) salts, $A^I_3Sb_2Sn_{1-x}Cl_6$ ($A^I = NH_4^+$, Cs^+ , and $MeNH_3^+$), and $Cs_2Sb^{III}_yIn^{III}_{3-y}Sb^V_3Cl_6$ have been prepared and characterised by chemical analysis, X-ray powder diffraction, and far-i.r. measurements. Visible and u.v. spectra of all the compounds were measured at room temperature by diffuse reflectance and, in the case of the $MeNH_3^+$ salts, by single-crystal transmission between room temperature and 6°K. The concentration-dependence of the spectra showed that the intensity of the visible mixed-valence band was proportional to the concentration of $Sb^{III}-Sb^V$ pairs in the hexachlorostannate(IV) lattice. From the absolute intensity of the mixed-valence transition it was found that delocalisation of the optical (5s) electrons of $SbCl_6^{3-}$ on to the neighbouring $SbCl_6^-$ was less than 0.1% in the ground state, in agreement with the far-i.r. results. The band, therefore, is almost purely charge-transfer in character. The temperature-dependence of the half-width of the band between 300 and 6°K could be accounted for in terms of broadening by a single effective frequency of 210 cm^{-1} . The relation between this optically derived frequency and the ground-state vibrational frequencies of $SbCl_6^{3-}$ and $SbCl_6^-$ is considered.

THE previous Parts,^{1,2} which were devoted to chlorocuprates, gave evidence that outer-sphere electron transfer between the mixed-valence anions in that lattice could be detected both as enhanced electrical con-

ductivity and increased light absorption. On the assumption that the migration of charge from one anion to another will lead to bond-length alterations between the anions of differing valency, one might hope to find a

¹ Part III, D. Culpin, P. Day, P. R. Edwards, and R. J. P. Williams, *J. Chem. Soc. (A)*, 1968, 1838.

² P. Day and D. W. Smith, *J. Chem. Soc. (A)*, 1967, 1045; P. Day, *ibid.*, 1968, 1835.

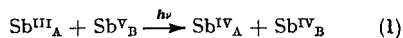
2424

J. Chem. Soc. (A), 1969

connection between the mobility of the charge carriers and the vibrational properties of the anions and the lattice.

The chlorocuprates provided an excellent series of compounds on which to test the hypothesis that enhanced conductivity could be unambiguously connected with the existence of two valency states in the same lattice, because solids could be prepared containing Cu^{I} and Cu^{II} in all mole ratios. Nevertheless, the peculiar structural circumstances which made this possible also made it impossible to apply quantitative models to them. In this and the following paper we report studies on a mixed-valence system chosen for its structural simplicity.

Many hexachloroantimonate(III,V) salts crystallise in lattices whose space-groups approximate very closely to those of the hexachlorostannates(IV) with the same cations. The first of these to be prepared³ was the dark blue compound Cs_2SbCl_6 , which has an almost cubic antiferroite structure. A historical survey of the evidence which led to its formulation as an $\text{Sb}^{\text{III,V}}$ compound was given in a recent review.⁴ The crystal structure⁵ of the related salt $(\text{NH}_4)_2\text{SbBr}_6$ reveals a superlattice of SbBr_6^- and SbBr_6^{3-} , and in Cs_2SbCl_6 the i.r.-active ν_3 vibration of SbCl_6^- can be detected at a frequency only 5 cm^{-1} from its position in CsSbCl_6 . U.v. electronic transitions in both salts are also observed at frequencies very close to those of the individual anions in single-valence lattices, such as $\text{Co}(\text{NH}_3)_6\text{SbCl}_6$, though in addition the mixed-valence salts have broad absorption bands covering the visible and near-i.r. regions. The latter, qualitatively investigated by diffuse reflectance spectroscopy,⁶ have been assigned to intermolecular charge transfer (1). We recently indicated⁴ how the



intensity of this type of absorption band could be used to estimate the electron delocalisation in the ground and excited states of such 'class II' mixed valency systems, and we therefore report measurements on the absolute intensity of the hexachloroantimonate(III,V) bands from single-crystal transmission spectra. Spectra have also been recorded down to 4°K, and a quantitative treatment of the variation of the band width with temperature enables an estimate to be made of the vibrational frequencies broadening the transitions. It is first necessary to assign the transitions unambiguously to intermolecular charge transfer, and this we do by examining the concentration-dependence of the intensity. Hexachlorostannate(IV) salts provide convenient host lattices for such experiments and, by varying the cation from ammonium to caesium, enable estimates to be made of the influence of the $\text{Sb}^{\text{III}}\text{-Sb}^{\text{V}}$ distance on both optical and thermal charge transfer.

³ C. Setterberg, *Oefversigt. K. Vetensk. Akad. Forhandl.*, 1882, No. 6, 23.

⁴ M. B. Robin and P. Day, *Adv. Inorg. Chem. Radiochem.*, 1967, 10, 247.

To delineate still more closely the concentration-dependence of these properties we have prepared a further set of compounds which permit the Sb^{III} concentration to be varied while the Sb^{V} concentration remains constant. These are based on partial replacement of Sb^{III} in the lattice of $\text{M}^{\text{I}}_2\text{Sb}^{\text{III}}_y\text{Sb}^{\text{V}}_x\text{Cl}_6$ by other trivalent ions such as In^{III} and Tl^{III} .

The present paper gives details of the preparation and characterisation of all the compounds, and the optical results; the following one concentrates on their electrical properties.

EXPERIMENTAL

Preparations.—Three series of compounds were prepared, with the general formulae $(\text{NH}_4)_2\text{Sb}_x\text{Sn}_{1-x}\text{Cl}_6$, $\text{Cs}_2\text{Sb}_x\text{Sn}_{1-x}\text{Cl}_6$, and $\text{Cs}_2\text{Sb}^{\text{III}}_y\text{In}^{\text{III}}_{1-y}\text{Sb}^{\text{V}}_x\text{Cl}_6$. Stock solutions of Sb_2O_3 , Sb_2O_5 , SnCl_4 , InCl_3 , CsCl , and NH_4Cl in 12M-HCl were employed; appropriate quantities of Sb^{III} , Sb^{V} , and dopant solutions were mixed with an equivalent or slight excess of the cation solution. The mixtures were warmed and sufficient 12M-HCl added to ensure complete solution at the b.p. The solutions were filtered hot through a sinter and immediately cooled until crystallisation began. After 5 min. the precipitates were filtered off and washed with a very small quantity of 12M-HCl. They were dried and stored over P_2O_5 in a vacuum desiccator. To avoid coprecipitation of CsSbCl_6 or NH_4SbCl_6 slight excesses of cation and M^{III} solutions were employed when the Sb^{V} concentration was high. The colours of the solids range from deep purple through light purple, grey, and green to white [$(\text{NH}_4)_2\text{SnCl}_6$ and Cs_2SnCl_6] or pale yellow ($\text{Cs}_2\text{In}_4\text{Sb}_4\text{Cl}_6$).

Crystals of the red-brown compound formulated by Weinland and Schmidt⁷ as $\text{Rb}_5\text{SbCl}_6 \cdot 2\text{Rb}_3\text{SbCl}_6$ were grown by dissolving 0.8 g. of Sb_2O_3 and 2.0 g. of RbCl in a total of 60 ml. of 12M-HCl. A dilute solution of Cl_2 in 12M-HCl was added dropwise until the resulting precipitate was brown. Recrystallisation from hot solution was allowed to take place in air.

$(\text{MeNH}_3)_2\text{Sb}_x\text{Sn}_{1-x}\text{Cl}_6$ and $(\text{EtNH}_3)_2\text{Sb}_x\text{Sn}_{1-x}\text{Cl}_6$.—To prevent precipitation of the sparingly soluble Sb^{V} compounds of these cations, Sb^{III} ; Sb^{V} ratios much greater than unity were employed. Sb^{III} and Sb^{V} saturated solutions were mixed in the ratio 2:1 v/v and various volumes of Sn^{IV} solution added. A few drops of alkylammonium hydrochloride solution in 12M-HCl were added, sufficient to cause precipitation. Recrystallisation gave well developed flat plates. An analogous series of $\text{Bi}^{\text{III}}\text{Sb}^{\text{V}}$ compounds was also prepared.

Analyses.—All Sn^{IV} doped compounds were analysed for total antimony, tin, and chlorine. Antimony was determined by bromate titration after Sb^{V} had been reduced to Sb^{III} by SO_2 . The end-point was detected potentiometrically. Tin was reduced to Sn^{II} by iron in strongly acid solution, followed by titration with iodine. Iron reduced the antimony to the metal, which could be filtered off with the excess of iron. To prevent oxidation of Sn^{II} an atmosphere of H_2 and CO_2 was maintained during the reduction. Chloride ion was determined by Volhard's method.

⁵ S. L. Lawton and R. A. Jacobson, *Inorg. Chem.*, 1966, 5, 743.

⁶ P. Day, *Inorg. Chem.*, 1963, 2, 452.

⁷ R. F. Weinland and H. Schmidt, *Ber.*, 1905, 38, 1080.

Inorg. Phys. Theor.

Results of the three analyses are given in Table 1. As the percentages of Sb and Sn are related independently to x , values of x calculated from both are given. The agreement between them is extremely good, even when the values of x are small, thus providing excellent evidence for the

TABLE 1
Analyses of $A^I_2Sb_2Sn_{1-x}Cl_6$ compounds

Compound	Sb (%)	Sn (%)	Cl (%)	x			
				from Sb + Sn	from % Sb	from % Sn	
$(NH_4)_2Sb_2Sn_{1-x}Cl_6$	9.19	23.4	57.2	57.6	0.28	0.27	
	7.76	24.8	57.3	57.3	0.24	0.24	
	6.02	26.2	57.4	57.6	0.19	0.19	
	3.15	29.2	57.9	57.8	0.10	0.10	
	2.81	29.6	58.0	57.9	0.08	0.09	
	2.31	30.2	57.9	57.6	0.07	0.07	
$(NH_4)_2SnCl_6$	Found	0	32.0	58.2	58.1	0	
	Calc.	0	32.2	58.0	58.0	0	
	Cs_2SbCl_6	Found	20.6	0	35.8	36.0	1
		Calc.	20.3	0	35.5	35.5	1
	$Cs_2Sb_2Sn_{1-x}Cl_6$	18.7	1.6	35.5	36.9	0.92	0.92
		12.8	7.4	35.7	35.6	0.63	0.63
4.9		15.1	35.2	35.5	0.24	0.25	
1.4		18.5	35.9	35.4	0.07	0.07	
Cs_2SnCl_6	Found	0	20.0	35.0	35.9	0	
	Calc.	0	19.8	35.7	35.7	0	
$(MeNH_3)_2Sb_2Sn_{1-x}Cl_6$	1.48	28.6	—	—	0.05	0.05	
	0.95	28.9	—	—	0.03	0.04	
$(EtNH_3)_2Sb_2Sn_{1-x}Cl_6$	4.83	23.2	—	—	0.17	0.17	
	1.24	26.9	—	—	0.04	0.04	

formulae suggested. This is of some importance as in a series of papers on the radioactive exchange between Sb^{III} and Sb^V in this type of solid, Turco and Mazzon⁸ found $Sb^{III} : Sb^V$ ratios much greater than unity in $(NH_4)_2Sb_2Sn_{1-x}Cl_6$ and $Cs_2Sb_2Sn_{1-x}Cl_6$. The analyses in Table 1 provide no evidence for any deviation from 1 : 1 in our samples.

Compounds in the $Cs_2Sb^{III}_yIn^{III}_{1-y}Sb^V_4Cl_6$ series were analysed by X-ray fluorescence for caesium, indium, and antimony. As calibration standards the end-members of the series, Cs_2SbCl_6 and $Cs_2In_4Sb_4Cl_6$, were mixed heterogeneously in various ratios to cover the range $0 < y < \frac{1}{2}$. Total weight of all samples was 0.150 g. with MgO added to a total weight of 3.000 g. so that the samples could be pressed into pellets. The analyses were performed on a Philips X-ray fluorescence apparatus in the Department of Geology, Oxford. The caesium content varies very little with y , and thus may be used as an approximate internal standard and check on sample preparation. On the other hand values of y may be calculated from both indium and antimony analyses, and the agreement between them provides a check on the suggested formulae. The results in Table 2 are judged accurate to about 1%, at which level the suggested formulae are obeyed.

X-Ray Measurements.—Powder diffraction patterns were obtained for all the compounds on a Philips diffractometer. The results were used both as a check on sample purity and identity, by examining the charts for lines due to impurities

⁸ A. Turco and L. Mazzon, *Ann. Chim. (Rome)*, 1953, **43**, 853, 865; 1955, **45**, 614.

⁹ G. C. Allen and N. S. Hush, *Progr. Inorg. Chem.*, 1967, **8**, 357.

TABLE 2
Analyses of $Cs_2Sb^{III}_yIn^{III}_{1-y}Sb^V_4Cl_6$ compounds

Sb (%)	In (%)	Cs (%)	y		
			Cs (%) from Sb + In	from Sb	from Sn
18.6	2.0	44.2	44.3	0.42	0.40
18.5	2.2	44.7	44.3	0.41	0.39
16.6	3.7	44.7	44.4	0.32	0.31
16.2	4.0	44.2	44.4	0.28	0.29
14.7	6.8	44.7	44.4	0.15	0.15
13.8	6.7	44.6	44.4	0.14	0.15
13.8	6.7	44.4	44.4	0.14	0.15
12.0	7.7	44.3	44.4	0.09	0.10
10.4	9.3	44.4	44.5	0.01	0.02

such as $CsSbCl_6$, and to calculate the unit-cell dimensions as a function of composition.

All the samples were indexed according to the space-group $O_h^2-Fm\bar{3}m$, the cubic antiferroite structure of Cs_2SnCl_6 , and unit-cell lengths, calculated from higher angle reflections only ($\theta > 18^\circ$), are recorded in Table 3. All

TABLE 3
Unit-cell lengths (Å) of $Cs_2Sb_2Sn_{1-x}Cl_6$ and $Cs_2Sb^{III}_yIn^{III}_{1-y}Sb^V_4Cl_6$

Compound	x or y	
Cs_2SnCl_6	0	10.38
	0.07	10.38
	0.24	10.39
$Cs_2Sb_2Sn_{1-x}Cl_6$	0.63	10.41
	0.92	10.44
Cs_2SbCl_6	1	10.47
$Cs_2In^{III}_4Sb^V_4Cl_6$	0	10.40
$Cs_2Sb^{III}_yIn^{III}_{1-y}Sb^V_4Cl_6$	0.01	10.41
	0.09	10.41
	0.14	10.42
	0.14	10.42
	0.28	10.43

standard deviations are less than 0.01 Å. Table 3 indicates that in both series of compounds the unit-cell lengths change more rapidly with composition at high antimony concentrations, contrary to Vegard's rule, which predicts a linear relationship of unit-cell length with concentration for random solid solutions. No evidence for superlattice ordering, such as that found⁶ in $Cs_2Sb^V_4Bi^{III}_4Cl_6$, was detected in any of the compounds examined here. Allen and Hush⁹ claimed a linear relationship between unit-cell length and x in the series $Rb_2Sb_2Sn_{1-x}Cl_6$, but the error limits in our own and Allen and Hush's work do not suggest that the origin of the discrepancy is experimental. The important conclusion for the present work is that the unit-cell lengths vary monotonically throughout both series of compounds with no major structural change.

Far-i.r. Spectra.—Because the vibrational properties of the anions and the lattice are important in determining the rate of intermolecular charge migration, the far-i.r. spectra of many of the mixed-valence and mixed-anion compounds prepared above were measured on a Beckman IR11 spectrometer. Samples were run between 600 and 40 cm^{-1} as Nujol mulls supported between Polythene discs, Polythene being transparent throughout the entire region except for a small peak at 73 cm^{-1} .

The solid-state Raman spectra of a number of the compounds, together with a limited amount of i.r. data, have been given.¹⁰

¹⁰ T. Barrowcliffe, I. R. Beattie, P. Day, and K. Livingston, *J. Chem. Soc. (A)*, 1967, 1810.

2426

J. Chem. Soc. (A), 1969

A complete list of all the frequencies observed is in Table 4. Because of interest¹⁰ in the possible differences on the half-widths of far-i.r. bands for 'inert-pair' and 'non-inert-pair' hexahalide ions, the second figure in each column of Table 4 is the band-width at a height where the transmission is double that at the peak maximum. The third figure is the peak-height relative to the highest peak. These band-heights and -widths are very approximate, since they depend somewhat on sample preparation, but it is thought that they are more informative than the purely qualitative description 'sharp', 'weak', etc. Further discussion leading to the assignments in Table 4 is presented below.

Electronic Spectra.—(i) *Diffuse reflectance spectra.* Crystals of hexachloroantimonate(III,V) doped in hexachlorostannate(IV) could not be grown large enough for crystal transmission spectroscopy when NH_4^+ and Cs^+ were

used as the cations. Hence, as in Part III,¹ diffuse reflectance spectra were employed quantitatively to examine the concentration-dependence of the intensity of the mixed-valence transitions. The spectra were measured manually on a Unicam SP 500 spectrophotometer with LiF as reference material.

120 seconds grinding time, then fell slowly, because of increasing Rayleigh scattering. Hence in all subsequent measurements 0.5 g. samples were ground for 120 sec. and used at once. Examination of the ground powders under a calibrated microscope showed no particle above 10 μ diameter. The spectra of two samples of each compound were measured. In no case did the percentage reflection at a given frequency vary by more than 2% between the two samples. It is therefore evident that with suitable care, diffuse reflectance measurements are capable of yielding quite accurate information about the relative absorbances of different samples.

Nevertheless, as a further test of the reliability of the diffuse reflectance technique, both powder reflectance and single crystal transmission spectra were recorded for a number of samples for which good crystals could be obtained. The method of measuring the transmission

TABLE 4
Far-i.r. spectra

Only metal-chlorine and lattice modes included. See text for explanation of symbols.

Cs_2SnCl_6	ν_2 309 * (40) 1	ν_4 174 (25) 0.95	ν_L 70 (15) 0.90			
Rb_2SnCl_6	316 * (40) 1	175 (25) 0.95	70 (15) 0.90			
$(\text{NH}_4)_2\text{SnCl}_6$	315 * (30) 1	181 (55) 0.95	124 (25) 0.80			
$(\text{MeNH}_3)_2\text{SnCl}_6$	317 * (30) 1	182 (46) 0.95	115 (46) 0.75		[75]br,w	
$(\text{EtNH}_3)_2\text{SnCl}_6$	310 * (40) 1	174 * (30) 0.95	107 (45) 0.45		[75]br,w	
CsSbVCl_6	ν_2 342 * (45) 1	ν_4 188 (25) 0.90	ν_L 57 (10) 0.55			
$\text{Cs}_2\text{Bi}^{\text{III}}\text{Cl}_6$	ν_3 187 * (85) 1	ν_4 (?) [129] -0.40	109 (25) 0.30	[71] 0.30	62 (15) 0.35	
$\text{Cs}_2\text{In}^{\text{III}}\text{Sb}^{\text{V}}\text{Cl}_6$	ν_2 (Sb ^V) 347 (30) 1	[329] 0.65	ν_3 (M ^{III}) 251 * (45) 0.90	ν_4 (Sb ^V) 187 (15) 0.95	ν_4 (M ^{III}) 161 * (40) 0.90	ν_L 73 (15) 0.70
Cs_2SbCl_6	347 * (25) 1	—	—	198 * (65) 1	—	68 (15) 0.75
$\text{Cs}_2\text{Tl}^{\text{III}}\text{Sb}^{\text{V}}\text{Cl}_6$	348 (20) 1	[329] 0.60	228 (35) 0.90	187 (15) 0.95	142 (40) 0.90	64 (15) 0.70
$\text{Cs}_2\text{Bi}^{\text{III}}\text{Sb}^{\text{V}}\text{Cl}_6$	350 (25) 1	[329] 0.30	196 * (65) 1	120 (35) 0.50	—	62 (15) 0.65
Rb_2SbCl_6	346 * (30) 1	—	—	208 * (75) 1	—	70 (20) 0.70
$\text{Rb}_2\text{Tl}^{\text{III}}\text{Sb}^{\text{V}}\text{Cl}_6$	353 (30) 1	[330] 0.75	239 * (40) 0.85	187 (15) 0.95	152 (40) 0.90	68 (15) 0.65
$\text{Cs}_2\text{Sb}_{0.45}\text{Sn}_{0.55}\text{Cl}_6$	ν_2 (Sb ^V) 348 * (20) 1	ν_3 (Sn ^{IV}) 313 (30) 0.85	187 * (45) 0.90	ν_L 69 (15) 0.55	—	—
$\text{Cs}_2\text{Sb}^{\text{III}}_{0.25}\text{In}^{\text{III}}_{0.75}\text{Sb}^{\text{V}}\text{Cl}_6$	ν_2 (Sb ^V) 348 * (25) 1	ν_4 (In ^{III}) 251 * (30) 0.60	191 * (25) 0.95	ν_4 (In ^{IV}) 160 (15) 0.60	ν_L 71 (15) 0.50	—

used as the cations. Hence, as in Part III,¹ diffuse reflectance spectra were employed quantitatively to examine the concentration-dependence of the intensity of the mixed-valence transitions. The spectra were measured manually on a Unicam SP 500 spectrophotometer with LiF as reference material.

To obtain reproducible results, comparable between different samples, it is essential to standardise the grinding procedure, so that powders of comparable particle size are produced. Likewise one must minimise the effect of specular reflection on the measured absorbance values by reducing the particle size of the sample, though not too much, for if the particles are small compared with the wavelength of the incident light, scattering becomes strongly frequency-dependent.¹¹ Under the latter conditions the recorded spectrum will clearly not be a true measure of the absorption characteristics of the solid.

To determine the optimum particle size, experiments were therefore performed on 0.5 g. samples of one of the compounds. The optical density at the frequency of the peak maximum was plotted against grinding time. The graph at first rose steeply, reaching a maximum at about

spectra is indicated below, but the results of two determinations, on concentrated and dilute samples of $(\text{MeNH}_3)_2\text{Sb}_2\text{Sn}_{1-x}\text{Cl}_6$, are shown in Figure 1. The diffuse reflectance spectra are plotted in units of $KM = (1 - R)^2/2R$, the Kubelka-Munk function,¹² where R is the percentage reflection, and the transmission spectra as α , the optical density per cm. of crystal. The excellent agreement between the two types of spectrum is indicated by the fact that the ratio $(KM)/\alpha$ is constant in each case over the entire spectral range to an accuracy better than 10%.

The frequencies of the band maxima reported in Table 5 were determined as the point at which a line joining the mid-points of the band at various peak-heights cuts the band. In samples with low antimony concentrations there is some contribution to the mixed-valence band shape from absorption on the high-energy side. Hence half-widths (H in Table 5) were taken as in equation (2), where ν_k is the

$$H = 2(\nu_{\text{max}} - \nu_k) \quad (2)$$

¹¹ G. Kortum and D. Oelkrug, *Z. Naturforsch.*, 1964, 19a, 28.

¹² W. W. Wendlandt and H. G. Hecht, 'Reflectance Spectroscopy,' Interscience, New York, 1966.

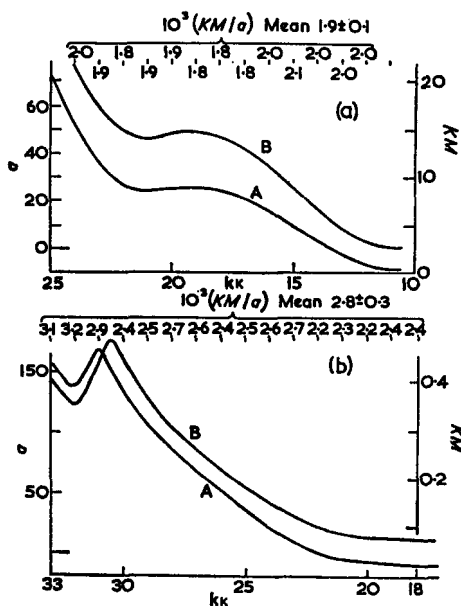


FIGURE 1 A, Diffuse reflectance and B, crystal transmission spectra of (a) concentrated and (b) dilute samples of $(\text{MeNH}_3)_2\text{Sb}_2\text{Sn}_{1-x}\text{Cl}_x$.

TABLE 5

Powder reflectance data: mixed-valence absorption band

Compound	x or y	Max. λ (kK)	H (kK)	$(KM)_{\text{max}}$
$(\text{NH}_4)_2\text{Sb}_2\text{Sn}_{1-x}\text{Cl}_x$	0.28	19.2	7.4	19.5
	0.24	18.9	7.4	12.9
	0.19	18.5	7.6	8.32
	0.10	18.3	7.4	1.62
	0.08	18.4	7.6	1.38
	0.07	18.1	7.6	0.692
	0.06	18.0	7.6	0.676
	0.02	17.9	7.6	0.068
Cs_2SbCl_6	1	18.5	7.0	20.4
	0.92	18.3	6.8	11.2
$\text{Vs}_2\text{Sb}_2\text{Sn}_{1-x}\text{Cl}_x$	0.63	18.1	7.0	6.76
	0.24	17.2	7.2	1.00
	0.07	15.5	7.4	0.071
$\text{Cs}_2\text{Sb}^{\text{III}}\text{In}^{\text{III}}_{1-y}\text{Sb}^{\text{V}}\text{Cl}_6$	0.42	18.2	6.8	17.0
	0.41	18.0	7.2	14.8
	0.32	17.7	7.2	11.5
	0.28	17.4	6.8	10.1
	0.15	17.2	7.0	5.89
	0.14	17.2	7.2	6.17
	0.14	17.1	7.4	5.75
	0.09	16.9	7.2	3.80
Rb_2SbCl_6		19.6	7.8	24.4
$(\text{MeNH}_3)_2\text{Sb}_2\text{Sn}_{1-x}\text{Cl}_x$		19.0	7.8	0.089
	(single crystal)	19.20	7.70)	
$(\text{MeNH}_3)_2\text{Sb}^{\text{V}}_{x/2}\text{Bi}^{\text{III}}_{x/2}\text{Sn}^{\text{IV}}_{1-x}\text{Cl}_6$		24.5	7.8	0.129
	(single crystal)	24.30	7.96)	
$\text{Rb}_2\text{SbCl}_6 \cdot 2\text{Rb}_2\text{SbCl}_6$		23.2	8.8	1.29
	(single crystal)	23.0	8.40)	

frequency at which $(KM) = \frac{1}{2}(KM)_{\text{max}}$ on the low-frequency side of the band.

(ii) *Crystal transmission spectra.* The spectra of crystals

belonging to the two series $(\text{MeNH}_3)_2\text{Sb}_2\text{Sn}_{1-x}\text{Cl}_6$ and $(\text{MeNH}_3)_2\text{Bi}^{\text{III}}_{x/2}\text{Sb}^{\text{V}}_{x/2}\text{Sn}_{1-x}\text{Cl}_6$ were measured between room temperature and 4°K on a Unicam SP 700 spectrophotometer equipped with a liquid-helium cryostat built by Oxford Instrument Co. The crystals, which were thin hexagonal plates about 2 mm.² in area, were mounted over a small hole approximately 1 mm. diameter drilled in a copper sheet. The crystals were fixed in position with 'Cryocon' copper conducting grease (Air Products Inc.) and the copper sheet was bolted to the base of the helium reservoir, an indium gasket ensuring good thermal contact. The temperature of the sample was monitored by a 0.03% w/w iron/gold-chromel thermocouple, the cold junction of which was firmly bolted between the indium gasket and the copper sheet. The other thermocouple junction was immersed in liquid nitrogen and the potential monitored by a 'Servoscribe' potentiometric recorder.

By pouring small amounts of liquid nitrogen into the helium reservoir the cryostat could be cooled from room temperature to 77°K in small steps, the thermal insulation of the sample from its surroundings being sufficiently good that a spectrum could be measured after each addition without the temperature varying more than 1–2°. Between 4 and 77°K, spectra were measured at intervals as the cryostat slowly warmed up.

To determine the linear absorption constants of the crystals, their thicknesses were measured with a microscope equipped with a Filar micrometer eyepiece. In addition, the spectra of a number of crystals of one of the more concentrated samples of $(\text{MeNH}_3)_2\text{Sb}_2\text{Sn}_{1-x}\text{Cl}_6$ were measured, and Lambert's law verified.

RESULTS

I.r. Spectra.—For an ion of regular octahedral point symmetry in a cubic lattice, three vibrations are normally i.r.-active: ν_3 , a stretch; ν_6 , a bend; and ν_8 , a lattice vibrational mode. Our results for A_2SnCl_6 ($\text{A} = \text{NH}_4, \text{Rb}, \text{Cs}$) agreed with those of Adams and Morris.¹³ Table 4 shows that the spectra of the $(\text{RNH}_3)_2\text{SnCl}_6$ compounds ($\text{R} = \text{Me}, \text{Et}$) are also very similar, suggesting that no great distortion of the octahedron occur in those lattices. These compounds belong¹⁴ to the space-groups $D_{3d}^2-R\bar{3}m$ ($\text{R} = \text{Me}$) and $D_{3d}^2-C\bar{3}m$ ($\text{R} = \text{Et}$), in which the SnCl_6^{2-} have D_{3d} site symmetry. If the distortion were substantial both ν_3 and ν_6 would be expected to split and ν_8 would become i.r.-allowed. The former bands show no sign of splitting, though the poorly resolved band at 75 cm^{-1} in both compounds could be the e_g component of ν_6 or a second lattice vibration.

The frequency of $\nu_4(\text{Sb}^{\text{V}})$ is the same in Cs_2SbCl_6 as in those mixed anion compounds in which it can be resolved, while $\nu_5(\text{Sb}^{\text{V}})$ develops a distinct shoulder in the mixed-anion compounds of $\text{In}^{\text{III}}, \text{Tl}^{\text{III}},$ and Bi^{III} . Its frequency, however, does not change by more than 5 cm^{-1} throughout the series of compounds, and is then consistent with the trend by Adams and Morris¹³ for a large number of hexahalides, *i.e.*, contraction of the lattice shifts it to higher frequency.

In their mixed-anion salts, the SbCl_6^{3-} and BiCl_6^{3-} ions have an unusually broad band which was previously assigned to ν_3 . $\text{Pb}^{\text{II}}, \text{Se}^{\text{IV}},$ and Te^{IV} hexachloroanions show similar broad bands¹⁰ and it was therefore suggested that

¹³ D. N. Adams and D. M. Morris, *J. Chem. Soc. (A)*, 1967, 1669.

¹⁴ R. W. G. Wyckoff, *Z. Krist.*, 1928, **68**, 231.

2428

J. Chem. Soc. (A), 1969

the broadening resulted from the presence of an 'inert pair'. The spectra have now been measured below 100 cm^{-1} , and in no case can ν_4 be assigned unambiguously. There remains a possibility, therefore, that the apparent broadening of ν_3 may simply result from ν_3 and ν_4 being close together and unresolved.

The two mixed-valence compounds Cs_2SbCl_6 and Rb_2SbCl_6 both contain a well resolved $\nu_3(\text{Sb}^{\text{V}})$ peak and a

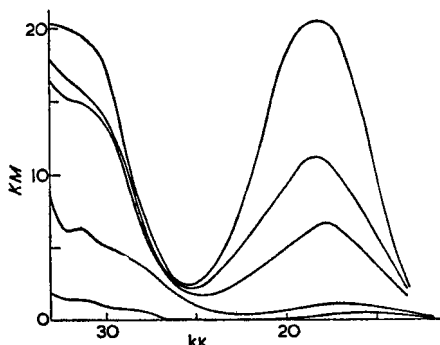


FIGURE 2 Diffuse reflectance spectra of $\text{Cs}_2\text{Sb}_2\text{Sn}_{1-x}\text{Cl}_6$ powders

lattice mode at a frequency very close to that in the corresponding SnCl_6^{2-} salts. The one remaining broad, asymmetric band presumably combines $\nu_3(\text{Sb}^{\text{III}})$ and ν_4 of both Sb^{III} and Sb^{V} . That $\nu_3(\text{Sb}^{\text{V}})$ appears so clearly in the mixed-valence compounds must be taken as evidence that the $\text{Sb}^{\text{III}}\text{-Sb}^{\text{V}}$ interaction in the ground state of these compounds is extremely small. We use this assumption in the analysis of the optical data on these compounds.

Diffuse Reflectance Spectra.—Figure 2 shows a typical set of reflectance spectra, for $\text{Cs}_2\text{Sb}_2\text{Sn}_{1-x}\text{Cl}_6$, and Table 5 collects the numerical results for all the compounds. They confirm that the deep colour of the mixed-valence compounds comes from a single broad absorption band in the red region, not present in either Sb^{III} or Sb^{V} hexahalogeno-compounds. This we call the mixed-valence band. The effect on its frequency and intensity of changing the cation is quite different from that of changing the antimony concentration. As the lattice contracts from Cs_2SbCl_6 to Rb_2SbCl_6 , $(KM)_{\text{max}}$, H , and ν_{max} , all increase, and a similar effect is observed in $\text{Cs}_2\text{Sb}_2\text{Sn}_{1-x}\text{Cl}_6$ and $(\text{NH}_4)_2\text{Sb}_2\text{Sn}_{1-x}\text{Cl}_6$ with similar values of x . In contrast, when the antimony concentration is decreased by introducing either indium or tin, the band-width remains constant and ν_{max} decreases, in spite of the contraction of the lattice (Table 3). Allen and Hush,⁹ who observed a similar effect in $\text{Cs}_2\text{Sb}_2\text{Pb}_{1-x}\text{Cl}_6$, ascribed it to the greater Madelung stabilisation of an excited state consisting of two Sb^{IV} ions in a lattice of Sn^{IV} than in one consisting of Sb^{III} and Sb^{V} . However, this cannot be the correct explanation since the same effect is observed in the indium-doped compounds where the lattice is composed of $3+$ and $5+$ ions for all compositions.

In Figure 3 are plotted $\log_{10}(KM)_{\text{max}}$ against $\log_{10} x$ for the tin-doped compounds and against $\log_{10} y$ for the indium-doped compounds. The points fall on good straight lines of slope 2.0 in the former and 1.0 in the latter, thus demonstrating very clearly that the intensity of the transi-

tion is proportional to the product $[\text{Sb}^{\text{III}}][\text{Sb}^{\text{V}}]$, as would be expected of an intermolecular charge-transfer transition. This result conflicts with measurements on $\text{Rb}_2\text{Sb}_2\text{Sn}_{1-x}\text{Cl}_6$ and $\text{Cs}_2\text{Sb}_2\text{Pb}_{1-x}\text{Cl}_6$ briefly reported by Allen and Hush.⁹ The latter found a discontinuity in their plots of (KM) against x at $x = 0.5$. On either side of this point (KM) varied linearly with x , but the slope when $0.5 < x < 1.0$ was about 11 times greater than when $0 < x < 0.5$. However, their work can be criticised on a number of grounds. First, the results of their analyses are inconsistent; values of x calculated independently from the antimony and tin or lead percentages are in much poorer agreement than those in Table 1. Secondly, the values of (KM) for a given value of x are generally higher than those reported here, suggesting that the particle size of the powders may have been larger than ours. Finally, the interpretation given for the break in the curve is not correct, since it involves the formation of a distinct ordered compound $\text{M}_2\text{Sb}_2\text{Sn}_4\text{Cl}_6$, for which we have found no experimental evidence, and in which each Sb^{III} has only one Sb^{V} neighbour. The latter situation is incompatible with the antifluorite structure, in which each anion has 12 near neighbours.

Brauer and Schnell¹⁵ measured powder reflectance spectra of a series of compounds $(\text{NH}_4)_2\text{Sb}_2\text{Sn}_{1-x}\text{Br}_6$ and found that at low concentrations (KM) was proportional to $[\text{Sb}]^2$. At higher concentrations their curve levelled off, but it is not clear whether they took precautions to ensure uniform particle size in the samples.

Crystal Transmission Spectra.—The spectra of two crystals of $(\text{MeNH}_4)_2\text{Sb}_2\text{Sn}_{1-x}\text{Cl}_6$ and one of $(\text{MeNH}_4)_2\text{Bi}^{\text{III}}\text{Sb}^{\text{V}}\text{Sn}_{1-x}\text{Cl}_6$, all measured at 300°K and at 6°K , are shown in Figures 4 and 5. In addition, Figures 6 and 7 show the variation of the half-widths of the visible bands

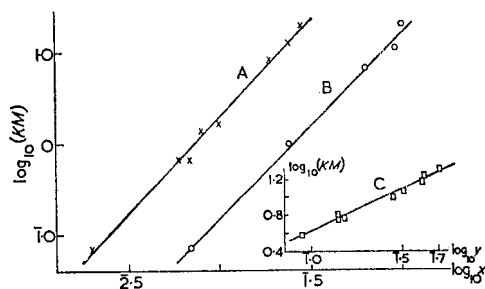


FIGURE 3 The intensity of the mixed-valence band of A, $(\text{NH}_4)_2\text{Sb}_2\text{Sn}_{1-x}\text{Cl}_6$; B, $\text{Cs}_2\text{Sb}_2\text{Sn}_{1-x}\text{Cl}_6$; and C, $\text{Cs}_2\text{Sb}^{\text{III}}\text{Bi}^{\text{III}}\text{Sn}_{1-x}\text{Sb}^{\text{V}}\text{Cl}_6$ plotted against x and y (log-log plot)

of both compounds with temperature. From room temperature to 6°K , the product $(H)_{\text{max}}$, which is proportional to the integrated intensity of the band, increases by approximately 10%. Thus the visible transition is electronically allowed, the increase at low temperature probably resulting from contraction of the lattice, thereby increasing the overlap between adjacent anions, on which the dipole strength of the transition depends. It is also noticeable that the bands in both the $\text{Sb}^{\text{III,V}}$ and $\text{Bi}^{\text{III}}\text{Sb}^{\text{V}}$ compounds shift monotonically to lower energy as the temperature is lowered. The shift between 300° and 6°K

¹⁵ G. Brauer and W. D. Schnell, *Z. anorg. Chem.*, 1956, **287**, 87.

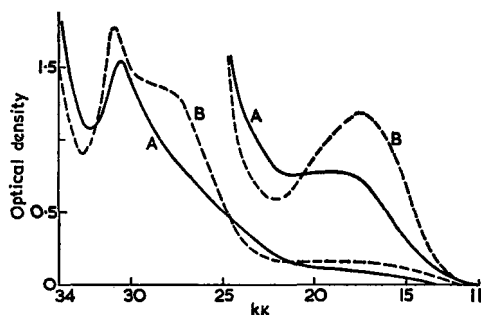


FIGURE 4 Transmission spectra of two crystals of $(\text{MeNH}_3)_2\text{Sb}_2\text{Sn}_{1-x}\text{Cl}_6$ A at 300°K and B at 6°K

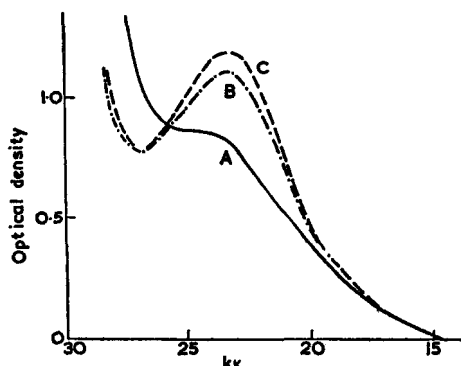


FIGURE 5 Transmission spectrum of a crystal of $(\text{MeNH}_3)_2\text{Bi}^{\text{III}}_{2/3}\text{Sb}^{\text{V}}_{2/3}\text{Sn}_{1-x}\text{Cl}_6$ A at 300°K , B at 80°K , and C at 4°K

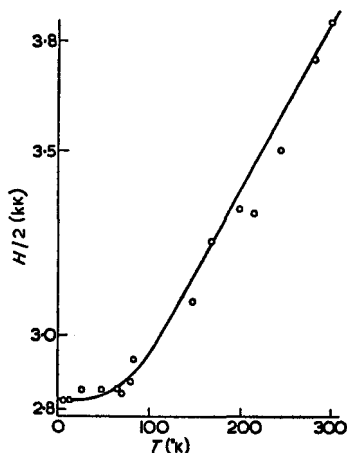


FIGURE 6 Variation in half-width (H) of the mixed-valence band in $(\text{MeNH}_3)_2\text{Sb}_2\text{Sn}_{1-x}\text{Cl}_6$ with temperature. The full line is calculated from equation (12) with $\omega = 210 \text{ cm}^{-1}$ and $S = 130$

is 1.78 kk in the former and 1.03 kk in the latter. From measurements at room temperature on a number of crystals of the more concentrated $(\text{MeNH}_3)_2\text{Sb}_2\text{Sn}_{1-x}\text{Cl}_6$ sample, a value of 48.5 cm^{-1} was calculated for the linear absorption constant at the maximum of the visible absorption band. In that sample $x = 0.15$, and from the density of 6.67 g./ions/l. the concentration of (III,V) chromophore is therefore $0.45 \text{ g.-ion pairs/l.}$, *i.e.*, an extinction coefficient of 110. This low figure, which lies in the same range as that found for the mixed-valence absorption band in the chlorocuprates(I,II),² suggests that the old generalisation¹⁶ that mixed-valency states lead to the appearance of intense absorption is not correct; mixed-valency solids often appear intensely coloured because the chromophore concentration is high in the solid state.

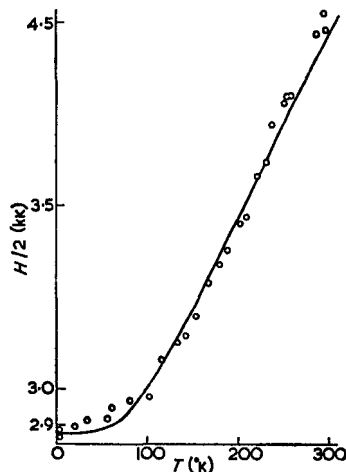


FIGURE 7 Variation in half-width (H) of the intermolecular charge transfer band in $(\text{MeNH}_3)_2\text{Bi}^{\text{III}}_{2/3}\text{Sb}^{\text{V}}_{2/3}\text{Sn}_{1-x}\text{Cl}_6$ with temperature. The full line is calculated from equation (12) with $\omega = 200 \text{ cm}^{-1}$ and $S = 150$

Apart from the mixed-valence visible band, two other more intense bands can be seen at higher energy in the more dilute crystal. These were previously seen in diffuse reflectance spectra,⁶ though Allen and Hush⁹ were apparently unable to detect them. The narrow band at 31 kk is the $5s^2(^1S_0) \rightarrow 5s^15p^1(^2P_1)$ transition of SbCl_6^{3-} , which occurs at 29.8 kk in $\text{Co}(\text{NH}_3)_4\text{SbCl}_6$, once again providing evidence for the identity of Sb^{III} and Sb^{V} in the compounds. The much broader band at 28 kk is most probably a second intermolecular charge transfer because SbCl_6^{3-} has no other internal transition in this region and the lowest-energy band of SbCl_6^- lies at 36.9 kk .¹⁷

DISCUSSION

Quantitative information about electron delocalisation in the ground and excited states of this mixed-valence

¹⁶ N. V. Sidgwick, 'The Chemical Elements and their Compounds,' Clarendon Press, Oxford, 1950.

¹⁷ C. K. Jørgensen, 'Absorption Spectra and Chemical Bonding,' Pergamon, Oxford, 1962.

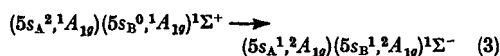
2430

J. Chem. Soc. (A), 1969

system can be obtained by considering the concentration-dependence, absolute intensity, and line-shape of the visible transition.

In the cubic antiferroite lattice of Cs_2SnCl_6 , each SnCl_6^{2-} has 12 near neighbours in a cubo-octahedral arrangement. If Sb^{III} replaces one of these when $\text{Sb}^{\text{III},\text{V}}$ is homogeneously doped into the lattice, the probability of any one of its neighbours being Sb^{V} is $x/2$ in the series $\text{Cs}_2\text{Sb}_x\text{Sn}_{1-x}\text{Cl}_6$ and $\frac{1}{4}$ in the series $\text{Cs}_2\text{Sb}^{\text{III}}\text{In}^{\text{III}}_{1-y}\text{Sb}^{\text{V}}_{\frac{1}{2}}\text{Cl}_6$. Since the Sb^{III} ion has a total of 12 neighbours it will form, on average, $6x$ $\text{Sb}^{\text{III}}\text{-Sb}^{\text{V}}$ pairs in the tin-doped series and 6 in the indium-doped. But if the total number of lattice points is N the total number of Sb^{III} ions is $N(x/2)$ or Ny . Hence the total number of $\text{Sb}^{\text{III}}\text{-Sb}^{\text{V}}$ pairs is $3Nx^2$ and $6Ny$. The results of Figure 3 then demonstrate that the absorption coefficient of the mixed-valence band is accurately proportional to the concentration of $\text{Sb}^{\text{III}}\text{-Sb}^{\text{V}}$ pairs over the whole range of composition, *i.e.*, to a good approximation the effect of changing the number of Sb^{V} ions around each Sb^{III} is additive. This implies that the ground-state wave-function of the optical electron is nearly independent of the number of Sb^{V} neighbours, and hence that interaction between neighbouring ions must be small.

From the close resemblance of the vibrational spectra of the single-valence and mixed-valence compounds we can infer that, in the ground state, delocalisation of the $5s$ electrons from the Sb^{III} to the Sb^{V} is small, so the mixed-valence absorption band must come from the intermolecular charge transfer (3), where the A-site ion



is SbCl_6^{3-} and the B-site one SbCl_6^- in the ground state. The states of the individual ions can be classified according to their octahedral point symmetry, but that of the mixed-valence chromophore, consisting of a pair of ions, is probably well classified simply according to linear symmetry, if the small admixture of halogen atomic wave-function into the (locally) totally symmetric antimony functions is neglected.

If we write the wave-function of the optical electron on an A-site as ϕ_A and on B as ϕ_B , the wave-function of the ground state in general becomes (4) and of an excited

$$\Psi_0 = \frac{1}{N} [\sqrt{(1-\alpha^2)}\phi_A + \alpha \sum_j C_{0j}\phi_{Bj}] \quad (4)$$

state (5), where each A-ion is surrounded by j B-ions

$$\Psi_k = \frac{1}{N} \cdot [\beta\phi_A + \sqrt{(1-\beta^2)} \sum_j C_{kj}\phi_{Bj}] \quad (5)$$

and the point symmetry of the set of ions formed by A and all its B neighbours determines the C. According to equation (3), α and β are both small. If, following the experimental evidence, we neglect any difference

between chromophores with different j , and only consider pairs of Sb^{III} and Sb^{V} , the absolute intensity of the transition $\Psi_0 \rightarrow \Psi_k$ yields direct estimates of α and β . The transition moment μ is given by equation (6), where

$$\mu = g^1 \langle \Psi_0 | M | \Psi_k \rangle \quad (6)$$

g is the orbital degeneracy of the transition. Substituting the simplified forms of (4) and (5) into (6) and ignoring all except one-centre terms (overlap between ϕ_A and ϕ_B being small), we have the very simple expression (7).

$$\mu = \frac{1}{2}e(\alpha + \beta)R \quad (7)$$

The transition moment we estimate from the transmission spectrum of $(\text{MeNH}_2)_2\text{Sb}_{0.15}\text{Sn}_{0.85}\text{Cl}_6$ (Figure 4) and R from the crystal structure of $(\text{MeNH}_2)_2\text{SnCl}_6$. The latter can be considered as being derived from the structure of Cs_2SnCl_6 by elongating the cubic unit-cell along its three-fold axis to accommodate the larger cation. Thus the packing of SnCl_6^{2-} ions within the (111) planes of the two crystals is identical [Sn-Sn distance in $(\text{NH}_4)_2\text{SnCl}_6$ is 7.11 Å and in $(\text{MeNH}_2)_2\text{SnCl}_6$ 7.07 Å].

From the measured extinction coefficient per mole of $\text{Sb}^{\text{III}}\text{-Sb}^{\text{V}}$ pairs, and the half-width at room temperature, we calculate that $(\mu/e)^2 = 0.019 \text{ Å}^2$, so that $\frac{1}{2}(\alpha + \beta)$ is 0.02. Hence in neither the ground nor the excited state is the optical electron delocalised by more than 0.1% from the A- or the B-sites, respectively. The transition thus has almost purely the character of a charge transfer. The constancy of the i.r. frequencies of the components in both the pure and diluted hexachloroantimonate(III,V) lattices, as well as the appearance of internal electronic transitions of the Sb^{III} ion, therefore become explicable.

By examining the temperature-dependence of the spectrum, we can derive still more information about the ground and excited state potential-energy surfaces. Even when the crystal is at liquid-helium temperature the mixed-valence absorption band does not show any vibrational fine structure, though it does become considerably narrower. This suggests that in the excited state the chromophore is strongly displaced from its equilibrium configuration, so that many vibrational quanta are excited. A similar situation has been observed in the spectra of F -centres¹⁸ and Tl^+ ions¹⁹ doped in alkali-metal halides, where the electronic excitation may couple both to local and to lattice modes. In the present case, however, the far-i.r. and Raman spectra of the crystals clearly indicate that local modes of the hexachloride octahedra are well separated in frequency from lattice modes. We therefore assume that broadening of the optical transition results from the difference in equilibrium geometry between SbCl_6^{3-} and SbCl_6^- in their ground states and the SbCl_6^{2-} formed in the excited state.

In general,²⁰ the shape function $G(v)$ of a broad

¹⁸ J. J. Markham, 'F-Centres in Alkali Halides,' Solid State Phys., Suppl. 8, Academic Press, New York, 1966.

¹⁹ F. E. Williams, *Phys. Rev.*, 1950, **80**, 306.

²⁰ J. J. Markham, *Rev. Mod. Phys.*, 1959, **31**, 956.

Inorg. Phys. Theor.

2431

absorption band is given by the sum of terms involving the overlap integrals between all the vibrational wavefunctions χ of the ground state and all those of the excited state weighted, for temperatures above absolute zero, by a Boltzmann factor relating to the population of the ground state levels, as in equation (8), where $P(v)$ is as in (9). On the assumption that the ground and excited

$$G(v) = \sum_{v,v'} P(v) |\langle \chi' | \chi \rangle|^2 \delta(v - (E_{v'} - E_v)/\hbar) \quad (8)$$

$$P(v) = \prod \left[\exp \frac{-v_j \hbar \omega_j(g)}{kT} \left(1 - \exp \frac{-\hbar \omega_j(g)}{kT} \right) \right] \quad (9)$$

state potential energy surfaces are harmonic, equations (10) and (11) follow. In practical applications, a further

$$E_v = E_0(g) + \hbar \omega_j(g)(v + \frac{1}{2}) \quad (10)$$

$$E_{v'} = E_0(u) + \hbar \omega_j(u)(v' + \frac{1}{2}) \quad (11)$$

drastic simplification of (8) has often been made by assuming that all the modes ω_j have the same frequency. The summation then leads to a Gaussian band shape, having a half-width given by equation (12), where ω is

$$H^2 = 8(\ln 2) \hbar^2 \omega^2 S \cdot \coth(\hbar \omega / 2kT) \quad (12)$$

the 'effective' frequency and S , the so-called 'Huang-Rhys factor',²¹ is the ratio between the vibrational energy excited in the upper state to the energy of a single vibrational quantum, *i.e.*, $S = (\frac{1}{2} \omega^2 \Delta q^2) / (\hbar \omega)$.

To test the applicability of equation (12) to our mixed-valence absorption band, $\coth^{-1}(H/H_0)^2$ was plotted against $1/T$. Good straight lines were obtained, both for $(\text{MeNH}_3)_2\text{Sb}_x\text{Sn}_{1-x}\text{Cl}_6$ and $(\text{MeNH}_3)_2\text{Bi}_{1/2}\text{Sb}_{1/2}\text{Sn}_{1-x}\text{Cl}_6$, yielding estimates for ω of 210 cm^{-1} and 200 cm^{-1} respectively. The curves drawn through the experimental points in Figures 6 and 7 were calculated from equation (12) by use of these values of ω , and it can be seen that the level of agreement over the whole temperature range is quite satisfactory. From the half-width H_0 at 0°K (*i.e.*, 4°K), a value for S , and hence Δq , the displacement of the oscillator, can be calculated. For the mixed-valence antimony compound we find $S = 130$ and $\Delta q = 8.3 \times 10^{-20}$ g.^{1/2} cm. These are within the same range as the values obtained for F -centres from the temperature-dependence of their absorption bands and correspond, on the assumption of a reduced mass equal to one chlorine atom, to a displacement of *ca.* 1 Å. The only direct information about the difference between Sb^{III} and Sb^{V} bond lengths to halide ions comes from the structure of $(\text{NH}_4)_2\text{SbBr}_6$, in which the SbBr_6^{3-} distance is 2.80 Å and the SbBr_6^{2-} 2.56 Å, a difference of 0.24 Å. When the drastic

approximations we have made are considered, the results are certainly of the right magnitude.

The figure of 210 cm^{-1} for ω_0 represents an average, with unknown weighting, over all the internal modes of SbCl_6^{3-} and SbCl_6^{2-} and over the modes of the unknown ion SbCl_6^{2-} . We do not believe, therefore, that at present there is any justification for elaborating the calculation any further, for example, by incorporating the frequencies of all the internal modes of the two ions in equation (12), or by removing the assumption that the ground- and excited-state frequencies of the two ions are the same. A simple way of parametrizing the latter possibility would be to take the excited-state frequencies of the two ions as equal, since they are both SbCl_6^{2-} after the electron transfer, and then assume that $\omega_j(u) = \frac{1}{2}[\omega_{\text{III}}(g) + \omega_{\text{V}}(g)]$. That such an assumption is not unreasonable can be seen by comparing the ω_j frequencies of SbCl_6^{3-} (329 cm^{-1})²² and SbCl_6^{2-} (267 cm^{-1})¹⁰ with those of SnCl_6^{2-} , a $5s^0$ ion (311 cm^{-1}),¹³ and TeCl_6^{2-} , a $5s^2$ ion (287 cm^{-1}).²³ The major problem is* that we have no clue to the weight which each mode must be given when forming the average. Nevertheless, it is certainly significant that if an average is taken over the frequencies of all the modes of SbCl_6^{3-} and SbCl_6^{2-} , weighting them solely according to their degeneracies, the resulting 'average vibrational frequencies' (163 cm^{-1} for SbCl_6^{3-} and 249 cm^{-1} for SbCl_6^{2-}) fall almost equally on both sides of the observed 'effective frequency' of 210 cm^{-1} . There can therefore be little doubt that it is indeed the dimensional changes within the two ions, accompanying the transfer of an electron from one to the other, which provide the major source of broadening of the mixed-valence absorption band. In the following paper we show how an examination of the electrical conductivity of these materials can lead to comparable information about adiabatic electron transfer.

Conclusions.—By examining the concentration-dependence, the absolute intensity, and the shape of the visible absorption band in hexachloroantimonate(III,V) doped in hexachlorostannate(IV), we have been able to demonstrate that the mixed-valence transition has the following characteristics: (i) its intensity is proportional to the number of adjacent pairs of SbCl_6^{3-} and SbCl_6^{2-} ; (ii) the transition, which is electronically allowed, has almost purely the character of an electron transfer from Sb^{III} to Sb^{V} ; delocalisation of Sb^{III} 5s electrons on to Sb^{V} in the ground state is less than 0.1%; (iii) the breadth of the transition results from the changes in internal dimensions of the two ions accompanying passage of an electron between them.

We thank the British Petroleum Company for financial support (to L.A.).

[9/704 Received, May 2nd 1969]

²¹ K. Huang and A. Rhys *Proc. Roy. Soc.*, 1950, **A**, 204, 403.
²² I. R. Beattie, T. Gilson, K. Livingston, V. Fawcett, and G. A. Ozin, *J. Chem. Soc. (A)*, 1967, 712.

²³ N. N. Greenwood and B. P. Straughan, *J. Chem. Soc. (A)*, 1966, 962.

Charge Transfer in Mixed-valence Solids. Part V.¹ Semiconductivity of Hexachloroantimonates(III,V)

By L. Atkinson and P. Day,* University of Oxford, Inorganic Chemistry Laboratory, South Parks Road, Oxford

Two-probe D.C. conductivity measurements are reported for the three series of hexachloroantimonates(III,V) whose optical properties were examined in the preceding paper: $A^I_xSb_xSn_{1-x}Cl_6$ ($A^I = NH_4^+$, Cs^+), $Cs_yIn^{III}_{1-y}Sb^{III}_yCl_6$, $Sb^{III}_yCl_6$. For values of x and y greater than about 0.1, the compounds behave as ohmic semiconductors. The specific conductivities at room temperature are proportional to x^2 and y respectively, while the activation energies are independent of the antimony concentration. Seebeck coefficients, determined at room temperature, indicate that for x and $y > 0.1$ the majority carriers are holes, but below 0.1, electrons. It is suggested that the conductivity of the compounds containing sufficient antimony to form a continuous path through the lattice is electronic while that of the dilute materials and single-valence host lattices is ionic. In the former, the magnitude of the conductivity is consistent with a diffusion mechanism in which carrier formation by electron transfer between $SbCl_6^{3-}$ and $SbCl_6^-$ is followed by migration of the resulting $SbCl_6^{2-}$ among the $SbCl_6^{3-}$. The charge-carrier formation step is the adiabatic analogue of the Franck-Condon intermolecular charge transfer process studied in the preceding paper. Relaxation frequencies calculated from the observed conductivity by use of the diffusion model are in the range of Sb-Cl vibrations. The relation between the semiconductor activation energy and the optical charge-transfer energy is discussed.

In Part IV¹ we described the preparation and characterisation of three series of mixed-valence antimony compounds designed to give information about thermal and photochemical charge transfer between ions of differing valency placed side by side in a crystal lattice, viz., $(NH_4)_2Sb_xSn_{1-x}Cl_6$, $Cs_xSb_xSn_{1-x}Cl_6$, and $Cs_yIn^{III}_{1-y}Sb^{III}_yCl_6$. By studying the concentration dependence, absolute intensity, and width of the visible absorption band in these compounds, we assigned it as the Franck-Condon charge transfer from $SbCl_6^{3-}$ to $SbCl_6^-$ and estimated the extent to which the optical electron is delocalised between the two antimony ions in the ground and excited states. We now describe experiments on the thermally activated charge migration in the same materials.

Very few experiments have been reported on the electrical conductivity of inorganic solids in which the charge migrates by what solution kineticists would term 'outer-sphere' electron transfer. In the more widely studied materials, such as non-stoichiometric mixed-valence oxides,² anions bridge from one metal ion to the next, forming a continuous path for charge migration which, by analogy with the solution redox process, might be called 'inner-sphere'. In an earlier paper³ on chlorocuprates(I,II) we showed that 'outer-sphere' charge transfer could occur in mixed-valence solids, but apart from an unsuccessful attempt by Fielding and Mellor⁴ to measure the conductivity of $(NH_4)_2SbBr_6$, no other experiment of this kind appears to have been carried out.

As well as measuring the conductivity of our materials as a function of concentration, we also performed Seebeck effect measurements on many of them, thus deriving the sign of the majority charge carriers. We also investigated the effect of adsorbed oxygen and hydrogen on the conductivity and searched for possible photoconductivity.

¹ L. Atkinson and P. Day, preceding paper.

² M. B. Robin and P. Day, *Adv. Inorg. Chem. Radiochem.*, 1967, **10**, 247.

³ D. Culpin, P. Day, P. R. Edwards, and R. J. P. Williams, *J. Chem. Soc. (A)*, 1968, 1838.

EXPERIMENTAL

Semiconductivity.—None of the compounds could be grown into crystals large enough for electrodes to be attached, so all the measurements were made on pellets of compressed powder. The sample holder, consisting of two flat nickel discs, making contact with the pellet by compression, has been described. No measurement was made until the pellets had been maintained in a vacuum of 10^{-4} – 10^{-5} torr for at least 12 hr.

The conductivity apparatus described more fully in Part III³ has been modified in two respects: temperature variation is now accomplished by passing compressed air, previously heated or cooled by an electrical heater or coolant bath, through a copper coil around the glass vacuum tube containing the sample holder. Since it is very important in this type of high resistance measurement to avoid injecting strong electrical signals into the sample from fluctuating external fields, this method of temperature control dispenses with the need for extra electrical connections inside the earthed shield surrounding the sample and its high-impedance leads. The second modification consists of feeding the output of the Vibron electrometer monitoring the conductivity of the sample, and the potential of the copper-constantan thermocouple, to the two channels of a Servoscribe recorder, so that heating or cooling runs could be performed automatically once the correct heating or cooling rate had been set by varying the flow-rate of compressed air. In this way temperatures between about -50 and 80° could be reached conveniently, the rate of temperature change being normally below 0.5° per minute. Such a slow variation is important when measuring high resistances as the time constant of the electrometer may be of the order of minutes.

Pellets of all the compounds whose preparations and analyses were recorded in Part IV¹ were made in an evacuable die. The powdered samples were evacuated for 1 min. and pressure applied for a further minute. To test the reproducibility and reliability of pellet conductivity measurements, several pellets of Cs_xSbCl_6 were made under different conditions. The lowest pressure at which pellets could be made was 1000 lb. in.⁻² so the densities and specific conductivities of pellets prepared between 1000 and 2000 lb. in.⁻² were measured. The densities increased over the range

⁴ P. E. Fielding and D. P. Mellor, *J. Chem. Phys.*, 1954, **22**, 1155.

Inorg. Phys. Theor.

1000—1250 lb. in.⁻² but above that were constant, and equal to more than 90% of the theoretical value for a single crystal. No trend in specific conductivity was observed when changing the pellet dimensions or density; the mean value for nine pellets of Cs₂SbCl₆ was 3.64×10^{-12} ohm⁻¹ cm.⁻¹ and the standard deviation 1.80×10^{-12} ohm⁻¹ cm.⁻¹.

The conductivities of at least two pellets of each compound were examined, after their ohmicity had been tested by measuring the current as the applied potential was varied through a cycle from +70 v to -70 v and back again. Pellets which showed signs of rectifying behaviour were rejected.

Seebeck Effect.—For high-resistance materials the Seebeck effect is a more convenient method than the Hall effect for determining the sign of majority charge carriers. The sample holder used in the conductivity measurements was replaced by that shown in Figure 1. To reduce the overall resistance of the circuit, silver paste was used to sandwich pellets between two copper rods, the lower of which, threaded so that firm contact could be made to the pellet, was connected to the high-impedance input of the electrometer. The upper, low-impedance electrode was heated by a non-

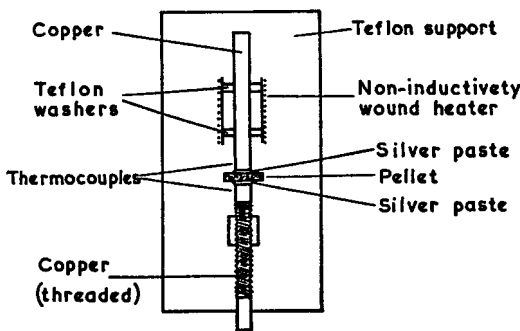


FIGURE 1 Sample holder for Seebeck coefficient measurements

inductively wound constantan coil surrounding the copper rod but insulated from it by Teflon washers. One end of the coil was earthed, and it was heated by a 12 v D.C. supply which caused no electrical noise in the electrometer.

The temperatures at the electrodes were measured by two independent copper-constantan thermocouples, an arrangement which was found preferable to a single thermocouple, differentially connected, because the temperature of the 'hot', low-impedance electrode could then be monitored continuously on one channel of the Servoscribe recorder. On the other channel, the Seebeck potential and the potential from the thermocouple attached to the high-impedance electrode were recorded alternately. Temperature differences up to 15° were employed and good straight-line plots of electrometer potential against ΔT were obtained. The noise level of the circuit and electrometer was less than 1 mv, even with pellets having resistances of 10^{14} ohm.

Few Seebeck coefficients of very high-resistance inorganic materials other than ionic conductors have been reported, though some data exist for organic semiconductors.⁵ To estimate the reliability of the method a number of measure-

⁵ F. Gutmann and L. E. Lyons, 'Organo Semiconductors,' J. Wiley and Sons, New York, 1967.

ments were performed on pellets of copper phthalocyanine, a semiconductor whose resistivity lies in the same range as the hexachloroantimonates, and for which several Seebeck measurements have been made. Our result, +0.92 mv/°c at 31°, is roughly the average of the rather discordant literature values.⁵

RESULTS

Conductivity.—The conductivity data for all the mixed-valence materials are in Table I. In each case the current-

TABLE I
Specific conductances and activation energies of hexachloroantimonates(III, V)

Compound	x	κ (300°K) (ohm ⁻¹ cm. ⁻¹)	E (ev)	Seebeck coefficients (mv/°C)	
(NH ₄) ₂ Sb ₂ Sn _{1-x} Cl ₆	0.24	9.36×10^{-14}	0.88		
		8.98×10^{-14}	0.87		
	0.19	2.74×10^{-14}	0.91		
		2.15×10^{-15}	0.95		
	0.10	9.43×10^{-16}	0.97		
		3.44×10^{-16}	0.87		
	0.08	5.15×10^{-16}	0.88		
		5.80×10^{-16}	0.88		
	0.07	1.19×10^{-15}	0.88		
		1.26×10^{-15}	0.95		
(NH ₄) ₂ SnCl ₆	0.06	1.16×10^{-15}	0.92		
		1.34×10^{-15}	0.90		
	0.02	$* 1.2 \times 10^{-16}$	0.98		
		$* 1.2 \times 10^{-16}$	0.99		
	0.01	$* 8.0 \times 10^{-17}$	0.79		
		$* 9.8 \times 10^{-17}$	0.79		
	0	$* 8.3 \times 10^{-17}$	0.71		
		$* 7.6 \times 10^{-17}$	0.72		
	Cs ₂ SbCl ₆	1	3.64×10^{-12}	0.75	1.2 ± 0.2
	Cs ₂ Sb ₂ Sn _{1-x} Cl ₆	0.92	5.02×10^{-12}	0.76	1.3
		2.62×10^{-12}	0.78		
		3.95×10^{-12}	0.78		
0.63		1.77×10^{-12}	0.76	1.1	
		1.06×10^{-12}	0.77		
0.24		2.04×10^{-12}	0.77	1.0	
Cs ₂ SnCl ₆	0.07	1.66×10^{-16}	0.78		
		4.95×10^{-16}	0.68	-0.5	
		9.90×10^{-16}	0.64		
	0	$* 3.2 \times 10^{-16}$	0.69	-2.0	
		$* 3.8 \times 10^{-16}$	0.60		
	Cs ₂ Sb ^{III} _{1-x} In ^{III} _x Sb ^V ₄ Cl ₆	0.42	3.27×10^{-12}	0.66	
			3.34×10^{-12}	0.69	
		0.41	3.85×10^{-12}	0.71	0.8
			1.84×10^{-12}	0.71	
		0.32	2.56×10^{-12}	0.68	
		1.48×10^{-12}	0.69		
0.28		2.03×10^{-12}	0.70	1.3	
		2.39×10^{-12}	0.70		
0.15		1.80×10^{-12}	0.76	0.8	
		1.00×10^{-12}	0.74		
Cs ₂ In ^{III} _{1-x} Sb ^V ₄ Cl ₆	0.14	9.09×10^{-12}	0.75	1.0	
		1.65×10^{-12}	0.72		
	0.09	4.17×10^{-12}	0.78	0.9	
		4.28×10^{-12}	0.78		
	0.01	4.17×10^{-16}	0.84	-0.5	
		4.70×10^{-16}	0.85		
	0	9.44×10^{-16}	0.93	-0.7	
		4.70×10^{-16}	0.97		
	Rb ₂ SbCl ₆	—	3.01×10^{-12}	0.85	1.3
		1.67×10^{-12}	0.88		
(MeNH ₃) ₂ Sb ₂ Sn _{1-x} Cl ₆	—	2.04×10^{-12}	0.93		
	1.68×10^{-12}	0.94			
Cs ₂ Bi ^{III} _{1-x} Sb ^V ₄ Cl ₆	—	1.65×10^{-15}	0.99		

* Indicates that R was too high to be measured accurately at room temperature. κ was obtained by extrapolation from higher temperatures assuming a constant activation energy.

2434

J. Chem. Soc. (A), 1969

voltage relation was used as an indication of the contribution of space-charge-limitation to the total current. In the absence of traps a space-charge-limited current is proportional to V^3 and in the presence of traps to V^n with $1 < n < 2$. The nine pellets of Cs_2SbCl_4 all had n in the 1.00–1.10, and for values of x and $y > ca. 0.1$, both indium and tin-doped compounds likewise obeyed Ohm's law quite closely. At lower antimony concentrations large divergences from Ohm's law occurred. Values of the specific conductivities κ in all cases in Table 1 are therefore given as the means for ± 50 v.

In Figure 2 $\log_{10} \kappa$ is plotted against $\log_{10} x$ or $\log_{10} y$ for each of the three series of doped compounds. There is some scatter among the points but it seems clear that above x and y values of 0.1, $\log \kappa$ varies linearly with $\log x$ or $\log y$. The lines on the plot have been drawn with slopes of 1.0 and 2.0, indicating that $\kappa \propto x^2$ in the tin-doped series and $\kappa \propto y$ in the indium-doped series. Hence we infer that $\kappa \propto [\text{Sb}^{\text{III}}][\text{Sb}^{\text{V}}]$, exactly as for the optical charge transfer in the preceding paper. When x and y are less than 0.1, the conductivity falls more rapidly, reaching the limiting values of Al_2SnCl_6 and $\text{Cs}_2\text{In}_{0.5}\text{Sb}_{0.5}\text{Cl}_6$. For light absorption near-neighbour antimony(III,V) pairs are presumably required but for electrical conductivity there is the additional requirement of a continuous conducting path of antimony ions between the electrodes. At lower antimony concentrations ionic conductivity is therefore expected to contribute increasingly.

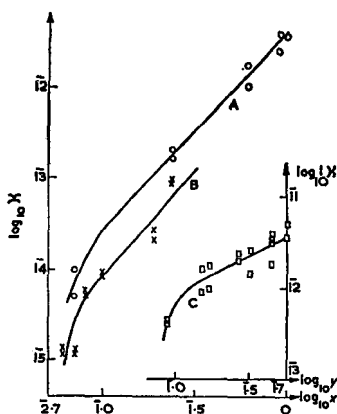


FIGURE 2 Concentration dependence of conductivity of hexachloroantimonates(III,V)
 A, $\text{Cs}_2\text{Sb}_2\text{Sn}_{1-x}\text{Cl}_6$; B, $(\text{NH}_4)_{1-x}\text{Sb}_2\text{Sn}_{1-x}\text{Cl}_6$; and
 C, $\text{Cs}_2\text{Sb}_2\text{In}_{1-y}\text{Sb}_1\text{Cl}_6$

All the compounds behaved as semiconductors, and the activation energies E calculated from equation (1) are in

$$\kappa = \kappa_0 \exp (E/kT) \quad (1)$$

Table 1. Plots of $\log \kappa$ against $1/T$ were good straight lines, heating and cooling runs producing coincident results (Figure 3). In each series, the activation energies of all the compounds with x or $y > 0.1$ are roughly equal, with no sign of any trend to higher or lower values except in the most dilute. It is noticeable, however, that E changes with changing cation in the same direction as the optical charge

transfer energy (preceding paper). On the other hand the specific conductivity at a given value of x is smaller in the NH_4^+ tin-doped series than in the Cs^+ one, although the intensity of mixed-valence absorption band is smaller in the latter.

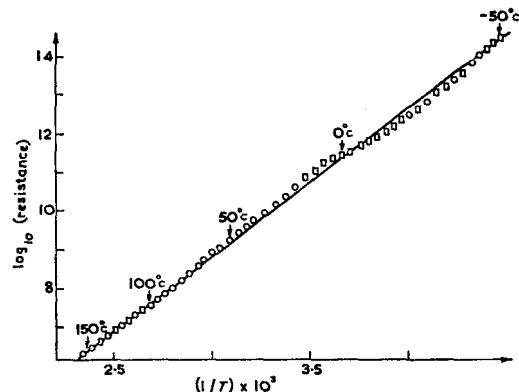


FIGURE 3 Temperature variation of conductivity of Cs_2SbCl_6 . Squares and circles represent cooling and heating measurements

Seebeck Effect.—Mean values for all the Seebeck coefficients are in Table 1. At least two pellets of each compound were examined, and two room-temperature Seebeck runs were carried out on each. The scatter of points on the Seebeck plots limited the accuracy of the slopes to about $0.1 \text{ mv}/^\circ\text{C}$. On Cs_2SbCl_6 itself, a total of 16 determinations were made, yielding a mean value for S of $+1.2 \pm 0.2 \text{ mv}/^\circ\text{C}$.

The most striking feature of the Seebeck results is that in the two series studied S changes sign from positive to negative with decreasing antimony concentration. Thus for values of x and y above 0.1 holes are the majority carriers, but in the single-valence and the most dilute mixed-valence samples the carriers are negatively charged. In ionic conductors such as the alkali-metal halides, where Schottky cation vacancies are the majority carriers, Seebeck coefficients have been found to be negative, and though there is some theoretical uncertainty surrounding the interpretation of the Seebeck effect in ionic conductors, because of difficulties about the process occurring at the electrodes, we assume that in our single-valence and dilute mixed-valence materials charge is transported by a similar ionic mechanism. The change in the sign of the Seebeck coefficient near x or $y = 0.1$ parallels the change in conductivity, and thus provides a further reason for believing that the charge-transfer mechanism changes from ionic to electronic with increasing antimony concentration.

Gas Effects.—Dry N_2 , H_2 , and O_2 at pressures from 10^{-4} torr to atmospheric had no detectable effect on the conductivity of a pellet of Cs_2SbCl_6 .

Photoconductivity.—A pellet of Cs_2SbCl_6 was examined for photoconductivity in the frequency range 5–19 kK. Above 6 kK, a very small photocurrent (roughly 0.001 of the dark current) could be detected. It was not caused by heating, because it decayed almost instantaneously when the light was turned off, but there was no increase in photo-

* A. Rose, *Phys. Rev.*, 1955, **97**, 1538.

current in the region of the mixed-valence absorption band. Thus there is no direct production of charge carriers from the optically excited charge transfer state.

DISCUSSION

In all except the most dilute samples, the conductivity of these mixed-valence compounds is not space-charge limited. The changing sign of the Seebeck coefficient and the fact that the specific conductivity is proportional to the concentration product $[Sb^{III}][Sb^V]$, like the light-absorption intensity, lead us to the conclusion that the charge-migration mechanism is electronic. We have shown¹ that there is negligible electron-delocalisation between $Sb^{III}Cl_6^{3-}$ and $Sb^VCl_6^-$ in the ground states of these materials and that the optical excited state is an electron transfer from Sb^{III} to Sb^V . In principle the conductivity could be described by a band model, in which the highest levels of valence band would be made up from Sb^{III} 5s functions, and the lowest levels of the conduction band from Sb^V 5s. But the conductivity is so low that such bands would be quite narrow, and it is therefore more appropriate to consider a diffusion model in which localised charge carriers migrate through the lattice in a series of discrete hops from one ion to the next. Conductivity can then be thought of as the thermally activated analogue of the optical process characterised in the preceding paper.¹

The 'hopping' model has been applied to a variety of semiconducting mixed-valence oxides, particularly by Heikes and his co-workers⁷⁻⁹ though recently¹⁰ the size of the Hall effect in these materials has been taken as evidence that, at least in $Li_xNi_{1-x}O$, a narrow band model may be more realistic. This is connected with the fact that local vibrational modes around the Ni^{III} impurities in the predominantly Ni^{II} lattice interact strongly with lattice modes in such infinite ionic lattices. In the present case, however, we can imagine that the lattice is a 'molecular' one, that is, that the internal modes of the $SbCl_6^{3-}$ and $SbCl_6^-$ lie at substantially higher frequencies than the lattice modes. Table 4 of the preceding paper shows that this is the case. In applying the fundamental conductivity equation (2) of the hopping model,⁷ where n is the density of charge

$$\kappa = \frac{ne^2a^2\omega_i}{kT} \exp(-E_m/kT) \quad (2)$$

carriers, a the distance between sites, and ω_i the vibrational frequency which equalizes the potential energy at the two sites and enables the carrier to hop, we therefore assume that ω_i is a good approximation to an Sb-Cl stretching frequency. Our model is then analogous to Marcus's approach¹¹ to outer-sphere redox reactions in solution, except that we have to consider the possibility that the carrier formation and migration steps are not the same. If there are N ions per unit volume of solid

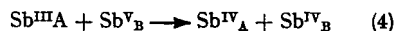
⁷ R. R. Heikes and W. D. Johnston, *J. Chem. Phys.*, 1956, **26**, 582.

⁸ R. R. Heikes, A. A. Maradudin, and R. C. Miller, *Ann. Phys.*, 1963, **8**, 773.

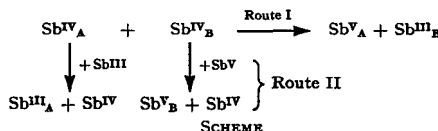
which are capable of becoming charge carriers on absorbing an energy E_t , $n = N \exp(-E_t/kT)$ and we obtain equation (3). If the carrier formation step is the thermal

$$\kappa = \frac{Ne^2a^2\omega_i}{kT} \exp[-(E_m + E_t)/kT] \quad (3)$$

analogue of the optical charge transfer (4) we could



envisage two kinds of migration process: either a second electron is transferred from site A to site B, or the single electrons remaining on the two sites after the formation step could each exchange electrons with a Sb^{III} ion, as shown in the Scheme. The Seebeck measurements



can be used to distinguish these routes. The Seebeck coefficient is related to the partial molal entropy of the charge carriers by $S = S/e$, where $-S$ contains a configurational contribution S_c arising from the distribution of n carriers on N sites and a so-called 'lattice relaxation entropy' S_r due to the change in lattice configuration as a carrier hops from one ion to another. S_r has been evaluated by Heikes *et al.*⁸ using several different models for hopping conductors and is always small. If both electron and hole migration takes place, equation (5) follows, where the t 's are transport numbers, e.g.,

$$S = -(1/e)(t_e S_e - t_h S_h) \quad (5)$$

$t_e = \mu_e/(\mu_e + \mu_h)$. Neglecting S_r , we find equation (6) from the hopping model for both the tin and indium-

$$S = -(k/e)(t_e - t_h)E_t/kT \quad (6)$$

doped series. Route I requires that $t_e = t_h$ and hence equation (6) predicts that S would be small, whereas the experimental value of about +1 mv/°c is quite large. We therefore confine our attention to route II.

Assuming that there is a random distribution of antimony in the tin or indium lattices, we showed in the preceding paper that the number of Sb^{III} - Sb^V pairs is $3Nx^2$ in the former and $6Ny$ in the latter. In the tin-doped series, for example, the conductivity equation (3) then becomes (7), where we have taken account of the

$$\kappa = \frac{e^2a^2\omega_i}{kT} \cdot 6Nx^2 [\exp(E_t + E_{me})/kT] + \exp[(E_t + E_{mb})/kT] \quad (7)$$

fact that electron transfer between Sb^{IV} and Sb^{III} represents the motion of holes while transfer between Sb^{IV} and Sb^V results in negative carrier migration. The

⁹ R. R. Heikes, in 'Transition Metal Compounds,' ed. E. R. Schatz, Gordon and Breach, New York, 1964.

¹⁰ A. J. Bosman and C. Crevecoeur, *Phys. Rev.*, 1966, **144**, 763; I. G. Austin, A. J. Springthorpe, B. A. Smith, and C. E. Turner, *Proc. Phys. Soc.*, 1967, **90**, 157.

¹¹ R. A. Marcus, *J. Chem. Phys.*, 1956, **24**, 966.

2436

J. Chem. Soc. (A), 1969

positive sign of the Seebeck coefficients implies that the first exponential term in equation (7) can be neglected.

Clearly, equation (7) agrees with the observed concentration-dependence of the room-temperature conductivity, provided that the antimony concentration is high enough for a continuous path of antimony ions to be formed. If the antimony were randomly distributed there would be on average $6x$ Sb^{III} neighbours to each Sb^{III} , so if charge migration occurs exclusively by transfer between Sb^{IV} and Sb^{III} the conductivity would cease when $6x$ fell below unity, that is, when x was *ca.* 0.17. Our observation (Figure 2) is that the conductivity falls when x is below *ca.* 0.1.

Since experimentally $\log \kappa$ varies linearly with $1/T$, the general equation (7) needs modifying in one of two ways. Either the two activation energies for migration, E_{me} and E_{mh} , are both small, and the formation of the Sb^{IV} carriers dominates, or E_{me} is very much larger than E_{mh} , when migration would occur mainly through Sb^{III} and the measured activation energy would be $(E_t + E_{\text{mh}})$. We also note that at concentrations above x or $y = 0.1$ neither the measured activation energy nor the Seebeck coefficients are concentration-dependent, indicating that the individual energy terms do not vary with the number of antimony ions surrounding a particular ion. This behaviour matches that of the optical charge-transfer process in the preceding paper,¹ and agrees with the assumptions of the diffusion model.

We can make a further test of the consistency of the diffusion model as applied to these compounds by using κ and E to calculate ω , in equation (7). Unfortunately the value of the pre-exponential factor in equation (1) is very sensitive to small experimental errors, and caution is also needed when making use of the absolute magnitudes of conductivities derived from powder measurements. Nevertheless, for all three series of doped compounds, as well as for Rb_2SbCl_6 and Cs_2SbCl_6 , ω , lies within the range 30–300 cm^{-1} , *i.e.*, the order of magnitude of a vibrational frequency.

The data do not allow us to calculate the individual contributions E_t , E_{mh} , and E_{me} to the measured activation energies but some indication of their magnitudes can be obtained by considering the two extreme situations we have mentioned. For Cs_2SbCl_6 , $E_{\text{obs}} = 0.76$ eV and $S = +1.2$ mV/°C. If we assume that E_{obs} is dominated by E_t , equation (6) yields $(t_h - t_e) = 0.48$ or t_h/t_e is approximately 3. On the other hand if migration occurred mainly through Sb^{III} , $(t_h - t_e)$ approached unity, and equation (6) provides an estimate of E_t . For those materials for which Seebeck and activation-energy data are available, it is therefore possible to state limits within which the activation energies for carrier formation and hole migration must lie. These are: Cs_2SbCl_6 , $0.36 < E_t < 0.76$; $0 < E_{\text{mh}} < 0.40$ eV; and Rb_2SbCl_6 , $0.39 < E_t < 0.87$; $0 < E_{\text{mh}} < 0.48$ eV. E_t thus makes a substantial contribution to the observed activation energy.

¹² N. S. Hush, *Progr. Inorg. Chem.*, 1968, 8, 391.

If E_t is indeed the energy required for the adiabatic transfer of one electron from an SbCl_6^{3-} to an SbCl_6^- , it is tempting to seek a correlation with the energy of the corresponding Franck-Condon process, derived from the optical spectrum. Assuming that the electron being transferred couples with a single harmonic oscillator which has the same frequency in both ground and excited states, Hush¹² recently derived a simple relation (8)

$$E_{\text{therm}} = E_{\text{opt}}^2/4(E_{\text{opt}} - E_0) \quad (8)$$

connecting the energies of adiabatic (E_{therm}) and Franck-Condon (E_{opt}) electron transfer. E_0 is the energy difference between the lowest vibrational states of the ground and excited states, that is, in the present example, of $\text{Sb}_A\text{Cl}_6^{3-} + \text{Sb}_B\text{Cl}_6^-$ and $\text{Sb}_A\text{Cl}_6^{2-} + \text{Sb}_B\text{Cl}_6^{2-}$. It seems likely that E_0 will be small compared with E_{opt} , and to estimate E_{therm} roughly from E_{opt} we therefore neglect it. Table 2 contains some results for a number

TABLE 2
Observed and calculated activation energies (eV)
(for definition of symbols, see text)

	E_{opt} (obs.)	$E_{\text{therm}} = \frac{1}{4}E_{\text{opt}}^2$	E_{obs}	E_t (min.)
Cs_2SbCl_6	2.30	0.57	0.76	0.36
Rb_2SbCl_6	2.43	0.61	0.87	0.39
Chlorocuprates(I,II) ^a ...	2.18	0.55	0.73	—
Crocidolite ^b	2.14	0.54	0.70	—

^a Ref. 3. ^b J. G. F. Littler and R. J. P. Williams, *J. Chem. Soc.*, 1965, 6368.

of mixed-valence solids, from which it is clear that E_{obs} is always larger than E_{therm} , when it is estimated as $E_{\text{opt}}/4$. As we have shown, at least part of the reason for this is that E_{obs} contains a contribution from carrier migration. Where E_{obs} and S enable minimum values of E_t to be estimated, E_{therm} calculated from Hush's relation falls within the required limits. Before Hush's model could be made more precise, however, both an experimental method for estimating E_t and a theoretical treatment of the coupling of the migrating electron with a variety of anharmonic vibrational modes would be needed.

Conclusions.—Outer-sphere electron transfer between SbCl_6^{3-} and SbCl_6^- has been observed in the solid state as electronic conductivity, both in Cs_2SbCl_6 and in compounds diluted with In^{III} and Sn^{IV} . In the latter, the conductivity varies with the antimony concentration in the same way as the light-absorption intensity. Both are proportional to the concentration of neighbouring $\text{Sb}^{\text{III}}\text{--Sb}^{\text{V}}$ pairs. The activation energies and Seebeck coefficients do not vary with concentration provided that the lattice contains sufficient antimony (*ca.* 10%) for a continuous path to be formed through the lattice between the electrodes. The magnitude of the conductivity is consistent with a diffusion mechanism in which, after carrier formation from a $\text{Sb}^{\text{III}}\text{--Sb}^{\text{V}}$ pair, migration occurs mainly through transfer of a hole (*i.e.*, Sb^{IV}) and the Sb^{III} ions.

[9/705 Received, May 2nd, 1969]

MIXED VALENCE CHEMISTRY—A SURVEY AND CLASSIFICATION

Melvin B. Robin

Bell Telephone Laboratories, Inc., Murray Hill, New Jersey

and

Peter Day

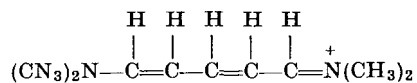
Inorganic Chemistry Laboratory, University of Oxford, Oxford, England

I. Introduction	248
II. Theory of Mixed Valence Effects	253
A. The Wave Functions and Mixed Valence Classification	254
B. Mixed Valence Spectra	258
C. Magnetism and Electron Transport	263
D. Molecular Geometry	269
III. Survey of the Elements	270
A. Titanium	271
B. Vanadium	275
C. Chromium	282
D. Manganese	288
E. Iron	291
F. Cobalt	305
G. Nickel	310
H. Copper	312
I. Zirconium and Hafnium	321
J. Niobium and Tantalum	321
K. Molybdenum and Tungsten	335
L. Technetium and Rhenium	344
M. Ruthenium and Osmium	345
N. Rhodium and Iridium	347
O. Palladium and Platinum	348
P. Silver	355
Q. Gold	361
R. Gallium	366
S. Indium	369
T. Thallium	371
U. Tin	374
V. Lead	375
W. Phosphorus and Arsenic	381
X. Antimony	382
Y. Bismuth	393
Z. Lanthanides	394
AA. Actinides	397
BB. Miscellaneous	401
IV. Conclusions	402
References	403

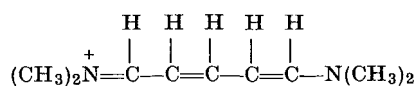
1. Introduction

This review is concerned with the neglected class of inorganic compounds which contain ions of the same element in two different formal states of oxidation. Although the number of references cited in our review shows that many individual examples of this class have been studied, yet they have very rarely been treated as a class, and there has never before, to our knowledge, been a systematic attempt to classify their properties in terms of their electronic and molecular structures. In the past, systems containing an element in two different states of oxidation have gone by various names, the terms "mixed valence," "nonintegral valence," "mixed oxidation," "oscillating valency," and "controlled valency" being used interchangeably. Actually, none of these is completely accurate or all-embracing, but in our hope to avoid the introduction of yet another definition we have somewhat arbitrarily adopted the phrase "mixed valence" for the description of these systems.

The concept of resonance among various valence bond structures is one of the cornerstones of modern organic chemistry. The most important feature of resonance among degenerate or near-degenerate structures is that the states resulting from the resonance have properties quite different from those expected of any one of the structures taken separately. Thus, for example, the pentamethinium ion requires the two degenerate structures



and



for an adequate description of its ground state, and, as a consequence of the resonance interaction between them, has a deep green color. On the other hand, either of the structures taken alone would be expected to have the color of 1,3,5-hexatriene, i.e., would be colorless. In this example, the resonance and the consequent green color spring from the fact that the nitrogen atoms can assume two valencies, 3+ and 4+, and are in equivalent positions in the ion so that on interchanging the nitrogen valencies, an equivalent structure results. There is ample reason to believe that exactly similar results would follow if a molecule could be synthesized in which the nitrogens were replaced by, say, Fe(II) and Fe(III). Thus it seems clear from the dramatic effects of resonance in organic chemistry that one can expect unusual properties in inorganic materials

possessing the same metal ion in different oxidation states, properties not to be found in the salts of either oxidation state taken separately.

Occasionally one finds examples of mixed valence among the inorganic nonmetals (the triiodide ion contains iodine atoms with formal valence zero and minus one). However, it is easily understood that by far the largest number and greatest variety of such compounds to be encountered in chemistry involve the transition and B subgroup metal elements, since many of these elements can exist in a variety of oxidation states. It is paradoxical, then, that the revitalization of transition metal chemistry brought about by the successes of the crystal field and ligand field theories has not been extended to the area of mixed valence compounds and their properties. It is the aim of this article to carry the renaissance of inorganic chemistry into this neglected area.

Mixed valence systems are, or should be, of great interest because their properties are rarely just the sum of the properties of the two metal ions taken separately; as with resonating organic molecules, there frequently is an "interaction" between the metal ions which results in the most dramatic changes in the physical properties of the system. Thus, as examples, $W^{VI}O_3$ and LiW^VO_3 ¹ are insulators whereas the mixed valence compound $Li_xW_x^VW_{1-x}^VO_3$ is a conductor, the crystals $K_4Fe^{II}(CN)_6$ and $Fe_2^{III}(SO_4)_3$ are pale yellow whereas $KFe^{III}Fe^{II}(CN)_6$ is deep blue, and paramagnetic substances may become ferromagnetic or diamagnetic, all by changing the oxidation state of a part of the metal ions in the system by one or more units. Thus, for those interested in the interrelationships between electronic structure, molecular structure, electronic spectra, electronic conduction, and molecular magnetism, the mixed valence systems offer a class of compounds unique in chemistry. As would be expected, a study of such mixed valence systems suggests a close correlation between their color, crystal structure, magnetism, and electronic conductivity, which hopefully will allow one to predict aspects of all the above properties, after determining any one of them.

The most obvious and striking feature of many mixed valence compounds is the presence of intense absorption in the visible region of the spectrum, not present in compounds containing either valence state alone. Thus, whereas the colors of almost all Fe(III) and Fe(II) compounds are colorless, pale orange, or pale green, the color of almost all mixed valence systems simultaneously containing Fe(III) and Fe(II) is deep blue to black. And there is another paradox here, for although the blue-black systems are being actively ignored today in the midst of a

¹ In this work, the Roman numeral which follows an atomic symbol refers to the formal oxidation state of the metal ion, and is not to be confused with similar numerals used differently by atomic spectroscopists for the same purpose.

flurry of quantum mechanical activity on the pale orange ones, in the dark ages of the prequantum mechanical days, when no one could guess the explanation for the color of the Fe(III) ion, there was presented a very reasonable rationale for the deep blue color of Prussian blue, $\text{KFe}^{\text{III}}\text{Fe}^{\text{II}}(\text{CN})_6$. Because the deep colors of mixed valence systems were so unexpected, they could not be ignored for long, with the result that an explanation of the effect was presented with which we today can find little fault.

Thus, Wells (759), describing with great insight the very dark colors of various Au(I), Au(III), Sb(III), Sb(V), Fe(II), Fe(III), and Cu(I), Cu(II) chromophoric groupings, wrote:

“The chromophore grouping that has been presented here is a very curious thing. In the cases of Au(I)–Au(III) and Sb(III)–Sb(V) there is a difference of two units of valency, while with Fe(II)–Fe(III) and Cu(I)–Cu(II) there is a difference of only one unit, and, furthermore, these four pairs of valencies are all different. It is particularly remarkable that the three chlorides, CsCl, SbCl_3 , and SbCl_5 , which constitute one of the examples of the chromophore grouping, are all of them colorless compounds.

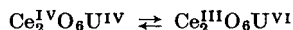
It seems possible that the action of this chromophore may be explained by exchanges of negative electrons between the atoms that differ in valency. It is supposed that in passing from one valency to another an atom gives up or takes on one or more electrons, and, if it is assumed that the atoms of a metal in two states of valency in the same molecule, instead of retaining fixed individual valencies, continually make these exchanges of electrons, it may be supposed that light, passing through such molecules, is in some way affected, so that colors or opacity are produced.”

As the reader will find on reading ahead, in a good many systems so little work has been done on this phenomenon that we can add little today to what Wells wrote over 45 years ago. It is interesting to note that Wells' idea predates the pioneering work of Bury (116) on resonance in organic dyes by over 10 years.

The history of mixed valence chemistry goes far beyond the work of the twentieth century chemists, beginning with the synthesis in 1704 of one of the first coordination compounds, Prussian blue (572). The early history of the mixed valence phenomenon can be clearly seen as consisting of two phases. In the first earlier phase, we have the slow recognition of the mixed valence color phenomenon and an appreciation of the conditions which must prevail for its appearance. Thus, as early as 1847, Berzelius (63) described the blue-black ink derived from tannin-containing gall nuts as a double salt of Fe(II) and Fe(III) ions, similar to the other blue iron salts then known to contain these ions simultaneously. Werner (764) also commented on the extraordinary colors and metallic sheen of certain Pt(II), Pt(IV) oxalate complexes he newly synthesized, comparing their colors to that of the tungsten bronzes and

hydroquinone, the common denominator in all these systems being the simultaneous presence of oxidizing and reducing species. Hofmann (365) followed shortly thereafter with convincing evidence that the blue color of Prussian blue and other iron cyanide complexes was due to the presence of iron in two different oxidation states in the molecule. The significance of the mixed valence phenomenon to the colors of certain iron-containing minerals was later elucidated by MacCarthy (470), who explained that the presence of Fe(II) and Fe(III) in minerals leads to deep colors, black if the mineral is anhydrous, blue if it is hydrated. In addition to these few examples, a long list of citations can be made of the appearance of transient dark colors in the course of oxidation and/or reduction of many transition metal compounds.

In the historical second phase, the seemingly logical inferences are drawn that in fact the different valences are not uniquely fixed, one to each ion, but oscillate rapidly in a mixed valence system, and that the result of this unique valence oscillation is a unique absorption of light, i.e., color. Thus, in 1915 Hofmann and Höschele (366) suggested that the blue color of "cerium-uranium blue," a mixed oxide of UO_2 and CeO_2 , was the result of the valence oscillation,

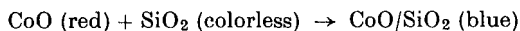


and coined the phrase "constitutive coloration" to describe this and other systems having colors which are not the sum of the colors of their components, but unexpectedly appear only on the union of these components:

"It is necessary that the distribution of oxidation states within the molecule can exchange under the influence of light so as to produce the light absorption and hence the color. This situation occurs most frequently in inorganic chemistry when the same element is present in different valence states in the same molecule."

Wells (759) shortly after, and without reference to the work of the Germans, came to the same conclusion quoted above, proposing in addition that the "spontaneous electronic activity" present in mixed valence compounds must also result in enhanced electrical conductivity. This latter conclusion of Wells made understandable the earlier work of Streintz (688), who found that white, yellow, red, and gray powders do not conduct electricity, whereas the deeply colored ones may show metallic conduction. Biltz (69) soon followed with an article outlining the origins of the colors of various inorganic materials, giving space to mixed valence colors and many examples of compounds wherein the same element occurs in two different oxidation states, and also to the situation wherein two different elements are present in different oxidation states.

This latter collection of examples is complicated by the possibility that the color change on mixing arises not from an oscillation of valence between different metal ions, but instead from a change in the ligand field about one of the components on going into the mixed crystal. Thus, the combination



is given as an example of the formation of a mixed valence, constitutive coloration. However, the red-to-blue color change given above could reasonably be interpreted as that expected for Co(II) in an octahedral site of CoO going into a tetrahedral site of SiO₂. The question raised here can obviously be settled by a study of the electronic spectrum, but until this is done there remains an ambiguity, which we take as an example of the fact that not *every* color change observed on mixing can be attributed to the mixed valence phenomenon.

Finally, the work of Stieglitz (687) must be mentioned as being of historical importance, for he expressed the thought that the deep color of many inorganic substances was intimately connected with the interatomic oxidation-reduction tendency of the compound. Thus, in mixed valence systems, he pointed out that intense colors can result from photochemical oxidation-reduction, the electrode potentials permitting, and that there is no compelling need to introduce an oscillation of the valences. As we shall see later, these two views are simply the extreme solutions of the same general problem, and many mixed valence systems can be found which support each of the two seemingly opposite positions.

Up to the present time, mixed valence phenomena have not very often been considered in the wider context of theories of spectroscopy and the solid state, but rather as peculiar occurrences occasionally met with here and there, their consequences here having no relationship to their consequences there. In fact, as we shall illustrate, mixed valence is found in a tremendous number of places, and it is hoped that a systematic study of the electronic phenomena related to its occurrence will serve to unite many seemingly unrelated facts. In Table I we list a number of the scientific areas in which mixed valence is encountered, together with examples. In a great many cases, the mixed valence introduces profoundly new effects.

Our first task is to cast the older, qualitative description of the mixed valence phenomena into a more modern, qualitative quantum mechanical one, relying heavily on ligand field theory. The accent here will be on the relationship between electronic spectra, electronic structure, and molecular structure. Following this, we will consider the experimental results at hand and attempt to apply our quantum

theoretical generalizations to them. Hopefully, by proceeding in this way, with all the data gathered in one place, we will uncover unexpected relationships and generalities, and, by pointing out where more work is needed, stimulate the completion of this work.

TABLE I
AREAS IN WHICH EXAMPLES OF MIXED VALENCE CAN BE FOUND

Area	Example
(1) Metal-metal bonding	$[\text{Ta}_6\text{Cl}_{12}]^{2+}$
(2) Nonstoichiometry	UO_{2-x}
(3) Coloration of glasses	Blue color of silicate glasses containing iron
(4) Biology	Hemocyanin
(5) Reaction intermediates	$\text{Fe}(\text{OH})_2$ (colorless) $\xrightarrow{\text{air}}$ (blue) $\xrightarrow{\text{air}}$ $\text{Fe}(\text{OH})_3$ (brown)
(6) Spot tests, qualitative analysis	$\text{Fe}^{\text{II}} + \text{Fe}^{\text{III}}(\text{CN})_6 \rightarrow$ blue solution
(7) Solid state	Self trapping, color centers, Na in NaCl (?)
(8) Electronic conduction	Controlled valency spinels
(9) Magnetic interactions	Ferromagnetic double exchange (LaMnO_3)
(10) Minerals	Biotite, Fe_3O_4
(11) Photochemistry, photography	Iron oxalate blueprint reaction, phosphotungstous acid images
(12) Metals in molten salts	Bi in BiI_3
(13) Intermetallics	$\text{In}^{\text{I}}\text{In}^{\text{III}}\text{Te}_2$
(14) Polyhalides	I_3^-
(15) Unusual oxidation states	Cs_2SbCl_6 , GaCl_2 , Pb_2O_3
(16) Statistical mechanics	Entropy-induced defect structures and shear phases
(17) Electrochemistry	AgO electrodes, Pb_2O_3
(18) Superconductivity	Tungsten bronze, Ag_2F
(19) Dyes, pigments, inks	Mo_3O_8 , W_3O_8 , Prussian blue
(20) Valence isomerization	$\text{Cu}^{\text{II}}\text{Ta}^{\text{IV}}\text{O}_3 = \text{Cu}^{\text{I}}\text{Ta}^{\text{V}}\text{O}_3$

II. Theory of Mixed Valence Effects

Our theory of mixed valence effects begins with a simple one-electron theory of the electronic structure of mixed valence systems, and then goes on to discussions of the electronic spectra, resistivity, and magnetic

interactions in such systems, followed by a few words about geometry and valence. The theory of mixed valence will use the concepts of ligand field theory as a basis, and is phrased in very broad and general terms. This is because there are very little quantitative data available on mixed valence compounds, and consequently very little need as yet for a detailed theory. The theory as outlined, however, is sufficient for drawing important preliminary qualitative conclusions about the electronic structures of these materials, and offers a foundation for a valuable classification scheme.

A. THE WAVE FUNCTIONS AND MIXED VALENCE CLASSIFICATION

Our initial concern is with the delineation of the mixed valence wave functions, the prime value of which is as a qualitative measure of the extent of delocalization of the valence shell electrons. Although these

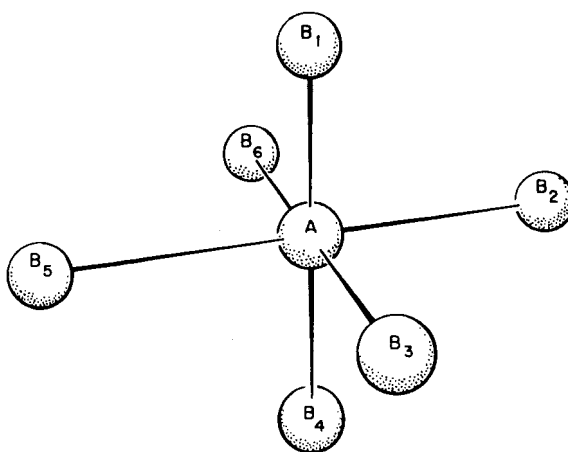


FIG. 1. A hypothetical mixed valence system consisting of the reduced metal ion at A, and six oxidized metal ions at the equivalent B sites. The ligands are not shown.

wave functions will not actually be used in a direct calculation of excitation energies, they can be of use in estimating other spectral properties, such as relative excitation energies, the number of excited states and their ordering, and spectral intensities. The extent of delocalization also correlates with the resistivity of mixed valence solids and their magnetic properties.

Consider the set of seven metal ions having the geometrical arrangement shown in Fig. 1. The metal ion in site A differs from those in the B sites not because of their relative geometrical arrangement, but because

the fields of the ligands, not shown, are supposed to be of different strengths and/or symmetries at the two sites. All the B sites are equivalent. Let us also suppose that the ion in the A site is of formal valence III [Ti(III), say] and that the ions in the B sites are all of formal valence IV [Ti(IV), say].

Neglecting explicit mention of the ligand wave functions, the ground state wave function of the system in *zeroth* order may be taken as

$$\Psi'_0 = \psi_A^{\text{III}} \psi_{B_1}^{\text{IV}} \psi_{B_2}^{\text{IV}} \cdots \psi_{B_s}^{\text{IV}} \quad (1)$$

where ψ_A^{III} is the wave function of the trivalent ion in the A site, and the $\psi_{B_i}^{\text{IV}}$ are the wave functions of the quadrivalent ions in the B sites. On transferring one electron from the A site to the B site, the A site and B site wave functions will change their oxidation state labels by +**(I)** and -**(I)**, respectively, yielding excited state wave functions, which may be written as:

$$\Psi_k = \psi_A^{\text{IV}} \sum_j C_{kj} \psi_{B_1}^{\text{IV}} \psi_{B_2}^{\text{IV}} \cdots \psi_{B_j}^{\text{III}} \cdots \psi_{B_s}^{\text{IV}} \quad (2)$$

There will be six Ψ_k 's, each with numerical coefficients C_{kj} chosen to normalize Ψ_k and chosen to guarantee that Ψ_k will transform according to one of the representations of the appropriate symmetry point group.

Suppose also that one of the Ψ_k 's, say Ψ_l , has a symmetry appropriate for mixing with Ψ'_0 , i.e., Ψ'_0 and Ψ_l belong to the same representation. The ground state, Ψ_0 , will then be taken as the linear combination

$$\begin{aligned} \Psi_0 &= \sqrt{1 - \alpha^2} \Psi'_0 + \alpha \Psi_l \\ &= \sqrt{1 - \alpha^2} \psi_A^{\text{III}} \psi_{B_1}^{\text{IV}} \psi_{B_2}^{\text{IV}} \cdots \psi_{B_s}^{\text{IV}} + \alpha \psi_A^{\text{IV}} \sum_j C_{lj} \psi_{B_1}^{\text{IV}} \psi_{B_2}^{\text{IV}} \cdots \psi_{B_j}^{\text{III}} \cdots \psi_{B_s}^{\text{IV}} \\ &= \sum_j \frac{\sqrt{1 - \alpha^2}}{6} \psi_A^{\text{III}} \pi_{B_j} \psi_{B_j}^{\text{IV}} + C_{lj} \alpha \psi_A^{\text{IV}} \pi_{B_j} \psi_{B_j}^{\text{III}} \end{aligned} \quad (3)$$

where π_{B_3} is defined as

$$\pi_{B_3} = \psi_{B_1}^{\text{IV}} \psi_{B_2}^{\text{IV}} \psi_{B_4}^{\text{IV}} \psi_{B_5}^{\text{IV}} \psi_{B_6}^{\text{IV}}, \quad (4)$$

and similarly for the other π_{B_j} 's. Thus,

$$\Psi_0 = \frac{1}{N} \sum_j \pi_{B_j} \left\{ \frac{\sqrt{1 - \alpha^2}}{6} \psi_A^{\text{III}} \psi_{B_j}^{\text{IV}} + C_{lj} \alpha \psi_A^{\text{IV}} \psi_{B_j}^{\text{III}} \right\} \quad (5)$$

where $1/N$ is a normalization factor.

At this point let us presume for simplicity that the reduced species in any site consists of one electron outside of a closed shell, so that we may take

$$\begin{aligned} \psi_A^{\text{IV}} &= \phi_A^C; & \psi_{B_j}^{\text{IV}} &= \phi_{B_j}^C \\ \psi_A^{\text{III}} &= \phi_A^C \phi_A^*; & \psi_{B_j}^{\text{III}} &= \phi_{B_j}^C \phi_{B_j}^* \end{aligned} \quad (6)$$

where ϕ^C represents the wave function for the closed-shell core, and ϕ^* is the only orbital outside the core. Using the above relations, one finds

$$\begin{aligned}\Psi_0 &= \frac{1}{N} \sum_j \pi_{B_j} \left\{ \frac{\sqrt{1-\alpha^2}}{6} \phi_A^C \phi_A^* \phi_{B_j}^C + \alpha C_{lj} \phi_A^C \phi_{B_j}^C \phi_{B_j}^* \right\} \\ &= \frac{1}{N} \sum_j \phi_A^C \phi_{B_j}^C \pi_{B_j} \left\{ \frac{\sqrt{1-\alpha^2}}{6} \phi_A^* + C_{lj} \alpha \phi_{B_j}^* \right\}\end{aligned}\quad (7)$$

The prefactor $\phi_A^C \phi_{B_j}^C \pi_{B_j}$ is simply the product of all the closed-shell core functions, κ , and can be carried along from this point onward without further comment. Thus,

$$\Psi_0 = \frac{\kappa}{N} \left[\sqrt{1-\alpha^2} \phi_A^* + \alpha \sum_j C_{lj} \phi_{B_j}^* \right] \quad (8)$$

We recognize the wave function in Eq. (8) as describing the optical electron in a *molecular orbital* written as a sum of atomic orbitals spanning both A and B positions. Notice that, since the A and B sites are distinguishably different and no symmetry operation will take a wave function centered on A into one centered on B, the two fragments ϕ_A^* and $\sum_j C_{lj} \phi_{B_j}^*$ must have the same symmetry if they are to be mixed. That is, the only Ψ_l which will be mixed in with Ψ'_0 must have its sum of $\phi_{B_j}^*$ orbitals transform like the ϕ_A^* orbital. Thus the electron will be delocalized from A onto the B sites only if the orbitals on A and B have the same point group symmetry, a result already well known in molecular orbital theory.

For normalized wave functions, the value of α^2 can be derived to be

$$\alpha^2 = N^2 \left[1 - \left\{ 1 + \frac{2E_l^2 - 2E_l \sqrt{E_l^2 + 4V^2} + 4V^2}{4V^2} \right\}^{-1} \right] \quad (9)$$

from the solution of the secular equation which expresses the mixing between Ψ'_0 and Ψ_l . In this equation, V is the mixing matrix element $\langle \Psi'_0 | V | \Psi_l \rangle$ and E_l is the energy of Ψ_l above Ψ'_0 . With an appropriate change of the zero of energy, the energies E_0 and E_l may be taken as approximately the valence state ionization potentials of the reduced ion at A and the reduced ion at B, respectively.

One sees from Eq. (9) that, as E_l approaches zero, both α and $\sqrt{1-\alpha^2}$ approach $(N\sqrt{2})/2$, whereas, for very large E_l , α tends to zero and $\sqrt{1-\alpha^2}$ to one. Thus if E_l is large, then α is small, and Eq. (8) reduces to the *zerth* order Eq. (1) for the wave function of the system in the ground state, but Eq. (8) becomes more appropriate the smaller is E_l and the larger is α . A large value of E_l may come about either because the ions in

the two sites are of different elements, or because the sites differ in ligand field strength or ligand field symmetry. Inasmuch as this review considers only mixed valence compounds in which the oxidation states involved are those of the same element, nonzero values of E_l will be associated only with differences in ligand field strength and/or ligand field symmetry.

We now propose a mixed valence classification scheme which is based essentially upon the strength and symmetry of the ligand fields about the metal ions, and their relationship to the value of α appropriate to a particular system. By definition, in a class I system, the ions of differing valence are in sites of very different symmetry and ligand field strength, so that E_l is large and α approaches zero. In a class I system the simple product function of Eq. (1) is used to describe the ground state. An example of a class I system would be a mixed valence cobalt compound in which the Co(III) ions were in octahedral ligand fields with low-spin configurations, and the Co(II) ions were in tetrahedral ligand fields with high-spin configurations.

On the other hand, if the Co(II) and Co(III) ions are in exactly equivalent sites, so that E_l is zero and $\alpha = (N\sqrt{2})/2$, then the system is class III, and the molecular orbital description, Eq. (8), is needed for the ground state of the system. Class III mixed valence systems can be further subdivided into classes III-A and III-B, depending upon whether or not discrete polynuclear ions can be distinguished in the crystal. An intermediate classification, class II, is defined for cases in which delocalization does take place ($\alpha > 0$), but the two types of site are still distinguishable, and so the optical electron does not spend equal times on them. As an example, a class II system might have both oxidized and reduced cations in octahedral sites, but with the metal-ligand distances shorter at one site than at the other. It is not easy to draw a precise demarcation between classes I and II, but, in the vast majority of cases, class II systems have at least one ligand which bridges the two ions of differing valency, whereas in class I systems the metal ions are either removed from one another by two or more ligands which are relatively non-interacting, or have very different coordinations.

A further point arising from Eq. (9), and relevant to our selection of compounds as examples of mixed valence, is that α can become large not only when E_l is small, but also when V becomes large. It is for this reason that we have, with very few exceptions, excluded sulfides, arsenides, and all other compounds in which there is likely to be extreme metal-ligand covalency. In many single valence examples of this type, electron delocalization can occur with such a small expenditure of energy that the resulting low-frequency absorption bands and high

electronic conductivity would be difficult to distinguish from that to be ascribed to mixed valence interaction. Our approach to mixed valence systems is thus predominantly an ionic one, in which electron delocalization, if it occurs, involves primarily the metal ions whose valences are under discussion, and the ligands to a much smaller extent.

The motivation for the classification scheme outlined above sprang from our observation that each of the classes as defined exhibits certain easily recognized physical properties which are characteristic of that class. Thus, by a measurement of a single property which is characteristic of one of the four classes, many of the other physical properties of the system can be guessed, or become understandable. Because compounds with properties common to more than one class are rare, the classification scheme is of rather greater utility and has been used extensively in the discussion of the mixed valence compounds (Section III).

B. MIXED VALENCE SPECTRA

Since we are neither capable nor desirous of calculating spectra in a review of this kind, our goal is to present some generalizations which, although they are phrased in the form of a theory, in fact were arrived at by a study of the experimental results reported in the literature. Thus our effort here is to rationalize "the truth" in terms of a simple model which, by its generality, will be of use in the discussion of the spectra of a wide variety of mixed valence compounds.

Our fundamental concern in this section is with the mixed valence electronic transition,

$$\frac{\kappa}{N} \left[\sqrt{1 - \alpha^2} \phi_A^* + \alpha \sum_j C_{lj} \phi_{B_j}^* \right] \rightarrow \frac{\kappa}{N'} \left[\beta \phi_A^* - \sqrt{1 - \beta^2} \sum_j C_{mj} \phi_{B_j}^* \right] \quad (10)$$

where β plays the same role for the excited state that α does for the ground state. It is electronic transitions of this sort that comprise the mixed valence absorption spectrum in all three classes. Because the classification scheme is based essentially on geometry, and since the nuclei in the excited state will be considered as fixed in the ground state configuration, the ground and excited states of mixed valence transitions are assumed to belong to the same mixed valence class.

A study of the literature shows that in systems which are known by their crystal structures to be mixed valence class I ($\alpha = \beta = 0$), the mixed valence absorption bands fall at frequencies higher than $27,000 \text{ cm}^{-1}$, for they are almost all colorless. Those class I systems that do show absorption in the visible invariably contain a colored ion as a constituent, their

visible spectra being merely sums of the spectra of the constituent ions, and nothing more. Virtually all the colorless class I systems involve nontransition metal ions, which are quite stable in the ground state as M^n and M^{n+2} , but which are relatively unstable in the M^{n+1}, M^{n+1} configuration of the mixed valence upper state. Actually, a mixed valence absorption has never been observed in a class I system, so there is no evidence as to where in the spectrum it might be found.

In contrast, the class II mixed valence systems are characterized by an absorption band in the visible region of the spectrum (14,000–27,000 cm^{-1}) which is absent in the spectra of the constituent ions taken separately. In the simplest approximation, the energy of this transition is

$$h\nu = E_A + E_B + E_{mad} \quad (11)$$

where E_A and E_B are the changes in internal energy at sites A and B, respectively, on transferring an electron from A to B, and E_{mad} is the Madelung energy expended in moving the optical electron from A to B in the electrostatic field of all the other charges in the crystal. This last term can be calculated from a cycle in which adjacent ions are removed from the crystal to infinity, an electron transferred adiabatically between them, and the ions then returned to their sites in the crystal. The two internal energy terms in Eq. (11), however, correspond to the ionization potential and electron affinity of sites A and B, respectively, and as yet cannot be estimated or measured for inorganic complexes. Inasmuch as a class II mixed valence transition is a photochemical oxidation-reduction, the possibility of somehow adapting half-cell potentials to the estimation of the internal energy terms is attractive. However, it should be mentioned that the only application of such potentials to mixed valence systems resulted in the incorrect valence assignment for the ground state of Prussian blue (754).

Although the various contributions to the energy of the lowest-frequency mixed valence absorption band in class II compounds cannot yet be interpreted in detail, certain other features of the spectrum are more readily understood. It seems clear that in class II compounds, even though α and β are nonzero, the perturbation of the wave function can be sufficiently small so that constituent ion absorptions can still be recognized, albeit not at exactly their normal frequencies. Thus the 29,000 cm^{-1} transition characteristic of the $\text{Sb}^{\text{III}}\text{Cl}_6$ group is identified at 31,000 cm^{-1} in the blue class II compound $\text{Cs}_4\text{Sb}^{\text{III}}\text{Sb}^{\text{V}}\text{Cl}_{12}$, and the 50,000 cm^{-1} charge transfer bands of the $[\text{Fe}^{\text{II}}(\text{CN})_6]^{4-}$ ion are observed at this frequency in the class II compound $\text{KFe}^{\text{III}}\text{Fe}^{\text{II}}(\text{CN})_6$. Because of this, the electronic spectrum holds promise for resolving ambiguities in the ground state valence configurations of many class II mixed valence

compounds. Similar constituent ion absorptions can be found in the infrared and Mössbauer spectra of class II compounds. For example, the ν_3 stretching frequency of the $[\text{Sb}^{\text{V}}\text{Cl}_6]^-$ ion in $\text{Cs}_4\text{Sb}^{\text{III}}\text{Sb}^{\text{V}}\text{Cl}_{12}$ is shifted only 5 cm^{-1} from its position in $\text{RbSb}^{\text{V}}\text{Cl}_6$.

A second interesting point, which also follows from the slight perturbation of the constituent ion levels in class II systems, involves the remaining mixed valence spectrum. For illustration, consider the d -orbital pattern of a hypothetical class II $\text{Cu}(\text{I}),\text{Cu}(\text{II})$ complex in which

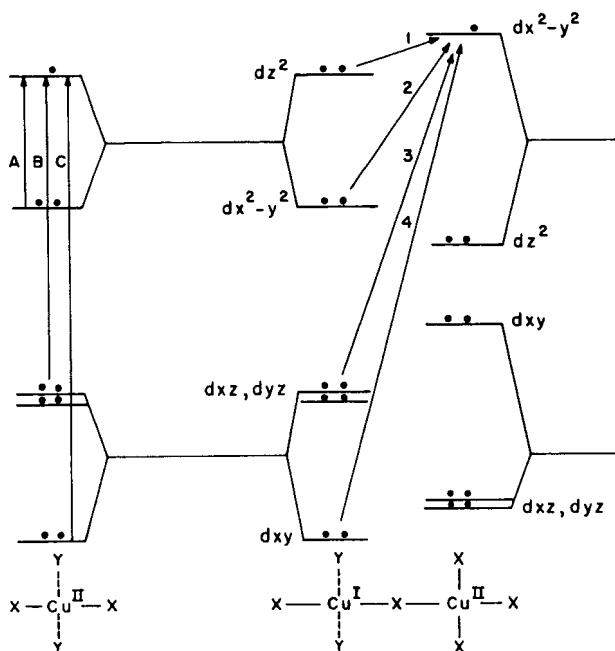


FIG. 2. The molecular orbital scheme for the hypothetical class II mixed valence system $\text{Cu}^{\text{I}}\text{Y}_2\text{X}_2\text{Cu}^{\text{II}}\text{X}_3$, showing how the energy difference between the two mixed valence transitions 2 and 1 is equal to the crystal field transition A in $\text{Cu}^{\text{II}}\text{X}_2\text{Y}_2$, etc.

the $\text{Cu}(\text{I})$ is in square coordination with two X and two Y ligands, and $\text{Cu}(\text{II})$ is in square coordination with four X ligands (Fig. 2). In such a simple system there will be four mixed valence absorption bands, labeled 1, 2, 3, and 4. The point of interest here is that the energy difference between mixed valence transitions 1 and 2 will be equal to the first crystal field excitation energy of the $\text{Cu}(\text{II})$ ion in the $\text{Cu}(\text{I})$ ion site, i.e., transition A ($dx^2 - y^2 \rightarrow dz^2$) in the oxidized ion. Similarly, mixed valence transition 3 will appear displaced from transition 1 by the $\text{Cu}(\text{II})$ crystal field excitation B ($dxz, dyz \rightarrow dz^2$). Thus in this case, the entire crystal field spectrum of the oxidized ion, $\text{Cu}(\text{II})$, in the reduced

ion site (A) appears in the mixed valence spectrum, shifted from where it ordinarily would appear by the energy of the lowest mixed valence transition. Other samples exist where the mixed valence spectrum consists of the crystal field spectrum of the reduced ion in the oxidized ion site, or of combinations of both kinds of spectrum. However, not all crystal field states will necessarily appear in the mixed valence spectrum, since many of the excited crystal field configurations require two-electron excitation when attained from the mixed valence ground state. Only one example of the shifting of the crystal field spectrum by the mixed valence excitation energy has so far been reported (591).

The intensities of electronically allowed transitions in class II systems are another interesting aspect of mixed valence spectra. In an electronically allowed transition, the orbital $\sum_j C_{mj} \phi_{B_j}^*$ of the upper state must transform differently under the operations of the symmetry point group than does $\sum_j C_{lj} \phi_{B_j}^*$, so that $\sum_j C_{mj} \phi_{B_j}^*$ cannot mix with ϕ_A^* , and thus β is zero. The intensity of such an electronically allowed mixed valence transition is proportional to the square of the transition moment integral,

$$\mu = \frac{g^{1/2}}{NN'} \int \left[\sqrt{1 - \alpha^2} \phi_A^* + \alpha \sum_j C_{lj} \phi_{B_j}^* \right] \mathbf{M} \sum_j C_{mj} \phi_{B_j}^* d\tau \quad (12)$$

where g is the orbital degeneracy of the transition, and \mathbf{M} is the electric moment operator. By neglecting overlap distributions between the A and B sites, the x component of Eq. (12) can be reduced to

$$\mu_x = \frac{\alpha g^{1/2}}{NN'} \int \sum_j C_{lj} \phi_{B_j}^* \text{ex} \sum_j C_{mj} \phi_{B_j}^* d\tau \quad (13)$$

$$= \frac{e\alpha g^{1/2}}{NN'} \sum_j C_{lj} C_{mj} x_j \quad (14)$$

in which x_j is the x coordinate of the j th site. Exactly similar equations hold for the y and z moments. The utility of Eq. (14) lies in the fact that, if the system is sufficiently regular geometrically so that the C_{lj} 's and C_{mj} 's are determined by symmetry, and the x_j 's are known from a crystal structure determination, α can be obtained from a measurement of μ ; μ is calculated from the equation

$$\mu^2 = 9.17 \times 10^{-4} \int \epsilon d \log \lambda \quad (15)$$

in which ϵ is the molar extinction coefficient of the mixed valence absorption band at wavelength λ , and μ^2 is measured in cm^2 .

There is one complication worth considering here, and that is the case where there are two types of orbital at each B site, call them

$\phi(z^2)_j^*$ and $\phi(x^2 - y^2)_j^*$, say. The possibility then arises for a transition involving the two types of orbital, leading to the transition moment:

$$\mu = \frac{\alpha g^{1/2}}{NN'} \int \sum_j C_{lj} \phi(z^2)_j^* \mathbf{M} \sum_j C_{mj} \phi(x^2 - y^2)_j^* d\tau \quad (16)$$

$$\mu = \frac{\alpha g^{1/2}}{NN'} \sum_j C_{lj} C_{mj} \int \phi(z^2)_j^* \mathbf{M} \phi(x^2 - y^2)_j^* d\tau \quad (17)$$

The transition moment integral in Eq. (17) is one between atomic orbitals on the same atom, and can be zero even though the selection rules predict an allowed transition between Ψ_0 and Ψ_m . This is possible because the selection rule allowing a transition between Ψ_0 and Ψ_m guarantees that the intensity generated in one part of the molecular system is not canceled by that in another part, but by itself does not guarantee that the intensity within this part of the molecular system is not itself zero. Inasmuch as the intensity of an electronically allowed mixed valence transition does depend upon α , it can readily be appreciated that there can be no *intense* ($\epsilon \geq 4000$) mixed valence absorption unless ϕ_A^* and some ϕ_B^* have a nonzero overlap.

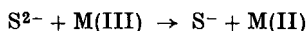
That highly hydrated mixed valence compounds have only the pale color of their constituent ions, but become more deeply colored as the water is removed, is one of the mixed valence facts of life. This is understandable, since water is not a bridging ligand and would promote the formation of a class I system when present in large proportions. However, as the water is removed, the empty sites must be filled by ligand anions which can bridge two metal ions and thereby turn the compound into a more deeply colored class II system.

Polynuclear mixed valence anions, cations, and neutral species in which the sites of all metal ions are equivalent are classified as III-A. The interpretation of the spectral properties of class III-A systems differs from that of class II systems, for in class III-A the distinction between A and B sites is lost completely, so that $E_A = -E_B$, and E_{mad} is zero. The excitation energies in class III-A are instead dependent upon ligand field splittings and molecular orbital resonance integrals, just as they are in an ordinary polynuclear complex having metal-metal bonds. Also, unlike class II, there will be no recognizable constituent ion spectra in class III-A compounds.

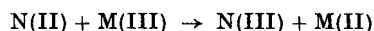
Class III-B systems are metals and as such show an absorption edge, usually in the infrared, and are opaque with a metallic reflex in the visible region.

In a broader sense, there is really nothing unique about mixed valence systems, for mixed valence properties are to be expected in any

system containing simultaneously an oxidizable and a reducible species in close contact. Thus, transition metal sulfides may have many properties in common with class II mixed valence systems, for the excitation



may be thought analogous to the excitation



in a mixed valence system. The difference between these two examples is one of degree only, for if the N and M ions are of the same element and are in identical ligand fields, then the energy difference between $N(\text{II}) + M(\text{III})$ and $N(\text{III}) + M(\text{II})$ will be as small as zero, whereas no such statement can be made for $S^{2-} + M(\text{III})$ versus $S^{-} + M(\text{II})$.

The relationship of inorganic mixed valence systems to the organic charge transfer complexes is also a close one. In fact, the charge transfer complex quinhydrone is mentioned in Biltz's early article on inorganic mixed valence systems (69). The unexpected deep black color of quinhydrone was correctly seen by Biltz to be a consequence of having formed a crystal containing an intimate mixture of the oxidized material (benzoquinone) and the corresponding reduced material (hydroquinone), in every way equivalent to the formation of a deep blue color in crystals which contain $\text{Fe}(\text{III})$ (an oxidized material) and $\text{Fe}^{\text{II}}(\text{CN})_6$ (a reduced material).

C. MAGNETISM AND ELECTRON TRANSPORT

The magnetic and electron transport properties of mixed valence compounds are closely related to one another, and the wide variations observed in their behavior give further weight to our proposed classification scheme. In particular, we can make operational distinctions between class I and class II compounds on the basis of these properties in a way not possible from a knowledge of the crystal structure alone.

In a class I mixed valence material, the electrons which distinguish the valence of one ion from another are so firmly trapped that virtually no magnetic coupling between partly filled shells on adjacent metal ions is possible, and these substances are paramagnetic down to very low temperatures. Thus a class I compound such as $\text{Co}^{\text{II}}\text{Co}_2^{\text{III}}\text{O}_4$ will have a molar magnetic susceptibility precisely that expected for a mixture of one mole of $\text{Co}(\text{II})$ in tetrahedral coordination and two moles of $\text{Co}(\text{III})$ in octahedral coordination. That electron transfer can occur only at the expense of a large amount of energy also means that class I materials are electrical insulators.

At the opposite extreme, when α in Eq. (9) has its maximum value, the odd electrons responsible for the mixed valence occupy a band spanning the entire cation sublattice (we are ignoring the possibility that they have any appreciable density on the anion sublattice, as mentioned above). In such a case, two electrons occupy each state of the energy band up to the Fermi surface so that, with completely filled inner shells and in the absence of a magnetic field, each atom has no net spin, and atomic moments exist only through induction by an applied field. By Lenz's law, such moments give a diamagnetic susceptibility, but for collective electrons there is a further possibility that an applied field might alter the populations of the electron states, producing what is known as temperature-independent Pauli paramagnetism. If each cation contributes either zero or two electrons to a band, then the band will be either completely empty or completely filled, and in either case the material will be an insulator. However, by their very nature of being mixed valence, the cations in class III-B materials will contribute, on the average, an intermediate number of electrons to the band, filling it only partially. Thus class III-B mixed valence materials will show metallic conductivity. The class III-B tungsten bronzes are good examples of these mixed valence effects, for they have temperature-independent paramagnetic susceptibilities and metallic conductivities. A second type of magnetic behavior in class III-B systems is described below.

The possibility of ferromagnetic ordering between the local magnetic moments in transition metals was first considered by Zener (812), who proposed that, in the metallic state, it was the conduction electrons which coupled the d -shell moments together. Since, according to Hund's rule, the lowest energy configuration within each d -shell has the spins of all of the unpaired electrons parallel, if the conduction electrons are to carry their spins unchanged from atom to atom, they must move in an environment of parallel spins, i.e., the moments of all the atoms must point in the same direction. Contrasting the Heusler alloys, which are conducting and ferromagnetic, with MnF_2 , which is an antiferromagnetic insulator, Zener concluded that ferromagnetism would never occur in the absence of conduction electrons (812). Shortly afterwards, the properties of a series of metallic mixed valence manganites, $\text{La}_{1-x}\text{Sr}_x\text{Mn}_{1-x}^{\text{III}}\text{Mn}_x^{\text{IV}}\text{O}_3$, were investigated by Jonker and van Santen (392, 393), and these have since become the classic examples of Zener's "double exchange" phenomenon. The relationship between ferromagnetism and conductivity is brought out most clearly by a simple example. In contrast to the metals described above, between each manganese ion in the perovskite structure of $\text{La}_{1-x}\text{Sr}_x\text{Mn}_{1-x}^{\text{III}}\text{Mn}_x^{\text{IV}}\text{O}_3$

there is an oxide ion, through which any electron transport must occur, although, as we have noted several times, the initial and final states of electron transfer are assumed to have very little unpaired spin density on any intervening ions. This is equivalent to saying that we could write wave functions for systems such as those described by Eqs. (1) and (2) as if their metal-ligand electronic configurations were $\text{Mn}_A^{\text{III}}\text{O}^{2-}\text{Mn}_B^{\text{IV}}$ and $\text{Mn}_A^{\text{IV}}\text{O}^{2-}\text{Mn}_B^{\text{III}}$. The magnetic exchange energy of such a system is given by

$$E_m = \int \psi_A^{\text{III}}\psi_0\psi_B^{\text{IV}}(H - E_0)\psi_A^{\text{IV}}\psi_0\psi_B^{\text{III}}d\tau \quad (18)$$

where H is the Hamiltonian for the entire system, and E_0 is the energy associated with the initial states, assumed degenerate. The dominant term of the exchange integral contains a product of wave functions $\psi_A(1)\psi_0(1)\psi_0(2)\psi_B(2)$, suggesting that one visualize the electron transfer from one manganese to the next as a transfer of electron (2) from the oxygen to the Mn_B^{IV} ion with a simultaneous transfer of electron (1) from Mn_A^{III} to the oxygen; a connection between ferromagnetic coupling and electronic conductivity is thus apparent. That the interaction in a mixed valence compound is ferromagnetic arises in the following way. Of the two antiparallel electron spins on the oxide ion, Hund's rule predicts that the oxide ion electron with spin parallel to those of the $3d^3$ Mn (IV) ion will be transferred the more readily, leaving behind the electron of opposite spin. Similarly, the $3d^4$ Mn(III) ion will transfer an electron to the O^- ion which has a spin opposite to that remaining on O^- . The net result is that the manganese ions are coupled via the oxide ligand only if the spins on the two metal ions are parallel, i.e., in ferromagnetic alignment.

If the magnetic exchange energy in the system discussed above is E_m , the "extra" electron, when placed on one of the manganese atoms, will oscillate between them with a frequency

$$\nu = 2E_m/h \quad (19)$$

and will have a diffusion coefficient

$$D = a^2E_m/h \quad (20)$$

where a is the cation-cation separation. Using the Einstein relation between electrical conductivity, σ , diffusion coefficient, and the number of ions per unit volume, n ,

$$\sigma = ne^2D/kT \quad (21)$$

one then finds that

$$\sigma = ne^2a^2E_m/hkT \quad (22)$$

If we further assume, along with Zener and Heikes (814), that $E_m \simeq kT_c$, where T_c is the ferromagnetic Curie temperature, then the resistivity at this temperature for a typical cation-cation separation of 3 Å is approximately 10^{-3} ohm cm. As we shall see, the resistivities of a number of class III-B mixed valence materials at room temperature are in order of magnitude agreement with this estimate. The number of charge carriers/cc in a class III-B metal is estimated simply from the density of the material and the difference in the formal oxidation states of the cations involved in the mixed valence.

We now want to consider the magnetic and electrical properties of the intermediate, mixed valence class II materials. Mott (519) was the first to point out that there should exist some critical interatomic separation at which the types of molecular orbital (or band, in the limit of an infinitely extended lattice), which we have set up, are no longer the best approximation for treating the interactions between cations. For large interatomic separations, a Heitler-London approach, which assigns a fixed integral number of electrons to each cation and does not permit polar states as does the molecular orbital model, would have to be used. This argument was originally proposed to account for the fact that transition metal oxides like NiO, with incompletely filled *d*-shells and bridging anions separating the cations, are not metals but insulators. As will be discussed below, it is this model which is most appropriate to class II materials.

Zener assumed that the two configurations $\text{Mn}^{\text{III}}\text{O}^{2-}\text{Mn}^{\text{IV}}$ and $\text{Mn}^{\text{IV}}\text{O}^{2-}\text{Mn}^{\text{III}}$ were indistinguishable, which is equivalent to setting $E_i = 0$ in Eq. (9), so that the system belongs to class III-B. If this were not the case and the "extra" electron were trapped by lattice polarization ($\text{Mn}^{\text{III}}\text{—O}$ and $\text{Mn}^{\text{IV}}\text{—O}$ bond lengths different), further work must be spent in rendering the bond lengths equal so that electron migration can occur. This activation energy corresponds to ΔG , the change in Gibbs free energy of the system, and the diffusion coefficient would then be:

$$D = a^2 \nu_0 e^{-\Delta G/kT} \quad (23)$$

Heikes and Johnston (351), who first derived expressions for the so-called "hopping model," identified ν_0 with the lattice vibration frequency, and values obtained from their work on lithium-doped mixed valence transition metal oxides are of the expected magnitude (about 10^{13} sec⁻¹).

The temperature dependence of conductivity implied by Eq. (23) is that of a semiconductor, and we thus expect this type of electronic activity in class II substances. Inasmuch as class II compounds have relatively low conductivities as compared with class III-B compounds, according to Eq. (22), they will have correspondingly weaker ferro-

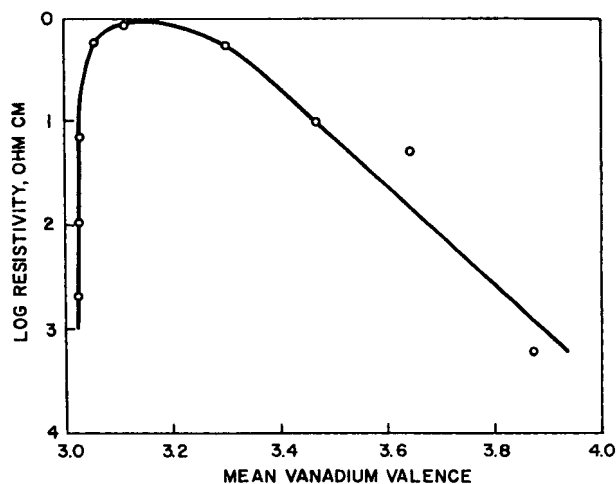


Fig. 3. The resistivity of mixed crystals of $MgV_2^{III}O_4$ and $Mg_2V^{IV}O_4$ as a function of the mean valence of the vanadium ions (581).

magnetic interactions. Thus they will remain paramagnetic down to much lower temperatures than will class III-B materials, and at low temperatures may go either ferromagnetic or antiferromagnetic, depending upon the relative strengths of the interactions between like and unlike valences.

TABLE II

CONTROLLED VALENCY SEMICONDUCTORS

Host	Dopant ^a	Valence introduced	Crystal lattice
Ni ^{II} O	Li ₂ O	Ni ^{III}	Rock salt
Mn ^{II} S	Li ₂ O	Mn ^{III}	Rock salt
CaTi ^{IV} O ₃	La ₂ O ₃	Ti ^{III}	Perovskite
BaTi ^{IV} O ₃	La ₂ O ₃	Ti ^{III}	Perovskite
CaMn ^{IV} O ₃	La ₂ O ₃	Mn ^{III}	Perovskite
LaMn ^{III} O ₃	CaO	Mn ^{IV}	Perovskite
LaFe ^{III} O ₃	SrO	Fe ^{IV}	Perovskite
Fe ₂ ^{III} ZnO ₄	TiO ₂	Fe ^{II}	Spinel
Fe ₂ ^{III} O ₃	SnO ₂	Fe ^{II}	Hematite
Ti ^{IV} O ₂	Ta ₂ O ₅	Ti ^{III}	Rutile
MgW ^{VI} O ₄	Cr ₂ O ₃	W ^V	Wolframite

^a In each of these systems, the dopant cation is thought to replace the cation listed first in the formula of the host crystal.

TABLE III
CHARACTERISTICS OF THE FOUR CLASSES OF MIXED VALENCE COMPOUNDS

Class I	Class II	Class III-A	Class III-B
(1) Metal ions in ligand fields of very different symmetry and/or strength, i.e., tetrahedral vs. octahedral	(1) Metal ions in ligand fields of nearly identical symmetry, differing from one another by distortions of only a few tenths Å	(1) Metal ions indistinguishable but grouped into polynuclear clusters	(1) All metal ions indistinguishable
(2) $\alpha = 0$; valences very firmly trapped	(2) $\alpha > 0$; valences distinguishable, but with slight delocalization	(2) α maximal locally	(2) α maximal; complete delocalization over the cation sublattice
(3) Insulator; resistivity of 10^{10} ohm cm or greater	(3) Semiconductor; resistivity in the range $10-10^7$ ohm cm	(3) Probably insulating	(3) Metallic conductivity; resistivity in the range $10^{-2}-10^{-6}$ ohm cm
(4) No mixed valence transitions in the visible region	(4) One or more mixed valence transitions in the visible region	(4) One or more mixed valence transitions in the visible region	(4) Absorption edge in the infrared, opaque with metallic reflectivity in the visible region
(5) Clearly shows spectra of constituent ions, IR, UV, Mössbauer	(5) Shows spectra of constituent ions at very nearly their normal frequencies	(5) Spectra of constituent ions not discernible	(5) Spectra of constituent ions not discernible
(6) Magnetically dilute, paramagnetic or diamagnetic to very low temperatures	(6) Magnetically dilute, with both ferromagnetic and antiferromagnetic interactions at low temperatures	(6) Magnetically dilute	(6) Either ferromagnetic with a high Curie temperature or diamagnetic, depending upon the presence or absence of local moments

Among the mixed valence manganites (392, 393), the connection between composition, Curie temperature, and resistivity is well established, and, in other systems in which the concentrations of two valence states can be varied, the conductivity also varies strongly (Fig. 3). Verwey and co-workers (730) have successfully altered these concentrations in a great many oxides, producing what are known as "controlled valency semiconductors." As illustrated in Table II, the addition of an insulating dopant to an insulating host crystal can alter the mean valency of the host's cations so as to render the system class II mixed valence and semiconducting.

The characteristics of the four classes of mixed valence compounds are compared in Table III.

D. MOLECULAR GEOMETRY

Inasmuch as the class of a mixed valence compound is intimately related to its crystal structure, the a priori prediction of the class of a mixed valence compound is equivalent to the a priori prediction of its crystal structure, a feat to which we can only aspire. The only mixed valence species upon which one can readily perform a calculation is the H_3^+ molecule-ion, which, from very complete calculations (147), would appear to be class III-A. A simple calculation on this molecule-ion reveals the two factors of importance in determining whether any mixed valence system will belong to class III or to a class of lower symmetry.

The total energy of the ground state of H_3^+ in various configurations was calculated, using as a basis nine *s*-type Gaussian orbitals on each proton, scaled to reproduce a Slater orbital with an effective nuclear charge of 1.414. In the first configuration (Fig. 4), the proton is situated 0.89 Å from each of the protons in H_2 (internuclear separation, 0.74 Å) and the two electrons are localized within the H_2 molecule. With the electrons still localized, the H_2 molecule is then stretched from 0.74 Å to 0.89 Å internuclear separation, raising the total energy by 24 kcal/mole and making all three protons equivalent. In the third configuration, the valence oscillates with the electrons moving over all three nuclei, and the total energy is then lowered by 135 kcal/mole.

This example of the H_3^+ molecule-ion illustrates the two opposing factors which must be considered in any problem of mixed valence geometry: (a) the reorganization energy which must be expended to stretch and/or compress certain bonds so as to make all the sites equivalent, and (b) the resonance energy stabilization which accrues from the oscillation of valence. If the second factor is larger than the first, then the system will belong to class III-A or III-B, whereas, if it is smaller than

the first, then the system will belong to class II or I. As explained in the previous section, if the reorganization energy is of the order of thermal energies, then the valence may oscillate via a hopping process.

Other attempts to predict which class a pair of mixed valence metal ions might prefer are frustrated by the fact that unusual coordinations can result in mixed valence compounds. Thus, for example one would ordinarily guess that Cu(I),Cu(II) systems would be class I or II, for

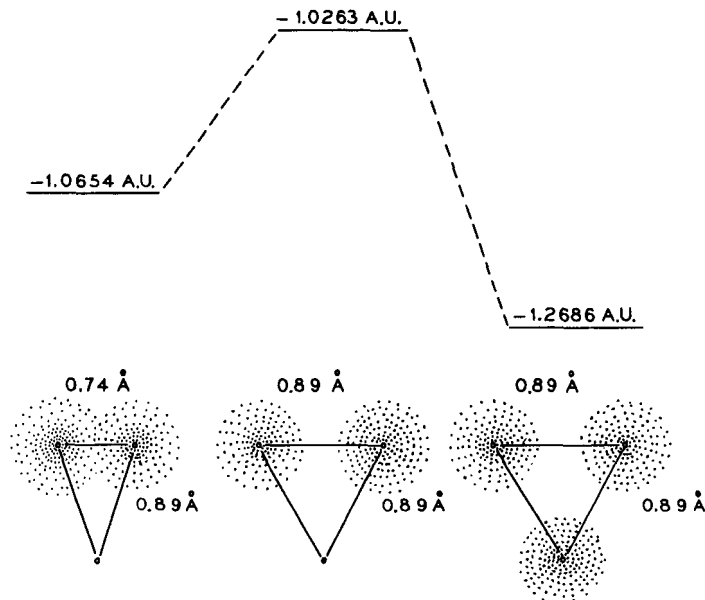


FIG. 4. The relative effects of reorganization and resonance on the total energy and geometry of the H_3^+ mixed valence molecule-ion.

these ions in general have very different coordination symmetries. However, in $\text{KCu}_3^{\text{I}}\text{Cu}^{\text{II}}\text{S}_3$, all the copper ions are in identical regular tetrahedral sites, a geometry never found for Cu(II) salts. There are other examples of unexpected geometries in class III systems.

III. Survey of the Elements

An indiscriminate study of mixed valence chemistry rapidly takes one from the simple salts and oxides into the realm of sulfides, tellurides, arsenides, and a vast array of other intermetallics. In an effort to keep this review of manageable length, we have arbitrarily ignored all but a very few compounds of this latter group, concentrating instead on the mixed valence oxides, halides, cyanides, and other simple salts, as well as coordination compounds. Many of the properties of mixed valence

compounds described in Section II can also be found in mixed metal complexes, such as $\text{KMn}^{\text{II}}\text{Fe}^{\text{III}}(\text{CN})_6$, which also have been ignored in this review. Similarly, we have neglected mention of all thermodynamic properties of mixed valence compounds, and have paid only slight attention to areas such as mixed valence kinetic and mechanism studies, fused salt chemistry, and the defect solid state.

In general, a mixed valence compound is most readily identified as such by its formula. However, there are certain difficulties in this, since in many cases the proposed formula is little more than a statement of analytical results, and a poor analysis might mistakenly turn a single valence material into a mixed valence one. A second problem, which arises most especially with oxides, is that of mixtures mistaken for pure mixed valence materials, and we mention this possibility wherever it seems advisable. Our emphasis throughout is first on structure, since this enables one to make a preliminary estimate of a compound's mixed valence class, and then on electronic properties as enumerated in Section II.

The order of presentation follows that of the Periodic Table, starting with the first-row transition elements, followed by the second- and third-row transition elements considered jointly, the groups III-A, IV-A, and V-A elements, and finally the lanthanide and actinide elements.

A. TITANIUM

The most extensively studied titanium mixed valence compounds are the oxides. That they provide a good example of the sensitivity of physical properties to stoichiometry is demonstrated by Verwey's early work on TiO_x (727), which has a resistivity of 10^{10} ohm cm when $x = 2.000$, decreasing to 10 when $x = 1.999$, and to 1.2 for $x = 1.995$. In addition to studies of the optical and electrical properties of $\text{Ti}^{\text{IV}}\text{O}_2$ containing small amounts of $\text{Ti}(\text{III})$, interest in the titanium mixed valence oxides has centered on the structures of the numerous oxides intermediate between Ti_2O_3 and TiO_2 , although it is unfortunate that rather less attention has been devoted to their physical properties.

The first X-ray phase analysis of the titanium-oxygen system, by Ehrlich (216), uncovered four phases with homogeneity ranges $\text{TiO}_{2.00}$ – $\text{TiO}_{1.90}$, $\text{TiO}_{1.80}$ – $\text{TiO}_{1.65}$, $\text{TiO}_{1.56}$ – $\text{TiO}_{1.46}$, and $\text{TiO}_{1.25}$ – $\text{TiO}_{0.6}$. After some disagreement (15, 349) as to whether the composition variation was due to random removal of some of the oxygen atoms or addition of extra titanium atoms to the parent TiO_2 , rutile lattice, it is now recognized that in the $x = 1.65$ – 1.80 range there are at least seven stable

oxides, all with the general formula Ti_nO_{2n-1} , with $n = 4-10$ (18). Members of the series with $n = 1, 2$, and 3 are also known. The occurrence of such "homologous series" or Magneli phases (474) among mixed valence transition metal oxides is quite frequent, and further examples are described in the sections on vanadium, niobium, and molybdenum and tungsten. In each case, blocks of the parent lattice structure (here rutile) are interrupted by regions of higher cation concentration, which can be thought of as resulting from the "shearing" (738) of one block past another. In the present example, blocks of the rutile (MO_2) structure are interleaved with layers of corundum (M_2O_3) structure. In the rutile structure, TiO_6 octahedra are joined through their corners and edges, but, in an oxide such as Ti_5O_9 (18) (Fig. 5), every fifth TiO_6 in one

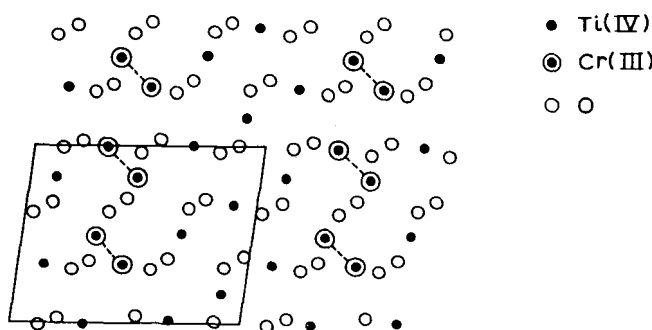


FIG. 5. The crystal structure of Ti_5O_9 and the isostructural compound $Cr_2Ti_3O_9$, viewed along [100] (18).

direction is joined to one of its neighbors by sharing one of their octahedral faces. The distance between the face-sharing pairs of titanium atoms in Ti_5O_9 is 2.81 Å, compared with 2.56 Å for the closest metal-metal distance in Ti_2O_3 , which has a corundum structure in which the TiO_6 units share both faces and edges. While there is no conclusive evidence that this series of oxides could be described as class II mixed valence systems of the sort $Ti_{n-2}^{IV}Ti_2^{III}O_{2n-1}$, there are two pieces of evidence that make the suggestion plausible. First, it has proved possible to isolate several mixed oxides of Ti(IV) and Cr(III), isostructural with the above homologous series, which have the general formula $Ti_{n-2}^{IV}Cr_2^{III}O_{2n-1}$ (8). Thus each block of rutile lattice, regardless of its size, accommodates only two chromium ions, and the question is whether these are randomly distributed or, as seems more likely, located in the face-sharing pairs of octahedral sites at the ends of each rutile block (the circled atoms in Fig. 5). ESR or static susceptibility measurements would settle the question if they could show whether or not the Cr(III) ions were mag-

netically coupled in pairs. The second piece of evidence bearing on the pairing of Ti(III) ions in Ti_nO_{2n-1} has to do with a set of magnetic susceptibilities determined by Ehrlich (216) on samples which, in the light of the more recent structural work, may have been phase mixtures. Measurements were made at -183°C and $+20^\circ\text{C}$ only, but the form of the plots of molar susceptibility against composition at the two temperatures suggests that, when $x = 1.95$ – 2.00 , the Curie-Weiss law applies. When larger amounts of Ti(III) were incorporated in the TiO_2 lattice, the molar susceptibility fell rapidly, and Ehrlich calculated that, in the region of Ti_nO_{2n-1} formation, the antiferromagnetic interaction between the Ti(III) ions was as marked at -183°C as in Ti_2O_3 , as might be expected if the magnetic Ti(III) ions were in face-sharing pairs. If we are right in regarding the shear structures of the Ti_nO_{2n-1} compounds as sheets of corundum-like Ti_2O_3 separating blocks of rutile TiO_2 , the mixed valence interaction is between cations situated in octahedra which share edges rather than faces. Because all the metal ions, regardless of valence, are in octahedral sites, the Ti_nO_{2n-1} compounds are catalogued as class II. However, more physical measurements will be needed before the picture can be made more precise. Although the Ti_nO_{2n-1} oxides are all dark blue to black, the facts that Ti_2O_3 is violet because of the $d-d$ transitions of the octahedrally coordinated Ti(III) ion (16), and also that the $Ti_{n-2}^{IV}Cr_2^{III}O_{2n-1}$ compounds are "graphite gray" (16), mean that no simple conclusions about the interaction absorption in these compounds can be drawn from the qualitative reports of their colors.

Although its formula fits the Ti_nO_{2n-1} sequence, Ti_3O_5 has a structure in which rutile and corundum fragments cannot be distinguished. Two forms of Ti_3O_5 exist, a high-temperature modification (anosovite), whose structure was determined by Zhdanov and Rusakov (815), and a black modification stable at room temperature, investigated by Asbrink and Magneli (26). These phases provide an interesting contrast, for anosovite appears to be a class III-B system with all the TiO_6 octahedra having somewhat similar distortions and all sharing six edges with their neighbors, whereas in the low-temperature phase there are three ways in which the octahedra, although similarly distorted, share edges with their neighbors. In anosovite there are no exceptionally close metal-metal contacts but, in low-temperature Ti_3O_5 , one pair of titanium atoms per unit cell is separated by only 2.61 Å, and other metal-metal distances are intermediate between this and 3.1 Å. Thus the system is class II, although the valence distribution cannot be unambiguously defined.

Since small deviations from stoichiometry in TiO_2 due to traces of Ti(III) darken the color of this white pigment, and are therefore extremely important to the paint industry, a number of optical studies

of reduced TiO_2 have been reported. Weyl (385) suggested that the discoloration of rutile on firing was due to reduction of some of the cations, and found that a similar result could be achieved by doping the rutile with pentavalent ions. Working with medium and strongly reduced rutile crystals, Cronemeyer (169) found a very broad absorption band near $10,000 \text{ cm}^{-1}$, whose intensity was proportional to the room temperature conductivity of the samples. An equally broad band also occurs at nearly the same frequency in samples containing only very small concentrations of Ti(III) (735). These results, as well as much of the earlier work on the optical and electrical properties of reduced TiO_2 (306), were interpreted on the assumption that the defect centers were oxygen vacancies acting as doubly charged donors. That the correct description involves interstitial Ti(III) ions is shown not only by the structural studies of the $\text{Ti}_n\text{O}_{2n-1}$ compounds, described above, but also by a good deal of ESR work (135, 136, 805). Reduced and niobium- and tantalum-doped samples of TiO_2 were studied, as well as centers produced by γ and ultraviolet irradiation, and in all cases the "extra" electrons were found trapped on titanium atoms, as shown also by the presence of weak hyperfine structure due to titanium nuclei with spins $5/2$ and $7/2$. To explain the results of his electrical conductivity, Hall effect, and thermoelectric power measurements on reduced rutile single crystals, Frederikse (260) therefore started from the assumption that, at very low temperatures, nearly all the electrons were self-trapped on cation sites by polarization of the surrounding lattice. The traps are sufficiently shallow to be thermally ionized, however, and so, at higher temperatures, conduction occurs in a narrow $3d$ band associated with the titanium ions, which is equivalent to a class III-B mixed valence system. This conclusion was broadly confirmed by recent high-temperature conductivity experiments over a wide range of oxygen pressure (76). If the energy required to discharge a trapped $3d$ electron into a conduction band is indeed within the range of thermal energies, there must be some doubt whether the system should be described as class II or III-B in our classification. Strictly speaking, therefore, the criteria of the classification ought to be applied at absolute zero.

Compounds which are more likely to belong in class III-B at all temperatures are the alkali metal (17, 739) and lanthanum (411) titanium bronzes, $\text{Na}_x\text{Ti}_4\text{O}_8$ and $\text{La}_{(2/3+x)}\text{TiO}_3$. Both series are said to form blue-black or black electrically conducting crystals with a metallic luster, but no detailed optical or conductivity experiments have been reported. A series of manganese titanates, $\text{Mn}_{(1+x)}^{\text{II}}\text{Ti}_{2(1-x)}^{\text{III}}\text{Ti}_x^{\text{IV}}\text{O}_4$, with spinel structures (459) might be class II or III-B mixed valence systems, according to the distribution of the cations. An X-ray study of the

$x = 0.48$ compound showed that the tetrahedral sites were exclusively occupied by Mn(II) (as indeed they are in MnTi_2O_4 and Mn_2TiO_4), suggesting that Ti(III) and Ti(IV) occupy the octahedral sites, but conductivity measurements have not been made on this apparently class III-B system.

In addition to the many Ti(III),Ti(IV) oxides, one oxide containing Ti(II) and Ti(III) has been reported. Both TiO and LiTiO_2 crystallize in rock salt lattices, and mixed crystals $\text{Li}_x\text{Ti}_{1-2x}^{\text{II}}\text{Ti}_x^{\text{III}}\text{O}$ can be prepared in which x lies between 0 and 0.5, and the cations are randomly distributed. The room temperature resistivity rises monotonically from 5×10^{-3} ohm cm for TiO, which is in any case a metal, up to 2 ohm cm for LiTiO_2 . Thus there appears to be no enhancement of conductivity over that of TiO due to the presence of the mixed valences.

Interaction absorption between Ti(III) and Ti(IV) has been detected in aqueous solutions as well as oxide lattices. Partial oxidation of sky blue Ti(III) solutions in 12 *M* HCl gives a deep purple coloration, which was studied by Jorgensen (395). The spectra of such solutions were said to be a superposition of the *d-d* bands of the Ti(III) ion (at 15,100 and 17,400 cm^{-1}) and an intense new absorption band at 20,200 cm^{-1} , which also had a shoulder at 16,100 cm^{-1} . Furthermore, absorption in the near-ultraviolet was very much intensified compared with single valence solutions. Arguing from the known formation constants of the Ti(III) and Ti(IV) chloro complexes, it was suggested that the interaction complex might be $[\text{Ti}^{\text{III}}\text{Cl}]^{2+}[\text{Ti}^{\text{IV}}\text{Cl}_6]^{2-}$, but there is no direct evidence that this is so. In 20% sulfuric acid a 1:1 Ti(III),Ti(IV) interaction complex is also formed, with an absorption maximum at 21,200 cm^{-1} (298), but is destroyed by higher concentrations of acid.

B. VANADIUM

The vanadium mixed valence compounds whose structural and electronic properties have received the greatest attention are the oxides intermediate between V_2O_3 and V_2O_5 . Hoschek and Klemm (370), who were the first to make a systematic study of the system, identified three mixed valence phases, α ($\text{VO}_{1.80}\text{-VO}_2$), α' ($\text{VO}_2\text{-VO}_{2.2}$), and β ($\text{VO}_{1.65}\text{-VO}_{1.8}$), in addition to V_2O_3 , which has a structure similar to corundum, and V_2O_5 , whose structure is based on very distorted octahedral VO_6 units (36). It is not immediately obvious whether the intermediate phases should all be formulated as V(III),V(V) compounds or whether the mixture of valences is V(III),V(IV) for compounds in the range $\text{VO}_{1.5}\text{-VO}_2$, and V(IV),V(V) in the range $\text{VO}_2\text{-VO}_{2.5}$. This problem has

attracted the attention of a number of investigators (318, 370, 437), who have attempted to resolve the dilemma by performing magnetic susceptibility measurements. However, since many of the compounds are strongly antiferromagnetic, such measurements are not easy to interpret without a detailed knowledge of the signs and magnitudes of the magnetic interactions between ions of like and unlike valence states.

The VO_2 - V_2O_5 phase region was examined in greater detail by Aebi (3), who found evidence for only one intermediate compound, with a formula $\text{VO}_{2.17}$, i.e., V_6O_{13} , and a structure which was considered to be derived from that of V_2O_5 by the regular removal of one third of the planes consisting solely of oxygen atoms (276). It is interesting that, of all the vanadium oxides, only products with compositions between V_2O_5 and V_6O_{13} are good oxidation catalysts, a result which may be explicable in terms of the ease with which oxygen atoms can migrate through channels in the lattice of V_2O_5 (276). V_6O_{13} forms needles of the same blue-black color as VO_2 (3). It is antiferromagnetic, with a Neel temperature of 154°K (437), above which it behaves as a semiconductor having a conductivity and activation energy not very different from V_2O_5 (318). Below the Neel point, the conductivity increases approximately 10-fold, in contrast to VO_2 and V_2O_3 , which at their Neel points undergo a transition from the metallic to the semiconducting state, accompanied by a decrease in conductivity of about five orders of magnitude. Above the Neel point in V_6O_{13} , the effective magnetic moment per paramagnetic vanadium atom is either 2.13 B.M. (437) or 1.95 B.M. (318) compared with either 2.16 B.M. (437) or 3.10 B.M. (318) for VO_2 above its Neel point. The very large divergence between these results, not to mention the difficulty in interpreting effective magnetic moments for substances having very large Weiss constants, makes it unprofitable to consider their significance any further. That the phase is paramagnetic and the conductivity low seem to indicate that in the ground state the valences are trapped. Alternative valence structures, $\text{V}_4^{\text{IV}}\text{V}_2^{\text{III}}\text{O}_{13}$ or $\text{V}_2^{\text{IV}}\text{V}_4^{\text{V}}\text{O}_{13}$, can be written, in both of which the two valence states are present in the stoichiometric ratio 2:1. A closer examination of Aebi's structure shows that there are indeed two types of metal ion sites present in this ratio, and Gillis' view (276) of the structural relationship with V_2O_5 leads to the conclusion that the minority sites are most likely to be occupied by the pentavalent ions. A neutron diffraction study of the magnetic ordering in this lattice would be of great value.

In the phase region labeled α by Klemm (370), a series of more accurate X-ray studies (13, 14, 18) has revealed the existence of a homologous series of Magneli shear phases, $\text{V}_n\text{O}_{2n-1}$, isostructural with the titanium-

(III,IV) series based on the rutile and corundum structures. Members of the series with $4 \leq n \leq 8$ have been identified. The two magnetic studies (318, 437) again disagree on the precise effective moments of these compounds, but agree that they lie in the range 2–3 B.M. and that all except V_6O_{11} and V_7O_{13} are antiferromagnetic, with Neel temperatures

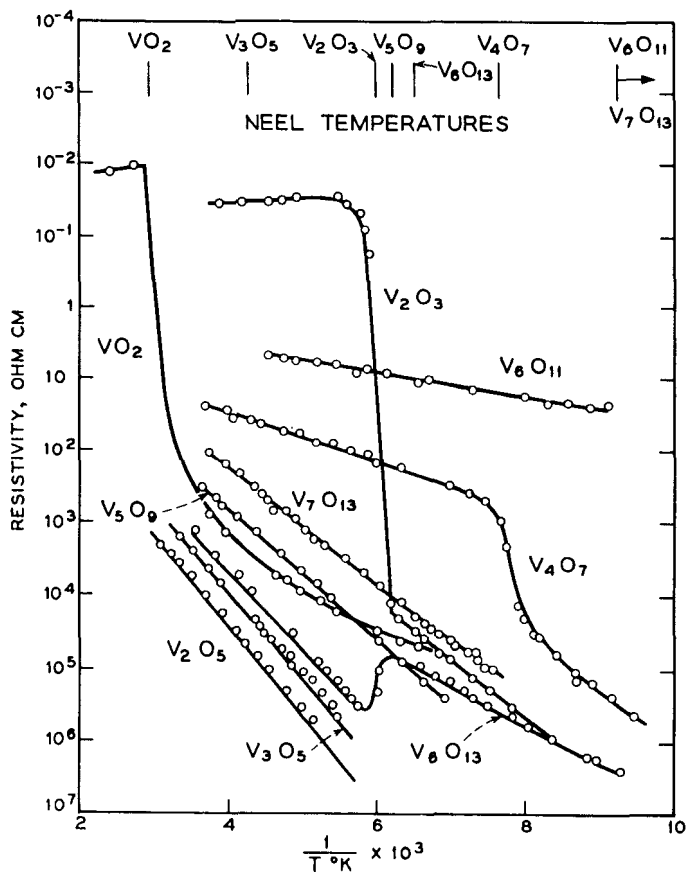
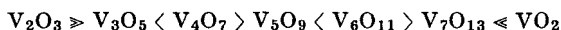


FIG. 6. The Neel temperatures and resistivity-temperature curves of various vanadium oxides (402).

somewhat lower than that of VO_2 . The two exceptions remained paramagnetic down to the lowest temperatures studied ($90^\circ K$). The compounds, which are all blue-black (13), behave as semiconductors, although with widely and apparently randomly varying resistivities and activation energies (402), as shown in Fig. 6. One feature apparent from this figure is that, among the mixed valence phases below their Neel temperatures, only V_4O_7 has a conductivity more than one order of magnitude greater than the single valence compounds V_2O_3 and VO_2 below their

Neel temperatures. Furthermore, at temperatures above their magnetic transitions, none of the mixed valence compounds conducts better than either V_2O_3 or VO_2 , although at all temperatures they all conduct better than V_2O_5 . It is therefore safe to say that, even when their spins are disordered, these remain class II systems. A further mysterious feature of the resistivity results is that, although one of the Magneli phases (V_4O_7) does undergo a discontinuous resistivity change at the Neel temperature, V_5O_9 shows no change in resistivity with magnetic ordering. Possibly this is connected with the fact that, for a given temperature above the Neel points of all the Magneli phases, there is a very marked alternation in conductivity with increasing size of the rutile-like slabs:



Clearly this interesting system deserves a very careful study.

There exist a number of V(IV), V(V) minerals, usually designated by the blanket term "vanadyl vanadates." The unit cell dimensions of several have been reported (601), but no other detailed structural or physical data are available.

The lower mixed valence oxides of vanadium have been of greater interest to metallurgists than to chemists. Oxygen dissolves interstitially in vanadium, yielding a number of different phases up to $VO_{0.57}$ (see Stringer (692) for a review). Vanadium monoxide is stable over a wide range of composition, since defects can occur at either cation or anion sites (13, 35, 641). Although stoichiometric VO has been shown to undergo a semiconductor-metal transition (35) at the Neel point, as do V_2O_3 and VO_2 , no physical properties of nonstoichiometric samples have been reported.

There exist two series of alkali metal vanadium bronzes with the general formulas $A_xV_2O_5$ and $A_xV_3O_8$, the structures of which have been determined by Wadsley (736, 737). Both contain double strings of octahedra sharing edges, and strings of octahedra distorted so much that they might almost be regarded as trigonal bipyramids. Since the formulas of the bronzes are continuously variable over wide limits, these two types of coordination can hardly correspond to the distribution of the valences in a class I or class II system, although in the compound LiV_2O_5 , where there are equal numbers of V(IV) and V(V) ions, this may well be the case. The latter compound contains two types of vanadium site (267), around one of which the oxygens approach more closely than around the other. LiV_2O_5 is also said to be blue, the characteristic color of V(IV) surrounded by oxygen atoms, so that there may be a smaller degree of mixed valence interaction in this class II compound than in the other bronzes. The first electrical measurements on the vanadium bronzes were made by

Flood (253), but more recently Ozerov (554) and Sienko (661) have studied these compounds. Ozerov found that, at room temperature, single crystals of $\text{Na}_{0.33}\text{V}_2\text{O}_5$ in the form of black needles showed very anisotropic resistivity, ρ being 0.046 ohm cm along and 20 ohm cm perpendicular to the needle axis. When measured between 400° and 600°C a compressed pellet of the same material behaved as a semiconductor, not a metal like the tungsten bronzes of comparable sodium content. Sienko also reports that $\text{Na}_{0.33}\text{V}_2\text{O}_5$ is a semiconductor, but with a room temperature resistivity and activation energy much lower than Ozerov's. The compound's magnetic susceptibility at room temperature is an order of magnitude higher than that of any sodium tungsten bronze, and actually agrees with expectation for a full spin-only contribution from the appropriate number of trapped V(IV), $3d^1$ ions. As in the tungsten bronzes, there is no detectable Knight shift in the ^7Li or ^{23}Na NMR spectra (273), so the mixed valence electrons are confined to the vanadium-oxygen framework. Since the observed g factors in the ESR spectra (1.96) are close to that reported for V(IV) in other compounds, we may confidently describe the vanadium bronzes as weakly trapped class II systems. Unfortunately, no hyperfine lines due to electron coupling with the ^{51}V nuclei could be detected in the ESR spectra.

The mixed valence vanadium oxide whose electronic structure is known in greatest detail is probably the black crystalline hydrate first prepared by Glemser (283) by reducing a suspension of V_2O_5 in concentrated ammonium chloride solution with zinc for several hours. Glemser gave the compound, which has an effective vanadium oxidation state of 4.66, the formula $\text{V}_3\text{O}_5(\text{OH})_4$, but a careful reexamination of the preparation under a variety of conditions suggested (59) that it should rather be written $\text{V}_6\text{O}_{20}\text{H}_{12}$. An X-ray powder photograph was compatible with a tetragonal unit cell. The electronic structure of this compound has recently been the subject of some magnetic studies (60, 701). First the intensity of the ESR spectrum of a powdered sample was measured as a function of temperature and shown to obey Curie's law between -150° and $+300^\circ\text{C}$. Thus by comparison with a sample of diphenylpicrylhydrazyl, the concentration of paramagnetic centers could be calculated and compared with that expected from the formula if the compound contained two V(IV) ($3d^1$) and four V(V) ($3d^0$) ions per mole. The agreement was excellent ($n_{\text{obs}} = 1.4 \times 10^{18}$ spins/mg, $n_{\text{calc}} = 1.9 \times 10^{18}$ spins/mg). Assuming that the V(IV) ion lies in a field of tetragonal symmetry with $dxy(b_2)$ lowest in energy, the observed g values (1.970 and 1.920) could be fitted by excitation energies $E_e(dxzdyz) - E_{b_2}(dxy)$ and $E_{b_1}(dx^2 - y^2) - E_{b_2}(dxy)$ of $10,000\text{ cm}^{-1}$ and $15,000\text{ cm}^{-1}$,

respectively, if the vanadium spin-orbit coupling constant was taken as 150 cm^{-1} . Hence the relative ordering of the $3d$ orbitals of the V(IV) ions is $b_2 < e < b_1 < a_1$, suggesting a tetragonally compressed octahedral environment. The spin-spin and spin-lattice relaxation times (t_2 and t_1) of the ESR signal in Glemser's oxide were measured by two independent methods, one involving rapid modulation and the other progressive saturation of the signal. The two methods agreed that t_2 is virtually invariant with temperature, and that t_1 varies only a little, both being in the region of 10^{-7} sec. Theobald (701) assumed that exchange played the dominant part in the relaxation processes, and, from the line width of the signal, calculated that the exchange integral J was large enough (3000 MHz) to act as a thermostat so that t_1 did not vary with temperature, and was close to t_2 . As a result of these experiments we therefore have the beginnings of a very satisfying view of the class II mixed valence interaction in Glemser's hydrate, but without a complete structure determination there is little more to be said at this stage. One point of great interest in relation to the role of water in mixed valence interactions (see subsection E on iron) is Theobald's statement (701) that the exchange interaction in other anhydrous vanadium(IV,V) oxides is almost zero.

Glemser's compound is probably a hydrate of one of the reduced isopolyvanadic acids. Further examples were prepared and their formulas characterized by Ostrowetsky (549, 550) in a comprehensive survey of the mixed valence chemistry of V(IV) and V(V) in acid and alkaline solutions. Above pH 10, no mixed valence absorption could be detected but, between pH 7 and 10, spectrophotometry revealed the existence of a single polyanion which was isolated as a dark gray-green sodium salt, $\text{Na}_3[\text{V}_6\text{O}_{15}\text{H}] \cdot 6\text{H}_2\text{O}$. In weakly acid solutions, six polyanions corresponding to varying degrees of reduction of $[\text{V}_{10}\text{O}_{28}]^{6-}$ were identified, although only two, formulated by Ostrowetsky as $[\text{V}_7^{\text{V}}\text{V}_3^{\text{IV}}\text{O}_{26}\text{H}]^{4-}$ and $[\text{V}_3^{\text{V}}\text{V}_7^{\text{IV}}\text{O}_{24}\text{H}]^{4-}$, are at all stable. Since these anions almost certainly retain the $\text{V}_{10}\text{O}_{28}$ skeleton, whose structure was determined by Evans (227), they are probably better written as $[\text{V}_{10}\text{O}_{28}\text{H}_5]^{4-}$ and $[\text{V}_{10}\text{O}_{28}\text{H}_4]^{4-}$. The others, which have V(V)/V(IV) ratios of 8/2, 6/4, 5/5, and 4/6, are formed only within very narrow ranges of pH, temperature, and concentration, and readily disproportionate into $[\text{V}_{10}\text{O}_{28}\text{H}_2]^{4-}$ and $[\text{V}^{\text{IV}}\text{O}]^{2+}$ or into mixtures of either of the latter and the 7/3 and 3/7 compound, according to their composition. The spectra of all these compounds, which vary in a most interesting way with degree of reduction, are collected in Fig. 7. Excepting the 5/5 and 4/6 compounds, they all have absorption maxima in the $13,000\text{--}20,000 \text{ cm}^{-1}$ region. In energy and width, these bands resemble the ligand field bands of vanadium(IV),

but, because they are at least an order of magnitude more intense, should probably be assigned as mixed valence absorptions. Their significance is not likely to become apparent until more is known of the structures of

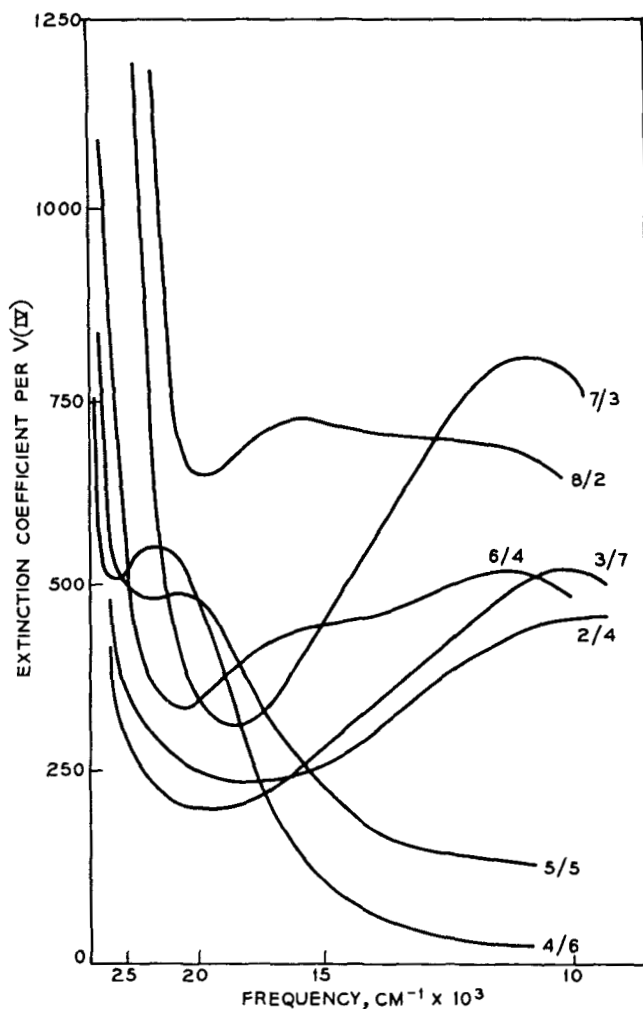


FIG. 7. Electronic spectra of the isopolyvanadate ions $[V_{10}O_{28}]^{4-}$ of various $V(V)/V(IV)$ ratios (550).

the polyanions. In particular, we have no information at this stage on whether the valences are trapped by distortion of the appropriate number of vanadium sites or, indeed, whether some are class II and others class III-A, except for the two compounds with no intense low-energy absorption, which must surely be class I. The low molar extinction coefficients of the mixed valence absorption bands in all cases indicate a

rather firm trapping of the valence. ESR measurements on glassy solutions would certainly help to decide the question. Another intriguing question is the exceptional stability of the 7/3 and 3/7 anions, for which the structure (227) of the parent ion $[V_{10}O_{28}]^{6-}$ suggests no obvious explanation.

The only other vanadium species detected in solution, which might be mixed valence, appears as an intermediate in the reaction between V(II) and V(IV) in acid perchlorate solutions (530). A dark color, which developed much more rapidly than the rate of the overall reaction to produce V(III), was shown to be due to the formation of the ion $[VOV]^{4+}$, identified by the author as a hydrolytic dimer of V(III). However, the intensity of the absorption (ϵ_{\max} calculated as 6800 at $23,200\text{ cm}^{-1}$) suggests that a V(II),V(IV) class II system is formed.

C. CHROMIUM

A discussion of the mixed valence compounds of chromium is hampered by the fact that this element can assume integral valences from 1+ to 6+. Thus, whereas Cr_3O_8 is clearly a mixed valence compound, the formula of KCr_3O_8 , for example, could be written as either $KCr_2^VI Cr^{III}O_8$, $KCr^{IV} Cr^V Cr^{IV}O_8$, or $KCr_3^VO_8$, for all four oxidation states, 3+, 4+, 5+, and 6+, are known for chromium. Although there are experiments (optical absorption, magnetic susceptibility, X-ray structure analysis, etc.) which will distinguish between these alternatives, they have not always been performed as yet and hence limit our discussion to the more obvious mixed valence compounds.

In contrast to titanium and vanadium, chromium forms mixed valence halides as well as oxides, two types of mixed valence chromium halide (Cr_2X_3 and Cr_2X_5) having been reported. The halides Cr_2Br_3 and Cr_2I_3 are formed as brown-black solids in the thermal degradation of the appropriate tetraphenylchromium halides, $(C_6H_5)_4CrX$ (352). Cr_2F_5 is formed as green translucent crystals from both the oxidation of CrF_2 and the incomplete reduction of CrF_3 (693). Since CrF_3 is yellow-green and CrF_2 is blue-green, and since the refractive indices of Cr_2F_5 are intermediate between those of CrF_2 and CrF_3 , there appears to be no low-lying mixed valence transition in this material. As a class I substance, Cr_2F_5 should therefore be an insulator. The crystal structure of Cr_2F_5 (Fig. 8) shows the expected trapping of the chromium valences as Cr(II) and Cr(III), for one half of the chromium ions are found at the centers of almost regular fluoride ion octahedra with an average Cr—F distance of 1.89 Å, whereas the other half occupy tetragonally distorted octahedral sites with four Cr—F distances at 1.96–2.01 Å and the remaining two

at 2.57 Å (683). That these are to be identified with Cr(III) and Cr(II) ions, respectively, follows not only from the Cr—F distances but also from the structures of CrF₃ and CrF₂ themselves, which contain, respectively, octahedrally and tetragonally coordinated chromium ions. Steinfink and Burns (683) explain that the three 3*d* electrons in the Cr(III) ion occupy nonbonding *t*_{2*g*} orbitals, but Cr(II) must place its fourth 3*d* electron in an antibonding *d**z*² orbital, thereby extending the octahedron in the *z*

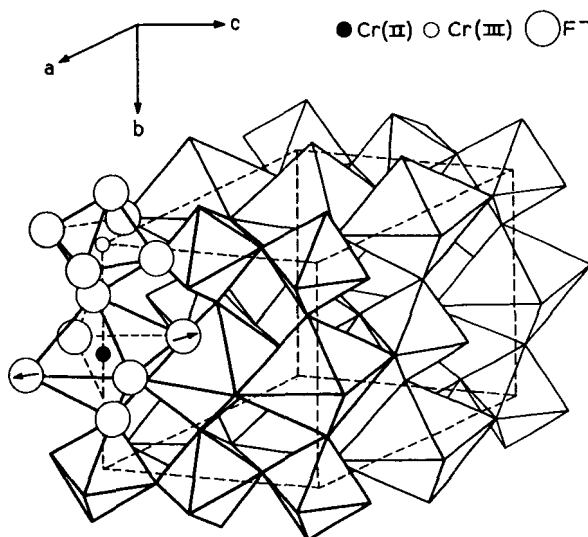


FIG. 8. The crystal structure of class I Cr₂F₅. In this substance, the Cr(III)—F distances in a Cr^{III}F₆ octahedron average 1.89 ± 0.01 Å, whereas the neighboring Cr^{II}F₆ octahedron is distorted, as shown by the arrows, four of the Cr(II)—F distances being 1.98 Å and the other two being 2.572 Å (683).

direction. Osmond (546) suggests that, according to qualitative superexchange considerations, the chains of cations in Cr₂F₅ should be ferromagnetically aligned in the (001) direction with neighboring chains coupled antiferromagnetically, resulting in an overall antiferromagnetic ground state. There are no experimental data on this point.

The oxides of chromium present a bewildering array of possible mixed valence compounds. Extrapolating from what very little is known, one can say, in general, that the ions involved in mixed valence chromium oxides are almost always Cr(VI) and Cr(III) in appropriate ratios, and that, since Cr(VI) appears always as a tetrahedrally coordinated species whereas the 3*d*³ configuration of Cr(III) prefers octahedral coordination, the oxides will be class I systems. The discussion begins with the better known oxides and then proceeds to the more speculative materials. It should be mentioned that, although little is known of the intermediate

chromium oxides, they have a great commercial value as catalysts for the polymerization of olefins.

Suchow *et al.* (695) were the first to point out that, although the chromium in KCr_3O_8 has an average valence of 5+, their preliminary crystal structure suggests that two of the chromium ions are of one type and one of the chromiums of another, suggesting in turn the formulation of the compounds as $\text{KCr}_2^{\text{VI}}\text{Cr}^{\text{III}}\text{O}_8$ with the Cr(III) ions in octahedral coordination and the Cr(VI) in tetrahedral coordination. Wilhelmi (775, 777) confirmed this view, demonstrating that the Cr(III) ions are in very nearly octahedral coordination with Cr—O distances averaging 1.97 Å,

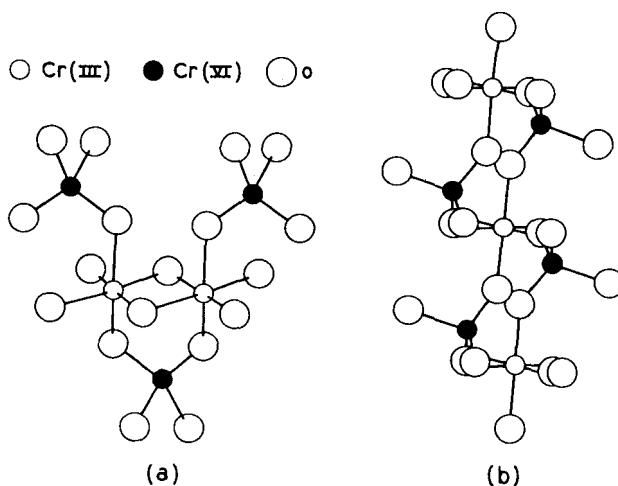


FIG. 9. The relative orientations of $\text{Cr}^{\text{VI}}\text{O}_4$ tetrahedra and $\text{Cr}^{\text{III}}\text{O}_6$ octahedra in the class I substances (a) Cr_5O_{12} , and (b) KCr_3O_8 (775, 778).

and that the Cr(VI) ions are surrounded tetrahedrally by oxide ions at an average distance of 1.60 Å, as in Fig. 9. Klemm (428) pointed out that the question of the chromium valences in KCr_3O_8 might also be answered by a measurement of the magnetic susceptibility, for magnetically dilute KCr_3O_8 would have an effective moment of 3.00 B.M., whereas $\text{KCr}_2^{\text{VI}}\text{Cr}^{\text{III}}\text{O}_8$ would have an effective moment of 3.87 B.M. His measurements yield an effective magnetic moment for KCr_3O_8 which varies from 4.09 to 4.36 B.M. over the temperature range 90°–295°K. Applying a correction for temperature-independent paramagnetism gives an upper limit of 3.97–4.23 B.M., which does not disagree with that expected for the Cr(III),Cr(VI) mixed valence formulation of KCr_3O_8 . The material is black and said to have a very high electrical resistivity (777). Wilhelmi (779) reports that the lithium and cesium salts of HCr_3O_8 similarly

contain octahedral $\text{Cr}^{\text{III}}\text{O}_6$ and tetrahedral $\text{Cr}^{\text{VI}}\text{O}_4$ groups sharing corners.

The alkaline earth chromium oxides, $\text{M}_3^{\text{II}}\text{Cr}_2\text{O}_8$, form another class of compounds in which the chromium has an average valence of 5+. Alternatively, one can write a mixed valence formula for the compound, $\text{M}_9^{\text{II}}\text{Cr}_4^{\text{IV}}\text{Cr}_2^{\text{III}}\text{O}_{24}$, which has a Cr(VI)/Cr(III) ratio of 2, as in KCr_3O_8 . Surprisingly, the evidence seems to be in favor of the single valence formulation, for not only do Ford and co-workers (256–258) and others (278) point out that $\text{Ca}_3\text{Cr}_2\text{O}_8$ has a powder pattern very much like that of $\text{Ca}_3(\text{P}^{\text{V}}\text{O}_4)_2$, but Klemm (640) finds an effective moment of 1.7 B.M. per chromium ion in $\text{Ba}_3\text{Cr}_2\text{O}_8$, where the pentavalent formula requires 1.73 B.M. and the mixed valence formula requires 2.24 B.M. Ford *et al.* and Vasenin (723) also describe the preparation of the oxides $\text{Ca}_2\text{Cr}_2\text{O}_7$, CaCr_2O_5 , $\text{Ca}_4\text{Cr}_3\text{O}_{10}$, and $\text{Ca}_6\text{Cr}_4\text{O}_{15}$, the last three of which are green, as is also $\text{Ca}_3\text{Cr}_2\text{O}_8$. Only a combination of optical, magnetic, and X-ray studies can settle the question of the chromium valence in these compounds.

Bashilova's (45) thallium chromate $\text{Tl}_2\text{Cr}_2\text{O}_8$, if taken as a salt of Tl(III), is analogous to the calcium salt mentioned above, for it can be written as either $\text{Tl}_2^{\text{III}}\text{Cr}_2^{\text{V}}\text{O}_8$ or $\text{Tl}_6^{\text{III}}\text{Cr}_4^{\text{VI}}\text{Cr}_2^{\text{III}}\text{O}_{24}$. Bashilova, however, maintains that it is the thallium mixed valence oxide, $\text{Tl}^{\text{I}}\text{Tl}^{\text{III}}\text{Cr}_2^{\text{VI}}\text{O}_8$. The latter formulation would be diamagnetic, whereas the other two would have effective magnetic moments of 1.73 B.M. and 2.24 B.M., depending on whether the chromium is, respectively, Cr(V) or Cr(III), Cr(VI).

Because of the difficulty of preparing pure intermediate chromium oxides, it seems probable that, of the large number of different anhydrous chromium oxides reported in the literature, a significant fraction will prove to be mixtures, or are in fact the same compound masquerading under different stoichiometries. The list of intermediate chromium oxides encompasses the following: Cr_2O_5 , Cr_3O_4 , Cr_3O_5 , Cr_3O_8 , Cr_4O_9 , Cr_5O_9 , Cr_5O_{12} , Cr_5O_{13} , Cr_5O_{19} , Cr_6O_{15} , Cr_7O_{18} , Cr_8O_{15} , Cr_8O_{21} , and $\text{Cr}_{32}\text{O}_{93}$, in addition to many "nonstoichiometric" materials of the formula CrO_x , which are not easily expressed as small whole number ratios of chromium and oxygen.

The materials described by Schwartz *et al.* (647) as Cr_3O_8 , and by Simon and Schmidt (664) as Cr_5O_{13} , are crystallographically identical, according to later work by Glemser and co-workers (281, 282), who feel that the formula Cr_5O_{13} better fits their analytical data. Cr_5O_{13} , as prepared by the thermal decomposition of CrO_3 , is a black substance and has a magnetic susceptibility consonant with the mixed valence description $\text{Cr}_3^{\text{VI}}\text{Cr}_2^{\text{IV}}\text{O}_{13}$ (8), although it has been said that its ESR

spectrum is characteristic of the Cr(III) ion (596). Rode *et al.* (596) first proposed that Cr_5O_{13} was really Cr_8O_{21} , and later work by Lorthioir and Michel (468) has confirmed Cr_8O_{21} as a product of the thermal decomposition of CrO_3 . According to their study, Cr_8O_{21} in water gives Cr(III) and Cr(VI) ions in 1 : 3 ratio, and has a magnetic susceptibility compatible with its formation as $\text{Cr}_2^{\text{III}}\text{Cr}_6^{\text{VI}}\text{O}_{21}$.

Cr_5O_{12} , also reported as Cr_2O_5 (281), is one of the few chromium oxides for which a crystal structure has been determined. Wilhelmi (778) found that Cr_5O_{12} contains structural units much like those found in KCr_3O_8 , i.e., octahedrally coordinated Cr(III) ions sharing ligands with tetrahedrally coordinated Cr(VI) ions. The structure is built up of Cr_5O_{18} units (Fig. 9), in which the Cr(VI)—O distances in the tetrahedral sites are 1.65 Å on the average, and the Cr(III)—O distances in the octahedral sites average 1.97 Å, as was found in KCr_3O_8 . Although this oxide is black, possibly suggesting a class II spectrum, its electrical resistivity is reported to be 1.78×10^{10} ohm cm at 360°C and 72 atm oxygen (446), as expected from the class I crystal structure. Cr_5O_{12} is ferromagnetic, with a Curie point at about 80°C (597), above which it shows an ESR signal attributable to the Cr(III) ion (596). An apparently related hydrated oxide, $\text{Cr}_5\text{O}_{12} \cdot 3\text{H}_2\text{O}$, is formed as a brown precipitate on mixing a solution of $\text{Cr}^{\text{III}}\text{Cl}_3$ with $\text{Ag}_2\text{Cr}^{\text{VI}}\text{O}_4$ (292).

Chromium dioxide, CrO_2 , presents a rather curious picture of conflicting claims, for, although CrO_2 has been said not to have a homogeneity region and to be quite stoichiometric (22, 647), materials ranging from $\text{CrO}_{1.89}$ (133) to $\text{CrO}_{2.14}$ (776) have been described in the literature as " CrO_2 ." Moreover, whereas Chapin *et al.* (776) have studied the electrical conductivities of samples in the range $\text{CrO}_{1.89}$ – $\text{CrO}_{2.02}$ and explained their quasi-metallic nature (ρ is approximately 3×10^{-3} ohm cm) on the basis of a *d*-band model involving Cr(IV) ions, Kubota (446) claims that the extraordinary conductivity results from the presence of Cr(III) and Cr(IV) ions in the rutile crystal lattice. In support of the mixed valence formulation, Rode *et al.* (596) interpret the ESR spectrum of CrO_2 above its Curie point (119°C) as showing that the oxide is a Cr(III),Cr(VI) compound. The saturation magnetization of CrO_2 at 0°K yields an effective moment of 2.07 B.M. per chromium atom (325), whereas Cr(IV) is expected to have an effective moment of 2.83 B.M. The decision as to whether CrO_2 is a mixed valence oxide or simply contains Cr(IV) clearly cannot be made without further physical measurements.

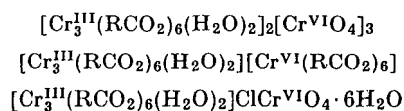
The hydrated material formed by mixing an aqueous solution containing Cr(III) with one containing $[\text{Cr}^{\text{VI}}\text{O}_4]^{2-}$ presents a situation related to that discussed above for CrO_2 . According to King and Neptune (423),

the mixing of Cr(III) and $[\text{Cr}^{\text{VI}}\text{O}_4]^{2-}$ in acidic solution leads to the formation of a 1:1 complex ion, $[\text{Cr}^{\text{III}}\text{Cr}^{\text{VI}}\text{O}_4]^+$, probably with sharing of oxo and/or hydroxyl ligands. Interestingly, the stoichiometry of this complex was determined, using its interaction absorption band at $14,300\text{ cm}^{-1}$, thereby showing that a class II absorption can occur in a Cr(III),Cr(VI) system. Krauss and Gnatz (440) confirmed the 1:1 nature of this complex by a conductivity titration, but also showed that the precipitate from the solution has the composition $\text{H}_4\text{Cr}_3\text{O}_8 \cdot x\text{H}_2\text{O}$ (x is continuously variable), which can be formulated as either $\text{H}_4\text{Cr}_3^{\text{IV}}\text{O}_8 \cdot x\text{H}_2\text{O}$ or $\text{H}_4\text{Cr}_2^{\text{III}}\text{Cr}^{\text{VI}}\text{O}_8 \cdot x\text{H}_2\text{O}$. Aten *et al.* (32) showed conclusively that the latter formulation is the proper one by mixing a solution of radioactive Cr(III) with inactive $[\text{Cr}^{\text{VI}}\text{O}_4]^{2-}$ ion, dissolving the $\text{H}_4\text{Cr}_3\text{O}_8$ so formed, and precipitating and counting the $[\text{CrO}_4]^{2-}$ as PbCrO_4 . As the PbCrO_4 showed less than 1% of the original activity, it is clear that the two types of chromium in this substance at no time were equivalent as they would be if they were all Cr(IV). Formulations of $\text{H}_4\text{Cr}_3\text{O}_8 \cdot x\text{H}_2\text{O}$ as a compound of Cr(IV) also demands an effective magnetic moment of 2.83 B.M. per chromium, whereas the calculated effective moment of the mixed valence compound is 3.16 B.M., in excellent agreement with the experimental value of 3.15 B.M. (440). The same dark brown material forms at the cathode on electrolysis of a 25% solution of CrO_3 in HClO_4 (450).

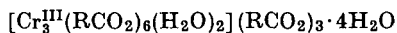
Sisler and co-workers (201, 669) have shown that liquid ammonia will partially reduce CrO_3 to a mixture containing, among other things, the brown polymeric materials $[\text{Cr}^{\text{III}}(\text{NH}_3)_3]_{2n}(\text{Cr}^{\text{VI}}\text{O}_4)_{3n}$ and $[\text{Cr}^{\text{III}}(\text{NH}_3)_3\text{NO}_2\text{Cr}^{\text{VI}}\text{O}_4]_n$, both of which are postulated to be class I systems with the Cr(III) ions in octahedral and the Cr(VI) ions in tetrahedral coordination, the two being joined by oxo bridges.

The thermal decomposition of chromyl chloride, $\text{Cr}^{\text{VI}}\text{O}_2\text{Cl}_2$, leads to the formation of a number of polychromyl chlorides having the general formula $(\text{CrO}_2)_n\text{Cl}_2$, where n is equal to 3, 4, 5, or 7 (479). Although a mixed valence formula for these substances can be written $(\text{Cr}^{\text{VI}}\text{Cr}^{\text{IV}}\text{O}_{2n}\text{Cl}_2)$, little is known of their physical properties, other than that they are brown-black in color and sensitive to moisture.

The formates and acetates of chromium offer further examples of class I mixed valence systems. Trivalent chromium forms a very stable trinuclear cationic species having the general formula $[\text{Cr}_3^{\text{III}}(\text{RCO}_2)_6(\text{H}_2\text{O})_2]^{3+}$, where RCO_2^- is an acetate or formate anion. Combinations of this trinuclear cation with chromium-containing anions yield salts (292), such as:



That the above are class I systems seems evident from the fact that they are all green, the color of the single valence compound :



Recoura (579) reports the preparation of the dark brown sulfates $\text{K}_{2n}\text{Cr}_2^{\text{III}}(\text{Cr}^{\text{VI}}\text{O}_4)_n(\text{SO}_4)_3$, where $n = 1, 2$, and 3. They are also most likely class I systems.

D. MANGANESE

As with most of the other elements of the first transition series, the most important examples of mixed valence in manganese compounds involve oxide lattices. At one time it was suggested (208a) that there existed a continuous series of oxides with formulas intermediate between MnO and MnO_2 , of which no less than eleven had been reported between 1862 and 1907! Very few of these nonstoichiometric oxides have survived the passage of time and closer scrutiny, and we shall therefore concentrate attention only on those based on stoichiometric phases. Of the latter, Mn_3O_4 , the mineral haussmannite, is the best known. When heated in air to 1000°C , all manganese oxides and hydroxides are converted to Mn_3O_4 , which forms as black crystals with a metallic sheen, or as a dark red powder when finally divided. Its electrical conductivity was studied many years ago (181, 731), using compressed pellets. Although behaving as a semiconductor, the fact that it is much less conducting than Fe_3O_4 at room temperature led de Boer and Verwey (181) to suggest that it was a normal spinel, ${}^2\text{Mn}^{\text{IV}}\text{Mn}_2^{\text{II}}\text{O}_4$ or $\text{Mn}^{\text{II}}\text{Mn}_2^{\text{III}}\text{O}_4$, and not of the inverse type $\text{Mn}^{\text{II}}(\text{Mn}^{\text{II}}, \text{Mn}^{\text{IV}})\text{O}_4$ or $\text{Mn}^{\text{III}}(\text{Mn}^{\text{II}}, \text{Mn}^{\text{III}})\text{O}_4$. This conclusion has been confirmed, but disagreement continues as to the valence structure of the compound. A recent magnetic susceptibility study (569) showed that, between 90° and 800°C , the susceptibility followed a Neel hyperbola, but below the Curie point it was consistent with a ferromagnetic model for an $\text{Mn}(\text{II}), \text{Mn}(\text{IV})$ normal spinel. On the other hand, the observed intensities of neutrons diffracted by powdered specimens at 4.2° , 77° , and 298°K (404) agree very well with those calculated for a model based on $\text{Mn}^{\text{II}}\text{Mn}_2^{\text{III}}\text{O}_4$. The latter results are probably the more reliable.

² A spinel compound has the formula AB_2O_4 and a lattice containing octahedral and tetrahedral cation sites in the ratio 2:1. In a normal spinel the B cations occupy the octahedral sites and the A the tetrahedral, whereas in an inverted spinel the tetrahedral sites are exclusively occupied by B cations so that the octahedral sites are occupied by equal numbers of A and B cations (see Fig. 16).

In a number of other instances, different methods of estimating the valence distributions in manganese oxides also appear to yield differing results. For example, X-ray analysis showed that the structure of manganite (γ -MnOOH) was based on sheets of O^{2-} and OH^- ions enclosing trivalent manganese ions (112, 237), but measurements of magnetic anisotropy appear to suggest that half of the manganese is divalent and half quadrivalent. Also the crystal structure of the mineral bixbyite (α -Mn₂O₃) agrees with a trivalent formulation (563), but it has been stated that chemical decomposition leads to divalent and quadrivalent ions (264). The latter result is of doubtful importance, however, when one considers the ease with which Mn(III) disproportionates in aqueous solution.

Another stoichiometric manganese oxide phase, which seems to have been fully characterized, has the formula Mn₅O₈. The X-ray diagram of the black powder indexes as monoclinic (551) with unit cell dimensions very similar to those of Cd₂Mn₃O₈, and approximate structure factor calculations show that the two compounds are isotypic. Thus the valence structure of Mn₅O₈ is clearly Mn₂^{II}Mn₃^{IV}O₈, and the compound belongs to either class I or class II.

In common with a number of other first series transition metals, mixed valence manganese oxide systems based on perovskite lattices may be prepared with formulas intermediate between M^{III}Mn^{III}O₃ and M^{II}Mn^{IV}O₃, where the trivalent metal is commonly lanthanum and the divalent metal is one of the alkaline earths. The magnetic (392) and electrical (722) properties of these compounds have been the subject of extensive study over the past 15 years. They are all ferromagnetic, but their Curie temperatures are very strongly dependent on composition, with maxima in the region 25–40% M(II) (392). Values of the saturation magnetization as a function of composition also showed that, over the same region of composition, all the 3d electrons contribute their full spin moments, although without appreciable orbital contribution. The form of the relationship between magnetization and composition can be understood qualitatively if one assumes that the Mn(III)–Mn(III) interaction is almost zero (very low Curie temperature), and that there is a very strong Mn(III)–Mn(IV) magnetic interaction with a positive exchange integral raising the Curie temperature with increasing Mn(IV) concentration. Finally, to explain the asymmetrical position of the maximum magnetization with respect to composition, it is necessary to assume a somewhat weaker negative interaction between Mn(IV) and Mn(IV). Elegant confirmation of this picture was obtained by Wollan and Koehler (791) from neutron diffraction experiments on (La_{1-x}Ca_x)MnO₃. They found that the phase is purely ferromagnetic only over a small range of

composition near $x = 0.35$, and that, from 0 to 0.25 and from 0.40 to 0.50, ferromagnetic and antiferromagnetic interactions were simultaneously present. Thus LaMnO_3 is ferromagnetic along all three axes. In the mixed valence phases many different kinds of spin superlattice are built up, according to the distribution of manganese valence in the lattice. Some of the possibilities are shown in Fig. 10. To explain the occurrence of these superlattices, Goodenough (295) used a valence bond model in which the Mn(III) ions have dsp^2 (square) and the Mn(IV) ions have

LABEL	ONE OCTANT OF MAGNETIC UNIT CELL	IONS PER UNIT CELL				
		$\text{Mn}^{3+} \rightarrow \uparrow$	6	4	2	0
		$\text{Mn}^{4+} \rightarrow \circ$	2	4	6	8
A						
B						
F						

FIG. 10. Some of the possible spin superlattices in mixed valence calcium lanthanum manganese perovskites (791).

d^2sp^3 (octahedral) hybridization, and invoked a concept called "semi-covalence." This is equivalent to saying that electron transfer from a filled anion p orbital to an unfilled cation d orbital occurs with greater probability for an electron having the same spin as those already occupying the d -shell of the cation. Similarly, electron transfer from the lower-valent cation to the oxidized anion will align their spins, thus resulting in a net coupling of the spins of the two mixed valence cations, as described more fully in Section II.

Since all the manganese ions of $(\text{La}_{1-x}\text{Ca}_x)\text{MnO}_3$ are in equivalent sites in the perovskite lattice, the series of compounds is class III-B and should have metallic resistivities. This is confirmed by the work of van Santen and Jonker (722), who found a minimal resistivity of 3×10^{-2} ohm cm at 100°K for samples of $(\text{La}_{1-x}\text{Sr}_x)\text{MnO}_3$ having x between 0.2 and 0.4.

It has been suggested (667) that CuMn_2O_4 has a normal rather than an inverse spinel structure, because the valence distribution is $\text{Cu}^{\text{I}}(\text{Mn}^{\text{III}}, \text{Mn}^{\text{IV}})\text{O}$ rather than $\text{Cu}^{\text{II}}\text{Mn}_2^{\text{III}}\text{O}_4$, which requires that $\text{Cu}(\text{II})$ occupy a tetrahedral site in preference to $\text{Mn}(\text{III})$. In the absence of resistivity measurements, which would readily distinguish between the two valence distributions, it is not possible to comment further on this interesting suggestion. The structure of another $\text{Mn}(\text{III}), \text{Mn}(\text{IV})$ oxide, $\text{DyMn}^{\text{III}}\text{Mn}^{\text{IV}}\text{O}_5$, has been deduced by Abrahams and Bernstein (1a) as being class I, with $\text{Mn}(\text{III})$ in penta-coordination and $\text{Mn}(\text{IV})$ in octahedral coordination. As expected from its class I structure, $\text{DyMn}^{\text{III}}\text{Mn}^{\text{IV}}\text{O}_5$ has a resistivity of 10^{10} ohm cm at room temperature.

Unlike the $\text{Mn}(\text{III}), \text{Mn}(\text{IV})$ perovskites, the $\text{Mn}(\text{II}), \text{Mn}(\text{III})$ lattice in the compounds $\text{Li}_x\text{Mn}_{1-x}\text{O}$ does not show ferromagnetic ordering (386). As the lithium content is increased, the susceptibility curves change from a typically antiferromagnetic to a paramagnetic form, merely as a result of diluting the magnetic cations.

The naturally occurring minerals braunite, $\text{Mn}_7\text{SiO}_{12}$ (119), and pinakolite, $\text{Mg}_3\text{Mn}^{\text{II}}\text{Mn}_2^{\text{III}}\text{B}_2\text{O}_{10}$ (698), are other $\text{Mn}(\text{II}), \text{Mn}(\text{III})$ compounds whose structures have been solved. The unit cell of braunite contains 48 octahedrally coordinated $\text{Mn}(\text{III})$ ions with average $\text{Mn}-\text{O}$ distances of 2.09 Å, and eight octa-coordinated $\text{Mn}(\text{II})$ ions with $\text{Mn}-\text{O}$ equal to 2.16 Å. Evidently the system is class I. Although all the manganese ions in pinakolite are in octahedral sites, the distortions of the sites are sufficient to render the system class II.

While studying the reduction of transition metal cyanide complexes by sodium in liquid ammonia, Kleinberg and co-workers (142, 175) isolated the only mixed valence manganese compound not containing oxide as a ligand. The dark brown product of the reduction had an empirical formula $\text{K}_{11}\text{Mn}_2(\text{CN})_{12} \cdot 2\text{NH}_3$, and was thought to contain equimolar proportions of $\text{Mn}(0)$ and $\text{Mn}(\text{I})$. It was paramagnetic, with a room temperature magnetic moment of 1.25 B.M., but no further experiments were carried out on it.

E. IRON

The mixed valence compounds of iron form by far the largest group presently known for any element. This group of compounds is exceptional not only for its size, but also for its variety, for it contains oxides, hydroxides, halides, sulfates, cyanides, phosphates, carbonates, acetates, silicates, borates, and sulfites. There is also no small historical interest here, for the mixed valence iron cyanides were among the earliest

coordination compounds investigated, and a large number of the qualitative ideas presently used in thinking about mixed valence chemistry arose first in consideration of mixed valence iron compounds.

The study of mixed valence iron chemistry has recently received impetus from the discovery of the Mössbauer effect. Because the Mössbauer spectrum is potentially capable of indicating the valences of the iron ions in a solid, as well as their amounts and their coordination, its use can take one a long way towards understanding the structural elements of an iron compound [see, for example, Fluck *et al.* (254)].

The preparations of the mixed valence fluorides $\text{Fe}_2\text{F}_5 \cdot 7\text{H}_2\text{O}$, $\text{Fe}_2\text{F}_5 \cdot 3\text{H}_2\text{O}$, and the anhydrous material Fe_2F_5 have recently been reported (93). The first of these compounds, $\text{Fe}^{\text{II}}\text{Fe}^{\text{III}}\text{F}_5 \cdot 7\text{H}_2\text{O}$, is but one member of a large class of compounds of general formula $\text{M}^{\text{II}}\text{Fe}^{\text{III}}\text{F}_5 \cdot 7\text{H}_2\text{O}$. Because the Fe(II) in this compound can be replaced readily by other M(II) ions and also because of its yellow color, it appears that $\text{Fe}_2\text{F}_5 \cdot 7\text{H}_2\text{O}$ is a class I crystal which, consequently, does not involve sharing of ligands, there being just six ligands per metal ion. Because water inhibits the formation of a deep mixed valence color, it is not surprising that dehydrating the yellow heptahydrate to the trihydrate yields crystals which are deep red. Further dehydration to Fe_2F_5 yields a steel-blue compound, which by its color and stoichiometry is at least class II, and may even be class III and metallic.

Deussen (192) first showed that the colorless iron fluoride thought to be $\text{FeF}_3 \cdot 4\frac{1}{2}\text{H}_2\text{O}$ in reality was the mixed valence salt $\text{Fe}^{\text{II}}\text{Fe}_2^{\text{III}}\text{F}_8 \cdot 10\text{H}_2\text{O}$. The chlorides (451) and bromides (288) of the $\text{Fe}^{\text{II}}\text{Fe}_2^{\text{III}}\text{X}_8 \cdot 10\text{H}_2\text{O}$ systems are also known and, as expected from the large amount of water in them, are yellow in color. There also exists a reduced chloride $\text{Fe}_2^{\text{II}}\text{Fe}^{\text{III}}\text{Cl}_7 \cdot 10\text{H}_2\text{O}$ with the expected yellow color (288). In the bromide series, dehydration of $\text{Fe}_3\text{Br}_8 \cdot 10\text{H}_2\text{O}$ to the hexahydrate changes its color from yellow to black (542), indicating a transformation from class I to class II. The mixed valence bromide Fe_3Br_8 forms a number of other interesting adducts; thus, $\text{Fe}_3\text{Br}_8 \cdot (\text{CN})_2 \cdot 3\text{BrCN}$ (brown-black), $\text{Fe}_3\text{Br}_8 \cdot 4\text{BrCN}$ (dark brown), $\text{Fe}_3\text{Br}_8 \cdot 5\text{HCN}$ (black-brown), and $\text{Fe}_3\text{Br}_8 \cdot [(\text{CN})_2]_x$ are all known (542). However, since $\text{Fe}^{\text{III}}\text{Br}_3 \cdot 4\text{BrCN}$ is itself almost black, nothing can yet be said of the colors of the mixed valence adducts.

The large number of $\text{Fe}_3\text{X}_8 \cdot \text{Y}$ compounds so far described (and others, see below) at first suggests the presence of a trinuclear Fe_3X_8 species. Such a polynuclear species would necessarily be at least class II because of the shared ligands, and should have the deep color characteristic of this class. That there are no polynuclear species involved here follows from the pale colors of several of the Fe_3X_8 hydrates, and also

from the crystal structure of $\text{Fe}_3\text{Br}_8 \cdot 16\text{H}_2\text{O}$ published by Zvonkova (820). In this substance, the bromide ions and water molecules form chains of octahedra ($2\text{Br}^- \cdot 4\text{H}_2\text{O}$) sharing corners. Three fourths of these octahedral sites are filled statistically with iron, the average Fe—Br distance being 2.60 Å and the average Fe—O distance being 2.01 Å. Although Zvonkova extrapolates from this *average* structure to the conclusion that $\text{Fe}_3\text{Br}_8 \cdot 16\text{H}_2\text{O}$ is a mixed valence class III-B system much as Fe_3O_4 (see below), more careful work will probably show that in fact the ligand-metal distances about the Fe(II) and Fe(III) ions in this compound are quite different, and that the valences are firmly trapped.

Walden (742) reports the preparation of the triple bromides $\text{KFe}_3\text{Br}_9 \cdot 3\text{H}_2\text{O}$ and $\text{RbFe}_3\text{Br}_9 \cdot 3\text{H}_2\text{O}$. As one can guess by the high proportion of iron to water in these substances, the crystals are deeply colored. Although rather unstable, the crystals of these iron bromides are deep green and opaque.

McConnell and Davidson (497) have investigated the mixed valence absorption of HCl solutions containing the Fe(II) and Fe(III) ions. As with antimony, tin, and copper, the mixtures of $\text{Fe}^{\text{II}}\text{Cl}_2$ and $\text{Fe}^{\text{III}}\text{Cl}_3$ in concentrated HCl showed an absorbance in the region 11,000–22,000 cm^{-1} , which was much greater than that measured for the sum of the FeCl_2 and FeCl_3 solutions taken separately. This enhancement of absorption was found to decrease on lowering the HCl concentration, so that, in aqueous solutions of $\text{Fe}^{\text{II}}(\text{ClO}_4)_2$ and $\text{Fe}^{\text{III}}(\text{ClO}_4)_3$, there is no noticeable mixed valence absorption. It was concluded that the mixed valence chromophore involves a chloride-containing species having equal numbers of Fe(II) and Fe(III) ions. There is a suggestive relationship between this work and electron exchange kinetic studies, in which it was found that the thermal electron transfer between Fe(II) and Fe(III) is accelerated by the presence of Cl^- ions (129). In fact, Weiss (755) quotes several such catalyzed reactions: the Cl^- -catalyzed exchange between Eu(II) and Eu(III), and the F^- -catalyzed exchange between Ce(III) and Ce(IV). It would be interesting to see if these systems show mixed valence absorption bands in solution analogous to that shown by HCl solutions of Fe(II) and Fe(III).

Hathaway and Holah (347) have found that the oxidation of elemental iron by halogens in various solvents leads to the formation of mixed valence compounds formulated as $[\text{Fe}^{\text{II}}(\text{Sol})_6][\text{Fe}^{\text{III}}\text{X}_4]_2$, where Sol is a solvent molecule and X is a halide ion. As expected from the class I geometry and the lack of shared ligands in these materials, the spectra show only the absorptions of the component ions.

The low ratio of ligand to iron in the mixed valence alkali iron carbonates $\text{M}^{\text{I}}\text{Fe}_2^{\text{II}}\text{Fe}^{\text{III}}(\text{CO}_3)_3(\text{OH})_2 \cdot \text{H}_2\text{O}$ (47, 288) demands a rather

intimate association of the ferric and ferrous ions. In accord with this, the crystals are green and their solutions in water test negative for free Fe(III).

A mixed valence iron acetate has been reported, which may be related to the carbonate described above. The acetate,

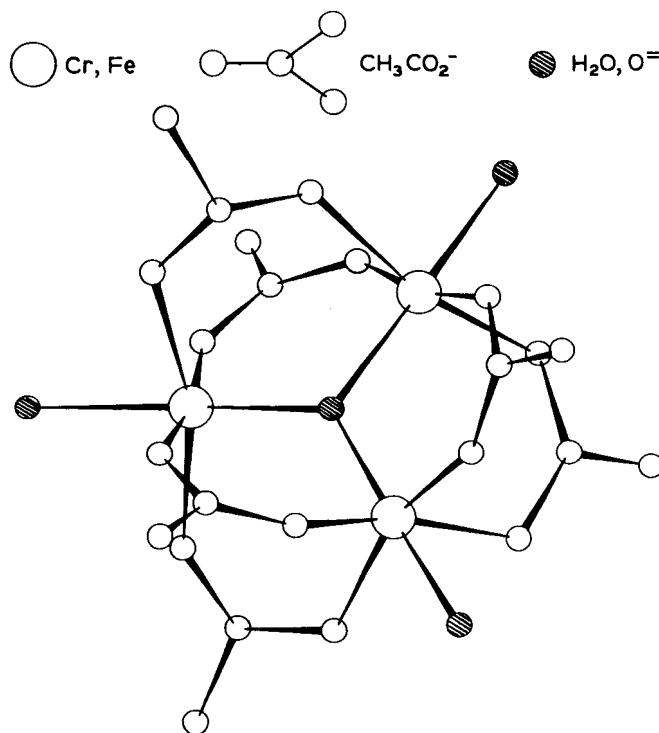
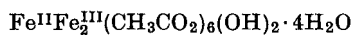
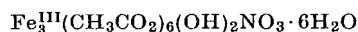


Fig. 11. The structure of the $[\text{M}_3(\text{CH}_3\text{CO}_2)_6\text{O} \cdot 3\text{H}_2\text{O}]^{n+}$ trinuclear ion.

is described as dark brown and, like the carbonate, yields a polynuclear ion in solution (141). There also exists here a possible connection with the ferric acetate with formula



which is known to involve a triangular array of Fe(III) ions in a cluster complex (Fig. 11) (251).

The mixed valence iron cyanides have been the object of constant study for over 250 years (572), a large part of their allure springing no doubt from their deep blue colors. Although it was long held that Prussian blue, made by adding Fe(III) to $[\text{Fe}^{\text{II}}(\text{CN})_6]^{4-}$, and Turnbull's

blue, made by adding Fe(II) to $[\text{Fe}^{\text{III}}(\text{CN})_6]^{3-}$, were distinct compounds, an overwhelming amount of evidence has since accumulated demonstrating that they are identical materials (66-68, 209, 225, 254, 753). We shall call this material Prussian blue. There are two kinds of Prussian blue, the first of which, soluble Prussian blue, is generally taken to be $\text{M}^{\text{I}}\text{Fe}_2(\text{CN})_6$, whereas insoluble Prussian blue is $\text{Fe}_4[\text{Fe}(\text{CN})_6]_3$. The earlier history of these "iron blues" has been reviewed by Holtzman (368).

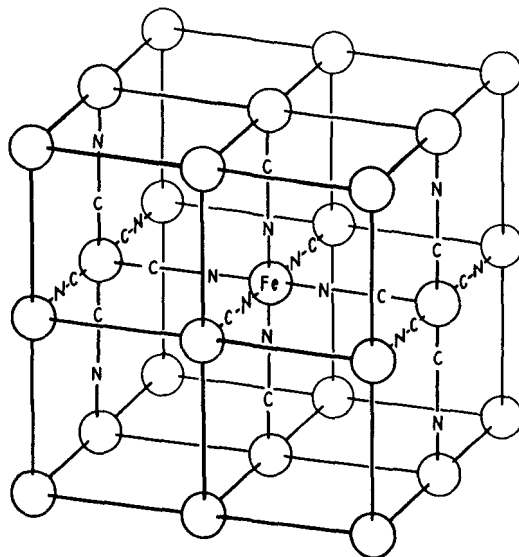


FIG. 12. The unit cell of Prussian blue-type crystals. In "soluble" Prussian blue ($\text{KFe}^{\text{III}}[\text{Fe}^{\text{II}}(\text{CN})_6]$), four potassium ions occupy octant sites and surround the body-centered ion tetrahedrally, whereas, in "insoluble" Prussian blue ($\text{Fe}_4^{\text{III}}[\text{Fe}^{\text{II}}(\text{CN})_6]_3$), hydrated Fe(III) ions are thought to occupy octant sites.

The crystal structures of soluble and insoluble Prussian blue are closely related to one another (409, 754), and to a large number of other heavy metal ferricyanides and ferrocyanides (588, 718) having face-centered cubic lattices with iron ions at the corners of a cube and cyanide ions bridging the irons along the cube edges. The centers of the cubes are filled with charge-compensating cations, if necessary, and/or water (Fig. 12). The iron-iron distance in Prussian blue is 5.1 Å as deduced from X-ray powder pattern data, which, however, were inadequate for determining the Fe—C, C—N, or N—Fe distances. Due to the roomy caverns at the cube centers, Prussian blue-type crystals are zeolitic and act as molecular sieves with channel diameters of ca. 3.2 Å (650). This is consistent with dehydration isotherm studies, which showed that Prussian blue is not a definite hydrate (753). Since the differentiation

between the Prussian blues as "soluble" and "insoluble" stems not from any real solubility of the "soluble" material, but instead from the ease with which it can be peptized to form a colloidal dispersion, knowledge of the crystal structure of soluble Prussian blue is essential to understanding the properties of its "solutions."

Both Thompson (703) and Korshunov and Lebedeva (436) have shown that, when Prussian blue is formed from inactive Fe(III) and radioactive $[\text{Fe}^{\text{II}}(\text{CN})_6]^{4-}$ and then decomposed by base, the resulting $\text{Fe}^{\text{III}}(\text{OH})_3$ is completely inactive. This demonstrates first that the Prussian blue crystal is not class III-B, as suggested indirectly by Emeleus and Anderson (221), and also that the cyanide ions do not rotate in the crystal or become carbon-bonded to the Fe(III) ions on forming the crystal. Thus, as can be readily seen from Fig. 12, there are two varieties of octahedral site in the class II Prussian blue crystal: those coordinated by the carbon ends of the cyanide ligands, and those coordinated by the nitrogen ends of these same ligands. It has been a problem of great interest to demonstrate which iron ion valence resides in which site, i.e., are the valences in Prussian blue trapped as ferric ferrocyanide or ferrous ferricyanide?

The magnetic susceptibility of Prussian blue, as measured by Davidson and Welo (176) and by Cambi (128), is consistent with either high-spin, $3d^5$ Fe(III) ions in the nitrogen sites and low-spin, $3d^6$ Fe(II) ions in the carbon sites, or high-spin, $3d^6$ Fe(II) ions in the nitrogen sites and low-spin, $3d^5$ Fe(III) ions in the carbon sites. On the basis of oxidation-reduction potentials in aqueous solutions, Weiser *et al.* (754) argue for the latter, claiming that Prussian blue is the ferrous salt of ferricyanic acid. A flood of more direct evidence has recently shown that, in fact, Prussian blue is better considered as the ferric salt of ferrocyanic acid. Thus, for example, on the basis of the fact that the C—N stretching frequencies of various ferrocyanides fall at 2090 cm^{-1} and below, whereas the C—N stretches in ferricyanides are found at 2150 cm^{-1} and above, Emschwiller (222) demonstrated that Prussian blue contained ferrocyanide ions since the C—N stretch in this compound lies at 2080 cm^{-1} . Again, Robin (591) has interpreted the first two bands at $14,700\text{ cm}^{-1}$ and $25,000\text{ cm}^{-1}$ in the electronic spectrum of Prussian blue as being associated with the transfer of an electron from a low-spin, $3d^6$ ferrocyanide ion to a high-spin, $3d^5$ ferric ion. The most compelling evidence for the formulation of Prussian blue as ferric ferrocyanide rests on the results of the many Mössbauer spectral studies of this material. As shown in Fig. 13, the Mössbauer spectrum of soluble Prussian blue consists of a pair of lines, 2 and 3, which are identified as the quadrupole split components of the high-spin Fe(III) ion in octahedral coordination,

and the single line, 1, due to the $[\text{Fe}^{\text{II}}(\text{CN})_6]^{4-}$ ion. The ratio of the intensities of lines 2 plus 3 to line 1 is 1.0 in soluble Prussian blue and almost 4/3 in insoluble Prussian blue (209, 225, 254, 410, 591).

Because the valences are firmly trapped, one can draw an orbital diagram for Prussian blue, using the orbitals of the $\text{Fe}^{\text{II}}(\text{CN})_6$ and $\text{Fe}^{\text{III}}(\text{NC})_6$ ions taken separately (591). This is shown in Fig. 14, where the mixed valence transition responsible for the blue color of Prussian blue ($14,700\text{ cm}^{-1}$, Fig. 15) is depicted by the arrow labeled 1. According to this assignment, the ground state of Prussian blue is $\text{KFe}^{\text{III}}\text{Fe}^{\text{II}}(\text{CN})_6$,

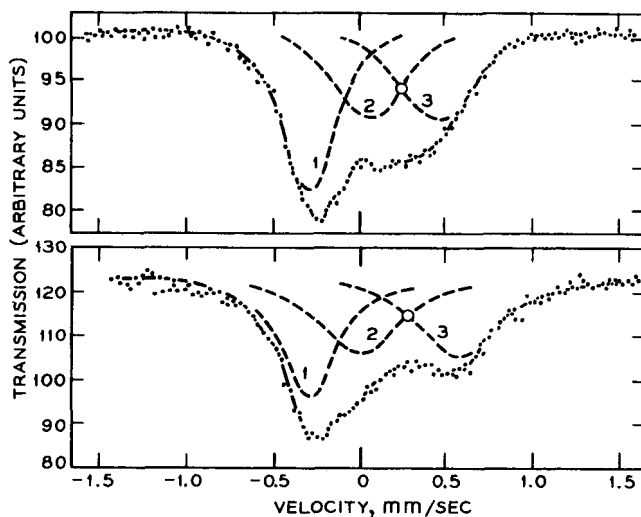


FIG. 13. The Mössbauer spectra of soluble Prussian blue ($\text{KFe}^{\text{III}}[\text{Fe}^{\text{II}}(\text{CN})_6]$), upper, and insoluble Prussian blue ($\text{Fe}_4^{\text{III}}[\text{Fe}^{\text{II}}(\text{CN})_6]_3$), lower, both at 143°K (254).

and the Turnbull's blue formulation, $\text{KFe}^{\text{II}}\text{Fe}^{\text{III}}(\text{CN})_6$, is more appropriate to the first excited state. Actually, because of configuration interaction, the system in the ground state is a mixture of the Prussian blue and Turnbull's blue configurations, in a proportion which can be estimated from the mixed valence absorption intensity. Application of Eq. (14) to the $14,700\text{ cm}^{-1}$ band of Prussian blue ($\epsilon = 9800$; $\mu = 1.23\text{ e}\text{\AA}$) yields a value of α^2 equal to 0.01, showing that the optical electron spends 99% of its time in a carbon hole and 1% in a nitrogen hole in the ground state.

Because Prussian blue is a class II crystal, with distinguishable oxidation states, its spectrum should contain not only the first mixed valence absorption (arrow 1), but a second band related to the first by a spectral interval in the high-spin $\text{Fe}(\text{II})$ ion, and also bands due to the $\text{Fe}(\text{III})$ and $[\text{Fe}^{\text{II}}(\text{CN})_6]^{4-}$ ions. The transition labeled 2 is assigned as the

band observed at $25,000\text{ cm}^{-1}$, for it is weak and separated from transition 1 by the $t_{2g} \rightarrow e_g$ separation ($10,000\text{ cm}^{-1}$) in the high-spin Fe(II) ion, as predicted for a class II system. The low intensity of this band follows from the fact that it is a transition between t orbitals on one center and e orbitals on another, and, according to Eq. (17), this is forbidden. The strong band in the $45,000\text{--}50,000\text{ cm}^{-1}$ region of the

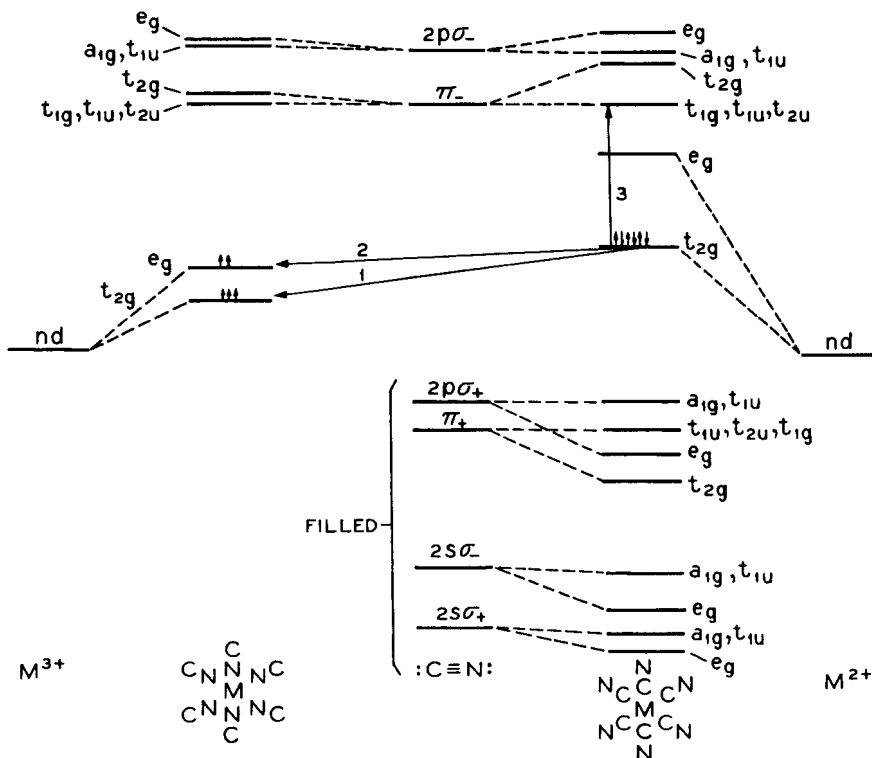


FIG. 14. A molecular orbital scheme for class II Prussian blue. The symmetry labels on any column of levels are appropriate only to the molecule listed at the foot of that column, and the transitions labeled 1, 2, and 3 correspond to the bands of Fig. 15 labeled in the same way (591).

Prussian blue spectrum is readily assignable as the intramolecular charge transfer excitation of the ferrocyanide ion (arrow 3 in Fig. 14). The bands at $35,000\text{--}40,000\text{ cm}^{-1}$ are tentatively assigned as transitions from a CN π -bonding orbital to the t_{2g} orbital of the Fe(III) ion. Braterman (85) has generalized the Prussian blue assignment scheme to include complexes in which the ions in the two holes are of different metals.

Also in accord with its class II assignment, Prussian blue has a room temperature resistivity of about 10^7 ohm cm, and is an intrinsic semi-

conductor with a negative temperature coefficient of resistance (250). Although ferromagnetic with a Curie temperature of 3.5°K (367), Prussian blue is not an example of mixed valence, Zener-type double exchange, for the Fe(II) ions in the ground state are diamagnetic.

There are numerous composition variations that can be made in the iron blues. A reduced form of Prussian blue, $\text{Fe}_2^{\text{II}}\text{Fe}^{\text{II}}(\text{CN})_6$, is colorless as one might expect, but the oxidized form, $\text{Fe}^{\text{III}}\text{Fe}^{\text{III}}(\text{CN})_6$, is green instead of the expected orange-brown color of $[\text{Fe}^{\text{III}}(\text{CN})_6]^{3-}$. Ibers and Davidson (373) present their spectrum of $\text{Fe}^{\text{III}}\text{Fe}^{\text{III}}(\text{CN})_6$ as well as those of Fe(III) and $[\text{Fe}^{\text{III}}(\text{CN})_6]^{3-}$, from which one sees clearly an "extraneous" absorption in $\text{Fe}^{\text{III}}\text{Fe}^{\text{III}}(\text{CN})_6$ centered at 20,000 cm^{-1} . DeWet and

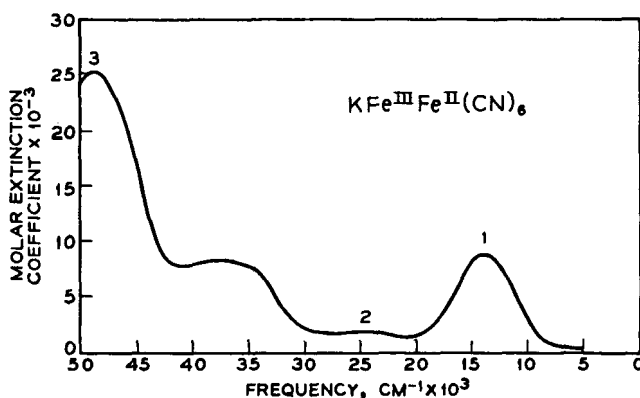


FIG. 15. The electronic spectrum of soluble Prussian blue as a colloidal dispersion in water (591).

Rolle (193), however, have demonstrated that $\text{Fe}^{\text{III}}\text{Fe}^{\text{III}}(\text{CN})_6$ is very readily reduced by water to a mixed valence Prussian blue-type compound, which no doubt is the cause of the 20,000 cm^{-1} band of " $\text{Fe}^{\text{III}}\text{Fe}^{\text{III}}(\text{CN})_6$." Both the oxidized and reduced compounds have the face-centered cubic lattice of Prussian blue (409).

Although Ibers and Davidson (373) were able to demonstrate a mixed valence absorption in solutions containing Fe(II) and Fe(III) ions, mixtures of the corresponding hexacyanides gave no such absorption. The lack of mixed valence absorption here is due in part to the impossibility of sharing ligands between these ions, and in part to the difficulty of forming pairs between ions of the same charge. However, they do exchange electrons rapidly in solution (703).

There are a large number of pentacyanide ions of the formula $[\text{Fe}^{\text{II}}(\text{CN})_5\text{X}]^{n-}$, where X is H_2O , NH_3 , AsO_2^- , SO_3^{2-} , NH_2NH_2 , or CO , all of which form deep blue precipitates with Fe(III) ion. On combining

the salts of $[\text{Ru}^{\text{II}}(\text{CN})_6]^{4-}$ or $[\text{Os}^{\text{II}}(\text{CN})_6]^{4-}$ with $\text{Fe}(\text{III})$ ion, blue to purple sols are formed which have electronic spectra virtually identical to that of Prussian blue (591).

As one might expect from the ubiquitous distribution of iron in nature, there are great numbers of naturally occurring minerals containing $\text{Fe}(\text{II})$ and $\text{Fe}(\text{III})$, both as major constituents and as impurities. As with the other iron compounds, the combination of X-ray crystallography and Mössbauer spectroscopy can be a great aid in determining the amounts, valencies, and coordinations of the iron ions in mixed valence minerals. From this information one can proceed to a qualitative understanding of their electronic structures. In this section, mixed valence iron minerals will be considered for which structures have been determined, together with only a few of the many other minerals which suggest themselves for future mixed valence study.

MacCarthy (470) many years ago presented the results of a study aimed at correlating the colors of a large number of iron-containing minerals with the oxidation state of the iron. Iron minerals as found in nature span the color spectrum, being colorless, yellow, red, brown, green, blue, purple, or black. MacCarthy showed that, in general, the colorless minerals contained only $\text{Fe}(\text{II})$, that the yellow, orange, and red ones were totally $\text{Fe}(\text{III})$, but that mixtures of these valence states led to blue materials if hydrated, black if anhydrous. The greens and purples were accounted for as physical mixtures of the other, more basic pigments. However, before one adjudges a naturally occurring mineral to be mixed valence on the basis of its unusual color, the possible contamination of the sample by colored impurities must be ruled out.

Both the partial reduction of colorless $\text{Fe}^{\text{III}}\text{PO}_4$ and partial oxidation of colorless $\text{Fe}_2^{\text{II}}(\text{PO}_4)_2$ lead to the formation of deeply colored $\text{Fe}(\text{II}), \text{Fe}(\text{III})$ phosphates (699). Thus, depending upon conditions, the reduction of slurried FePO_4 in H_2O with H_2 under pressure leads to green, blue, or black crystals (374). Vivianite, a naturally occurring mineral with composition $\text{Fe}_3^{\text{II}}(\text{PO}_4)_2 \cdot 8\text{H}_2\text{O}$, presents a dramatic example of the development of a deep color on attaining mixed valence, for the mineral is colorless until cleaved and exposed to the air, whereupon it oxidizes and develops a dark blue color. Since the reduced mineral contains pairs of ferrous ions in oxygen octahedra sharing an edge (514), it is clear how a chromophoric grouping can result on partial oxidation. A similar situation holds for iron in silicate and borate glasses (767) in which, for example, ferrous iron is colorless and ferric iron is brown, but glasses of intermediate oxidation are blue. The blue-color centers in these glasses must be "dimers" in the sense that no mixed valence color can develop if the $\text{Fe}(\text{II})$ and $\text{Fe}(\text{III})$ ions are too far separated.

Iron lazulite is another basic iron phosphate mineral. It is described as being "shiny, jewel-like black in color," and contains Fe(II) and Fe(III) in face-sharing octahedral coordination (407). The close approach of the Fe(II) and Fe(III) ions to class III geometry suggests that iron lazulite will have a low electrical resistivity, a quantity which is unmeasured as yet. A similar situation holds for barbosolite (462), $\text{Fe}_2^{\text{II}}\text{Fe}_4^{\text{III}}(\text{PO}_4)_4(\text{OH})_4$, a material in which the oxygen octahedra surrounding the Fe(II) and Fe(III) ions share faces and corners.

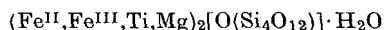
There are a great many silicate minerals containing iron in two valence states. Crocidolite is a bright blue, fibrous silicate containing Fe(II) and Fe(III) in octahedral coordination. The Mössbauer spectrum of crocidolite shows the presence of discrete Fe(II) and Fe(III) ions, as expected for a class II mixed valence system (275). That its blue color is due to a mixed valence interaction is apparent both from the fact that when the Fe(II) fraction is oxidized to Fe(III) the band responsible for the blue color at $16,000\text{ cm}^{-1}$ disappears, and from the fact that this band is polarized along the fiber axis, which is also the direction of shortest Fe(II)–Fe(III) separation (465). Crocidolite is a semiconductor along the fiber axis, but has a very high resistivity perpendicular to this axis.

Biotite is a micaceous mineral in which variable amounts of Al(III) and Mg(II) have been replaced by Fe(III) and Fe(II). As a result of this substitution into the layered mica structure, biotite appears quite black in light polarized with its electric vector within the layers but is colorless perpendicular thereto. Because of the mixed valence aspect of this material and the obvious related electronic conduction mechanism, it is clear why the best insulating micas are lowest in iron. Because the Mössbauer spectrum of biotite shows absorption due to clearly defined Fe(II) and Fe(III) ions, the system is mixed valence class II, as is also clear from its crystal structure (83).

Lievrite is a black mineral having the composition

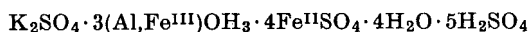


with both the Fe(II) and Fe(III) ions in distorted octahedra sharing edges (53). Taramellite, another iron-containing silicate, also contains chains of octahedral Fe(II) and Fe(III) ions sharing edges, and has the overall formula (490):



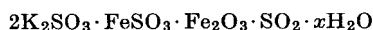
Cronstedtite is a layered mineral, $\text{Fe}_2^{\text{II}}\text{Fe}_2^{\text{III}}\text{SiO}_5(\text{OH})_4$, which has both Fe(II) and Fe(III) ions in octahedral coordination as well as Fe(III) in tetrahedral sites (354). The mineral is black in thick sections and emerald green in thinner ones.

Voltaite is an interesting mixed valence iron sulfate mineral with the composition



which is easily synthesized in the laboratory (300). Consistent with a class II mixed valence formulation, voltaite has a deep black color in massive form, but is green when viewed by transmission in thin sections. Synthesis of the corresponding material having $\text{Cd}^{\text{II}}\text{SO}_4$ replacing $\text{Fe}^{\text{II}}\text{SO}_4$ results in an almost colorless solid, as expected. In contrast to the black color of voltaite, the mixed valence iron sulfate mineral romerite ($\text{Fe}^{\text{II}}\text{Fe}_2^{\text{III}}(\text{SO}_4)_4 \cdot 14\text{H}_2\text{O}$) has only a reddish brown color (634, 635). However, dehydration of romerite to the dihydrate yields a blue-black material, just as in the case of the ferrous-ferric fluorides mentioned above. Pending a report of the structures of these minerals, one might guess that in voltaite the Fe(II) and Fe(III) ions are in rather close association with their octahedra probably sharing ligands, whereas in hydrated romerite these ions are effectively separated by "insulating" water molecules.

Gmelin (288) lists a number of synthetic mixed valence iron sulfates of rather similar composition: $\text{FeSO}_4 \cdot \text{Fe}_2(\text{SO}_4)_3 \cdot 2\text{H}_2\text{SO}_4$ (rose colored), $4\text{FeSO}_4 \cdot \text{Fe}_2(\text{SO}_4)_3 \cdot 12\text{H}_2\text{O}$ (yellow-green), $6\text{FeSO}_4 \cdot \text{Fe}_2(\text{SO}_4)_3 \cdot 10\text{H}_2\text{O}$ (pale green), and $3\text{FeSO}_4 \cdot 2\text{Fe}_2(\text{SO}_4)_3 \cdot 3\text{H}_2\text{O}$ (colorless). There is also an Fe(II),Fe(III) sulfite (57a),



which is a colorless material.

A cursory look through a modern book of mineralogy (172) will reveal a large number of other iron-containing substances of potential mixed valence interest. For example, the ferrous minerals augite (black, distinctly dichroic), riebeckite (dark blue, dichroic), glaucophane (blue, dichroic), hornblende (dark green to black), tourmaline (all colors, strongly dichroic), ludwigite (black, dichroic), and osumilite are all thought to contain ferrous and ferric ions.

The mineral magnetite, Fe_3O_4 , offers many illustrative examples of mixed valence effects. On the basis of its stoichiometry, Gay-Lussac first described Fe_3O_4 as involving a "special" valence state of iron. Shortly thereafter, Dalton and Berzelius proposed instead that Fe_3O_4 was a compound of $\text{Fe}^{\text{II}}\text{O}$ and $\text{Fe}_2^{\text{III}}\text{O}_3$ in 1:1 ratio. As we shall see, there is a certain amount of truth in both of these ideas. Fe_3O_4 is a cubic spinel, consisting of a cubic close-packed arrangement of oxide ions which define both octahedral and tetrahedral sites (Fig. 16). In a normal spinel with eight molecules per unit cell, eight of the tetrahedral holes are filled by M(II) metal ions, while sixteen of the octahedral holes are filled by

M(III) metal ions. In magnetite, however, because of the propensity of Fe(III) for tetrahedral coordination, all eight tetrahedral sites are filled by Fe(III) and the remaining sixteen edge-sharing octahedral sites are filled by eight Fe(II) ions and eight Fe(III) ions (726, 728). Thus if it were a normal spinel, magnetite clearly would be a class I mixed valence system, but the inverse spinel structure described above results in class III-B behavior within the octahedral sites and class I behavior between octahedral and tetrahedral sites.

Verwey *et al.* (729) felt that the rapid electron exchange implied by the mixed valence occupation of the octahedral sites in magnetite was

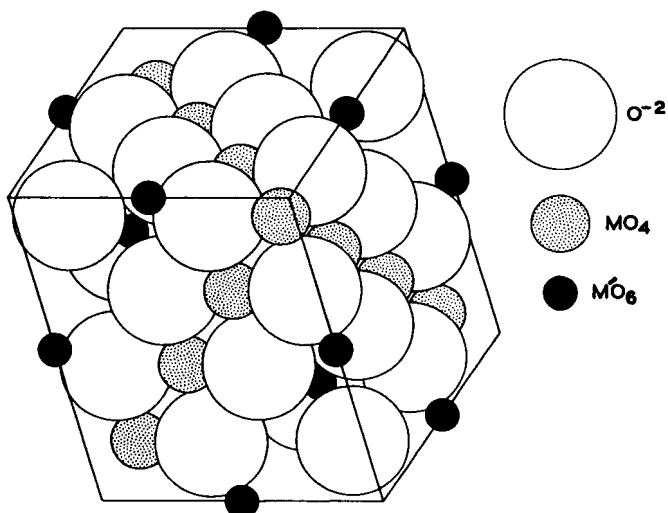


FIG. 16. The unit cell of the spinel MM'_2O_4 , in which the M cations are in tetrahedral and the M' in octahedral sites.

responsible for its unusually low resistivity (4×10^{-3} ohm cm at 300°K). Unlike many oxides which show maximal resistance when stoichiometric and a decreasing resistance as the composition departs from stoichiometry, Fe_3O_4 is just the opposite, for the addition of defects and other valences of iron only act to trap the valence locally and thereby increase the activation energy for conduction (726).

Fe_3O_4 is ferrimagnetic with a Curie point at 500°–600°C. Neutron diffraction experiments (660) show that the Fe(II) in the tetrahedral sites is antiferromagnetically coupled to the ferromagnetically coupled Fe(II), Fe(III) ions in the octahedral sites, the net ferrimagnetism resulting from the larger numbers of octahedral sites.

Verwey *et al.* (729) reported that, on cooling Fe_3O_4 below 120°K, the resistivity rose abruptly by two orders of magnitude and became

distinctly anisotropic whereas above 120°K it is isotropic. They suggested that above 120°K the Fe(II) and Fe(III) in the octahedral sites are in "dynamic disorder," but that below this temperature the crystal is orthorhombic and the Fe(II) and Fe(III) ions become ordered, occupying perpendicular rows of octahedral sites. We can paraphrase Verwey and presume that the octahedral Fe—O distances alter abruptly at 120°K so as to trap the Fe(II) and Fe(III) valences, thereby making the octahedral system more class II, i.e., insulating. If the valences are partly trapped at room temperature through the introduction of Fe₂O₃ into the crystal, then the 120°K transition is absent. Careful neutron diffraction work by Hamilton (335) fully confirmed Verwey's conjectures, for Hamilton showed not only that the low temperature form of Fe₃O₄ was orthorhombic but that, whereas the Fe—O distance in the octahedral sites at 300°K is uniformly 2.0590 ± 0.0016 Å, in the low temperature phase there are two octahedral sites, one having Fe(III)—O equal to 2.00 Å, and one having Fe(II)—O equal to 2.123 Å. These Fe(II) and Fe(III) ions are in perpendicular rows, as predicted. Calhoun's resistivity measurements show that the anisotropy increases with decreasing temperature, indicating a firmer trapping at lower temperatures (126).

The Mössbauer spectra of Fe₃O₄ at 300°K and 85°K offer striking confirmation for the views expressed above (49). At room temperature, the Mössbauer spectrum of Fe₃O₄ shows that the magnetic fields at the octahedral sites are indistinguishable, indicating an oscillation of valence more rapid than 10⁸/sec. On the other hand, at 85°K, the Fe(II) and Fe(III) ions in the octahedral holes can be distinguished as expected for a class II system.

Magnetite can be brominated to yield a dark brown material of the composition (Fe₃O₄)₃Br₂ (360). This bromide still possesses a spinel lattice like Fe₃O₄ and although ferromagnetic, is less so than Fe₃O₄.

The binary oxides of barium and iron contain, among their number, two mixed valence materials. Derbyshire *et al.* (190) and Fraker (259) have shown that the barium iron oxide thought to be BaFeO₃ really contains only 76% of its iron as Fe(IV), the remainder being Fe(III). This leads to a probable formula Ba(Fe^{III},Fe^{IV})O_{2.9}. A second oxide, BaFe₂^{II}Fe₁₆^{III}O₂₇, has a spinel-type structure (95) and, like magnetite, is an electrical conductor and ferromagnet (763).

We will present here only one of many examples of the dramatic effects that low-level doping can produce through mixed valence. In yttrium iron garnet, 3Y₂O₃·5Fe₂O₃, three fifths of the Fe(III) ions are found in tetrahedral sites and two fifths in octahedral sites, the stoichiometric crystal being an insulator with a resistivity of about 10¹¹ ohm cm.

On doping such crystals with approximately 0.02 atom of silicon per formula weight, an equivalent amount of Fe(III) is reduced to Fe(II) and the resistivity decreases by seven orders of magnitude (792). It is not yet known whether the Fe(II) ions reside in the tetrahedral or the octahedral sites of the garnet.

The process of iron corrosion has been shown to proceed through an intermediate "green rust" of composition $2\text{FeO} \cdot \text{Fe}_2\text{O}_3 \cdot \text{H}_2\text{O}$, which precedes the formation of brown rust, $\gamma\text{-Fe}_2\text{O}_3 \cdot \text{H}_2\text{O}$ (1, 174, 803). Abe (1) showed that $2\text{FeO} \cdot \text{Fe}_2\text{O}_3 \cdot \text{H}_2\text{O}$, when made by the combination of $\gamma\text{-Fe}_2\text{O}_3 \cdot \text{H}_2\text{O}$ and $\text{Fe}(\text{OH})_2$, is really a blue material, and that "green rust" is probably a mixture of this blue compound and the brown rust. Shively and Weyl (659) also report that the partial oxidation of $\text{Fe}(\text{OH})_2\text{-Al}(\text{OH})_3$ coprecipitates yields dark blue materials. In a more detailed study, Feitknecht and Keller (238) report that the air oxidation of colorless $\text{Fe}(\text{OH})_2$ leads to the formation of a deep green material, which has the crystal structure of $\text{Fe}(\text{OH})_2$ although containing up to 10% Fe(III). Air oxidation of buffered FeCl_2 solutions yields a dark green mixed valence oxychloride of ideal composition $\text{Fe}_4^{\text{II}}\text{Fe}^{\text{III}}\text{Cl}(\text{OH})_{10} \cdot x\text{H}_2\text{O}$, which, however, can have appreciable amounts of its Fe(II) replaced by Fe(III) (238). Selwood (652) mentions that ferromagnetic gels can be formed by addition of base to solutions containing mixtures of ferric and ferrous ions.

There are two biologically important iron-containing materials of potential interest to our study. The first, photosynthetic pyridine nucleotide reductase, contains two nonheme Fe(III) ions per molecule. On photoreduction, one of the two Fe(III) ions is reduced to Fe(II) and the protein *decolorizes* (263). This fact suggests strongly that the two iron ions are not closely associated in the photoreduced protein. Ferredoxin contains seven iron ions per molecule, all of which appear to be Fe(III) (74). However, it is postulated that these ions are involved in electron transport, and that some of the Fe(III) is reduced on reduction of the protein.

F. COBALT

Like manganese and iron, cobalt forms a mixed valence oxide with a spinel structure, Co_3O_4 , and, as with the other two oxides, there has been a good deal of discussion about the distribution of the valency in it. In principle, four possibilities exist: normal or inverse Co(II),Co(III) spinels and normal or inverse Co(II),Co(IV) spinels. In common with Mn_3O_4 and in contrast to Fe_3O_4 , Co_3O_4 has a high resistivity (458, 741),

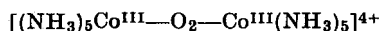
suggesting that the manganese and cobalt compounds are normal spinels (725). Cossee (158) measured the magnetic susceptibilities of tetrahedral Co(II) in $(\text{Co}^{\text{II}}, \text{Zn})\text{O}$, of Co(III) octahedrally coordinated in the spinel $\text{ZnCo}_2^{\text{III}}\text{O}_4$, and of Co_3O_4 from 77° to 1000°K and found that the effective magnetic moment per Co(II) in ZnO was 4.05 B.M., but that the moment of Co(III) in ZnCo_2O_4 was zero, as expected for a low-spin $3d^6$ configuration. The effective magnetic moment per mole of Co_3O_4 , 4.14 B.M., can then be interpreted in terms of the structure $\text{Co}^{\text{II}}\text{Co}_2^{\text{III}}\text{O}_4$ with Co(II) in tetrahedral and Co(III) in octahedral coordination. At 40°K, Co_3O_4 becomes antiferromagnetic (602), and the spin interaction between the Co(II) ions is an order of magnitude stronger than in the spinel CoAl_2O_4 , possibly as a result of indirect exchange involving the empty e_g orbitals of the Co(III) ions. The nuclear magnetic resonance chemical shift of ^{59}Co in Co_3O_4 (403, 509) contains a temperature-independent contribution due to mixing of the low-lying excited configuration $t_{2g}^5 e_g^1$ with the t_{2g}^6 ground state, and a temperature-dependent part attributed to hyperfine coupling between the nuclear spins of the diamagnetic Co(III) ions and the electron spins of the Co(II) ions at the tetrahedral sites.

Cobalt(III,IV) perovskites can be prepared with formulas intermediate between $\text{LaCo}^{\text{III}}\text{O}_3$ and $\text{SrCo}^{\text{IV}}\text{O}_3$, just as was found for the Mn(III),Mn(IV) manganites (394). In contrast to the octahedrally coordinated, low-spin Co(III) in Co_3O_4 , that in LaCoO_3 is high-spin, and all the mixed valence phases are ferromagnetic, with Curie temperatures that rise sharply with increasing Co(IV) concentration. LaCoO_3 behaves as a semiconductor, but when doped with strontium the room temperature resistivity drops sharply and the temperature coefficient of resistivity finally becomes positive. As in the case of the Mn(III),Mn(IV) manganites, the ferromagnetism of the mixed valence cobaltites is attributed to a strong positive Co(III)–Co(IV) interaction. As described in Section II, Zener (813) showed that the resonance energy between the canonical structures $\text{Co}^{3+}\text{—O}^{2-}\text{—Co}^{4+}$ and $\text{Co}^{4+}\text{—O}^{2-}\text{—Co}^{3+}$ is larger if the electron spins on the metal atoms are parallel. Since the integrals determining the interaction in Zener's model are those involving simultaneous electron transfer from O^{2-} to Co^{4+} and Co^{3+} to O^- , the spin correlation and electrical resistivity would both be accounted for by mixed valence interaction, were it not for the fact that there is no anomaly in the resistivity at the Curie temperature. This observation has not yet been satisfactorily explained.

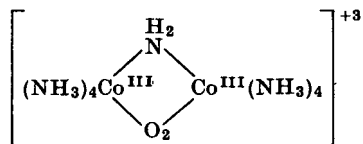
A further interesting example of a Co(II),Co(III) system with oxide ligands occurs among the class of heteropolytungstates. Powerful oxidizing agents, such as hot persulfate solution, oxidize the emerald

green anion $[\text{Co}_2^{\text{II}}\text{W}_{12}\text{O}_{42}]^{8-}$ to a mixed valence anion, the alkali metal salts of which form very dark brown to black cubic crystals. The anion was at first (37) formulated as $[\text{Co}^{\text{II}}\text{Co}^{\text{III}}\text{W}_{12}\text{O}_{42}]^{7-}$, with an "extra" Co(II) attached to the outside of the Keggin structure (408) characteristic of polytungstates. Very recently, however, the evidence for this formula has been reexamined (38) and the anion is now considered to be $[\text{Co}^{\text{II}}\text{Co}^{\text{III}}\text{W}_{11}\text{O}_{40}]^{9-}$, in which Co(II) replaces one of the tungsten atoms of the $\text{W}_{12}\text{O}_{40}$ framework, and is thus octahedrally coordinated by oxygen. The paramagnetic susceptibility of the potassium salt of this anion exhibits a most curious dependence on temperature, changing only 13% between -143° and 23°C , so that, although the two cobalt ions are in octahedral and tetrahedral coordinations and the system belongs to class I, there appears to be appreciable intraionic interaction. An ESR study would be rewarding.

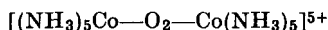
Peroxo-bridged binuclear cobalt complexes have been known for over 100 years (262) and were systematically investigated by Werner (765, 766). Diamagnetic cations such as



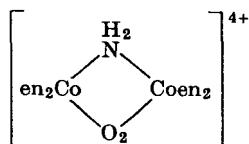
and



undergo one-electron oxidations (702), forming paramagnetic species, and the question is whether Werner's formulation with one Co(III) and one Co(IV) is correct, or whether the electron has been removed from the bridging peroxo group, i.e., is the oxidized cation a mixed valence species belonging to class II or III-A, or a single valence species containing the radical ligand O_2^- ? A number of workers established that the complexes



and



had magnetic moments corresponding to one unpaired spin (287, 480), but were unable to distinguish between the alternative formulations and, indeed, Malatesta (480) envisaged a resonance between them.

In 1938 Mathieu (488) measured the rotatory dispersion and circular

dichroism of the optically active ethylenediamine compounds of the peroxo-bridged cobalt complexes, but, in the absence of a quantum mechanical theory of rotational strengths in metal complexes, was unable to interpret them. Mathieu (488) and Ohyagi (544) reported some solution absorption spectra, but the most reliable available appears to

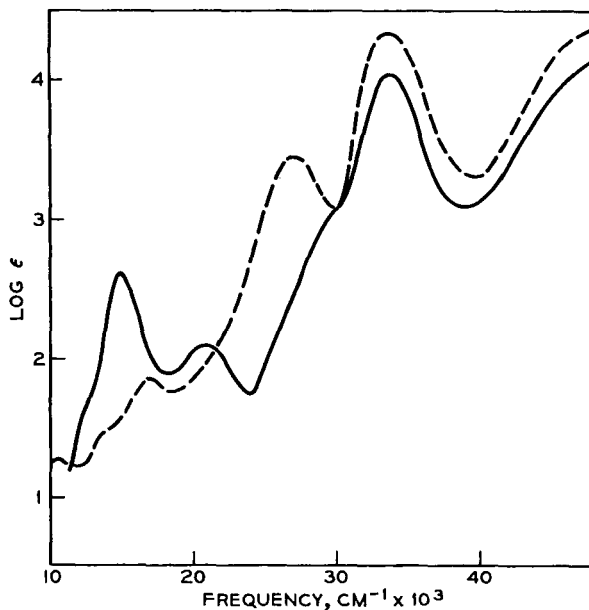
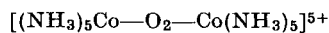
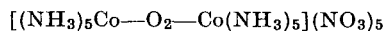


FIG. 17. The electronic absorption spectra of the $[(\text{NH}_3)_5\text{CoO}_2\text{Co}(\text{NH}_3)_5]^{5+}$ (—) and $[\text{Co}(\text{NH}_3)_5\text{I}]^{2+}$ (---) ions in aqueous solution (463, 464).

be that of Linhard and Weigel (463, 464) (Fig. 17), who also were the first to note that the spectrum of

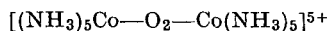


resembled the ligand field spectrum of an octahedral $\text{Co}(\text{III})$ complex, $\text{Co}^{\text{III}}(\text{NH}_3)_5\text{X}$, in which the ligand field strength of X was very different from that of NH_3 . Yamada *et al.* (797) had previously measured the polarized crystal spectrum of

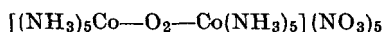


and concluded that the first absorption band was polarized parallel to what they call the $\text{Co}-\text{O}-\text{O}-\text{Co}$ direction, but, as the crystal structure of the compound had not been determined at that time, it is difficult to see how they arrived at this conclusion.

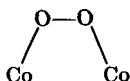
Dunitz and Orgel (210) attempted to rationalize the electronic structure of



using qualitative arguments based on π -bonding between t_{2g} orbitals on the cobalt atoms and $2p$ orbitals on the oxygens, with the assumption that the Co—O—O—Co unit was linear. Unfortunately, the first crystal structure determination (721) revealed that the O—O bond was at right angles to the metal-metal line. In either case, the two cobalt atoms would be equivalent, and the complex would be a class III-A system. That the two cobalt atoms are magnetically equivalent was clearly shown by the ESR spectrum of the cation in concentrated sulfuric acid solution (58). The fifteen observed hyperfine lines result from the interaction of the single unpaired electron with both cobalt nuclei ($I = 7/2$). The spectra of both peroxy- and peroxy-imino-bridged complexes were asymmetrical and varied with the acidity, viscosity, and temperature of the solvent in a manner which could be explained by a relaxation effect depending on protonation of the oxygen atoms (214). A further relaxation mechanism might come from rotation or torsional oscillations about the O—O bond, an effect made more likely by the fact that unpublished crystallographic work by Okaya, cited in (214), showed that in



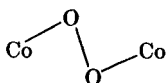
the two cobalts are cis to one another :



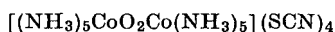
The crystal structure determination of Vannerberg and Brosset (721), in which both oxygen atoms were equidistant from the two cobalts, has been criticized recently by Schaefer and Marsh (623), who pointed out that it was based on only 234 reflections and refined to an R factor of only 19 %, even after assuming that there was disorder in the lattice. Schaefer and Marsh measured 1458 reflections from



and refined their proposed structure to an R value of 7.7 %. In this crystal, each oxygen is bonded to one cobalt as in Okaya's structure but in a trans



rather than a cis arrangement, which parallels that found in the diamagnetic compound (720):



The cobalt and oxygen atoms all lie in a plane, the Co—O—O angles are almost 120° , and the O—O bond length ($1.31 \pm 0.02 \text{ \AA}$) is close to what one would expect for the O_2^- superoxide ion. The Schaefer and Marsh structure appears to be well substantiated, but without further details of Okaya's work it is not possible to state for certain whether there are two geometrical isomers of this cation. One can say that it is in fact not a class II or class III-A mixed valence system at all, but rather an example of the extremely small group of metal complexes which have a radical ligand. Polarographic reduction studies have been reported for the various peroxy and peroxy-imino complexes (302, 415), but the reduction reactions are complicated and difficult to interpret. The complexes have also been considered as potential semiconductors (249) on the basis of the ease of transferring electrons to or from them, but it is clear from dielectric constant measurements that they are not.

A binuclear cyanide complex $[(\text{CN})_5\text{CoO}_2\text{Co}(\text{CN})_5]^{5-}$ has also been prepared (333) as a deep red potassium salt. The intense absorption band at $32,000 \text{ cm}^{-1}$ ($\epsilon = 6800$) probably corresponds to the band at $33,800 \text{ cm}^{-1}$ ($\epsilon = 10,000$) in $[(\text{NH}_3)_5\text{CoO}_2\text{Co}(\text{NH}_3)_5]^{5+}$, although, because of the higher position of cyanide in the spectrochemical series, no ligand field bands like those of the amine complex are seen.

By the action of HCN on Co(II) solution in an inert atmosphere, one obtains a rose-colored precipitate with a Co:CN ratio of 1:2.4 and an effective magnetic moment of 3.2–3.6 B.M. per cobalt atom (127, 555, 584). Numerous crystallographic studies of this (716, 717) and a related hydrate (247) have led to the conclusion that the compound is cobaltous cobalticyanide, i.e., that the valences are firmly trapped and the system is class II. $\text{Co}_3^{\text{II}}[\text{Co}^{\text{III}}(\text{CN})_6]_2$ has a cubic lattice isomorphous with the cobalticyanides of other divalent first transition metals and closely resembles that of Prussian blue. The diffuse reflectance spectrum of the compound (85) has been interpreted as a simple superposition of the ligand field bands of $[\text{Co}^{\text{III}}(\text{CN})_6]^{3-}$ and Co(III) octahedrally coordinated by the nitrogen ends of the cyanides. That there is no mixed valence absorption like that found in Prussian blue (591) indicates the greater difficulty of reducing a low-spin, $3d^6$ Co(III) ion than a high-spin, $3d^5$ Fe(III) ion.

G. NICKEL

Being almost the only mixed valence compound of nickel, the lithium-doped nickel oxide system has played a central role in our understanding of the electrical properties of mixed valence solids (described in Section

II). Pure, stoichiometric NiO is a green compound with a room temperature resistivity greater than 5×10^{14} ohm cm and an absorption spectrum in the visible region closely resembling that of $\text{Ni}(\text{H}_2\text{O})_6^{2+}$. When heated with lithium carbonate at 800°C , however, Li^+ ions replace a variable number of Ni(II) ions in the rock salt lattice, and a corresponding number of Ni(II) ions are oxidized to Ni(III). The solids so produced range from gray to black and are semiconductors with activation energies and room temperature resistivities which decrease sharply with increasing lithium content. Thus, the presence of 2% lithium in NiO lowers the room temperature resistivity of a pressed pellet to only 10^2 ohm cm (719). De Boer and Verwey (182) first suggested that such enhanced conductivity would arise only when ions of differing valency were present at crystallographically indistinguishable sites, and since then many others have applied this idea, both to Ni_{1-x}O (348, 351, 730) and to many other systems (see subsections D and F on manganese and cobalt, for example).

As regards the mixed valence classification of Ni_{1-x}O , the question is whether, in the ground state at absolute zero, the Ni(II) and Ni(III) ions can be distinguished, in which case the system belongs to class II, or whether it would be more appropriate to speak of holes in a conduction band consisting of $3d$ orbitals on the metal ions (class III-B). There have been several magnetic studies of lithium-doped nickel oxides (239, 378, 566), but the observed ferromagnetism of some samples (378, 566), which might have been correlated with coupling between the bound $3d$ electrons and the conduction electrons (813), most probably results from impurities. The most comprehensive study to date (296) reveals that, when less than 30% of the nickel has been replaced by lithium, the lattice is antiferromagnetic and cubic above the Curie temperature; but when the lithium content is higher, the lattice is rhombohedral and ferrimagnetic, probably because the lithium and nickel ions are partly ordered in alternate (111) planes. The moments within each plane are either ferromagnetically coupled or paramagnetic. On the assumption that all Ni—O—Ni interactions are antiferromagnetic, the variation in magnetization per molecule with composition is explained much better by assuming that the Ni(III) ions are low-spin, with the $t_{2g}^6 e_g^1$ configuration. Such a configuration, however, having only one electron in the e_g orbitals, will promote a tetragonal elongation (see the earlier example in Cr_2F_5), which will trap the valence and make the system class II. Thus, even though the presence of Ni(III) results in a vast decrease in resistivity, the indirect exchange mechanisms providing antiferromagnetic coupling between near neighbors appear to be of lower energy than Zener-type double exchange.

Although the ground state electronic structure of these oxides places them firmly in class II, there remains the question of the conduction mechanism. Verwey *et al.* (730) thought that conduction arose by the motion of a positive hole from Ni(III) to Ni(II), the activation energy being that required to ionize the hole on Ni(III) from neighboring lithium ions. That this is not the case follows from the fact (351) that, at very high lithium concentrations, the activation energy, although decreasing, does not tend to zero. Heikes and Johnston (351) later proposed that conduction should be regarded as a thermally activated diffusion process, in which the activation energy comes from the self-trapping of the hole by its polarization field (802) (described in Section II). Extensive series of conductivity and Seebeck effect measurements as a function of temperature and lithium content (719) were held to confirm Heikes and Johnston's view, but all these considerations have recently been placed in question by measurements of the Hall effect (816), which show it to be much larger than those calculated using the thermal diffusion (hopping) model. Further, and more damaging, the Hall mobility does not increase exponentially with temperature as the hopping model requires. A reconsideration of the previous Seebeck measurements, which were carried out on heavily lithium-doped samples, and new measurements on very lightly doped samples (80), have also led to the same conclusion. Whether these observations spell the demise of the hopping model altogether, or only for this system, remains very much to be seen. There is the possibility that a model similar to the one proposed by Frederikse (260) for slightly reduced rutile (see Section III,A on titanium) may prove appropriate, but a further factor that has to be kept in mind is the possibility of compound formation in the lightly doped nickel oxides. Thus semiconductivity plots have been published (433) for pellets of Ni_{1-x}O , with x as large as 0.12, giving room temperature resistivities as low as 10^2 ohm cm. However, a study (77) of the nickel-oxygen phase diagram does not reveal the existence of stoichiometric higher oxides, such as Ni_3O_4 .

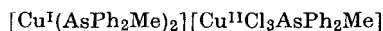
In addition to the Ni(II),Ni(III) oxides, one Ni(III),Ni(IV) system is known (453). The compounds $\text{BaNi}^{\text{IV}}\text{O}_3$ and $\text{Ba}_2\text{Ni}_2^{\text{III}}\text{O}_5$ are both black materials having low resistivities and magnetic moments, so the properties of the intermediate mixed valence phase $\text{Ba}_3\text{Ni}_2^{\text{III}}\text{Ni}^{\text{IV}}\text{O}_8$ will not be a clear guide to its classification.

H. COPPER

A wide variety of mixed valence copper compounds have been described, the majority containing halide ligands, although examples

with oxygen, nitrogen, and sulfur donors exist. Of the halides, a large number appear to fall into class I, in which the environments of the metal ions in the two oxidation states are very different and there are no bridging ligands. Thus, salts with empirical formulas $\text{Cu}_3\text{Br}_4(\text{pyr})_2$ and $\text{Cu}_3\text{Br}_4(\text{ant})_5(\text{H}_2\text{O})_6$ [pyr = dipyramidon, ant = antipyrine] were prepared some time ago by Souchay (672), who measured the conductivities of their solutions in acetone and concluded that they contained, for example, $[\text{Cu}^{\text{II}}(\text{pyr})_2]^{2+}$ and $[\text{Cu}^{\text{I}}\text{Br}_2]^-$. The colors of the solids (reported as dark green and yellow-green, respectively) are what one would expect for such a formulation. More recently, a large number of similar complexes were prepared (341–343) with simpler ligands, such as ammonia and ethylenediamine, which have the general formula $[\text{Cu}^{\text{II}}\text{A}_4][\text{Cu}^{\text{I}}\text{X}_2]_2$ or $[\text{Cu}^{\text{II}}\text{A}_4][\text{Cu}^{\text{I}}\text{X}_3]$. Compounds with similar formulas and presumably similar structures can also be prepared containing Cu(II) and Ag(I) (344–346), which, when vigorously shaken with water, decompose to AgX leaving $[\text{CuA}_4]^{2+}$ in solution. The chlorides and bromides were reported as deep blue or violet, but the iodides were all brown or black. Further compounds of the same type were prepared by Brauer and Eichner (90). Compounds in which X is CN^- have also been recognized for many years (513, 706) and other examples have been added more recently (506). Their colors suggest that they are all class I systems, with formulas analogous to those of the halides. Another class I cyanide containing one Cu(II) and two Cu(I) ions per mole has been reported by Cooper and Plane (146).

Attempts to prepare cupric complexes of methyldiphenylarsine (AsPh_2Me) always result in reduction of the copper to Cu(I), but Burrows and Sandford (115) isolated two compounds from the reaction, one blue and one brown, both of which appeared to have the empirical formula $\text{Cu}_2\text{Cl}_3 \cdot 3\text{AsPh}_2\text{Me}$. The original explanation offered for the apparent isomerism was in terms of ionic structures such as

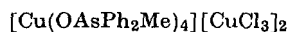


but, reinvestigating the reaction, Nyholm (540) found that the arsine had been oxidized, and that the analyses were much better described by the empirical formula $\text{Cu}_3\text{Cl}_4(\text{OAsPh}_2\text{Me})_4$. In nitrobenzene, the blue compound was an electrolyte, and the structural formula would appear to be



i.e., similar to the compounds containing ammonia and ethylenediamine discussed above. Because the blue compound became brown on storage, and also when exposed to chlorine gas, Nyholm concluded that the anion was oxidized to $[\text{Cu}^{\text{II}}\text{Cl}_3]^-$. Although the intensity of color of the brown

compound suggests that it may result from mixed valence absorption, this may perhaps be misleading, since on prolonged exposure to chlorine a red compound analyzing as



was isolated. Since all the copper in this compound is divalent, the color of this and possibly the other mixed valence compound may be related to that of red CsCuCl_3 .

A series of chlorocuprates (I,II) in which the color is clearly due to mixed valence absorption was first prepared by Mori (516). When hexaminecobalt(III) chloride solution is added to an aqueous solution of either CuCl or CuCl_2 containing excess chloride ions, orange-yellow crystals are obtained, but if the solution contains both CuCl and CuCl_2 the resulting crystals are brown or black, depending on the mole fraction of each valence state present. By measuring diffuse reflectance spectra, Mori found the new absorption band in the mixed valence material to be near $17,000 \text{ cm}^{-1}$ (518), and its intensity was shown by the same method to be proportional to the product of the mole fractions of the two valence states (171). The crystal structures of the two single valence compounds are closely related, so that both valence states may be present in a crystal in any proportion with only minor structural variations. The chlorocuprate(II) has the formula $\text{Co}(\text{NH}_3)_6\text{CuCl}_5$, with a structure based on a cubic rock salt lattice of $[\text{Co}(\text{NH}_3)_6]^{3+}$ and $[\text{Cu}^{\text{II}}\text{Cl}_5]^{3-}$ ions (517), but the cuprous salt has the much more complicated formula, $[\text{Co}(\text{NH}_3)_6]_4\text{Cu}_5^{\text{I}}\text{Cl}_{17}$. Its crystal structure, however, is also cubic with $[\text{Co}(\text{NH}_3)_6]^{3+}$ and $\text{Cu}(\text{I})$ ions forming a rock salt lattice. Each $\text{Cu}(\text{I})$ is surrounded by four chloride ions, one of which forms a bridge to a $\text{Cu}(\text{I})$ at the body center of the cubic unit cell (522) (Fig. 18). Thus, the anion is a pentamer, $[\text{Cu}_5\text{Cl}_{16}]^{11-}$, considered as derived formally from condensation of four $[\text{CuCl}_4]^{3-}$ anions through addition of a fifth $\text{Cu}(\text{I})$. When compounds are formed containing only a small mole fraction of $\text{Cu}(\text{I})$, it may be presumed that it enters the $[\text{Cu}^{\text{II}}\text{Cl}_5]^{3-}$ lattice as $[\text{Cu}^{\text{I}}\text{Cl}_4]^{3-}$, but at higher mole fractions of $\text{Cu}(\text{I})$ there is an increased probability of finding four $[\text{CuCl}_4]^{3-}$ ions on adjacent, tetrahedrally related sites, and then $[\text{Cu}_5\text{Cl}_{16}]^{11-}$ may be formed by incorporating an extra $\text{Cu}(\text{I})$ and a chloride ion at another site (Fig. 19). The formula variation with mixed valence composition which this model suggests is substantiated by chemical analyses (179). It is worth noting that, apart from nonstoichiometric and doped oxides, these class II chlorocuprates(I, II) are among the very small number of systems in which the proportions of two valence states may be varied over the whole range of composition from 100% of one to 100% of the other.

MIXED VALENCE CHEMISTRY

315

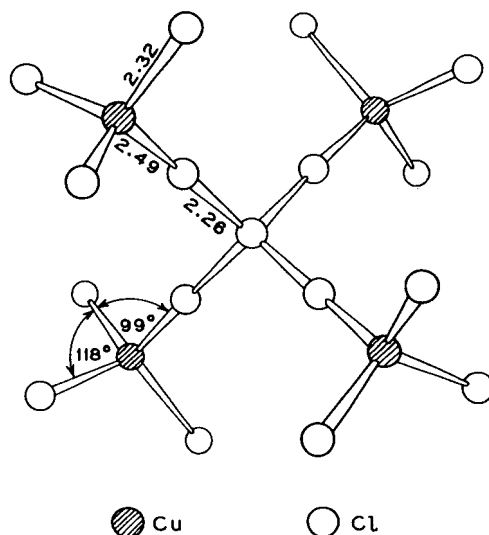


FIG. 18. Bond distances (Å) and angles in the $[\text{Cu}_5\text{Cl}_{16}]^{11-}$ ion (522).

The electrical resistivities of the chlorocuprates(I,II) have also been investigated (171). They are high resistance semiconductors, and at room temperature the specific conductivities, like the interaction absorption intensities, were proportional to the product of the mole fractions

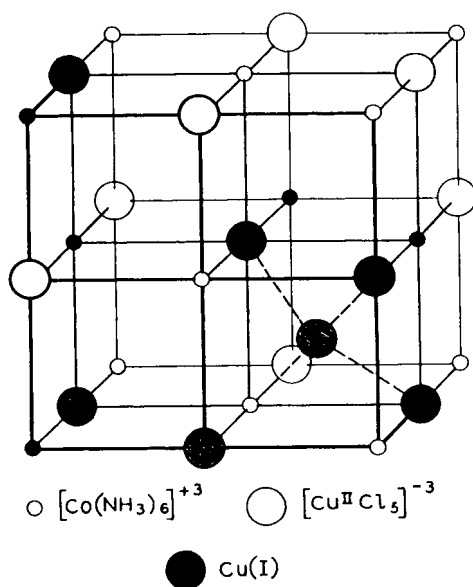


FIG. 19. The distribution of metal atoms in the mixed valence hexamminecobalt chlorocuprate(I,II) crystal.

of the two valence states. Plots of the mixed valence absorption intensity and room temperature resistivity as a function of the mole fraction of Cu(I) are shown in Fig. 20. As was also found with the interaction absorption energy, the semiconduction activation energy did not vary with mixed valence composition, although the value obtained was different from that for either of the single valence chlorocuprates. It was also reported that, unlike either single valence salt, all the mixed valence chlorocuprate salts obeyed Ohm's law quite accurately.

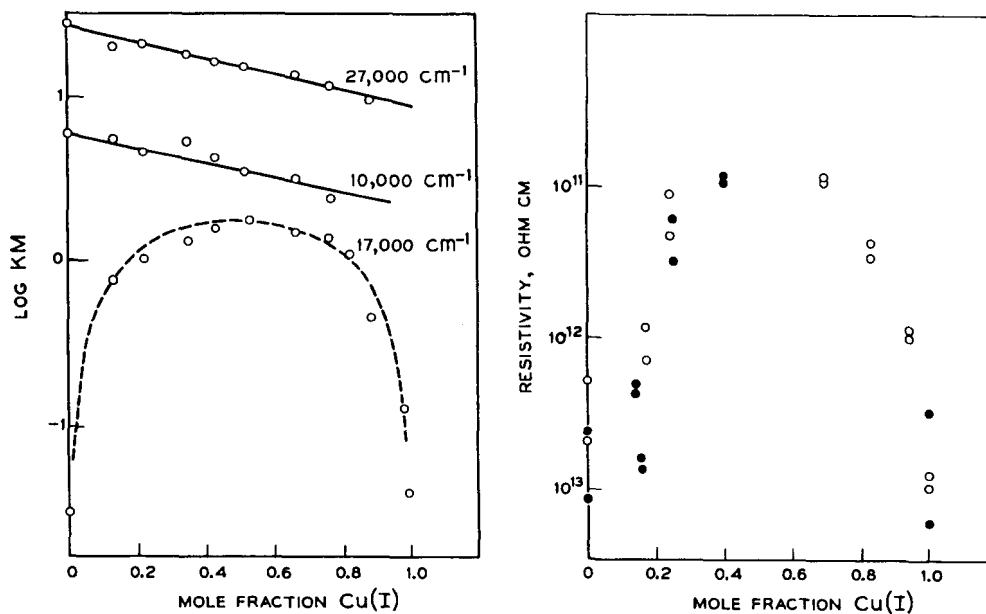
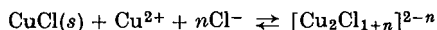


FIG. 20. The intensity of reflected light at three frequencies, and the room temperature resistivity of solid hexaminecobalt(III) chlorocuprates(I,II) as a function of the mole fraction of copper as Cu(I) in the sample (171).

Mixed valence copper chloro complexes have also been extensively studied in aqueous solution. Doehlemann and Fromherz (200) were the first to show that addition of CuCl to a solution of CuCl₂ in 10 M HCl caused a marked increase in absorption in the visible region (Fig. 21). It is of interest that the difference in the spectra of a mixed valence solution and two single valence solutions of equivalent concentration has a maximum at 18,000 cm⁻¹, close to that of the solid chlorocuprates(I,II) discussed above. It is clear from this figure and from Fig. 20 that the bands at 10,000 cm⁻¹ and 27,000 cm⁻¹ are Cu(II) constituent ion absorptions. Diehl *et al.* (195) demonstrated that the interaction complex contained equal amounts of Cu(I) and Cu(II). In an effort to determine the formula and association constant of the species responsible

for the mixed valence light absorption, McConnell and Davidson (496) worked at higher dilutions so that they could make use of previously determined association constants for the single valence chloro complexes. For solutions saturated with CuCl, they assumed that the equilibrium was



and found that, in solutions containing up to 0.30 *M* Cu(II) and 0.40 *M* chloride ion, *n* was very close to 2. At higher copper and chloride concentrations, *n* began to increase, and it was noticeable that the difference

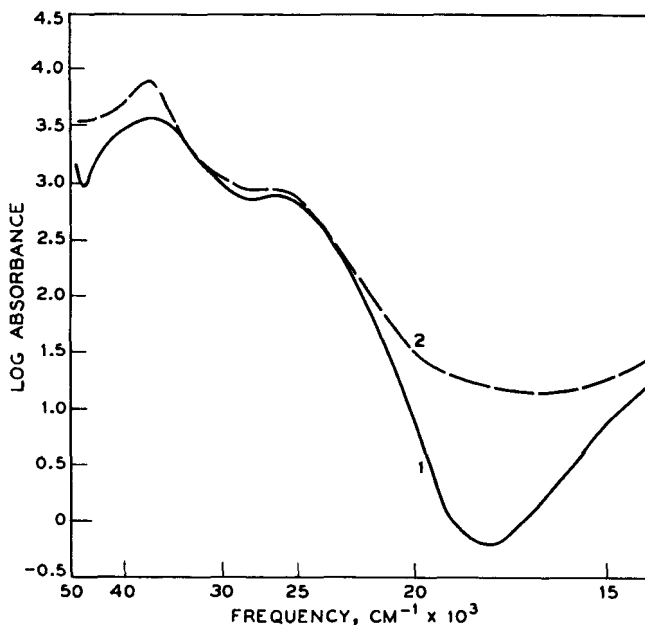


FIG. 21. The electronic spectra of 5.18 *M* solutions of CaCl_2 containing (1) 0.47 *M* Cu(II), and (2) 0.235 *M* Cu(II) and 0.273 *M* Cu(I) (200).

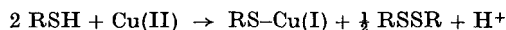
spectrum shifted to lower energy, approaching that found by Doehlemann and Fromherz. The formula of the interaction complex, Cu_2Cl_3 , alone does not permit a distinction between bridged or outer-sphere arrangements, since there is no indication of the manner in which the coordination spheres of the two metal ions are completed by water molecules. If the absorption band in the solid chlorocuprates(I, II) is due to an intermolecular (outer-sphere) charge transfer between $[\text{Cu}^{\text{II}}\text{Cl}_5]^{3-}$ and either $[\text{Cu}^{\text{I}}\text{Cl}_4]^{3-}$ or $[\text{Cu}_5^{\text{I}}\text{Cl}_{16}]^{11-}$, depending on the composition, then the fact that its energy is so similar to that of the mixed valence complex in solution suggests that the latter may also be an outer-sphere complex.

The rate of electron transfer between Cu(I) and Cu(II) in concentrated HCl solution was measured by McConnell and Weaver (498) in one of the first experiments to use NMR line broadening for this purpose. The ^{63}Cu resonance in a 1 *M* solution of CuCl in concentrated HCl was completely flattened by adding Cu(II) ions to a concentration of 10^{-2} *M*, which, using the theory worked out by McConnell and Berger (499), gave a bimolecular rate constant equal to 0.5×10^8 liter mole $^{-1}$ sec $^{-1}$, one of the highest ever measured up to that time. Unfortunately, however, it is not clear to which transition state this rate constant refers.

One of the first mixed valence copper compounds to be prepared was Chevreul's salt, $\text{Cu}_2\text{SO}_3 \cdot \text{CuSO}_3 \cdot 2\text{H}_2\text{O}$ (91a, 137). A recent determination of the crystal structure (418) places the compound in class I since the Cu(II) ions are surrounded by a distorted octahedron of oxygen atoms, two from water molecules at 1.92 Å and four from the sulfite ions, two at 2.03 Å and two at 2.47 Å, whereas the Cu(I) ions have a very different environment from the Cu(II) ions, being within a distorted tetrahedron consisting of three sulfite oxygen atoms (2.11–2.14 Å) and a sulfur atom (2.14 Å). The compound is reported to be red, but since the crystal structure shows it to be class I the color is most likely that of the constituent cupric sulfite. A related compound, Rogojski's salt, $\text{Cu}_2\text{SO}_3 \cdot \text{H}_2\text{O}$, was found by X-ray powder photography to be a mixture of Chevreul's salt and metallic copper (173).

A mixed valence copper thiosulfate salt, $\text{NaCu}^{\text{II}}\text{Cu}^{\text{I}}(\text{S}_2\text{O}_3)_2$, has been reported (663), but its blue-green color suggests that it belongs to class I, like the aminothiosulfate salt prepared by Ferrari *et al.* (243, 248). The structure of the latter, recently determined, contains well separated $[\text{Cu}^{\text{II}}(\text{NH}_3)_4]^{2+}$ square planar ions and $[\text{Cu}_n^{\text{I}}(\text{S}_2\text{O}_3)_{2n}]^{3n-}$ polyanions in which each Cu(I) is surrounded by four thiosulfate groups while each thiosulfate bonds two Cu(I) ions.

Because of their intense colors, a number of biological copper-containing compounds have been thought to contain the element in both valence states. Klotz *et al.* (429) investigated the reaction between thiomalic acid, $\text{HOOC}-\text{CH}_2-\text{CH}(\text{SH})-\text{COOH}$, and Cu(II) ions as a model system for hemocyanin, an oxygen-carrying protein. The intense violet color, similar to that of hemocyanin, appeared only when the Cu(II): thiomalate ratio reached 0.5, so assuming that the initial reaction was



the color could have been due to a mixed valence complex $\text{Cu}^{\text{II}}(\text{RSCu}^{\text{I}})_4$. About 20% of the copper in the violet complex could be extracted with penten, following which the violet color was replaced by the blue color

of the Cu(II)-penten complex. The absorption spectrum of the violet complex has a single broad band at $19,200\text{ cm}^{-1}$ with an extinction coefficient of 6000 per $\text{Cu}_5(\text{SR})_4$ unit, indicating the presence of a class II species with appreciable delocalization, if indeed this band is a mixed valence absorption. From the violet solution a gray solid has been isolated (668), which is reported to have a Cu:SR ratio of 5:4, and a room temperature magnetic moment of 2.13 B.M. per Cu(II). Thio-glycolic acid and β -mercaptoethylamine both give similar violet colors, but β -mercaptopropionic acid and cysteine do not.

Ceruloplasmin, another intensely blue copper protein, contains eight copper atoms per molecule, of which approximately four could be exchanged with ionic Cu(II) and four reacted with biquinolyl, as is characteristic of Cu(I) (75). When all the copper is in the reduced state, the compound is colorless and diamagnetic, but in partially reduced samples the intensity of the visible absorption band at $16,400\text{ cm}^{-1}$ is proportional to that of the ESR absorption. The hyperfine splitting of the latter shows that the Cu(II) are magnetically dilute, but there remained the possibility that the color was due to mixed valence absorption, with the Cu(I) and Cu(II) in slightly different environments (class II) (75). However, a number of instances have since been discovered of copper proteins having optical and ESR properties similar to those of ceruloplasmin, but which contain only one copper atom per molecule (487). Thus, if ceruloplasmin is a mixed valence compound, the metal atoms of differing valence are sufficiently separated for there to be no detectable interaction between them in the ground or excited state, i.e., the system is class I.

For reasons set out at the beginning of this section, we have not generally included sulfides among the mixed valence systems reviewed here. Nevertheless, there are a number of copper sulfides whose mixed valence nature is clear enough to be worth mentioning. Of these, the most famous is probably the mineral covellite, CuS, the structure of which was investigated in some detail by Berry (61). This deep blue compound is not, as the formula implies, a simple Cu(II) salt, but contains both S^{2-} and S_2^{2-} ions as well as copper atoms in two distinctly different coordination sites, one planar triangular and the other tetrahedral. It appears from the crystal structure that the correct formulation is $\text{Cu}_4^{\text{I}}\text{Cu}_2^{\text{II}}(\text{S}_2)_2\text{S}_2$. The fact that covellite is a metal, and below 1.35°K a superconductor (111), shows either that covellite is an inverse structure (class III-B) with both Cu(I) and Cu(II) in the tetrahedral sites, or that one cannot draw firm conclusions about mixed valence class behavior from the crystal structures of highly covalent materials.

The series of dark blue mixed valence compounds $\text{Na}_2\text{Cu}_3\text{S}_3$,

$K_3Cu_8S_6$, KCu_4S_3 , and $RbCu_4S_3$ can be made by fusing copper metal, an alkali metal carbonate, and sulfur at various temperatures (605). Whereas the stoichiometries of these materials suggest that, of the m copper ions in each molecule, one is Cu(II) and $m-1$ are Cu(I), the crystal structures of isostructural KCu_4S_3 and $RbCu_4S_3$ (Fig. 22) show that all the copper atoms in these crystals are in equivalent ligand fields of sulfur atom tetrahedra, which form sheets separated by the alkali

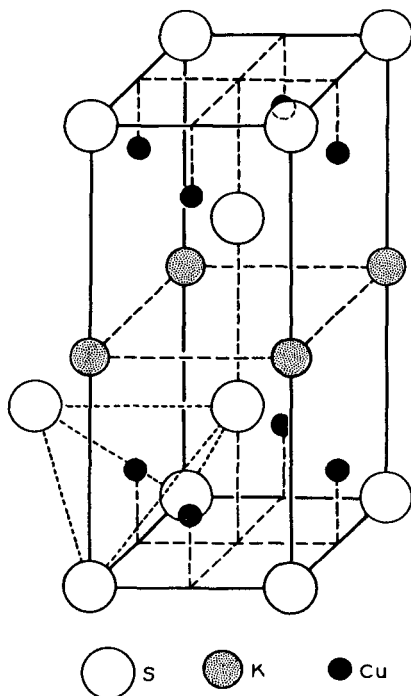


FIG. 22. The class III-B crystal structure of KCu_4S_3 , demonstrating the equivalence of the Cu(I,II) ions in the tetrahedral sites (605).

metal ions. Within the sheets, the copper-copper spacing is 2.76 Å, and not surprisingly these class III-B compounds are good conductors, with resistivities at 20°C of 2.5×10^{-2} and 1.7×10^{-2} ohm cm for KCu_4S_3 and $RbCu_4S_3$, respectively. Inasmuch as $Na_2Cu_3S_3$ and $K_3Cu_8S_6$ have resistivities comparable to those of KCu_4S_3 and $RbCu_4S_3$, these compounds may also have class III-B structures.

Gmelin's *Handbuch* lists many other supposed Cu(I),Cu(II) compounds, including sulfites and amino-cyanides, as well as more bizarre compounds such as $Cu_2Cl(VO_3)_2$, the majority of which were prepared over 50 years ago, and have not been investigated since. A random example is $Cu_7^I Cu_2^{II} Fe_3(CN)_{14} \cdot 2H_2O$ (?) (*sic*), prepared (645) as a black

shiny mass in 1856! We are unable to pass judgement on the status of these substances.

I. ZIRCONIUM AND HAFNIUM

Doubtless as a result of the extremely reducing character of the lower oxidation states of these two elements, there are no compounds of either which have ever been considered as possible mixed valence systems.

J. NIOBIUM AND TANTALUM

The mixed valence halides of niobium and tantalum, numbering over twenty with many as yet only briefly investigated, offer an interesting area for the experimental and theoretical study of mixed valence chemistry. It has become apparent during the last 5–10 years that a remarkable number of these compounds have in common a structural unit of high stability and most interesting electronic structure. It is with the properties of this structural unit that we will be almost totally occupied in dealing with the halides.

The first of the niobium and tantalum mixed valence halides synthesized have since proved to have the composition $M_6X_{14} \cdot 7H_2O$. The fact that the niobium and tantalum compounds of this composition yield only one seventh of their halide ions to aqueous silver nitrate (134, 340) was an early indication that these solutions contain the $[M_6X_{12}]^{2+}$ complex ion. In support of this conclusion, Vaughan, Sturdivant, and Pauling (724) later found that the X-ray diffraction patterns obtained from alcoholic solutions of $Nb_6Cl_{14} \cdot 7H_2O$, $Ta_6Cl_{14} \cdot 7H_2O$, and $Ta_6Br_{14} \cdot 7H_2O$ were interpretable as due to scattering by a polynuclear ion, the idealized structure of which has six metal ions at the face centers of a cube and twelve halide ions at the midpoints of the cube edges (Fig. 23). Single crystal X-ray work has since confirmed this structure of the $[M_6X_{12}]^{2+}$ ion and proved its presence in a number of other niobium and tantalum subhalides. Most recently it has been found that many of the $[M_6X_{12}]^{2+}$ ions can be oxidized to net charge 3+, 4+, and, in one case, a reported 5+, without change of the basic geometry, thereby increasing considerably the number of compounds containing the mixed valence M_6X_{12} structural unit. Many of these mixed valence niobium and tantalum subhalides are discussed in the recent metal-metal bonding review of Schäfer and Schnering (627).

According to the X-ray scattering data (724), the $[\text{Nb}_6\text{Cl}_{12}]^{2+}$ ion in solution has cis Nb—Nb distances of 2.85 Å and Nb—Cl distances of 2.41 Å, the former indicating appreciable metal-metal interaction in view of the 2.86-Å Nb—Nb distance in niobium metal. The authors admit, however, that there is little evidence that the symmetry of the complex ion is as high as they describe it. Indeed, the single crystal study of the anhydrous salt $\text{Nb}_6\text{Cl}_{14}$ (665) shows that in this material the $[\text{Nb}_6\text{Cl}_{12}]^{2+}$ octahedron is compressed along a fourfold axis so as to yield cis Nb—Nb distances from 2.89 to 2.95 Å, and Nb—Cl distances from 2.40 to 2.58 Å.

$\text{Nb}_6\text{Cl}_{14}$ has no free spins, its paramagnetism being of the temperature-independent type ($\chi_{\text{mol}} = 579 \times 10^{-6}$ cgs, corrected for diamagnetism) (665). The heptahydrate, however, has been reported to have an effective moment of 1.48 B.M. as deduced from the Curie-Weiss behavior of the susceptibility (443). Robin and Kuebler (593), however, found this material to have a temperature-independent paramagnetism ($\chi_{\text{mol}} = 850 \times 10^{-6}$ cgs, corrected for diamagnetism) in the temperature range 42°–290°K. In support of a closed-shell ground state configuration for the $[\text{Nb}_6\text{Cl}_{12}]^{2+}$ ion, Mackay and Schneider (471) also find a temperature-independent paramagnetism ($\chi_{\text{mol}} = 456 \times 10^{-6}$ cgs, corrected for diamagnetism) in the double salt $[(\text{C}_2\text{H}_5)_4\text{N}]_4\text{Nb}_6\text{Cl}_{18}$.

Chemically, $[\text{Nb}_6\text{Cl}_{12}]^{2+}$ is rather stable and can be used as a cationic species for the formation of compounds such as $\text{Nb}_6\text{Cl}_{12}(\text{OH})_2 \cdot 8\text{H}_2\text{O}$ and $\text{Nb}_6\text{Cl}_{12}\text{Br}_2 \cdot 7\text{H}_2\text{O}$ (340). The $[\text{Nb}_6\text{Cl}_{12}]^{2+}$ ion has also found use as a "heavy atom" in the X-ray analysis of the structure of wet lysozyme chloride (157). It has been suggested (10) that in alkaline solution the $[\text{Nb}_6\text{Cl}_{12}(\text{OH})_4]^{2-}$ ion forms, and that hydroxyl groups may even be introduced as bridges replacing the chloride ions. The deep green aqueous solution of $\text{Nb}_6\text{Cl}_{14}$ can be oxidized with I_2 in a two-electron step (493), with only the first electron being lost, however, in alcoholic solutions (471).

The oxidized species $[\text{Nb}_6\text{Cl}_{12}]^{3+}$ has been isolated as the double salt $[(\text{C}_2\text{H}_5)_4\text{N}]_3\text{Nb}_6\text{Cl}_{18}$ (471), and has an effective magnetic moment (1.61 B.M.) corresponding closely to that expected for one unpaired electron. The ESR spectrum of the $[\text{Nb}_6\text{Cl}_{12}]^{3+}$ ion shows a symmetrical 49-line pattern, which is that expected if the unpaired electron has the same hyperfine interaction with all six niobium nuclei (spin 9/2). Further oxidation yields $[(\text{C}_2\text{H}_5)_4\text{N}]_2\text{Nb}_6\text{Cl}_{18}$, a compound with an effective moment of 0.47 B.M. Because Mackay and Schneider presume that this compound is, in fact, diamagnetic but contains a large amount of paramagnetic impurity, its true susceptibility is still open to question.

In alcoholic solution, the $[\text{Ta}_6\text{Cl}_{12}]^{2+}$ ion also has the structure shown

in Fig. 23, with the cis Ta—Ta distances amounting to 2.88 Å and the Ta—Cl distances to 2.44 Å (724). The recent crystallographic study of the heptahydrate $\text{Ta}_6\text{Cl}_{14} \cdot 7\text{H}_2\text{O}$ by Burbank (113) shows that the crystal contains one molecule per unit cell (probably $P\bar{3}1m$) with both disorder and stacking faults present. In this material, the $[\text{Ta}_6\text{Cl}_{12}]^{2+}$ ion appears as a distorted octahedron, principally tetragonally extended, with the nonbridging chloride ions coordinated to the tantalums on the tetragonal fourfold axis. The cis Ta—Ta bond distances range from 2.63 to 3.27 Å and the bridging Cl to Ta distances range from 2.28 to 2.72 Å, thereby demonstrating not only a distortion of the $[\text{Ta}_6\text{Cl}_{12}]^{2+}$ ion, which is much larger than that measured (665) for the $[\text{Nb}_6\text{Cl}_{12}]^{2+}$ ion, but which also

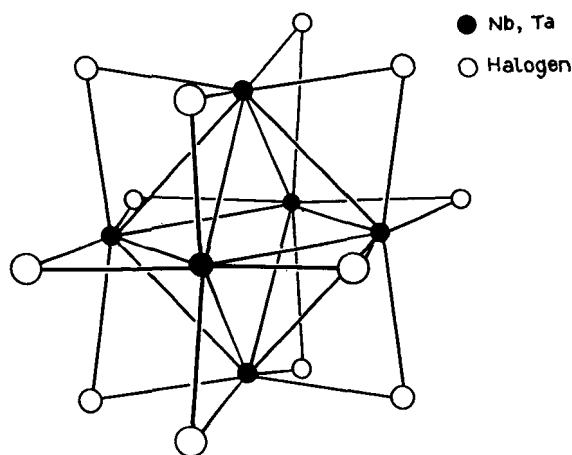


FIG. 23. The idealized geometry of the niobium and tantalum subhalide ions, $[\text{M}_6\text{X}_{12}]^{n+}$, showing the metal atom octahedron and bridging halide ions.

has a different sense to the tetragonality. Careful analytical work on the "heptahydrate" of $\text{Ta}_6\text{Cl}_{14}$ suggests that the true formula is instead $\text{Ta}_6\text{Cl}_{14} \cdot 8\text{H}_2\text{O}$ (630).

As with $\text{Nb}_6\text{Cl}_{14} \cdot 7\text{H}_2\text{O}$, the tantalum analog was first reported to have an effective moment of 1.39 B.M. (443), whereas later work (593) showed that this substance had a zero susceptibility, implying a temperature-independent paramagnetism equal to the diamagnetic correction. The close similarity in properties of the niobium and tantalum subhalides suggests that, like $\text{Nb}_6\text{Cl}_{14} \cdot 7\text{H}_2\text{O}$, $\text{Ta}_6\text{Cl}_{14} \cdot 7\text{H}_2\text{O}$ has a closed-shell ground state.

Reduction of TaCl_5 with aluminum foil in the appropriate temperature gradient yields the greenish brown material $\text{Ta}_6\text{Cl}_{15}$ (447). X-ray (626) and magnetic susceptibility (626, 665) measurements show the presence of the $[\text{Ta}_6\text{Cl}_{12}]^{3+}$ ion having one free spin. The same species is

produced as a stable ion in solution by the oxidation of $[\text{Ta}_6\text{Cl}_{12}]^{2+}$ by either Fe^{3+} or Cl_2 , and probably by O_2 as well (226, 493). Ferric ion can further oxidize the 3+ ion to 4+ in aqueous solution, from which the diamagnetic salt $\text{Ta}_6\text{Cl}_{16} \cdot 9\text{H}_2\text{O}$ can be recovered (226, 494).

Air oxidation of ethanolic solutions of $\text{Nb}_6\text{Cl}_{14} \cdot 8\text{H}_2\text{O}$ results in the formation of $\text{Nb}_6\text{Cl}_{16} \cdot 3\text{C}_2\text{H}_5\text{OH}$, which was demonstrated to contain the $[\text{Nb}_6\text{Cl}_{12}]^{4+}$ ion by the close similarity of its optical spectrum to that of the $[\text{Nb}_6\text{Cl}_{12}]^{2+}$ ion (681). More will be said of this similarity below. Surprisingly, the anhydrous, green niobium subhalide $\text{Nb}_6\text{Cl}_{16}$ does not contain the M_6X_{12} structural unit, but rather has a layered lattice much like that of CdI_2 with only 3/4 of the metal sites filled (733). The Nb—Nb distance within the metal atom layer is 2.78 Å (638), a distance significantly smaller than that in $\text{Nb}_6\text{Cl}_{14}$. The substance, better written as Nb_3Cl_8 , however, may not be metallic as is Ag_2F with the anti- CdI_2 structure (class III-B), for it is reported (638, 666) that the niobiums are grouped into triplets (class III-A), and that the effective magnetic moment amounts to 1.83 B.M., as expected for an isolated Nb_3Cl_8 molecule containing an odd number of d electrons. Actually, Nb_3Cl_8 is the end member of a homogeneous mixed valence system of considerable breadth, the other end member being NbCl_4 . This presents the interesting possibility that NbCl_3 is really a mixed valence compound, being composed of equal parts of Nb_3Cl_8 and NbCl_4 (638, 648).

The niobium oxychloride $\text{Nb}_3\text{O}_7\text{Cl}$ presents another possibility as a mixed valence system, for when it is prepared in an oxidizing atmosphere it is colorless, as expected for a $4d^0$ system, but when prepared in the absence of O_2 the product presumably contains lower oxides of niobium and is colored blue. Identical color changes have been observed in the preparation of the $4d^0$ systems Nb_2O_5 and NbOCl_3 (624).

The mixed valence niobium and tantalum subbromides present little that is new and interesting. $\text{Nb}_6\text{Br}_{14} \cdot 7\text{H}_2\text{O}$ possesses a temperature-independent paramagnetism, as does the corresponding tantalum compound (593). Just as was found with the chloride of this composition, $\text{Ta}_6\text{Br}_{15}$ has one free spin (628, 629) and the $[\text{Ta}_6\text{Br}_{12}]^{2+}$ ion in aqueous solution can be oxidized with Fe^{3+} or Br_2 to $[\text{Ta}_6\text{Br}_{12}]^{4+}$ (593). An extensive phase study revealed that, in addition to the $\text{Ta}_6\text{Br}_{14}$ (green) and $\text{Ta}_6\text{Br}_{15}$ (black) compounds, an even higher bromide, $\text{Ta}_6\text{Br}_{17}$, can exist (492), but there is no other information on this substance.

$\alpha\text{-Nb}_3\text{Br}_8$ is isostructural with the chloride, and our comment about "NbCl₃" would apply also to "NbBr₃" (56, 625). Simon and von Schnering (666) report the preparation and properties of a second form of Nb_3Br_8 , the β -form. The black crystals of this substance have a temperature-dependent effective magnetic moment (0.5 B.M. at 90°K, 1.95 B.M.

at 573°K), and a structure composed of Nb_3 triangular units having an irregular octahedron of halide ions about each niobium ion. As with $\text{Nb}_6\text{Br}_{14}$, there appears to be appreciable metal-metal bonding in the $\beta\text{-Nb}_3\text{Br}_8$ system, judging from the 2.88-Å separation between niobium atoms. The system is class III-A.

The preparation and properties of the mixed valence fluoride Nb_6F_{15} have recently been described (629). In this material, the $[\text{Nb}_6\text{F}_{12}]^{3+}$ groups have full octahedral symmetry, with all six of the niobiums of an octahedron being bridged to niobium atoms of other octahedra by fluoride ions. Within an octahedron, the cis Nb—Nb distance is 2.80 Å, and Nb—F equals 2.05 Å. The magnetic properties of Nb_6F_{15} have not yet been reported, but one expects one free spin per Nb_6 , just as has been found for $\text{Ta}_6\text{Cl}_{15}$, $\text{Ta}_6\text{Br}_{15}$, and $[(\text{C}_2\text{H}_5)_4\text{N}]_3\text{Nb}_6\text{Cl}_{18}$. The diamagnetism of the niobium and tantalum tetrahalides $\text{M}^{\text{IV}}\text{X}_4$ has recently been explained as due to a spin-pairing dimer formation, and not to the mixed valence M(III),M(V) configuration suggested earlier (600). However, since NbF_4 does not have the dimer structure and yet has a temperature-independent paramagnetism (299, 629), the mixed valence formulation is a possibility here. As described above for the chlorides, a niobium oxyfluoride $\text{Nb}(\text{O},\text{F})_3$ also exists as a blue material (629).

The lower iodide of niobium, Nb_6I_{11} , presents an interesting variation of the subhalide structural unit (46, 48, 631, 665). In this material the six niobiums are approximately at the face centers of a cube, with the bridging halogen not at the centers of the cube edges, but instead at the cube corners, each iodide thereby bridging three niobium ions. This ideal structure is in fact distorted in the crystal to symmetry C_i , with an average Nb—Nb distance of 2.85 Å. This is surprisingly close to the Nb—Nb distances found in the $[\text{Nb}_6\text{X}_{12}]^{2+}$ ions. A more regular geometry prevails for the lower tantalum iodide. Ta_6I_{14} , the only lower iodide of tantalum (447, 492, 628), is structurally isotypic with $\text{Nb}_6\text{Cl}_{14}$ and shows a weak temperature-independent paramagnetism (48, 665). The black solid gives a green aqueous solution containing the $[\text{Ta}_6\text{I}_{12}]^{2+}$ ion, which, however, is not as stable as those of the other halides in this series. Whereas it was first thought that Nb_3I_8 might be composed of diamagnetic $[\text{Nb}_6\text{I}_{12}]^{4+}$ units, it is now known to have a trinuclear class III-A structure identical to that of $\beta\text{-Nb}_3\text{Br}_8$ and, like this substance, has a temperature-dependent effective magnetic moment (666).

The $[\text{M}_6\text{X}_{12}]^{2+}$ unit contains 16 metal d electrons in molecular orbitals formed from combinations of the metal atom d orbitals and the halide ligand p orbitals. If all the metal ions are in equivalent sites so as to form a class III-A system, then each metal atom has a formal valence of $2\frac{1}{3}+$. If, however, the $[\text{M}_6\text{X}_{12}]^{2+}$ ion is distorted so as to distinguish

two of the metal atoms from the other four, then these two may be assigned an integral valence of 3+ and the other four an integral valence of 2+, making the system class II. A trapping of the valence could almost be guaranteed in the mixed ion $[\text{Ta}_4\text{Nb}_2\text{X}_{12}]^{2+}$ if it could be made. Schäfer and Spreckelmeyer (632) made a start in this direction, having prepared a substance of the overall composition $\text{Ta}_{3.6}\text{Nb}_{2.4}\text{Br}_{14} \cdot 8\text{H}_2\text{O}$ with an optical spectrum different from that of a simple mixture of $\text{Nb}_6\text{Br}_{14} \cdot 8\text{H}_2\text{O}$ and $\text{Ta}_6\text{Br}_{14} \cdot 8\text{H}_2\text{O}$. To date, the determination of the mixed valence class and valence configurations of the $[\text{M}_6\text{X}_{12}]^{2+}$ polynuclear ions has been attempted using a simplified ligand-field theory analysis of optical spectra and magnetic susceptibility data together with X-ray structure analysis.

Cotton and Haas (159) first derived the molecular orbital ordering appropriate to the $[\text{M}_6\text{X}_{12}]^{2+}$ unit on the assumption that this ordering is determined, with one exception, solely by the various metal-metal interactions. From overlap considerations, they decided that the level ordering depended upon the internuclear separation and the effective nuclear charge, but that, for reasonable values of these parameters, a ground state³ with occupation

$$dxzdyz(t_{1u})^6 dz^2(a_{1g})^2 dxzdyz(t_{2g})^6 dxy(a_{2u})^2$$

was predicted, which is diamagnetic, as observed for the $[\text{M}_6\text{X}_{12}]^{2+}$ ions. The Cotton-Haas orbital diagram (Fig. 24) is derived under the assumption that the orbitals arising from $dx^2 - y^2$ are too high to be of any consequence, due to σ -bonding with the ligands. Kettle (414) concurs with Cotton and Haas as to the symmetries of the occupied levels. A second calculation on this system, which considered not only metal-metal but metal-ligand interactions as well (593), showed that the relative positions of the Cotton-Haas orbitals can depend not only upon the metal-metal interaction, but also upon the metal-ligand interaction. Thus, for example, for the MO's composed of metal atom dxy orbitals only, the level ordering is $a_{2u} < t_{2g} < e_u$, whereas, with the introduction of ligand orbitals into the calculation, an inverted ordering $e_u < t_{2g} < a_{2u}$ can be obtained. The MO's resulting from the "metal d plus ligand orbitals" calculations are shown in Fig. 25, for comparison with the original Cotton-Haas scheme. This second scheme, as proposed

³ Each molecular orbital of the ground state is composed of a linear combination of only certain of the d orbitals of the metal atoms. Thus, for example, taking z as the locally out-of-plane direction, a linear combination of dxz and dyz metal orbitals can be found which transforms like t_{1u} in the octahedral group, and, if it contains six electrons, is written as $dxzdyz(t_{1u})^6$. Similarly, in the ground state the a_{1g} combination of dz^2 orbitals has two electrons in it, etc.

originally, was constructed so as to give a reasonable explanation of the electronic spectra of the $[M_6X_{12}]^{2+}$ ions. In order to do this, it was found that an apparently low-lying $dz^2(a_{1g})$ orbital had to be left unoccupied in the ground state. This undesirable feature arises from the assumption

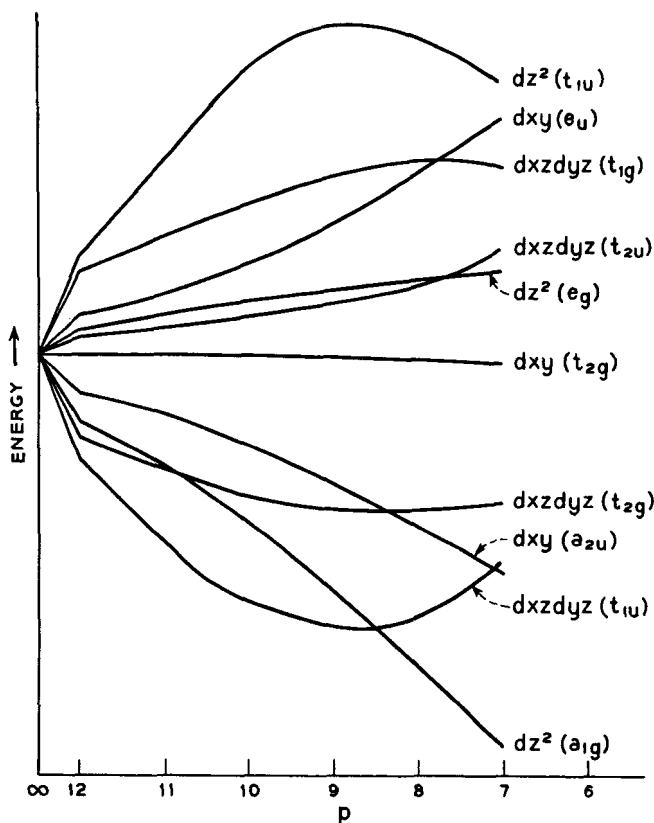


FIG. 24. The molecular orbital scheme for the $[M_6X_{12}]^{2+}$ ion as derived by Cotton and Haas (159). p is a variable equal to the product of the Slater orbital exponent of the metal d orbitals and the metal-metal distance.

that each metal atom is in the plane of the four halide ligands nearest it (local symmetry C_{4h}), when in fact the metal atoms are known to be displaced inward toward each other. As a result, the local symmetry is lowered to C_{4v} , and two of the three p orbitals on each ligand interact with the dz^2 manifold, raising it by an undetermined amount. Thus the closed-shell ground state configuration



is attained without occupying $dz^2(a_{1g})$.

On oxidation to $[M_6X_{12}]^{3+}$, both Figs. 24 and 25 predict an ion having one free spin, as observed experimentally. The real test between these two diagrams rests on the prediction for the ion $[M_6X_{12}]^{4+}$. According to

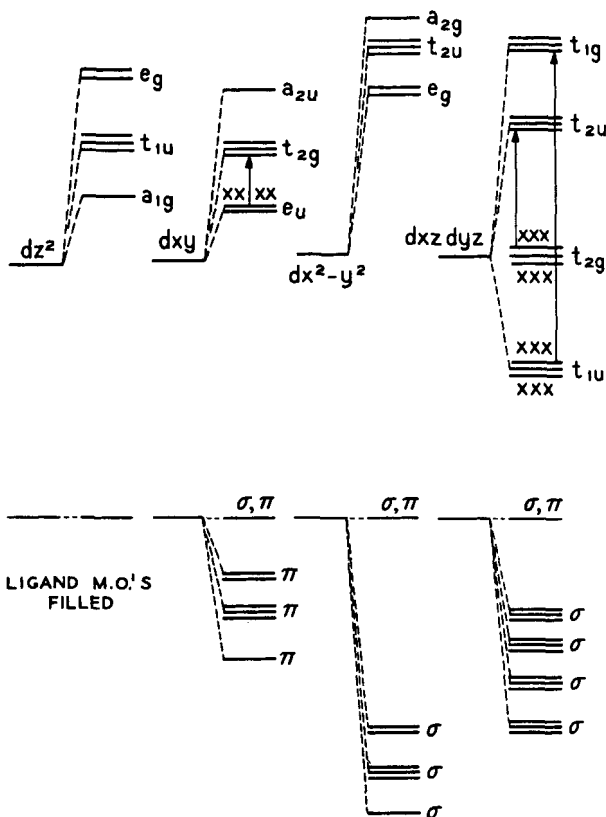


FIG. 25. The molecular orbital scheme for the $[M_6X_{12}]^{2+}$ ion according to Robin and Kuebler (593), as derived from the electronic spectrum.

Fig. 24, for p greater than 8.5, the $[M_6X_{12}]^{4+}$ ion has the closed-shell ground state configuration

$$dxzdyz(t_{1u})^6 dz^2(a_{1g})^2 dxzdyz(t_{2g})^6$$

whereas Fig. 25 predicts a triplet ground state

$$dxzdyz(t_{1u})^6 dxzdyz(t_{2g})^6 dxy(e_u)^2$$

provided that the $4+$ ion is not distorted so that the dxy (e_u) level is split and the electrons paired. Since the $[M_6X_{12}]^{4+}$ ions are claimed to be diamagnetic (471, 494), it would seem that the Cotton-Haas orbital ordering offers more hope for explaining the magnetic properties of these ions, provided that they are not badly distorted.

Electronic spectra of the niobium and tantalum subhalides have been recorded in the 10,000–50,000 cm^{-1} region by a number of invest-

igators (10, 447, 471, 593), but with only one attempt at interpretation (593). The electronic spectra of polynuclear complexes are complicated by the fact that the metal-metal transitions can be as strong as the

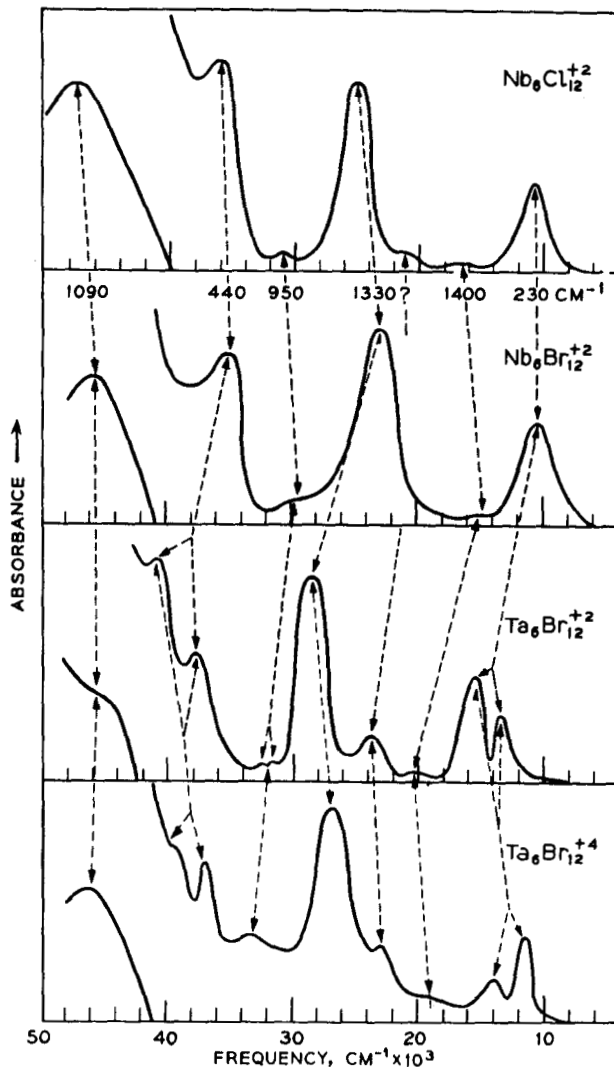


FIG. 26. Correlation of the electronic bands of oxidized and reduced $[M_6X_{12}]^{n+}$ ions in ethanol at -100°C (593).

ligand-metal charge transfer bands, so that a simple intensity argument cannot be used for their identification. In the $[M_6X_{12}]^{2+}$ series, the distinction, however, can be made by changing the ligand from, say, Cl to Br, so that the ligand-metal bands will identify themselves by a larger shift than the metal-metal bands. Figure 26 shows the spectra

of $[\text{Nb}_6\text{Cl}_{12}]^{2+}$ and $[\text{Nb}_6\text{Br}_{12}]^{2+}$ ions in alcohol at -100°C , from which it can be seen that the bands at $11,000\text{ cm}^{-1}$ and $36,000\text{ cm}^{-1}$ are allowed metal-metal transitions (${}^1A_{1g} \rightarrow {}^1T_{1u}$), all others being ligand \rightarrow metal charge transfer bands, on the basis of their much larger shift. The extinction coefficients of the various bands in aqueous solutions are given by Allen and Sheldon (10).

On comparing the spectra of the $[\text{Nb}_6\text{X}_{12}]^{2+}$ ions with the corresponding $[\text{Ta}_6\text{X}_{12}]^{2+}$ ions (Fig. 26), it is seen that the two metal-metal bands in the tantalum complexes have split into two components, each with intensity ratio 1:2. This splitting was interpreted as that expected of the triply degenerate ${}^1T_{1u}$ state for $[\text{Ta}_6\text{X}_{12}]^{2+}$ ions having an extended tetragonal distortion in solution. Spectra of the oxidized ions $[\text{Ta}_6\text{X}_{14}]^{4+}$ are very much like those of the reduced species, except that the intensity ratio of the split components is reversed, being 2:1, signaling a tetragonal distortion of the opposite sense (Fig. 26). The spectral similarities of the 2+ and 4+ ions in both the niobium and tantalum subhalides have been explained as the consequence of removing electrons from previously filled, triply degenerate levels on going from 2+ to 4+.

On the basis of this simple interpretation of the optical spectra, Robin and Kuebler concluded that, in ethanol solution, the $[\text{Nb}_6\text{X}_{12}]^{2+}$ ions are class III-A systems with all metal ions of formal charge $2\frac{1}{3}+$, whereas the $[\text{Ta}_6\text{X}_{12}]^{2+}$, $4+$ ions tend to trap integral valences through a tetragonal distortion. One might hope for some verification of these ideas through crystal structure analysis of a number of systems containing the M_6X_{12} ions. Figure 27 shows that there is no obvious regularity in the geometries of these species, except that, wherever a halogen coordinates to an M from outside the M_6X_{12} unit, the result is a displacement of that M atom outward from the symmetrical position. As concluded from the spectral study, it also appears that the distortions are larger in the tantalum complexes than in the niobium ones. The fact that the $[\text{Ta}_6\text{Cl}_{12}]^{2+}$ and $[\text{Ta}_6\text{I}_{12}]^{2+}$ octahedra have tetragonal distortions of the opposite sense demonstrates that these distortions are in large part due to crystal forces and not to any particular preferred electronic configuration of the ions.

An amazingly large number of stable compounds have been found in the niobium-oxygen system within the range $\text{NbO}_{2.50}$ – $\text{NbO}_{2.33}$. As compiled most recently by Gruehn and Schäfer (319, 320) and by Gruehn *et al.* (321), the following mixed valence oxides of niobium have been identified:

$\text{NbO}_{2.489}$ – $\text{NbO}_{2.500}$, $\text{NbO}_{2.482}$, $\text{NbO}_{2.480}$ ($\text{Nb}_{25}\text{O}_{62}$), $\text{NbO}_{2.467}$ – $\text{NbO}_{2.480}$, $\text{NbO}_{2.467}$, $\text{NbO}_{2.474}$ ($\text{Nb}_{19}\text{O}_{47}$?), $\text{NbO}_{2.466}$ – $\text{NbO}_{2.460}$, $\text{NbO}_{2.454}$ ($\text{Nb}_{22}\text{O}_{54}$), $\text{NbO}_{2.417}$ ($\text{Nb}_{12}\text{O}_{29}$), $\text{NbO}_{2.333}$ (Nb_9O_{21})

At present, the structures of only a few of these substances have been solved, yet certain regularities are already apparent.

On the basis of a determination of the crystal structure of the high temperature modification of the single valence material Nb_2O_5 ,

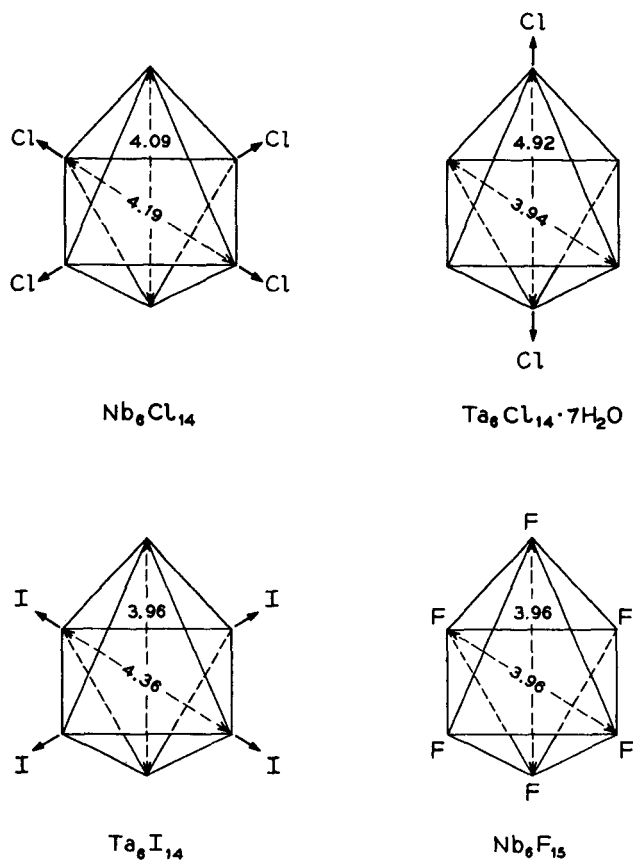


FIG. 27. Distortions of various M_6X_{12} octahedra induced apparently by the placement of halide ions on the fourfold axes of certain M ions, thereby lengthening the trans M-M distance in that direction.

Gatehouse and Wadsley (271) proposed that it is but a member of the general series $\text{Nb}_{3n+1}\text{O}_{8n-2}$, having $n = 9$. This structure consists of ReO_3 -type slabs of edge-sharing octahedra joined at the slab boundaries so as to form tetrahedral holes which are partly, but systematically, occupied by niobium atoms. Of the 28 niobium atoms in the Nb_2O_5 ($\text{Nb}_{28}\text{O}_{70}$) unit cell, 27 are in octahedral sites and one is in a tetrahedral site. It is proposed by them that the $n = 7$ mixed valence compound,

$\text{Nb}_{22}\text{O}_{54}$ ($\text{NbO}_{2.46}$), consists of smaller ReO_3 -type slabs, joined so that 21 of the niobiums are in octahedral sites and one is in a tetrahedral site, and that the $n = 5$ mixed valence compound, $\text{Nb}_{16}\text{O}_{38}$ ($\text{NbO}_{2.375}$), should it exist, would have one tetrahedrally and 15 octahedrally coordinated niobium atoms per unit cell. Although the two compounds $\text{NbO}_{2.48}$ ($\text{Nb}_{25}\text{O}_{62}$) and $\text{NbO}_{2.42}$ ($\text{Nb}_{19}\text{O}_{46}$) fit the formula for $n = 8$ and 6, respectively, Gatehouse and Wadsley point out that the members with even n will have a different crystal structure. Since the proposed $\text{Nb}_{3n+1}\text{O}_{8n-2}$ crystal structures would appear to trap valences readily, one is tempted immediately to try and assign valences to the various sites. The formula $\text{Nb}_{21}^{\text{V}}\text{Nb}^{\text{IV}}\text{O}_{54}$ fits nicely for $\text{Nb}_{22}\text{O}_{54}$, for it is postulated to have two sites in 21 : 1 ratio. However, $\text{Nb}_{16}\text{O}_{38}$ by this reasoning would have to be written as $\text{Nb}_{15}^{\text{V}}\text{Nb}^{\text{IV}}\text{O}_{38}$.

A straightforward accounting of electrons in $\text{Nb}_{25}\text{O}_{62}$ shows that it must be written formally as $\text{Nb}^{\text{IV}}\text{Nb}_{24}^{\text{V}}\text{O}_{62}$. Although the structure of this mixed valence oxide has not been determined in detail, it is known to be isostructural with the titanoniobate $\text{Ti}^{\text{IV}}\text{Nb}_{24}\text{O}_{62}$ (538). Moreover, although there are 24 octahedral sites to every tetrahedral one in the titanoniobate, the analysis indicates that the structure is partly inverted, in that all the sites appear to be occupied by either niobium or titanium in a random manner. If this is also true for $\text{Nb}_{25}\text{O}_{62}$, then it is a class II or class III system, rather than class I as intimated by the one-to-one correspondence of the numbers of the two types of site available and the numbers of niobium atoms of valency 5+ and 4+. Accepting a class II electronic structure for $\text{Nb}_{25}\text{O}_{62}$, it is reasonable then to postulate that its black color is in large part due to an Nb(IV) ($4d^1$), Nb(V) ($4d^0$) mixed valence class II transition, whereas $\text{TiNb}_{24}\text{O}_{62}$ is colorless due to the substitution of Nb(IV) ($4d^1$) by Ti(IV) ($3d^0$) and the consequent loss of the optical electrons.

Norin (539) has found monoclinic $\text{Nb}_{12}\text{O}_{29}$ to be an example of a Magneli phase containing corner-sharing blocks of NbO_6 octahedra, as in the ReO_3 -type structure, with edgesharing between blocks. This finding raises the possibility that $\text{Nb}_{12}\text{O}_{29}$ is but one member of a family of mixed valence niobium oxide Magneli phases. The titanoniobate $\text{Ti}_2^{\text{IV}}\text{Nb}_{10}^{\text{V}}\text{O}_{29}$ is isostructural with $\text{Nb}_{12}\text{O}_{29}$ (538), and, as with the $\text{Nb}_{25}\text{O}_{62}$, $\text{TiNb}_{24}\text{O}_{62}$ pair mentioned above, $\text{Nb}_{12}\text{O}_{29}$ is black but $\text{Ti}_2\text{Nb}_{10}\text{O}_{29}$ is colorless.

Similarly, Nb_9O_{21} , recognizable as $\text{Nb}_3^{\text{IV}}\text{Nb}_6^{\text{V}}\text{O}_{21}$, is isostructural with $\text{Ti}_3^{\text{IV}}\text{Nb}_6^{\text{V}}\text{O}_{21}$ (740), a substance in which the titanium and niobium sites are both distorted octahedral. Thus, this compound is a class II system, bordering on class III. There are, however, no short metal-metal distances here so the substance may not show metallic conductivity. Although the

oxide $\text{Nb}_{22}\text{O}_{54}$ (537) can be written as $\text{Nb}_2^{\text{IV}}\text{Nb}_{20}^{\text{V}}\text{O}_{54}$, there is no evidence that its valences are trapped. Structural work has yet to be done on the other oxides mentioned above.

An electron diffraction study of oxidized thin films of niobium reveals the existence of Nb_3O_5 , a cubic compound thought to contain the niobium ions in distorted octahedral coordination (424).

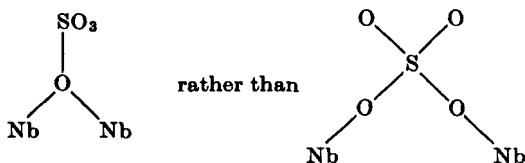
In the tantalum-oxygen system, Schönberg (642) reports a black phase (ϵ) of composition intermediate between TaO_2 and Ta_2O_5 having a complicated crystal structure. The only other compounds in this system of possible mixed valence interest are the metallic lower oxides TaO_x , having x much smaller than 1. Niebuhr has recently presented a critical evaluation of the properties of these substances (532), as well as of the oxides of niobium (533).

The importance of recognizing that such seemingly nonstoichiometric substances as the niobium oxides are, like the titanium, vanadium, molybdenum, and tungsten oxides, stoichiometric mixed valence compounds in disguise, is amply demonstrated by the studies of the electrical conductivity of "nonstoichiometric $\alpha\text{-Nb}_2\text{O}_5$ " [(377) and references cited therein]. Extensive work on materials ranging in composition from $\text{NbO}_{2.4996}$ to $\text{NbO}_{2.4284}$ shows that their resistivity is 0.1–0.01 ohm cm at 1000°C with an average carrier mobility of 0.22 $\text{cm}^2\text{V}^{-1}\text{sec}^{-1}$. These data have been interpreted in detail, using a model which presumes that the materials contain electron pairs trapped in oxygen ion vacancies, and that the electrical conductivity arises from the thermal excitation of electrons from these traps into a narrow $4d$ conduction band. We can see now that Nb(IV), Nb(V) compounds were in fact involved here, and that the conductivity might be more properly explained as arising from the thermal ionization of Nb(IV) ions.

Krylov *et al.* (445) report the mixed metal oxide, NbCuO_3 , in which both of the valence isomers can exist as stable phases. Thus, the sintering of Cu_2O with Nb_2O_5 yields diamagnetic $\text{Cu}^{\text{I}}\text{Nb}^{\text{V}}\text{O}_3$, whereas the sintering of CuO with NbO_2 yields paramagnetic $\text{Cu}^{\text{II}}\text{Nb}^{\text{IV}}\text{O}_3$ ($\mu_{\text{eff}} = 1.10$ B.M.). Powder patterns confirm the individuality of these valence isomers as well as those in the corresponding TaCuO_3 system.

The very large number of stable halide complexes built upon the Nb_6 octahedral framework suggests the possibility of formation of Nb_6 polynuclear complexes with other than halide ligands. The red compound $\text{K}_8\text{Nb}_6\text{O}_3(\text{SO}_4)_{12} \cdot 21\text{H}_2\text{O}$ (294, 417, 444) and the corresponding ammonium salt $(\text{NH}_4)_8\text{Nb}_6\text{O}_3(\text{SO}_4)_{12} \cdot 12\text{H}_2\text{O}$ (297, 508) would seem to be examples of just such complexes. Although no structural work has been done on these systems, it seems reasonable to predict that the niobium sulfates contain the Nb_6 octahedron with bridging sulfate

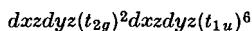
groups, and quite possibly OH^- ions situated on the fourfold axes of the niobium ions. In order to maintain the all-important Nb—Nb direct metal-metal bonding, it is necessary to postulate bridges of the form



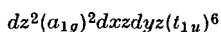
The niobium sulfates are soluble in sulfuric acid and in this solvent the red ions migrate to the anode in an electric field, thus demonstrating their negative charge. If the colored ions are indeed M_6X_{12} species, the overall negative charge can result only if X is SO_4^{2-} , and not if X is OH^- .

Krylov and Kalugina (444) have measured the magnetic susceptibility of the crystalline salt $\text{K}_8\text{Nb}_6\text{O}_3(\text{SO}_4)_{12} \cdot 21\text{H}_2\text{O}$ and found an effective moment of 2.0 B.M. per molecule. However, this value is uncorrected for temperature-independent paramagnetism, a factor which seems to be large in the niobium polynuclear complexes (471). Application of a temperature-independent paramagnetism correction, amounting to 600×10^6 cgs, reduces Krylov and Kalugina's effective moment to 1 B.M., a value sufficiently low that it raises doubt as to whether the substance is really paramagnetic or is simply diamagnetic but impure. The latter seems possible for it is known that the substance in question can react further to produce blue substances thought to contain Nb(III) (417).

The hypothetical $[\text{Nb}_6(\text{SO}_4)_{12}]^{2-}$ unit contains eight niobium 4d electrons in metal-metal bonds. According to the scheme of Robin and Kuebler (593) (Fig. 25), the metal-metal electronic configuration for such a system would be



giving a triplet ground state. On the other hand, the Cotton and Haas (159) ground state would be



which is a spin singlet. Should an X-ray crystallographic study show the presence of *symmetrical* Nb_6X_{12} complexes in the niobium sulfates, an accurate determination of the magnetic susceptibility then would be of great value in deciding between the Robin-Kuebler and Cotton-Haas orbital schemes, although as it stands the Cotton-Haas scheme seems to be the better one.

K. MOLYBDENUM AND TUNGSTEN

With very few exceptions, the mixed valence compounds of molybdenum and tungsten have oxide ion as ligand. The existence of well-defined phases with formulas intermediate between MO_2 and MO_3 has been recognized for many years, but it is primarily as a result of the extensive crystallographic investigations of Hägg, Magneli, Kihlberg, and their collaborators that the structural principles governing their

TABLE IV
MIXED VALENCE MOLYBDENUM OXIDES

MoO_x	Formula	Phase	Structure	Resistivity (ohm cm, 300°K)
3.000	MoO_3	α	MoO_3	$> 10^7$ (419)
2.889	$\text{Mo}_{18}\text{O}_{52}$	ξ	MoO_3	250 (419), 932 (279)
2.889	Mo_9O_{26}	β'	ReO_3	3.7 (419), 3.95 (279)
2.875	Mo_8O_{23}	β	ReO_3	1.2 (419)
2.800	Mo_5O_{14}	θ	Mixed polygonal	< 0.05 (419)
2.765	$\text{Mo}_{17}\text{O}_{47}$	χ	Mixed polygonal	0.2 (419), 0.59 (279)
2.750	Mo_4O_{11}	η	ReO_3	0.25 (419), 1.50 (279)
2.750	Mo_4O_{11}	γ	ReO_3	
2.000	MoO_2	δ	Distorted rutile	

formation are now well established. The most important results of these labors have been several times reviewed (328, 422, 474), and we shall therefore include only a brief outline here.

The seven mixed valence compounds within the composition range $\text{MoO}_{2.75}$ – MoO_3 which have been identified from phase analyses based on X-ray powder (279, 419) and single crystal measurements (422), as well as differential thermal analysis (598), are listed in Table IV. Within this composition range, three basic structure types may be distinguished: ReO_3 , MoO_3 , and what Kihlberg (422) has called the “mixed-polygonal” type. In the “homologous” (476) series with the general formula $\text{M}_n\text{O}_{3n-1}$, based on the ReO_3 lattice, examples having $n = 8$ and 9 have been prepared which contain only molybdenum, but by incorporating increasing concentrations of tungsten it is possible to obtain further members with $n = 10, 11, 12,$ and 14. The ReO_3 structure, which can be regarded as built up from MO_6 octahedra linked exclusively at the corners, extends

infinitely along only one axis in the compounds belonging to the M_nO_{3n-1} series, thus forming finite slabs whose width is determined by the value of n . In Fig. 28, the structure of Mo_8O_{23} shows how the slabs are connected through sharing of edges between the octahedra at the slab boundaries. In this way, clusters of four octahedra sharing edges occur throughout the structure, as indicated by the heavy lines. The other structures based on ReO_3 are the two forms of Mo_4O_{11} , in which the slabs of connected octahedra are joined by tetrahedra which share corners with the octahedra of two neighboring slabs. No tetrahedra or octahedra share edges in this structure.

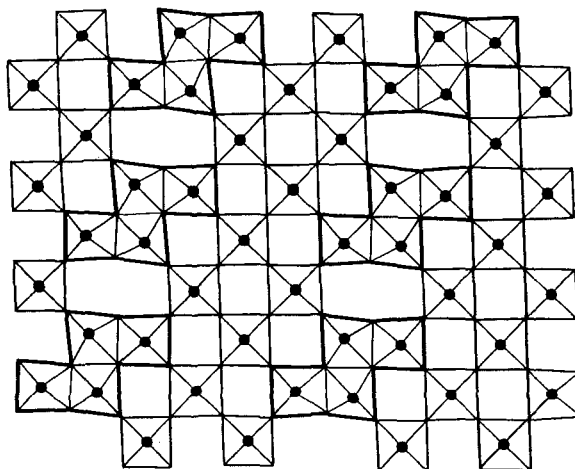


FIG. 28. The crystal structure of Mo_8O_{23} (422). The metal atom clusters are outlined in *bold lines*, while the metal atoms themselves are represented by the *filled circles*, and the oxygen atoms are found above and below the metal atoms and at the apices of the squares.

In the structures based on MoO_3 , e.g., $Mo_{18}O_{52}$, slabs of the basic lattice are once again connected by edgesharing, but, in addition, some of the metal atoms occur in tetrahedral sites. The lattices called "mixed polygonal" are distinguished by a complicated connection of coordination polyhedra in two dimensions, in which not only distorted octahedra but pentagonal bipyramids occur. This class includes mixed valence compounds such as Mo_5O_{14} and $W_{18}O_{49}$ (473), as well as single valence mixed oxides such as $MoW_{11}O_{36}$ and $MoW_{14}O_{45}$ (304). It is also interesting to note the similarity with the tunnel lattices occurring among the tetragonal and hexagonal tungsten bronzes. In the mixed polygonal oxides, the equatorial edges of the pentagonal bipyramids are shared with octahedra so that there exist pronounced metal atom clusters

(Fig. 29), which are still further condensed in $\text{Mo}_{17}\text{O}_{47}$ and $\text{W}_{18}\text{O}_{49}$ by edgesharing between pairs of octahedra attached to neighboring pentagonal clusters. Considerable variations in metal-oxygen and metal-metal distances are needed to accommodate these structural complexities, although it should be noted that they are not necessarily the result of mixed valence interactions, since MoO_2 and WO_2 are themselves distorted from rutile lattices in such a way that the metal atoms appear to form pairs (472).

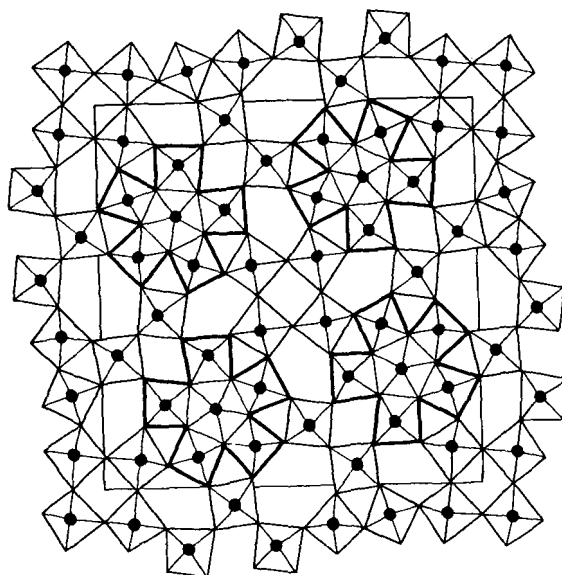


FIG. 29. The crystal structure of Mo_5O_{14} (422). The *filled circles* represent the metal atoms, and oxygen atoms are found above and below the metal atom and at the apices of the squares. The "mixed polygonal" metal clusters are indicated by the *bold lines*.

In contrast to the effort devoted to structure determinations in this series of compounds, very little has been reported which might enable one to rationalize their electronic structures with their complicated stereochemistries and stoichiometries. In closing his most recent review of the structural chemistry of the molybdenum oxides (422), Kihlberg remarks that definite conclusions about the variations in the distortion of the Mo—O coordination with valence state cannot be drawn until reliable measurements of basic physical properties, such as magnetism, have been made. Some of the distortions from regular octahedral coordination may perhaps be accounted for by "rattling" of the small cations, as originally proposed by Orgel (545). Ionic radii of Mo(IV) and Mo(VI) are in the range where this might be expected to occur.

Attempts have been made (422) to fit the observed bond lengths d_n in many of the compounds to a logarithmic relationship with bond number, n , of the kind proposed by Pauling (564)

$$d_n - d_1 = 2k \log n$$

using values for d_1 and k which fit the observed lengths in MoO_3 , and the assumption that $\Sigma n = 2$ for each oxygen atom. The sums Σn_{Mo} for the two modifications of Mo_4O_{11} were taken to suggest that there is a gradual increase in the valence state of the metal atoms from the middle of the basic ReO_3 slab toward the outside, in accord with a previous suggestion (477) that decreasing valency favors the occurrence of higher coordination numbers. However, the tenuous theoretical basis of Pauling's equation makes it difficult to use the "bond number" criterion to decide whether the valences are partly or wholly trapped. From the low resistivities of all except one of the mixed valence oxides (279, 419), one is tempted to conclude that no definite lattice sites or coordination numbers are to be allocated to specific valence states in these compounds, i.e., the compounds are very close to class III-B. Thus in Mo_4O_{11} , for example, 3/4 of the molybdenums are octahedrally coordinated and 1/4 are tetrahedrally coordinated and, furthermore, the formula is compatible with the existence of one Mo(IV) for every three Mo(VI), so at first glance the compound might appear to be a class I mixed valence system. On the other hand, the room temperature resistivity of this compound is less than 1 ohm cm (279, 419) and the bond length arguments of Kihlberg (422) suggest that the tetrahedral sites might be preferentially occupied by Mo(VI). The valence distribution would then be rather like that of an inverse as compared with a normal spinel. Nevertheless, it might prove possible to rationalize the occurrence of blocks of ReO_3 structure, together with regions of metal atom clustering in oxides such as Mo_8O_{23} or Mo_5O_{14} , by deriving bonding schemes similar to those suggested by Cotton (160) for the trinuclear single valence cluster in $\text{Zn}_2\text{Mo}_3\text{O}_8$. If we start from the assumption that the octahedra joined only through their apices contain metal ions trapped as hexavalent, and then apportion the extra electrons corresponding to the Mo(IV) or Mo(V) to the region of the clusters, we find that two d electrons are to be distributed within each cluster of four edgesharing octahedra in the $\text{M}_n\text{O}_{3n-1}$ series. Similarly, four d electrons would have to be assigned to each cluster of six molybdenums in the "mixed polygonal" series. Overlap between d orbitals on adjacent metal atoms in the former case is expected to be greatest for the dxy orbitals, which are nonbonding between metal and oxygen, but which could form σ bonds within the metal cluster. The orbital combination with the phases

shown in Fig. 30 is strongly σ -bonding and nondegenerate, and would therefore accommodate the two "extra" electrons. Unfortunately, the metal-metal distances within the clusters are not notably shorter than that expected for two normally bonded octahedra sharing edges, and there is no evidence that spin pairing of the kind postulated here actually occurs.

All the mixed valence molybdenum oxides are described as blue or blue-violet (422), but no spectra have been reported and care is needed in interpreting their colors as MoO_2 is itself reddish brown. Finally, there

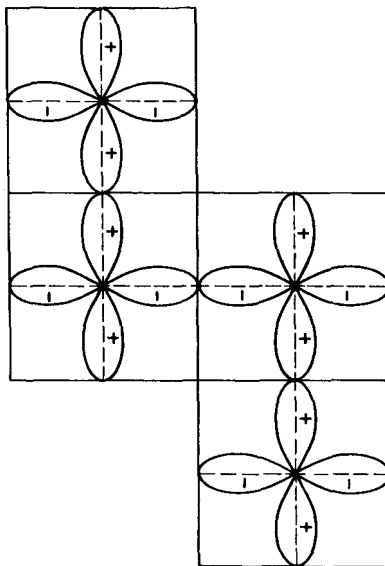


FIG. 30. A possible mode of d_{xy} bonding within the metal atom clusters of Mo_8O_{23} .

is not even conclusive evidence that these systems involve the 4+ and 6+ rather than 5+ and 6+ oxidation states. Once again, unfortunately, our conclusion must be that a great deal more physical evidence will be needed before definite conclusions can be drawn about the electronic structures of these interesting compounds. Magnetic and spectroscopic measurements will be the most profitable lines of attack.

A much more highly reduced mixed valence oxide, Mo_3O , was reported to form when mixtures of Mo and MoO_2 were heated (643), but the preparation could not be repeated (420).

When polymolybdate(VI) and polytungstate(VI) anions are reduced in aqueous solution, the dark blue colors of the products suggest that their electronic structures may be related to those of the mixed valence

molybdenum and tungsten oxides. The photochemical reduction of polymolybdates and tungstates has been studied in connection with photographic processes (132, 789). Molybdenum blue was prepared as long ago as 1805 (110) and since then very many investigations have been reported (289), but little progress could be made in sorting out the variety of products until the structures of the parent iso- and hetero-polyanions had been determined. It was Keggin (408) who first showed that anions with the general formula $[A^{n+} X_{12}O_{40}]^{(8-n)-}$, where A may be a transition or main group element and X is Mo(VI) or W(VI), consisted of compact groups of XO_6 octahedra sharing edges and surrounding the central ion A with a tetrahedron of oxygen atoms. Further members of the series are described and illustrated by Wells (756).

Many of the attempts to characterize solid molybdenum blue compounds have been frustrated by the colloidal nature of the reduction products and the difficulty of isolating them with reproducible amounts of water. Thus Sacconi and Cini (613) claimed to have prepared a continuous series of amorphous blues with Mo(VI):Mo(V) ratios between 3.4 and 6, and Glemser and Lutz (280) showed that not only blue anhydrous oxides, but crystalline hydrates as well, could be prepared by solid phase reactions. However, only the products $Mo_4O_{10}(OH)_2$ and $Mo_8O_{15}(OH)_{16}$ were characterized by X-ray analysis. Both were insoluble in water and stable to alkali, but a range of water-soluble, amorphous products was also prepared. The final reduction product of MoO_3 with zinc in concentrated HCl is a crystalline olive-green Mo(IV) compound, $Mo_5O_5(OH)_{10}$, which when placed in vacuum loses hydrogen to give a red mixed valence compound $Mo_5O_7(OH)_8$ (284). By reducing $WO_3 \cdot H_2O$ and $WO_3 \cdot 2H_2O$ with zinc and HCl, Glemser *et al.* (285) have also succeeded in preparing a series of blue tungsten oxide hydrates which they related to the molybdenum oxides, using X-ray powder diagrams.

In contrast to the variety of solid molybdenum blues, evidence has accumulated that, in homogeneous aqueous solution, reduced species based on the isopolymolybdate structure exist in very limited numbers. When molybdic acid solutions were reduced electrolytically and extracted with butanol, the ratio Mo(VI):Mo(V) in aqueous solutions of the extract was 2.0 (23), a result in accord with the variation in the optical density at $13,300\text{ cm}^{-1}$ as a function of Mo(VI):Mo(V) ratio (675). At higher pH than is needed to form blue solutions, there is also spectrophotometric evidence for a brown hexamolybdate anion with Mo(VI):Mo(V) = 1, which has an absorption maximum at $22,200\text{ cm}^{-1}$ (547), and another having Mo(VI):Mo(V) = 0.5, in which the absorption maximum has shifted even further to the ultraviolet, to $30,800\text{ cm}^{-1}$ (548).

The reduction of 12-heteropolymolybdates and tungstates in aqueous solution has proved rather easier to study than that of the isopolyacids either in solution or in the solid state. It is now quite clear, as a result of polarographic (309–311, 571, 673, 674) and potentiometric (571, 690, 691) work, that these anions can accept limited numbers of electrons, e.g., up to four, without decomposition, and, in a number of instances, salts of the reduced anions have been isolated (331, 332). The values (571) of the reduction potentials for addition of the first electron to $[\text{PW}_{12}\text{O}_{40}]^{3-}$, $[\text{SiW}_{12}\text{O}_{40}]^{4-}$, $[\text{Fe}^{\text{III}}\text{W}_{12}\text{O}_{40}]^{5-}$, and $[\text{Co}^{\text{II}}\text{W}_{12}\text{O}_{40}]^{6-}$ vary with the charges in a way consistent with a model that treats the anion simply as a charged sphere. This suggests that the first electron goes into an orbital whose energy is nearly independent of the central atom. The fact that the spectra of silicomolybdates, to which two and four electrons have been added, remain very similar as to both energy and intensity (676) also suggests that the electrons are entering orbitals that are localized on particular metal atoms. There has been some disagreement about the existence of one- and three- in addition to two- and four-electron reduction products; only the latter have been isolated as solid salts (331, 332), and had been detected by Souchay (673) in his original polarographic work. However, more recently, waves due to the one-electron step have been located by two groups (571, 677). The absorption spectra of various reduced 12-silicomolybdates (676, 677) are shown in Fig. 31.

In one case at least there is clear evidence for the occurrence of Mo(V) in a reduced polymolybdate. By γ -irradiation of polycrystalline ammonium heptamolybdate, $(\text{NH}_4)_6\text{Mo}_7\text{O}_{24} \cdot 6\text{H}_2\text{O}$ (562), paramagnetic centers are formed which, from their ESR spectra, can be identified with NH_3^+ and Mo(V) ions. Irradiation at room temperature gave Mo(V) spectra which were almost isotropic, the major absorption coming from isotopes with $I = 0$, with a smaller contribution from Mo^{95} and Mo^{97} with $I = 5/2$. The most interesting feature, however, is the presence of a further hyperfine interaction between the unpaired electron of the Mo(V) and the $I = 5/2$ isotope of a neighboring Mo(VI). We therefore conclude that this system at least belongs to class II of our classification, and that the first electronic transition will contain an appreciable component of charge transfer. Similar experiments on the crystalline heteropoly-blue salts or their frozen solutions would be extremely interesting. Proton nuclear magnetic resonance spectra of a number of heteropoly-blue acids have recently been measured in the solid state (484), and interpreted as resulting from fast exchange between protons bound to oxygen atoms of the anions and those attached to crystal water molecules. That a nuclear magnetic resonance spectrum can be observed at all in these substances

seems to imply that the anions are diamagnetic. Once again, magnetic measurements would be valuable.

It is not our intention to attempt a review of the very large amount of work carried out on the other class of mixed valence molybdenum and

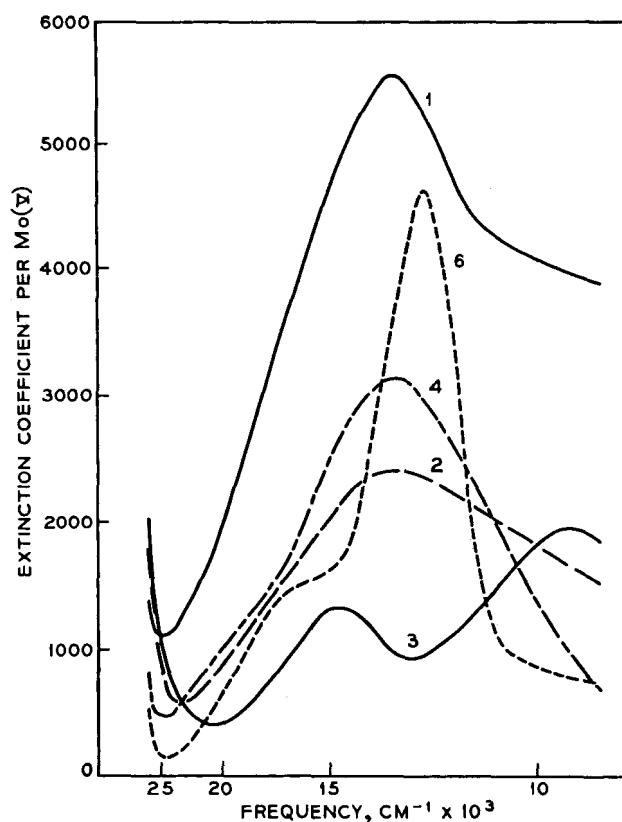


FIG. 31. The electronic spectra of 12-silicomolybdates reduced by 1-6 electrons, as indicated by the labels on the spectral curves (676).

tungsten oxides, the bronzes, since this has recently been done quite thoroughly by others (421, 694). Nevertheless it is worth emphasizing that the volume of physical measurements on these compounds far surpasses that reported for the other reduced group VI-B oxide systems considered here, and that the level of understanding of the electronic properties is correspondingly higher. We will merely record some of the more important conclusions about the crystal and electronic structures of these interesting compounds.

Hägg (326) was the first to show that the bronzes could be given a general formula $A_x\text{WO}_3$, where A was an alkali metal and x varied continuously from about 0.3 to nearly 1.0. At the latter extreme the structure approximates that of a perovskite, while for low values of x the structure goes through various lower symmetry modifications, all based on the lattice of WO_3 . At all A concentrations the tungsten atoms are equivalent and the lattice is a clear example of a class III-B mixed valence system. Ionization of the alkali metal atoms produces electrons which are evenly distributed among all the tungsten atoms. In agreement with this, the sodium bronzes in which x lies between 0.5 and 0.9 behave as metallic conductors between 4° and 800°K (217), with Hall effect coefficients which suggest that each sodium atom contributes one free electron to the conduction band (268). Further evidence that the sodium atoms lose their valence electrons completely into a conduction band that extends only across the tungsten atoms comes from nuclear magnetic resonance experiments (391), which show that the ^{23}Na resonance has an extremely small Knight shift. At high temperatures, the conductivity is nearly proportional to the sodium concentration (217), and the mobility is independent of the electron concentration. The fact that the conductances of lithium, sodium, and potassium tungsten bronzes lie on the same curve when plotted against x (421) also suggests that the alkali metal atoms do not participate directly in the conduction process.

Attempts to prepare molybdenum bronzes by reducing MoO_3 with alkali metal vapors always lead to MoO_2 , and it was only very recently that the first compounds of this type were prepared by electrolyzing fused mixtures of K_2MoO_4 and MoO_3 (789). Two samples have been definitely characterized: $\text{K}_{0.26}\text{MoO}_3$, which formed reddish plates and behaved as a typical semiconductor, and $\text{K}_{0.23}\text{MoO}_3$, a blue compound that conducted like a metal above -100°C . Despite their similarity in composition, the structures of the two compounds were different; the former contained subunits of six and the latter of ten MoO_6 octahedra sharing edges (305, 684). The subunits formed layers by sharing corners and the layers were linked together by the potassium ions. A sodium molybdenum bronze in the same composition range has also been reported (685).

The only other mixed valence molybdenum and tungsten compounds beside the oxides are a small number of halides. When yellow $[\text{W}_6^{11}\text{Br}_8]\text{Br}_4$ is reacted with bromine at various temperatures (633, 662), compounds such as W_6Br_{14} , W_6Br_{16} , and W_6Br_{18} can be isolated. These dissolve in ethanol to give intensely red solutions, whose spectra are by no means the superposition of those of W_6Br_{12} and Br_2 . The suggestion is that

$[\text{W}_6\text{Br}_8]^{n+}$ mixed valence ions with structures like $[\text{Nb}_6\text{I}_8]^{3+}$ may be formed. The other mixed valence halide results from reactions between MoF_6 and various main group chlorides, e.g., CCl_4 , and, on the basis of conductance, infrared, and magnetic measurements, has been assigned the formula $[\text{Mo}_3^{\text{IV}}\text{Cl}_9][\text{Mo}^{\text{V}}\text{F}_6]_3$ (543, 686). The trinuclear $[\text{Mo}_3^{\text{IV}}\text{Cl}_9]^{3+}$ cation is assumed to have a similar core structure to that found in $[\text{Re}_3\text{Cl}_{12}]^{3-}$ and $\text{Re}_3\text{Cl}_{12}$. Since the anion is colorless and the cation itself is orange, the reported orange color of the salt suggests that there is no interaction absorption in the visible region and that the salt is a simple class I example.

L. TECHNETIUM AND RHENIUM

No mixed valence compounds of either of these elements appear to have been prepared, with the single exception of $(\text{NH}_4)_3\text{Tc}_2\text{Cl}_8 \cdot 2\text{H}_2\text{O}$ (213). The compound forms shiny black crystals which dissolve in HCl to give a turquoise blue solution having a broad absorption band at $16,300 \text{ cm}^{-1}$. Cotton has published a preliminary account of an X-ray diffraction study of this compound (162), which shows the presence of $[\text{Tc}_2\text{Cl}_8]^{3-}$ groups essentially isostructural with $[\text{Re}_2\text{Cl}_8]^{2-}$ (163). Each technetium atom lies at the center of a square of chlorine atoms, and a distorted octahedral coordination is completed by one of the water molecules and the other technetium atom at a distance of 2.13 \AA , a full 0.6 \AA shorter than the $\text{Tc}-\text{Tc}$ distance in the metal. Cotton has described the electronic structure of diamagnetic $[\text{Re}_2\text{Cl}_8]^{2-}$ in terms of a σ bond, two π bonds, and a δ bond between the metal atoms (161), and a comparable description would serve for the technetium analog, which has one more d electron and whose susceptibility is consistent with one unpaired spin per $[\text{Tc}_2\text{Cl}_8]^{3-}$ ion. An ESR measurement on the technetium compound would be exceptionally interesting, as Cotton's bonding scheme for $[\text{Re}_2\text{Cl}_8]^{2-}$ (161) assumes that the relative ordering of the σ , π , and δ orbitals of the metal-metal bond is entirely due to the difference in overlap between the pairs of, respectively, dz^2 , $dxzdyz$, and dxy orbitals on each metal atom. A more detailed consideration of the bonding, taking into account π -bonding between $dxzdyz$ and the chlorine atoms, and σ -bonding between dz^2 and the water molecule, might very easily alter this relative ordering, as we noted in the case of the niobium and tantalum subhalides. It is only fair to say, however, that since the lowest empty orbital, δ^* , is not appreciably antibonding, Cotton's scheme does suggest that the $\sigma^2\pi^4\delta^2$ configuration of $[\text{Re}_2\text{Cl}_8]^{2-}$ might easily add an extra electron, forming a mixed valence system isoelectronic

with $[\text{Tc}_2\text{Cl}_8]^{3-}$. Oxidation and reduction experiments on $[\text{Re}_2\text{Cl}_8]^{2-}$ and the other rhenium halide cluster complexes might lead to other interesting class III-A mixed valence clusters.

M. RUTHENIUM AND OSMIUM

Easily the most famous ruthenium mixed valence compound is the one called "ruthenium red." It is usually prepared by allowing aqueous ruthenium trichloride to react with an excess of ammonia (388), or by exposing solutions of $\text{Ru}(\text{NH}_3)_6\text{Cl}_3$ in aqueous ammonia to air (252). Solutions of the compound have an extremely intense rose color; indeed, it has been said that a $2 \times 10^{-7} M$ solution is clearly pink. The color becomes fixed to silk, although not to wool or cotton, and has been used commercially as a dyestuff. Joly (388) formulated ruthenium red as $\text{Ru}_2\text{Cl}_4(\text{OH})_2 \cdot 7\text{NH}_3 \cdot 3\text{H}_2\text{O}$ and Morgan and Burstall (512), who prepared from it compounds which they thought were monomeric, formulated it as $[\text{Ru}(\text{OH})\text{Cl}(\text{NH}_3)_4]\text{Cl} \cdot \text{H}_2\text{O}$. Gleu and Breuel (286) showed that the latter could not be correct, as $[\text{Ru}(\text{OH})\text{Cl}(\text{NH}_3)_4]^+$ would have an effective magnetic moment of almost 2 B.M. and would be virtually colorless, whereas ruthenium red is only very weakly paramagnetic, if at all, and shows a most intense coloration.

In a very careful investigation, Fletcher *et al.* (252) found that ruthenium red contains no complexed chloride ions, and behaves as a trinuclear cation with a ruthenium:ammonia ratio of 3:14. The average oxidation number of the ruthenium, 10/3, then points to a formula



containing two oxo bridges. The molar extinction coefficient per ruthenium atom is 21,000 at the band maximum, $18,800 \text{ cm}^{-1}$, but in acid solution a reversible oxidation leads to the formation of a brown compound, whose spectrum appears to contain the same band shifted to higher energy ($21,700 \text{ cm}^{-1}$, $\epsilon = 14,100$) (Fig. 32). Ruthenium red has an effective magnetic moment of 0.77 B.M. per metal atom if no diamagnetic correction is made, whereas the moment of the brown compound is 1.13 B.M. per metal atom. The difference, $3(1.13 - 0.77) = 1.1 \text{ B.M.}$, is nearly equivalent to one electron per molecule. The spectra of both the red and brown compounds shift slightly to lower energy with increasing pH, suggesting that in basic solution they were being partly deprotonated.

Jorgensen and Orgel (399) explained the stability of the presumed linear ruthenium red framework as the result of π -bonding between the t_{2g} orbitals of the metal atoms and the $2p \pi$ orbitals of the oxygen atoms.

Aside from the σ -bonding in the linear cation, ten π molecular orbitals can be formed which group themselves as five pairs of doubly degenerate levels, with two pairs bonding, two antibonding, and one nonbonding. As there are 16 π electrons in the system, the π manifold in the ground state is filled up to and including the second highest antibonding pair, so that the net effect is a π -bonding stabilization in addition to the σ bonds. In such a linear system, the first transition is allowed, but the

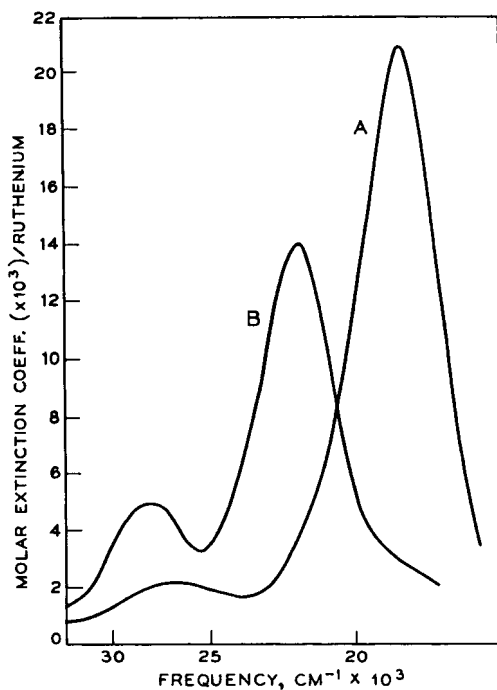
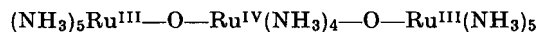


FIG. 32. The electronic spectrum of the ruthenium red cation $[\text{Ru}_3\text{O}_2(\text{NH}_3)_{14}]^{6+}$ in water (A), and the brown cation $[\text{Ru}_3\text{O}_2(\text{NH}_3)_{14}]^{7+}$ in 0.01 *N* HNO_3 (B) (252).

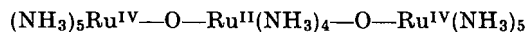
second is forbidden (as observed in Fig. 32, curve A). However, because the intensity of the first band decreases whereas that of the second band increases on bending the molecule, the spectrum of the oxidized ion (curve B) suggests that it is more bent than the reduced ruthenium red.

Regardless of whether ruthenium red is linear or bent, the ion at first appears to be class II, with the terminal ruthenium atoms in principle being clearly distinguishable from the bridging one. However, the unusually high molar extinction coefficient of 61,500 for the first band of ruthenium red in water suggests that α is very large indeed (Eq. 14), and that the delocalization of valences approaches that for

class III-A. This is confirmed by the magnetic susceptibility study, for if ruthenium red were class II with valences trapped as either



or



it would have an effective magnetic moment per ruthenium of 2.2 or 2.3 B.M., whereas 0.77 B.M. is observed, a large part of which may be temperature-independent paramagnetism. The large depression of the effective magnetic moment follows from the strong interaction between the ruthenium atoms via both π and σ bonds.

Other ruthenium mixed valence materials have been suggested as forming when RuO_4 in aqueous solution is reduced in the presence of trifluoroacetic acid (124), and it seems possible that the very dark blue-green precipitate obtained when solutions of $\text{K}_4\text{Ru}(\text{CN})_6$ are acidified after oxidation by chlorine (184, 439) may be the ruthenium analog of Prussian blue, for it analyzes as $\text{Ru}^{\text{II}}\text{Ru}^{\text{III}}(\text{CN})_5 \cdot \text{H}_2\text{O}$.

The literature appears to contain only one reference to a mixed valence compound of osmium, and doubt has been raised as to its constitution. $\text{Os}^{\text{III}}\text{Os}^{\text{IV}}\text{Cl}_7 \cdot 7\text{H}_2\text{O}$ is a red material, said to be possibly a mixture of OsCl_4 and OsOHCl_3 (290).

N. RHODIUM AND IRIDIUM

No rhodium compounds have been shown conclusively to be of mixed valence type. In ice-cold solution, ceric nitrate oxidizes a suspension of Cs_3RhCl_6 to a dark blue-green substance thought to be $\text{Cs}_2\text{Rh}^{\text{IV}}\text{Cl}_6$ (211, 212), but, since it appears that ozone oxidizes Rh(III) solutions to Rh(V) in the presence of excess chloride ions (57), the suggestion was therefore made that the Cs_2RhCl_6 salt may contain equimolar proportions of Rh(III) and Rh(V), like the isomorphous antimony compound. However, the diffuse reflectance spectrum of the blue-green compound, and its dilution in Cs_2PtCl_6 , sufficiently resemble that of Cs_2IrCl_6 to make it certain that the compound is indeed one of Rh(IV) (397, 398). Solutions of rhodium perchlorate of average oxidation number 4.5–5.3 (57) were said to exhibit further intense absorption bands in addition to those of Rh(III) and Rh(V), which may be taken as indicating the presence of mixed valence species in some of these solutions. The only other rhodium compound which is perhaps a mixed valence system is the dichloride (787) for which, as Kettle (413) pointed out, the original analyses agree much more closely with the formula $\text{Rh}_6\text{Cl}_{14}$. This is thus a potential example of the group of mixed valence compounds based on octahedral metal clusters, such as $[\text{Ta}_6\text{Cl}_{12}]^{2+}$.

Numerous mixed valence iridium compounds are based on a trimeric arrangement of iridium atoms bridged by sulfate groups. Lecoq de Boisbaudran (460) prepared what he thought was an Ir(III) double sulfate, $\text{Ir}_2(\text{SO}_4)_3 \cdot 3\text{K}_2\text{SO}_4$, which, unlike most Ir(III) salts, was not green but blue. His formulation was questioned by Delépine (187), whose analyses agreed better with the formula $\text{K}_{10}\text{Ir}_3(\text{SO}_4)_9$ and who also demonstrated that reducing agents turned the blue solution of the salt green. The original salt therefore apparently contained Ir(IV) as well as Ir(III). Delépine also prepared a green nitrido-iridium sulfate (186), which he showed, 60 years later (188), had the formula $\text{K}_4[\text{N}\{\text{Ir}(\text{H}_2\text{O})(\text{SO}_4)_2\}_3]$, i.e., it contained one Ir(III) atom and two Ir(IV) atoms per anion. Having examined the solution spectrum of the nitrido compound, Jorgensen (396) proposed that the formulas of that and Lecoq's salt were related to those of the trimeric Cr(III) acetates, $[\text{O}\{\text{Cr}(\text{H}_2\text{O})(\text{CH}_3\text{CO}_2)_2\}_3]^+$ (251), in which the oxygen atom and the three chromium atoms are found in a planar triangular arrangement, and octahedral coordination about each metal is completed by bridging acetate groups and the water molecules (Fig. 11). A rationalization of the electronic structures of these unusual compounds can be achieved by considering that, if the t_{2g} orbitals of the iridium atoms and the $2p \pi$ orbital of oxygen were fully occupied, there would be room for twenty electrons, but that one linear combination

$$\frac{1}{\sqrt{3}}[(t_{2g})_1 + (t_{2g})_2 + (t_{2g})_3]$$

forms not only a $d\pi-p\pi$ bonding orbital with the $2pz$ oxygen orbital, but a strongly antibonding orbital as well. Thus by losing two electrons and becoming mixed valence, an eighteen-electron system results which does not require occupation of the energetically unfavourable antibonding orbital. Delépine's formula (187) for Lecoq's salt becomes analogous to that of the nitrido compound, if one assumes that the three iridium atoms are in that case coordinated to an oxygen atom. If these trinuclear complexes do have the equilateral triangular geometry, then they belong to class III-A, and should be diamagnetic.

Ray and Adhikari (578) report the preparation of $\text{Ir}^{\text{II}}\text{Ir}^{\text{III}}\text{Cl}_5 \cdot 4\text{R}_2\text{S}$, where R_2S is either $\text{S}(\text{CH}_3)_2$ or $\text{S}(\text{C}_2\text{H}_5)_2$, as pale yellow crystals.

O. PALLADIUM AND PLATINUM

These two elements form mixed valence compounds with a wider range of ligands than many others, and intensive studies of their molecular structures and physical properties over many years have provided

us with a clear view of their electronic structures. A few simple compounds such as oxides and halides are known, but the majority of examples contain complex ions or neutral molecules, typically with halide and amine ligands.

Hydrates of the simple oxides Pd_2O_3 and Pt_2O_3 were first prepared by Wöhler and Martin (783, 784). They are reported to be brown-black, but, since PdO_2 and PtO_2 are also black, this fact gives no information about the possibility of an M(II),M(IV) mixed valence interaction. Some controversy has surrounded the formulation and structure of another oxide, Pt_3O_4 . Galloni and Ruffo (265) described the structure as body-centered cubic, with all the platinum ions in equivalent sites (class III-B), and a Pt-Pt spacing of 3.11 Å. An oxide prepared by Waser and McClanahan (745, 746) using the same method, however, contained enough sodium to suggest the formula NaPt_3O_4 . A powder diagram of the latter revealed a simple cubic lattice in which each platinum has four oxygen neighbors and two other platinum ions at 2.85 Å. Since the structure contains infinite chains of platinum atoms, the conductivity was investigated. The volume resistivity at room temperature was about 10^4 ohm cm, but the occurrence of polarization suggested that the conductivity was ionic. The powder pattern of this preparation was quite different than Galloni and Ruffo's, whose results were said to resemble the pattern of PtO_2 . Galloni and Busch (266) reiterated that their product contained no sodium, so one must accept the compromise suggestion (747) that there exists a series of compounds with the general formula $\text{Na}_x\text{Pt}_3\text{O}_4$, based on the platinum and oxygen lattice found by Waser and McClanahan (746). It should perhaps be mentioned that, according to our classification scheme, the high resistivity reported for NaPt_3O_4 is at variance with its proposed class III-B structure.

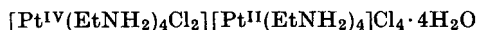
Oxidation of PdCl_2 with BrF_3 gives black PdF_3 (608, 655), but Pt(II) salts are oxidized to PtF_4 by this reagent. The magnetic moment of PdF_3 was at first interpreted (541) in terms of a Pd(III) ion with a configuration $t_{2g}^6e_g^1$, but Bartlett and Rao (43) have recently shown that the compound is in fact $\text{Pd}^{\text{II}}[\text{Pd}^{\text{IV}}\text{F}_6]$, in which Pd(II) is assigned a high-spin configuration $t_{2g}^6e_g^2$. When Pd(II) salts react with BrF_3 in the presence of quadrivalent oxides, isostructural compounds such as PdGeF_6 and PdSnF_6 are formed. No structural studies of the other simple PtX_3 halides with $X = \text{Cl}, \text{Br}, \text{or I}$ (784, 788) have been reported, but it seems probable that they are related to the fluoride. However, they cannot be precisely the same since the divalent metal ions in these halides are low-spin (697), and thus, no doubt, in square planar coordination. Mixed valence halides such as K_2PdCl_5 (783) and Cs_2PtCl_5 (785) may perhaps contain $[\text{M}^{\text{II}}\text{Cl}_4]^{2-}$ and $[\text{M}^{\text{III}}\text{Cl}_6]^{2-}$ ions, which, if the

350

MELVIN B. ROBIN AND PETER DAY

compounds belong to class II, will exhibit their own characteristic absorption bands in addition to any mixed valence absorption. Unfortunately, no information on this point is available, except for the single observation that Cs_2PtCl_5 is green (785).

One of the first mixed valence platinum compounds containing halide and amine ligands to be prepared was the red salt of Wolfram (790):



Its mixed valence character was recognized first from the method of preparation, for mixing solutions of the compounds $[\text{Pt}^{\text{IV}}(\text{EtNH}_2)_4\text{Cl}_2]\text{Cl}_2$ and $[\text{Pt}^{\text{II}}(\text{EtNH}_2)_4]\text{Cl}_2$ (580) precipitates the red salt from the colorless solutions. Propylamine is the only other amine which forms similar salts. Wolfram (790) also has described similar mixed valence materials which apparently did not contain halide, for example, a nitrate, sulfate, and oxalate. The red chloride could be recovered from these salts by adding HCl solution, but no work on them has been described since 1907 (384).

Because they were able to prepare a salt with the formula $\text{Pt}(\text{EtNH}_2)_4\text{Cl}(\text{NCS})_2$, which they thought was a dimer, Drew and Tress (205) thought that Wolfram's red salt was also a dimer rather than a double salt, but a crystal structure determination (165) has confirmed the earlier conclusion. The crystal structure contains chains of platinum atoms with alternately square planar coordinated Pt(II) ions and octahedrally coordinated Pt(IV) ions. Chlorine atoms lie between the platinum atoms, 2.26 Å from the quadrivalent platinum and 3.13 Å from the divalent (as shown in Fig. 33); the compound clearly belongs to class II. The structure could not be fully refined because of the occurrence of stacking faults due to the chains slipping past one another. Craven and Hall (166) recently attempted to resolve this difficulty by determining the structure of the corresponding bromide, but these crystals also proved to be disordered.

Yamada and Tsuchida (800) studied the polarized crystal spectrum of Wolfram's red salt, and also the isomorphous bromide, which is green. Whereas neither $[\text{Pt}^{\text{IV}}(\text{EtNH}_2)_4\text{Cl}_2]\text{Cl}_2$ nor $[\text{Pt}^{\text{II}}(\text{EtNH}_2)_4]\text{Cl}_2$ showed absorption in the visible, the red salt had an absorption band near $17,000\text{ cm}^{-1}$ which was strongly polarized in the direction of the metal atom chain. The first two bands polarized normal to this direction appear to be internal transitions of the quadrivalent complex (Fig. 34), but the $17,000\text{ cm}^{-1}$ band is likely to be the class II mixed valence absorption band due to the transfer of an electron from the highest filled $5d$ orbital of $[\text{Pt}^{\text{II}}(\text{EtNH}_2)_4]^{2+}$ (probably d_{z^2} since the ligands are purely σ -bonding) to the unfilled d_{z^2} orbital of $[\text{Pt}^{\text{IV}}(\text{EtNH}_2)_4\text{Cl}_2]^{2+}$. Since the d_{z^2} orbitals on

the two centers point at one another and can overlap via the $3 p\sigma$ orbital of the intervening chloride ion, the α of Eq. (15) is nonzero and the transition will be electronically allowed (although not necessarily strong), with a polarization along the Pt-Pt chain.

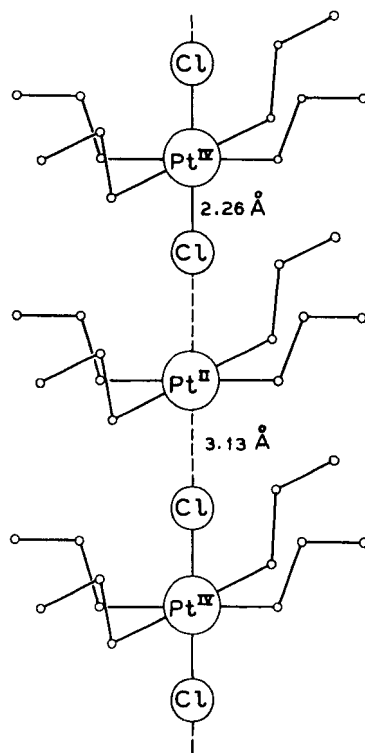
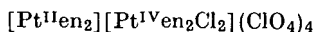


FIG. 33. The platinum atom chain in Wolfram's red salt, $[\text{Pt}^{\text{IV}}(\text{NH}_2\text{C}_2\text{H}_5)_4\text{Cl}_2]^{2+}[\text{Pt}^{\text{II}}(\text{NH}_2\text{C}_2\text{H}_5)_4]^{2+}\text{Cl}_4 \cdot 4\text{H}_2\text{O}$ (165).

A compound which appears to be related to Wolfram's red salt was recently prepared by Kida (416). Chemical analysis suggested the formula



and the compound forms dichroic needles which are red parallel to, and light yellow perpendicular to, the needle axis. A structure determination and polarized spectrum would be of interest.

The other type of mixed valence compound with halide and amine ligands has the general formula $[\text{Ma}_2\text{X}_2][\text{M}'\text{A}_2\text{X}_4]$, where M and M' may be either Pt or Pd, A is an amine, and X a halogen. The palladium salt, with an empirical formula $\text{Pd}(\text{NH}_3)_2\text{Cl}_3$, was first prepared in 1878 (614),

but many others have since been prepared containing palladium or platinum, ammonia or ethylenediamine, and either chloride, bromide, or iodide (202, 204, 205, 314, 708). The compounds are diamagnetic (376, 379, 380, 697) and, as was the case with Wolfram's salt, Drew and his coworkers (203) first thought that they contained metal-metal bonds. However, numerous crystal structure determinations (100, 334, 612, 743) have since shown that the correct formulations are as class II mixed valence compounds. Square planar MA_2X_2 and octahedral $M'A_2X_4$ molecules are stacked in chains with a halogen atom between each pair

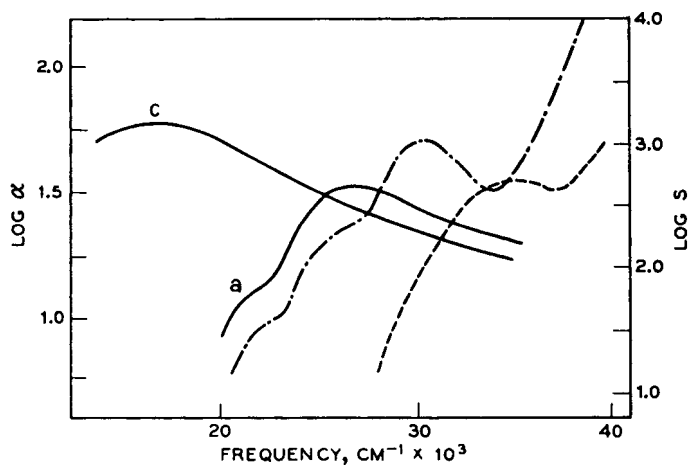


FIG. 34. The polarized absorption spectrum of crystalline $[Pt^{II}(NH_2C_2H_5)_4][Pt^{IV}(NH_2C_2H_5)_4]Cl_6 \cdot 4H_2O$ with the electric vector along the chain direction (c), and perpendicular to it (a). Spectra of the components $[Pt^{II}(NH_2C_2H_5)_4]Cl_2$ (---) and $[Pt^{IV}(NH_2C_2H_5)_4]Cl_2$ (-.-) are also shown for comparison (800).

of metal atoms within the chains (Fig. 35). The most recent determinations (612, 743) agree that the Pt(II)—Br and Pt(IV)—Br bonds at right angles to the chain are slightly longer than the Pt(IV)—Br bond within the chain, and also that the distance between the Pt(II) and the bromine atom attached to Pt(IV) is somewhat smaller than expected from covalent radii. To the degree of approximation obtainable in these determinations, the Pt(II)—Br and Pt(IV)—Br bond lengths appeared identical. Greater precision could not be achieved because of disorder in the crystals resulting from the very weak interactions between neighboring stacks, which enables them to slip past one another. As with Wolfram's salt, the lowest mixed valence absorption in the class II $[MA_2X_2][M'A_2X_4]$ salts should be $dz^2 \rightarrow dz^2$, and allowed with a polarization along the Pt-Pt chain.

In agreement with the formulation of this class of compounds as molecular crystals, the infrared spectrum of Pt_nBr_3 is a superposition of those of Pt_nBr_2 and Pt_nBr_4 (750). In the visible, however, all compounds in the series have intense absorption bands not present in either of their components. Cohen and Davidson (145) reported that $\text{Pd}(\text{NH}_3)_2\text{Cl}_3$ was highly dichroic, being lemon-yellow when the electric vector was perpendicular to the needle axis and black (even for the smallest crystals) when parallel, just as predicted above. When Pt_nBr_3 , reportedly green, is finely ground the powder appears black (750), but

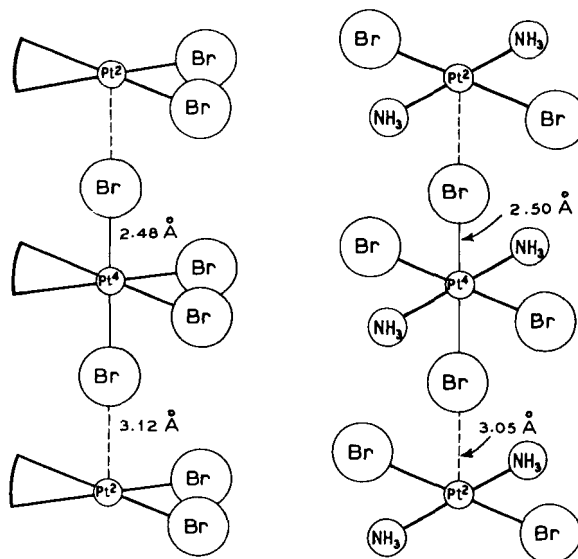
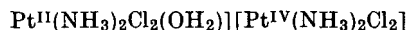


FIG. 35. The alternating $\text{Pt}^{\text{II}}, \text{Pt}^{\text{IV}}$ chains in $[\text{Pt}^{\text{II}}(\text{NH}_2\text{CH}_2\text{CH}_2\text{NH}_2)_2\text{Br}_2]$ $[\text{Pt}^{\text{IV}}(\text{NH}_2\text{CH}_2\text{CH}_2\text{NH}_2)_2\text{Br}_4]$, left, and $[\text{Pt}^{\text{II}}(\text{NH}_3)_2\text{Br}_2]$ $[\text{Pt}^{\text{IV}}(\text{NH}_3)_2\text{Br}_4]$, right (612).

when viewed in thin sections the transmitted color is purple. The green color is therefore caused by metallic reflection, indicating that the mixed valence absorption is very strong and that therefore α is very large. Attempts to measure the polarized crystal spectra of some of these compounds (798, 799) were not very successful because of the extremely intense absorption, but all the examples studied had a broad absorption band between $15,000$ and $20,000 \text{ cm}^{-1}$, polarized in the direction of the metal-metal chains. Like the band in Wolfram's red salt, this transition is probably a mixed valence absorption band involving transfer of an electron from the divalent to the quadrivalent ion, but more refined experimental and theoretical work would be required to make the assignment more precise.

As with Wolfram's red salt, compounds of the type $[\text{MA}_2\text{X}_2][\text{MA}_2\text{X}_4]$ have also been prepared containing X groups other than halogens. For example, the salt

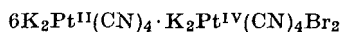


first prepared by Tschugajeff and Tschernjajeff (709) is so strongly dichroic that it has been suggested (78) for use as a polarizer. The dichroism (from black to white in the visible region) is said to extend at least from 12,000 to 29,000 cm^{-1} .

In view of the variety of solid mixed valence halides of palladium and platinum, one might expect that some mixed valence interaction would be detectable in halide-containing solutions. However, Cohen and Davidson (145) were unable to detect a change in the spectrum on mixing solutions of $[\text{Pd}^{\text{II}}\text{Cl}_4]^{2-}$ and $[\text{Pd}^{\text{IV}}\text{Cl}_6]^{2-}$, or $[\text{Pt}^{\text{II}}\text{Cl}_4]^{2-}$ and $[\text{Pt}^{\text{IV}}\text{Cl}_6]^{2-}$. Trivalent platinum has been suggested as an intermediate in the exchange of $[\text{PtCl}_6]^{2-}$ and chloride ions, which proceeds by a chain mechanism (583) but the reaction is catalyzed by $[\text{PtCl}_4]^{2-}$, possibly via a symmetrical transition state. Similarly, electron exchange between $\text{Pt}^{\text{II}}\text{Br}_2$ and $\text{Pt}^{\text{IV}}\text{Br}_4$ is catalyzed by bromide ions, which would also allow a symmetrical transition state to be formed (491).

Mixed valence platinum oxalate complexes were first prepared 70 years ago by Werner, who reacted oxalic acid with sodium platinite, and obtained a salt whose copper color contrasted with the yellow color of the normal $\text{Pt}(\text{II})$ oxalate (764). This interesting compound has recently been reexamined by Krogmann and his co-workers (441, 442). The crystal structure of $\text{K}_2\text{Pt}(\text{C}_2\text{O}_4)_2 \cdot 2\text{H}_2\text{O}$ contains isolated planar oxalato complexes (489) but, in the compound $\text{K}_{1.6}\text{Pt}(\text{C}_2\text{O}_4)_2 \cdot 2.5\text{H}_2\text{O}$, the complex anions are stacked one above the other so that the Pt—Pt distance is only 2.75 Å. It is not possible to distinguish $\text{Pt}(\text{II})$ and $\text{Pt}(\text{IV})$ ions in the structure (441) and, on this basis, the compound is a class III-B system. Krogmann suggests that, whereas in $\text{K}_2\text{Pt}(\text{C}_2\text{O}_4)_2 \cdot 2\text{H}_2\text{O}$ the dz^2 band is filled, on oxidation electrons are drawn off from that band, and an overall bonding results.

The oxidation of potassium platinocyanide with bromine or nitric acid was first investigated over 100 years ago (430), but there appears to be considerable disagreement about the nature of the products. Knop (430) assigned the formula $\text{K}_2\text{Pt}(\text{CN})_5$ to the metallic-looking coppery crystals, but, according to Levy (461), there are two products of the bromine oxidation, one a $\text{Pt}(\text{IV})$ salt $\text{K}_2\text{Pt}(\text{CN})_4\text{Br}_2$ and the other a copper-colored mixed valence salt:



Oxidation by hydrogen peroxide gave another mixed valence salt with a bronze luster, to which analysis assigned the formula $K_{1.5}Pt(CN)_4$. Hydrated lithium cyanoplatinites undergo remarkable color changes when cooled in liquid air (582), which may be related to partial oxidation and formation of a mixed valence chromophore. No work has been done on these interesting compounds since 1912.

P. SILVER

The mixed valence chemistry of silver is limited apparently to its oxides and halides, the latter being mostly mixed compounds with the Au(III) ion. Silver distinguishes itself from its congener element gold in that, whereas the most common valence states of gold are Au(I) and Au(III) and all its mixed valence compounds are formed from these, with silver the most common oxidation states are Ag(I) and Ag(II), yet the mixed valence compounds involve the valence pairs Ag(I)–Ag(0) or Ag(I)–Ag(III). Although we will treat the silver and gold compounds separately, they are closely related in that a large number of Ag(I)–Au(III) complexes have Au(I)–Au(III) counterparts.

Of the silver oxides of potential mixed valence interest, AgO is of prime importance. Reviews of the chemistry of this substance have been presented by McMillan (503) and Dirkse (198). AgO has been prepared in the past in a variety of ways, both chemical and electrochemical, and has been reported to have a variety of conflicting properties. However, AgO preparations made in six different ways by Schwab and Hartmann (646) were shown to have identical X-ray powder patterns. Apparently the purity of the sample varies with its mode of preparation.

The early suggestions that AgO is a peroxide of univalent silver of the form $Ag_2^I O_2$ has been discredited repeatedly by reports of its inability to show reactions thought to be characteristic of peroxides (39, 303). As for AgO being a divalent oxide as its formula implies, one would then expect paramagnetism due to the $4d^9$ Ag(II) ions, yet it is generally agreed that AgO is diamagnetic (425, 528, 622, 651, 696). An obvious suggestion is that AgO should be written as $Ag^I Ag^{III} O_2$, with the $4d^8$ Ag(III) ions in square coordination, thereby making them diamagnetic. Crystal structure analysis demonstrates that this indeed is the case.

It is not entirely clear whether or not AgO can be obtained as a face-centered cubic crystal as well as a monoclinic one, as some have claimed. Although several reports of face-centered cubic AgO have appeared (97, 390, 682), the possibility exists that these are higher or lower oxides

of silver, and not AgO. The monoclinic variety of AgO has been studied extensively by both X-ray and neutron diffraction techniques. Unfortunately, due to the disparity in scattering power of silver and oxygen, the X-ray experiments on powdered AgO do not permit an adequate direct determination of the oxygen positions, but silver positions can be obtained accurately and the oxygen positions then deduced from packing considerations. As determined by Scatturin *et al.* (619, 620), AgO consists of Ag(II) ions in approximately square coordination, forming infinite chains via bridging oxide ions. McMillan (502), on the other hand, finds a distinct difference in the coordination about the silver ions, half of the silver ions being four-coordinated (square) and half two-coordinated (linear). The final word would appear to be that of Scatturin *et al.* (621, 622), who turned to neutron diffraction, wherein silver and oxygen have comparable scattering power, and found that there are indeed two types of silver ion in AgO, one, presumably Ag(III), in square oxygen coordination with Ag—O equal to 2.01–2.05 Å, and the other, presumably Ag(I), in linear coordination having Ag—O equal to 2.18 Å. Monoclinic AgO by this criterion is thus a class I mixed valence system.

Owing no doubt to its importance to the battery industry, there have been a number of studies of electronic conduction in AgO, with some disagreement as to its resistivity. Le Blanc and Sachse (458) found that, whereas the resistivity of Ag₂O is 10⁸ ohm cm, a sample of *approximate* composition AgO had a resistivity of only 10 ohm cm. More recent measurements on pressed pellets of AgO at various pressures yield a resistivity of 0.012 ohm cm (390) when extrapolated to infinite pressure. This material, however, is claimed to be the face-centered cubic variety of AgO. A pellet of monoclinic AgO pressed at 12,000 kg/cm² had a resistivity of 14 ohm cm and the positive temperature coefficient expected for a semiconductor (528). The resistivity of an AgO film formed electrolytically on a metallic silver sheet is 5×10^3 ohm cm (125). These values, although disparate, all indicate a rather high electronic conductivity for AgO, much higher in fact than expected for a class I system. It must be mentioned, however, that pure AgO is a rather unstable compound and the low resistivity reported for it may be due to the presence of impurities.

There are two other compounds which must be mentioned in a discussion of the mixed valence oxides of silver. Unstable, paramagnetic Ag₄O₅, perhaps better written as Ag^IAg₃^{III}O₅, has been described as one of the materials resulting from ozonization of an acidified solution of AgClO₄ (651). It has been claimed, however, that the powder pattern attributed by the original workers to Ag₄O₅ is in fact due to a mixture of Ag₂O₃, AgO, and Ag₂CO₃ (524). A second oxide of presumed composi-

tion Ag_4O_3 has been studied by the analysis of X-ray powder patterns (732), and was said to consist of Ag_4 tetrahedra having three oxide ions bonded symmetrically to each of the silver ions. It remains to be shown if this is a genuine compound, or, as often is the case with silver oxides, simply a mixture of the better known oxides of silver (556).

Electrolysis of an acidic solution of silver nitrate leads to the formation of a black, crystalline substance at the anode having the composition $\text{Ag}_7\text{NO}_{11}$. Although this material has been the subject of a great many studies, its crystal structure only recently has been solved and its electronic structure is still in some doubt. Following the earlier crystallographic work (82, 819), more complete studies by Chou Kung-Du (140) and Naray-Szabo and co-workers (525) finally led to an acceptable structure for $\text{Ag}_7\text{NO}_{11}$. This last study, involving single crystal X-ray work and neutron diffraction on the powdered material, gave a face-centered cubic cell containing polyhedral structural units (as shown in Fig. 36). Each polyhedron (cubo-octadodecahedron) is formed from six square planar AgO_4 units (Fig. 36) and has an NO_3^- ion at its center. The polyhedra themselves are joined by a sharing of the AgO_4 faces, and the smaller cubes formed between polyhedra have Ag(I) ions at their centers. Thus there are two types of silver ion in this structure, one type having eight oxygens about it at the corners of a cube with an Ag-O distance equal to 2.52 Å, and a second type which is in square planar oxygen coordination having Ag-O distances equal to 2.05 Å. The stoichiometry of $[\text{Ag}_7\text{O}_8]^+\text{NO}_3^-$ demands that the ratio $\text{Ag(I)}/\text{Ag(III)}$ be 2/5, whereas the ratio of cubic sites to square planar sites in such a structure is 1/6. Since the cubic sites are occupied only by Ag(I) , and since all the square planar sites are equivalent, the one Ag(I) and the five Ag(III) ions in the square coordination within a polyhedral unit form a two-electron, class III mixed valence system, the metal ions of which are joined by bridging oxygen atoms. Moreover, since each polyhedral unit is joined to twelve similar units by sharing its square AgO_4 faces (Fig. 36), the class III mixed valence system encompasses the entire crystal without involving any of the cubically coordinated silver, and is therefore class III-B.

The mixed valence $[\text{Ag}_7\text{O}_8]^+\text{NO}_3^-$ system involves $4d^8$ and $4d^{10}$ ions in square coordination. Although there is considerable argument as to the ordering of the d levels in square planar systems such as these, there is universal agreement that the uppermost orbital is $dx^2 - y^2$, which thus forms the valence shell of the mixed valence system, together with the $2p\sigma$ orbitals of the bridging oxide ions through which $dx^2 - y^2$ orbitals on adjacent silver ions interact. As was discussed above, the most dramatic properties of a class III-B system are its electrical conductivity and

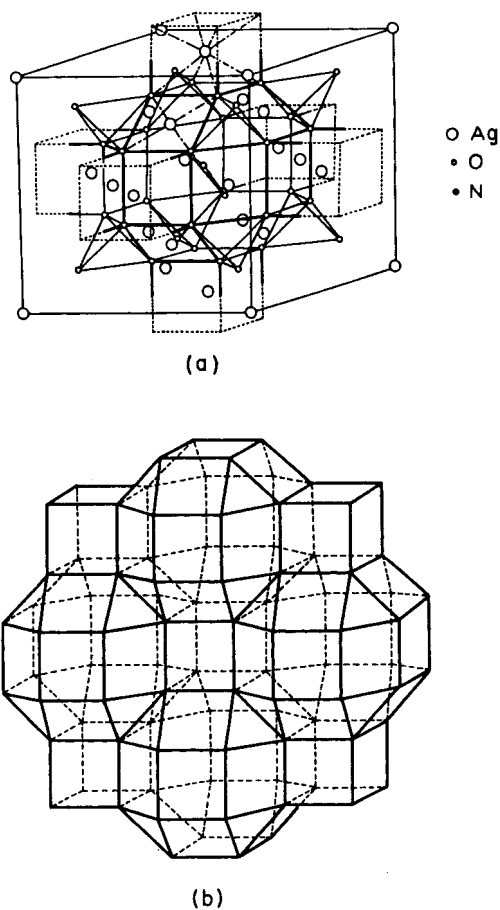


FIG. 36. The unit cell of $\text{Ag}_7\text{O}_8\text{NO}_3$ showing (a) the polyhedral cage with the NO_3^- ion at its center, and (b) the fusion of Ag_6O_8 polyhedra through sharing of the square AgO_4 faces (140, 525).

reflectivity, both of which should be metallic. McMillan (503) first reported that $\text{Ag}_7\text{O}_8\text{NO}_3$ was only semiconducting, but later work on single crystals (594) has shown that it is metallic ($\rho = 2.5 \times 10^{-3}$ ohm cm at 300°K) and is superconducting below 1.04°K . The reflectivity of $\text{Ag}_7\text{O}_8\text{NO}_3$ is also metallic, the crystals being shiny black and quite opaque. The molar susceptibility of $\text{Ag}_7\text{NO}_{11}$ has been reported by various authors as 398×10^{-6} (524), 688×10^{-6} (528), and $6379 \pm 1750 \times 10^{-6}$ (651) cgs, suggesting that the substance as ordinarily synthesized may contain a variable amount of paramagnetic impurity and that the pure substance is only feebly paramagnetic, if at all.

The NO_3^- anion of $\text{Ag}_7\text{NO}_{11}$ apparently can be replaced while keeping

the Ag_7O_8^+ framework intact, for the salts $\text{Ag}_7\text{O}_8\text{F}$ (303, 503), $\text{Ag}_7\text{O}_8\text{ClO}_4$ (503), $\text{Ag}_7\text{O}_8\text{BF}_4$ (594), and $\text{Ag}_7\text{O}_8\text{HSO}_4$ (503, 528) also have been reported, the fluoride, fluoroborate, and bisulfate having unit cell dimensions almost exactly those of the nitrate. Because crystals of the same unit cell dimensions form regardless of the radii of the anions within the polyhedral cages, the systems can be considered as clathrate salts, with mononegative ions as guests within the very rigid Ag_6O_8 cages. Careful analytical work on the fluoride and perchlorate (524) suggests that, unlike the nitrate and bisulfate, these substances may not have a fixed composition. All these substances are metals (594).

Earlier doubts as to the exact composition of Ag_2F and its existence as a stoichiometric compound were settled by the work of Wöhler (786), who showed that there is no oxygen in the substance and that, on dissolution in water, it gives equimolar amounts of AgF and metallic silver, as expected for Ag_2F . Silver subfluoride, Ag_2F , as prepared either electrolytically or by the reaction of silver metal with an AgF solution, is formed as large crystals described as being yellow to yellow-green with a bright metallic, brassy reflex (358).

Bruno and Santoro (109) have performed isotope exchange experiments on Ag_2F in an effort to determine whether or not the silver ions in this substance are equivalent. They found that, following the formation of Ag_2F from inactive AgF and radioactive ^{110}Ag metal and decomposition in H_2O , the resulting Ag metal and AgF had equal activities, indicating the equivalence of the silver atoms. However, a second experiment, in which inactive Ag_2F exchanged heterogeneously with active $^{110}\text{AgNO}_3$ in acetone solution, showed that virtually all the radioactive Ag doped into the compound could be recovered as Ag metal on H_2O decomposition.

X-ray analysis reveals the crystal structure of Ag_2F to be a simple one, having one molecule per hexagonal cell in the anti-cadmium iodide structure (552, 700) (Fig. 37). The structure may be looked upon as consisting of alternate layers of silver and fluoride ions. Within the silver layer, adjacent silver ions are separated by 2.84 Å within the unit cell and 2.989 Å between unit cells, these distances being nearly equal to the Ag-Ag separation of 2.28 Å in metallic silver. All silver atoms are in equivalent sites, and each is coordinated symmetrically by three fluoride ions at a distance of 2.44 Å, equal to the silver-fluoride distance in AgF . Since the Ag_2F stoichiometry demands that half the silver atoms be univalent and half zero-valent, the equivalence of the silver sites and the short repeat distance a lead to a class III-B mixed valence system, which should be an insulator in the c direction and metallic perpendicular thereto.

The resistivity of Ag_2F has been measured, using a four-probe technique at temperatures between 1.4° and 300°K . It increases monotonically from a value of 0.4×10^{-5} to 2.4×10^{-5} ohm cm in this temperature range (359); for comparison, the resistivity of metallic lead is 22×10^{-5} ohm cm at 300°K . Experimental (138) and theoretical (139) studies of the ^{19}F NMR spectra of AgF and Ag_2F show that the spin lattice relaxation time t_1 varies with temperature, as would be expected for relaxation by hyperfine interaction of the ^{19}F nuclei with the conduction electrons. A Knight shift calculated on this assumption is in good agreement with the shift observed between Ag_2F and AgF . The magnetic

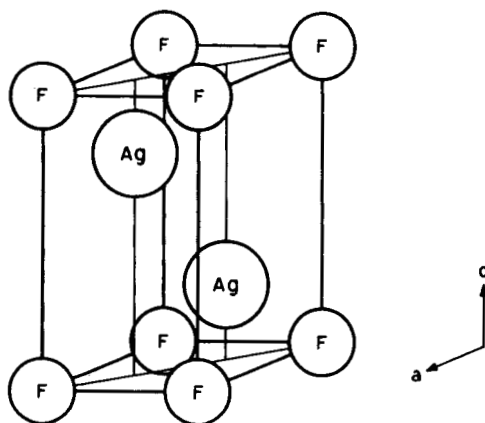


FIG. 37. The hexagonal unit cell of class III-B silver subfluoride, Ag_2F , with $a = 2.989 \text{ \AA}$, $c = 5.710 \text{ \AA}$, and $\text{Ag}-\text{Ag} = 2.84 \text{ \AA}$ (700).

susceptibility of Ag_2F has also been studied (261); the molar susceptibility of -64.3×10^{-6} cgs appears understandable only if the conduction electrons move in an anisotropic potential, in accord with the anisotropic structure of the crystal. Hall measurements (707) on Ag_2F demonstrate that there is one carrier per pair of silver atoms, as one would expect from the $\text{Ag}^0\text{Ag}^{\text{I}}\text{F}$ formulation. Ag_2F is superconducting below 0.058°K (20).

There is a second silver fluoride of interest to us. Fluorination of AgCl results in the formation of a black substance of the composition AgF_2 (609), nominally a divalent silver fluoride. In support of this, it is claimed to be strongly paramagnetic ($\chi_{\text{mol}} = 45 \times 10^{-6}$ cgs at room temperature), as a magnetically dilute divalent silver salt must be. A more detailed study of the magnetic susceptibility of samples of AgF_2 , prepared in three different ways, confirmed the above value of the molar susceptibility and in addition showed that the material is weakly ferromagnetic at 90°K (324). Through the action of fluorine on metallic

silver, a yellow form of AgF_2 is produced (383). The yellow form is poorer in fluoride than the black and has a lower magnetic susceptibility, suggesting perhaps that the black form is contaminated with paramagnetic Ag(III) salts (44). The black form has a face-centred orthorhombic, distorted CaF_2 structure with all the silver ions in equivalent sites (44). The problem as to whether AgF_2 is a salt of Ag(II) or is a mixed valence Ag(I),Ag(III) class III-B system could be clarified perhaps through a study of its resistivity. A similar question exists in regard to the "divalent" black fluoride BaAgF_4 (369).

Solution of the crystal structure of $\text{Ag}_5\text{Pb}_2\text{O}_6$ has revealed it to be a substance containing the Ag_2^+ dimer ion (123). In $\text{Ag}_5\text{Pb}_2\text{O}_6$, the quadrivalent lead ions are surrounded octahedrally by oxygen at 2.19 Å, and three of the five silver ions in the unit cell are univalent and linearly coordinated with oxygen. The two remaining silver atoms form Ag_2^+ dimers having an internuclear separation of 3.04 Å, with each silver of this pair in turn coordinated by three oxygens, much as each silver ion of Ag_2F is coordinated to three fluoride ions. However, unlike the situation in Ag_2F where short Ag-Ag distances imply a very strong interaction between silver ions of adjacent pairs, in the $\text{Ag}_5\text{Pb}_2\text{O}_6$ crystal the Ag_2^+ groups are aligned in chains with 3.39 Å separating the atoms of adjacent pairs. Thus the crystal structure suggests that the system is overall class III-A. Because the Ag_2^+ ion is an odd-electron species, a study of the magnetic susceptibility of $\text{Ag}_5\text{Pb}_2\text{O}_6$ would be of great use in determining just how strongly the Ag_2^+ ions are interacting. If the interaction were strong, then the Ag_2^+ ions form a class III-B system which would be a one-dimensional analog of the two-dimensional silver layer of Ag_2F . There are no data available on the optical, magnetic, or electrical properties of $\text{Ag}_5\text{Pb}_2\text{O}_6$, but the Ag_2^+ ion has been observed by ESR in organic glasses (658).

Q. GOLD

The best known mixed valence gold compounds are the halides of Au(I) and Au(III) and the corresponding compounds having Ag(I) in substitution for the Au(I) ion. Insofar as crystal structures have been determined, these compounds contain the trivalent gold as square coplanar AuX_4 and the univalent gold (silver) as linear bicoordinated AuX_2 (AgX_2) groups, the systems being, in general, class I or class II. The recent report of a genuine, paramagnetic Au(II) complex (749) suggests that one must use some caution in presuming that all nominally divalent gold compounds are univalent-trivalent mixed valence materials.

The AuCl–AuCl₃ system has been studied by Corbett and Druding (150), who conclude that their phase diagram and powder pattern results show no evidence for the formation of the mixed valence compound Au^IAu^{III}Cl₄. However, the silver salt Ag^IAu^{III}Cl₄ (deep red) (355) and the corresponding fluoride Ag^IAu^{III}F₄ (541) have been reported. There also exists a report on the preparation of Au₂I₄, an unstable, ether-soluble substance (106). Although the double chloride Au^IAu^{III}Cl₄ has not been prepared, salts of Au(I),Au(III) and Ag(I),Au(III) with alkali metal cations abound.

One of the first mixed valence triple salts of gold and silver reported was Pollard's salt (570), originally thought to be (NH₄)₈Ag₃Au₄Cl₂₃, but later revised to (NH₄)₆Ag₂Au₃Cl₁₇ (760). A rubidium-silver-gold chloride having the same atomic ratios as Pollard's ammonium salt also has been reported (50, 761). The dark red crystals of the ammonium salt show a black-to-red pleochroism, in which the black color is most likely due to the mixed valence absorption between the [Au^{III}Cl₄][−] and [Ag^ICl₂][−] groups. The crystal structure of this material has not been determined, but unit cell parameters are known (245).

The most famous mixed valence double salts of gold are Wells' cesium salt, Cs₂Au^IAu^{III}Cl₆, and its silver analog, Cs₂Ag^IAu^{III}Cl₆ (50, 758). The structures of these two isomorphous mixed valence halides have not yet been settled, for there are two different interpretations of the experimental X-ray diffraction data. Elliott and Pauling (219, 220) propose a tetragonal structure containing [Au^{III}Cl₄][−] square planar ions and [Ag^ICl₂][−] or [Au^ICl₂][−] linear ions stacked alternately within columns. One sees from Fig. 38 that each Au(III) ion is in a nominally octahedral field with a tetragonal extension, whereas each Ag(I) or Au(I) ion is nominally octahedral with a tetragonal compression. As is well known, such a tetragonal field about the 5d⁸ Au(III) ion leads to a singlet ground state, in agreement with the diamagnetism of Wells' salts (219). On the other hand, Ferrari and co-workers (240, 242) propose that the Au(III) ions in these compounds exist as octahedral [Au^{III}Cl₆]^{3−} ions in a cubic unit cell. That this is inappropriate follows from the fact that the 5d⁸ Au(III) ion in an octahedral field would have a triplet ground state, in contradiction to the observed diamagnetism of these compounds. In support of the M(I),M(III) formulas of these materials, both the Ag and Au salts are described as "astonishingly" jet black in color (758), as expected for a mixed valence salt containing shared ligands. Related materials have been reported in which the two univalent cations of a double formula are replaced by a single divalent cation (242, 244, 758). Thus the triple salts Cs₄M^{II}Au₂^{III}Cl₁₂, wherein M is Zn(II), Pd(II), Cd(II), Hg(II), and Cu(II), have been prepared, but

their colors are little different than the sum of the colors of the M(II) and Au(III) ions.

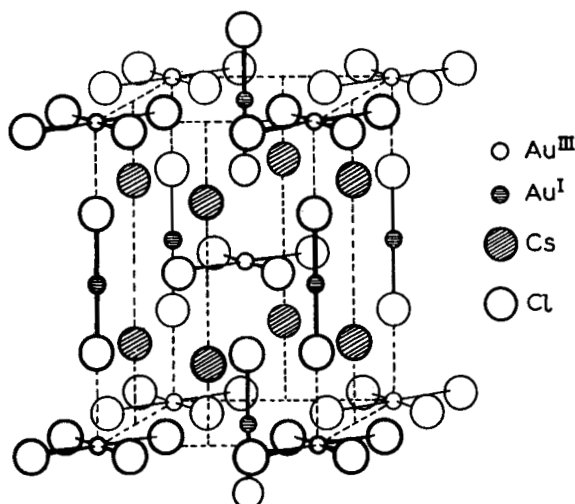
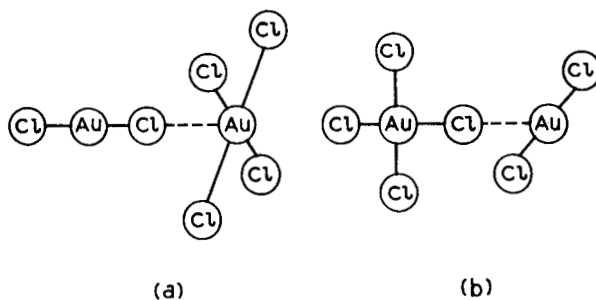


FIG. 38. The tetragonal unit cell proposed by Elliott and Pauling (220) for $\text{Cs}_2\text{Au}^{\text{I}}\text{Au}^{\text{III}}\text{Cl}_6$.

The black color of $\text{Cs}_2\text{Au}^{\text{I}}\text{Au}^{\text{III}}\text{Cl}_6$ undoubtedly arises from the class II mixed valence interaction between the $[\text{Au}^{\text{III}}\text{Cl}_4]^-$ and $[\text{Au}^{\text{I}}\text{Cl}_2]^-$ groups. As can be seen from Fig. 38, there are two relative orientations of these groups in the crystal, redrawn below as configurations (a) and (b):



Regardless of the geometric orientations of the groups, the optical electron in the mixed valence transition can safely be regarded as originating in the axially symmetrical d_{z^2} orbital of the $[\text{Au}^{\text{I}}\text{Cl}_2]^-$ ion and terminating in the $dx^2 - y^2$ orbital of the $[\text{Au}^{\text{III}}\text{Cl}_4]^-$ ion. As explained in Section II, class II mixed valence systems are characterized by a non-zero value of α , which means that the donor and acceptor orbitals must have a nonzero overlap. Inasmuch as this is the case for the chromophore

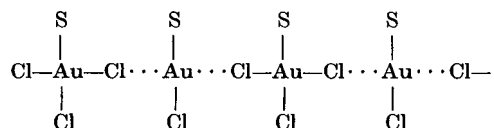
configuration (b), but not for (a), we must assume that it is configuration (b) which is responsible for the mixed valence absorption in $\text{Cs}_2\text{Au}^{\text{I}}\text{Au}^{\text{III}}\text{Cl}_6$, and that this absorption will be polarized in the ab plane.

Preliminary spectra of both $\text{Cs}_2\text{AgAuCl}_6$ and $\text{Cs}_2\text{AuAuCl}_6$ (595) show the mixed valence transition as a rather weak but distinct feature at $15,500\text{ cm}^{-1}$ followed by a stronger absorption centered at $23,500\text{ cm}^{-1}$, having the opposite polarization. The latter band is also found at $23,500\text{ cm}^{-1}$ in the salt $\text{CsAu}^{\text{III}}\text{Cl}_4$ and is due no doubt to the $[\text{Au}^{\text{III}}\text{Cl}_4]^-$ ion. Since Yamada and Tsuchida (798) report that the visible absorption of the triple salts is polarized along the c axis, perpendicular to the planes of the $[\text{Au}^{\text{III}}\text{Cl}_4]^-$ ions, the $23,500\text{ cm}^{-1}$ band must be polarized in the $[\text{Au}^{\text{III}}\text{Cl}_4]^-$ plane. The fact that the absorption spectra are polarized in Wells' salt also argues for the Elliott and Pauling tetragonal unit cell, and against the cubic cell proposed by Ferrari. However, the disagreement between the predicted ab polarization of the first mixed valence absorption band in $\text{Cs}_2\text{Au}^{\text{I}}\text{Au}^{\text{III}}\text{Cl}_6$ and the observed c polarization is still a puzzle requiring further research.

Yamada and Tsuchida (710, 799) also report the polarized crystal spectrum of an ammonium salt of composition $(\text{NH}_4)_3\text{Ag}^{\text{I}}\text{Au}^{\text{III}}\text{Cl}_7$, which has a spectrum much like that mentioned above for $\text{Cs}_2\text{Ag}^{\text{I}}\text{Au}^{\text{III}}\text{Cl}_6$, i.e., two bands, centered at $18,000\text{ cm}^{-1}$ and $23,500\text{ cm}^{-1}$, with opposite polarizations. The spectral similarities suggest that the ammonium salt also contains $[\text{Ag}^{\text{I}}\text{Cl}_2]^-$ and $[\text{Au}^{\text{III}}\text{Cl}_4]^-$ groups sharing halide ions.

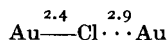
The syntheses of the bromide (241) and iodide (246) salts of the $\text{M}_2(\text{Ag}^{\text{I}}, \text{Au}^{\text{I}})\text{Au}^{\text{III}}\text{X}_6$ mixed valence system have been reported but little is known of them other than that they are black, as expected. According to Ferrari and Cecconi (241), the salt $\text{Cs}_2\text{AgAuBr}_6$ is only an end member in a series of general composition $\text{Cs}_2\text{Ag}_y\text{Au}_{(1-y)/3}\text{AuBr}_6$, as is the corresponding chloride $\text{Cs}_2\text{AgAuCl}_6$.

The properties of an interesting mixed valence compound of gold involving dibenzylsulfide as ligand have been described in detail (84). The compounds $(\text{C}_6\text{H}_5\text{CH}_2)_2\text{SAuCl}_2$ and $(\text{C}_6\text{H}_5\text{CH}_2)_2\text{SAuBr}_2$ are diamagnetic, have molecular weights in bromoform or benzene equal to those of the formulas as written above, and are nonconducting solutes in nitrobenzene. Solution of the crystal structure revealed $(\text{C}_6\text{H}_5\text{CH}_2)_2\text{SAuCl}_2$ to be composed of equal parts of the two neutral species $(\text{C}_6\text{H}_5\text{CH}_2)_2\text{SAu}^{\text{I}}\text{Cl}$ and $(\text{C}_6\text{H}_5\text{CH}_2)_2\text{SAu}^{\text{III}}\text{Cl}_3$, having the mutual orientation:

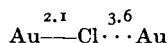


Along the chain direction in this structure, the Au—Cl distance is about 2.1 Å and Au···Cl is about 3.6 Å, but the chains are stacked in such a way in the crystal that the intrachain chloride appears crystallographically to be disordered between Au—Cl and Au···Cl. The structure of the dibromide is closely related, and a dibenzylsulfide gold diiodide has also been prepared (671) but not investigated crystallographically.

As both the component complexes, the monohalo- and the trihalo-gold dibenzylsulfide, can be prepared separately, it is not surprising that the dihalide can be prepared by mixing the components and that the dihalide dissolves to yield the component complexes. There does not appear to be much mixed valence interaction in spite of the bridging chloride ions, for the color of the dihalide is not very different from that of the trihalide, $(C_6H_5CH_2)_2SAuBr_3$ being ruby red and $(C_6H_5CH_2)_2SAuBr_2$ being brown. The reason why Wells' salt is black, whereas the dibenzylsulfides have no apparent mixed valence color, may be related to the fact that in Wells' salt the distances (in angstroms) within the chromophoric grouping are



whereas in the dibenzylsulfides they are



Thus, by comparison, the chlorine is not really bridging in the dibenzylsulfides, and the system is more class I than is Wells' salt.

$[Au^{III}(DMG)_2][Au^ICl_2]$, where DMG is the dimethylglyoxime monoanion, is another mixed valence complex of gold containing an organic ligand. This complex, first synthesized by Rundle (611), was found by him to contain linear chains of $Au(III) \cdots Au(I) \cdots Au(III)$ ions having the internal structure shown in Fig. 39. The Au(I)-Au(III) separation in the chain is 3.26 Å.

The polarized absorption spectrum of $[Au^{III}(DMG)_2][Au^ICl_2]$ has been recorded (798, 801), and it is interesting to compare it with similar spectra of single crystals of $CsAu^{III}Cl_4$ (799). The spectra show what appear to be only minor differences, suggesting that in both cases the spectrum can be attributed to Au(III) ions in square planar coordination, and that there is no visible mixed valence absorption in $[Au^{III}(DMG)_2][Au^ICl_2]$. That this is so seems reasonable, considering the very large difference in the ligand fields at the two gold sites, and also from the fact that, given the geometrical arrangement shown above, the highest-energy, filled orbital of $[Au^ICl_2]^-$, dz^2 , is orthogonal to the lowest-energy,

unfilled orbital of $[\text{Au}(\text{DMG})_2]^+$, $dx^2 - y^2$, as in configuration (a) of $\text{Cs}_2\text{Au}^{\text{I}}\text{Au}^{\text{III}}\text{Cl}_6$, above. The symmetry of the orbitals thus makes the



optical transition forbidden, and the system belongs to class I, its amber-red color being merely that of the $[\text{Au}^{\text{III}}(\text{DMG})_2]^+$ ion.

There is only one example of a mixed valence gold oxide in the literature. Lux and Niedermaier (469) report that the dissolution of metallic gold in molten KOH in a dry O_2 atmosphere leads to the formation of a deep blue polynuclear complex containing approximately

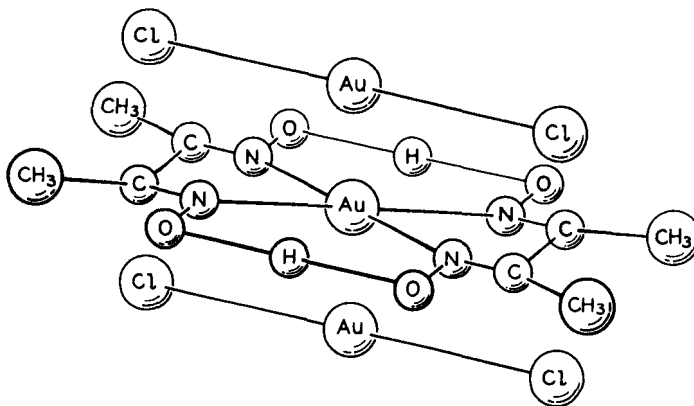


FIG. 39. The class I crystal structure of $[\text{Au}^{\text{III}}(\text{DMG})_2]^+[\text{Au}^{\text{I}}\text{Cl}_2]^{-}$ (611).

equal amounts of Au(I) and Au(III), as determined spectrophotometrically. Analogous complexes also were said to result in aqueous solution, but there is no evidence for their structure in either case.

R. GALLIUM

Gallium, indium, and thallium are all found in a univalent and a trivalent oxidation state. Although this simple generalization at first appears challenged by the existence of several halides of the composition MX_2 , the possibility that they are M(I),M(III) mixed valence compounds rather than compounds of M(II) is a good one. The exact constitution of these salts has been a matter of recent interest, and has been approached from a number of directions.

Klemm and Tilk (426) argued that, unlike the diamagnetic $\text{M}^{\text{I}}\text{X}$ and $\text{M}^{\text{III}}\text{X}_3$ salts, $\text{M}^{\text{II}}\text{X}_2$ compounds will be paramagnetic provided the M(II) ions are not dimerized. Their susceptibility measurements on GaCl_2 and InCl_2 showed that these compounds are diamagnetic and, therefore, are either dimerized like the Hg_2^{2+} ion or are M(I),M(III) mixed valence

compounds. GaI_2 was later shown also to be diamagnetic (148). The first unambiguous structural evidence on the nominally divalent gallium salts was presented by Woodward, Garton, and Roberts, whose Raman spectra of molten GaCl_2 clearly showed the presence of large amounts of the $[\text{Ga}^{\text{III}}\text{Cl}_4]^-$ ion, as recognized from earlier solution work on GaCl_3 in HCl solution (795). On the basis of this, the melt was held to be that of the salt $\text{Ga}^{\text{I}}[\text{Ga}^{\text{III}}\text{Cl}_4]$. This conclusion is also in accord with the high ionic conductivity of the melt (336) and the high resistivity (4.5×10^7 ohm cm) of solid GaCl_2 .

Any doubt still remaining as to the mixed valence nature of GaCl_2 was removed by the determination of the GaCl_2 crystal structure (269).

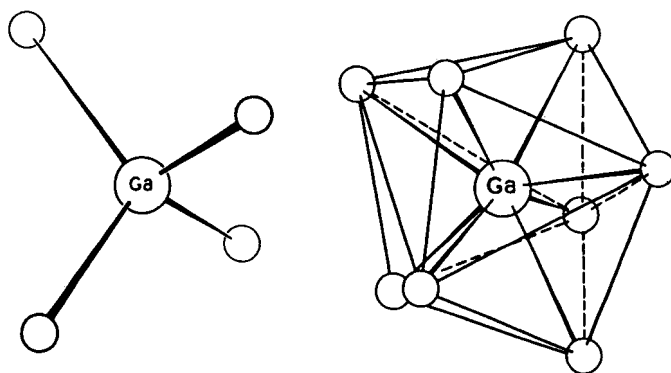


FIG. 40. The coordination about the Ga(III), *left*, and Ga(I) ions, *right*, in crystalline $\text{Ga}^{\text{I}}[\text{Ga}^{\text{III}}\text{Cl}_4]$.

In crystalline GaCl_2 , half of the gallium ions are surrounded tetrahedrally by chloride ions with Ga—Cl distances equal to 2.19 Å, and are undoubtedly trivalent, whereas the other half of the gallium ions, presumably univalent, are surrounded by an irregular dodecahedron of eight chloride ions with Ga—Cl distances equal to 3.2–3.3 Å (Fig. 40). The unusually large Ga^{I} —Cl distance is due perhaps to the Cl—Cl repulsions. GaCl_2 is thus an extreme example of class I mixed valence and, as expected, the crystal is a diamagnetic insulator having essentially the color of the constituent ions. Measurement of the vapor pressure above molten Ga_2Cl_4 suggests the presence of large quantities of genuinely divalent $\text{Ga}^{\text{II}}\text{Cl}_2$ (454), as does the optical spectrum of the vapor (751). A colorless substance of the composition Ga_4Cl_9 has been uncovered by a phase study of the Ga— GaCl_3 system (559); if it is a mixed valence compound it must have Ga(III)/Ga(I) equal to 5/3.

Experiments similar to those described for Ga_2Cl_4 have been directed at elucidating the structure of GaBr_2 . Inasmuch as the Raman spectrum

of molten GaBr_2 shows the presence of large amounts of the $[\text{Ga}^{\text{III}}\text{Br}_4]^-$ ion (796), the melt has a conductance typical of a molten salt consisting of a large anion and a small cation (312), and solid GaBr_2 is colorless and diamagnetic, the compound must be formulated as $\text{Ga}^{\text{I}}[\text{Ga}^{\text{III}}\text{Br}_4]$.

Relatively little is known about the mixed valence iodides of gallium. Diamagnetic, yellow GaI_2 was reported by Corbett and McMullan (148) and later by Chadwick *et al.* (131) as being most likely $\text{Ga}^{\text{I}}[\text{Ga}^{\text{III}}\text{I}_4]^-$, in accord with the formulation of the corresponding chloride and bromide. The electrical conductivities and vapor pressures of the molten iodides of gallium have been studied by Riebling and Erickson (585, 586), who found that, whereas GaI_3 is a low conductance molecular melt, GaI_2 is highly ionic and probably contains the ions $(\text{Ga}^{\text{I}})^+$ and $[\text{Ga}^{\text{III}}\text{I}_4]^-$. Chadwick *et al.* (131) also described the intensely colored, diamagnetic compounds Ga_2I_3 and Ga_3I_5 as being mixed valence materials with formulas $\text{Ga}_3^{\text{I}}\text{Ga}^{\text{III}}\text{I}_6$ and $\text{Ga}_2^{\text{I}}\text{Ga}^{\text{III}}\text{I}_5$, respectively.

There appear to be no lower gallium fluorides (337). In this regard, it is pertinent to note that, unlike the tetrahedral coordination found for the Ga(III) ion in the Ga_2X_4 salts having $\text{X} = \text{Cl}, \text{Br}, \text{or I}$, the complex fluorides of trivalent gallium are octahedrally coordinated (574), as expected from the radius ratio.

Chemically, the salts Ga_2Cl_4 and Ga_2Br_4 are soluble in benzene from which solvent they can be recrystallized as the mixed valence complexes $\text{Ga}_2\text{X}_4 \cdot \text{C}_6\text{H}_6$ (130). Dielectric measurements on solutions of Ga_2Cl_4 in benzene are interpreted as showing the formation of the ion pair $[\text{Ga}^{\text{I}}]^+[\text{Ga}^{\text{III}}\text{Cl}_4]^-$ ($\mu = 8.9$ Debye units) at low concentrations, with aggregation at higher concentrations (504). Addition of basic ligands such as organic amines, ethers, sulfides, selenides, or arsines to the benzene solution of GaCl_2 leads to the immediate precipitation of $[\text{Ga}^{\text{I}}\text{L}_4]^+[\text{Ga}^{\text{III}}\text{Cl}_4]^-$, where L is a monodentate ligand (9, 96, 657). As expected, these mixed valence compounds are all diamagnetic and colorless, except for the 2,2'-dipyridyl complex which is red (9). As the dipyridyl ligands are relatively easily reduced, and Ga(I) is easily oxidized, the red color of the complex may be due to a Ga^{I} -dipyridyl charge transfer absorption. Water immediately hydrolyzes GaCl_2 to a dark brown substance analyzed to be $\text{GaClOH} \cdot \frac{1}{2}\text{H}_2\text{O}$ (97). If this substance indeed is a mixed valence material, it would appear to be one of the few reported which show a Ga(I), Ga(III) mixed valence absorption band in the visible region. Dehydration of this substance gives colorless GaClOH , analogous to the GaClSH formed by addition of H_2S to a GaCl_2 solution in benzene (97).

Although in the case of the nominally divalent gallium halides, GaX_2 , the possibility of spin pairing by dimer formation ($\text{X}_2\text{Ga}-\text{GaX}_2$)

is never realized, it is interesting to note, however, that, in the diamagnetic substances GaS and GaSe, dimer pairs of gallium ions are found, each gallium having three sulfide or selenide ions and one other gallium ion about it in a tetrahedral arrangement (330). Inasmuch as the gallium ions in these structures are equivalent, the systems are technically class III-A mixed valence, although in fact it is just as correct to consider them simply as divalent gallium compounds.

S. INDIUM

Unlike the situation with gallium, almost nothing has been done toward elucidating the structures of the mixed valence compounds of indium. Aside from a few isolated reports of magnetic susceptibility and qualitative reports of color, the only works of mixed valence interest are phase studies showing the existence of certain mixed valence indium halides.

The halides InF_2 (337), InCl_2 (6, 94, 144, 234), InBr_2 (94, 744), and InI_2 (567) have been described briefly. The first three have been shown to be diamagnetic, as would be expected for either $\text{In}^{\text{I}}[\text{In}^{\text{III}}\text{X}_4]$ salts or $\text{X}_2\text{In}-\text{InX}_2$ dimers, but not for $\text{In}^{\text{II}}\text{X}_2$ itself. Although the close analogy with the gallium compounds suggests that the InX_2 compounds are $\text{In}(\text{I}), \text{In}(\text{III})$ mixed valence salts, the possibility that the $\text{In}(\text{II})$ halides are really dimers is worth considering on the basis of the colors of the compounds involved (427). The trihalides InCl_3 and InBr_3 are colorless, whereas the monohalides InCl and InBr are, respectively, yellow-red and carmine red. If the InCl_2 and InBr_2 salts are class I mixed valence compounds, one would expect them to be red, the sum of the colors of their constituent ions. In fact, the dichloride and dibromide of indium are colorless, suggesting either that these compounds contain no $\text{In}(\text{I})$ and are therefore to be taken as dimers, or more probably that the $\text{In}(\text{I})$ in InX is complexed by halide ion and has either a ligand \rightarrow metal charge transfer transition or an atomic $5s^2 \rightarrow 5s^15p^1$ transition in the visible, but is complexed much more weakly in the InX_2 compounds, so that these transitions fall in the ultraviolet. It is to be remembered that, in $\text{Ga}^{\text{I}}[\text{Ga}^{\text{III}}\text{Cl}_4]$, the $\text{Ga}(\text{I})$ cation is essentially uncomplexed. The lack of color in the substance $\text{In}^{\text{I}}[\text{Al}^{\text{III}}\text{Cl}_4]$, however, does make the lack of color in In_2Cl_4 (144) rather less surprising. If InBr_2 is a mixed valence compound, it at first seems likely that the $\text{In}(\text{III})$ would be found in the crystal as $[\text{In}^{\text{III}}\text{Br}_4]^-$, just as is found in GaBr_2 . However, it is to be noted that, unlike the corresponding $\text{Ga}(\text{III})$ salt (794), InBr_3 in concentrated HBr does not form the tetrahedral tetrahalide ion $[\text{InBr}_4]^-$,

although such a species is said to form in an ether extract of the aqueous solution (793). Burns and Hume, on the other hand, have found spectrophotometrically an indium bromide species in aqueous solutions of high Br^- content having $\text{Br}/\text{In} = 4$, which they suggest is the octahedral ion $[\text{InBr}_4(\text{H}_2\text{O})_2]^-$ (114).

The phase diagram of the $\text{In}-\text{InCl}_3$ system has been studied rather extensively by a number of investigators, and a large number of mixed valence compounds have been uncovered. To date the list includes InCl_2 (mentioned above), In_4Cl_6 (144, 230, 231, 234, 558), In_4Cl_5 (144), In_4Cl_7 (144, 231), In_5Cl_9 (558), and several other possibilities of undetermined composition. In the $\text{In}-\text{InBr}_3$ system, the corresponding bromides In_4Br_6 and In_4Br_7 as well as In_5Br_7 have been found to exist (94, 511, 744). Of the compounds on this list, Clark *et al.* (144) propose that InCl_2 is not a genuine compound, but simply a mixture of In_4Cl_6 and InCl_3 , whereas Chadwick *et al.* (131) claim to have "reestablished the existence" of InCl_2 on the basis of a redetermination of the indium chloride phase diagram. On the other hand, Fedorov and Fadeev (234) can find no evidence for In_4Cl_5 , a compound claimed by Clark *et al.* Surprisingly, In_4Cl_7 exists as such in the gas phase over solid In_4Cl_7 at 450°C , according to the results of a vapor pressure study.

Clark *et al.* (144) present an interesting geometrical argument for the existence of certain but not all indium halides of a given stoichiometry. In_4Cl_6 is formulated as $\text{In}_3^{\text{I}}[\text{In}^{\text{III}}\text{Cl}_6]$, the radius ratio (565) of $\text{In}(\text{III})$ and Cl^- being such as to allow octahedral coordination as well as tetrahedral coordination. Thus, the salt $\text{In}^{\text{I}}[\text{In}^{\text{III}}\text{Cl}_4]$ also forms. In the case of the lower indium iodides, the radii are such that tetrahedral $[\text{In}^{\text{III}}\text{I}_4]^-$ can be realized but octahedral $[\text{In}^{\text{III}}\text{I}_6]^{3-}$ cannot, in agreement with Peretti's (567) finding that In_2I_4 is the only mixed valence lower iodide of indium. As Clark *et al.* point out, both tetrahedral $[\text{In}^{\text{III}}\text{Br}_4]^-$ and octahedral $[\text{In}^{\text{III}}\text{Br}_6]^{3-}$ ions can meet the radius ratio test, so that both InBr_2 and In_4Br_6 should exist, as they do (744). Applying these tests to the In_4X_7 series, it would appear that these substances contain octahedral $[\text{In}^{\text{III}}\text{X}_6]^{3-}$ ions, since they are found as the chloride and bromide, but not the iodide.

There are reports of the synthesis of mixed metal halides having compositions equivalent to several of the mixed valence halides mentioned above. Thus, corresponding to $\text{In}_3^{\text{I}}[\text{In}^{\text{III}}\text{Cl}_6]$, the salts $\text{Ag}_3^{\text{I}}[\text{In}^{\text{III}}\text{Cl}_6]$ and $\text{Tl}_3^{\text{I}}[\text{In}^{\text{III}}\text{Cl}_6]$ have been reported (235), and the salt $\text{In}^{\text{I}}[\text{Al}^{\text{III}}\text{Cl}_4]$ (144) corresponds to $\text{In}^{\text{I}}[\text{In}^{\text{III}}\text{Cl}_4]$.

Both In_2I_4 and In_2Br_4 can be ammoniated to yield the compounds $\text{In}_2\text{X}_4 \cdot 6\text{NH}_3$ and $\text{In}_2\text{X}_4 \cdot 8\text{NH}_3$ (131, 432). The fact that the iodide ammoniates are bright red and the bromides orange-red as compared

with the colorless ammonia-free In_2X_4 compounds is interesting, but perhaps not totally unexpected in view of the red color of the $\text{In}^{\text{I}}\text{X}$ compounds. However, because of the supposed instability of the $[\text{In}^{\text{I}}(\text{NH}_3)_6]^+$ cation, it has been argued that the ammoniates are $\text{In}(\text{II})$ dimers rather than mixed valence materials (431).

There is little evidence about the colors of the indium halides. If the indium dihalides are mixed valence, there is very little tendency toward class II behavior as evidenced by their lack of color. It is important to note that the dihalides of both gallium and indium can appear colored due to trace impurities of the corresponding monohalides. Thus, the report that $\text{In}-\text{InCl}_3$ mixtures give dark red to black, transparent crystals in the composition range 50–100 mole % InCl_3 (558) is of questionable importance to our discussion. Inasmuch as, in a class II system, the electron affinity of the oxidized species in the ground state is of consequence to the development of a mixed valence color in the visible region, the lack of color in the GaX_2 and InX_2 systems may be attributable in part to a low electron affinity of the $\text{Ga}(\text{III})$ and $\text{In}(\text{III})$ species. This suggestion is compatible with the very high energy of the ligand-to-metal charge transfer absorption in the $[\text{In}^{\text{III}}\text{Cl}_4]^-$ ($46,500\text{ cm}^{-1}$) (615) and $[\text{In}^{\text{III}}\text{Br}_4]^-$ ($42,600\text{ cm}^{-1}$) (114) ions. Spectra of InCl_2 , InBr_2 , and InI_2 in the gas phase have been reported (762), but the absorbing species are triatomic and most likely are the genuine divalent halides.

The action of H_2 and HCN on indium metal has been found to lead to the formation of $\text{In}(\text{CN})_2$, a white solid formulated as $\text{In}^+[\text{In}(\text{CN})_4]^-$ (293).

T. THALLIUM

In contrast to gallium and indium, a very large number and variety of thallium mixed valence compounds have been synthesized, although no more is known of their constitution than has been determined in the cases of gallium and indium. Crystallographically, the structures of three mixed valence thallium compounds have been solved, with surprising results. TlBr_2 (350) is isostructural with $\text{Ga}^{\text{I}}[\text{Ga}^{\text{III}}\text{Cl}_4]$ (269), discussed above. Thus, in TlBr_2 there are tetrahedral $[\text{Tl}^{\text{III}}\text{Br}_4]^-$ ions having $\text{Tl}-\text{Br}$ distances equal to 2.51 Å, and $\text{Tl}(\text{I})$ ions in irregular dodecahedral sites having eight bromines at a mean distance of 3.46 Å. Surprisingly, in the isostructural diamagnetic compounds TlS and TlSe (329, 412) there are two types of thallium, one determined to be $\text{Tl}(\text{III})$ in tetrahedral coordination with, for example, the $\text{Tl}-\text{Se}$ distance equal to 2.68 Å, and one being $\text{Tl}(\text{I})$ having eight Se atoms as nearest neighbors,

with Tl—Se distances equal to 3.42 Å! In fact, in the gallium, indium, thallium group, only four mixed valence compounds have been studied crystallographically, and each has as its structural units the $M^{III}X_4$ tetrahedron and the M^IX_8 dodecahedron. More structures must be solved before one can see how general this combination of coordinations is in the mixed valence compounds of these elements. A preliminary investigation of Tl_2Cl_3 has shown it to have a complex structure with 32 molecules per cell (327).

The thallium halides Tl_2X_3 are probably better written as $Tl_3[Tl^{III}X_6]$. That Tl_4Cl_6 is not a class III mixed valence compound is indicated by the radiochemical exchange experiments of McConnell and Davidson (468, 771), which demonstrated that Tl_4Cl_6 , synthesized from radioactive $^{204}TlCl_3$ and inactive $TlCl$ in HCl solution, when decomposed and analyzed, yielded almost all its radioactivity as $Tl(III)$. This result was interpreted as showing that the $Tl(I)$ and $Tl(III)$ ions of crystalline Tl_4Cl_6 are nonequivalent. The same conclusion was reached following similar experiments with Tl_4Br_6 .

A study of the thallium NMR spectra of several thallium compounds including $TlCl_2$ and $TlBr_2$ has been reported (603). It was found that, as expected from the crystal structure of $Tl^I[Tl^{III}Br_4]$, the molten tetrachloride and tetrabromide yield ionic melts which showed two thallium resonances, the one due to $Tl(I)$ being at higher field than that due to $Tl(III)$. As the temperature of the melt was raised, the two lines fused into one, indicating exchange between the two thallium species with an average lifetime of about 10^{-5} sec at $500^\circ K$. In similar experiments, crystalline and molten $Tl(I)$ salts showed only one line at all temperatures up to $720^\circ K$.

A study of the $TlCl-TlCl_3$ phase diagram by Fadeev and Fedorov (232) demonstrated the existence of only two mixed valence compounds, Tl_2Cl_4 and Tl_4Cl_6 , the first being described by earlier investigators as colorless to yellow, and the second as yellow to red, depending upon the mode of preparation. It is to be noted that $TlCl$ and $TlCl_3$ are colorless and that Tl_4Cl_6 is colorless at the temperature of liquid air. Thus the maximum of the Tl_4Cl_6 mixed valence transition must lie in the ultra-violet region. The corresponding mixed valence bromides, Tl_2Br_4 and Tl_4Br_6 , are respectively yellow and red (54, 55).

Reaction of I_2 with TlI leads to the formation of black Tl_3I_4 (55, 448, 449, 656), a mixed valence iodide having a metal/halogen ratio unlike any reported in the gallium or indium halides. Sharpe (656) proposes $[Tl_2]^+[Tl^{III}I_4]^-$ as the assignment of valences in Tl_3I_4 , but $Tl_5^+Tl^{III}I_8$ seems more reasonable. A third possibility exists that it is the iodine that is mixed valence and not the thallium, i.e., Tl_6I_8 is $Tl_6^+I_5^-(I_3^-)$.

The deep black color of this substance is certainly consistent with a composition containing triiodide or higher polyiodide ions. This third possibility seems attractive since I^- is known to reduce Tl(III) to Tl(I) with the formation of I_3^- , thus leading one to expect that thallium iodides will not contain Tl(III), but may contain I_3^- or higher polyiodides. Such an explanation is similar to that given by Lawton and Jacobson (456) for some of the antimony halides, which were first thought to be Sb(III), Sb(V) compounds and were later shown by them to be polyhalides of Sb(V).

One finds a similar problem in the assignment of valences in the compound $Tl_3Sb_2Cl_{13}$ (223), which may be taken to be either $Tl_3^I Sb_2^V Cl_{13}$ or $Tl_2^I Tl^{III} Sb^{III} Sb^V Cl_{13}$. The deep black color of this substance argues strongly for the latter formulation, since the mixed valence absorption of Sb(III), Sb(V) halides lies at very low energy (see subsection X on antimony). In the same way, the dark violet compound $Tl_2Sb_2Cl_{10}$ (223) is more likely $Tl_2^I Sb^{III} Sb^V Cl_{10}$ than $Tl^I Tl^{III} Sb_2^{III} Cl_{10}$. Similar problems formally exist in the compounds $InTl_2Cl_5$ (557), $InTl_3Cl_6$ (557), and $TlGaCl_4$ (236) although their reactivity toward water should show immediately which of the ions is univalent and which is trivalent.

Evidence for the mixed valence interaction between Tl(I) and Tl(III) in perchloric acid solution was sought by McConnell and Davidson (495) in the spectral region 33,000–42,000 cm^{-1} , but no mixed valence absorption was found. However, their solution contained no halide ions which might act as bridging groups in a mixed valence complex. In this regard, it is perhaps pertinent to note that the charge exchange between Tl(I) and Tl(III) ions is considerably accelerated by the presence of bridging anions in the solution (104, 105, 339, 774).

Peroxide oxidation of an alkaline thallos salt solution precipitates TlO as an unstable, deep blue material (575, 617), which has been formulated as $Tl_2^I Tl_2^{III} O_4$. Scatturin *et al.* (618) report on various oxides TlO_x , having $x > 1.5$, which were said to contain Tl(I), Tl(III), and Tl(IV), and which had numerous reflection maxima in the 10,000–25,000 cm^{-1} region.

A fast ruffle through the thallium volume of Gmelin's *Handbuch* (291) uncovers the following mixed valence compounds: $TlN_3 \cdot Tl(N_3)_3$ (yellow needles yielding Tl(I) and Tl(III) in solution), $2TlNO_3 \cdot Tl(NO_3)_3$ (colorless prisms blackening in moist air), $Tl_2SO_4 \cdot Tl_2(SO_4)_3$ (colorless crystals), $5Tl_2SO_4 \cdot Tl_2(SO_4)_3$ (pale yellow crystals) and the corresponding selenates $Tl_2SeO_4 \cdot Tl_2(SeO_4)_3$ (colorless crystals) and $5Tl_2SeO_4 \cdot Tl_2(SeO_4)_3$ (yellow crystals), $Tl_2Cl_2SO_4$ and $Tl_2Br_2SO_4$ (both yellow), $Tl_2Cl_2SeO_4$ and $Tl_2Br_2SeO_4$ (both yellow), $TlCN \cdot Tl(CN)_3$ (colorless crystals yielding Tl(I) and Tl(III) in base), $Tl_2C_2O_4 \cdot$

$\text{Tl}_2(\text{C}_2\text{O}_4)_3 \cdot 6\text{H}_2\text{O}$ (colorless crystals), $\text{Tl}_2\text{C}_2\text{O}_4 \cdot \text{Tl}_2(\text{C}_2\text{O}_4)_3 \cdot 4\text{NH}_3$, and $[\text{NH}_4, \text{Tl(I)}]_3\text{Tl(III)}(\text{SO}_4)_3$, a mixed crystal. The compound believed to be $\text{Tl}_2\text{Cl}_4 \cdot 2\text{NOCl}$ (28) is really $\text{TlCl}_3 \cdot \text{NOCl}$ (561).

U. TIN

The interesting work of Davidson and co-workers on the interaction between the Sb(III) and Sb(V) ions in concentrated HCl solution was later extended by them to the Sn(II), Sn(IV) system. It was found that mixing Sn(II) and Sn(IV) solutions in concentrated HCl results once more in a mixed valence absorption, although much further in the ultraviolet than was found with antimony (770). As before, the intensity of the mixed valence absorption was proportional to the product of the concentrations of Sn(II) and Sn(IV), showing that in the ground state, at least, the colored species was an Sn(II), Sn(IV) dimer and not an ion containing Sn(III). In addition to the composition study, an investigation was made of the thermal isotope exchange rate (103, 771) and the effect on this of irradiation in the region of the mixed valence absorption (164). It was found that the exchange reaction, which was bimolecular, proceeded in the dark at a rate sufficiently slow to demonstrate that the mixed valence dimer was unsymmetrical in the ground state if, indeed, it had anything at all to do with the exchange process. More interestingly, it was found that irradiation of the solution in the region of the mixed valence absorption ($25,000\text{--}30,000\text{ cm}^{-1}$) at ca. 2°C substantially enhanced the exchange rate, the quantum yield of the photochemically induced exchange being estimated to be 0.2. Since a quantum yield of 0.5 is expected for such a three-level system if the excited state is symmetrical (class III-A), the significantly lower yield may be taken as evidence for an unsymmetrical upper state, as well.

The quantum yield can be interpreted within the framework of the mixed valence model in the following way. Although there is no evidence for the geometry or composition of the unsymmetrical Sn(II), Sn(IV) complex, for the sake of illustration it is represented by configuration A in Fig. 41. The starred atom is radioactive. On excitation in the mixed valence absorption band, an electron is transferred from left to right and both tin atoms become Sn(III) with a simultaneous rearrangement of ligands being quite probable, but in any case not to a symmetrical geometry (configuration B). On relaxation from the excited state B, either the system can go back to the original ground state A by transfer of an electron from right to left, or a second electron may be transferred again from left to right giving the exchanged configuration C. The

quantum yield of photoinduced exchange is thus seen to be related to the relative probabilities of transitions to the terminal states A and C from the intermediate state B. A relative probability of four to one for the $B \rightarrow A$ and $B \rightarrow C$ transitions would then explain the quantum yield of 0.2 observed for the Sn(II),Sn(IV) exchange. More precisely, the intermediate state B is really two states, one a spin singlet and one a spin triplet, and the quantum yield will depend upon the relative rates of reaching A and C from both of the B surfaces, and also on the rate of excited state singlet-triplet intersystem crossing. By whatever mechanism the relaxation from the intermediate state proceeds, it seems clear that Franck-Condon factors play an important role in determining the relative probabilities involved in the photoinduced exchange

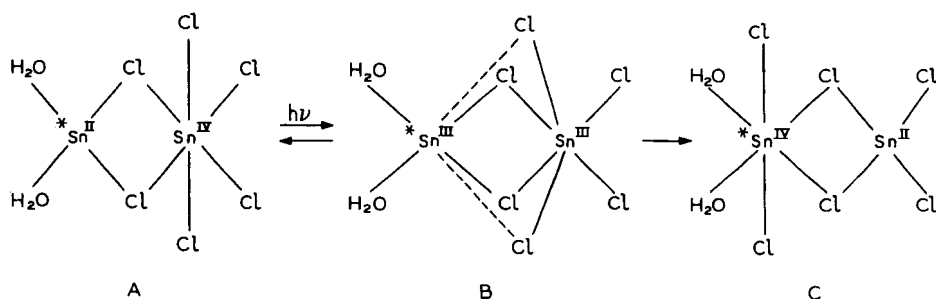


FIG. 41. Configurations involved in photochemical isotope exchange in the three-level system $\text{Sn}_2\text{Cl}_6(\text{H}_2\text{O})_2$.

phenomenon; that terminal state with the larger Franck-Condon overlap with the intermediate state will be favored.

The mixed valence tin oxide Sn_3O_4 has been identified in various thermochemical studies of SnO (678, 679). However, preliminary work on the powder pattern of Sn_3O_4 showed that it could not be indexed as tetragonal (272), this being the crystal system of the analogous lead compound Pb_3O_4 . Similar studies in the Sn-S system (7) indicate the formation of Sn_2S_3 and Sn_3S_4 , mixed valence compounds which may be related to the mixed valence lead oxides of the same stoichiometry. The preparation of the oxide $\text{Sn}^{\text{II}}\text{Sn}^{\text{IV}}\text{O}_6$ by heating SnO at 475°C is described by Decroly and Ghodsi (183).

V. LEAD

The study of the mixed valence oxides of lead is confused by a number of reports on substances thought to be unique compounds, but which may well be mixtures. The mixed valence oxides of lead which

have been authenticated to date have been described most recently by White and Roy (769), who find experimental evidence for Pb_3O_4 , Pb_2O_3 , and $\text{Pb}_{12}\text{O}_{19}$. Byström (121) also discusses the structures and compositions of these compounds and others of less certain stoichiometry.

Pb_3O_4 (red lead) is obtained as transparent scarlet crystals from a solution of PbCO_3 in molten KNO_3 - NaNO_3 flux. According to the X-ray studies of Gross (317) and of Byström and Westgren (118, 122) and the neutron diffraction study of Fayek and Leciejewicz (233), Pb_3O_4 has a class I crystal structure in which lead ions in very different environments

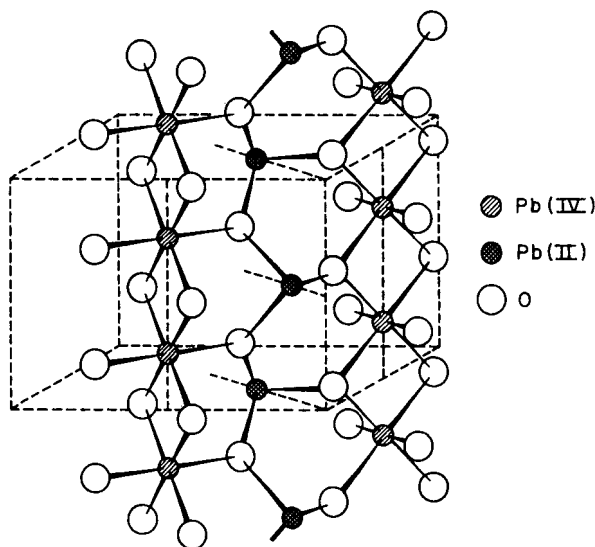


FIG. 42. The class I crystal structure of Pb_3O_4 (756).

share oxide ligands. As shown in Fig. 42, the Pb(IV) ions lie at the centers of oxygen atom octahedra which share edges to form chains and have $\text{Pb(IV)}-\text{O}$ distances equal to 2.15 Å, whereas the Pb(II) are inserted between the $\text{Pb}^{\text{IV}}\text{O}_6$ chains in such a way that each has three oxygen atoms at about 2.2–2.3 Å, the next nearest oxygen neighbor being at 3.0 Å. The $\text{O}-\text{Pb(II)}-\text{O}$ angles are all approximately 90°. Consonant with the class I structure, polycrystalline $\text{Pb}_2^{\text{II}}\text{Pb}^{\text{IV}}\text{O}_4$ has a resistivity of 10^{12} ohm cm (769), and a color (red) which would appear to be just the sum of the colors of $\text{Pb}^{\text{II}}\text{O}$ (red) and $\text{Pb}^{\text{IV}}\text{O}_2$ (red). The bonding and hybridization in Pb_3O_4 have been discussed by Dickens (194).

An anhydrous form of lead sesquioxide, Pb_2O_3 , can be produced by hydrothermal synthesis as large crystals of a lustrous jet black color (143). The striking difference between the colors of Pb_2O_3 and Pb_3O_4 at

first suggests that the lead ion environments are not nearly as dissimilar in Pb_2O_3 as they are in Pb_3O_4 . The structure of Pb_2O_3 has been only partially solved, the all-important positions of the oxygen atoms still being in some doubt (120, 127). It appears that one type of lead atom is at the center of a distorted square with a mean Pb—O distance of 2.1 Å, whereas the second type of lead atom is at the center of a distorted octahedron with four Pb—O distances equal to 2.39 Å, and two additional oxygens at 2.81 Å. If this is so, the two types of lead ion in Pb_2O_3 would seem to form a class I system, judging from our limited experience. On the other hand, the black color of Pb_2O_3 would seem more understandable if it were a class II system. However, the black color may be due to a constituent ion absorption. Because there are two ions of lower valence for every ion of higher valence in Pb_3O_4 , and because the crystal contains twice as many metal ion sites of one type as of the other, the stoichiometry clearly suggests which oxidation states occupy which metal ion sites. Such is not the case in Pb_2O_3 . However, although the question of which oxidation state of lead occupies which type of site in Pb_2O_3 cannot be answered a priori, the bond distances suggest that the Pb(IV) ions are in the distorted square sites and the Pb(II) ions are in the distorted octahedral sites.

The resistivity of Pb_2O_3 is reported as 10^{12} ohm cm, a value which is a composite of bulk resistance, surface resistance, contact resistance, and grain-contact resistance values (769). The fact that the reported resistivities of Pb_2O_3 and class I Pb_3O_4 are of the same order of magnitude demonstrates either the difficulty of divining the significance of resistivities as measured on powders, or that Pb_2O_3 really is a class I system as intimated by its crystal structure. Only further work can decide which is the case.

An experiment widely quoted as refuting the "oscillating valence" concept was preformed by Zintl and Rauch (817) on the mixed valence hydrate $\text{Pb}_2\text{O}_3 \cdot 3\text{H}_2\text{O}$. This yellow-orange material was synthesized, using radioactive Pb(II) and inactive Pb(IV) in a way previously shown not to exchange the Pb(II) and Pb(IV) ions. The solid was irradiated for 3 hours and then decomposed, again without exchange, and the two types of lead were separated and then assayed for radioactivity. It was found that, after irradiation and decomposition, the Pb(IV) was only 1.3% as radioactive as the Pb(II). From this, the conclusion was drawn that in this compound, the valences did not oscillate on irradiation with light and, by analogy, that they did not oscillate in any other mixed valence compound. With the advantage of hindsight, one can point out that, although no structure is available for this hydrated oxide, its lack of an intense, low-energy mixed valence color suggests that the

lead ions are in very different environments in the crystal and that, although it is a three-level system (see tin, subsection U), the excited state reached in a mixed valence absorption will always relax to the no-exchange ground state. This will be especially true in crystals where nuclear rearrangements are difficult. Although the Zintl and Rauch experiment performed on $\text{Pb}_2\text{O}_3 \cdot 3\text{H}_2\text{O}$ therefore sheds no light on the problem of "oscillating valence," the experimental idea has been used with interesting results by Craig and Davidson (164) in the aqueous Sn(II),Sn(IV) system.

A brown-black mixed valence lead oxide, earlier known as $\alpha\text{-PbO}_x$ (122) and now known to have the stoichiometry $\text{Pb}_{12}\text{O}_{19}$, has been briefly described. A crystal structure, deduced both from a single crystal X-ray study (122) and from studies of the lead-oxygen phase equilibria and powder patterns (12, 769), shows that the structure of $\text{Pb}_{12}\text{O}_{19}$ is derived from that of tetragonal PbO by the insertion of a layer of oxygen atoms between the Pb—O—Pb layers. The result is a face-centered, nominally cubic cell having a small monoclinic distortion in which all lead atoms are in nearly equivalent, cubic, eightfold coordination. Because the lead atoms in $\text{Pb}_{12}\text{O}_{19}$ occupy slightly dissimilar sites (class II), its resistivity will not be metallic, but should be considerably lower than those of Pb_3O_4 and Pb_2O_3 . This expectation is fulfilled, for the resistivity of $\text{Pb}_{12}\text{O}_{19}$ is reported to be eight orders of magnitude smaller than that of Pb_3O_4 and Pb_2O_3 (769).

As expected, orthorhombic PbO is an insulator. Strangely, although $\text{Pb}_{12}\text{O}_{19}$ appears to be a relatively good conductor of electricity, it is to be noted that, according to the data of White and Roy (769), the single valence material $\text{Pb}^{\text{IV}}\text{O}_2$ has a resistivity which is three orders of magnitude smaller still than that of $\text{Pb}_{12}\text{O}_{19}$. However, it is pertinent to note that a sample of analytical reagent grade PbO_2 has been analyzed earlier to be of the composition $\text{PbO}_{1.98} \cdot 0.04\text{H}_2\text{O}$ (117), thus demonstrating that " PbO_2 " may well be nonstoichiometrically mixed valence, although nominally it is not. Byström (121) also reports a nonstoichiometric composition for commercial " PbO_2 ." There are many examples of the difficulty of getting oxide crystals of many metals free of interfering, extraneous oxidation states. Because of this, it is difficult to assess the true meaning of powder conductivities in oxides.

Infrared spectra of the mixed valence oxides are given by Roy and co-workers (768) in a paper concerned primarily with their high pressure-high temperature polymorphism.

The addition of a solution of $[\text{M}^{\text{III}}(\text{NH}_3)_6]\text{Cl}_3$ to an HCl solution containing Pb(IV) precipitates a pale colored Pb(IV) salt, which subsequently evolves Cl_2 to form darkly colored mixed valence chloro-

plumbates(II,IV). The salts $[\text{Co}^{\text{III}}(\text{NH}_3)_6]\text{PbCl}_6$ and $[\text{Co}^{\text{III}}(\text{NH}_3)_5\text{H}_2\text{O}]\text{PbCl}_6$ have been investigated by Mori (515), who found them to be diamagnetic. This lack of paramagnetism suggests that, as in the Sb(III),Sb(V) halides, the lead in these compounds is in fact an equimolar mixture of the diamagnetic ions Pb(II) and Pb(IV). The corresponding chromium salts $[\text{Cr}^{\text{III}}(\text{NH}_3)_6]\text{PbCl}_6$ and $[\text{Cr}^{\text{III}}(\text{NH}_3)_5\text{H}_2\text{O}]\text{PbCl}_6$ are strongly paramagnetic owing to the presence of the Cr(III) ion. This series of four salts present an interesting situation in that the two aquopentammines are pale red, as might be expected for a $\text{Pb}^{\text{II}}\text{Cl}_6$ - $\text{Pb}^{\text{IV}}\text{Cl}_6$ system, but the hexammines are reported to be violet-black. The suggestion is that the two types of salt have rather different crystal structures.

The crystal structure of the black-violet $[\text{Co}^{\text{III}}(\text{NH}_3)_6]\text{PbCl}_6$ was investigated by Atoji and Watanabe (34), who found it to be closely related to that of $[\text{Co}^{\text{III}}(\text{NH}_3)_6]\text{TlCl}_6$, a compound studied by them earlier (748). In the latter substance, the $[\text{TlCl}_6]^{3-}$ and $[\text{Co}(\text{NH}_3)_6]^{3+}$ ions form a cubic sodium chloride type lattice with four formula weights per unit cell. Each $[\text{TlCl}_6]^{3-}$ octahedron is surrounded by eight $[\text{Co}(\text{NH}_3)_6]^{3+}$ groups as nearest neighbors and eight $[\text{TlCl}_6]^{3-}$ groups as second nearest neighbors at $2^{1/2}$ times the Co—Tl distance. The powder pattern of the hexachloroplumbate compound was interpreted as showing a cubic cell much like that of the hexachlorothallate, in spite of several lines observed in the former which are not present in the latter. If the hexachloroplumbate is indeed cubic as claimed, then either all lead ions must have the intermediate valence 3+ and be paramagnetic, or the system is metallic. The situation is completely analogous to the dilemma discussed in the case of the M_2SbX_6 salts, where a cubic structure implied a paramagnetic species, yet the compounds are observed to be diamagnetic. And just as the solution to that dilemma rested on showing that the crystals were in fact tetragonal, not cubic, it seems a good guess that a more careful study of $[\text{Co}(\text{NH}_3)_6]\text{PbCl}_6$ will show that it too is tetragonal, with valences trapped as $\text{Pb}^{\text{II}}\text{Cl}_6$ and $\text{Pb}^{\text{IV}}\text{Cl}_6$. Indeed, some of the weak lines in the powder pattern of the lead compound index as reflections not allowed in the cubic space group reported for it (180).

If the valences are really trapped, then the PbCl_6 sublattice of $[\text{Co}(\text{NH}_3)_6]\text{PbCl}_6$ is probably related quite closely to the SbBr_6 superlattice of $(\text{NH}_4)_2\text{SbBr}_6$ (Fig. 46). The analogy between the lead and antimony mixed valence halides can be carried further, since Sb(III) and Sb(V) are isoelectronic with Pb(II) and Pb(IV), except for a difference in principal quantum number, and hence should have quite similar mixed valence spectra. The powder reflection spectrum of $[\text{Co}(\text{NH}_3)_6]\text{PbCl}_6$ (shown in Fig. 43) contains intense bands at lower frequencies

than the absorptions of the component ions, which should probably be assigned as class II mixed valence transitions, although in this case some care is needed to distinguish the mixed valence absorption from absorption due to the $[\text{Co}(\text{NH}_3)_6]^{3+}$ ion.

In this regard, it is of interest that the narrow band at $36,300 \text{ cm}^{-1}$ corresponds very closely in energy to the $^1S_0 \rightarrow ^3P_1$ ($6s^2 \rightarrow 6s^16p^1$) transition of the Pb(II) ion in KCl (807). Again, as with the corresponding antimony halides, the frequency and intensity of the mixed valence transition in the chloroplumbates(II, IV) would appear to depend upon

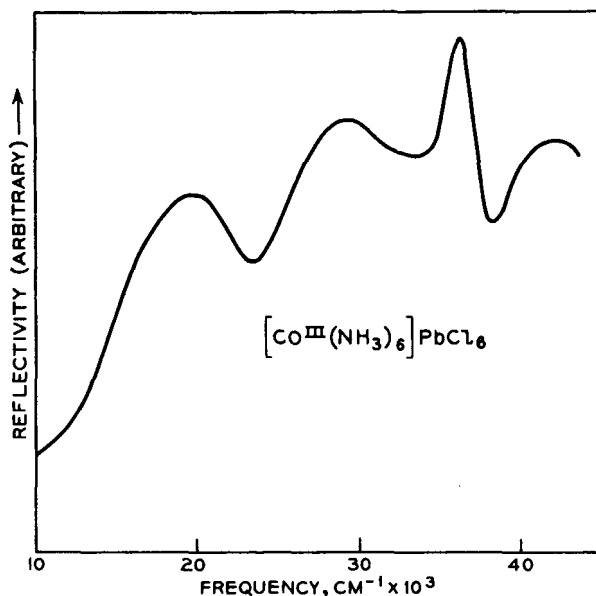


FIG. 43. The diffuse reflectance spectrum of $[\text{Co}^{\text{III}}(\text{NH}_3)_6]\text{PbCl}_6$ (180).

the overlap of halide orbitals on neighboring MX_6 groups transforming the system into class II. Not unexpectedly, the far infrared spectrum of $[\text{Co}(\text{NH}_3)_6]\text{PbCl}_6$ (42) contains a band coincident with that of $[\text{Pb}^{\text{IV}}\text{Cl}_6]^{2-}$, as well as bands at lower frequencies presumably due to $[\text{Pb}^{\text{II}}\text{Cl}_6]^{4-}$.

Arguing by analogy with the Bi_9^{5+} ion characterized by Hershaff and Corbett (356, 357), Britton (98) had proposed that the isoelectronic ion Pb_9^{4-} of Zintl and co-workers (818) also has the tripyramidal structure (Fig. 44). The suggestion of Marsh and Shoemaker (483) that the Pb_9^{4-} ion is formed of three Pb_4 tetrahedra sharing two vertices each is readily seen to be equivalent to Britton's description with allowances for distortion.

A brief note by Gasperin (270) describes the structure of a mixed

valence lead oxychloride of the composition $\text{Pb}_{3.6}\text{Cl}_{1.8}\text{O}_4$, in which 10% of the metal ion sites are empty, 50% of these sites being filled with Pb(II) and 32% with Pb(IV). In the ideal structure, all metal ion sites are equivalent, having as nearest neighbors four oxygen atoms and one chlorine atom in a square bipyramidal arrangement. As the material is reported to be yellow, it appears that the true structure involves considerable distortion from the ideal, such that the lead valences are firmly trapped as in a class I system.

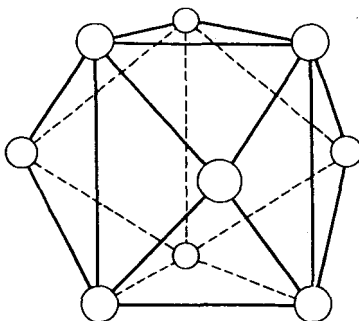


FIG. 44. The structure proposed for the Pb_9^{4-} ion and observed in the iso-electronic Bi_9^{6+} ion in crystalline $\text{Bi}_{12}\text{Cl}_{14}$.

A second compound of apparently nonintegral stoichiometry, $\text{Pb}_3\text{Sb}_2\text{O}_{8.47}$, is discussed by Kuznetsov and Koz'min (452). In this substance, the ratio $\text{Sb(V)}:\text{Pb(IV)}:\text{Pb(II)}$ is equal to 4.0:1:5.0, and the two valences of lead appear trapped, the ions being in different environments. The Pb(IV) is eight-coordinated with six oxygens at 2.19 Å and two at 2.30 Å, whereas the Pb(II) is six-coordinated with oxygens at 2.43 Å. There is no description of the physical properties of $\text{Pb}_3\text{Sb}_2\text{O}_{8.47}$.

A nominally trivalent lead fluoride, PbF_3 , has been mentioned (371), but nothing appears to be known about it.

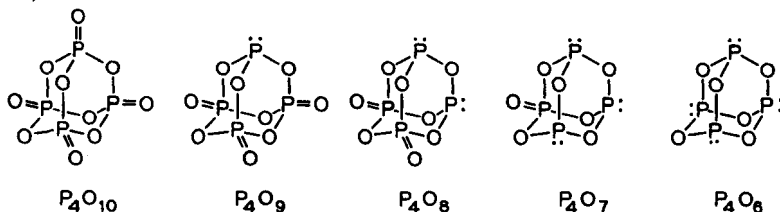
W. PHOSPHORUS AND ARSENIC

Between the two phosphorus oxides, P_4O_{10} and P_4O_6 , there exist three intermediate oxides, P_4O_9 , P_4O_8 , and P_4O_7 , each of which contains P(III) and P(V) oxidation states in the same molecule. As can be seen from the structures given below, the valences in these molecules are

382

MELVIN B. ROBIN AND PETER DAY

firmly trapped as P(III) and P(V), and so the crystals are class I (353, 400, 401):



These mixed valence oxides are colorless and diamagnetic, as expected. Similar mixed valence oxides are reported in the arsenic oxide (466) and the phosphorus sulfide (199) systems. As might be expected from the lack of color in the solid mixed valence arsenic oxides, a concentrated HCl solution containing As(III) and As(V) failed to give a mixed valence absorption band in the 14,000–31,000 cm^{-1} region (772).

X. ANTIMONY

There are two general types of mixed valence system thought to contain Sb(III) and Sb(V) ions. The double halides of Sb(III) and Sb(V) are, with one exception, of a very dark violet, blue, or black color and all present interesting problems in electronic structure, color, magnetism, and molecular structure. The mixed valence antimony oxides, on the other hand, are colorless, and, in the light of the deeply colored halides, present yet another problem in the study of color and constitution.

Salts of antimony of the kind Cs_2SbX_6 were long ago regarded as examples of the 4+ oxidation state of antimony. Although the possibility of the presence of Sb(IV) in such halide salts now appears quite remote, there still remains considerable confusion as to the molecular and electronic structures of the component ions, in spite of recent efforts to rationalize seemingly contradictory experimental results. Setterberg (654) first synthesized the intensely blue salt Cs_2SbCl_6 from the colorless components CsCl , SbCl_3 , and SbCl_5 , and raised the question as to whether it was a salt of Sb(IV) or was to be formulated as the mixed valence compound $\text{Cs}_4\text{Sb}^{\text{III}}\text{Sb}^{\text{V}}\text{Cl}_{12}$. For comparison, the salts $\text{Rb}_3\text{Sb}^{\text{III}}\text{Cl}_6$ and $\text{RbSb}^{\text{V}}\text{Cl}_6$ are colorless and pale yellow-green, respectively. The first indication that Cs_2SbCl_6 was a salt of Sb(IV) came from the work of Wells and Metzger (757), who showed that it was isostructural with $\text{Cs}_2\text{Pb}^{\text{IV}}\text{Cl}_6$, forming mixed crystals with it having a pale to dark green color depending upon the Sb/Pb ratio. Following this, black Rb_2SbCl_6 was found to give violet-colored mixed crystals with $\text{Rb}_2\text{Pt}^{\text{IV}}\text{Cl}_6$, as did the corresponding potassium salts, and the unstable $(\text{NH}_4)_2\text{SbCl}_6$ was

obtained readily as a deeply colored mixed crystal with either $(\text{NH}_4)_2\text{Pt}^{\text{IV}}\text{Cl}_6$ or $(\text{NH}_4)_2\text{Sn}^{\text{IV}}\text{Cl}_6$ (752). That these salts contain Sb(IV) was apparently confirmed by X-ray powder diffraction work on $(\text{NH}_4)_2\text{SbBr}_6$, Rb_2SbBr_6 , and Rb_2SbCl_6 , in which consideration of extinctions and intensities led to the conclusion that each of the salts is face-centered cubic (381), having the anti-fluorite structure of the $\text{M}_2\text{Pt}^{\text{IV}}\text{Cl}_6$ salts. Thus, in these salts all antimony ions appeared to be crystallographically equivalent, and the unusual colors were therefore ascribed to the Sb(IV) ion in octahedral coordination.

The Sb(IV) ion has the outer electronic configuration $5s^1$ and as such should show the paramagnetism characteristic of a 2S state, whereas the ions Sb(III) and Sb(V), being $5s^2$ and $5s^0$, respectively, are diamagnetic. Repeated magnetic susceptibility measurements on the M_2SbX_6 salts and on $(\text{NH}_4)_2(\text{Sb},\text{Sn})\text{Cl}_6$ have shown them in every case to be diamagnetic with $\chi_\sigma \sim 0.3 \times 10^{-6}$ cgs (28, 29, 218, 381, 382). Although demonstrating that these substances do not contain magnetically dilute Sb(IV) ions, the observed diamagnetism may not rule out a strongly antiferromagnetic aggregation of Sb(IV). The latter possibility, however, is a remote one, for the crystal structure determination shows that neither direct Sb—Sb interactions nor bridged configurations of the type Sb—X—Sb are present, but, instead, only SbX_6 — X_6Sb contacts with a center-to-center distance of about 7 Å, a grouping which has never been found to give antiferromagnetic ordering at 300°K. On the other hand, the observed diamagnetism of these compounds agrees with the Sb(III),-Sb(V) formulation.

The high resistivity of the salts (29, 382) demonstrates that, if they are indeed mixed valence, the valences are firmly trapped, although it should be marked that thermally activated electron transfer remains a possibility in class II mixed valence systems. Indeed, $(\text{NH}_4)_2(\text{Sb}_x\text{Sn}_{1-x})\text{Cl}_6$ mixed crystals behave as high resistance semiconductors (33), with a room temperature resistivity which drops sharply with increasing antimony concentration. On the other hand, the thermal activation energy for conductivity is almost independent of composition, suggesting that it is dominated by the energy of mobility rather than production of charge carriers, as in mixed valence hopping semiconductors like $\text{Li}_x\text{Ni}_{1-x}\text{O}$ (Section III, G).

In an interesting application of the continuous variation technique to the problem of the valences in the solid state, Brauer and Schnell (91) attempted to refute the presence of Sb(IV) in these complexes. In this experiment, the intensity of light reflected from powdered samples was measured as the concentration of $(\text{NH}_4)_2\text{SbBr}_6$ was increased in the host crystal $(\text{NH}_4)_2\text{SnBr}_6$. Here, as in the solution work (*vide infra*), it

was found that, at low antimony concentrations, the reflectivity varied as the square root of the $(\text{NH}_4)_2\text{SbBr}_6$ concentration and not linearly as would be expected if the chromophoric grouping were $[\text{Sb}^{\text{IV}}\text{Br}_6]^{2-}$. At higher antimony concentrations, the variation of the reflected light intensity with antimony concentration was not so marked. Such solid state spectrophotometry can sometimes yield useful results when

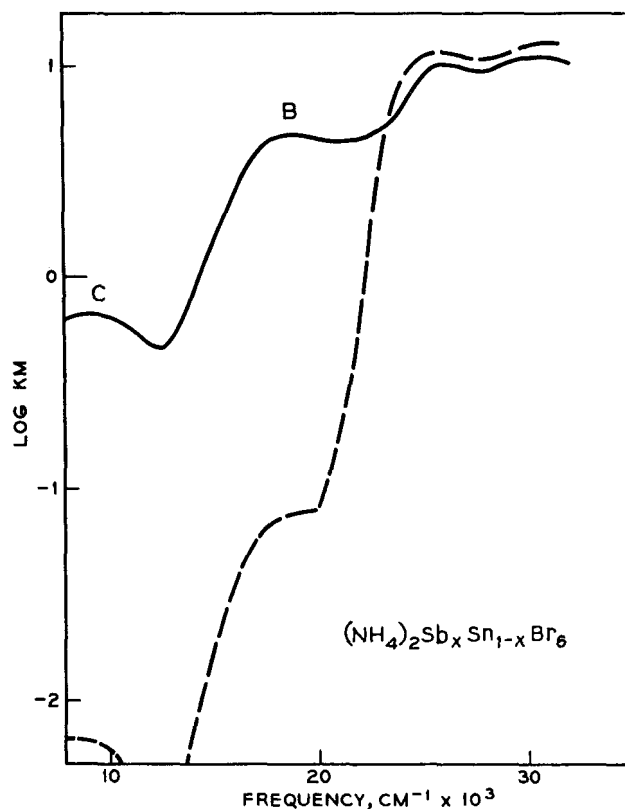


FIG. 45. The diffuse reflectance spectrum of solid solutions of $(\text{NH}_4)_2\text{SbBr}_6$ in $(\text{NH}_4)_2\text{SnBr}_6$ at high (—), and low (---) concentrations. The bands B and C are mixed valence transitions.

comparisons are made between sets of very similar samples and precautions are taken to ensure uniform particle sizes. However, it is not clear whether such precautions were taken in this case, and since the frequency at which measurements were made ($21,300\text{ cm}^{-1}$) does not correspond to the interaction absorption frequency (Fig. 45), it is difficult to draw conclusions from the experiment.

Further evidence of the mixed valence nature of the hexahaloantimonates was provided by Turco and co-workers (711-714), who have shown in a series of studies that the introduction of radioactive

Sb(III) into these salts does not yield equal amounts of radioactive Sb(III) and Sb(V) on decomposition, as would be expected if all the antimony ions in the crystal were equivalent. They also report that Rb_2SbCl_6 can be made with Sb(V)/Sb(III) ratios as large as 1.6, while still maintaining the color and external form of the 1:1 substance. Even larger deviations of the Sb(V)/Sb(III) ratio from 1.0 were reported for the mixed crystals of $(\text{NH}_4)_2\text{SbCl}_6$ in $(\text{NH}_4)_2\text{SnCl}_6$, but a recent study of this system (33) did not confirm this result.

The major objection to the Sb(III),Sb(V) mixed valence model of the M_2SbX_6 crystals was removed by Tovborg Jensen and Rasmussen (705), who found that the crystals reported as cubic by Jensen (381) are in fact tetragonal with $c/a = 1.43$, whereas this ratio is 1.414 for a cubic cell. In particular, it was found that $(\text{NH}_4)_2\text{SbBr}_6$, Rb_2SbBr_6 , and Cs_2SbBr_6 are tetragonal and that Rb_2SbCl_6 is strictly cubic but has an anomalous X-ray intensity distribution, which suggests disorder among the Sb(III) and Sb(V) ions. Recent confirmation of Tovborg Jensen and Rasmussen's powder measurements has come from single crystal X-ray work by Lawton and Jacobson (456) on $(\text{NH}_4)_2\text{SbBr}_6$. They found a small tetragonal distortion of the cubic cell resulting from ordering of the $[\text{Sb}^{\text{V}}\text{Br}_6]^-$ and $[\text{Sb}^{\text{III}}\text{Br}_6]^{3-}$ units, as shown in Fig. 46. In this structure, each $[\text{SbBr}_6]^{3-}$ is surrounded by eight $[\text{SbBr}_6]^-$ and four $[\text{SbBr}_6]^{3-}$ ions, and vice versa. The average Sb(III)—Br and Sb(V)—Br bond lengths were 2.795 Å and 2.564 Å, respectively. Thus, the sites of the two types of antimony ion are quite similar, which, when taken with the mixed valence absorption in the visible, strongly suggests that the system is class II. However, it is not immediately obvious how this can be, since there do not appear to be any shared ligands.

Experimentally, the only spectra available are those obtained by diffuse reflection by Day (178) in the systems $\text{M}_2[\text{Sb},\text{Sn}]\text{X}_6$, where $\text{M} = \text{K}, \text{NH}_4, \text{N}(\text{CH}_3)_4, \text{N}(\text{C}_2\text{H}_5)_4, \text{Rb},$ or Cs , and X is Cl or Br (Figs. 45 and 47). The latter was recorded as the difference spectrum between samples of differing dilutions and thus accentuates the visible absorption. In these spectra, the host lattice absorptions are assigned as those bands which do not lose intensity on lowering the concentration of antimony in the solid solution. In the cesium stannic chloride mixed crystal, the sharp band at $31,000 \text{ cm}^{-1}$ (marked A) is most probably the $^1S_0 \rightarrow ^3P_1$ component of the $5s^2 \rightarrow 5s^15p^1$ transition in Sb(III), which occurs at $29,000 \text{ cm}^{-1}$ in $[\text{Co}(\text{NH}_3)_6][\text{Sb}^{\text{III}}\text{Cl}_6]$. The first absorption band of $[\text{Sb}^{\text{V}}\text{Cl}_6]^-$, which occurs at $37,000 \text{ cm}^{-1}$ in solution (772), is hidden under the host lattice absorption. The lower frequency bands (marked B and C in Figs. 45 and 47) are clearly the interaction bands responsible for the mixed valence color in M_2SbX_6 systems.

Day (178) suggested that the two mixed valence transitions B and C are the singlet and triplet components of the lowest symmetry-allowed excitation, but it does not now seem likely that an exchange interaction

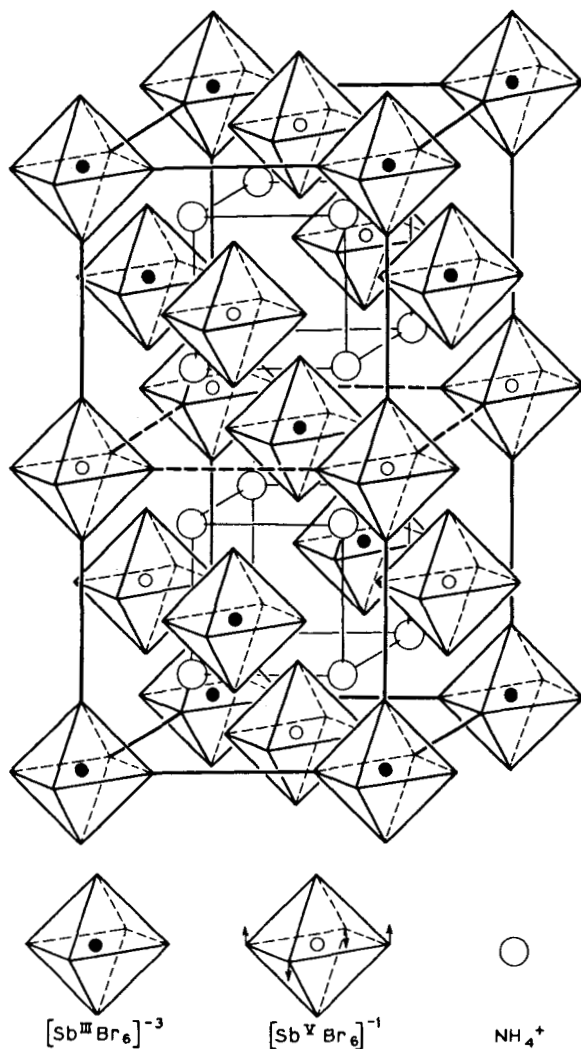


FIG. 46. The class II tetragonal unit cell of $(NH_4)_4Sb^{III}Sb^VBr_{12}$, showing the relative disposition of Sb^VBr_6 and $Sb^{III}Br_6$ octahedra. The distortion of the Sb^VBr_6 octahedron is as indicated at the bottom (456).

between two $5s$ orbitals separated by about 7 \AA could produce a singlet-triplet separation of 9000 cm^{-1} . Two other explanations present themselves. As can be seen from Fig. 46, each $Sb(III)$ ion in $(NH_4)_2SbBr_6$ is surrounded by four $Sb(V)$ ions in a plane, and by four $Sb(V)$ ions at the

vertices of a tetrahedron. If the salts that Day investigated also have this structure and are sufficiently tetragonal, then two symmetry-allowed mixed valence absorption bands would be expected, one, a doubly degenerate, in-plane-polarized transition involving the Sb(III) ion and the planar array of Sb(V) ions, and the second a nearly triply degenerate, weakly polarized transition involving the Sb(III) ion and the tetrahedral array of Sb(V) ions. Another explanation for the second band is that electron transfer occurs to higher orbitals on the Sb(V). The transition

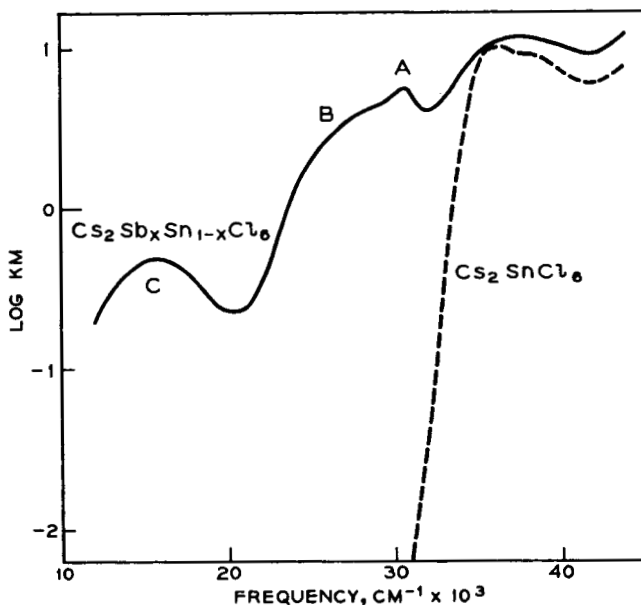


FIG. 47. The diffuse reflectance spectra of Cs_2SnCl_6 (---), and of Cs_2SbCl_6 doped into Cs_2SnCl_6 (—) (180).

$\psi_A 5s^2 \psi_B 5s^0 \rightarrow \psi_A 5s^1 \psi_B 5p^1$ is expected to lie above $\psi_A 5s^2 \psi_B 5s^0 \rightarrow \psi_A 5s^1 \psi_B 5s^1$ by an amount corresponding to the excitation $\psi_B 5s^1 \rightarrow \psi_B 5p^1$, which is about $86,000 \text{ cm}^{-1}$ in the Sb(IV) free ion (510), but could be considerably less when the Sb(IV) is imbedded in a crystal as a hexahalogen anion.

As was seen in Section II, for a mixed valence transition in the trapped valence case, the transition moment cannot be large unless there is overlap between the functions,

$$\Psi_A(5s) \text{ and } \sum C_i \Psi_{B_i}(5s)$$

The former function is that of the $5s$ orbital on the central antimony ion, and the sum is taken over the $5s$ orbitals of the surrounding antimony

ions, with the signs of the coefficients C_i taken so as to give a function which has a single nodal plane. Thus the qualitative reports, which describe the M_2SbX_6 mixed valence colors as very intense, necessitate a significant overlap between the antimony ion wave functions of neighboring $Sb^{III}X_6$ and Sb^VX_6 groups. This is rather unexpected since the Sb—Sb distance is approximately 7 Å in all cases. The required overlap between the antimony could be imagined to arise from delocalization of the 5s orbitals through σ -bond formation with the halide $p\sigma$ orbitals. If the halide ions on adjacent $[SbX_6]^-$ and $[SbX_6]^{3-}$ ions have a nonzero overlap, there is then formed a path over which an electron could be transferred from Sb(III) to Sb(V). That such an SbX_6-X_6Sb overlap may exist was first suggested by Jensen (382), but Lawton and Jacobson state specifically that there is nothing in the least unusual about the $SbBr_6-SbBr_6$ distances in $(NH_4)_2SbBr_6$ (456). Since it is notoriously difficult to assess absorption intensities in solids from visual depth of color, it may well be that the transition moment of the mixed valence absorption and the associated overlap are really quite small, and that it is this small ligand-ligand overlap which turns the formally class I system into a class II system with a visible mixed valence absorption. Charge transfer from halide to metal in adjacent hexahalogen anions has been proposed already by Owen to explain the antiferromagnetic interaction between the Ir(IV) ions in the lattice of K_2IrCl_6 (553).

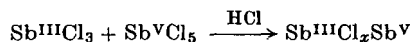
As might be expected, the substitution of the Sb(III) in $M_4Sb^{III}Sb^VCl_{12}$ by the ions Fe(III) or In(III) changes the color from black to pale yellow, since all metal ions are then fully oxidized and there is no electron readily available for low-energy transfer. Day (178) reports the intermolecular charge transfer transition of $Cs_4In^{III}Sb^VCl_{12}$ to fall at 30,800 cm^{-1} , and that of the Tl(III) analog to fall at 29,600 cm^{-1} . The corresponding Bi(III) compound has a deep red color with a maximum at 24,000 cm^{-1} in the diffuse reflectance spectrum.

Many other halide salts have been described as containing Sb(III) and Sb(V). Brauer and Schnell (89) have prepared black $Rb_3Sb_2Br_{11}$ and also mention the salt $TlSbCl_5$. Since this latter substance is reported to have only a pale color, and in view of the fact that the mixed valence thallium chloride compounds are never deeply colored, it may be more reasonable to consider it as being $Tl^ITl^{III}Sb_2^{III}Cl_{10}$ rather than $Tl_2^{III}Sb^{III}Sb^VCl_{10}$. The materials $Rb_8Sb_3Cl_{18}$, $(NH_4)_5Sb_2Cl_{12}$, $(pyH)_5Sb_3Cl_{18}$, and $(pyH)_{11}Sb_5Cl_{30}$ (752) are all brown-black crystalline solids of apparent mixed valence constitution, but a recent X-ray study of $[N(CH_3)_4]_3Sb_2Br_{11}$ (455) reveals that the compound is not an example of antimony mixed valence, for $[Sb_2^{III}Br_9]^{3-}$ groups alternate with

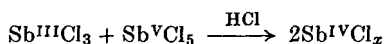
bromine molecules in the lattice. The only mixed valence antimony fluorides reported to date have the compositions $\text{Sb}_2^{\text{III}}\text{Sb}^{\text{V}}\text{F}_{11}$ and $\text{Sb}_5^{\text{III}}\text{Sb}^{\text{V}}\text{F}_{20}$ (607), and are low melting, colorless solids.

Ephraim and Weinberg (224) report a thermochromic effect in an Sb(III),Sb(V) halide system which certainly deserves more exploration, both crystallographically and spectroscopically. Addition of NH_4Cl in sufficient quantity to a molten mixture of SbCl_3 and SbCl_5 leads to the formation of a black mass which on cooling becomes colorless. Heating then restores the black color, and the white-black cycle can be repeated indefinitely. Clearly, more crystallographic and spectroscopic work will be needed before a clear picture emerges of the relationship between the color and constitution of the many mixed valence antimony halides.

The "interaction color" of concentrated HCl solutions containing both SbCl_3 and SbCl_5 , first observed by Weinland and Schmid (752), has since been studied by a very large number of workers. Hydrochloric acid solutions of SbCl_3 and SbCl_5 are colorless and pale yellow, respectively, and both obey Beer's law, showing that there are no Sb(III)-Sb(III) or Sb(V)-Sb(V) interactions in the solutions. However, the HCl solution containing both Sb(III) and Sb(V) is a deep lemon-yellow to brown color, and continuous variation studies show that the concentration of the species responsible for the mixed valence absorption, as measured by the optical density of the solutions at frequencies where the components are only weakly absorbing, is a maximum for $[\text{Sb(III)}]/[\text{Sb(V)}] = 1$. Moreover, the concentration of this colored species varies as the product $[\text{Sb(III)}][\text{Sb(V)}]$ (177, 215, 770, 772). These facts are consistent with a color-producing reaction of the sort



but inconsistent with the reaction



It is to be noted, however, that, since the two antimony atoms in a mixed valence dimer complex in solution might very well have identical ligand fields, the spectrophotometric studies do not rule out the formation of $\text{Sb}^{\text{IV}}\text{Cl}_x\text{Sb}^{\text{IV}}$ in these solutions. The susceptibilities of the Sb(III),Sb(V) solutions have not been measured.

Studies of electrochemical redox reactions (101, 102) as well as radiochemical exchange experiments (79, 434, 529) also point to the formation of an Sb(III),Sb(V) dimer in concentrated HCl solutions. Bonner and Goishi (79) made a careful study of the rate of electron exchange in HCl solutions, using ^{124}Sb as a tracer. The exchange rate increased steadily

with increasing HCl concentration, reaching a maximum at approximately 9.3 *M* HCl and decreasing again in 12 *M* HCl. Up to 8 *M* HCl, complex exchange curves were observed and explained by slow interconversion among two complexes of Sb(V) which exchange at different rates with Sb(III). To discover whether the interaction absorption complex in solution was also the reaction intermediate for exchange, they made qualitative observations on the interaction absorption in non-equilibrium solutions. Their conclusion was that the interaction absorption, which occurs only between $[\text{Sb}^{\text{III}}\text{Cl}_4]^-$ and $[\text{Sb}^{\text{V}}\text{Cl}_6]^-$ ions, does not result from a symmetrical dimer, nor does it lead to a symmetrical excited state, because there is no correlation with the rate of electron exchange. Transition states such as $[\text{Cl}_5\text{Sb}^{\text{III}}\text{ClSb}^{\text{V}}\text{Cl}_5]^{3-}$, $[\text{Cl}_4\text{Sb}^{\text{III}}\text{Cl}_2\text{Sb}^{\text{V}}\text{Cl}_4]^{2-}$, and $[\text{Cl}_4\text{Sb}^{\text{III}}\text{Cl}_2\text{Sb}^{\text{V}}\text{Cl}_3]^-$ have been suggested for the thermochemical electron exchange (434, 529), but no unequivocal choice has been made between them. However, the fact that the mixed valence dimer has a class II absorption suggests that the coordinations about the two antimony ions are very similar.

Under the influence of an electric field, the colored Sb(III),Sb(V) species in 12 *M* HCl was found to migrate to the positive electrode (215), showing that it had a negative charge. Thus, there are more than eight chloride ions in the mixed valence complex $[\text{Sb}^{\text{III}}\text{Sb}^{\text{V}}\text{Cl}_x]^{n-}$. Although a high formal concentration of HCl is required to form the complex, a brown color is also reported to form on heating a mixture of pure SbCl_3 and SbCl_5 ⁴ (224). Usanovitch *et al.* (715) studied this system and concluded that the components reacted to form the ion pair $[\text{SbCl}_4]^-[\text{SbCl}_4]^+$.

Solution of metallic antimony in the molten halides SbX_3 might be expected to lead to the formation of reduced species in the presence of the oxidized SbX_3 , and thence to mixed valence compounds. However, Corbett and students (107, 151) have studied the product of dissolution of antimony in SbI_3 and found it to be diamagnetic Sb_2I_4 .

The oxides of antimony present a most interesting contrast, for although the mixed valence halides are black, the mixed valence oxides are colorless! The difference is even more striking when one realizes that

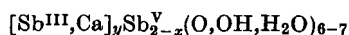
⁴ Whitney and Davidson (772) report that there is no perceptible color change on cooling the concentrated HCl solution of SbCl_3 and SbCl_5 to -80°C , and conclude that the reaction forming the colored species has a very low heat. An alternate explanation rests on the fact that, in any case, one sees only the band edge as the source of color and the intensity of absorption in the band edge will decrease rapidly with a decrease in temperature. The experimental result is then understandable as the simultaneous decrease of visible absorption intensity per absorbing molecule, and increase of the number of absorbing species as the temperature is decreased. According to such an explanation, the heat of dimer formation could be appreciable.

the oxides contain anions bridging the mixed valence antimony whereas, formally, the halides do not. As expected, the difference in color of the oxides and halides can be traced directly to differences in structure.

The primary product formed on heating hydrated Sb_2O_5 is $\text{Sb}_3\text{O}_6\text{OH}$, which contains two gram ions of Sb(V) and one gram ion of Sb(III) per formula weight, and is reported to be colorless to pale yellow, suggesting a class I crystal structure. After a few near misses (185, 527), the crystal structure of $\text{Sb}_3\text{O}_6\text{OH}$ was finally deduced by Dählström and Westgren (196) from the powder pattern. They found a face-centered, cubic cell in which all the Sb(V) ions lie at the centers of oxide ion octahedra having an Sb(V)—O distance of 2.02 Å, whereas each of the Sb(III) ions is surrounded by six oxide ions at a distance of 2.48 Å and two OH^- ions at 2.23 Å. Since a normal Sb(III)—O distance is 2.02–2.1 Å, the Sb(III) is in effect only two-coordinated and the other six oxygens, which simultaneously surround the Sb(III) ion and form octahedra with the Sb(V) ions, have only a very weak interaction with the former. Thus it appears possible to rationalize the lack of color in this compound as the consequence of a class I crystal structure.

On further dehydration of $\text{Sb}_3\text{O}_6\text{OH}$ by prolonged heating at 900°C, the colorless, diamagnetic, insulating, mixed valence oxide $\alpha\text{-Sb}_2\text{O}_4$ is formed. Although a structure had been advanced for $\alpha\text{-Sb}_2\text{O}_4$ in which both the Sb(III) and Sb(V) ions were octahedrally coordinated (197), Wells (756) has criticized it, pointing out that the four shortest Sb(III)—O distances were 0.5 Å longer than the 2.0 Å expected. The validity of this criticism is now apparent from the work of Skapski and Rogers (599, 670), who solved the crystal structures of $\alpha\text{-Sb}_2\text{O}_4$ and of a second polymorph $\beta\text{-Sb}_2\text{O}_4$. In both the α and β forms of Sb_2O_4 the Sb(V) ions are found in layers, each Sb(V) being at the center of a slightly deformed octahedron with Sb—O distances ranging from 1.956 to 1.990 Å. On the other hand, the Sb(III) ions form columns between the layers with each Sb(III) ion having two oxide ions at 2.032 Å and two at 2.218 Å (as shown in Fig. 48). Although the color of $\beta\text{-Sb}_2\text{O}_4$ is not given, one presumes that it is colorless, like the $\alpha\text{-Sb}_2\text{O}_4$ from which it is made, and that both are class I systems. Titration of solutions of Sb_2O_4 in mineral acids is said to show that the antimony in such solutions is present as Sb(III) and Sb(V) in equal amounts (435).

There is a naturally occurring mixed valence mineral, stibiconite, which has the general formula



in which x varies from zero to almost one, and y is approximately one (486). Because this yellow mineral has been shown to be isostructural

392

MELVIN B. ROBIN AND PETER DAY

with the pyrochlore minerals (5, 389, 810), it no doubt has a structure closely related to that of $\text{Sb}_2\text{O}_6\text{OH}$, described above, with Sb(III) and Sb(V) ions in distinctly different environments.

Thus, in the mixed valence antimony oxides, the Sb(V) ion prefers a sixfold, octahedral coordination, whereas the Sb(III) ion has only four

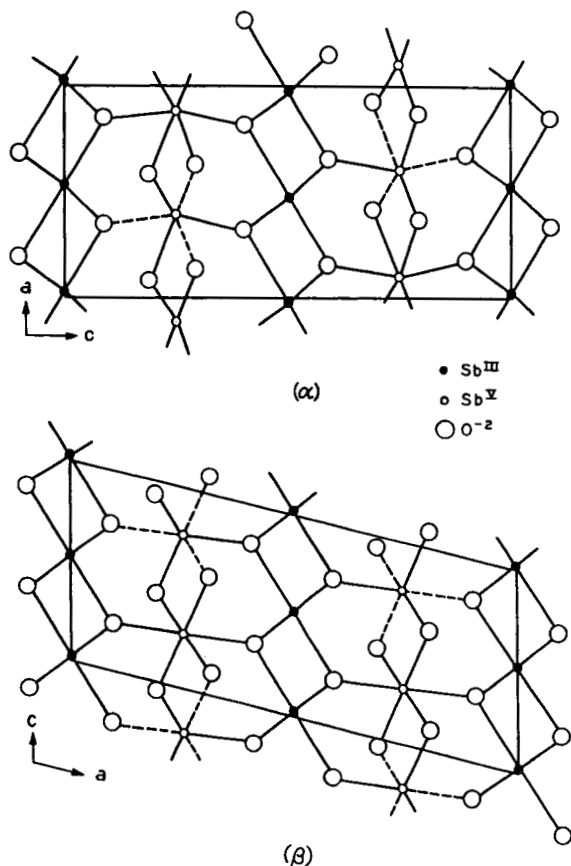


FIG. 48. The class I crystal structures of $\alpha\text{-Sb}_2\text{O}_4$, upper, and $\beta\text{-Sb}_2\text{O}_4$, lower (599, 670).

near neighbors. The fact that no mixed valence optical transition is observed in the visible region in these compounds, even though there are Sb(III)-O-Sb(V) bridges, may result not only from the difference in site symmetries, but also from the very high stability of the Sb(III) ion in fourfold coordination and its consequent resistance to thermal or photochemical oxidation. The mixed valence oxide $\beta\text{-Sb}_2\text{O}_4$ can be heated to over 1000°C in oxygen without oxidation of the Sb(III).

Y. BISMUTH

Metallic bismuth has long been known to dissolve in molten bismuth trichloride, forming lower halides of debatable composition (149). Although BiCl is a predominant species in the gas phase reaction, the condensed phase reaction has been shown by a single crystal X-ray study to yield a compound of the stoichiometry $\text{Bi}_{12}\text{Cl}_{14}$ (356, 357). The compound was shown to consist of two $[\text{BiCl}_5]^{2-}$, one-half $[\text{Bi}_2\text{Cl}_8]^{2-}$, and one mole of the mixed valence cation Bi_9^{5+} per formula weight. This latter cation is a tripyramid of nominal symmetry D_{3h} , having six bismuth atoms at the vertices of a trigonal prism and a bismuth atom placed symmetrically above each of the three rectangular faces of the prism (Fig. 44). Although the observed structure of Bi_9^{5+} is of a symmetry lower than D_{3h} , it approximates the ideal arrangement wherein all nine bismuth atoms are equidistant from a central point. As there are two types of bismuth atom in the complex (the six prism atoms and the three equatorial ones), one might at first attempt to assign integral valences in accord with the trapped valence model. However, this is not possible if the overall charge is to be $5+$. Thus the ion is a class III-A system in spite of certain inequivalences between atoms, and is best considered by using molecular orbital theory. This has been done by Corbett and Rundle (153), who found that the MO theory, using $6p$ orbitals only, predicts a diamagnetic ground state, as observed, and that the equatorial atoms are much less positive than the prism atoms.

Spectroscopically, there are no quantitative data for $\text{Bi}_{12}\text{Cl}_{14}$, but it is reported to form shiny black prisms, the color being due no doubt to the Bi_9^{5+} cation. Because the mixed valence Bi_9^{5+} units are separated by essentially insulating material, the $\text{Bi}_{12}\text{Cl}_{14}$ crystals will probably be found to be insulators, unless, however, there is an additional mixed valence interaction between the reduced Bi_9^{5+} and oxidized $[\text{Bi}^{\text{III}}\text{Cl}_5]^{2-}$ groups.

Spectra of Bi-BiCl_3 melts recorded by Boston and Smith (81) in the visible region show a large absorption tail in the $20,000\text{--}25,000\text{ cm}^{-1}$ region due to hot BiCl_3 (BiCl_3 in a KCl matrix shows a transition centered at $30,500\text{ cm}^{-1}$) (277) and a broad band centered at $17,860\text{ cm}^{-1}$ with a weak shoulder claimed at $16,400\text{ cm}^{-1}$, the combination of the three acting to make the melt black. The large deviation from Beer's law observed by them in the visible region was felt to be due to the presence of two species of unknown structure, each absorbing in the same spectral region. It is to be remembered, however, that, although the black substance $\text{Bi}_{12}\text{Cl}_{14}$ is a solid recovered from a solution of bismuth in BiCl_3 , there is in fact no evidence for the Bi_9^{5+} ion in the melt. In a later spectral

study, Bjerrum *et al.* (71) found that solution of metallic bismuth in dilute solutions of BiCl_3 in liquid $\text{AlCl}_3\text{-NaCl}$ and $\text{ZnCl}_2\text{-KCl}$ eutectics resulted in the formation of Bi^+ ions with three bands in the 10,000–16,000 cm^{-1} region, and Bi_5^{3+} ions with major bands at 12,000 and 25,000 cm^{-1} . This latter mixed valence species may be further coordinated by halide ions.

The magnetic susceptibility of Bi-BiCl_3 solutions has been measured by Nachtrieb (523). In accord with the observed lack of electronic conduction in the dilute melts (30, 31), the Bi-BiCl_3 solutions are diamagnetic, indicating that there are neither metallic conduction electrons nor neutral ground state Bi atoms ($^4S_{3/2}$) in the melt. Thus the dissolved metallic bismuth is associated with itself and/or the BiCl_3 solvent. The susceptibilities and conductivities of solutions of bismuth metal in molten BiBr_3 (308) and BiI_3 (307, 576, 704) have also been studied recently.

There are a few bismuth oxides about which little can be said, but which may later prove to be of mixed valence interest. Zemmann (811) has described the preparation and results of a crystal structure study of an orange-red "bismuth acid," thought to contain Bi(III) and Bi(IV) in a structure like that of "antimony acid," $\text{Sb}^{\text{III}}\text{Sb}_2^{\text{V}}\text{O}_8\text{OH}$. In addition to the red and brown-black forms of $\text{Bi}_2\text{O}_4 \cdot x\text{H}_2\text{O}$ (639), anhydrous BiO has been reported (809). BiO has a slightly distorted sphalerite structure and probably contains equal numbers of Bi(I) and Bi(III) ions.

Z. LANTHANIDES

The reduction of $\text{Ce}^{\text{IV}}\text{O}_2$ by H_2 at high temperatures results in the formation of lower oxides of cerium having a deep blue-black color, which fades to pale yellow-green as the reduction proceeds to $\text{Ce}_2^{\text{III}}\text{O}_3$ (64, 65, 86, 92, 587). Similar lower mixed valence oxides can be produced by firing mixtures of $\text{Ce}^{\text{IV}}\text{O}_2$ and $\text{Ce}_2^{\text{III}}\text{O}_3$ (88, 108). Studies of the phase diagram in the region $\text{CeO}_2\text{-CeO}_{1.50}$ show the presence of three stoichiometric intermediate phases, $\text{Ce}_{11}\text{O}_{20}$, Ce_9O_{16} , and Ce_7O_{12} , and two other regions of composition $\text{CeO}_{1.70}\text{-CeO}_{1.67}$ and $\text{CeO}_{1.67}\text{-CeO}_{1.50}$ (64, 65, 88). There is no evidence for the earlier reported compound Ce_4O_7 . The stoichiometric intermediate phases have rhombohedral structures based on that of fluorite with an extension along a cube diagonal. In these structures, the cation lattice is complete, but there is presumed to be an ordering of vacancies in the anion lattice. The other two regions of lower oxide homogeneity have the type-C and type-A rare earth oxide structures, respectively (64). The lower cerium oxides are most likely

class II systems, but no other physical measurements on them have been reported as yet.

Numerous mixed valence oxides of the other lanthanide elements known to exist in oxidation states higher than 3+, i.e., praseodymium and terbium, have also been widely studied. The best known praseodymium oxide is Pr_6O_{11} , which is formed when any other praseodymium oxide or oxy-salt is strongly heated in air. There was once speculation (573) that praseodymium could be oxidized beyond 4+ in the presence of other trivalent rare earths, and, on this basis, Pr_6O_{11} was given the formula $2\text{Pr}_2^{\text{III}}\text{O}_3 \cdot \text{Pr}_2^{\text{V}}\text{O}_5$, and $\text{Pr}^{\text{IV}}\text{O}_2$ was thought to be $\text{Pr}_2^{\text{III}}\text{O}_3 \cdot \text{Pr}_2^{\text{V}}\text{O}_5$. Marsh (482), however, was able to oxidize praseodymium only to the 4+ oxidation state, a conclusion many times reconfirmed (229, 485, 500, 501). The major features of the phase diagram between $\text{PrO}_{1.5}$ and PrO_2 were mapped by Martin (485), who found two types of phase, one cubic, with essentially the fluorite lattice of PrO_2 systematically deficient in oxygen, and the other hexagonal, based on the A-type Pr_2O_3 lattice. Since 1950 many structural investigations of the PrO_x system have been made by Brauer (88) and by Eyring and his associates, whose results have recently been reviewed (229). We shall not go into details here, except to say that, for carefully annealed samples, it now seems likely that the entire range of composition between $\text{PrO}_{1.5}$ and PrO_2 will be resolved into definite compounds with narrow composition ranges separated by two-phase regions. The existence of a homologous series $\text{M}_n\text{O}_{2n-1}$ has been proposed (229), with slabs of MO_2 joined by facesharing of their coordination polyhedra, as in A-type M_2O_3 .

Similar conclusions would apply to the terbium oxides, of which Tb_4O_7 and Tb_6O_{11} were characterized by Prandtl and Rieder (573) and confirmed by Gruen *et al.* (322), and may also be relevant to the so-called solid solutions of La_2O_3 , Nd_2O_3 , and Sm_2O_3 in CeO_2 and PrO_2 . The latter were said (167, 168) to show a region of homogeneity from MO_2 to about 60% M_2O_3 , but closer examination might reveal details of ordering comparable to that found with the mixed valence transition metal oxides (compare $\text{Ti}_n\text{O}_{2n-1}$ and $\text{Cr}_2^{\text{III}}\text{Ti}_{n-2}^{\text{IV}}\text{O}_{2n-1}$, for example).

Measurements of the physical properties of the lanthanide(III,IV) oxides began with the observation of Foëx (255) that Pr_6O_{11} had a conductivity at 500°C at least 10^7 times greater than that of Pr_2O_3 , and further careful work on all the trivalent lanthanide oxides (535, 536), as well as Pr_6O_{11} and Tb_4O_7 , showed that the latter two compounds were very much more conducting than any of the others. It was also concluded that the conductivity was electronic and not ionic. In his work on the PrO_x phase diagram, Martin (485) used thermoelectric measurements to show that, while type-A Pr_2O_3 is a *p*-type semiconductor, indicating

that the Pr_2O_3 lattice can accommodate small amounts of additional oxygen, Pr_6O_{11} is *n*-type, suggesting that it is effectively PrO_2 with an oxygen deficiency, rather than Pr_2O_3 with excess oxygen. Eyring and his collaborators (228) as well as Honig [quoted in Eyring and Baenziger (228)] have begun to make electrical measurements on the praseodymium oxides as a function of temperature and oxygen pressure, but their results as reported up to the present add little to the earlier qualitative conclusions, except that the transition from *n*-type conduction in PrO_x occurs when *x* is between 1.65 and 1.83.

All the praseodymium(III,IV) oxides are reported as black (229) and those of terbium as dark brown, but, in the oxides closest in composition to Pr_2O_3 , *f-f* transitions of Pr(III) are clearly seen (734) against a background of absorption steadily increasing into the ultraviolet. There is also an extremely broad absorption in the near infrared, beginning at about $12,000\text{ cm}^{-1}$. In the terbium(III,IV) oxides, there is a very broad absorption centered near $15,000\text{ cm}^{-1}$, extending into the near infrared and as far as the ultraviolet cut-off of Tb_2O_3 . From the available structural and physical evidence it therefore appears that all these oxides are class II systems.

Mixed valence oxides of those lanthanides which form stable divalent states have been much less investigated than the quadrivalent ones. One of the best characterized compounds of this type is Eu_3O_4 (2), which, with the isomorphous compound SrEu_2O_4 (40), is related structurally to CaFe_2O_4 . A recent structure analysis (577) showed that each Eu(III) was surrounded by six oxide ions and each Eu(II) by eight, so the compound, which is dark red by transmitted light (577), belongs to class I. Nothing has been reported about its electrical properties. Another mixed valence europium oxide, LiEu_3O_4 (41), has been described as isomorphous with $\text{LiSr}_2\text{Eu}^{\text{III}}\text{O}_4$.

By melting some lanthanide metals with their respective sesquioxides, compounds LnO_x with $1.450 < x < 1.500$ were prepared for Gd, Y, Er, and Lu (507), and their dark colors were attributed to the presence of high concentrations of color centers. Whether this is the case, or whether the excess electrons are trapped on metal ions, forming Ln(II),Ln(III) mixed valence systems, remains to be seen.

Although a mixed valence cerium chloride and fluoride have been mentioned in the literature, it appears that, to the moment, the only genuine mixed valence cerium halide is an iodide. Asker and Wylie (27) mention the double fluoride $(\text{NH}_4)_2\text{Ce}^{\text{III}}\text{Ce}^{\text{IV}}\text{F}_9$, but give no details or references about it; it may well exist only as a misprint. On the basis of e.m.f. studies, Senderoff and Mellors (653) have suggested that the dissolution of Ce metal in molten CeCl_3 results in the formation of

$\text{Ce}^{\text{I}}[\text{Ce}^{\text{III}}\text{Cl}_4]$, analogous to the $\text{Ga}^{\text{I}}[\text{Ga}^{\text{III}}\text{X}_4]$ compounds. On quenching the Ce/CeCl₃ melt, an intensely black solid phase resulted which analyzed for large amounts of both metallic cerium and CeCl₃ (170). Later work (99), however, convincingly refutes the conclusions of the e.m.f. study, and so it would appear that there is no evidence for a mixed valence cerium chloride.

A phase study of the Ce–CeI₃ system by Corbett *et al.* (152) shows that, in addition to CeI₂, a lower iodide of composition CeI_{2.4} can be made. The compound is isomorphous with PrI_{2.5} and can be formulated as $\text{Ce}_2^{\text{III}}\text{Ce}_3^{\text{II}}\text{I}_{12}$. Although nothing more is known of this material, it may well be a metallic conductor, for CeI₂ itself is metallic (152) due to the fact that the Ce(II) ion prefers to put its second 4*f* electron into a conduction band of the solid, thereby becoming Ce(III). According to Sallach and Corbett (616), there are no intermediate mixed valence cerium bromides.

There are a number of lower-valent halides of the other lanthanides which may be of mixed valence interest. By dissolving lanthanide metals in the appropriate molten trihalides, the following “nonstoichiometric” phases have been detected (152, 206–208, 505, 616): NdCl_{2.37}, NdI_{1.95}, PrCl_{2.31}, PrBr_{2.33}, PrI_{2.50}, and GdCl_{1.58}. Scandium (154), yttrium, and erbium (155) do not form such compounds. Like cerium, the diiodides of praseodymium and neodymium are metals, so the corresponding mixed valence compounds may be class III-B systems with partly filled conduction bands based on 5*d* orbitals. In contrast, the other mixed valence halides have very low electrical conductivities including, surprisingly, GdCl_{1.6}, which has a magnetic moment of 7.89 ± 0.03 B.M. per gadolinium (313), very close to that expected if all the gadoliniums had effective 4*f*⁷ configurations (7.94 B.M.). What has happened to the “extra” 1.4 electrons per metal atom has by no means been determined, but the close proximity of the configurations 4*f*⁷5*d*¹ and 4*f*⁸ for Gd(II) suggests that spin pairing might have occurred through the formation of metal-metal bonds using 5*d* orbitals. The compound would then be a member of our class III-A.

AA. ACTINIDES

Stimulated in large part by their potential use as nuclear fuels, large areas of the complicated uranium oxide phase diagram have been studied, revealing many mixed valence materials. Makarov (478) attempted to bring some order to the wealth of data collected by 1961, by suggesting that the uranium oxides form a related series of compounds,

just as was found with the titanium, vanadium, molybdenum, and niobium oxides. In the case of uranium, the general formula U_nO_{2n+2} accounts for a number, but not all the reported oxides. The most studied region of the uranium oxide phase diagram (70, 72, 362, 364, 481, 589, 590) lies between UO_3 ($n = 2$) and UO_2 ($n = \infty$), wherein five members of the series with mixed valence stoichiometry have been located so far.

UO_2 , the end member of the series, is a readily oxidizable material which, at low temperature, can incorporate oxygen into its fluorite lattice up to a composition of $UO_{2.3}$ (24, 316, 568). On annealing, this oxide decomposes to a mixture of UO_2 and U_4O_9 (25, 316, 438, 481, 589). Further oxidation leads to the formation of U_7O_{16} (568), U_6O_{14} (189, 191, 364, 387, 636, 637), U_5O_{12} (636, 637), U_4O_{10} (361, 481, 610), and U_3O_8 (191, 316, 481). In addition to these compounds, the compositions $UO_{2.90}$ (51, 363, 689), U_5O_{13} (72, 637), U_3O_4 (806), $UO_{2.61}$ (589), and U_8O_{17} (481) have been reported. Many of these phases listed above have polymorphic forms and are of appreciable breadth.

In the UO_{2+x} phase, in the region $0 < x < 0.3$, the excess oxygen ions occupy interstitial sites in the host UO_2 fluorite-type lattice in a random manner (24, 781). The contraction of the UO_2 unit cell as oxygen is added to it was interpreted by Anderson *et al.* (11) to result from the partial oxidation of U(IV) to the smaller U(V) ions. Because the interstitial oxide ions form part of the uranium ions' coordination sphere, these ions effectively trap the uranium valence, turning UO_{2+x} into a class II system. Over wide variations of x , the systems all seem to have a resistivity of approximately 10^5 ohm cm at 300° K (521). The color of " UO_2 " has been reported variously as all shades between green and black, due no doubt to the ease with which UO_{2+x} is formed even at room temperature.

U_4O_9 has a structure much like that of the UO_{2+x} phase, except that the interstitial positions are filled in an orderly way (52, 782). Like UO_{2+x} , U_4O_9 is a semiconductor ($E_{act} = 0.46$ eV) (521) and is paramagnetic from 1.4° to 500° K with a maximum susceptibility at 6.4° K (301, 457). The effective magnetic moment of U_4O_9 is 2.06 B.M. per uranium, to be compared with 2.83 B.M. in pure UO_2 . Gotoo *et al.* (301) have computed the effective magnetic moment of U_4O_9 on the assumption that the valences are trapped as either $U_2^{IV}U_2^{V}O_9$ or $U_3^{IV}U^{VI}O_9$, and find 2.10 B.M. for the former and 1.42 B.M. for the latter. Although appearing to support a U(IV),U(V) configuration for U_4O_9 , it must be said that the calculation is based upon a simplified model of the structure. The compound CaU_3O_9 also has a face-centered cubic structure and very nearly the resistivity of U_4O_9 (804).

The application of X-ray (315) and neutron diffraction (467)

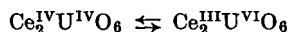
techniques to the problem of the structure of U_3O_8 was successful in showing the positions of both the uranium and oxygen atoms in the unit cell. There are two types of uranium site in U_3O_8 (467), the first having six oxygens at 2.07–2.23 Å and a seventh at 2.44 Å, and a second with six oxygens at 2.07–2.23 Å and a seventh at 2.71 Å, there being twice as many of the latter as the former. Such a structure allows one to assign the valences in U_3O_8 as either $U^{VI}U_2^{IV}O_8$ or $U_2^{VI}U^{IV}O_8$. Whereas the U(VI),U(V) formulation is suggested by Loopstra (467), the U(VI),U(IV) formula is compatible with the general formula $U_2^{VI}U_{n-2}^{IV}O_{2n+2}$ for the uranium oxide series. The green color of U_3O_8 is also that expected for a material containing the U(IV) ion. A radiochemical exchange experiment on U_3O_8 , using first radioactive UO_2 and then radioactive UO_3 in the preparation of U_3O_8 , yielded equal amounts of uranium radioactivity in both oxidation states, suggesting at first that all the uranium atoms were equivalent in the structure (73). The authors admit, however, that it is more likely that an isotopic exchange occurred on formation of the U_3O_8 . Reported resistivity measurements on U_3O_8 differ by a factor of 10^6 , due no doubt to the fact that U_3O_8 and UO_3 readily form solid solutions which upset the stoichiometry. The resistivity of stoichiometric α - U_3O_8 would seem to be 10^5 ohm cm at 300°K, with a semi-conduction activation energy of 0.6–0.7 eV (274, 521). U_3O_8 is paramagnetic with a susceptibility anomaly at 4.2°K (457), and an effective magnetic moment per mole of 1.39 B.M. (338). Assuming that the electron spin is the only source of paramagnetism, $U^{VI}U_2^{IV}O_8$ has an expected moment of 1.41 B.M., and $U_2^{VI}U^{IV}O_8$ has one of 1.63 B.M., both in acceptable agreement with the experimental value.

The α - and β -forms of U_3O_7 have structures much like that of UO_2 , except that they are tetragonally deformed. As with many of the other mixed valence uranium oxides, the material is paramagnetic with a maximum susceptibility at 6.4°K (457), and, as with the others, the resistivity has been reported to be as low as 3×10^2 (780) and as high as 3×10^6 ohm cm (521) for different samples at 300°K.

There are indications that spectral studies on the uranium oxides might be of value in understanding their molecular and electronic structures, particularly as regards the distribution of valence. Thus, Narbutt and Laputina (526) have studied the X-ray fluorescence M spectra of UO_2 , U_3O_8 , and UO_3 , and find small but distinct differences between UO_2 and UO_3 , with U_3O_8 occupying an intermediate position. Gruen's study of the optical spectrum of UO_2 in ThO_2 (323) clearly shows the presence of the U(IV) ion, and his technique might be of value in determining the presence of this valence state in other class II oxides. Finally, Hoekstra and Siegel (363) report that the infrared spectra of

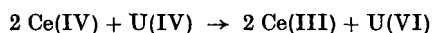
U_3O_8 and $UO_{2.9}$ show that neither of these substances contains the isolated $[U^{VI}O_2]^{2+}$ group.

Hofmann and Hörschele (366) first reported the preparation of the deep blue materials "cerium-uranium blue," having the approximate composition $2 CeO_2 \cdot UO_2$, and a dihydrate having the same Ce/U ratio. Because $U^{IV}O_2$ is brown and $Ce^{IV}O_2$ is colorless, these authors ascribed the blue color of the mixed oxides as due to an oscillation of valence:

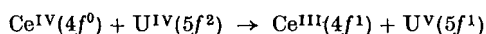


Later investigators (87, 372, 475, 604, 606) have since shown that, because both CeO_2 and UO_2 have the fluorite lattice with only a very small difference in their lattice parameters, mixed crystals of UO_2 and CeO_2 are to be expected over a wide range of composition, and that the Ce_2UO_6 composition is but one unexceptional example of these solid solutions. In addition to the Ce/U ratio, the water content of the cerium-uranium blue "dihydrate" is also variable continuously (87). In spite of extensive X-ray work on the CeO_2-UO_2 system, a disagreement still remains as to the upper limit of UO_2 solubility in CeO_2 , Hund *et al.* (372) claiming that a solid solution forms only in the range 0–63% UO_2 , while Magneli and Kihlberg (475) and Rüdorff and Valet (604, 606) find unlimited UO_2 solubility, with the Vegard law very nearly obeyed.

In $HClO_4-NaClO_4$ solutions, the Ce(IV) ion rapidly oxidizes the U(IV) ion, according to the reaction (36a):



If such a redox reaction were to occur during the formation of cerium-uranium blue, then, depending upon whether the Ce(IV) or U(IV) ions were in excess in the crystal, there would arise the possibility of either Ce(III),Ce(IV) or U(IV),U(VI) mixed valence optical transitions. However, at the $2Ce(IV):1U(IV)$ stoichiometry there would be no excess ions for mixed valence interaction and the blue color should fade at this composition. In fact, the intensity of the blue color is maximal at approximately the 2:1 composition (87), showing that the blue color is instead due to a Ce-U interaction. Now the U(VI) ion when in eightfold oxygen coordination, as it would be in the fluorite lattice of cerium-uranium blue, is known to always draw two of the oxygens toward itself so as to form the $[UO_2]^{2+}$ ion (756). However, were such to happen in cerium-uranium blue, the lattice would no longer be that of fluorite. Thus it appears that the blue color is due to the transfer of an electron between Ce(IV) and U(IV):



Solution of UO_2 in the not easily reduced host ThO_2 results in brownish solids, as expected (87). Pressed pellets of cerium-uranium blue of

various Ce/U ratios show a minimum resistivity of 1.6×10^2 ohm cm at about 40% CeO₂ with maximal resistivity at pure CeO₂ and UO₂ (606).

Oxidation of cerium-uranium blue leads to the formation of CeO₂-U₃O₈ mixed crystals containing up to 45 mole % U₃O₈ while still maintaining the fluorite structure. As determined from density measurements, the excess oxygen ions in CeO₂-U₃O₈ mixed crystals occupy both interstitial and cation sites. The CeO₂-U₃O₈ crystals are described as being dark green to black (606).

The mixed valence halides of uranium have been investigated but very little. There are two chlorides of possible mixed valence interest, $2U^{IV}Cl_4 \cdot U^{VI}Cl_6 \cdot 6POCl_3$, described as dark green crystals (560), and the dark brown prismatic crystals formed by the action of CCl₄ on U₃O₈, formulated as either $2U^{IV}Cl_4 \cdot U^{VI}O_2Cl_2$, or $3U^{IV}Cl_4 \cdot U^{IV}OCl_2 \cdot 2U^{VI}O_2Cl_2$ (375).

Uranium enneaffluoride, U₂F₉, is a black substance formed in varying yield in many fluorination reactions (4, 531, 534). According to Zachariasen (808), U₂F₉ has a class III-B crystal structure with all uranium atoms in structurally equivalent positions. The unit cell is body-centered cubic with the uranium in ninefold coordination, the average U-F distance of 2.30 Å being intermediate between the U(IV)-F and U(V)-F distances of UF₄ and UF₅. However, the same cannot be said for the black color of U₂F₉, for UF₄ is green and UF₅ is colorless. An effective magnetic moment of 2.11 B.M. per uranium atom has been measured for U₂F₉ (595). The resistance of U₂F₉ has not been measured, but would be very interesting as it might suggest whether the system is really class III-B or class II. A second black mixed valence uranium fluoride, U₄F₁₇, has a structure described as "distorted UF₄," and a specific susceptibility of 8.8×10^{-6} cgs at 22°C (4, 531).

The physical and chemical properties of many of the uranium halides and oxides have been described in detail in reference works (406) and (649). Of the other actinide elements, there are only a few oxides whose stoichiometry suggests that they are mixed valence (649). Protactinium forms the oxide Pa₄O₉ which is cubic, as is U₄O₉, but which is white, whereas U₄O₉ is black. The lower oxides PaO_{2.25}-PaO_{2.20} (cubic), Pa₅O₁₁ (tetragonal), and PaO_{2.20}-PaO_{2.00} (cubic) are all black, however. Neptunium forms a chocolate-brown oxide Np₃O₈ isomorphous with U₃O₈ (405), and plutonium forms an oxide phase PuO_{1.50}-PuO_{1.75} isomorphous with Mn₂O₃.

BB. MISCELLANEOUS

Those elements which have as yet only a scant mixed valence chemistry are brought together in this section. The most surprising of

these is xenon, which forms a stable yellow oxide of the apparent composition $K_4Xe^{VIII}Xe^{VI}O_{12}$, which by its color is most likely class I (21, 680). A possible mixed valence compound of aluminum, $Al_4B[N(CH_3)_2]_3(CH_3)_6$, has been reported as a yellow solid having an average aluminum oxidation number of 1.5+ (644). Solutions of cadmium metal in molten $CdCl_2$ have been shown repeatedly to contain species formed from one cadmium atom and from one to three $Cd(II)$ ions (520), but no mixed valence compounds have yet been isolated.

Considerably more can be said about the mixed valence polyhalides; however, we shall limit our remarks to the triiodide ion, and refer the interested reader to the review by Wiebenga *et al.* (773) for information on the other polyhalides. The triiodide ion, I_3^- , is a nominally linear species with ends which are more or less equivalent, depending upon the environment in which it finds itself. Its bonding has been investigated and its electronic spectrum in water explained on the basis of a slightly bent, class III-A system (91). The blue starch-iodine complex has been described as both a class III-A (592) and class III-B (62) polymer of the triiodide ion.

IV. Conclusions

At this point, a survey study of mixed valence chemistry is rather frustrating, because the data for virtually every substance are too meager to allow the deduction and testing of firm conclusions. The reason for this lies in the fact that mixed valence compounds up to now seem to have been studied only by chance, without a real appreciation of their uniqueness and the complementary nature of their various properties. The future is bright, however, in that papers on mixed valence chemistry are presently appearing at the healthy rate of about 60 per year and could easily double, once mixed valence chemistry becomes fashionable. As it stands now, though, the dearth of information is not only in a way frustrating, but also stimulating, we think, and it is our hope that this article will prompt the work in the near future needed to build a proper understanding of this phenomenon. Moreover, the thermodynamic, kinetic, and mechanistic aspects of mixed valence are all important ones which we have not mentioned, along with mixed metal mixed valence, covalent materials, and intermetallics.

It appears that until the properties of mixed valence substances have been more completely investigated, the classification scheme presented here can be used profitably to predict the properties of a substance, given any one of them. One imagines that, in the future, as mixed valence

becomes more and more understandable, it will prove as rewarding to inorganic chemistry as the concept of resonance has been to organic chemistry.

ACKNOWLEDGMENT

P.D. is very grateful to Bell Telephone Laboratories, Inc., for their hospitality during the summer of 1966, when most of this review was written. We both wish to acknowledge the assistance of Mr. N. A. Kuebler with the clerical work, and to thank Dr. H. Basch for performing the H_3^+ calculation for us.

REFERENCES

1. Abe, R., *J. Phys. Soc. Japan* **6**, 345 (1951).
- 1a. Abrahams, S. C., and Bernstein, J. L., *J. Chem. Phys.* **46**, 3776 (1967).
2. Achard, J. C., *Compt. Rend.* **250**, 3025 (1960).
3. Aebi, F., *Helv. Chim. Acta* **31**, 8 (1948).
4. Agron, P., Grenall, A., Kunin, R., and Weller, S., *U.S. At. Energy Comm. Rept. MDDC-1588* (1948).
5. Aia, M. A., Mooney, R. W., and Hoffman, C. W. W., *J. Electrochem. Soc.* **110**, 1048 (1963).
6. Aiken, J. K., Haley, J. B., and Terrey, H., *Trans. Faraday Soc.* **32**, 1617 (1936).
7. Albers, W., and Schol, K., *Philips Res. Rept.* **16**, 329 (1961).
8. Albrecht, W. H., and Wedekind, E., *Z. Anorg. Allgem. Chem.* **210**, 105 (1933).
9. Ali, S. M., Brewer, F. M., Chadwick, J. L., and Garton, G., *J. Inorg. & Nucl. Chem.* **9**, 124 (1959).
10. Allen, R. J., and Sheldon, J. C., *Australian J. Chem.* **18**, 277 (1965).
11. Anderson, J. S., Edgington, D. N., Roberts, L. E. J., and Wait, E., *J. Chem. Soc.* p. 3324 (1954).
12. Anderson, J. S., and Sterns, M., *J. Inorg. & Nucl. Chem.* **11**, 272 (1959).
13. Andersson, G., *Acta Chem. Scand.* **8**, 1599 (1954).
14. Andersson, G., *Acta Chem. Scand.* **10**, 623 (1956).
15. Andersson, S., Collén, B., Kuylenstierna, V., and Magneli, A., *Acta Chem. Scand.* **11**, 1641 (1957).
16. Andersson, S., Sundholm, A., and Magneli, A., *Acta Chem. Scand.* **13**, 989 (1959).
17. Andersson, S., and Wadsley, A. D., *Acta Cryst.* **15**, 201 (1962).
18. Andersson, S., and Jahnberg, L., *Arkiv Kemi* **21**, 413 (1963).
19. Andes, M. T. N. S., *Z. Astrobot.* **17A**, 612 (1939).
20. Andres, K., Kuebler, N. A., and Robin, M. B., *J. Phys. Chem. Solids* **27**, 1747 (1966).
21. Appelman, E. H., and Malm, J. G., *J. Am. Chem. Soc.* **86**, 2141 (1964).
22. Ariya, S. M., Shchukarev, S. A., and Glushkova, V. B., *Zh. Obshch. Khim.* **23**, 1241 (1953).
23. Arnold, R., and Walker, S. M., *J. S. African Chem. Inst.* **9**, 80 (1956).
24. Aronson, S., and Belle, J., *J. Chem. Phys.* **29**, 151 (1958).
25. Aronson, S., and Clayton, J. C., *J. Inorg. & Nucl. Chem.* **7**, 384 (1958).
26. Asbrink, S., and Magneli, A., *Acta Cryst.* **12**, 575 (1959).

27. Asker, W. J., and Wylie, A. W., *Australian J. Chem.* **18**, 959 (1965).
28. Asmussen, R. W., *Z. Anorg. Allgem. Chem.* **243**, 127 (1939).
29. Asmussen, R. W., *Z. Elektrochem.* **45**, 698 (1939).
30. Aten, A. H. W., *Z. Physik. Chem.* **66**, 641 (1909).
31. Aten, A. H. W., *Z. Physik. Chem.* **73**, 578 (1910).
32. Aten, A. H. W., Jr., Steinberg, H., Heymann, D., and Fontijn, A., *Rec. Trav. Chim.* **72**, 94 (1953).
33. Atkinson, L., and Day, P., unpublished results (1966).
34. Atoji, M., and Watanabe, T., *J. Chem. Phys.* **20**, 1045 (1952).
35. Austin, I. G., *Phil. Mag.* [8] **7**, 961 (1962).
36. Bachmann, H. G., Ahmed, F. R., and Barnes, W. H., *Z. Krist.* **115**, 110 (1961).
- 36a. Baker, F. B., Newton, T. W., and Kahn, M., *J. Phys. Chem.* **64**, 109 (1960).
37. Baker, L. C. W., and McCutcheon, T. P., *J. Am. Chem. Soc.* **78**, 4503 (1956).
38. Baker, L. C. W., Baker, V. S., Eriks, K., Pope, M. T., Shibata, M., Rollins, O. W., Fang, J. H., and Koh, L. L., *J. Am. Chem. Soc.* **88**, 2329 (1966).
39. Barbieri, G. A., *Ber. Deut. Chem. Ges.* **60**, 2424 (1927).
40. Bärnighausen, H., and Brauer, G., *Acta Cryst.* **15**, 1059 (1962).
41. Bärnighausen, H., *Angew. Chem.* **77**, 1014 (1965).
42. Barrowcliffe, C., Beattie, I. R., Day, P., and Livingstone, K., *J. Chem. Soc.* (1967) (to be published).
43. Bartlett, N., and Rao, P. R., *Proc. Chem. Soc.* p. 393 (1964).
44. Bartlett, N., private communication (1966).
45. Bashilova, N. I., *Dokl. Akad. Nauk SSSR* **141**, 1083 (1961).
46. Bateman, L. R., Blount, J. F., and Dahl, L. F., *J. Am. Chem. Soc.* **88**, 1082 (1966).
47. Baudisch, O., and Welo, L. A., *J. Biol. Chem.* **61**, 261 (1924).
48. Bauer, D., Schnering, H. G., and Schäfer, H., *J. Less-Common Metals* **8**, 388 (1965).
49. Bauminger, R., Cohen, S. G., Marinov, A., Ofer, S., and Segal, E., *Phys. Rev.* **122**, 1447 (1961).
50. Bayer, E., *Monatsh. Chem.* **41**, 223 (1920).
51. Beketov, A. R., Strekalovskii, V. N., and Vlasov, V. G., *J. Struct. Chem. (USSR) (English Transl.)* **6**, 64 (1965).
52. Belbeoch, B., Piekarski, C., and Pério, P., *Acta Cryst.* **14**, 837 (1961).
53. Belov, N. V., and Mokeeva, V. I., *Tr. Inst. Kristallogr., Akad. Nauk SSSR* **9**, 47 (1954).
54. Benrath, A., *Z. Anorg. Allgem. Chem.* **93**, 161 (1915).
55. Benrath, A., *Z. Anorg. Allgem. Chem.* **136**, 358 (1924).
56. Berdonosov, S. S., and Lapitskii, A. V., *Zh. Neorgan. Khim.* **10**, 2812 (1965).
57. Berecki-Biedermann, C., *Arkiv. Kemi* **19**, 35 (1962).
- 57a. Berglund, E., *Ber. Deut. Chem. Ges.* **7**, 470 (1874).
58. Bernal, I., Ebsworth, E. A. V., and Weil, J. A., *Proc. Chem. Soc.* p. 57 (1959).
59. Bernard, J., and Theobald, F., *Compt. Rend.* **256**, 4916 (1963).
60. Bernard, J., Theobald, F., and Theobald, J. G., *Compt. Rend.* **260**, 873 (1965).
61. Berry, L. G., *Am. Mineralogist* **39**, 504 (1954).
62. Bersohn, R., and Isenberg, I., *J. Chem. Phys.* **35**, 1640 (1961).
63. Berzelius, J. J., "*Lehrbuch*", 5th ed., Vol. 4, p. 422 (1847); quoted in Biltz (69).
64. Bevan, D. J. M., *J. Inorg. & Nucl. Chem.* **1**, 49 (1955).
65. Bevan, D. J. M., and Kordis, J., *J. Inorg. & Nucl. Chem.* **26**, 1509 (1964).
66. Bhattacharya, A. K., and Dhar, N. R. Z., *Z. Anorg. Allgem. Chem.* **213**, 240 (1933).

67. Bhattacharya, A. K., *J. Indian Chem. Soc.* **12**, 143 (1935).
68. Bhattacharya, A. K., *J. Indian Chem. Soc.* **18**, 85 (1941).
69. Biltz, W., *Z. Anorg. Allgem. Chem.* **127**, 169 (1923).
70. Biltz, W., and Müller, H., *Z. Anorg. Allgem. Chem.* **163**, 257 (1927).
71. Bjerrum, N. J., Boston, C. R., Smith, G. P., and Davis, H. L., *Inorg. Nucl. Chem. Letters* **1**, 141 (1965).
72. Blackburn, P. E., *J. Phys. Chem.* **62**, 897 (1958).
73. Blinova, N. I., and Tolmachev, Yu. M., *Radiokhimiya* **4**, 447 (1962).
74. Blomstrom, D. C., Knight, E., Jr., Phillips, W. D., and Weiher, J. F., *Proc. Natl. Acad. Sci. U.S.* **51**, 1085 (1964).
75. Blumberg, W. E., Eisinger, J., Aisen, P., Morell, A. G., and Scheinberg, I. H., *J. Biol. Chem.* **238**, 1675 (1963).
76. Blumenthal, R. N., Coburn, J., Baukus, J., and Hirthe, W. M., *J. Phys. Chem. Solids* **27**, 643 (1966).
77. Bogackij, D. P., *Zh. Obshch. Khim.* **21**, 3 (1951).
78. Bokii, G. B., and Distler, G. I., *Dokl. Akad. Nauk. SSSR* **56**, 923 (1947).
79. Bonner, N. A., and Goishi, W., *J. Am. Chem. Soc.* **83**, 85 (1961).
80. Bosman, A. J., and Crevecoeur, C., *Phys. Rev.* **144**, 763 (1966).
81. Boston, C. R., and Smith, G. P., *J. Phys. Chem.* **66**, 1178 (1962).
82. Braekken, H., *Kgl. Norske Videnskab. Selskabs. Forh.* **7**, 143 (1935).
83. Bragg, W. L., "Atomic Structure of Minerals." Cornell Univ. Press, Ithaca, New York, 1937.
84. Brain, F. H., Gibson, C. S., Jarvis, J. A. J., Phillips, R. F., Powell, H. M., and Tyabji, A., *J. Chem. Soc.* p. 3686 (1952).
85. Braterman, P. S., *J. Chem. Soc. A. Inorg., Phys., Theoret.* p. 1471 (1966).
86. Brauer, G., and HOLTschmidt, U., *Z. Anorg. Allgem. Chem.* **265**, 105 (1951).
87. Brauer, G., and Tiessler, R., *Z. Anorg. Allgem. Chem.* **271**, 273 (1953).
88. Brauer, G., and Gradinger, H., *Z. Anorg. Allgem. Chem.* **277**, 89 (1954).
89. Brauer, G., and Schnell, W. -D., *Z. Anorg. Allgem. Chem.* **283**, 49 (1956).
90. Brauer, G., and Eichner, M., *Z. Anorg. Allgem. Chem.* **285**, 118 (1956).
91. Brauer, G., and Schnell, W. -D., *Z. Anorg. Allgem. Chem.* **287**, 87 (1956).
- 91a. Brauer, G., and Eichner, M., *Z. Anorg. Allgem. Chem.* **287**, 95 (1956).
92. Brauer, G., and Gingerich, K., *Angew. Chem.* **69**, 480 (1957).
93. Brauer, G., and Eichner, M., *Z. Anorg. Allgem. Chem.* **296**, 13 (1958).
94. Brauer, G., and Morawietz, H., *Z. Anorg. Allgem. Chem.* **340**, 133 (1965).
95. Braun, P. B., *Nature* **170**, 708 (1952).
96. Brewer, F. M., Chadwick, J. R., and Garton, G., *J. Inorg. & Nucl. Chem.* **23**, 45 (1961).
97. Brewer, F. M., Chadwick, J. R., and Garton, G., *J. Inorg. & Nucl. Chem.* **25**, 322 (1963).
98. Britton, D., *Inorg. Chem.* **3**, 305 (1964).
99. Bronstein, H. R., Dworkin, A. S., and Bredig, M. A., *J. Phys. Chem.* **64**, 1344 (1960).
100. Brosset, C., *Arkiv Kemi, Mineral. Geol.* **25A**, No. 19 (1948).
101. Brown, R. A., and Swift, E. H., *J. Am. Chem. Soc.* **71**, 2717 (1949).
102. Brown, R. A., and Swift, E. H., *J. Am. Chem. Soc.* **71**, 2719 (1949).
103. Browne, C. I., Craig, R. P., and Davidson, N., *J. Am. Chem. Soc.* **73**, 1946 (1951).
104. Brubaker, C. H., Jr., Groves, K. O., Mickel, J. P., and Knop, C. P., *J. Am. Chem. Soc.* **79**, 4641 (1957).
105. Brubaker, C. H., Jr., and Mickel, J. P., *J. Inorg. & Nucl. Chem.* **4**, 55 (1957).

106. Brüll, L., and Griffi, F., *Ann. Chim. Appl.* **28**, 536 (1938).
107. Bruner, B. L., and Corbett, J. D., *J. Inorg. & Nucl. Chem.* **20**, 62 (1961).
108. Bruno, M., *Ric. Sci.* **20**, 645 (1950).
109. Bruno, M., and Santoro, V., *Gazz. Chim. Ital.* **86**, 1095 (1956).
110. Bucholz, C. F., *Gehlen J.* **4**, 626 (1805).
111. Buckel, W., and Hilsch, R., *Z. Physik* **128**, 324 (1950).
112. Buerger, M. J., *Z. Krist.* **95**, 163 (1936).
113. Burbank, R. D., *Inorg. Chem.* **5**, 1491 (1966).
114. Burns, E. A., and Hume, D. N., *J. Am. Chem. Soc.* **79**, 2704 (1957).
115. Burrows, G. J., and Sandford, E. P., *J. Proc. Roy. Soc. N. S. Wales* **69**, 182 (1936).
116. Bury, C. R., *J. Am. Chem. Soc.* **57**, 2115 (1935).
117. Butler, G., and Copp, J. L., *J. Chem. Soc.* p. 725 (1956).
118. Byström, A., and Westgren, A., *Arkiv Kemi. Mineral. Geol.* **16B**, No. 14 (1943).
119. Byström, A., and Mason, B., *Arkiv Kemi, Mineral. Geol.* **16B**, No. 15 (1943).
120. Byström, A., *Arkiv Kemi, Mineral. Geol.* **18A**, No. 23 (1944).
121. Byström, A., *Arkiv Kemi, Mineral. Geol.* **20A**, No. 11 (1945).
122. Byström, A., *Arkiv Kemi, Mineral. Geol.* **25A**, No. 13 (1947).
123. Byström, A., and Evers, L., *Acta Chem. Scand.* **4**, 613 (1950).
124. Cady, H. H., Ph.D. Thesis, University of California, Berkeley, California (1957).
125. Cahan, B. D., Ockerman, J. B., Amlie, R. F., and Ruetschi, P., *J. Electrochem. Soc.* **107**, 725 (1960).
126. Calhoun, B. A., *Phys. Rev.* **94**, 1577 (1954).
127. Cambi, L., *Rend. Ist. Lombardo Sci. Lettere* **A68**, 182 (1935).
128. Cambi, L., *Gazz. Chim. Ital.* **77**, 575 (1947).
129. Champion, R. J., Conocchioli, T. J., and Sutin, N., *J. Am. Chem. Soc.* **86**, 4591 (1964).
130. Carlston, R. C., Griswold, E., and Kleinberg, J., *J. Am. Chem. Soc.* **80**, 1532 (1958).
131. Chadwick, J. R., Atkinson, A. W., and Huckstepp, B. G., *J. Inorg. & Nucl. Chem.* **28**, 1021 (1966).
132. Chalkley, L., *J. Opt. Soc. Am.* **44**, 699 (1954).
133. Chapin, D. S., Kafalas, J. A., and Honig, J. M., *J. Phys. Chem.* **69**, 1402 (1965).
134. Chapin, W. H., *J. Am. Chem. Soc.* **32**, 323 (1910).
135. Chester, P. F., *J. Appl. Phys.* **32**, 866 (1961).
136. Chester, P. F., *J. Appl. Phys.* **32**, 2233 (1961).
137. Chevreul, M., *Ann. Chim. (Paris)* [1] **83**, 181 (1812).
138. Choi, Q. W., *J. Am. Chem. Soc.* **82**, 2686 (1960).
139. Choi, Q. W., and Clark, W. G., *J. Chem. Phys.* **34**, 1584 (1961).
140. Chou Kung-du, *Sci. Sinica (Peking)* **12**, 139 (1963).
141. Chretien, A., and Lous, E., *Bull. Soc. Chim. France* **11**, 446 (1944).
142. Christensen, V. J., Kleinberg, J., and Davidson, A. W., *J. Am. Chem. Soc.* **75**, 2495 (1953).
143. Clark, G. L., Schieltz, N. C., and Quirke, T. T., *J. Am. Chem. Soc.* **59**, 2305 (1937).
144. Clark, R. J., Griswold, E., and Kleinberg, J., *J. Am. Chem. Soc.* **80**, 4764 (1958).
145. Cohen, A. J., and Davidson, N., *J. Am. Chem. Soc.* **73**, 1955 (1951).
146. Cooper, D., and Plane, R. A., *Inorg. Chem.* **5**, 1677 (1966).

147. Conroy, H., *J. Chem. Phys.* **41**, 1341 (1964).
148. Corbett, J. D., and McMullan, R. K., *J. Am. Chem. Soc.* **77**, 4217 (1955).
149. Corbett, J. D., *J. Am. Chem. Soc.* **80**, 4757 (1958).
150. Corbett, J. D., and Druding, L. F., *J. Inorg. & Nucl. Chem.* **11**, 20 (1959).
151. Corbett, J. D., and Albers, F. C., *J. Am. Chem. Soc.* **82**, 533 (1960).
152. Corbett, J. D., Druding, L. F., Burkhard, W. J., and Lindahl, C. B., *Discussions Faraday Soc.* **32**, 79 (1961).
153. Corbett, J. D., and Rundle, R. E., *Inorg. Chem.* **3**, 1408 (1964).
154. Corbett, J. D., and Ramsey, B. N., *Inorg. Chem.* **4**, 260 (1965).
155. Corbett, J. D., Pollard, D. L., and Mee, J. E., *Inorg. Chem.* **5**, 761 (1966).
156. Cordite, B. A. M., and Phires, G. L. O., *Heat Combust* **17**, 123 (1946).
157. Corey, R. B., Stanford, R. H., Marsh, R. E., Leung, Y. C., and Kay, L. M., *Acta Cryst.* **15**, 1157 (1962).
158. Cossee, P., *J. Inorg. & Nucl. Chem.* **8**, 483 (1958).
159. Cotton, F. A., and Haas, T. E., *Inorg. Chem.* **3**, 10 (1964).
160. Cotton, F. A., *Inorg. Chem.* **3**, 1217 (1964).
161. Cotton, F. A., *Inorg. Chem.* **4**, 334 (1965).
162. Cotton, F. A., and Bratton, W. K., *J. Am. Chem. Soc.* **87**, 921 (1965).
163. Cotton, F. A., and Harris, C. B., *Inorg. Chem.* **4**, 330 (1965).
164. Craig, R. P., and Davidson, N., *J. Am. Chem. Soc.* **73**, 1951 (1951).
165. Craven, B. M., and Hall, D., *Acta Cryst.* **14**, 475 (1961).
166. Craven, B. M., and Hall, D., *Acta Cryst.* **21**, 177 (1966).
167. Croatto, U., and Bruno, M., *Gazz. Chim. Ital.* **78**, 83 (1948) (and references cited therein).
168. Croatto, U., and Bruno, M., *Gazz. Chim. Ital.* **78**, 95 (1948).
169. Cronmeyer, D. C., *Phys. Rev.* **113**, 1222 (1959).
170. Cubicciotti, D., *J. Am. Chem. Soc.* **71**, 4119 (1949).
171. Culpin, D., Day, P., Edwards, P. R., and Williams, R. J. P., *Chem. Commun.* No. 19, p. 450 (1965).
172. Dana, E. S., and Ford, W. E., "A Textbook of Mineralogy." Wiley, New York, 1958.
173. Dasent, V. E., and Morrison, D., *J. Inorg. & Nucl. Chem.* **26**, 1122 (1964).
174. Dasgupta, D. R., and Mackay, A. L., *J. Phys. Soc. Japan* **14**, 932 (1959).
175. Davidson, A. W., and Kleinberg, J., *J. Phys. Chem.* **57**, 571 (1953).
176. Davidson, D., and Welo, L. A., *J. Phys. Chem.* **32**, 1191 (1928).
177. Davidson, N., *J. Am. Chem. Soc.* **73**, 2361 (1951).
178. Day, P., *Inorg. Chem.* **2**, 452 (1963).
179. Day, P., Ph.D. Thesis, Oxford University (1965).
180. Day, P., unpublished observations (1966).
181. de Boer, J. H., and Verwey, E. J. W., *Rec. Trav. Chim.* **55**, 541 (1936).
182. de Boer, J. H., and Verwey, E. J. W., *Proc. Phys. Soc.* **49**, Suppl., 59 (1937).
183. Decroly, C., and Ghodsi, M., *Compt. Rend.* **261**, 2659 (1965).
184. DeFord, D. D., and Davidson, A. W., *J. Am. Chem. Soc.* **73**, 1469 (1961).
185. Dehlinger, U., *Z. Krist.* **66**, 108 (1928).
186. Delépine, M., *Compt. Rend.* **120**, 152 (1895).
187. Delépine, M., *Compt. Rend.* **142**, 1525 (1906).
188. Delépine, M., *Ann. Chim. (Paris)* [13] **4**, 1115 (1959).
189. DeMarco, R. E., Heller, H. A., Abbott, R. C., and Burkhardt, W., *Am. Ceram. Soc. Bull.* **38**, 360 (1959).

190. Derbyshire, S. W., Fraker, A. C., and Stadelmaier, H. H., *Acta Cryst.* **14**, 1293 (1961).
191. Deshpande, V. V., Saxena, R. P., Daroowalla, S. H., and Karkhanavala, M. D., *Indian J. Chem.* **1**, 511 (1963).
192. Deussen, E. *Monatsh. Chem.* **28**, 163 (1907).
193. de Wet, J. F., and Rolle, R., *Z. Anorg. Allgem. Chem.* **336**, 96 (1965).
194. Dickens, B., *J. Inorg. & Nucl. Chem.* **27**, 1509 (1965).
195. Diehl, H., Carlson, P. A., Christian, D., Dewel, E. H., Emerson, M. R., Heumann, F. K., and Standage, H. W., *Proc. Iowa Acad. Sci.* **55**, 241 (1948).
196. Dihlström, K., and Westgren, A., *Z. Anorg. Allgem. Chem.* **235**, 153 (1937).
197. Dihlström, K., *Z. Anorg. Allgem. Chem.* **239**, 57 (1938).
198. Dirkse, T. P., *J. Electrochem. Soc.* **106**, 453 (1959).
199. Dixon, D. T., Einstein, F. W. B., and Penfold, B. R., *Acta Cryst.* **18**, 221 (1965).
200. Doehlemann, E., and Fromherz, H., *Z. Physik. Chem.* **A171**, 353 (1934).
201. Drago, R. S., and Sisler, H. H., *J. Am. Chem. Soc.* **79**, 1811 (1957).
202. Drew, H. D. K., Pinkard, F. W., Wardlaw, W., and Cox, E. G., *J. Chem. Soc.* p. 1004 (1932).
203. Drew, H. D. K., Pinkard, F. W., Preston, G. H., and Wardlaw, W., *J. Chem. Soc.* p. 1895 (1932).
204. Drew, H. D. K., and Tress, H. J., *J. Chem. Soc.* p. 1335 (1933).
205. Drew, H. D. K., and Tress, H. J., *J. Chem. Soc.* p. 1244 (1935).
206. Druding, L. F., and Corbett, J. D., *J. Am. Chem. Soc.* **81**, 5512 (1959).
207. Druding, L. F., and Corbett, J. D., *J. Am. Chem. Soc.* **83**, 2462 (1961).
208. Druding, L. F., Corbett, J. D., and Ramsey, B. N., *Inorg. Chem.* **2**, 869 (1963).
- 208a. Dubois, P., *Ann. Chim. (Paris)* **5**, 411 (1936).
209. Duncan, J. F., and Wigley, P. W. R., *J. Chem. Soc.* p. 1120 (1963).
210. Dunitz, J. D., and Orgel, L. E., *J. Chem. Soc.* p. 2594 (1953).
211. Dwyer, F. P. J., and Nyholm, R. S., *Nature* **160**, 502 (1947).
212. Dwyer, F. P. J., Nyholm, R. S., and Rogers, L. E., *J. Proc. Roy. Soc. N.S. Wales* **81**, 267 (1947).
213. Eakins, J. D., Humphreys, D. G., and Mellish, C. E., *J. Chem. Soc.* p. 6012 (1963).
214. Ebsworth, E. A. V., and Weil, J. A., *J. Phys. Chem.* **63**, 1890 (1959).
215. Edwards, F. C., Voigt, A. F., and Diehl, H., *Proc. Iowa Acad. Sci.* **55**, 247 (1948).
216. Ehrlich, P., *Z. Elektrochem.* **45**, 362 (1939).
217. Ellerbeck, L. D., Shanks, H. R., Sidles, P. H., and Danielson, G. C., *J. Chem. Phys.* **35**, 298 (1961).
218. Elliott, N., *J. Chem. Phys.* **2**, 298 (1934).
219. Elliott, N., *J. Chem. Phys.* **2**, 419 (1934).
220. Elliott, N., and Pauling, L., *J. Am. Chem. Soc.* **60**, 1846 (1938).
221. Emeleus, H. J., and Anderson, J. S., "Modern Aspects of Inorganic Chemistry." Routledge, London, 1938.
222. Emschwiller, G., *Compt. Rend.* **238**, 1414 (1954).
223. Ephraim, F., and Barteczko, P., *Z. Anorg. Allgem. Chem.* **61**, 238 (1909).
224. Ephraim, F., and Weinberg, S., *Ber. Deut. Chem. Ges.* **42**, 4447 (1909).
225. Epstein, L. M., *J. Chem. Phys.* **36**, 2731 (1962).
226. Espenson, J. H., and McCarley, R. E., *J. Am. Chem. Soc.* **88**, 1063 (1966).
227. Evans, H. T., Jr., *Inorg. Chem.* **5**, 967 (1966).
228. Eyring, L., and Baenziger, N. C., *J. Appl. Phys.* **33**, 428 (1962).

229. Eyring, L., and Holmberg, B., *Advan. Chem. Ser.* **39**, 46 (1963).
230. Fadeev, V. N., and Fedorov, P. I., *Russ. J. Inorg. Chem. (English Transl.)* **8**, 1046 (1963).
231. Fadeev, V. N., and Fedorov, P. I., *Russ. J. Inorg. Chem. (English Transl.)* **9**, 209 (1964).
232. Fadeev, V. N., and Fedorov, P. I., *Russ. J. Inorg. Chem. (English Transl.)* **9**, 1094 (1964).
233. Fayek, M. K., and Leciejewicz, J., *Z. Anorg. Allgem. Chem.* **336**, 104 (1965).
234. Fedorov, P. I., and Fadeev, V. N., *Russ. J. Inorg. Chem. (English Transl.)* **9**, 207 (1964).
235. Fedorov, P. I., and Il'ina, N. I., *Russ. J. Inorg. Chem. (English Transl.)* **9**, 659 (1964).
236. Fedorov, P. I., and Tsimbalist, V. V., *Russ. J. Inorg. Chem. (English Transl.)* **9**, 908 (1964).
237. Feitknecht, W., and Marti, W., *Helv. Chim. Acta* **28**, 129 (1945).
238. Feitknecht, W., and Keller, G., *Z. Anorg. Allgem. Chem.* **262**, 61 (1950).
239. Fensham, P. J., *J. Am. Chem. Soc.* **76**, 969 (1954).
240. Ferrari, A., *Gazz. Chim. Ital.* **67**, 94 (1937).
241. Ferrari, A., and Cecconi, R., *Gazz. Chim. Ital.* **72**, 170 (1942).
242. Ferrari, A., Cecconi, R., and Cavalca, L., *Gazz. Chim. Ital.* **73**, 23 (1943).
243. Ferrari, A., Cavalca, L., and Coghi, L., *Gazz. Chim. Ital.* **82**, 385 (1952).
244. Ferrari, A., Cavalca, L., and Nardelli, M., *Gazz. Chim. Ital.* **85**, 137 (1955).
245. Ferrari, A., Cavalca, L., and Nardelli, M., *Gazz. Chim. Ital.* **85**, 1551 (1955).
246. Ferrari, A., and Tani, M. E., *Gazz. Chim. Ital.* **89**, 502 (1959).
247. Ferrari, A., Tani, M. E., and Magnano, G., *Gazz. Chim. Ital.* **89**, 2512 (1959).
248. Ferrari, A., Braibanti, A., and Tiripicchio, A., *Acta Cryst.* **21**, 605 (1966).
249. Fielding, P. E., *J. Chem. Phys.* **22**, 1153 (1954).
250. Fielding, P. E., and Mellor, D. P., *J. Chem. Phys.* **22**, 1155 (1954).
251. Figgis, B. N., and Robertson, G. B., *Nature* **205**, 694 (1965).
252. Fletcher, J. M., Greenfield, B. F., Hardy, C. J., Scargill, D., and Woodhead, J. L., *J. Chem. Soc. p.* 2000 (1961).
253. Flood, H., Krog, T., and Sorum, H., *Tidsskr. Kjemi, Bergvesen Met.* **3**, 32 (1946).
254. Fluck, E., Kerler, W., and Neuwirth, W., *Angew. Chem. Intern. Ed. English* **2**, 277 (1963).
255. Foëx, M., *Compt. Rend.* **220**, 359 (1945).
256. Ford, W. F., and Rees, W. J., *Trans. Brit. Ceram. Soc.* **47**, 207 (1948).
257. Ford, W. F., and Rees, W. J., *Trans. Brit. Ceram. Soc.* **48**, 291 (1949).
258. Ford, W. F., and White, J., *Trans. Brit. Ceram. Soc.* **48**, 417 (1949).
259. Fraker, A. C., *J. Phys. Chem.* **69**, 4395 (1965).
260. Frederikse, H. P. R., *J. Appl. Phys.* **32**, Suppl., 2211 (1961).
261. Freed, S., Sugarman, N., and Metcalf, R. P., *J. Chem. Phys.* **8**, 225 (1940).
262. Fremy, E., *Ann. Chem.* **83**, 240 (1852).
263. Fry, T. K., Lazzarini, R. A., and San Pietro, A., *Proc. Natl. Acad. Sci. U.S.* **50**, 652 (1963).
264. Fyfe, W. S., *Nature* **164**, 790 (1949).
265. Galloni, E. E., and Roffo, A. E., Jr. *J. Chem. Phys.* **9**, 875 (1941).
266. Galloni, E. E., and Busch, R. H., *J. Chem. Phys.* **20**, 198 (1952).
267. Galy, J., and Hardy, A., *Acta Cryst.* **19**, 432 (1965).
268. Gardner, W. R., and Danielson, G. C., *Phys. Rev.* **93**, 46 (1964).
269. Garton, G., and Powell, H. M., *J. Inorg. & Nucl. Chem.* **4**, 84 (1957).

270. Gasperin, M., *Bull. Soc. Franc. Mineral. Crist.* **87**, 278 (1964).
271. Gatehouse, B. M., and Wadsley, A. D., *Acta Cryst.* **17**, 1545 (1964).
272. Gauzzi, F., *Ann. Chim. (Rome)* **53**, 1503 (1963).
273. Gendell, J., Cotts, R., and Sienko, M. J., *J. Chem. Phys.* **37**, 220 (1962).
274. George, A. M., and Karkhanavala, M. D., *J. Phys. Chem. Solids* **24**, 1207 (1963).
275. Gibb, T. C., and Greenwood, N. N., *Trans. Faraday Soc.* **61**, 1317 (1965).
276. Gillis, E., *Compt. Rend.* **258**, 4765 (1964).
277. Glasner, A., and Reisfeld, R., *J. Chem. Phys.* **32**, 956 (1960).
278. Glasser, F. P., and Osborn, E. F., *J. Am. Ceram. Soc.* **41**, 358 (1958).
279. Glemser, O., and Lutz, G., *Z. Anorg. Allgem. Chem.* **263**, 2 (1950).
280. Glemser, O., and Lutz, G., *Z. Anorg. Allgem. Chem.* **264**, 17 (1951).
281. Glemser, O., Hauschild, U., and Trüpel, F., *Naturwissenschaften* **40**, 317 (1953).
282. Glemser, O., Hauschild, U., and Trüpel, F., *Z. Anorg. Allgem. Chem.* **277**, 113 (1954).
283. Glemser, O., and Schwarzmann, E., *Z. Anorg. Allgem. Chem.* **278**, 249 (1955).
284. Glemser, O., Lutz, G., and Meyer, G., *Z. Anorg. Allgem. Chem.* **285**, 173 (1956).
285. Glemser, O., Weidelt, J., and Freund, F., *Z. Anorg. Allgem. Chem.* **332**, 299 (1964).
286. Gleu, K., and Breuel, W., *Z. Anorg. Allgem. Chem.* **237**, 350 (1937).
287. Gleu, K., and Rehm, K., *Z. Anorg. Allgem. Chem.* **237**, 79 (1938).
288. "Gmelins Handbuch der Anorganischen Chemie," Iron, Part 59B, 8th ed. Verlag Chemie, Weinheim, 1932.
289. "Gmelins Handbuch der Anorganischen Chemie," Molybdenum, Part 53, 8th ed. Verlag Chemie, Weinheim, 1935.
290. "Gmelins Handbuch der Anorganischen Chemie," Osmium, Part 66, 8th ed. Verlag Chemie, Weinheim, 1939.
291. "Gmelins Handbuch der Anorganischen Chemie," Thallium, Part 38, 8th ed. Verlag Chemie, Weinheim, 1940.
292. "Gmelins Handbuch der Anorganischen Chemie," Chromium, Part 52, 8th ed. Verlag Chemie, Weinheim, 1962.
293. Goggin, P. L., and McColm, I. J., *J. Less-Common Metals* **11**, 292 (1966).
294. Golibersuch, E. W., and Young, R. C., *J. Am. Chem. Soc.* **71**, 2402 (1949).
295. Goodenough, J. B., *Phys. Rev.* **100**, 564 (1957).
296. Goodenough, J. B., Wickham, D. G., and Croft, W. J., *Phys. Chem. Solids* **5**, 107 (1958).
297. Goroshchenko, Ya. G., Andreeva, M. I., and Babkin, A. G., *Zh. Prikl. Khim.* **32**, 1664 (1959).
298. Goroshchenko, Ya. G., and Godneva, M. M., *Russ. J. Inorg. Chem. (English Transl.)* **6**, 744 (1961).
299. Gortsema, F. P., and Didchenko, R., *Inorg. Chem.* **4**, 182 (1965).
300. Gossner, B., and Arm, M., *Z. Krist.* **72**, 202 (1929).
301. Gotoo, K., Nomura, S., and Naito, K., *J. Phys. Chem. Solids* **26**, 1679 (1965).
302. Graff, H., and Wilmarth, W. K., *Proc. Symp. Co-ord. Chem., Tihany, Hungary, 1963* p. 255 (1964).
303. Graff, W. S., and Stadelmaier, H. H., *J. Electrochem. Soc.* **105**, 446 (1958).
304. Graham, J., and Wadsley, A. D., *Acta Cryst.* **14**, 379 (1961).
305. Graham, J., and Wadsley, A. D., *Acta Cryst.* **20**, 93 (1966).
306. Grant, F. A., *Rev. Mod. Phys.* **31**, 646 (1959).
307. Grantham, L. F., and Yosim, S. J., *J. Chem. Phys.* **38**, 1671 (1963).
308. Grantham, L. F., *J. Chem. Phys.* **43**, 1415 (1965).

309. Grasshoff, K., and Hahn, H., *Z. Anal. Chem.* **168**, 247 (1959).
310. Grasshoff, K., and Hahn, H., *Z. Anal. Chem.* **180**, 18 (1961).
311. Grasshoff, K., and Hahn, H., *Z. Anal. Chem.* **187**, 328 (1962).
312. Greenwood, N. N., and Worrall, I. J., *J. Chem. Soc.* p. 1680 (1958).
313. Greiner, J. D., Smith, J. F., Corbett, J. D., and Jelinek, F. J., *J. Inorg. & Nucl. Chem.* **28**, 971 (1966).
314. Grinberg, A. A., and Filinov, F. M., *Bull. Acad. Sci. URSS, Classe Sci. Math., Ser. Chim.* p. 1245 (1937).
315. Gronvold, F., *Nature* **162**, 70 (1948).
316. Gronvold, F., *J. Inorg. & Nucl. Chem.* **1**, 357 (1955).
317. Gross, S. T., *J. Am. Chem. Soc.* **65**, 1107 (1943).
318. Grossmann, G., Proskurenko, O. W., and Ariya, S. M., *Z. Anorg. Allgem. Chem.* **305**, 121 (1960).
319. Gruehn, R., and Schäfer, H., *Naturwissenschaften* **50**, 642 (1963).
320. Gruehn, R., and Schäfer, H., *J. Less-Common Metals* **10**, 152 (1965).
321. Gruehn, R., Bergner, D., and Schäfer, H., *Angew. Chem.* **77**, 1082 (1965).
322. Gruen, D. M., Koehler, W. C., and Katz, J. J., *J. Am. Chem. Soc.* **73**, 1475 (1951).
323. Gruen, D. M., *J. Am. Chem. Soc.* **76**, 2117 (1954).
324. Gruner, E., and Klemm, W., *Naturwissenschaften* **22**, 59 (1937).
325. Guillaud, E., Michel, A., Bénard, J., and Fallot, M., *Compt. Rend.* **219**, 58 (1944).
326. Hägg, G., *Z. Physik. Chem.* **29B**, 192 (1935).
327. Hägg, G., and Jerslev, B., *Experientia* **2**, 495 (1946).
328. Hägg, G., and Magneli, A., *Rev. Pure Appl. Chem.* **4**, 235 (1955).
329. Hahn, H., and Klinger, W., *Z. Anorg. Allgem. Chem.* **260**, 110 (1949).
330. Hahn, H., and Frank, G., *Z. Anorg. Allgem. Chem.* **278**, 340 (1955).
331. Hahn, H., and Schmidt, G., *Naturwissenschaften* **49**, 513 (1962).
332. Hahn, H., and Becker, W., *Naturwissenschaften* **50**, 402 (1963).
333. Haim, A., and Wilmarth, W. K. J., *J. Am. Chem. Soc.* **83**, 509 (1961).
334. Hall, D., and Williams, P. P., *Acta Cryst.* **11**, 624 (1958).
335. Hamilton, W. C., *Phys. Rev.* **110**, 1050 (1958).
336. Hampe, W., *Jahresber.* Part I, p. 388 (1888).
337. Hannebohn, O., and Klemm, W., *Z. Anorg. Allgem. Chem.* **229**, 337 (1936).
338. Haraldsen, H., and Bakken, R., *Naturwissenschaften* **28**, 127 (1940).
339. Harbottle, G., and Dodson, R. W., *J. Am. Chem. Soc.* **73**, 2442 (1951).
340. Harned, H. S., *J. Am. Chem. Soc.* **35**, 1078 (1913).
341. Harris, C. M., *J. Proc. Roy. Soc. N. S. Wales* **82**, 218 (1948).
342. Harris, C. M., *J. Proc. Roy. Soc. N. S. Wales* **84**, 111 (1950).
343. Harris, C. M., *J. Proc. Roy. Soc. N. S. Wales* **85**, 138 (1952).
344. Harris, C. M., *J. Proc. Roy. Soc. N. S. Wales* **85**, 142 (1952).
345. Harris, C. M., and Schafer, H. N. S., *J. Proc. Roy. Soc. N. S. Wales* **85**, 145 (1952).
346. Harris, C. M., and Schafer, H. N. S., *J. Proc. Roy. Soc. N. S. Wales* **85**, 148 (1952).
347. Hathaway, B. J., and Holah, D. G., *J. Chem. Soc.* p. 2408 (1964).
348. Hauffe, K., and Block, J., *Z. Physik. Chem. (Leipzig)* **196**, 438 (1950).
349. Hauffe, K., "Reactionen in und am festen Stoffen." Springer, Berlin, 1955.
350. Hazell, A. C., *J. Chem. Soc.* p. 3459 (1963).
351. Heikes, R. R., and Johnston, W. D., *J. Chem. Phys.* **26**, 582 (1957).
352. Hein, F., and Pauling, H., *Z. Anorg. Allgem. Chem.* **273**, 209 (1953).

353. Heinz, D., *Z. Anorg. Allgem. Chem.* **336**, 137 (1965).
354. Hendricks, S. B., *Am. Mineralogist* **24**, 529 (1939).
355. Herrmann, F., *Ber. Deut. Chem. Ges.* **27**, 596 (1894).
356. Hershaf, A., and Corbett, J. D., *J. Chem. Phys.* **36**, 551 (1962).
357. Hershaf, A., and Corbett, J. D., *Inorg. Chem.* **2**, 979 (1963).
358. Hettich, A., *Z. Anorg. Allgem. Chem.* **167**, 67 (1927).
359. Hilsch, R., von Minnigerode, G., and von Wartenberg, H., *Naturwissenschaften* **44**, 463 (1957).
360. Hilpert, R. S., Hoffmann, A., and Schacht, R., *Ber. Deut. Chem. Ges.* **71**, 82 (1938).
361. Hoekstra, H. R., Siegel, S., Fuchs, L. H., and Katz, J. J., *J. Phys. Chem.* **59**, 136 (1955).
362. Hoekstra, H. R., and Siegel, S., *Proc. Intern. Conf. Peaceful Uses At. Energy, Geneva, 1955* Vol. 7, p. 394. Columbia Univ. Press (I.D.S.), New York, 1955.
363. Hoekstra, H. R., and Siegel, S., *J. Inorg. & Nucl. Chem.* **18**, 154 (1961).
364. Hoekstra, H. R., Santoro, A., and Siegel, S., *J. Inorg. & Nucl. Chem.* **18**, 166 (1961).
365. Hofmann, K. A., and Resenscheck, F., *Ann. Chem.* **342**, 364 (1905).
366. Hofmann, K. A., and Hörschele, K., *Ber. Deut. Chem. Ges.* **48**, 20 (1915).
367. Holden, A. N.; Matthias, B. T., Anderson, P. W., and Lewis, H. W., *Phys. Rev.* **102**, 1463 (1956).
368. Holtzman, H., *Ind. Eng. Chem.* **37**, 855 (1945).
369. Hoppe, R., *Z. Anorg. Allgem. Chem.* **292**, 28 (1957).
370. Hoschek, E., and Klemm, W., *Z. Anorg. Allgem. Chem.* **242**, 63 (1939).
371. Huckel, W., *Nachr. Akad. Wiss. Goettingen, IIa. Math.-Physik.-Chem. Abt. Math.-Phys. Kl.*, No. 1, p. 36 (1946).
372. Hund, F., Wagner, R., and Peetz, U., *Z. Elektrochem.* **56**, 61 (1952).
373. Ibers, J. A., and Davidson, N., *J. Am. Chem. Soc.* **73**, 476 (1951).
374. Ipatiew, W., and Nikolajew, W., *Ber. Deut. Chem. Ges.* **59**, 1423 (1926).
375. Iwase, E., Nishiyama, S., Kobayashi, I., and Matsuda, K., *Rika Gaku Kenkyusho Hokoku* **36**, 714 (1960).
376. Janes, R. B., *J. Am. Chem. Soc.* **57**, 471 (1935).
377. Janninek, R. F., and Whitmore, D. H., *J. Chem. Phys.* **37**, 2750 (1962).
378. Janusz, T. P., Heikes, R. R., and Johnston, W. D., *J. Chem. Phys.* **26**, 973 (1957).
379. Jensen, K. A., *Z. Anorg. Allgem. Chem.* **229**, 252 (1936).
380. Jensen, K. A., *Z. Anorg. Allgem. Chem.* **229**, 261 (1936).
381. Jensen, K. A., *Z. Anorg. Allgem. Chem.* **232**, 193 (1937).
382. Jensen, K. A., *Z. Anorg. Allgem. Chem.* **252**, 317 (1944).
383. Jockusch, H., *Naturwissenschaften* **22**, 561 (1934).
384. Johnsen, A., *Neues Jahrb. Mineral.* **1**, 89 (1907).
385. Johnson, G., and Weyl, W. A., *J. Am. Ceram. Soc.* **32**, 398 (1949).
386. Johnston, W. D., and Heikes, R. R., *J. Am. Chem. Soc.* **78**, 3255 (1956).
387. Jolibois, P., *Compt. Rend.* **224**, 1395 (1947).
388. Joly, M. A., *Compt. Rend.* **115**, 1299 (1892).
389. Jona, F., Shirane, G., and Pepinsky, R., *Phys. Rev.* **98**, 903 (1955).
390. Jones, P., and Thirsk, H. R., *Trans. Faraday Soc.* **50**, 732 (1954).
391. Jones, W. H., Garbaty, E. A., and Barnes, R. G., *J. Chem. Phys.* **36**, 494 (1962).
392. Jonker, G. H., and van Santen, J. H., *Physica* **16**, 337 (1950).
393. Jonker, G. H., and van Santen, J. H., *Physica* **16**, 599 (1950).
394. Jonker, G. H., and van Santen, J. H., *Physica* **19**, 120 (1953).

395. Jorgensen, C. K., *Acta Chem. Scand.* **11**, 73 (1957).
396. Jorgensen, C. K., *Acta Chem. Scand.* **13**, 196 (1959).
397. Jorgensen, C. K., *Mol. Phys.* **4**, 231 (1961).
398. Jorgensen, C. K., *Mol. Phys.* **4**, 235 (1961).
399. Jorgensen, C. K., and Orgel, L. E., *Mol. Phys.* **4**, 215 (1961).
400. Jost, K.-H., *Acta Cryst.* **21**, 34 (1966).
401. Jost, K.-H., *Acta Cryst.* **17**, 1593 (1964).
402. Kachi, S., Takada, T., and Kosuge, K., *J. Phys. Soc. Japan* **18**, 1839 (1963).
403. Kamimura, H., *J. Phys. Soc. Japan*, **21**, 484 (1966).
404. Kasper, J. S., *Bull. Am. Phys. Soc.* [2] **4**, 178 (1959).
405. Katz, J. J., and Gruen, D. M., *J. Am. Chem. Soc.* **71**, 2106 (1949).
406. Katz, J. J., and Rabinowitch, E., "The Chemistry of Uranium." McGraw-Hill, New York, 1951.
407. Katz, L., and Lipscomb, W. N., *Acta Cryst.* **4**, 345 (1951).
408. Keggin, J. F., *Proc. Roy. Soc.* **A144**, 75 (1934).
409. Keggin, J. F., and Miles, F. D., *Nature* **137**, 577 (1936).
410. Kerler, W., Neuwirth, W., Fluck, E., Kuhn, P., and Zimmermann, B., *Z. Physik* **173**, 321 (1963).
411. Kestigian, M., and Ward, R., *J. Am. Chem. Soc.* **77**, 6199 (1955).
412. Ketelaar, J. A. A., t'Hart, W. H., Moerel, M., and Polder, D., *Z. Krist.* **101**, 396 (1939).
413. Kettle, S. F. A., *Nature* **207**, 1384 (1965).
414. Kettle, S. F. A., *Theoret. Chim. Acta* **3**, 211 (1965).
415. Khakhan, I. B., and Reibel, I. M., *Tr. Kishinevsk. Sel'skokhoz. Inst.* **11**, 159 (1956).
416. Kida, S., *Bull. Chem. Soc. Japan* **38**, 1804 (1965).
417. Kiehl, S. J., Fox, R. L., and Hardt, H. B., *J. Am. Chem. Soc.* **59**, 2395 (1937).
418. Kierkegaard, P., and Nyborg, B., *Acta Chem. Scand.* **19**, 2189 (1965).
419. Kihlberg, L., *Acta Chem. Scand.* **13**, 954 (1959).
420. Kihlberg, L., *Acta Chem. Scand.* **16**, 2458 (1962).
421. Kihlberg, L., *Advan. Chem. Ser.* **39**, 37 (1963).
422. Kihlberg, L., *Arkiv Kemi* **21**, 471 (1964).
423. King, E. L., and Neptune, J. A., *J. Am. Chem. Soc.* **77**, 3186 (1955).
424. Klechkovskaya, V. V., Troitskaya, N. V., and Pinsker, Z. G., *Soviet Phys.-Cryst. (English Transl.)* **10**, 28 (1965).
425. Klemm, W., *Z. Anorg. Allgem. Chem.* **201**, 32 (1931).
426. Klemm, W., and Tilk, W., *Z. Anorg. Allgem. Chem.* **207**, 175 (1932).
427. Klemm, W., and von Vogel, H. U., *Z. Anorg. Allgem. Chem.* **219**, 45 (1934).
428. Klemm, W., *Z. Anorg. Allgem. Chem.* **301**, 323 (1959).
429. Klotz, I. M., Czerlinski, G. H., and Fiess, H. A., *J. Am. Chem. Soc.* **80**, 2920 (1958).
430. Knop, W., *Ann. Chem.* **43**, 111 (1842).
431. Kochetkova, A. P., Tronev, V. G., and Gilyarov, O. N., *Dokl. Akad. Nauk SSSR* **147**, 1373 (1962).
432. Kochetkova, A. P., and Gilyarov, O. N., *Zh. Neorgan. Khim.* **11**, 1239 (1966).
433. Koide, S., and Takei, H., *J. Phys. Soc. Japan* **18**, 319 (1963).
434. Kolditz, L., and Rochusch, W., *Z. Anorg. Allgem. Chem.* **318**, 17 (1962).
435. Konopik, N., and Zwiauer, J., *Monatsh. Chem.* **83**, 189 (1952).
436. Korshunov, I. A., and Lebedeva, Z. M., *Zh. Neorgan. Khim.* **1**, 1912 (1956).
437. Kosuge, K., Takada, T., and Kachi, S., *J. Phys. Soc. Japan* **18**, 318 (1963).

438. Kovba, L. M., Kuz'micheva, E. U., and Ippolitova, E. A., *Vestn. Mosk. Univ., Ser. II: Khim.* **19**, 34 (1964).
439. Krauss, F., and Schrader, G., *Z. Anorg. Allgem. Chem.* **165**, 59 (1927).
440. Krauss, H. L., and Gnatz, G., *Chem. Ber.* **92**, 2110 (1959).
441. Krogmann, K., *Angew. Chem. Intern. Ed. English* **3**, 147 (1964).
442. Krogmann, K., Dodel, P., and Hansen, H. D., *Proc. 8th Intern. Conf. Coord. Chem., Vienna, 1964* p. 157.
443. Krylov, E. I., *Nauchn. Dokl. Vysshei Shkoly, Khim. i Khim. Tekhnol.* p. 676 (1958).
444. Krylov, E. I., and Kalugina, N. N., *Zh. Neorgan. Khim.* **4**, 2476 (1959).
445. Krylov, E. I., Samarina, V. A., and Shtol'ts, A. K., *Dokl. Akad. Nauk SSSR* **130**, 556 (1960).
446. Kubota, B., *J. Am. Ceram. Soc.* **44**, 239 (1961).
447. Kuhn, P. J., and McCarley, R. E., *Inorg. Chem.* **4**, 1482 (1965).
448. Kul'ba, F. Ya., and Mironov, V. E., *Zh. Neorgan. Khim.* **2**, 19 (1957).
449. Kul'ba, F. Ya., and Mironov, V. E., *Zh. Neorgan. Khim.* **2**, 46 (1957).
450. Kunze, J., *Chem. Tech. (Berlin)* **5**, 392 (1953).
451. Kurkjian, C. R., and Lefort, J., *Compt. Rend.* **69**, 169 (1869).
452. Kuznetsov, V. G., and Koz'min, P. A., *Russ. J. Inorg. Chem. (English Transl.)* **3**, 182 (1958).
453. Lander, J. J., and Wooten, L. A., *J. Am. Chem. Soc.* **73**, 2452 (1951).
454. Laubengayer, A. W., and Schirmer, F. B., *J. Am. Chem. Soc.* **62**, 1578 (1940).
455. Lawton, S. L., personal communication (1966).
456. Lawton, S. L., and Jacobson, R. A., *Inorg. Chem.* **5**, 743 (1966).
457. Leask, M. J. M., Roberts, L. E. J., Walter, A. J., and Wolf, W. P., *J. Chem. Soc.* p. 4788 (1963).
458. Le Blanc, M., and Sachse, H., *Physik. Z.* **32**, 887 (1931).
459. Lecerf, A., Rault, M., and Villers, G., *Compt. Rend.* **261**, 749 (1965).
460. Lecoq de Boisbaudran, P. E., *Compt. Rend.* **96**, 1406 (1883).
461. Levy, L. A., *J. Chem. Soc.* **101**, 1081 (1912).
462. Lindberg, M. L., and Christ, C. L., *Acta Cryst.* **12**, 695 (1959).
463. Linhard, M., and Weigel, M., *Z. Physik. Chem. (Frankfurt) [N.S.]* **11**, 312 (1957).
464. Linhard, M., and Weigel, M., *Z. Anorg. Allgem. Chem.* **308**, 254 (1961).
465. Littler, J. G. F., and Williams, R. J. P., *J. Chem. Soc.* p. 6368 (1965).
466. Long, L. H., and Sackman, J. F., *J. Inorg. & Nucl. Chem.* **25**, 79 (1963).
467. Loopstra, B. O., *Acta Cryst.* **17**, 651 (1964).
468. Lorthioir, G., and Michel, A., *Compt. Rend.* **258**, 4560 (1964).
469. Lux, H., and Niedermaier, T., *Z. Naturforsch.* **11a**, 613 (1956).
470. MacCarthy, G. R., *Am. J. Sci.* **12**, 16 (1926).
471. Mackay, R. A., and Schneider, R. F., *Inorg. Chem.* **6**, 549 (1967).
472. Magneli, A., *Arkiv Kemi, Mineral. Geol.* **24A**, No. 2 (1946).
473. Magneli, A., *Arkiv Kemi* **1**, 223 (1949).
474. Magneli, A., *Nova Acta Regiae Soc. Sci. Upsaliensis* **14**, 8 (1950).
475. Magneli, A., and Kihlberg, L., *Acta Chem. Scand.* **5**, 578 (1951).
476. Magneli, A., *Acta Cryst.* **6**, 495 (1953).
477. Magneli, A., *J. Inorg. & Nucl. Chem.* **2**, 330 (1956).
478. Makarov, E. S., *Proc. Acad. Sci. USSR, Chem. Sect. (English Transl.)* **139**, 720 (1961).
479. Makarov, S. Z., and Vakrushev, A. A. *Izv. Akad. Nauk SSSR, Otd. Khim. Nauk* No. 10, p. 1731 (1960).

480. Malatesta, L., *Gazz. Chim. Ital.* **72**, 287 (1942).
481. Margotin, P., Stuckens, W., and Durand, R., *Compt. Rend.* **252**, 4005 (1961).
482. Marsh, J. K., *J. Chem. Soc.* p. 15 (1946).
483. Marsh, R. E., and Shoemaker, D. P., *Acta Cryst.* **6**, 197 (1953).
484. Marsmann, H., and Hahn, H., *Z. Naturforsch.* **21b**, 188 (1966).
485. Martin, R. L., *Nature* **165**, 202 (1950).
486. Mason, B., and Vitaliano, C. J., *Mineral. Mag.* **30**, 100 (1953).
487. Mason, H. S., *Biochem. Biophys. Res. Commun.* **10**, 11 (1963).
488. Mathieu, J. P., *Bull. Soc. Chim. France* **5**, 105 (1938).
489. Mattes, R., and Krogmann, K., *Z. Anorg. Allgem. Chem.* **332**, 247 (1964).
490. Mazzi, F., and Rossi, G., *Z. Krist.* **121**, 243 (1955).
491. McCarley, R. E., Martin, D. J., Jr., and Cox, L. T., *J. Inorg. & Nucl. Chem.* **7**, 113 (1958).
492. McCarley, R. E., and Boatman, J. C., *Inorg. Chem.* **4**, 1486 (1965).
493. McCarley, R. E., Hughes, B. G., Cotton, F. A., and Zimmerman, R., *Inorg. Chem.* **4**, 1491 (1965).
494. McCarley, R. E., quoted in MacKay and Schneider (471).
495. McConnell, H. M., and Davidson, N., *J. Am. Chem. Soc.* **71**, 3845 (1949).
496. McConnell, H. M., and Davidson, N., *J. Am. Chem. Soc.* **72**, 3168 (1950).
497. McConnell, H. M., and Davidson, N., *J. Am. Chem. Soc.* **72**, 5557 (1950).
498. McConnell, H. M., and Weaver, H. E., Jr., *J. Chem. Phys.* **25**, 307 (1956).
499. McConnell, H. M., and Berger, S. B., *J. Chem. Phys.* **27**, 230 (1957).
500. McCullough, J. D., *J. Am. Chem. Soc.* **72**, 1386 (1950).
501. McCullough, J. D., and Britton, J. D., *J. Am. Chem. Soc.* **74**, 5225 (1952).
502. McMillan, J. A., *J. Inorg. & Nucl. Chem.* **13**, 28 (1960).
503. McMillan, J. A., *Chem. Rev.* **62**, 65 (1962).
504. McMullan, R. K., and Corbett, J. D., *J. Am. Chem. Soc.* **80**, 4761 (1958).
505. Mee, J. E., and Corbett, J. D., *Inorg. Chem.* **4**, 88 (1965).
506. Mikhalevich, K. N., and Litvinchuk, V. M., *Zh. Neorgan. Khim.* **9**, 2391 (1964).
507. Miller, A. E., and Daane, A. H., *J. Inorg. & Nucl. Chem.* **27**, 1955 (1965).
508. Milyutina, M. I., and Sharova, A. K., *Tr. Inst. Khim. Akad. Nauk SSSR, Ural'sk. Filial* p. 85 (1963).
509. Miyatani, K., Kohn, K., Kamimura, H., and Iida, S., *J. Phys. Soc. Japan* **21**, 464 (1966).
510. Moore, C. E., *Nat. Bur. Std. (U.S.), Circ.* **467**, 94.
511. Morawietz, W., Morawietz, H., and Brauer, G., *Z. Anorg. Allgem. Chem.* **316**, 220 (1962).
512. Morgan, G. T., and Burstall, F. H., *J. Chem. Soc.* p. 41 (1936).
513. Morgan, G. T., and Burstall, F. H., *J. Chem. Soc.* p. 2018 (1926).
514. Mori, H., and Ito, T., *Acta Cryst.* **3**, 1 (1950).
515. Mori, M., *Bull. Chem. Soc. Japan* **24**, 285 (1951).
516. Mori, M., *Bull. Chem. Soc. Japan* **33**, 985 (1960).
517. Mori, M., Saito, Y., and Watanabe, T., *Bull. Chem. Soc. Japan* **34**, 295 (1961).
518. Mori, M., *Bull. Chem. Soc. Japan* **34**, 1249 (1961).
519. Mott, N. F., *Nuovo Cimento* [10] **7**, Suppl., 312 (1958).
520. Munday, T. C. F., and Corbett, J. D., *Inorg. Chem.* **5**, 1263 (1966).
521. Murat, M., Chevreton, M., Berodias, G., and Eyraud, C., *J. Chim. Phys.* **61**, 812 (1964).
522. Murray-Rust, P., Day, P., and Prout, C. K., *Chem. Commun.*, p. 277 (1966).
523. Nachtrieb, N. H., *J. Phys. Chem.* **66**, 1163 (1962).
524. Naray-Szabo, I., and Popp, K., *Z. Anorg. Allgem. Chem.* **322**, 286 (1963).

525. Naray-Szabo, I., Argay, G., and Szabo, P., *Acta Cryst.* **19**, 180 (1965).
526. Narbutt, K. I., and Laputina, I. P., *Bull. Acad. Sci. USSR, Phys. Ser. (English Transl.)* **26**, 410 (1962).
527. Natta, G., and Baccaredda, M., *Z. Krist.* **85**, 271 (1933).
528. Neiding, A. B., and Kazarnovskii, I. A., *Dokl. Akad. Nauk. SSSR* **78**, 713 (1951).
529. Neumann, H. M., and Brown, H., *J. Am. Chem. Soc.* **78**, 1843 (1956).
530. Newton, T. W., and Baker, F. B., *Inorg. Chem.* **3**, 569 (1964).
531. Nguyen-Nghi, H., Plurien, P., Mme. Baggioni-Escoubes, and Eyraud, C., *Bull. Soc. Chim. France* p. 72 (1963).
532. Niebuhr, J., *J. Less-Common Metals* **10**, 312 (1966).
533. Niebuhr, J., *J. Less-Common Metals* **11**, 191 (1966).
534. Nikolaev, N. S., and Shishkov, Yu. D., *Proc. Acad. Sci. USSR, Chem. Sect. (English Transl.)* **143**, 168 (1962).
535. Noddack, W., and Walsh, H., *Z. Physik. Chem. (Leipzig)* **211**, 194 (1959).
536. Noddack, W., and Walsh, H., *Z. Elektrochem.* **63**, 269 (1959).
537. Norin, R., and Magneli, A., *Naturwissenschaften* **47**, 354 (1960).
538. Norin, R., *Naturwissenschaften* **52**, 300 (1965).
539. Norin, R., *Acta Chem. Scand.* **20**, 871 (1966).
540. Nyholm, R. S., *J. Chem. Soc.* p. 1767 (1951).
541. Nyholm, R. S., and Sharpe, A. G., *J. Chem. Soc.* p. 3579 (1952).
542. Oberhauser, F., and Schormuller, J., *Ber. Deut. Chem. Ges.* **62**, 1482 (1929).
543. O'Donnell, T. A., and Stewart, D. F., *Inorg. Chem.* **5**, 1434 (1966).
544. Ohyagi, Y., *Bull. Chem. Soc. Japan* **15**, 186 (1940).
545. Orgel, L. E., *Discussions Faraday Soc.* **26**, 138 (1958).
546. Osmond, W. P., *Proc. Phys. Soc. (London)* **87**, 767 (1966).
547. Ostrowetsky, S., and Souchay, P., *Compt. Rend.* **251**, 373 (1960).
548. Ostrowetsky, S., *Compt. Rend.* **251**, 1068 (1960).
549. Ostrowetsky, S., *Bull. Soc. Chim. France* No. 5, p. 1012 (1964).
550. Ostrowetsky, S., *Bull. Soc. Chim. France* No. 5, p. 1018 (1964).
551. Oswald, H. R., Feitknecht, W., and Wampetich, M. J., *Nature* **207**, 72 (1965).
552. Ott, H., and Seyfarth, H., *Z. Krist.* **67**, 430 (1928).
553. Owen, J., *Discussions Faraday Soc.* **26**, 53 (1958).
554. Ozerov, R. P., *Soviet Phys.-Cryst. (English Transl.)* **2**, 219 (1957).
555. Paglia, E., and Sironi, C., *Gazz. Chim. Ital.* **88**, 541 (1958).
556. Palagyi, T., and Naray-Szabo, I., *Acta Chim. Acad. Sci. Hung.* **30**, 1 (1962).
557. Palkin, A. P., Vigutova, T. N., and Glotova, L. I., *Russ. J. Inorg. Chem. (English Transl.)* **8**, 128 (1963).
558. Palkin, A. P., Ostrikova, N. V., and Vigutova, T. N., *Russ. J. Inorg. Chem. (English Transl.)* **8**, 1344 (1963).
559. Paklin, A. P., and Ostrikova, N. V., *Russ. J. Inorg. Chem. (English Transl.)* **9**, 1104 (1964).
560. Panzer, R. E., and Suttle, J. F., *J. Inorg. & Nucl. Chem.* **20**, 229 (1961).
561. Partington, J. R., and Whynes, A. L., *J. Chem. Soc.* p. 1952 (1948).
562. Pascaru, I., Constantinescu, O., Constantinescu, M., and Arizan, D., *J. Chim. Phys.* **62**, 1283 (1965).
563. Pauling, L., and Shappell, M. D., *Z. Krist.* **75**, 128 (1930).
564. Pauling, L., *J. Am. Chem. Soc.* **69**, 542 (1947).
565. Pauling, L., "The Nature of the Chemical Bond." 3rd ed. Cornell Univ. Press, Ithaca, New York, 1960.

566. Perakis, N., Serres, A., Parravano, G., and Wucher, J., *Compt. Rend.* **242**, 1275 (1956).
567. Peretti, E. A., *J. Am. Chem. Soc.* **78**, 5745 (1956).
568. Pério, P., *Bull. Soc. Chim. France*, p. 256 (1953).
569. Perthiel, R., and Jahn, H., *Phys. Status Solidi* **5**, 563 (1964).
570. Pollard, W. B., *J. Chem. Soc.* **117**, 99 (1920).
571. Pope, M. T., and Varga, G. M., Jr., *Inorg. Chem.* **5**, 1249 (1966).
572. Powell, H. M., *Proc. Chem. Soc.* p. 73 (1959).
573. Prandl, W., and Rieder, G., *Z. Anorg. Allgem. Chem.* **238**, 225 (1938).
574. Pugh, W., *J. Chem. Soc.* p. 1959 (1937).
575. Rabe, O., *Z. Anorg. Allgem. Chem.* **58**, 23 (1908).
576. Raleigh, D. O., *J. Chem. Phys.* **38**, 1677 (1963).
577. Rau, R. C., *Acta Cryst.* **20**, 716 (1966).
578. Ray, P. C., and Adhikari, N., *J. Indian Chem. Soc.* **9**, 254 (1932).
579. Recoura, A., *Bull. Soc. Chim. France* **17**, 934 (1897).
580. Reihlen, H., and Flohr, E., *Ber. Deut. Chem. Ges.* **67**, 2010 (1934).
581. Reuter, B., Jaskowsky, J., and Riedel, E., *Z. Elektrochem.* **63**, 937 (1959).
582. Reynolds, J. E., *Proc. Roy. Soc.* **A82**, 380 (1909).
583. Rich, R. L., and Taube, H., *J. Am. Chem. Soc.* **76**, 2608 (1954).
584. Richardson, J., and Elliott, N., *J. Am. Chem. Soc.* **62**, 3182 (1940).
585. Riebling, E. F., and Erickson, C. E., *J. Phys. Chem.* **67**, 307 (1963).
586. Riebling, E. F., and Erickson, C. E., *J. Phys. Chem.* **67**, 509 (1963).
587. Rienäcker, G., and Birckenstaedt, M., *Z. Anorg. Allgem. Chem.* **265**, 99 (1951).
588. Rigamonti, R., *Gazz. Chim. Ital.* **67**, 137 (1937).
589. Roberts, L. E. J., and Walter, A. J., *J. Inorg. & Nucl. Chem.* **22**, 213 (1961).
590. Roberts, L. E. J., *Advan. Chem. Ser.* **39**, 66 (1963).
591. Robin, M. B., *Inorg. Chem.* **1**, 337 (1962).
592. Robin, M. B., *J. Chem. Phys.* **40**, 3369 (1964).
593. Robin, M. B., and Kuebler, N. A., *Inorg. Chem.* **4**, 978 (1965).
594. Robin, M. B., Andres, K., Geballe, T. H., Kuebler, N. A., and McWhan, D. B., *Phys. Rev. Letters* **17**, 917 (1966).
595. Robin, M. B., unpublished results (1962).
596. Rode, T. V., Kazanskii, V. B., and Pecherskaya, Yu. I., *Russ. J. Phys. Chem. (English Transl.)* **35**, 1170 (1961).
597. Rode, T. V., and Rode, V. E., *Russ. J. Phys. Chem. (English Transl.)* **35**, 1225 (1961).
598. Rode, E. Ya., and Lysanova, G. V., *Dokl. Akad. Nauk SSSR* **145**, 351 (1962).
599. Rogers, D., and Skapski, A. C., *Proc. Chem. Soc.* p. 400 (1964).
600. Rolsten, R. F., *J. Am. Chem. Soc.* **80**, 2952 (1958).
601. Ross, M., *Am. Mineralogist* **44**, 322 (1959).
602. Roth, W. L., *J. Phys. Chem. Solids* **25**, 1 (1964).
603. Rowland, T. J., and Bromberg, J. P., *J. Chem. Phys.* **29**, 626 (1958).
604. Rüdorff, W., and Valet, G., *Z. Naturforsch.* **7b**, 57 (1952).
605. Rüdorff, W., Schwarz, H. G., and Walter, M., *Z. Anorg. Allgem. Chem.* **269**, 141 (1952).
606. Rüdorff, W., and Valet, G., *Z. Anorg. Allgem. Chem.* **271**, 257 (1953).
607. Ruff, O., and Plato, W., *Ber. Deut. Chem. Ges.* **37**, 673 (1904).
608. Ruff, O., and Ascher, E., *Z. Anorg. Allgem. Chem.* **183**, 193 (1929).
609. Ruff, O., and Giese, M., *Z. Anorg. Allgem. Chem.* **219**, 143 (1934).
610. Rundle, R. E., Baenziger, N. C., Wilson, A. S., and McDonald, R. A., *J. Am. Chem. Soc.* **70**, 99 (1948).

611. Rundle, R. E., *J. Am. Chem. Soc.* **76**, 3101 (1954).
612. Ryan, T. D., and Rundle, R. E., *J. Am. Chem. Soc.* **83**, 2814 (1961).
613. Sacconi, L., and Cini, R., *J. Chem. Phys.* **18**, 1124 (1950).
614. Sainte-Claire Deville, H., and Debray, H., *Compt. Rend.* **86**, 927 (1878).
615. Sakellaridis, P., and Coromanzou, M., *Bull. Soc. Chim. France* p. 769 (1962).
616. Sallach, R. A., and Corbett, J. D., *Inorg. Chem.* **2**, 457 (1963).
617. Scatturin, V., *Atti, Ist. Veneto Sci., Lettere Arti, Classe Sci. Mat. Nat.* **109**, 109 (1951).
618. Scatturin, V., Zannetti, R., and Censolo, G., *Ric. Sci.* **26**, 3108 (1956).
619. Scatturin, V., Bellon, P. L., and Zannetti, R., *Ric. Sci.* **27**, 2163 (1957).
620. Scatturin, V., Bellon, P. L., and Zannetti, R., *J. Inorg. & Nucl. Chem.* **8**, 462 (1958).
621. Scatturin, V., Bellon, P. L., and Salkind, A. J., *Ric. Sci.* **30**, 1034 (1960).
622. Scatturin, V., Bellon, P. L., and Salkind, A. J., *J. Electrochem. Soc.* **108**, 819 (1961).
623. Schaefer, W. P., and Marsh, R. E., *J. Am. Chem. Soc.* **88**, 178 (1966).
624. Schäfer, H., Sibbing, E., and Gerken, R., *Z. Anorg. Allgem. Chem.* **307**, 163 (1961).
625. Schäfer, H., and Dohmann, K.-D., *Z. Anorg. Allgem. Chem.* **311**, 134 (1961).
626. Schäfer, H., Scholz, H., and Gerken, R., *Z. Anorg. Allgem. Chem.* **331**, 154 (1964).
627. Schäfer, H., and Schnering, H. G., *Angew. Chem.* **76**, 833 (1964).
628. Schäfer, H., Gerken, R., and Scholz, H., *Z. Anorg. Allgem. Chem.* **335**, 96 (1965).
629. Schäfer, H., von Schnering, H. G., Niehues, K.-J., and Nieder-Vahrenholz, H. G., *J. Less-Common Metals* **9**, 95 (1965).
630. Schäfer, H., and Bauer, D., *Z. Anorg. Allgem. Chem.* **340**, 62 (1965).
631. Schäfer, H., von Schnering, H. G., Siepman, R., Simon, A., Giegling, D., Bauer, D., and Spreckelmeyer, B., *J. Less-Common Metals* **10**, 154 (1966).
632. Schäfer, H., and Spreckelmeyer, B., *J. Less-Common Metals* **11**, 73 (1966).
633. Schäfer, H. S., and Siepman, R., *J. Less-Common Metals* **11**, 76 (1966).
634. Scharizer, R., *Z. Krist.* **37**, 530 (1903).
635. Scharizer, R., *Z. Krist.* **43**, 113 (1907).
636. Scheibe, H., and Ermischer, W., *Kernenergie* **6**, 178 (1963).
637. Scheibe, H., and Ermischer, W., *Kernenergie* **7**, 95 (1964).
638. Schnering, H. G., and Wöhrle, H., *Angew. Chem. Intern. Ed. English* **2**, 558 (1963).
639. Scholder, R., and Stobbe, H., *Z. Anorg. Allgem. Chem.* **247**, 392 (1941).
640. Scholder, R., and Klemm, W., *Angew. Chem.* **66**, 461 (1954).
641. Schönberg, N., *Acta Chem. Scand.* **8**, 221 (1954).
642. Schönberg, N., *Acta Chem. Scand.* **8**, 240 (1954).
643. Schönberg, N., *Acta Chem. Scand.* **8**, 617 (1954).
644. Schramm, E. P., *Inorg. Chem.* **5**, 1291 (1966).
645. Schultz, C., *J. Prakt. Chem.* **68**, 257 (1856).
646. Schwab, G.-M., and Hartmann, G., *Z. Anorg. Allgem. Chem.* **281**, 183 (1955).
647. Schwartz, R. S., Fankuchen, I., and Ward, R., *J. Am. Chem. Soc.* **74**, 1676 (1952).
648. Seabaugh, P. W., and Corbett, J. D., *Inorg. Chem.* **4**, 176 (1965).
649. Seaborg, G. T., and Katz, J. J., "The Actinide Elements." McGraw-Hill, New York, 1954.
650. Seifer, G. B., *Russ. J. Inorg. Chem. (English Transl.)* **7**, 621 (1962).

651. Selbin, J., and Usategui, M., *J. Inorg. & Nucl. Chem.* **20**, 91 (1961).
652. Selwood, P. W., "Magnetochemistry," Wiley (Interscience), New York, 1956.
653. Senderoff, S., and Mellors, A. S., *J. Electrochem. Soc.* **105**, 224 (1958).
654. Setterberg, C., *Oefversigt K. Vetensk. Akad. Forhandl.* No. 6, p. 23 (1882).
655. Sharpe, A. G., *J. Chem. Soc.* p. 3444 (1950).
656. Sharpe, A. G., *J. Chem. Soc.* p. 2165 (1952).
657. Sheka, I. A., Chaus, I. S., and Mityureva, T. T., "The Chemistry of Gallium." Elsevier, Amsterdam, 1966.
658. Shields, L., and Symons, M. C. R., *Mol. Phys.* **11**, 57 (1966).
659. Shively, R. R., Jr., and Weyl, W. A., *J. Phys. Chem.* **55**, 512 (1951).
660. Shull, C. G., Wollan, E. O., and Koehler, W. C., *Phys. Rev.* **84**, 912 (1951).
661. Sienko, M. J., *Advan. Chem. Ser.* **39**, 224 (1963).
662. Siepman, R., and Schäfer, H., *Naturwissenschaften* **52**, 344 (1965).
663. Sil'nichenko, V. G., *Uch. Zapisk. Mosk. Obl. Ped. Inst.* **84**, 119 (1959).
664. Simon, A., and Schmidt, T., *Z. Anorg. Allgem. Chem.* **153**, 191 (1926).
665. Simon, A., Schnering, H. G., Wöhrle, H., and Schäfer, H., *Z. Anorg. Allgem. Chem.* **339**, 155 (1965).
666. Simon, A., and von Schnering, H. G., *J. Less-Common Metals* **11**, 31 (1966).
667. Sinha, A. P. B., Sanjana, N. R., and Biswas, B. A., *J. Phys. Chem.* **62**, 191 (1958).
668. Sinha, S. C., and Nigam, H. L., *Current Sci. (India)* **35**, 63 (1966).
669. Sisler, H. H., and Jirik, F. E., *J. Am. Chem. Soc.* **66**, 1344 (1944).
670. Skapski, A. C., and Rogers, D., *Chem. Commun.* p. 611 (1965).
671. Smith, G. McP., *J. Am. Chem. Soc.* **44**, 1769 (1922).
672. Souchay, P., *Bull. Soc. Chim. France* **7**, 875 (1940).
673. Souchay, P., *Ann. Chim. (Paris)* [12] **18**, 73 (1943).
674. Souchay, P., *Ann. Chim. (Paris)* [12] **18**, 169 (1943).
675. Souchay, P., and Ostrowetsky, S., *Compt. Rend.* **250**, 4168 (1960).
676. Souchay, P., and Massart, R., *Compt. Rend.* **253**, 1699 (1961).
677. Souchay, P., and Herve, G., *Compt. Rend.* **261**, 2486 (1965).
678. Spandau, H., and Kohlmeyer, E. J., *Z. Anorg. Allgem. Chem.* **254**, 65 (1947).
679. Spinedi, P., and Gauzzi, F., *Ann. Chim. (Rome)* **47**, 1305 (1957).
680. Spittler, T. M., and Jaselskis, B., *J. Am. Chem. Soc.* **88**, 2942 (1966).
681. Spreckelmeyer, B., and Schäfer, H., *J. Less-Common Metals* **11**, 74 (1966).
682. Stehlik, B., and Weidenthaler, P., *Collection Czech. Chem. Commun.* **24**, 1416 (1959).
683. Steinfink, H., and Burns, J. H., *Acta Cryst.* **17**, 823 (1964).
684. Stephenson, N. C., and Wadsley, A. D., *Acta Cryst.* **19**, 241 (1965).
685. Stephenson, N. C., *Acta Cryst.* **20**, 59 (1966).
686. Stewart, D. F., and O'Donnell, T. A., *Nature* **210**, 836 (1966).
687. Stieglitz, J., *Proc. Natl. Acad. Sci. U.S.A.* **9**, 308 (1923).
688. Streintz, F., in "Sammlung elektrotechnischer Vorträge," Vol. 4, Stuttgart, Enke, 1903; quoted in Biltz (69).
689. Strekalovskii, V. N., Beketov, A. R., and Vlasov, V. G., *Russ. J. Inorg. Chem. (English Transl.)* **9**, 1347 (1964).
690. Strickland, J. D. H., *J. Am. Chem. Soc.* **74**, 862 (1952).
691. Strickland, J. D. H., *J. Am. Chem. Soc.* **74**, 868 (1952).
692. Stringer, J., *J. Less-Common Metals* **8**, 1 (1954).
693. Sturm, B. J., *Inorg. Chem.* **1**, 665 (1962).
694. Subbarao, E. C., in "Non-Stoichiometric Compounds" (L. Mandelcorn, ed.), p. 268. Academic Press, New York, 1964.

695. Suchow, L., Fankuchen, I., and Ward, R., *J. Am. Chem. Soc.* **74**, 1678 (1952).
696. Sugden, S., *J. Chem. Soc.* p. 161 (1932).
697. Syrkin, Ya. K., and Belova, V. I., *Zh. Fiz. Khim.* **23**, 664 (1949).
698. Takéuchi, Y., Watanabé, T., and Ito, T., *Acta Cryst.* **3**, 98 (1950).
699. Tammann, G., and von Samson-Himmelstjerna, H. O., *Z. Anorg. Allgem. Chem.* **207**, 319 (1932).
700. Terrey, H., and Diamond, H., *J. Chem. Soc.* p. 2820 (1928).
701. Theobald, J. G., *Compt. Rend.* **261**, 2185 (1965).
702. Thompson, L. R., and Wilmarth, W. K., *J. Phys. Chem.* **56**, 5 (1952).
703. Thompson, R. C., *J. Am. Chem. Soc.* **70**, 1045 (1948).
704. Topol, L. E., and Ransom, L. D., *J. Chem. Phys.* **38**, 1663 (1963).
705. Tovborg Jensen, A., and Rasmussen, S. E., *Acta Chem. Scand.* **9**, 708 (1955).
706. Treadwell, F. P., and von Girssewald, C., *Z. Anorg. Allgem. Chem.* **39**, 84 (1904).
707. Trzebiatowski, W., and Rozyczka, J., *Roczniki Chem.* **32**, 183 (1958).
708. Tschugajeff, L., Chlopin, W., and Fritzmann, E., *Z. Anorg. Allgem. Chem.* **151**, 253 (1926).
709. Tschugajeff, L., and Tschernjajeff, J., *Z. Anorg. Allgem. Chem.* **182**, 159 (1929).
710. Tsuchida, R., and Yamada, S., *Nature* **174**, 1064 (1954).
711. Turco, A., and Mazzon, L., *Ann. Chim. (Rome)* **43**, 853 (1953).
712. Turco, A., and Sordillo, G., *Ann. Chim. (Rome)* **43**, 865 (1953).
713. Turco, A., and Sordillo, G., *Ric. Sci.* **24**, 831 (1954).
714. Turco, A., and Sordillo, G., *Ann. Chim. (Rome)* **45**, 614 (1955).
715. Usanovitch, M. I., Sumarokova, T. N., and Beketov, M. B., *Izv. Akad. Nauk Kaz. SSR, Ser. Khim.* **123**, 3 (1953).
716. Vaciago, A., and Mugnoli, A., *Atti. Accad. Nazl. Lincei, Rend., Classe Sci. Fis., Mat. Nat.* [8] **25**, 531 (1958).
717. Vaciago, A., and Mugnoli, A., *Atti. Accad. Nazl. Lincei, Rend., Classe Sci. Fis., Mat. Nat.* [8] **26**, 517 (1959).
718. Van Bever, A. K., *Rec. Trav. Chim.* **57**, 1259 (1939).
719. Van Houten, S., *Phys. Chem. Solids* **17**, 7 (1960).
720. Vannerberg, N.-G., *Acta Cryst.* **18**, 449 (1965).
721. Vannerberg, N.-G., and C. Brosset, *Acta Cryst.* **16**, 247 (1963).
722. van Santen, J. H., and Jonker, G. H., *Physica* **16**, 599 (1950).
723. Vasenin, F. I., *Zh. Prikl. Khim.* **21**, 429 (1948).
724. Vaughan, P. A., Sturdivant, J. H., and Pauling, L., *J. Am. Chem. Soc.* **72**, 5477 (1950).
725. Verwey, E. J. W., and de Boer, J. H., *Rec. Trav. Chim.* **55**, 531 (1936).
726. Verwey, E. J. W., and Haayman, P. W., *Physica* **8**, 979 (1941).
727. Verwey, E. J. W., *Phillips Tech. Rev.* **9**, 46 (1947).
728. Verwey, E. J. W., and Heilmann, E. L., *J. Chem. Phys.* **15**, 174 (1947).
729. Verwey, E. J., Haayman, P. W., and Romeijn, F. C., *J. Chem. Phys.* **15**, 181 (1947).
730. Verwey, E. J. W., Haaijamn, P. W., Romeijn, F. C., and van Oosterhout, G. W., *Phillips Res. Rept.* **5**, 173 (1950).
731. Viel, S., *Ann. Chem.* **6**, 136 (1925).
732. Vlach, J., and Stehlik, B., *Collection Czech. Chem. Commun.* **25**, 676 (1960).
733. von Schnering, H.-G., Wöhrle, H., and Schäfer, H., *Naturwissenschaften* **48**, 159, (1961).
734. Vratny, F., Tsai, M., and Honig, J. M., *J. Inorg. & Nucl. Chem.* **16**, 263 (1961).
735. Vratny, F., and Micale, F., *Trans. Faraday Soc.* **59**, 2739 (1963).

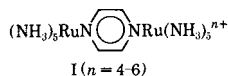
736. Wadsley, A. D., *Acta Cryst.* **8**, 695 (1955).
737. Wadsley, A. D., *Acta Cryst.* **10**, 261 (1957).
738. Wadsley, A. D., *J. Proc. Roy. Soc. N. S. Wales* **92**, 25 (1958).
739. Wadsley, A. D., and Andersson, S., *Nature* **192**, 551 (1961).
740. Wadsley, A. D., *Acta Cryst.* **14**, 660 (1961).
741. Wagner, C., and Koch, E., *Z. Physik. Chem.* **B32**, 439 (1936).
742. Walden, P. T., *Am. J. Sci.* **48**, 283 (1894).
743. Wallen, J., Brosset, C., and Vannerberg, N.-G., *Arkiv Kemi* **18**, 541 (1962).
744. Walter, P. H. L., Kleinberg, J., and Griswold, E., *J. Inorg. & Nucl. Chem.* **19**, 223 (1961).
745. Waser, J., and McClanahan, E. D., *Experientia* **6**, 379 (1950).
746. Waser, J., and McClanahan, E. D., Jr., *J. Chem. Phys.* **19**, 413 (1951).
747. Waser, J., and McClanahan, E. D., Jr., *J. Chem. Phys.* **20**, 199 (1952).
748. Watanabe, T., Atoji, M., and Okazaki, C., *Acta Cryst.* **3**, 405 (1950).
749. Waters, J. H., and Gray, H. B., *J. Am. Chem. Soc.* **87**, 3534 (1965).
750. Watt, G. W., and McCarley, R. E., *J. Am. Chem. Soc.* **79**, 4585 (1957).
751. Wehrli, M., and Wenk, W., *Helv. Phys. Acta* **12**, 559 (1939).
752. Weinland, R. F., and Schmid, H., *Ber. Deut. Chem. Ges.* **38**, 1080 (1905).
753. Weiser, H. B., Milligan, W. O., and Bates, J. B., *J. Phys. Chem.* **45**, 701 (1941).
754. Weiser, H. B., Milligan, W. O., and Bates, J. B., *J. Phys. Chem.* **46**, 99 (1942).
755. Weiss, J., *Proc. Roy. Soc.* **A222**, 128 (1954).
756. Wells, A. F., "Structural Inorganic Chemistry," 3rd ed. Oxford Univ. Press (Clarendon), London and New York, 1962.
757. Wells, H. L., and Metzger, F. J., *Am. Chem. J.* **26**, 268 (1901).
758. Wells, H. L., *Am. J. Sci.* **3**, 315 (1922).
759. Wells, H. L., *Am. J. Sci.* **3**, 417 (1922).
760. Wells, H. L., *Am. J. Sci.* **4**, 257 (1922).
761. Wells, H. L., *Am. J. Sci.* **4**, 476 (1922).
762. Wenk, W., *Helv. Phys. Acta* **14**, 355 (1941).
763. Went, J. J., Rathenau, G. W., Gorter, E. W., and van Oosterhout, G. W., *Philips Tech. Rev.* **13**, 194 (1952).
764. Werner, A., *Z. Anorg. Allgem. Chem.* **12**, 46 (1896).
765. Werner, A., *Ber. Deut. Chem. Ges.* **40**, 4605 (1907).
766. Werner, A., *Ann. Chem.* **375**, 1 (1910).
767. Weyl, W. A., *J. Soc. Glass Technol.* **27**, 265 (1943).
768. White, W. B., Dachille, F., and Roy, R., *J. Am. Ceram. Soc.* **44**, 170 (1961).
769. White, W. B., and Roy, R., *J. Am. Ceram. Soc.* **47**, 242 (1964).
770. Whitney, J. E., and Davidson, N., *J. Am. Chem. Soc.* **69**, 2076 (1947).
771. Whitney, J. E., Browne, C. I., McConnell, H. M., and Davidson, N., *Brookhaven Conf. Rept.* **2**, 196 (1948).
772. Whitney, J. E., and Davidson, N., *J. Am. Chem. Soc.* **71**, 3809 (1949).
773. Wiebenga, E. H., Havinga, E. E., and Boswijk, K. N., *Advan. Inorg. Chem. Radiochem.* **3**, 133 (1961).
774. Wiles, D. R., *Can. J. Chem.* **36**, 167 (1958).
775. Wilhelmi, K.-A., *Naturwissenschaften* **44**, 580 (1957).
776. Wilhelmi, K.-A., and Jonsson, O., *Acta Chem. Scand.* **12**, 1532 (1958).
777. Wilhelmi, K.-A., *Acta Chem. Scand.* **12**, 1965 (1958).
778. Wilhelmi, K.-A., *Acta Chem. Scand.* **19**, 165 (1965).
779. Wilhelmi, K.-A., *Chem. Commun.* p. 437 (1966).
780. Willardson, R. K., Moody, J. W., and Goering, H. L., *J. Inorg. & Nucl. Chem.* **6**, 19 (1958).

781. Willis, B. T. M., *Nature* **197**, 755 (1963).
782. Willis, B. T. M., *J. Phys. Radium* **25**, 431 (1964).
783. Wöhler, L., and Martin, F., *Z. Anorg. Chem.* **57**, 398 (1908).
784. Wöhler, L., and Martin, F., *Ber. Deut. Chem. Ges.* **42**, 3958 (1909).
785. Wöhler, L., and Martin, F., *Ber. Deut. Chem. Ges.* **42**, 4100 (1909).
786. Wöhler, L., *Z. Anorg. Chem.* **78**, 239 (1912).
787. Wöhler, L., and Müller, W., *Z. Anorg. Allgem. Chem.* **149**, 125 (1925).
788. Wöhler, L., and Müller, F., *Z. Anorg. Allgem. Chem.* **149**, 377 (1925).
789. Wold, A., Kunmann, W., Arnott, R. J., and Ferretti, A., *Inorg. Chem.* **3**, 545 (1964).
790. Wolfram, H., Dissertation, Königsberg (1900).
791. Wollan, E. O., and Koehler, W. C., *Phys. Rev.* **100**, 545 (1957).
792. Wood, D. L., and Remeika, J. P., *J. Appl. Phys.* **37**, 1232 (1966).
793. Woodward, L. A., and Bill, P. T., *J. Chem. Soc.* p. 1699 (1955).
794. Woodward, L. A., and Nord, A. A., *J. Chem. Soc.* p. 2655 (1955).
795. Woodward, L. A., Garton, G., and Roberts, H. L., *J. Chem. Soc.* p. 3723 (1956).
796. Woodward, L. A., Greenwood, N. N., Hall, J. R., and Worrall, I. J., *J. Chem. Soc.* p. 1505 (1958).
797. Yamada, S., Shimura, Y., and Tsuchida, R., *Bull. Chem. Soc. Japan* **26**, 72 (1953).
798. Yamada, S., and Tsuchida, R., *Ann. Rept. Sci. Works, Fac. Sci., Osaka Univ.* **4**, 79 (1956).
799. Yamada, S., and Tsuchida, R., *Bull. Chem. Soc. Japan* **29**, 421 (1956).
800. Yamada, S., and Tsuchida, R., *Bull. Chem. Soc. Japan* **29**, 894 (1956).
801. Yamada, S., and Tsuchida, R., *Bull. Chem. Soc. Japan* **30**, 715 (1957).
802. Yamashita, J., and Kurosawa, T., *Phys. Chem. Solids* **5**, 34 (1958).
803. Yoshioka, H., *J. Phys. Soc. Japan* **4**, 270 (1949).
804. Young, A. P., and Schwartz, C. M., *J. Inorg. & Nucl. Chem.* **25**, 1133 (1963).
805. Young, C. G., Shuskus, A. J., Gilliam, O. R., and Levy, P. W., *Bull. Am. Phys. Soc.* [2] **6**, 248 (1961).
806. Young, R. C., *J. Inorg. & Nucl. Chem.* **7**, 418 (1958).
807. Yuster, P., and Delbecq, C., *J. Phys. Chem.* **21**, 892 (1953).
808. Zachariasen, W. H., *Acta Cryst.* **2**, 390 (1949).
809. Zav'yalova, A. A., Imamov, R. M., and Pinsker, Z. G., *Soviet Phys.-Cryst. (English Transl.)* **10**, 401 (1966).
810. Zedlitz, O., *Z. Krist.* **81**, 253 (1932).
811. Zemann, J., *Mineral. Petrog. Mitt.* **1**, 361 (1950).
812. Zener, C., *Phys. Rev.* **81**, 440 (1951).
813. Zener, C., *Phys. Rev.* **82**, 403 (1951).
814. Zener, C., and Heikes, R. R., *Rev. Mod. Phys.* **25**, 191 (1953).
815. Zhdanov, G. S., and Rusakov, A. A., *Tr. Inst. Kristallogr., Akad. Nauk SSSR* **9**, 165 (1954).
816. Zhuze, V. P., and Shelykh, A. I., *Soviet Phys.-Solid State (English Transl.)* **5**, 1278 (1963).
817. Zintl, E., and Rauch, A., *Ber. Deut. Chem. Ges.* **57**, 1739 (1924).
818. Zintl, E., and Harder, A., *Z. Physik. Chem.* **154**, 47 (1931).
819. Zvonkova, Z. V., and Zhdanov, G. S., *Zh. Fiz. Khim.* **22**, 1284 (1948).
820. Zvonkova, Z. V., *Zh. Fiz. Khim.* **28**, 453 (1954).

Trapping of Valence States in a Ruthenium(II,III)-Pyrazine Complex

Sir:

Creutz and Taube¹ have measured the electronic spectra of the ions I in which valence states of the ru-



thenium atoms may be written as (II,II), (II,III), and (III,III). They concluded that an absorption band at 6.5 kK in the (II,III) complex, which is not present in either of the other two complexes, arises from a specific interaction between the mixed-valence Ru atoms. A band about 17.5 kK observed in the (II,II) and, with approximately half the intensity, in the (II,III) complex, but not present in the (III,III) complex, was ascribed to Ru(II) \rightarrow pyrazine π^* charge transfer. That this band should be present in both the single valence (II,II) and mixed valence (II,III) complexes indicates that in the latter the valences are "trapped," *i.e.*, that the complex belongs to class II in the classification of Robin and Day.²

Since identical ligands surround each Ru atom in the (II,III) complex, it seems surprising at first sight that the two Ru valences should be firmly localized. In this note, we wish to indicate a general condition for valence trapping in a mixed valence system and also to show that the condition is indeed satisfied by the ruthenium complex I. Figure 1 shows the reaction coordinates for a valence interchange $\text{M}(\text{X},\text{Y}) \rightleftharpoons \text{M}(\text{Y},\text{X})$. Electron transfer by a Frank-Cóndon process at the points $x = 0, 1$ produces a Y^+ ion in the environment of an X^+ ion, and *vice versa*. If the coordination spheres about the mixed-valence atoms A and B are distorted by Δq_A and Δq_B

$$E_{\text{FC}} = k(\Delta q_A^2 + \Delta q_B^2) \quad (1)$$

On the other hand, if the electron transfer is adiabatic, at $x = 1/2$ the distortions of the coordination spheres about atoms A and B are $\Delta q_A/2, \Delta q_B/2$ ($= -\Delta q_A/2$). Now $E_{\text{Ad}} = k[(\Delta q_A/2)^2 + (\Delta q_B/2)^2]$ and with eq 1

$$E_{\text{Ad}} = E_{\text{FC}}/4 \quad (2)$$

a relationship originally demonstrated by Hush.³ At the point $x = 1/2$ the complex is in a delocalized state formed by an equal combination of states (X,Y) and (Y,X). If the resonance interaction between (X,Y)

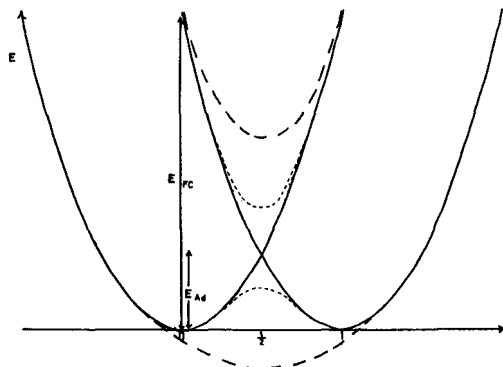


Figure 1. Reaction coordinates for valence interchange (X,Y) \rightleftharpoons (Y,X): (a) (—) energy surface for (X,Y), (Y,X) in the absence of resonance interaction between the sites; (b) (---) energy surface with $H_{\text{res}} > E_{\text{Ad}}$; (c) (- - -) energy surface with $H_{\text{res}} < E_{\text{Ad}}$.

and (Y,X) is H_{res} , the energy of this point is given by

$$E(x = 1/2) = E_{\text{Ad}} - H_{\text{res}} = E_{\text{FC}}/4 - H_{\text{res}} \quad (3)$$

and the energy of any point between $x = 0$ and $x = 1$ by the solution of a secular determinant. Then it is clear that if $H_{\text{res}} > E_{\text{Ad}}$ we have complete delocalization and hence class III² behavior, but if $H_{\text{res}} < E_{\text{Ad}}$ we have valence trapping and class II behavior. This criterion is analogous to the one which determines whether a small polaron or band model is most appropriate to describe the conduction properties of a crystal.⁴

In principle an *a priori* calculation of the class of a mixed-valence complex is therefore possible. The trapping energy E_{Ad} depends upon the relaxation of the metal coordination spheres upon the valence change $\text{X} \rightleftharpoons \text{Y}$. E_{Ad} is then calculable in terms of metal-ligand force constants and the differences in metal-ligand stretching frequencies and bond lengths between the valence states X and Y. The resonance stabilization energy of the delocalized state ($x = 1/2$) might also be estimated by a molecular orbital calculation for the complex.

Unfortunately, for the particular case of the diruthenium(II,III)-pyrazine complex the only relevant data relate to the difference in Ru-N stretching frequencies in Ru(II) and Ru(III) hexaammine complexes^{5,6} so that a *a priori* calculation of the mixed-valence class is not yet possible. However, for the special case of a binuclear complex in which the ligands sur-

(1) C. Creutz and H. Taube, *J. Amer. Chem. Soc.*, **91**, 3988 (1969).
(2) M. B. Robin and P. Day, *Advan. Inorg. Chem. Radiochem.*, **10**, 247 (1967).

(3) N. Hush, *Progr. Inorg. Chem.*, **8**, 391 (1967).
(4) I. G. Austin and N. F. Mott, *Science*, **168**, 71 (1970).
(5) W. P. Griffiths, *J. Chem. Soc. A*, 899 (1966).
(6) M. B. Fahey and R. J. Irving, *Spectrochim. Acta*, **22**, 359 (1966).

2886

rounding each metal ion are identical, one may demonstrate that there is a definite maximum limit to the valence delocalization which is compatible with the existence of two sites with differing nuclear configurations. Using the spectral data of Creutz and Taube¹ we can then show that the extent of valence delocalization in compound I lies well below this limit.

For a class II system regarded formally as $A^{X+} B^{Y+}$ the ground state may be written

$$\Psi_G = [\Psi(A^X B^Y) + \alpha \Psi(A^Y B^X)] / \sqrt{1 - \alpha^2} \quad (4)$$

and the excited state

$$\Psi_{MV} = [\Psi(A^Y B^X) - \alpha' \Psi(A^X B^Y)] / \sqrt{1 - \alpha'^2} \quad (5)$$

The dipole length transition moment governing the spectral intensity of the transition $\Psi_G \rightarrow \Psi_{MV}$ is

$$\mu = 1/2(\alpha + \alpha') R_{AB} \quad (6)$$

R_{AB} is the distance separating the two centers A and B, and α and α' are given by first-order perturbation theory as

$$\alpha = \beta / (E_{MV} - E_G) \quad (7a)$$

$$\alpha' = \beta' / (E_{MV} - E_G) \quad (7b)$$

where $(E_{MV} - E_G)$ is approximately equal to the energy of the mixed-valence absorption band, while β and β' are resonance energies in the ground and excited states, respectively. Since $\Psi(A^X B^Y)$ and $\Psi(A^Y B^X)$ are effectively orthogonal when A and B are well separated, they may interact only *via* mutually nonorthogonal $A \rightarrow (\text{ligand})^*$, $(\text{ligand}) \rightarrow B$ charge-transfer states. This situation is quite analogous to that occurring in the theory of superexchange.⁷ Since the metal-ligand charge-transfer states are closer in energy to Ψ_{MV} than to Ψ_G , perturbation theory yields the result $\beta' > \beta$, $\alpha' > \alpha$. The experimentally observed quantity $(\alpha + \alpha')/2$ is then greater than α , which in turn equals β/E_{FC} (eq 7a). However, for trapping of valence, $\beta < E_{FC}/4$, so that

$$\alpha < 1/4 \quad (8)$$

In a class III system $\alpha^2 = 0.5$ so that any experimentally determined value of α^2 between 0.07 and 0.5 would invalidate the valence-trapping criterion suggested above.

From the data of Taube and Creutz¹ the transition dipole μ of the mixed-valence band in I may be estimated at roughly 1.07 eÅ, yielding a value of about 0.15 for $1/2(\alpha + \alpha')$. Thus $\alpha^2 \leq 0.025$, which satisfies

(7) P. W. Anderson, *Phys. Rev.*, **79**, 350 (1950).

(8) B. Mayoh and P. Day, to be published.

the criterion for trapping (8). From the same data a resonance integral for valence interaction at the point $x = 0$ in the energy surface of Figure 1 may be estimated as $\beta \leq 975 \text{ cm}^{-1}$ (0.12 eV). Resonance interaction H_{res} at the point $x = 1/2$ will be of similar magnitude, and the energy of adiabatic charge-transfer E_{Ad} is 1625 cm^{-1} .

We can also show that our estimate of the resonance integral β is realistic by another simple theoretical approach. If the states $\Psi[Ru_A^{2+} Ru_B^{3+}]$ and $\Psi[Ru_A^{3+} Ru_B^{2+}]$ are considered to be orthogonal, interacting only by a second-order mechanism involving nonorthogonal ligand $\pi \rightarrow Ru^{3+}$ and $Ru^{2+} \rightarrow$ ligand π^* charge-transfer states,⁸ the resonance integral β is given by perturbation theory as

$$\beta = \sum_i \frac{\langle \Psi_0 | H | \Psi_{CT_i} \rangle \langle \Psi_{CT_i} | H | \Psi_{CT} \rangle}{E_{CT_i} - E_0}$$

where $\Psi_0 = \Psi[Ru_A^{2+} Ru_B^{3+}]$, $\Psi_{CT} = [Ru_A^{3+} Ru_B^{2+}]$, and Ψ_{CT_i} are all other ligand $\pi \rightarrow Ru^{3+}$, $Ru^{2+} \rightarrow$ ligand π^* charge-transfer states; β' is given by a similar expression having denominator $(E_{CT_i} - E_{CT})$. The integrals defining β may be estimated semiempirically from the energies and intensities of observed metal(II) \rightarrow ligand π^* and ligand $\pi \rightarrow$ metal(III) charge-transfer bands. We have employed the method used by Sanders and Day⁹ in the assignment of the charge-transfer spectra of iron complexes with conjugated ligands. The value of β calculated by this method is 1040 cm^{-1} . This estimate involves the assumption that the unpaired electron density in the Ru(III) d^5 system is distributed almost equally over the d_{xy} , d_{zx} , d_{yz} orbitals, which seems reasonable in view of the high spin-orbit coupling constant for Ru(III) (1000 cm^{-1})¹⁰ and the similar ligand field strengths of ammonia and pyrazine.¹⁰ Such a distribution of spin-unpaired electron density gives a good agreement between calculated and observed intensities for the ligand $\pi \rightarrow$ Ru(III) charge-transfer absorption at 28.5 kK in the (III,III) complex when $\beta_{Ru(III)N}$ is set equal to $\beta_{Ru(II)N}$. Using our calculated values of β and β' we estimate the transition dipole of the mixed-valence absorption band as 1.4 eÅ. The observed value is 1.07 eÅ.

(9) N. Sanders and P. Day, *J. Chem. Soc. A*, 1191 (1970); 2303 (1969); 1530, 1536 (1967).

(10) B. N. Figgis, "An Introduction to Ligand Fields," Wiley, New York, N. Y., 1966.

Bryan Mayoh, Peter Day*

University of Oxford, Inorganic Chemistry Laboratory
Oxford, England

Received January 24, 1972

Charge Transfer in Mixed-valence Solids. Part VIII.¹ Contribution of Valence Delocalisation to the Ferromagnetism of Prussian Blue

By **Bryan Mayoh** and **Peter Day**,* University of Oxford, Inorganic Chemistry Laboratory, South Parks Road, Oxford OX1 3QR

Reprinted from

JOURNAL
OF
THE CHEMICAL SOCIETY

DALTON TRANSACTIONS

1976

Charge Transfer in Mixed-valence Solids. Part VIII.¹ Contribution of Valence Delocalisation to the Ferromagnetism of Prussian Blue

By Bryan Mayoh and Peter Day,* University of Oxford, Inorganic Chemistry Laboratory, South Parks Road, Oxford OX1 3QR

The contribution of mixed-valence electron delocalisation to the ferromagnetic exchange between the iron(III) ions in Prussian Blue $\{\text{Fe}^{\text{III}}_4[\text{Fe}^{\text{II}}(\text{CN})_6]_3 \cdot 14\text{H}_2\text{O}\}$ has been estimated theoretically. Agreement between the calculated and observed values of the Curie temperature is quite good.

PRUSSIAN BLUE, $\text{Fe}^{\text{III}}_4[\text{Fe}^{\text{II}}(\text{CN})_6]_3 \cdot 14\text{H}_2\text{O}$, is an interesting compound not only because it is one of the classical examples of a Class II² mixed-valence compound whose physical properties have been very comprehensively investigated but also because at low temperatures the iron(III) spins order ferromagnetically. Ionic transition-metal compounds, especially co-ordination complexes, which order as three-dimensional ferromagnets, are extremely rare,³ so any insight which can be gained into the mechanism of the exchange interaction in Prussian Blue would be valuable.

¹ Part VII, B. Mayoh and P. Day, *J.C.S. Dalton*, 1974, 846.

² M. B. Robin and P. Day, *Adv. Inorg. Chem. Radiochem.*, 1967, **10**, 247.

³ For some examples, see A. K. Gregson, P. Day, D. H. Leech, M. J. Fair, and W. E. Gardner, *J.C.S. Dalton*, 1975, 1306.

The first report on the low-temperature magnetic properties of Prussian Blue⁴ gave the Curie temperature as 3.5 K, and the Mössbauer spectrum recorded at 1.3 K certainly shows⁵ the magnetic hyperfine structure expected of a ferromagnet. However, in neither of these studies was the chemical composition of Prussian Blue particularly well characterised, especially with regard to the potassium content of the samples. More recently, Ludi and his co-workers⁶ prepared and analysed single crystals of Prussian Blue. They verified that the

⁴ A. N. Holden, B. T. Matthias, P. W. Anderson, and H. W. Lewis, *Phys. Rev.*, 1956, **102**, 1463.

⁵ A. Ito, M. Suenaga, and K. Ono, *J. Chem. Phys.*, 1968, **48**, 3597.

⁶ H. J. Buser, A. Ludi, W. Petter, and D. Schwartzbach, *J.C.S. Chem. Comm.*, 1972, 1299.

1484

limiting formula was $\text{Fe}^{\text{III}}[\text{Fe}^{\text{II}}(\text{CN})_6]_{13} \cdot 14\text{H}_2\text{O}$ and determined the crystal structure by single-crystal X-ray diffraction. For their samples, powder neutron diffraction⁷ suggested that the Curie temperature was ca. 10 K and indeed, at 4.2 K, the Mössbauer spectrum⁸ showed fully developed magnetic hyperfine structure and the magnetic circular dichroism⁹ saturated in very small applied fields. The existence of these more recent data make it worth examining the magnetic-ordering mechanism in more detail.

Most mixed-valence compounds which order as ferromagnets, for example the well known¹⁰ series of manganites(III,IV) such as $\text{La}_x\text{Sr}_{1-x}\text{MnO}_3$, are also metallic conductors. In that case the ferromagnetism arises from the 'double-exchange' mechanism first proposed by Zener:¹¹ coupling occurs between the unpaired electron spins localised on the metal ions *via* the delocalised conduction electrons. A perturbation procedure similar to the one we used earlier to calculate valence-delocalisation coefficients would then serve to derive the relevant coupling integrals. However, the ferromagnetism of Prussian Blue cannot come from this mechanism because, being a class II mixed-valence compound, it is not a metal, but a high-resistance semiconductor. Furthermore, in the cubic lattice the high-spin iron(III) ions are separated along each axis of the unit cell by low-spin diamagnetic Fe^{II} , and are thus no less than 10.16 Å apart. Consequently the basic mechanism of the exchange interaction must lie in what we^{1,12} have called 'valence delocalisation' in the ground state between the Fe^{II} and Fe^{III} .

In essence the mechanism we envisage relies on the partial delocalisation of electrons formally occupying t_{2g} orbitals on Fe^{II} on to neighbouring high-spin iron(III) sites. Since each iron(III) site may only accept electron density of one particular spin, because the t_{2g} and e_g orbitals are both exactly half occupied, a t_{2g} electron with α spin originating on Fe^{II} may spend a larger fraction of its time on iron(III) sites than one of β spin. Some of the coulomb- and exchange-repulsion terms are sensitive to differences in the extent of delocalisation of α and β spins. The effect of this is that it is energetically more favourable to delocalise only one type of spin (either α or β) from Fe^{II} to Fe^{III} . In the crystal, however, each Fe^{II} is surrounded by six equivalent Fe^{III} , over which the spin density originating on the central Fe^{II} must therefore be correlated. The ferromagnetic coupling energy is the difference between the energy per iron(II) centre when the spins of the neighbouring Fe^{III} are ordered parallel to one another, compared to the energy when they are arranged randomly. It is this energy difference which we shall calculate.

THEORY

Spin Orientations and Wavefunctions.—If the spins of the six Fe^{III} around an iron(II) centre are randomly oriented

⁷ H. J. Buser, A. Ludi, P. Fischer, T. Studach, and B. W. Dale, *Z. phys. Chem. (Frankfurt)*, 1974, **92**, 354.

⁸ A. Ludi and B. W. Dale, personal communication.

⁹ H. U. Güdel and E. R. Krausz, personal communication.

the statistical weights of all the possible spin-coupling schemes are respectively 1/64 for 6α or 6β , 6/64 for $5\alpha + 1\beta$ or $5\beta + 1\alpha$, 15/64 for $4\alpha + 2\beta$ or $4\beta + 2\alpha$, and 20/64 for $3\alpha + 3\beta$. A general Slater-determinant wavefunction for the optical electrons, which we assume to be $\text{Fe}^{\text{II}} t_{2g}$, in the ground state is as in equation (1) where i labels the coupling case and $t_n^{\alpha,\beta}$ take the forms (2a) and (2b) where t_C are t_{2g}

$$\Psi_G = |t_{1i}^{\alpha} t_{1j}^{\beta} t_{2k}^{\alpha} t_{2l}^{\beta} t_{3m}^{\alpha} t_{3n}^{\beta}| \quad (1)$$

$$t_n^{\alpha} = [(1 - kc^2)t_C^2 + kc^2\phi(t_N)^2]^{\frac{1}{2}} \quad (2a)$$

$$t_n^{\beta} = [(1 - jc^2)t_C^2 + jc^2\phi(t_N)^2]^{\frac{1}{2}} \quad (2b)$$

orbitals on Fe^{II} at the carbon ends of the cyanide groups, $\phi(t_N)$ is an appropriate combination of t_{2g} orbitals on Fe^{III} at the nitrogen ends of the cyanides, and $h/(h+j)$ is the fraction of the delocalised electron density c^2 which has α spin [$j/(h+j)$ is the similar fraction for β spin], and $h+j=1$. In writing equations (2a) and (2b) we have made use of the small degree of overlap between t_C and $\phi(t_N)$, *i.e.* (3). In the various spin-coupling combinations acces-

$$t_n^{\alpha} = (1 - kc^2)t_C + (kc^2)^{\frac{1}{2}}\phi(t_N) \quad (3)$$

sible to the six Fe^{III} around our reference Fe^{II} the appropriate values of h and j are as in equations (4)–(10). In

$$6\alpha : k = 0, \quad j = 1 \quad (4)$$

$$6\beta : k = 1, \quad j = 0 \quad (5)$$

$$5\alpha + 1\beta : k = 1/6, \quad j = 5/6 \quad (6)$$

$$5\beta + 1\alpha : k = 5/6, \quad j = 1/6 \quad (7)$$

$$4\alpha + 2\beta : k = 1/3, \quad j = 2/3 \quad (8)$$

$$4\beta + 2\alpha : k = 2/3, \quad j = 1/3 \quad (9)$$

$$3\alpha + 3\beta : k = 1/2, \quad j = 1/2 \quad (10)$$

order to write the wavefunctions of the different coupling combinations in the form of Slater determinants, it is now convenient to rewrite $t_n^{\alpha,\beta}$ as in (11) and (12) where $\phi(t_C, t_N) =$

$$t_n^{\alpha} = [t_C^2 - kc^2\phi(t_C, t_N)^2]^{\frac{1}{2}} \quad (11)$$

$$t_n^{\beta} = [t_C^2 - jc^2\phi(t_C, t_N)^2]^{\frac{1}{2}} \quad (12)$$

$[t_C^2 - \phi(t_N)^2]^{\frac{1}{2}}$, again assuming small overlap between t_C and $\phi(t_N)$.

Since for our purposes the energies of $(x-6)\alpha + x\beta$ and $x\alpha + (6-x)\beta$ are the same, we shall write only one component of each, for example $k=1, j=0$. Then substituting into equation (1), we have:

Case (a) ($6\alpha, 6\beta$):

$$\Psi_{G_a} = |[t_C^2 - c^2\phi(t_C, t_N)^2]_1^{1\alpha} t_{C_1}^{\beta} [t_C^2 - c^2\phi(t_C, t_N)^2]_2^{\alpha} - t_{C_2}^{\beta} [t_C^2 - c^2\phi(t_C, t_N)^2]_1^{1\alpha} t_{C_3}^{\beta}| \quad (13)$$

Case (b) ($5\alpha + 1\beta, 5\beta + 1\alpha$):

$$\Psi_{G_b} = |[t_C^2 - \frac{5}{6}c^2\phi(t_C, t_N)^2]_1^{1\alpha} [t_C^2 - \frac{1}{6}c^2\phi(t_C, t_N)^2]_1^{1\beta} \text{ etc.}] \quad (14)$$

Case (c) ($4\alpha + 2\beta, 4\beta + 2\alpha$):

$$\Psi_{G_c} = |[t_C^2 - \frac{2}{3}c^2\phi(t_C, t_N)^2]_1^{1\alpha} [t_C^2 - \frac{2}{3}c^2\phi(t_C, t_N)^2]_1^{1\beta} \text{ etc.}] \quad (15)$$

Case (d) ($3\alpha + 3\beta$):

$$\Psi_{G_d} = |[t_C^2 - \frac{1}{3}c^2\phi(t_C, t_N)^2]_1^{1\alpha} [t_C^2 - \frac{1}{3}c^2\phi(t_C, t_N)^2]_1^{1\beta} \text{ etc.}] \quad (16)$$

¹⁰ G. H. Jonker and J. H. van Santen, *Physica*, 1950, **16**, 337, 599.

¹¹ C. Zener, *Phys. Rev.*, 1951, **81**, 440.

¹² B. Mayoh and P. Day, *Inorg. Chem.*, 1974, **13**, 2273.

1976

1485

Ferromagnetic Coupling Energy.—In order to find the ferromagnetic coupling energy the energies of the four cases (a)—(d) must be compared, that is, the values of (17) for $i = a, b, c, d$, and d . Energy differences between the

$$E_{Gi} = \langle \Psi_{Gi} | \mathcal{H} | \Psi_{Gi} \rangle \quad (17)$$

various states i arise from differences in the coulomb- and exchange-repulsion integrals $\langle t_n^\alpha t_n^\alpha | e^2/r_{12} | t_n^\beta t_n^\beta \rangle$, $\langle t_n^\alpha t_p^\alpha | e^2/r_{12} | t_n^\alpha t_p^\alpha \rangle$, and $\langle t_n^\beta t_p^\beta | e^2/r_{12} | t_n^\beta t_p^\beta \rangle$. In fact, if we define equations (18) and (19), we find the energy differences (20)—(22)

$$J_{11} = \langle \phi^2(t_C, t_N)_1 | e^2/r_{12} | \phi^2(t_C, t_N)_1 \rangle \quad (18)$$

$$K_{12} = \langle \phi(t_C, t_N)_1 \phi(t_C, t_N)_2 | e^2/r_{12} | \phi(t_C, t_N)_1 \phi(t_C, t_N)_2 \rangle \quad (19)$$

between the different coupling cases (a)—(d). The ferro-

$$E_{Ga} - E_{Gb} = (15c^4/36)J_{11} + (30c^4/36)K_{12} \quad (20)$$

$$E_{Ga} - E_{Gc} = (6c^4/9)J_{11} + (12c^4/9)K_{12} \quad (21)$$

$$E_{Ga} - E_{Gd} = (3c^4/4)J_{11} + (6c^4/4)K_{12} \quad (22)$$

magnetic coupling energy depends not only on these energy differences but also on the weighting to be given to each case. Relative to case (a) the weighting factor w_i of (b) is 12/64, of (c) is 30/64, and of (d) is 20/64. Then the total ferromagnetic coupling energy resulting from the mixed-valence interaction is (23).

$$E_{fm} = \sum_{i=b,c,d} (E_{Ga} - E_{Gi})w_i = (1/8)(5J_{11} + 10K_{12})c^4 \quad (23)$$

Evaluation of J_{11} and K_{12} .—The next step in calculating E_{fm} is to evaluate J_{11} and K_{12} explicitly. Substituting into equations (18) and (19) we obtain (24) and (25). In order

$$J_{11} = \langle t_{C1}^2 - \phi_1(t_N)^2 | e^2/r_{12} | t_{C1}^2 - \phi_1(t_N)^2 \rangle \quad (24)$$

$$K_{12} = \langle [t_{C1}^2 - \phi_1(t_N)^2]^\dagger [t_{C2}^2 - \phi_2(t_N)^2] | e^2/r_{12} | [t_{C1}^2 - \phi_1(t_N)^2]^\dagger [t_{C2}^2 - \phi_2(t_N)^2] \rangle \quad (25)$$

to expand these expressions in terms of single-centre Fe^{II} and Fe^{III} t_{2g} functions we need to define the axis of the Fe^{II} -(CN)₆ Fe^{III} cluster. Fortunately an axis definition is already available from our previous paper¹ on the optical spectrum of Prussian Blue. Using the labels we used in that paper, and arbitrarily fixing t_{C1} as d_{xy} and t_{C2} as d_{zx} , we obtain equations (26) and (27). In order to simplify

$$\phi_1(t_N) = (1/2)[d_{xy_4} + d_{xy_5} + d_{xy_6} + d_{xy_7}] \quad (26)$$

$$\phi_2(t_N) = (1/2)[d_{zx_1} + d_{zx_2} + d_{zx_3} + d_{zx_4}] \quad (27)$$

the expressions for J_{11} and K_{12} , all the interactions between d_{xy} on Fe^{II} and the d_{xy_i} on the surrounding Fe^{III} are generalised in terms of d_{xy} . All the Fe^{III} - Fe^{III} interactions are expressed in terms of either one-centre (d_i - d_i), adjacent two-centre (d_i - d_j ; $i = 1, j = 2$), or distant two-centre (d_i - d_j ; $i = 1, j = 6$) interactions. The resulting expressions are (28) and (29). In deriving these expressions we have also

$$J_{11} = \langle d_{xy}d_{xy} | e^2/r_{12} | d_{xy}d_{xy} \rangle - 2\langle d_{xy}d_{xy} | e^2/r_{12} | d_{xy}d_{xy} \rangle + (1/4)[\langle d_{xy_1}d_{xy_1} | e^2/r_{12} | d_{xy_1}d_{xy_1} \rangle + 2\langle d_{xy_1}d_{xy_2} | e^2/r_{12} | d_{xy_1}d_{xy_2} \rangle + \langle d_{xy_1}d_{xy_6} | e^2/r_{12} | d_{xy_1}d_{xy_6} \rangle] \quad (28)$$

$$K_{12} = \langle d_{xy}d_{zx} | e^2/r_{12} | d_{xy}d_{zx} \rangle + (1/8)[\langle d_{xy_1}d_{zx_1} | e^2/r_{12} | d_{xy_1}d_{zx_1} \rangle + \langle d_{xy_1}d_{zx_2} | e^2/r_{12} | d_{xy_1}d_{zx_2} \rangle] \quad (29)$$

¹ 1 eV $\approx 1.60 \times 10^{-19}$ J.

² R. G. Parr, 'Quantum Theory of Molecular Electronic Structure,' Benjamin, New York, 1964.

used the Mulliken approximation to set all other terms of the type $\langle d_i d_j | d_i d_j \rangle$, where d_i and d_j are on different centres, equal to zero.

Numerical Estimates of J_{11} and K_{12} .—The final stage in our calculation of E_{fm} is to estimate some numerical magnitudes for the various coulomb- and exchange-repulsion integrals which appear in (28) and (29). As our aim is only to obtain a rough idea of the magnitudes of the various terms which enter into the magnetic coupling, we used the point-charge approximation $f_{ij} = 14.4/R_{ij}$, where R_{ij} is the distance between the two centres, to estimate the two-centre repulsion integrals between orbitals localised on different iron(III) centres. The one-centre Fe^{II} and one-centre Fe^{III} coulomb integrals correspond to the γ_{11} terms of Pariser-Parr-Pople ZDO-MO theory,¹³ while the one-centre exchange integrals are assumed to be proportional to the γ_{11} as in the INDO approximation.¹⁴ The two-centre Fe^{II} - Fe^{III} exchange integral is set equal to zero. With these approximations, we obtain (30) and (31), k being the proportionality constant just mentioned.*

$$J_{21} = \gamma_{11}(Fe^{II}) + (1/4)\gamma_{11}(Fe^{III}) - 4.30 \text{ eV} \quad (30)$$

$$K_{12} = k\gamma_{11}(Fe^{II}) + (1/8)k\gamma_{11}(Fe^{III}) \quad (31)$$

Values of γ_{11} may of course be obtained from atomic Hartree-Fock calculations. However, it is well known that when they are used in molecular-orbital (m.o.) calculations they usually predict singlet-triplet separations much greater than those observed. Consequently, following other semiempirical m.o. calculations¹⁵ we use the energy of the 'Pariser disproportionation reaction' to find γ_{11} . As a function of the charge q on a metal ion, γ is given by the difference between two valence-orbital ionisation potentials

$$\gamma(q) = \text{VOIP}(q-1) - \text{VOIP}(q) \quad (32)$$

as in (32). Published tabulations¹⁵ of VOIP(q) then lead to estimates for both $\gamma_{11}(Fe^{II})$ and $\gamma_{11}(Fe^{III})$ of 12.4 eV. Finally Watson's self-consistent-field calculations of γ_{dd} , $\gamma_{dd'}$, and $K_{dd'}$ for neutral atoms of the first transition series indicate that the ratio of γ_{dd} to $K_{dd'}$ (*i.e.* the proportionality factor k) is 0.0388. When the values of all these parameters are substituted into (30) and (31) the resulting estimates of J_{11} and K_{12} are 11.2 and 0.54 eV respectively. The ferromagnetic coupling energy E_{fm} from (23) is therefore equal to 7.675 c^4 eV.

RESULTS AND DISCUSSION

Calculation of the Curie Temperature.—In order to relate the magnitude of E_{fm} which we have calculated to the observed Curie temperature we assume that $E_{fm} \sim k_B T_c$, from which T_c is predicted to be $(8.9 \times 10^4)c^4$ K. The coefficient c , which we have called 1.12 the 'valence delocalisation coefficient,' can be approached in one of two ways. Either one can estimate it from the intensity of the mixed-valence absorption band or, for cases such as Prussian Blue, where the two metal ions of differing valency are bridged by an intervening ligand, it can be calculated from a perturbation model, mixing $Fe^{II} \rightarrow CN$ and $CN \rightarrow Fe^{III}$ local charge-transfer states into the ground state. In our earlier paper¹ on the perturbation

¹³ J. A. Pople, D. P. Santry, and G. A. Segal, *J. Chem. Phys.*, 1965, **43**, 5129.

¹⁵ H. Basch, A. Viste, and H. B. Gray, *Theor. Chim. Acta*, 1965, **3**, 458.

model for valence delocalisation we used Prussian Blue as a test case, and obtained estimates of the ground-state delocalisation coefficient in both ways, for comparison: that estimated from the intensity of the mixed-valence band was 0.106, while the estimate based on the perturbation calculation was 0.083. The former value leads to a calculated Curie temperature of 11.2 K and the latter to 6.6 K.

A number of comments can be made on this result. First, the fact that the iron(III) ions in Prussian Blue are so far apart, and yet magnetic ordering is found at a modestly accessible temperature, strongly implicates the intervening diamagnetic iron(II) ions in the interaction process. Secondly, that the interaction should be ferromagnetic is highly unusual, and the fact that it occurs in a mixed-valence compound suggests that it is the mixed-valence interaction which provides the dominant exchange path. The calculations described above give strong support to both these hypotheses. We have demonstrated not only that the mixed-valence delocalisation mechanism indeed predicts ferromagnetic coupling but, further, that the extent of ground-state valence delocalisation as estimated from the optical spectrum or a perturbation calculation leads to a calculated Curie temperature very close to that observed. Of course, the level of agreement between the calculated and observed Curie temperatures is very remarkable, especially when

one remembers that in our model T_c is proportional to c^4 . Obviously it would be very interesting to examine the low-temperature magnetic properties of related compounds, such as the ruthenium and osmium analogues of Prussian Blue, and other heavy-metal ferro- and ferri-cyanides in which interionic charge-transfer states, though not strictly of the mixed-valence type, might make an important contribution to the exchange mechanism.

Finally it is worth mentioning that no direct correlation between the calculated magnetic interaction energy and any electrical-conductivity properties is to be expected in Prussian Blue and related class II mixed-valence compounds. In this kind of compound conduction is limited by electron trapping as a result of lattice polarisation. The diffusion coefficient in the hopping model depends on $\nu_0 \exp(-\Delta G/kT)$, where ν_0 is the frequency of the lattice mode and ΔG the work which must be done to bring the energies of the carbon-hole and nitrogen-hole sites to equivalence, so that electron transfer can take place.

We thank the S.R.C. for a studentship (to B. M.), and Professor Ludi and Drs. Güdel and Krausz for discussions and for communicating results to us in advance of publication.

[6/179 Received, 27th January, 1976]

Separatum
HELVETICA CHIMICA ACTA
Vol. 63, Fasc. 1, p. 148–153 (1980)

14. Valence Delocalization in Prussian Blue $\text{Fe}_4^{\text{III}}[\text{Fe}^{\text{II}}(\text{CN})_6]_3 \cdot x\text{D}_2\text{O}$, by Polarized Neutron Diffraction

by **Peter Day**

Inorganic Chemistry Laboratory, Oxford University, Oxford, England

Fritz Herren, Andreas Ludi, Hans Ulrich Güdel

Institut für Anorganische Chemie, Universität Bern, Bern, Switzerland

Fritz Hulliger

Institut für Festkörperphysik, ETH, Zürich, Switzerland

and **Dominique Givord**

Institut Laue-Langevin, Grenoble, France

(26. X. 79)

Summary

Polarized neutron diffraction has been used to investigate the spin delocalization from the high-spin Fe(III) sites to the low-spin Fe(II) in deuteriated Prussian Blue, $\text{Fe}_4[\text{Fe}(\text{CN})_6]_3 \cdot x\text{D}_2\text{O}$. Measurements of the 111, 200, and 400 reflections were made on a powdered sample at 3 K and 4.8 T using a neutron wavelength of 1.074 Å. The expectation value of S at the Fe(II) site is -0.008 ± 0.028 corresponding to an upper limit of about 5% of an electron for the spin delocalization.

Introduction. – Prussian Blue, $\text{Fe}_4[\text{Fe}(\text{CN})_6]_3 \cdot x\text{D}_2\text{O}$ ($x=14-16$), is a classical mixed valence compound, belonging to Class II of the *Robin-Day* classification [1]. The overall structure of the cubic Fe(III)–N–C–Fe(II) framework corresponds to the face-centered space group $\text{Fm}\bar{3}\text{m}$ [2]. That there is substantial interaction between the two kinds of Fe-ions is indicated by the appearance of a broad intense absorption band at 14100 cm^{-1} , assigned as the Fe(II) \rightarrow Fe(III) charge transfer transition [3]. Another feature of Prussian Blue is that at 5.5 K the Fe(III) spins order ferromagnetically [4], behaviour which is highly unusual for a coordination complex. Furthermore, the shortest superexchange pathway between the Fe(III)-ions is no less than 10.16 Å so the existence of magnetic ordering even at 5.5 K requires some explanation. A plausible mechanism [5] is the mixed-valence interaction, *i.e.*, mixing of the Fe(II)-to-Fe(III) charge-transfer excited state into the ground state. One consequence of such mixing would be a small transfer of spin density from Fe(III) to the low-spin Fe(II) which, to a first approximation, carries no net spin.

One of the most sensitive and direct methods for determining the distribution of unpaired electron-spin density in solids is by diffraction of polarized neutrons [6].

In brief, the cross-section for elastic scattering of neutrons by unpaired electrons depends on the relative orientation of the electron and neutron spins. Since the cross-section for scattering by the nuclei is independent of the neutron-spin orientation, one can separate the nuclear and magnetic contributions to the total scattering cross-section by aligning the electron spins and then carrying out two diffraction experiments with the spins of the incident neutrons polarized parallel and antiparallel to the spins of the unpaired electrons in the solid. The earliest experiments of this kind were performed on ferromagnetic elements and alloys [7] and only very few have concerned non-metallic inorganic compounds [8]. Although in principle, one could magnetically saturate most paramagnetic substances by using a sufficiently high applied magnetic field at a sufficiently low temperature, compounds which order spontaneously as ferromagnets have a substantial advantage. This encouraged us to search for spin transfer from the high-spin Fe(III) to the low-spin Fe(II) in Prussian Blue by means of polarized neutron-diffraction. Unfortunately, because of its polymeric structure which makes it extremely insoluble, Prussian Blue has only been grown into single crystals of, at most, 0.1 mm on edge. This is too small for single crystal polarized neutron diffraction so our experiments had to be performed on polycrystalline samples. Prussian Blue is cubic so the number of reflections available is in any case limited.

Experimental Part. - The microcrystalline sample of Prussian Blue was prepared by slowly diffusing H₂O-vapour into a solution of FeCl₃ and H₄Fe(CN)₆ in concentrated HCl-solution [2]. Deuteration was achieved by stirring a suspension of Prussian Blue (14.6 g) in D₂O (100 ml, 99.9%) at 80° for two days and collecting the solid by filtration. This procedure was repeated twice to yield a

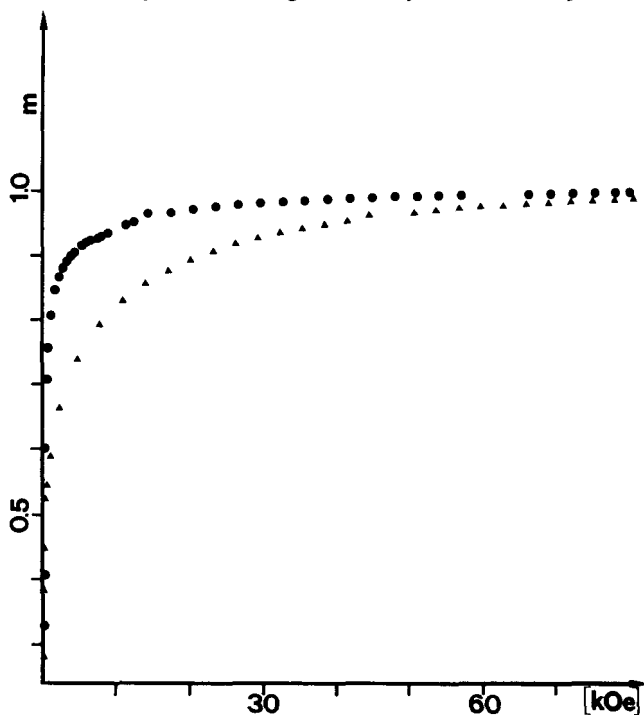


Fig. 1. Magnetization isotherms of Prussian Blue powder at 1.7 K (○) and 4.4 K (△)

sample deuteriated to 97.9% (by atoms) as determined by mass spectrometry. It has previously [2] been characterized by chemical analysis and x-ray powder diffraction. The sample contains a small amount of $\text{Fe}(\text{CN})_6^{3-}$ which can be detected in the IR. spectrum showing a weak signal at 2130 cm^{-1} . This amount was determined by dissolving the sample in $2N$ KOH, filtering and measuring the absorbance at 420 nm . A calibration curve was obtained by measuring the absorbance of mixtures of $\text{Fe}(\text{CN})_6^{3-}$ and $\text{Fe}(\text{CN})_6^{4-}$ (in the same ratio as expected in the Prussian Blue sample) in $2N$ KOH.

The magnetic susceptibility was measured by a moving sample magnetometer [9] between 1.3 and 300 K. It shows perfect *Curie-Weiss* behaviour between 10 and 300 K with a *Curie* constant of $17.92 \pm 0.02\text{ cm}^3/\text{mol}$ and $\theta = 6.74 \pm 0.07\text{ K}$. This gives a $\mu_{\text{eff}} = 2.828 \sqrt{C/4} = 5.98 \pm 0.02\text{ B.M.}$ per Fe(III) corresponding to the spin-only moment of high-spin Fe(III). Two magnetization isotherms were measured at 1.7 and 4.4 K, respectively (Fig. 1). In a field of 4.8 T the magnetization m is 0.99 at 1.7 K and 0.96 at 4.4 K.

The polarized neutron-diffraction measurements were carried out on the D5 instrument at the *Institut Laue-Langevin* high flux reactor, Grenoble, using a neutron wavelength of 1.074 \AA . The polarization measured at two positions in the beam with a Fe-Co single crystal was $P = 0.970 \pm 0.002$. At 4.2 K no depolarization by the sample was detected, but after pumping the cryostat a depolarization of $\beta = 7.3 \pm 0.4 \times 10^{-2}\text{ cm}^{-1}$ was measured, giving $P_{\text{eff}} = 0.928 \pm 0.003$ [10]. The efficiency of the flipping coil was $E = 0.99$. The counting time for the two polarizations was chosen approximately inversely proportional to the expected intensities. The sample was placed in a vanadium container

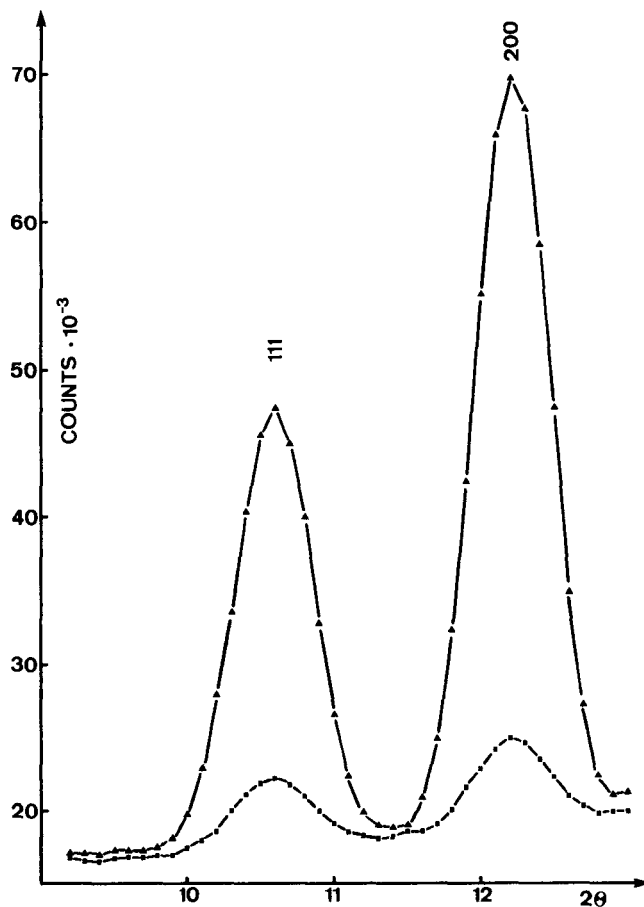


Fig. 2. Neutron diffraction profiles of Prussian Blue powder for neutron spin up (\uparrow ; \blacktriangle) and down (\downarrow ; \blacksquare) at 3 K and 4.8 T. I^{\downarrow} has been scaled to the same monitor count as I^{\uparrow} .

(diameter = 12 mm) in a superconducting cryomagnet (4.8 T). The magnetic field was perpendicular to the scattering vector and the neutron spins were polarized parallel (\uparrow) and antiparallel (\downarrow) to the magnetic field. The temperature, measured with a carbon resistor, was 3 K. Interpolating the magnetic data between 1.7 and 4.4 K gives a magnetization $m = 0.98 \pm 0.01$ at 3 K. The maximum signal/background ratio was 4.1 and the linear absorption coefficient μ of the sample was 0.166 cm^{-1} , giving a negligible absorption correction.

Initially, powder diffraction profiles were scanned out to $2\theta = 30^\circ$. However, given the limited number of reflections observable, any possibility of obtaining a spin-density map of the entire unit cell by the usual *Fourier* transformation procedure is out of the question. Owing to the rapid decrease of the magnetic form factor with increasing *Bragg* angle, we concentrated our measurements on the low angle region. Moreover, only reflections with odd indices have intensities which depend on the spin transfer to Fe(II) (cf. eqn. (4)). The single well resolved peak that meets both these requirements is the 111 reflection. We therefore measured this reflection and the equally well resolved 200 and 400 reflections in 0.1° steps using long counting times in order to obtain a reliable scale factor. A portion of this data is shown in *Figure 2*.

Reduction and Evaluation of Data. - Because the nuclear structure is not known to sufficient accuracy it was not possible to make use of conventional flipping ratio measurements. The intensities for each spin state were measured and normalized point by point and fitted as *Gaussians* by a least-squares procedure (together with a 3-parameter background) by means of a computer program provided by *Wolfers* [11] which also gives standard deviations σ of the intensities. The σ 's describing the deviation from a *Gaussian*-line shape computed by this program exceed the statistically determined standard deviations by a factor of about 4, but are considered to be a better estimate of the real uncertainties [11].

The left hand side of the *Table* shows the observed intensities I^\uparrow and I^\downarrow for the two directions of neutron polarization, normalized and corrected for multiplicity, together with their standard deviations. Allowing for incomplete magnetization, the intensities are given by

$$I^\uparrow = F_N^2 + 2mPF_NF_M + \left(\frac{2}{3} + \frac{1}{3}m^2\right)F_M^2$$

$$I^\downarrow = F_N^2 + 2mP(1-2E)F_NF_M + \left(\frac{2}{3} + \frac{1}{3}m^2\right)F_M^2$$
(1)

where F_N and F_M are the observed nuclear and magnetic structure factors, respectively [6]. From eqn. (1) the relative nuclear and magnetic structure factors, shown with their standard deviations on the right hand side of the *Table*, may now be evaluated. Throughout these calculations the standard deviations of results were determined according to $\sigma_y(x_i) = \sqrt{\sum_i ((\partial y / \partial x_i) \sigma_{x_i})^2}$.

To obtain the magnitude of the spin on the Fe(II), we note that neglecting the *Debye-Waller* factor the magnetic structure factor is given by

$$F_M^{hkl} = (e^2\gamma/mc^2) \sum_i \langle S_i \rangle f_i^{hkl} \exp \left[2\pi i \left(\frac{hx + ky + lz}{a} \right) \right]$$
(2)

where $\langle S_i \rangle$ is the expectation value of S_z at site i . In order to find $\langle S_{Fe(II)} \rangle$, we used the form factor for high-spin Fe(III) to describe the magnetic scattering from all the Fe-ions and neglected all orbital contributions. The magnetic form factors were determined graphically from tabulated literature values [12] as: (111) 0.936, (200) 0.918, (400) 0.732. The small amount of ferricyanide present was assumed to

Table. Polarized neutron-diffraction intensities and structure factors for Prussian Blue at 3 K and 4.8 T for $m = 0.98$ (σ is standard deviation)

	I^\uparrow	σ	I^\downarrow	σ	F_N	σ	F_M	σ
111	4.135	0.0797	0.675	0.0310	0.717	0.0320	1.410	0.0483
200	12.86	0.188	1.478	0.0545	2.286	0.0318	1.383	0.0354
400	103.6	3.25	66.0	1.50	9.13	0.133	1.14	0.102

occupy the same position in the crystal lattice as ferrocyanide, giving the following occupancies for the space group Fm3m: 4 high-spin Fe(III) on 4a, 3 low-spin Fe(II) and q low-spin Fe(III) on 4b; q as determined by chemical analysis was 0.07 ± 0.005 . It was further assumed that the spin of the low-spin Fe(III) was parallel to that on the 4a sites.

Excluding the ferricyanide the total spin in each unit cell is:

$$4\langle S_{\text{Fe(III)}} \rangle + 3\langle S_{\text{Fe(II)}} \rangle = 10. \quad (3)$$

Furthermore, the absolute values of the geometric parts of the structure factors are the same for all contributions (that of 4b to the odd peaks being negative) so the resulting magnetic structure factors for odd (ooo) and even (eee) peaks are

$$\begin{aligned} F_{\text{M}}^{\text{ooo}} &= (\text{constant}) (10 - 6\langle S_{\text{Fe(II)}} \rangle - \frac{1}{2}q) f^{\text{ooo}} \\ F_{\text{M}}^{\text{eee}} &= (\text{constant}) (10 + \frac{1}{2}q) f^{\text{eee}} \end{aligned} \quad (4)$$

The observed magnetic structure factors F_{M} were subjected to a least-squares refinement [13] using the scale factor and $\langle S_{\text{Fe(II)}} \rangle$ as parameters. The function minimized was $\sum w(|F_{\text{obs.}}| - |F_{\text{cal.}}|)^2$ where the weighting function was represented by $\sigma(F_{\text{obs.}})^{-2}$.

Results and Discussion. - The least-squares treatment of F_{M} for the 111, 200, and 400 reflections converges to a value of $\langle S_{\text{Fe(II)}} \rangle$ of -0.008 ± 0.028 . The standard deviation of $\langle S_{\text{Fe(II)}} \rangle$ is disappointingly high. Nevertheless, we consider it to be realistic by taking into account various possible sources of errors, e.g. slight distortions in the geometry of the experiment from ideal alignment, deviations of the diffraction peaks from *Gaussian* shape, etc.

The magnitude of $\langle S_{\text{Fe(II)}} \rangle$ is very sensitive to the value of magnetization m . This dependence is most clearly illustrated by the same calculations but using $m = 0.975 \pm 0.01$ instead of $m = 0.98 \pm 0.01$. In this case the result is $\langle S_{\text{Fe(II)}} \rangle = 0.003 \pm 0.026$. It must be pointed out that a negative value of $\langle S_{\text{Fe(II)}} \rangle$ is physically unreasonable. A negative sign would imply that the spin on the 4b site is antiparallel to that on 4a. Since we know that the high-spin Fe(III)-spins are ferromagnetically aligned, each with a half-filled d-shell, only a spin antiparallel to the Fe(III)-spins can be transferred to them from the Fe(II), leaving behind an unpaired electron spin directed parallel to the uncompensated Fe(III).

It is worth noting that there is a simple connection between $\langle S_{\text{Fe(II)}} \rangle$ and the valence delocalization coefficient a . Let us write the ground state wavefunction as [14]

$$\psi_{\text{G}} = (1 - a^2)^{1/2} \psi_0 + a \psi_1 \quad (5)$$

where $\psi_0 = [\text{C}^6\text{N}^{30}]$ symbolizes the zero order ground state in which a low-spin Fe(II) with six d-electrons at the site surrounded by six C-atoms has six high-spin Fe(III) neighbours, each with five d-electrons, at the nitrogen ends of the same cyanide groups. In the intervalence charge transfer excited state $\psi_1 = [\text{C}^5\text{N}^{31}]$ an electron has been transferred from the Fe(II) to an appropriate linear combination of the surrounding Fe(III). Full details of the symmetry arguments used to construct these wavefunctions are given in [14] but it is sufficient to point out here that in the zero order ground state $\langle \psi_0 | S_{z\text{Fe(III)}} | \psi_0 \rangle = 5/2$ and $\langle \psi_0 | S_{z\text{Fe(II)}} | \psi_0 \rangle = 0$, while in the intervalence charge transfer excited state, we have $\langle \psi_1 | S_{z\text{Fe(III)}} | \psi_1 \rangle_{\text{av}} = 5/2 - 1/6 \cdot 2$ and $\langle \psi_1 | S_{z\text{Fe(II)}} | \psi_1 \rangle = 1/2$, where 'av' expresses an average over all six Fe(III) sites. Thus, for the true ground state ψ_{G} , we have $\langle \psi_{\text{G}} | S_{z\text{Fe(III)}} | \psi_{\text{G}} \rangle = 5/2 - 1/12 a^2$ and $\langle \psi_{\text{G}} | S_{z\text{Fe(II)}} | \psi_{\text{G}} \rangle = 1/2 a^2$, i.e. in the nomenclature used above $a^2 = 2\langle S_{\text{Fe(II)}} \rangle$.

The result of our polarized neutron diffraction on Prussian Blue gives a value for a^2 of -0.016 ± 0.056 . The spin delocalization in the ground state corresponds to less than about 5% of an electron. This upper limit can be compared with the predictions of different models of valence delocalization in mixed valence compounds [14]. A perturbation model in which 'local' CN (π) \rightarrow Fe(III) and Fe(II) \rightarrow CN (π^*) states provide the means of mixing ψ_0 in (5) with ψ_1 , gave a^2 as 0.011 [14]. The intensity of the intervalence transition of Prussian Blue has also been used to derive a value of 0.01 for a^2 [3]. Owing to the difficulties of reliably measuring the optical density of colloidal solutions and to analytical uncertainties, this value reflects only the order of magnitude of a^2 . Both these figures lie within the standard deviation of our experiment. However, we cannot exclude the possibility that the theoretical predictions for a^2 are too high. The fact that we are looking for a very small amount of spin density at a particular site in a unit cell containing a large number, *i.e.* 20, of unpaired electrons is a severe limitation in the present application. It must be emphasized, however, that polarized neutron diffraction is the only method to directly determine spin delocalization. In contrast to a^2 values deduced from other experiments, our result does therefore not depend on approximations and assumptions of a particular theoretical model. We have demonstrated that it is possible, in principle, to determine spin transfer in a high symmetry lattice from polarized neutron diffraction of a powder. The high standard deviation of our result, on the other hand, clearly reveals the limitations of the method.

This work was supported by the *U.K. Science Research Council*, the *Swiss National Science Foundation*, and the *Berner Hochschulstiftung*. We thank the staff of the *Institut Laue-Langevin* for their assistance and for allocations of beam time.

REFERENCES

- [1] *M.B. Robin & P. Day*, *Adv. Inorg. Chem. Radiochem.* 10, 247 (1967).
- [2] *H.J. Buser, A. Ludi, W. Petter & D. Schwarzenbach*, *Inorg. Chemistry* 16, 2704 (1977).
- [3] *M.B. Robin*, *Inorg. Chemistry* 1, 337 (1962).
- [4] *H.J. Buser, A. Ludi, P. Fischer, T. Studach & B.W. Dale*, *Z. Phys. Chem.* 92, 354 (1974); *A. Ito, M. Suenaga & K. Ono*, *J. Chem. Physics* 48, 3597 (1968).
- [5] *B. Mayoh & P. Day*, *J. chem. Soc. Dalton* 1976, 1483.
- [6] *W. Marshall & S.W. Lovesey*, 'Theory of Thermal Neutron Scattering', Clarendon Press, Oxford 1971.
- [7] *E.g., J. Moss & P.J. Brown*, *J. Physics F12*, 358 (1972); a recent review is *J.B. Forsyth*, *Physica Scripta* 15, 69 (1977).
- [8] For a recent example, see *F.A. Wedgwood*, *Proc. Roy. Soc. A349*, 447 (1976).
- [9] *J.P. Rebouillat*, Ph. D. thesis, C.N.R.S., Grenoble, 1972.
- [10] *P.J. Brown & J.B. Forsyth*, *Brit. J. Appl. Phys.* 15, 1529 (1964).
- [11] *P. Wolfers*, Manual for INT 2 Program, ILL Internal Report.
- [12] *R.E. Watson & A.J. Freeman*, *Acta crystallogr.* 14, 27 (1961).
- [13] 'International Tables for X-Ray Crystallography', Vol. II, pp 326, The Kynoch Press, Birmingham 1959.
- [14] *B. Mayoh & P. Day*, *J. chem. Soc. Dalton* 1974, 846.

International Reviews in Physical Chemistry (1981) 1, (149–193)
© 1981 Butterworths

MIXED VALENCY CHEMISTRY: A SURVEY OF 10 YEARS PROGRESS

PETER DAY

*Inorganic Chemistry Laboratory, Oxford University,
South Parks Road, Oxford OX1 3QR, UK*

INTRODUCTION: HISTORICAL BACKGROUND

Mixed valency chemistry is literally as old as the hills. Minerals such as vivianite, crocidolite, voltaite and above all magnetite testify to the existence of lattices containing an element (in this case Fe) in two different oxidation states on the geological time scale. Only slightly more recently primitive microorganisms began to see the evolutionary advantages of employing mixed valency clusters of Fe bound to S as oxidation-reduction enzymes, no doubt because the small atom rearrangements which accompany the change in oxidation state, further described below, mean that the activation energy of the process is suitably low. In historical times mixed valency came into technology via dyestuffs such as Prussian Blue (17th–18th century). The latter half of the 19th century saw preparative inorganic chemists like Alfred Werner (1896) taking a strong interest in the phenomenon, for example in his pioneering work on the bis-oxalatoplatinates which we now know as among the first linear-chain molecular metals. Indeed, it was he who recognized the analogy between these compounds and the tungsten bronzes, prepared some 20 years earlier by Biltz.

Qualitative theories connecting colour with chemical constitution, and giving prominence to charge transfer from one ion to another in mixed oxidation state compounds, were common in the first 20 years of the present century (e.g. Hofmann and Hoschele, 1916). Starting in the 1930s, and continuing after the Second World War, solid state physicists like Verwey at the Philips Laboratory, Eindhoven, uncovered the connections between conductivity and mixed valency in oxides such as $\text{Li}_x\text{Ni}_{1-x}\text{O}$ and $\text{La}_{1-x}\text{SrMnO}_3$, known as 'controlled valency semiconductors' (e.g. Verwey *et al.*, 1950). At the same time, in a parallel development, came work on the oxidation-reduction mechanisms of metal complexes in solution which drew attention to mixed valency oligomers as potentially tractable models for studying redox phenomena. Still, in spite of the long history of mixed valency in chemistry just described, there appeared to be no general realization by physical inorganic chemists that mixed valency compounds might have interesting and rewarding properties as a class, rather than haphazardly encountered individual examples. In 1967 two reviews (Robin and Day, 1967; Allen and Hush, 1967) appeared which aimed to remedy this situation, in the event, it can now be seen, successfully. Of the two accounts published in 1967 that by Hush related mixed valency phenomena to theories of inner- and outer-sphere electron transfer in solution while that of Robin and the present author collected a large body of examples from all over the Periodic Table, and showed how their physical properties could be related to molecular and crystal structures in terms of the degree of similarity, or difference, between the coordination sites occupied by the ions of different oxidation states.

During the last 10 years there has been an explosion of interest in mixed valency chemistry, ranging from preparative inorganic and organometallic chemistry, through the

physical chemistry of electron transfer processes, into the solid state physics of one-dimensional metals, and in other quite disparate directions such as biology and mineralogy. The present article aims to give a synoptic view of these new developments, taking account of advances in theory, in the results of new physical measurements and in the elucidation of new types of mixed valency compound, most of which did not exist in 1967. It is certainly not comprehensive, and very likely is biased. For much greater detail on particular aspects, the Proceedings of a NATO Advanced Study Institute entitled 'Mixed Valency Compounds' (Brown, 1980) should be consulted, while for brief and popular accounts, see articles by the present author in *Endeavour* (1970), *La Recherche* (1981) and *Comments on Inorganic Chemistry* (1981). There have also been a number of review articles on specific aspects of mixed valency chemistry, such as the coupling mechanisms in binuclear Ru(II,III) and other complexes, organometallic compounds, intervalence optical transitions in minerals and one-dimensional compounds. A selection from these is listed separately from the main body of references at the end of this article, to give an entry into the now very extensive primary literature. In what follows, we shall first describe some of the recent theoretical approaches to the statics and dynamics of intervalence interactions and then summarize the present state of knowledge about particular categories of mixed valency compound.

THEORIES OF MIXED VALENCY

Preliminaries

In Fig. 1 is shown a schematic picture of the most general kind of mixed valency situation. Two neighbouring metal ions A and B, each surrounded by a coordination environment which may consist of similar or different numbers and types of ligand, are connected by a pathway often consisting of a common ligand. A and B ions are of the same element but, on a time-scale to be discussed, have different oxidation states.

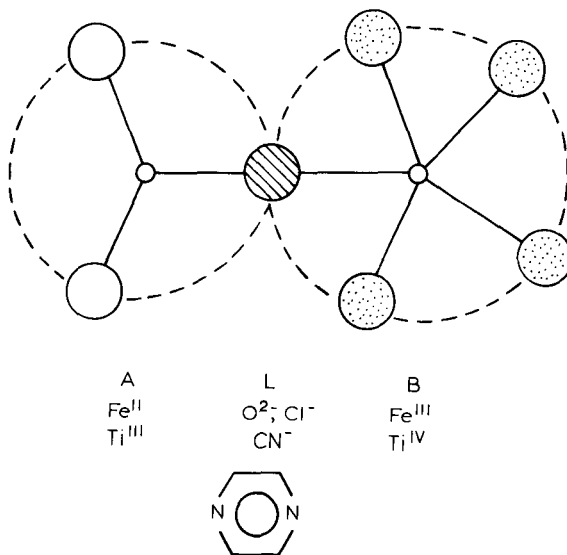


FIG. 1. Schematic view of two mixed valency ions with their ligand environments and a bridging group.

Li	Be											B	C	N	O	F	Ne
Na	Mg											Al	Si	P	S	Cl	Ar
K	Ca	Sc	Ti	V	Cr	Mn	Fe	Co	Ni	Cu	Zn	Ga	Ge	As	Se	Br	Kr
			[III, IV]	[III, IV] [IV, V]	[II, III] [III, VI]	[II, III] [III, IV] [IV, VII]	[II, III]	[II, III] [III, IV]	[II, III]	[I, II]		[I, III]					
Rb	Sr	Y	Zr	Nb	Mo	Tc	Ru	Rh	Pd	Ag	Cd	In	Sn	Sb	Te	I	Xe
			[II, III] [IV, V]	[V, VI]	[II, III]	[II, III] [III, IV]	[II, III]	[II, III]	[II, IV]	[0, I] [I, III]		[I, III]	[II, IV]	[III, V]			[VI, VIII]
Cs	Ba	La	Hf	Ta	W	Rc	Os	Ir	Pt	Au	Hg	Tl	Pb	Bi	Po	At	Rh
			[II, III]	[V, VI]			[II, III]	[III, IV]	[II, IV]	[I, III]		[I, III]	[II, IV]	[III, V]			
Fr	Ra	Ac															
			Ce	Pr	Nd	Pm	Sm	Eu	Gd	Tb	Dy	Ho	Er	Tm	Yb	Ln	
			[III, IV]	[III, IV]				[II, III]		[III, IV]							
			Th	Pa	U	Np	Pu	Am	Cm	Bk	Cf	Es	Fm	Md			
			[IV, V]	[IV, V] [IV, VI]	[IV, V]	[V, VI]	[III, IV]										

FIG. 2. Elements forming mixed valency compounds, with oxidation states.

Elements known to form at least one mixed valency compound are displayed in Fig. 2, with the combinations of oxidation state most commonly found. Over a third of the Periodic Table is represented, with the bulk of the examples concentrated, not very surprisingly, in d- and f-block elements. Numerous cases also exist among the B-subgroups, where the Group oxidation state N often co-exists with $(N-2)$. Bridging ligands in Fig. 1 range from monoatomic anions like O^{2-} , or Cl^- through diatomic (CN^-) to bifunctional aromatic molecules like pyrazine, 4,4'-bipyridyl and others even more elaborate, some of which are listed later (Table 3).

In terms of their stoichiometry two types of mixed valency compound can be distinguished. On the one hand are those in which an element clearly has a non-integral average oxidation state, on the ground of stoichiometry alone, e.g. Fe_3O_4 , where (since the most loosely bound electrons are certainly largely of Fe 3d type) the choice is to have 5.33 d-electrons on each Fe, or 6 on one and 5 on the other two. However, quite a lot of mixed valency compounds have an apparently integral average oxidation state, though one which would be very unusual for the element in question, e.g. $Pt(NH_3)_2Cl_3$ or SbO_2 . Here there are other structural and physical grounds for believing that we do not, in any sense, have Pt(III) and Sb(IV), but Pt(II,IV) and Sb(III,V). It is also important at the outset to realize that what we are calling 'mixed valency' here is quite a different phenomenon from the one which many physicists recently call by the same name, that is, the fluctuation of electron configuration between say $4f^6$ and $4f^55d^1$ in such purely stoichiometric compounds as SmS (see e.g., Campagna *et al.*, 1974).

In deciding on the most appropriate theoretical format for describing the electronic states, and hence the physical and chemical properties, of mixed valency systems a couple of preliminary points need clearing up.

1. How should we treat electron exchange between the two centres? If the intervalence interaction were weak we could treat it as a perturbation on the single valence wavefunctions, as in the valence-bond approximation. The ground state might then be written as $(Fe_A^{II}Fe_B^{III} + \lambda Fe_A^{III}Fe_B^{II})$ for example, where A and B are the two sites in Fig. 1 and λ is small. In fact that was the starting point of our own model (Robin and Day, 1967). On the other hand if electron exchange between A and B were a dominant feature one would move to the molecular orbital limit and construct LCAO one-electron wavefunctions from Fe 3d orbitals, or tight-binding band functions in the case of continuous solids. It is precisely because examples exist in mixed valency chemistry covering both these limiting cases, and all stages in between, that the field has proved so fascinating.
2. Do we aim at a static or a dynamic model? In some mixed valency systems electron exchange is slow enough on the time-scale of the vibrational motion that one can treat the electrons as trapped, and consider the wavefunctions appropriate to a fixed static nuclear framework. On the other hand, as we shall illustrate later, there are certainly cases where the 'extra' electron exchanges between the two centres of differing oxidation state on a time-scale comparable to that of a molecular skeletal vibration, and in which, therefore, the nuclear and electronic motions are inextricably connected, i.e. we have *par excellence* systems where the Born–Oppenheimer approximation does not apply.

The Robin–Day model

It was a static model which formed the basis of the Robin–Day (RD) classification scheme. Suppose the oxidation states of ions at A and B in Fig. 1 are n and $n + 1$. A first approximation to the ground state might be $\Psi_0 = A^n B^{n+1}$. But if the ligand fields around

the two sites are quite similar (though distinguishable) the valence bond configuration $\Psi_1 = A^{n+1}B^n$ will not have a very much greater energy than Ψ_0 . If there exists a suitable perturbation matrix element to mix them together the correct ground state wavefunction is the combination

$$\Psi_G = (1 - \alpha^2)^{1/2} \Psi_0 + \alpha \Psi_1. \quad (1)$$

The magnitude of the 'valence delocalization coefficient' α is determined by the energy $E_1 = \langle \Psi_1 | \mathcal{H} | \Psi_1 \rangle$ of Ψ_1 relative to Ψ_0 and the off-diagonal matrix element $V_{01} = \langle \Psi_0 | \mathcal{H} | \Psi_1 \rangle$ which mixes the two configurations together. Focusing first on E_1 , it is clear that for a one-electron transfer between A and B , only a difference between the ligand fields round the two sites can lead to $E_1 \neq 0$, because in the gas phase the ionization potential $A^n \rightarrow A^{n+1}$ is equal and opposite to the electron affinity $B^{n+1} \rightarrow B^n$. Thus the more different the sites are in geometry, in ligands or in bond lengths the larger is E_1 and the smaller is α . Compounds in which the sites are so different that α is negligible are called class I, while ones which have similar, but still distinguishable sites are class II. If we know from the stoichiometry that the average oxidation state is non-integral, but find all the metal ion sites crystallographically indistinguishable, α takes its maximum value (class III). Some examples of the three classes are given in Table 1.

As far as physical properties are concerned, in class I all properties determined by local forces, e.g. core-shell photoionization energies, Mössbauer chemical shifts, etc. are just a superposition of those of the two oxidation states taken separately. Direct optical transitions $E_0 \rightarrow E_1$ are at very high energy, and likewise thermally activated electron transfer requires too great an energy to observe conductivity in the solid state.

In class II compounds α has a small but finite value so 'local' properties are still close to those of the individual single oxidation states. However, optical transitions $E_0 \rightarrow E_1$ now

TABLE 1. Some examples of the three Robin-Day classes of mixed valency compound

	Site A	Site B	Formal oxidation states	
			A	B
<i>Class I</i>				
Sb ₂ O ₄	Distorted tetrahedral Av. Sb-O 2.13 Å	Octahedral Sb-O	III	V
GaCl ₂	Distorted 8-coord Ga-Cl 3.2 Å	Tetrahedral Ga-Cl 2.19 Å	I	III
<i>Class II</i>				
V ₇ O ₁₃	Octahedral V-O 1.964 Å	Octahedral V-O 1.945 Å	III	IV
Fe ₄ [Fe(CN) ₆] ₁₄ H ₂ O	Octahedral Fe-C 1.92 Å	Octahedral Fe-N 2.03 Å	II	III
(NH ₄) ₂ SbBr ₆	Octahedral Sb-Br 2.795 Å	Octahedral Sb-Br 2.564 Å	III	V
Mn ₂ O ₂ (bipy) ₄ ³⁺	Distorted octahedral Av. Mn-N 2.174 Å	Distorted octahedral Av. Mn-N 2.048 Å	III	IV
<i>Class III</i>				
Na _x WO ₃	Octahedral Av. W-O 2.1 Å	Octahedral	VI-V	VI-V
Fe ₄ S ₄ (SCH ₂ Ph) ₄ ²⁻	Tetrahedral Av. Fe-S 2.277 Å	Tetrahedral	2.5	2.5
K ₂ Pt(CN) ₄ Br _{0.30} 3H ₂ O	Planar Pt-Pt 2.89 Å	Planar	2.30	2.30

appear at lower energy, often in the visible, giving the bright colours so characteristic of many mixed valency compounds. Such compounds are also semiconductors.

If they are continuous lattice solids class III compounds are expected to be metallic, since the 'extra' electrons are spread out over all sites with equal probability, and they will have no 'local' properties characteristic of the integral oxidation states n , $n + 1$ but of something intermediate. On the other hand numerous discrete metal clusters are of class III type but cannot, of course, be metallic since intercluster electron hopping is not favoured. Their excited states, too, do not form a continuous band but are found at discrete energies corresponding to electronic transitions between molecular orbitals delocalized over the cluster.

A perturbation model for bridging groups

The utility of the simple static RD model has been demonstrated by applying it to a very large number of compounds. We have not, however, mentioned the role of V , which emphasizes the part played by the intervening ligands in the interaction. In most mixed valency compounds A and B are at least 5–6 Å apart so direct overlap between, e.g., d-orbitals on each centre must be very small. Consider two such orbitals χ_A , χ_B separated by a bridging ligand L with highest occupied and lowest unoccupied orbitals ϕ_L and ϕ_L^* . Suppose (Mayoh and Day, 1972, 1973) that the ground state mixed valency configuration is $\phi_L^2 \chi_A^2 \chi_B^1(\Psi_0)$ and the intervalence charge transfer excited state $\phi_L^2 \chi_A^1 \chi_B^2(\Psi_1)$. Assuming zero differential overlap $V_{01} \sim \langle \chi_A | \mathcal{H} | \chi_B \rangle \sim 0$. Any interaction between Ψ_0 and Ψ_1 must therefore take place via interaction with 'local' charge transfer configurations such as $\phi_L^1 \chi_A^2 \chi_B^2(\Psi_2)$ or $\phi_L^2 \chi_A^1 \chi_B^1 \phi_L^* \phi_L^*(\Psi_3)$. Normally these lie higher in energy than Ψ_1 but have much larger matrix elements V_{02} , V_{03} , V_{12} and V_{13} than V_{01} . Second-order perturbation theory gives

$$\alpha = \sum_{n=2,3} (V_{0n} V_{1n}) / (E_1 - E_0)(E_n - E_0) \quad (2)$$

$$\beta = \sum_{n=2,3} - (V_{0n} V_{1n}) / (E_1 - E_0)(E_n - E_1) \quad (3)$$

where β is the excited state valence delocalization coefficient in

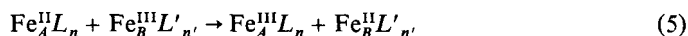
$$\Psi_E = (1 - \beta^2)^{1/2} \Psi_1 + \beta \Psi_0. \quad (4)$$

It is also possible to extend the summation over all configurations of the type $\chi_A \rightarrow \phi_L^*$ and $\phi_L \rightarrow \chi_B$. The many-electron matrix elements V_j can be expressed in terms of one-electron matrix elements which, in turn, become metal-ligand resonance integrals. The latter may be evaluated from appropriate atomic wavefunctions using the Linderberg method or, more empirically, chosen to reproduce the observed oscillator strengths of identifiable $\chi_A \rightarrow \phi_L^*$ and $\phi_L \rightarrow \chi_B$ transitions, either in the mixed valency complex itself or in the corresponding monomeric single valency fragments. In any case it is best to take the E_n where possible from the measured absorption peaks. Proceeding in this way values of α of the magnitude 10^{-1} have been obtained for several typical bridged class II complexes such as Prussian Blue and the related dimer $[(\text{NC})_5\text{Fe}(\text{CN})\text{Fe}(\text{CN})_5]^{6-}$ and somewhat smaller ones (3×10^{-2}) for Fe(II,III) compounds bridged by oxide ions (e.g. biotite micas), where the $\chi_A \rightarrow \phi_L^*$ charge transfer states lie at very high energy. The calculated values are validated by comparing the oscillator strength of the $\Psi_0 \rightarrow \Psi_1$ intervalence transition obtained from them with the observed ones. Agreement for strongly trapped class II systems is quite good (Mayoh and Day, 1973; Richardson, 1981).

Other experimental measures of α are ones which observe the degree of spin transfer from A to B in the ground state, for example transferred hyperfine interactions in Mössbauer spectroscopy or, even more directly, the magnetization density distribution found by polarized neutron diffraction (Day *et al.*, 1980). In the case of Prussian Blue both methods agree on an upper limit of 10^{-1} for α , but unfortunately were not sensitive enough to give a precise value.

Dynamics of electron transfer: adiabatic and Franck–Condon processes

Although the static model just described gives quite a satisfying picture of intervalence charge transfer mixing in terms of the energy difference between E_0 and E_1 and the magnitude of V_{01} , there is plenty of evidence that coupling between the electronic and vibrational motion has fundamental importance in both thermal and optical intervalence transfer. Most immediately obvious is the fact that intervalence optical transitions invariably have a very large Franck–Condon width, full widths at half height of 5000 cm^{-1} being by no means exceptional. Thus, the relaxed excited state is displaced very far from the minimum in the ground state potential energy surface. In fact, as Hush (1967) pointed out, the relaxed excited state after a one-electron intervalence transfer is electronically very similar to the original ground state, and most of the energy of the optical transition goes into vibrational excitation. For instance in a transfer



the only electronic contribution comes from the difference in the ligand fields exerted by L and L' , just as in the RD model. Assuming harmonic potentials the most general situation is as shown in Fig. 3 where the left-hand potential surface represents the variation with the vibrational coordinates of the electron configuration on the left-hand side of Eq. (5) and

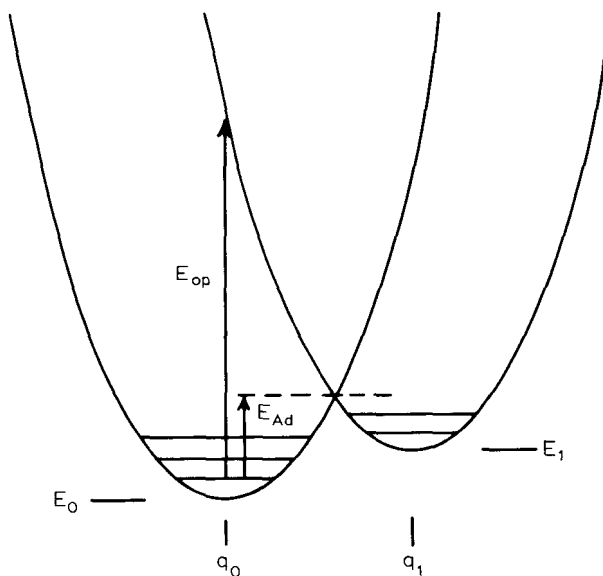


FIG. 3. Potential energy surfaces of Ψ_0 and Ψ_1 (defined in the text). E_{op} and E_{Ad} are the optical (Franck–Condon) and adiabatic intervalence electron transfer energies.

the right surface that on the right-hand side of Eq. (5). The vertical line E_{op} is the Franck–Condon maximum of the optical intervalence transition while E_{Ad} is the energy of a thermally activated electron transfer. In the case that $(q_1 - q_0)$ was small compared to $(E_1 - E_0)$ we would return towards the RD static limit but if the mixed valency complex were symmetrical ($L = L'$, $n = n'$ in Eq. (5)) one would have the simple geometrical relationship

$$E_{op} = 4E_{Ad} \quad (6)$$

Very few direct tests of Eq. (6) have been made because the activation free energy measured from the rate of a self-exchange process like (5) taking place in solution includes contributions from other processes such as the energy required to bring the reactants together and reorganize the solvent. If adiabatic electron transfer could be observed in the solid state this problem would be circumvented but only one study of a direct comparison between semiconduction activation energy and optical intervalence frequency appears to have been reported (Culpin *et al.*, 1965, 1968). In that case, a series of chlorocuprate(I,II) salts, E_{op} was 17 500 cm^{-1} while E_{Ad} was 6000 cm^{-1} .

Clearly, however, neither Franck–Condon nor adiabatic electron transfer can take place between A and B if the two surfaces in Fig. 3 are orthogonal. In the vicinity of the intersection there must be an ‘avoided crossing’ brought about by a matrix element like V_{01} . The situation is no longer a static one and the relevant matrix element is a function of the vibrational as well as the electronic coordinates. If we invoke the Born–Oppenheimer approximation, $\Psi_{0i} = \psi_0 \chi_{0i}$ and $\Psi_{1j} = \psi_1 \chi_{1j}$ where the ψ s are the electronic functions and χ s the vibrational ones. Then

$$V_{0i,1j} = \langle \psi_0 \chi_{0i} | \mathcal{H} | \psi_1 \chi_{1j} \rangle = V \langle \chi_{0i} | \chi_{1j} \rangle. \quad (7)$$

Application of time-dependent perturbation theory leads to the result that the rate of transition from Ψ_{0i} to any of the vibrational levels χ_{1j} of Ψ_1 is

$$W_{0i} = (2\pi/\hbar) V^2 \langle \chi_{0i} | \chi_{1j} \rangle^2 \rho(E_{0i} = E_{1j}) \quad (8)$$

where ρ is the density of vibrational levels in the state near the energy E_{0i} . This is the so-called Fermi ‘Golden Rule’. The total transition probability W_{0i} , proportional to the rate-constant for crossing between the two potential energy surfaces of Ψ_0 and Ψ_1 is then obtained by making a thermal average over all the vibrational levels χ_{0i} which have the greatest overlap with the χ_{1j} having the same energy, $E_{0i} = E_{1j}$. That can only be those vibrational levels lying at, or close to, the crossing point between the two potential energy surfaces. To carry out the summations involved in evaluating W_{0i} , it is normally assumed that the energy intervals between the vibrational levels are small enough to use a semi-classical treatment (e.g. Levich, 1970). Then the total adiabatic transition probability is given by

$$W_{0i} = (2\pi/\hbar) V^2 [\pi/kT(E_{op} - E_1)] \exp(-E_{Ad}/kT). \quad (9)$$

The formidable list of assumptions used to derive this expression are:

1. Weak electronic coupling.
2. Harmonic potential energy surfaces.
3. Identical normal mode frequencies in both potential energy surfaces.
4. Strong vibrational-electronic interactions.
5. Vibrational intervals which are much smaller than kT .

Equation (9) is already familiar from theories of the rates of electron transfer reactions in solution but Meyer (1979), in particular, has pointed out a great advantage which mixed-valency dimers have over collision complexes in solution when attempts are made

to estimate the various quantities which enter the equation. Meyer's principal point is that the frequency and intensity of the optical intervalence transition carry information respectively on E_{Ad} and V_{01} . In the symmetrical case ($E_0 = E_1$ in Fig. 3) Eq. (6) applies, or otherwise

$$E_{Ad} = E_{op}^2/4[E_{op} - (E_1 - E_0)]. \quad (10)$$

Assuming zero overlap between donor and acceptor orbitals the transition dipole moment of the intervalence absorption $\Psi_G \rightarrow \Psi_E$ (Eqs. (1) and (4)) is

$$M_{GE} = \langle \Psi_G | er | \Psi_E \rangle = \frac{1}{2}e(\alpha + \beta)R \quad (11)$$

where R is the distance between the sites A and B and V_{01} can then be evaluated from the experimental values of α and β , for example, via Eqs. (2) and (3). Some numerical values of W_{01} estimated from intervalence absorption spectra are given in Table 2. They refer to acetonitrile at 23°C, and appear to have quite reasonable orders of magnitude compared with outer-sphere self-exchange reactions of the corresponding monomeric Ru^{II} and Ru^{III} complexes.

TABLE 2. Values of W_{01} (eq. (9)) in acetonitrile at 23°C calculated from the properties of intervalence optical transitions of $[(\text{bipy})_2\text{ClRu}^{\text{II}}(\text{L})\text{Ru}^{\text{III}}(\text{bipy})_2\text{Cl}]^{3+}$ (Meyer, 1979)

L	E_{op} (eV)	E_{Ad} (eV)	V_{01} (eV)	W_{01} (s^{-1})
pz	0.95	0.24	0.049	2.4×10^{10}
4,4'-bipy	1.26	0.32	0.017–0.025	$(1.0\text{--}2.8) \times 10^8$
BPE	1.34	0.34	0.016–0.023	$(5.1\text{--}10) \times 10^7$

A complication arising from attempts to estimate adiabatic electron transfer rates from optical data for mixed valency dimers concerns the respective contributions of intramolecular skeletal vibrational modes and solvent reorganization to E_{Ad} . For solvent vibrations, assumption (5) above is very likely to be correct, but much less likely so for molecular vibrations, which may have frequencies above 200 cm^{-1} . One method which has been proposed for separating the two contributions is to measure the frequency of the intervalence band E_{op} as a function of solvent dielectric constant since the variation should be entirely the result of the solvent reorganization (Tom *et al.*, 1974). In the dielectric continuum approximation (Marcus, 1956, 1965; Hush, 1961) the contribution E_s to E_{op} from solvent reorganization is

$$E_s = e^2 \left(\frac{1}{2a_A} + \frac{1}{2a_B} - \frac{1}{d} \right) \left(\frac{1}{D_{op}} - \frac{1}{D_s} \right) \quad (12)$$

if the charge distributions around the two sites A , B are assumed to be spheres of radius a_A , a_B with centres separated by d . D_{op} and D_s are the optical and static dielectric constants. Some examples of the application of Eq. (12) are given below. A better approximation than a pair of charged spheres is a charged ellipsoid, as treated originally by Kirkwood and Westheimer (1938) and applied to mixed valency dimers by Cannon (1977). It is also worth noting in passing that Eq. (12) also contains a simple prediction about the distance dependence of E_{op} , which has been verified for a series of $\text{Ru}^{\text{II,III}}$ dimers bridged by ligands of increasing length (Powers *et al.*, 1976), and also in some biferrocenium ions (Powers and Meyer, 1978). It has also been found recently to apply to shifts in intervalence absorption bands in crystals on lowering the temperature from 300 to 4 K, as a result of contracting the lattice (Prassides, 1980).

Building on the theories developed originally to describe the interaction of point defects in crystals with localized and lattice vibrations (e.g. Huang and Rhys, 1951), the frequencies of the skeletal modes which couple to mixed valency electron transfer can also be estimated by measuring the temperature dependence of the intervalence absorption band profile. Because the relaxed excited state in an intervalence transition (q_1 in Fig. 3) lies very far from the ground state q_0 in the configuration coordinate diagram, such absorption bands are always very wide, and do not become dramatically narrower on cooling. In particular, no vibrational fine-structure has ever been observed in an intervalence band. Quite generally the shape function $G(\nu)$ of a broad absorption band is given by the sum of terms involving the overlap integrals between all the vibrational wavefunctions χ_{oi} in the ground state Ψ_0 and χ_{1j} in the excited state Ψ_1 weighted by the thermal occupancy $P(i)$ of χ_{oi} (e.g. Markham, 1959):

$$G(\nu) = \sum_{ij} P(i) \langle \chi_{oi} | \chi_{1j} \rangle^2 \delta[\nu - (E_{1j} - E_{0i})/\hbar] \quad (13)$$

$$P(i) = \prod \left\{ \exp\left(\frac{-i\hbar\omega_0}{kT}\right) \left[1 - \exp\left(\frac{-\hbar\omega_0}{kT}\right) \right] \right\} \quad (14)$$

if the force field is harmonic

$$E_{0i} = E_0 + \hbar\omega_0(i + \frac{1}{2}) \quad (15)$$

$$E_{1j} = E_1 + \hbar\omega_1(j + \frac{1}{2})$$

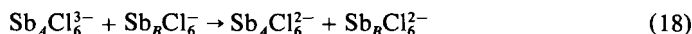
where ω_0 and ω_1 are vibrational frequencies in states 0 and 1. Of course, there may be many modes in both states but we assume for simplicity that there is only one 'effective' mode. If it is further assumed that $\omega_0 = \omega_1$ then $G(\nu)$ is a Gaussian with a halfwidth H given by

$$H^2 = 8(\ln 2) \hbar^2 \omega^2 S \coth(\hbar\omega_0/2kT) \quad (16)$$

where S is the Huang–Rhys factor, the ratio between the vibrational energy excited in the upper state to the energy of a single vibrational quantum

$$S = (1/2) \omega_0^2 (q_1 - q_0)^2 / \hbar\omega. \quad (17)$$

Equations (16) and (17) are equivalent to assuming that one can neglect quantization of the vibrations in the upper state so that there is a continuum of upper state vibrational levels so the probability of a Franck–Condon transition from the ground state is proportional to $|\chi_0|^2$. Equation (16) was first investigated experimentally for mixed valency compounds by Atkinson and Day (1969), who found a good fit was obtained for $\omega = 210 \text{ cm}^{-1}$ and $S = 130$ in the $\text{Sb}^{\text{III}} \rightarrow \text{Sb}^{\text{V}}$ transition in crystals of $(\text{CH}_3\text{NH}_3)_2\text{Sb}_{1-x}\text{Sn}_x\text{Cl}_6$. Analogous measurements on $[(\text{CN})_5\text{Fe}(\text{pyrazine})\text{Fe}(\text{CN})_5]^{5-}$ (Felix and Ludi, 1978) and Prussian Blue (Ludi, 1980) yielded values of $\omega = 490$ and 430 cm^{-1} (Fig. 5). Clearly these figures lie within the range expected for metal–ligand stretching vibrations, but only in the case of the $\text{Sb}^{\text{III,V}}$ system was it possible to make a direct comparison with known normal mode frequencies. In that example the intervalence transition is



and it is known from the crystal structures of related compounds (Lawton and Jacobson, 1966; Birke, Latscha and Pritzkow, 1976) that the SbCl_6 units approximate very closely to octahedra in both oxidation states, with a bond length difference of 0.1–0.3 Å. The a_{1g} stretching modes of the $\text{Sb}(\text{III})$ and $\text{Sb}(\text{V})$ have frequencies of 267 and 329 cm^{-1} respectively (Barrowcliffe *et al.*, 1967), i.e. both higher than the effective frequency broadening

PETER DAY

159

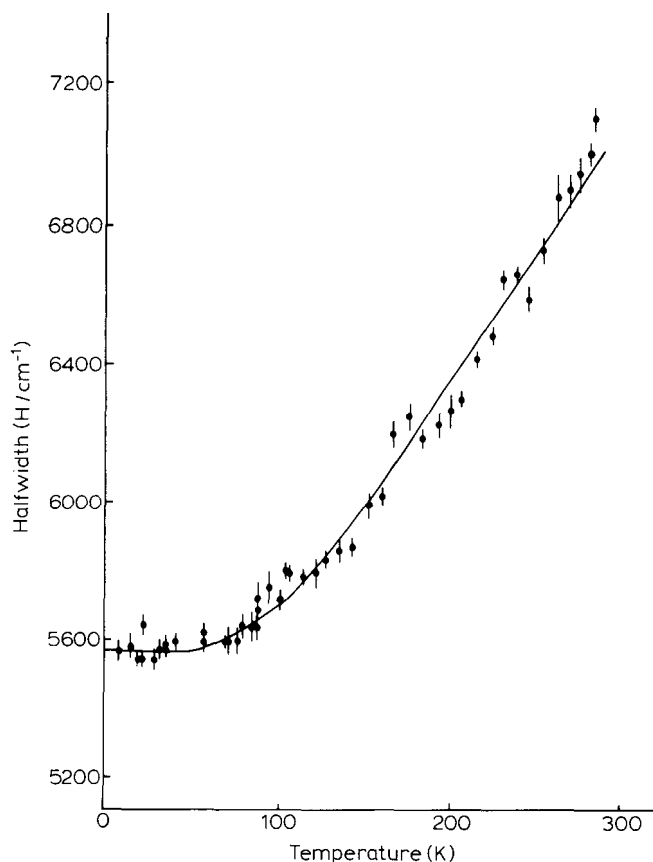


FIG. 4. Halfwidth of the intervalence electron transfer band in $(\text{CH}_3\text{NH}_3)_2\text{Sb}_{1-x}\text{Sn}_x\text{Cl}_6$ as a function of temperature. The full line is calculated from Eq. (16) with $\omega = 234 \text{ cm}^{-1}$ (Prassides, 1980).

the intervalence absorption band. However, there is no direct evidence about the extent to which each individual mode of the two octahedra couples to the electronic transition. In fact, if the assumption is made that all internal modes contribute equally, weighted only by their degeneracy, the resulting averages (163 cm^{-1} for SbCl_6^{3-} and 249 cm^{-1} for SbCl_6^-) fall on either side of the 'effective' frequency observed. A better assumption would be that there are two 'effective' ground state frequencies, one for each ion, and that the effective excited state vibrational frequency was not necessarily equal to that of the ground state. Under these circumstances Markham (1959) showed that the half-width of the absorption band (strictly speaking, the second moment) was

$$H^2 = \hbar^2 \omega_1^2(A) S_A \coth(\beta_A/2) + \hbar^2 \omega_1^2(B) S_B \coth(\beta_B/2) \quad (19)$$

where

$$\beta_A = (\hbar/kT) \omega_0(A); \quad \beta_B = (\hbar/kT) \omega_0(B) \quad (20)$$

and A and B refer to the two ions. If we take $\omega_0(A)$ and $\omega_0(B)$ as 163 and 249 cm^{-1} and $\omega_1(A) = \omega_1(B) = \omega_1 = (1/2)(\omega_0(A) + \omega_0(B))$, because the two relaxed excited state ions

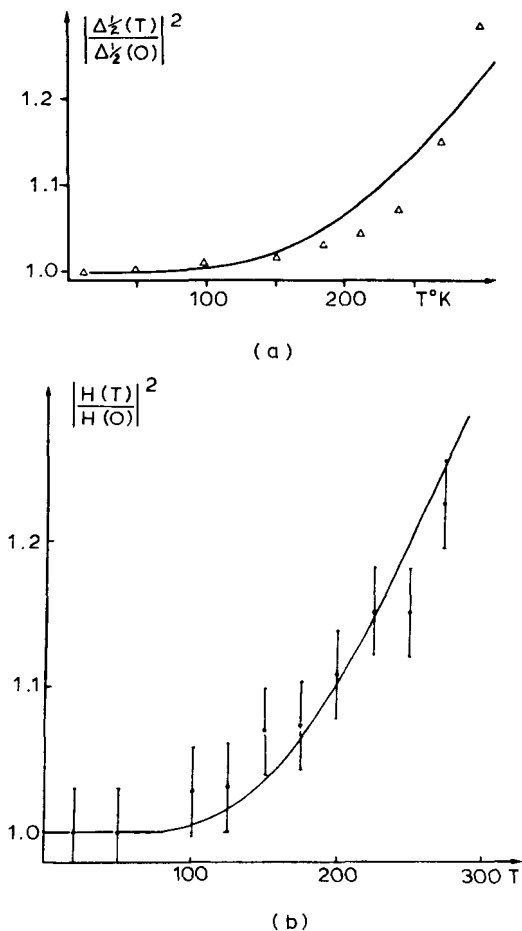


FIG. 5. Temperature variation of halfwidths of intervalence bands in (a) $[(\text{CN})_5\text{Fe}(\text{pz})\text{Fe}(\text{CN})_5]^{6-}$ (Felix and Ludi, 1978) and (b) Prussian Blue (Ludi, in Brown, 1980). The full lines are calculated from Eq. (16) with $\omega = 490$ and 430 cm^{-1} respectively.

on the righthand side of Eq. (18) are identical, the limiting halfwidth of the Gaussian band at 0 K is

$$H(O)^2 = 8(\ln 2) \hbar^2 \omega_1^2 (S_A + S_B). \quad (21)$$

Experimentally $H(O)$ is 5550 cm^{-1} (Prassides, 1980) which, taking into account the reduced masses associated with all the modes, yields an estimate of 0.3 \AA for the difference between the bond lengths of SbCl_6^{3-} and SbCl_6^- in their ground states, in quite good agreement with what is observed (Fig. 4).

Class II or class III dimers: V_{01} versus E_{Ad}

There can be no doubt that the very large width and lack of resolved vibrational structure in intervalence charge transfer spectra is the result of the large changes of

PETER DAY

161

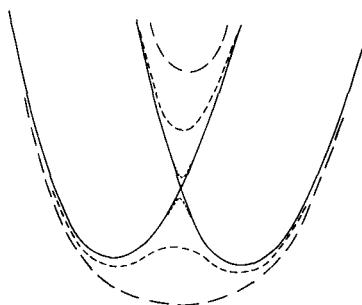


FIG. 6. Potential energy surfaces for a symmetrical mixed valency dimer. The dotted, short dashed and long dashed lines represent the surfaces for $E_{Ad} \gg V_{01}$, $E_{Ad} \sim V_{01}$ and $E_{Ad} \ll V_{01}$ (see text).

bond lengths taking place when electrons are transferred into and out of a localized orbital. In strongly trapped class II examples there is only very limited mixing between the donor and acceptor wavefunctions so the 'avoided crossing' at the intersection of the two potential energy surfaces in Fig. 3 is a small perturbation and the semiclassical theories we have just described cope quite satisfactorily with the main experimental characteristics of both adiabatic and Franck–Condon electron transfer. On the other hand there is no reason *a priori* why V_{01} should be small compared with E_{Ad} , a thought which was highlighted in a particularly stark fashion by the preparation of the dimeric cationic complex $[(\text{NH}_3)_5\text{Ru}(\text{pyrazine})\text{Ru}(\text{NH}_3)_5]^{5+}$, now known as the Creutz–Taube (CT) complex (Creutz and Taube, 1969). In this ion each Ru has a distorted octahedral ligand field exerted by five NH_3 nitrogen atoms and one nitrogen from the pyrazine so as far as the ligand environments are concerned the two Ru could be identical. Whether they are or not remains controversial and the evidence is reviewed later, but in related ions containing bipyridyl and Cl in place of the NH_3 it seems clear that there is no inversion centre (Powers *et al.*, 1976).

With identical ligands around each metal ion it might be thought that the complex would inevitably belong in class III of the RD classification. However, it was first pointed out by Mayoh and Day (1972) how it might still be possible for such a complex to be in class II if the vibrations of the ligands around the sites *A* and *B* were taken into account. To each wavefunction Ψ_0 , Ψ_1 defined in the RD static model corresponds a potential energy surface. As shown in Fig. 6 they are identical, but displaced along the normal coordinate which carries the equilibrium configuration of $A^n B^{n+1}$ to $A^{n+1} B^n$. The mixing between these two surfaces via the matrix element V_{01} produces two new ones separated, as shown, by $2V_{01}$. If $V_{01} \ll E_{Ad}$ the lower surface retains two minima close to the positions in the configuration coordinate space which they would have occupied in the absence of the interaction. Thus the minimum of energy corresponds to an unsymmetrical valence distribution. In contrast, if $V_{01} \gg E_{Ad}$ there is now a single minimum in the lower potential energy surface at a symmetrical configuration, so we have a qualitative criterion for localization or delocalization. For the model case of two orthonormal electron wavefunctions linearly coupled to a doubly degenerate vibration the quantitative criterion for localization is $V_{01} < 2E_{Ad}$ (Hush, 1975).

The Piepho–Krausz–Schatz model

Figure 6 makes it clear that there is a strong analogy between the potential energy surfaces of a dimeric mixed valency complex and those generated by the interaction of a doubly

degenerate electronic state with a vibrational mode, i.e. the Jahn–Teller effect. The main difference, of course, stems from the fact that the electronic degeneracy in the mixed valency problem is associated with oscillations of an electron between two orbitals centred on different atoms, while Jahn–Teller degeneracy is about a single centre. Piepho, Krausz and Schatz (PKS) (1978) recently worked out the vibronic problem explicitly for the mixed valency case and derived eigen values and vibronic coefficients using a formalism originally developed by Fulton and Gouterman (1961) to describe the excited states of symmetrical dimers such as $(C_6H_6)_2^+$. Defining Ψ_0 and Ψ_1 in the same way as we did in the RD static model, they use the harmonic approximation and consider only the totally symmetric normal coordinates Q_A , Q_B of each subunit. The vibrational potential energy of A in oxidation state n is

$$W_n^A(Q_A) = W_n^0 + L_n^A Q_A + (1/2) k_n^A Q_A^2 \quad (22)$$

and similarly for W_{n+1}^A , W_n^B and W_{n+1}^B . Putting $k_n^A = k_n^B = k_n$, etc.,

$$\begin{aligned} W_0 &= W_n^A(Q_A) + W_{n+1}^B(Q_B) = lQ_A + (1/2) k_n Q_A^2 + (1/2) k_{n+1} Q_B^2 \\ W_1 &= W_{n+1}^A(Q_A) + W_n^B(Q_B) = lQ_B + (1/2) k_{n+1} Q_A^2 + (1/2) k_n Q_B^2. \end{aligned} \quad (23)$$

If one introduces new vibrational coordinates

$$Q_{\pm} = (1/\sqrt{2})(Q_A \pm Q_B) \quad (24)$$

and makes the rather drastic assumption that $k_n = k_{n+1} = k$

$$\begin{aligned} W_0 &= (1/\sqrt{2})lQ_- + (1/2)kQ_-^2 + (1/\sqrt{2})lQ_+ + (1/2)kQ_+^2 \\ W_1 &= (-1/\sqrt{2})lQ_- + (1/2)kQ_-^2 + (1/\sqrt{2})lQ_+ + (1/2)kQ_+^2 \end{aligned} \quad (25)$$

the problem is separable into Q_+ and Q_- (or q) terms, of which only the latter is important for spectroscopic and other properties connected with intervalence transfer. PKS now define dimensionless variables

$$q = 2\pi(\nu_-/h)^{1/2} Q_-; \quad \lambda = (8\pi^2 h\nu_-^3)^{-1/2} l \quad (26)$$

whence

$$W_0/h\nu_- = \lambda q + (1/2)q^2; \quad W_1/h\nu_- = -\lambda q + (1/2)q^2. \quad (27)$$

The next stage is to allow A and B to interact via V_{01} so that new wavefunctions such as Ψ_G and Ψ_E (Eqs. (1) and (4)) are generated, but it is important to note that V_{01} is now a function of both the electronic and vibrational coordinates around A and B . In fact, to make the problem tractable it has to be assumed that $V_{01} = V_{01}^0$, its value when all the nuclei are fixed at their equilibrium configurations. A further parameter to describe the electronic coupling is now defined as

$$(h\nu_-) \varepsilon = V_{01}^0 \quad (28)$$

so first-order perturbation theory yields the secular determinant

$$\begin{vmatrix} \lambda q + (1/2)q^2 & \varepsilon \\ \varepsilon & -\lambda q + (1/2)q^2 - W_k \end{vmatrix} = 0 \quad (29)$$

$$\Psi_k = c_0 \Psi_0 + c_1 \Psi_1 \quad (30)$$

whence

$$W_{0,1} = (1/2)q^2 \mp (\varepsilon^2 + \lambda^2 q^2)^{1/2}. \quad (31)$$

For an unsymmetrical complex (RD class II) $W_n^A \neq W_n^B$ and $W_{n+1}^A \neq W_{n+1}^B$ so, defining one extra parameter W , roughly related to $E_1 - E_0$ in Fig. 3, to take account

of the difference between the minima in the two originally non-interacting potential energy surfaces,

$$W_{0,1} = (1/2)q^2 \mp [\varepsilon^2 + (\lambda q + W)^2]^{1/2}. \quad (32)$$

To emphasize the relationship between the RD and PKS models (Wong, Schatz and Piepho, 1979), one can write the PKS wave functions corresponding to the RD Ψ_G , Ψ_E of Eqs. (1) and (4) in the static limit (zero nuclear kinetic energy) as

$$\begin{aligned} \Psi_G^{PKS} &= -(1/N\sqrt{2})[(\varepsilon - \kappa + \sigma)\Psi_0 + (\varepsilon - \kappa - \sigma)\Psi_1] \\ \Psi_E^{PKS} &= (1/N\sqrt{2})[-(\varepsilon - \kappa - \sigma)\Psi_0 + (\varepsilon - \kappa + \sigma)\Psi_1] \end{aligned} \quad (33)$$

where $N = [\sigma^2 + (\varepsilon - \kappa)^2]^{1/2}$, $\kappa = [\varepsilon^2 + \sigma^2]^{1/2}$, $\sigma = (\lambda q + W)$, all being functions of q . If q is set equal to λ there is a direct relationship with Eq. (1) such that

$$\alpha^2 = \frac{1}{2} \left[1 - \left\{ \frac{(\lambda^2 + W)^2}{\varepsilon^2 + (\lambda^2 + W)^2} \right\}^{1/2} \right]. \quad (34)$$

In this equation, as W becomes large α tends to zero, exactly as in the RD model. The three RD classes I, II and III correspond respectively to the cases $|\varepsilon| \ll (\lambda^2 + W)$, $|\varepsilon| \lesssim (\lambda^2 + W)$ and $|\varepsilon| > (\lambda^2 + W)$. In a purely static model such as the RD one a complex in which $W=0$ (or $E_1 = E_0$) could not be other than delocalized. The PKS model, on the other hand, taking account of the vibrational-electronic coupling, would allow such a complex to be localized or delocalized to an extent determined by the ratio $|\varepsilon|/\lambda^2$. The same point, though with somewhat different nomenclature, has also been made by Hush (1975).

Now it is most important to observe that although account has been taken of the interaction between the electronic wavefunctions and the vibrational motion, equations such as (30)–(33), not to mention earlier ones such as Eqs. (9) and (13), remain within the adiabatic Born–Oppenheimer approximation, that is, the nuclear kinetic energy has not yet been included in the Hamiltonian. To take advantage of the interchange symmetry ($A = B$) it is convenient to use electronic functions Ψ_{\pm} defined as

$$\Psi_{\pm} = (1/\sqrt{2})(\Psi_0 \pm \Psi_1) \quad (35)$$

and define a general vibronic function

$$\Phi_v(r, q) = \Psi_+(r) \chi_{+,v}(q) + \Psi_-(r) \chi_{-,v}(q) \quad (36)$$

where χ_{\pm} are also linear combinations of $\chi_{0,1}$. In the unsymmetrical case, where interchange symmetry is lost, the vibronic function is

$$\Phi_v(r, q) = \sum_{n=0}^{\infty} (c_{vn} \Psi_+ \chi_n + c'_{vn} \Psi_- \chi_n). \quad (37)$$

The intervalence band is now the envelope of all the transitions $\Phi_v \rightarrow \Phi_v$, weighted by their differences in thermal population, as in Eq. (13). In the weak-coupling (class II) limit $\lambda^2 + W \gg |\varepsilon|$ it is found that the band should be gaussian, with a halfwidth (second moment) which varies with temperature according to a $\coth(\hbar\nu_-/2kT)$ function as in Eq. (16). When the coupling $|\varepsilon|$ becomes stronger, and particularly in symmetrical complexes such as the CT ion the intervalence band becomes narrower and distinctly asymmetric. Observed and calculated band envelopes for the CT ion from the PKS model are shown in Fig. 7a and the corresponding potential energy surfaces in Fig. 7b. Agreement is quite good for values of ε and λ of -6 and 2.7 in units of a q quantum $\nu_- = 500 \text{ cm}^{-1}$. On the other hand it has been suggested by Hush (1980) that symmetric expansion of the excited state ought to be taken into account in addition to the coupling to ν_- .

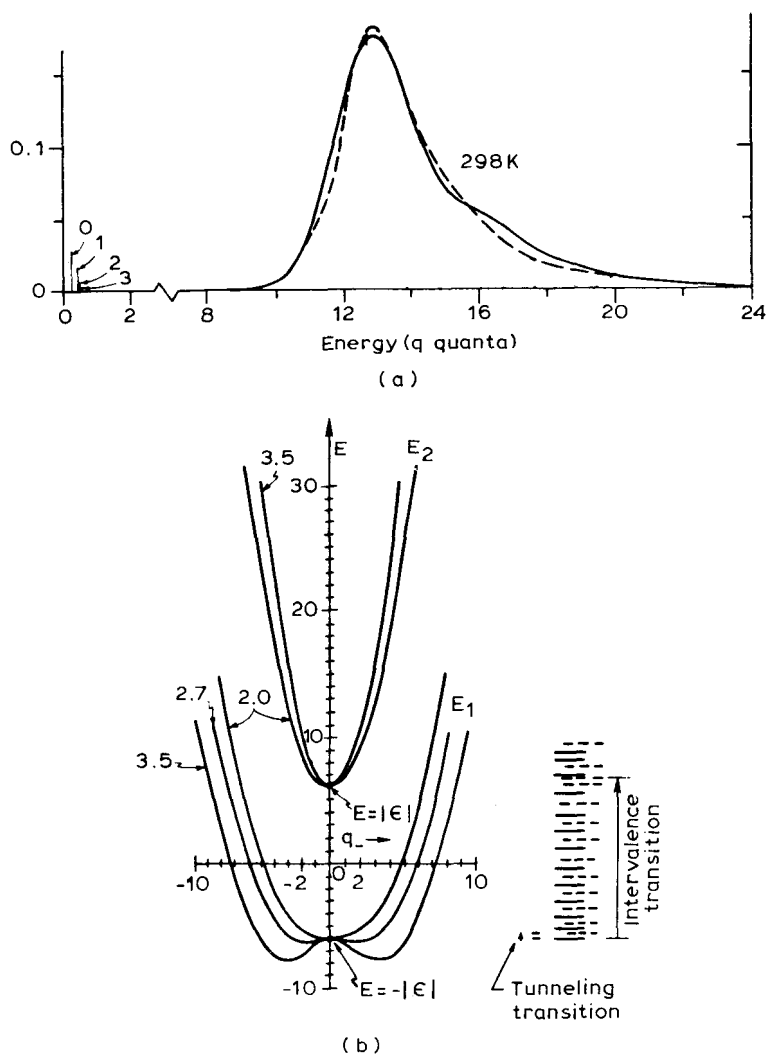


FIG. 7. The PKS model applied to the Creutz-Taube complex. (a) Observed (----) and calculated (—) intervalence band profiles at room temperature. The calculation used $\epsilon = -6$, $\lambda = 2.7$ (Piepho *et al.*, 1978). Also shown are the predicted infrared tunnelling transitions. (b) Potential energy surfaces calculated for $\epsilon = -6$, $\lambda = 2.0, 2.7, 3.5$. The intervalence transition is shown for the $\lambda = 2.7$ case.

Adding a fourth parameter S to indicate the energy of coupling $Sh\nu_+$ to the symmetric mode, assumed to have the same frequency as ν_- Hush finds that he, too, can get reasonable agreement with the observed intervalence band shape for the CT ion (Fig. 8) but with parameter values suggesting a delocalized ground state, with a single minimum in the lower potential energy surface. Clearly this remains an open question (*see later for further discussion of other experimental evidence about the CT complex*) but it is worth noting that Hush's point may give the answer to a puzzling dilemma arising from

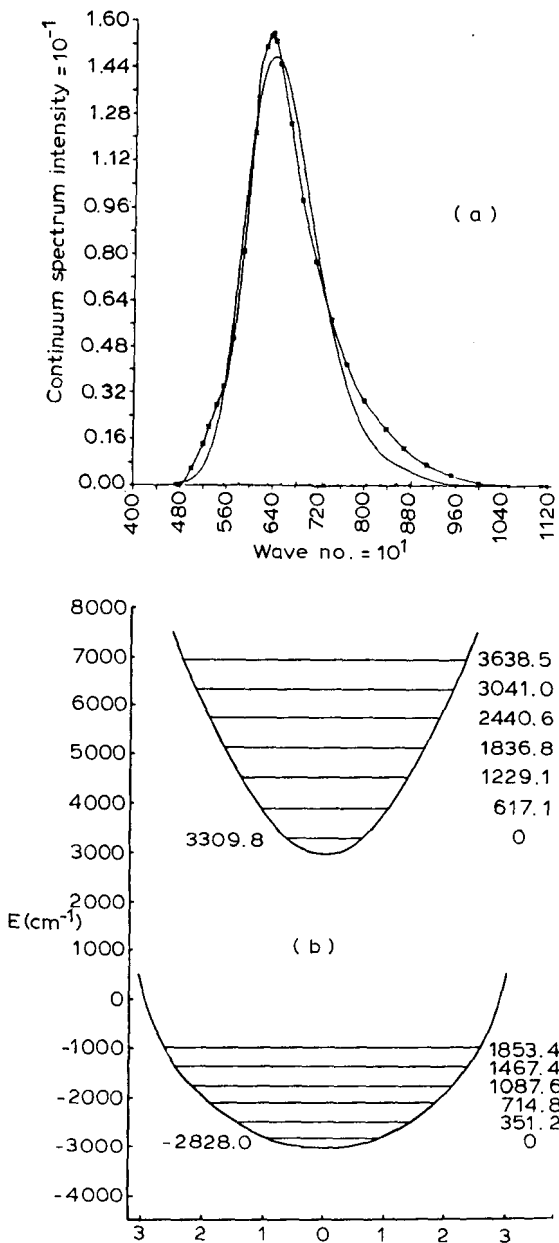


FIG. 8. Hush's (1980) calculation for the Creutz-Taube complex. (a) Observed (■) and calculated intervalence band envelopes. (b) Potential energy surfaces used to calculate (a).

the PKS treatment of the CT ion, namely, why has it not proved possible to observe 'tunnelling' transitions in the far infrared? From Fig. 7b one sees that in addition to the transitions between the upper and lower potential energy surfaces which give rise to the intervalence band there should exist transitions between adjacent levels in the lower surface. Since they have something of the character of an electronic charge transfer as well as a vibrational transition they ought to be much more intense than the ordinary vibrational bands, but no sign of any abnormal absorption has been seen in the CT complex at 4.2 K down to 20 cm^{-1} (Schatz *et al.*, 1978).

TYPES OF MIXED VALENCY COMPOUNDS

In the previous section some recent theoretical advances in understanding ground and excited states of mixed valency compounds have been described. In the second part of this review we shall survey experimental work on particular types of compound to exemplify the variety and vitality of the field and show how the theoretical models work out in practice.

Discrete dimers and oligomers

Evidence from structures

Following Creutz and Taube's (1969) isolation of their pyrazine-bridged Ru(II,III) ammine dimer, many other binuclear complexes $L_nM_A L_b M_B L'_n$ have been synthesized, some of which are listed in Table 3. Evidence about the classification of all these compounds comes from many different kinds of experiment. Crystal structure determinations are the most direct, but are not available in many cases. For example $[(bipy)_2Mn(O)_2Mn(bipy)_2]^{3+}$ (Plaksin *et al.*, 1972) has two quite distinct types of Mn coordination (Fig. 9). On the other hand there is always the possibility that small differences between the sites in an oligomer might not exceed the thermal ellipsoids in a room temperature crystal structure or, alternatively, that a molecule which almost, but not quite, has a centre of inversion or some other symmetry element, might be disordered in the crystal. Thus the CT complex, in a mixed chloride/bromide salt (Beattie *et al.*, 1977) appears to lie on such a centre (Fig. 10) though the difference between Ru(II)-N and Ru(III)-N bond lengths in the respective single valency hexammine salts is in any case no greater than 0.04 \AA (Stynes and Ibers, 1971). A similar example is the trimeric complex

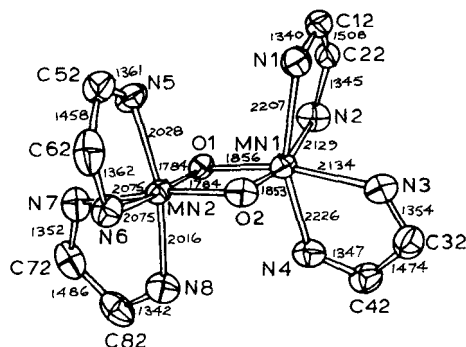

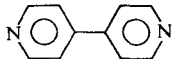
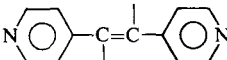
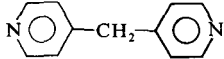
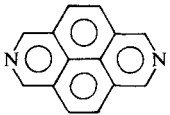
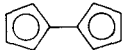
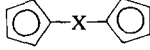
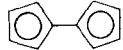
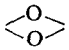


FIG. 9. The molecular structure of $[(bipy)_2MnO_2Mn(bipy)_2]^{3+}$ (Plaksin *et al.*, 1972).

PETER DAY

167

TABLE 3. Some ligand-bridged mixed valency dimeric molecules $L_nM_A L_b M_B L'_n$

				R-D class	Ref.
Ru(II,III)	$(NH_3)_5$	$(NH_3)_5$	 (pz)	II-III	a, b
			 (4,4' bipy)	II	c
			 (BPE)	II	d
				II	e
				II	d
Ru(II,III)	$(bipy)_2Cl$	$(bipy)_2Cl$	NC-CN	III	c
			NC-C(R)-CN	III	g
			pz	II	h
			4,4'-bipy	II	h
			BPE	II	h
			$Ph_2PCH_2PPh_2$	II	i
Ru(II,III)	$(NH_3)_5$	$(bipy)_2Cl$	4,4'-bipy	II	j
Os(II,III)	$(NH_3)_4Cl$	$(NH_3)_4Cl$	N_2	III	k
Fe(II,III)	$(CN)_5$	$(CN)_5$	CN	II	l
			pz, BPE	II	m
Fe(II,III)	$\eta-C_5H_5$	$\eta-C_5H_5$		II	n
				II	o
			(X=CH, -C=C-Hg)	I	o
Fe(II,III)			—	III	p
Mn(III,IV)	$(bipy)_2$	$(bipy)_2$		II	q

a, Creutz and Taube, 1969. b, Creutz and Taube, 1973. c, Tom *et al.*, 1974. d, Fischer *et al.*, 1976. e, Rieder and Taube, 1977. f, Tom and Taube, 1975. g, Krentzien and Taube, 1976. h, Powers *et al.*, 1976. i, Sullivan and Meyer, 1980. j, Powers *et al.*, 1976. k, Magnuson and Taube, 1972. l, Glauser *et al.*, 1973. m, Felix and Ludi, 1978. n, Morrison and Hendrickson, 1973. o, Morrison *et al.*, 1973. p, Mueller-Westerhoff and Eilbracht, 1972; LeVanda *et al.*, 1976. q, Plaksin *et al.*, 1972; Cooper and Calvin, 1977.

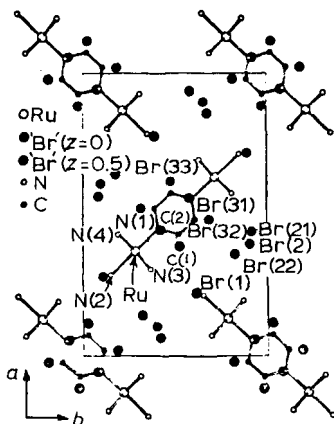


FIG. 10. The crystal structure of $[(\text{NH}_3)_5\text{Ru}(\text{pz})\text{Ru}(\text{NH}_3)_5]\text{Br}_{10/3}\text{Cl}_{5/3}\cdot 4\text{H}_2\text{O}$ (Beattie *et al.*, 1977).

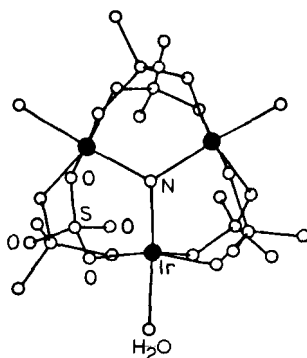
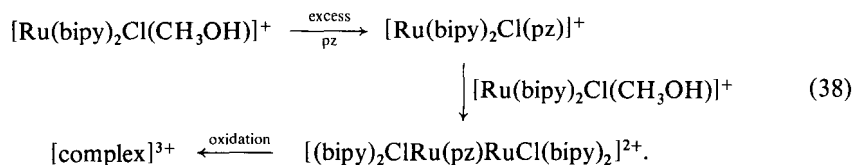


FIG. 11. The molecular structure of $[\text{Ir}_3\text{N}(\text{SO}_4)_6(\text{H}_2\text{O})_3]^{4-}$ (Ciechanowicz *et al.*, 1971).

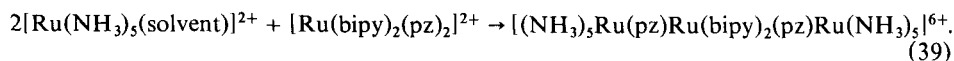
$[\text{Ir}_3\text{N}(\text{SO}_4)_6(\text{H}_2\text{O})_3]^{4-}$ (Fig. 11) in which the three Ir atoms appear to have identical environments (Ciechanowicz *et al.*, 1971) although the optical and Mössbauer spectra were interpreted as consistent with a trapped Ir(III,III,IV) formulation (Brown *et al.*, 1970).

Preparation and thermodynamics

Preparation of binuclear complexes, principally by Taube, Meyer, Ludi and their coworkers, is normally accomplished by combining appropriate mononuclear complexes containing labile solvent molecules and taking advantage, where possible, of the substitution-inertness of low spin d^6 ions, for example (Meyer, 1978)



Longer chains can also be built up in this way (Powers *et al.*, 1976):



Another method would be to mix two single valence binuclear complexes, e.g. Ru(III,III) and Ru(II,II) and take advantage of a favourable conproportionation constant K_c :



Values of K_c are derived from the difference between the reduction potentials of the two reactions $(\text{III,III}) + e \rightarrow (\text{II,III})$ and $(\text{II,III}) + e \rightarrow (\text{II,II})$, the latter usually obtained by cyclic voltammetry. Measured K_c 's range all the way from the statistical value for 4 for $[(\text{CN})_5\text{Fe}(\text{BPE})\text{Fe}(\text{CN})_5]^{5-}$ (Felix and Ludi, 1978) through intermediate ones, e.g. 4×10^6 for the CT complex (Taube, 1978), up to 10^{20} for $[(\text{NH}_3)_5\text{Os}(\text{N}_2)\text{Os}(\text{NH}_3)_5]^{5+}$.

It is tempting to ascribe increasing values of K_c to increased interaction between the two metal ion sites, thus stabilizing the mixed valency complex, and in the case of the Os complex this is clearly true since $[(\text{NH}_3)_5\text{Os}(\text{N}_2)]^{3+}$ loses N_2 in aqueous solution at room temperature at a specific rate of 2×10^{-2} seconds (Elson *et al.*, 1970) while the mixed valency complex is produced from a solution heated at 70°C for 36 hours! Furthermore the N-N stretch in $[(\text{NH}_3)_5\text{Os}(\text{N}_2)\text{Os}(\text{NH}_3)_5]^{5+}$ is inactive in the infrared, though it appears strongly in the Raman spectrum at 1993 cm^{-1} (compare 2037 cm^{-1} in $[(\text{NH}_3)_5\text{Os}(\text{N}_2)]^{2+}$ and 2217 cm^{-1} in $[(\text{NH}_3)_5\text{Os}(\text{N}_2)]^{3+}$). Add to this the complexity of the near infrared electronic transitions which bear no resemblance to any in the Os(II) and Os(III) monomeric precursor complexes, and it seems quite clear that we have a RD class III system.

On the other hand, as Taube (1978) has pointed out, the seemingly high value of K_c for the CT complex must be interpreted with care. Consider the reduction potentials in Table 4. Adding a cation to the terminal N atom of the pyrazine renders the monomeric Ru(III) complex more oxidizing since $d \rightarrow \pi^*$ donation is enhanced in the corresponding Ru(II) state. Thus, adding CH_3 to the pyrazine increases the $3+/2+$ potential from 0.49 to 0.90 V. The Ru(III),Rh(III) complex likewise has a higher potential for reduction, while the Rh(IV) \rightarrow Rh(III) and Rh(III) \rightarrow Rh(II) couples are respectively much more oxidizing and reducing. Note, however, that the reduction potential of the CT complex is only 0.05 V lower than that of the Ru(III), Rh(III) dimer, suggesting that stabilization of the Ru(III,II) dimer by the hole in the πd is only about 1.2 kcal. Considering also the Ru(III,II) \rightarrow Ru(II,II) couple in the CT complex, the low value of 0.37 V shows that it is actually easier to extract an electron than from the monomeric Ru(II) complex, perhaps by as much as 0.2 V if the inductive effect of the other cation is taken into account. This suggests that there is some electronic factor, possibly electron repulsion arising from simultaneous delocalization of two πd electrons from opposite ends of the Ru(II,II) dimer into the pyrazine π^* -system, which is serving to destabilize the (II,II) oxidation, and that

TABLE 4. Reduction potentials of Ru(III), Ru(III,III) and Ru(II,III) complexes (Taube, 1978)

		E_f
I	$(\text{NH}_3)_5\text{Ru}(\text{pz})^{3+/2+}$	0.49
II	$(\text{NH}_3)_5\text{Ru}(\text{pz}-\text{CH}_3)^{3+/2+}$	0.90
III	$(\text{NH}_3)_5\text{Ru}(\text{pz})\text{Rh}(\text{NH}_3)_5^{6+/5+}$	0.79
IV	$(\text{NH}_3)_5\text{Ru}(\text{pz})\text{Rh}(\text{NH}_3)_5^{6+/5+}$	0.74
V	$(\text{NH}_3)_5\text{Ru}(\text{pz})\text{Rh}(\text{NH}_3)_5^{5+/4+}$	0.37

it is this effect, rather than any intrinsic stability in the (II,III) state, which accounts for the high K_c .

Nevertheless, in general smaller values of K_c correspond to weaker interaction between the two centres so that, in the limit that they behave independently, and oxidation at one end of the molecule is not correlated with oxidation of the other, the two oxidation potentials are governed only by statistical considerations. Such an evolution was observed in the cyclic voltammograms of a series of biferrocenes with different bridging groups, as in Table 5.

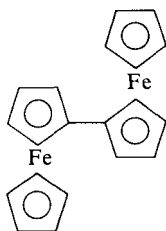
TABLE 5. Differences ($\Delta E_{1/2}$) between successive reduction potentials (III,III) \rightarrow (III,II) and (III,II) \rightarrow (II,II) of $(C_5H_5)Fe(C_5H_4)-X-(C_5H_4)-Fe(C_5H_5)$

X	$\Delta E_{1/2}(V)$	Ref.
$-C(CH_3)_2-C(CH_3)_2-$	0	a
$-CH=CH- \quad O \quad CH=CH-$	0	a
$-Hg-$	0	a
$-CH_2-CH_2-$	0.04	a
$-C\equiv C-C\equiv C-$	0.10	b
$-C\equiv C-$	0.13	b
$-CH_2-$	0.17	a
directly bonded (noX)	0.33, 0.35	a, b
two direct bonds (bis-fulvalene-diiron)	0.59	a, b

a. Morrison *et al.*, 1973.

b. LeVanda *et al.*, 196

For biferrocene itself, or when the bridging group between the two cyclopentadienyl (cp) rings is conjugated, e.g. $-C\equiv C-$, two separate one-electron oxidation waves are seen, but when it is larger, e.g. $-CH_2CH_2-$, only a single wave is observed (Morrison, Krogsund and Hendrickson, 1973). Even when there is direct bonding between the two cp rings, other physical evidence such as Mössbauer (Morrison and Hendrickson, 1973) infrared and optical spectroscopy suggests that the Fe(II,III) biferrocenes remain class II, probably because the two subunits are connected in a *trans* fashion:



If both cp rings are fused together, though, as in the bis(fulvalene) diiron monocation, it appears that the two Fe atoms are equivalent, at least on the time-scale of Mössbauer spectroscopic transitions, i.e. the dimer is now class III, despite the fact that the Fe atoms remain separated by almost 4 Å. Clearly interaction through the π - and π^* -orbitals of the ligand must play an important role (LeVanda *et al.*, 1976).

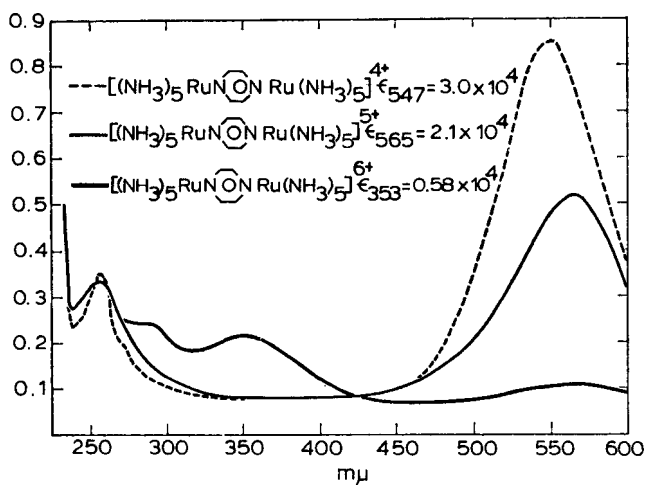
The Creutz-Taube complex: class II or III?

Most notoriously difficult of the mixed valency dimers to classify as class II or class III has been the Creutz-Taube (CT) complex itself, for which a host of conflicting evidence and views now exists. A brief summary of the present state of knowledge is appropriate.

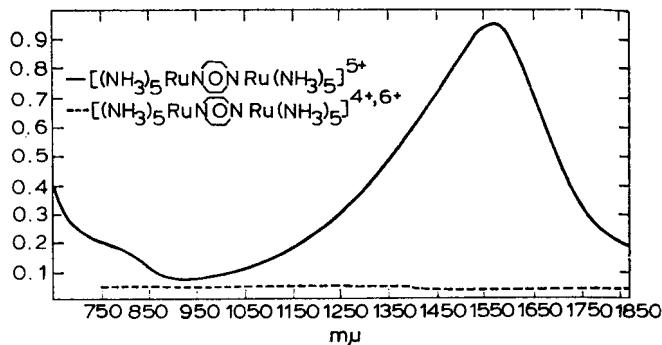
PETER DAY

171

1. *Optical properties.* Like all Ru(II) complexes with aromatic heterocyclic ligands, the Ru(II,II) CT complex has an intense absorption in the visible assigned as a $d \rightarrow \pi^*$ charge transfer, which is also present in the monomeric Ru(II) pz complexes such as I and II in Table 4. As shown in Fig. 12 the band is absent from the Ru(III,III) CT complex but does appear, with roughly half the Ru(II,II) intensity, in the Ru(II,III) spectrum (Creutz and Taube, 1973). This certainly appears to support the idea that on the timescale of an optical transition (say 10^{-14} seconds) a distinct Ru(II) entity can be identified. However, the intervalence band centred at 6400 cm^{-1} (absent, of course, from the (II,II) and (III,III) complexes) is almost invariant to changes in the solvent's dielectric constant, in contrast to the bands in more weakly coupled Ru(II,III) dimers, such as those bridged by 4,4'-bipyridyl, whose energies follow Eq. (12) quite satisfactorily (Tom, Creutz and Taube, 1974). It is also worth noting that the intervalence band is quite a bit narrower than in Ru(II,III) known to be of class II type.



(a)



(b)

FIG. 12. Absorption spectra (a) in the visible and (b) in the near infrared of the Creutz-Taube complex (Creutz and Taube, 1969).

2. *Photoelectron spectrum.* Citrin (1973) measured the XPS spectrum of the CT complex in the Ru 3d region for all three levels of oxidation. Unfortunately the C 1s ionization from the pyrazine and organic counterion obscured part of the spectrum, which had to be 'deconvoluted'. Nevertheless the spectra of the (II,II) and (III,III) complexes each appear to consist of a doublet, due to $3d_{3/2}$ and $3d_{5/2}$ while in the (II,III) there are two doublets separated by 2 eV. Thus it appears at first sight that on this timescale (10^{-16} seconds) individual oxidation states can be distinguished. Quite recently Citrin and Ginsberg (1981) remeasured the XPS spectra, extending the data to the Ru 3p peaks, which are not covered by ionization peaks from other elements, and also taking particular care to avoid radiation damage. They confirm that there are indeed two sets of core level ionization peaks in the (II,III) complex, with equal intensities and with binding energies close to those in the (II,II) and (III,III). A naïve interpretation of these facts is that the CT complex is class II, but a further subtlety must be remarked.

Hush (1975) has argued that two sets of ionization peaks might still be observed even if there were complete charge delocalization. Upon creation of a core hole by photoionization the valence shell orbital relaxes strongly, even if originally delocalized, and the system becomes localized. Then there are two final states of photoionization, a lower one having the valence electron localized on the same centre as the core hole and one of higher energy in which the valence electron is on the other centre. In Hush's treatment the intensities of the two peaks depend on the extent to which the charge is localized and the observed ratio of 1.0 would indicate localization. However, Citrin and Ginsberg (1981) note that the electronic coupling integral, V_{01} (or ϵ in the PKS model) is bound to be different in the photoionized state than in the ground state. If, as is likely, it is much smaller then it turns out that the ratio of the intensities of the two photoionization peaks should be 1.0 irrespective of whether the complex is class II or III, i.e. core-shell photoelectron spectroscopy cannot be used to distinguish the extent of the localization or delocalization in the valence shell. It is interesting to note that the idea of localization by core hole polarization in a photoionized state was suggested by Friedel (1969) for metals and has also been used to account for splittings in the XPS of metallic (i.e. indubitably class III) tungsten bronzes (Chazalviel *et al.*, 1977).

3. *Vibrational spectra.* The first infrared spectra of the CT complex were measured on the tosylate salt (Creutz and Taube, 1973) and there was some difficulty in disentangling parts of the spectrum of the cation from that of the anion. Some indication was found, however, that the symmetric NH_3 rocking frequency in the (II,III) complex was intermediate between (II,II) and (III,III) rather than a superposition of the two. Later measurements by Beattie, Hush and Taylor (1976) on the bromide salt confirmed that the rocking mode was at 800 cm^{-1} in the (II,III) ion compared with 750 and 840 cm^{-1} in (II,II) and (III,III), and a further Ru– NH_3 band at 449 , compared with 438 and 461 cm^{-1} . Similarly, a band attributed to an Ru–pz stretching mode was at 316 cm^{-1} compared with 310 and 320 in the two single valence ions, though in this case the energy difference between the bands is not much greater than their halfwidths. Thus there appears to be some evidence that the CT complex is delocalized on the timescale 10^{-12} – 10^{-13} seconds. However, it has been claimed (Strekas and Spiro, 1976) that irradiating into the visible electronic absorption band, assigned above to Ru(II)d \rightarrow pz π^* charge transfer, causes resonance enhancement of a Raman transition corresponding to an Ru(II)–pz stretching mode. Further experiments of this kind would be most welcome.

4. *Mössbauer spectrum.* In principle one could use the Mössbauer spectrum to distinguish whether the electron transfer rate (given, for example, by Eq. (9)) is greater or less than the nuclear excited state decay time for the element in question. Clear-cut instances of both extremes are found among Fe(II,III) compounds— $\text{Fe}_2\text{F}_5\cdot 7\text{H}_2\text{O}$ is class I (Walton *et al.*, 1976) and bis(fulvalene)diiron monocation (Morrison and Hendrickson, 1973) is class III

for example—but application of the technique to the CT complex has been less than satisfying. ^{99}Ru has only a low recoilless fraction above 4.2 K so spectra can only be recorded at that temperature. Furthermore the only published spectrum of the CT complex was obtained with a very small sample (Creutz, Good and Chandra, 1973), and consequently poor statistics. Nevertheless it proved possible to fit it to a convolution of three peaks, one assigned to low-spin Ru(II) with a 1A_1 ground state and the other pair to Ru(III), split by the quadrupole interaction in the $I = 3/2$ nuclear excited state. It would be very desirable to repeat these measurements to improve the signal-to-noise ratio, but even so, there seems little doubt that a class II ground state has been observed at 4.2 K.

5. *Magnetic susceptibility.* No data are available for the (II,III) ion but the moment of the (III,III) dimer varies with temperature from 300 down to 15 K in a manner which parallels that of $\text{Ru}(\text{NH}_3)_6\text{Cl}_3$ (Bunker *et al.*, 1978). This has been taken as evidence, first that the oxidized dimer contains two unpaired electrons of essentially Ru 4d type and, second, that there is only a very weak interaction between them. The moment of the dimer falls very rapidly below 15 K but it is not known whether this is due to intramolecular or intermolecular antiferromagnetic coupling. In either case the argument is that since the unpaired spins in the (III,III) complex scarcely interact, it would be remarkable if the single unpaired spin in the (II,III) dimer were delocalized between the two metal atoms.

6. *Paramagnetic resonance.* The first e.p.r. measurements on the CT complex to be published were those of Bunker *et al.* (1978) who used frozen solutions in Me_2SO : glycerol at 24 K. They found that the (III,III) dimer had $g_{\perp} = 2.68$, almost the same as that of a Ru(III) pz monomeric complex and also $\text{Ru}(\text{ethylenediamine})_3^{3+}$ which had been measured earlier in a single crystal. The four NH_3 ligands around each Ru in the CT complex lie at 45° to the pyrazine plane so with X as the Ru–Ru axis, Z normal to the pz plane and Y within the plane the relevant one-electron orbitals are

$$\begin{aligned} |a\rangle &= (1/\sqrt{2})(|z^2 - y^2\rangle + i|xy\rangle) \\ |b\rangle &= (1/\sqrt{2})(|z^2 - y^2\rangle - i|xy\rangle). \end{aligned} \quad (41)$$

Expressions relating the observed g-values to the splitting of an octahedral $^2T_{2g}$ ground term by tetragonal distortion and spin-orbit coupling were given by Stevens (1953) in the form

$$\begin{aligned} g_{\parallel} &= 2|(1+k)\cos^2\alpha - \sin^2\alpha| \\ g_{\perp} &= 2|\sqrt{2}k\cos\alpha\sin\alpha + \sin^2\alpha| \end{aligned} \quad (42)$$

where $\tan 2\alpha = \sqrt{2}(\frac{1}{2} - t/\zeta)^{-1}$. The parameter t is the energy difference between the $^2B_{2g}$ and 2E_g components of $^2T_{2g}$ in the tetragonal field, ζ is the spin-orbit coupling constant, equal to -1050 cm^{-1} and k is the orbital reduction factor. The predicted variation of g_{\parallel} and g_{\perp} with t/ζ is shown in Fig. 13 for $k = 1.0$ and 0.96 . The measured g_{\perp} was 2.68. Bunker *et al.* could not observe g_{\parallel} and therefore they assumed that it was very low, corresponding to $t/\zeta \sim 1$, a value consistent with a localized ground state having g_{\parallel} aligned parallel to the X (Ru–Ru) axis, along which the crystal structure demonstrates that there is indeed an axial compression. Quite recently, however, Hush, Edgar and Beattie (1980) re-examined the e.p.r. spectrum of the CT complex using a single crystal instead of a frozen solution. They confirmed $g_{\perp} = 2.632 \pm 0.005$ but in addition found $g_{\parallel} = 1.334 \pm 0.010$. From Fig. 13 these values would define $t/\zeta \sim 2.3$. Furthermore the g_{\parallel} component is actually aligned along the Z axis, i.e. perpendicular to the plane of the pz and to the Ru–Ru axis. Hush *et al.* (1980) note that this is exactly what would be expected if the electronic structure were dominated by strong $d\pi$ – $p\pi$ bonding, and is hence quite compatible with a delocalized ground state. What is not clear, however, is that the result is definitely incompatible with a weakly delocalized state.

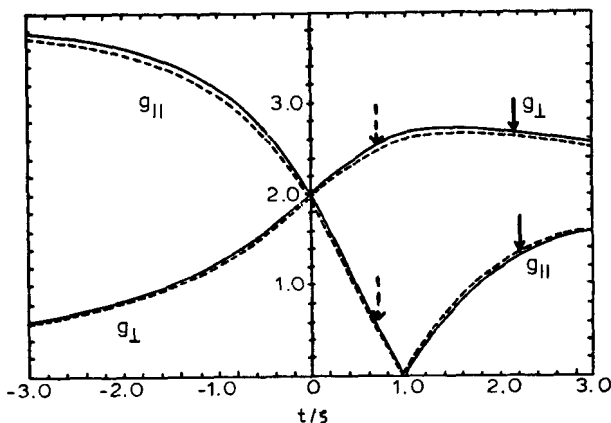


FIG. 13. Calculated g_{\parallel} and g_{\perp} for the Creutz-Taube complex as a function of t/ζ . (—) orbital reduction factor $k = 1.0$ and (---) for $k = 0.96$. (---) indicate g -values from Bunker *et al.* (1978) and (—) from Hush *et al.*, 1980.

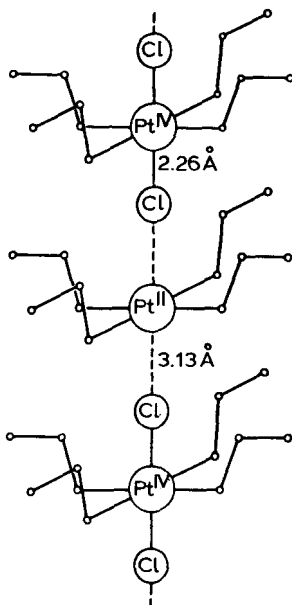


FIG. 14. The structure of Wolfram's Red Salt (Craven and Hall, 1961).

7. *Nuclear magnetic resonance.* Methanol- Me_2SO solutions of the CT complex in all three states of oxidation show a single broad resonance due to the p protons, that in the (II,III) ion being intermediate both in chemical shift and linewidth between those of the two single valency ions (Bunker *et al.*, 1978). Consequently the (II,III) is delocalized on the n.m.r. timescale (say 10^{-6} seconds) at -80°C .

We have gone into considerable detail about the evidence obtained from a wide range of physical methods about the extent of electron delocalization in the CT complex because,

PETER DAY

175

TABLE 6. Estimates of the ground state of the Creutz-Taube complex $[(\text{NH}_3)_5\text{Ru}(\text{pz})\text{Ru}(\text{NH}_3)_5]^{5+}$ by various experimental methods

	Timescale (seconds)		Ref.
Core-shell photoionization	10^{-16}	Uncertain	a
Pz π - π^* and Ru d \rightarrow π^* absorption	10^{-14}	Localized	b
Intervallence transition	10^{-13}		
Solvent dependence		Delocalized	c
Bandshape		Borderline, delocalized	d
Infrared spectrum	10^{-12}	Uncertain, probably localized	e
Resonance Raman spectrum	10^{-12}	Localized	f
Paramagnetic resonance	10^{-9}	Uncertain, probably delocalized	g
NMR	10^{-7}	Delocalized	h
Mössbauer spectroscopy	10^{-6}	Localized	i
Crystal structure		Delocalized	j

a, Citrin, 1973; Hush, 1975; Citrin and Ginsberg, 1981. b, Creutz and Taube, 1969; Mayoh and Day, 1972, 1974. c, Creutz and Taube, 1973. d, Piepho *et al.*, 1978; Beattie *et al.*, 1976. e, Creutz and Taube, 1973; Beattie *et al.*, 1976. f, Streckas and Spiro, 1976. g, Bunker *et al.*, 1978; Hush *et al.*, 1980. h, Bunker *et al.*, 1978. i, Creutz *et al.*, 1973. j, Beattie *et al.*, 1977.

in the minds of many workers in the field, it has evidently taken on the character of a paradigm case. Some of the lines of evidence certainly conflict, partly because of the enormous range of timescales they encompass but partly, too, because of problems about the detailed interpretation of the experiments themselves (e.g. XPS and e.p.r.). Table 6 attempts a summary of the conclusions now current concerning the nature of the CT ion, together with the timescales sampled by the various techniques. The best that can be said at present is that the electron transfer rate is certainly greater than 10^5 seconds $^{-1}$ and probably greater than 10^{12} seconds $^{-1}$. It must be emphasized very forcibly, though, that the very existence of such a conflict of evidence as we have described means that the CT complex certainly lies near the borderline between classes II and III and thus is very far from being a typical case. In almost all other dimeric or oligomeric mixed valency complexes the various strands of evidence agree quite firmly on localization over the longest timescales available experimentally, or delocalization over the shortest. Indeed, given the very large number of mixed valency complexes whose properties have now been studied it is quite remarkable how few have electron transfer rates lying within the range spanned by the various spectroscopic methods. Interesting recent exceptions to this generalization are the temperature dependent Mössbauer spectra of the trinuclear basic acetate $\text{Fe(II)Fe(III)}_2\text{O}(\text{CH}_3\text{COO})_6(\text{H}_2\text{O})$ (Dziobkowski, Wroblewski and Brown, 1981) and the temperature dependent e.p.r. of the Mo(V,VI) heteropolyblue anion $\text{Mo}_6\text{O}_{19}^{3-}$ (Che, Fournier and Launay, 1979), in both of which one finds evidence for rapid electron hopping at room temperature, but localization on to a single site at 77 K.

One-dimensional complexes

After discrete dimeric or oligomeric molecules, the infinite lattice systems containing interacting mixed valency metal ions which might be expected to be the easiest to understand in detail are those in which the interactions extend only in one dimension, i.e.

linear chain compounds. Very many inorganic and metal-organic compounds form lattices containing chains of closely-spaced metal ions, and their physical properties cover the whole gamut from insulators containing essentially non-interacting metal ions, through substances with appreciable magnetic exchange interactions all the way to the now famous one-dimensional metallic conductors. It is the peculiar properties of the latter which has focused so much attention on one-dimensional mixed valency compounds. I have drawn attention to correlations between structure and physical properties in both single and mixed valency metal chain compounds in other articles (Day, 1974, 1975, 1977, 1978), and will not repeat the discussion here. Suffice it to say, in the present context, that there are two major categories of mixed valency metal chain complexes, namely those in which the metal atoms along the chain alternate with bridging anions, and those in which the chain is composed solely of metal atoms. Evidence to be briefly summarized here leads to the conclusion that all the former are of class II type while all the latter belong to class III.

Class II complexes with bridging anions: Wolfram's Red Salt

The prototype mixed valency chain compound with anion bridging groups is Wolfram's Red Salt, $[\text{Pt}(\text{C}_2\text{H}_5\text{NH}_2)_4][\text{Pt}(\text{C}_2\text{H}_5\text{NH}_2)_4\text{Cl}_2]\text{Cl}_4 \cdot 4\text{H}_2\text{O}$, (WRS) whose structure is shown in Fig. 14. Like so many of the mixed valency compounds first prepared in the last century, its trivial name emphasizes its colour, which is in striking contrast to the colours of its two constituent complexes of Pt(II) and Pt(IV). In all the compounds of this kind the dominant structural motif is a square of ligands around each Pt, with its plane perpendicular to the axis of the chain. The ligands may be NH_3 , RNH_2 ($\text{R} = \text{alkyl}$), $\text{H}_2\text{N}(\text{CH}_2)_2\text{NH}_2$ or halide ions as in $\text{Pt}(\text{NH}_3)_2\text{Cl}_3$. In every case however, the stacking of these planar units is accomplished via halide ion bridges, so that the 'operative' part of the linear structure consists of a diatomic chain. However, the feature of greatest importance in determining the electronic behaviour of the chain is that the chain is not uniform, but dimerized. The Pt-X distances alternate so as to produce two distinct Pt sites, one with four planar ligands and two axial halide ions much more distant, the other also with four planar ligands but now with the two axial halide ions much closer. Table 7 collects structural data about some of these compounds. Although there is some variation within each set with the counter-ion or equatorial ligands, there is a clear trend towards equalizing the Pt-X and Pt...X bond lengths as one passes from Cl to Br to I (average values of ρ are 0.72 ± 0.10 for Cl, 0.82 ± 0.14 for Br and 0.93 ± 0.02 for I). Nevertheless, in all compounds of the WRS type the two Pt sites are clearly distinguishable, so class II mixed valency behaviour is to be expected. Briefly we now survey the evidence from physical properties.

1. *Photoelectron spectroscopy.* Burroughs *et al.* (1975) made a very careful study of $(\text{Pt}(\text{en})\text{Cl}_2)(\text{Pt}(\text{en})\text{Cl}_4)$ (en = ethylenediamine) in the Pt 4f region. They found that the spectrum consisted of three peaks (Fig. 15) which, however, could be deconvoluted into two pairs arising from 4f(5/2) and 4f(7/2) spin-orbit components from Pt(II) and Pt(IV). In Fig. 15 we also reproduce the 4f region of $\text{Pt}(\text{en})\text{Cl}_4$, showing the single pair of spin-orbit components from Pt(IV). Interpretation of the XPS of this type of compound is not quite so straightforward as it may appear because, as is well known, the technique is extremely sensitive to surface impurities and mixed-valency compounds especially are liable to oxidize or reduce superficially, either in the atmosphere or under X-ray bombardment. Indeed, starting with $\text{Pt}(\text{en})\text{Cl}_4$, Burroughs *et al.* were able to demonstrate that increasing exposure to the Al K α exciting radiation produced XPS signals first of $\text{Pt}(\text{en})\text{Cl}_4$, then of the mixed valency compound $(\text{Pt}(\text{en})\text{Cl}_2)(\text{Pt}(\text{en})\text{Cl}_4)$ and finally of

PETER DAY

177

TABLE 7. Structural data on compounds of the Wolfram's Red Salt (WRS) type

Axial bridging ligand	Equatorial ligand(s)	Counter-ion	Pt-X(Å) ^a	Pt...X(Å) ^a	Pt-Pt ^b	ρ^c	Ref.
Cl	C ₂ H ₅ NH ₂	Cl, H ₂ O	2.26	3.13	5.39	0.72	d
Cl	H ₂ N(CH ₂) ₃ NH ₂	BF ₄	2.30	3.10	5.40	0.74	e
Cl	H ₂ N(CH ₂) ₂ NH ₂	CuCl ₄	2.33	2.93	5.26	0.79	f
Cl	NH ₃ , Cl	—	2.03	3.30	5.33	0.61	g
Br	C ₂ H ₅ NH ₂	Br	2.28, 2.68	3.41, 3.81	6.09	0.69	h
Br	C ₂ H ₅ NH ₂	Br, H ₂ O	2.45, 2.48	3.11, 3.14	5.59	0.79	i
Br	H ₂ N(CH ₂) ₂ NH ₂	ClO ₄	2.71	2.76	5.47	0.98	j
Br	H ₂ N(CH ₂) ₂ NH ₂	ClO ₄	2.55	2.96	5.51	0.86	e
Br	H ₂ NCH(CH ₃)CH ₂ NH ₂	Cu ₃ Br ₅	2.55	3.07	5.62	0.83	k
Br	NH ₃ , Br	—	2.50	3.03	5.53	0.83	l
Br	H ₂ N(CH ₂) ₂ NH ₂ , Br	—	2.48	3.12	5.60	0.79	m
I	I	K	2.74	3.00	5.74	0.91	n
I	H ₂ N(CH ₂) ₂ NH ₂	ClO ₄	2.79	3.04	5.83	0.92	o
I	H ₂ NCH(CH ₃)CH ₂ NH ₂	ClO ₄	2.77	2.96	5.73	0.93	p
I	H ₂ NCH(CH ₃)CH ₂ NH ₂	I	2.81	2.99	5.80	0.94	j

a, Short and long Pt-halide distances along the chain. b, closest Pt-Pt distance along the chain. c, (Pt-X)/(Pt...X). d, Craven and Hall, 1961. e, Matsumoto *et al.*, 1978. f, Endres *et al.*, 1979. g, Wallen *et al.*, 1962. h, Endres *et al.*, 1980. i, Brown and Hall, 1976. j, Endres *et al.*, 1980. k, Keller *et al.*, 1978. l, Hall and Williams, 1958. m, Ryan and Rundle, 1961. n, Thiele, 1977. o, Endres *et al.*, 1980. p, Breer *et al.*, 1978.

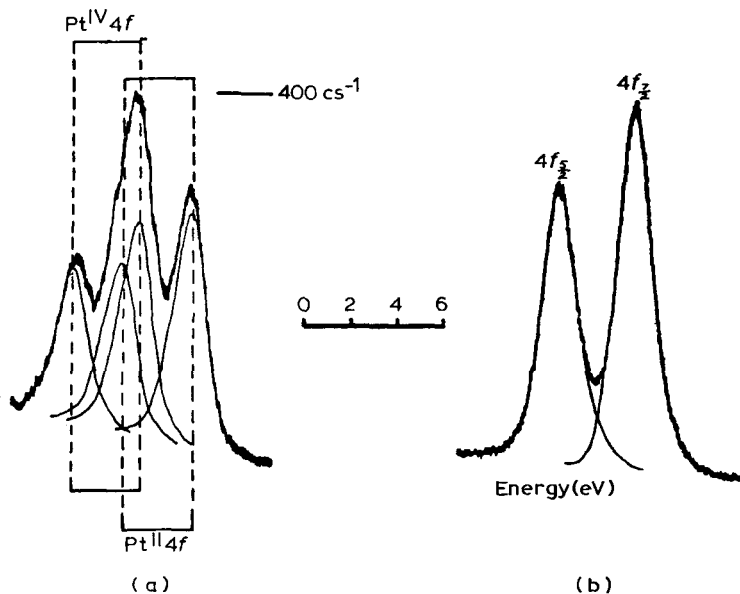


FIG. 15. XPS of (a) [Pt(en)Cl₂][Pt(en)Cl₄], (b) Pt(en)Cl₂ in the Pt 4f region (Burroughs *et al.*, 1975).

Pt(en)Cl₂. Such radiation-induced reactions at the surface are quite common, and constitute a hazard to interpreting the XPS of many other mixed valency compounds. Examples which have been investigated quite thoroughly in this way include Cs₂SbCl₆ (Tricker *et al.*, 1972, Burroughs *et al.*, 1974) and Sb₂O₄ (Orchard and Thornton 1977). Nevertheless, it seems quite clear that all the WRS group of compounds have separate

XPS signals from Pt(II) and Pt(IV), though it has been claimed by Yamashita *et al.* (1978) that the difference in 4f bridging energy at the two sites decreases as the bridging anion is changed from Cl to Br to I, following the diminished difference between the Pt–X and Pt...X bond lengths.

2. *Optical spectroscopy.* The red colour of WRS (and the green colour of Reihlen's Green Salt, its bromide analogue!) has its origin in an extremely intense absorption band covering most of the visible region of the spectrum. Because the absorption is so strong the transmission spectra of single crystals of these compounds are very hard to measure. The early work of Yamada and Tsuchida (1956) in this field is marred by stray light, which entered their spectrometer and obscured the upper parts of the absorption bands. More recently it proved possible to record the polarized transmission spectrum of a microscopic single crystal of WRS (Fig. 16) using condensing optics and cooling the crystal in a helium gas flow tube (Crabtree, 1972). The absorption in the visible is almost entirely confined to the spectrum recorded with the electric vector parallel to the metal chains, with the exception of the small band at 3900 Å, assigned as the first ligand field transition of the $[\text{Pt}(\text{C}_2\text{H}_5\text{NH}_2)_4\text{Cl}_2]^{2+}$ moiety. The intense absorption with $E//c$ appears composite (a point of some importance in interpreting the resonance Raman enhancement profiles, see below) but it does not seem to be an artifact resulting from stray light or incomplete polarization. The most convenient way to derive the optical properties of highly absorbing materials is to measure normal-incidence reflectivity spectra, a technique which has been applied to salts of the WRS type by Breer *et al.* (1978) and Papavassiliou and Zdetis (1980). One such spectrum is shown in Fig. 17. With the electric vector of the incident light perpendicular to the chain axis the reflectivity is low and constant throughout the visible and near infrared but when it is parallel to the chain axis there is a broad peak. The reflectivity can be written (e.g. Anex and Simpson, 1960) in terms of the complex dielectric constant ϵ as

$$R = \frac{1 + |\epsilon| - [2(|\epsilon| + \epsilon_1)]^{1/2}}{1 + |\epsilon| + [2(|\epsilon| + \epsilon_1)]^{1/2}} \quad (43)$$

where ϵ_1 and ϵ_2 are the real and imaginary parts of ϵ , i.e.

$$|\epsilon| = (\epsilon_1^2 + \epsilon_2^2)^{1/2}. \quad (44)$$

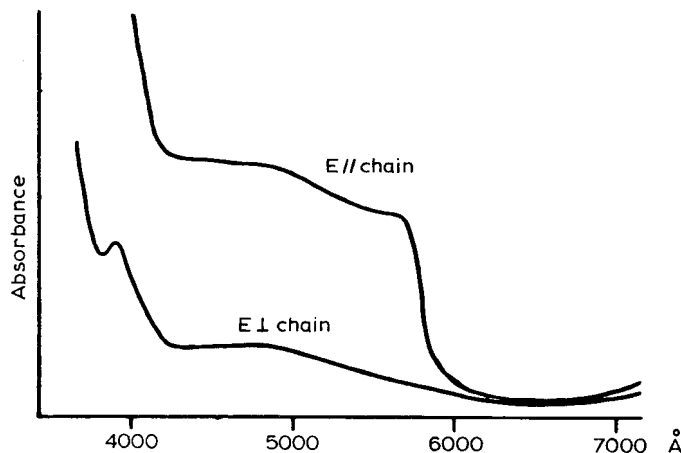


FIG. 16. Polarized absorption spectrum of Wolfram's Red Salt at 4.2 K (Crabtree, 1972).

PETER DAY

179

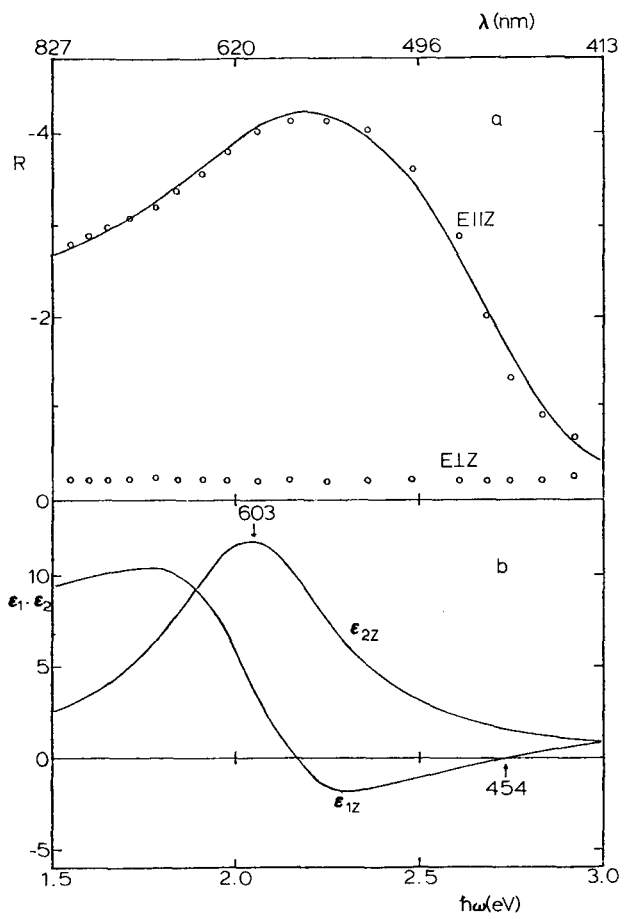


FIG. 17. (a) Polarized reflectivity of $[\text{Pt}(\text{dapn})_2\text{Pt}(\text{dapn})_2\text{Br}_2](\text{ClO}_4)_4$. The circles are experimental points and the full line calculated with the parameters listed in Table 8. (b) Calculated frequency dependence of ϵ_1 and ϵ_2 (Pappavassiliou and Zdetsis, 1980).

It is customary to assume that the frequency dependence of ϵ obeys a damped Lorentzian function:

$$\epsilon(\omega) = \epsilon(\infty) + \frac{\omega_p^2}{\omega_g^2 - \omega^2 - (i\omega/\tau)} \quad (45)$$

where ω_p is the plasma frequency, given by $\omega_p^2 = 4\pi N_0 e^2/m$ (N_0 is the effective electron density and in the effective electron lines), ω_g is the gap frequency and τ is a damping factor, essentially the electronic relaxation time. Pappavassiliou and Zdetsis (1980) used a least-squares procedure to fit the observed reflectivity to Eqs. (43) and (45) so as to derive the optical constants. Their results for $[\text{Pt}(\text{dapn})_2\text{Pt}(\text{dapn})_2\text{Br}_2](\text{ClO}_4)_4$ are shown in Fig. 17b and the full line in Fig. 17a shows the quality of the fit. In Table 8 we give the optical parameters for all three members of this series.

TABLE 8. Optical parameters of the linear chain mixed valency compounds $[\text{Pt}(\text{dapn})_2\text{Pt}(\text{dapn})_2\text{X}_2](\text{ClO}_4)_4$ (dapn = 1,2 diaminopropane) (Pappavassiliou and Zdetsis, 1980)

X	$\epsilon(\infty)$	$\epsilon(0)$	$h\nu_g$ (eV)	$\tau(10^{-13}$ s)
Cl	1.62	2.60	2.61	3.20
Br	3.55	6.81	2.06	1.77
I	1.99	9.07	1.13	1.89

Most striking among the data in Table 8 is the strong dependence of the gap frequency on the bridging halide ion. Given that in their other physical and structural properties the WRS salts are typical class II compounds the excited states listed in Table 8 should be assigned as intervalence transitions, Pt(II) \rightarrow Pt(IV). There has been a lot of discussion since the mid-1960s about the relative ordering of the 5d-based valence shell orbitals in square planar d^8 complexes (e.g. Day *et al.*, 1965; Martin, 1971) but there is now a good consensus that in most cases where strong σ - and π -donor ligands are concerned, the order is as shown on the left hand side of Fig. 18. It is important to notice that both the Pt(II) and Pt(IV) sites in the WRS compounds have D_{4h} point symmetry, and the relative valence shell orbital ordering in a tetragonally distorted six-coordinate Pt(IV) complex is shown on the right hand side of Fig. 18. Appropriate donor and acceptor orbitals for the electron transfer between Pt(II) and Pt(IV) are the respectively filled and empty z^2 orbitals. Note, however, that the Pt–Pt distance along the chain (Table 7) is between 5 and 6 Å, so direct overlap between these orbitals is negligible. Just as in the Ru(II,III) dimers (page 166) we must invoke participation of orbitals on the bridging ligands, most appropriately through the perturbation model for bridging ligands (page 154). The ‘local’ charge transfer excited states which provide the intervalence interaction in that model certainly fall in energy in the order $\text{Cl} > \text{Br} > \text{I}$, and it may be significant that the intervalence transition energies themselves in the $[\text{Pt}(\text{dapn})_2\text{Pt}(\text{dapn})_2\text{X}_2](\text{ClO}_4)_4$ salts (Table 8) decrease by nearly the same amount from X = Cl to Br and X = Br to I as the X \rightarrow M charge transfer transitions in transition metal halide complexes (e.g. Jørgensen, 1970).

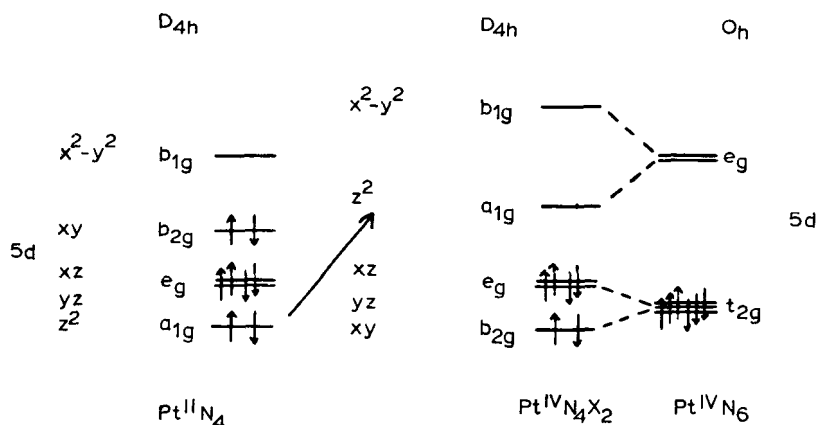


FIG. 18. Ligand field levels of Pt(II) and Pt(IV) in Wolfram's Red Salt. The postulated intervalence transfer is arrowed.

Nevertheless, two points about the intervalence transitions in one-dimensional Pt(II,IV) compounds must be borne in mind. First, the lattices *are* one-dimensional, i.e. they contain infinite chains of metal atoms. Consequently the intervalence states must be treated, strictly speaking, as excitons. Thus, if the ground state of the chain is written as

$$\phi_0 = \phi_1^{\text{II}} \phi_2^{\text{IV}} \phi_3^{\text{II}} \cdots \phi_{2N-1}^{\text{II}} \phi_{2N}^{\text{IV}} \quad (46)$$

where the ϕ are 5d z^2 -based molecular orbitals on the alternating Pt(II) and Pt(IV) centres, a single site intervalence excited state wavefunction would be

$$\phi_n = \phi_1^{\text{II}} \phi_2^{\text{IV}} \cdots \phi_n^{\text{II}} \phi_{n+1}^{\text{IV}} \cdots \phi_{2N-1}^{\text{II}} \phi_{2N}^{\text{IV}} \quad (47)$$

and the exciton wavefunction

$$\phi_n(\mathbf{k}) = N^{-1/2} \sum \exp(i\mathbf{k}\mathbf{r}_n) \phi_n \quad (48)$$

Since transfer of an electron from ϕ_n^{II} to ϕ_{n-1}^{IV} is completely equivalent to transfer to ϕ_{n+1}^{IV} , the exciton wavefunction is a linear combination of the two, so for $\mathbf{k} = 0$

$$\psi_{\pm n}(0) = 2^{-1/2} [\phi_{n+1}(0) \pm \phi_{n-1}(0)]. \quad (49)$$

From the local symmetry one can see that only the transition to $\psi_{-n}(0)$ would be electric-dipole-allowed. The second point which distinguishes these excited states from, e.g. the Ru(II,III) ones, is that the oxidation states of the two metal ions in the ground states differ by two units instead of one. Pairs of potential energy surfaces of the type shown in Fig. 3 are not appropriate, therefore, and have to be replaced by a set of three surfaces as in Fig. 19. Those labelled (II,IV) and (IV,II), in an obvious nomenclature, are orthogonal since they differ by two electrons but either can interact with (III,III), whose minimum lies symmetrically between the other two in the configuration coordinate diagram, but at an unknown energy above them. The same kind of diagram would be needed, of course, to rationalize the optical spectra of other mixed valency compounds in which the oxidation states differ by two units, e.g. Sb(III,V) (page 158).

3. *Vibrational spectra.* The infrared and normal Raman spectra of the WRS compounds are precisely what one would expect of class II mixed valency, namely, vibrational transitions close to being a superposition of those of the Pt(II) and Pt(IV) complexes making up the chains. What is really exceptional and remarkable, however, is the appearance of the resonance Raman spectra excited at frequencies lying inside the intervalence absorption band envelope. A typical example is shown in Fig. 20. The spectrum, which only appears with such enhancement when the electric vector of the exciting light is parallel to the chain, is dominated by a very long progression (up to 18 members) in one

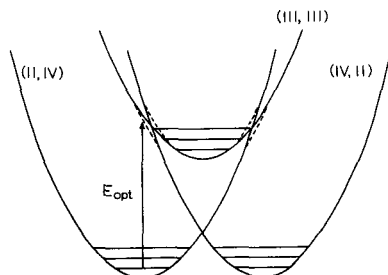


FIG. 19. Potential energy surfaces for Wolfram's Red Salt. The dashed lines indicate regions of 'non-crossing'.

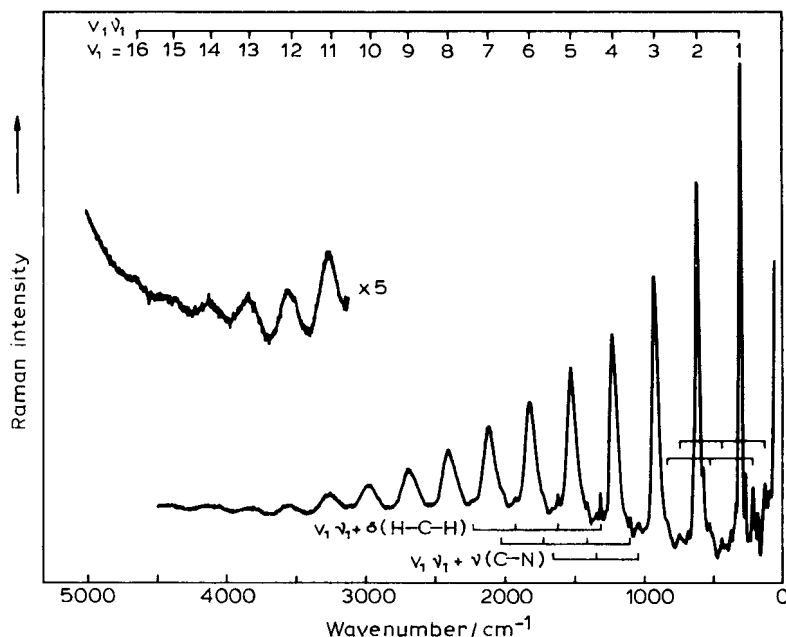


FIG. 20. Resonance Raman spectrum of Wolfram's Red Salt at 80 K (Clark, 1978).

single mode, namely the axial ν_1 X–Pt–X symmetric stretching mode. Clark (1977, 1980) and Pappavassiliou, Layek and Theophanides, (1980) have measured many spectra of this kind which, from the theory of the resonance Raman effect, betoken a very large displacement of the electronically excited state along this particular vibrational coordinate. Of course, this is exactly what one would expect if the excitation is to an intervalence state such as that of Eq. (47) because its relaxed configuration (Fig. 19) would have the axial bridging halide ion midway between the two Pt(III) ions.

Mingardi and Siebrand (1975) showed how to estimate how much the excited state is displaced along the ν_1 vibrational coordinate by measuring the intensities $I_{0(n+1)}/I_{0n}$ of successive resonance Raman lines in the progression. Application of their theory to the WRS compounds is most instructive. Labelling the minimum energies of the ground and excited state potential energy surfaces as E_{00} and E_{10} (as in Fig. 3) the equations of the two surfaces are

$$\begin{aligned} E_0(q) &= E_{00} + (1/2) \mu_0 \omega_0^2 q^2 \\ E_1(q) &= E_{10} + (1/2) \mu_1 \omega_1^2 (q - q_1)^2 \end{aligned} \quad (50)$$

where the μ s are reduced masses, the ω s are the vibrational frequencies in the two states and we assume that E_{00} lies at $q = 0$ while E_{10} is displaced by q_1 along the vibrational coordinate concerned. With these definitions Mingardi and Siebrand (1975) show that

$$(I_{02}/I_{01})^2 \sim g\gamma(0.61g^2 + \gamma)^{-2} \quad (51)$$

where

$$\begin{aligned} g &= (E_{opt} - E_{inc} - i\Gamma)/\hbar\omega_1 \\ \gamma &= (1/2) \mu_1 \omega_1^2 q_1^2/\hbar\omega. \end{aligned} \quad (52)$$

In Eq. (52) E_{opt} is the energy of the Franck–Condon maximum of the intervalence band, as in Fig. 3, while E_{inc} is the energy of the exciting radiation, and Γ is a damping function describing the widths of the individual vibronic lines. Of course, such lines are never observed in intervalence transitions, as we pointed out, so Γ must be estimated. Nevertheless, combining the observed values of E_{opt} ($21\,000\text{ cm}^{-1}$) and ω (319.5 cm^{-1}) for WRS at room temperature, with I_{02}/I_{01} of 0.55 at an excitation frequency of $19\,436\text{ cm}^{-1}$ (Clark, Franks and Trumble, 1976) one finds that $q_1 \sim 0.50\text{ \AA}$. This estimate should be compared with the difference of 0.87 \AA between the Pt(II)–Cl and Pt(IV)–Cl bond lengths in WRS at room temperature, and serves to show that they are indeed almost equalized in the relaxed intervalence excited state. At low temperatures (80 K, Clark, 1980) the ratios I_{02}/I_{01} become even larger, but we have no information on the bond lengths under these conditions.

The theory of Mingardi and Siebrand (1975) was designed to deal with the electronic and vibrational states of molecules, but just as we wrote the wavefunctions of the electronic excited states of the infinite mixed valency chains as Frenkel excitons (Eq. (48)) so it is also strictly correct to write those of the vibrational states as phonons rather than individual X–Pt–X modes. The classical problem of the vibrational modes of a dimerized diatomic chain was solved recently by Paraskevaidis and Papatriantafillou (1980), and should form the basis for the correct solid state solution of the resonance Raman effect in these compounds, taking account of the interactions of the excitons and phonons, much as in continuous lattice semiconductors such as CdS. Such a programme has not yet been carried out, but may provide the answer to a puzzling feature of the resonance Raman spectra, namely, that their excitation profiles do not follow the intervalence absorption profile, at least as measured by powder diffuse reflectance spectroscopy (Fig. 21). On the other hand it may simply be that the excitation profile is following the profile of the imaginary part of the refractive index (compare the excitation profile of Reihlen's Green Salt in Fig. 21 with the ϵ_2 curve of a similar bromide salt in Fig. 17b).

4. *Electrical conductivity.* Corresponding to adiabatic electron transfer in the dimeric Ru(II,III) complexes described earlier, electron transfer along an infinite chain might be detectable as electrical conductivity. Given their highly anisotropic structures, it is no surprise that the conductivity of crystals of WRS type is much larger parallel than perpendicular to the chains. For example $\sigma_{\parallel}/\sigma_{\perp} \sim 300$ was reported for $[\text{Pd}(\text{NH}_3)_2\text{Cl}_2]_n$ – $[\text{Pd}(\text{NH}_3)_2\text{Cl}_4]_m$ by Thomas and Underhill (1969, 1971) but the absolute specific conductivity σ_{\parallel} was low ($3 \times 10^{-9}\text{ }\Omega^{-1}\text{ cm}^{-1}$ at room temperature), as anticipated for a class II compound. With pressure, however, the conductivity rises dramatically, and at 130 kbar has reached $0.2\text{ }\Omega^{-1}\text{ cm}^{-1}$ (Interrante, Browall and Bundy, 1974). Most likely, the increase in conductivity with pressure comes about because the Pt(II)–X and Pt(IV) \cdots X bond lengths move closer to equivalence, so reducing $(E_1 - E_0)$ in Fig. 3. No information has been published about the structures of WRS crystals at high pressure, but it is worth pointing out that in another halide-bridged mixed valency chain compound $\text{Cs}_2[\text{AuCl}_4]_n$ – $[\text{AuCl}_2]_m$ (Well's Salt) there is definite evidence for a shift in the Au(I)–Cl and Au(III)–Cl bond lengths with pressure (Day, Vettier and Parisot, 1978), so that at 60 kbar they become equal (Denner, Schulz and d'Amour, 1978) and the substance is then a metal (Keller, Fenner and Holzapfel, 1974).

Class III chains with directly interacting metal atoms: KCP

In the mixed valency metal chains with halide bridging groups, the halide bridges cause the valence trapping, and hence class II behaviour, in two ways. First they simply separate the metal ions, so they are never less than 5 \AA apart (Table 7). This is much too great a distance for any direct overlap between metal orbitals. The second role of the bridging

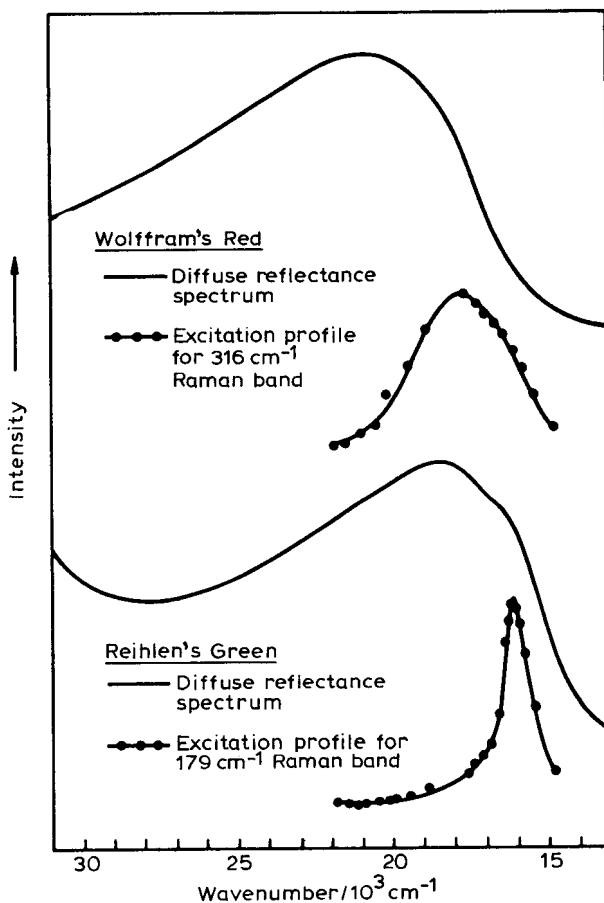


FIG. 21. Resonance Raman enhancement profiles of Wolfram's Red and Reihlen's Green Salts compared with their intervalence band profiles (Clark, 1978).

groups is to introduce the possibility of longitudinal electron-phonon interactions. One may view this question most simply against the background of the Mott-Hubbard model (Hubbard, 1963). If one visualizes a chain of atoms, each having a single unpaired electron, then depending on whether the overlap integral between adjacent orbitals is the dominant factor or, alternatively, the repulsion energy which ensues when one attempts to put two electrons on to the same site, so the ground state wavefunction will either be that of a metal or of a magnetic insulator. There is no room in the simplest version of the Hubbard model for a ground state of the kind actually found in the WRS compounds, namely, a chain containing orbitals which are alternately empty and doubly filled. The only way one could arrive at such a ground state is to include the possibility of trapping the charge fluctuation by relaxing the ligands. This is where the bridging groups come in: remove them and (unless there are differences in the equatorial ligands around the metal sites) the way is open to a metallic ground state.

Still, however, there remains the problem of the one-centre Coulomb repulsion. In a chain containing an integral number of electrons per atom it still costs energy to transfer an electron from one site to another, to create the kind of charge fluctuation needed to

get conduction. But if, on average, the number of electrons per site is not integral, the charge fluctuation is built in already, and the only energy required to get conduction is the energy required to move the fluctuation along the chain. Thus the recipe for metallic conduction in a one-dimensional compound is to have no bridging ligands but directly interacting metal ions, and to ensure that there is a genuinely non-integral number of valence electrons per atom. This is precisely what is found in practice.

Following the first work on the structure and physical properties of the prototype one-dimensional metallic conductor $\text{K}_2\text{Pt}(\text{CN})_4\text{Br}_{0.30}\cdot 3\text{H}_2\text{O}$ (KCP) in the later 1960s (Krogmann and Hausen, 1968; Krogmann, 1969) a very large number of similar compounds have now been prepared and examined. Some reviews on the class of material are listed among the general references at the end of the present review, but it is certainly worth remarking at this point on the extraordinary upsurge of interest in this field among both chemists and physicists. In part this stems from what may, in the end, turn out to be a chimera, namely the realization in practical terms of Little's (1964) recipe for an excitonic (and hence high temperature) superconductor.

Little's model has been subjected to searching theoretical scrutiny over the last 17 years, but has not been found logically wanting. It calls for an electronically conducting chain, at right angles to which are placed groups of polarizable material, for example conjugated organic ligands. Excitons within these side-chains then couple with the electrons moving along the chain (*see* chapters by Little, and Gutefreund and Little, in Keller, 1977, for a recent description of the model). A second reason for the physicists' interest in the KCP salts is that many years ago Peierls (1955), in a very simple and elegant theorem, demonstrated that one-dimensional metallic conductors ought to be inherently unstable to distortions which would open a gap in the electron density-of-states at the Fermi surface, thus rendering them semiconductors. In a word, purely one-dimensional metallic conductors ought not to exist! Here, we shall do no more than review very briefly the evidence about the KCP series, emphasizing the role played by mixed-valency.

A feature common to all compounds of the KCP type is a chain of closely spaced metal atoms formed by stacking square-planar ML_4 complexes, where M is Ni, Pd or Pt and L a ligand such as CN^- , oxalate, diphenylglyoximate or a planar macrocycle like phthalocyanine. Mixed valency is achieved by partially oxidizing the metal ions to an average oxidation state $(\text{II} + x)$, x being usually about 0.3. Partial oxidation is accomplished in two ways. Counter-ions, both cations and anions, occupy channels between the stacks of planar complex ions, often accompanied by water molecules which create a hydrogen-bonded framework and hence link the one-dimensional metallic chains. Mixed valency in the metal chains comes about either by introducing extra anions (as, for example, on going from $\text{K}_2\text{Pt}(\text{CN})_4\cdot 3\text{H}_2\text{O}$ to $\text{K}_2\text{Pt}(\text{CN})_4\text{Cl}_{0.32}\cdot 3\text{H}_2\text{O}$, Fig. 22) or by removing some of the cations (e.g. in $\text{K}_{1.75}\text{Pt}(\text{CN})_4\cdot 1.5\text{H}_2\text{O}$, Fig. 23). Metal complexes of more highly conjugated ligands can be partly oxidized by iodine, which is incorporated in the channels between the metal chains as I_3^- (Gleizes, Marks and Ibers, 1975; Schramm *et al.*, 1980). An example is shown in Fig. 24. If we write a general formula for compounds of this kind as $\text{A}_m\text{ML}_n\text{X}_p(\text{H}_2\text{O})_q$, Table 9 gives a survey of known examples.

Not surprisingly in view of the fact that the average oxidation state has increased, the metal-metal spacings in the mixed valency compounds are all less than in the parent divalent compounds. Average oxidation states in the KCP series cluster around 2.30, and there is quite a good correlation between this quantity and the Pt-Pt spacing, as shown in Fig. 25.

Whilst in a few of the compounds the metal atoms lie on special points in the unit cell, so that the metal-metal spacings are constrained to be equal, in the majority of the KCP series this is not the case (Stucky, Schultz and Williams, 1977). Nevertheless, in most examples the spacings are almost equal within experimental error (e.g. Fig. 23). No differ-

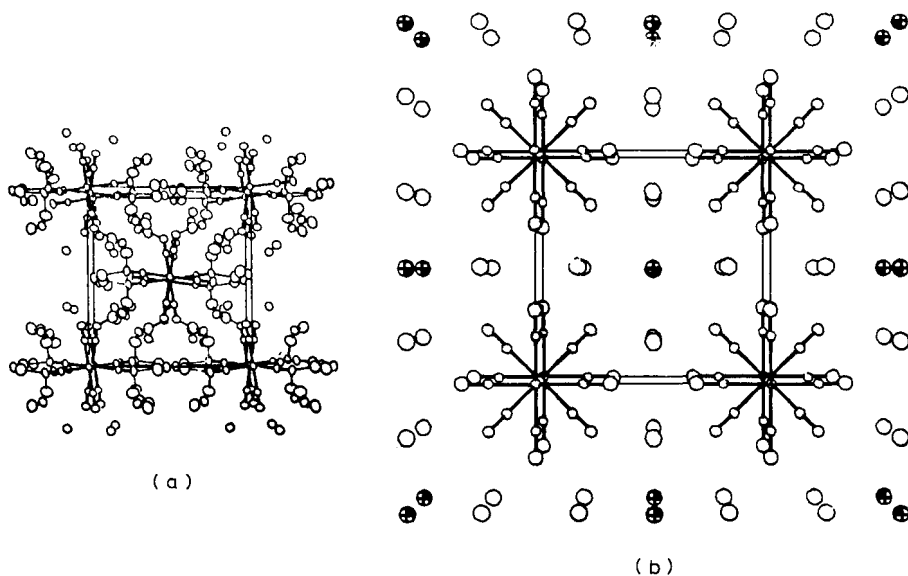


FIG. 22. The crystal structures of (a) $\text{K}_2\text{Pt}(\text{CN})_4 \cdot 3\text{H}_2\text{O}$, (b) $\text{K}_2\text{Pt}(\text{CN})_4\text{Cl}_{0.32} \cdot 3\text{H}_2\text{O}$ (Williams *et al.*, 1974; Washecheck *et al.*, 1976).

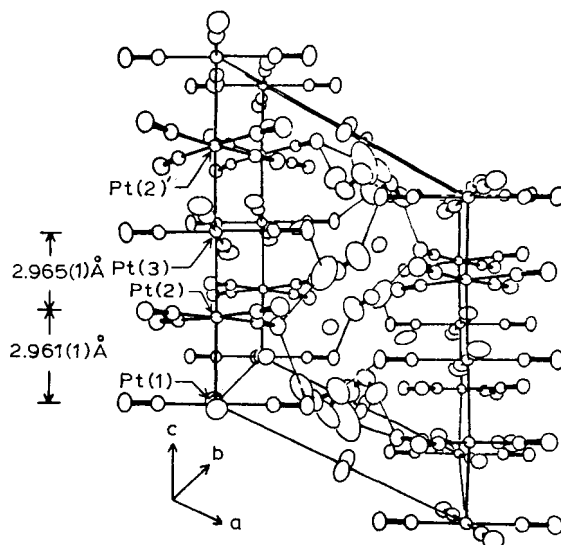


FIG. 23. The crystal structure of $\text{K}_{1.75}\text{Pt}(\text{CN})_4 \cdot 1.5\text{H}_2\text{O}$ (Keefer *et al.*, 1976).

ences in the Pt–C, or other bond lengths and angles within the complexes have ever been detected so the average oxidation state of the metal is genuinely non-integral and the compounds should be considered as RD class III. Other physical evidence pointing in the same direction includes infrared and Raman spectroscopy (Rousseau *et al.*, 1974) showing only one type of Pt–C and C–N modes, Mössbauer spectroscopy (Ruegg, Kuse and Zeller, 1973) showing only a single broad ^{195}Pt line, and ^{195}Pt NMR, which has a Knight

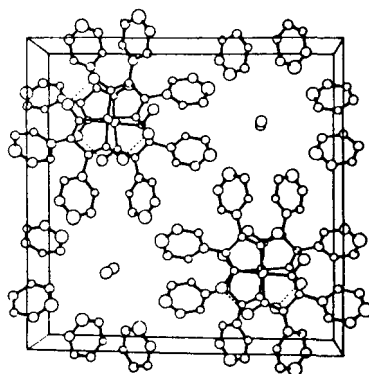


FIG. 24. The crystal structure of $\text{Ni}(\text{dpg})_2(\text{I}_3)_{0.33}$ (Gleizes *et al.*, 1975).

TABLE 9. The formulae of conducting metal chain compounds $\text{A}_m\text{ML}_n\text{X}_p(\text{H}_2\text{O})_q$ (Reis and Petersen, 1978; Underhill and Watkins, 1980)

(1) Anion non-stoichiometry

(a) $\text{M} = \text{Pt}, \text{L} = \text{CN}, n = 4$									
A:	K	K	NH_4	Rb	Rb	Cs	Cs	$\text{C}(\text{NH}_2)_3$	
X:	$\text{Br}_{0.30}$	$\text{Cl}_{0.32}$	$\text{Cl}_{0.30}$	$\text{Cl}_{0.30}$	$(\text{HF}_2)_{0.26-0.4}$	$\text{F}_{0.19}$	$(\text{N}_3)_{0.25}$	$\text{Cl}_{0.25}$	
q:	3	3	3	3	0-1.67	0		1	
(b) $\text{A} = \text{O}, \text{M} = \text{Ni}, \text{L} = \text{planar macrocycle}, \text{X} = \text{I}_3, q = 0$									
L:	OMTBP	TBP	PC	DPG	OMTBP				
p:	0.35	0.33	0.33	0.33	0.97				

(2) Cation non-stoichiometry

(a) $\text{M} = \text{Pt}, \text{L} = \text{CN}, \text{X} = \text{---}$				
A:	K	Rb	Cs	
m:	1.75	1.73	1.72	
q:	1.5	x	x	
(b) $\text{M} = \text{Pt}, \text{L} = \text{oxalate}, \text{X} = \text{---}$				
A:	K	Rb	Co	Mg
m:	1.6	1.67	0.83	0.82
q:	1.2	1.5	6	6

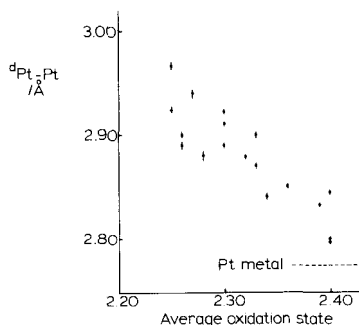


FIG. 25. Variation of Pt-Pt spacing in KCP analogues with average oxidation state.

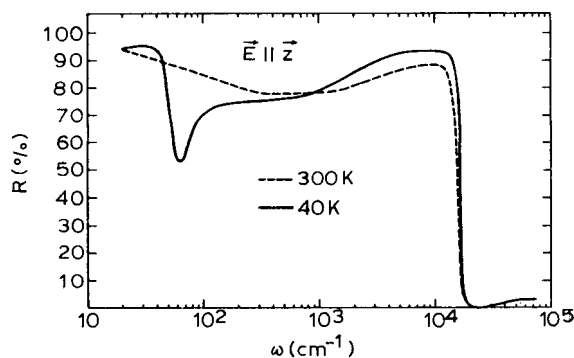


FIG. 26. Reflectivity of KCP with $E//z$ from the far infrared to the ultraviolet (Bruesch *et al.*, 1975).

shift relative to the divalent precursor salts, but again only a single line (Niedoba *et al.*, 1973). Finally, the XPS shows all the Pt atoms in KCP are equivalent (Butler, Rousseau and Buchanan, 1973).

Like the WRS compounds, the optical properties of the KCP salts are extremely anisotropic, and it has even been suggested that they could be used as infrared polarizers. With the incident electric vector parallel to the chains they have a high reflectivity from the far infrared up to $15\,000\text{ cm}^{-1}$, giving the crystals a copper-bronze colour (Fig. 26).

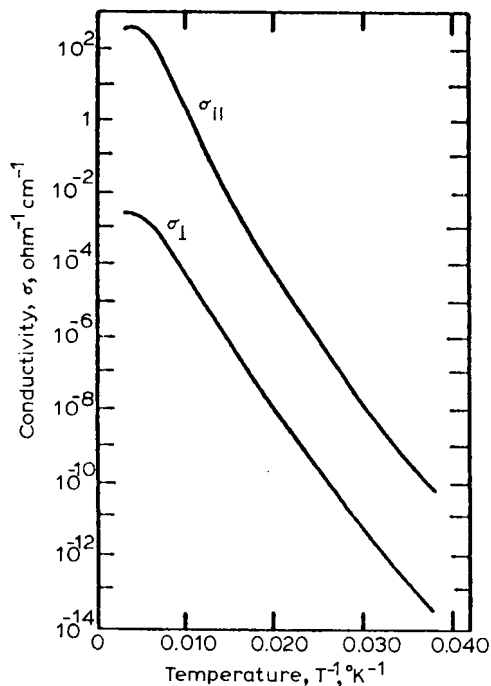


FIG. 27. Specific conductivity of KCP parallel and perpendicular to the metal chain axis as a function of temperature (Zeller and Beck, 1974).

Using Eqs. (43)–(45), but with $\omega_g = 0$ because we are dealing with a metal, the reflectivity has been analysed to give the plasma frequency $\omega_p \sim 2.0$ eV, $\epsilon_1(\infty) = 2.1$ and τ , the electron relaxation time, is 3.2×10^{-15} seconds (Wagner *et al.*, 1973; Bruesch, Strassler and Zeller, 1975). These figures should be compared with those in Table 8. Complications occur at low frequencies, where modes arising from the instability of the one-dimensional metal envisaged by Peierls (1955) come into play. We will not discuss these here, but refer the reader to other reviews (e.g. Keller, 1975, 1977).

As expected for class III mixed valency compounds both the KCP and partly oxidized Ni macrocyclic compounds have high electrical conductivities at room temperature, which are also markedly anisotropic (Fig. 27). In the KCP salts the conductivity falls with decreasing temperature, indicating that at low temperature there is, indeed, a gap in the electron density-of-states as required by Peierls' theorem. The NiLi_x compounds, on the other hand, become more conducting at low temperatures though in one instance there is evidence for a sharp metal-insulator transition.

In this brief account we have not been able to do justice to the range and subtlety of the structural and physical experiments on the class III metal chain compounds. Neither have we mentioned any of the other class III mixed valency compounds containing chains, such as $\text{Hg}_{2.86}\text{AsF}_6$ and $\text{M}_x\text{Pt}_3\text{O}_4$ whose properties (including, in the former case, superconductivity) are under intensive investigation. For recent accounts, see Hatfield (1979).

CONCLUSION

This review has tried to bring together some of the very disparate strands in contemporary mixed valency chemistry. In doing so many aspects have been ignored, or mentioned only briefly in passing. For example, mixed valency plays an important part in the colouring of minerals and rocks, and is now widely studied by mineralogists (e.g. Burns, 1970; Smith and Strens, 1976). Examples of mixed valency have even been found in moon rocks! (Loeffler, Burns and Tossell, 1975). Other fields which I have scarcely mentioned here, but which have proved a fruitful source of mixed valency materials, are the biological metal clusters such as the ferredoxins and the purely inorganic clusters found in many 'metal rich' phases, e.g. $\text{Nb}_6\text{Cl}_{14}$ and $\text{M}_x\text{Mo}_6\text{S}_8$, the latter of exceptional interest because they are superconductors with relatively high T_c (up to 14 K) and the highest critical fields presently known (Odermott *et al.*, 1974). Nevertheless, the static and vibronic models described provide a useful framework for understanding many of the physical properties of mixed valency compounds though some questions, particularly on the application of the quantitative models to extended lattice compounds, remain to be answered. It can be predicted quite confidently that there will be ample new material for another review of this topic in 10 years' time.

REFERENCES

- Reviews on aspects of mixed valency chemistry and physics.
- BROWN, D. B. (ed.) (1980). *Mixed Valence Compounds: Theory and Applications in Chemistry, Physics, Geology and Biology*, D. Reidel Publishing Co. Articles on many aspects of mixed valency.
- COWAN, D. O., LEVANDA, C., PARK, J. and KAUFMAN, F. (1973). *Acc. Chem. Res.*, 6, 1. Mixed valency ferrocene chemistry.
- HATFIELD, W. E. (ed.) (1979). *Molecular Metals*, Plenum Press. Contains many reviews of conducting chain compounds.
- HOLM, R. H. (1977). *Acc. Chem. Res.*, 10, 427. Mixed-valency iron-sulphur clusters related to ferredoxins.

- KELLER, H. J. (ed.) (1975). *Low-dimensional Cooperative Phenomena*, Plenum Press. Contains several reviews about one-dimensional mixed valency compounds.
- KELLER, H. J. (ed.) (1977). *Chemistry and Physics of One-dimensional Metals*, Plenum Press.
- MILLER, J. S. and EPSTEIN, A. J. (1976). *Prog. Inorg. Chem.*, **20**, 1. One-dimensional complexes.
- MILLER, J. S. and EPSTEIN, A. J. (eds.) (1978). *Ann. N.Y. Acad. Sci.*, **313**. Many articles on mixed-valency dimers and chains.
- SMITH, G. and STRENS, R. G. J. (1976). *The Physics and Chemistry of Minerals and Rocks*, Wiley. Mixed valency absorption in minerals.
- UNDERHILL, A. E. and WATKINS, D. M. (1980). *Chem. Soc. Rev.*, **9**, 429. One-dimensional class III mixed-valency compounds.
- WONG, E. Y. and SCHATZ, P. N. (1981). *Prog. Inorg. Chem.*, **28**. Review of the PKS vibronic model of mixed valency.
- ALLEN, G. C. and HUSH, N. S. (1967). *Prog. Inorg. Chem.*, **8**, 357.
- ANEX, B. G. and SIMPSON, W. T. (1960). *Rev. Mod. Phys.*, **32**, 466.
- ATKINSON, L. and DAY, P. (1969). *J. Chem. Soc., A*, 2423.
- BARROWCLIFFE, T., BEATTIE, I. R., DAY, P. and LIVINGSTONE, K. (1967). *J. Chem. Soc. A*, 1810.
- BEATTIE, J. K., HUSH, N. S. and TAYLOR, P. R. (1976). *Inorg. Chem.*, **15**, 992.
- BEATTIE, J. K., HUSH, N. S., TAYLOR, P. R., RASTON, C. L. and WHITE, A. H. (1977). *J. Chem. Soc., Dalton Trans.*, 1121.
- BREER, H., ENDRES, H., KELLER, H. J. and MARTIN, R. (1978). *Acta Cryst.*, **B34**, 2295.
- BROWN, D. B., ROBIN, M. B., MCINTYRE, J. D. E. and PECK, W. E. (1970). *Inorg. Chem.*, **9**, 2315.
- BROWN, K. L. and HALL, D. (1976). *Acta Cryst.*, **B32**, 279.
- BRUESCH, P., STRASSLER, S. and ZELLER, H. R. (1975). *Phys. Rev.*, **B12**, 219.
- BUNKER, B. C., DRAGO, R. S., HENDRICKSON, D. N., RICHMAN, R. M. and KESSEL, S. L. (1978). *J. Amer. Chem. Soc.*, **100**, 3805.
- BURKE, G., LATSCHA, H. P. and PRITZKOW, H. (1976). *Z. Naturforsch.*, **31b**, 1285.
- BURNS, R. G. (1970). *Mineralogical Applications of Crystal Field Theory*, Cambridge University Press.
- BURROUGHS, P., HAMNETT, A., MCGILP, J. F. and ORCHARD, A. F. (1975). *J. Chem. Soc., Faraday Trans. II*, **71**, 177.
- BURROUGHS, P., HAMNETT, A. and ORCHARD, A. F. (1974). *J. Chem. Soc., Dalton Trans.*, 565.
- BUTLER, M. A., ROUSSEAU, D. L. and BUCHANAN, D. N. E. (1973). *Phys. Rev.*, **B7**, 61.
- CAMPAGNA, M., BUCHER, E., WERTHEIM, G. K., and LONGINOTTI, L. D. (1974). *Phys. Rev. Lett.*, **33**, 165.
- CANNON, R. D. (1977). *Chem. Phys. Lett.*, **49**, 299.
- CHAZALVIEL, J. N., CAMPAGNA, M., WERTHEIM, G. K. and SHANKS, H. R. (1977). *Phys. Rev.*, **B16**, 697.
- CHE, M., FOURNIER, M. and LAUNAY, J. P. (1979). *J. Chem. Phys.*, **71**, 1954.
- CIECHANOWICZ, M., GRIFFITH, W. P., PARSON, D., SKAPSKI, A. C. and CLEARE, M. J. (1971). *Chem. Commun.*, 876.
- CITRIN, P. H. (1973). *J. Amer. Chem. Soc.*, **95**, 6472.
- CITRIN, P. H. and GINSBERG, A. P. (1981). *J. Amer. Chem. Soc.*, (in press).
- CLARK, R. J. H., FRANKS, M. L. and TRUMBLE, W. R. (1976). *Chem. Phys. Lett.*, **41**, 287.
- CLARK, R. J. H. (1977). *Ann. N.Y. Acad. Sci.*, **313**, 672.
- CLARK, R. J. H. (1980). In: *Mixed Valency Compounds*, (Ed. by D. B. Brown), p. 271. D. Reidel: Dordrecht.
- COOPER, S. R. and CALVIN, M. (1977). *J. Amer. Chem. Soc.*, **99**, 6623.
- CRABTREE, A. N. (1972). Chemistry Part II Thesis, Oxford (unpublished).
- CRAVEN, B. M. and HALL, D. (1961). *Acta Cryst.*, **14**, 475.
- CREUTZ, C. and TAUBE, H. (1969). *J. Amer. Chem. Soc.*, **91**, 3988.
- CREUTZ, C. and TAUBE, H. (1973). *J. Amer. Chem. Soc.*, **95**, 1086.
- CREUTZ, C., GOOD, M. L. and CHANDRA, S. (1973). *Inorg. Nucl. Chem. Lett.*, **9**, 171.
- CULPIN, D., DAY, P., EDWARDS, P. R. and WILLIAMS, R. J. P. (1965). *Chem. Commun.*, 450.
- idem.* (1968), *J. Chem. Soc. A*, **1**, 838.
- DAY, P. (1963). *Inorg. Chem.*, **2**, 452.
- DAY, P. (1970). *Endeavour*, **29**, 45.

- DAY, P. (1974). *Extended Interactions Between Transition Metal Ions*, p. 234. *Amer. Chem. Soc. Symp. Ser.*, no. 5.
- DAY, P. (1975). *Low-dimensional Cooperative Phenomena* (ed. H. J. Keller), p. 191. Plenum Press: New York.
- DAY, P. (1977). *Chemistry and Physics of One-dimensional Metals* (ed. H. K. Keller), p. 197. Plenum Press: New York.
- DAY, P. (1978). *Ann. N.Y. Acad. Sci.*, 313, 9.
- DAY, P. (1981). *La Recherche*, 12, 304.
- DAY, P. (1981). *Comments on Inorg. Chem.* (in press).
- DAY, P., ORCHARD, A. F., THOMSON, A. J. and WILLIAMS, R. J. P. (1965). *J. Chem. Phys.*, 42, 1973.
- DAY, P., HERREN, F., LUDI, A., GUDEL, H. U., HULLIGER, F. and GIVORD, D. (1980). *Helv. Chim. Acta*, 63, 148.
- DAY, P., VETTER, C. and PARISOT, G. (1978). *Inorg. Chem.*, 17, 2319.
- DENNER, W., SCHULZ, H. and D'AMOUR, H. (1978). *Naturwissenschaften*, 65, 257.
- DZIOBKOWSKI, C. T., WROBLESKI, J. T. and BROWN, D. B. (1981). *Inorg. Chem.*, 20, 671, 679.
- ELSON, C. M., GULENS, J. G., ITZKOVITCH, I. J. and PAGE, J. A. (1970). *Chem. Commun.*, 875.
- ENDRES, H., KELLER, H. J., MARTIN, R. and TRAEGER, U. (1979). *Acta Cryst.*, B35, 2880.
- ENDRES, H., KELLER, H. J., MARTIN, R., GUNG, H. N. and TRAEGER, U. (1979). *Acta Cryst.*, B35, 1885.
- ENDRES, H., KELLER, H. J., KEPPLER, B., MARTIN, R., STEIGER, W. and TRAEGER, U. (1980). *Acta Cryst.*, B35, 760.
- ENDRES, H., KELLER, H. J., MARTIN, R., TRAEGER, U. and NOVOTNY, M. (1980). *Acta Cryst.*, B36, 35.
- FELIX, F. and LUDI, A. (1978). *Inorg. Chem.*, 17, 1782.
- FISCHER, H., TOM, G. M. and TAUBE, H. (1976). *J. Amer. Chem. Soc.*, 98, 5512.
- FRIEDEL, J. (1969). *Comments on Sol. State Phys.*, 2, 21.
- FULTON, R. L. and GOUTERMAN, M. (1861). *J. Chem. Phys.*, 35, 1059.
- GLAUSER, R., HAUSER, U., HERREN, F., LUDI, A., RODER, P., SCHMIDT, E., SIEGENTHALER, H. and WENK, F. (1973). *J. Amer. Chem. Soc.*, 95, 8457.
- GLEIZES, A., MARKS, T. J. and IBERS, J. A. (1975). *J. Amer. Chem. Soc.*, 97, 3545.
- HALL, D. and WILLIAMS, P. P. (1959). *Acta Cryst.*, 11, 624.
- HOFMANN, K. A. and HOSCHELE, K. (1916). *Ber. dt. Chem. Ges.*, 48, 20.
- HUANG, K. and RHYS, A. (1951). *Proc. Roy. Soc. A*, 204, 413.
- HUBBARD, J. (1963). *Proc. Roy. Soc. A*, 276, 238.
- HUSH, N. S. (1961). *Trans. Faraday Soc.*, 57, 557.
- HUSH, N. S. (1967). *Prog. Inorg. Chem.*, 8, 391.
- HUSH, N. S. (1975). *Chem. Phys.*, 10, 361.
- HUSH, N. S. (1980). In: *Mixed Valence Compounds*, (ed. D. B. Brown), p. 151. Dordrecht: D. Reidel.
- HUSH, N. S., EDGAR, A. and BEATTIE, J. K. (1980). *Chem. Phys. Lett.*, 69, 128.
- INTERRANTE, L. V., BROWALL, K. W. and BUNDY, F. B. (1974). *Inorg. Chem.*, 13, 1158.
- JØRGENSEN, C. K. (1970). *Prog. Inorg. Chem.*, 12, 101.
- KEEFER, K. D., WASHECHECK, D. M., ENRIGHT, N. P. and WILLIAMS, J. M. (1976). *J. Amer. Chem. Soc.*, 98, 233.
- KELLER, R., FENNER, J. and HOLZAPFEL, W. B. (1974). *Mat. Res. Bull.*, 9, 1363.
- KIRKWOOD, J. G. and WESTHEIMER, F. H. (1938). *J. Chem. Phys.*, 6, 509.
- KRENTZIEN, H. and TAUBE, H. (1976). *J. Amer. Chem. Soc.*, 98, 6379.
- KROGMANN, K. and HAUSEN, H. D. (1968). *Z. anorg. Chem.*, 358, 67.
- KROGMANN, K. (1969). *Angew. Chem. Int. Ed.*, 8, 35.
- LAWTON, S. L. and JACOBSON, R. A. (1966). *Inorg. Chem.*, 5, 743.
- LEVANDA, C., BECHGAARD, K. and COWAN, D. O. (1976). *J. Org. Chem.*, 41, 2700.
- LEVANDA, C., BECHGAARD, K., COWAN, D. O., MUELLER-WESTERHOFF, U. T., EILBRACHT, P., CANDELA, G. A. and COLLINS, R. A. (1976). *J. Amer. Chem. Soc.*, 98, 3181.
- LEVICH, V. G. (1970). *Physical Chemistry, an Advanced Treatise* (ed. H. Eyring, D. Hendrickson and W. Jost), vol. 9B. New York: Academic Press.
- LITTLE, W. A. (1964). *Phys. Rev.*, 134, A1416.
- LOEFFLER, B. M., BURNS, R. G. and TOSSELL, J. A. (1975). *Proc. 6th Lunar Sci. Conf.*, p. 2663.

- LUDI, A. (1980). In: *Mixed Valence Compounds*, (ed. D. B. Brown), p. 25. Dordrecht: D. Reidel.
- MAGNUSON, R. H. and TAUBE, H. (1972). *J. Amer. Chem. Soc.*, **94**, 7213.
- MARCUS, R. A. (1956). *J. Chem. Phys.*, **24**, 966.
- MARCUS, R. A. (1965). *J. Chem. Phys.*, **43**, 679.
- MARKHAM, J. J. (1959). *Rev. Mod. Phys.*, **31**, 956.
- MARTIN, D. S. (1971). *Inorg. Chim. Acta Rev.*, **5**, 107.
- MATSUMOTO, N., YAMASHITA, M. and KIDA, S. (1978). *Bull. Chem. Soc. Japan*, **51**, 3514.
- MAYOH, B. and DAY, P. (1972). *J. Amer. Chem. Soc.*, **94**, 2885.
- MAYOH, B. and DAY, P. (1973). *J. Chem. Soc., Dalton Trans.*, 846.
- MAYOH, B. and DAY, P. (1974). *Inorg. Chem.*, **13**, 2273.
- MEYER, T. J. (1978). *Ann. N.Y. Acad. Sci.*, **313**, 496.
- MEYER, T. J. (1979). *Chem. Phys. Lett.*, **64**, 417.
- MINGARDI, M. and SIEBRAND, W. (1975). *J. Chem. Phys.*, **62**, 1074.
- MORRISON, W. H. and HENDRICKSON, D. N. (1973). *J. Chem. Phys.*, **59**, 380.
- MORRISON, W. H., KROGSUND, S. and HENDRICKSON, D. N. (1973). *Inorg. Chem.*, **12**, 1998.
- MUELLER-WESTERHOFF, U. T. and EILBRACHT, P. (1972). *J. Amer. Chem. Soc.*, **94**, 9272.
- NIEDOBA, H., LANNOIS, H., BRINKMANN, D., BRUGGER, R. and ZELLER, H. R. (1973). *Phys. Stat. Sol.*, (b) **58**, 309.
- ODERMATT, R., FISCHER, O., JONES, H. and BONGI, G. (1974). *J. Phys.*, **C7**, L13.
- ORCHARD, A. F. and THORNTON, G. (1977). *J. Chem. Soc., Dalton Trans.*, 1238.
- PAPPAVASSILIOU, G. C., LAYEK, D. and THEOPHANIDES, T. (1980). *J. Raman Spect.*, **9**, 69.
- PAPPAVASSILIOU, G. C. and ZDETSIS, A. D. (1980). *J. Chem. Soc., Faraday Trans., II*, **76**, 104.
- PARASKEVAIDIS, C. E. and PAPATRIANTAFILLOU, C. (1980). *Chem. Phys.*, **45**, 393.
- PIERLS, R. E. (1955). *Quantum Theory of Solids*, p. 108, Oxford University Press.
- PIEPHO, S. B., KRAUSZ, E. R. and SCHATZ, P. N. (1978). *J. Amer. Chem. Soc.*, **100**, 2996.
- PLAKSIN, P. M., STONFER, R. C., MATHEW, M. and PALENIK, G. J. (1972). *J. Amer. Chem. Soc.*, **94**, 2121.
- POWERS, M. J., CALLAHAN, R. W., SALMON, D. J. and MEYER, T. J. (1976). *Inorg. Chem.*, **15**, 894.
- POWERS, M. J., CALLAHAN, R. W., SALMON, D. J. and MEYER, T. J. (1976). *Inorg. Chem.*, **15**, 1457.
- POWERS, M. J., SALMON, D. J., CALLAHAN, R. W. and MEYER, T. J. (1976). *J. Amer. Chem. Soc.*, **98**, 6731.
- POWERS, M. J. and MEYER, T. J. (1978). *J. Amer. Chem. Soc.*, **100**, 4393.
- PRASSIDES, K. (1980). Chemistry Part II Thesis, Oxford (unpublished).
- RICHARDSON, D. (1981). PhD. Thesis, Stanford University, California.
- RIEDER, K. and TAUBE, H. (1977). *J. Amer. Chem. Soc.*, **99**, 789.
- ROBIN, M. B. and DAY, P. (1967). *Adv. Inorg. Chem. and Radiochem.*, **10**, 247.
- ROUSSEAU, D. L., BUTLER, M. A., GUGGENHEIM, H. J., WEISMAN, R. B. and BLOCH, A. N. (1974). *Phys. Rev.*, **B10**, 2281.
- RUEGG, W., KUSE, D. and ZELLER, H. R. (1973). *Phys. Rev.*, **B8**, 952.
- RYAN, T. D. and RUNDLE, R. E. (1961). *J. Amer. Chem. Soc.*, **83**, 2814.
- SCHATZ, P. N., PIEPHO, S. B. and KRAUSZ, E. R. (1978). *Chem. Phys. Lett.*, **55**, 539.
- SCHRAMM, C. J., SCARINGE, R. P., STOJAKOVIC, D. R., HOFMANN, B. M., IBERS, J. A. and MARKS, T. J. (1980). *J. Amer. Chem. Soc.*, **102**, 6702.
- STEVENS, K. W. H. (1953). *Prog. Roy. Soc.*, **A219**, 542.
- STREKAS, T. C. and SPIRO, T. G. (1976). *Inorg. Chem.*, **15**, 974.
- STUCKY, G. D., SCHULTZ, A. J. and WILLIAMS, J. M. (1977). *Ann. Rev. Mat. Sci.*, **7**, 301.
- STYNES, H. C. and IBERS, J. A. (1971). *Inorg. Chem.*, **10**, 2304.
- SULLIVAN, B. P. and MEYER, T. J. (1980). *Inorg. Chem.*, **19**, 321.
- TAUBE, H. (1978). *Ann. N.Y. Acad. Sci.*, **313**, 481.
- THIELE, G. (1977). Quoted by Clark, R. J. H., *Ann. N.Y. Acad. Sci.*, **313**, 672.
- THOMAS, T. W. and UNDERHILL, A. E. (1969). *Chem. Commun.*, 725.
- THOMAS, T. W. and UNDERHILL, A. E. (1971). *J. Chem. Soc. A*, 512.
- TOM, G. M., CREUTZ, C. and TAUBE, H. (1974). *J. Amer. Chem. Soc.*, **96**, 7827.
- TOM, G. and TAUBE, H. (1975). *J. Amer. Chem. Soc.*, **97**, 5310.
- TRICKER, M. J., ADAMS, I. and THOMAS, J. M. (1972). *Inorg. Nucl. Chem. Lett.*, **8**, 633.

PETER DAY

193

- VERWEY, E. J. W., HAAYMAN, P. J., ROMELJN, F. C. and VAN OOSTERHOUT, G. W. (1950). *Philips Res. Report*, 5, 173.
- WAGNER, H., GESERICH, H. P., BALTZ, R. V. and KROGMANN, K. (1973). *Sol. State Commun.*, 13, 659.
- WALLEN, J., BROSSET, C. and VANNERBERG, N. G. (1962). *Arkiv. Kem.*, A18, 541.
- WALTON, E. G., CORVAN, P. J., BROWN, D. B. and DAY, P. (1976). *Inorg. Chem.*, 15, 1737.
- WASHECHECK, D. M., PETERSEN, S. W., REIS, A. H. and WILLIAMS, J. M. (1976). *Inorg. Chem.*, 15, 74.
- WERNER, A. (1896). *Z. anorg. Chem.*, 12, 46.
- WILLIAMS, J. M., PETERSON, J. L., GERDES, H. M. and PETERSEN, S. W. (1974). *Phys. Rev. Lett.*, 33, 1079.
- WONG, K. Y., SCHATZ, P. N. and PIEPHO, S. B. (1979). *J. Amer. Chem. Soc.*, 101, 2793.
- YAMADA, S. and TSUCHIDA, R. (1956). *Bull Chem. Soc. Japan*, 29, 894.
- YAMASHITA, M., MATSUMOTO, N. and KIDA, S. (1978). *Inorg. Chim. Acta*, 31, L381.
- ZELLER, H. R. and BECK, A. (1974). *J. Phys. Chem. Sol.*, 35, 77.

Vibronic Coupling Model for Mixed-Valence Compounds. Extension to Two-Site Two-Electron Systems

Kosmas Prassides,^{*†} Paul N. Schatz,^{*‡} Kin Y. Wong,^{†§} and Peter Day[†]

The Inorganic Chemistry Laboratory, Oxford University, Oxford OX1 3QR, England, and the Chemistry Department, University of Virginia, Charlottesville, Virginia 22901 (Received: March 10, 1986)

The two-site one-electron vibronic coupling model of Piepho, Krausz, and Schatz (PKS) for mixed-valence systems is extended to two-site two-electron dimeric systems. The full dynamic problem is solved and characterization of the system reduces to a simple matrix diagonalization. For strong vibronic coupling, a perturbation treatment is also presented which leads to simple analytical expressions for the eigenvalues and eigenfunctions. The model is used to fit the absorption, resonance Raman, and luminescence spectra of the one-dimensional chlorine-bridged mixed-valence compound $[\text{Pt}^{\text{II}}\text{L}_4][\text{Pt}^{\text{IV}}\text{L}_4\text{Cl}_2]\text{Cl}_4 \cdot 4\text{H}_2\text{O}$ (L = ethylamine), Wolfram's Red Salt.

I. Introduction

Mixed valency is one of the various names used to describe compounds that contain ions of the same element in two different formal states of oxidation. The first models of mixed-valence systems were proposed by Allen and Hush¹ and by Robin and Day.² The latter also proposed a classification scheme which is

now widely used. The full vibronic problem for a mixed-valence dimer was later solved by Piepho, Krausz, and Schatz³ (PKS). Since then the PKS model has been used to calculate a variety of mixed-valence properties, including intervalence band contours,^{3,4} electron transfer,^{5,6} magnetic susceptibilities,^{5,7} resonance

[†]University of Oxford.

[‡]University of Virginia.

[§]Present address: General Electric Company, Seminole Trail, Charlottesville, VA 22906.

(1) Allen, G. C.; Hush, N. S. *Prog. Inorg. Chem.* **1967**, *8*, 357-444.

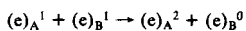
(2) Robin, M. B.; Day, P. *Adv. Inorg. Chem. Radiochem.* **1967**, *10*, 247-422.

(3) Piepho, S. B.; Krausz, E. R.; Schatz, P. N. *J. Am. Chem. Soc.* **1978**, *100*, 2996-3005.

Vibronic Coupling Model for Two-Electron Systems

Raman spectra,⁸⁻¹⁰ and solvent effects.¹¹ Its formulation and use, however, has been largely restricted to dimeric systems which contain a single electron (or hole).

Recently, Prassides and Day¹² solved the PKS model in the static limit (zero nuclear kinetic energy) for dimeric mixed valence systems which contain two electrons. The interest in these systems in which there is a two-electron difference between ions of differing oxidation states stems from the fact that they are simple examples of the so-called "negative-U" effect,¹³ i.e., valency disproportionation of the following form has taken place:



In this paper we solve the full vibronic problem for this case and show that the model can be used to calculate a variety of mixed-valence properties. We explicitly consider the absorption, resonance Raman, and luminescence spectra of Wolfram's Red Salt as an illustration of the applicability of the model. For such cases of strong vibronic coupling, a perturbation treatment is also presented which leads to simple analytical results.

II. Naive Formulation of the Problem

We proceed in close analogy with an earlier treatment⁵ and start with the following simple picture. Suppose we have two moieties A and B associated with formal oxidation states N and $N-2$, respectively. We write the electronic Hamiltonian operators associated with the two moieties as H_{el}^A and H_{el}^B , respectively. Then

$$\begin{aligned} H_{el}^A \psi_N^A &= W_N^A \psi_N^A \\ H_{el}^B \psi_{N-2}^B &= W_{N-2}^B \psi_{N-2}^B \end{aligned} \quad (1)$$

If we assume that there is no interaction between the two subunits, the electronic Schrödinger equation for the system is given by

$$(H_{el}^A + H_{el}^B) \psi_N^A \psi_{N-2}^B \equiv (H_{el}^A + H_{el}^B) \psi_a = (W_N^A + W_{N-2}^B) \psi_a \equiv W_a \psi_a \quad (2)$$

If one or two electrons are transferred from B to A, the zeroth-order electronic wave functions of the new states are respectively

$$\begin{aligned} \psi_b &= \psi_{N-1}^A \psi_{N-1}^B \\ \psi_c &= \psi_{N-2}^A \psi_N^B \end{aligned} \quad (3)$$

Then equations exactly analogous to (2) apply if the interchanges $a \rightarrow b$, $(N-2) \rightarrow (N-1)$, $N \rightarrow (N-1)$, and $a \rightarrow c$, $A \rightarrow B$, $B \rightarrow A$ are made, respectively.

We make the harmonic approximation and assume that the subunits have the same point group symmetry in all three oxidation states. Then it is only necessary to consider totally symmetric normal coordinates. We restrict ourselves to a single totally symmetric normal coordinate on each moiety (Q_A and Q_B). The vibrational potential energy of subunit j in oxidation state i can then be written

$$W_i^j = W_i^{0j} + \frac{1}{2} Q_j + \frac{1}{2} k_j Q_j^2, \quad j = A, B; \quad i = N, N-1, N-2 \quad (4)$$

where $W_i^{0j} \equiv W_i^j(Q_j = 0)$. Let us initially assume that centers A and B are equivalent (the symmetrical case). The hexa-

The Journal of Physical Chemistry, Vol. 90, No. 22, 1986 5589

chloroantimonate(III,V) compounds and Wolfram's Red Salt (and analogues) are examples of such systems with $N = 5$ and 4, respectively. We define the zero of energy by $W_N^{0A} + W_{N-2}^{0B} = W_{N-2}^{0A} + W_N^{0B} = 0$ and define $2W \equiv (W_{N-1}^{0A} + W_{N-1}^{0B}) - (W_N^{0A} + W_{N-2}^{0B})$. As before,⁵ we introduce the sum and difference coordinates

$$Q_{\pm} = (1/2^{1/2})(Q_A \pm Q_B) \quad (5)$$

We now make the crucial assumptions (which also apply for $A \rightarrow B$)

$$\begin{aligned} k_N^A &= k_{N-1}^A = k_{N-2}^A \equiv k \\ I_{N-1}^A &= \frac{1}{2}(I_N^A + I_{N-2}^A) \equiv I \end{aligned} \quad (6)$$

With eq 6, W_a , W_b , and W_c give identical parabolas in Q_{\pm} space. Thus the Q_{\pm} coordinate decouples from the problem and may be dropped.⁵ We choose origins by setting Q_A and Q_B to zero at the minima of W_{N-2}^A and W_N^B , respectively. Introducing the dimensionless variables

$$\begin{aligned} q &= 2\pi(\nu/h)^{1/2} Q_{-} \\ \lambda &= (8\pi^2 h\nu_{-}^3)^{-1/2} l \\ 2W &= 2\bar{W}/h\nu_{-} + \lambda^2/2 \end{aligned} \quad (7)$$

where $\nu_{-} = (2\pi)^{-1} k^{1/2}$ is the vibrational frequency associated with the crucial coordinate Q_{-} , we obtain (after changing the energy zero by $\lambda^2/2$)

$$\begin{aligned} W_a/h\nu_{-} &= \frac{1}{2}(q + \lambda)^2 \\ W_b/h\nu_{-} &= 2W + \frac{1}{2}q^2 \\ W_c/h\nu_{-} &= \frac{1}{2}(q - \lambda)^2 \end{aligned} \quad (8)$$

Now let us remove the assumption that there is no interaction between centers A and B. We hold the nuclei at $q = 0$ and define

$$V_{ij}^0 \equiv \langle \psi_i^A | V^A | \psi_j^B \rangle^0; \quad i, j = a, b, c \quad (9)$$

In the symmetrical case, $V_{aa}^0 = V_{cc}^0$. We define the parameters ϵ and ϵ' by the relations

$$\begin{aligned} \epsilon &\equiv V_{ab}^0/h\nu_{-} \\ \epsilon' &\equiv V_{ac}^0/h\nu_{-} \end{aligned} \quad (10)$$

Changing the zero of energy by $V_{aa}^0/h\nu_{-}$ and substituting the above definitions and eq 8 into eq 2, we obtain the vibronic matrix in the ψ_a, ψ_b, ψ_c electronic basis:

$$\begin{pmatrix} \frac{1}{2}(q + \lambda)^2 & \epsilon & \epsilon' \\ \epsilon & 2W + \frac{1}{2}q^2 & \epsilon \\ \epsilon' & \epsilon & \frac{1}{2}(q - \lambda)^2 \end{pmatrix} \quad (11)$$

The constant term $(V_{bb}^0 - V_{aa}^0)/h\nu_{-}$ has been absorbed into $2W$. Matrix (11) becomes identical with the one proposed by Prassides and Day¹² if ϵ' is set to zero. In the following section, we demonstrate that this vibronic matrix has a more general physical meaning.

III. Exact Equivalence with the Two-Site Two-Electron Model¹⁴

(4) Wong, K. Y.; Schatz, P. N.; Piepho, S. B. *J. Am. Chem. Soc.* **1979**, *101*, 2793-2803.

(5) Wong, K. Y.; Schatz, P. N. *Prog. Inorg. Chem.* **1981**, *28*, 369-449.

(6) Wong, K. Y.; Schatz, P. N. *Chem. Phys. Lett.* **1980**, *71*, 152-157.

(7) Schatz, P. N. In *Mixed Valence Compounds*, Brown, D. B., Ed.; Reidel: New York, 1980; pp 115-150.

(8) Wong, K. Y.; Schatz, P. N. *Chem. Phys. Lett.* **1980**, *73*, 456-460.

(9) Wong, K. Y.; Schatz, P. N. *Chem. Phys. Lett.* **1981**, *80*, 172-177.

(10) Wong, K. Y.; Schatz, P. N. *Chem. Phys. Lett.* **1984**, *108*, 484-489.

(11) Wong, K. Y.; Schatz, P. N. In *Mechanistic Aspects of Inorganic Reactions*, Rorabacher, D. B., Endicott, J. F., Eds.; American Chemical Society: Washington, DC, 1982; ACS Symp. Ser. No. 198, pp 281-299.

(12) Prassides, K.; Day, P. *J. Chem. Soc., Faraday Trans. 2* **1984**, *80*, 85-95.

(13) Anderson, P. W. *Phys. Rev. Lett.* **1975**, *34*, 953-955.

Consider a general system consisting of two closed-shell moieties, two additional electrons, and the surrounding deformable lattice medium (a mixed-valency dimer in which there is a two-electron difference between oxidation states is a special case of such a system).

Electronic basis functions with associated spin for moieties A and B are simply $\psi^{\alpha}\alpha, \psi^{\alpha}\beta, \psi^{\beta}\alpha$ and $\psi^{\beta}\beta$, where α and β represent the spin functions. The zeroth-order electronic wave functions of the system are

singlets:

$$\begin{aligned}\psi_a^s &= |\psi^B \alpha \psi^B \beta\rangle \\ \psi_b^s &= (1/2^{1/2})(|\psi^A \alpha \psi^B \beta\rangle + |\psi^B \alpha \psi^A \beta\rangle) \\ \psi_c^s &= |\psi^A \alpha \psi^A \beta\rangle\end{aligned}$$

triplets:

$$\begin{aligned}\psi_a^T &= |\psi^A \alpha \psi^B \alpha\rangle \\ \psi_b^T &= (1/2^{1/2})(|\psi^A \alpha \psi^B \beta\rangle - |\psi^B \alpha \psi^A \beta\rangle) \\ \psi_c^T &= |\psi^A \beta \psi^B \beta\rangle\end{aligned}\quad (12)$$

where the two-electron kets are normalized Slater determinants.

The electronic Hamiltonian for the dimeric system is

$$H_{el} = H_{el}^A + H_{el}^B + V^{AB} + \frac{e^2}{r_{12}}\quad (13)$$

where H_{el}^A , H_{el}^B , and V^{AB} have the same meaning as before and e^2/r_{12} is the electron repulsion operator. We construct the singlet vibronic matrix elements by evaluating $\langle \psi_i^s | H_{el} | \psi_j^s \rangle$; $i, j = a, b, c$. To connect this procedure to the previous treatment, make the identifications, $\psi_{N-1}^A \psi_{N-2}^B \rightarrow \psi_a^s$, $\psi_{N-2}^A \psi_{N-1}^B \rightarrow \psi_c^s$, $\psi_{N-1}^A \psi_{N-1}^B \rightarrow \psi_b^s$. We use $(H_{el}^A + H_{el}^B)$ in the sense of eq 2 and make the usual approximation of zero overlap between centers, $\langle \psi^A | \psi^B \rangle = 0$. We again consider one totally symmetric mode for each site (Q_A, Q_B) and make the harmonic approximation. As before, Q_+ decouples from the system when we assume equal force constants and $I_{N-1} = (I_N + I_{N-2})/2$. Changing to dimensionless variables as before with energy in units of $h\nu_-$ we obtain

$$\begin{aligned}\langle \psi_a^s | H_{el} | \psi_a^s \rangle &= 1/2(q + \lambda)^2 - \lambda^2/2 + V_{aa}^0/h\nu_- + U \\ \langle \psi_b^s | H_{el} | \psi_b^s \rangle &= 1/2q^2 + V_{bb}^0/h\nu_- + U \\ \langle \psi_c^s | H_{el} | \psi_c^s \rangle &= 1/2(q - \lambda)^2 - \lambda^2/2 + V_{cc}^0/h\nu_- + U \\ \langle \psi_a^s | H_{el} | \psi_b^s \rangle &\equiv \epsilon = \langle \psi_b^s | H_{el} | \psi_c^s \rangle \\ \langle \psi_a^s | H_{el} | \psi_c^s \rangle &\equiv \epsilon'\end{aligned}\quad (14)$$

in which

$$\begin{aligned}V_{aa}^0 &\equiv \langle \psi_a^s | V^{AB} | \psi_a^s \rangle = V_{cc}^0 \\ V_{bb}^0 &\equiv \langle \psi_b^s | V^{AB} | \psi_b^s \rangle \\ U h\nu_- &\equiv \left\langle \psi_a^s \left| \frac{e^2}{r_{12}} \right| \psi_a^s \right\rangle = \left\langle \psi_c^s \left| \frac{e^2}{r_{12}} \right| \psi_c^s \right\rangle \\ U' h\nu_- &\equiv \left\langle \psi_b^s \left| \frac{e^2}{r_{12}} \right| \psi_b^s \right\rangle\end{aligned}\quad (15)$$

We assume that centers A and B are sufficiently separated that the intersite electron repulsion is negligible. Thus $U' = 0$. Note that if we now add $(\lambda^2/2 - V_{aa}^0/h\nu_- - U)$ to the diagonal elements in eq 14, we obtain (11), with the identification

$$2W = \lambda^2/2 - U\quad (16)$$

The quantity $(1/2)\lambda^2$ represents the lattice stabilization energy due to the electron-phonon interaction and hence the parameter W is a direct measure of the competition between the on-site component U of the interelectronic Coulomb repulsion and the electron-phonon interaction. If we set $\epsilon' = 0$, matrix (11) is identical with the result of Toyozawa¹⁴ and the relation between our parameters and his is easily established:

$$\lambda^2 = 2c^2 = 2S; \quad \epsilon = -2^{1/2}T\quad (17)$$

The energy of the triplet state in eq 12 is also readily evaluated and is equal to $\langle \psi_c^s | H_{el} | \psi_b^s \rangle$ if exchange terms are neglected. We

do not consider the triplet state further despite the possibility of spin-orbit interaction with the singlets. This interaction is in fact a higher order effect because implicit in eq 12 is the assumption that the orbital ψ (ψ^A or ψ^B) is nondegenerate and thus has no orbital angular momentum. Thus for example in our later applications to Wolfram's Red Salt, ψ is the nondegenerate (a_{1g}) Pt d_{z^2} orbital.

IV. "Exact" Solution of the Dynamic Problem

The two-site two-electron system has been studied by Rice¹⁵ within the small λ region (weak electron-phonon coupling) with particular application to organic charge-transfer salts. Toyozawa¹⁴ has studied the same system over the whole region of λ , ϵ , and W in the adiabatic approximation. We proceed in the spirit of the PKS model to solve the full dynamic problem, i.e.

$$(H_{el} + T_n(q))\Phi_\nu = E_\nu \Phi_\nu\quad (18)$$

$T_n(q)$ is the kinetic energy operator for the crucial coordinate q .

A. *The Symmetrical Case.* To take advantage of the interchange symmetry ($A = B$), we use the electronic basis:

$$\begin{aligned}\psi_\pm &= \frac{1}{2^{1/2}}(\psi_a \pm \psi_c) \\ \psi_0 &= \psi_b\end{aligned}\quad (19)$$

$T_n(q)$ commutes with ψ_\pm , ψ_0 (i.e. $\langle \psi_i | T_n | \psi_j \rangle = \delta_{ij} T_n$ for $i, j = +, -, 0$) with $\langle \psi_i | \psi_j \rangle = \delta_{ij}$. We write the vibronic wave functions as

$$\Phi_\nu = \psi_+ \chi_{j,\nu} + \psi_0 \chi_{0,\nu} + \psi_- \chi_{-, \nu}\quad (20)$$

The $\chi_{j,\nu}$ ($j = +, -, 0$) are expanded in the complete orthonormal set of harmonic oscillator functions $\chi_n(q)$, $n = 0, 1, 2, \dots, \infty$:

$$\chi_{j,\nu} = \sum_{n=0}^{\infty} C_{j,\nu n} \chi_n(q)\quad (21)$$

We separate the vibronic wave functions into those that change (Φ_ν^+) and those that do not change (Φ_ν^+) sign under interchange:

$$\begin{aligned}\Phi_\nu^+ &= \psi_+ \sum_{n=\text{even}} r_{\nu n} \chi_n + \psi_- \sum_{n=\text{odd}} r_{\nu n} \chi_n + \psi_0 \sum_{n=\text{even}} s_{\nu n} \chi_n \\ \Phi_\nu^- &= \psi_+ \sum_{n=\text{odd}} r'_{\nu n} \chi_n + \psi_- \sum_{n=\text{even}} r'_{\nu n} \chi_n + \psi_0 \sum_{n=\text{odd}} s'_{\nu n} \chi_n\end{aligned}\quad (22)$$

Proceeding in exact analogy to the simple PKS treatment,⁵ we find that the coefficients $r_{\nu n}$ and $s_{\nu n}$ are determined by the following secular equations:

$$\begin{aligned}\sum_{n=0}^{\infty} r_{\nu n} (H_{mn} - \delta_{mn} E_\nu^+) + \sum_{n=0}^{\infty} s_{\nu n} H''_{mn} &= 0 \\ \sum_{n=0}^{\infty} s_{\nu n} (H'_{mn} - \delta_{mn} E_\nu^+) + \sum_{n=0}^{\infty} r_{\nu n} H''_{mn} &= 0 \\ m = 0, 1, 2, \dots; \nu = 0, 1, 2, \dots\end{aligned}$$

with

$$H_{mn} = \left(m + \frac{1}{2} + \frac{1}{2} \lambda^2 + (-1)^m \epsilon' \right) \delta_{mn} + \lambda \left[\left(\frac{m}{2} \right)^{1/2} \delta_{m,n+1} + \left(\frac{m+1}{2} \right)^{1/2} \delta_{m,n-1} \right]$$

$$H''_{mn} = 2^{1/2} \epsilon \delta_{mn}, \quad m = \text{even}; \quad H''_{mn} = 0, \quad m = \text{odd}$$

$$\begin{aligned}H'_{mn} &= (m + 1/2 + 2W) \delta_{mn}, \quad m = \text{even}; \\ H'_{mn} &= 0, \quad m = \text{odd}\end{aligned}\quad (23)$$

The coefficients $r'_{\nu n}$ and $s'_{\nu n}$ are likewise obtained by making the substitutions $r_{\nu n} \rightarrow r'_{\nu n}$, $s_{\nu n} \rightarrow s'_{\nu n}$, $E_\nu^+ \rightarrow E_\nu^-$, $\epsilon' \rightarrow -\epsilon'$ and interchanging the roles of odd and even m in the definitions for H'_{mn} and H''_{mn} , i.e., H''_{mn} and $H'_{mn} = 0$ when m is even and can be different from zero when m is odd.

Thus the solution to the dynamic problem has been reduced to the diagonalization of a simple matrix. Four parameters, ϵ ,

(14) Toyozawa, Y. *J. Phys. Soc. Jpn.* **1981**, *50*, 1861-1867.

(15) Rice, M. J. *Solid State Commun.* **1979**, *31*, 93-98.

Vibronic Coupling Model for Two-Electron Systems

ϵ' , λ , and W , completely define the eigenvalues and eigenfunctions of the ground vibronic manifold which spans all three potential surfaces. With this information we can calculate a variety of observables including intervalence bands and resonance Raman and luminescence spectra (see Section VI). Of particular importance is the dipole strength of a vibronic line. $\Phi_{\nu'}^{\pm} \rightarrow \Phi_{\nu}^{\pm}$, which, following ref 3 and 5, is given by

$$D(\nu' \rightarrow \nu) = \left(\frac{N_{\nu'} - N_{\nu}}{N} \right) \mathcal{S}_{\nu\nu'}^2 \langle \psi_{\pm} | m_z | \psi_{\pm} \rangle^2 \quad (24)$$

where

$$N_{\nu} = \exp(-E_{\nu}/kT), \quad N = \sum_{\nu} N_{\nu}$$

$$\mathcal{S}_{\nu\nu'} = \sum_{n=0}^{\infty} r_{\nu\nu'} r_{\nu n}^{\prime} \quad (25)$$

and m_z is the molecule-fixed electric dipole operator component along the dimer axis. Note particularly that the simple form (24) results because $\langle \psi_0 | m_z | \psi_{\pm} \rangle \approx 0$ when overlap between the two centers is neglected.

The basis size required for acceptable accuracy in such calculations depends strongly on the value of the electron-phonon coupling λ . For large values of λ (e.g. ≈ 10), it is necessary to use a basis of 180 quanta on each surface. This requires the diagonalization of two 270×270 matrices. For small values of λ (e.g. for typical organic radical-ion molecular solids like TCNQ salts), acceptable accuracy can be achieved with considerably smaller bases.

B. The Unsymmetrical Case. If the two sites are not symmetrically equivalent, as for example in the $\text{Bi}^{\text{III}}\text{Cl}_6^{3-} - \text{Sb}^{\text{V}}\text{Cl}_6^{-}$ systems or the $\text{Pd}^{\text{II}} - \text{Pt}^{\text{IV}}$ analogues of Wolfram's Red Salt, the dynamic problem can still be solved with the introduction of one additional parameter:

$$2W'/h\nu_{-} \equiv (W_{N-2}^{\text{OA}} + W_{N-2}^{\text{OB}}) - (W_{N-2}^{\text{OA}} + W_{N-2}^{\text{OB}}) \quad (26)$$

However, it is no longer a symmetry requirement that $k_i^{\text{A}} = k_i^{\text{B}}$, $I_i^{\text{A}} = I_i^{\text{B}}$ ($i = N, N-1, N-2$). These are the additional assumptions required to decouple the Q_+ coordinate from the problem. Then proceeding as before we obtain

$$W_a/h\nu_{-} = 1/2(q + \lambda)^2$$

$$W_b/h\nu_{-} = 1/2q^2 + 2W$$

$$W_c/h\nu_{-} = 1/2(q - \lambda)^2 + 2W' \quad (27)$$

Equations 21 are replaced by

$$\Phi_{\nu} = \sum_{n=0}^{\infty} (\psi_{+n} r_{\nu n} \chi_n + \psi_{0n} s_{\nu n} \chi_n + \psi_{-n} r'_{\nu n} \chi_n) \quad (28)$$

and the secular equations are

$$\sum_{n=0}^{\infty} r_{\nu n} (H_{nn}^{(1)} - \delta_{nn} E_{\nu}) + \sum_{n=0}^{\infty} r'_{\nu n} H_{nn}^{(2)} + \sum_{n=0}^{\infty} s_{\nu n} H_{nn}^{(3)} = 0$$

$$\sum_{n=0}^{\infty} r'_{\nu n} (H_{nn}^{(4)} - \delta_{nn} E_{\nu}) + \sum_{n=0}^{\infty} r_{\nu n} H_{nn}^{(2)} = 0$$

$$\sum_{n=0}^{\infty} s_{\nu n} (H_{nn}^{(5)} - \delta_{nn} E_{\nu}) + \sum_{n=0}^{\infty} r_{\nu n} H_{nn}^{(3)} = 0$$

where

$$H_{nn}^{(1)} = \left(m + \frac{1}{2} + \frac{1}{2} \lambda^2 + W' + \epsilon' \right) \delta_{nn}$$

$$H_{nn}^{(2)} = \lambda \left[\left(\frac{m}{2} \right)^{1/2} \delta_{m,n+1} + \left(\frac{m+1}{2} \right)^{1/2} \delta_{m,n-1} \right] - W \delta_{nn}$$

$$H_{nn}^{(3)} = 2^{1/2} \epsilon \delta_{nn}$$

$$H_{nn}^{(4)} = \left(m + \frac{1}{2} + \frac{1}{2} \lambda^2 + W' - \epsilon' \right) \delta_{nn}$$

$$H_{nn}^{(5)} = \left(m + \frac{1}{2} + 2W \right) \delta_{nn} \quad (29)$$

The Journal of Physical Chemistry, Vol. 90, No. 22, 1986 5591

Hence it is necessary to diagonalize a single block twice the size of the two separate blocks of the symmetrical case.

The dipole strength of a vibronic line $\Phi_{\nu'} \rightarrow \Phi_{\nu}$, is again given by eq 23 if $\mathcal{S}_{\nu\nu'}$ is replaced by $\mathcal{S}'_{\nu\nu'}$, where

$$\mathcal{S}'_{\nu\nu'} = \sum_{n=0}^{\infty} (r_{\nu n} r'_{\nu n} + r'_{\nu n} r_{\nu n}) \quad (30)$$

V. Perturbational Solution of the Dynamic Problem in the Strong Electron-Phonon Coupling Regime

The "exact" solution of the dynamic problem requires a matrix diagonalization (eq 23 or 29), and the required basis (and matrix) becomes increasingly large as λ increases. Fortunately, a simple perturbational treatment becomes increasingly applicable under just these circumstances. Furthermore, such an approach is easy to extend to the many-mode case¹⁶ where the direct diagonalization rapidly becomes intractable.

A. The Symmetrical Case ($A = B$). Examining eq 11, we note that if $\epsilon = \epsilon' = 0$, W_a , W_b , and W_c (eq 8) are three independent harmonic potential surfaces, and the exact vibronic eigenfunctions are $\Phi_a^0 = \psi_a \chi_{aa}(q + \lambda)$, $\Xi_b^0 = \psi_b \chi_{bb}(q)$, $\Phi_c^0 = \psi_c \chi_{cc}(q - \lambda)$, where χ_{aa} , χ_{bb} , and χ_{cc} are harmonic oscillator functions centered about $q = -\lambda$, 0, and λ , respectively. The corresponding eigenenergies are $E_{a\nu}^0 = E_{c\nu}^0 = (\nu + 1/2)$, $E_{b\nu}^0 = (\nu + 1/2) + 2W$. It is thus natural to use Φ_a^0 , Ξ_b^0 , Φ_c^0 as the unperturbed basis and to treat V^{AB} as the perturbation. The treatment is increasingly applicable as $|\epsilon|, |\epsilon'| \ll \lambda^2$. This type of approach was used by Fulton and Gouterman many years ago.¹⁷

To make use of the interchange symmetry, we write

$$\Phi_{\nu}^{0+} = (1/2^{1/2})(\psi_a \chi_{aa} + (-1)^{\nu} \psi_c \chi_{cc})$$

$$\Phi_{\nu}^{0-} = (1/2^{1/2})(\psi_a \chi_{aa} - (-1)^{\nu} \psi_c \chi_{cc})$$

$$\Xi_{\nu}^{0+} = \psi_b \chi_{bb}, \quad \nu = \text{even}$$

$$\Xi_{\nu}^{0-} = \psi_b \chi_{bb}, \quad \nu = \text{odd} \quad (31)$$

and the perturbation can only couple (+) with (+) or (-) with (-). The energies to first order are ($2W$ noninteger):

$$E_{\Phi_{\nu}^{\pm}} = (\nu + 1/2) \pm (-1)^{\nu} \epsilon' \langle \chi_{aa} | \chi_{cc} \rangle$$

$$E_{\Xi_{\nu}^{\pm}} = (\nu + 1/2) + 2W \quad (32)$$

and the corresponding eigenfunctions are

$$\Phi_{\nu}^{\pm} =$$

$$\Phi_{\nu}^{0\pm} = (-1)^{\nu} \epsilon' \sum_{\alpha} r'_{\nu \alpha} \Phi_{\alpha}^{0\pm} \frac{\langle \chi_{aa} | \chi_{cc} \rangle}{\alpha - \nu} - 2^{1/2} \epsilon \sum_{\substack{\alpha = \text{even}(+) \\ \text{or odd}(-)}} \Xi_{\alpha}^{0\pm} \frac{\langle \chi_{ba} | \chi_{ba} \rangle}{\alpha - \nu + 2W}$$

$$\Xi_{\nu}^{\pm} = \Xi_{\nu}^{0\pm} - 2^{1/2} \epsilon \sum_{\alpha} r_{\nu \alpha} \Phi_{\alpha}^{0\pm} \frac{\langle \chi_{aa} | \chi_{bb} \rangle}{\alpha - \nu - 2W} \quad (33)$$

where either all upper or all lower signs apply. The quantities $\langle \chi_{aa} | \chi_{bb} \rangle$, $\langle \chi_{aa} | \chi_{cc} \rangle$, etc. are the well-known overlap integrals between displaced harmonic oscillators of equal force constant which can be conveniently expressed in terms of associated Laguerre polynomials (see, for example, eq A4.1, ref 17).

We may now immediately use these wave functions to calculate transition moments through first order. The results are (using the abbreviation, $M \equiv \langle \psi_{+} | m_z | \psi_{-} \rangle$)

$$\langle \Phi_{\nu}^{\pm} | m_z | \Phi_{\nu'}^{\mp} \rangle = M$$

$$\langle \Phi_{\nu}^{\pm} | m_z | \Phi_{\nu'}^{\pm} \rangle = \pm (-1)^{\nu} (2\epsilon' M) \langle \chi_{aa} | \chi_{cc} \rangle / (\nu' - \nu) \quad (35)$$

$$\langle \Phi_{\nu}^{\pm} | m_z | \Xi_{\nu'}^{\mp} \rangle = (-2^{1/2} \epsilon M) \langle \chi_{aa} | \chi_{bb} \rangle / (\nu' - \nu - 2W) \quad (36)$$

Equation 34 describes the so-called tunneling transition^{3,18} (infrared-enhanced transition in the delocalized limit¹⁰) between

(16) Prassides, K.; Schatz, P. N.; Wong, K. Y., to be published.
 (17) Fulton, R. L.; Gouterman, M. *J. Chem. Phys.* **1961**, *35*, 1059-1071.
 (18) Schatz, P. N.; Piepho, S. B.; Krausz, E. R. *Chem. Phys. Lett.* **1978**, *55*, 539-542.

the Φ_{ν}^{\pm} split pair. Equations 35 and 36 describe intervalence transitions.

Finally, we note that if $2W$ is an integer, there will be accidental degeneracies between $E_{a\nu}^0 = E_{c\nu}^0$ and $E_{b\nu}^0$. In that case it is straightforward to start by diagonalizing the degenerate pairs in the perturbation.

B. The Unsymmetrical Case ($A \neq B$). The previous treatment is easy to extend to this case. Starting with eq 27, the obvious unperturbed vibronic functions are $\Phi_a^0 = \psi_a \chi_{a\nu}(q + \lambda)$, $\Phi_b^0 = \psi_b \chi_{b\nu}(q)$, $\Phi_c^0 = \psi_c \chi_{c\nu}(q - \lambda)$ with corresponding eigenenergies $E_a^0 = \nu + 1/2$, $E_b^0 = (\nu + 1/2) + 2W$, $E_c^0 = (\nu + 1/2) + 2W'$. If we choose $2W$ and $2W'$ noninteger to avoid accidental degeneracy, the E_i^0 ($i = a, b, c$) are unchanged to first order. It is straightforward to write the perturbed wave functions. The corresponding transition moment matrix elements are then found to be:

$$\begin{aligned} \langle \Phi_{a\nu} | m_z | \Phi_{c\nu} \rangle &= 2\epsilon M \langle \chi_{a\nu} | \chi_{c\nu} \rangle / (\nu' - \nu - 2W) \\ \langle \Phi_{a\nu} | m_z | \Phi_{b\nu} \rangle &= -\epsilon M \langle \chi_{a\nu} | \chi_{b\nu} \rangle / (\nu' - \nu - 2W) \end{aligned} \quad (37)$$

VI. Applications of the Model

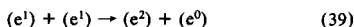
A. Potential Energy Surfaces. As has been stressed before,^{3,5} the adiabatic potential surfaces offer physical insight into the mixed valence problem (or, in general, into the phase diagram¹⁴ of the two-site two-electron problem), but they can be used only in a qualitative fashion to predict absorption profiles and other physical observables.

Equations for the potential energy surfaces are obtained by diagonalization of eq 11; this also leads to the electronic eigenfunctions associated with these surfaces. These functions are eigenfunctions of the electronic Hamiltonian and thus apply only if the kinetic energy operators are omitted³ (i.e. in the "static" limit); they do not commute with T_n and that is why we do not use them as basis functions in the dynamic treatment. However, in the special cases where ϵ (and/or ϵ') and λ are not simultaneously nonzero, they do not depend on the vibrational coordinate q . Then we can separate the nuclear from the electronic problem in the Born-Oppenheimer approximation.

In Figure 1 we show the potential energy surfaces for certain special cases. If we start by assuming that $\epsilon = \epsilon' = 0$, eq 8 gives the adiabatic potentials (Figure 1a):

$$\begin{aligned} W_a/h\nu &= 1/2(q + \lambda)^2 \\ W_b/h\nu &= 1/2q^2 + 1/2\lambda^2 - U \\ W_c/h\nu &= 1/2(q - \lambda)^2 \end{aligned} \quad (38)$$

(Henceforth, we abbreviate ν as ν if there is no ambiguity.) The energy term $(1/2)\lambda^2$ represents the stabilization due to electron-phonon coupling of the mixed-valence states (or the double occupancy states) relative to the single-valence state (or the one-by-one occupancy state). The parameter $2W$ ($\equiv (1/2)\lambda^2 - U$) directly measures their relative stabilities. If $W > 0$, the mixed-valence state is stabilized at the expense of the single-valence one, or disproportionation of the type



has taken place with the electron-pair localized on one site only. This is the so-called "negative- U " effect.¹³ If $W < 0$, the "delocalized" (single-valence) state is more stable. Furthermore, the existence of a potential barrier¹⁴ between the localized and delocalized state persists for values of W greater than $-(1/4)\lambda^2$.

A second limiting case is $\lambda = 0$ (or $2W = -U$). Then (eq 11) the adiabatic potentials are

$$\begin{aligned} W_a/h\nu &= 1/2(q^2 - U) - 1/2(U^2 + 8\epsilon^2)^{1/2} \\ W_b/h\nu &= 1/2q^2 \\ W_c/h\nu &= 1/2(q^2 - U) + 1/2(U^2 + 8\epsilon^2)^{1/2} \end{aligned} \quad (40)$$

when $\epsilon' = 0$. Note that the ground state tends to the valence bond or molecular orbital state of the hydrogen molecule as $|q|/U \rightarrow 0$ or ∞ , respectively.¹⁴

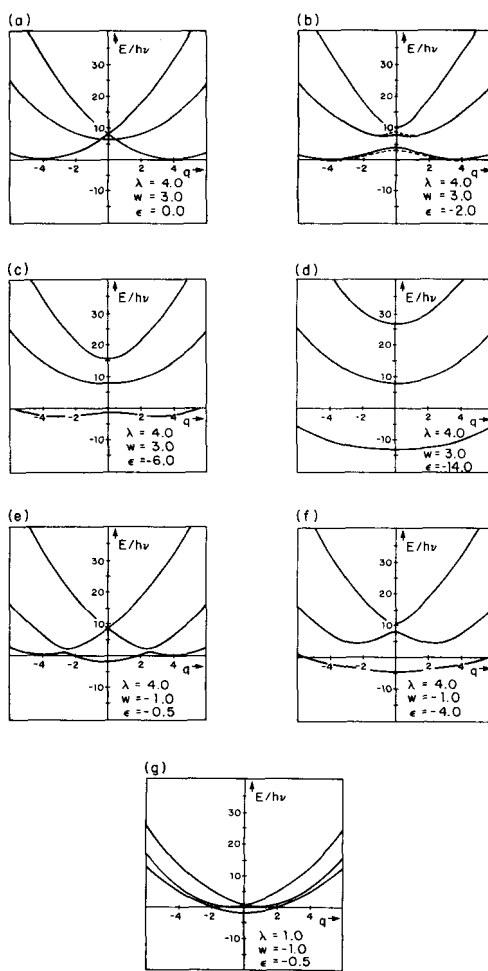


Figure 1. Potential energy surfaces (in units of $h\nu$) in q space for a range of values of λ , W , and ϵ . The solid curves apply for $\epsilon' = 0$ and the dashed curve in (b) applies for $\epsilon' = -2.0$.

In general, the surfaces are no longer harmonic when both ϵ and λ are nonzero. A variety of such cases are presented in Figure 1. Keeping $\epsilon' = 0$ when $W > 0$, the ground-state potential surface W_1 has three minima for small values of $|q|$, a shallow one at $q = 0$, and a pair of deeper ones at $\pm q_1$. As $|q|$ becomes larger, the minimum at $q = 0$ disappears and $|q_1|$ becomes smaller. For values of $|q| \gg (1/4)\lambda^2 + W$, W_1 has a single minimum at $q = 0$ (Figure 1d). The first excited-state surface W_2 shows two minima at $\pm q_2$ for small values of $|q|$ that eventually coalesce as $|q|$ increases (Figure 1, c and d). W_3 , the second excited state surface, has a single minimum at $q = 0$ in all cases. A similar pattern is followed in the case $W < 0$ (Figure 1, e, f, and g). If $0 < (1/4)\lambda^2 + W$, W_1 has a single minimum at $q = 0$ for large $|q|$; otherwise it has three minima, the one at $q = 0$ being deepest. If $0 > (1/4)\lambda^2 + W$, W_1 always has a single minimum at $q = 0$. A nonzero value for ϵ' will lead to a smaller potential barrier in the ground surface (Figure 1b). An illuminating discussion of the "phase diagram" of these systems has been given by Toyozawa¹⁴ (for the case $\epsilon' = 0$).

B. The Absorption Band. A characteristic feature of mixed-valence systems (classes II and III)² is the existence of an ab-

Vibronic Coupling Model for Two-Electron Systems

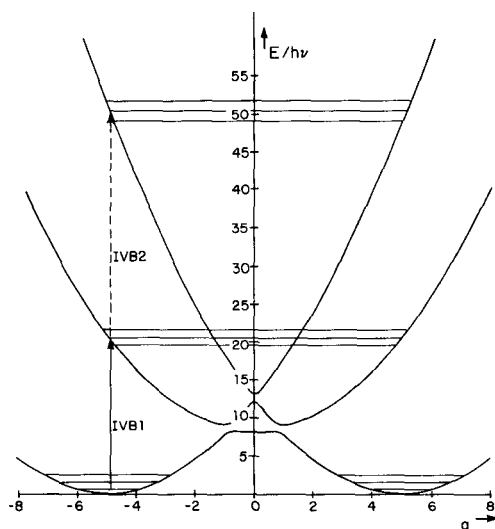
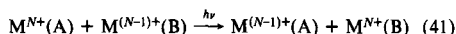
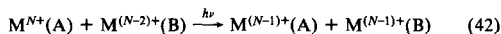


Figure 2. Potential energy surfaces (units of $h\nu$) in q space for $\epsilon = -0.5$, $\epsilon' = -0.5$, $\lambda = 5.0$, $W = 4.1$. The vertical arrows indicate the approximate energies of the first (IVB1) and second (IVB2) intervalence bands described, respectively, by eq 42 and 43. The horizontal lines show the location of three of the vibronic levels "on" each surface. The tunneling splittings of the vibronic lines are too small to be seen to the scale of the figure for this strongly localized case.

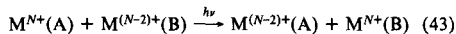
sorption band (the so-called intervalence band) which is not present in the absorption spectrum of either of the single-valence moieties. If there is a one-electron difference between the two centers, the intervalence band is associated with the intermolecular charge-transfer process



whence an electron is transferred from the donor site B to the acceptor site A. In the two-site, two-electron case, two such processes and hence two intervalence bands are possible, namely the one-electron charge transfer governed by ϵ



and the two-electron charge transfer governed by ϵ'



The absorption spectrum corresponding to these processes is readily calculated in our treatment because we can calculate the eigenfunctions and eigenvalues associated with the interacting potential surfaces. The band intensity as a function of frequency can be written

$$I(\nu) = C\nu \sum_i D_i f_i(\nu) \quad (44)$$

in which D_i is the dipole strength of the i th transition whose line shape is given by $f_i(\nu)$, and the summation is over all transitions. C is a constant which depends upon the units used and simply serves as a scaling factor in our case since we only calculate relative intensities. In our calculations we choose $f_i(\nu) = (1/\Delta\pi^{1/2}) \exp[-(\nu - \nu_i)^2/\Delta_i^2]$, a normalized Gaussian which is supposed to represent the various interactions which give each line its breadth. Δ_i is chosen to produce a smooth band and is usually assigned a fixed value for all lines in a band. In the symmetrical case, \mathcal{F}_{ν_i} of eq 25 is calculated from eq 23 if the diagonalization ("exact") procedure is used or from eq 34–36 if the perturbation treatment is applicable. Likewise, eq 29 or eq 37 is used in the unsymmetrical case. [A very important check of both our exact and perturbational approaches was explicit numerical confirmations that both

The Journal of Physical Chemistry, Vol. 90, No. 22, 1986 5593

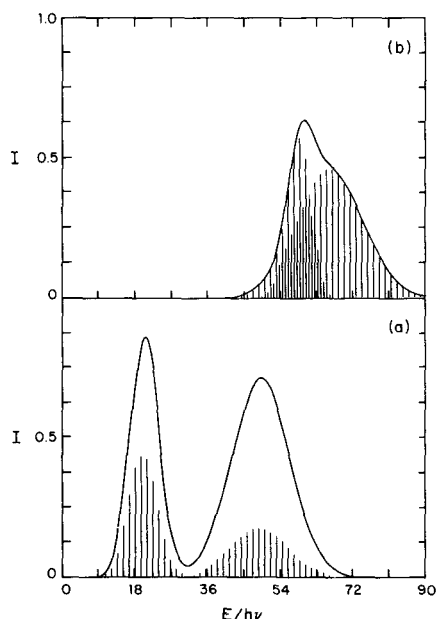


Figure 3. Calculated absorption contours at 4.2 K showing the two sets of intervalence transitions in the case of nonzero electronic coupling constants ϵ and ϵ' . Each vibronic transition (vertical bar) is assumed to be a Gaussian with half-width 1.2 ν : (a) $\nu = \nu_1 = \nu_2$ (see eq 47) with parameters $\lambda = 5.0$, $W = 4.1$, $\epsilon = -0.5$, $\epsilon' = -0.5$; (b) $\nu = \nu_1 \neq \nu_2$ (see eq 47 and 48) with parameters $\lambda = 5.8$, $W = 23.4$, $\nu = 307.4 \text{ cm}^{-1}$, $\tau = 0.84$, and $\epsilon = \epsilon'$ anywhere in the range 0 to -1.0 . The very low energy infrared (tunneling) transitions are of negligible intensity to the scale of the figure.

gave (essentially) the same eigenvalues, eigenvectors, and dipole strengths for strongly localized cases ($\epsilon, \epsilon' \ll \lambda^2$).

In general, one can divide the absorption spectrum into three regions (Figure 2). The first involves transitions in the infrared, the charge-transfer-induced (or so-called "tunneling") transitions since they occur between split levels on the lower potential surface. (For experimental confirmation of their existence in delocalized systems, see ref 10, 15, and 19.) The second involves transitions "between" the ground and the first excited-state potential surfaces and the third "between" the ground and second excited-state potential surfaces. Thus if both ϵ and ϵ' are nonzero, the existence of two intervalence bands is predicted. In Figure 3a, we show the calculated absorption (intervalence) spectrum of the system depicted in Figure 2 ($\lambda = 5.0$, $W = 4.1$, $\epsilon = -0.5$, $\epsilon' = -0.5$).

We note that in strongly localized systems (either in the simple PKS or present extension) the "tunneling" splittings will be extremely small. By eq 32, this splitting is $2\epsilon' \langle \chi_{a0} | \chi_{a0} \rangle = 2\epsilon' \times \exp(-\lambda^2)$. Likewise, the ratio of "tunneling" to intervalence intensity will be minute because of the presence of $(N_\nu - N_\nu)$ in eq 24 and the presence of ν in eq 44.

VII. Wolfram's Red Salt

Wolfram's Red Salt (WRS), $[\text{Pt}^{\text{II}}(\text{EtNH}_2)_4][\text{Pt}^{\text{IV}}(\text{EtNH}_2)_4\text{Cl}_2]\text{Cl}_4 \cdot 4\text{H}_2\text{O}$, is the prototype of a large class of quasi-one-dimensional mixed-valence compounds²⁰ which consist of linear chains of halogen-bridged alternating Pt(II) and Pt(IV) subunits. Recently, this series has been further enriched with the preparation of Pd^{II}-Pd^{IV} mixed-valence and Pd^{II}-Pt^{IV} mixed-metal

(19) Rice, M. J.; Yartsev, V. M.; Jacobsen, C. S. *Phys. Rev. B* **1980**, *21*, 3437–3446.

(20) Clark, R. J. H. In *Mixed-Valence Compounds*, Brown, D. B., Ed.; Reidel: New York, 1980; pp 271–292.

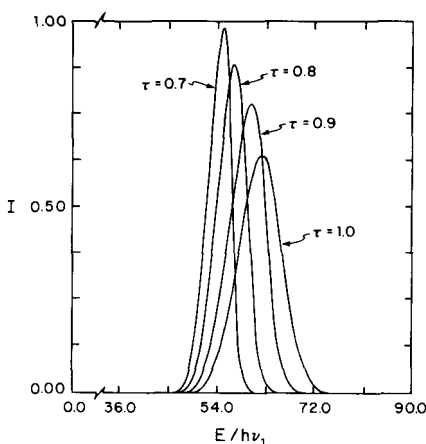
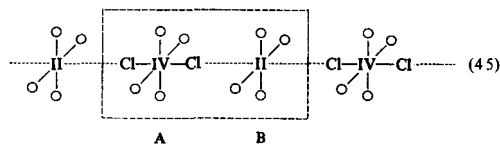


Figure 4. Calculated intervalence absorption profiles in the low temperature limit for the unequal force constant case with parameters $\lambda = 5.5$, $W = 23.1$, and $\epsilon = -0.5$. The profiles are synthesized from Gaussian vibronic transitions of half-width $1.2\nu_1$: $\tau = \nu_2/\nu_1$.

analogues.^{21,22} A rich variety of spectroscopic evidence (e.g., far-infrared and Raman,^{23,24} ultraviolet and visible,^{25,26} and photoelectron²⁷ spectra) together with conductivity²⁸ measurements show that WRS (and its analogues) are Robin-Day class II² mixed-valence systems. Of particular interest is the impressive resonance Raman spectrum^{20,26} of WRS which is produced by excitation into the intervalence band and which is dominated by a long harmonic progression (up to 16 quanta) in ν_1 , the symmetric Cl-Pt^{IV}-Cl stretching fundamental (307.4 cm⁻¹ at 4 K).²⁶ This rather conclusively demonstrates the small electronic coupling between the Pt(II) and Pt(IV) centers.

A. The Model Hamiltonian. The structure of WRS is schematically represented as follows: We concentrate our analysis



on one "unit cell" along the chain (the dashed box in (45)). In principle, the two-site two-electron system should be replaced by an N -site N -electron system using an electronic basis of Bloch functions to take account of the translational symmetry of the infinite one-dimensional chain. However, the experimental evidence strongly suggests that coupling between "unit cells" along the chain is small. Thus for the calculation of the optical properties of interest it seems an excellent approximation to consider a single "unit cell" (cf. the three-dimensional mixed-valence hexachloro-antimonate(III,V) systems¹² in which treating a single dimer, Sb^{III}Cl₆³⁻-Sb^VCl₆⁻, seems a less satisfactory assumption).

In our analysis, we closely follow previous theoretical treatments of these systems,³ but we extend the two-center one-electron model

to take explicit account of the intrasite electron-electron repulsion. In analogy to eq 2 and 3, we define our valence states as

$$\begin{aligned}\psi_a &= \psi_{IV}^A \psi_{II}^B \\ \psi_b &= \psi_{III}^A \psi_{III}^B \\ \psi_c &= \psi_{II}^A \psi_{IV}^B\end{aligned}\quad (46)$$

We choose an origin halfway between A and B in (45) and designate the position of the closer Cl atom with respect to this origin by the variable x . Then following section II, we obtain⁵

$$\begin{aligned}W_a &= 4\pi^2\nu_1^2 M_{Cl}(x - x_0^A)^2 \\ W_b &= 4\pi^2\nu_2^2 M_{Cl}x^2 + 2W\hbar\nu_1 \\ W_c &= 4\pi^2\nu_1^2 M_{Cl}(x - x_0^B)^2\end{aligned}\quad (47)$$

where x_0^A , x_0^B , and zero are the equilibrium positions of the Cl atom in states ψ_a , ψ_c , and ψ_b , respectively; note that $x_0^A = -x_0^B$ and that, in general, $\nu_2 \neq \nu_1$. The problem can be reduced to the standard form, eq 8, if we make the following definitions:⁵

$$\begin{aligned}q &= 2(2^{1/2})\pi M_{Cl}^{1/2}(\nu_1/\hbar)^{1/2}x \\ \lambda &= \left(\frac{8\pi^2 M_{Cl}\nu_1}{h}\right)^{1/2} |x_0^A| \\ \tau &= \nu_2/\nu_1\end{aligned}\quad (48)$$

Then eq 47 becomes

$$\begin{aligned}W_a/\hbar\nu_1 &= \frac{1}{2}(q + \lambda)^2 \\ W_b/\hbar\nu_1 &= \frac{1}{2}\tau^2 q^2 + 2W \\ W_c/\hbar\nu_1 &= \frac{1}{2}(q - \lambda)^2\end{aligned}\quad (49)$$

Note particularly that unequal force constants have been introduced and this does not couple a Q_+ mode back into the problem as would be the case in the general treatment (see eq 6 et seq.). This is so because the system is modeled as a linear chain, and no analogue of the Q_+ mode occurs. In general, we would expect $\tau < 1$ in view of the longer Pt-Cl bond in the III-III state. If $\tau = 1$ (the equal force constant case), the perturbation treatment of section V or the "exact" treatment of sections II and IVA for a symmetrical system ($W = 0$) applies identically. If $\tau \neq 1$ (the unequal force constant case), the perturbation treatment of section V can be easily modified. Equations 34 and 35 continue to apply and eq 36 becomes

$$\langle \Phi_{\nu'}^* | m_z | \bar{\Psi}_{\nu'} \rangle = (-2^{1/2}\epsilon M) \langle \chi_{a\nu'}(\nu_1) | \chi_{b\nu'}(\nu_2) \rangle / (\nu' - \tau\nu - 2W) \quad (50)$$

where $\langle \chi_{a\nu'}(\nu_1) | \chi_{b\nu'}(\nu_2) \rangle$ is the overlap integral between two displaced harmonic oscillators of different frequencies. An explicit analytic expression for this integral exists in terms of Hermite polynomials.²⁹ Likewise, in the "exact" treatment, eq 22 and 23 still apply if only H'_{mn} is replaced by

$$\begin{aligned}H'_{mn} &= [(m + \frac{1}{2})\tau + 2W]\delta_{mn}, \quad m = \text{even}; \\ H'_{mn} &= 0, \quad m = \text{odd}\end{aligned}\quad (51)$$

In Figure 4, we illustrate the effect on the intervalence band of varying τ from unity.

B. Absorption, Resonance Raman, and Luminescence Spectra. In Figure 5a we reproduce the Raman spectrum of WRS obtained by Tanino and Kobayashi²⁶ following excitation into the intervalence band. Both the exciting and scattered light are polarized parallel to the z axis (the Pt^{II}-Pt^{IV} chain axis). The spectrum consists of three parts: (i) the well-known harmonic progression (labeled R) in $\nu_1 = 307.4$ cm⁻¹, the Cl-Pt^{IV}-Cl stretching fundamental, (ii) a flat, broad emission band (labeled B) that shows up immediately below the excitation energy, most prominently

(21) Clark, R. J. H.; Croud, V. B.; Kurmoo, M. *Inorg. Chem.* **1984**, *23*, 2499-2504.

(22) Clark, R. J. H.; Croud, V. B. *Inorg. Chem.* **1985**, *24*, 588-592.

(23) Clark, R. J. H.; Franks, M. L.; Trumble, W. R. *Chem. Phys. Lett.* **1976**, *41*, 287-292.

(24) Clark, R. J. H.; Turtle, P. C. *Inorg. Chem.* **1978**, *17*, 2526-2531.

(25) Day, P. In *Low-Dimensional Cooperative Phenomena*, Keller, H. J., Ed.; Plenum: New York, 1975; pp 191-214.

(26) Tanino, H.; Kobayashi, K. *J. Phys. Soc. Jpn.* **1983**, *52*, 1446-1456.

(27) Cahen, D.; Lester, J. E. *Chem. Phys. Lett.* **1973**, *18*, 108-111.

(28) Interrante, L. V.; Browall, K. W.; Bundy, F. B. *Inorg. Chem.* **1974**, *13*, 1158-1162.

(29) Sidors, P.; Marcus, R. A. *J. Am. Chem. Soc.* **1981**, *103*, 741-747.

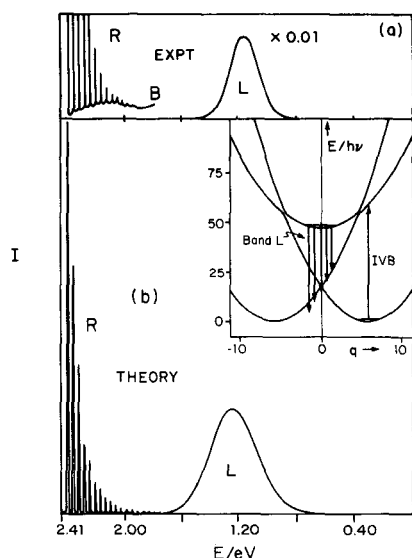


Figure 5. (a) 4.2 K Raman spectrum of Wolfram's Red Salt using laser excitation at 2.410 eV from Tanino and Kobayashi.²⁶ (For a quantitative depiction of band R, see ref 8, 23, and 24.) The abscissa is the energy of the scattered light. (b) Calculated spectrum using the parameters: ϵ in the range 0 to -1.0 , $\epsilon' = 0$, $\lambda = 5.8$, $W = 23.4$, $\tau = 0.84$, $\nu_1 = 307.4 \text{ cm}^{-1}$, $\Gamma_E = 6.0\nu_1$ (eq 53). Individual transitions are represented by Gaussians of half-width of $0.12\nu_1$ (band R) and $1.2\nu_1$ (band L). The inset shows the potential energy surfaces for these parameters choosing $\epsilon = -1.0$. The vertical arrows symbolize the excitation (IVB) and emission (band L) processes.

observed when both the exciting and scattered light are polarized parallel to the z axis, and (iii) an intense, unstructured, and slightly asymmetric emission band at 1.15 eV (labeled L).

In a series of papers,⁸⁻¹⁰ Wong and Schatz used the two-center one-electron PKS model to calculate resonance Raman spectra and resonance Raman excitation profiles. The relative intensities of the Raman lines are calculated from

$$I_s \sim \nu_s^4 \sum_{\rho\sigma} |(\alpha_{\rho,\sigma})_{G \rightarrow F}|^2 \quad (52)$$

where ν_s is the frequency of the scattered light and $(\alpha_{\rho,\sigma})_{G \rightarrow F}$ is the polarizability tensor for the transition $G \rightarrow F$, with ρ and σ the polarizations of the incident and scattered radiation:

$$(\alpha_{\rho,\sigma})_{G \rightarrow F} = (hc)^{-1} \sum_E \left[\frac{\langle F|m_\rho|E\rangle \langle E|m_\sigma|G\rangle}{\nu_{GE} - \nu_L + i\Gamma_E} + \frac{\langle F|m_\sigma|E\rangle \langle E|m_\rho|G\rangle}{\nu_{FE} + \nu_L + i\Gamma_E} \right] \quad (53)$$

m_α is the component of the electric dipole operator, ν_L is the frequency of the incident light, and Γ_E is a damping factor associated with intermediate state $|E\rangle$. In principle, the summation runs over the complete vibronic manifold of all electronic states $|E\rangle$ but is restricted in the resonance case to the electronic state in resonance with the exciting light. Since the PKS model yields a "complete" set of vibronic eigenfunctions and eigenvalues if the parameters ϵ , λ , W , and ν are specified, one can routinely evaluate eq 53 for a specified value of Γ_E and thus explore the predicted characteristics of mixed-valence resonance Raman spectra. These calculations show that in strongly localized systems, in addition to the expected long harmonic vibrational progression (band R, Figure 5), another series of Raman lines can occur whose Stokes shifts correspond to transitions between the two vibronically coupled surfaces. The intensity of these "electronic" Raman transitions relative to the vibrational progression depends critically on the magnitude of ϵ . It was thus argued¹⁰ that band L originates

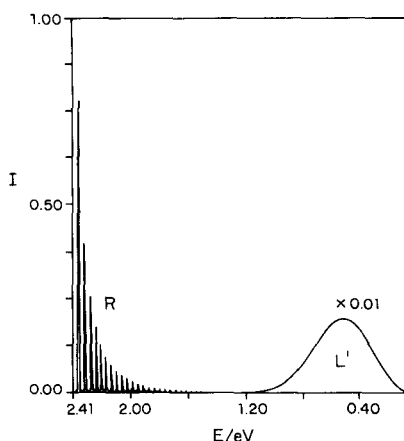


Figure 6. Calculated resonance Raman spectrum at 4.2 K using parameters: $\epsilon = -0.1$, $\lambda = 10.0$, $W = 4.1$, $\tau = 1.0$, $\nu_1 = 307.4 \text{ cm}^{-1}$, $\Gamma_E = 3.0\nu_1$, $\nu_L = 63.24\nu_1$. Band R is the vibrational progression with individual transitions represented by Gaussians of half-width $0.12\nu_1$. Band L' is the "electronic" Raman band synthesized from Gaussians of half-width $1.2\nu_1$.

from these "electronic" Raman transitions. Tanino and Kobayashi had, on the other hand, proposed that band L be identified as an emission from a self-trapped state to which the system has relaxed following excitation into the intervalence band.²⁶ A difficulty with the "electronic" Raman assignment¹⁰ arises when the location and width of band L is calculated. While parameters can be found that correctly locate the intervalence band and correctly describe band R and the relative intensities of bands R and L, the calculations consistently overestimate the band R-band L separation, and the width of the latter. It was suggested¹⁰ that these discrepancies might be accounted for in a treatment which properly included the $\text{Pt}^{\text{III}}\text{-Pt}^{\text{III}}$ surface (W_b), i.e. the treatment we have done in earlier sections of this paper.

We have therefore repeated the resonance Raman calculations using eq 52 and 53. $|G\rangle$, $|F\rangle$, and $|E\rangle$ all correspond to the eigenfunctions we obtain by coupling the surfaces in eq 49 in accord with the treatment in sections IV.A and/or V.A (taking note of eq 50 and 51 when $\tau \neq 1$). We use a sufficient basis that truncation of the sum in eq 53 does not significantly affect our results. Despite strenuous efforts, the difficulties encountered in the simpler model persist. Figure 6 shows a typical case where the parameters ($\epsilon = -0.10$, $\lambda = 10.0$, $W = 4.1$, $\tau = 1.0$, $\nu_1 = 307.4 \text{ cm}^{-1}$) have been chosen. These account correctly for the location of the intervalence band and the relative intensities within band R and between bands R and L. However, the calculated separation between the first line of band R and the maximum of band L remains substantially higher than observed, viz. $\approx 50\nu_1 = 1.906 \text{ eV}$ vs. $\approx 33\nu_1 = 1.258 \text{ eV}$ for excitation frequency $\nu_L = 63.24\nu_1 = 2.410 \text{ eV}$. The calculated width is also about twice that observed. All attempts to move band L closer to band R fail if the correct location of the intervalence band is maintained. (If $\epsilon' \neq 0$, a second electronic Raman band is predicted with a still larger Stokes shift.) We thus conclude that the present model also cannot account for the location of band L on the basis of an electronic Raman effect. We therefore now use our model to examine the proposal of Tanino and Kobayashi.²⁶

Following excitation into the intervalence band, let us suppose the system relaxes rapidly to the ground vibrational level of the (III,III) potential energy surface (see inset, Figure 5b). We then assume that emission from this state is responsible for band L. (Band B could then be assigned to hot luminescence during the above relaxation process.) We can easily synthesize band L since, by choosing values of ϵ , ϵ' , λ , W , τ , and ν_1 , we determine the "complete" vibronic manifold. For a strongly localized system like WRS, the perturbation treatment (section VA) can be used.

The intensity of each vibronic emission line $\Xi_0^+ \rightarrow \Phi_r^-$ is obtained from

$$I(\Xi_0^+ \rightarrow \Phi_r^-) \propto E_{0r}^4 |\langle \Xi_0^+ | m_z | \Phi_r^- \rangle|^2 \quad (54)$$

where E_{0r} is the difference in energy between the emitting and the final vibronic state, and the transition moment matrix element is given by eq 50. Each emission line is convoluted with a Gaussian broadening function of the same width arbitrarily chosen to obtain a smooth, unstructured profile. In Figure 5b we show a typical attempt to account for the observed spectrum (but not band B). The agreement is quite good. The relative intensities within band R and the separation of bands R and L are accounted for well although the calculated width of band L is about 50% greater than observed. It is not possible to calculate the relative intensities of bands R and L, and these have been arbitrarily scaled. The parameters used also correctly locate the intervalence band. [In fact the separation between bands R and L can be correctly predicted for a range of values of our parameters ($\lambda = 5.4-6.0$, $W = 22.3-23.4$, $\tau = 0.77-1.0$) which also correctly locate the intervalence band.]

We thus conclude that the Tanino-Kobayashi hypothesis provides a basis for explaining the observed WRS spectrum (Figure 5a). There are, however, difficulties in the details of our treatment. First, the value of λ used, $\approx 5.4-6.0$, predicts a value of $|\chi_0^A|$ which is only about half the observed value (see eq 167 et seq., ref 5). Second, using the parameters giving rise to Figure 5b, we obtain $U \approx -30\nu_1 \approx -1.1$ eV from eq 16. A simple view of the model requires $U > 0$, but we have neglected intersite electron repulsion and considered only one coordinate q . It could well be that a positive U would emerge when all degrees of freedom are considered, as in calculations³⁰ on the mixed-valence salt Cs_2SbCl_6 where all vibrational degrees of freedom and the lattice coulomb energy were included. Clearly, in the present approximate calculations we must regard parameters such as U and λ as *effective quantities*. We note in a recent treatment of WRS and related systems that Nasu³¹ suggested the parameters $2T \sim S$ with $2T$, U , and S all of the order of 1 eV. Translating to our units via eq 17, this is equivalent to $\lambda^2 \approx 2(2^{1/2})|e|$, i.e. an intermediate case where vibronic and electronic coupling are comparable. It seems to us that such a possibility can be dismissed because it is incompatible with the observed vibrational resonance Raman spectrum of WRS. Specifically, the latter spectrum shows a very *harmonic* progression in ν_1 going up to 16 quanta. This means that the lower potential surface is *very harmonic* up to at least $16\nu_1 = 4900 \text{ cm}^{-1} \approx 0.61$ eV, which would not be compatible with the parameters suggested by Nasu (see, for example, Figure 5b, ref 31). It would also seem difficult to understand the low electrical conductivity²⁸ of WRS with such a large electronic coupling (e).

Our treatment will not account for the observed²⁶ slight shift of band L with excitation frequency. Tanino and Kobayashi suggest that this is due to motion of the excited III-III state along the chain, a phenomenon outside the scope of our model. We do note that, in a number of similar II-IV systems, no shift of band L with excitation frequency is observed.³²

The prediction⁹ of a possible electronic Raman effect in WRS and similar systems remains unconfirmed. Our calculations (Figure 6) indicate that such a band will be Stokes shifted an additional ≈ 0.65 eV with respect to band L. In addition, the predicted intensity of this band decreases rapidly in intensity relative to band R as $|e|$ increases.⁹ Thus if $|e|$ is appreciably greater than 0.1, the intensity of this band may be very small.

C. The Composite Nature of the Intervalence Band in WRS. The intervalence band in WRS has a rather strange shape. It rises very sharply at ≈ 2.1 eV and then stays almost flat to ≈ 3 eV where it is obscured by a strongly rising background absorption (see Figure 2, ref 26 and Figure 9, ref 33). (The latter also reports

an unexplained smaller band at ~ 1.63 eV which appears at low temperature.) The shape of the band suggests overlapping transitions. We can model this possibility by allowing $e' \neq 0$. Such a calculation is illustrated in Figure 3b for the case $e'/e = 1.0$. (The calculation is sensitive to the ratio but not to the numerical values of e and e' over the range 0 to -1.0 .) It is not possible to compare this contour quantitatively with the experimental band because of the background absorption. But there is a quite reasonable qualitative resemblance. (The parameters used to obtain Figure 3b are the same as those used to obtain Figure 5b except that $e' = e$ instead of $e' = 0$. Because $|e|, |e'| \ll \lambda^2$, this change to a nonzero e' does not appreciably alter the calculated spectrum in Figure 5b.)

Two distinct intervalence bands, at ~ 2 and 3.5 eV, have been observed by Prassides and Day for the $\text{Sb}^{\text{III}}\text{Cl}_6^{3-}-\text{Sb}^{\text{V}}\text{Cl}_6$ system.¹² The lower energy band was assigned¹² to the one-electron transfer, eq 42. Recently Dubicki³⁴ proposed that the second band be associated with the process in eq 43, i.e. $e' \neq 0$, or even that these two assignments be interchanged since the higher energy band is sharper and more intense.³⁵ For the analogous InCl_2 mixed-valence salt, however, it has been shown that the first optical excitation is to the paramagnetic $\text{In}^{\text{II}}-\text{In}^{\text{I}}$ state.³⁶

Examination of the definitions of e and e' (eq 14) and the form of the functions ψ_a^s and ψ_b^s (eq 12) implies that $e'/e \sim \langle \psi^A | \psi^B \rangle \ll 1$. Thus whether $e' \neq 0$ can play a significant role in these systems remains open to question and requires further investigation.

VIII. Conclusion

It has been shown that a three surface treatment of dimer mixed-valence systems whose moieties can differ by two in oxidation number is equivalent to a two-electron, two-site model. With appropriate assumptions, solution of the model can be reduced to a one-mode problem for which we have given the explicit secular equations in both the symmetrical and unsymmetrical case. A simple perturbational solution has also been given for strongly localized systems (strong vibronic coupling). Some general characteristics of the potential energy surfaces and intervalence band have been explored.

The model has been applied to the resonance Raman and luminescence spectrum of Wolfram's Red Salt with quite reasonable success. In particular, model parameters can be found which account for the vibrational resonance Raman spectrum and can also explain as a luminescence from the III-III state, the strong emission band observed by Tanino and Kobayashi. This latter band cannot be accounted for in our model by an electronic Raman effect as some of us previously suggested.¹⁰ The parameters obtained from our model cannot, in general, be given a literal interpretation but must rather be regarded as effective quantities. This is probably not surprising in view of the simplicity of the model—the assumption of equal force constants in different oxidation states (except in the linear chain case), choosing the vibronic coupling of the III oxidation state as the mean of the II and IV states, the use of a single effective mode, and the harmonic approximation—all are required to make a general solution tractable. Despite these simplifications, we believe the model provides a very useful framework within which to view $N, N-2$ mixed-valence systems. The model can also be readily extended to the many-mode case in both the localized and delocalized limits using perturbation theory.¹⁶ In the latter case, an analytic description of the infrared enhanced (charge oscillation¹⁵) modes in organic charge-transfer salts is perfectly feasible. (In effect, such a treatment has already been given by Wong using the simple PKS model.³⁷ Though his treatment is for the single-mode case, the extension to many modes is immediate since each mode

(33) Tanaka, M.; Kurita, S.; Kojima, T.; Yamada, Y. *Chem. Phys.* **1984**, *91*, 257-265.

(34) Dubicki, L., personal communication.

(35) Day, P. *Inorg. Chem.* **1963**, *2*, 452-456.

(36) Warren, Jr., W. W.; Schönherr, G.; Hensel, F. *Chem. Phys. Lett.* **1983**, *96*, 505-508.

(37) Wong, K. Y. *Inorg. Chem.* **1984**, *23*, 1285-1290.

(30) Prassides, K.; Day, P. *Inorg. Chem.* **1985**, *24*, 1109-1110.

(31) Nasu, K. *J. Phys. Soc. Jpn.* **1984**, *53*, 427-437.

(32) Wada, Y.; Mitani, T.; Yamashita, M.; Koda, T. *J. Phys. Soc. Jpn.* **1985**, *54*, 3143-3153.

contributes independently to first order.³⁸⁾

It would be interesting to apply the present model to other $\text{Pt}^{\text{II}}-\text{Pt}^{\text{IV}}$ systems and also to the spectra of the mixed-metal $\text{Pd}^{\text{II}}-\text{Pt}^{\text{IV}}$ systems recently reported by Clark and Croud²² where

(38) Schatz, P. N., unpublished calculation.

the unsymmetrical case ($W' \neq 0$) is applicable.

Acknowledgment. This work was supported by the S.E.R.C. (K.P. and P.D.) and by the National Science Foundation (P.N.S. and K.Y.W.) under Grants CHE8400423 and INT-8510077. We acknowledge many useful discussions with Professor S. B. Piepho and Dr. M. Kurmoo.

Charge Transfer in Mixed-valence Solids. Part I. Crystal Spectra of Chlorocuprates(I, II)

By P. Day and D. W. Smith, Inorganic Chemistry Laboratory, South Parks Road, Oxford

Reprinted from
JOURNAL
OF
THE CHEMICAL SOCIETY

SECTION A
Inorganic, Physical and Theoretical Chemistry

1967

Charge Transfer in Mixed-valence Solids. Part I. Crystal Spectra of Chlorocuprates(I, II)

By P. Day and D. W. Smith, Inorganic Chemistry Laboratory, South Parks Road, Oxford

The intensity of the mixed-valence absorption in a series of mixed-valence chlorocuprates has been measured as a function of the mole fraction of copper(I). The low intensity of the band agrees with its assignment as an intermolecular charge transfer from a chlorocuprate(I) anion to a chlorocuprate(II).

INORGANIC solids which contain the same element in two oxidation states often have absorption bands not present in related solids containing either oxidation state alone. These have been assigned to intermolecular charge transfer,¹ but very little information is available about their intensities. Yamada and Tsuchida² measured polarised crystal spectra of platinum(II, IV) and gold(I, III) compounds without giving any indication whether their samples obeyed the Lambert-Beer law and their spectra may be affected by stray light. Further, in compounds such as $[\text{Pt}^{\text{II}}(\text{NH}_3)_2\text{Cl}_2][\text{Pt}^{\text{IV}}(\text{NH}_3)_2\text{Cl}_4]$ the proportions of the two oxidation states are fixed stoichiometrically. As part of a study of the charge-transfer properties of mixed-valence solids by electronic spectroscopy and semiconductivity, we now report quantitative intensity data on the mixed-valence absorption in single crystals of hexamminecobalt(III) chlorocuprates(I, II) as a function of the mole fraction of copper(I). The latter may take any value between zero in $\text{Co}(\text{NH}_3)_6\text{CuCl}_5$ and unity in $[\text{Co}(\text{NH}_3)_6]_4\text{Cu}_5\text{Cl}_{17}$, depending on the composition of the solution from which the product is crystallised.³ Both single-valence compounds are orange, but the mixed-valence compounds are much darker, even black when equal mole fractions of copper(I) and copper(II) are present, owing to the appearance of an absorption band at about 17kk. Powder reflectance measurements⁴ suggested that the intensity of the band was proportional to the product of the mole fractions of the two oxidation states but this method cannot give quantitative inform-

ation about intensities, for which transmission measurements on single crystals are required. The use of polarised light does not yield additional information in this case since the crystal structures are cubic throughout the range of composition.⁵⁻⁷

The pure copper(II) and copper(I) compounds and mixed-valence compounds containing up to 50% Cu^{I} are readily crystallised as large octahedra. Compounds containing more than 50% of Cu^{I} have only been obtained as powders, since the mother-liquor tends to deposit a mixture of the pure Cu^{I} compound and a mixed-valence compound containing less than 50% of Cu^{I} when allowed to stand. Octahedral crystals are unsuitable for crystal spectroscopy; thin sections were cut from large crystals for our measurements, which were made with a single-crystal microspectrophotometer designed in this laboratory.⁸

The crystal spectrum of $\text{Co}(\text{NH}_3)_6\text{CuCl}_5$ in the visible region is dominated by an intense band which appears at 25kk in the powder reflectance spectrum and is assigned to an intramolecular charge transfer band of CuCl_5^{3-} .⁶ Like that of CuCl_4^{2-} , its molar extinction coefficient is likely to be several thousand. $[\text{Co}(\text{NH}_3)_6]_4\text{Cu}_5\text{Cl}_{17}$ showed only two bands, at 21.0 and 27.0kk, which are assigned to the ${}^1A_{1g} \rightarrow {}^1T_{1g}, {}^1T_{2g}$ transitions, respectively, of the hexamminecobalt(III) cation. The intensity of the 21.0kk band was identical with that in $\text{Co}(\text{NH}_3)_6\text{Cl}_3$ ($\epsilon = 60$).⁹ Analysis of the low-frequency tail of the visible absorption of $\text{Co}(\text{NH}_3)_6\text{CuCl}_5$ showed that up to about 20kk the

¹ M. B. Robin and P. Day, *Adv. Inorg. Chem. Radiochem.*, in press.

² S. Yamada and R. Tsuchida, *Bull. Chem. Soc. Japan*, 1956, **29**, 421.

³ M. Mori, *Bull. Chem. Soc. Japan*, 1960, **33**, 985; 1961, **34**, 1249.

⁴ D. Culpin, P. Day, P. R. Edwards, and R. J. P. Williams, *Chem. Comm.*, 1965, 450.

3 Y

⁵ M. Mori, Y. Saito, and T. Watanabe, *Bull. Chem. Soc. Japan*, 1961, **34**, 295.

⁶ P. Day, D.Phil. Thesis, Oxford, 1965.

⁷ P. Murray-Rust, P. Day, and C. K. Prout, *Chem. Comm.*, 1966, 277.

⁸ J. C. Barnes and A. J. Thomson, *J. Sci. Instr.*, in press.

⁹ Y. Kondo, *Sci. Light (Tokyo)*, 1960, **10**, 166; 1961, **11**, 88.

1046

J. Chem. Soc. (A), 1967

intensity could be attributed to the hexamminecobalt(III) ${}^1A_{1g} \rightarrow {}^1T_{1g}$ band alone. In the mixed-valence compounds studied, ϵ at 20kk was constant within the experimental error incurred in measuring the crystal thicknesses. Hence in these compounds the absorption at 20kk is solely that of hexamminecobalt(III), and has the same intensity as in $\text{Co}(\text{NH}_3)_6\text{Cl}_3$ at 20kk. It is not possible to define a molar extinction coefficient for the intermolecular charge-transfer band since it is not clear how to determine the molar concentration of the chromophore for a transition from a donor to a linear combination of acceptor orbitals on adjacent molecules. We therefore use α , the optical density for a 1 cm. path-length, as a measure of intensity.

Figure 1 shows the crystal spectrum of a mixed-valence chlorocuprate crystal containing 50% of Cu^{I} . The intermolecular charge-transfer band appears as a shoulder at 17.2kk. The ratio of the optical densities at 17.2 and 20kk, which gives a measure of the intensity of the charge-transfer band, is plotted against composition

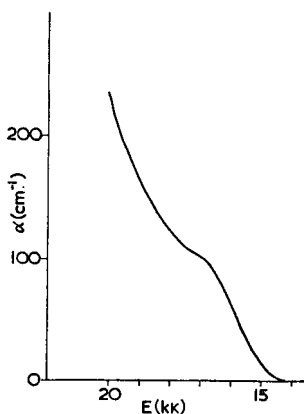


FIGURE 1 Crystal spectrum of mixed-valence chlorocuprate containing 50% of copper(I)

for a number of samples in Figure 2. The intensity variation with composition confirms that found by powder reflectance measurements,⁴ but the single-crystal data also give an indication of the absolute intensity of the charge-transfer band. The ratio of the optical densities at 17.2 and 20.0kk reaches a maximum value of 0.45, corresponding to $\alpha = 150 \text{ cm}^{-1}$. The low intensity of the charge-transfer band is sur-

prising in relation to the striking change which it produces in the visible colour of the crystals, but since no other result is available on the intensities of intermolecular charge-transfer bands in inorganic crystals, we

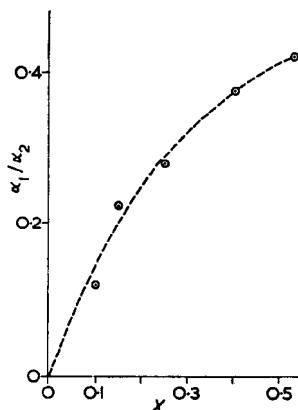


FIGURE 2 Plot of α_1/α_2 , the ratio of optical densities at 17.2 and 20.0 kk, against X , the mole fraction of copper(I)

have no basis for comparing our results. The apparently intense colour of the mixed-valence compounds is mainly a consequence of the breadth of the charge-transfer band, the half-width of which is about 3kk. That the band is so broad can be readily understood if we regard it as an electron transfer from $\text{Cu}^{\text{I}}\text{Cl}_4^{3-}$ to $\text{Cu}^{\text{II}}\text{Cl}_5^{3-}$ since $\text{Cu}^{\text{II}}\text{Cl}_4^{2-}$ will be formed in the excited state as a regular tetrahedron, far from its equilibrium geometry. When the minima in the potential energy surfaces for the ground and excited states occur at appreciably different values of the nuclear co-ordinates, broad absorption bands usually result. Further, a low intensity is to be expected of such a transition, which can only gain intensity through electron delocalisation from the metal to the chlorine orbitals, the latter forming a pathway from a Cu^{I} complex to a neighbouring Cu^{II} . In the more familiar examples of intermolecular charge transfer encountered in organic molecular complexes, there exists direct overlap between donor and acceptor orbitals, and extinction coefficients of the order of 10^3 are encountered.

D. W. S. thanks the S.R.C. for a Research Studentship.

[7/002 Received, January 2nd, 1967

Temperature Variation of the Intervalence Absorption Band of Hexachloroantimonate(III, V) Ions in a Crystal Lattice

BY KOSMAS PRASSIDES AND PETER DAY*

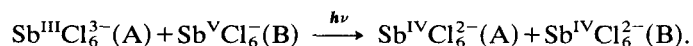
University of Oxford, Inorganic Chemistry Laboratory, South Parks Road, Oxford OX1 3QR

Received 28th June, 1983

The bandshape of the intervalence absorption of SbCl_6^{3-} and SbCl_6^- has been measured from 300 to 4 K in a crystal of $(\text{CH}_3\text{NH}_3)_2\text{Sb}_x\text{Sn}_{1-x}\text{Cl}_6$ in order to study the variation of the zeroth, first and second moments. At all temperatures the bandshape is Gaussian, as required by the vibronic model of Piepho, Krausz and Schatz (P.K.S.) in the weak-interaction limit. From the temperature dependence of the second moment, we estimate the electron-phonon coupling constant (and hence the displacement in vibrational coordinate from the ground state to the intervalence charge-transfer state), together with the effective phonon frequency coupled to the transition. The latter is very close to the mean of the ground-state totally symmetric Sb—Cl stretching modes of SbCl_6^{3-} and SbCl_6^- , and the displacement in the vibrational coordinate is also about half the difference between the Sb—Cl crystallographic bond lengths in the two complex ions. To explain the temperature dependence of the zeroth and first moments anharmonicity must be involved. A simple model for the variation of intervalence excitation energy with interionic distance, combined with an isotropic model of the thermal lattice expansion, gives a quantitative account of the change in first moment with temperature and a qualitative description of the change in zeroth moment.

One of the most characteristic features of class II¹ mixed-valency compounds is the appearance of an intervalence optical transition as a structureless broad absorption band in the visible or near-infrared. Considerable theoretical work on these transitions has appeared^{1–3} and in particular Piepho, Krausz and Schatz⁴ (P.K.S.) developed a vibronic coupling model for calculation of mixed-valency absorption profiles. Their one-dimensional model for the potential-energy surface of mixed-valency systems can be solved exactly, and consequently it is possible to describe the whole range of behaviour of such systems as they vary from strongly localized to strongly delocalized.

As examples of weak-interaction mixed valency, the hexachloroantimonates(III, V) are valuable prototypes with high-symmetry structures. Cs_2SbCl_6 is the parent member of this series and its crystal structure⁵ reveals a superlattice of SbCl_6^{3-} and SbCl_6^- . A great deal of spectroscopic evidence (*e.g.* Mössbauer,⁶ far-infrared,⁷ Raman,⁸ ultraviolet⁹ and photoelectron spectra¹⁰) also confirms the existence of distinguishable SbCl_6^- and SbCl_6^{3-} , while semiconductivity¹¹ and visible-absorption^{9–12} measurements show that Cs_2SbCl_6 and related hexachloroantimonates(III, V) are classical Robin–Day¹ class II mixed-valency compounds. Their colour is usually dark blue and arises from the intermolecular charge transfer:



Dilution of the effective chromophore concentration can be successfully achieved by using isostructural non-absorbing host lattices like the hexachlorostannates(IV).

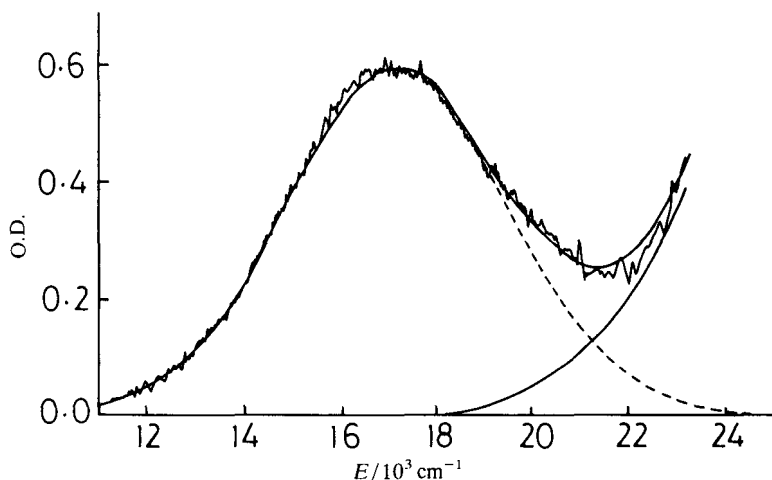


Fig. 1. Mixed-valency band in $(\text{CH}_3\text{NH}_3)_2\text{Sb}_x\text{Sn}_{1-x}\text{Cl}_6$ at 55.5 K (baseline subtracted).

In view of the development of the P.K.S. model we have re-examined in greater detail the temperature dependence of the single-crystal absorption-band profile of the $(\text{CH}_3\text{NH}_3)_2\text{Sb}^{\text{III}}_{x/2}\text{Sb}^{\text{V}}_{x/2}\text{Sn}^{\text{IV}}_{1-x}\text{Cl}_6$ compound ($0 < x < 1$), whose properties were first investigated by Atkinson and Day,⁹ with the aim of testing the application of both the configuration coordinate model¹³ and the P.K.S. model to $\text{Sb}^{\text{V}}\text{-Sb}^{\text{III}}$ charge transfer.

EXPERIMENTAL

Crystals of $(\text{CH}_3\text{NH}_3)_2\text{Sb}^{\text{III}}_{x/2}\text{Sb}^{\text{V}}_{x/2}\text{Sn}^{\text{IV}}_{1-x}\text{Cl}_6$ were synthesized by previously published methods⁹ from HCl solutions of the constituent ions. Their colour ranged from purple to light green, depending on the antimony concentration, and high antimony concentration was sought. Their integrity was checked by examining them under a polarizing microscope and single crystals of exceptionally high quality were found.

The absorption spectra were recorded at *ca.* 5 K intervals between room temperature and 4 K using a McPherson R.S.10 spectrophotometer and an Oxford Instruments CF 100 liquid-helium cryostat. The temperature of the crystal was measured with a compensated linear-temperature-sensor resistance thermometer and the temperature varied by an Oxford Instruments 'Harwell' temperature controller. The spectral output was digitized by a Stogate A/D converter.

The choice of baseline to be subtracted from the digitized spectral output was of major importance. The baseline was estimated by least-squares fitting a straight line to a portion of the spectrum to the low-energy side of the intervalence absorption which was then extrapolated to the higher-energy side. The resulting spectrum after the subtraction of the baseline (fig. 1) can be considered as resulting from the superposition of two components: the intervalence band at low energy and the tail of a second high-energy charge-transfer band. A computer program was used to fit two Gaussians to the absorption spectra of the form

$$(\text{O.D.})_k = (1/\pi^{1/2}\Delta_k) \exp[-(\hbar\nu - \hbar\nu_{0,k})^2/\Delta_k^2]; \quad k = 1, 2 \quad (1)$$

where (O.D.) is the optical density, ν_0 is the energy in cm^{-1} of the maximum absorption and Δ is the half-width at the point where the optical density is $1/e$ of the maximum absorption. The quality of the fits were excellent (fig. 1) through the whole temperature range. The

R-factors† were between 4 and 5%, mainly limited by the uncertainty arising from the small number of spectral points available for the high-energy band.

THEORY

CONFIGURATIONAL-COORDINATE MODEL

The intervalence absorption band can be considered as consisting of a series of lines arising from transitions to and from different vibrational levels of the ground and excited electronic states. Every line has a finite width due to a variety of interactions and the absorption consists of a series of bands which merge into a single broad structureless profile.

The intensity of a transition of energy $h\nu_{vv'}$ is proportional to the square of the Franck-Condon factor of vibrational levels v, v' . In order to carry out the summation over all the possible vibrational states of the electronic ground and excited states, the configuration-coordinate model can be used. This assumes that the optical electron is firmly trapped on an ion and interacts with a small number of local vibrational modes and that there are one or several 'effective' frequencies associated with these eigenmodes.

The absorption band shape can be analysed by the method of moments.¹⁴ If $\alpha(E)$ is some function describing the line shape, the n th moment of $\alpha(E)$ is given by

$$M_n = \int \alpha(E) E^n dE.$$

The zeroth moment is simply the area under the band. The mean band energy is given by $\bar{E} = (M_1/M_0)$, while the mean band width is given by

$$m^2 = (1/M_0) \int \alpha(E)(E - \bar{E})^2 dE.$$

In the case of a Gaussian band shape: $\bar{E} = E_{\max}$ and $m^2 = (1/8 \ln 2)H^2$, where E_{\max} is the maximum band energy and H is the full halfwidth of the band.

On the assumption that the ground and excited potential-energy surfaces are harmonic:

$$E_v = E_0(g) + h\nu_j(g)(v + \frac{1}{2})$$

$$E_{v'} = E_0(u) + h\nu_j(u)(v' + \frac{1}{2})$$

the expressions for the moments become¹³

$$\bar{E} = \Delta E(T) + \frac{1}{4} \sum [h\nu_j(g)] \left(\frac{\nu_j^2(u) - \nu_j^2(g)}{\nu_j^2(g)} \right) \coth [h\nu_j(g)/2kT] \quad (2)$$

† The *R*-factor was defined by

$$R = \left[\sum \left(\frac{\nu_{\text{obs}} - \nu_{\text{calc}}}{\nu_{\text{obs}}} \right)^2 \right]^{1/2} \times 100.$$

88

INTERVALENCE ABSORPTION OF SbCl_6^{3-} AND SbCl_6^-

and

$$m^2 = \sum_j S_j [\mathbf{h}\nu_j(u)]^2 \coth [\mathbf{h}\nu_j(g)/2kT] + \frac{1}{8} \sum_j [\mathbf{h}\nu_j(g)]^2 \left(\frac{\nu_j^2(u) - \nu_j^2(g)}{\nu_j^2(g)} \right) \coth^2 [\mathbf{h}\nu_j(g)/2kT] \quad (3)$$

where S_j is the Huang-Rhys¹⁵ factor, with the zeroth moment independent of temperature.

THE P.K.S. MODEL

In the P.K.S. formalism⁴ a mixed-valency system consists of two subunits designated by A and B, which in the case of the SbCl_6^{3-} (A)– SbCl_6^- (B) dimer are associated with formal oxidation states III and V, respectively. Making the harmonic approximation and assuming that the subunits have the same point-group symmetry in all oxidation states, one need only consider the totally symmetric normal coordinates Q_A , Q_B . In the harmonic approximation the vibrational potential energy of subunit i in oxidation state j can be written as

$$W_j^i(Q_i) = W_j^0 + l_j^i Q_i + \frac{1}{2} k_j^i Q_i^2.$$

By introducing new dimensionless variables q_+ , λ and W_i and assuming $k_j^i = k$ for all $i = \text{A, B}$ and $j = \text{III, IV, V}$ and $l_{iV}^i = \frac{1}{2}(l_{iIII}^i + l_{iV}^i)$, the potential surfaces in q_- ($\equiv q$) space consist of three parabolas, each one corresponding to an $\text{Sb}^{\text{V}}\text{--Sb}^{\text{III}}$, an $\text{Sb}^{\text{IV}}\text{--Sb}^{\text{IV}}$ and an $\text{Sb}^{\text{III}}\text{--Sb}^{\text{V}}$ oscillator. Note that q_+ does not enter the calculations in the case of equal force constants and when l_{iV}^i is the average of l_{iIII}^i and l_{iV}^i . The $\text{Sb}^{\text{V}}\text{--Sb}^{\text{III}}$ and $\text{Sb}^{\text{III}}\text{--Sb}^{\text{V}}$ energy surfaces are displaced horizontally and are symmetrical about the $\text{Sb}^{\text{IV}}\text{--Sb}^{\text{IV}}$ energy minimum while the $\text{Sb}^{\text{IV}}\text{--Sb}^{\text{IV}}$ surface is displaced vertically from the other two surfaces (fig. 2). Furthermore if the electronic coupling is switched on and if it is assumed that there is no interaction between the (V, III) and (III, V) surfaces, then the vibronic matrix is of the form

$$\begin{pmatrix} \frac{1}{2}(q+2\lambda)^2 & \varepsilon & 0 \\ \varepsilon & \frac{1}{2}q^2 + 2W & \varepsilon \\ 0 & \varepsilon & \frac{1}{2}(q-2\lambda)^2 \end{pmatrix}$$

with all energies expressed in units of $\nu = (2\pi)^{-1}\sqrt{k}$, the fundamental vibrational frequency associated with q , and where ε is the electronic coupling constant, W measures the difference in zero-point energy between the $\text{Sb}^{\text{III,V}}$ (or $\text{Sb}^{\text{V,III}}$) and $\text{Sb}^{\text{IV,IV}}$ surfaces and λ is related directly to the differences (assumed to be equal) in the equilibrium displacement between Sb^{III} , Sb^{IV} and Sb^{IV} , Sb^{V} .

The intervalence band⁴ is the totality of vibronic lines $v \rightarrow v'$ arising from transitions between the surfaces, and the effect of temperature is incorporated through the Boltzmann population factors of v, v' . By using a theoretical absorption profile

$$\alpha(E) = \sum_{\gamma, g, u} \frac{(N_g - N_u)}{N} |\langle g | m_\gamma | u \rangle|^2 f_{gu}(E)$$

where $\int f_{gu}(E) dE = 1$, explicit expressions for the moments of the intervalence band can be obtained.⁴

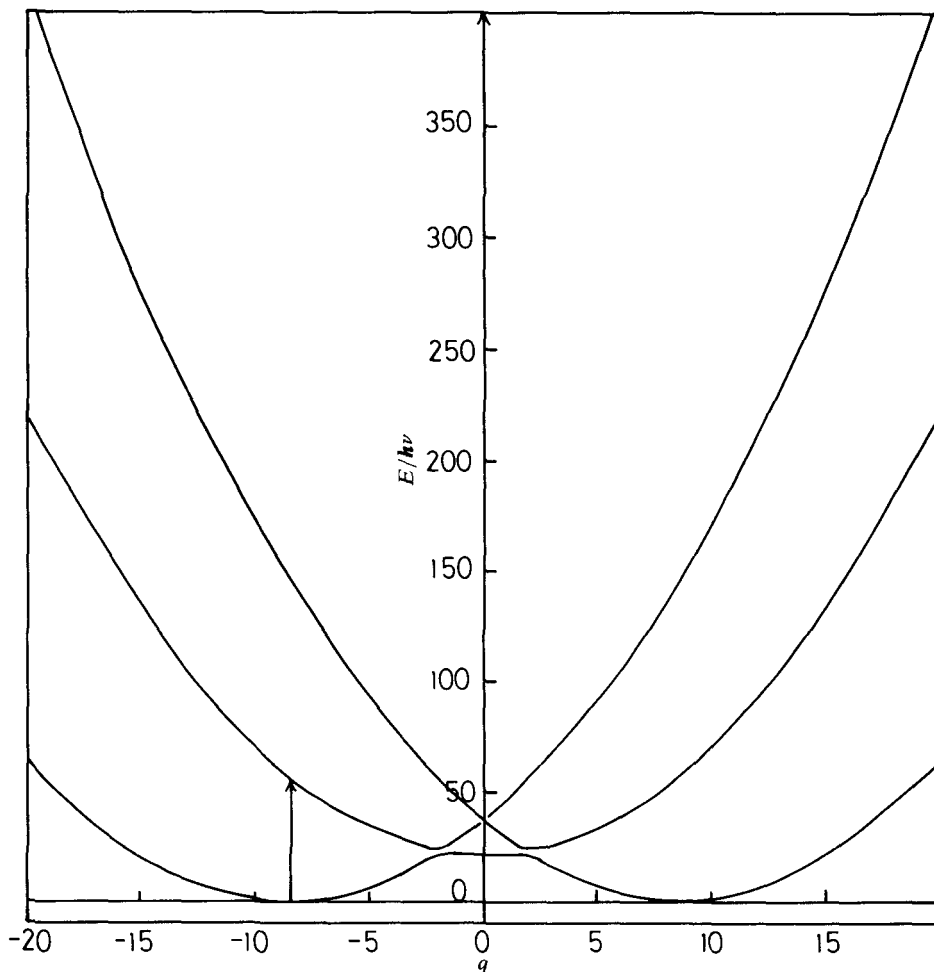


Fig. 2. Potential-energy surfaces for the oscillator $\text{Sb}^{\text{III}}\text{Cl}_6^{3-} - \text{Sb}^{\text{V}}\text{Cl}_6^- \rightarrow \text{Sb}^{\text{IV}}\text{Cl}_6^{2-} - \text{Sb}^{\text{IV}}\text{Cl}_6^{2-}$ in $(\text{CH}_3\text{NH}_3)_2\text{Sb}_x\text{Sn}_{1-x}\text{Cl}_6$ ($\lambda = 4.3$, $W = 10.5$, $\epsilon = -1.8$ and $\nu = 298 \text{ cm}^{-1}$).

RESULTS

A typical single-crystal absorption spectrum of $(\text{CH}_3\text{NH}_3)_2\text{Sb}_{x/2}\text{Sb}_{x/2}\text{Sn}_{1-x}^{\text{IV}}\text{Cl}_6$ is shown in fig. 1. As already discussed, the intervalence band can be described very well by a Gaussian shape over the entire temperature range. In addition, in fig. 3 and 4 we give the variation of the halfwidth and the band maximum with temperature. The zeroth moment of the band (integrated intensity) increases considerably (*ca.* 20%) on going from 280 to 8 K.

The observation of a second intermolecular charge-transfer band at $27\,500 \text{ cm}^{-1}$ by Day¹² is also confirmed in the more dilute crystals of $(\text{CH}_3\text{NH}_3)_2\text{Sb}_x\text{Sn}_{1-x}\text{Cl}_6$.

DISCUSSION

It is clear from fig. 1 that the intervalence charge-transfer band shows no vibrational fine structure, although it becomes narrower by *ca.* 1500 cm^{-1} . Since

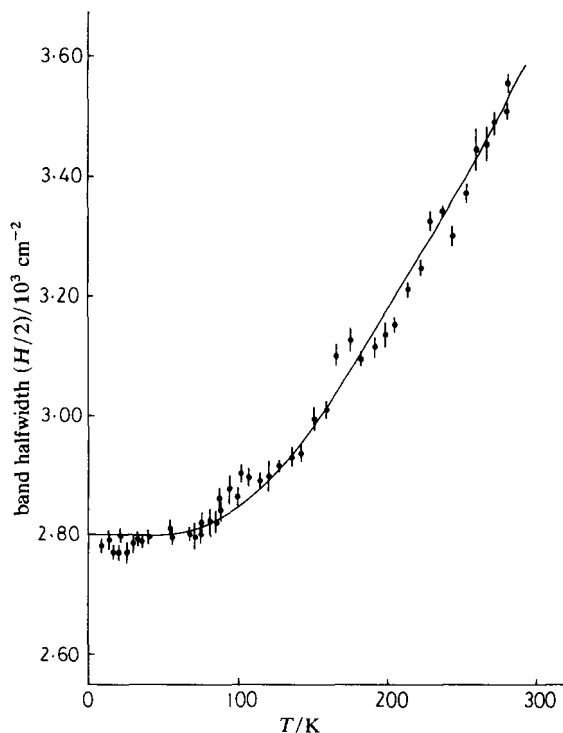


Fig. 3. Variation in halfwidth of the intervalence band with temperature. The line is calculated from eqn (4) with $\nu = 290 \text{ cm}^{-1}$ and $\lambda = 5.8$.

intramolecular vibrational modes and lattice modes are well separated in frequency in the Sb mixed-valency salt, the assumption that the major contribution to the broadening of the optical absorption results from the difference in equilibrium geometry between SbCl_6^{3-} and SbCl_6^- in the ground state and SbCl_6^{2-} in the excited state is immediately justified. Recognizing the difficulty of deciding which of the many vibrational modes in a solid interact with the optical electrons, we limit ourselves to a single 'effective' frequency, ν .

The P.K.S. model uses the parameters ϵ , λ , W and ν to define the potential-energy surfaces between which the optical transitions occur and to describe the shape of the intervalence band. We shall use these parameters throughout our discussion.

Based on the above assumptions, consider the situation where the system is in the lowest vibrational state, *i.e.* at 0 K. If $\lambda = 0$, the only transition that is allowed is to the lowest vibrational level of the excited state and the spectrum consists of a single line. If, however, $\lambda^2 + W \gg |\epsilon|$, then the quantization of vibrational levels in the upper state can be neglected. In this case a continuum of energy levels can be postulated in the upper state and the probability of the vertical Franck-Condon transition is simply proportional to $|\chi_0|^2$. At finite temperatures the P.K.S. model approaches the semiclassical treatment and the expression for the second moment of the band becomes

$$m^2 = 2\lambda^2(\hbar\nu)^2 \coth(\hbar\nu/2kT) \quad (4)$$

on the assumption of equal force constants in the ground and excited states.

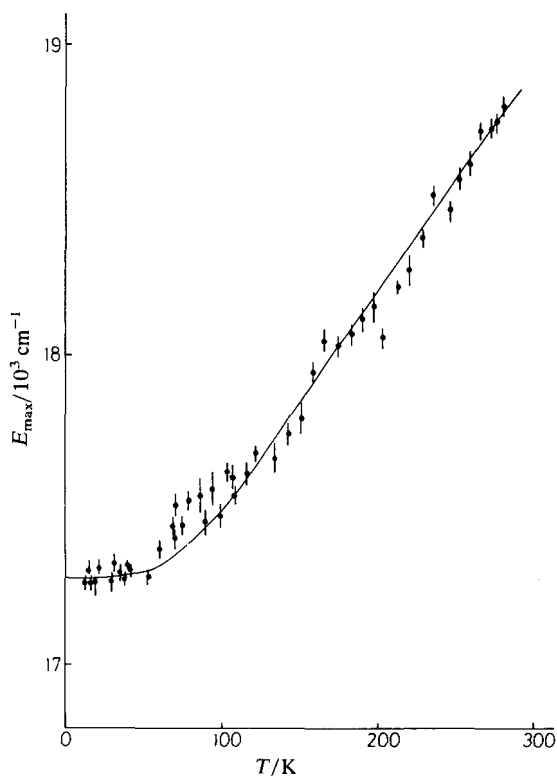


Fig. 4. Variation in maximum energy of the intervalence band with temperature. The line is calculated from eqn (6) and (7).

Eqn (4) was used to fit the observed halfwidths by employing a derivative-free non-linear regression computer program. The best fit† was obtained for the following parameter values: $(H_0/2) = 2801 \pm 6 \text{ cm}^{-1}$; $\nu = 290 \pm 3 \text{ cm}^{-1}$; $\lambda = 5.8 \pm 0.1$. This fit is shown in fig. 3 and the agreement between observed and fitted values is very good. The value of the 'effective' frequency, ν , falls within the range of intramolecular vibrations of the SbCl_6^- and SbCl_6^{3-} species. More specifically, the A_{1g} modes of SbCl_6^- and SbCl_6^{3-} (327 and 267 cm^{-1} , respectively)⁷ fall on either side of the observed 'effective' frequency, ν . For the hypothetical ion SbCl_6^{2-} , a value for A_{1g} equal to $[\frac{1}{2}(\nu_{\text{III}}^2 + \nu_{\text{V}}^2)]^{1/2} = 298 \text{ cm}^{-1}$ is not unreasonable and indeed is very close to the observed effective frequency. Further, the oscillator considered here is $\text{Sb}^{\text{V}}\text{Cl}_6 - \text{Sb}^{\text{III}}\text{Cl}_6 \rightarrow \text{Sb}^{\text{IV}}\text{Cl}_6 - \text{Sb}^{\text{IV}}\text{Cl}_6$, and hence from the electron-phonon coupling constant, λ , we can get an estimate of Δr , which represents half the difference between the $\text{Sb}^{\text{V}} - \text{Cl}$ and $\text{Sb}^{\text{III}} - \text{Cl}$ equilibrium bond lengths. If the point symmetry of the SbCl_6^{2-} species is assumed to be octahedral, a value of Δr equal to $0.19 \pm 0.01 \text{ \AA}$ is obtained. Structural studies of Cs_2SbCl_6 ⁵ give a value for Δr of 0.131 \AA at 4.7 K , while in $(\text{C}_3\text{H}_7\text{NH}_3)_4\text{Sb}_{1/2}^{\text{III}}\text{Sb}_{1/2}^{\text{V}}\text{Cl}_6(\text{Cl})_2$,¹⁶ which has a rather different structure, Δr is 0.14 \AA at room temperature. In Cs_2SbCl_6 ⁵ also the deviation from O_h symmetry is small (a 0.5° angular distortion of SbCl_6^- and a $2.5^\circ D_{2d}$ distortion of the lone-pair

† The smallest value of the sum $\sum_{i=1}^{48} (H_{\text{pred}}^2 - H_{\text{obs}}^2)^2$ was 1.1976.

SbCl_6^{3-} ion). Thus besides all the drastic approximations the results show an encouraging agreement between theory and experiments, indicating that coupling of the electron transfer to antisymmetric combination of the A_{1g} totally symmetric modes of the subunits plays a major role in determining the broadening of the intervalence charge-transfer band and that indeed the $\text{Sb}^{\text{V}}\text{Cl}_6\text{-Sb}^{\text{III}}\text{Cl}_6$ solids belong to the valency-trapped case (Robin-Day class II).

However, the situation changes dramatically if we continue the interpretation one stage further. If the band shape is a Gaussian, then the first moment of the band is exactly equal to the maximum band energy; hence by elementary consideration of the potential-energy surfaces in the case of $\lambda^2 + W \gg |\epsilon|$ we obtain $\bar{E} = E_{\text{max}} \approx 2(\lambda^2 + W)(h\nu)$. However, $E_{\text{max}}(0 \text{ K}) \approx E_{\text{max}}(8 \text{ K}) = 17\,290 \text{ cm}^{-1}$, and the value of W which measures the energy difference between the potential minima of the ground and excited states can be evaluated by substituting values for λ and ν . This gives values of W which are negative ($W = -3.8$); obviously this is not acceptable since the equilibrium energy of the ground state should be less than that of the excited state. However, we note that W is very sensitive to the value of the vibronic coupling constant λ , which in turn is a very sensitive function of the difference in equilibrium bond lengths of the SbCl_6^{n-} subunits. Thus if Δr is varied from 0.19 to 0.18 Å, λ changes from 5.5 to 5.8 and W from -3.8 to 0. Further, for the value of $\Delta r = 0.13$ found from the crystal structure λ is 4.0 and W is 13.8. So even if we are not able to assign a value to W , we may nevertheless conclude that the difference in energy between the equilibrium configurations of the ground-state oscillator $\text{SbCl}_6^{3-}\text{-SbCl}_6^-$ and the excited-state oscillator $\text{SbCl}_6^{2-}\text{-SbCl}_6^-$ is very small. Using a two-dimensional P.K.S. model¹⁷ by including a second 'effective' frequency led to an unacceptably high value of ν_2 or λ_2 and no improvement in the value of W .

From fig. 4 it is noticeable that the band in the $\text{Sb}^{\text{V}}\text{-Sb}^{\text{III}}$ compound shifts monotonically to lower energy as the temperature is lowered. The shift between 300 and 8 K is *ca* 1500 cm^{-1} . The P.K.S. model predicts that the temperature dependence of the first moment of the band will be small in all cases.⁴ The semiclassical treatment predicts a blue shift with decreasing temperatures. One way of introducing temperature dependence into the first moment is by considering the ground- and excited-state potentials to have different curvatures. Then in the case of a single 'effective' frequency in both ground and excited states, eqn (2) transforms into

$$\bar{E} = \Delta E(T) + \frac{1}{4}[h\nu(g)] \left(\frac{\nu^2(u) - \nu^2(g)}{\nu^2(g)} \right) \coth [h\nu(g)/2kT]. \quad (5)$$

Hence a red shift with decreasing temperature is predicted when the excited-state potential-energy surface has a larger curvature than the ground-state one. Fitting eqn (5) to our data yields unreasonably large values for the ratio $[\nu^2(u)/\nu^2(g)]$, so the explanation for the temperature dependence of E must be sought in the term $\Delta E(T)$.

All attempts to discuss the variation of the bandshape of the intervalence charge transfer have been limited in the potential energy to terms quadratic in the interatomic displacements. This is the harmonic theory and a major consequence is the prediction of no thermal expansion of the crystal lattice. In real crystals, however, this prediction is not accurately satisfied. The deviations may be attributed to the neglect of anharmonic (higher than quadratic) terms. We present here a very approximate and empirical treatment of the effect of temperature on thermal

expansion of the crystal and consequently on the mean band energy of the charge-transfer band. The empirical nature of the treatment stems from the fact that no data are available on the thermal properties of molecular ionic crystals of Sb.

Powers and Meyer¹⁸ have reported a study of the optical and electron-transfer properties of a series of Ru^{II}-Ru^{III} compounds in solution. By changing the distance l of Ru^{II}-Ru^{III} in successive complexes they established that the maximum energy of the intervalence charge-transfer band in solution increases as the Ru^{II}-Ru^{III} distance increases. To explain their results, they considered a dielectric continuum model³ and used the relationship¹⁹

$$E_{\max} = \varepsilon_i + e^2 \left(\frac{1}{2a_1} + \frac{1}{2a_2} - \frac{1}{l} \right) \left(\frac{1}{D_{\text{op}}} - \frac{1}{D_s} \right) \quad (6)$$

where D_{op} and D_s are the optical and static dielectric constants of the solvent medium, respectively, and a_1 and a_2 are radii of two charged spherical ions: ε_i is the inner-sphere contribution to the vibrational trapping free energy of the electrons in the localized mixed-valency ion. A plot of E_{\max} against $(1/l)$ gave a straight line.

In our case the crystal lattice is considered as the dielectric medium. Again the lattice environment of the two ions between which electron transfer occurs is regarded as continuous dielectric. Hence the maximum band energy can be separated into a part arising from lattice vibrational modes of the medium and a part arising from localized (metal-ligand) vibrational modes. Again for an ion in an octahedral hole in a lattice, eqn (6) applies with a_1 , a_2 and l identified as the Sb^V-Cl, Sb^{III}-Cl and Sb^{III}-Sb^V distances, respectively. The temperature dependence of l can be approximately established by considering the thermal expansion of the lattice to be isotropic. Then²⁰

$$l = \tilde{l}(1 + D_0 \bar{\varepsilon}) \quad (7)$$

where \tilde{l} is the distance between nearest neighbours at 0 K for the harmonic approximation, D_0 is a constant which depends on the lattice type and $\bar{\varepsilon}$ is the mean energy per oscillator. For the variation of the internal energy $\bar{\varepsilon}$ with temperature the Debye spectrum is taken as a basis with a Debye temperature of *ca.* 100 K. A plot of E_{\max} against $(1/l)$ gives a straight line (fig. 5). The exact values of the slope and the intercept are not of importance since they are very approximate, but it is noticeable that E_{\max} is a very steep function of $l(T)$. The curve drawn through the experimental points in fig. 4 was calculated from eqn (6) and (7), and it can be seen that the level of agreement is satisfactory. Still, however, $[(1/D_{\text{op}}) - (1/D_s)]$ is evaluated to be *ca.* 4.4, which is of the correct order of magnitude.³ Unfortunately if the localized contribution ε_i is evaluated, it turns out to be negative. So while anharmonic contributions appear to play a role in determining the behaviour of the band maximum as a function of temperature, their contribution is probably overestimated in the above approach.

Any anharmonic contributions will be expected to manifest themselves to a lesser degree in the temperature dependence of the second moment, but they should be more visible in the temperature dependence of the integrated band intensity. Thus contraction of the lattice will increase the overlap between adjacent SbCl₆³⁻ and SbCl₆⁻ units, on which the dipole strength of the transition depends. So the integrated band intensity will increase as the temperature is lowered. This is indeed observed; as mentioned above, this increase is *ca.* 20%, well beyond experimental error that might have arisen due to uncertainties in the baseline subtraction. Note that both the semiclassical treatment and the P.K.S. model in general predict negligible temperature dependence of the zeroth moment of the band.

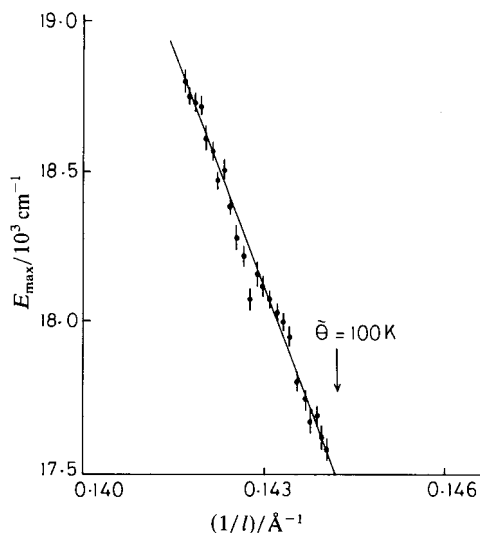


Fig. 5. Variation in maximum energy of the intervalence band with inverse distance between nearest Sb^{III} , Sb^{V} neighbours.

Finally, Atkinson and Day⁹ have calculated an upper limit for the degree of delocalization of the optical electron between the SbCl_6^- and SbCl_6^{3-} sites of *ca.* 0.001. Using this value we may calculate an upper limit for the value of the electronic coupling constant $|\epsilon|^4$ of the P.K.S. model between the subunits in the case of strong localization of *ca.* 1.8.

CONCLUSIONS

We have shown that between 300 and 4 K the intervalence absorption band in a hexachloroantimonate(III, V) crystal approximates very closely to a Gaussian bandshape, as required by the P.K.S. model for a weakly interacting system. Moreover, the temperature dependence of the second moment follows a hyperbolic cotangent law, leading to a value of the effective vibrational frequency coupled to the transition which is very close to the mean of the totally symmetric stretching frequencies of SbCl_6^{3-} and SbCl_6^- in their electronic ground states. The difference in bond lengths between SbCl_6^- , SbCl_6^{3-} and the hypothetical excited-state SbCl_6^{2-} derived from the optical spectrum is also near to half the difference between the observed bond lengths in Cs_2SbCl_6 . On the other hand both the first moment and the zeroth moment vary considerably with temperature, a result which is not compatible with the P.K.S. model if one retains the harmonic approximation. A simplified treatment of the variation of intervalence band energy with interionic spacing,²⁰ combined with an isotropic model for the lattice expansion, provides a satisfactory picture of the temperature dependence of the first moment. The sense of the variation of the zeroth moment with temperature is compatible with the lattice expansion model, but to explain it quantitatively requires precise knowledge of the way in which the donor and acceptor orbitals overlap, which is not available at the present time.

We thank S.E.R.C. for partial support of this work. K.P. thanks Christ Church, Oxford, for a Senior Scholarship. We acknowledge many helpful discussions with Dr P. A. Cox.

- ¹ M. B. Robin and P. Day, *Adv. Inorg. Chem. Radiochem.*, 1967, **10**, 248.
- ² *Proc. NATO-ASI on Mixed-valence Compounds in Chemistry, Physics and Biology*, ed. D. B. Brown (D. Reidel, Dordrecht, 1980).
- ³ N. S. Hush, *Prog. Inorg. Chem.*, 1967, **8**, 391.
- ⁴ S. B. Piepho, E. R. Krausz and P. N. Schatz, *J. Am. Chem. Soc.*, 1978, **100**, 2996; K. Y. Wong, P. N. Schatz and S. P. Piepho, *J. Am. Chem. Soc.*, 1979, **101**, 2793; K. Y. Wong and P. N. Schatz, *Prog. Inorg. Chem.*, 1981, **28**, 369.
- ⁵ K. Prassides, P. Day and A. K. Cheetham, *J. Am. Chem. Soc.*, 1983, **105**, 3366.
- ⁶ G. Longworth and P. Day, *Inorg. Nucl. Chem. Lett.*, 1976, **12**, 451.
- ⁷ H. W. Clark and B. I. Swanson, *J. Am. Chem. Soc.*, 1981, **103**, 2929; T. Barrowcliffe, I. R. Beattie, P. Day and K. Livingston, *J. Chem. Soc. A*, 1967, 1810.
- ⁸ R. J. H. Clark and W. R. Trumble, *J. Chem. Soc., Dalton Trans.*, 1976, 1145.
- ⁹ L. Atkinson and P. Day, *J. Chem. Soc. A*, 1968, 2423.
- ¹⁰ P. Burroughs, A. Hamnett and A. F. Orchard, *J. Chem. Soc., Dalton Trans.*, 1974, 565.
- ¹¹ L. Atkinson and P. Day, *J. Chem. Soc. A*, 1968, 2432.
- ¹² P. Day, *Inorg. Chem.*, 1963, **2**, 452.
- ¹³ J. J. Markham, *Rev. Mod. Phys.*, 1959, **31**, 956; J. J. Markham, *F-Centres in Alkali Halides, Solid State Physics, Supplement 8* (Academic Press, New York, 1966).
- ¹⁴ M. Lax, *J. Chem. Phys.*, 1952, **20**, 1752.
- ¹⁵ K. Huang and A. Rhys, *Proc. R. Soc. London, Ser. A*, 1950, **204**, 403.
- ¹⁶ G. Birke, H. P. Latshcha and H. Pritzkow, *Z. Naturforsch., Teil B*, 1976, **31**, 1285.
- ¹⁷ K. Y. Wong and P. N. Schatz, *A.C.S. Symp. Ser.*, 1982, **198**, 281.
- ¹⁸ M. J. Powers and T. J. Meyer, *J. Am. Chem. Soc.*, **102**, 1289.
- ¹⁹ N. S. Hush, *Trans. Faraday Soc.*, 1961, **57**, 557.
- ²⁰ G. Leibfried and W. Ludwig, *Solid State Phys.*, 1961, **12**, 276.

(PAPER 3/1117)

This page intentionally left blank

CHAPTER 4

This page intentionally left blank

Transparent Ferromagnets: Structures and Optical Properties

One of the roles of a chemist venturing into the field of novel materials is to uncover new kinds of physical behaviour not found in the simpler paradigm cases espoused by our physics colleagues. Chemists can identify and construct new arrangements of atoms that lead to combinations of properties never associated with each other before. I once called this a game of nouns and adjectives [1]. When most people think of a magnet, they imagine a lump of iron that is hard, heavy, opaque and shiny, which goes ‘clang’ if you drop it on the floor. It is undoubtedly true that most magnets are such, but do they have to be? Until the 1980s, practically all known ferromagnets were metals but other mechanisms exist for ferromagnetic exchange between localised atomic moments that ought to make it possible to synthesise ferromagnets which are electrical insulators. There is then no reason why they should not be optically transparent. If the lattice can be built in such a way that the orbitals containing the unpaired spins are all orthogonal, Hund’s rule guarantees that the lowest energy state of the ensemble is the one having all the atomic moments parallel. The question then is how to do it chemically.

Envisaging that mono- or poly-atomic anions form bridges between the transition metal or lanthanide ions carrying the unpaired spins, two ways present themselves. The orbital symmetry rules governing magnetic exchange between neighbouring localised moments, based on the Anderson model for superexchange through an intervening anion bridge, were established by Kanamori [2] and Goodenough [3] approximately forty years ago. They implied that to obtain ferromagnetic exchange, there are two possible scenarios of requiring 180° metal-anion-metal links and 90° links. In the first instance, overlap occurs between a half-filled d-orbital [e.g. $d(z^2)$] on one metal and a p-orbital on the ligand, which transfers spin to an empty orbital [e.g. $d(x^2-y^2)$] on the second metal, also through σ -overlap. If there is a half-filled — and orthogonal — $d(z^2)$ on the second metal, then its moment is coupled parallel to the transferred moment on the first one by intra-atomic exchange (Hund’s rule). The issue for a chemist is how to mould the lattice to ensure that the $d(z^2)$ orbitals on neighbouring metal ions are orthogonal, while preserving the 180° M-X-M angle. The answer lies in the Jahn–Teller effect.

The general theorem due to Jahn and Teller [4], the latter also better known as the ‘father of the hydrogen bomb’, states that in a non-linear polyatomic molecule, any orbitally degenerate electronic state is inherently unstable to a distortion that

removes the degeneracy. In essence, it is a theorem about two potential energy surfaces crossing; the point where two such surfaces intersect (i.e. the point in configuration space where they are degenerate is most unlikely to be at either of their minima. In the particular case of d-orbital configurations where $d(x^2-y^2)$ and $d(z^2)$ have different electron occupancies in an octahedral environment, there will be some distortion that renders one or the other the singly-occupied frontier orbital. Such a situation arises when an octahedrally coordinated transition-metal ion has either a d^4 or d^9 configuration [5]. Jahn–Teller distortions in Cu^{II} salts ($3d^9$) are widespread and well-known, and had even given rise to examples of ferromagnetic exchange [6]. More interestingly, because the larger number of unpaired d-electrons leads to stronger exchange and hence higher ordering temperatures, the d^4 case is found in Cr^{II} and Mn^{III} .

In 1973, we found a simple ternary Cr^{II} salt, K_2CrCl_4 , that was ferromagnetic at 53 K [7], because a superlattice ordering of the Jahn–Teller distorted the CrCl_6 octahedra within the overall K_2NiF_4 layer structure guarantees that the half-occupied $d(z^2)$ orbitals on neighbouring Cr^{II} are orthogonal. It comes about by displacing the anion separating all the nearest neighbour Cr^{II} on a square two-dimensional lattice away from the midpoint, thus, $\text{Cr-Cl} \dots \text{Cr}$. The CrCl_6 octahedra are thereby elongated within the plane of the layer, their long axes being orthogonal on neighbouring sites [8]. The same exact thing occurs in the mixed valence $\text{La}_x\text{Sr}_{1-x}\text{MnO}_3$ perovskites famous for their so-called ‘colossal magneto-resistance’, but the situation is greatly complicated by the presence of two oxidation states, Mn^{III} (the d^4 Jahn-Teller ion) and Mn^{IV} (undistorted d^3) [9].

As is often the case in materials chemistry, when a new compound is found to have unusual physical properties, in this instance, ferromagnetism and optical transparency, other properties arose that had not previously been the object of the original enquiry. In the present case, the compound is transparent in the visible because the spin-allowed ligand-field absorption band expected for a high-spin d^4 ion lies in the near infrared, and because Cr^{II} is far from being oxidising, any ligand-to-metal charge transfer transitions are confined to the ultraviolet. However, there are two narrow spin-forbidden ligand-field transitions in the visible which give the crystals their green colour. What is quite unprecedented and remains unique to this class of compound is that below the Curie temperature, when the localised Cr^{II} moments are ordered ferromagnetically, the crystals changed colour! It is gratifying, but unfortunately quite rare, to observe a quantum effect manifested to the naked eye. One could point to the case of superconductivity in Chap. 6, where a transition to a different kind of ordered state also produces a dramatic change in the properties. The intensities of the spin-forbidden (quintet-triplet) transitions fall by a factor of 100 from 50 K to 5 K, and moreover, vary precisely as T^2 . [10]

The reason for this extraordinary behaviour lies in the mechanism which gives the absorption bands their intensity [11]. As the spin decreases when a Cr^{II} ion is excited from the quintet to a triplet state, intensity can be gained by coupling the electronic excitation with a positive spin deviation in the magnetically ordered ground state. Since the lattice is ferromagnetically ordered, it is only possible if a thermally populated negative spin deviation is annihilated. Thus, the intensity of optical absorption mirrors the thermal population, and hence density-of-states, of the spin deviations known as spin-waves or magnons by physicists, in what turns out to be an excellent approximation to a two-dimensional square-planar Heisenberg ferromagnet [12]. All this has been validated very precisely by measuring the spin-wave density-of-states using inelastic neutron scattering [13]. It is also worth pointing out that these spin-waves can be populated not only thermally, but also by microwave pumping, when the crystal changes colour likewise! Given the fortunate chance that one of the visible absorption bands coincides with the wavelength of a He-Ne laser (632 nm), we showed how an optical frequency can be amplitude-modulated at a microwave frequency, sadly only at low temperature or modulators based on this principle might well be found in many telecommunications devices [14].

Apart from combining ferromagnetism with optical transparency for the first time, the layer perovskite halides of Cr^{II} lead to a further innovation with potentially far-reaching consequences for magnetic materials processing, namely the concept of a soluble magnet. The ternary halides like K_2CrCl_4 have to be grown into single crystals from a melt at a high temperature of 850°C , usually by the Bridgman method [15]. However, if the Group 1 cation is replaced by an organic cation, in particular, mono- n -alkylammonium, an analogous series of salts $(\text{C}_n\text{H}_{2n+1}\text{NH}_3)_2\text{CrCl}_4$ with the same Jahn–Teller distorted ferromagnetic layers results, but they are soluble in ethanol and can be re-crystallised at room temperature [16]. Their T_c s and optical behaviour are very similar to those of their purely inorganic counterparts [17], except for the extra flexibility that the inter-layer spacing can be modulated by changing the length of the alkyl-chain. This is interesting for people who seek test-beds for examining the mechanisms of phase transitions to long-range order in low-dimensional magnetic lattices. It also renders it possible to incorporate functional groups into the organic chains in a search for synergy between the magnetic order and other properties of molecular solids such as mesomorphism or chain-melting [18]. It is worth noting that all these developments took place some years before what is nowadays known as ‘molecular magnets’, a fashionable research field.

As to the other recipes referred to at the outset for generating near-neighbour ferromagnetic exchange between localised moments, involving 90° M-X-M bridges, some remarkably simple inorganic examples can indeed be found and their optical behaviour mirrors that of the A_2CrX_4 series. Most numerous are the binary halides MX_2 of 3d elements, which have CdCl_2 or CdI_2 crystal structures. These too are

layer compounds and they provide the classic examples of 'metamagnetism', the circumstance where ferromagnetically ordered layers are weakly coupled antiferromagnetically. That leads to the intriguing situation recognised earlier, that while the crystal as a whole is an antiferromagnet, the strongest near-neighbour interactions are ferromagnetic. Thus, the question is which is going to dominate their optical properties, in particular, the temperature-dependence of the spin-forbidden ligand field transitions in the visible? Surveying the dihalides of Mn, Fe, Co and Ni, it appears that near-neighbour ferromagnetic exchange dominates the weaker antiferromagnetic inter-plane interaction, so that the visible absorption bands due to spin-forbidden ligand field transitions gain intensity with increasing temperature in a manner similar to the Cr^{II} ferromagnets. The precise form of temperature-dependence varies from T^2 when the system is Ising-like to T^3 when it is XY [19].

The special case of NiBr₂ deserves separate consideration because it shows how a simple chemical system can have quite remarkably complicated properties when interactions beyond the near-neighbours have to be taken into account. The nearest-neighbour interaction in the CdCl₂ structure is ferromagnetic, and that would be the end of the story if it were not for the fact that the second- and third-nearest-neighbour exchange is antiferromagnetic. Competition between these opposing forces means that the lowest energy arrangement near absolute zero temperature is a compromise, i.e. a spiral structure [20]. Neighbouring moments in the layers find their equilibrium not when the spins are parallel, but when they are canted by some 8°. From the n th to the $(n + 1)$ th, we see the moments rotating in the basal plane by 8°, 16°, . . . , generating a helix. Since the angle in question is not a simple sub-multiple of 180° (because it originates from the arbitrary ratio of the exchange constants), the repeat length of the helix is not a straightforward multiple of the lattice spacing, i.e. it is incommensurate.

Even more bizarre is the observation that the pitch of the helix changes with temperature, or to put it succinctly, the helix unwinds till it has disappeared and a collinear ferromagnetic structure is re-established above 27 K. These strange goings-on surfaced first in a close look at the optical spectrum, where a mysterious 'cold band' accompanied the hot band anticipated from the ferromagnetic ferromagnetic near-neighbour exchange [21]. However, the subtle details were only laid bare by neutron scattering. In fact, the complete story behind such complicated and unusual behaviour in an apparently simple lattice (needing the full complement of optical, magnetic and neutron techniques to unravel it) fully justifies the sub-title *A Magnetic Detective Story* [22].

References

- [1] P. Day, ch. in C. R. A. Catlow and A. K. Cheetham, *New Trends in Materials Chemistry*, Dordrecht: Kluwer Academic Publishers, 1997, pp. 1.

-
- [2] J. Kanamori, *J Phys Chem Solids* **10**: 87 (1959).
- [3] J. B. Goodenough, *Magnetism and the Chemical Bond*, New York, Interscience, 1963.
- [4] H. A. Jahn and E. Teller, *Proc Roy Soc A* **161**: 220 (1937).
- [5] F. A. Cotton and G. Wilkinson, *Advanced Inorganic Chemistry*, New York: J. Wiley & Co., 4th ed., 1980.
- [6] L. J. de Jongh and A. R. Miedema, *Adv Phys* **23**: 1 (1974).
- [7] P. Day, A. K. Gregson and D. H. Leech, *Phys Rev Lett* **30**: 19 (1973).
- [8] P. Day, M. T. Hutchings, E. Janke and P. J. Walker, *Chem Comm* **711** (1979).
- [9] For a review see A. Maignan, V. Caijnaent, Ch. Simon, M. Herveau, and B. Raveau, *J Mater Chem* **5**: 1089 (1995).
- [10] P. Day, E. Janke, T. E. Wood and D. Woodwork, *J Phys C: Sol St Phys* **12**: L329 (1979).
- [11] P. Day, *Acc Chem Res* **12**: 236 (1979) [Reprint 4.1].
- [12] M. T. Hutchings, M. J. Fair, P. Day and P. J. Walker, *J Phys C: Sol St Phys* **9**: L55 (1976).
- [13] M. J. Fair, A. K. Gregson, P. Day and M. T. Hutchings, *Physica B* **657**: 86–88 (1977).
- [14] P. J. Fyne, P. Day, M. T. Hutchings, S. Depinna, B. C. Cavenett and R. Pynn, *J Phys C: Sol St Phys* **17**: L245 (1984).
- [15] Bridgman method.
- [16] C. Bellitto and P. Day, *J Chem Soc Dalton Trans* **1207** (1978) [Reprint 4.2]; *idem J Cryst Growth* **58**: 641 (1982).
- [17] C. Bellitto and P. Day, *J Chem Soc Chem Commun* **511** (1978) [Reprint 4.3]; *idem J Mater Chem* **2**: 265 (1992) [Reprint 4.4].
- [18] P. Day, *Phil Trans Roy Soc A* **314**: 145 (1985).
- [19] D. J. Robbins and P. Day, *J Phys C: Sol St Phys* **9**: 867 (1976) [Reprint 4.5].
- [20] P. Day and K. R. A. Ziebeck, *J Phys C: Sol St Phys* **13**: L523 (1980).
- [21] M. W. Moore, T. E. Wood and P. Day, *J Chem Soc Faraday Trans II* **77**: 1611 (1981).
- [22] P. Day, *Acc Chem Res* **21**: 250 (1988) [Reprint 4.6].

New Transparent Ferromagnets

PETER DAY

Oxford University, Inorganic Chemistry Laboratory, Oxford, OX1 3Q, England

Received September 14, 1978

This Account describes a wide-ranging set of experiments to prepare and characterize a new series of transport ionic ferromagnets with the general formulae A_2CrX_4 , where A is either an organic or an inorganic unipositive cation and X is a halide ion.

The large majority of ferromagnets are metallic conductors. Conversely, by far the largest proportion of ionic transition-metal or lanthanide compounds, including oxides, halides, sulfates, and many complexes, are antiferromagnets. In its simplest terms, ferromagnetism in metals arises from the coupling of localized electrons on neighboring centers, such as those in partly occupied 3d shells, via the mobile conduction electrons.¹ In insulators, the interaction between the unpaired electrons on neighboring cations is normally mediated by an intervening ligand bridge, usually an anion. In that case the sign of the resulting exchange integral depends on a variety of competing superexchange pathways involving delocalization of the unpaired spin on the metal toward the ligand as a result of covalency.² It turns out that in the great majority of cases the sum total of all the superexchange pathways is an antiferromagnetic coupling.

Peter Day was born at Wrotham, Kent, England, in 1938. His first degree and D.Phil. are from Oxford University, where he was a Scholar at Wadham College. At present he is a Science Research Council Senior Research Fellow and Fellow of St. John's College, Oxford, having, until 1977, been University Lecturer in Inorganic Chemistry. In 1971 he was awarded the Corday-Morgan Medal of The Chemical Society.

Are there then any ionic transition-metal salts which order as simple ferromagnets? The answer is very few. In fact, Table I contains close to an exhaustive list. A striking feature of this list³⁻¹¹ is how chemically disparate the various substances are, embracing simple cubic lattices, coordination complexes, and lanthanide and transition-metal compounds. Having such diverse crystal structures and ground-state electron configurations, it would be surprising if the superexchange pathways giving rise to the ferromagnetic ordering had very much in common. However, at least between the

- (1) C. Zener, *Phys. Rev.*, **81**, 440 (1951).
- (2) P. W. Anderson, *Phys. Rev.*, **79**, 350 (1950).
- (3) H. L. Davis and A. Narath, *Phys. Rev. A*, **134**, 433 (1964).
- (4) B. J. Matthias, R. M. Bozorth, and J. H. Van Vleck, *Phys. Rev. Lett.*, **7**, 160 (1961); J. R. McGuire and M. W. Shafer, *J. Appl. Phys.*, **35**, 984 (1964).
- (5) C. A. Catanese, A. J. Skjeltorp, H. E. Meissner, and W. P. Wolf, *Phys. Rev. B*, **8**, 4223 (1973).
- (6) A. N. Holden, B. T. Matthias, P. W. Anderson, and H. W. Lewis, *Phys. Rev.*, **102**, 1463 (1956); H. J. Buser, A. Ludi, P. Fischer, T. Studach, and B. W. Dale, *Z. Phys. Chem. (Frankfurt am Main)*, **92**, 354 (1974); B. Mayoh and P. Day, *J. Chem. Soc., Dalton Trans.*, 1483 (1976).
- (7) I. Yamada, *J. Phys. Soc. Jpn.*, **33**, 979 (1972); W. Kleeman and Y. Farge, *J. Phys. (Paris), Lett.*, **35**, 135 (1974).
- (8) L. J. De Jongh and W. D. Van Amstel, *J. Phys. (Paris), Colloq.*, **1**, C1-880 (1971); L. J. De Jongh and A. R. Miedema, *Adv. Phys.*, **23**, 1 (1974).
- (9) C. G. Barraclough, A. K. Gregson, and S. Mitra, *J. Chem. Phys.*, **60**, 962 (1974); H. Miyoshi, *J. Phys. Soc. Jpn.*, **37**, 50 (1974).
- (10) W. M. Reiff and S. Foner, *J. Am. Chem. Soc.*, **95**, 260 (1973).
- (11) W. P. Wolf, M. J. M. Leask, B. W. Mangum, and A. F. G. Wyatt, *J. Phys. Soc. Jpn., Suppl. B.*, **1**, 487 (1961).

Table I
Ionic Ferromagnets

	T_c/K	color	spin-forbidden crystal-field states	ref
CrBr ₃	33	red-purple	yes	3
EuO	69	black	no	4
Tb(OH) ₃	3.7	-	no	5
Fe[Fe(CN) ₆] ₃ · 14H ₂ O	5.5	blue-black	no	6
K ₂ CuF ₆	6.25	yellow	no	7
(RNH ₃) ₂ CuCl ₄	8-8	yellow	no	8
Mn-phthalocyanine	-	black	no	9
Fe(<i>o</i> -phenanthroline) ₂ Cl ₂	5	dark red	no	10
GdCl ₃	2.2	red	no	11
A ₂ CrX ₄	50-60	green	yes	this work

Cu^{II} examples and the Cr^{II} compounds there are some close analogies.

A significant word in the title of this Account is "transparent". Except in the thinnest sections metals are quite opaque to all visible and infrared frequencies, but insulators may have extended regions of transparency at frequencies lower than the band gap. Ligand-field and charge-transfer excited states are the commonest source of visible light absorption in the insulating ferromagnets, though in the two Eu examples the lowest excited states are most likely $4f \rightarrow 5d$.⁴ Like $f \rightarrow d$ transitions, charge-transfer transitions, being electric dipole allowed, result in absorption bands with peak linear absorption constants of some tens of thousands of cm^{-1} and also several thousand cm^{-1} wide. Compounds in which these bands appear in the visible are deeply colored or black. The energies of charge-transfer transitions depend on "optical electronegativities",¹² so there is little point in looking for compounds transparent in the visible when the metal is in a high oxidation state or the anion has a low electronegativity. Thus CrI₃ is black, and so is the mixed oxide Y₃Fe₅O₁₂, better known as YIG, which, although long famous as a transparent ferromagnet,¹³ is really neither appreciably transparent in the visible nor a true ferromagnet. It is actually ferrimagnetic because Fe(III) ions occupy both octahedral and tetrahedral sites.

When one is looking for visible transparency, therefore, it is better to choose compounds of metals in lower oxidation states with ligands of high electronegativity, such as the lighter halogens. Even then, spin-allowed ligand-field transitions need to be considered. They usually have peak linear absorption constants of a few hundred cm^{-1} and widths nearly as big as charge-transfer bands, and so can obscure much of the visible region. CrBr₃ is dark, not because of charge-transfer bands, but because the two broad ligand-field bands ${}^4A_{2g} \rightarrow {}^4T_{1g}$ and ${}^4A_{2g} \rightarrow {}^4T_{2g}$ overlap strongly.

Spin-forbidden ligand-field bands are not only weaker, but usually much narrower. In magnetic lattices, whether ferro- or antiferromagnetic, they also have an intrinsic interest because most of their intensity derives from creation or annihilation of spin waves (magnons) accompanying the electronic excitations, or excitons.¹⁴ The intensities, polarizations, and band shapes of such exciton-magnon combination bands thus

contain detailed information about the densities of states and dispersion of the excitons and magnons and the thermal populations of the magnon states, which are related directly to the ordering process.

So much for the wider background to our experiments on the tetrahalogenochromates. They provide important new examples of the small class of visibly transparent ferromagnetic compounds. Furthermore, they are unique in having well-resolved spin-forbidden crystal-field transitions in the visible, whose properties can be used to probe the magnetic excitations. Uniquely, too, these bands are the only ones in the visible. Consequently when the crystals go through their Curie temperature, they change color!

The binary phase diagrams ACl-CrCl₂, where A is K, Rb, Cs, were first determined by Siefert and Klatyk,¹⁵ who showed from X-ray powder patterns that in each case there were two compounds, ACrCl₃ and A₂CrCl₄. The former had the hexagonal perovskite structure, the latter the K₂NiF₄ structure. All the compounds had room temperature magnetic moments close to that expected for an $S = 2$ ground state. Later measurements at 80 K,¹⁶ however, gave slightly lower moments for the hexagonal perovskite phases, but very much larger ones for the ones with the K₂NiF₄ structures. Using the simple Curie formula a value of 11.3 μ_B was calculated for the moment of Rb₂CrCl₄! Clearly this is much bigger than for any magnetically dilute d^n ground state and must mean that at 80 K the compound is on the point of becoming ferromagnetically ordered. Siefert and Klatyk reported that the A₂CrCl₄ salts were yellow-green, implying small visible absorption. From these facts it seemed that the compounds were additions to the select group of transparent ferromagnets.

Preparation and Crystal Growing

The published ACl-CrCl₂ phase diagrams¹⁵ show that the K₂CrCl₄ and Rb₂CrCl₄ phases are congruently melting while Cs₂CrCl₄ melts incongruently. In principle, therefore, crystals of the two former salts could be prepared by slowly cooling a melt of the alkali metal chloride and CrCl₂ with the correct stoichiometric composition. The simplest way of doing this is to seal the powdered material in a silica ampule and, after evacuating and carefully flaming it out, to heat it above the melting point in a vertical tube furnace and lower it slowly (1-2 mm/h) through a temperature gradient (Bridgman method). For optical measurements and elastic neutron scattering, crystals of a few millimeters on edge are sufficient, but for inelastic neutron scat-

(12) C. K. Jørgensen, "Orbitals in Atoms and Molecules", Academic Press, New York, 1962.

(13) R. Pauthenet, *Ann. Phys.*, **3**, 424 (1958); G. B. Scott, D. E. Lacklinton, and J. L. Page, *Phys. Rev. B*, **10**, 1971 (1974).

(14) D. Sell, R. L. Greene, and R. M. White, *Phys. Rev.*, **158**, 489 (1967).

(15) H. J. Siefert and K. Klatyk, *Z. Anorg. Allg. Chem.*, **334**, 113 (1964).

(16) L. F. Larkworthy and J. K. Trigg, *Chem. Commun.*, 1221 (1970).

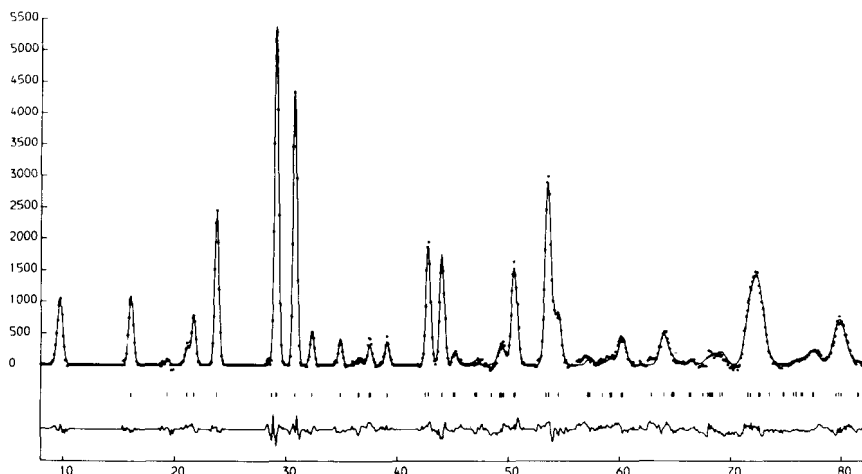


Figure 1. Powder neutron diffraction profile of Cs_2CrCl_4 at 4.2 K. The vertical lines show calculated peak positions and the lowest line in each case is the residual of the profile analysis.

tering one needs single crystals of at least 1 cm^3 . Furthermore, one's ability to measure spin waves close to the Brillouin zone center is determined by the width of the elastic scattering peaks, and hence by crystal perfection. A low mosaic spread is thus desirable. Large crystals suitable for inelastic neutron scattering experiments were grown by the Crystal Growing Group in the Clarendon Laboratory, Oxford, using the Czochralski method.¹⁷ Extreme care is needed to exclude oxygen and water from all stages in the preparation and crystal growing as the powdered Cr(II) chlorides are both hygroscopic and very easily oxidized. On the other hand the cleaved surfaces of larger single crystals remain shiny in air for some hours. However, all starting materials and crystals are handled exclusively under dry oxygen-free nitrogen. The CrCl_2 was prepared either from Cr and HCl or from CrCl_3 by reduction with Cr metal or Ga.¹⁸

More recently, we found that ferromagnetic compounds of the same general type can be made by replacing the group 1A cations by monoalkylammonium cations.^{19,20} Compounds with the general formula $(\text{RNH}_3)_2\text{CrCl}_4$ ($\text{R} = \text{CH}_3$ to $\text{C}_{12}\text{H}_{25}$) are not prepared from melts but by precipitation on slowly cooling an ethanol solution.

Crystal and Magnetic Structures

First experiments on the crystal and magnetic structures of A_2CrCl_4 salts used powder neutron diffraction.²¹ A powerful method of determining structures from powder neutron data is the Rietveld profile refinement method²² by which the structure is refined, not simply from the angles and intensities of the diffraction peaks, but by treating each individual data point, as the diffraction profile is scanned in 0.1° steps, as a separate item of input to the least-squares re-

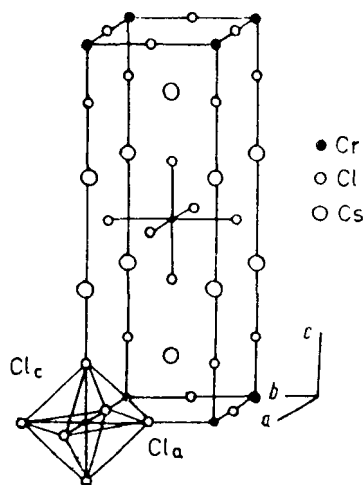


Figure 2. The K_2NiF_4 structure.

finement process. Figure 1 shows the diffraction profile of Cs_2CrCl_4 at 4 K with, underneath, the residual of the least-squares fit represented by the full line through the data points. By comparing the 4 K profile with one measured at 300 K, a simple indication of the fact that the compound is ferromagnetically ordered is that no purely magnetic peaks appear in the 4 K profile; the magnetic cell coincides with the crystallographic cell.

The powder diffraction profiles of Rb_2CrCl_4 and Cs_2CrCl_4 index in the D_{4h}^{17} space group, the same as K_2NiF_4 (Figure 2). Since K_2CrCl_4 has an orthorhombic unit cell and Cs_2CrCl_4 is incongruently melting, most of our detailed structural experiments centered on the Rb salt, which is both tetragonal and congruently melting, so that single crystals can be grown. Single-crystal diffraction measurements were needed for three reasons. First, the powder profiles were not unambiguous regarding the direction of the magnetic mo-

(17) P. J. Walker and G. Garton, *J. Cryst. Growth*, **36**, 351 (1976).

(18) G. Garton and P. J. Walker, *J. Cryst. Growth*, **33**, 331 (1976).

(19) C. Bellitto and P. Day, *J. Chem. Soc., Chem. Commun.*, 870 (1976).

(20) C. Bellitto and P. Day, *J. Chem. Soc., Dalton Trans.*, 1207 (1978).

(21) M. T. Hutchings, A. K. Gregson, P. Day, and D. H. Leech, *Solid State Commun.*, **15**, 313 (1974).

(22) H. M. Rietveld, *J. Appl. Crystallogr.*, **2**, 65 (1969).

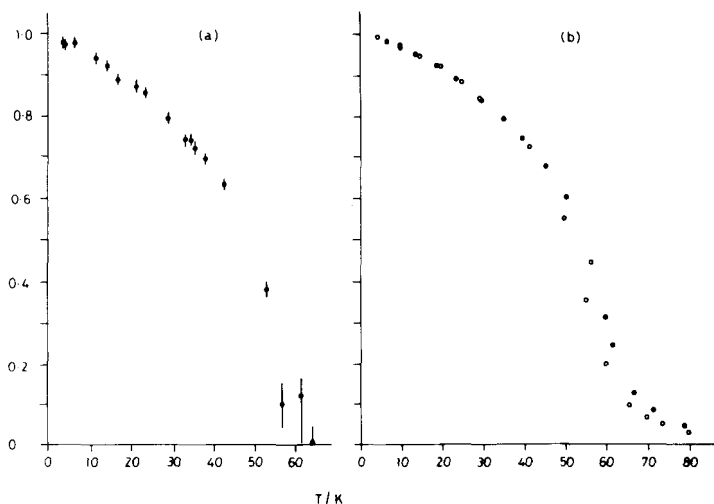


Figure 3. Temperature variation of magnetization of Rb_2CrCl_4 from (a) neutron diffraction and (b) susceptibility measurements.

ment: with a single crystal the intensities of (101) and (004) peaks were therefore measured with a magnetic field of 1.8 T applied perpendicular to the scattering plane, which coincided with the (010) plane of the crystal.²³ The diffracted intensity is proportional to $\sin^2 \alpha$, where α is the angle between the moment and the scattering vector. Within experimental error $\alpha(004)$ was constant at 90° , that is, the moments lie in the basal plane, within which they are rotated by the applied field.

The second reason for carrying out single-crystal neutron diffraction was to determine the variation of the magnetization with temperature. Whereas measurements of magnetization by susceptibility methods require a magnetic field, the magnetic contribution to the elastic neutron scattering intensity is a direct measure of the spontaneous (zero-field) magnetization. Integrated intensities of (002), (101), and (004) were recorded from liquid helium temperature up to 90 K; we found that the Curie temperature of Rb_2CrCl_4 was 57 ± 2 K. To subtract the nuclear contribution to the total scattering, we used the intensities recorded above T_c and found the variation in magnetization with temperature (Figure 3a). It should be compared with the magnetization curves measured with a Faraday susceptibility balance (Figure 3b).

Finally, only single-crystal measurements could reveal the more subtle features of the structure. As we have noted, powder X-ray and neutron diffraction suggested a K_2NiF_4 structure for Rb_2CrCl_4 . Best values of the positional parameters for the Cl atoms obtained in this way require that the coordination around the Cr atoms be that of an octahedron flattened along the tetragonal c axis. Cr^{2+} is formally $3d^4$, and hence in octahedral coordination should be subject to a strong Jahn-Teller distortion. The situation here is very analogous to that obtaining in K_2CuF_4 . For many years the latter was thought to be the only example of a Cu^{2+} compound in which the tetragonal Jahn-Teller distortion was a

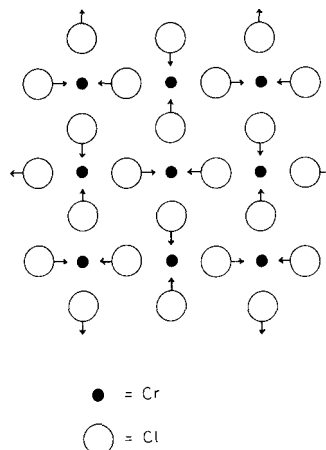


Figure 4. Jahn-Teller distortion within the basal plane of K_2CuF_4 and Rb_2CrCl_4 .

flattening rather than an elongation.²⁴ Recently, however, it has been established that the structure contains an antiferro-distortive displacement of the F atoms away from the centers of the lines joining each pair of Cu atoms in the basal plane, so that the coordination around each Cu is tetragonally elongated. The principal axes of all the CuF_6 units lie within the basal plane, but at right angles to one another (Figure 4). Clearly such a possibility must be considered in Rb_2CrCl_4 . A search for reflections which would be allowed in the D_{2d}^{10} space group, the one proposed for K_2CuF_4 by Haegele and Babel,²⁵ revealed nothing, but a more recent proposal²⁶ suggests a different ordering of the distorted planes in K_2CuF_4 . Weak reflections

(24) For example, F. A. Cotton and G. Wilkinson, "Advanced Inorganic Chemistry", 2nd ed., Interscience, New York, 1966, p 899.

(25) R. Haegele and D. Babel, *Z. Anorg. Allg. Chem.*, **409**, 11 (1974).

(26) Y. Ito and J. Akamitsu, *J. Phys. Soc. Jpn.*, **40**, 1333 (1976).

(23) M. J. Fair, A. K. Gregson, P. Day, and M. T. Hutchings, *Physica (Utrecht)*, **86-88B**, 657 (1977).

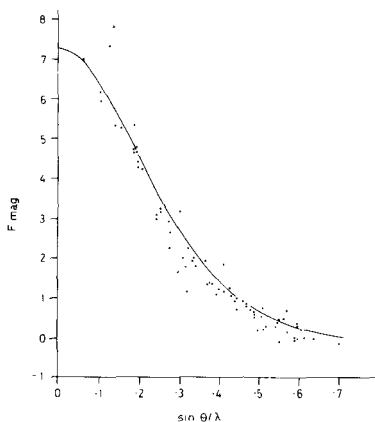


Figure 5. Magnetic form factor of Cr^{2+} from polarized neutron diffraction of Rb_2CrCl_4 . The full line is the calculated form factor³² scaled to $3.6 \mu_B$.

compatible with this new suggestion have now been observed in Rb_2CrCl_4 .²⁷ Independent confirmation that the lattice contains two Jahn-Teller distorted metal ion sites with their principal axes at right angles within the basal plane comes from the angular variation of the resonance frequency in the ^{53}Cr NMR spectrum.²⁸

A further structural aspect concerns the unpaired spin distribution. A powerful method for determining spatial distributions of unpaired spin density in magnetic crystals is the diffraction of polarized neutrons by the lattice of aligned spins.²⁹ While the cross section for magnetic scattering depends on the angle between the neutron spin and the electron spin, nuclear scattering is independent of this angle. Consequently by measuring the intensity of a reflection when the neutron and electron spins are first parallel, then antiparallel, the nuclear contribution to the scattered intensity is eliminated. Fourier transformation of the purely magnetic reflection intensities then gives the unpaired spin density distribution in the unit cell. To carry out such an experiment the unpaired electron spins have to be aligned. While this can be done for a magnetically dilute compound by applying a big enough external field at a low enough temperature, the experiment can obviously be done more effectively on substances having a spontaneous magnetization, ferromagnets, ferrimagnets, or canted antiferromagnets.

Leaving aside experiments on ferromagnetic alloys, only a handful of inorganic compounds have so far been examined by polarized neutron diffraction.³⁰ At the I.L.L. high flux reactor we collected polarization data on 102 independent reflections of Rb_2CrCl_4 at 4.2 K, measuring polarization ratios of the $(h0l)$ peaks to $\sin \theta/\lambda = 0.6$ at two different neutron wavelengths, to check for extinction.³¹ Our spin-density map is not complete yet, but Figure 5 shows a comparison between the

(27) M. T. Hutchings and E. Janke, personal communication.

(28) K. Le Dang, P. Veillet, and P. J. Walker, *J. Phys. (Paris)*, C, 10, 4593 (1977).

(29) W. Marshall and S. W. Lovesey, "Theory of Thermal Neutron Scattering", Clarendon Press, Oxford, 1971.

(30) For a well-documented recent example see F. A. Wedgwood, *Proc. R. Soc. London, Ser. A*, 349, 447 (1976).

(31) M. J. Fair, J. B. Forsyth, and P. Day, *I. L. L. Annu. Rep.*, 149 (1975).

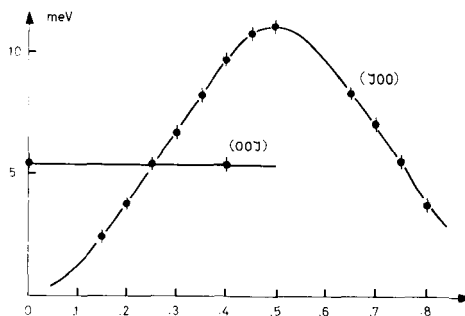


Figure 6. Dispersion of magnons propagating in the basal plane (100) and along the c axis (001) of Rb_2CrCl_4 at 5 K. The lines through the experimental points are the best fit to eq 1 with $J_1 = 5.3 \pm 0.1 \text{ cm}^{-1}$ and $D = 0$.³⁸

observed magnetic form factor and one computed theoretically³² for Cr^{2+} , scaled to $3.7 \mu_B$.

Magnetic Susceptibility and Magnetization

First we measured the susceptibilities and magnetizations of the three compounds A_2CrCl_4 ($\text{A} = \text{K}, \text{Rb}, \text{Cs}$) to 4 K, using powder samples and a Faraday balance.³³ We also repeated the earlier susceptibility measurements from 77 K to room temperature^{34,35} to fit them to a high-temperature series expansion^{36,37} and hence calculate the near-neighbor exchange constants.

The large positive Weiss constants (70–80 K) indicate qualitatively that the compound must be ferromagnetic. Best fit to the series expansion are given by positive exchange constants J in the range $3.5\text{--}4.5 \text{ cm}^{-1}$ and g values close to 2. However, inelastic neutron scattering measurements of the spin-wave dispersion can provide much more precise estimates of J . The variation with temperature of the magnetization curve was obtained from neutron diffraction. The applied field in the magnetic experiment rounds off the phase transition, making it harder to get an accurate estimate of T_c . The value obtained in this way for Rb_2CrCl_4 ($62 \pm 2 \text{ K}$) is a little higher than that found by neutron diffraction.

Inelastic Neutron Scattering

The ultimate stage in characterizing the magnetic parameters of a new substance is to measure the dispersion relations of its magnons, preferably as a function of temperature up to T_c . Coherent inelastic neutron scattering measurements on Rb_2CrCl_4 were made on the Pluto triple axis spectrometer at Harwell³⁸ and the IN2 and IN8 instruments at the I.L.L.³⁹ To record the very small energy and momentum transfers from magnons close to the zone center, a long wave-

(32) E. J. Lisher and J. B. Forsyth, *Acta Crystallogr., Sect. A*, 27, 545 (1971).

(33) A. K. Gregson, P. Day, D. H. Leech, M. J. Fair, and W. E. Gardner, *J. Chem. Soc., Dalton Trans.*, 1306 (1975).

(34) D. H. Leech, Ph.D. Thesis, Manchester, 1971.

(35) D. H. Leech and D. Machin, *J. Chem. Soc., Chem. Commun.*, 866 (1974).

(36) G. S. Rushbrooke and P. J. Wood, *Mol. Phys.*, 1, 257 (1958).

(37) M. E. Lines, *J. Phys. Chem. Solids*, 31, 101 (1970).

(38) M. T. Hutchings, M. J. Fair, P. Day, and P. J. Walker, *J. Phys. (Paris)*, C, 9, L55 (1976).

(39) M. J. Fair, M. T. Hutchings, P. Day, R. Ghosh, and P. J. Walker, *J. Phys. (Paris)*, C, 11, L813 (1978).

length triple axis instrument at the Danish Atomic Energy Research Establishment, Risø, has also been used.⁴⁰

If we add an anisotropy term $D_i \sum_i S_i^z$ to the Heisenberg Hamiltonian, the spin wave energies are given³⁸ by

$$h\omega_q = 2S\{[J(0) - J(q)][J(0) - J(q) + D]\}^{1/2} \quad (1)$$

where

$$J(q) = \sum_{i,r} J_i \exp(iqr) \quad (2)$$

the sum being taken over the i nearest neighbor ions positioned at r_i . Experimental spin wave energies, shown in Figure 6, were least-squares-fitted to eq 1 to give values of J_1 , the nearest neighbor exchange constant, and D . J_1 was estimated as $5.3 \pm 0.1 \text{ cm}^{-1}$, a much more precise value than the one obtained from the series expansion. Two points about Figure 6 are noteworthy: first, the value of D which gave the best fit to the spin-wave dispersion in the basal plane was zero, and second, there was no detectable dispersion of the spin waves propagating along the c axis, equivalent to zero J between successive layers. The K_2NiF_4 structure is a layer lattice, but both observations focus attention on the three-dimensional ordering mechanism. Thus Mermin and Wagner⁴¹ have given a rigorous theoretical proof that a two-dimensional lattice with purely Heisenberg interactions cannot undergo a phase transition to an ordered state at any non-zero temperature, although in practice this could be relaxed by introducing anisotropy or an interaction between the planes.⁴² Experiment suggests that both the in-plane anisotropy and the interplanar interaction must be very small, yet Rb_2CrCl_4 orders at 63 K. The dilemma has been resolved by further neutron-scattering experiments with a particularly good crystal having a low mosaic spread. Because the boule used to obtain the results in Figure 6 consisted of several slightly misaligned domains, measurements could only be made down to $q = 0.15$. New measurements⁴⁰ at lower q reveal that the dispersion curve does not go to zero energy at $q = 0$, but to approximately 0.7 cm^{-1} , equivalent to about 1 K.

Optical Properties

Expectation of finding unusual optical properties was a substantial driving force in our preoccupation with these ionic ferromagnets. The ground term of a $3d^4$ ion in an octahedral ligand field would be 5E_g , with only one other quintet term, ${}^5T_{2g}$, in the manifold of ligand-field states. However, the relevant Tanabe-Sugano diagram⁴³ shows a large number of triplet terms which, for all reasonable values of the ligand-field splitting parameter Δ and the Racah parameter B , are at higher energies than the quintet. Almost all 6-coordinate Cr(II) compounds have a strong Jahn-Teller distortion, splitting the E and T_2 terms, but in general the absorption corresponding to ${}^3E_g \rightarrow {}^3T_{2g}$ is an envelope of overlapping bands in the near-infrared. Transitions to the various triplets are found across the visible and

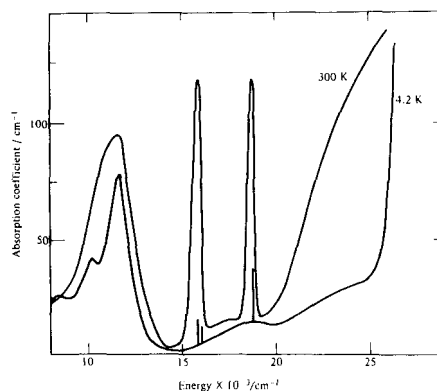


Figure 7. Absorption spectrum of K_2CrCl_4 at 300 K and 4 K with unpolarized light incident parallel to the c axis.⁴⁴

since Cr(II) has a low optical electronegativity the intense absorption edge resulting from ligand-to-metal charge transfer is on the edge of the ultraviolet.

Figure 7 shows the transmission spectrum of K_2CrCl_4 at room temperature and at 4.2 K.⁴⁴ In the visible only two of the anticipated triplet states appear, but they are sharp and well resolved even at room temperature. On lowering the temperature, a remarkable change occurs: in the near-infrared the group of bands assigned to the spin-allowed ligand-field transitions diminish a little because most of their intensity comes from vibronic coupling; in the visible though, the two spin-forbidden bands all but vanish! To our knowledge no such effect had ever been observed before; it can be seen with the naked eye since the two bands in question provide the only absorption in the visible region, and removing them changes the crystal from dark olive green to pale yellow. At low temperatures the chlorochromates are therefore easily the most transparent ferromagnets known. The Rb and monoalkylammonium salts behave in the same way.⁴⁵

Such behavior poses two questions. Why, out of the large number of possible triplet transitions, are there only two with appreciable intensity? And why does their intensity vary so much with temperature? To answer the first question ligand-field calculations were carried out over a wide region of parameter space involving Δ , B , and a tetragonal field component.⁴⁶ In the relevant part of the d^4 Tanabe-Sugano diagram for O_h symmetry we find ${}^3T_{1g}$, 3E_g , ${}^3T_{1g}$, and ${}^3T_{2g}$ from 3H , ${}^3A_{2g}$ (3F), and ${}^3A_{1g}$ (3G). Of these, 3E_g (3H) and ${}^3A_{1g}$ (3G) do not vary with Δ ; i.e., in the strong field limit they are pure "spin flips". A similar conclusion is reached on applying a tetragonal perturbation which splits the 5E_g ground state into ${}^5B_{1g}$ and ${}^5A_{1g}$. Transitions which do not involve any changes in orbital occupancy, for instance the well-known ${}^4A_{1g}$, 4E_g bands of Mn(II) compounds,⁴⁷ are always narrow because they do not change the molecule's potential-energy surface. Furthermore, in a variety of d^4 compounds, whether ferromagnetic or antiferromagnetic (e.g., binary and

(40) J. Als-Neilsen, M. T. Hutchings, and P. A. Lindgard, personal communication.

(41) N. D. Mermin and H. Wagner, *Phys. Rev. Lett.*, **17**, 1133 (1966).

(42) For example, M. E. Lines, *Phys. Rev.*, **B**, **3**, 1749 (1971).

(43) E. N. Figgis, "Introduction to Ligand Fields", Interscience, New York, 1967, p 162.

(44) P. Day, A. K. Gregson, and D. H. Leech, *Phys. Rev. Lett.*, **30**, 19 (1973).

(45) C. Bellitto and P. Day, *J. Chem. Soc., Chem. Commun.*, 511 (1978).

(46) A. K. Gregson, unpublished.

(47) L. E. Orgel, *J. Chem. Phys.*, **23**, 1824 (1955).

ternary Cr(II) fluorides^{48,49} and chlorides,³⁴ CrI₂⁵⁰ and MnF₂,⁵¹ there are two relatively intense spin-forbidden bands between 15 000 and 20 000 cm⁻¹. Using magnetic circular dichroism, which is much more sensitive to weak transitions than ordinary absorption spectroscopy, we also located the baricenters of other cubic field components of ³H and ³G.⁵²

The most interesting question, however, concerns the temperature dependence. In magnetic insulators spin-forbidden ligand-field transitions gain intensity by coupling to spin fluctuations in the ordered lattice. Qualitatively the decrease in the crystal's spin projection when one of the ions undergoes a transition from a quintet to an excited triplet state is compensated either by creating a positive spin deviation within the array of ions remaining in their ground states or by annihilating a thermally excited negative deviation.⁵³ The former process is very well-known in antiferromagnets.⁵⁴ In ferromagnets only the latter process contributes to the absorption because, in proportion as the lattice is magnetized, no positive spin deviation, further increasing the spin projection of the lattice, is possible. Thus the intensity of an exciton-magnon combination band in a ferromagnet depends on the thermal population of magnons. Quantitatively:

$$I(\omega) = \sum_k I_k(\omega) = \sum_k |M_k|^2 \langle n_k \rangle \delta(\hbar\omega + E_k - \lambda_k) \quad (3)$$

where the summation is over the Brillouin zone, M_k is the electric dipole transition moment, $\langle n_k \rangle$ is the thermal population of magnons with the same wave-vector as the exciton, E_k is the energy of the magnon, λ_k is that of the exciton and the δ function ensures equality between the photon energy and the sum of the exciton and magnon energies.¹⁴ At thermal equilibrium $\langle n_k \rangle$ is given by the Planck distribution

$$\langle n_k \rangle = [\exp(E_{sw}/k_B T) - 1]^{-1} \quad (4)$$

and the total number of magnons excited at temperature T is

$$\sum_k \langle n_k \rangle = \int D(\omega) \langle n(\omega) \rangle d\omega \quad (5)$$

$D(\omega)$ being the magnon density of states in frequency units. Both $D(\omega)$ and E_{sw} are experimentally accessible from inelastic neutron scattering, but as a rough approximation we could take just the magnons close to the zone center, since only these are populated at low temperatures. For a two-dimensional easy-plane ferromagnet with negligible anisotropy the limiting form⁵⁵ of the magnon dispersion at small k is $E_{sw} \propto k^2$. When this approximation is used in eq 4 and 5 to calculate $\langle n_k \rangle$ and $D(\omega)$ and the results are substituted in eq 3, the integrated intensity of our exciton-magnon bands should vary at low temperature as T^2 , as shown in Figure 8 for the 530-nm band of Rb₂CrCl₄.⁵⁶ Note,

(48) A. Earnshaw, L. F. Larkworthy, and K. S. Patel, *J. Chem. Soc. A*, 363 (1966).

(49) W. W. Holloway and M. Kestigian, *Spectrochim. Acta*, **22**, 1381 (1966).

(50) S. Jermin, Chemistry Part II Thesis, Oxford, 1972, unpublished.

(51) R. J. H. Clark, *J. Chem. Soc.*, 417 (1964).

(52) M. J. Fair, Chemistry Part II Thesis, Oxford, 1973, unpublished.

(53) For a review, see D. S. McClure in "Optical Properties of Ions in Solids", B. di Bartolo, Ed., Plenum, New York, 1975, p 259.

(54) K. Shinagawa and Y. Tanabe, *J. Phys. Soc. Jpn.*, **30**, 1280 (1971).

(55) D. J. Robbins and P. Day, *J. Phys. (Paris)*, **C**, **9**, 867 (1976).

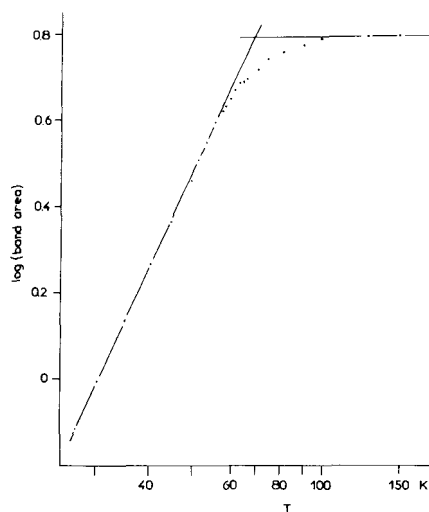


Figure 8. Intensity of the 530-nm absorption band in Rb₂CrCl₄ as a function of temperature.⁵⁶

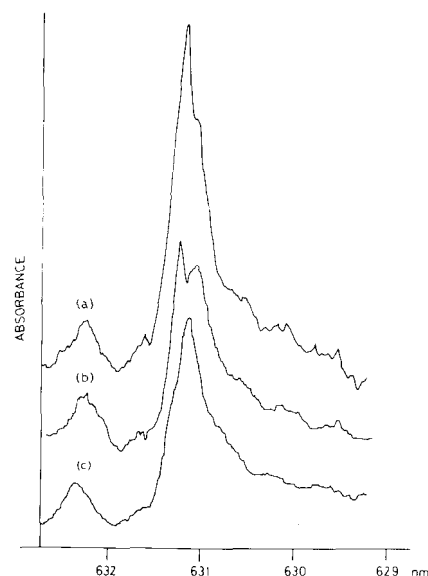


Figure 9. Axial absorption spectrum of Rb₂CrCl₄ in the 630-nm region at very low temperatures.⁵⁶ (a) 1.38 K, (b) 1.15 K, (c) 0.83 K.

however, that the T^2 dependence persists almost up to T_c and also that even above T_c the intensity continues to grow, presumably because short range order still persists. Strictly speaking, one should perform the integration in eq 3 over the whole Brillouin zone using magnon dispersion relations which are either obtained experimentally or fitted to the observed exchange parameters. This we have done for K₂CrCl₄,⁵⁷ and

(56) P. Day, *Collog. Int. C.N.R.S.*, **255**, 237 (1977).

(57) A. K. Gregson, P. Day, A. Okiji, and R. J. Elliott, *J. Phys. (Paris)*, **C**, **9**, 4497 (1976).

Vol. 12, 1979

243

found good agreement with experiment from 4.2 K upward.

If there is a gap in the magnon spectrum at $k = 0$, as suggested by neutron scattering, the intensity of the optical absorption bands should begin to deviate from the T^2 law as the temperature becomes comparable to the gap energy. We therefore measured the sharp 632-nm band down to the limit of pumped ^4He , about 0.7 K.⁵⁸ Some of the results, obtained using a nitrogen laser pumped tunable dye laser⁵⁹ are shown in Figure 9. The sharp band at 631.3 nm, which dominates the band envelope at 3 K and upward, disappears rapidly below 1 K and can be quantitatively fitted to a gap energy equivalent to 1.0–1.5 K.

From these experiments we now have a good picture of the crystal and magnetic structures of the chlorochromates, the reasons why they are ferrimagnetic, and the effect this has on their optical properties. Although

(58) P. Day, E. Janke, T. E. Wood, and D. R. Woodwark, *J. Phys. C*, **12**, L329 (1979).

(59) C. Ironside, K. Gardner, D. R. Woodwark, P. Day, and R. G. Denning, to be published.

they are the most visible transparent ferromagnets known at present, their relatively low Curie temperatures will limit technological application of their curious properties, whether to optical modulation or to magnetic data storage with optical readout. Nevertheless they have provided intriguing problems for magnetic theory and an object lesson in applying a wide range of physical techniques. A further dimension of chemical variation, only touched on in this account, concerns replacement of the alkali metal cations by organic groups, increasing the spacing between the layers up to as much as 25 Å.²⁰ With their simpler prototypes they too are good examples of how preparative inorganic chemistry can bring forward new systems to challenge the skills both of the experimental and of the theoretical physicist.

The experiments described here were carried out in collaboration with many colleagues, postdoctorates, and graduate students whose names appear in the references; my best thanks for all their help. Our group has been supported by the U.K. Science Research Council, A.E.R.E. Harwell, and the National Research Development Corporation.

Magnetic Susceptibility and Optical Spectra of the Organic-intercalated Two-dimensional Ferromagnets Bis(monomethylammonium)- and Bis-(monoethylammonium) Tetrachlorochromate(II)

By Carlo Bellitto and Peter Day,* Oxford University, Inorganic Chemistry Laboratory, South Parks Road, Oxford OX1 3QR

The title compounds have been prepared and characterised by chemical analysis and X-ray diffraction. By magnetic-susceptibility and magnetisation measurements they are shown to order ferromagnetically at $T_c = 58 \pm 2$ and 55 ± 2 K respectively. Up to ca. $0.7 T_c$ the magnetisation $M(T)$ obeys the equation $1 - [M(T)/M(0)] = CT^\gamma$ where $\gamma = 1.5 \pm 0.1$. The optical spectra of both compounds contain sharp absorption bands at 533 and 626 nm, assigned as quintet-triplet ligand-field transitions. Up to $0.9 T_c$ their intensities vary with temperature as T^2 , as predicted for 'hot' exciton-magnon combination bands in a two-dimensional easy-plane ferromagnet.

In the last few years there has been much interest, both among chemists and physicists, in the magnetic properties of compounds containing layers or chains of metal ions.¹ This activity has been motivated in part by a search for model systems on which to test the predictions of statistical thermodynamic theories of collective magnetic behaviour which take their simplest form where only one- or two-dimensional interactions have to be considered. In part, too, it has stemmed from a desire to probe the three-dimensional ordering mechanism in compounds in which the interactions are essentially low-dimensional. Thus, for example, Mermin and Wagner² showed theoretically that a two-dimensional array of spins, with near-neighbour interactions described by an isotropic Heisenberg Hamiltonian, does not undergo a phase transition to a ferromagnetic or antiferromagnetic state above absolute zero. On the other hand, introducing anisotropy into the Hamiltonian raises T_c to a finite level.

From the experimental point of view one of the most attractive groups of low-dimensional magnetic compounds are the layer perovskites $[\text{NRH}_3]_2[\text{MX}_4]$ (R = an alkyl or aryl group, M = a $3d$ ion, X = halide). Varying R permits variation of the distance between the MX_2 layers. In all these compounds, even when the inter-layer distance is as great as 25 Å, spontaneous magnetic order in three dimensions is established between 10 and 90 K. The manganese³ and iron⁴ members have anti-ferromagnetic near-neighbour coupling, the copper has ferromagnetic.⁵ The purpose of the present paper is to report the synthesis, characterisation, and magnetic properties of the corresponding chromium salts. Not only are they ferromagnetic, and hence an addition to the very small group of ionic insulators which order ferromagnetically,⁶ but they are unique among optically transparent ferromagnets in showing well resolved spin-forbidden ligand-field transitions, whose intensity variation with temperature provides a direct probe of the magnetic order.

¹ For an excellent review, see L. J. de Jongh and R. A. Miedema, *Adv. Phys.*, 1974, **23**, 1.

² N. D. Mermin and H. Wagner, *Phys. Rev. Letters*, 1966, **17**, 1133.

³ W. D. Van Amstel and L. J. de Jongh, *Solid State Comm.*, 1972, **11**, 1423.

A preliminary communication of these results has appeared.⁷

EXPERIMENTAL

B.D.H. Monoalkylammonium chlorides were dried *in vacuo* over P_2O_{10} for several hours. Since the tetrachlorochromates(II) are hygroscopic and very easily oxidised, all the preparations and sample handling were carried out under oxygen-free nitrogen. To a hot solution of Cr^{II} in dry ethanol, prepared by passing dry HCl gas through a suspension of finely divided Cr metal, was slowly added a stoichiometric quantity of monoalkylammonium chloride in dry ethanol solution. On cooling, pale green plates of the bis(monalkylammonium) tetrachlorochromate(II) crystallised. Larger crystals could be grown by slow recrystallisation (Found: C, 9.70; H, 4.70; Cl, 54.1; Cr, 20.8; N, 10.9. Calc. for $\text{C}_2\text{H}_{12}\text{Cl}_4\text{CrN}_2$: C, 9.30; H, 4.65; Cl, 55.0; Cr, 20.15; N, 10.85. Found: C, 16.8; H, 5.80; Cl, 49.7; Cr, 18.25; N, 9.65. Calc. for $\text{C}_4\text{H}_{16}\text{Cl}_4\text{CrN}_2$: C, 16.8; H, 5.60; Cl, 49.6; Cr, 18.2; N, 9.80%).

X-Ray powder photographs were obtained using a Philips W 1024 camera (nickel-filtered $\text{Cu-K}\alpha$ radiation), the samples being sealed in Lindemann tubes. Single-crystal transmission spectra were recorded either by a Cary 14R spectrophotometer equipped with an Oxford Instruments CF 100 continuous-flow helium cryostat and Harwell temperature controller, or a McPherson RS 10 high-resolution double-beam spectrophotometer together with a Thor Cryogenics cryostat containing a 5-T split-coil superconducting solenoid. The latter is equipped with a Thor Cryogenics temperature controller and carbon resistance thermometer, providing temperatures from 1.5 to 150 K controllable to ± 0.1 K.

Magnetic-susceptibility measurements were made from 150 to 80 K using a Faraday balance at the Materials Physics Division, A.E.R.E., Harwell, and from 80 to 4.2 K using Oxford Instruments Faraday balances at the Inorganic Chemistry Laboratory, Oxford, and the Laboratorio di Teoria e Struttura Elettronica dei Composti di Coordinazione, Rome. The powdered samples were contained in 'Rislan' spheres and suspended by quartz fibres from a Sartorius microbalance. Temperatures were measured with a Au (0.03 atom % Fe) vs. chromel thermocouple with its

⁴ F. M. Mostafa and R. D. Willett, *Phys. Rev.*, 1971, **B3**, 2213.

⁵ L. J. de Jongh and W. D. Van Amstel, *J. Phys. (Paris)*, *Colloq.*, 1971, **1**, C1-880.

⁶ For a brief review see P. Day, *Colloques Int. C.N.R.S.*, 1977, No. 255, 237.

⁷ C. Bellitto and P. Day, *J.C.S. Chem. Comm.*, 1976, 870.

1208

J.C.S. Dalton

reference junction in a liquid-helium bath. The balances were calibrated with Pt.

RESULTS

Crystal Structure.—The X-ray powder photographs could be indexed in the space group $Cmca (D_{2h}^{18})$, the same as that of the corresponding compounds of Mn²⁺ and Cd²⁺ at room

inverse susceptibilities of $[NMeH_3]_2[CrCl_4]$ and $[NEtH_3]_2[CrCl_4]$ as a function of temperature from 150 K down to the ordering temperature. At *ca.* > 90 K the Curie-Weiss law is obeyed, with values of the Weiss constant θ of 61 and 58 K respectively. The observed susceptibilities were corrected for the diamagnetism of the constituent atoms and for temperature-independent paramagnetism (t.i.p.). For the

TABLE I
Powder X-ray diffraction data (unit-cell parameters are given in the text)

<i>h</i> <i>k</i> <i>l</i>	$[NMeH_3]_2[CrCl_4]$			$[NEtH_3]_2[CrCl_4]$		
	$\sin^2\theta$ (obs.)	Intensity	$\sin^2\theta$ (calc.)	$\sin^2\theta$ (obs.)	Intensity	$\sin^2\theta$ (calc.)
0 0 2	0.006 07	vs	0.006 67	0.004 68	vs	0.005 19
	0.007 05	vs		0.005 38	vs	
1 1 1	0.022 68	vs	0.023 69	0.022 87	s	0.022 60
0 0 4	0.024 40	vs	0.026 67	0.022 23	s	0.020 76
1 1 3	0.035 98	m		0.032 74	s	0.032 97
	0.037 95	m	0.037 03	0.033 36	s	
2 0 0	0.042 22	m	0.043 09	0.041 64	m	0.041 29
0 2 0	0.044 89	m	0.045 00	0.044 29	m	0.043 91
2 0 2	0.048 94	w	0.049 76	0.046 66	w	0.046 48
	0.051 42	w				
0 2 2	0.053 95	w	0.051 67			0.049 10
	0.056 74	w				
0 0 6	0.058 98	m	0.060 00	0.046 66	w	0.046 69
1 1 5	0.060 21	m	0.063 70	0.053 70	w	0.053 73
2 0 4	0.068 77	s	0.069 76	0.062 05	m	0.062 04
0 2 4	0.071 67	s	0.071 67	0.064 60	m	0.064 66
2 2 0	0.085 98	vs	0.088 10	0.084 75	vs	0.085 20
	0.088 44	vs				
2 2 2	0.093 45	m	0.094 76	0.090 67	s	0.090 39
	0.095 49	m				
2 0 6	0.103 84	m	0.103 10	0.086 70	s	0.087 98
0 2 6			0.105 01	0.099 63	w	0.090 60
0 0 8	0.106 78	m	0.106 69	0.080 66	w	0.083 08
3 1 1	0.110 30	w	0.109 87	0.106 80	w	0.105 18
1 3 1	0.112 50	w	0.113 70	0.110 05	w	0.110 42
3 1 3	0.122 89	w	0.123 20			0.115 66
			0.127 03	0.124 08	w	0.120 79
2 2 6	0.147 91	m	0.148 48			
3 1 5	0.149 77	w	0.149 70	0.132 24	w	0.133 10
1 1 9	0.153 67	m	0.157 05	0.126 39	w	0.126 36
4 0 0	0.172 50	w	0.172 35	0.168 38	m	0.156 16
0 4 0	0.178 14	m	0.180 01			
4 0 4	0.199 62	w	0.199 19			
2 4 0	0.221 64	m	0.223 10	0.213 90	m	0.216 94

temperature. The results are given in Table I and least-squares values of the unit-cell dimensions below:

Compound	a_0	b_0	c_0
$[NMeH_3]_2[CrCl_4]$	7.27	7.43	18.89
$[NEtH_3]_2[CrCl_4]$	7.59	7.35	21.41

The full crystal and magnetic structures at 300 K and low temperatures are currently under investigation.¹⁰ However, preliminary powder neutron-diffraction scans obtained at 87 and 4.2 K, using the Curran diffractometer at A.E.R.E., Harwell, indicate that, like its cadmium analogue, $[NMeH_3]_2[CrCl_4]$ undergoes a transition to a monoclinic phase, $P2_1/c (C_{2h})$, between 300 and 87 K. The low-temperature unit-cell dimensions of $[NMeH_3]_2[CrCl_4]$ are as follows:

T/K	a_0	b_0	c_0	$\beta/^\circ$
87	7.19	7.43	18.80	90.0
4.2	7.16	7.42	18.82	90.9

High-temperature Susceptibility.—Figure 1 shows the

¹⁰ H. Arend, R. Hofmann, and F. Waldner, *Solid State Comm.*, 1973, **9**, 1629.

¹¹ G. Chapuis, H. Arend, and R. Kind, *Phys. Stat. Sol.*, 1975, **31**, 449.

⁵ E cubic-field ground state of a high-spin d^4 ion the t.i.p. correction is $4N\mu_B^2/10Dq$, where Dq is the ligand-field splitting parameter. Taking $10Dq$ as $10\ 000\text{ cm}^{-1}$, the t.i.p. correction is $10^{-4}\text{ cm}^3\text{ mol}^{-1}$. With these corrections, the room-temperature susceptibilities of the methyl- and ethylammonium salts are respectively 5.62 and 4.98 μ_B , values which are to be compared with 4.89 μ_B at 300 K in a magnetically dilute chromium(II) compound such as $Rb_2[CrCl_4(OH_2)_2]$,¹¹ very close to the spin-only value of 4.90 μ_B .

To analyse the temperature dependence of the susceptibility at temperatures well above T_c we use the series-expansion method of Rushbrooke and Wood,¹² as refined by Lines¹³ specifically for the quadratic-layer Heisenberg magnet. Writing the exchange Hamiltonian as (1) where

$$H = \sum_{n,m} J S_n S_m \quad (1)$$

the summation n,m covers all pairs of near-neighbour ions i,j , the susceptibility is given by a power series (2). In equation (2) $\phi = kT/J(S+1)$ and the coefficients C_n

¹² P. Battle, C. Daul, and P. Day, unpublished work.

¹³ L. F. Larkworthy and J. K. Trigg, *Chem. Comm.*, 1970, 1221.

¹⁴ G. S. Rushbrooke and P. J. Wood, *Mol. Phys.*, 1958, **1**, 267.

¹⁵ M. E. Lines, *J. Phys. Chem. Solids*, 1970, **31**, 101.

1978

1209

depend on the value of the spin S . When the exchange is ferromagnetic the C_n are multiplied by $(-1)^n$, so for $S = 2$ equation (2) becomes (3) where $x = J/kT$. Equation (3)

$$\frac{Ng^2\mu_B^2}{\chi J} = 3\phi + \sum_{n=1}^{\infty} \frac{C_n}{\phi^{n-1}} \quad (2)$$

$$Ng^2\mu_B^2/\chi = \frac{1}{2}kT + J(-4 + 9x - 9.072x^2 + 55.728x^3 - 160.704x^4 + 116.640x^5) \quad (3)$$

is the same as the one we used earlier to analyse the high-temperature susceptibility of the ferromagnets $A_2[\text{CrCl}_4]$ ($A = \text{K, Rb, or Cs}$).¹⁴

Figure 1 shows the susceptibilities of the two salts, plotted as $1/\chi$ against temperature, together with the best-fit curves calculated according to equation (3). For the methylammonium salt the best agreement between theory

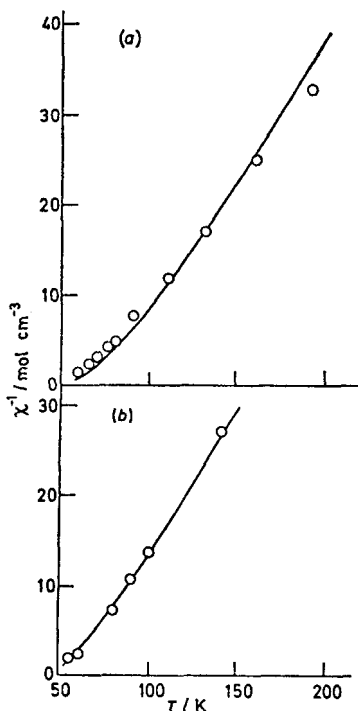


FIGURE 1 Plots of inverse susceptibility against temperature for (a) $[\text{NMeH}_3]_2[\text{CrCl}_4]$ and (b) $[\text{NEtH}_3]_2[\text{CrCl}_4]$. The lines are fits to equation (3) for (a) $J = 9 \text{ cm}^{-1}$, $g = 2.00$ and (b) $J = 7 \text{ cm}^{-1}$, $g = 1.95$.

and experiment is obtained for a value of $J = 9 \text{ cm}^{-1}$ and $g = 2.00$, while for the ethylammonium salt a slightly lower J (7 cm^{-1}) and a g value reduced to 1.95 give an excellent account of the data from 60 to 150 K. An average g value slightly below 2.00 is quite typical of chromium(II) salts, e.g. $\text{Cr}[\text{SO}_4] \cdot 5\text{H}_2\text{O}$.¹⁵ Further evidence

¹⁴ A. K. Gregson, P. Day, D. H. Leech, M. J. Fair, and W. E. Gardner, *J.C.S. Dalton*, 1975, 1306.

¹⁵ K. Ono, S. Koide, H. Sekiyama, and H. Abe, *Phys. Rev.*, 1964, **88**, 38.

of a higher exchange constant in the monomethylammonium salt is provided by the apparently larger magnitude of the high-temperature magnetic moment (see above).

Low-temperature Magnetisation.—At 4.2 K polycrystalline samples of both salts were already essentially saturated by the lowest field (0.1 T) which could be applied conveniently with the superconducting solenoid using the available power supplies. The variation of the magnetisation with temperature for the two salts, measured at 0.3 T, is shown in Figure 2. In both cases the curves show appreciable

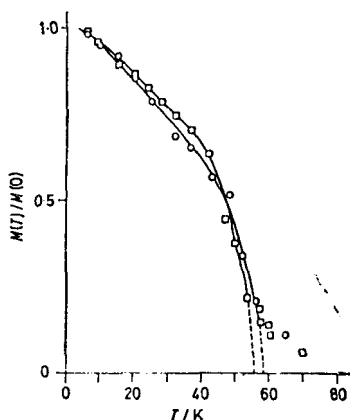


FIGURE 2 Plots of reduced magnetisation against temperature for $[\text{NMeH}_3]_2[\text{CrCl}_4]$ (O) and $[\text{NEtH}_3]_2[\text{CrCl}_4]$ (□)

rounding in the vicinity of T_c , reflecting the field-induced ordering above the spontaneous-ordering temperature characteristic of low-dimensional magnets. It is therefore difficult to be very precise about T_c , although a reasonable estimate would be 58 ± 2 and 55 ± 2 K for the methyl- and ethyl-ammonium salts respectively. We shall see below that this value agrees quite closely with that obtained from the optical spectrum, which is of course a zero-field measurement.

An alternative way to express the variation of magnetisation with temperature is through equation (4). In

$$1 - [M(T)/M(0)] = CT^\gamma \quad (4)$$

Figure 3 magnetisation data for both compounds in terms of equation (4) are plotted on a logarithmic scale. Equation (4) is obeyed almost up to T_c . Least-squares fits to the two straight lines yield values of C and γ as follows: $[\text{NMeH}_3]_2[\text{CrCl}_4]$, $C = 0.00155$, $\gamma = 1.50 \pm 0.10$; $[\text{NEtH}_3]_2[\text{CrCl}_4]$, $C = 0.00086$, $\gamma = 1.64 \pm 0.15$. To a reasonable approximation, therefore, the exponent is $\frac{3}{2}$. Only in a low-dimensional magnet would one expect such a simple power law to apply up to a high fraction of T_c , since the high density of low-lying magnon modes near the centre of the Brillouin zone (*i.e.* with long wavelengths) means that magnon-magnon interaction effects are less important than they would be in a three-dimensional ferromagnet. In the latter, the Bloch $T^{\frac{3}{2}}$ law¹⁶ applies only to *ca.* $0.1-0.2 T_c$.¹⁷ Again, one may note that analogous behaviour is found in

¹⁶ F. Bloch, *Z. Physik*, 1931, **61**, 206.

¹⁷ C. Kittel, 'Introduction to Solid State Physics', 4th edn., Wiley, New York, 1971, p. 635.

the two-dimensional ferromagnets $K_3[CuF_4]$ ¹⁸ and $Rb_3[CrCl_4]$.^{14,19}

Optical Spectra.—Both monoalkylammonium salts grow

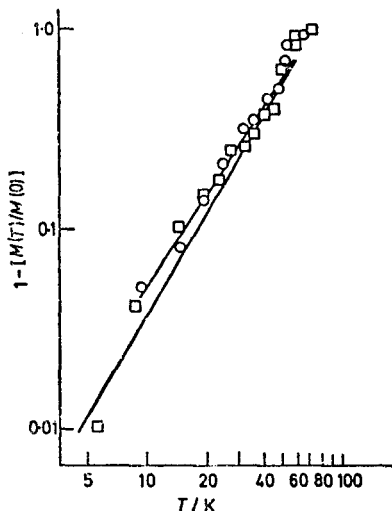


FIGURE 3 Magnetisation of $[NMeH_3]_2[CrCl_4]$ (O) and $[NEtH_3]_2[CrCl_4]$ (□)

as thin flat plates, so optical spectra can only be recorded with the incident light parallel to the *c* axis, *i.e.* perpendicular to the sheets of exchanged-coupled metal ions. Figure 4

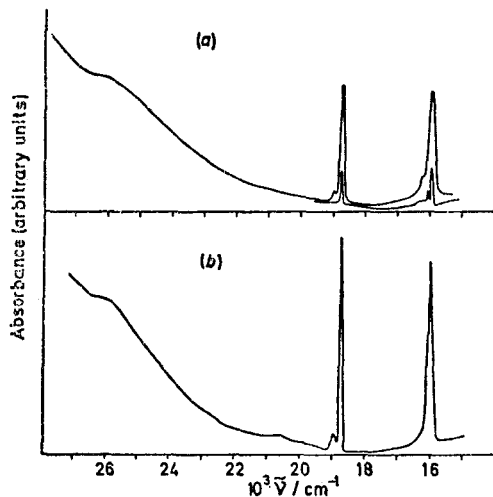


FIGURE 4 Visible absorption spectra of (a) $[NMeH_3]_2[CrCl_4]$ at 130 and 20 K and (b) $[NEtH_3]_2[CrCl_4]$ at 38 K

shows the spectra of the two salts in the visible region. For the methylammonium example we also show spectra measured at two different temperatures. The major

¹⁸ K. Hirakawa and H. Ikeda, *J. Phys. Soc. Japan*, 1973, **35**, 1323.

spectral features are a pair of sharp well resolved bands at 15 800 and 18 760 cm^{-1} , almost at the same frequency as the bands in the alkali-metal analogues.^{4,20} Otherwise the whole visible region is remarkably featureless. Also in common with the alkali-metal tetrachlorochromates(II), the intensities of the two visible bands in the present compounds vary very strongly with temperature. Figure 5

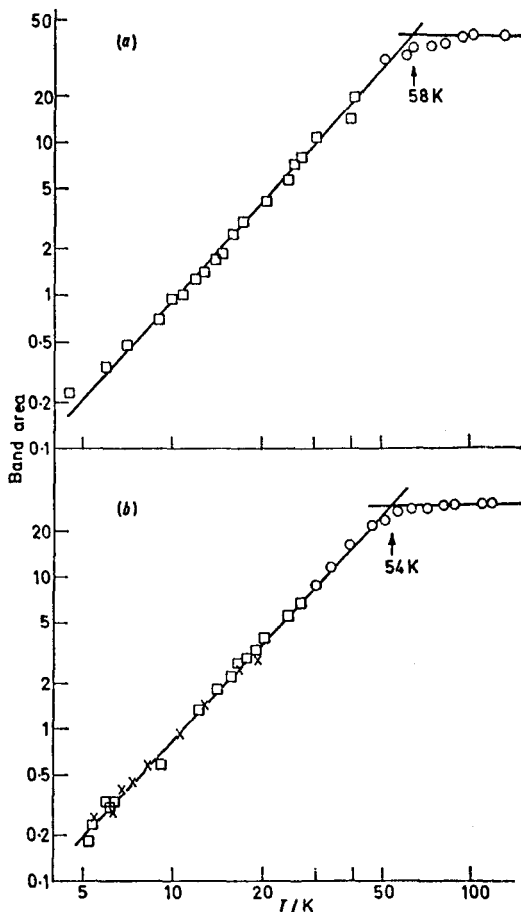


FIGURE 5 Temperature variation of the area of the band at 18 800 cm^{-1} for (a) $[NMeH_3]_2[CrCl_4]$ and (b) $[NEtH_3]_2[CrCl_4]$

demonstrates that for temperatures nearly up to T_c the integrated area of the band at 18 760 cm^{-1} is quite accurately described by a simple power law T^β with $\beta = 2.0 \pm 0.1$. Qualitatively, the consequence of this variation is that at < 10 K the compounds are all but colourless, while at higher temperatures they become olive-green. It can also be seen from Figure 5 that above T_c the intensities of the two visible bands become constant.

¹⁹ M. J. Fair, A. K. Gregson, P. Day, and M. T. Hutchings, *Physica*, 1977, **B30**—88, 657.

²⁰ P. Day, A. K. Gregson, and D. H. Leech, *Phys. Rev. Letters*, 1973, **30**, 19.

DISCUSSION

The space group and unit-cell parameters of the bis-(monoalkylammonium) tetrachlorochromates(II) are very similar to those of their Mn, Fe, Cu, and Cd analogues, whose structures have been determined in detail. Thus one may safely assume that they too contain layers of metal ions bridged by chloride ions, separated from one another by the organic groups, in a manner approximating to the $K_2[NiF_4]$ structure. A potentially complicating feature of the chromium salts is the Jahn-Teller effect, which is assumed to be operative in these

metal analogues, thus demonstrating that the temperature for three-dimensional magnetic ordering is not very sensitive to the distance separating the layers of ferromagnetically coupled ions. On the assumption (the validity of which was discussed above) that the structures of the bis-(monoalkylammonium) tetrachlorochromates(II) are very similar to those of the corresponding cuprates(II), we find the correlation given in Table 2, *i.e.* for a 35% increase in interplanar spacing T_c decreases by *ca.* 14%. Nevertheless, it is interesting to notice that the T_c values of the tetrachlorocuprates(II) are even

TABLE 2
Magnetic and structural parameters of tetrachlorochromates(II)

Compound	Interplanar Cr-Cr (Å)	J/cm^{-1}	$T_c(\text{obs.})/K$	$T_c(\text{calc.})/K$			
				Molecular field	Ref. 26	Ref. 27	Ref. 29
$K_2[CrCl_4]$	9.07	7	60-75	80	33	22	36
$Rb_2[CrCl_4]$	9.41	10.7	63	123	51	34	55
$Cs_2[CrCl_4]$	9.73	6.5	61	75	31	21	33
$[NMeH_3]_2[CrCl_4]$	10.78	9	58	103	43	29	45
$[NEtH_3]_4[CrCl_4]$	11.93	7	55	80	33	22	36

high-spin $3d^4$ ions. Although the detailed structures of the tetrachlorochromates(II) are still under investigation,¹⁰ it seems likely that the co-ordination around the chromium(II) ions will be similar to that found in the corresponding copper(II) salts,²¹ *i.e.* a tetragonally distorted octahedron of chloride ions with its long axis within the plane of the metal ions. Such an arrangement would account for the ferromagnetic sign of the near-neighbour magnetic interaction by superexchange between a half-filled z^2 and an empty $x^2 - y^2$ orbital at right angles to each other.²² A similar explanation has been given for the ferromagnetism of $K_2[CuF_4]$ ²³ and the bis-(monoalkylammonium) tetrachlorocuprates(II). It is also worth noting that in $Rb_2[CrCl_4]$ the same kind of tetragonal distortion has been inferred from the angular variation of the ^{53}Cr n.m.r. frequency within the *ab* plane.²⁴

That the near-neighbour exchange is indeed ferromagnetic is confirmed by the high-temperature series-expansion fits to the susceptibility of both compounds from 80 to 150 K. The exchange constants which give the best fit to the high-temperature susceptibility data are similar in magnitude to those derived in a similar fashion for the alkali-metal tetrachlorochromates(II) (J 7, 8.5, and 6.5 cm^{-1} for K, Rb, and Cs salts respectively).¹⁴ A more accurate value of J for $Rb_2[CrCl_4]$ obtained by fitting the spin-wave dispersion curve determined by inelastic neutron scattering was 10.7 \pm 0.1 cm^{-1} .²⁵

Likewise the Curie temperatures of the two organic-intercalated salts are quite close to those of their alkali-

less sensitive to interplanar separation. Thus on passing from the $[NMeH_3]^+$ to the $[N(C_6H_{11})H_3]^+$ salt the interplanar spacing increases by almost 80% while T_c diminishes from 8.9 to 7.3 K, *i.e.* by 18%.⁵

As mentioned at the outset, there exists² a rigorous proof that two-dimensional lattices with purely Heisenberg or XY -like interactions cannot possess long-range order above absolute zero. On the other hand, Stanley and Kaplan²⁶ found evidence from high-temperature series expansions that, at least for $S > \frac{1}{2}$, some kind of transition might be possible at a temperature $T_c^{(2)}$ to a state in which the susceptibility diverged, but there was no truly long-range order. Further arguments for²⁷ and against²⁸ Stanley and Kaplan's proposal have been given, but what does seem clear²⁹ is that a small Ising-like anisotropy or, of course, a small interplanar interaction³⁰ is sufficient to bring about three-dimensional ordering in a layer compound at a finite temperature. However, in such cases the predicted three-dimensional T_c is very close to $T_c^{(2)}$. Consequently, it is of interest to correlate the values of T_c and J in the tetrachlorochromates(II) according to the various theories available. The relevant equations are as follows:

$$\begin{aligned} \text{Molecular field } T_c &= \frac{1}{2} zJS(S+1) \\ \text{Ref. 26 } T_c^{(2)} &= \frac{1}{10} J(z-1)[2S(S+1) - 1] \\ \text{Ref. 27 } T_c^{(2)} &\sim 0.55JS^2 \\ \text{Ref. 29 } T_c^{(2)} &= 0.595JS(S+1) \end{aligned}$$

Clearly none of the theories gives particularly good agreement between J and T_c , although as expected the mean-field theory prediction is too high (Table 2). Of

¹¹ J. P. Steadman and R. D. Willett, *Inorg. Chim. Acta*, 1970, **4**, 367.

¹² J. B. Goodenough, 'Magnetism and the Chemical Bond,' Interscience, New York, 1966, p. 222.

¹³ D. I. Khomskii and K. I. Kugel, *Solid State Comm.*, 1973, **13**, 763.

¹⁴ K. Le Dang, P. Veillet, and P. J. Walker, *J. Phys. (C)*, 1977, **10**, 4593.

¹⁵ M. T. Hutchings, M. J. Fair, P. Day, and P. J. Walker, *J. Phys. (C)*, 1976, **9**, L55.

¹⁶ H. E. Stanley and T. A. Kaplan, *Phys. Rev. Letters*, 1966, **17**, 913.

¹⁷ J. Villain, *J. Phys. (Paris)*, 1975, **36**, 581.

¹⁸ K. Yamaji and J. Kondo, *J. Phys. Soc. Japan*, 1973, **35**, 25.

¹⁹ M. E. Lines, *Phys. Rev.*, 1971, **B3**, 1749.

²⁰ L. J. de Jongh, *Physica*, 1976, **B52**, 247.

the experimental values of J , that for $\text{Rb}_2[\text{CrCl}_4]$, obtained by fitting the spin-wave spectrum, is much the most precise while the others, obtained from high-temperature series expansions, may be in error by as much as $\pm 1 \text{ cm}^{-1}$. Nevertheless, all the other equations predict $T_c^{(2)}$ distinctly lower than the observed T_c in all cases. It should also be pointed out that the values of T_c listed in Table 2 were measured in an applied field of 0.3 T which, in a weakly coupled layer magnet, might easily be sufficient to change the ordering temperature. Some measure of the initial (zero-field) magnetisation is therefore needed. We contend that the optical spectrum provides such a measure.

In earlier papers^{6,31,32} we have demonstrated that in a wide variety of low-dimensional ionic ferromagnets exciton-magnon combination bands associated with spin-forbidden ligand-field transitions gain their intensity primarily through the annihilation of a thermally created 'spin-down' magnon simultaneous with creation of the exciton. The oscillator strength of such a band at a particular temperature is therefore related directly to the initial magnetisation at that temperature. We also showed³² that by taking into account explicitly the magnon dispersion, and hence the density of magnon states as a function of energy, one could calculate simple analytic expressions for the variation of oscillator strength with temperature. For instance, for a two-dimensional easy-plane ferromagnet with negligible anisotropy one finds that the oscillator strength should be proportional to T^2 , precisely as found for $\text{Rb}_2[\text{CrCl}_4]$ ⁶ and the monoalkylammonium salts described in this

paper. From Figure 5 we see that the T^2 law is obeyed by the band at $18\,650 \text{ cm}^{-1}$ of the monoalkylammonium salts up to ca. $0.9 T_c$, but that from ca. $1.1 T_c$ upwards the oscillator strength of the band becomes constant. A simple linear interpolation therefore gives quite a good estimate of T_c in zero applied field. In fact, from Figure 5, T_c values estimated in this way are 53 ± 1 and $54 \pm 1 \text{ K}$ for the monomethyl- and monoethylammonium salts respectively. These values agree closely with those obtained from the magnetisation measurements, suggesting that the applied field in the latter experiment does not influence the magnitude of T_c noticeably. To our knowledge, the tetrahalogenochromates(II) are the only ferromagnetic substances in which spin-forbidden ligand-field transitions are fully resolved, and in which the 'hot-band' exciton-magnon combination mechanism can be tested. Consequently, they provide a unique opportunity to use a combination of optical and magnetic methods to probe the ordering mechanism in a low-dimensional magnet. Further experiments on these and other members of the same series will be reported in due course.

We thank the Italian Consiglio Nazionale delle Ricerche and the Royal Society for support (to C. B.), the S.R.C. for an equipment grant and a Senior Research Fellowship (to P. D.), and Dr. T. E. Wood for valuable assistance with the optical measurements. The preliminary magnetic measurements were made at the Materials Physics Division, A.E.R.E., Harwell, with the help of Mr. N. Hance.

[8/050 Received, 12th January, 1978]

³¹ D. J. Robbins and P. Day, *J. Phys. (C)*, 1976, **9**, 867.

³² A. K. Gregson, P. Day, A. Okiji, and R. J. Elliott, *J. Phys. (C)*, 1976, **9**, 4497.

Correlation of Magnetic and Optical Properties in the Organic-intercalated Two-dimensional Ionic Ferromagnet Bis(monomethylammonium) Tetrachlorochromate(II)

By CARLO BELLITTO and PETER DAY

(Oxford University, Inorganic Chemistry Laboratory, South Parks Road, Oxford OX1 3QR)

Summary A simple correlation exists between the intensity of a quintet-to-triplet transition in the visible absorption spectrum of $(\text{MeNH}_2)_2\text{CrCl}_4$ (T_C 58 K) and the magnetic order; from 6 to 50 K the oscillator strength of the optical transition is proportional to T^2 and from 70 to 125 K it is nearly constant.

COMPOUNDS with the general formulae $(\text{RNH}_2)_2\text{MX}_4$, where R is an alkyl or aryl group, M a 3d ion, and X a halide ion, have excited interest in the last few years because, although their lattices contain layers of ferromagnetically (M = Cu) or antiferromagnetically (M = Mn, Fe) coupled metal ions, separated by as much as 25 Å from one another by organic material, they nevertheless undergo transitions to three-dimensional magnetic order at finite temperatures.¹ The Cu members of the series have had the added interest of belonging to the very small group of ionic transition metal salts which order as three-dimensional ferromagnets.² We recently showed³ that the previously unknown Cr salts with similar formulae also contain layers of ferromagnetically coupled spins and furthermore, that their Curie temperatures are much higher than those of the Cu salts containing the same R groups (50–80 K compared with 7–10 K). Like their alkali-metal analogues,⁴ the bis(monomethylammonium)tetrachlorochromates have two particularly sharp absorption bands in the visible region, assigned as spin-forbidden ligand field transitions. Indeed, the tetrachlorochromates are unique even among the small number of three-dimensional ionic ferromagnets in showing

such well resolved optical transitions. In this note we report that the temperature dependence of one of these transitions in the first member of the series, $(\text{MeNH}_2)_2\text{CrCl}_4$, correlates with the onset of three-dimensional ferromagnetic order. Thus the optical spectrum measured without an applied magnetic field is an excellent probe of the magnetic order in this important class of organic-intercalated ionic ferromagnets.

Complex $(\text{MeNH}_2)_2\text{CrCl}_4$ was prepared as described previously³ and crystals were grown by slowly cooling an ethanolic solution. Both the crystals themselves and the Cr^{II} solutions are extremely sensitive to air oxidation and all manipulations including crystal mounting were carried out exclusively under nitrogen. The crystals which are orthorhombic at room temperature^{3,5} grow as thin flat plates and the spectra were measured with the light propagating along the *c*-axis.

In the visible region of the spectrum $(\text{MeNH}_2)_2\text{CrCl}_4$ has two prominent absorption bands at 533 and 626 nm with halfwidths at 120 K of only 3 and 7 nm respectively. This compares with 535 and 629 nm for the wavelengths of the corresponding bands in K_2CrCl_4 .⁴ The d^4 Tanabe-Sugano diagram indicates that from 700 to 400 nm in octahedrally co-ordinated metal ions quintet-to-triplet transitions are to be expected and because the wavelengths of the two bands observed vary so little from one Cr^{II} salt to another we attribute them to pure 'spin-flip' transitions. Our earlier assignment⁴ of the K_2CrCl_4 bands [${}^3B_{1g}(D_{4h})$ of ${}^3E_g(O_h)$ (3H) and ${}^3E_{1g}(D_{4h})$ of ${}^3A_{1g}(O_h)$ (a^3F)] would therefore still stand in the monomethylammonium salt.

The most striking feature of the spectrum of $(\text{MeNH}_3)_2\text{-CrCl}_4$ is that below *ca.* 70 K the two visible absorption bands lose their intensity very rapidly. In the Figure we plot the integrated area of the 533 nm band as a function of temperature. From 6 to 50 K the variation is described by a simple power law T^x with $x = 2.1 \pm 0.1$. In the same Figure is plotted the reduced magnetisation $1 - [M(T)/M(0)]$, measured by the Faraday method for a powdered sample at 0.3 T. The latter also obeys a power law up to at least $0.9 T_c$, with an exponent of 1.5 ± 0.1 . From magnetization measurements the Curie temperature of $(\text{MeNH}_3)_2\text{-CrCl}_4$ has been estimated³ as 58 ± 2 K, which is within 2 K of the temperature extrapolated from the high temperature and low temperature behaviour of the intensity of the 533 nm absorption band, as shown in the Figure.

We demonstrated previously that both in the metamagnetic transition metal dihalides and in compounds like K_2CrCl_4 which, though they have layer structures, order as three-dimensional ferromagnets, the temperature dependence of the intensity of spin-forbidden ligand field transition can be thought of as arising solely from coupling between excitons and magnons propagating within the layers. In other words, as far as the limiting optical properties at low temperatures are concerned, those interactions between the layers which determine the nature of the three dimensional ordering are unimportant. For example, using the calculated magnon dispersion relation for a two-dimensional easy-plane ferromagnet we derived a T^2 law for the intensity of the exciton-magnon combination bands in ferromagnetic K_2CrCl_4 ⁶ and metamagnetic NiBr_2 ,⁷ in both cases in excellent agreement with observation at lower temperatures compared to T_c . The result reported in this note is important because, having extended the intensity data on an exciton-magnon band in a layer ferromagnet to temperatures well above T_c one can see, first that the T^2 law appropriate to a two-dimensional easy-plane ferromagnet remains valid almost up to T_c and, second, that it rapidly becomes invalid above T_c , although in an essentially two-dimensional magnetic system one would expect substantial intra-layer correlations to persist above the three-dimensional ordering temperature. It is clear that the uniquely well resolved optical transitions in this new class of organic-intercalated layer ferromagnets will provide the

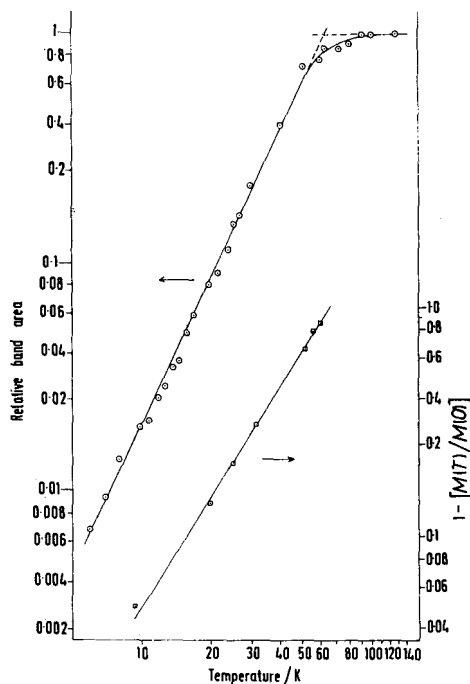


FIGURE. Intensity of the 533 nm absorption band and magnetization of $(\text{MeNH}_3)_2\text{CrCl}_4$ vs. temperature.

basis for a variety of experiments on the onset of the ordering process.

We thank the S.R.C. for an equipment grant and the Italian Consiglio Nazionale delle Ricerche for support to C.B.

(Received, 3rd April 1978; Com. 355.)

¹ For a review, see L. J. de Jongh and R. A. Miedema, *Adv. Phys.*, 1974, **23**, 1.

² L. J. de Jongh and W. D. van Amstel, *J. Phys. (Paris)*, 1971, **32**, Suppl. C-1, 880.

³ C. Bellitto and P. Day, *J.C.S. Chem. Comm.*, 1976, 870.

⁴ P. Day, A. K. Gregson, and D. H. Leech, *Phys. Rev. Letters*, 1973, **30**, 19.

⁵ P. Battle, C. Daul, and P. Day, unpublished results.

⁶ A. K. Gregson, P. Day, A. Okiji, and R. J. Elliott, *J. Phys.*, 1976, **C9**, 4497.

⁷ P. Day, A. Dinsdale, E. R. Krausz, and D. J. Robbins, *J. Phys.*, 1976, **C9**, 2481.

FEATURE ARTICLE

Organic-intercalated Halogenochromates(II): Low-dimensional Magnets

Carlo Bellitto^a and Peter Day^b^a Istituto di Teoria, Struttura Elettronica e Comportamento Spettrochimico dei Composti di Coordinazione del CNR, Area della Ricerca di Roma, Via Salaria km. 29.5, 00016 Monterotondo Staz., Roma, Italy^b The Royal Institution of Great Britain, 21 Albemarle Street, London W1X 4BS, UK

Ferromagnetism in non-metallic solids is quite a rare property. In solids containing molecular building blocks it is even rarer. One strategy for preparing ionic ferromagnets is to combine a low-dimensional continuous lattice containing transition-metal ions with organic molecular ions. In this article we review the synthesis, structures and magnetic and optical properties of halogenochromate(II) salts with substituted ammonium cations. The shape of the latter has a striking influence on the bulk magnetic behaviour of the solids. Monosubstituted cations yield tetrahalogenochromates(II) with layer structures which are ferromagnets with Curie temperatures up to 60 K. On the other hand, tetramethylammonium trihalogenochromates(II) are one-dimensional antiferromagnets. The striking difference in the intensities of the visible absorption spectra of the two classes of materials can be explained by an exchange-induced electric-dipole mechanism.

Keywords: Ferromagnetism; Antiferromagnetism; Chromium; Feature article

A major goal of contemporary synthetic strategy in the chemistry of magnetic compounds is to make molecular-based materials that exhibit spontaneous magnetisation (for a survey, see ref. 1). The boldest efforts in this direction have been in attempts to make molecular-based ferromagnets, but the number of successes has been small and the Curie temperatures disappointingly low. In any case, electrical insulators that order ferromagnetically are quite rare. Among continuous lattice compounds can be cited EuO ($T_c = 69$ K) as a three-dimensional example (NaCl structure) and CrBr₃ ($T_c = 33$ K) as two-dimensional.² Purely molecular examples are confined to [Fe(Cp*)₂][TCNE] ($T_c = 4.8$ K), [Mn(Cp*)₂][TCNE] ($T_c = 8.8$ K)^{3a} and [Mn(Cp*)₂][TCNQ] ($T_c = 6.2$ K)^{3b†} though a recent report presents intriguing evidence for ferromagnetic interactions in a fullerene salt.^{3c} Intermediate between these extremes are compounds whose structures contain both molecular and low-dimensional continuous lattice constituents. The latter are especially interesting because near-neighbour magnetic exchange between metal centres in the non-molecular array may be larger than one could achieve when the exchange interaction involves overlap between orbitals on neighbouring molecules. At the same time, one can take advantage of the chemical flexibility so characteristic of the molecular solid state by using organic (or perhaps even organometallic) cations as spacers between the infinite anionic chains or layers. This article summarizes the preparation, structures and both the magnetic and optical properties of one extensive series of such materials, the halogenochromates (II). An additional feature of particular importance in this series is the manner in which the bulk magnetic behaviour varies with the lattice dimensionality: whereas tetramethylammonium trihalogenochromates(II) are quasi-one-dimensional antiferromagnets, the monoalkylammonium tetrahalogenochromates(II) are bulk ferromagnets exhibiting strong two-dimensional correlations.

Ternary chromium halides of composition A₂CrX₄ (A =

Cs⁺, Rb⁺, K⁺, X = Cl) have been the subject of numerous reports during the past few years because they are among the few examples of ionic insulators which show long-range ferromagnetic order⁴ (e.g. for Rb₂CrCl₄ $T_c = 52.4$ K).⁵ They crystallize in the well known K₂NiF₄ structure⁶ and their magnetic properties show marked two-dimensionality. It has proved possible to replace A in A₂CrX₄ by a variety of organic cations, and a large group of salts having general formula (RNH₃)₂CrX₄ where X = Cl, Br have been prepared.⁶⁻¹² The group R can be *n*-alkyl (C_{*n*}H_{2*n*+1}) or C₆H₅CH₂. They belong to a more general family of salts (C_{*n*}H_{2*n*+1}NH₃)₂MX₄ where M is a divalent metal ion, X = halogen.¹³

This family, which has the so-called layer perovskite structure (see Fig. 1), has played an important part in the study of two-dimensional magnetism and crystallographic phase transitions.¹⁴ The introduction of the organic cation into the lattice creates the opportunity of modulating the distance between the inorganic layers and establishing van der Waals forces in between them, giving rise to features characteristic of a molecular system. Recently, mixed-halide derivatives (RNH₃)₂CrX_{4-x}Y_x, where X = Br and Y = Cl or I, *x* = 0.7 were also isolated.^{12,15,16}

In contrast to the Group I₁ tetrachlorochromates(II), which are prepared from the melt at high temperatures, the organic-intercalated analogues have been synthesised from solution close to room temperature. All the examples made to date have been found to order ferromagnetically at temperatures as high as 60 K. An advantage of introducing molecular chemistry is that one can also control the spatial dimensionality of the exchange interaction by tailoring the shape of the organic cation. In the present case we find that by passing from long-chain monoalkylammonium salts, RNH₃⁺, to the tetrahedral R₄N⁺ it proves possible to obtain compounds containing chains of Cr^{II}. In contrast to the layer compounds they show antiferromagnetic nearest-neighbour exchange interactions between the Cr, and at low temperatures the chloride derivative orders antiferromagnetically in three dimensions ($T_N = 5.8$ K).¹⁷ The following sections of this paper

† Cp* = pentamethylcyclopentadienyl; TCNQ = tetracyanoquinodimethane; TCNE = tetracyanoethylene.

266

J. MATER. CHEM., 1992, VOL. 2

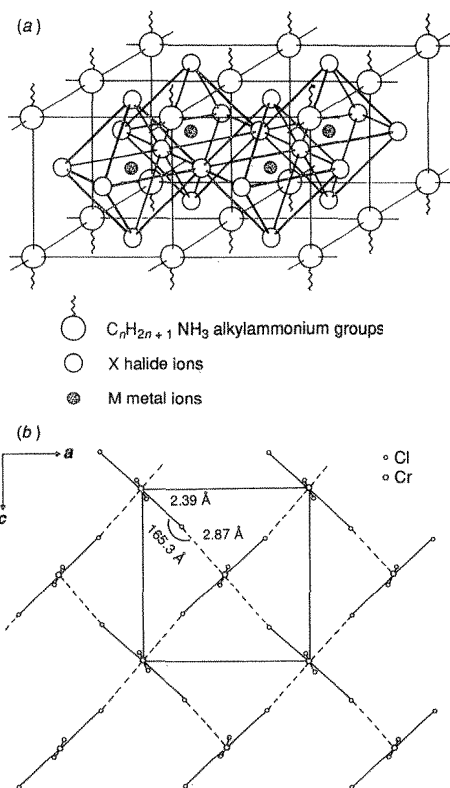
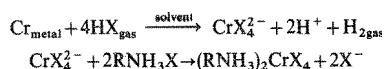


Fig. 1 (a) Schematic representation of a single MX₄ layer of (RNH₃)₂MX₄. (b) The CrCl₄ layer in 1,3-propanediammonium tetrachlorochromate(II)

review properties of all these compounds and discuss the change of the magnetic and optical properties from the one- to the two-dimensional examples.

Syntheses

Two different methods of preparation of the A₂CrX₄ layer compounds have been reported;^{6,7,9} the first starts from solvated tetrachloro- and tetrabromo-chromates(II), which have been isolated from concentrated aqueous solutions of the constituent salts in the corresponding halogen acid. The A₂CrX₄ phases are obtained by thermal dehydration of the bis(hydrates) A₂CrX₄(H₂O)₂ *in vacuo* at 130 °C for several hours,⁷ and therefore only microcrystalline products are obtained. The second preparative route, much more suitable for preparing the organic-intercalated derivatives, involves the two reactions:



where X=Cl, Br, R=alkyl or aryl group, and the solvent is methanol, ethanol or glacial acetic acid. This method also permits preparation of mixed-halide derivatives, just by using the appropriate RNH₃X in different ratios. Large crystals of some of them have been obtained from saturated solutions in sealed tubes¹⁰ by careful control of the temperature (Fig. 2).

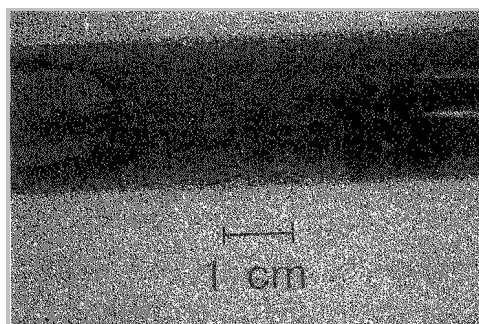


Fig. 2 Crystals of bis(benzylammonium) tetrachlorochromate(II) (after ref. 10)

The longer chain alkyl derivatives become increasingly soluble, e.g. in ethanol. It should be noted that Group 1 tetrabromochromates(II) cannot be prepared from the melt because the ACrBr₃ phase dominates the phase diagram. In contrast, in the case of the alkylammonium compounds, the bromo-derivatives crystallize easily from solution in glacial acetic acid¹¹ in the form of platelets, which vary from pale yellow-green to golden yellow. Twinned crystals are easily isolated. Mixed bromo-iodo derivatives have likewise been prepared as dark-brown polycrystalline powder.^{12,15} All these Cr^{II} compounds are hygroscopic and oxidise easily. Storage under inert atmosphere is essential for maintaining the crystal quality over long periods.

The synthesis of the one-dimensional Cr^{II} compounds is similar to that of the layer phases, though in general the latter are more soluble. Thus, in the case of the first member of the series, [(CH₃)₄N]CrX₃, where X=Cl, Br, crystals suitable for X-ray diffraction were obtained by slow diffusion of a solution of a tetramethylammonium salt in ethanol into a solution of Cr^{II} through a frit.^{17,18} The bromide derivative was synthesized in a similar way except for the solvent which was glacial acetic acid.¹⁹ For both the chain and layer compounds, deuterated products for neutron-scattering purposes are easily prepared.

Crystal Structures

The bis(monoalkylammonium) tetrahalogenochromate(II) complexes belong to a more general class of salts, (RNH₃)₂MX₄, where M is a divalent metal,¹³ known as layered perovskites. MX₄ layers form the basic structural element of this family, consisting of more or less regular halide octahedra, sharing corners in two dimensions. RNH₃⁺ groups are hydrogen bonded to the halide atoms in the cavity formed by four adjacent MX₆ octahedra, so that the fourfold symmetry of the parent K₂NiF₄-type crystal lattice is broken by the threefold symmetry of the RNH₃⁺ group. The inorganic layers are not perfectly planar, the MX₆ octahedra are puckered and the M—X—M bonds are no longer linear. The RNH₃⁺ chains are connected to the network of MX₆ octahedra *via* weak hydrogen bonds [see Fig. 1(a)]. The organic layers are bound together only by van der Waals forces. Table 1 lists structural parameters of (RNH₃)₂CrX₄ salts reported to date. Full single-crystal X-ray structure determinations of trimethylenediammonium tetrachlorochromate(II), [H₃N(CH₂)₃NH₃]CrCl₄ and bis(benzylammonium) tetrabromochromate(II) have been reported.^{20,21} For the remaining members of the series only the unit-cell parameters and space group are known from X-ray powder diffraction. The separation between the MX₄

Table 1 Structural parameters of $(\text{RNH}_3)_2\text{CrX}_4^a$

	$a/\text{\AA}$	$b/\text{\AA}$	$c/\text{\AA}$	space group	ref.
$\text{Rb}_2\text{CrCl}_4^b$	7.184(18)	7.194(18)	15.67(4)	<i>Cmca</i>	29
$(\text{CH}_3\text{NH}_3)_2\text{CrCl}_4$	7.43	7.27	18.89	<i>Cmca</i>	6
$[\text{H}_3\text{N}(\text{CH}_2)_3\text{NH}_3]\text{CrCl}_4^b$	7.517	7.235	18.535	<i>Pnma</i>	20
$(\text{C}_2\text{H}_5\text{NH}_3)_2\text{CrCl}_4$	7.59	7.36	21.41	<i>Cmca</i>	6
$(\text{C}_3\text{H}_7\text{NH}_3)_2\text{CrCl}_4$	7.61	7.36	24.7	<i>Cmca</i>	6
$(\text{C}_6\text{H}_5\text{CH}_2\text{NH}_3)_2\text{CrCl}_4$	7.60	7.44	31.45	<i>Cmca</i>	6
$(\text{C}_6\text{H}_5\text{CH}_2\text{NH}_3)_2\text{CrBr}_{3.3}\text{Cl}_{0.7}$	7.80	7.60	32.20	<i>Pacb</i>	12
$(\text{C}_6\text{H}_5\text{CH}_2\text{NH}_3)_2\text{CrBr}_4^b$	7.909(3)	7.760(1)	32.06(1)	<i>Pacb</i>	21
$(\text{C}_6\text{H}_5\text{CH}_2\text{NH}_3)_2\text{CrBr}_{3.3}\text{I}_{0.7}$	7.90	7.80	32.20	<i>Pacb</i>	16

^a X-Ray powder studies. ^b X-Ray single-crystal studies.

layers is half the c -axis parameter [Fig. 1(b)]. The most significant feature of the crystal structures is the presence of an antiferrodistortive ordering of the Jahn–Teller distorted CrX_6 similar to that found previously in Rb_2CrCl_4 by single-crystal neutron diffraction.²² In both the Rb and the organic-intercalated compounds, the halide ions in the basal plane are displaced away from the centres of the lines joining each pair of Cr atoms, so that the co-ordination around each Cr is tetragonally elongated. The axes of elongation of all the $[\text{CrX}_6]$ units lie in the basal plane but those of neighbouring CrX_6 are at right angles to one another.

At room temperature, tetramethylammonium trichlorochromate(II) (TMCrC) and tetramethylammonium tribromochromate(II) (TMCrB) are isostructural with their well known manganese and nickel analogues,^{23,24} except for the coordinate of the halogen atom X parallel to the CrX_3 chains, as a consequence of statistical distribution of three equivalent halogen atoms among six positions, above and below the mirror plane. Thus the crystal structure¹⁸ of $[(\text{CH}_3)_4\text{N}]\text{CrX}_3$ consists of infinite linear chains of face-sharing octahedra of CrX_6 parallel to the c axis (Fig. 3), separated by tetramethylammonium ions. At room temperature, both the chloride and bromide compounds have a hexagonal structure (space group $P6_3/m$) and two molecules per unit cell, which represents an average structure. The one-dimensional character is reflected in the longer Cr–Cr distance perpendicular to the c axis (9.129 Å for TMCrC) rather than along it.¹⁹ Deviations from the parent hexagonal structure have been observed in the

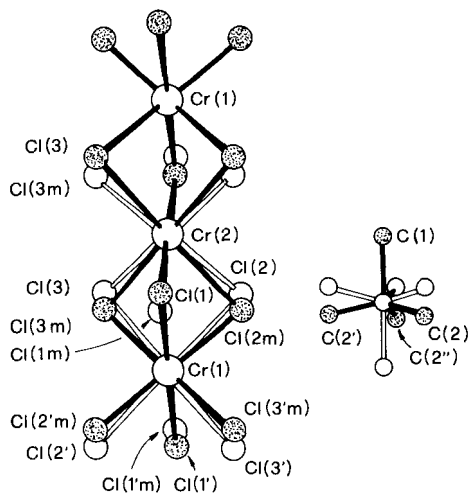


Fig. 3 Crystal structure of $[(\text{CH}_3)_4\text{N}]\text{CrCl}_3$ (after ref. 18)

corresponding alkali-metal derivatives,²³ arising from the fact that Cr^{II} is a Jahn–Teller active ion. In TMCrC there is a crystallographic phase transition to a triclinic space group at 120 K,¹⁷ no doubt analogous to the ones found in TMCu^{25} and RbCrCl_3 .²⁶

Magnetic Properties

Two-dimensional Tetrahalogenochromates(II)

The ferromagnetic behaviour of the $(\text{RNH}_3)_2\text{CrX}_4$ compounds is observed in the susceptibility χ and magnetisation M of powdered samples, measured using both the Faraday and a.c. mutual inductance techniques down to liquid-helium temperature.^{3,6,8,11,27} At temperatures above 100 K the reciprocal magnetic susceptibility follows the Curie–Weiss law with large positive values of the Weiss constant θ , indicating that ferromagnetic near-neighbour interactions dominate. The effective moment $\mu_{\text{eff}} = 2.828\sqrt{C}$, where C is the Curie constant, is considerably larger than the spin-only value, *i.e.* $4.90 \mu_B$, and it increases as the temperature is lowered. The susceptibilities at higher temperatures can be fitted quite accurately to the high-temperature series expansion for an $S=2$, two-dimensional square Heisenberg ferromagnet as modified by Lines:²⁸

$$N_A^2 g^2 \mu_B^2 / \chi = 1/2k_B T + J(-4 + 9x - 9.072x^2 + 55.728x^3 - 160.704x^4 + 116.640x^5) \quad (1)$$

where $x = J/k_B T$, k_B is the Boltzmann constant, N_A is Avogadro's number and g is the Landé factor, to obtain estimates of the nearest-neighbour exchange constants J . A typical fit is shown in Fig. 4 and the values of J are reported in Table 2

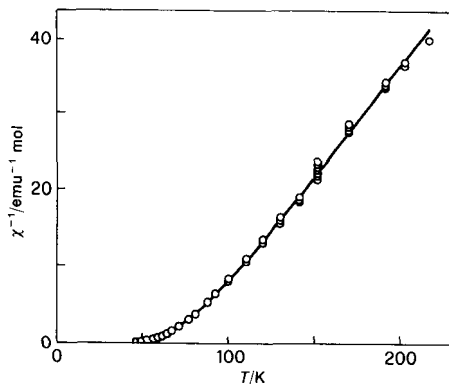


Fig. 4 Fit of susceptibility of bis(benzylammonium) tetrabromochromate(II) to Curie–Weiss law and eqn. (1) (after ref. 11)

268

J. MATER. CHEM., 1992, VOL. 2

together with the other magnetic and structural parameters. Note that the J values are all positive, indicating the presence of a nearest-neighbour ferromagnetic exchange, and the J values found for the chloro derivatives are smaller than those of the bromides, *i.e.* the ferromagnetic coupling strength through the bridging halide increases with chromium-halogen covalency. The other important feature is that the J values are independent of the interlayer separation since the geometry of the CrX_4 layer is essentially unaffected by the nature of the organic side chain.

The temperature dependence of reduced magnetisation, $m = M(T)/M(0)$ of the first compound in the series [Fig. 5(a)] is typical of a ferromagnet, *i.e.* the spontaneous magnetisation drops to zero at the Curie temperature, T_C . These compounds are very soft ferromagnets, as one can see from the very narrow hysteresis loops observed [Fig. 5(b)]. In the example shown, the coercive field (*i.e.* the applied field at which M becomes zero) is only 130 G. In the same material *ca.* 80% of the saturation magnetisation is attained at 6 K (*i.e.* $T/T_C = 0.12$) in an applied field of 5 T. The a.c. (*i.e.* zero-field) susceptibility of a typical member of the series, measured as a function of the temperature in the region of the magnetic phase transition, is shown in Fig. 6. The data in this figure represent the in-phase susceptibility, but the behaviour of the out-of-phase component is quite similar. In principle the a.c. susceptibility should be constant below T_C but Fig. 6 indicates that there is a decrease. This kind of behaviour occurs when the domain walls are no longer able to follow the applied a.c. field.⁴ Furthermore, when an external field is applied, domains tend to grow larger and align with the external magnetic field. The peak in χ_{ac} is then associated with the onset of three-dimensional ferromagnetic order, *i.e.* T_C . It is noteworthy that the values of T_C within a given series are only weakly dependent on the separation between the magnetic planes, but do vary with halogen, in common with J (see Table 2). Finally, a.c. susceptibility measurements on a single crystal of the mixed-halide bis(benzylammonium) tetra(bromo, chloro)chromate(II)¹⁵ reveal a strong anisotropy between the susceptibilities parallel and perpendicular to the c axis of the unit cell. Below T_C , χ_{\parallel} is constant and *ca.* 2 orders of magnitude smaller than that when the applied field is perpendicular to the c -axis. Such behaviour can be explained if the moments lie in the (001) plane, as in the Group 1 tetrachlorochromates(II).²⁹

One-dimensional Trihalogenochromates(II)

The magnetic properties of the one-dimensional ternary trihalogenochromates(II) have likewise been studied by using Faraday and SQUID magnetometry.¹⁷⁻¹⁹ Above 200 K the magnetic susceptibility follows the Curie-Weiss law with parameters that are listed in Table 3. The effective magnetic moment is slightly bigger than the expected spin-only value for a high-spin d^4 configuration. Further evidence that the compounds are paramagnetic in this region comes from magnetisation measurements. The experimental values fit the

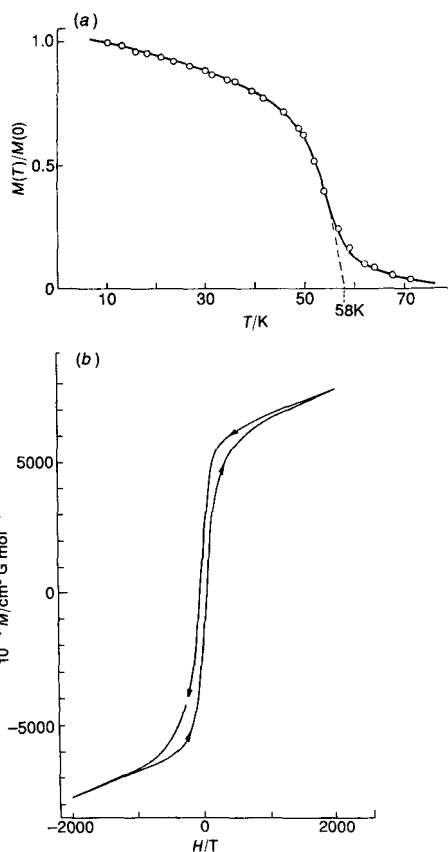


Fig. 5 (a) Reduced magnetisation vs. temperature for bis(monomethylammonium) tetrachlorochromate(II) (after ref. 6). (b) Magnetic hysteresis loop for $(\text{C}_6\text{H}_5\text{CH}_2\text{NH}_3)_2\text{CrBr}_{3.3}\text{I}_{0.7}$ (after ref. 16)

theoretical magnetisation for a paramagnet:

$$M_{\text{at}} = \frac{N_A g^2 \mu_B^2 S(S+1)}{3k_B(T-\theta)} H \quad (2)$$

for $S=2$, $g=1.98$ and $\theta = -158$ K.

At lower temperatures the magnetic susceptibility shows a broad maximum centred at 100 K in the trichloride derivative and 70 K in the tribromide derivative. In principle, such a maximum is expected either for an antiferromagnetic chain or an isolated cluster, but since the crystal structure is that of a hexagonal perovskite, the most appropriate model to calculate the magnetic functions is that of an infinite chain

Table 2 Magnetic parameters and interlayer spacings of $(\text{RNH}_3)_2\text{CrX}_4$, R = alkyl and X = Cl, Br, I

compound	T_C/K	$(J/k_B)/\text{K}$	θ/K	$d/\text{\AA}$	ref.
$(\text{CH}_3\text{NH}_3)_2\text{CrCl}_4$	42	13.0	59	9.44	5
$(\text{C}_2\text{H}_5\text{NH}_3)_2\text{CrCl}_4$	41	10.1	58	10.71	5
$(\text{C}_3\text{H}_7\text{NH}_3)_2\text{CrCl}_4$	39.5	9.3	57	12.35	5
$(\text{C}_6\text{H}_5\text{CH}_2\text{NH}_3)_2\text{CrCl}_4$	37	10.6	58	15.71	5
$(\text{C}_6\text{H}_{11}\text{NH}_3)_2\text{CrCl}_4$	—	9.3	57	17.81	5
$(\text{C}_6\text{H}_5\text{CH}_2\text{NH}_3)_2\text{CrBr}_{3.3}\text{Cl}_{0.7}$	49	12.5	62	16.10	15
$(\text{C}_6\text{H}_5\text{CH}_2\text{NH}_3)_2\text{CrBr}_4$	52	13.1	77	16.03	11
$(\text{C}_6\text{H}_5\text{CH}_2\text{NH}_3)_2\text{CrBr}_{3.3}\text{I}_{0.7}$	51	11.0	69	16.15	16

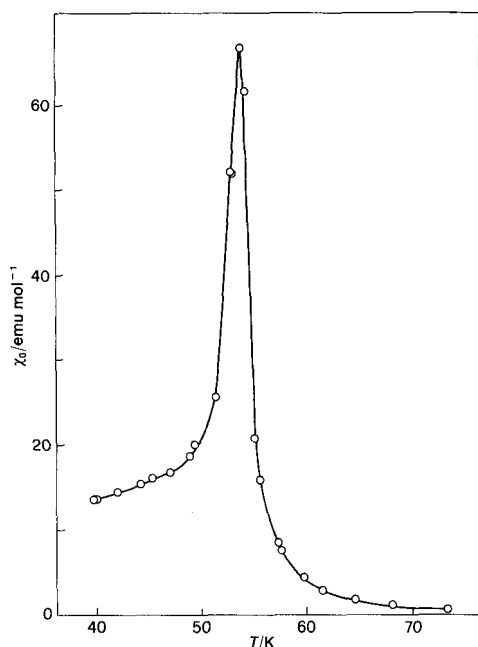


Fig. 6 The a.c. magnetic susceptibility χ_0 of bis(benzylammonium) tetrabromochromate(II) in the region of T_C (after ref. 11)

with an exchange Hamiltonian of isotropic Heisenberg type:

$$H_{ex} = 2J \sum S_i S_j \quad (3)$$

Fisher³⁰ solved this problem for the classical infinite-spin case, while Smith and Friedberg³¹ have shown that the infinite-spin results may be scaled to the leading terms of a high-temperature expansion to yield

$$\chi(T) = \frac{N_A^2 g^2 \mu_B^2 S(S+1)}{3k_B T} \frac{(1+U)}{(1-U)} \quad (4)$$

where $U = \coth K - 1/K$ and $K = 2JS(S+1)/k_B T$.

For $S=2$ the susceptibility exhibits a maximum when $k_B T (\chi_{max})/J$ is 7.1. The best fit to eqn. (4) gives negative J values indicating antiferromagnetic nearest-neighbour exchange coupling (see Table 3).

Magneto-structural Correlations

Chromium(II) in an octahedral ligand field may be high-spin ($t_{2g}^3 e_g^1$ configuration) or low-spin (t_{2g}^4). In the $[R_4N]CrX_3$ and $(RNH_3)_2CrX_4$ series it is high-spin, as found experimentally by magnetic susceptibility measurements. Taking into account the electronic configuration for Cr^{II} , antiferromagnetic interaction in the one-dimensional trihalogenochromates(II) could take place through two possible exchange pathways, a direct t_{2g} overlap between two adjacent Cr^{II} ions, or *via* superex-

change involving e_g - σ - e_g overlap. Strong evidence for the importance of the first of these mechanisms comes from comparing the J values for $CsCrCl_3$ and $TMCrC$ (in which the intrachain Cr—Cr distance increases from 3.11 to 3.26 Å), where we observe a decrease of the antiferromagnetic interactions, due to the decrease of the t_{2g} - t_{2g} direct overlap. Furthermore, if we assume that the tribromide has the same hexagonal perovskite structure as the trichloride, the Cr—Cr distance is even bigger (3.40 Å) and indeed the J value is still less negative. In the case of $[(CH_3)_4N]CrCl_3$, a kink is observed in the temperature variation of the susceptibility at 5.8 K, which is associated with the three-dimensional magnetic ordering temperature, T_N . The presence of this magnetic phase transition has been confirmed by neutron diffraction and solid-state NMR experiments.¹⁷ This value of T_N is distinctly lower than in $CsCrCl_3$,³² a fact that may be related to the greater interchain separation or larger intrachain Cr—Cr distance in the tetramethylammonium derivative compared to the caesium one.³³ No transition has been observed in $[(CH_3)_4N]CrBr_3$ down to 1.8 K because of the presence of a strong Curie tail in the magnetic susceptibility.

The sensitivity of the Cr—X and Cr—Cr distances in the one-dimensional trihalides to the nature of the counter ion contrasts with the relative insensitivity of the corresponding distances in the two-dimensional tetrahalides to the size of the R-group in the RNH_3^+ . Thus, in the layer compounds the J values are likewise nearly independent of R.

In an octahedral (O_h) ligand field the ground term of high-spin Cr^{II} is 5E_g , i.e. it is orbitally degenerate. The Jahn–Teller theorem states that, for a non-linear system, an orbitally degenerate ground state is unstable against at least one distortion which removes such degeneracy in first order. The distortion can be static or dynamic and in the present case the octahedron can distort along the four-fold axis by elongation or compression. In solids such as the present ones, distortion is co-operative and could in principle result in a ferrodistorptive or antiferrodistorptive superstructure. As mentioned above, in A_2CrCl_4 , where A is Rb, trimethylenediammonium and methylammonium ion, an antiferrodistorptive displacement is found in the basal plane so that the adjacent $[CrX_6]$ octahedra are elongated alternately along the [100] and [010] directions of the parent K_2NiF_4 crystal structure.²⁹

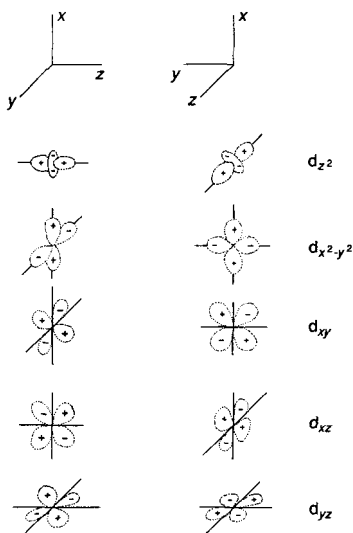
In a ligand field of D_{4h} symmetry, corresponding to a tetragonally elongated octahedron, the e_g subshell is split in such a way that the d_{z^2} orbital is half filled and $d_{x^2-y^2}$ is empty, where z is the local elongation axis (Fig. 7). Since the fourfold axes of adjacent octahedra are orthogonal, the filled halogen p orbital overlaps with a half-filled d_{z^2} orbital on one side and an empty $d_{x^2-y^2}$ on the other. If the first metal ion has a spin up, there will be a net transfer of spin-up density into the empty orbital of the other. The intra-atomic exchange interaction between electrons in different d orbitals on this second atom then lowers the total energy if the electron in the occupied orbital also has a spin up. The net result is therefore a ferromagnetic exchange between neighbouring Cr^{II} ions.^{29,33} In summary, there is a direct correlation between the electronic structure of the 3d ion, the ordered Jahn–Teller distortion observed in the crystal structure and the ferromagnetism of the layered perovskite tetrahalogenochromates(II).

Table 3 Structural and magnetic parameters for $[CrX_3]^-$ chain compounds

compound	M—M/Å	M—B—M/degrees	M—M'/Å	(J/k_B)/K	T_N /K	ref.
$CsCrCl_3$	3.112	76.2	7.256	−24.0	16	32
$[(CH_3)_4N]CrCl_3$	3.256	79	9.129	−15.2	5.8	17
$[(CH_3)_4N]CrBr_3$	3.40	—	9.40	−13.1	—	17

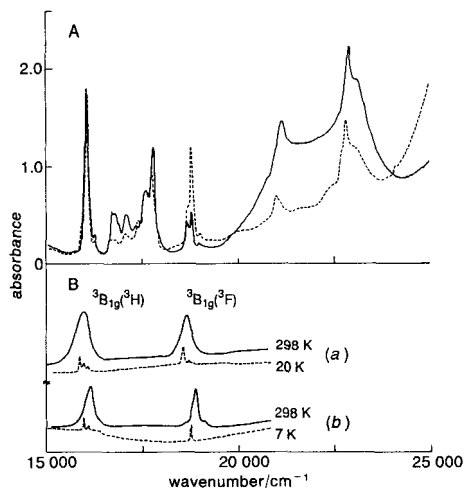
270

J. MATER. CHEM., 1992, VOL. 2

Fig. 7 Orbital ordering in $(RNH_3)_2CRX_4$ (after ref. 33)

Optical Properties

The optical absorption spectra of the two-dimensional tetrahalogenochromates(II) are quite unusual and make a striking contrast to the one-dimensional trihalogenochromates(II). In general the absorption spectra of Cr^{II} compounds in the visible region consist only of spin-forbidden transitions, while the spin-allowed transitions are located in the near infrared and the charge-transfer in the ultraviolet.³⁴ The intensity of the spin-allowed transitions varies with temperature in a fashion typical of vibronically induced transitions. Assuming the crystal field scheme already mentioned, and a D_{4h} notation, the two overlapping bands observed are assigned to the transitions ${}^5B_{1g}(E_g) \rightarrow {}^5B_{2g}(T_{2g})$ and ${}^5E_g(T_{2g})$.²⁷ Their energy difference corresponds to the splitting of the octahedral ${}^5T_{2g}$ state as a result of the local Jahn-Teller distortion. The lowest energy absorption, due to the ${}^5B_{1g}(E_g) \rightarrow {}^5A_{1g}(E_g)$ transition, lies at 7800 cm^{-1} . However, in spite of having similar ligand fields, the visible spectra of the one and two-dimensional Cr^{II} compounds are strikingly different (Fig. 8). Whereas the former show a large number of sharp bands, the latter show only two regions of intense absorption around $16\,000\text{ cm}^{-1}$ and $18\,800\text{ cm}^{-1}$ in the chloride and *ca.* $16\,000\text{ cm}^{-1}$ and $18\,600\text{ cm}^{-1}$ in the bromide. Both sets of bands show typical

Fig. 8 Visible absorption spectra of (a) $(CH_3)_4NCrCl_3$ and (b) $(C_2H_5NH_3)_2CrCl_4$ (after ref. 33)

'hot-band' behaviour,³⁴ with the intensity increasing proportional to T^2 at low temperatures.

In such magnetically ordered materials as the halogenochromates, spin-forbidden transitions can acquire intensity through an exchange mechanism. Tanabe and Ebara worked out the consequences of such a mechanism for exchange-coupled chains and derived expressions for the temperature dependence of the spin-forbidden bands.^{35,36} The starting point is the local cluster consisting of a pair of cations with their surrounding ligand fields. The selection rules for spin-forbidden transitions in these clusters are derived from the procedure of ref. 35. Finally, the cluster selection rules are transformed into crystal selection rules, which are then directly comparable with experiment. Table 4 gives a summary of the crystal selection rules. From these results we would expect more bands than are observed. Thus, in the layer compounds some of the orbital pathways for gaining intensity are blocked by the lack of overlap between d orbitals on nearest neighbours. Fig. 8 shows the relative disposition of tetragonal d orbitals on neighbouring Cr^{II} ions in A_2CrX_4 . As mentioned above, it is the dominant overlap between the d_{z^2} orbital of the given Cr^{II} ion and the unoccupied $d_{x^2-y^2}$ on its neighbour that is mainly responsible for the ferromagnetic coupling within the layers in this type of structure. All the overlaps between singly occupied orbitals on adjacent Cr are either

Table 4 Selection rules for exchange-induced spin-forbidden transitions^a

		$\gamma\text{-CsCrCl}_3$			
excited state	$E_{\parallel\text{chain}}$	$E_{\perp\text{chain}}$	excited state	$E_{\parallel\text{chain}}$	$E_{\perp\text{chain}}$
${}^3A_{1g}$	—	+	${}^3B_{2g}$	—	+
${}^3A_{2g}$	+	+	${}^3E_{g(xz)}$	—	+
${}^3B_{1g}$	+	+	${}^3E_{g(yz)}$	+	+
		A_2CrX_4			
excited state	$E_{\perp\text{layer}}$	$E_{\text{within layer}}$	excited state	$E_{\perp\text{layer}}$	$E_{\text{within layer}}$
${}^3A_{1g}$	—	+	${}^3B_{2g}$	+	—
${}^3A_{2g}$	+	—	${}^3E_{g(xz)}$	+	—
${}^3B_{1g}$	—	+	${}^3E_{g(yz)}$	—	+

^a All notations are in D_{4h} . The ground state is ${}^5B_{1g}$.

zero by symmetry or small. The two non-vanishing overlaps involving $p(\pi)$ on the halogen ion ($d_{yz}-d_{xz}$ and $d_{xy}-d_{xy}$) should be much smaller than the $d_{xz}-d_{xz-yz}$ overlap. They contribute to the kinetic exchange but too little to override the ferromagnetic contribution.

The strong-field wavefunction for the ground state of Cr^{II} in a tetragonal field is given by:

$${}^5\text{B}_{1g}(M_s=2)=|z^2xyxz| \quad (5)$$

Flipping the spin of the electron in one of the half-occupied orbitals, thus creating a triplet state, corresponds to an electronic excitation, the intensity of which is strongly enhanced by the exchange mechanism. The configuration z^2xyxz contributes to the following triplet function:

$$\bar{z}^2xy({}^3\text{B}_{2g})xz yz({}^3\text{A}_{2g}) \quad {}^3\text{B}_{1g}(M_s=1) \quad (6)$$

$$\bar{z}^2xy({}^1\text{B}_{2g})xz yz({}^3\text{A}_{2g}) \quad {}^3\text{B}_{1g}(M_s=1) \quad (7)$$

The excited states, whose functions have dominant contributions from (6) and (7) are ${}^3\text{B}_{1g}({}^3\text{H})$ and ${}^3\text{B}_{1g}({}^3\text{F})$. We have therefore assigned the two absorption bands to the ${}^3\text{B}_{1g}({}^3\text{H})$ and ${}^3\text{B}_{1g}({}^3\text{F})$ excitations. In conclusion, the absence of any other bands in the visible region in these ferromagnets is accounted for by the above arguments.³³

Conclusions

Compared with the alkali-metal tri- and tetra-halogenochromates(II), the corresponding derivatives containing mono- or tetra-alkylammonium cations present some interesting contrasts. Amongst the small group of known ferromagnets containing molecular components the $(\text{RNH}_3)_2\text{CrX}_4$ series have by far the highest T_c s presently known. Of course the use of organic cations as 'spacers' between the infinite anionic inorganic layers permits a much greater variation of interlayer distance than with alkali-metal cations. In addition, it could permit a larger range of functionalised side chains, though apart from phenyl groups this aspect has not been explored to date. The mild preparative route to the organic-intercalated salts also renders it easier to make bromo- and iodo-substituted examples, and hence map the variation of T_c with halogen. Operation of the selection rules for exchange-induced intensity of the visible absorption spectrum in the spin-forbidden ligand field transitions is demonstrated beautifully by the temperature dependence in the ferromagnets and also by the contrast with the spectra of the one-dimensional antiferromagnet.

Thanks are due to our many collaborators named in the references and to the UK Science and Engineering Research Council and Italian Consiglio Nazionale delle Ricerche for support.

References

- 1 *Mol. Cryst. Liq. Cryst.*, 1989, **176**.
- 2 P. Day, *Acc. Chem. Res.*, 1979, **12**, 236.
- 3 (a) J. S. Miller, A. J. Epstein and W. M. Reiff, *Acc. Chem. Res.*, 1988, **21**, 114; (b) W. E. Broderick, J. A. Thompson, E. P. Day and B. M. Hoffman, *Science*, 1990, **249**, 401. (c) P. M. Allemand, K. C. Khemani, A. Koch, F. Wudl, K. Holczer, S. Donovan, G. Graher and J. D. Thompson, *Science*, 1991, **253**, 301.
- 4 R. L. Carlin, *Magnetochemistry*, Springer-Verlag, Berlin, 1986, p. 143.
- 5 P. Day, *J. Magn. Magn. Mater.*, 1986, **54-56**, 1442.
- 6 C. Bellitto and P. Day, *J. Chem. Soc., Chem. Commun.*, 1976, 870; C. Bellitto and P. Day, *J. Chem. Soc., Dalton Trans.*, 1978, 1207.
- 7 L. F. Larkworthy and A. Yavari, *J. Chem. Soc., Dalton Trans.*, 1978, 1236.
- 8 M. A. Babar, L. F. Larkworthy and A. Yavari, *J. Chem. Soc., Dalton Trans.*, 1981, 27.
- 9 C. Bellitto, *Inorg. Synth.*, 1986, **24**, 188.
- 10 C. Bellitto and P. Day, *J. Cryst. Growth*, 1982, **38**, 641.
- 11 C. Bellitto, P. Filaci and S. Patrizio, *Inorg. Chem.*, 1987, **26**, 191.
- 12 D. M. Halepoto and L. F. Larkworthy, *Trans. Met. Chem.*, 1988, **13**, 104.
- 13 H. Arend, W. Huber, F. H. M. Mischgofsky and G. H. Richter van Loeven, *J. Cryst. Growth*, 1978, **32**, 213.
- 14 L. J. de Jongh and A. R. Miedema, *Adv. Phys.*, 1974, **24**, 1.
- 15 C. Bellitto, *Mol. Cryst. Liq. Cryst.*, 1989, **176**, 465.
- 16 G. Staulo and C. Bellitto, *J. Mater. Chem.*, 1991, **1**, 915.
- 17 C. Bellitto, L. Regnault and J. P. Renard, *J. Magn. Magn. Mater.*, in the press.
- 18 C. Bellitto, G. Dessy, V. Fares, D. Fiorani and S. Viticoli, *J. Phys. Chem. Solids*, 1984, **45**, 1129.
- 19 C. Bellitto, D. Fiorani and S. Viticoli, *Inorg. Chem.*, 1985, **24**, 1939.
- 20 M. A. Babar, M. F. C. Ladd, L. F. Larkworthy, D. C. Povey, K. J. Proctor and L. J. Summers, *J. Chem. Soc., Chem. Commun.*, 1981, 1046.
- 21 D. O. Halepoto, L. F. Larkworthy, D. C. Povey and V. Ramdas, *Inorg. Chim. Acta*, 1989, **162**, 71.
- 22 M. T. Hutchings, J. Als-Nielsen, P. A. Lindgaard and P. J. Walker, *J. Phys. C., Solid State Phys.*, 1978, **32**, 213.
- 23 B. Morosin and E. J. Graeber, *Acta Crystallogr.*, 1967, **23**, 766.
- 24 G. D. Stucky, *Acta Crystallogr., Sect. B*, 1968, **24**, 330.
- 25 W. G. Haije and W. J. A. Maaskant, *J. Phys. C.: Solid State Phys.*, 1988, **21**, 5337.
- 26 W. J. Crama and W. J. A. Maaskant, *Physica B*, 1983, **121**, 219.
- 27 C. Bellitto, P. Day and T. E. Wood, *J. Chem. Soc., Dalton Trans.*, 1986, 847.
- 28 M. E. Lines, *J. Phys. Chem. Solids*, 1970, **31**, 101.
- 29 P. Day, M. Hutchings, E. Janke and P. J. Walker, *J. Chem. Soc., Chem. Commun.*, 1979, 711.
- 30 M. E. Fisher, *Am. J. Phys.*, 1964, **32**, 343.
- 31 T. Smith and S. A. Friedberg, *Phys. Rev.*, 1968, **176**, 660.
- 32 P. Day, A. K. Gregson, D. H. Leech, M. T. Hutchings and B. D. Rainford, *J. Magn. Magn. Mater.*, 1979, **14**, 166.
- 33 C. Bellitto, H. Brunner and H. U. Güdel, *Inorg. Chem.*, 1987, **26**, 2750.
- 34 E. Janke, T. E. Wood, C. Ironside and P. Day, *J. Phys. C.*, 1982, **15**, 3809.
- 35 Y. Tanabe and K. Ebara, *J. Phys. Soc. Jpn.*, 1971, **30**, 886.
- 36 K. Ebara and Y. Tanabe, *J. Phys. Soc. Jpn.*, 1974, **36**, 93.

Temperature variation of exciton–magnon absorption bands in metamagnetic transition-metal dihalides

D J Robbins† and P Day

Oxford University, Inorganic Chemistry Laboratory, South Parks Road, Oxford OX1 3QR, UK

Received 31 October 1975

Abstract. This paper reports an experimental and theoretical study of the temperature dependence of the oscillator strengths of exciton–magnon absorption bands in the optical spectra of FeCl_2 , CoBr_2 and NiBr_2 , representative examples of the class of metamagnetic transition-metal layer compounds in which strong intralayer ferromagnetic exchange interactions are combined with much weaker antiferromagnetic exchange between layers. FeCl_2 and CoBr_2 have large anisotropy, the former being an easy-axis system, the latter easy-plane, while in NiBr_2 the anisotropy is small and of easy-plane type. In all three compounds at low temperatures the form of the temperature dependence of the exciton–magnon absorption bands, associated with spin-forbidden ligand-field transitions, is dominated by coupling of the electronic excited states with magnons propagating within the ferromagnetic planes. In FeCl_2 the intensity of the exciton–magnon band at 4270 Å varies as $T^2 \exp(-A/kT)$ over the temperature range 4.0–7.2 K, extending the range previously examined by Schnatterly and Fontana. We have also improved their resolution and found a band which we assign as the pure exciton. In CoBr_2 , bands at 4940 Å have intensities varying approximately as T^3 , in agreement with theory, while in NiBr_2 the band at 6070 Å varies as T^2 . The effect of zero-point spin fluctuations on the limiting form of the exciton–magnon combinations at low temperature is also discussed.

1. Introduction

Much has been written about the optical properties of ionic compounds of the 3d elements in which the exchange interactions are predominantly antiferromagnetic, but comparatively little about compounds in which the dominant interactions are ferromagnetic, though in many respects the behaviour of the latter is expected to be quite different. The most striking difference is that, in a three-dimensional ferromagnetic lattice, excitons associated with ligand-field transitions which take place with a decrease of the overall spin projection of the crystal (e.g. quintet-to-triplet) can only gain electric-dipole intensity by simultaneously annihilating thermally excited magnons that are also associated with a decrease in the total spin projection of the crystal. Thus, in place of the combination of 'hot' and 'cold' mechanisms envisaged by Shinagawa and Tanabe (1971) for the antiferromagnetic case, in a ferromagnet only 'hot' exciton–magnon combinations are allowed. Such combination bands should therefore lose their intensity completely at low temperature. Recently, we were able to verify this prediction by examining the visible spectrum of the ionic ferromagnet K_2CrCl_4 (Day *et al* 1973). In this compound,

† Present address: Royal Radar Establishment, St Andrews Road, Great Malvern, Worcs, WR14 3PS, UK.

which approximates to the K_2NiF_4 structure, one has reasonably well separated layers of ions, and the coupling both within and between the layers is ferromagnetic (Hutchings *et al* 1974, Gregson *et al* 1975).

Three-dimensional ferromagnetism in ionic transition-metal compounds is extremely rare, and in our search for further examples of optically transparent salts in which ferromagnetic interactions were dominant we were led to consider the series of transition-metal dihalides. These compounds, dubbed 'metamagnetic' by Landau (1933) because they are antiferromagnets which can be ferromagnetically saturated by relatively weak external magnetic fields, have either $CdCl_2$ or CdI_2 structures in which the intralayer exchange coupling is strong and ferromagnetic while that between layers is weak and antiferromagnetic. In addition to their interest in having near-neighbour ferromagnetic coupling, this series of compounds thus poses the question of whether the temperature dependence of the exciton-magnon absorption should be determined by the two-dimensional ferromagnetic interactions of the layers or by the overall three-dimensional antiferromagnetism of the entire crystal lattice. Within the series too, one can find examples of both easy-axis ($FeCl_2$) and easy-plane systems ($CoCl_2$, $CoBr_2$, $NiCl_2$, $NiBr_2$) and examples with large ($FeCl_2$, $CoCl_2$, $CoBr_2$) and small ($NiCl_2$, $NiBr_2$) single-ion anisotropies. The magnetic properties have been studied in great detail, both by susceptibility methods (e.g. Bizette *et al* 1956) and elastic (Wilkinson *et al* 1959) and inelastic (Birgeneau *et al* 1972, Hutchings 1973, Lindgard *et al* 1975) neutron scattering. Previous optical work on $FeCl_2$ has centred mainly on the effect of externally applied magnetic fields (Robbins and Day 1973, Griffin *et al* 1974), leading to the establishment of the phase diagram in the $H-T$ plane, though Schnatterly and Fontana (1972) report the temperature variation of the 4270 Å band from 6.7 to 17 K, i.e. 0.3 to 0.7 T_N . Since the theory described below takes its simplest form at lower temperatures, we report here our own measurements on $FeCl_2$ from 0.1 to 0.4 T_N , and at somewhat higher resolution. For $CoCl_2$ and $CoBr_2$, low-resolution survey scans of the axial spectra at 20 K were given by Ferguson *et al* (1963) and for $NiCl_2$ and $NiBr_2$ by Kozielski *et al* (1974) and Ackerman *et al* (1974). In this paper we report the temperature variation of the intensity of exciton-magnon lines at 4940 Å and 5680 Å in $CoBr_2$ from 3.7 to 18 K, and of the line at 6070 Å in $NiBr_2$ from 3.7 to 21 K. In all cases we find intensities which increase sharply with increasing temperature, indicating that it is the 'hot' exciton-magnon combination mechanism which dominates and that the excitons thus couple preferentially to magnons propagating within the ferromagnetic layers. Starting from that assumption, we derive expressions for the oscillator strengths of the exciton-magnon lines as a function of temperature for both the easy-axis and easy-plane cases in the low-temperature limit (i.e. only magnons near the zone-centre populated). Agreement with experiment is satisfactory.

2. Experimental

Crystals of $FeCl_2$, $CoBr_2$ and $NiBr_2$ were grown from the melt in silica ampoules by the Bridgman method. Because of the two-dimensional nature of the crystal structure, they all readily cleave perpendicular to the hexagonal c axis. Thus, for the present purpose, only axial spectra were recorded. Spectra were measured using a McPherson RS10 double-beam spectrophotometer equipped with an Oxford Instruments CF 100 continuous-flow helium cryostat and temperature controller utilizing a CLTS temperature sensor, which was calibrated by immersion in liquid helium. The base temperature of the

cryostat was 2.9 K, and up to about 20 K the temperature control was stable to about ± 0.1 K. The slit of the monochromator, which has a reciprocal dispersion of 8.33 \AA mm^{-1} , was set either to 5 or 10 μm , and under these conditions all the bands examined were fully resolved. The areas of the bands were measured using a Dupont Curve Analyser.

3. Spin-wave dispersion in layer metamagnets

The temperature dependence of the exciton-magnon combination bands derives from the variation in the populations of the magnon states. We must therefore begin by considering the forms of the magnon dispersion in these two-dimensional systems.

From the neutron diffraction work cited above, we know that in the compounds which concern us the intra-plane exchange is ferromagnetic and strong while the inter-plane exchange is antiferromagnetic and much weaker. As an example of an easy-axis system we take FeCl_2 , and of an easy-plane system, CoBr_2 . The cubic single-ion ground states of the metal ions in these two compounds are respectively ${}^5T_{2g}$ and ${}^4T_{1g}$ which, under the action of spin-orbit coupling in first order, give $T_{2g}(J = 1)$ and $E'_g(J = \frac{1}{2})$. Further, the T_{2g} spinor ground state of Fe^{2+} is split by the trigonal field component in the CdCl_2 structure, though of course the Kramers degeneracy of the E'_g ground state of Co^{2+} cannot be so lifted. In the effective spin-Hamiltonian formalism, we may therefore write the exchange Hamiltonians of the two ions as:

$$\text{Fe}^{2+}: \quad \mathcal{H}'_{\text{ex}} = \sum_{\text{NN}} (-J_1 \mathbf{S}_i \cdot \mathbf{S}_j - D_1 S_{iz} S_{jz}) + \sum_{\text{NNN}} (J_2 \mathbf{S}_i \cdot \mathbf{S}_j + D_2 S_{iz} S_{jz}) - \sum_i \Delta [(S_{iz})^2 - \frac{1}{3} S(S+1)] \quad (1)$$

$$\text{Co}^{2+}: \quad \mathcal{H}'_{\text{ex}} = \sum_{\text{NN}} (-J_1 \mathbf{S}'_i \cdot \mathbf{S}'_j + D'_1 S'_{ix} S'_{jx}) + \sum_{\text{NNN}} (J_2 \mathbf{S}'_i \cdot \mathbf{S}'_j - D'_2 S'_{ix} S'_{jx}) \quad (2)$$

where, in the former, the effective spin of the ground state is $S = 1$ and in the latter $S' = \frac{1}{2}$. In (1) and (2) the subscripts 1 and 2 indicate intra- and inter-plane exchange, respectively. $J(J')$ and $D(D')$ are isotropic and anisotropic exchange parameters, and Δ is the trigonal field anisotropy parameter. The z axis is the axis of preferred spin orientation, and only nearest-neighbour intra- (NN) and inter-plane (NNN) interactions are included. Hamiltonians of this form have been used for FeCl_2 by Birgeneau *et al* (1972) and for CoCl_2 by Lines (1963) and Hutchings (1973). Lines also showed that the magnetic properties of NiCl_2 could be treated by a Hamiltonian of the form of equation (2), but with $D_1 = D_2 = 0$. The latter approximation arises because the ${}^3A_{2g}$ ground state of Ni^{2+} is split only in second-order by the trigonal field and spin-orbit interaction. In fact, the experimentally determined anisotropy is very small (Katsumata and Yamasaka (1973) estimate $D_1 = D_2 = 0.40$ K for NiCl_2) and on this basis we assume that an isotropic Hamiltonian can be used as a first approximation for the Ni^{2+} case.

The next stage of the treatment is to transform the Hamiltonians (1) and (2) to spin-wave variables. We shall consider the two cases separately.

The Hamiltonian (1), applicable to FeCl_2 , is that of a simple two-sublattice antiferromagnet with the anisotropy field directed along the preferred spin axis. The form of the transformed Hamiltonian therefore follows that given by Keffer (1966), from which the spin-wave energies are derived as:

$$E_{\text{sw}} = \bar{S} \left[\left(A + z_1 J_1 + z_2 J_2 - \sum_{\text{NN}} J_1 \exp [ik \cdot \delta(1)] \right)^2 - \left(\sum_{\text{NNN}} J_2 \exp [ik \cdot \delta(2)] \right)^2 \right]^{1/2} \quad (3)$$

870 *D J Robbins and P Day*

where A includes all anisotropy terms, z is the number of neighbours in the summation, δ is a vector connecting the original ion with the neighbours included in the summation and \bar{S} is the mean effective spin. Since $J_1 > J_2$ we have

$$E_{\text{sw}} \sim \bar{S} \left(A + z_1 J_1 + z_2 J_2 - \sum_{\text{NN}} J_1 \exp [ik \cdot \delta(1)] \right). \quad (4)$$

Now, for a centrosymmetric system, we define

$$z_1 \gamma_{k1} = \sum_{\text{NN}} \exp [ik \cdot \delta(1)] = \sum_{\text{NN}} \cos [k \cdot \delta(1)], \quad (5)$$

so that

$$E_{\text{sw}} \sim \bar{S} (A + z_1 J_1 + z_2 J_2 - J_1 z_1 \gamma_{k1}). \quad (6)$$

This is just the dispersion relation for a simple two-dimensional ferromagnet with strong axial anisotropy, as would be expected when the dominant interactions are ferromagnetic and in-plane. The spin-waves on each sublattice are doubly degenerate, and at the same time the spin-wave modes on the two sublattices of the antiferromagnet are degenerate in the absence of an external field.

In Hamiltonian (2) the anisotropy field directed along the x axis makes the solution more difficult, but this case has previously been treated by Lines (1963) and Hutchings (1973). In this case the degeneracy of the spin-waves on each sublattice is lifted by the anisotropy field, and Lines (1963) gives the energies of the modes as

$$E_{\text{sw}}^{(1)} = \bar{S} [(\mu + \lambda)(\mu - \lambda + \rho_1 + \rho_2)]^{1/2}. \quad (7a)$$

$$E_{\text{sw}}^{(2)} = \bar{S} [(\mu - \lambda)(\mu + \lambda + \rho_1 - \rho_2)]^{1/2} \quad (7b)$$

where

$$\mu = z_1 J_1 + z_2 J_2 - \sum_{\text{NN}} J_1 \exp [ik \cdot \delta(1)] = z_2 J_2 + z_1 J_1 (1 - \gamma_{k1}) \quad (8a)$$

$$\lambda = \sum_{\text{NNN}} J_2 \exp [ik \cdot \delta(2)] = z_2 J_2 \gamma_{k2} \quad (8b)$$

$$\rho_1 = \sum_{\text{NN}} D'_1 \exp [ik \cdot \delta(1)] = z_1 D'_1 \gamma_{k1} \quad (8c)$$

$$\rho_2 = \sum_{\text{NNN}} D'_2 \exp [ik \cdot \delta(2)] = z_2 D'_2 \gamma_{k2}. \quad (8d)$$

Note that neglecting the anisotropy terms ρ_1 and ρ_2 , as we shall do when we consider the Ni^{2+} case, has the effect of making the modes degenerate again. We are then back to the case of the isotropic antiferromagnet, i.e. to the expression we shall use for FeCl_2 , though now with very small anisotropy energy. In the same way as in equation (5), the summations of equations (8) can also be simplified when the space group of the crystal is centrosymmetric.

As the experiments described in this paper were performed at temperatures below $0.5T_N$, at which only the lower-energy magnon states are likely to be populated, i.e. those near the zone centre, we put

$$\cos (\mathbf{k} \cdot \delta) \sim 1 - \alpha k^2 \quad (9)$$

where α is a constant of order of magnitude 1 whose precise value depends on the crystal structure. Then, for FeCl_2 , the spin-wave dispersion equation (6) becomes

$$E_{\text{sw}} \sim A'(1 + \alpha'k^2). \quad (10)$$

Temperature variation of exciton-magnon absorption bands

871

There is an energy gap at $k = 0$ whose magnitude depends on the anisotropy parameter A' . For CoBr_2 , the two spin-wave dispersions of equation (7) take rather different forms. The first, $E_{\text{sw}}^{(1)}$ is as follows:

$$E_{\text{sw}}^{(1)} \sim \bar{S}' \{ [2J_2 z_2 + (J_1 z_1 \alpha - J_2 z_2 \beta) k^2] [D_1' z_1 + D_2' z_2 + z_1 \alpha (J_1 - D_1') k^2 + z_2 \beta (J_2 - D_2') k^2] \}^{1/2}. \tag{11a}$$

In the cobalt halides, $J_1' > D_1' > J_2' > D_2'$, so that

$$E_{\text{sw}}^{(1)} \sim (B_1 + \gamma k^2)^{1/2} \sim B_1' (1 + \gamma' k^2) \tag{11b}$$

where we have neglected terms of higher order in k and made use of the binomial expansion. In equation (11b), B_1' is of course determined by D_1' and J_2' . We see that equation (11b) has the same form as equation (10) for FeCl_2 . As k tends to zero, the energy of $E_{\text{sw}}^{(1)}$ tends to a finite limit governed by the anisotropy field, and the dependence of the energy on k is quadratic, a result typical of ferromagnetic systems. Further, as J_2' tends to zero, $E_{\text{sw}}^{(1)}$ itself varies as k^2 .

The second spin-wave mode, $E_{\text{sw}}^{(2)}$, at small k becomes

$$E_{\text{sw}}^{(2)} \sim \bar{S}' \{ [(J_1 z_1 \alpha + J_2 z_2 \beta) k^2] [2J_2 z_2 + D_1' z_1 - D_2' z_2 + z_1 \alpha (J_1 - D_1') k^2 - z_2 \beta (J_2 - D_2') k^2] \}^{1/2} \sim (B_2 k^2 + \dots)^{1/2} \sim B_2' k, \tag{12}$$

again neglecting terms of higher order in k . Here B_2' is determined largely by the anisotropy D_1' and also, to a lesser extent, by J_1' . From equation (12) we see that, as k tends to zero, the energy of this second mode also tends to zero, and further, that its energy is linear in k , a characteristic usually associated with antiferromagnetic ordering. This type of behaviour for the easy-plane ferromagnet has been discussed by Semura and Huber (1973). Finally, as J_2' tends to zero, $E_{\text{sw}}^{(2)}$ is still linear in k .

Although no experimental work has been reported on the spin-wave dispersion of CoBr_2 , the easy-plane system whose optical behaviour concerns us in this paper, the inelastic neutron scattering results of Hutchings (1973) on CoCl_2 clearly show the two modes with the behaviour predicted by equations (11) and (12). If the inter-plane coupling were vanishingly small compared with that within the planes, the energies of $E_{\text{sw}}^{(1)}$ and $E_{\text{sw}}^{(2)}$ become degenerate and assume the form typical of a two-dimensional easy-plane ferromagnet with no energy gap and a linear dependence of energy on k . Clearly, however, in practice some small inter-plane interaction or anisotropy field is needed to maintain the long-range order of the system.

Turning to the nickel dihalides, in view of their orbital singlet ground states, the appropriate Hamiltonian is now that of an isotropic antiferromagnet, i.e. either equation (1) with $D_1 = D_2 = \Delta = 0$ or equation (2) with $D_1' = D_2' = 0$. Then

$$E_{\text{sw}} \sim \bar{S}'' \{ [z_2 J_2' + z_1 J_1' (1 - \gamma_{k1})]^2 - (z_2 J_2 \gamma_{k2})^2 \}^{1/2} \sim \bar{S}'' [2z_2 J_2' (z_1 J_1' \alpha + z_2 J_2' \beta) k^2 + (z_1 J_1' \alpha + z_2 J_2' \beta) (z_1 J_1' \alpha - z_2 J_2' \beta) k^4]^{1/2}. \tag{13}$$

Now J_1' is much bigger than J_2' and α and β are of the order of unity, so

$$E_{\text{sw}} \sim \bar{S}'' (2z_1 z_2 J_1' J_2')^{1/2} k \left(1 + \frac{z_1 J_1'}{2z_2 J_2'} k^2 \right)^{1/2}. \tag{14}$$

For very small k , this equation has the form typical of an antiferromagnet, i.e. E_{sw} proportional to k . On the other hand, for larger values of k , as J'_2 becomes smaller and smaller relative to J'_1 , E_{sw} again becomes proportional to k^2 .

4. Temperature dependence of exciton–magnon bands

For magnon-assisted optical transitions, the absorption intensity is given by summing contributions from excitons and magnons across the Brillouin zone, since the incident photon excites an exciton of wavevector k and a magnon of wavevector $-k$ (Sell *et al* 1967). Thus

$$I(\omega) = \sum_k I_k(\omega).$$

For antiferromagnetic crystals

$$I_k(\omega) \propto |M_k^A|^2 \delta(\hbar\omega - E_k - \lambda_k) \quad (15a)$$

where M_k^A is the electric-dipole matrix element, which depends on both the symmetry of the exciton and magnon and on the crystal symmetry, E_k is the energy of the magnon and λ_k that of the exciton. For ferromagnetic crystals, on the other hand,

$$I_k(\omega) \propto |M_k^F|^2 \langle n_k \rangle \delta(\hbar\omega + E_k - \lambda_k). \quad (15b)$$

The magnon occupation number now enters, since, as we noted earlier, for $\Delta S = -1$ electronic transitions, e.g. quintet-to-triplet, allowed exciton–magnon combinations only arise from creation of an exciton together with annihilation of a thermally created $\Delta S = -1$ magnon. Let us now consider the various terms in equation (15b).

In the low-temperature limit, when only magnons of small k are thermally populated, only matrix elements M_k having small k need to be taken into account. For a centrosymmetric system, the leading terms in M_k are proportional to $\sin(\mathbf{k} \cdot \boldsymbol{\delta})$, i.e. approximately to k (Loudon 1967). At thermal equilibrium, the average value of n_k , the second term, is given by the Planck distribution

$$\langle n_k \rangle = [\exp(\hbar\omega/k_B T) - 1]^{-1} \quad (16)$$

and the total number of magnons excited at temperature T is

$$\sum_k \langle n_k \rangle = \int D(\omega) \langle n(\omega) \rangle d\omega \quad (17)$$

where $D(\omega)$ is the number of magnon modes per unit frequency. (Note that the integral may be taken from 0 to ∞ , since in the low-temperature limit $\langle n(\omega) \rangle \rightarrow 0$ as $\omega \rightarrow \infty$.) Further,

$$D(\omega) = \frac{V}{(2\pi)^3} \int \frac{dS_\omega}{|d\omega/dk|} \quad (18)$$

(Kittel 1971), where V is the volume of the sample and dS_ω is an element of area on the surface of constant frequency in k -space. If we assume that only magnons propagating within the layers are important, we can write $\int dS_\omega \propto 2\pi k$ and also, if $\omega \propto |k|^m$ where m is some power, then $(d\omega/dk) \propto mk^{m-1}$. For the two-dimensional easy-axis ferromagnet, we noted above that $m = 2$ at small k , so $D(\omega)$ becomes a constant, independent of k . In contrast, in the two-dimensional easy-plane system, the low-energy mode has $m = 1$,

Temperature variation of exciton–magnon absorption bands

873

giving $D(\omega) \propto k$. Later we compare the predictions based on these simple considerations with the form of temperature variation of $I(\omega)$ actually observed.

A final theoretical point which requires comment concerns the possible influence of zero-point spin fluctuations on the temperature variation of the exciton–magnon combination bands. In this connection, it should be noticed that the calculation of the magnon occupation numbers at low temperatures is intrinsically different for an isotropic or easy-axis ferromagnet compared with an easy-plane ferromagnet. In the former, the rotational symmetry about the z axis ensures that the total magnetization is a constant of the motion, but in the latter the anisotropy field along the x axis destroys the rotational symmetry and can thus lead to zero-point fluctuations in the magnetization along the z axis. This could clearly have important consequences for the exciton–magnon spectra in the low-temperature limit. In this respect, the easy-plane ferromagnet is analogous to the isotropic antiferromagnet, in which the degeneracy associated with the two sublattices also permits zero-point deviations via the interaction terms. To examine this point further it is convenient to write the Hamiltonians in terms of second quantization operators (Kittel 1963). That for the isotropic antiferromagnet can be applied to FeCl_2 , which has an axial anisotropy field. Retaining the antiferromagnetic inter-plane interactions in the Hamiltonian, the terms bilinear in magnon variables may be written

$$\mathcal{H} = \sum_{\mathbf{k}} \omega_0 (c_{\mathbf{k}}^\dagger c_{\mathbf{k}} + d_{\mathbf{k}}^\dagger d_{\mathbf{k}}) + \sum_{\mathbf{k}} \omega_1 (c_{\mathbf{k}}^\dagger d_{\mathbf{k}}^\dagger + c_{\mathbf{k}} d_{\mathbf{k}}) \quad (19)$$

in which $c_{\mathbf{k}}^\dagger, c_{\mathbf{k}}$ are the magnon creation and annihilation operators, respectively, on sublattice 1 and $d_{\mathbf{k}}^\dagger, d_{\mathbf{k}}$ are defined analogously for sublattice 2. Also

$$\omega_0 = \bar{S}[A + z_2 J_2 + z_1 J_1(1 - \gamma_{k1})] \quad (20)$$

$$\omega_1 = z_2 J_2 \bar{S} \gamma_{k2},$$

the $\gamma_{k\alpha}$ ($\alpha = 1, 2$) having been defined in equation (5). We see from equation (19) that it is the second term which mixes magnons on the two sublattices (neighbouring planes in the case of FeCl_2) and gives rise to the zero-point fluctuations.

In contrast to the easy-axis case, in the easy-plane ferromagnet zero-point fluctuations may arise from intra-layer interactions, even when inter-layer interactions are assumed negligible. For example, putting $J_2 = D_2 = 0$, the Hamiltonian of equation (2) may be written in magnon variables as

$$\begin{aligned} \mathcal{H} = & \sum_{\mathbf{k}} [z_1 J_1 S'(1 - \gamma_{k1}) + \frac{1}{2} D_1' z_1 S' \gamma_{k1}] (b_{\mathbf{k}}^\dagger b_{\mathbf{k}} + b_{-\mathbf{k}}^\dagger b_{-\mathbf{k}}) \\ & + \sum_{\mathbf{k}} \frac{1}{2} D_1' z_1 S' \gamma_{k1} (b_{\mathbf{k}} b_{-\mathbf{k}} + b_{\mathbf{k}}^\dagger b_{-\mathbf{k}}^\dagger) \end{aligned} \quad (21)$$

where $b_{\mathbf{k}}^\dagger, b_{\mathbf{k}}$ are the magnon creation and annihilation operators within a single layer. This Hamiltonian may be rewritten in a form comparable to equation (19), i.e.

$$\mathcal{H} = \sum_{\mathbf{k}} \omega'_0 (b_{\mathbf{k}}^\dagger b_{\mathbf{k}} + b_{-\mathbf{k}}^\dagger b_{-\mathbf{k}}) + \sum_{\mathbf{k}} \omega'_1 (b_{\mathbf{k}} b_{-\mathbf{k}} + b_{\mathbf{k}}^\dagger b_{-\mathbf{k}}^\dagger) \quad (22)$$

with

$$\left. \begin{aligned} \omega'_0 &= z_1 J_1 S'(1 - \gamma_{k1}) + \frac{1}{2} D_1' z_1 S' \gamma_{k1} \\ \omega'_1 &= \frac{1}{2} D_1' z_1 S' \gamma_{k1}. \end{aligned} \right\} \quad (23)$$

Just as in equation (19), it is the second term in (22) which causes interactions between magnons, and hence zero-point spin fluctuations, although now the magnons reside on

874 *D J Robbins and P Day*

the same sublattice. To determine the effect of these interactions on the magnon occupation numbers at low temperature, for example in CoBr_2 , we diagonalize the Hamiltonian (22), first transforming to new variables

$$\left. \begin{aligned} \beta_k &= u_k b_k - v_k b_{-k}^\dagger \\ \beta_k^\dagger &= u_k b_k^\dagger - v_k b_{-k} \end{aligned} \right\} (u_k^2 - v_k^2 = 1; u_k = \cosh \chi_k; v_k = \sinh \chi_k). \quad (24)$$

The Hamiltonian (22) is then diagonal if

$$\tanh 2\chi_k = -\omega'_1/\omega'_0 \quad (25)$$

and the eigenfunctions are given by

$$(\epsilon'_k) = (\omega'_0)^2 - (\omega'_1)^2 \quad (26a)$$

i.e.

$$\epsilon'_k = S' \{ [z_1 J_1 (1 - \gamma_{k1})] [z_1 J_1 (1 - \gamma_{k1}) + D'_1 z_1 \gamma_{k1}] \}^{1/2}. \quad (26b)$$

This is just the equation for $E_{\text{sw}}^{(2)}$ given by Lines, though as we noted before, when inter-layer terms are neglected (equation 21), $E_{\text{sw}}^{(1)}$ and $E_{\text{sw}}^{(2)}$ become degenerate.

The ground state of the easy-plane system has the property

$$\beta_k |\psi_0\rangle = 0$$

for all k , and the number of spin deviations in the system is given by terms of the type $(b_k^\dagger b_k)$. In terms of the new variables,

$$b_k^\dagger b_k = u_k^2 \beta_k^\dagger \beta_k + v_k^2 \beta_{-k} \beta_{-k}^\dagger. \quad (27)$$

Writing $|\psi_{n_k}\rangle$ as a state with a magnon occupancy n_k we have

$$\begin{aligned} \beta_k^\dagger \beta_k |\psi_{n_k}\rangle &= n_k |\psi_{n_k}\rangle \\ \beta_k \beta_k^\dagger |\psi_{n_k}\rangle &= (n_k + 1) |\psi_{n_k}\rangle. \end{aligned} \quad (28)$$

Therefore

$$\begin{aligned} \langle \psi_{n_k} | b_k^\dagger b_k | \psi_{n_k} \rangle &= n_k (u_k^2 + v_k^2) + v_k^2 \\ &= n_k \cosh 2\chi_k + \sinh^2 \chi_k. \end{aligned} \quad (29)$$

Thus, even when all $n_k = 0$, the second term in (29) introduces spin fluctuations which might permit some magnon-induced absorption intensity in a two-dimensional easy-plane ferromagnet even as T approaches 0 K. It is important to notice, however, that any such exciton-magnon absorption allowed by this mechanism will be found at higher energy than the corresponding exciton line since the ground state, with inclusion of the zero-point fluctuations, is the lowest state of the system. When evaluating the temperature dependence of the hot exciton-magnon lines, the effective magnon occupation number in equation (15b) would have to be replaced by $\langle n_k \rangle \cosh 2\chi_k$, where

$$\cosh 2\chi_k = \frac{\omega'_0}{(\omega'_0{}^2 - \omega'_1{}^2)^{1/2}}, \quad (30)$$

the ω 's being defined by equation (23). Combining equations (23) and (30) tells us that, for magnon states of small k , the leading terms have the k -dependence

$$\cosh 2\chi_k = (a/k) + \dots \quad (31)$$

in the easy-plane case.

Temperature variation of exciton–magnon absorption bands

875

A similar diagonalization procedure applied to the easy-axis Hamiltonian (19) yields an expression for the spin-wave energies identical to equation (26a). For FeCl_2 , we know that $\omega_0 \gg \omega_1$ so that neglecting inter-plane interaction terms, $\epsilon_k \sim \omega_0$, which brings us back to equation (6). The system thus behaves to a good approximation as a two-dimensional ferromagnet, and the single sublattice spin-waves closely approximate the true spin-waves. Any zero point spin deviation within a plane as a result of the antiferromagnetic coupling between the planes would be expected to be very small or, put another way, $\sinh \chi_k \sim 0$. We shall see later, however, that there may be some evidence for a small contribution in FeCl_2 from this effect.

5. Experimental results and discussion

5.1. FeCl_2

The temperature variation of the band which appears in the absorption spectrum of FeCl_2 near 4270 \AA has been examined by Schnatterly and Fontana (1972). It is clear from their spectra that their crystals were rather thin (probably sublimation flakes) and they were therefore restricted to looking at the temperature dependence of the band area at rather high temperatures ($> 10 \text{ K}$). By using a thicker crystal, we have extended the temperature range over which the band area can be measured down to 2.9 K . Further, the spectrophotometer used in the present work has a higher resolution than the Cary 14 used by Schnatterly and Fontana, so we are able to resolve more detail in the spectrum.

Figure 1 shows axial absorption spectra of FeCl_2 in the 4270 \AA region, measured over the lower temperature range, on a high sensitivity (0 to 0.1) optical density scale. Band A is clearly the hot band, the relative intensities of the other two varying only very slightly over this range of temperature. Band B, which is much narrower than either A or C, occurs 17.0 cm^{-1} higher than band A. From inelastic neutron scattering, Birgeneau *et al* (1972) found that the gap in the spin-wave dispersion of FeCl_2 at the zone centre was $17.2 + 0.4 \text{ cm}^{-1}$ at 5 K , so we may plausibly assign band B as the exciton line corresponding to the hot exciton–magnon band A. One possible assignment of band C is that it is a second exciton component arising from the trigonal crystal-field splitting. On the other hand, it is much broader than band B, and so might be a cold exciton–magnon combination band whose intensity comes from zero-point spin fluctuations in the two-dimensional spin system brought about by the weak antiferromagnetic coupling between the layers in the manner described in the previous section. As we have already remarked, such a band would indeed occur at a higher energy than the exciton line.

We treat the temperature dependence of the hot exciton–magnon band A in a fashion analogous to Schnatterly and Fontana. From equations (10), (15b), (16) and (17), recalling at the same time that, for the two-dimensional easy-axis ferromagnet, $D(\omega)$ is independent of k at small k , and neglecting the small inter-plane interactions, we have

$$\sum_{\mathbf{k}} I_{\mathbf{k}}(\omega) = \int_0^{\infty} k^2 \exp(-E_{\text{sw}}/k_{\text{B}}T) d\omega = \int_0^{\infty} \omega' \exp[-(A' + \hbar\omega)/k_{\text{B}}T] d\omega' \quad (32)$$

or, putting $x = \omega'/T$,

$$\sum_{\mathbf{k}} I_{\mathbf{k}}(\omega) = C \exp(-A'/k_{\text{B}}T) T^2 \int_0^{\infty} x \exp(-ax) dx = W(T). \quad (33)$$

876

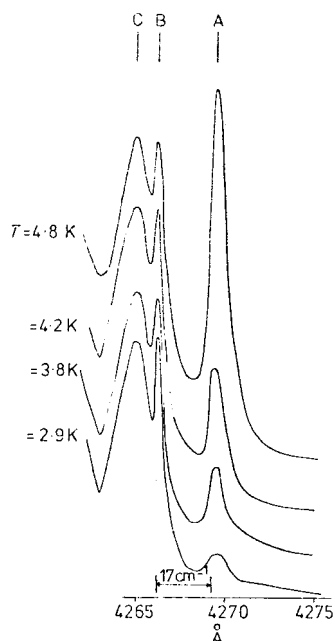
D J Robbins and P Day

Figure 1. Axial absorption spectrum of FeCl_2 in the 4270 Å region from 2.9 to 4.8 K.

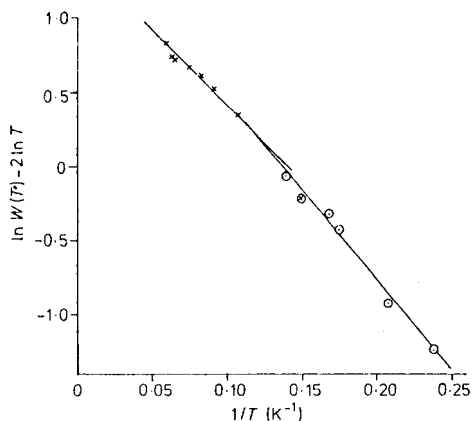


Figure 2. Temperature variation of the intensity of the 4270 Å band in FeCl_2 . The points marked \times are those of Schnatterly and Fontana (1972) and those marked \circ are from the present work. The two sets have been normalized together at the point \otimes .

The integral in x is a definite integral and A' is the energy gap in the spin-wave dispersion. It follows from equation (33) that a plot of $\ln W(T) - 2 \ln T$ against $1/T$ should be a straight line whose slope depends on A' . Such a plot was made by Schnatterly and Fontana (1972) who found a linear relation over the temperature range 9–15 K. However, the function of equation (33) is a good approximation to the intensity of the exciton–magnon band only if equation (10) represents a good approximation to the spin-wave energy, a situation prevailing only close to the zone centre.

In figure 2 we have plotted our own data on the 4270 Å hot band from 4.0 to 7.2 K together with the Schnatterly and Fontana data, having normalized the two sets together by means of the fortuitous fact that each contains a measurement taken at 6.7 K. The best straight line through our data points yields an energy gap of $19 \pm 1 \text{ cm}^{-1}$ while Schnatterly and Fontana quote a value of 16 cm^{-1} for theirs. Recalling that the energy gap at 5 K from inelastic neutron scattering was 17.2 cm^{-1} , we consider that these various figures are in reasonable agreement with one another, particularly since the neutron work indicates renormalization leading to a reduction of the gap at higher temperatures.

Our temperature-dependence measurements were made solely on band A, but reference to figure 3, which contains data recorded up to 9.9 K, reveals that, while band A continues to increase in intensity, a second hot band labelled D (at 4266 Å) begins to appear at approximately 6 K. This band grows up rapidly to dominate the spectrum above about 10 K. Comparing figure 3 with the spectra taken over the corresponding temperature range by Schnatterly and Fontana, we note that in their experiments band A

Temperature variation of exciton-magnon absorption bands

877

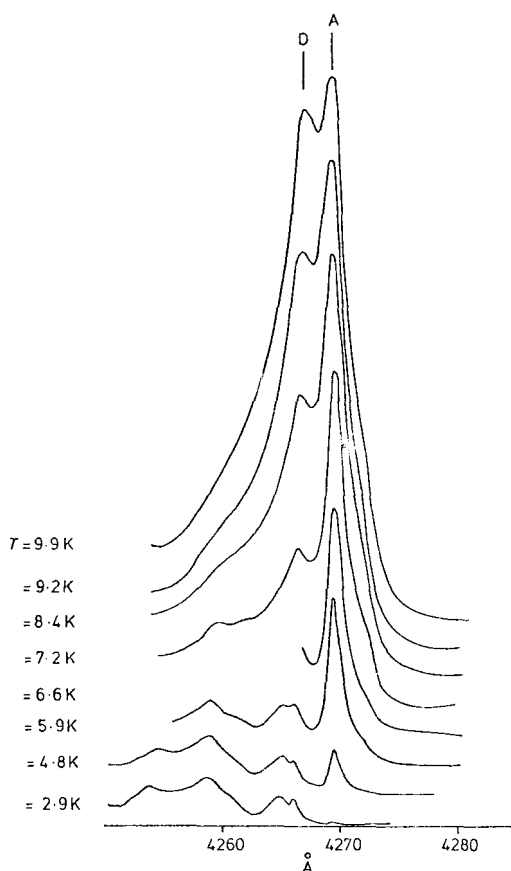


Figure 3. Axial absorption spectrum of FeCl_2 in the 4270 Å region from 2.9 to 9.9 K.

still dominates the spectrum up to about 17–18 K. Hence, although their measurements of band intensity were made over a higher temperature range than ours, it was presumably still predominantly the area of band A which they were measuring. This is a question of some importance in interpreting their data, since equation (33) is only expected to apply to band A, which is the simple one-magnon sideband.

What, therefore, is the origin of band D? The fact that the relative intensities of bands A and D vary from one sample to another might suggest that band D is sensitive to some aspect of crystal morphology, or to the concentration either of defects and dislocations or of impurity centres. Our own sample was cleaved from a melt-grown boule. Unfortunately, Schnatterly and Fontana do not record whether their crystal was grown from the melt or by sublimation, a point which may be important because, in general, vapour-grown crystals are expected to contain a smaller concentration of defects than those grown from melts. Another structural variable which may enter into any comparison of results obtained on crystals of different origins concerns polytypism. There do not appear to have been any studies of this phenomenon in FeCl_2 , but formation of superstructures which differ in repeat distances is a well known feature of layer structures

and has been very extensively studied in CdI_2 (e.g. Prasad 1974). The effect of such superstructures on magnetic and optical properties is uncharted territory.

As well as apparently being sensitive to sample, other relevant properties of the band D are, first, that it has a steeper dependence on temperature than band A, and second, that it appears at a frequency almost identical to that of the exciton line B. The latter implies that it comes from a transition which conserves spin-wave energy. One conceivable mechanism which has this property is that of 'spin-wave confluence', discussed by Keffer (1966). Two magnons annihilate to create a third, conserving momentum and energy:

$$\mathbf{k}_1 + \mathbf{k}_2 = \mathbf{k}_3, \quad \epsilon_1 + \epsilon_2 = \epsilon_3. \quad (34)$$

The probability of such a process would be related to the square of the magnon occupancy number and to the magnon density of states. Applied to the present instance of an exciton-magnon combination created by absorption of a photon,

$$\begin{aligned} \epsilon_{\text{photon}} + \epsilon_1 + \epsilon_2 &= \epsilon_{\text{exciton}} + \epsilon_3 \\ \mathbf{k}_1 + \mathbf{k}_2 &\sim \mathbf{k}_{\text{exciton}} + \mathbf{k}_3. \end{aligned} \quad (35)$$

Such a second-order process would indeed have a steeper dependence on temperature than a first-order one, but it could only be brought about by higher-order terms in the spin-wave expansion or perhaps as a result of a breakdown in the translational symmetry of the lattice by, for example, dislocations. Evidently, further experiments, particularly on the variation in relative intensities of the two bands A and D with sample, are going to be needed before anything more precise can be said about the origin of band D.

5.2. CoBr_2

Our measurements on CoBr_2 were made on the zero-phonon line at 4940 Å, which is the best resolved of the doublet states in this compound, and on the zero-phonon line at 5670 Å. The latter, though not so well resolved as the 4940 Å band system, is of interest because it is a component of the same electronic excited state, ${}^2T_{1g}(H)$, whose single-ion and pair spectra we previously studied in the isomorphous host lattice CdBr_2 (Bailey *et al* 1974). Figure 4(a) shows the axial absorption spectrum of CoBr_2 in the 4940 Å region, at temperatures between 3.7 and 18 K. Three features are apparent. The band labelled A is 'hot' and lies to the low-energy side of the weak feature B, whose intensity does not vary noticeably with temperature. A is therefore the expected 'hot' exciton-magnon combination band and B the exciton origin band. In addition, there is a broad cold band labelled C at a higher energy than the exciton, which may perhaps be the exciton-magnon combination resulting from the zero-point spin fluctuations introduced by the anisotropy terms in the easy-plane system in the manner which we described in the previous section.

In the low-temperature limit, the temperature dependence of band A, the hot one-magnon sideband, may be predicted by assuming that the exciton concerned couples to the low-energy spin-wave branch in the easy-plane case, $E_{\text{sw}}^{(2)}$ of equation (12). Then combining equations (12), (15b), (18), (29) and (31), we have

$$\begin{aligned} \sum_{\mathbf{k}} I_{\mathbf{k}}(\omega) &= \int_0^\infty k^2(1/k) [\exp(E_{\text{sw}}/k_{\text{B}}T) - 1]^{-1} k \, d\omega \\ &\propto \int_0^\infty \omega^2 [\exp(\hbar\omega/k_{\text{B}}T) - 1]^{-1} d\omega. \end{aligned} \quad (36)$$

Temperature variation of exciton-magnon absorption bands

879

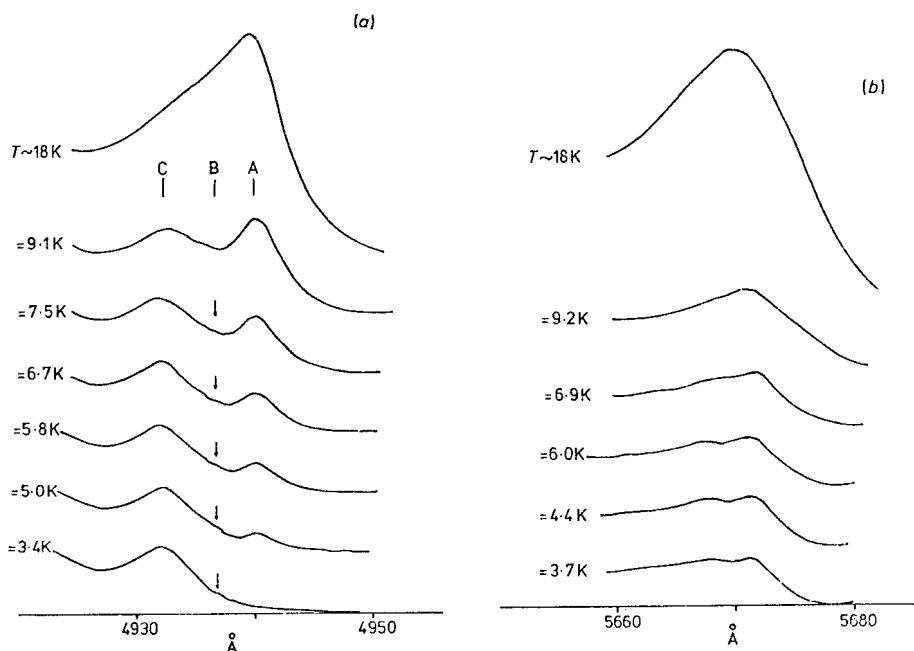


Figure 4. Axial absorption spectra of CoBr₂ from 3.7 to 18 K: (a) near 4940 Å; (b) near 5680 Å.

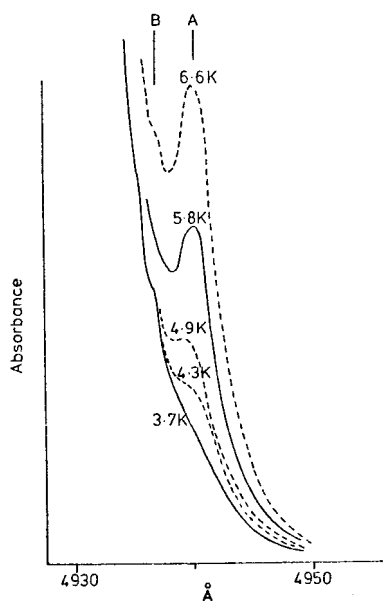


Figure 5. Axial absorption spectrum of CoBr₂ near 4940 Å from 3.7 to 6.6 K on expanded optical density scale.

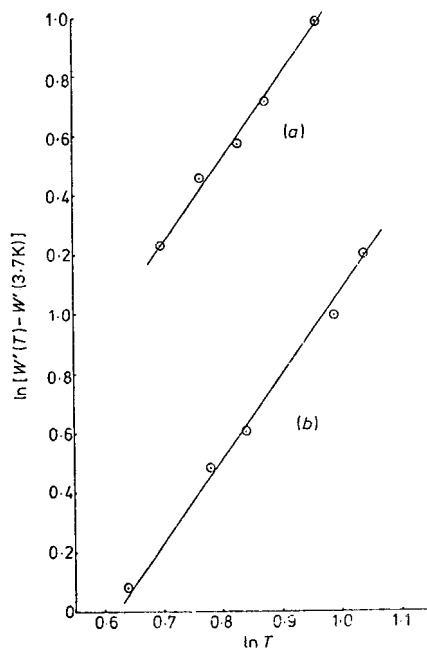


Figure 6. Temperature variation of the intensity of (a) the 4940 Å band and (b) the 5680 Å band in CoBr₂.

880 *D J Robbins and P Day*

Letting $x = \omega/T$, as in equation (33),

$$\sum_k I_k(\omega) = CT^3 \int_0^\infty x^2 [\exp(ax) - 1]^{-1} dx = W'(T). \quad (37)$$

In equation (36), the four terms originate respectively from the electronic matrix element M_k , the zero-point fluctuation, the magnon occupancy number n_k and the magnon density of state $D(\omega)$. The final outcome is a prediction that the intensity of the hot one-magnon sideband will vary as T^3 .

Figure 5 displays this sideband on the lower-temperature range on an optical density scale expanded ten-fold compared to figure 4(a). At the base temperature of our continuous flow cryostat (3.7 K), one can see that band A has almost entirely disappeared. Therefore, to analyse the temperature dependence, we integrated the area of band A between 4950 and 4932.5 Å, taking the 3.7 K curve as the baseline. In figure 6(a) we show the resulting plot of $\ln [W'(T) - W'(3.7 \text{ K})]$ versus $\ln T$. The straight line of best fit has a slope of 2.8. The zero-phonon line at 5670 Å is rather poorly resolved compared with the one at 4940 Å, but we show its temperature variation in figure 4(b) and a log-log plot of its area versus temperature in figure 6(b). Again the line of best fit has a slope of 2.8. Equation (37), and the assumptions underlying it, therefore represent a reasonable approximation to the behaviour of the hot exciton-one-magnon sideband in the easy-plane ferromagnet, with large anisotropy.

5.3. *NiBr₂*

Our final example is an easy-plane ferromagnet with small single-ion anisotropy. The single-ion ground state is $^3A_{2g}$ and near 6100 Å is a weak highly-structured band system which is either $^1A_{1g}$ or $^1T_{2g}$. Its zero-phonon line, a single asymmetric hot band about 10 Å wide, is at 6070 Å, but no absorption corresponding to a pure exciton line could be found. At 3.7 K the hot band had negligibly small intensity, so as in the case of *CoBr₂*, we plot $\ln [W''(T) - W''(3.7 \text{ K})]$ versus $\ln T$, here for temperatures up to 21 K. The Néel temperature of *NiBr₂* is reported as 60 K. The resulting plot (figure 7) is a good straight line of slope 2.0.

If we neglect inter-plane exchange and any in-plane anisotropy, then, as described in §3, an isotropic Hamiltonian (equation 13) as discussed by Lines (1963) is appropriate and $E_{sw} \propto k^2$. Then

$$\begin{aligned} \sum_k I_k(\omega) &\propto \int_0^\infty k_2 [\exp(E_{sw}/k_B T) - 1]^{-1} d\omega \\ &\propto \int_0^\infty \omega [\exp(h\omega/k_B T) - 1]^{-1} d\omega \\ &\propto C'' T^2 \int_0^\infty x [\exp(ax) - 1]^{-1} dx = W''(T) \end{aligned}$$

where x is defined as before. Figure 7 is thus in good agreement with theoretical expectations. Indeed, a similar T^2 dependence of intensity on temperature has also been found to hold at low temperature for the quintet-triplet transitions in the two-dimensional easy-plane ferromagnet *Rb₂CrCl₄* (A Okiji 1974, private communication, Fair *et al* 1975), while the introduction of a small degree of anisotropy produces a temperature dependence between T^2 and T^3 , as found experimentally in *K₂CrCl₄* (Day *et al* 1973).

Temperature variation of exciton–magnon absorption bands

881

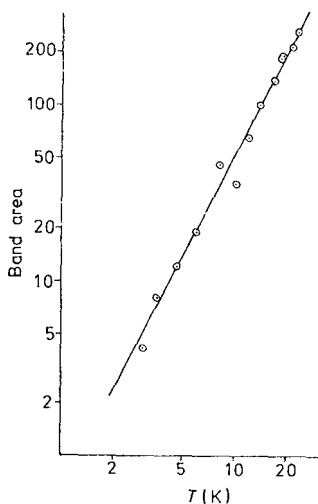


Figure 7. Temperature variation of the intensity of the 6070 Å band in NiBr₂ from 3.7 to 21 K.

A final point which will need to be taken into account in any more-extended treatment of the exciton–magnon absorption in NiBr₂ concerns the precise nature of the magnetic structure of the compound at low temperature. A number of independent lines of evidence, for example antiferromagnetic resonance (Katsumata and Date 1969) and neutron diffraction (Dinsdale 1975), suggest that around 22 K a magnetic phase transition takes place from the simple metamagnetic spin structure, with the spins lying in the basal plane, to a closely related, but lower-symmetry structure. Accompanying this phase transition, a number of new sharp weak absorption lines appear near 6080 Å. Experiments on the temperature dependence of these lines and their behaviour when an external magnetic field is applied parallel to the basal plane will be reported later.

6. Conclusions

The compounds FeCl₂, CoBr₂ and NiBr₂ are representative of the three main classes of magnetic behaviour to be found within the group of metamagnetic 3d layer halides MX₂, and thus provide examples of three different kinds of temperature variation of exciton–magnon absorption. In all three, the most intense magnon sidebands associated with spin-forbidden ligand field transitions have intensities which increase steeply with increasing temperature. Thus, in each case, the allowed exciton–magnon combinations are those in which the creation of an exciton with a spin-projection lower than that of the ground state is accompanied by the annihilation of a thermally created magnon. The magnons thus annihilated propagate within the ferromagnetic planes and correspond to a decrease in the spin-projection of each plane.

The hot exciton–magnon absorption intensity varies in a different way with temperature in all three compounds because of differences in the functional forms of the magnon dispersions and of the gap energies near the centres of the Brillouin zones. In FeCl₂, which has axial anisotropy and a large gap, we find that the expression $T^2 \exp(-A/kT)$ (where A is the gap energy) is obeyed. In CoBr₂, the magnon energies are to a good

approximation those of an easy-plane two-dimensional ferromagnet with large anisotropy and the intensity varies as T^3 . On the other hand, NiBr_2 , exemplifying the two-dimensional easy-plane ferromagnet with small anisotropy, shows an intensity dependence close to T^2 . Our experiments therefore demonstrate that the way the intensity of an exciton-magnon combination band varies with temperature is a valuable probe to the magnetic structure of the lattice in metamagnetic layer compounds or, indeed, in other compounds in which ferromagnetic exchange plays a dominant role. Other examples taken from one- and two-dimensional ferromagnets will be reported later.

Acknowledgment

We are grateful to the Science Research Council for an equipment grant and a Fellowship (to DJR).

References

- Ackerman J, Fouassier C, Holt E M and Holt S L 1972 *Inorg. Chem* **11** 3118
Bailey A, Robbins D J and Day P 1974 *Molec. Phys.* **28** 1519
Birgeneau R J, Yelon W B, Cohen E and Makovsky J 1972 *Phys. Rev.* **B5** 2607
Bizette H, Terrier C and Tsai B 1956 *C.R. Acad. Sci., Paris* **243** 1295
Day P, Gregson A K and Leech D H 1973 *Phys. Rev. Lett.* **30** 19
Dinsdale A 1975 *Chemistry Part II Thesis* Oxford University
Fair M J, Gregson A K, Day P, Okiji A and Elliott R J 1975 unpublished work
Ferguson J, Wood D L and Knox K 1963 *J. Chem. Phys.* **39** 116
Gregson A K, Day P, Leech D H, Fair M J and Gardner W E 1975 *J. Chem. Soc. Dalton Trans.* 1306
Griffin J A, Schnatterly S E, Farge Y, Regis M and Fontana M P 1974 *Phys. Rev.* **B10** 1960
Hutchings M T 1973 *J. Phys. C: Solid St. Phys.* **6** 3143
Hutchings M T, Gregson A K, Day P and Leech D H 1974 *Solid St. Commun.* **15** 313
Katsumata K and Date M 1969 *J. Phys. Soc. Japan* **27** 1360
Katsumata K and Yamasaka K 1973 *J. Phys. Soc. Japan* **34** 346
Keffler F 1966 *Handb. Phys.* **XVIII/2** 1
Kittel C 1963 *Quantum Theory of Solids* (New York: Wiley) ch 4
——— 1971 *Introduction to Solid State Physics* 4th edn (New York: Wiley) p 210
Kozielski M, Pollini I and Spinolo G 1972 *J. Phys. C: Solid St. Phys.* **5** 1253
Landau L 1933 *Z. Phys. Sowietunion* **4** 675
Lindgard P A, Birgeneau R J, Als-Nielsen J and Guggenheim H J 1975 *J. Phys. C: Solid St. Phys.* **8** 1059
Lines M E 1963 *Phys. Rev.* **131** 540, 546
Loudon R 1967 *Adv. Phys.*
Prasad R 1974 *Z. Kristallogr.* **139** 136
Robbins D J and Day P 1973 *Chem. Phys. Lett.* **19** 529
Schnatterly S E and Fontana M 1972 *J. Physique* **33** 691
Sell D, Greene R L and White R M 1967 *Phys. Rev.* **158** 489
Semura J S and Huber D L 1973 *Phys. Rev.* **B7** 2154
Shinagawa K and Tanabe Y 1971 *J. Phys. Soc. Japan* **30** 1280
Wilkinson M K, Cable J W, Wollan E O and Koehler W C 1959 *Phys. Rev.* **113** 497

Nickel Dibromide: A Magnetic Detective Story

PETER DAY

Inorganic Chemistry Laboratory, Oxford University, South Parks Road, Oxford OX1 3QR, England

Received July 21, 1987 (Revised Manuscript Received March 16, 1988)

Ferro- and antiferromagnetism are the commonplace types of long-range magnetic order in inorganic solid-state chemistry. The first occurs in a lattice containing localized moments, for example arising from unpaired d or f electrons, when the interaction between neighboring (n) moments, measured by the exchange constant J_n , is such as to couple them parallel. At low temperatures, when thermally induced disorder cannot disrupt the near-neighbor interactions, the free energy of the ensemble of moments is minimized when they are all parallel, and the magnetization of the whole lattice is saturated. Conversely, when the interaction between near neighbors couples them antiparallel, there is no net moment in zero field at low temperature. In any real lattice, though, there are not only the immediate neighbors of a magnetic ion to be considered, but next nearest (nn), next next nearest (nnn), etc. Clearly, if the interactions between all these are ferromagnetic, the long-range order must be ferromagnetic. What, though, if the (n) interaction is ferromagnetic (J_n positive) and the (nn) and (nnn) are antiferromagnetic (J_{nn} and J_{nnn} negative)?

Fortunately this problem does not arise very often in ionic lattices because the unpaired electrons are quite firmly localized onto individual cations and J_n dominates J_{nn} , even if there are more (nn) than (n). Nevertheless, occasionally the metal-ligand covalency combined with a favorable lattice topology may be sufficient to strengthen the (nn) superexchange to the point where it begins to compete with J_n in determining the long-range order. Such a case, occurring in the simple binary compound NiBr_2 , is the subject of this Account.

NiBr_2 has a simple layer structure isomorphous with CdCl_2 , but it turns out that because of competition between ferromagnetic J_n and antiferromagnetic J_{nn} and J_{nnn} , its magnetic ordering is highly unusual. In fact it changes from a collinear structure to an incommensurate helical one with decreasing temperature and moreover with a helix repeat length that varies with temperature and pressure. This Account is also a detective story, since the indicators for the existence of unusual magnetic order were at first indirect. Evidence from a variety of physical methods has to be combined to produce a coherent picture of the ordering process. In particular optical spectroscopy and neutron scattering were employed to measure the magnetic phase diagram and interpret the unique magnetic behavior. Chemical substitution was also used extensively to probe the effect of varying the electron configuration

of the transition-metal ion and the nature of the anions bridging between them.

Noncollinear Magnetic Structures

The simplest example of a magnetic structure whose periodicity differs from that of the nuclear structure is the two-sublattice antiferromagnet. A relevant example is provided by the transition-metal dihalides exhibiting the CdCl_2 or CdI_2 layer structures. These were dubbed metamagnetic by Landau^{1a} because despite being antiferromagnetic below their ordering temperatures, they may be ferromagnetically saturated above a relatively small critical magnetic field applied in the *ab* plane (CoX_2 , NiX_2) or parallel to the *c* axis (FeX_2). Landau proposed a model in which moments are ferromagnetically aligned within the *ab* plane, either parallel or perpendicular to the *c* axis, with weak antiferromagnetic coupling between adjacent planes. This was subsequently confirmed by neutron diffraction.^{1b}

Figure 1 displays the CdCl_2 structure of NiBr_2 , clearly showing that exchange between neighboring ions within each layer (J_n) occurs via a single bridging halide ion whereas interlayer exchange (J') occurs via two bridging halide ions. The latter is expected to be very much smaller in magnitude, thus explaining the observed predominantly two-dimensional magnetism. Figure 1 also illustrates how the (n), (nn), and (nnn) pairs of metal ions within the layers are coupled by J_n , J_{nn} , and J_{nnn} .

More complex antiferromagnetic structures can arise where there is competition between magnetic interactions that favor the alignment of magnetic moments in different directions in the lattice.² Five separate types of competition have been identified. First, there may be competing exchange interactions between a magnetic species and its first and further crystallographically equivalent nearest-neighbor shells. Second, competing exchange interactions may occur between a magnetic species and its nearest neighbors, if they occupy crystallographically inequivalent sites. Third, there could be competition in exchange involving different magnetic species. Fourth, in metallic systems competing long-range exchange interaction can take place via the conduction electrons, and itinerant exchange between the conduction electrons themselves, and finally competition is set up between exchange and dipolar interactions, when the former are very weak.

In low-dimensional magnetic materials, it is easier to identify the sources of competing interactions because such interactions are fewer in number. NiBr_2 ,³ NiI_2 ,⁴

Peter Day received his D.Phil. from Oxford University in 1965 for work initiating the modern-day study of mixed-valency compounds. He worked with C. K. Jorgensen at the Cyanamid Institute in Geneva, Switzerland, and briefly at Bell Laboratories, Murray Hill, NJ. Since 1967 he has been a lecturer in Inorganic Chemistry at Oxford University and Fellow of St. John's College. He received the Corday-Morgan Medal of the Royal Society of Chemistry in 1971 and their Award for Solid State Chemistry in 1986. In 1986 he was elected a Fellow of the Royal Society.

(1) (a) Landau, L. D. *Phys. Z. Sowjetunion* 1933, 4, 675. (b) Wilkinson, M.; Cable, J. W.; Wollan, E. O.; Koehler, W. C. *Phys. Rev.* 1959, 113, 497.

(2) Villain, J. *J. Phys. Chem. Solids* 1959, 11, 303.

(3) Day, P.; Dinsdale, A. T.; Krausz, E. R.; Robbins, D. J. *J. Phys. C* 1976, 9, 2481.

(4) Kuindersma, S. R.; Sanchez, J. P.; Haas, C. *Physica B* 1981, 111B, 231.

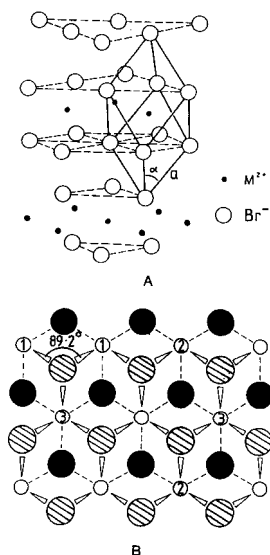


Figure 1. (A) Elevation and (B) plane view of the crystal structure of NiBr_2 ; (1,1), (2,2), and (3,3) are the (n), (nn), and (nnn) pairs of cations.

and $\text{BaCo}_2(\text{AsO}_4)_2$ ⁵ are examples of nearly two-dimensional systems where the competition is of the first type and helical magnetic phases exist. Certain members of the series of one-dimensional hexagonal perovskites $\text{A}^{\text{II}}\text{B}^{\text{III}}\text{X}_3$ (A = Cs, Rb; B = Fe, Mn; X = Br, Cl)⁶⁻⁸ have triangular spin arrays, and the competition is essentially of the second type. Both the third and fourth types of competition also exist in magnetic insulators with the spinel ($\text{A}^{\text{II}}\text{B}^{\text{III}}_2\text{O}_4$) and garnet ($\text{A}^{\text{III}}_3\text{B}^{\text{III}}_2\text{B}^{\text{III}}_3\text{O}_{12}$) structures; for example, MnCr_2O_4 ⁹ and $\text{Ho}_3\text{Fe}_2\text{Fe}_3\text{O}_{12}$ ¹⁰ exhibit magnetic phases with complex spiral spin structures.

Among metals, the rare earths have long been known to show a wide variety of noncollinear magnetic phases, caused by the fourth type of competition, while HoP, which is believed to become ordered almost entirely by dipolar interactions, has a spiral magnetic phase and thus falls into the fifth category.

In most instances, a number of magnetic phase transitions take place as the temperature or applied magnetic field is raised. NiBr_2 is unique among the metamagnetic transition-metal dihalides, and probably among all magnetic insulators, because with decreasing temperature it undergoes a transition (at $T_{\text{IC}} = 23$ K) from a collinear magnetic phase to a phase with a helical modulation of the moments, and the vector describing the helical phase increases smoothly in magnitude from zero at T_{IC} to a limiting value at about 4 K.

(5) Regnault, L. P.; Bulet, P.; Rossat-Mignod, J. *Physica B* 1977, 86-88B, 660.

(6) Davidson, G. R.; Minkiewicz, V. J.; Cox, D. E.; Khattak, C. P. *AIP Conf. Proc.* 1971, 5, 483.

(7) Eibschuetz, M.; Sherwood, R. C.; Hsu, F. S. L.; Cox, D. E. *AIP Conf. Proc.* 1973, 18, 386.

(8) Wada, N.; Ubukashi, K.; Hirakawa, K. *J. Phys. Soc. Jpn.* 1982, 51, 2833.

(9) Hastings, K. M.; Corliss, L. M. *Phys. Rev.* 1962, 126, 556.

(10) Herpin, A.; Koehler, W.; Meriel, P. *Bull. Am. Phys. Soc.* 1960, 5, 457.

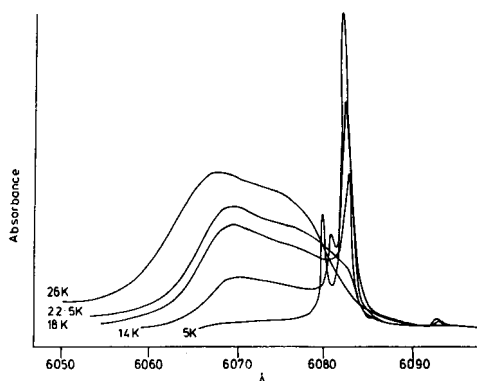


Figure 2. Temperature variation of the ligand field absorption spectra of NiBr_2 near 6000 Å. The cold bands are A and B.¹⁴

Optical Spectra

The story begins with a project on the temperature dependence of exciton-magnon absorption bands in the family of metamagnetic dihalides MX_2 (M = Mn, Fe, Co, Ni; X = Cl, Br, I).¹¹ In the large majority of cases J_n within the layers is ferromagnetic while the much smaller J' between layers is antiferromagnetic. Thus while the (n) interaction is ferromagnetic, the lattice as a whole is antiferromagnetic. We had already demonstrated that in purely ferromagnetic lattices, spin-forbidden ligand field transitions gain electric-dipole intensity by combining the creation of the electronic excited state (exciton) with the annihilation of thermally populated spin fluctuations (magnons).¹² The result of this mechanism is that the absorption intensity is strongly temperature dependent, disappearing at low temperature when the magnon states are no longer populated. This contrasts with the situation in purely antiferromagnetic compounds, where the exciton-magnon absorption bands become more intense with decreasing temperature.¹³ The question we posed to ourselves was whether the temperature behavior of the corresponding absorption bands in the metamagnets would mimic that of a two-dimensional ferromagnet or a three-dimensional antiferromagnet.

In the event, for M = Fe, Co and X = Cl, Br, I the answer was clear: the two-dimensional ferromagnetism dominated, and "hot"-band behavior was seen.¹¹ In the single case of NiBr_2 , however, not only was there a hot band in the region of the ${}^3\text{A}_{2g} \rightarrow {}^1\text{A}_{1g}, {}^1\text{T}_{2g}$ ligand field transition, but also next to it there were two much sharper bands that decreased rapidly in intensity with increasing temperature until at 23 K they had completely disappeared (Figure 2).¹⁴ The widths of exciton-magnon combination bands depend on the energy dispersion of both exciton and magnon since the incoming photon creates an exciton with a wave vector \mathbf{k} combined with either creation or annihilation of a magnon with a corresponding wave vector $-\mathbf{k}$.^{13,15} In

(11) Robbins, D. J.; Day, P. *J. Phys. C* 1976, 9, 867.

(12) For a brief review, see: Day, P. *Acc. Chem. Res.* 1979, 12, 236.

(13) Sell, D.; Greene, R. L.; White, R. M. *Phys. Rev.* 1967, 158, 489.

(14) Day, P.; Dinsdale, A.; Krausz, E. R.; Robbins, D. J. *J. Phys. C* 1976, 9, 2481.

(15) McClure, D. S. In *Optical Properties of Ions in Solids*; di Bartolo, B., Ed.; Plenum: New York, 1974.

252

Day

Accounts of Chemical Research

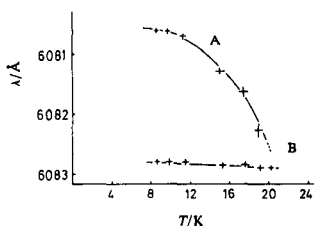


Figure 3. Temperature variation of the wavelengths of absorption bands A and B.¹⁶

halides such absorption bands are usually about 50–100 cm^{-1} wide, corresponding to the energy difference between the Brillouin zone center and zone edge magnons of zJ_nS , where z is the number of (n) neighbors, J_n is the exchange constant, and S is the spin. However, in Figure 2, one can see that the "cold" bands are very much narrower, suggesting that they arise from coupling between the exciton and a magnetic fluctuation that only has a very weak dispersion. The alternative explanation, that the bands corresponded to absorption by creating the exciton alone, could be ruled out by their polarization.

Although it is difficult to polish the mica-like crystals perpendicular to the easy cleavage plane, we measured polarized spectra with the incident light parallel and perpendicular to the layers. We found that they were allowed by the electric-dipole mechanism, like the nearby hot exciton–magnon combination, rather than magnetic-dipole, as expected if they were pure exciton lines. Another unusual feature is that the separation between the cold bands changes with temperature; in fact the most intense one remains almost fixed while the weaker one moves toward it as the temperature rises (Figure 3). Extrapolating, the temperature at which they would both have the same energy turns out to be that where their intensities both tend to zero, i.e., about 23 K.

That the two sharp cold bands signal a peculiarity in the magnetic structure is strongly indicated by their behavior when a magnetic field is applied.^{14,16} In fields applied perpendicular to the layers the bands are almost unaffected, except for a small shift to higher frequency that only starts to become appreciable above 10 T. (Measurements in such high fields, up to 15 T, were made with a pulsed magnet.) Contrastingly, with the field parallel to the layers there is a dramatic effect: the bands remain unchanged up to a critical value of the field H_c at which they vanish sharply. H_c is also a function of temperature, decreasing from 2.7 T at 4 K smoothly toward zero at 23 K (Figure 4). Figure 4 therefore defines a phase diagram in the H, T plane and delineates the existence region of a magnetic phase that we have labeled A_2 . But what is it? The method of choice for determining magnetic structures is neutron diffraction, so it was to this that we turned next.

Neutron Diffraction

Single-crystal neutron diffraction measurements^{14,17} showed that below its Neel temperature of 52 K, NiBr_2 adopts a magnetic structure in which the $S = 1$ ($3d^8$)

(16) Moore, M. W.; Wood, T. E.; Day, P. *J. Chem. Soc., Faraday Trans. 2* 1981, 77, 1611.

(17) Day, P.; Ziebeck, K. R. *A. J. Phys. C* 1980, 13, L623.

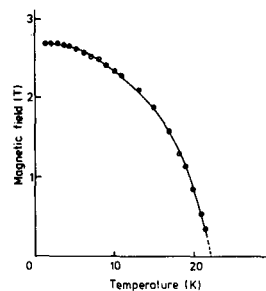


Figure 4. Temperature variation of the critical field at which bands A and B (Figure 3) disappear.¹⁴

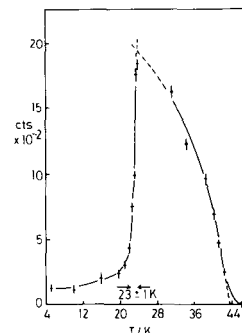


Figure 5. Temperature dependence of the maximum scattered neutron intensity at (003/2) in $\text{Ni}_{0.94}\text{Fe}_{0.06}\text{Br}_2$.¹⁸

moments localized on each Ni^{2+} lie parallel to one another within the planes of the layers, with alternate layers being antiparallel. That is, ferromagnetic layers are weakly coupled antiferromagnetically as in the other MX_2 halides. In the rhombohedral (D_{3d}^5) space group of the CdCl_2 crystal structure, (00 l) nuclear Bragg reflections are allowed for $l = 3n$. The antiferromagnetic order between the planes perpendicular to the c axis doubles the unit cell along this axis below 52 K, and magnetic Bragg reflections (003/2), (005/2), etc. are observed with intensities that increase with decreasing temperature following the spontaneous magnetization (Figure 5). Below 23 K, however, a remarkable change occurs, and the intensity at (003/2) suddenly drops. Where has it gone?

With a classical single-detector diffractometer, such as D15 at the high-flux beam reactor of the Institut Laue-Langevin (ILL), Grenoble, France, the most convenient way to monitor the intensity in the neighborhood of (003/2) as a function of temperature is by setting the neutron detector to the Bragg angle 2θ , corresponding to the center of the reflection, and rocking the crystal angle ω with the c axis in the horizontal plane. In that way we found that below 23 K the reflection broadens and splits into two satellite peaks that shift smoothly with decreasing temperature as shown in Figure 6 for a crystal doped with a small concentration of Fe^{2+} .¹⁸ The magnetic Bragg intensity no longer peaks at (003/2), but at ($\delta\delta$ 3/2), where δ reaches a limiting value of 0.027 at 4 K. This means that within the layers the spins are no longer parallel

(18) Moore, M. W.; Day, P. *J. Solid State Chem.* 1985, 59, 23.

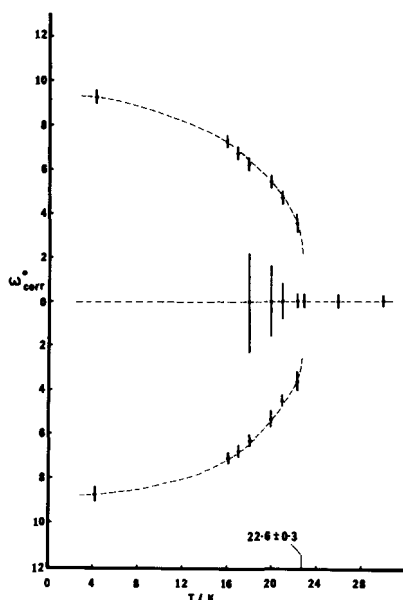


Figure 6. Temperature dependence of the separation $\omega^{\circ}_{\text{corr}}$ in crystal angle between the magnetic satellite neutron diffraction peaks around (003/2) in $\text{Ni}_{0.99}\text{Fe}_{0.01}\text{Br}_2$.¹⁸

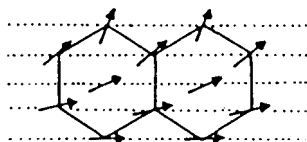


Figure 7. Helical arrangement of spins in the basal plane of NiBr_2 .

but that a new repeat distance of δ^{-1} has become established. Careful searching for higher order reflections ($n\delta$, $n\delta$, $3/2$) revealed none, so the arrangement of the moment vectors along (110) is sinusoidal. Another way of putting it is that the moments in each plane perpendicular to (110) are all parallel, but that on passing from each layer to the next there is a turn angle of $\pi\delta$, or about 5° , thus describing a helix (Figure 7).

To make quite sure that the direction of the helix is along (110) and that there are no other satellite peaks, one should scan over all crystal and scattering angles or, put in other words, search the whole region of the reciprocal lattice around (003/2), a tedious undertaking with a single-detector diffractometer that has to step and count through successive small solid angles. Fortunately, multidetectors for neutrons are now becoming available, thus permitting simultaneous counting at many reciprocal lattice points. For example, the D16 diffractometer at ILL has a ^3He detector containing 64×16 elements, subtending a maximum total angle of some 10° about the sample. With this instrument one can set the angle of the crystal and get good counting statistics for a mesh of 1024 reciprocal lattice points in about 5–10 min. Stepping the crystal angle and repeating the count, one may quickly search a large volume of reciprocal space.¹⁹ The result is shown as

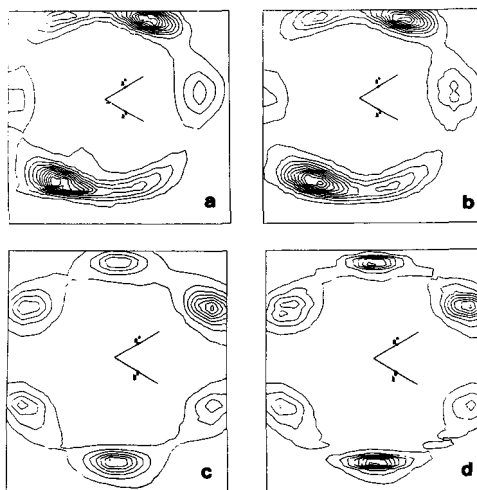


Figure 8. Neutron scattering intensity contours of magnetic satellites around (003/2): (a, b) NiBr_2 , observed and simulated; (c, d) $\text{Ni}_{0.91}\text{Fe}_{0.09}\text{Br}_2$, observed and simulated.¹⁹

a contour diagram in Figure 8a.

There are six satellite peaks forming a regular hexagon because in the absence of an applied magnetic field there are three equivalent spin orientations, along (110), ($\bar{1}10$), and (1 $\bar{1}0$). Actually the three pairs of satellites in Figure 8a do not have equal intensities, probably because the crystal was slightly strained on mounting. Above 23 K, the temperature of the incommensurate-commensurate transition T_{IC} , the hexagon vanishes and is replaced by a single peak centered at (003/2). Since only the temperature is changed, and the mosaic spread of the crystal and the resolution of the diffractometer remain the same, we can safely assume that the shape of the single (003/2) peak arising in the commensurate phase is the same as that of each of the ($\delta\delta 3/2$) satellites in the incommensurate phase. Without making any assumptions about how many pairs of satellites there are, we can model the total intensity by placing pairs of peaks around a ring of radius δ , varying their number and relative intensity to optimize the fit. The result of this procedure (Figure 8b) is in excellent agreement with the observed profile.

Our conclusion from neutron diffraction is therefore that from 52 to 23 K NiBr_2 has a collinear easy plane metamagnetic structure, but that at 23 K the spins begin to cant about the (110) direction, so that the angle between successive spins increases smoothly from zero to a maximum of about 5° . So far as is known, such behavior is unique among nonmetallic compounds. Why does NiBr_2 do it?

The Magnetic Phase Diagram

Superimposed on the layer structure in Figure 1B are the three types of near neighbors. In common with the other MX_2 having predominantly 90° superexchange pathways between the nearest neighbors, the J_n in NiBr_2 should be ferromagnetic. If J_{nn} and J_{nnn} are antiferromagnetic, however, the ground state could be

(19) Day, P.; Moore, M. W.; Wilkinson, C.; Ziebeck, K. R. A. *J. Magn. Mater.* 1985, 50, 1.

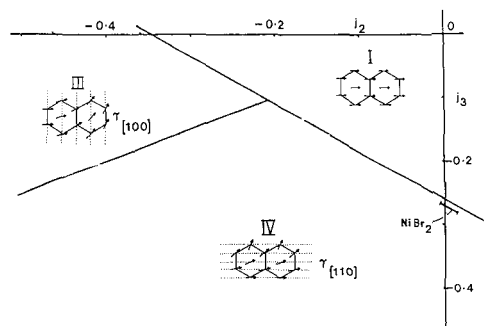


Figure 9. Calculated phase diagram for a planar hexagonal Heisenberg antiferromagnetic.²⁰ Phase II (not shown) is collinear antiferromagnetic.

a canted one. Some years ago Rastelli et al.²⁰ calculated the phase diagram for a planar triangular lattice as a function of $j_i = z_i J_i / z_{nn} J_{nn}$, where i represents (nn) and (nnn), with the result shown in Figure 9. Clearly, when j_{nn} and j_{nnn} are both positive, the lattice is ferromagnetic, but when either or both are negative, helical or antiferromagnetic phases are predicted. NiBr₂ lies within phase IV of Figure 9. To find the experimental values of the J_i , inelastic neutron scattering was carried out by using long-wavelength neutrons to concentrate on the lowest energy part of the magnon dispersion.²¹ We found that J_{nn} was zero within experimental error but that J_{nnn} was indeed negative, placing NiBr₂ just inside phase IV, but very close to the boundary of the collinear phase I.

The helical magnetic structure found in NiBr₂ at low temperature results from a very delicate and fortuitous balance of the various J_i . Raising the temperature forces the system across the boundary from phase IV to phase I. To see whether this was the result of lattice expansion altering J_i , we performed single-crystal neutron diffraction as a function of hydrostatic pressure.²² The result was surprising: δ decreases with increase of pressure, just as it does with increasing temperature, so the temperature-induced transition is not due to lattice expansion. The theorists' belief at the moment is that thermally excited spin fluctuations change the effective values of J_i .²³

Chemical Substitution

Given the extreme sensitivity of the magnetic structure to J_{nn} and J_{nnn} , chemical substitution should have some interesting effects. NiCl₂ is collinear (phase I, Figure 9) at all temperatures,²⁴ and NiI₂ has a temperature-independent helical structure,²⁵ though in

- (20) Rastelli, E.; Tassi, A.; Reatto, L. *Physica B*, 1979, 97B, 1.
 (21) Day, P.; Moore, M. W.; Wood, T. E.; Paul, D. Mc.; Ziebeck, K. R. A.; Regnault, L. P.; Rossat-Mignod, J. *Solid State Commun.* 1984, 51, 627.
 (22) Day, P.; Vettier, C. *J. Phys. C* 1981, 17, L195.
 (23) Rastelli, E.; Tassi, A. *J. Magn. Magn. Mater.* 1986, 54-57, 1147.
 (24) Lindgard, P. A.; Birgeneau, R. J.; Als-Neilsen, J.; Guggenheim, H. *J. Phys. C* 1975, 8, 1059.
 (25) Kuindersma, S. R.; Sanchez, J. P.; Haas, C. *Physica B* 1981, 111B, 231.

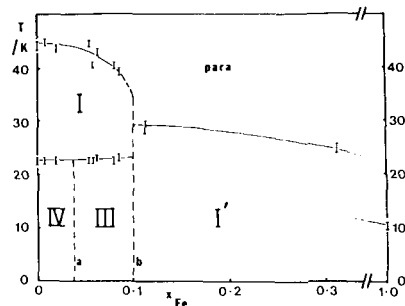


Figure 10. Observed magnetic phase diagram of Ni_{1-x}Fe_xBr₂ from neutron diffraction.¹⁸ The Roman numerals correspond to Figure 9.

neither case are j_{nn} and j_{nnn} known. Doping NiBr₂ with Cl⁻ rapidly reduces both δ and T_{IC} until above 10% substitution, no helical phase is seen.²⁶ Conversely, I⁻ increases both δ and T_{IC} .²⁷ Diluting the moments by substituting 8% Zn²⁺ for Ni²⁺ has virtually no effect on δ and only slightly reduces T_{IC} , but an exploration of the magnetic satellite structure around (003/2) showed that there was no longer any preferred direction of the helix within the layers. Instead of a hexagon of satellite peaks as in Figure 8, the scattering contours were fitted best by a ring.²⁸ Equally remarkable is the effect of Fe²⁺.²⁸ In FeBr₂ itself the moments lie parallel to the c axis, i.e., orthogonal to the Ni²⁺ moments in NiBr₂. Up to 3% Fe²⁺ doping, the NiBr₂ magnetic structure is unaffected, both as to T_{IC} and the magnitude and direction of δ . However, doping between 3 and 9% Fe²⁺ changes the direction of the helix from (110) to (100), although δ still has the same magnitude. This can be seen from the rotation of the satellite hexagon (Figure 8c,d).¹⁹ We have thus passed from phase IV to III. Above 9% Fe²⁺ the entire magnetic structure changes over the easy axis structure of FeBr₂ itself, because of the strong axial anisotropy of Fe²⁺ in this lattice geometry. The x, T phase diagram of Ni_{1-x}Fe_xBr₂ is shown in Figure 10.

Conclusion

This Account has described how a combination of optical spectroscopy and neutron scattering, combined with chemical substitution, has led to a better understanding of the unique magnetic behavior of NiBr₂. Structurally it is a very simple compound, but a delicate balance of competing ferro- and antiferromagnetic interactions produces a gamut of strange magnetic behavior.

Our group has been supported by the UK SERC, and access to neutron beams was provided by AERE Harwell and ILL Grenoble.

- (26) Day, P.; Turner, K.; Visser, D.; Wood, T. E. *Phys. Status Solidi B* 1982, 113, 623.
 (27) Moore, M. W.; Day, P.; Wilkinson, C.; Ziebeck, K. R. A. *Solid State Commun.* 1985, 53, 1009.
 (28) Day, P.; Moore, M. W.; Wilkinson, C.; Ziebeck, K. R. A. *J. Phys. C* 1981, 14, 3423.

Optical Properties of Ferromagnetic K_2CrCl_4

P. Day, A. K. Gregson, and D. H. Leech

University of Oxford, Inorganic Chemistry Laboratory, Oxford, England

(Received 7 November 1972)

The optical absorption spectrum of the ferromagnetic insulator K_2CrCl_4 has been measured from 8000 to 25 000 cm^{-1} and for temperatures between 4.2 and 300°K.

Ferromagnetic materials having discrete optical absorption bands, and hence regions of relative transparency in the visible, are rather uncommon. Indeed, in all the insulating ferromagnetic transition-metal compounds examined hitherto, the entire visible region is covered by a succession of broad overlapping ligand-field¹ or charge-transfer² bands. We now report preliminary optical studies of the three-dimensional ferromagnet K_2CrCl_4 , the visible absorption of which is almost entirely concentrated into two narrow spectral regions, sufficiently resolved from each other to permit quantitative measurements of the temperature variation of their oscillator strengths.

K_2CrCl_4 is a member of an extensive series of ternary halides formed by alkali metals and divalent 3d elements.^{3,4} X-ray powder photographs³ indicated a structure very similar to that of Cs_2CrCl_4 , which has the K_2NiF_4 structure. This conclusion is confirmed by a single-crystal x-ray study,⁵ which demonstrated that the unit cell is in fact orthorhombic ($a = 7.13$, $b = 7.34$, $c = 14.97$ Å), though the deviation from the tetragonal cell of the parent K_2NiF_4 structure is small. The magnetic susceptibility of a powder sample measured between 80–300°K has been extrapolat-

ed to give a Weiss constant of $+67 \pm 1$ °K.³ Further analysis^{3,6} of the same data using high-temperature series-expansion techniques^{7,8} applicable to a Heisenberg ferromagnet having a plane square lattice with $S = 2$ yielded an exchange integral of 5.0 ± 0.5 cm^{-1} . Magnetization measurements over the range 4.2–80°K⁹ confirm that the compound becomes ferromagnetic below 65°K.

Crystals of K_2CrCl_4 were grown from the melt in a Bridgman furnace. Because the plane of easy cleavage is perpendicular to the c axis, and thin crystals were needed for measurements of the two intense sharp visible transitions, good quality spectra were only obtained for light propagated along this axis (Fig. 1). Poorer-quality spectra recorded with the incident light perpendicular to c showed that while the axial and σ spectra were very similar, the π absorption was much weaker.¹⁰ By comparison with other Cr(II) spectra,¹¹ we assign the three broad bands between 8000 and 14 000 cm^{-1} to the low-symmetry components of 5D . If, in common with all other Cr(II) salts having strongly Jahn-Teller distorted ground states, we assume that the Cr site in K_2CrCl_4 is tetragonally elongated, the three bands are assigned to transitions from ${}^5B_{1g}({}^5E_g)$ to ${}^5A_{1g}({}^5E_g)$ and $({}^5B_{1g} + {}^5E_g)({}^5T_{2g})$.

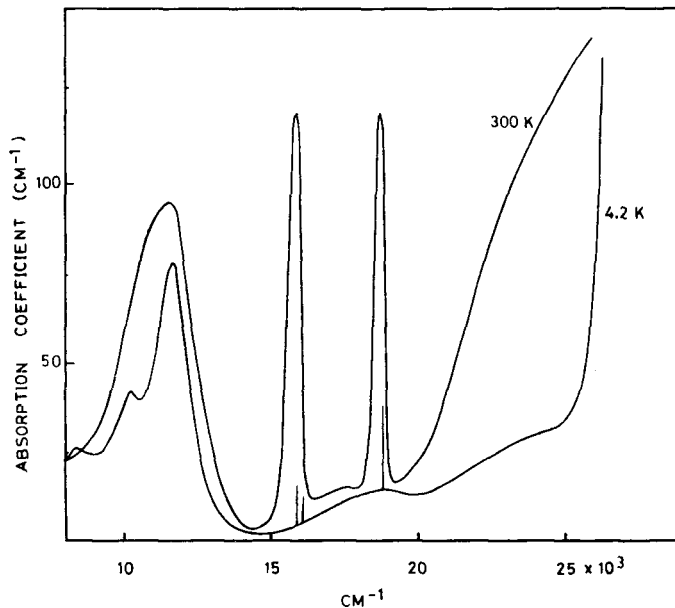


FIG. 1. Absorption spectra of a crystal of K_2CrCl_4 at 300 and 4.2°K. The incident light is propagated parallel to the c axis.

The most remarkable features in the optical spectrum of K_2CrCl_4 at 300°K are the two intense narrow lines at 15900 and 18700 cm^{-1} . They are much more intense relative to the quintet transitions than is normally observed in Cr(II) salts. Apart from these two lines, there are no other discrete absorption maxima in the visible region except for a weak and very ill-defined peak at about 17500 cm^{-1} . Even more remarkable is the behavior of the two narrow lines on lowering the temperature. As indicated in Fig. 1, at 4.2°K the intensity of the lines all but disappears. The band at 15900 cm^{-1} collapses to an extremely narrow line at 15892 cm^{-1} together with another, slightly broader line at 16062 cm^{-1} . The band at 18700 cm^{-1} becomes a narrow doublet, centered at 18726 cm^{-1} , with a splitting of 21 cm^{-1} . As the temperature is raised, all the narrow lines increase in intensity, and further lines appear at 16215 cm^{-1} and 18690 cm^{-1} when the temperature reaches about 23°K. At liquid-nitrogen temperature all the lines have coalesced into the two band envelopes seen at room temperature. The detailed temperature variation of the total oscillator strength of the 15900 cm^{-1} transition is shown in Fig. 2. The inset in this figure indicates that the limiting behavior of the oscillator

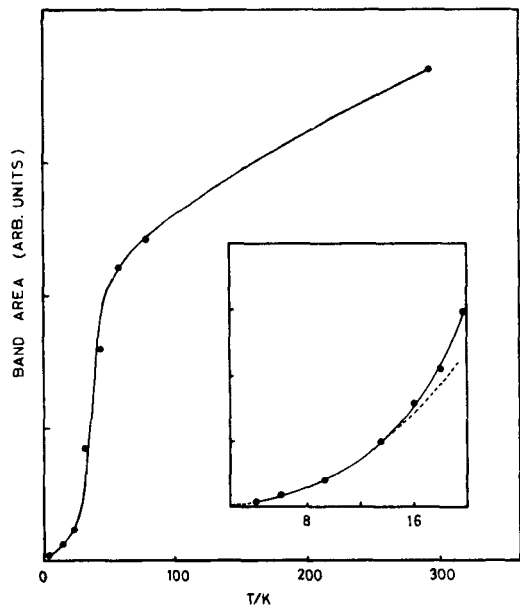


FIG. 2. Temperature variation of the intensity of the 15900 cm^{-1} transition in K_2CrCl_4 . The inset shows the detailed intensity variation from 4.2 to 20°K. The dashed line is $f = aT^2$.

strength below 20°K is quite well approximated as T^2 , drawn as the dashed line, normalized to 4.2°K, and to 0°K on the assumption that the oscillator strength is then zero. The temperature variation of the 18 700-cm⁻¹ band is somewhat similar, though there are differences in the detailed behavior below 65°K.

From the d^4 Tanabe-Sugano diagram¹² it is clear that any transitions in this spectrum between 14 000 and 25 000 cm⁻¹ are of triplet parentage. A phonon-assisted mechanism for the dipole strength of the 15 900- and 18 700-cm⁻¹ bands is ruled out by the unusual form of their temperature dependence, which bears no resemblance to a hyperbolic-cotangent function. On the other hand, second-order spin-orbit mixing with the components of ${}^5T_{2g}$ would not account for the unusually high intensity of the two lines. In fact, it appears qualitatively that their intensity is related to the magnetization. In antiferromagnets such as KNiF₃ the intensities of spin-forbidden ligand-field transitions follow the sublattice magnetization $M(T)$ quite closely, and depend on short-range order above T_N .¹³ In the present ferromagnetic example a more appropriate function, at least as a first approximation, would appear to be $1 - M(T)/M(0)$. Short-range order above T_c , and the contribution of vibronic intensity, could account for the departure of the experimental curve (Fig. 2) from this simple function. We believe, therefore, that the main contribution to the intensity of our two lines is an exchange-induced electric dipole mechanism. Since all the lines so far observed in the 14 000–20 000-cm⁻¹ region have similar temperature dependence, it seems likely that they are all exciton-magnon combinations and that with the equipment used to record the spectra in Fig. 1 (Cary type 14 spectrometer), the pure exciton lines remain undetected.

In contrast to the situation in antiferromagnets, which have been very widely studied, in ferromagnets only "hot-band"¹⁴ exciton-magnon absorption is possible. Either creation of an exciton is accompanied by annihilation of a thermally created magnon or the electronic excitation takes place from a thermally populated magnon state. Indeed, the temperature variation of the oscillator strength in Fig. 2 is remarkably similar to that calculated by Shinagawa and Tanabe¹⁴ for the "hot-band" contribution to the exciton-magnon electric dipole strength in an antiferromagnet. It is also worth noting that the energies of the sharp lines in K_2CrCl_4 remain invariant up to

78°K, an observation which is also consistent with absorption by the "hot-band" mechanism.

Precise assignments of the ligand-field excited states responsible for the two narrow absorption bands in K_2CrCl_4 are difficult to decide because of the density of triplet levels in the relevant region of the Tanabe-Sugano diagram. In O_h symmetry these are ${}^3T_{1g}$, 3E_g , ${}^3T_{1g}$, and ${}^3T_{2g}$ from 3H , ${}^3A_{2g}(a^3F)$, and ${}^3A_{1g}({}^3G)$. However, surveying known examples of d^4 ligand-field spectra, we find that in those compounds in which magnetic interactions, ferromagnetic or antiferromagnetic, are present [i.e., various binary and ternary Cr(II) fluorides^{15,16} and chlorides,⁴ CrI_2 ¹⁷ and MnF_3 ¹⁸], two relatively intense spin-forbidden transitions are always observed, between 15 000 and 20 000 cm⁻¹ in the Cr(II) compounds, and at 19 100 and 23 200 cm⁻¹ in MnF_3 . To aid the assignment we have diagonalized the d^4 ligand-field matrices with and without the assumption of tetragonal symmetry and including spin-orbit coupling. We find that with the assumption that the two intense bands result from analogous transitions in each case, their positions are well represented simply by the nephelauxetic variation of the Racah parameters B and C even though the compounds surveyed represent a wide variety of metal-ion site symmetries. This implies either (i) the ligand-field states retain their cubic symmetry, or (ii) the lower than cubic symmetry states are insensitive to distortions in the ligand field. For (i) the assignment would be ${}^3E_g - {}^3E_g({}^3H)$ and ${}^5E_g - {}^3A_{1g}({}^3G)$. If (ii) applied, and with the assumption that the sign of the tetragonal distortion is such that the ${}^5B_{1g}$ component of the ${}^5E_g(O_h)$ ground state lies lowest, the two tetragonal components of the excited O_h triplet states listed above would be ${}^3B_{1g}$ of ${}^3E_g({}^3H)$ and ${}^3B_{1g}$ of ${}^3A_{2g}(a^3F)$.

Further detailed investigations on K_2CrCl_4 and other members of the M_2CrX_4 series are in progress, and will be reported in due course.

We are grateful to the National Research Development Corporation for financial support, and to Imperial Chemical Industries Ltd. for a Postdoctoral Fellowship to A.K.G.

¹J. F. Dillon, H. Kamimura, and J. P. Remeika, Phys. Rev. Lett. **9**, 161 (1962).

²A. M. Clogston, J. Appl. Phys. **31**, 1985 (1960).

³H. J. Stefert and K. Klatyk, Z. Anorg. Chem. **334**, 113 (1954).

⁴D. H. Leech, Ph. D. thesis, Manchester University,

1971 (unpublished).

⁵T. S. Cameron, personal communication.

⁶D. H. Leech and D. Machin, to be published.

⁷G. S. Rushbrooke and P. J. Wood, *Mol. Phys.* **1**, 257 (1958).

⁸H. E. Stanley, *Phys. Rev.* **158**, 546 (1967).

⁹W. E. Gardner and A. K. Gregson, paper presented at the Tenth Conference on Vacuum Microbalance Technology, London, 1972 (to be published).

¹⁰Although K_2CrCl_4 is orthorhombic, we use the labels appropriate to a uniaxial crystal as an approximation because the a and b unit cell lengths are so nearly equal.

¹¹J. Ferguson, *Prog. Inorg. Chem.* **12**, 159 (1970).

¹²Y. Tanabe and S. Sugano, *J. Phys. Soc. Jap.* **9**, 753 (1964).

¹³V. V. Druzhinin, R. V. Pisarev, and G. A. Karamyshева, *Fiz. Tverd. Tela* **12**, 2239 (1970) [*Sov. Phys. Solid State* **12**, 1789 (1971)].

¹⁴K. Shinagawa and Y. Tanabe, *J. Phys. Soc. Jap.* **30**, 1280 (1971).

¹⁵A. Earnshaw, L. F. Larkworthy, and K. S. Patel, *J. Chem. Soc., A* **1966**, 363.

¹⁶W. W. Holloway and M. Kestigian, *Spectrochim. Acta* **22**, 1381 (1966).

¹⁷S. Jermin, Chemistry Part II thesis, Oxford, 1972 (unpublished).

¹⁸R. J. H. Clark, *J. Chem. Soc., London* **1964**, 417.

Magnetic Susceptibility and Magnetization of the Ionic Ferromagnets Dipotassium, Dirubidium, and Dicaesium Tetrachlorochromate(II)

By Anthony K. Gregson, Peter Day,* David H. Leech, and Malcolm J. Fair, Inorganic Chemistry Laboratory, South Parks Road, Oxford
W. E. Gardner, Materials Physics Division, A.E.R.E., Harwell, Didcot

High-temperature (300–80 K) susceptibility data are reported for polycrystalline samples of the ionic ferromagnets M_2CrCl_4 ($M = K, Rb, \text{ or } Cs$) and interpreted using the high-temperature series-expansion method for the quadratic-layer Heisenberg $S = 2$ ferromagnet to yield estimates of 7.0, 8.5, and 6.5 cm^{-1} for the nearest-neighbour exchange integrals. Low-temperature (80–4.2 K) magnetization measurements are also reported for polycrystalline Rb_2CrCl_4 and Cs_2CrCl_4 . In both compounds the magnetization obeys the equation $\{1 - [M(T)/M(0)]\} = CT^\gamma$ with $\gamma = 1.54$ up to 60 K, *i.e.* ca. $0.9 T_c$. Saturation magnetizations are ca. 0.4 B.M. lower than expected for $S = 2$ ions.

THREE-DIMENSIONAL ferromagnetism in ionic compounds is extremely rare, and the small number of examples available up till now have been intensively studied, both for their intrinsic interest, and for technological reasons.¹ The first ionic ferromagnet to be discovered was $Y_3Fe_5O_{12}$ (YIG),² followed by EuO ³ and $CrBr_3$ ⁴ and more recently by K_2CuF_4 ⁵ and $[Fe(\text{phen})_2Cl_2]$ (phen = 1,10-phenanthroline).⁶ Recent magnetic-susceptibility measurements^{7–9} on the series M_2CrCl_4 ($M = K, Rb, \text{ or } Cs$) suggested that they too ordered ferromagnetically, with Curie temperatures in the region of 65 K. We therefore decided to examine their physical properties in more detail, particularly the relation between the magnetic ordering and the optical properties in the visible region of the spectrum.

Neutron diffraction from powdered Cs_2CrCl_4 ¹⁰ and single-crystal Rb_2CrCl_4 ⁹ confirms the ferromagnetic ordering in these two compounds. In the latter,^{9,11} as also in K_2CrCl_4 ,¹² the onset of ferromagnetic ordering is accompanied by some very startling changes in the visible absorption spectrum. At 300 K several of the spin-forbidden ligand-field transitions are quite intense, but below the Curie temperature their intensity falls rapidly. Thus at 4.2 K the entire visible region from

14 000 to 25 000 cm^{-1} is very nearly transparent. Qualitatively, this effect may be explained by an exchange-coupled electric-dipole-intensity mechanism since in a ferromagnet electronic transitions which lead to a decrease in the spin projection of the crystal (*e.g.* quintet-to-triplet ligand-field excitations) can only become electric-dipole allowed if thermally excited magnons which also decrease the spin projection are simultaneously annihilated. To understand such effects in detail, a more complete analysis of the magnetic susceptibility is clearly needed. On the other hand there are also good reasons why the magnetic properties of the M_2CrCl_4 series are interesting and important in their own right.

The compounds have the K_2NiF_4 structure^{10,13} so that in Cs_2CrCl_4 , for example, there is a two-dimensional network of Cr and Cl atoms, each Cr being surrounded by four others, with 180° Cr–Cl–Cr bonds. Each layer is separated from the next by two layers with the stoichiometry CsCl, each Cl completing the octahedral coordination about a Cr ion (Figure 1). The resulting anisotropy in the exchange interaction is evident in the high-temperature ($T > T_c$) susceptibility and low-temperature ($T < T_c$) magnetization data. The properties of these compounds may also be relevant to the

¹ See, for example, D. F. Nelson, *Sci. Amer.*, 1968, **218**, 17.

² R. Pauthenet, *Ann. Physique*, 1958, **3**, 424.

³ B. T. Mathias, R. M. Bozorth, and J. H. Van Vleck, *Phys. Rev. Letters*, 1961, **7**, 160.

⁴ For example, see H. L. Davis and A. Narath, *Phys. Rev.*, 1964, **A124**, 433.

⁵ I. Yamada, *J. Phys. Soc. Japan*, 1972, **23**, 979.

⁶ W. M. Reiff and S. Foner, *J. Amer. Chem. Soc.*, 1973, **95**, 260.

⁷ L. F. Larkworthy and J. K. Trigg, *Chem. Comm.*, 1970, 1221.

⁸ D. H. Leech, Ph.D. Thesis, Victoria University of Manchester, 1971.

⁹ M. J. Fair, Chemistry Part II Thesis, Oxford, 1973.

¹⁰ M. T. Hutchings, A. K. Gregson, P. Day, and D. H. Leech, *Solid-State Comm.*, 1974, **15**, 313.

¹¹ A. K. Gregson, P. Day, and M. J. Fair, Autumn Meeting, The Chemical Society (Dalton Division), University of East Anglia, September 1973.

¹² P. Day, A. K. Gregson, and D. H. Leech, *Phys. Rev. Letters*, 1973, **30**, 19.

¹³ H. J. Seifert and K. Klatky, *Z. anorg. Chem.*, 1964, **334**, 113.

1975

1307

current controversy¹⁴ about the existence or otherwise of phase transitions in two-dimensional lattices.

In the present paper we report susceptibility measurements on powdered samples of M_2CrCl_4 ($M = K, Rb, \text{ or } Cs$) from 300 to 80 K, which we analyse by high-temperature series-expansion methods, and also magnetization measurements at 4.2 K. Single-crystal neutron-diffraction, including polarized, measurements, and an extended description of the optical properties will be published separately. A brief preliminary account of the high-temperature (300–80 K) powder-susceptibility data on K_2CrCl_4 and Cs_2CrCl_4 has recently appeared.¹⁵

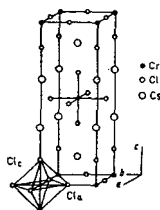


FIGURE 1. Crystal structure of Cs_2CrCl_4 . The Cr^{2+} ion is surrounded by a tetragonally compressed octahedron of chlorine atoms. Bond distances are $Cr-Cl_a$ 2.609 and $Cr-Cl_c$ 2.399 Å where Cl_a and Cl_c are the chlorine atoms on the a and c axes respectively.¹⁰

EXPERIMENTAL

Samples used for the susceptibility measurements were prepared by two different methods: K_2CrCl_4 and Rb_2CrCl_4 were obtained by melting $CrCl_3$ and the appropriate alkali-metal halide together in the correct stoichiometric ratio;⁶ in the second method, which was employed for K_2CrCl_4 and Cs_2CrCl_4 , molten $CrCl_3$ was treated with the alkali-metal halide in the presence of excess of chromium metal, the excess of unchanged metal being removed by high-temperature filtration.⁸ Crystalline samples of the congruently melting salts K_2CrCl_4 and Rb_2CrCl_4 were grown from the melt in a Bridgeman furnace and then finely ground.

The magnetic-susceptibility measurements on K_2CrCl_4 and Cs_2CrCl_4 from 300 to 77 K were made using a Gouy balance, at field strengths in the range 1.5–6.5 kOe.* All measurements on Rb_2CrCl_4 , and those on K_2CrCl_4 and Cs_2CrCl_4 below 77 K, were made on a Faraday balance at the Materials Physics Division, A.E.R.E., Harwell.¹⁶ For the latter, the samples were placed inside a Perspex sphere and suspended by a fine silica wire from a Sartorius vacuum microbalance. The magnetic field was furnished by a superconducting solenoid. The crystallites were free to orientate themselves inside the Perspex sphere, and it is therefore anticipated that the direction of easy magnetization lies parallel to the magnetic field. The Faraday measurements were made down to 4.2 K and at field strengths up to 41 kOe.

* 1 Oe = $(10^{21}N)^{1/2}$ cm⁻¹, 1 B.M. $\approx 9.27 \times 10^{-24}$ A m².

¹⁴ For example, recent evidence for and against is presented respectively in (a) H. K. Charles and R. I. Joseph, *Phys. Rev.*, 1973, **B7**, 2046; (b) K. Yamaji and J. Kondo, *J. Phys. Soc. Japan*, 1973, **35**, 25.

¹⁵ D. H. Leech and D. J. Machin, *J.C.S. Chem. Comm.*, 1974, 866.

RESULTS

High-temperature Susceptibility—The Table records the effective magnetic moments of K_2CrCl_4 , Rb_2CrCl_4 , and Cs_2CrCl_4 at 300 and 90 K. The small differences between our results and Larkworthy's⁷ are most likely due to preparative difficulties and impurities. To investigate the detailed temperature dependence using the high-temperature

	Magnetic-moment data		θ °/K	Ref.
	$\mu(300 \text{ K})$ / B.M.	$\mu(90 \text{ K})$ / B.M.		
K_2CrCl_4	5.34	8.90		7
	5.54	8.93	67.5	8 ^b
	5.61	9.32	64.5	8 ^c
	5.80	11.30		7
Rb_2CrCl_4	5.80	11.65	82	d
Cs_2CrCl_4	5.78	11.60		7
	5.53	10.05	77	8

* Curie-Weiss θ in $\chi = C/(T - \theta)$. ^{b,c} Two different preparations. ^d This work; normalized to data at 300 K in ref. 1.

series-expansion method, we therefore used the average values of the magnetic moments of the three compounds. Corrections for both the diamagnetism of the constituent atoms and temperature-independent paramagnetism (t.i.p.) were made. For the formal 5E ground state of the high-spin d^4 configuration, the t.i.p. contribution is $4N\beta^3/10Dq$ ¹⁷ (usual symbols) and with $10Dq$ ca. $10\,000 \text{ cm}^{-1}$ ¹⁸ we take this to be $100 \times 10^{-6} \text{ cm}^3 \text{ mol}^{-1}$. Apart from the t.i.p. contributions, any departures from Curie behaviour should only be due to the effect of the exchange interaction because even in formal octahedral symmetry the ground 5E state behaves magnetically as an orbital singlet, any orbital contributions being absorbed into the variation of the g value from 2.0023. Room-temperature magnetic-moment values of 5.8 B.M. of, for example, Rb_2CrCl_4 are to be compared with magnetic moments of 4.89 B.M. at 300 K for the magnetically dilute $Rb_2[CrCl_4(H_2O)_2]$,⁷ quite close to the spin-only value of 4.90 B.M. Even more striking are the moments at 90 K, which for $Rb_2[CrCl_4(H_2O)_2]$ is 4.91 B.M. whereas for the ferromagnetic anhydrous compound it is 11.3 B.M.⁷

To examine the temperature variation of the susceptibility above T_c we made use of series expansions. Assuming a Heisenberg-exchange Hamiltonian, and confining the exchange to nearest neighbours, Rushbrooke and Wood calculated exact series-expansion formulae for the paramagnetic susceptibility in powers of reciprocal temperature up to six for arbitrary spin and wide range of lattice structures.¹⁸ More recently, Lines¹⁹ re-examined the series for the quadratic-layer Heisenberg antiferromagnet using the

$$H = \sum_{n,m} J_{nm} S_i \cdot S_j \quad (1)$$

exchange Hamiltonian (1) where n,m covers all pairs of nearest-neighbour spins i and j . The power series in reciprocal susceptibility is then given by (2) where $\theta =$

$$\frac{Ng^2\beta^2}{\chi J} = 3\theta + \sum_{n=1}^{\infty} \frac{C_n}{\theta^{n-1}} \quad (2)$$

$kT/JS(S+1)$ and the coefficients C_n depend on the value

¹⁸ W. E. Gardner and A. K. Gregson, *Proc. Vac. Microbalance Techniques*, 1973, **2**, 183.

¹⁷ B. N. Figgis, 'Introduction to Ligand Fields,' Interscience, 1968, p. 266.

¹⁹ G. S. Rushbrooke and P. J. Wood, *Mol. Phys.*, 1968, **1**, 257.

¹⁸ M. E. Lines, *J. Phys. and Chem. Solids*, 1970, **31**, 101.

1308

of the spin S , other symbols having their usual meanings. Remembering that for the ferromagnetic interaction the coefficients C_n are to be multiplied by $(-1)^n$, the series for $Ng^2\beta^2/\chi = \frac{1}{2}kT + J(-4 + 9x - 9.0720x^2 + 55.7280x^3 - 160.7040x^4 + 116.64x^5)$ (3)

$S = 2$ becomes (3) where $x = J/kT$. Choosing $g = 1.98$ (appropriate to the average g value of a typical Cr^{II} compound such as $\text{CrSO}_4 \cdot 5\text{H}_2\text{O}$)²⁰ equation (3) gave an excellent fit to the high-temperature susceptibility data on K_2CrCl_4 with $J = 7 \text{ cm}^{-1}$ (Figure 2). The non-linearity

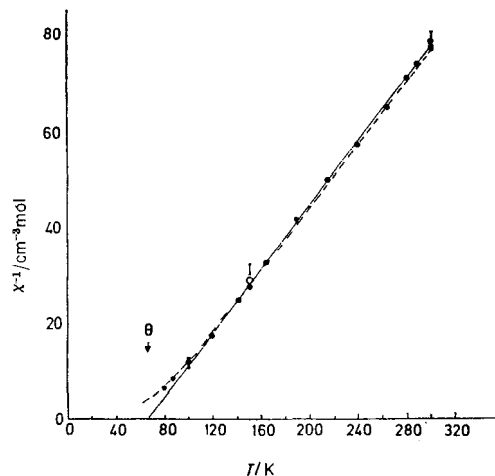


FIGURE 2 Plot of reciprocal susceptibility against temperature for K_2CrCl_4 : (●), Gouy data; (○), Faraday data; (—), Curie-Weiss plot; and (---), equation (3) with $g = 1.98$ and $J = 7.0 \text{ cm}^{-1}$

of the reciprocal susceptibility against temperature plot below *ca.* 115 K is characteristic of ferromagnetic interactions with the presence of short-range order.

Equation (3) gave only a fair fit to the high-temperature susceptibility data on Rb_2CrCl_4 and Cs_2CrCl_4 (Figures 3 and 4), the optimum values of J being 8.5 and 6.5 cm^{-1} respectively. To improve the gradient of the plot of χ^{-1} against T for Cs_2CrCl_4 a g value of 1.90 and $J = 8 \text{ cm}^{-1}$ was sufficient for acceptable agreement down to *ca.* 115 K, but 1.90 is rather low for normal paramagnetic Cr^{II} compounds. Other possible reasons for the poorer fit to the Rb_2CrCl_4 and Cs_2CrCl_4 data are that the interaction may have some three-dimensional character or, alternatively, that the Heisenberg interaction may have a small XY-like anisotropy. However, the magnetic properties of K_2CuF_4 , another ferromagnet with the K_2NiF_4 structure,⁵ were accurately described by the series expansion for the strictly two-dimensional plane-square lattice with $S = \frac{1}{2}$, and furthermore the interaction had only *ca.* 1% XY-like anisotropy. Thus we conclude that these two factors are probably not responsible for the difference in gradient between the calculated and experimental χ^{-1} against T plots. The difference in gradient might also be caused by a slight error in the mass of the very small amount of sample used. However, we do not think this likely as the limiting saturation magnetizations of the three polycrystalline compounds at 4.2 K (see below) are very similar.

The saturation magnetizations are reduced from the normal value of 4.0 B.M. for the $S = 2 \text{ Cr}^{\text{II}}$ ion to *ca.* 3.6 B.M., another fact which may be responsible for the departures from the ideal isotropic Heisenberg interaction in

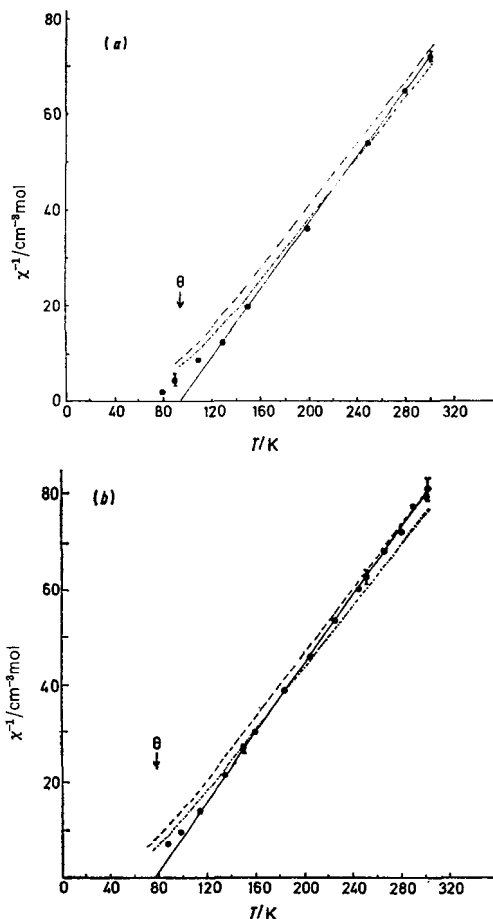


FIGURE 3 Plots of reciprocal susceptibility against temperature for Rb_2CrCl_4 (a) and Cs_2CrCl_4 (b): (●), Gouy data; (○), Faraday data; (—), Curie-Weiss plot; (---), and (···), equation (3) with $g = 1.98$ and $J = 8.0$ and 9.0 cm^{-1} respectively [J 6.0 and 7.0 cm^{-1} for (b)]

the two-dimensional lattice. However, rather than speculate further, at this point we merely conclude that the high-temperature susceptibility data on K_2CrCl_4 appears to be well described by the isotropic Heisenberg series expansion appropriate to the square lattice with J *ca.* 7.0 cm^{-1} whereas in Rb_2CrCl_4 and Cs_2CrCl_4 $J = 8.5$ and 6.5 cm^{-1} , respectively, although the agreement is not as good. These values of J may be compared with that of *ca.* 7 cm^{-1} obtained by Okiji²¹ from the temperature variation about T_c of the oscillator strengths of the two quintet-triplet ligand-field transitions,

²⁰ K. Ono, S. Koide, H. Sekiyama, and H. Abe, *Phys. Rev.*, **1954**, **96**, 38.

²¹ A. Okiji, personal communication and unpublished work.

1975

1309

using the simple pairwise approximation. A value of J of similar magnitude also gives a good account of the complicated temperature-dependent intensities of the same transitions between 4 and 10 K.²¹

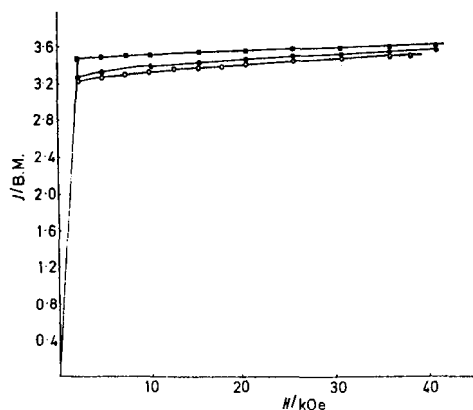


FIGURE 4 Plot of magnetization against applied magnetic field for polycrystalline samples of K_2CrCl_4 (●), Rb_2CrCl_4 (○), and Cs_2CrCl_4 (■), at 4.2 K

Low-temperature Magnetization.—At 4.2 K polycrystalline samples of all three compounds saturated in applied fields greater than 2 kOe in a manner characteristic of simple

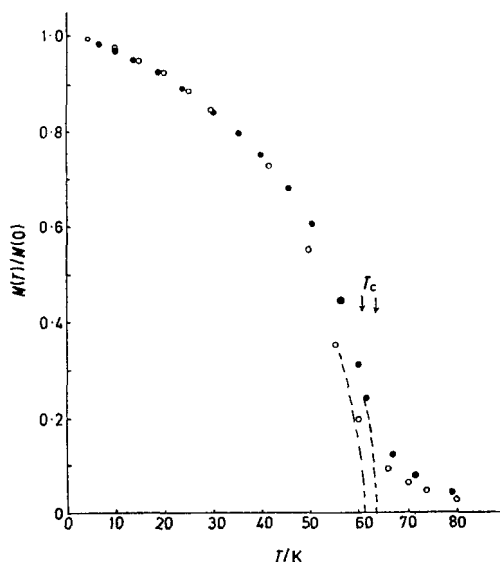


FIGURE 5 Plot of reduced magnetization against temperature for polycrystalline samples of Rb_2CrCl_4 (●) and Cs_2CrCl_4 (○), measured in 2.31 kOe

ferromagnets. The saturated magnetic moments of 3.5–3.6 B.M. (Figure 4) are rather lower than the value of 4.0 expected for the $S = 2 Cr^{II}$ ion. Both the very small amounts

²¹ K. Hirakawa and H. Ikeda, *J. Phys. Soc. Japan*, 1973, **35**, 1328.

of metal-halide impurity detected in the powder neutron-diffraction pattern¹⁰ and experimental error in the measurements would tend to reduce the observed magnetic moment. However, the major factor responsible for reducing the saturated magnetization below 4.0 B.M. is probably covalency, as discussed later.

Temperature Variation of the Magnetization.—A sensitive test of the effect of dimensionality on the magnetic properties of a ferromagnet is the temperature variation of the magnetization from zero to ca. $0.5 T_c$ and then, to test theories concerning critical phenomena, around T_c itself. The reduced magnetizations $M(T)/M(0)$ for Rb_2CrCl_4 and Cs_2CrCl_4 are plotted in Figure 5, $M(0)$ being the magnetization between 4.2 and 10 K extrapolated to 0 K and $M(T)$ the magnetization between 4.2 and 80 K. The data on these two compounds are very similar except near T_c where the larger value of J deduced from the high-temperature series expansion for Rb_2CrCl_4 reflects the higher T_c . The large ‘tails’ in the magnetizations for both compounds between 60 and 80 K make it difficult to obtain precise values for T_c . No data on K_2CrCl_4 have been included in Figure 5 since we could not obtain consistent results for this compound.

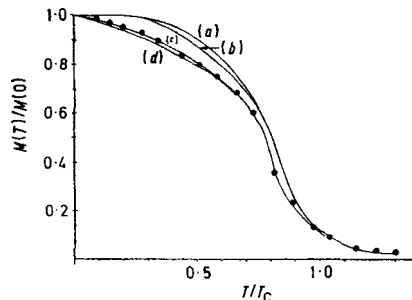


FIGURE 6 Plot of reduced magnetization against temperature for Rb_2CrCl_4 : (—), calculated using Weiss molecular-field theory and the Brillouin function, after Smart;²² $S = \infty$ (a), 1 (b), 2 (c), and 20 (d)

For both Rb_2CrCl_4 and Cs_2CrCl_4 the reduced magnetization may be expressed empirically as a function of temperature by (4). With $C = 0.0091$ and $\gamma = 1.54$ this expression represents the reduced magnetization quite well up to

$$\{1 - [M(T)/M(0)]\} = CT^\gamma \quad (4)$$

nearly 60 K, i.e. ca. $0.9 T_c$. That equation (4) fits the reduced magnetization up to such a high fraction of T_c is quite remarkable because in most magnetic compounds the reduced magnetization against temperature curves depart from such a simple expression by at most $0.5 T_c$ and often at much lower temperatures. An exception relevant to the present example is K_2CuF_4 ,²³ the reduced magnetization

$$\{1 - [M(T)/M(0)]\} = 0.0299 T^{3/2} \quad (5)$$

of which could be expressed as in (5) up to ca. $0.64 T_c$ (T_c 6.25 K).

The simplest method of relating reduced magnetization to temperature is through the Weiss molecular-field model, using a Brillouin function, as described, for example, by Smart.²² Curves calculated using the experimental values of $M(T)/M(0)$ are illustrated for Rb_2CrCl_4 in Figure 6. At

²² J. S. Smart, ‘Effective Field Theories of Magnetism,’ W. B. Saunders Company, 1966, p. 25.

1310

temperatures well below T_c the experimental reduced magnetization is much smaller than expected for an $S = 2$ system; in fact the best fit is for $S = 20!$ Clearly no physical significance can be attached to this value of S , which simply illustrates the inadequacy of the molecular-field approximation for the present series of compounds. For temperatures well below T_c , particularly near zero, a spin-wave description of the magnetization behaviour is much more appropriate. In the spin-wave description of three-dimensional magnetic behaviour the magnetization decreases much more rapidly at temperatures just above zero than predicted by molecular-field theory. Bloch's

$$\frac{M(T)}{M(0)} = 1 - \frac{T^{3/2}}{T_B} - \text{etc.} \quad (6)$$

equation, (6), where $T_B = 21 S^{5/3} J/k$ for the body-centred cubic lattice, agrees well with experiment at temperatures much less than $0.5 T_c$. At higher temperatures, and especially in three-dimensional systems, spin-wave interactions lead to higher terms in equation (6), which can be derived by considering spin-wave renormalization.

DISCUSSION

In all three M_2CrCl_4 compounds we have examined the strongly rising magnetic moments with decreasing temperature provide clear evidence of ferromagnetic interactions, amply confirmed by the magnetization measurements at 4.2 K and up to T_c . The existence of magnetic order at finite temperatures in predominantly two-dimensional materials such as those with K_2NiF_4 structures has in the past posed several theoretical problems. The original prediction for two-dimensional spin arrays with isotropic Heisenberg interactions was that no long-range order could be established above absolute zero²⁴ so there would be no phase transition. However, numerical evidence from high-temperature series-expansion techniques supports the existence of a phase transition in the two-dimensional Heisenberg model.^{14a,25} The formula (7) reproduces these latest

$$kT_c^{(2)}/J = (12/5)[z - (5/z)](4S + 3)^{-1} \quad (7)$$

numerical results^{14a} and hence, for the square lattice ($z = 4$) and $S = 2$, we would anticipate that $kT_c^{(2)}/J = 0.33$, a result which clearly does not hold for Rb_2CrCl_4 and Cs_2CrCl_4 . On the other hand it must be recognized that in real systems there is often an anisotropy in the exchange interaction which will normally induce a magnetic ordering, even when the superexchange is dominated by a one- or two-dimensional path.

Of course any interlayer exchange automatically gives the system three-dimensional character and so the question of a two-dimensional phase transition does not arise. On the other hand, using a Green's function approach with wave-vector-dependent magnon renormalization, Lines²⁶ showed that, in a two-dimensional system and for any spin, $kT_c^{(2)}$ is *ca.* $1.19JS(S+1)$ which in the present case would predict T_c to be 87 or 67 K for

²⁴ N. D. Mermin and H. Wagner, *Phys. Rev. Letters*, 1966, **17**, 1133.

²⁵ H. E. Stanley and T. A. Kaplan, *Phys. Rev. Letters*, 1966, **17**, 913.

²⁶ M. E. Lines, *Phys. Rev.*, 1971, **3**, 1749.

Rb_2CrCl_4 and Cs_2CrCl_4 respectively, close to the observed critical temperatures. It is interesting to compare the predicted two-dimensional ordering temperatures with those predicted for three-dimensional body-centred cubic lattices. In the latter¹⁸ equation (8) is applicable and so $T_c^{(3)}$ would be 62 and 47 K for Rb_2CrCl_4 and Cs_2CrCl_4 .

$$kT_c^{(3)}/J = (5/192)(z-1)[11S(S+1)-1] \quad (8)$$

These theoretical relations between T_c and J do not lead to estimates of T_c which are very sensitive to the dimensionality of the exchange. For example, the anisotropy energy, which is difficult to predict, probably provides the reason for the stability of the long-range order. Nevertheless, the effect of the dimensionality of the exchange is brought out clearly by several other experimental observables. The first is the temperature dependence of the magnetization above 4.2 K. As Figure 6 shows, the Weiss molecular-field theory, which assumes an isotropic Heisenberg interaction in three dimensions, is by no means an adequate description of the magnetization of Rb_2CrCl_4 and Cs_2CrCl_4 . This is because two-dimensional systems have a much larger proportion of low-energy magnons than three-dimensional ones so the magnetization decreases much more rapidly as the temperature is raised. At higher temperatures no simple theory is likely to be really adequate, even with renormalization modifications, because excitation processes near the transition or critical region become important. In two-dimensional lattices such processes extend over a much wider temperature range, both above and below the transition temperature, than in three-dimensional lattices, and are responsible for the pronounced short-range-order effects observed, for example, in Figures 2, 3, and 5. In Figures 2 and 3 the reciprocal susceptibility diverges from the Curie-Weiss behaviour well above the predicted T_c ; in Figure 5 the magnetization does not continue to fall towards zero but retains a sizeable value well past the temperature at which $M(T)$ goes to zero by simple extrapolation of the low-temperature magnetization. Both types of behaviour are quite characteristic of two-dimensional systems. Finally, the reduction in the moments of the M_2CrCl_4 compounds is most plausibly attributed to covalency. Thus, for example, a moment reduction of 4.1% due to covalency alone has been found in MnO ²⁷ while the total reduction of 13% in the moment of K_2CuF_4 ²² has been ascribed to covalency, as demonstrated by paramagnetic diffuse neutron scattering.²⁸

The only other ferromagnetic compound in any way related to those we have described in this paper is K_2CuF_4 ,^{5,22,28} which also has the K_2NiF_4 structure. Both magnetic and neutron-scattering measurements have been made on K_2CuF_4 and, as in the chromium compounds, the magnetization can be represented by a

²⁷ A. J. Jacobson in 'Chemical Applications of Thermal Neutron Scattering,' ed. B. T. M. Willis, Oxford University Press, 1973, ch. 12.

²⁸ K. Hirakawa and H. Ikeda, *J. Phys. Soc. Japan*, 1973, **35**, 1608.

1975

1311

simple $T^{3/2}$ dependence up to $0.86 T_c$ (T_c 6.25 K). Again this is a result of the low dimensionality of the system so that magnon interactions, and hence renormalization effects, are small. In Figure 7 the magnetization curves for K_2CuF_4 , K_2NiF_4 , and K_2MnF_4 are

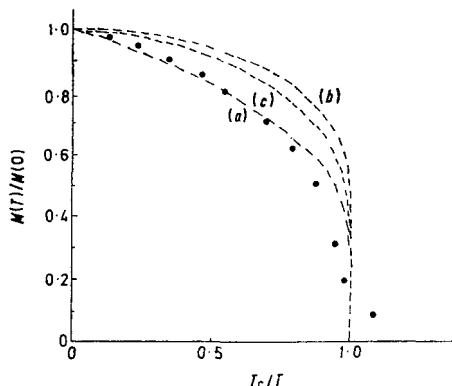


FIGURE 7 Comparison of the reduced magnetizations for K_2CuF_4 (a), K_2NiF_4 (b), and K_2MnF_4 (c) with Rb_2CrCl_4 (●)

plotted for comparison with data for Rb_2CrCl_4 . The similarity between the two ferromagnets is very noticeable, at least in the low-temperature region. In K_2CuF_4 the three-dimensional ordering is apparently due to inter-layer coupling because the single-ion anisotropy is zero and dipole-dipole interactions are very small. Because the contributions to the anisotropy energy are either zero or small, the spins in K_2CuF_4 are aligned perpendicular to the c axis. However, it should be noted that in the M_2CrCl_4 compounds an analysis of the unpolarized neutron-diffraction data on powders and single crystals

²⁹ J. B. Goodenough, 'Magnetism and the Chemical Bond,' Interscience, 1966, p. 222.

shows that the magnetic moment lies at an angle of 34° to the c plane,³⁰ presumably because of the various competing contributions to the anisotropy field.

The actual mechanism of the intralayer ferromagnetism in M_2CrCl_4 must lie in the $180^\circ 3d^4$ -anion- $3d^4$ interaction, corresponding to half-filled e_g -empty e_g cation-anion-cation superexchange. According to Goodenough's description the ferromagnetic interaction arises from Jahn-Teller effects, approximating to his 'quasistatic' limit,²⁹ a situation which has been re-examined recently by Khomskii and Kugel.³⁰

In summary, the compounds K_2CrCl_4 , Rb_2CrCl_4 , and Cs_2CrCl_4 appear to be typical two-dimensional ferromagnets. Although the actual critical temperatures may not reflect their dimensionality very precisely, the magnitude and temperature dependence of the susceptibility can be explained at least qualitatively using relatively simple theory appropriate to the two-dimensional lattice. In contrast, both in the M_2CrCl_4 series and in K_2CuF_4 , the $T^{3/2}$ dependence of the magnetization is more in line with a three-dimensional isotropic Heisenberg-interaction model although the significance of the proportionality constant C remains unclear. However, in the three-dimensional Heisenberg ferromagnet the description of the magnetization in terms of a single temperature exponent is in any case expected to hold only up to a small fraction of T_c whereas in the present compounds and K_2CuF_4 the simple $T^{3/2}$ dependence holds nearly up to T_c . Experiments now in progress on the spin-wave dispersion in Rb_2CrCl_4 may throw further light on this question.

We are grateful to the National Research Development Corporation for support and to Imperial Chemical Industries Ltd. for the award of a postdoctoral fellowship (to A. K. G.).

[4/2267 Received, 4th November, 1974]

³⁰ D. I. Khomskii and K. I. Kugel, *Solid-State Comm.*, 1973, **13**, 763.

This page intentionally left blank

CHAPTER 5

This page intentionally left blank

Molecule-Based Magnets

Although it is now a cornerstone of the new discipline of materials chemistry, the phrases 'molecular magnetism' and 'molecule-based magnets' remains wreathed in ambiguity. Molecules may be magnetic (i.e. paramagnetic) if they are organic radicals containing unpaired p-electrons or metal complexes containing unpaired d- or f-electrons, but that is not the import of the word 'magnetism' in that context. In practice, it denotes lattices of paramagnetic molecular entities assembled in such a way that they interact ferro- or anti-ferromagnetically to give long-range magnetic order. The phrase 'molecule-based magnets' first sprang to prominence in the 1980s as a result of the proselytising efforts principally by Kahn [1] and Miller [2], but in a wider historical perspective, it can be seen as a natural extension of coordination complexes into the realm of supramolecular chemistry.

In fact, the first examples of ferromagnetic lattices built from molecular building blocks (what Kahn expressively called 'bricks') dated back to earlier days, even though their importance was not recognised widely at the time; even the ferromagnetic tetrahalogeno-chromates described in Chap. 4 might be construed as molecular, in the sense that they were crystallised from complexes in solution. In fact, the first ferromagnet made from unambiguously molecular units was discovered serendipitously more than a decade earlier and was characterised by all the conventional physical means short of neutron scattering [3]. Even before that, the grand-daddy of all mixed valency compounds, Prussian Blue, was also surprisingly shown to be a ferromagnet [4], a curious circumstance that was already explained quantitatively in 1976 [5] (see Chap. 3). Prussian Blue, $\text{Fe}^{\text{III}}_4[\text{Fe}^{\text{II}}(\text{CN})_6]_3 \cdot 14\text{H}_2\text{O}$ in its crystalline form, is one of those compounds that prompts the question of what is a molecular magnet?, since it consists of a simple cubic lattice of alternating Fe^{II} and Fe^{III} , bridged by CN^- . Many comparable lattices are formed by other ambidentate ligands such as NCS^- and $[\text{C}_2\text{O}_4]^{2-}$, the oxalato- and dithio-oxalato series being particularly rich and varied. The present chapter outlines our own studies of just two specific groups of molecule-based magnets, one based on oxalate bridging groups and the other on ion-radical salts. In each instance, we found quite unusual magnetic properties, quite distinct from those of continuous lattice solids.

As far as the oxalates are concerned, we showed that the series of bimetallic salts $\text{A}[\text{M}^{\text{II}}\text{Fe}^{\text{III}}(\text{C}_2\text{O}_4)_3]$, where A is an organic mono-cation and M^{II} a 3d ion had a complicated and subtle relationship between bulk magnetism and structural detail.

These compounds, the first examples of which were made in Japan in the early 1990s [6], consist of hexagonal honeycomb layers of alternating M^{II} and Fe^{III} bridged by oxalate anions, so that each metal ion is surrounded by a trigonally-distorted octahedron of O atoms. This structural arrangement, while basically quite simple, contains several subtle features. Firstly, the overall symmetry of the inorganic layer opens the possibility of finding magnetic frustration, which occurs when there is no unique long-range-ordered ground state, but rather a plethora of different spin arrangements with more or less equal energies. Secondly, because there are three bidentate ligands around each metal ion, the coordination resembles that of a three-bladed propeller or screw. This means that the sense of the screw can be either right- or left-handed, or the metal ion environment is chiral. In fact, a moment's reflection will show that such a two-dimensional honeycomb structure can only be built up when alternate metal ion environments have opposing chirality; that if all the M^{II} are Λ , all the Fe^{III} are Δ or *vice versa*. The '*vice versa*' is interesting too. If we make the solid from racemic starting materials (as is clearly the simplest thing to do), alternate layers can be expected to have different distributions of Δ and Λ like $[M^{II}(\Delta)Fe^{III}(\Lambda)]_A[M^{II}(\Lambda)Fe^{III}(\Delta)]_B \dots$, where AB... describes the stacking of the layers. Suppose we use only one stereoisomeric form of $[Fe^{III}(C_2O_4)_3]^{3-}$, there could then be a chance to make a new state of matter that still remains elusive and is not likely to be found in anything other than a molecular solid, namely a chiral magnet.

Finally, as if that is not enough, we come to the organic cation A^+ interleaving the layers. More than a decade earlier, we have pointed out how exceptionally interesting the generic class of organic-inorganic layer compounds could be, from the standpoint of combining physical properties not normally found together in simple inorganic lattices. In that context, the bimetallic tris-oxalato-metallate lattice proves an exceptionally flexible template. A remarkable variety of A^+ can be inserted between the bimetallic layers, from tetra-alkylammonium to species containing aromatic rings and even organometallic sandwich molecules [7]. Among the aromatic cations are the ones such as tetrathiafulvalene (TTF) that also appear in molecular conductors, thus creating superb examples of co-existing properties such as magnetism and superconductivity, an aspect addressed in the next chapter. For now, we concentrate on insulators, where the principal focus is the many facets of magnetic order.

Given the wide choice of 2+ and 3+ cations forming oxalato-bridged materials, instances exist of both ferro- and antiferromagnetic near-neighbour exchange interactions. In all the $M^{II}Fe^{III}$ cases, however, the interaction is antiferromagnetic, so the ordered state is a ferrimagnet, i.e. there is spontaneous magnetisation below the ordering temperature T_c [8]. The $Mn^{II}Fe^{III}$ compounds are unusual ferrimagnets in their own right, as both metal ions share the same electron configuration (high spin

d^5), so the bulk properties closely mimic those of an antiferromagnet. Yet, it is this mixed-valent $\text{Fe}^{\text{II}}\text{Fe}^{\text{III}}$ series that we find the most strikingly unusual properties. In the tetraphenylphosphonium salt, the magnetisation varies with temperature in the conventional way: in zero field, it increases as the temperature is lowered towards T_c and spin correlations develop, then falls again below T_c as magnetic domains develop. Cooling in higher fields leads to monotonically increasing magnetisation below T_c as a single domain orientation comes to dominate. Changing the cation to tetrabutylammonium, however, transforms the situation dramatically.

In zero field, there is still a maximum in the magnetisation at T_c , but when a field is applied, instead of the magnetisation increasing monotonically with decreasing temperature below T_c , it falls to zero and then becomes negative! [9] When we first observed this, we thought that someone had reversed the current leads to the magnet power supply. A magnetic moment aligning itself *anti*-parallel to the applied field is distinctly counterintuitive: still more so that merely changing the organic cation should bring about such an effect. In fact, we were in the presence of an extremely rare example of Neel's class N ferrimagnetism [10]. Neutron diffraction and magnetisation studies [11] show that it is in fact the 'normal' (class Q) behaviour of the tetraphenylphosphonium that is less common in this series. Furthermore, the class Q lattice is not completely ordered. Frustration between domains with contrarily ordered magnetisation directions leaves a fraction of the atomic moments isolated and paramagnetic, as revealed by a powerful (but somewhat esoteric) technique named neutron polarisation analysis, applied for the first time to a molecular magnet [12].

Another novel kind of magnet that never existed at all before molecular-based materials came along is the purely organic magnet, one in which the individual moments in the lattice arise from unpaired p-electrons. Otherwise known as 'solid free-radicals', the first purely organic ferromagnet only emerged in the early 1990s, but it suggests the further possibility of an organic ferrimagnet. Nevertheless, up till 2000, all the ferrimagnets known were composed from combinations of d- and f-block elements. However, aromatic molecules, and especially the ones containing Group 6 hetero-atoms (like TTF, mentioned above) can be persuaded to form stable radical cations, and combining these with transition-metal complex anions leads to salts in which localised p- and d-moments co-exist to form ferrimagnets with long-range order [13]. Engineering the crystal lattice to prevent the radical cations forming dimers or stacks remains tricky, as is also the inter-molecular overlap pathway transmitting the required antiferromagnetic interaction [14]. Yet, the key examples have all the classic signatures of bulk ferrimagnetism, i.e. minimum in the susceptibility-temperature curve, hysteresis, etc.

The two very different classes of ferrimagnets described in the articles that follow should be enough to exemplify how making magnetic materials from molecular

building blocks leads to new kinds of physical behaviour, with structural subtleties transcending those oxides and intermetallics beloved by generations of magneticians.

References

- [1] O. Kahn, *Molecular Magnetism*, VCH: New York, 1993.
- [2] J. S. Miller, A. J. Epstein and W. M. Reiff, *Chem Rev* **88**: 201 (1988).
- [3] H. H. Wickman, A. M. Trozzolo, H. J. Williams, G. W. Hull and F. R. Merritt, *Phys Rev* **155**: 563 (1967); *idem ibid* **163**: 526 (1967); P. Day, *Notes Rec Roy Soc* **56**, 95 (2002).
- [4] A. N. Holden, B. T. Matthias, P. W. Anderson and H. W. Lewis, *Phys Rev* **102**: 1463 (1956).
- [5] B. Mayoh and P. Day, *J Chem Soc Dalton Trans* 1483 (1976).
- [6] H. Tamaki, J. Zhong, M. Matsumoto, S. Kida, N. Koikawa, Y. Achiwa, Y. Hashimoto and H. Okawa, *J. Amer Chem Soc* **114**, 6974 (1992).
- [7] E. Coronado, J. R. Galan-Mascaros, C. Ruiz-Peros and S. Triki, *Adv Mat* **8**: 737 (1996).
- [8] C. Mathoniere, C. J. Nuttall, S. G. Carling and P. Day, *Inorg Chem* **35**: 1201 (1996); **Reprint 5.1**.
- [9] C. Mathoniere, S. G. Carling, Y. Dou and P. Day, *J. C. S. Chem Commun* 1551 (1994).
- [10] L. Neel, *Ann Phys (Paris)* **1**: 137 (1948).
- [11] C. J. Nuttall and P. Day, *Inorg Chem* **37**: 3885 (1998), **Reprint 5.2**; *idem Chem Mat* **10**: 3050 (1998), **Reprint 5.3**.
- [12] S. G. Carling, D. Visser, D. Hautot, I. D. Watts, P. Day, J. Ensling, P. Guetlich, G. J. Long and F. Grandjean, *Phys Rev* **B66**: 104407 (2002); **Reprint 5.4**.
- [13] S. S. Turner, C. Michaut, S. Durot, P. Day, T. Gelbrich and M. B. Hursthouse, *J Chem Soc Dalton Trans* 905 (2000); **Reprint 5.6**.
- [14] S. S. Turner and P. Day, *J Mater Chem* **15**: 23 (2005); **Reprint 5.5**.

Ferrimagnetic Mixed-Valency and Mixed-Metal Tris(oxalato)iron(III) Compounds: Synthesis, Structure, and Magnetism

Corine Mathonière,[†] Christopher J. Nuttall, Simon G. Carling, and Peter Day*

Davy Faraday Research Laboratory, The Royal Institution of Great Britain,
21 Albemarle Street, London W1X 4BS, U.K.

Received June 7, 1995[⊗]

The synthesis and structural and magnetic characterization of 16 compounds $\text{AM}^{\text{II}}\text{Fe}^{\text{III}}(\text{C}_2\text{O}_4)_3$ ($\text{A} = \text{N}(n\text{-C}_3\text{H}_7)_4$, $\text{N}(n\text{-C}_4\text{H}_9)_4$, $\text{N}(n\text{-C}_5\text{H}_{11})_4$, $\text{P}(n\text{-C}_4\text{H}_9)_4$, $\text{P}(\text{C}_6\text{H}_5)_4$, $\text{N}(n\text{-C}_4\text{H}_9)_3(\text{C}_6\text{H}_5\text{CH}_2)$, $(\text{C}_6\text{H}_5)_3\text{PNP}(\text{C}_6\text{H}_5)_3$, $\text{As}(\text{C}_6\text{H}_5)_4$; $\text{M}^{\text{II}} = \text{Mn, Fe}$) are reported. X-ray powder diffraction profiles are indexed in $R3c$ or its subgroup $P6_522$ or $P6/mmm$ to derive unit cell constants. The structures of all the compounds consist of two-dimensional honeycomb networks $[\text{M}^{\text{II}}\text{Fe}^{\text{III}}(\text{C}_2\text{O}_4)_3]_{\infty}$. The $\text{M}^{\text{II}} = \text{Fe}$ compounds behave as ferrimagnets with T_c between 33 and 48 K, but five exhibit a crossover from positive to negative magnetization near 30 K when cooled in a field of 10 mT. The compounds exhibiting this unusual magnetic behavior are those that have the highest T_c . Within the set $\text{N}(n\text{-C}_n\text{H}_{2n+1})_4\text{Fe}^{\text{II}}\text{Fe}^{\text{III}}(\text{C}_2\text{O}_4)_3$ ($n = 3-5$), T_c increases with interlayer separation and the low-temperature magnetization changes from positive ($n = 3$) to negative ($n = 4, 5$). In the $\text{M} = \text{Mn}^{\text{II}}$ compounds, the in-plane cell parameter a_0 is $\sim 0.03 \text{ \AA}$ greater than in the corresponding $\text{M} = \text{Fe}^{\text{II}}$ ones while the interlayer separation ($c_0/6$) is on average 0.08 \AA smaller. All members of the $\text{M}^{\text{II}} = \text{Mn}$ series have magnetic susceptibilities showing broad maxima at 55 K characteristic of two-dimensional antiferromagnetism, but the magnetization of several of the salts increases sharply below 27 K due to the onset of spin canting, the magnitude of which varies significantly with A.

Introduction

The occurrence of long-range magnetic order in lattices composed of molecular transition metal complexes has been attracting increasing attention in recent years.¹ Such compounds are of interest because they are insulating, and hence frequently transparent, and offer the opportunity of creating novel lattice architectures. They also offer the chemist the opportunity to investigate how magnetic exchange interactions are propagated through extended polyatomic ligands. Prominent among the latter is the ambidentate oxalate ion, and numerous dimeric and trimeric oxalate complexes have been prepared as models.² However, in view of their simplicity and potential magnetic interest, it is surprising that only in the last two years have infinitely extended networks based on transition metal oxalato complexes been prepared.³ The crystal structures of compounds $\text{AM}^{\text{II}}\text{Cr}(\text{C}_2\text{O}_4)_3$ with $\text{M}^{\text{II}} = \text{Mn}$ and $\text{A} = \text{N}(n\text{-C}_4\text{H}_9)_4$ and $\text{P}(\text{C}_6\text{H}_5)_4$ consist of infinitely extended sheets of hexagonal symmetry containing alternating Mn and Cr octahedrally coordinated on each side of every oxalato anion.^{4,5} The $\text{N}(n\text{-C}_4\text{H}_9)_4$ compounds show transitions to long-range magnetic order at temperatures between 6 and 14 K depending on M^{II} .³

In the search for chemical correlations between structure and properties in this interesting class of compounds, an important

aspect is to extend the range of examples from four points of view. First, since they form layer structures, systematically varying A should modulate the separation between the layers, and hence the physical properties. Second, in view of the fact that three-dimensional as well as layer compounds of the type $\text{AMM}'(\text{C}_2\text{O}_4)_3$ have been reported,⁴ it is important to delineate the extent to which the template cation A determines the crystal chemistry. Third, varying M^{III} as well as M^{II} gains access to a wider range of magnetic behavior; in particular, replacing Cr^{III} ($S = 3/2$) with Fe^{III} ($S = 5/2$) increases the moment and hence alters the ordering temperature, which scales with $J_S(\text{M}^{\text{II}}) \cdot S(\text{M}^{\text{III}})$, though of course J itself is sensitive to the orbital occupancy and the numbers of exchange pathways. Finally, in an earlier paper⁶ we reported that $\text{N}(n\text{-C}_4\text{H}_9)_4\text{Fe}^{\text{II}}\text{Fe}^{\text{III}}(\text{C}_2\text{O}_4)_3$ exhibits a giant negative magnetization at low temperature unprecedented in molecular-based magnetic materials. It is therefore of great interest to find out how widespread this phenomenon is and whether a connection can be drawn with the cation A.

With these four issues in mind, we have therefore prepared polycrystalline samples of $\text{AM}^{\text{II}}\text{Fe}^{\text{III}}(\text{C}_2\text{O}_4)_3$ with layer structures analogous to those of $\text{AMnCr}(\text{C}_2\text{O}_4)_3$ ($\text{A} = \text{N}(n\text{-C}_4\text{H}_9)_4$, $\text{P}(\text{C}_6\text{H}_5)_4$), which have been determined.^{4,5} Eight phases with different A are reported, each with $\text{M}^{\text{II}} = \text{Fe}$ and Mn. The former are interesting because they are mixed-valency materials⁷ while the latter are unusual in containing two different elements having the same electron configuration (high-spin $3d^5$). The crystallographic cell parameters were refined by least-squares-fitting X-ray powder diffraction data, and the susceptibilities and magnetizations were determined from 4 to 300 K. Several further examples of giant negative magnetization at low temperature have been found in the $\text{M}^{\text{II}} = \text{Fe}$ series, and a qualitative explanation for the phenomenon is given in terms of the molecular field approach to ferrimagnetism.

* Corresponding author. FAX: +44 71 629 3569.

[†] Present address: Labo des Science Moléculaires, ICMCB, Chateau de Brivazac, Avenue du Dr. A. Schweitzer, 33608 Pessac Cedex, France.

[⊗] Abstract published in *Advance ACS Abstracts*, February 1, 1996.

- (1) See e.g.: Kahn, O., *Molecular Magnetism*; VCH: New York, 1994.
- (2) Julve, M.; Fans, J.; Verdager, M.; Gleizes, A. *J. Am. Chem. Soc.* **1984**, *106*, 8306. Pei, Y.; Journeax, Y.; Kahn, O. *Inorg. Chem.* **1989**, *28*, 100.
- (3) Zhong, Z. J.; Matsumoto, N.; Okawa, H.; Kida, S. *Chem. Lett.* **1990**, 87. Tamaki, H.; Mitsumi, M.; Nakamura, K.; Matsumoto, N.; Kida, S.; Okawa, H.; Iijima, S. *Chem. Lett.* **1992**, 1975. Tamaki, H.; Zhong, Z. J.; Matsumoto, N.; Kida, S.; Koikawa, N.; Achiwa, Y.; Hashimoto, Y.; Okawa, H. *J. Am. Chem. Soc.* **1992**, *114*, 6974.
- (4) Decurtins, S.; Schmalie, H. W.; Oswald, H. R.; Linden, A.; Ensing, J.; Gütlisch, P.; Hauser, A. *Inorg. Chim. Acta* **1994**, *216*, 65.
- (5) Atovmyan, L. O.; Shilov, G. V.; Lyubovskaya, R. N.; Zhilyaeva, E. I.; Ovanesyan, N. S.; Pirumova, S. I.; Gusakovskaya, I. G. *JETP Lett.* **1993**, *58*, 766.

(6) Mathonière, C.; Carling, S. G.; Dou, Y.; Day, P. *J. Chem. Soc., Chem. Commun.* **1994**, 1551.

(7) Robin, M. B.; Day, P. *Adv. Inorg. Chem. Radiochem.* **1967**, *10*, 248. Day, P. *Int. Rev. Phys. Chem.* **1981**, *1*, 149.

Table 1. Refined Unit Cell Constants of $AM^{\text{II}}\text{Fe}^{\text{III}}(\text{C}_2\text{O}_4)_3$ (1–8, $M^{\text{II}} = \text{Fe}$; 9–16, $M^{\text{II}} = \text{Mn}$)

compd	A	a_0 , Å	c_0 , Å	no. of peaks fitted
1	$N(n\text{-C}_3\text{H}_7)_4$	9.334(2)	49.31(3)	14
2	$N(n\text{-C}_4\text{H}_9)_4$	9.402(3)	53.88(5)	17
3	$N(n\text{-C}_5\text{H}_{11})_4$	9.406(6)	61.4(2)	13 ^a
4	$\text{P}(\text{C}_6\text{H}_5)_4$	9.375(4)	57.45(5)	15
5	$N(\text{C}_6\text{H}_5\text{CH}_2)(n\text{-C}_4\text{H}_9)_3$	9.38(2)	57.8(2)	12 ^b
6	$(\text{C}_6\text{H}_5)_3\text{PNP}(\text{C}_6\text{H}_5)_3$	9.38(1)	86.6(2)	13 ^b
7	$\text{P}(n\text{-C}_4\text{H}_9)_4$	9.47(1)	55.9(2)	8
8	$\text{As}(\text{C}_6\text{H}_5)_4$	9.365(2)	57.93(4)	12
9	$N(n\text{-C}_3\text{H}_7)_4$	9.372(3)	49.11(6)	16
10	$N(n\text{-C}_4\text{H}_9)_4$	9.461(2)	53.62	17
11	$N(n\text{-C}_5\text{H}_{11})_4$	9.457(5)	60.95(1)	11 ^a
12	$\text{P}(\text{C}_6\text{H}_5)_4$	9.428(4)	57.15(1)	11
13	$N(\text{C}_6\text{H}_5\text{CH}_2)(n\text{-C}_4\text{H}_9)_3$	9.470(4)	56.6(1)	12
14	$(\text{C}_6\text{H}_5)_3\text{PNP}(\text{C}_6\text{H}_5)_3$	9.413(3)	87.1(2)	13 ^b
15	$\text{P}(n\text{-C}_4\text{H}_9)_4$	9.52(5)	55.17(8)	11
16	$\text{As}(\text{C}_6\text{H}_5)_4$	9.445(6)	57.4(1)	9

^a $P6_322$. ^b $P6/mmm$.

Experimental Section

Chemicals were standard reagents from Aldrich (99% or higher purity). Solvents were reagent grade, deoxygenated where necessary by freeze–thaw cycles under vacuum. All manipulations of air-sensitive compounds were carried out by standard Schlenk techniques or in a N_2 dry box. N_2 was purified through columns containing BTS catalyst and 5 Å molecular sieves.

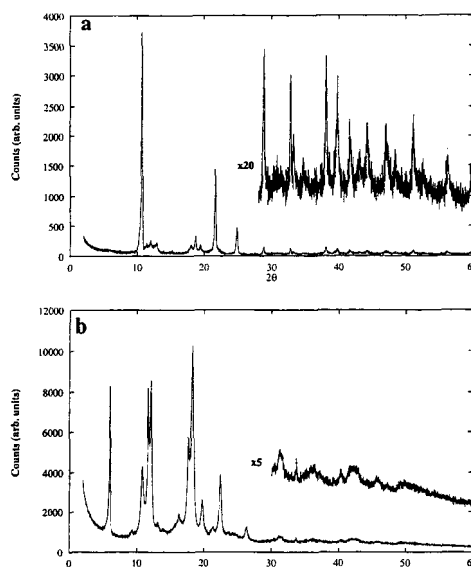
Elemental analyses were performed by the Microanalytical Departments at the Inorganic Chemistry Laboratory, Oxford, and University College, London.

X-ray powder diffraction profiles were recorded at room temperature on a Siemens D500 diffractometer in reflection mode using Cu K α radiation with the monochromator set at 30° takeoff angle. Magnetic susceptibility and magnetization measurements were made using a Quantum Design MPMS 7 SQUID magnetometer. Polycrystalline samples were contained within gelatin capsules. The customary measuring protocol was to cool the sample in a field of 10 mT from ambient temperature to 2 K and record the susceptibility while warming. To estimate the Curie and Weiss constants, data from 150 to 300 K were used in every case. To render the results more comparable, the same number of data points and similar sample masses were employed. Correction for core diamagnetism of the sample was made using Pascal's constants and for the sample capsule by comparison with a standard measurement.

In a typical preparation, an aqueous solution (5 mL) of $\text{K}_3\text{Fe}(\text{C}_2\text{O}_4)_3 \cdot 3\text{H}_2\text{O}$ is added to an aqueous solution (5 mL) of $\text{FeSO}_4 \cdot 7\text{H}_2\text{O}$ or $\text{MnSO}_4 \cdot 7\text{H}_2\text{O}$ with stirring at room temperature. After 30 min, the solution is filtered to remove the small amount of $\text{Fe}(\text{C}_2\text{O}_4)_2 \cdot 2\text{H}_2\text{O}$ which forms, and a methanol solution (5 mL) of AX (X = halide) is added to the filtrate, whereupon a precipitate begins to form. The solution is left for a period at room temperature before filtering. Optimum quantities of reagents and the reaction times are different for different A, varying from 1 to 2 mmol and from 1 h to several days, respectively. The longer the precipitation time, the less crystalline the resulting product is, as determined by XRD.

The following compounds were prepared in this way: for $M^{\text{II}} = \text{Fe}$, A = $N(n\text{-C}_3\text{H}_7)_4$ (1), $N(n\text{-C}_4\text{H}_9)_4$ (2), $N(n\text{-C}_5\text{H}_{11})_4$ (3), $\text{P}(\text{C}_6\text{H}_5)_4$ (4), $N(\text{C}_6\text{H}_5\text{CH}_2)(n\text{-C}_4\text{H}_9)_3$ (5), $(\text{C}_6\text{H}_5)_3\text{PNP}(\text{C}_6\text{H}_5)_3$ (6), $\text{P}(n\text{-C}_4\text{H}_9)_4$ (7), $\text{As}(\text{C}_6\text{H}_5)_4$ (8); $M^{\text{II}} = \text{Mn}$, with the same sequence of cations, compounds numbered 9–16 (Table 1). Elemental analyses showed that all the products had the formula $AM^{\text{II}}\text{Fe}(\text{C}_2\text{O}_4)_3$. The analytical data are available as Supporting Information. Attempts to prepare similar compounds with several other cations A were unsuccessful, as follows: $N(n\text{-C}_6\text{H}_{13})_4$ ($n = 1, 2, 6, 7$), $N(n\text{-C}_{16}\text{H}_{33})(\text{CH}_3)_3$, and $\text{P}(\text{C}_6\text{H}_5)_3\text{H}$.

An alternative preparative route is to generate the $\text{Fe}(\text{C}_2\text{O}_4)_3^{3-}$ complex *in situ*. An aqueous solution (5 mL) of $\text{FeCl}_3 \cdot 6\text{H}_2\text{O}$ is added to one (5 mL) of $\text{FeSO}_4 \cdot 7\text{H}_2\text{O}$, and an aqueous solution (3 mmol in 5 mL) of oxalic acid is added dropwise. Upon addition of 5 mL of an

**Figure 1.** X-ray powder diffraction profiles for $AMn^{\text{II}}\text{Fe}^{\text{III}}(\text{C}_2\text{O}_4)_3$. A: (a) $N(n\text{-C}_3\text{H}_7)_4$; (b) $(\text{C}_6\text{H}_5)_3\text{PNP}(\text{C}_6\text{H}_5)_3$.

aqueous or methanolic solution of $N(n\text{-C}_4\text{H}_9)_4\text{I}$, a green precipitate of **2** is formed immediately. It is also possible to carry out the reaction entirely in methanol solution.

Crystals of **9**, were also prepared by placing 1 or 2 mmol of $\text{K}_3\text{Fe}(\text{C}_2\text{O}_4)_3$ and $\text{MnSO}_4 \cdot 7\text{H}_2\text{O}$ in one arm of an H-shaped tube and 1 mmol of $N(n\text{-C}_3\text{H}_7)_4\text{Cl}$ in the other, filling the cell carefully with water to prevent mixing, and allowing the reactants to diffuse together over a 2 month period.

Results

Crystal Structures. All the phases prepared were characterized by X-ray powder diffraction. In some preparations, peaks assignable to a few percent of $\text{Fe}(\text{C}_2\text{O}_4)_2 \cdot 2\text{H}_2\text{O}$ were visible, but filtering the mixed M^{2+} , Fe^{3+} , $\text{C}_2\text{O}_4^{2-}$ solution before adding the A⁺ eliminated them. Typical diffraction profiles are shown in Figure 1. For each compound, the reflections were indexed and unit cell constants were refined on a hexagonal cell as reported in refs 4 and 5. The values of the cell constants obtained are listed in Table 1. That the lattice constants in the basal plane are all so similar shows that the structures of all the compounds are similar and resemble those found by X-ray single-crystal diffraction for $AMn\text{Cr}(\text{C}_2\text{O}_4)_3$ with A = $\text{P}(\text{C}_6\text{H}_5)_4$ ⁴ and $N(n\text{-C}_4\text{H}_9)_4$.⁵ However, varying the organic cation changes the spacing between the layers as anticipated. The structures of the $\text{Mn}^{\text{II}}\text{Fe}^{\text{III}}$ and $\text{Fe}^{\text{II}}\text{Fe}^{\text{III}}$ series correlate closely, as indicated by the cell parameters c_0 plotted in Figure 2a. The a_0 cell parameter varies little, as expected (Table 1 and Figure 2b). Refinement of the unit cell parameters for compounds 1, 2, 4, 7–10, 12, 15, and 16 was successfully accomplished within the space group $R3c$ assumed in refs 4 and 5. [We were informed by a reviewer that the structure of a compound **10** has been refined from single-crystal X-ray data in the space group $P6_3$ (Decurtins, S., et al. Manuscript in preparation). However, for comparison with the other compounds, we use the larger hexagonal supercell.] However in several other cases, attempts to refine the cell constants in this space group left a number of intense peaks unassigned. The latter could only be fitted by assuming a lower symmetry space group, $P6_522$ for compounds **3** and **11** and $P6/mmm$ for compounds **5**, **6**, **13**, and

(8) Bailer, J. C.; Jones, E. M. *Inorg. Synth.* 1939, 1, 37.

Ferrimagnetic Tris(oxalato)iron(III) Compounds

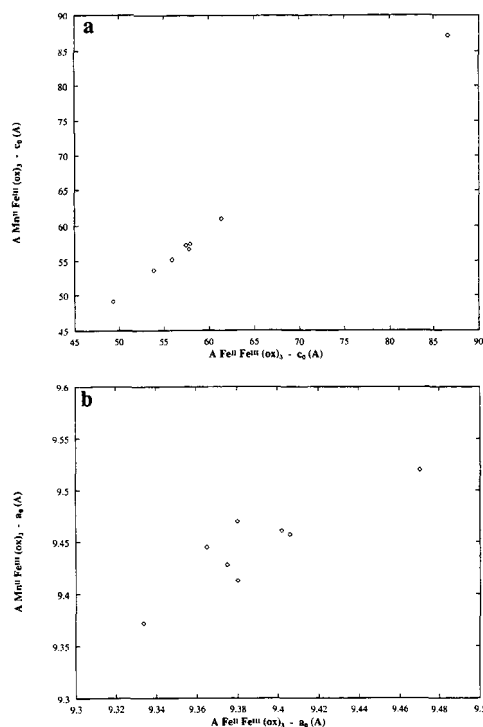


Figure 2. Unit cell parameters of $AM^{\text{II}}\text{Fe}^{\text{III}}(\text{C}_2\text{O}_4)_3$ ($M = \text{Mn}^{\text{II}}, \text{Fe}^{\text{II}}$): (a) c_0 ; (b) a_0 . For numbering of compounds, see text.

14. In all three space groups, the separation between $\text{MM}^{\text{II}}(\text{C}_2\text{O}_4)_3^-$ layers is $c_0/6$ so cation variation induces a change from 8.18 Å ($\text{Mn}^{\text{II}}\text{Fe}^{\text{III}}$) and 8.22 Å ($\text{Fe}^{\text{II}}\text{Fe}^{\text{III}}$) in the $N(n\text{-C}_3\text{H}_7)_4$ compounds, the smallest separation observed, to 14.52 Å ($\text{Mn}^{\text{II}}\text{Fe}^{\text{III}}$) and 14.43 Å ($\text{Fe}^{\text{II}}\text{Fe}^{\text{III}}$) in $(\text{C}_6\text{H}_5)_3\text{PNP}(\text{C}_6\text{H}_5)_3$, the largest found so far.

Magnetic Properties. The magnetic susceptibilities of polycrystalline samples of all the compounds, measured in a field of 10 mT, closely obeyed the Curie–Weiss law between room temperature and 150 K. The values of Curie (C) and Weiss constants (Θ) extracted by least-squares-fitting the data after subtraction of a correction for diamagnetism are listed in Table 2. The large negative values of the Weiss constants clearly indicate antiferromagnetic interaction between Mn^{II} or Fe^{II} and Fe^{III} in every case. In the $\text{Fe}^{\text{II}}\text{Fe}^{\text{III}}$ series, the values of Θ vary markedly with A , but among the $\text{Mn}^{\text{II}}\text{Fe}^{\text{III}}$ compounds, they span a smaller range, indicating that the near-neighbor exchange pathway is less sensitive to a change of organic cation. This is to be expected from the similar values of the unit cell parameter a_0 .

Below 100 K the behavior of the $\text{Mn}^{\text{II}}\text{Fe}^{\text{III}}$ and $\text{Fe}^{\text{II}}\text{Fe}^{\text{III}}$ compounds must be examined separately. Considering first the $\text{Fe}^{\text{II}}\text{Fe}^{\text{III}}$ series, the compounds fall into two sets with sharply contrasting behavior. Adopting the measurement protocol defined in the Experimental Section, we find that in compounds 1, 4, and 8 the magnetization increases abruptly at 35, 37, and 33 K, respectively, corresponding to the onset of long-range order, increasing further in a conventional monotonic fashion down to 4 K (Figure 3). In striking contrast, in compounds 2, 3, and 5–7, the onset of sharply increasing magnetization occurs at higher temperature (between 44 and 48 K), while at lower

Inorganic Chemistry, Vol. 35, No. 5, 1996 1203

Table 2. Magnetic Parameters of $AM^{\text{II}}\text{Fe}^{\text{III}}(\text{C}_2\text{O}_4)_3^a$

compd	T_c , K	Curie const C , emu K mol^{-1}	Weiss const Θ , K	negative magnetizn
1	35	8.0	−97	no
2	45	9.5	−120	yes
3	48	7.1	−140	yes
4	37	6.3	−86	no
5	44	7.7	−102	yes
6	45	10.2	−146	yes
7	45	8.5	−106	yes
8	33	7.3	−113	no
9	28	10.4	−127	
10	28	10.6	−121	
11	27	10.5	−124	
12	25	8.9	−128	
13	26	9.6	−117	
14	29	10.3	−136	
15	26	8.9	−124	
16	27	10.6	−122	

^a For numbering of compounds, see text.

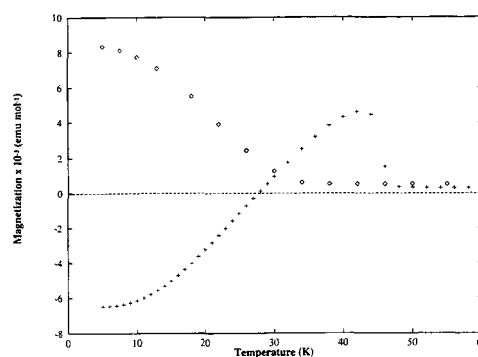


Figure 3. Temperature dependence of the magnetization of $A\text{Fe}^{\text{II}}\text{Fe}^{\text{III}}(\text{C}_2\text{O}_4)_3$ in a field of 10 mT: (\diamond) $\text{As}(\text{C}_6\text{H}_5)_3$; ($+$) $(\text{C}_6\text{H}_5)_3\text{PNP}(\text{C}_6\text{H}_5)_3$.

temperature the magnetization reaches a maximum, followed by a monotonic decrease down to 4 K, becoming strongly negative below about 30 K (Figure 3). This remarkable behavior is observed consistently in numerous samples, including ones which had been prepared by the *in situ* synthesis of $\text{Fe}(\text{C}_2\text{O}_4)_3^{3-}$ rather than previously prepared $\text{K}_3\text{Fe}(\text{C}_2\text{O}_4)_3$. It is discussed further below.

From room temperature to 150 K, the susceptibilities of polycrystalline samples of the $\text{Mn}^{\text{II}}\text{Fe}^{\text{III}}$ compounds likewise obey the Curie–Weiss Law, with negative Weiss constants indicating near-neighbor antiferromagnetic exchange. At lower temperature, the susceptibilities pass through a broad maximum near 55 K of the kind seen in low-dimensional antiferromagnets. In the $\text{P}(\text{C}_6\text{H}_5)_4$ compound 12, the susceptibility below 55 K continues to fall monotonically to below 10 K, but in the other $\text{Mn}^{\text{II}}\text{Fe}^{\text{III}}$ compounds, there is a discontinuous jump in susceptibility at 27 K (Figure 5), suggesting the onset of spin canting. A small single crystal of 9 was studied as a function of temperature at applied magnetic fields of 100, 500, and 1000 G with the results shown in Figure 6. It is apparent from the single-crystal data that the 27 K transition is not first but second order.

Discussion

Crystal Chemistry. The existence of such a large number of compounds sharing the stoichiometry $AM^{\text{II}}\text{Fe}^{\text{III}}(\text{C}_2\text{O}_4)_3$ invites discussion of their crystal chemistry as a prelude to rationalizing their magnetic properties. Since the full structure cannot be resolved from powder X-ray data, we base the discussion on the variation in the unit cell parameters.

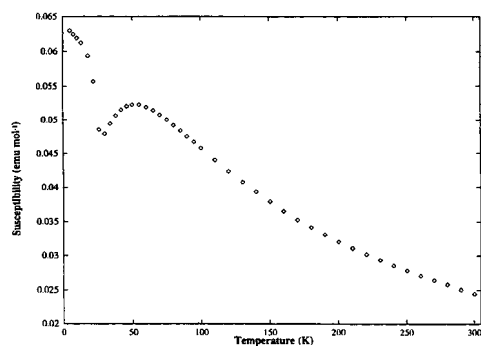


Figure 4. Temperature dependence of the susceptibility of polycrystalline $N(n\text{-C}_4\text{H}_9)_4\text{Mn}^{\text{II}}\text{Fe}^{\text{III}}(\text{C}_2\text{O}_4)_3$ from 10 to 300 K.

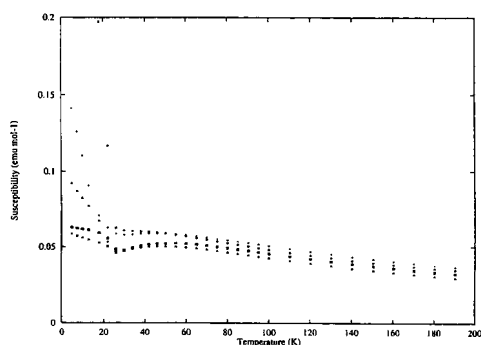


Figure 5. Temperature dependence of the susceptibility of several polycrystalline $\text{AMn}^{\text{II}}\text{Fe}^{\text{III}}(\text{C}_2\text{O}_4)_3$ compounds showing spin canting at low temperature: (◆) $(\text{C}_6\text{H}_5)_2\text{PNP}(\text{C}_6\text{H}_5)_2$; (+) $\text{As}(\text{C}_6\text{H}_5)_4$; (▲) $(\text{C}_6\text{H}_5\text{-CH}_2)\text{N}(n\text{-C}_4\text{H}_9)_2$; (■) $\text{N}(n\text{-C}_4\text{H}_9)_4$; (×) $\text{P}(n\text{-C}_4\text{H}_9)_4$.

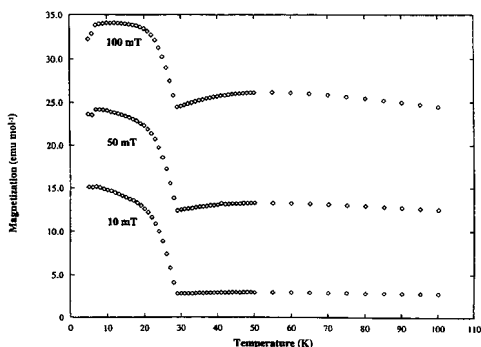


Figure 6. Temperature dependence of the magnetization of a single crystal of $\text{N}(n\text{-C}_3\text{H}_7)_4\text{Mn}^{\text{II}}\text{Fe}^{\text{III}}(\text{C}_2\text{O}_4)_3$ in fields of 10, 50, and 100 mT.

On the basis of model building and topological arguments, it is possible to envisage two modes of connectivity between octahedral tris-bidentate $\text{M}^{\text{II}}(\text{C}_2\text{O}_4)_3^{3-}$ groups mediated by M^{II} , each of which in turn is coordinated by three octahedrally disposed (C_2O_4) .^{2,3} These two modes correspond to each octahedron being connected to its neighbors through three edges. If, in a trigonally distorted octahedron having D_3 symmetry, the edges in question are related by a 3-fold screw axis, polymerization can take place, in principle, in two ways. One alternative leads to an infinite honeycomb layer in which the 3-fold screw axes of all the octahedra are aligned perpendicular

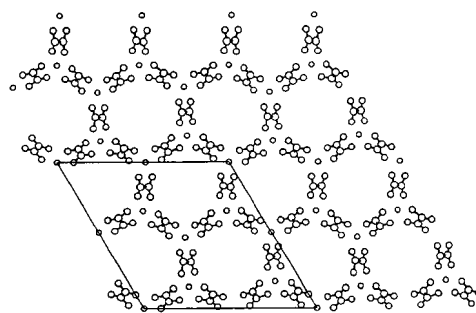


Figure 7. The honeycomb layer arrangement of $[\text{MM}'(\text{C}_2\text{O}_4)_3]^-$.

to the plane (Figure 7). In the other possible arrangement, the octahedra are connected in helical ribbons so that their 4-fold axes are all aligned. The crystal structures of two examples of $\text{AMM}'(\text{C}_2\text{O}_4)_3$ compounds containing monovalent A cations determined to date both reveal honeycomb layer arrangements.^{4,5} On the other hand, when $\text{A} = [\text{Fe}(\text{bipy})_3]^{2+}$ and $\text{M} = \text{M}' = \text{Fe}^{\text{II}}$, a cubic lattice is found ($P4_332$) with the second form of connectivity.⁹ Clearly, therefore, the organic cation A^+ is capable of acting as a template to direct the polymerization in a manner analogous to zeolites.

All the template cations A used in the present work are of quaternary ammonium, phosphonium, or arsonium type. They give rise to compounds having a layer honeycomb structure, although they include both alkyl- and phenyl-substituted species as well as one containing the two types of substituent together. Equally of interest is the range of XR_4^+ for which no bimetallic tris(oxalato) compounds could be synthesized. For example in the $\text{N}(n\text{-C}_n\text{H}_{2n+1})_4^+$ sequence for $n = 1-7$, only $n = 3-5$ gave crystalline products, while highly asymmetrically substituted species such as the surfactant $(\text{C}_{16}\text{H}_{33})\text{N}(\text{CH}_3)_3^+$ and $(\text{C}_6\text{H}_5)_3\text{-PH}^+$ did not.

In the crystal structure of $\text{P}(\text{C}_6\text{H}_5)_4\text{MnCr}(\text{C}_2\text{O}_4)_3$, the organic cations occupy sites interleaved between the $[\text{MnCr}(\text{C}_2\text{O}_4)_3]_\infty$ layers in such a way that one P-C bond of each cation lies parallel to the 3-fold axis of the hexagonal unit cell, i.e. perpendicular to the anion layer. The C_6H_5 ring in question resides within the cavity formed by six $(\text{C}_2\text{O}_4)^{2-}$ while the remaining three extend between the anion layer.⁴ Unfortunately the only N and one C atom of the organic cations were located in the structure determination of $\text{N}(n\text{-C}_4\text{H}_9)_4\text{MnCr}(\text{C}_2\text{O}_4)_3$ ⁵ though the assumption of the $R3c$ space group requires the N to be placed on a 3-fold axis with one C-N bond parallel to the axis. The remaining C atoms were assumed to be fully disordered. A reasonable hypothesis, however, is that one C_4H_9 chain extends into the cavity in the $[\text{MnCr}(\text{C}_2\text{O}_4)_3]_\infty$ layer in a fashion analogous to the phenyl group in the $\text{P}(\text{C}_6\text{H}_5)_4$ compound. On that basis, the increments of interlayer spacing in the $\text{N}(n\text{-C}_n\text{H}_{2n+1})_4$ compounds for $n = 3-4$ and $4-5$ ought to correspond to the interpolation of a C-C bond. The increments in question are respectively 0.76 and 1.25 Å in the $\text{Fe}^{\text{II}}\text{Fe}^{\text{III}}$ case and 0.75 and 1.22 Å in the $\text{Mn}^{\text{II}}\text{Fe}^{\text{III}}$.

The increments in c_0 correspond precisely to the well-known "alternation effect" in the unit cell constants of n -alkanes or compounds containing extended aliphatic hydrocarbon chains such as the layer perovskite halide salts $(n\text{-C}_n\text{H}_{2n+1}\text{NH}_3)_2\text{MX}_4$.¹⁰ In the latter, the increment in interlayer spacing on extending the chain by one CH_2 unit is smaller when one passes from odd to even than when one passes from even to odd, exactly as

(9) Decurtins, S.; Schmale, H. W.; Schneuwly, P.; Ensling, J.; Gütlich, P. *J. Am. Chem. Soc.* **1994**, *116*, 9521.

Ferrimagnetic Tris(oxalato)iron(III) Compounds

Inorganic Chemistry, Vol. 35, No. 5, 1996 1205

found here. Indeed, adopting the same geometrical argument as in other organic-inorganic layer systems,^{11,12} we can use the observed increments to estimate the angle that the N-C bond of A⁺ in the present series makes with the [M^{II}Fe(C₂O₄)₃]⁻ layer. With the C_nH_{2n+1} chains fully extended, and taking the C-C bond length as 1.54 Å and the C-C-C angle as the normal tetrahedral one, the "axial" C-C bonds make angles of approximately 60° with the anion layer. The a₀ parameters also increase from n = 3 to n = 4 by 0.07 and 0.09 Å (Fe^{II} and Mn^{II}) but remain constant within experimental error from n = 4 to n = 5. On the other hand, there is a marked increase in a₀ (0.06 Å) from N(n-C₄H₉)₄ to P(n-C₄H₉)₄, the latter having the largest a₀ of the series. For comparison, the difference in N-C and P-C bond lengths is 0.36 Å. Finally, it is significant that the c-axis parameters of the P(C₆H₅)₄ and N(C₆H₅CH₂)(n-C₄H₉)₃ compounds are almost equal, suggesting that in both cases the plane of a phenyl group is aligned perpendicular to the anion layer.

In view of the large number of new compounds AM^{II}Fe(C₂O₄)₃ reported in Table 1, further structural correlations can be established. The Mn^{II}Fe^{III} and Fe^{II}Fe^{III} compounds containing the same A⁺ are isostructural, but while the c₀ cell parameters in the two series correlate closely (Figure 2a), examination of the a parameters shows that the correlation is less precise (Figure 2b). However, in every case, the parameter a₀ of the Mn^{II}Fe^{III} compound is larger than that of the corresponding Fe^{II}Fe^{III} one, the mean difference among eight A being 0.054 Å. By contrast, for all A except (C₆H₅)₃PNP-(C₆H₅)₃ (compounds 6 and 14), the c₀ parameter of the Mn^{II}Fe^{III} compound is smaller than the corresponding Fe^{II}Fe^{III} one, by an average of 0.50 Å, i.e. a difference in interlayer spacing of 0.083 Å. The variation in a₀ is sufficiently explained by a decrease in size of M^{II} from Mn to Fe, the ionic radii being respectively 0.82 and 0.77 Å.¹³ On the other hand, we explain the change in c₀ by noting that expanding the hexagonal cavities in the [M^{II}Fe(C₂O₄)₃]⁻ layers on replacing Fe^{II} by Mn^{II} permits the alkyl or aryl side chain of the A⁺ to enter further, thus creating a more densely packed structure.

Magnetic Properties. We consider first the Fe^{II}Fe^{III} series. Referring to the data in the paramagnetic region, the mean value of the measured Curie constant (8.0 emu K mol⁻¹) is consistent with the presence of high-spin Fe^{II} and Fe^{III}, the value of C calculated on the assumption S(Fe^{II}) = 5/2, S(Fe^{III}) = 2, and g = 2 for both ions being 7.4 emu K mol⁻¹. The measured Curie and Weiss constants span a wide range, the largest values of C being (with one exception) correlated with the largest Θ (Table 2). This can be explained by noting that the highest measurement temperature accessible in the present study was 300 K, i.e. only 2-3Θ, so it is arguable that the true Curie-Weiss regime has not been accessed. Second, the Fe^{II} ground state is complex, since the degeneracy of the cubic field ⁵T_{2g} term is lifted, not only by first-order spin-orbit coupling but also by a trigonal field component, which can also vary with the organic template cation. Furthermore, the spin-orbit coupling constant of Fe^{II} is comparable in magnitude to kT in the temperature range covered by the measurements,¹⁴ so an orbital contribution to the observed moment is expected. It might be thought that the strong antiferromagnetic near-neighbor exchange indicated by the large negative values of Θ could be examined by considering the interactions between the orbitals carrying the unpaired electrons. However, the problem is greatly compli-

cated by the presence of unquenched orbital angular momentum on one of the ions (Fe^{II}), and no generally applicable formalism for such a case has yet been given (see ref 1, section 9.6).

A subset of the Fe^{II}Fe^{III} series that permits some precise magneto-structural correlations is the one with A = N(n-C_nH_{2n+1})₄ having n = 3-5, in which there is a monotonic increase in Θ and T_c with increasing n, i.e. with increasing c₀. Such a variation is extremely unusual, since for organic-inorganic layer compounds¹⁵ in which inorganic magnetic layers are interleaved by aliphatic carbon chains, the 3D ordering temperatures (while not very sensitive to interlayer separation) universally decrease as the distance between the layers increases.^{16,17} In the Fe^{II}Fe^{III} series, there is a marked correlation between the measured Weiss constant Θ determined from the susceptibility in the paramagnetic region above the onset of long range order and the ordering temperature T_c, those compounds having the largest Θ also having the highest T_c (Table 2). The existence of that correlation requires that exchange between metal ions in neighboring layers is important, as well as exchange within the layers. Consequently, though the crystal structure is clearly two-dimensional, the exchange interactions are not. More detailed experiments on single crystals will be needed to clarify the issue.

The most striking feature of the magnetic behavior of the Fe^{II}Fe^{III} series is the occurrence of apparently negative magnetization at low temperature. We found this phenomenon in the N(n-C₄H₉)₄ compound,⁶ but the extended series of examples reported in the present paper enables us to confirm that it is a widespread but not universal feature of this class of material. Such behavior is unprecedented in molecular-based magnets, though cases have been known for many years in the ferrites^{17,18} where the concentration of magnetic ions on the tetrahedral (A) and octahedral (B) sites in the AB₂O₄ spinel lattice may vary as a result of forming solid solutions, e.g. in NiFe_{2-4x}V_xO₄ where the cation distribution is Fe[NiFe_{1-x}V_x]O₄.¹⁷ In his classic theory of ferrimagnets, Neel¹⁹ envisaged the possibility that the spontaneous magnetization might change sign at a so-called "compensation temperature" T_{comp}, when the net magnetizations of the two sublattices cancelled each other. The phenomenon can arise when the two sublattice magnetizations have different temperature dependences. The situation is shown schematically in Figure 8. Since the Fe^{III} ground state is orbitally nondegenerate, the magnetization of the Fe^{III} sublattice follows a Brillouin curve in the molecular field approximation, but in view of its orbital degeneracy, that of the Fe^{II} will not. Furthermore, the Fe^{II} ion shows single-ion anisotropy due to spin-orbit coupling so the orientation of the Fe^{II} moments is pinned to the Fe^{II} should the latter exert the larger molecular field in the temperature range immediately below T_c.

Evidence that the Fe^{II} and Fe^{III} sublattices do not become magnetized to an equivalent extent at the same temperature comes from temperature-dependent Mössbauer spectroscopy. At 4.2 K compound 2 shows a six-line Fe^{III} spectrum corresponding to an internal field of 53 T, while the Fe^{II} component of the spectrum was fitted to an internal field of only 4 T, though the analysis was complicated by an impurity of a few percent Fe(C₂O₄)·2H₂O.²⁰ Temperature-dependent measurements on a sample of 2 uncontaminated by Fe(C₂O₄)·2H₂O reveal that, while the internal field at the Fe^{III} site is clearly established at

- (10) Arend, H.; Huber, W.; Mischgofsky, F. H.; Richter van-Leeuwen, G. K. *J. Cryst. Growth* 1978, 42, 213.
 (11) Beneke, K.; Lagaly, G. *Clay Miner.* 1982, 17, 175.
 (12) Buckley, A. M.; Bramwell, S. T.; Visser, D.; Day, P. *J. Solid State Chem.* 1987, 69, 240.
 (13) Shannon, R. D.; Prewitt, W. *Acta Crystallogr.* 1969, B25, 925.

- (14) Figgis, B. N. *Introduction to Ligand Field Theory*; Interscience: New York, 1966.
 (15) Day, P. *Philos. Trans. R. Soc.* 1985, A314, 145.
 (16) Bellitto, C.; Day, P. *J. Mater. Chem.* 1992, 2, 265.
 (17) Blasse, G.; Gorter, E. W. *J. Phys. Soc. Jpn., Suppl. B-1* 1962, 17, 176. Gorter, E. W. *Philips Res. Rep.* 1954, 9, 403.
 (18) Goodenough, J. B. *Magnetism and the Chemical Bond*; Interscience: New York, 1963.
 (19) Neel, L. *Ann. Phys.* 1948, 3, 137.

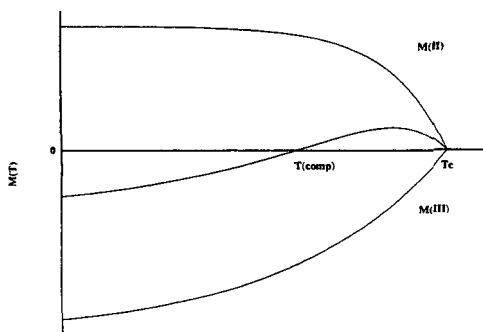


Figure 8. Temperature-dependent magnetization of a two-sublattice ferrimagnet, showing the occurrence of a compensation temperature T_{comp} .

35 K, the field at the Fe^{II} site is still small at 10 K.²¹ Given the topology of the 2D honeycomb lattice (Figure 7), the largest component of the molecular field experienced by the Fe^{III} is due to the neighboring Fe^{II} and vice versa. Thus the Mössbauer results confirm the hypothesis that the Fe^{II} sublattice magnetization increases more steeply below T_c than that of the Fe^{III} sublattice. Qualitatively, therefore, the situation in those compounds exhibiting negative magnetization at low temperature must indeed be as shown in Figure 8.

Finally, we address the question of why some of the $\text{AFe}^{\text{II}}\text{Fe}^{\text{III}}(\text{C}_2\text{O}_4)_3$ compounds show negative low-temperature magnetization while others do not. First of all, reference to Tables 1 and 2 shows that the phenomenon is not confined to those compounds with either the smallest or the largest interlayer separation. On the other hand, the compounds showing the effect are those with the highest T_c and (with one exception (5)) the largest Θ . The first of these observations requires that something more than interlayer interaction is responsible, while the second reveals the importance of the magnitude of the near-neighbor exchange interaction. The latter is a function of the intraplanar cation–cation separation, as well as the “bite” angle subtended by the bidentate $\text{C}_2\text{O}_4^{2-}$ bridging group and the degree of trigonal distortion around the cation sites. The sign and magnitude of the trigonal distortion, which is modulated by the intercalated organic template cations A, also determine the single ion anisotropy at the Fe^{II} site, which in turn affects the temperature dependence of the spontaneous magnetization of the Fe^{II} sublattice. Definition of all these parameters must await a full set of crystal structure determinations. Other physical methods, especially neutron diffraction, will be required to determine the distribution of the cations and their moments in the $\text{Fe}^{\text{II}}\text{Fe}^{\text{III}}$ tris(oxalate) series, but a final observation from the present study should be noted. Although the samples were synthesized under anaerobic conditions, their elemental analyses reveal a small deficiency in Fe. This may be due to a small fraction of the Fe^{II} becoming oxidized to Fe^{III} , despite the anaerobic conditions. Thus the ratio of Fe^{II} to Fe^{III} may deviate slightly from the ideal 1:1, introducing a small fraction of metal vacancies (cf. wustite, Fe_{1-x}O).

The magnetic properties of $\text{Mn}^{\text{II}}\text{Fe}^{\text{III}}$ tris(oxalate) series also reveal a number of highly unusual features. First, we have the unique situation that both metal ions have the same electronic ground state, ${}^6\text{A}_1$ in the D_3 point group. The Curie and Weiss

constants (Table 2) span a much smaller range than those of the $\text{Fe}^{\text{II}}\text{Fe}^{\text{III}}$ series, though the former (mean value $10.0 \text{ emu K mol}^{-1}$) are larger than the value of $8.75 \text{ emu K mol}^{-1}$ calculated for $S(\text{Mn}^{\text{II}}) = S(\text{Fe}^{\text{III}}) = 5/2$ and $g = 2$. Likewise the T_c 's vary only over about half the range as in the $\text{Fe}^{\text{II}}\text{Fe}^{\text{III}}$ series, with the same set of A. Apart from differences in the g values, which are very small since both ions have orbital singlet ground states, the compounds are expected to mimic antiferromagnetic rather than ferrimagnetic behavior. This is borne out by the temperature dependence of the susceptibility, which is indeed that of a classic 2D antiferromagnet,²² reaching a broad maximum at 55 K. An example is shown in Figure 4, but similar behavior is found in all eight compounds studied, indicating that the in-plane near-neighbor exchange constant does not vary significantly with changing organic cation A. In contrast, the degree of spin canting evidenced by the sharp rise in magnetization below 27 K varies very markedly with organic cation. The magnitude of the uncompensated moment, as indicated by the magnetization at 5 K, increases in the sequence $\text{N}(n\text{-C}_4\text{H}_9)_4 > \text{P}(\text{C}_6\text{H}_5)_4 < \text{P}(n\text{-C}_4\text{H}_9)_4 < \text{N}(n\text{-C}_3\text{H}_7)_4 < \text{As}(\text{C}_6\text{H}_5)_4 < (\text{C}_6\text{H}_5)_3\text{-PNP}(\text{C}_6\text{H}_5)_3$ (Figure 5). This order does not follow that of increasing interlayer separation (Table 1), so the spin canting arises from more subtle variations in the structure than those of the a_0 and c_0 parameters alone.

Conclusion

In this paper we have shown that 2D ferrimagnets $\text{AM}^{\text{II}}\text{Fe}^{\text{III}}(\text{C}_2\text{O}_4)_3$ ($\text{M}^{\text{II}} = \text{Mn, Fe}$) are formed by a wide variety of organic template cations A, giving material for extensive crystal chemical and magneto–structural correlation. In all, unit cell and magnetic parameters for 16 compounds are presented. In the series $\text{N}(n\text{-C}_n\text{H}_{2n+1})_4\text{Fe}^{\text{II}}\text{Fe}^{\text{III}}(\text{C}_2\text{O}_4)_3$ ($n = 3\text{--}5$), Θ and T_c increase with increasing n , as does the interlayer separation, the latter in the manner expected for intercalated n -alkyl groups. Several of the $\text{Fe}^{\text{II}}\text{Fe}^{\text{III}}$ compounds show negative magnetization at low temperature together with a “compensation temperature” at which the net magnetization vanishes, reminiscent of that found in ferromagnetic solid solutions.¹⁷ A qualitative explanation for the negative magnetization is found in Neel’s theory of two-sublattice ferrimagnets.¹⁹ This phenomenon is seen in the compounds with the largest measured Θ and T_c . Nevertheless there is no correlation between these magnetic parameters and interlayer separation. The corresponding $\text{Mn}^{\text{II}}\text{Fe}^{\text{III}}$ compounds mimic 2D antiferromagnets, though with a degree of spin canting at low temperature which varies strongly with the organic template cation. While the present work reveals many unusual features in the properties of the compounds $\text{AM}^{\text{II}}\text{Fe}^{\text{III}}(\text{C}_2\text{O}_4)_3$ with honeycomb layer structures, much remains to be done to understand the detailed relation of these properties with crystal structure, for which further X-ray and magnetic experiments with single crystals will be necessary. Our work is continuing in this direction.

Acknowledgment. We acknowledge the U.K. Engineering and Physical Sciences Research Council for an equipment grant and support to C.J.N. and S.G.C. and the European Union for an Institutional Fellowship (C.M.) and support through the Network on Molecular-based Magnets. We are grateful to Dr. J. Ensling (Mainz) for measuring Mössbauer spectra of compound 2 and to one of the reviewers for pointing out the unpublished structure determination of compound 10.

Supporting Information Available: A table of analytical data for $\text{AM}^{\text{II}}\text{Fe}^{\text{III}}(\text{C}_2\text{O}_4)_3$ (1 page). Ordering information is given on any current masthead page.

IC950703V

(20) Iijima, S.; Katsura, T.; Tamaki, H.; Mitsumi, M.; Matsumoto, N.; Okawa, H. *Mol. Cryst. Liq. Cryst.* **1993**, *233*, 263. Reiff, W. M.; Kreis, J.; Meda, L.; Kirss, R. U. *Mol. Cryst. Liq. Cryst.* **1995**, *273*, 181.

(21) Ensling, J. Personal communication.

(22) de Jongh, L. J.; Miedema, A. R. *Adv. Phys.* **1974**, *24*, 1.

The Magnetic Structures of the Layer Ferromagnets $P(C_6D_5)_4M^{II}Fe(C_2O_4)_3$ ($M^{II} = Mn, Fe$)

Christopher J. Nuttall and Peter Day*

Davy Faraday Research Laboratory, The Royal Institution of Great Britain, 21 Albemarle Street, London W1X 4BS

Received February 24, 1998

The bimetallic trisoxalato-metal(II,III) salts with the general formula $AMM'(C_2O_4)_3$, first reported by Tamaki et al.,¹ form a fascinating series in which to establish structure–property relationships in two-dimensional molecular-based lattices. The organic cation A can be varied widely, so that interlayer separations range from 8.5 to 14.5 Å;² the transition metal ions M and M' are also capable of wide variation, leading to ferro- or antiferromagnetic near-neighbor exchange and either ferro- or ferrimagnetic bulk properties. The oxalate ions bridge M and M', which, having 6-fold coordination, therefore form honeycomb layers.^{3–5} Within this broad series the compounds having $M' = Fe(III)$ are especially interesting from a magnetic point of view. When $M = Mn(II)$ we have the rare situation of a bimetallic lattice in which both metal ions have the same electronic ground state, $3d^5$, $S = 5/2$, 6A_1 . In case of antiferromagnetic near-neighbor exchange, the bulk properties should mimic those of an antiferromagnet rather than a ferrimagnet, since the two ions only differ marginally in their g values. This is indeed so,² though the magnitude of the uncompensated moment, while small, is extremely sensitive to the organic counterion A. When $M = Fe(II)$ an even more fascinating situation arises: not only are the compounds mixed valency (albeit of class II,⁶ i.e., valence-trapped, type) but since the Fe(II) ion has a large anisotropy the bulk magnetic behavior is highly unusual, with strong negative magnetization at low fields for some A.^{2,7} Definitive evidence on the ordered magnetic structures of solids comes from neutron diffraction. To date the only published work on the magnetic structure of a layer bimetallic trisoxalate salt using this method refers to a Mn^{II} - Cr^{III} phase which is ferromagnetic.⁸ In the present note we report a neutron powder diffraction study of the two antiferromagnetic phases $P(C_6D_5)_4M^{II}Fe(C_2O_4)_3$ with $M^{II} = Mn$ and Fe.

Experimental Section

Neutron powder diffraction data were collected using three instruments at the Institut Laue-Langevin, Grenoble, France. The D1B diffractometer is a high-intensity, medium-resolution, multidetector diffractometer. The wavelength is fixed at 2.52 Å, by a graphite

focusing monochromator. Counts are collected in steps of 0.2°, as defined by the distance between adjacent detector cells in the PSD bank. D1A has a high takeoff angle of 122° giving a good resolution over $2\theta = 6–160^\circ$. Scans are taken in 0.05° steps. The wavelength employed was 2.9811 Å, Ge[113]. A graphitic filter between the monochromator and the sample significantly reduced higher-order wavelength contaminations ($\lambda/\lambda < 0.1\%$). D2B is a very high resolution constant-wavelength diffractometer. Data collection is by step scans of 0.05°. A graphitic filter similar to that of D1A allowed collection at the relatively high wavelength of 2.398 Å (Ge[331]) without significant contamination from higher-order wavelengths. The instrument was set in its high-intensity mode.

The deuterated tetraphenylphosphonium cation $P(C_6D_5)_4^+$ was prepared as its bromide salt by a method modified from that originally proposed by Michealis⁹ and Dodanov^{10,11} for the synthesis of $P(C_6H_5)_4Br$. Bromobenzene(d_5) and triphenylphosphine(d_3) were used as purchased from Aldrich Chemicals Ltd. (deuteration >99.8%). The prepared $P(C_6D_5)_4Br$ was confirmed to be >99% deuterated by mass spectrometry (performed by John Hill at UCL).

$P(C_6D_5)_4MnFe(C_2O_4)_3$ and $P(C_6D_5)_4FeFe(C_2O_4)_3$ were prepared as follows.

$P(C_6D_5)_4MnFe(C_2O_4)_3$. A solution containing 3.344 g of $Fe(NO_3)_3 \cdot 6H_2O$ (9.56 mmol) and 1.885 g of $MnCl_2 \cdot 6H_2O$ (9.56 mmol) in 64 mL of H_2O was prepared; 3.671 g of $H_2C_2O_4 \cdot 2H_2O$ was dissolved in it. After 1 h the solution was filtered, and 2.65 g of $P(C_6D_5)_4Br$ (6.38 mmol), dissolved in 11 mL of 70:30 MeOH/ H_2O , was added dropwise to the filtrate. The precipitated $P(C_6D_5)_4MnFe(C_2O_4)_3$ was removed by filtration and dried {yield = 3.55 g (80%)}.
 $P(C_6D_5)_4FeFe(C_2O_4)_3$. A solution containing 2.271 g of $Fe(NO_3)_3 \cdot 6H_2O$ (6.5 mmol) and 1.804 g of $FeSO_4 \cdot 6H_2O$ (6.5 mmol) in 50 mL of H_2O was prepared; 2.496 g of $H_2C_2O_4 \cdot 2H_2O$ was dissolved in it. After 1 h the solution was filtered, and 1.9 g of $P(C_6D_5)_4Br$ (4.329 mmol), dissolved in 11 mL of 70:30 MeOH/ H_2O , was added dropwise to the filtrate. The precipitated $P(C_6D_5)_4FeFe(C_2O_4)_3$ was removed by filtration and dried {yield = 2.05 g (71.7%)}.
X-ray diffraction profiles of the two compounds verified that they were free of $M^{II}C_2O_4 \cdot 2H_2O$ peaks.

Results

The neutron powder diffraction profile of the MnFe compound recorded on D1A at 40 K is displayed in Figure 1a, and that of the FeFe compound, recorded at 50 K on D2B, is in Figure 1b. Using profile matching,¹² i.e., iterative fitting of structure factors, both were fitted with a Gaussian peak shape and $R3c$ unit cell { $\chi^2(MnFe) = 0.53$, $\chi^2(FeFe) = 0.47$ }. The fit gave lattice parameters of $a, b = 18.831(4)$ and $18.674(8)$ Å and $c = 55.511(8)$ and $56.289(14)$ Å, respectively, which correspond well with those obtained by room-temperature X-ray diffraction,^{2,8} with the expected contraction in c (~2 Å) and a, b (~0.5 Å) on decreasing the temperature. The intensity not fitted by the profile matching procedure is attributed to a small fraction of $P6(3)$ stacking phase identified in X-ray diffraction profiles. The 1.5 K profiles revealed no significant change in lattice parameters between 1.5 and 40 K. However, in the MnFe compound a number of reflections had increased intensity in the 1.5 K profile due to magnetic diffraction arising from long-range magnetic order. In contrast, in the FeFe compound, the only extra intensity at 1.5 K was a weak shoulder to the [202] nuclear reflection.

- (1) Tamaki, H.; Zhong, Z. J.; Matsumoto, N.; Kida, S.; Koikawa, M.; Achiwa, N.; Hashimoto, Y.; Okawa, H. *J. Am. Chem. Soc.* **1992**, *114*, 6974.
- (2) Mathonière, C.; Nuttall, C. J.; Carling, S. G.; Day, P. *Inorg. Chem.* **1996**, *35*, 1201.
- (3) Decurtins, S.; Schmalte, H. W.; Oswald, H. R.; Linden, A.; Ensling, J.; Güthlich, P.; Hauser, A. *Inorg. Chim. Acta* **1994**, *216*, 65.
- (4) Atovmyan, L. O.; Shilov, G. V.; Lyobovskaya, R. N.; Zhilyaeva, E.; Ovanesyan, N. S.; Pirumova, S. A.; Gusakovskaya, I. G. *JETP Lett.* **1993**, *58*, 766.
- (5) Carling, S. G.; Mathonière, C.; Day, P.; Malik, K. M.; Coles, S. J.; Hursthouse, M. B. *J. Chem. Soc., Dalton Trans.* **1996**, 1839.
- (6) Robin, M. B.; Day, P. *Adv. Inorg. Chem. Radiochem.* **1966**, *10*, 247.
- (7) Mathonière, C.; Carling, S. G.; Yusheng, D.; Day, P. *J. Chem. Soc., Chem. Commun.* **1994**, 1551.
- (8) Pellaux, R.; Schmalte, H. W.; Huber, R.; Fischer, P.; Hauss, T.; Ouladladi, B.; Decurtins, S. *Inorg. Chem.* **1997**, *36*, 2301.

- (9) Michaelis, D.; Soden, V. *Annales* **1885**, 229, 298.
- (10) Dodanov, R.; Medox, S. *Ber.* **1928**, *61*, 907.
- (11) Nuttall, C. J. Thesis, University of London, 1998.
- (12) Rodriguez-Carvajal, J. *FULLPROF: Reference Guide to the Program 3.2*; CEA-CNRS: Paris, 1997.

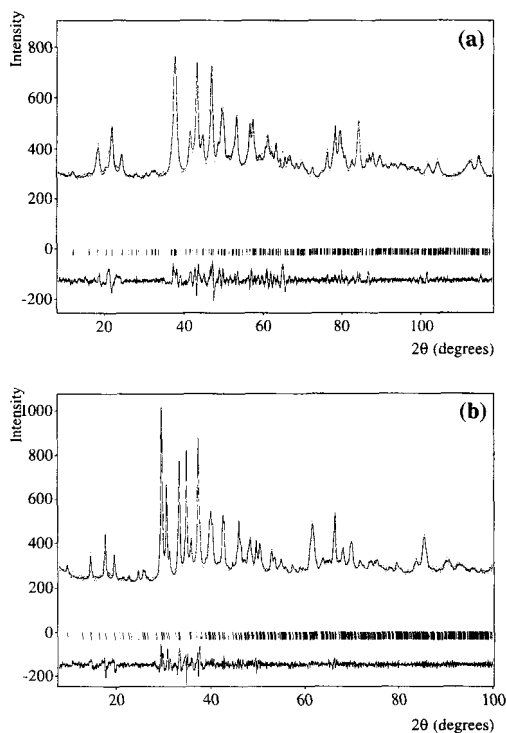


Figure 1. Neutron diffraction profiles of $P(C_6D_5)_4M^{II}Fe(C_2O_4)_3$ fitted with pattern matching to an $R3c$ cell: (a) $M^{II} = Mn$, 40 K (D1A) ($10 < 2\theta < 120^\circ$); (b) $M^{II} = Fe$, 50 K (D2B) ($10 < 2\theta < 120^\circ$).

The magnetic diffraction intensity was investigated in greater detail by means of difference plots obtained with the higher-flux D1B diffractometer. The intensity difference ($[I(1.7\text{ K}) - I(T > T_c)]$) is plotted in Figure 2. The magnetic reflections are quite weak compared to the large fluctuations in the difference background; however, the magnetic intensity can be indexed using an $R3c$ cell. The most intense magnetic reflection [201] observed in the difference plots was integrated, and its temperature dependence is plotted in Figure 3. The sharp decrease of the magnetic intensity at 24 and 39 K for the MnFe and FeFe compounds, respectively, compares well with the ordering temperatures estimated by bulk susceptibility measurements. While the temperature dependence of the FeFe magnetic intensity approximates a Brillouin function, that of MnFe is more complex and probably contains a contribution from short-range order above T_c which cannot be deconvoluted from powder data.

The indices of the magnetic reflections of MnFe (Figure 2a) indicate that the chemical and magnetic cells are coincident, i.e., the magnetic structure has the propagation vector $\kappa = 0$, and also that the moments lie close to the c axis, since no intensity is found for [00] reflections. In the $R3c$ cell both antiferromagnetic and ferromagnetic magnetic ordering models with $\kappa = 0$ can be envisaged with moments aligned parallel to the c axis. However, ferromagnetic ordering can be discounted as susceptibility measurements indicate antiferromagnetic ordering in the hydrogenous compound $P(C_6H_5)_4MnFe(C_2O_4)_3$.² Possible antiferromagnetic ordering models with moments parallel to the c axis may be further defined by considering the character of axial spins with respect to the symmetry operations

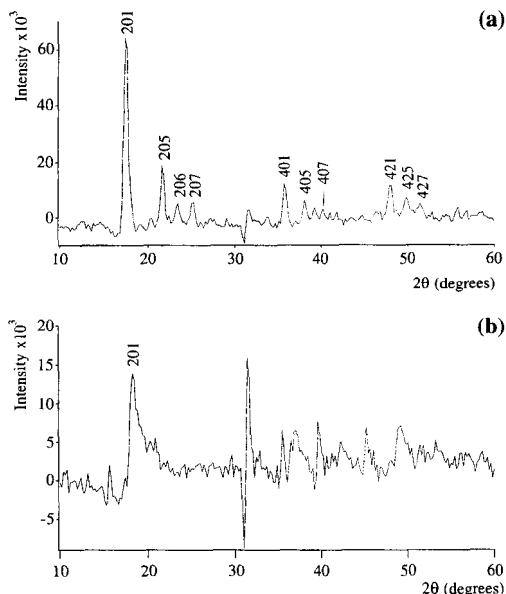


Figure 2. Intensity difference $[I(1.7\text{ K}) - I(T > T_c)]$ for $P(C_6D_5)_4M^{II}Fe(C_2O_4)_3$ with magnetic reflections ($R3c$ cell) indicated: (a) $M^{II} = Mn$, $T = 30\text{ K}$; (b) $M^{II} = Fe$, $T = 50\text{ K}$.

of the group. Two models are generated by considering the moment characters associated with the c glide plane operation in $R3c$, namely, antiferromagnetism with and without inversion of axial components of the moment along the c glide plane; respectively these are $R3c$ and $R3c'$ according to the Shubnikov definition. They differ in that $R3c$ requires the orientations of Mn and Fe moments to alternate from up to down in adjacent layers while in $R3c'$ they have the same relative orientation in all layers.

Using the FULLPROF program,¹² profiles were generated for the antiferromagnetic models $R3c$ and $R3c'$ using the metal positions³ from the structure of $P(C_6H_5)_4MnCr(C_2O_4)_3$ and the fitted low-temperature cell constants from the neutron data. For each model a moment of $5\mu_B$ was placed antiparallel along the c axis on the $Mn^{2+}(1)$ and $Fe^{3+}(4)$ sites. The predicted profiles are plotted in Figure 4.

By comparing the observed and predicted patterns, it is clear that the $R3c$ Shubnikov group provides the best representation of the low-temperature magnetic order in the MnFe compound. The proposed magnetic structure is illustrated in Figure 5. There are a few reflections in the magnetic profile which are not predicted by this model, the most prominent being [206]. The extra magnetic intensity could result from either the presence of a small amount of a $P6(3)$ stacking phase previously identified or from magnetic order in $R3c$ with moments not exactly aligned along the c axis. The first alternative was investigated by constructing a cell in $P6(3)$ using the metal atom positions from the $P6(3)$ half-cell structure of $N(C_4H_9)_4MnFe(C_2O_4)_3$.⁸ Calculated profiles for this structure, with antiferromagnetic alignment along the c axis for either $P6(3)$ or $P6(3)'$ stacking, predict a high intensity for the [102(206)] reflection, but [100(200)] is predicted to have even higher intensity although it is not observed. Hence the first alternative can be discounted, i.e., labeling reflections in both $P6(3)$ and the $R3c$ super cell as $[P6(3)(R3c)]$.

Notes

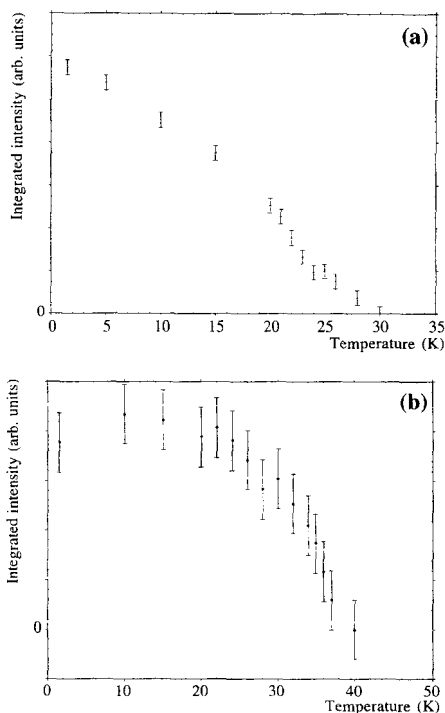


Figure 3. Integrated intensity of the [201] magnetic reflection of $P(C_6D_5)_4M^II Fe(C_2O_4)_3$ versus temperature: (a) $M^{II} = Mn$; (b) $M^{II} = Fe$.

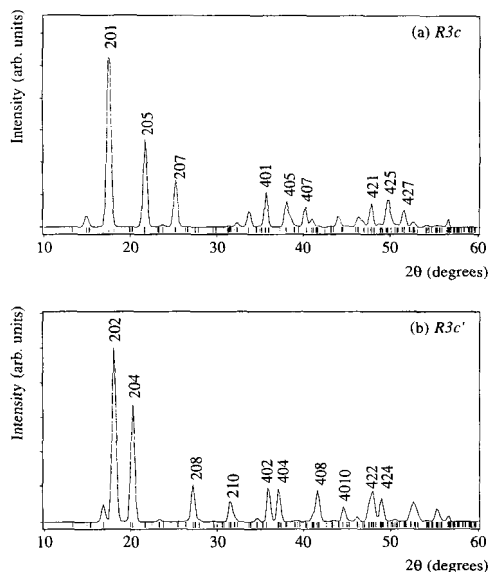


Figure 4. Predicted magnetic diffraction patterns for antiferromagnetic alignment along the c axis in $P(C_6D_5)_4MnFe(C_2O_4)_3$: (a) $R3c$; (b) $R3c'$.

The alternative of antiparallel antiferromagnetic ordering with moments oriented away from the c axis was investigated by

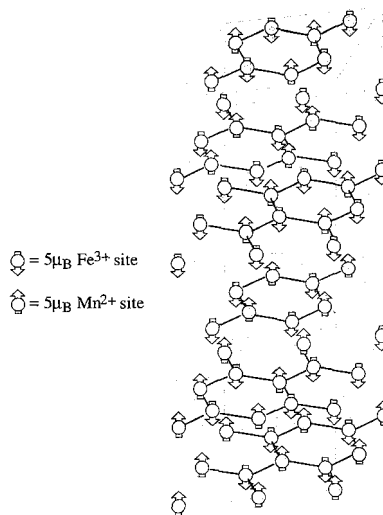


Figure 5. Proposed magnetic structure of $P(C_6D_5)_4MnFe(C_2O_4)_3$.

generating magnetic profiles with moments on $Mn(\uparrow)$ and $Fe(\downarrow)$ inclined at various angles to the c axis (using the $R3c$ Shubnikov group), with nonaxial moment components parallel to the a axis. Altering the nonaxial spin direction between the a and b axes caused little change in the predicted pattern because of the almost exact hexagonal arrangement of the metal atoms in the (a,b) plane. The intensity of the [206] magnetic reflection does not increase significantly, while those of [006] and [204], which we do not observe, increase greatly. Thus there is no evidence that the moments are aligned other than parallel to the c axis.

In striking contrast to the $MnFe$ compound, the intensity difference plot [$I(1.7\text{ K}) - I(50\text{ K})$] of the $FeFe$ compound (Figure 2b) reveals only extremely weak magnetic scattering. That the single clearly observed peak indexes as [201] indicates antiferromagnetic order of the $Fe(II)$ and $Fe(III)$ moments parallel to the c axis. However, the [201] reflection is highly asymmetric, which strongly suggests that there is disorder between the layers. Nevertheless, the bulk susceptibility measurements suggested a transition to long-range order at 34 K.² In view of these facts, one possible view of the magnetic order is that the behavior is glassy as a result of the strong single-ion anisotropy of the $Fe(II)$ ions: below 39 K ferrimagnetic correlations develop with anisotropy directions randomly oriented in different layers. Finally the correlated regions become blocked by each other so that, while the majority of the moments are fixed by anisotropy pinning, a fraction remains mobile down to 5 K.

Conclusion

Neutron powder diffraction reveals contrasting low-temperature magnetic order in the bimetallic layer ferrimagnets $P(C_6D_5)_4M^II Fe(C_2O_4)_3$ ($M^{II} = Mn, Fe$). In the $MnFe$ compound the observed magnetic diffraction agrees very well with that predicted for a simple collinear antiferromagnetic alignment of $Mn(II)$ and $Fe(III)$ moments parallel to the c axis (i.e. perpendicular to the layers) with Shubnikov $R3c$ symmetry. This model correctly describes the relative intensities of the four most intense magnetic reflections, and also the presence of weaker

3888 *Inorganic Chemistry, Vol. 37, No. 15, 1998*

Notes

observed peaks predicted by the model. In contrast, in the FeFe compound the magnetic diffraction is much weaker and only a single reflection [201] is observed. Absence of [00l] intensity indicates that, like the MnFe compound, the moments in FeFe are aligned antiferromagnetically along or close to the *c* axis. However, the asymmetric line shape of the [201] reflection suggests that full long-range order is not fully established, even

at 5 K, possibly because randomly oriented domains with differing anisotropy directions develop and become blocked.

This work has been supported by the UK Engineering and Physical Sciences Research Council (studentship to C.J.N.). We are grateful to the Institut Laue-Langevin, Grenoble, for access to neutron facilities and to Dr A. Hewat for help and discussions.

IC980201S

Magnetization of the Layer Compounds $AFe^{II}Fe^{III}(C_2O_4)_3$ (A = Organic Cation), in Low and High Magnetic Fields: Manifestation of Néel N and Q Type Ferrimagnetism in a Molecular Lattice[†]

Christopher J. Nuttall and Peter Day*

Davy Faraday Research Laboratory, The Royal Institution of Great Britain,
21 Albemarle Street, London W1X 4BS, U.K.

Received March 23, 1998. Revised Manuscript Received June 5, 1998

Detailed bulk magnetization and magnetic susceptibility measurements are reported for representative examples of the series of ferrimagnetic tris-oxalato-ferrate(II,III) salts with general formula $AFe^{II}Fe^{III}(C_2O_4)_3$ (A = quaternary ammonium, phosphonium, or arsonium). The compounds all crystallize in two-dimensional hexagonal honeycomb lattices, but while some show conventional low field positive magnetization at low temperature (Néel type Q), others show a large negative magnetization below a compensation temperature T_{comp} (Néel type N) under the same measurement protocol. Isothermal and temperature-dependent magnetizations are measured after zero field and field cooling. Temperature-dependent hysteresis measurements are also presented. In compounds that exhibit negative magnetization a discontinuity in the magnetization is observed at T_t ($T_{comp} < T_t < T_c$) which correlates with the onset of a giant anisotropy and is indicative of a magnetostrictive transition. In compounds that exhibit positive magnetization, hysteresis behavior and frequency-dependent ac susceptibility data indicate a glassy magnetic order at low temperatures, possibly arising from the frustration of random anisotropy domains below a characteristic blocking temperature or imbalance and disorder of Fe(II) and Fe(III).

Introduction

One of the most remarkable features of molecular-based materials is the way that the magnetic properties may be transformed by quite small and subtle variations in the molecular chemistry.¹ A striking example of this general statement is the elegant and diverse series of two-dimensional molecular-based magnetic materials formed by tris-oxalato salts containing both divalent and trivalent transition metal ions and a wide range of organic cations, principally tetraalkyl- and tetraarylphosphonium, -arsonium, and -ammonium.² The common formula is $AM^{II}M^{III}(C_2O_4)_3$ (A = organic cation), and the M and M' alternate in a hexagonal planar honeycomb lattice, bridged by the ambidentate oxalate ions.^{3–5} Depending on M and M' the near-neighbor exchange may be ferro- or antiferromagnetic, leading to bulk ferro- or ferrimagnetic behavior. We surveyed the structures and magnetic properties of a large number of $Mn^{II}Fe^{III}$

and $Fe^{II}Fe^{III}$ examples with different A and found that the magnetic ground state was extremely sensitive to small chemical variations in A.⁶ In particular, we found that in the $Fe^{II}Fe^{III}$ series the low field magnetization became large and negative at low temperature for some A's, but not others.⁷ Essentially, the compounds behaved as N type or Q type according to Néel's classification of ferrimagnets.⁸ In the present article we present a more detailed magnetic study with a focus on one example of each order type (A = $N(n-C_4H_9)_4$ and $P(C_6H_5)_4$), in an endeavor to find the factors determining the characteristics of the two types of behavior, in particular the negative magnetization. Magnetization, susceptibility, and hysteresis data have been determined over a wide range of temperature and applied magnetic field, paying special attention to the zero field or field cooling protocols.

Experimental Section

The compounds were prepared and characterized as described in ref 5. dc magnetic measurements were performed on a MPMS7 Quantum Design SQUID magnetometer equipped with a 7 T magnet in the temperature range 2–300 K. Powder samples of ~30 mg (~3 × 3 × 6 mm³) were loaded into gel caps and placed in tight fitting transparent straws, periodically

[†] Dedicated to the memory of Jean Rouxel, pioneer of layer materials.

(1) For numerous recent examples, see, e.g.: Kahn, O., Ed. *Magnetism a Supramolecular Function*; Kluwer Academic Publishers: Dordrecht, 1996.

(2) Tamaki, H.; Zhong, Z. J.; Matsumoto, N.; Kida, S.; Koikawa, M.; Achiwa, N.; Hashimoto, Y.; Ookawa, H. *J. Am. Chem. Soc.* **1992**, *114*, 6974–6979.

(3) Decurtins, S.; Schmalle, H. W.; Oswald, H. R.; Linden, A.; Enslin, J.; Gutlich, P.; Hauser, A. *Inorg. Chim. Acta* **1994**, 65–73.

(4) Atovymann, O. L.; Shilov, G. V.; Lyubovskaya, R. N.; Zhilyaeva, E. I.; Ovanesyan, N. S.; L., P. S.; Gusakovskaya, I. G.; G., M. Y. *JETP Lett.* **1993**, *58*, 767–768.

(5) Carling, S. G.; Mathonière, C.; Day, P.; Malik, K. M. A.; Coles, S. J.; Hursthouse, M. B. *J. Chem. Soc., Dalton Trans.* **1996**, 1839.

(6) Mathoniere, C.; Nuttall, C. J.; Carling, S. G.; Day, P. *Inorg. Chem.* **1996**, *35*, 1201–1207.

(7) Mathoniere, C. C., S. G.; Yusheng, D.; Day, P. *J. Chem. Soc., Chem. Commun.* **1994**, 1551–1552.

(8) Néel, L. *Ann. Phys. (Paris)* **1948**, *3*, 137–198.

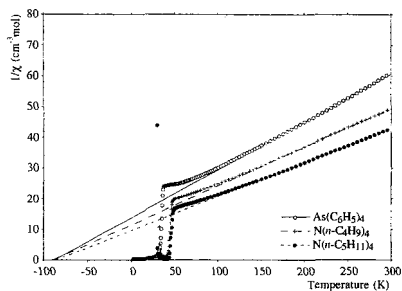


Figure 1. Inverse susceptibility vs temperature of $AFe^{II}Fe^{III}(C_2O_4)_2$ fitted to the Curie–Weiss law.

punctured with tiny holes along their length. The straws were then loaded with three compensatory empty gel caps on either side of the one containing the sample.

Low Field dc SQUID Magnetometry. Remanent fields in the magnetometer were reduced and calibrated before (and after) measurement. Large remanent fields (~ 1 – 10 G) were reduced via the magnet reset option. Persistent remanence was calibrated by measuring samples in a paramagnetic regime, in a range of applied fields above and below ($+10$ G \leftrightarrow -10 G). By this means zero effective field could be accurately achieved in the magnetometer down to ± 0.05 G. Remanent field creep during prolonged measurement was monitored by recalibrating remanence after completing the measurement. Low field measurements were carried out with the magnet in its oscillation field setting mode.

High Field DC SQUID Magnetometry. High field hysteresis measurements were carried out with the magnet set in the no-overshoot field setting mode, using the hysteresis option. In all high field measurements samples were rigidly held in the sample mount by pressing and placing in an inverted gel cap.

AC Magnetometry. ac susceptibility measurements were performed at the Institute of Molecular Science in Okazaki National Science Park, Japan, on a MPMS2 SQUID magnetometer fitted with an ac measurement option. Measurements were recorded between 0.01 and 1500 Hz, from 2 to 100 K. The driving field was maintained at 5 G for all measurements and zero applied dc field was rigorously maintained.

Results

Survey of Magnetic Properties. The basic magnetic characterization of all members of the series was carried out by cooling polycrystalline samples in 100 G field (100 G FC) to 2 or 5 K and measuring the magnetization at 100 G while warming to 300 K. The susceptibilities were fitted to the Curie–Weiss law from 150 to 300 K, after correcting for sample diamagnetism. Figure 1 shows the susceptibilities of the $As(C_6H_5)_4$, $N(n-C_4H_9)_4$, and $N(n-C_8H_{11})_4$ compounds. Those of other members of the series will be found in ref 6. The Curie–Weiss parameters extracted from these data will be found in Table 1.

The temperature dependence of the molar magnetizations of several of the compounds from 5 to 50 K is shown in Figure 2 and the resulting magnetic parameters in Table 1. From Figure 2, it is clear that there are two quite different kinds of temperature dependence. The magnetization of the $P(C_6H_5)_4$ and $As(C_6H_5)_4$ compounds increases abruptly below about 35 K and continues to increase monotonically, tending to saturation with $M/T \rightarrow 0$ at the lowest temperature. In striking contrast, the $N(n-C_3H_7)_4$, $N(n-C_4H_9)_4$, $N(n-$

$C_5H_{11})_4$, $P(n-C_4H_9)_4$, and PPN compounds behave quite differently after 100 G FC. Below $T_c \sim 45$ K, the magnetization increases abruptly to reach a rounded maximum at $T_{max} \approx 40$ K ($\delta^2 M/\delta T^2$ is negative in the region 35 K $< T < 42$ K). It then falls rapidly and monotonically until, at about 30 K (T_{comp}), it reaches zero. At lower temperatures the magnetization becomes large and negative with respect to the applied field, tending to saturation at the lowest temperature, with $M/T \rightarrow 0$. To throw more light on this peculiar magnetic behavior, detailed magnetization measurements were made on the $N(n-C_4H_9)_4$ compound, which exhibits a negative magnetization at low temperature, and the $P(C_6H_5)_4$ compound, which has a positive magnetization.

Negative Low Temperature Magnetization. Low Applied Fields. The $N(n-C_4H_9)_4$ sample was cooled in fields between 0 and 100 G and the magnetization measured from 5 to 50 K in a field of 100 G. Both the ZFC and 100 G FC magnetizations increase at $T_c = 45$ K but they diverge at 43.5 K, indicating the onset of hysteresis. The ZFC magnetization reaches a maximum at 42 K and then falls, with a pronounced shoulder at 40 K, to a minimum around 35 K, after which it rises slowly toward lower temperatures. Cooling in very small fields ($H < 1$ G) results in negative magnetization. For example, an applied field of only 2 G during cooling gave the same negative saturation magnetization as the 100 G FC measurement (Figure 3).

The shoulder in the ZFC magnetization at 40 K was also evident as a slight discontinuity in 100-G FC magnetizations of all the compounds that showed low temperature negative magnetization. To examine this effect in more detail the $N(n-C_4H_9)_4$ compound was cooled from the paramagnetic regime to 45 K in 100 G applied field and the magnetization measured from 45 to 35 K in small temperature intervals. The resulting magnetization curve (Figure 4) has a pronounced discontinuity at 40.0 K (T_c), without significant temperature hysteresis between cooling and warming (Figure 4 inset).

To investigate the sensitivity of the low temperature magnetization to the temperature at which the field was applied, the sample was cooled successively in zero field to 45 K ($T > T_c$), 43 K ($T_t < T < T_c$), and 40 K ($T = T_t$) before further field cooling in 100 G to 5 K. Applying the field from 45 and 43 K resulted in behavior almost identical to the 100-G FC case, while field cooling from 40 K gave a magnetization curve intermediate between the FC and ZFC behavior, indicating that the sample had been cooled partially in magnetized and demagnetized states.

High Applied Field. To probe the stability of the negative magnetization state the $N(n-C_4H_9)_4$ compound was cooled in fields from 100 to 70 000 G, measuring the magnetization during warming from 5 to 50 K in an applied field of 100 G. Cooling in fields from 100 to 2000 G increased the negative saturation magnetization at 5 K, while in higher cooling fields, the saturation magnetization became progressively more positive, as shown in Figure 5. Only at the highest cooling fields (60 000–70 000 G) did the magnetization curves tend to the inverse of the 100-G FC case, with a compensation temperature at 32 K and magnetization becoming positive on decreasing temperature. Above 37 K the

Table 1. Magnetic Parameters of $\text{AFe}^{\text{II}}\text{Fe}^{\text{III}}(\text{C}_2\text{O}_4)_3$ (100-G FC)

A	T_c^a (K)	T_{comp} (K)	C ($\text{cm}^3 \text{mol}^{-1} \text{K}$) (150–300 K)	θ (K) (150–300 K)	μ_{eff} (μB) (300 K)	M_{sat} (at T_{min}) ($\text{cm}^3 \text{G mol}^{-1}$)
$\text{N}(n\text{-C}_3\text{H}_7)_4$	44.5	34	7.79(13)	-92.2(5.0)	6.88	-385 (2 K)
$\text{N}(n\text{-C}_4\text{H}_9)_4$	45	31.5	7.88(1)	-90.24(30)	6.87	-404 (5 K)
$\text{N}(n\text{-C}_6\text{H}_{11})_4$	46	29.5	9.05(1)	-86.92(6)	7.45	-850 (5 K)
$\text{P}(\text{C}_6\text{H}_5)_4$	34		6.71(12)	-88.4(2)	6.43	243 (2 K)
$\text{As}(\text{C}_6\text{H}_5)_4$	36		6.41(10)	-88.5(5.8)	6.27	290 (2 K)
$\text{P}(n\text{-C}_4\text{H}_9)_4$	44.5	33.5	7.761(10)	-89.9(2)	6.93	-392 (5 K)
PPN	43	30.5	7.758(10)	-88.4(2)	6.92	-235.5 (5 K)

^a T_c chosen as the temperature of the abrupt increase in 100-G FC magnetisation.

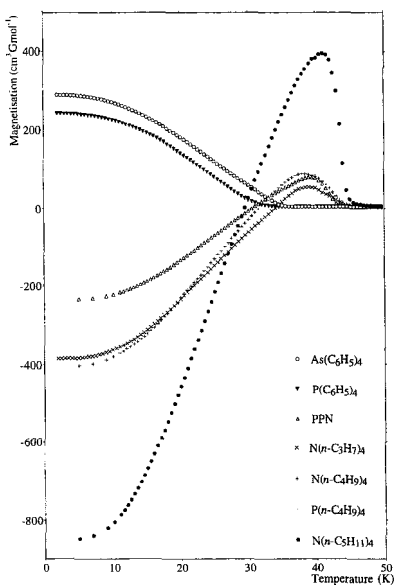


Figure 2. Temperature dependence of the magnetization of $\text{AFe}^{\text{II}}\text{Fe}^{\text{III}}(\text{C}_2\text{O}_4)_3$ after 100-G field cooling.

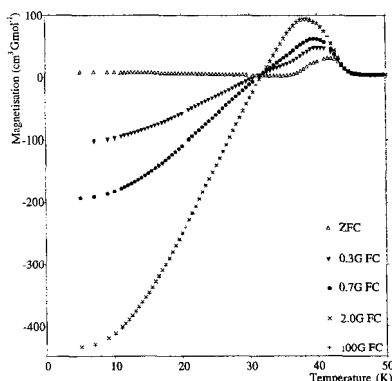


Figure 3. Temperature dependence of the ZFC and FC (0–100 G) magnetization of $\text{N}(n\text{-C}_4\text{H}_9)_4\text{Fe}^{\text{II}}\text{Fe}^{\text{III}}(\text{C}_2\text{O}_4)_3$ below 50 K.

magnetization returned to the direction of the field with a second $T_{\text{comp}} = 39.5$ K.

Hysteresis loops (± 70 000 G) were recorded at 5 K after 100-G FC, 70 000-G FC, and ZFC. The hysteresis curve after 100-G FC (Figure 6) is asymmetrically

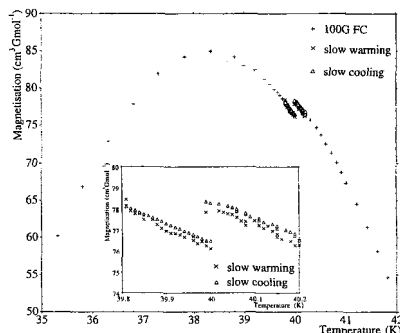


Figure 4. Magnetization of $\text{N}(n\text{-C}_4\text{H}_9)_4\text{Fe}^{\text{II}}\text{Fe}^{\text{III}}(\text{C}_2\text{O}_4)_3$ (100-G FC) showing the discontinuity at 40 K. The inset shows slow warming and slow cooling cycles.

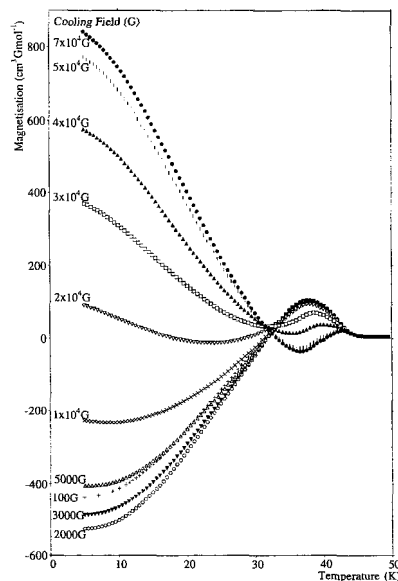


Figure 5. Temperature dependence of the FC (100–70 000 G) magnetization of $\text{N}(n\text{-C}_4\text{H}_9)_4\text{Fe}^{\text{II}}\text{Fe}^{\text{III}}(\text{C}_2\text{O}_4)_3$, on warming in 100.G.

displaced toward negative magnetization, indicating that the sample retains a memory of its field cooling history, despite field cycling between ± 70 000 G. The fact that the hysteresis loop opens over the field cycle indicates that irreversible magnetization processes occur, although it shows no coercive field (H_c). The

Magnetization of Layer Compounds

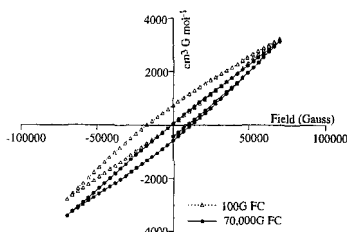


Figure 6. Hysteresis of $N(n\text{-C}_4\text{H}_9)_4\text{Fe}^{\text{II}}\text{Fe}^{\text{III}}(\text{C}_2\text{O}_4)_3$ at 5K after (a) 100-G FC and (b) 70 000-G FC.

Table 2. Temperature Dependence of the Coercivity (H_c) and Remanence (R_M) of $\text{AFe}^{\text{II}}\text{Fe}^{\text{III}}(\text{C}_2\text{O}_4)_3$

temp (K)	cooling field (G)	H_c (G)	R_M ($\text{cm}^3 \text{ G mol}^{-1}$)		$ \Delta R_M $ ($\text{cm}^3 \text{ G mol}^{-1}$)
			dec field	inc field	
(a) $\text{A} = (n\text{-C}_4\text{H}_9)_4$					
42	100	188	18	-22	40
40	100	400	60	-58	118
38	100	581	75	-75	150
36	100		69	-39	108
33	100		22	14	8
31	100		5	-13	18
29	100		-20	-64	44
5	100		58	-585	643
5	0		744	42	702
5	70000		330	-330	660
(b) $\text{A} = \text{P}(\text{C}_6\text{H}_5)_4$					
25	100		0	0	40
20	100	541	140	-130	118
15	100	1200	280	-280	150
5	100	11500	890	-890	108

remnant magnetizations R_M are recorded in Table 2a for both increasing and decreasing applied fields. In contrast, the 70 000-G FC hysteresis curve at 5 K is asymmetrically displaced toward positive magnetization, indicating a memory effect in the opposite direction to the 100-G FC one, with respect to the cooling field, while the shape is almost identical to that after 100-G field cooling, with similar asymmetry and remanence values. Thus, the ground-state reached after cooling in 70 000 G is similar to the one arrived at cooling in 100 G, though with a reversal in the direction of the remanent magnetization.

The 100-G FC hysteresis loop opens below T_c and between 42 and 38 K retains a conventional S-shape, is symmetric with respect to the magnetization axis, and exhibits a coercive field (H_c). Such behavior is consistent with the growth of magnetic domains in the direction of applied field. Below 38 K, the hysteresis curve changes shape, becomes asymmetric, and has no observed coercivity $\pm 10\,000$ G (Figure 7). On further cooling the hysteresis narrows and reduces its asymmetric shift until at 32 K (T_{comp}) it vanishes. Finally at 29 K it resembles the one recorded at 5 K. The temperature dependence of the magnetic coercivity and remanence constants are listed in Table 2a.

AC Susceptibility. Figure 8 shows the dispersion (χ') and the absorption (χ'') of the ac susceptibility at 0.1 Hz. Above T_c , χ' follows the dc susceptibility and $\chi'' = 0$, consistent with the measured quantity being the isothermal susceptibility, i.e., $\chi' = c_T = c_{\text{dc}}$ ($\omega t \ll 1$). Below 47 K χ' begins to rise, reaching a maximum at ~ 44 K, in parallel with the onset of divergence between

Chem. Mater., Vol. 10, No. 10, 1998 3053

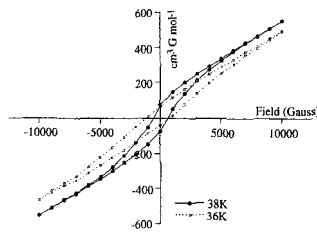


Figure 7. Variation of hysteresis of $N(n\text{-C}_4\text{H}_9)_4\text{Fe}^{\text{II}}\text{Fe}^{\text{III}}(\text{C}_2\text{O}_4)_3$ (100-G FC) with temperature.

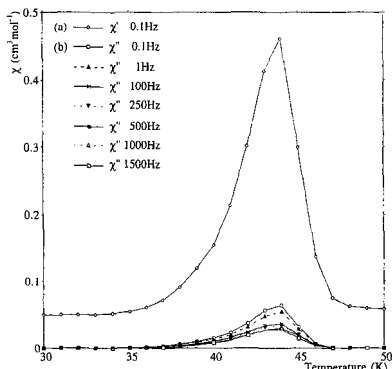


Figure 8. AC susceptibilities of $N(n\text{-C}_4\text{H}_9)_4\text{Fe}^{\text{II}}\text{Fe}^{\text{III}}(\text{C}_2\text{O}_4)_3$ in ordering region: (a) χ' at 0.1 Hz; (b) frequency dependence of χ'' (0.1–1500 Hz).

the dc FC and ZFC susceptibilities. At lower temperature χ' falls, with a broad but weak shoulder at 40 K, analogous to that seen in the dc ZFC data. At 35 K χ' follows the ZFC χ_{dc} , consistent with the measured quantity now being the adiabatic susceptibility $\chi' = \chi_S$ ($\omega t \gg 1$). Below 46 K χ'' rises from zero to a maximum at ~ 44 K before falling to zero around 40 K. The nonzero χ'' between 40 and 46 K indicates that relaxational processes are active ($\omega t \sim 1$) and confirms the transition to a state with a spontaneous magnetization. The maximum in χ'' at ~ 44 K reduces in magnitude and broadens with increasing measurement frequency from 0.1 to 1500 Hz, though the temperature of the maximum remains constant (Figure 8).

Positive Low Temperature Magnetization. Low Applied Field. As an example of a compound showing positive low temperature magnetization, the magnetization of the $\text{P}(\text{C}_6\text{H}_5)_4$ salt was investigated under the same protocols as the $N(n\text{-C}_4\text{H}_9)_4$ compound. Both the ZFC and 100 G FC magnetizations rise at $T_c \sim 34$ K but begin to diverge at 28 K. The ZFC magnetization reaches a broad maximum at around 25 K and then decreases toward lower temperatures reaching $6 \text{ cm}^3 \text{ G mol}^{-1}$ at 5 K (Figure 9). Magnetization curves measured after cooling in fields higher than 10 G have no maxima at 25 K. The saturation magnetization at 5 K increased monotonically with the cooling field, in each case with $\delta M / \delta T \rightarrow 0$.

High Field Studies. The high field hysteresis behavior of $\text{P}(\text{C}_6\text{H}_5)_4\text{Fe}^{\text{II}}\text{Fe}^{\text{III}}(\text{C}_2\text{O}_4)_3$ at 5 K (100-G FC) is plotted in Figure 10a, while the temperature evolution of hysteresis between $\pm 10\,000$ G at 15, 20, and 25 K

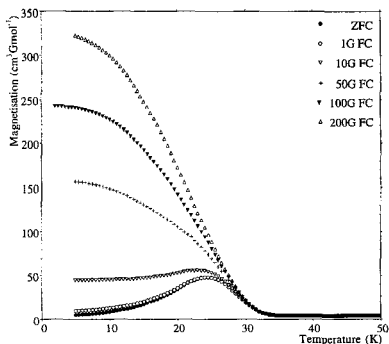


Figure 9. Temperature dependence of the ZFC and FC (1–200 G) magnetization of $P(C_6H_5)_4Fe^{II}Fe^{III}(C_2O_4)_3$.

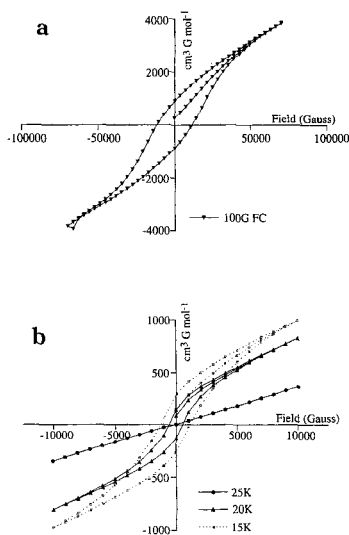


Figure 10. Hysteresis of $P(C_6H_5)_4Fe^{II}Fe^{III}(C_2O_4)_3$ (100-G FC): (a) 5 K; (b) variation with temperature.

(100-G FC) is shown in Figure 10b. The hysteresis loop at 5 K is symmetric, indicating no field cooling memory, and has a coercive field (H_c) of 11 500 G. The temperature dependence of the hysteresis is unusual: at 25 K (corresponding to roughly the magnetization maximum in the ZFC data (Figure 9) and 9 K below T_c) there is no measurable opening of the hysteresis, but at lower temperatures it opens, resembling the 5 K curve (Figure 10b). The temperature-dependent magnetic coercivity and remanence constants are listed in Table 2b.

AC Susceptibility. Figure 11 shows the ac susceptibilities (χ' and χ'') measured at 0.1 Hz. At 45 K $\chi' \approx \chi_{dc}$ and the absorption $\chi'' = 0$ ($wt \ll 1$). Upon lowering the temperature, χ' rises to a very small maximum at around 40 K and falls; χ' begins to rise gradually again at 35 K, with a shoulder near 30 K and a maximum ~ 18 K. At 5 K, χ' decreases to become equal to the ZFC dc magnetization. At its peak, χ' is considerably smaller than ZFC χ_{dc} . Furthermore, since χ' has no sharp peak it is not possible to estimate T_c from ac measurements.

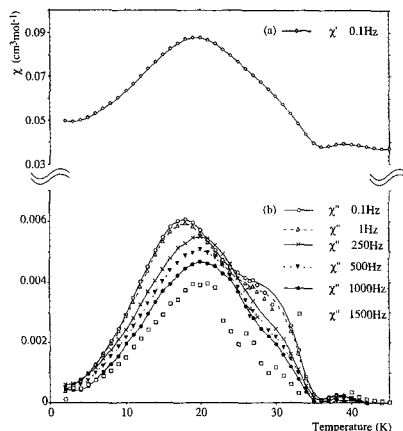


Figure 11. AC susceptibilities of $P(C_6H_5)_4Fe^{II}Fe^{III}(C_2O_4)_3$ in ordering region: (a) χ' at 0.1 Hz; (b) frequency dependence of χ'' (0.1–1500 Hz).

The absorption, χ'' , varies with temperature in the same way as χ' but with much smaller susceptibility. The behavior of both χ' and χ'' is extremely unusual and the fact that χ'' remains finite between 5 and 40 K indicates that at least some relaxation processes are active ($wt \sim 1$) down to low temperature. Figure 11b displays the frequency dependence of χ'' . The maximum at 18 K becomes weaker and shifts to higher temperatures with increasing measuring frequency, the high temperature shoulder being present only at frequencies lower than 1 Hz. If we assume that there is a single time constant t for magnetic relaxation, the maximum in χ'' corresponds to a freezing temperature (T_f), below which the magnetization cannot follow the oscillating field. A test for Arrhenius magneto-dynamics indicated that the magneto-dynamics of this material are more complicated than that predicted by a single activation energy.

Discussion

Paramagnetic Region. As a background to looking in more detail at the unusual magnetic properties of the $AFe^{II}Fe^{III}(C_2O_4)_3$ compounds in their ordered state we first consider their behavior in the paramagnetic region. The susceptibilities of all members of the series obey the Curie–Weiss law from 150 to 300 K. The mean value of the Curie constant across the series ($7.662 \text{ cm}^3 \text{ mol}^{-1} \text{ K}$) is consistent with the presence of high spin Fe^{III} and Fe^{II} ions: assuming spin-only moments $S(Fe^{III}) = 5/2$ and $S(Fe^{II}) = 2$ and an isotropic Landé splitting factor, $g = 2$, for both ions calculates $C = 7.375 \text{ cm}^3 \text{ mol}^{-1} \text{ K}$.

While it is a good approximation to the ${}^6A_{1g}$ ground state of the Fe^{III} ion, the assumption of a spin-only moment is a poor approximation for Fe^{II} . The 5D ($L = 2$) free-ion state of $Fe^{II}(d^6)$ ions has orbital degeneracy and in a cubic ligand field the ${}^5T_{2g}$ ground term retains an orbital contribution to the total moment, so that the lowest spin–orbit state has $J = 1$. Introducing a trigonal distortion from the three bidentate oxalate ligands causes a further splitting of the $J = 1$ state so

Magnetization of Layer Compounds

that the resulting ground state is either a singlet ($M_J = 0$) or doublet ($M_J = \pm 1$).⁹ The energy separation between the spin-orbit components in Fe^{II} is on the order of 200 cm^{-1} , so we expect an orbital contribution to the Fe^{II} moment, which could explain the high value of the Curie constant. The Curie constants of $\text{N}(n\text{-C}_3\text{H}_7)_4$, $\text{N}(n\text{-C}_4\text{H}_9)_4$, and $\text{P}(n\text{-C}_4\text{H}_9)_4$ compounds are all in excess of the spin-only value by approximately $0.43 \text{ cm}^3 \text{ G mol}^{-1}$; however, for $\text{N}(n\text{-C}_5\text{H}_{11})_4\text{Fe}^{\text{II}}\text{Fe}^{\text{III}}(\text{C}_2\text{O}_4)_3$, $C = 9.05 \text{ cm}^3 \text{ G mol}^{-1}$, corresponding to an excess of approximately $1.6 \text{ cm}^3 \text{ G mol}^{-1}$ (Table 1). This might result from the different symmetry of the Fe^{II} sites: for $\text{N}(n\text{-C}_3\text{H}_7)_4$, $\text{N}(n\text{-C}_4\text{H}_9)_4$, and $\text{P}(n\text{-C}_4\text{H}_9)_4$ compounds the powder X-ray diffraction is modeled by a hexagonal cell with C_3 site symmetry of the $\text{Fe}^{\text{II}}(\text{C}_2\text{O}_4)_3$ unit,⁶ while the site symmetry of Fe^{II} in the $\text{N}(n\text{-C}_5\text{H}_{11})_4$ compound is C_2 .⁵

The Weiss constants θ are all large and negative, indicating a mean antiferromagnetic interaction between Fe moments. From the small spread in θ values (-86.9 to -92.2 K), we see that the magnetic exchange is of similar strength in all the compounds, as expected, given the close similarity between the structures. In most of the compounds $|T_c/\theta| \sim 0.5$, although for $\text{P}(\text{C}_6\text{H}_5)_4$ and $\text{As}(\text{C}_6\text{H}_5)_4$ it is ~ 0.4 . Molecular field theory predicts $|T_c/\theta| = 1$, but large deviations are expected in low dimensional magnets because of the buildup of short-range correlations above T_c . Indeed, for a two-dimensional Ising ferromagnet on a honeycomb lattice $|T_c/\theta|$ has been calculated as 0.506 .¹⁰ The reduced $|T_c/\theta|$ in the $\text{P}(\text{C}_6\text{H}_5)_4$ and $\text{As}(\text{C}_6\text{H}_5)_4$ compounds may therefore signal a change in the effective dimensionality.

Low-Temperature Magnetic Behavior. Below 100 K the magnetization of this series of compounds varies dramatically with the cation A. When measuring the magnetization after cooling in a 100 G field, a magnetic compensation point (T_{comp}) and low-temperature negative magnetization with respect to the field are observed in the $\text{A} = \text{N}(n\text{-C}_3\text{H}_7)_4$, $\text{N}(n\text{-C}_4\text{H}_9)_4$, $\text{N}(n\text{-C}_5\text{H}_{11})_4$, $\text{P}(n\text{-C}_4\text{H}_9)_4$, and PPN compounds, while the $\text{P}(\text{C}_6\text{H}_5)_4$ and $\text{As}(\text{C}_6\text{H}_5)_4$ compounds show a positive magnetization at low temperature. Since all the compounds are ferrimagnetic, with Fe^{III} and Fe^{II} ions ordered antiferromagnetically, it is useful to compare the temperature dependence of the magnetization with that predicted by Néel: the "normal" positive magnetization curves of the $\text{P}(\text{C}_6\text{H}_5)_4$ and $\text{As}(\text{C}_6\text{H}_5)_4$ compounds resemble the Néel type Q ferrimagnetic order, while the negative magnetization curves exhibit a variant of Néel type N order.

According to Néel, the ground state of a ferrimagnet is determined by the saturation magnetizations of each magnetic sublattice ($M_s(T = 0 \text{ K})$) and their relative ordering rates with respect to temperature. A compensation temperature (T_{comp}) should occur in the magnetization if the sublattice with the smaller saturation magnetization initially orders more rapidly with decreasing temperature than the one with the larger saturation magnetization. In the honeycomb lattice

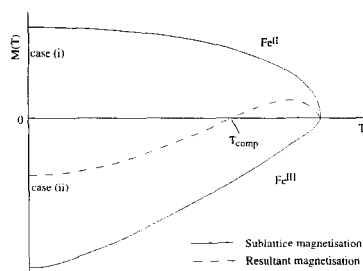


Figure 12. Magnetic sublattice ordering in a ferrimagnet containing Fe^{II} and Fe^{III} with Néel type N order.

with alternating Fe^{II} and Fe^{III} ions, this situation corresponds to an initially steeper ordering on the Fe^{II} sublattice, as shown schematically in Figure 12.

Evidence concerning the sublattice ordering in the $\text{Fe}^{\text{II}}\text{Fe}^{\text{III}}$ compounds comes from the Mössbauer spectra of the $\text{N}(n\text{-C}_4\text{H}_9)_4$ and $\text{P}(\text{C}_6\text{H}_5)_4$ compounds, from which the hyperfine field at the Fe^{III} nucleus has been extracted as a function of temperature for both compounds.¹¹ Within the molecular field approximation, the field experienced at the Fe^{III} nucleus is the sum of exchange fields which, to a first approximation, originate from the neighboring Fe^{II} ions. Hence, the development of a hyperfine field at the Fe^{III} nucleus provides a measure of the magnetization of the Fe^{II} sublattice and *vice versa*. The Mössbauer data indicate that there is a sharp increase in the Fe^{II} sublattice magnetization in the $\text{N}(n\text{-C}_4\text{H}_9)_4$ compound below 40 K . The temperature dependence of the Fe^{II} hyperfine field was not extracted from the data, although there was some indication that it was not fully developed ($H_{\text{int}} \sim 5 \text{ T}$ at 1.9 K). This provides evidence that the Fe^{II} sublattice does indeed order at a higher temperature than Fe^{III} in the $\text{N}(n\text{-C}_4\text{H}_9)_4$ compound. The situation in the $\text{P}(\text{C}_6\text{H}_5)_4$ case is more complex, with a hyperfine splitting at the Fe^{III} nucleus occurring only below 25 K .

The molecular field model predicts that the 0 K saturation magnetization of a two-sublattice ferrimagnet is the difference between the saturation magnetizations on each sublattice, which, in the magnetic order types N and Q, are both fully saturated. Therefore, in the hypothetical spin-only $\text{Fe}^{\text{II}}\text{Fe}^{\text{III}}$ case the saturation moment at 0 K would be $M_s(0 \text{ K}) = \pm g_I S(\text{Fe}^{\text{II}}) - S(\text{Fe}^{\text{III}}) m_B = \pm 1 m_B$ (i.e., 1 spin per $\text{Fe}^{\text{II}}\text{Fe}^{\text{III}}$ unit) for type Q and type N ferrimagnetic order. In the negative magnetization compounds, we find saturation magnetization at 5 K (after 100-G FC) between -235 (PPN) and $-850 \text{ cm}^3 \text{ G mol}^{-1}$ ($\text{N}(n\text{-C}_5\text{H}_{11})_4$), which corresponds to moments of between $0.0422 m_B$ and $0.1522 m_B$. In the compounds with positive magnetization the (100-G FC) saturation moment was $0.0435 m_B$ and $0.052 m_B$ for $\text{P}(\text{C}_6\text{H}_5)_4$ and $\text{As}(\text{C}_6\text{H}_5)_4$, respectively, much smaller than predicted by molecular field theory. However, in polycrystalline samples, crystallite orientations, non-crystallinity, and/or domain effects all contribute to reduce the saturation magnetization, though we note that in the $\text{N}(n\text{-C}_4\text{H}_9)_4$ compound a saturation moment of $\sim 0.07 m_B$ was reached at 5 K after cooling in fields between 2 and 5000 G .

(9) Figgis, B. N. *Introduction to Ligand Fields*; Interscience Publishers: New York, 1961.

(10) De Jongh, L. J. *Magnetic Properties of Layered Transition Metal Compounds*; Kluwer Academic Press: Dordrecht, 1990; Vol. 9.

(11) Ensling, J.; Nuttall, C. J.; Day, P., to be published.

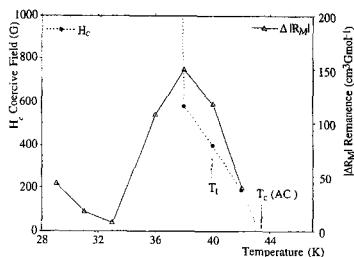


Figure 13. Temperature-dependent hysteresis parameters of $N(n\text{-C}_4\text{H}_9)_4\text{Fe}^{\text{II}}\text{Fe}^{\text{III}}(\text{C}_2\text{O}_4)_3$.

For a variety of reasons it is not appropriate to attempt a quantitative evaluation of the molecular field model to extract molecular field parameters. First, the honeycomb lattice is two-dimensional and therefore deviates considerably from the molecular field approximation as can be seen by the fact that $|T\chi/\theta| = 0.5$. Furthermore, the Fe^{II} ion exhibits an orbital moment and hence its magnetization does not follow a Brillouin function. Finally, spin-orbit coupling in Fe^{II} introduces considerable anisotropy into the system that is not accounted for by the molecular field model.

Figure 12 illustrates two ways in which the magnetization in Néel type N ferrimagnets can vary with temperature. In case (i) the magnetization curve "bounces", as the magnetic pole reverses, i.e., $\{\text{Fe}^{\text{II}}(\uparrow)\text{-Fe}^{\text{III}}(\downarrow) \rightarrow \text{Fe}^{\text{II}}(\downarrow)\text{Fe}^{\text{III}}(\uparrow)\}$ at T_{comp} , resulting in positive magnetization at low temperature, while in case (ii) the initial magnetic pole direction is maintained and the magnetization becomes negative below T_{comp} . $N(n\text{-C}_4\text{H}_9)_4\text{Fe}^{\text{II}}\text{Fe}^{\text{III}}(\text{C}_2\text{O}_4)_3$ behaves like case (ii), although thermodynamically, positive magnetization is favored over negative at low temperature. In the molecular field approximation with fully isotropic exchange fields, there is no energy barrier to magnetic pole reversal, leading to magnetization similar to case (i). The fact that the $N(n\text{-C}_4\text{H}_9)_4$ salt conforms to case (ii) indicates that there is a barrier due to anisotropy sufficient to hinder pole reversal at T_{comp} .

The magnetic hysteresis loops of the $N(n\text{-C}_4\text{H}_9)_4$ compound reflect the anisotropy and stability of the negative magnetization, because a negative magnetization should be unstable to alignment with field above the anisotropy field H_a . However, the 5 K hysteresis of the $N(n\text{-C}_4\text{H}_9)_4$ compound shows no magnetic transition or coercive field (H_c) during field cycling between $\pm 70\,000$ G but remains centered about the negative remanence, indicating a magnetic memory effect. The shape of the hysteresis and absence of a coercive field $= 70\,000$ G indicate that there is a giant anisotropy in the magnetization.

Parameters describing the temperature-dependent hysteresis in the $N(n\text{-C}_4\text{H}_9)_4$ compound are displayed in Figure 13, from which it is clear that the onset of giant anisotropy ($H_c > 10\,000$ G) and the magnetic memory effect both occur between 36 and 38 K. Also the divergence in coercivity clearly correlates with narrowing of the hysteresis. In a ferrimagnet, the coercivity should diverge and the hysteresis narrow on

approaching a compensation temperature¹² since $M_s(T = T_{\text{comp}}) = 0$. While the hysteresis loop in the $N(n\text{-C}_4\text{H}_9)_4$ salt is closed at T_{comp} , the pronounced change in magnetic characteristics between 36 and 38 K indicates that some form of magnetostrictive transition occurs between T_c and T_{comp} . Further evidence that there is such a transition comes from the low field measurements. The shoulder at 40 K in the ZFC magnetization is revealed as a discontinuity in the 100-G FC case. Indeed, we find similar discontinuities in the FC magnetization in all members of the series with negative magnetization at low temperature. However, it is important to note that it is the field cooling history through T_t and not T_c that is critical in determining the low-temperature negative magnetization: the negative magnetization is only reversed after cooling through T_c and T_t in fields $= 60\,000$ G. The resulting positively magnetized state is identical to that obtained after 100-G FC, as indicated by the fact that the temperature dependence of magnetization is almost the inverse of the 100-G FC curve below T_t and that the hysteresis at 5 K is similar to the 100-G FC one, but asymmetrically displaced to positive magnetization.

Clearly the first-order discontinuity in the magnetization at T_t is the factor determining the low temperature magnetization properties of $\text{AFe}^{\text{II}}\text{Fe}^{\text{III}}(\text{C}_2\text{O}_4)_3$ compounds with negative magnetization. However, the physical origin of the transition has not been identified. One possibility is that at T_t the Fe^{II} moments lock due to an orbital ordering. If this is so, then cooling through T_t in small applied fields would provide the Fe^{II} moments with a preferred ordering direction. Provided the ferrimagnetic order conforms to the Néel type N, the magnetization will then become negative at low temperatures. The anisotropy developing below T_c due to a magnetostrictive orbital ordering of the Fe^{II} moments would be very large, as observed. A structural phase transition should also occur at T_t as the Fe^{II} moments couple to the lattice, but to date there are no low temperature structural data on any of these compounds. Nevertheless, the discontinuity in the magnetization points strongly to such a phase transition. Orbital ordering transitions occur when unquenched orbital moments align cooperatively below a magnetic ordering transition as a consequence of the spin-orbit coupling interaction. The theory developed by Goodenough¹³ has been used to explain the negative magnetization and anisotropy behavior in the ferrimagnetic spinel¹⁴ $\text{Co}[\text{CoV}]\text{O}_4$ ¹⁴ and in the antiferromagnet LaVO_3 .^{15,16}

Returning to the magnetization behavior in $\text{P}(\text{C}_6\text{H}_5)_4$ and $\text{As}(\text{C}_6\text{H}_5)_4$ compounds, which correspond to Néel type Q ferrimagnetic order, one question remaining is why there is such a large difference between the magnetic behavior in these compounds and those behaving like Néel type N. It is therefore pertinent to examine the behavior of the $\text{P}(\text{C}_6\text{H}_5)_4$ compound more closely and contrast it with the $N(n\text{-C}_4\text{H}_9)_4$ case. First, the transition to long-range magnetic order is less

(13) Goodenough, J. B. *Phys. Rev.* **1968**, *171*, 466-479.

(14) Menyuk, N.; Dwight, K.; Wickam, D. G. *Phys. Rev. Lett.* **1996**, *4*, 119-120.

(15) Goodenough, J. B.; Nguyen, H. C. *C. R. Acad. Sci. Paris* **1994**, *319 (II)*, 1285-1291.

(16) Nguyen, H.; Goodenough, J. B. *Phys. Rev. B* **1995**, *52*, 325-335.

(12) Standley, K. J. *Oxide Magnetic Materials*; Clarendon Press: Oxford, 1962.

Magnetization of Layer Compounds

Chem. Mater., Vol. 10, No. 10, 1998 3057

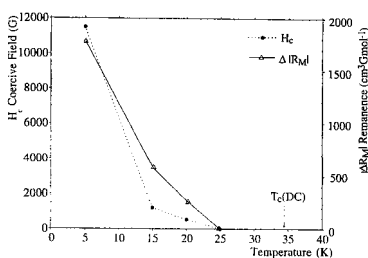


Figure 14. Temperature-dependent hysteresis parameters of $P(C_6H_5)_4Fe^{II}Fe^{III}(C_2O_4)_3$.

abrupt than in the $N(n-C_4H_9)_4$ compound. The increase in dc magnetization occurs at 34 K, which we assign as T_c . However, the ac susceptibility shows no sharp peak, either in dispersion or absorption. Furthermore, the ac susceptibility is strongly frequency dependent, while hysteresis is only observed below 25 K. This behavior contrasts with the $N(n-C_4H_9)_4$ case where ac susceptibility, Mössbauer, and hysteresis measurements all indicate a sharp magnetic transition between 43.5 and 40 K. The temperature dependence of the hysteresis parameters of the $P(C_6H_5)_4$ salt (Figure 14) are quite different from those of the $N(n-C_4H_9)_4$ one (Figure 13).

Neutron powder diffraction of $P(C_6D_5)_4Fe^{II}Fe^{III}(C_2O_4)_3$ reveals only weak asymmetric magnetic scattering intensity below 38 K at the [201] reciprocal lattice point, attributed to moments ordering parallel to the *c*-axis.¹⁷ Although coherent magnetic scattering is evidence of long-range magnetic order, the weak scattering in $P(C_6D_5)_4Fe^{II}Fe^{III}(C_2O_4)_3$, in comparison to $P(C_6D_5)_4Mn^{II}Fe^{III}(C_2O_4)_3$, indicates that long-range magnetic order is not completely developed in the former, even at 5 K, either as a result of a finite spin correlation length or because only part of the sample undergoes a transition to long-range magnetic order. From these diverse strands of evidence the most consistent view of the magnetic order in $P(C_6H_5)_4Fe^{II}Fe^{III}(C_2O_4)_3$ is that it is glassy. Below 34 K, ferrimagnetic correlations begin to develop with randomly oriented anisotropy, so that at 22–25 K the correlated regions become blocked by one another and hysteresis develops. Below the blocking temperature the bulk of the moments are fixed by anisotropy pinning, while a fraction remains mobile down to 5 K. The reasons for such glassy magnetic ordering could lie in a small deficiency of Fe and the charge compensating oxidation process $Fe^{II} \rightarrow Fe^{III}$, which introduces disorder in the magnetic sublattices. Such disorder would produce random anisotropies among

the Fe^{II} moments. Hence, ferrimagnetically correlated regions of random anisotropy may develop, pinned to the Fe^{II} moments. When the correlated regions of different anisotropy interact, magnetic frustration and consequent glassy ordering would occur.

Conclusions

We have undertaken a comprehensive study of the temperature dependent magnetization of two members of the series of layer molecular based ferrimagnets $AFe^{II}Fe^{III}(C_2O_4)_3$ ($A = N(n-C_4H_9)_4$ and $P(C_6H_5)_4$) in a range of zero field and applied field protocols. Our aim has been to map and then identify the reason for the appearance of negative magnetization at low temperature in the $N(n-C_4H_9)_4$ salt but not in the $P(C_6H_5)_4$ one. The two types of behavior correspond to Néel's type N and Q categories of ferrimagnetism. The negative magnetization becomes established above very low cooling fields (2 G) and increases in magnitude until around 2000 G. It is progressively reversed with higher cooling fields and becomes completely reversed above 60 000 G. As a result of the field cooling, the magnetization remanence at 5 K displays an asymmetric hysteresis with a giant anisotropy. The onset of giant anisotropy is identified with the presence of a discontinuity in the magnetization at $T_i = 40$ K ($T_{comp} < T_i < T_c$), which is assigned to a magnetostrictive transition, accompanied by alignment of the Fe^{II} local anisotropy axes. It is this transition, in low cooling fields, that is responsible for the stability of the negative magnetization. By contrast, in the $P(C_6H_5)_4$ compound, where no such discontinuity is found, full long-range magnetic order is not achieved, but a proportion of the moments remain mobile well below T_c . We ascribe this to the buildup of domains of correlated moments with randomly oriented anisotropy axes, which become fixed below a blocking temperature. More detailed crystallographic studies at low temperature will be needed to answer the final key question as to why the substitution of one organic cation by another should trigger such a profound change in the magnetic order in these otherwise very similar lattices.

Acknowledgment. We thank Dr. Simon Carling for help with the SQUID measurements at the RI and Professor K. Yakushi and Dr. Y. Nakazawa of the Institute of Molecular Sciences, Okazaki, Japan, for assisting with the AC susceptibility work. The project is supported by the U.K. Engineering and Physical Sciences Research Council. C.J.N. is also grateful for a MONBUSHO fellowship, awarded through the auspices of the British Council.

(17) Nuttall, C. J.; Day, P. *Inorg. Chem.*, in press.

Polarized neutron diffraction and Mössbauer spectral study of short-range magnetic correlations in the ferrimagnetic layered compounds $(\text{PPh}_4)[\text{Fe}^{\text{II}}\text{Fe}^{\text{III}}(\text{ox})_3]$ and $(\text{NBu}_4)[\text{Fe}^{\text{II}}\text{Fe}^{\text{III}}(\text{ox})_3]$

Simon G. Carling,¹ Dirk Visser,^{2,3,4} Dimitri Hautot,¹ Ian D. Watts,¹ Peter Day,¹ Jürgen Ensling,⁵ Phillip Gütllich,⁵ Gary J. Long,⁶ and Fernande Grandjean⁷

¹Royal Institution of Great Britain, London W1S 4BS, United Kingdom

²Department of Physics, University of Warwick, Coventry CV4 7AL, United Kingdom

³NWO-EW, ISIS Facility, Rutherford Appleton Laboratory, Chilton, Didcot, OX11 0QX, United Kingdom

⁴IRI, TU-Delft, Mekelweg 15, 2629 JB Delft, Netherlands

⁵Institut für Anorganische Chemie und Analytische Chemie, J. Gutenberg-Universität Mainz, Staudinger Weg 9, D-55099 Mainz, Germany

⁶Department of Chemistry, University of Missouri-Rolla, Rolla, Missouri 65409-0010

⁷Institut de Physique, B5, Université de Liège, B-4000 Sart-Tilman, Belgium

(Received 27 November 2001; revised manuscript received 2 July 2002; published 9 September 2002)

Short-range antiferromagnetic correlations have been studied in the layered compounds $(\text{PPh}_4)[\text{Fe}^{\text{II}}\text{Fe}^{\text{III}}(\text{ox})_3]$ and $(\text{NBu}_4)[\text{Fe}^{\text{II}}\text{Fe}^{\text{III}}(\text{ox})_3]$ by neutron polarization analysis and Mössbauer spectroscopy. Polarized neutron diffraction profiles obtained between 2 and 50 K on $(d_{20}\text{-PPh}_4)[\text{Fe}^{\text{II}}\text{Fe}^{\text{III}}(\text{ox})_3]$ show no magnetic Bragg scattering; the lack of such scattering indicates the absence of long-range magnetic order. However, a broad asymmetric feature observed at a Q of ca. 0.8 \AA^{-1} is attributed to two-dimensional short-range magnetic correlations, which are described by a Warren function. The correlation length is ca. 50 Å between 2 and 30 K and then decreases to ca. 20 Å at 50 K. The Mössbauer spectra of $(\text{PPh}_4)[\text{Fe}^{\text{II}}\text{Fe}^{\text{III}}(\text{ox})_3]$ and $(\text{NBu}_4)[\text{Fe}^{\text{II}}\text{Fe}^{\text{III}}(\text{ox})_3]$ have been measured between 1.9 and 293 K and 1.9 and 315 K, respectively, and are very similar. The paramagnetic spectra exhibit both high-spin Fe^{II} and Fe^{III} doublets with relative areas which indicate a 5% and 2% excess, respectively, of Fe^{III} . The coexistence in $(\text{PPh}_4)[\text{Fe}^{\text{II}}\text{Fe}^{\text{III}}(\text{ox})_3]$ between 10 and 30 K of broad sextets and doublets in the Mössbauer spectra and the paramagnetic scattering observed in the polarized neutron measurements indicate the coexistence of spin-correlated and spin-uncorrelated regions in the layers of this compound. The polarized neutron scattering profiles and the Mössbauer spectra yield the magnetic exchange correlation length and lifetime, respectively, and the combined results are best understood in terms of layers composed of random frozen, but exchange correlated domains of ca. 50 Å diameter at the lowest temperatures, of spin-correlated domains and spin-uncorrelated regions at intermediate temperatures, and of largely spin-uncorrelated regions above the Néel temperature as determined from magnetometry. The similarity of the Mössbauer spectra of $(\text{PPh}_4)[\text{Fe}^{\text{II}}\text{Fe}^{\text{III}}(\text{ox})_3]$ and $(\text{NBu}_4)[\text{Fe}^{\text{II}}\text{Fe}^{\text{III}}(\text{ox})_3]$ leads to the conclusion that similar magnetic exchange correlations are present in the latter compound.

DOI: 10.1103/PhysRevB.66.104407

PACS number(s): 75.25.+z, 76.80.+y, 75.30.Kz

I. INTRODUCTION

The layered molecular-based ferromagnets and ferrimagnets $(A)[M^{\text{II}}M^{\text{III}}(\text{ox})_3]$, where A is an organic cation, M^{II} and M^{III} are 3d ions, and (ox) is the oxalate anion, $\text{C}_2\text{O}_4^{2-}$, are attractive systems in which to observe the establishment of magnetic correlations in two-dimensional honeycomb lattices, and as such they have been the subject of numerous studies.¹⁻⁶ In these insulating materials, the M^{II} and M^{III} cations are disposed in an alternating honeycomb array, bridged by oxalates so that each metal has a trigonally distorted octahedral environment, and the A cations lie in between the metal-oxalate layers, often with one or more side chains penetrating into the hexagonal cavities between the oxalates. Among the many compounds of this type, those containing Fe^{II} and Fe^{III} have proved particularly fascinating. Both metal ions are in the high-spin state and the near-neighbor magnetic exchange is antiferromagnetic. For many A , the bulk magnetization of the resulting compounds resembles that of a Néel class- N ferrimagnet⁷ with a compensation temperature and a negative magnetization at low tem-

perature in small applied field. In contrast, where the A cation is tetraphenyl-phosphonium or tetraphenyl-arsonium, the bulk magnetization resembles⁷ Néel's class Q with monotonically increasing magnetization below the apparent ordering temperature T_N and no compensation behavior. Examples of the magnetization of each class of materials can be found in Fig. 1, which shows recent magnetization measurements on compounds whose behavior we have reported earlier.⁶ Néel ascribed such differences in bulk magnetization to different ordering rates of the two sublattices in a ferrimagnet. Recent magnetometry and Monte Carlo studies⁸ on compounds doped with diamagnetic ions suggest that the apparently type- N behavior is inhibited and then destroyed by increasing deficiency on the divalent magnetic sublattice. Unpolarized powder neutron diffraction measurements performed on $(d_{20}\text{-PPh}_4)[\text{Fe}^{\text{II}}\text{Fe}^{\text{III}}(\text{ox})_3]$ (Ref. 9) showed a broad magnetic feature below 35 K; unfortunately this feature overlapped with a strong nuclear Bragg peak and could not be thoroughly analyzed. The temperature dependence of the intensity of this feature resembled that expected for a sublattice magnetization.

SIMON G. CARLING *et al.*

PHYSICAL REVIEW B 66, 104407 (2002)

In this paper we present detailed Mössbauer spectral data measured between 295 and 1.9 K for one example of each type, $A^+ = PPh_4^+$ [type Q , $PPh_4^+ = P(C_6H_5)_4^+$] and $A^+ = NBu_4^+$ [type N , $NBu_4^+ = N(n-C_4H_9)_4^+$] to probe the reasons for the difference in the ordering process in the two types. This study is complemented by neutron polarization analysis measurements on $(d_{20}\text{-}PPh_4)[Fe^{II}Fe^{III}(ox)_3]$ which directly monitor the buildup of short-range exchange correlations above T_c and the coexistence of correlated and paramagnetic regions below T_c . The neutron measurements of the spatial magnetic exchange correlation, with a time scale of $\sim 10^{-11}$ s, serve to supplement the time-dependent magnetic exchange correlation observed in the Mössbauer results, for which the time scale is $\sim 10^{-8}$ s. Preliminary polarization analysis measurements on $(d_{20}\text{-}PPh_4)[Fe^{II}Fe^{III}(ox)_3]$ at 5 K have already been reported.¹⁰

Although there have been no detailed reports on the Mössbauer spectral properties of $(PPh_4)[Fe_2(ox)_3]$, the spectral properties of $(NBu_4)[Fe_2(ox)_3]$ as well as of the related $(NBu_4)[M^{II}M^{III}(ox)_3]$ compounds have been studied^{1,3,5,11-15,17} in detail (Table I). There is good agreement in both the iron(II) and iron(III) hyperfine parameters for the compounds in the paramagnetic state. Below the magnetic ordering temperature, the agreement is also good for the iron(II) site and most authors report a quadrupole interaction of ca. 1.8 mm/s and negative V_{zz} and a surprisingly small hyperfine field of ca. 35–52 kOe for this site. In contrast, for the iron(III) site there are reports of both positive and negative quadrupole interactions of ca. 0.60 mm/s and both positive and negative signs of V_{zz} , although the hyperfine fields are typical of iron(III): the angle θ between this field and the principal axis of the electric field gradient V_{zz} has been reported to have both large and/or small values. These trends are further complemented by studies^{14,15} of mixed-metal complexes, such as $(NBu_4)[(Fe_xMn_{1-x})^{II}Cr^{III}(ox)_3]$, $(NBu_4)[(Fe_xNi_{1-x})^{II}Fe^{III}(ox)_3]$, and $(NBu_4)[Mn^{II}(Fe_xCr_{1-x})^{III}(ox)_3]$, in which two different metals of the same oxidation state occupy the same site.

There have been fewer Mössbauer spectral studies with other A cations, but Iijima and Mizutani¹³ have studied $(NBu_4)[Fe^{II}Fe^{III}(ox)_3]$, $(Nn\text{-propyl}_4)[Fe^{II}Fe^{III}(ox)_3]$, $(Nn\text{-propyl}_4)[Fe^{II}Cr^{III}(ox)_3]$, and $(Nn\text{-propyl}_4)[Mn^{II}Cr^{III}(ox)_3]$ in some detail, the latter of which contains small amounts of iron-57 on the Mn^{II} site and Ovanesyan *et al.*¹⁷ and Bottyán *et al.*¹⁸ have studied $(Nn\text{-pentyl}_4)[Mn^{II}Fe^{III}(ox)_3]$ and $(Nn\text{-pentyl}_4)[Fe^{II}Fe^{III}(ox)_3]$. Finally, the very unusual bulky cations $[Co^{III}(Me_5Cp)_2]^+$ and $[Fe^{III}(Me_5Cp)_2]^+$, which form layered oxalate compounds $[M^{III}(Me_5Cp)_2][M^{II}M^{III}(ox)_3]$, have been studied by Coronado *et al.*¹⁹ The spectra of many of these compounds will be discussed below as is appropriate.

In order to better understand the complex but virtually unstudied Mössbauer spectral properties of $(PPh_4)[Fe_2(ox)_3]$, we have carried out a parallel study of $(NBu_4)[Fe_2(ox)_3]$, which has proved extremely valuable in understanding the more complex spectra of $(PPh_4)[Fe_2(ox)_3]$. The results of both of these studies are reported and compared herein.

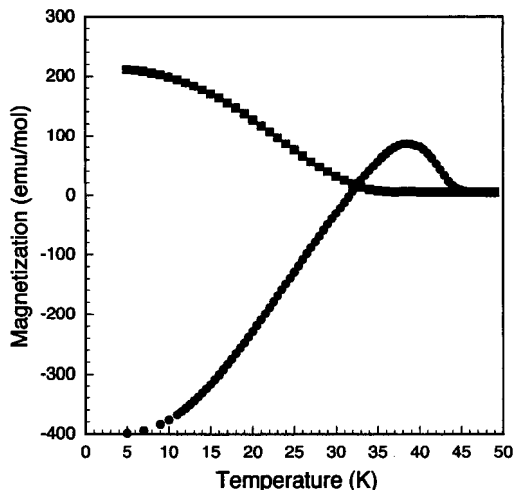


FIG. 1. The temperature dependence of the field-cooled magnetization of $(PPh_4)[Fe_2(ox)_3]$ (■) and $(NBu_4)[Fe_2(ox)_3]$ (●) measured in an applied field of 100 Oe.

II. EXPERIMENT

A. Preparation

The $(d_{20}\text{-}PPh_4)[Fe^{II}Fe^{III}(ox)_3]$ and $(NBu_4)[Fe^{II}Fe^{III}(ox)_3]$ samples were prepared as reported earlier.^{6,9} One of the $(d_{20}\text{-}PPh_4)[Fe^{II}Fe^{III}(ox)_3]$ samples was the same as that used in an earlier unpolarized neutron diffraction study.⁹ Earlier chemical analysis^{20,21} of related $(A)[Fe^{II}Fe^{III}(ox)_3]$ compounds have shown a ca. 1%–7% deficiency of iron cations relative to the number of oxalate anions. Because of the extremely high cost of the $(d_{20}\text{-}PPh_4)^+$ cation, no chemical analysis of $(d_{20}\text{-}PPh_4)[Fe^{II}Fe^{III}(ox)_3]$ was performed, but as discussed below, the Mössbauer spectra show a 5% deficiency in iron(II) content relative to the total iron content. This deficiency no doubt results in iron(II) vacancies in the honeycomb lattice, which may be occupied by simple H_3O^+ cations because the complex is made in acidic solution.

B. Magnetization

dc bulk magnetization measurements were performed using a Quantum Design MPMS7 superconducting quantum interference device (SQUID) magnetometer. Samples were accurately weighed to a precision of $\pm 1 \mu g$ and loaded in gelatine capsules which were then mounted in a plastic drinking straw. Magnetization was measured as a function of temperature between 5 and 50 K in an applied field of 100 Oe. The measured data were corrected for diamagnetic contributions using Pascal's constants. Figure 1 shows the magnetizations of $(d_{20}\text{-}PPh_4)[Fe^{II}Fe^{III}(ox)_3]$ and $(NBu_4)[Fe^{II}Fe^{III}(ox)_3]$ as a function of temperature.

C. Neutron diffraction

Polarized neutron diffraction experiments were performed on the diffuse scattering spectrometer D7 at the Institut

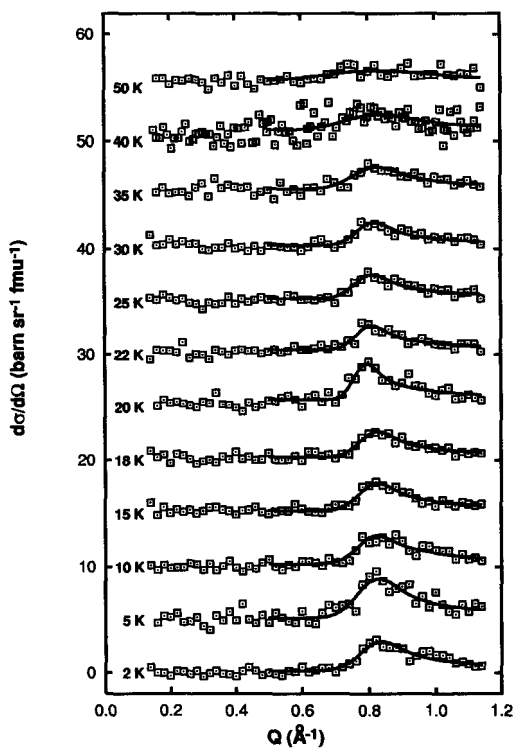


FIG. 2. The differential magnetic scattering cross-section $d\sigma/d\Omega$ of $(d_{20}\text{-PPh}_4)[\text{Fe}_2(\text{ox})_3]$. The solid lines correspond to a fit to a Warren function as is discussed in the text.

Laue-Langevin (ILL), Grenoble, France. The incident beam of cold neutrons, wavelength 4.84 \AA , is polarized by a supermirror. Thirty-two ^3He detectors, arranged in four banks, each have their own supermirror analyzer. A set of three Helmholtz coils allows the polarization direction of the incident beam to be defined along x , y , or z . The disk chopper which permits time-of-flight energy analysis was not present for these measurements.

Two polycrystalline samples of $(d_{20}\text{-PPh}_4)[\text{Fe}^{\text{II}}\text{Fe}^{\text{III}}(\text{ox})_3]$ of mass 3.58 and 7.30 g were mounted in an ILL Orange cryostat in a cylindrical vanadium can. Measurements were performed at 2, 5, 10, 15, 18, 20, 22, 25, 30, 35, 40, and 50 K. At each temperature, full xyz polarization analysis²² was carried out, the spin-flip and non-spin-flip scattering being measured with the incident beam polarization direction along each of the three axes. This enables the total scattering to be separated into its nuclear coherent, spin incoherent, and magnetic components. Data were collected over the range $0.15 \leq Q \leq 2.5 \text{ \AA}^{-1}$, and parts of these data, the fits of which are discussed below, are shown in Fig. 2. The data are to scale but each successive profile is vertically displaced by 5 b sr^{-1} per formula unit at each temperature. All measurements were corrected for the scattering of the vanadium can and normalized to the scattering of a known

mass of vanadium powder or foil, giving an absolute measure of the scattering intensity as a function of Q .

D. Mössbauer spectra

The Mössbauer spectral absorbers contained 75 mg/cm^2 of powder and the spectra were measured between 1.9 and 293 or 315 K on a constant-acceleration spectrometer which utilized a room-temperature rhodium matrix cobalt-57 source and was calibrated at room temperature with α -iron foil. The estimated absolute errors are $\pm 0.01 \text{ mm/s}$ for the isomer shifts, $\pm 0.02 \text{ mm/s}$ for the quadrupole splittings and line-widths, and $\pm 2\%$ for the percentage areas of the spectral components. The relative errors are estimated to be smaller by a factor of about one-half.

III. RESULTS AND DISCUSSION

A. Magnetization

The magnetization of $(\text{NBu}_4)[\text{Fe}^{\text{II}}\text{Fe}^{\text{III}}(\text{ox})_3]$ has been reported earlier,^{4,6,20,23} and its magnetization and that of $(d_{20}\text{-PPh}_4)[\text{Fe}^{\text{II}}\text{Fe}^{\text{III}}(\text{ox})_3]$ used herein have been measured and are shown in Fig. 1. As expected the magnetization of $(d_{20}\text{-PPh}_4)[\text{Fe}^{\text{II}}\text{Fe}^{\text{III}}(\text{ox})_3]$ corresponds to that of a Néel class- Q ferrimagnet⁷ and shows a constant, essentially zero value above 30 K and a monotonically increasing value reaching ca. $210 \text{ erg Oe}^{-1} \text{ mol}^{-1}$ under 100 Oe below 30 K, a small value as expected for the ferrimagnetic coupling between high-spin iron(II) and high-spin iron(III). In contrast the magnetic properties of $(\text{NBu}_4)[\text{Fe}^{\text{II}}\text{Fe}^{\text{III}}(\text{ox})_3]$ are quite different, as discussed earlier,^{4,6,20,23} and correspond to a Néel class- N ferrimagnet.⁷

B. Polarized neutron diffraction

Figure 2 shows the differential magnetic cross section $d\sigma/d\Omega$ of $(d_{20}\text{-PPh}_4)[\text{Fe}^{\text{II}}\text{Fe}^{\text{III}}(\text{ox})_3]$ at temperatures between 2 K and 50 K. Because no structure is observed in the magnetic scattering for $0.15 \leq Q \leq 0.5 \text{ \AA}^{-1}$, the observed intensity must be due to paramagnetic scattering. The numerical integration of the magnetic intensity over the Q range $0.15 \leq Q \leq 0.50 \text{ \AA}^{-1}$ gives an estimate of the relative proportion of fluctuating, uncorrelated spins present. The percentage of the paramagnetic scattering that is expected to fall in this Q range can be calculated from the magnetic form factors for Fe^{II} and Fe^{III} as 12.72%.²⁴ Normalizing to this percentage and the total magnetic scattering over the whole Q range gives the percentage of uncorrelated magnetic moments, shown in Fig. 3.

While the uncertainties in this measurement are high, it is still clear that three different scattering regimes can be distinguished. At low temperatures $T \leq 10 \text{ K}$, the paramagnetic intensity is very low. In the intermediate regime $10 < T \leq 30 \text{ K}$, it becomes somewhat higher, while for $T > 30 \text{ K}$ it is higher still. This result is in clear agreement with the analysis of the Mössbauer spectra presented in the following section.

As can be seen in Fig. 2 even at 2 K, the lowest temperature studied, no magnetic Bragg scattering was found over the entire Q range studied. This indicates the absence of any

SIMON G. CARLING *et al.*

PHYSICAL REVIEW B 66, 104407 (2002)

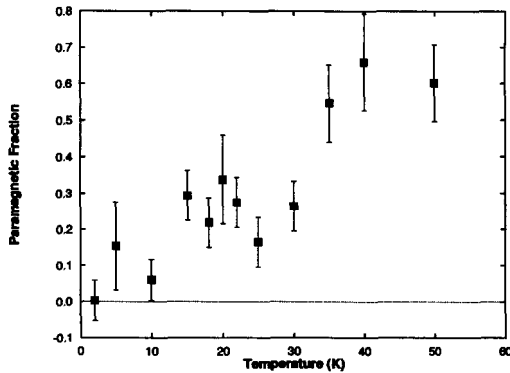


FIG. 3. The paramagnetic intensity integrated over the Q range of $0.15 \leq Q \leq 0.50 \text{ \AA}^{-1}$, normalized to give the fraction of paramagnetic scattering, as a function of temperature for $(d_{20}\text{-PPh}_4)[\text{Fe}_2(\text{ox})_3]$.

three-dimensional long-range magnetic order in $(d_{20}\text{-PPh}_4)[\text{Fe}^{\text{II}}\text{Fe}^{\text{III}}(\text{ox})_3]$. However, a broad and asymmetric feature is apparent at $Q_0 \approx 0.8 \text{ \AA}^{-1}$, a feature which becomes weaker and broader above 35 K but is still present at 50 K. This non-Bragg scattering is ascribed to quasi-two-dimensional (2D) short-range magnetic correlations and can be described by a Warren function^{25,26}

$$p(\theta) = Km F_{hk}^2 \frac{(1 + \cos^2 2\theta)}{2(\sin \theta)^{3/2}} \left(\frac{\xi}{\lambda \sqrt{\pi}} \right)^{1/2} F(a), \quad (1)$$

where λ is the neutron wavelength, K is a scale factor, m is the multiplicity of the 2D reflection $[hk]$ whose structure factor is F_{hk} and whose position is θ_0 , ξ is the spin-spin correlation length, and

$$F(a) = \int_0^\infty \exp[-(x^2 - a)^2] dx, \quad (2)$$

where

$$a = \frac{2\xi\sqrt{\pi}}{\lambda} (\sin \theta - \sin \theta_0). \quad (3)$$

Based on the unit cell parameters determined from the previous, unpolarized neutron diffraction measurements,⁹ the scattering intensity at 0.8 \AA^{-1} was assigned as [20]. Because the integral in Eq. (2) cannot be solved analytically, the function was integrated numerically to an upper limit of 20 with results that compare favorably with those given in Ref. 26. Fitting the Warren-like feature therefore yields the temperature dependence of the 2D correlation length. Fits were performed for each temperature in the Q range $0.5 \leq Q \leq 1.15 \text{ \AA}^{-1}$ and are shown at each temperature in Fig. 2.

The variation of the magnetic exchange correlation length with temperature in $(d_{20}\text{-PPh}_4)[\text{Fe}^{\text{II}}\text{Fe}^{\text{III}}(\text{ox})_3]$ is shown in Fig. 4.

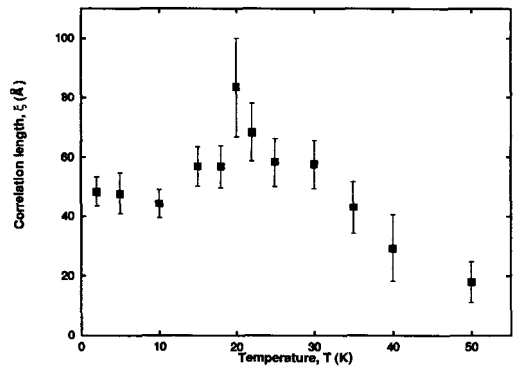


FIG. 4. The two-dimensional magnetic correlation length ξ as a function of temperature for $(d_{20}\text{-PPh}_4)[\text{Fe}_2(\text{ox})_3]$.

As expected, above 30 K the correlation length decreases with increasing temperature in the paramagnetic phase. Below 30 K, rather unexpectedly, the correlation length increases only slightly and reaches a maximum of only ca. 80 Å at 20 K. These results seem to indicate a small decrease in the correlation length, a decrease that may be an artifact of the two samples used for this study; most likely the correlation length is unchanging at ca. 50 Å below 20 K. This distance corresponds to between five and six honeycomb units.

The diffraction observed here, while not conclusive, is compatible with an orientation of the magnetic moments in the basal plane. On the basis of their unpolarized neutron diffraction work on $(d_{20}\text{-PPh}_4)\text{Mn}^{\text{II}}\text{Fe}^{\text{III}}(\text{ox})_3$, which does exhibit long-range magnetic order, Nuttall and Day⁹ concluded that the moments in this compound are axial, an orientation that seems reasonable for a magnetic compound with an ${}^6A_{1g}$ ground state for both ions and, hence, no orbital contribution to the magnetic anisotropy. In contrast, in $(d_{20}\text{-PPh}_4)[\text{Fe}^{\text{II}}\text{Fe}^{\text{III}}(\text{ox})_3]$ the iron(II) ion does have a significant orbital contribution to the magnetic moment, as discussed below, and hence its contribution to the magnetic anisotropy may be quite different. As a consequence the magnetic moments in $(d_{20}\text{-PPh}_4)[\text{Fe}^{\text{II}}\text{Fe}^{\text{III}}(\text{ox})_3]$ may be basal, an orientation which would lead to a threefold degeneracy, giving rise to three energetically equivalent easy directions of magnetization. In this case the spin configurational entropy may limit the exchange correlation length and the direction of the exchange-correlated moments may be different, depending on their nucleation site.

C. Mössbauer spectral analysis

1. Paramagnetic spectra

The Mössbauer spectra of $(\text{PPh}_4)[\text{Fe}_2(\text{ox})_3]$ and $(\text{NBu}_4)[\text{Fe}_2(\text{ox})_3]$ have been measured as a function of temperature and selected paramagnetic spectra are shown in Figs. 5 and 6, respectively.

The experimental data shown in these figures clearly indicate the presence of two quadrupole doublets, which may

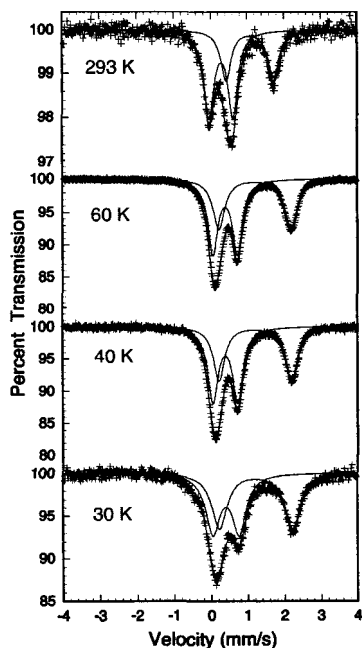


FIG. 5. Selected paramagnetic Mössbauer spectra of $(\text{PPh}_4)[\text{Fe}_2(\text{ox})_3]$ obtained at the indicated temperatures.

be assigned to iron(II) and iron(III) ions. Although the fits shown in these figures are not unique in terms of the placement of the two lines found at ca. 0.0 mm/s, they do yield hyperfine parameters which are consistent both with earlier studies, summarized in Table I, and with the parameters obtained for the magnetically ordered spectra, which are discussed in detail in the next section. Further, these fits yield hyperfine parameters which are physically realistic for high-spin iron(II) and iron(III) ions in the distorted octahedral coordination environment expected in these compounds. The resulting hyperfine parameters are given in Tables II and III for $(\text{PPh}_4)[\text{Fe}_2(\text{ox})_3]$ and $(\text{NBu}_4)[\text{Fe}_2(\text{ox})_3]$, respectively.

The Mössbauer spectra of $(\text{PPh}_4)[\text{Fe}_2(\text{ox})_3]$ shown in Fig. 5 clearly indicate that this compound is paramagnetic between 293 and 40 K. Although the spectrum observed at 30 K is similar to the 40 K spectrum, the lines are clearly broader, an indication of the onset of magnetic exchange correlations. As will be seen in the next section, the spectra of $(\text{PPh}_4)[\text{Fe}_2(\text{ox})_3]$ clearly show the influence of magnetic exchange correlations at 25 K and below. In contrast, the spectra of $(\text{NBu}_4)[\text{Fe}_2(\text{ox})_3]$ shown in Fig. 6 indicate that it is paramagnetic between 315 and 50 K. Although the spectrum observed at 42.5 K is similar to the 50 K spectrum, the lines are broader, again an indication of the onset of magnetic exchange correlations. As will be seen in the next section, the spectra of $(\text{NBu}_4)[\text{Fe}_2(\text{ox})_3]$ clearly show the influence of magnetic exchange correlations at 40 K and below.

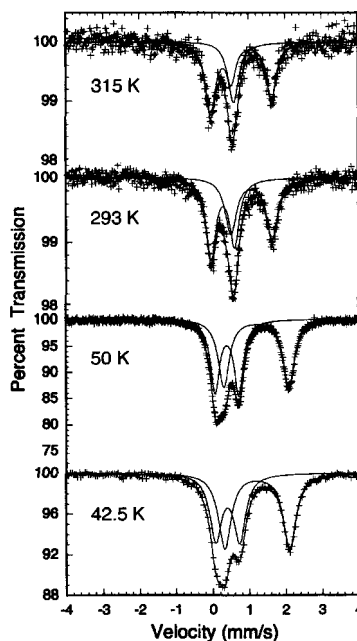


FIG. 6. Selected paramagnetic Mössbauer spectra of $(\text{NBu}_4)[\text{Fe}_2(\text{ox})_3]$ obtained at the indicated temperatures.

The isomer shifts of the iron(II) sites in the two compounds are very similar at 1.12 and 1.16 mm/s at 293 K, values which are characteristic of high-spin iron(II). The isomer shifts of the iron(III) sites in the two compounds are virtually identical at 0.39 and 0.38 mm/s at 293 K, values which are characteristic of high-spin iron(III). The isomer shift values are very similar to those observed²⁷⁻²⁹ for iron(II) in $\text{Fe}(\text{ox}) \cdot 2\text{H}_2\text{O}$ and iron(III) in $\text{K}_3\text{Fe}(\text{ox})_3$ and confirm the assignments presented in Tables II and III. Further, the paramagnetic spectra are very similar to those reported earlier^{3,13,15} and the spectra reported by Coronado *et al.*¹⁹ for $[\text{FeCp}_2^*][\text{Fe}_2(\text{ox})_3]$ except for the presence of an additional line due to the (FeCp_2^*) cation. The observed decrease in the isomer shifts of $(\text{PPh}_4)[\text{Fe}_2(\text{ox})_3]$ and $(\text{NBu}_4)[\text{Fe}_2(\text{ox})_3]$ with increasing temperature (see Tables II and III) results from the second-order Doppler-shift contribution to the isomer shift and validate the analysis.

As is revealed in Tables II and III, the quadrupole splittings of the iron(III) sites are similar and almost independent of temperature in both $(\text{PPh}_4)[\text{Fe}_2(\text{ox})_3]$ and $(\text{NBu}_4)[\text{Fe}_2(\text{ox})_3]$ with respective values of -0.64 and -0.65 mm/s at 293 K. The values are negative as is required to obtain the *best* fit of the magnetically ordered spectra, but the equivalent positive values may be equally acceptable; see discussion below. The slightly larger magnitude of the quadrupole splittings observed for $(\text{PPh}_4)[\text{Fe}_2(\text{ox})_3]$ at lower temperatures may indicate that larger distortions in its iron(III) coordination environment are produced on cooling; the same trend is observed for the iron(II) site in this complex.

SIMON G. CARLING *et al.*PHYSICAL REVIEW B **66**, 104407 (2002)TABLE I. Previous Mössbauer spectral studies of (NBu₄)[M^{II}M^{III}(ox)₃].

Site	M ^{II}	M ^{III}	T (K)	δ (mm/s) ^b	ΔE _Q (mm/s)	V _{zz} ^a	H _{eff} (kOe)	θ (deg)	Ref.	
Fe ^{II}	Fe	Fe	78	1.30	1.79	±	0		3	
			4.2	1.32	1.92	-	52	90	11	
	Fe	Cr	298	1.18	1.26	±	0		3	
			12	1.33	1.82	±	0			
			10	1.32	1.85	-	35	90		
			4.2	1.33	1.86	-	38	90		
	Fe	Cr	293	1.18	1.23	±	0		15	
			4.2		1.78	-	45	90		
	Fe ^{III}	Fe	Fe	78	0.51	0.60	±	0		3
				4.2		0.60	+	537	81	11
					0.60	-	537	37		
Mn		Fe	78	0.49	0.62	±	0		11	
			30	0.50	0.62	±	0			
			25	0.50	0.62	+	320	52		
			20	0.51	0.62	+	380	58		
				15	0.49			432		
				4.2	0.50			502		
Ni		Fe	78	0.49	0.68	±	0		11	
	25		0.51	0.71	±	0				
	20		0.50	0.71	+	391	28	13		
	4.2		0.50	0.71	+	509	28			

^a± indicates that either the sign was unknown or not reported.^bThe isomer shifts are given relative to room-temperature α-iron foil.

In contrast to the iron(III) sites and, as expected³⁰ for a high-spin iron(II) ion with the approximate $t_{2g}^4 e_g^2$ electronic configuration in a distorted octahedral coordination environment, the quadrupole splittings for the iron(II) sites in both (PPh₄)[Fe₂(ox)₃] and (NBu₄)[Fe₂(ox)₃] are rather different and decrease dramatically with increasing temperature above ca. 50 K, the change being larger for (PPh₄)[Fe₂(ox)₃] than for (NBu₄)[Fe₂(ox)₃]. The temperature dependence for both compounds is shown in Fig. 7, where again the quadrupole splitting values are taken to be negative as is required to best fit the ordered spectra.

The temperature dependence of the iron(II) quadrupole splitting ΔE_Q in a distorted environment may be fitted with the Ingalls model³⁰ in which

$$\Delta E_Q = \Delta E_Q(0) \tanh\left(\frac{\Delta}{2kT}\right), \quad (4)$$

where ΔE_Q(0) is the quadrupole splitting at 0 K and Δ is the splitting of the orbital triplet ⁵T_{2g} octahedral iron(II) ground state by low-symmetry components of the crystal field. The solid lines shown in Fig. 7 correspond to the best fits of the quadrupole splittings with this model. For (PPh₄)[Fe₂(ox)₃] the best-fit parameters are ΔE_Q(0) = 1.98 mm/s, V_{zz} = -9.06 × 10²¹ V/m², and Δ = 292 cm⁻¹ and for (NBu₄)[Fe₂(ox)₃] they are ΔE_Q(0) = 1.79 mm/s, V_{zz} = -8.19 × 10²¹ V/m², and Δ = 312 cm⁻¹. The fits with

TABLE II. Mössbauer spectral hyperfine parameters for (PPh₄)[Fe₂(ox)₃].

Site	T (K)	δ (mm/s) ^a	ΔE _Q (mm/s)	V _{zz} (10 ²¹ V/m ²)	H _{max} (kOe)	Γ (mm/s)	Area (%)	
Fe ^{II}	293	1.123	1.30	-5.95		0.34	39	
	240	1.169	1.42	-6.50		0.25	40	
	190	1.217	1.55	-7.09		0.29	42	
	140	1.248	1.70	-7.78		0.30	41	
	90	1.275	1.88	-8.60		0.33	43	
	60	1.299	1.97	-9.02		0.38	45	
	40	1.307	1.98	-9.06		0.35	45	
	30	1.317	2.00	-9.15		1.12	51	
	25	1.307	1.98 ^b	-9.06	40	1.40	52	
	22.5	1.307	1.98 ^b	-9.06	55	1.23	54	
	20	1.304	1.98 ^b	-9.06	61	0.95	51	
	15	1.337	1.98 ^b	-9.06	68	0.85	46	
	10	1.306	1.98 ^b	-9.06	68	0.84	43	
	6	1.338	1.98 ^b	-9.06	65	0.91	45	
	4.2	1.316	1.98 ^b	-9.06	65	0.83	44	
	1.9	1.329	1.98 ^b	-9.06	68	0.78	43	
	Fe ^{II}	293	0.390	0.65	-2.98		0.33	61
		240	0.410	0.60	-2.75		0.35	60
		190	0.440	0.60	-2.75		0.35	58
		140	0.467	0.62	-2.84		0.32	59
90		0.479	0.63	-2.88		0.33	57	
60		0.486	0.67	-3.07		0.32	55	
40		0.488	0.68	-3.11		0.35	55	
30		0.500	0.72	-3.30		0.47	49	
25		0.493	0.72	-3.30	460	0.98	48	
22.5		0.479	0.72	-3.30	485	1.02	46	
20	0.494	0.75	-3.43	500	1.24	49		
15	0.507	0.75	-3.43	520	0.64	54		
10	0.512	0.75	-3.43	526	0.52	57		
6	0.517	0.78	-3.57	527	0.56	55		
4.2	0.532	0.74	-3.39	540	0.38	56		
1.9	0.527	0.72	-3.30	541	0.42	57		

^aThe isomer shifts are given relative to room-temperature α-iron foil.^bParameter constrained to the value given.

this model are not fully adequate, most probably because of small changes in Δ with temperature, which are ignored by the Ingalls model. Changes in Δ with temperature are not unexpected in complexes of the type studied here, as a result of anisotropic changes in the coordination environment of the iron(II) sites.

2. Magnetically ordered spectra

The magnetically ordered Mössbauer spectra of (PPh₄)[Fe₂(ox)₃] and (NBu₄)[Fe₂(ox)₃] are shown in Figs. 8 and 9, respectively. It should be noted that the spectra shown in Figs. 8 and 9 are again qualitatively very similar to those reported earlier^{3,13,15,16,18} and by Coronado *et al.*¹⁹ for [FeCp₂]⁺[Fe₂(ox)₃] except for the presence of an additional line due to the (FeCp₂)⁺ cation.

TABLE III. Mössbauer spectral hyperfine parameters for $(\text{NBu}_4)[\text{Fe}_2(\text{ox})_3]$.

Site	T (K)	δ (mm/s) ^a	ΔE_Q (mm/s)	V_{zz} (10^{21} V/m ²)	H_{max} (kOe)	Γ (mm/s)	Area (%)
Fe ^{II}	315	1.162	1.12	-5.13		0.33	44
	293	1.164	1.14	-5.22		0.38	48
	240	1.204	1.34	-6.13		0.32	46
	190	1.235	1.42	-6.50		0.31	47
	140	1.265	1.60	-7.32		0.31	47
	90	1.291	1.72	-7.87		0.30	49
	50	1.290	1.79	-8.19		0.36	53
	45	1.306	1.78	-8.15		0.39	52
	42.5	1.306	1.79	-8.19		0.43	55
	40	1.306	1.79 ^b	-8.19	38	0.82	58
	39	1.315	1.79 ^b	-8.19	38	0.98	65
	38	1.312	1.79 ^b	-8.19	45	0.81	60
	35	1.275	1.79 ^b	-8.19	40	0.75	52
	30	1.319	1.79 ^b	-8.19	50	1.10	50
	10	1.331	1.79 ^b	-8.19	58	0.68	47
	4.2	1.327	1.79 ^b	-8.19	57	0.59	47
1.9	1.329	1.79 ^b	-8.19	58	0.59	48	
Fe ^{III}	315	0.363	0.63	-2.88		0.33	56
	293	0.380	0.64	-2.93		0.32	52
	240	0.416	0.65	-2.98		0.40	54
	190	0.435	0.65	-2.98		0.35	53
	140	0.461	0.64	-2.93		0.32	53
	90	0.486	0.64	-2.93		0.29	51
	50	0.481	0.65	-2.98		0.36	47
	45	0.489	0.65	-2.98		0.37	48
	42.5	0.495	0.66	-3.02		0.39	45
	40	0.504	0.67	-3.07	360	0.78	42
	39	0.518	0.64	-2.93	405	0.92	35
	38	0.518	0.64	-2.93	405	1.08	40
	35	0.518	0.64	-2.93	428	1.02	48
	30	0.518	0.67	-3.07	462	0.72	50
	10	0.503	0.68	-3.11	530	0.44	53
	4.2	0.520	0.67	-3.07	544	0.31	53
1.9	0.520	0.66	-3.02	545	0.29	52	

^aThe isomer shifts are given relative to room-temperature α -iron foil.

^bParameter constrained to the given value.

The spectra shown in Figs. 8 and 9 have been fitted with a minimization program³¹ which calculates the eigenvalues and eigenvectors of the ground- and excited-state Hamiltonians describing the combined quadrupolar and magnetic interactions. The adjustable hyperfine parameters for a given component in the spectral fits are the isomer shift δ , the effective hyperfine field H_{eff} , the quadrupole interaction ΔE_Q , the angle θ between the principle axis of the electric field gradient and the magnetization direction, and the line-width Γ . In all fits reported herein $\eta = 0.0$ as is expected for the axially symmetric trigonal iron(II) and iron(III) sites in these complexes. Further, any attempt to increase the value of the asymmetry parameter η above zero leads to substan-

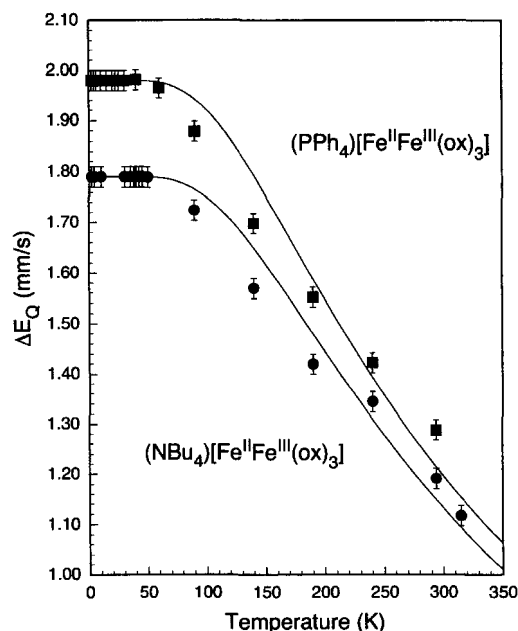


FIG. 7. The temperature dependence of the iron(II) quadrupole interactions of $(\text{PPh}_4)[\text{Fe}_2(\text{ox})_3]$ (■) and $(\text{NBu}_4)[\text{Fe}_2(\text{ox})_3]$ (●). The absolute error bars are shown. The solid lines represent a fit of the quadrupole splittings based on the Ingalls model as is discussed in the text.

tially poorer fits. Thus the spectra were fit by adjusting the five adjustable parameters for each spectral component and by using enough spectral components to reproduce the experimental spectrum. In addition, at a given temperature, the δ , ΔE_Q , and Γ values associated with a given iron oxidation state have been constrained to be equal. In contrast, in none of the fits have the relative areas of the iron(II) and iron(III) components been constrained.

In the spectra shown in Figs. 8 and 9 it is immediately apparent that the iron(III) ions exhibit a sextet with a large hyperfine field. In contrast, the iron(II) ions exhibit a relatively small hyperfine field. The presence of these sextets would seem to indicate the presence of long-range magnetic order in these complexes, a presence which initially appears inconsistent with the polarized neutron diffraction results presented above for $(\text{PPh}_4)[\text{Fe}_2(\text{ox})_3]$.

Below 10 K for $(\text{PPh}_4)[\text{Fe}_2(\text{ox})_3]$ and below 30 K for $(\text{NBu}_4)[\text{Fe}_2(\text{ox})_3]$ the Mössbauer spectra show sharp sextets, which indicate that the short-range magnetic exchange correlations observed in the polarized neutron scattering study yield an apparently static hyperfine field at both iron sites. Between 10 and 30 K for $(\text{PPh}_4)[\text{Fe}_2(\text{ox})_3]$ and between 30 and 45 K for $(\text{NBu}_4)[\text{Fe}_2(\text{ox})_3]$, the Mössbauer spectra are a superposition of broadened sextets and paramagnetic doublets. We believe that this behavior results from the dynamic behavior of the short-range magnetic exchange correlations. Each layer within a compound can be envisaged

SIMON G. CARLING *et al.*

PHYSICAL REVIEW B 66, 104407 (2002)

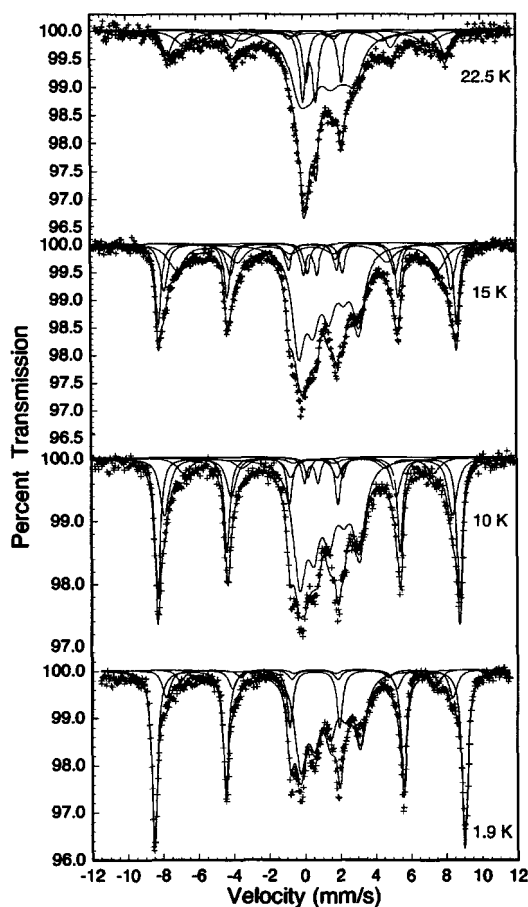


FIG. 8. Selected Mössbauer spectra of $(\text{PPh}_4)[\text{Fe}_2(\text{ox})_3]$ obtained at the indicated temperatures.

as composed of small regions of ca. 50 Å diameter, in which there is magnetic exchange correlation. The Mössbauer spectrum will depend on the lifetime of this correlation. At the lowest temperatures, the lifetime is longer than the Larmor period of the nuclear moment and the Mössbauer spectra show sharp sextets. As the temperature increases, the lifetime decreases and a given iron nucleus then sees a relaxing hyperfine field which gives rise to the broadened sextets or the paramagnetic doublets, depending upon the relaxation rate. Hence the Mössbauer spectra probe the time domain of the short-range magnetic exchange correlations observed by polarized neutron scattering. More specifically, at 1.9 K the relaxation time of the hyperfine field is longer than the Larmor precession period of the nuclear moment, a period which can be obtained from the splitting of the outer lines of the Fe(III) sextet. In other words, the relaxation time is at least one order of magnitude longer than the Larmor period of 0.5×10^{-8} s. As the temperature increases, the relaxation

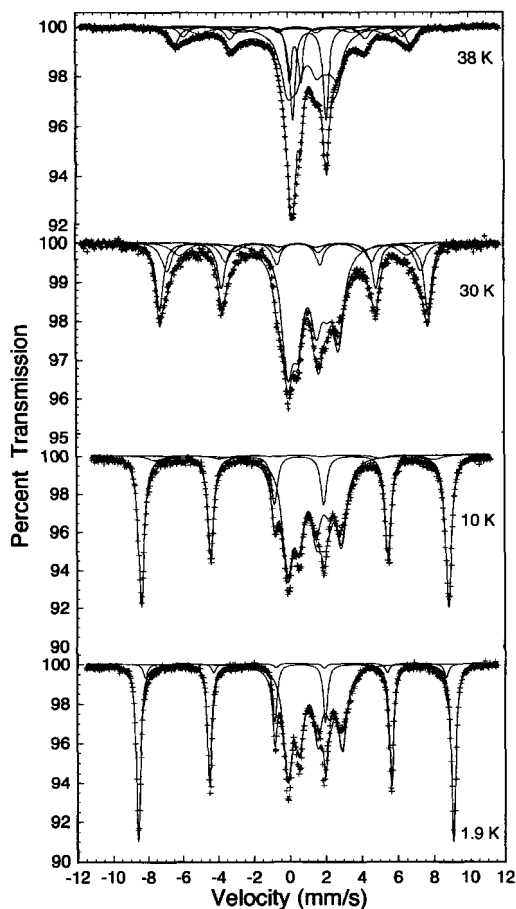


FIG. 9. Selected Mössbauer spectra of $(\text{NBu}_4)[\text{Fe}_2(\text{ox})_3]$ obtained at the indicated temperatures.

time becomes smaller and paramagnetic doublets are observed if the relaxation time is at least one order of magnitude shorter than the Larmor period of 0.5×10^{-8} s. The broadened sextets correspond to intermediate relaxation times between 10^{-7} and 10^{-9} s. Because a superposition of sextets and doublets is observed, there is a distribution of relaxation times within the layer. As expected, the relative area of the paramagnetic doublets increases as the temperature approaches the critical temperature.

The preliminary fits also indicated that more than one magnetic sextet was required to fit the spectral components associated with the iron(III) ions, even at the lowest temperatures of 4.2 and 1.9 K. At higher temperatures these magnetic sextets are quite broad, presumably because of differing relaxation rates of the hyperfine fields due to the dynamic nature of the short-range magnetic exchange correlations within the layers. In contrast to the iron(III) site, only one magnetic component was required to fit the iron(II) contri-

bution to the spectra but in this case, the very much reduced hyperfine field would be less sensitive to variations in the magnetic environment. Further, the failure of our model to more adequately fit the observed spectral profile of the iron(II) sextet is an indication of the presence of some variation in the magnetic environment.

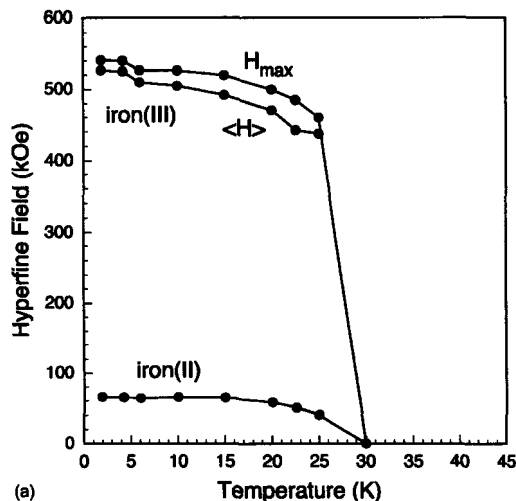
As expected from the quadrupole splitting observed in the paramagnetic spectra, the magnetic spectra of $(\text{PPh}_4)[\text{Fe}_2(\text{ox})_3]$ and $(\text{NBu}_4)[\text{Fe}_2(\text{ox})_3]$ exhibit quadrupole shifts (QS's). These quadrupole shifts are most easily observed in the spectra as a difference in the splitting of 1 and 2 and 5 and 6 iron(III) lines at 1.9 K. Because the quadrupole shift is determined by both the quadrupole splitting ΔE_Q and θ through the equation

$$\text{QS} = \frac{1}{2} \Delta E_Q (3 \cos^2 \theta - 1), \quad (5)$$

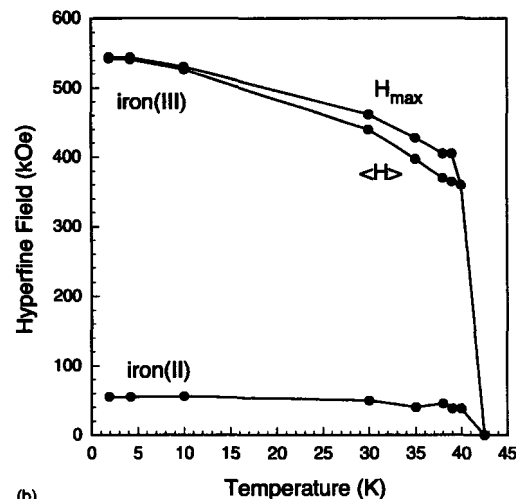
it is not possible to determine both ΔE_Q and θ from the magnetic spectra. Fortunately, it is well known³¹ that ΔE_Q approaches a constant value at low temperatures. Hence, in fitting the iron(II) component of the magnetic spectra, ΔE_Q was constrained to be equal to the value observed in the lowest-temperature paramagnetic spectrum and the θ value was adjusted to yield the observed quadrupole shift. Essentially the same approach was used for the iron(III) components except that it was found unnecessary to fix the ΔE_Q and θ values, which could easily be estimated from the observed spectra. For the iron(II) sextet the best fits always corresponded to $V_{zz} < 0$ and θ values of 90° ; no acceptable fits could be obtained with positive V_{zz} . Further, for the iron(III) sextets the best fits always corresponded to a negative V_{zz} and θ values of ca. 40° ; the results of these best fits are shown in Figs. 10 and 11. However, for the iron(III) sextets it was found that alternative fits with a positive V_{zz} and θ values which are much closer to 90° were almost as good as the best fits. At 1.9 K the alternative fit for $(\text{PPh}_4)[\text{Fe}_2(\text{ox})_3]$ corresponds to $\Delta E_Q = 0.75$ mm/s, $V_{zz} > 0$, and $\theta = 72.4^\circ$ and the alternative fit for $(\text{NBu}_4)[\text{Fe}_2(\text{ox})_3]$ corresponds to $\Delta E_Q = 0.67$ mm/s, $V_{zz} > 0$, and $\theta = 81.1^\circ$. A comparison of these alternative fits with the fits shown in Figs. 10 and 11 indicates that the alternative fit is potentially acceptable.

If the principal axis of the electric field gradient tensor at the iron site is reasonably assumed to be the c axis, the θ angle of 90° for the iron(II) site indicates that the iron(II) hyperfine field is within the plane of the layer. A similar conclusion was reached by Iijima and Mizutani¹¹ for $(\text{NBu}_4)[\text{Fe}_2(\text{ox})_3]$. If the effective hyperfine field is assumed to be parallel to the iron moment, then the iron(II) Mössbauer spectral fit and hyperfine parameters are fully consistent with a basal orientation of the moments.

In the case of the iron(III) sextet, if the negative quadrupole interaction values are used, the θ angles are $40^\circ \pm 1^\circ$ and ca. $37^\circ \pm 1^\circ$ for $(\text{PPh}_4)[\text{Fe}_2(\text{ox})_3]$ and $(\text{NBu}_4)[\text{Fe}_2(\text{ox})_3]$, respectively, and indicate that the iron(III) hyperfine fields and moments are canted from the c axis. If the positive quadrupole interaction values are used, the θ angles are $72^\circ \pm 1^\circ$ and ca. $81^\circ \pm 1^\circ$ for



(a)



(b)

FIG. 10. The temperature dependence of the maximum hyperfine field H_{max} and the weighted average hyperfine field $\langle H \rangle$ for iron(III) and the hyperfine field for iron(II) in $(\text{PPh}_4)[\text{Fe}_2(\text{ox})_3]$ (a) and in $(\text{NBu}_4)[\text{Fe}_2(\text{ox})_3]$ (b).

$(\text{PPh}_4)[\text{Fe}_2(\text{ox})_3]$ and $(\text{NBu}_4)[\text{Fe}_2(\text{ox})_3]$, respectively, and indicate that the iron(III) hyperfine field and moments are close to the basal plane. In either case, there is a component of the moments in the basal plane. So the magnetically ordered Mössbauer spectra are certainly consistent with a basal orientation of the iron magnetic moments in both $(\text{PPh}_4)[\text{Fe}_2(\text{ox})_3]$ and $(\text{NBu}_4)[\text{Fe}_2(\text{ox})_3]$. They suggest that perhaps there is either some canting of the moments or some noncollinearity of the iron(II) and iron(III) moments.

In attempting to fit the spectra obtained just below the apparent freezing temperature, it was found that no accept-

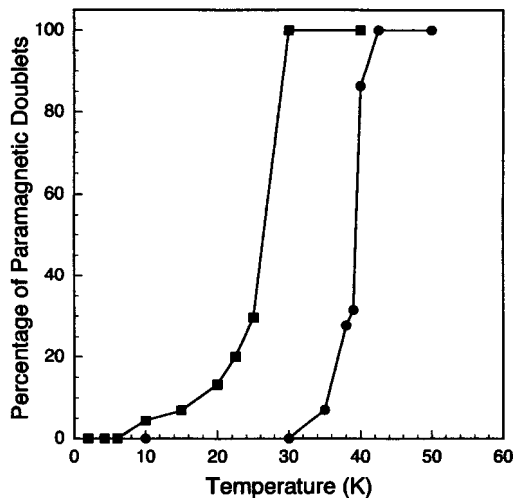


FIG. 11. A comparison of the percentage area of the paramagnetic quadrupole doublets observed in the Mössbauer spectra of $(\text{PPh}_4)[\text{Fe}_2(\text{ox})_3]$ (■) and $(\text{NBu}_4)[\text{Fe}_2(\text{ox})_3]$ (●) as a function of temperature.

able fits could be obtained unless the fit also included paramagnetic components, which were constrained to have the same δ , ΔE_Q , and Γ values as the magnetic components of the spectra. The necessity of including these paramagnetic components is most easily observed in the 22.5 K spectrum of $(\text{PPh}_4)[\text{Fe}_2(\text{ox})_3]$ shown in Fig. 8 and the 38 K spectrum of $(\text{NBu}_4)[\text{Fe}_2(\text{ox})_3]$ shown in Fig. 9. The presence of these paramagnetic components is consistent with the magnetic properties discussed above. At the temperatures requiring these components, a portion of the iron ions experience a rapidly fluctuating hyperfine field because of the dynamic nature of the exchange correlated regions within the layers.

The fits of the magnetic spectra yield isomer shifts and quadrupole splittings that are reasonable and consistent with the values obtained from the paramagnetic spectra: see Tables II and III and Fig. 7. Further, in all cases, the unconstrained ratio of iron(II) to iron(III) spectral areas is close to 50:50 in agreement with the small iron(II) deficiency observed experimentally in these compounds.²³ The 0 K extrapolated values of the iron(II) percentages are 48% and 45% in $(\text{NBu}_4)\text{Fe}_2(\text{ox})_3$ and $(\text{PPh}_4)\text{Fe}_2(\text{ox})_3$, respectively.

The magnetic hyperfine fields are shown as a function of temperature in Fig. 10, which shows for the iron(III) spectral components both the maximum field H_{max} and the weighted average field $\langle H \rangle$. For both $(\text{PPh}_4)[\text{Fe}_2(\text{ox})_3]$ and $(\text{NBu}_4)[\text{Fe}_2(\text{ox})_3]$ the iron(III) hyperfine fields approach 540 kOe at low temperatures and are typical of high-spin iron(III) with an $S = \frac{5}{2}$ electronic ground state. In contrast, the iron(II) ions in the two compounds have saturation hyperfine fields of ca. 65 and 55 kOe, fields which are much lower than the values of ca. 440 kOe expected of high-spin iron(II) with an $S = 2$ electronic ground state. Similar very small iron(II) fields have been reported^{3,12} earlier for $(\text{NBu}_4)[\text{Fe}_2(\text{ox})_3]$.

The effective magnetic hyperfine field, H_{eff} , at the iron site is given³² by

$$H_{\text{eff}} = H_{\text{core}} + H_{\text{orb}} + H_{\text{dip}}, \quad (6)$$

where H_{core} is the Fermi contact term and is typically -440 kOe, and H_{dip} and H_{orb} are the fields produced by the dipolar interaction of the nuclear magnetic moment with the electronic and orbital spin moment, respectively. Usually these last two terms are small. However, in $(\text{PPh}_4)[\text{Fe}_2(\text{ox})_3]$ and $(\text{NBu}_4)[\text{Fe}_2(\text{ox})_3]$, the iron(II) orbital moment is not quenched by the trigonal symmetry at the iron(II) site^{16,18} and, further, its contribution is expected³³ to oppose that of H_{core} . Thus, from the observed effective hyperfine fields H_{eff} , which are known¹⁵ to be positive, we calculate that $H_{\text{orb}} + H_{\text{dip}}$ is ca. $+500$ kOe.

A comparison of Figs. 10(a) and 10(b) indicates that the 30 K ordering temperature of $(\text{PPh}_4)[\text{Fe}_2(\text{ox})_3]$ is substantially lower than the 45 K value observed for $(\text{NBu}_4)[\text{Fe}_2(\text{ox})_3]$. The latter value is very similar to the 43 K ordering temperature observed¹⁹ for $[\text{FeCp}_2^+][\text{Fe}_2(\text{ox})_3]$.

Figures 10(a) and 10(b) show that both sublattices order at the same temperature. Further, both hyperfine fields increase at the same rate, contrary to the prediction of Nuttall and Day. For instance, at 30 K just below the compensation temperature of $(\text{NBu}_4)[\text{Fe}_2(\text{ox})_3]$, both fields have reached 85% of their saturation value. Hence, we do not find any evidence in the temperature dependence of the hyperfine fields to explain the negative magnetization of $(\text{NBu}_4)[\text{Fe}_2(\text{ox})_3]$. However it is difficult to relate directly the hyperfine fields to the sublattice magnetization, especially for the iron(II) ions because of the large orbital contribution to this field.

It should be noted that the three regions of differing paramagnetic intensity observed in the polarized neutron diffraction results shown in Fig. 3 are also reflected in the percentage area of the paramagnetic doublets observed in the Mössbauer spectra of $(\text{PPh}_4)[\text{Fe}_2(\text{ox})_3]$ and shown in Fig. 11. Below 10 K, virtually no paramagnetic doublets were observed. Between 10 and 25 K, paramagnetic doublets are required and are consistent with the intermediate intensity of the paramagnetic scattering observed in the polarized neutron diffraction results. Above 30 K, only paramagnetic doublets are observed and the intensity of the paramagnetic scattering is the highest. The analogous results for $(\text{NBu}_4)[\text{Fe}_2(\text{ox})_3]$ are also shown in Fig. 11 and seem to indicate a parallel behavior to that observed in the $(\text{PPh}_4)[\text{Fe}_2(\text{ox})_3]$, a parallel behavior which is shifted to higher temperature by ca. 15 K. The similarity would seem to indicate that the magnetic exchange correlations are very similar in the two compounds but the different cations and the presence of additional vacancies in $(\text{PPh}_4)[\text{Fe}_2(\text{ox})_3]$, as compared to $(\text{NBu}_4)[\text{Fe}_2(\text{ox})_3]$, lowers the onset of the magnetic exchange correlations by ca. 15 K.

IV. DISCUSSION

The polarized neutron diffraction results reported herein give the first description of the onset of magnetic interactions

in (d_{20} -PPh₄) [Fe^{II}Fe^{III}(ox)₃]. The unexpected result is the absence of long-range magnetic order. In contrast, short-range magnetic correlations are present below ca. 50 K. The existence of small magnetically correlated regions, or domains of ca. 50 Å diameter, within the layer plane is incompatible with iron magnetic moments parallel to the *c* axis. Hence, the iron magnetic moments must lie within the layer plane or at least have a component within the layer plane. This conclusion is in agreement with the analysis of the magnetically ordered Mössbauer spectra. While no neutron diffraction data are available for (NBu₄)[Fe₂(ox)₃], the similarities between the Mössbauer spectra of (PPh₄)[Fe₂(ox)₃] and (NBu₄)[Fe₂(ox)₃] lead to the conclusion that the magnetic behaviors of the two compounds are similar. Particularly, regions of differing paramagnetic intensity are found in both compounds. This suggests that a similar freezing process is involved in the ordering of both compounds. Without polarized neutron diffraction data, however, the spatial extent of the correlated domains in (NBu₄)[Fe₂(ox)₃] cannot be determined.

The magnetic behavior of (NBu₄)[Fe₂(ox)₃] has been interpreted in terms of a spin-glass-like behavior in several previous papers.^{11,34-36} This spin-glass-like behavior and the short-range magnetic correlation model proposed herein can be reconciled as follows. As indicated by the chemical analyses both (PPh₄)[Fe₂(ox)₃] and (NBu₄)[Fe₂(ox)₃] are iron deficient, a deficiency which results in a shortage of iron(II) in agreement with the 45% and 48% of iron(II) observed in the Mössbauer spectra of (PPh₄)[Fe₂(ox)₃] and (NBu₄)[Fe₂(ox)₃], respectively. When the temperature decreases below the freezing temperature, small regions or domains of correlated spins form most likely at nucleation sites, sites which may be located near one of the iron(II) vacancies. Because of the three magnetically equivalent directions within the layer plane, these spin-correlated domains grow with a spin direction parallel to one of three equivalent directions. Between these domains, there are regions of uncorrelated spins observed as the paramagnetic scattering in the polarized neutron diffraction profiles and as the paramagnetic doublets in the Mössbauer spectra. As the temperature decreases further, the exchange-correlated spin domains grow at the expense of the uncorrelated regions, as is indicated by the temperature dependence of the paramagnetic contribution to the Mössbauer spectra: see Fig. 11. Below ca. 10 K for (PPh₄)[Fe₂(ox)₃] and 30 K for (NBu₄)[Fe₂(ox)₃] the random spin structure freezes and no paramagnetic doublets are observed in the Mössbauer spectra. In these temperature regions, the spin structure can be viewed as a glass formed by small domains of magnetically correlated spins randomly aligned parallel to one of the three equivalent directions within the layer plane. The average size of these regions is ca. 50 Å as is indicated by the polarized neutron diffraction profiles. This description of the onset of the magnetic structure may also explain the small maximum in the correlation length that may be present at 20 K in the polarized neutron diffraction measurements on (d_{20} -PPh₄)[Fe₂(ox)₃]. When the compound is heated from its frozen spin structure, the smaller spin correlated regions are more likely to lose their correlations first and, as a con-

sequence, the average observed correlation length increases between 10 and 20 K. Above 20 K the larger exchange correlated domains begin to lose their correlation because of thermal agitation and the correlation length again decreases. Finally, it is interesting to note that a magnetic transition at 16.3 K has been observed³⁴ in the heat capacity of (NBu₄)[Fe₂(ox)₃] and the proximity of the temperatures of 16.3 and 20 K may indicate that these magnetic transitions have the same origin.

V. CONCLUSIONS

Neutron polarization analysis and Mössbauer spectroscopy have been used to study the short-range antiferromagnetic correlations in the layered insulators (PPh₄) [Fe^{II}Fe^{III}(ox)₃] and (NBu₄) [Fe^{II}Fe^{III}(ox)₃]. The absence of magnetic Bragg scattering in the polarized neutron diffraction profiles obtained between 2 and 50 K on (d_{20} -PPh₄) [Fe^{II}Fe^{III}(ox)₃] indicates the absence of long-range magnetic order. However, a broad asymmetric feature observed at a *Q* of ca. 0.8 Å⁻¹ is attributed to two-dimensional short-range magnetic correlations, which are described by a Warren function. The correlation length is ca. 50 Å between 2 and 30 K and then decreases to ca. 20 Å at 50 K. The Mössbauer spectra of (PPh₄) [Fe^{II}Fe^{III}(ox)₃] and (NBu₄) [Fe^{II}Fe^{III}(ox)₃] have been measured between 1.9 and 293 K and 1.9 and 315 K, respectively, and are very similar. Between 10 and 30 K, paramagnetic scattering in the polarized neutron diffraction profiles of (PPh₄) [Fe^{II}Fe^{III}(ox)₃] and the coexistence of broad sextets and doublets in the Mössbauer spectra both indicate the coexistence of spin-correlated and spin-uncorrelated regions in the layers of this compound on the time scales of both techniques. The polarized neutron scattering profiles yield the spatial correlation length, while the Mössbauer spectra yield the time autocorrelation function, and the combined results are best understood in terms of layers composed of random frozen, but exchange-correlated domains, of ca. 50 Å diameter at the lowest temperatures, of spin-correlated domains and spin-uncorrelated regions at intermediate temperatures, and of largely spin-uncorrelated regions above the apparent Néel temperature as determined from bulk magnetometry. The similarity of the Mössbauer spectra of (PPh₄) [Fe^{II}Fe^{III}(ox)₃] and (NBu₄) [Fe^{II}Fe^{III}(ox)₃] leads us to conclude that similar processes occur in the both compounds.

ACKNOWLEDGMENTS

The authors thank Dr. H. Spiering for useful discussions and ideas during the course of this work and Dr. J. R. Stuart and Dr. K. H. Andersen for valuable assistance with the neutron scattering experiments. G.J.L. thanks the National Science Foundation for Grant No. DMR-9521739 and the Belgian "Fonds National de la Recherche Scientifique" for support during a sabbatical leave. This work is supported by the UK EPSRC and EC TMR network "Molecular Magnets." Thanks are due to the Institut Laue-Langevin, Grenoble, for access to neutron facilities.

SIMON G. CARLING *et al.*PHYSICAL REVIEW B **66**, 104407 (2002)

- ¹H. Tamaki, M. Mitsumi, K. Nakamura, N. Matsumoto, S. Kida, H. Okawa, and S. Iijima, *Chem. Lett.* **1992**, 1975 (1992).
- ²H. Tamaki, Z. Zhong, N. Matsumoto, S. Kida, M. Koikawa, N. Aihwa, Y. Hashimoto, and H. Okawa, *J. Am. Chem. Soc.* **114**, 6974 (1992).
- ³S. Iijima, T. Katsura, H. Tamaki, M. Mitsumi, N. Matsumoto, and H. Okawa, *Mol. Cryst. Liq. Cryst. Sci. Technol., Sect. A* **233**, 263 (1993).
- ⁴C. Mathonière, S. G. Carling, Y. Dou, and P. Day, *J. Chem. Soc. Chem. Commun.* **1994**, 1554.
- ⁵W. M. Reiff, J. Kreis, L. Meda, and R. U. Kirss, *Mol. Cryst. Liq. Cryst. Sci. Technol., Sect. A* **273**, 181 (1995).
- ⁶C. Mathonière, C. J. Nuttall, S. G. Carling, and P. Day, *Inorg. Chem.* **35**, 1201 (1996).
- ⁷L. Néel, *Ann. Phys. (Paris)* **3**, 137 (1948).
- ⁸I. D. Watts, S. G. Carling, and P. Day, *Phys. Chem. Chem. Phys.* **3**, 4418 (2001).
- ⁹C. J. Nuttall and P. Day, *Inorg. Chem.* **37**, 3885 (1998).
- ¹⁰D. Visser, S. G. Carling, I. D. Watts, P. Day, and K. H. Andersen, *Physica B* **268**, 266 (1999).
- ¹¹H. Okawa, N. Matsumoto, H. Tamaki, and M. Ohba, *Mol. Cryst. Liq. Cryst. Sci. Technol., Sect. A* **233**, 257 (1993).
- ¹²S. Iijima, F. Mizutani, M. Mitsumi, N. Matsumoto, and H. Okawa, *Inorg. Chim. Acta* **253**, 47 (1996).
- ¹³S. Iijima and F. Mizutani, *Mol. Cryst. Liq. Cryst. Sci. Technol., Sect. A* **306**, 227 (1997).
- ¹⁴S. Iijima and F. Mizutani, *Mol. Cryst. Liq. Cryst. Sci. Technol., Sect. A* **335**, 143 (1999).
- ¹⁵S. Iijima and F. Mizutani, *Mol. Cryst. Liq. Cryst. Sci. Technol., Sect. A* **343**, 199 (2000).
- ¹⁶N. S. Ovanesyan, G. V. Shilov, L. O. Atovmyan, R. N. Lyubovskaya, A. A. Pyalling, and Y. G. Morozov, *Mol. Cryst. Liq. Cryst. Sci. Technol., Sect. A* **273**, 175 (1995).
- ¹⁷N. S. Ovanesyan, G. V. Shilov, N. A. Sanina, A. A. Pyalling, L. O. Atovmyan, and L. Bottyán, *Mol. Cryst. Liq. Cryst. Sci. Technol., Sect. A* **335**, 91 (1999).
- ¹⁸L. Bottyán, L. Kiss, N. S. Ovanesyan, A. A. Pyalling, N. A. Sanina, and A. B. Kashuba, *JETP Lett.* **70**, 697 (1999).
- ¹⁹E. Coronado, J. R. Galán-Mascarós, C. J. Gómez-García, J. Ensling, and P. Gütllich, *Chem.-Eur. J.* **6**, 552 (2000).
- ²⁰C. J. Nuttall, Ph.D. thesis, University of London, 1998.
- ²¹I. D. Watts, Ph.D. thesis, University of London, 2000.
- ²²O. Schärpf and H. Capellmann, *Phys. Status Solidi A* **135**, 359 (1993).
- ²³C. J. Nuttall and P. Day, *Chem. Mater.* **10**, 3050 (1998).
- ²⁴P. J. Brown, in *International Tables for Crystallography*, edited by A. J. C. Wilson (Kluwer Academic, Dordrecht, 1999), Vol. C, p. 450.
- ²⁵J. E. Greedan, M. Bieringer, J. F. Britten, G. M. Giaquinta, and H. C. Zurloye, *J. Solid State Chem.* **116**, 118 (1995).
- ²⁶B. E. Warren, *Phys. Rev.* **59**, 693 (1941).
- ²⁷J. Fenger, K. E. Siekierska, and A. G. Maddock, *J. Chem. Soc. A* **1970**, 1456.
- ²⁸M. J. Halsey and A. M. Pritchard, *J. Chem. Soc. A* **1968**, 2878.
- ²⁹H. Sato and T. Tominaga, *Bull. Chem. Soc. Jpn.* **52**, 1402 (1979).
- ³⁰R. Ingalls, *Phys. Rev.* **133**, A787 (1964).
- ³¹G. J. Long and F. Grandjean, in *Supermagnets, Hard Magnetic Materials*, edited by G. J. Long and F. Grandjean (Kluwer Academic, Dordrecht, 1991) p. 355.
- ³²T. E. Cranshaw and G. Longworth, in *Mössbauer Spectroscopy Applied to Inorganic Chemistry*, edited by G. J. Long (Plenum, New York, 1984), Vol. 1, p. 171.
- ³³M. F. Thomas and C. E. Johnson, in *Mössbauer Spectroscopy*, edited by D. P. E. Dickson and F. J. Berry (Cambridge University Press, Cambridge, England, 1986), p. 143.
- ³⁴A. Bhattacharjee, Y. Miyazaki, and M. Sorai, *J. Phys. Soc. Jpn.* **69**, 479 (2000).
- ³⁵A. Bhattacharjee, K. Saito, and M. Sorai, *Solid State Commun.* **113**, 543 (2000).
- ³⁶A. Bhattacharjee, S. Iijima, F. Mizutani, T. Katsura, N. Matsumoto, and H. Okawa, *Jpn. J. Appl. Phys., Part 1* **34**, 1521 (1995).

Ion-radical salts: a new type of molecular ferrimagnet

Scott S. Turner^a and Peter Day^{a,b}

DOI: 10.1039/b412696n

Long-range ferrimagnetic order in which one magnetic sub-lattice is formed from partly-occupied p-orbitals and the other from d-orbitals can be achieved in molecular ion-radical salts where the cations are oxidised organo-chalcogen donors and the anions are 3d-metal complexes containing both N-bonded NCS and planar N-heterocyclic ligands. Overlaps between p-orbitals of the radical cations and those of the heterocycle are implicated in the cation-anion exchange pathway.

When Néel¹ published his seminal theoretical paper defining the characteristics of ferrimagnets in 1948, he envisaged that the localised atomic moments making up the two antiferromagnetically coupled sub-lattices would be furnished by partly-filled d-shells. Specifically, he had in mind spinels AB₂O₄ where A is a 2+ and B a 3+ transition-metal ion. Since then, hundreds (if not thousands) of ferrimagnetic phases have been prepared and characterised, based not only on d- but also on f-atomic moments² but, until quite recently, no three-dimensional examples were known where one of the magnetic sub-lattices consisted of moments originating from partly-filled

p-shells. The reason for this deficiency is obvious: paramagnetic p-electron systems are normally highly reactive and immediately combine with one another to form dimers and polymers, hence losing the magnetism in electron-pair bonds.

The proliferation of ion-radical salts (D_n)⁺(X)⁻ over the last 20 years might be useful in addressing this problem because they are formed by oxidising an aromatic donor molecule D to a radical cation and stabilising it in a crystal lattice through combining it with an anion, X.³ However, in the vast majority of cases, overlap between p-orbitals of neighbouring (D_n)⁺ is great enough to form a conduction band (albeit usually a narrow one) so the resulting solid is

a strongly-correlated metal or a semiconductor.⁴ Indeed, most of the presently known organic superconductors are drawn from the families of ion-radical salts based on organo-chalcogen donors like TMTSF (tetramethyl tetraselenofulvalene)⁵ and BEDT-TTF (bis-ethylenedithiotetrathiafulvalene).⁶ To make molecular ion-radical salts that show long-range magnetic order rather than coherent electron transport, we must therefore use crystal engineering principles to devise structures that inhibit D...D overlap. Furthermore, to make bulk ferrimagnets where one sub-lattice is formed from p-electrons and the other from d-electrons, we also need to enhance D...X overlap, while incorporating the d-moments into X. Those requirements have now been fulfilled

*pday@ri.ac.uk



Scott Turner

Scott Turner received a BSc (1990) in chemistry and PhD (1993) in inorganic chemistry from the University of Manchester, UK. His doctoral studies were undertaken with Dr F. Mabbs in the field of the EPR spectroscopy of oligomeric vanadyl species. Subsequently he joined the group of the late Prof. O. Kahn, in Paris and then Bordeaux, as a NATO research fellow for two years. During this time he worked on a wide variety of molecule-based magnetic materials. From 1996 to 2004 he worked with Prof. Day as a post-doctoral researcher, synthesising and characterising novel molecule-based

conductors and magnets. Recently Dr Turner has become a lecturer of Inorganic Chemistry at the University of Exeter, UK. His current research activities focus on bistable and multifunctional molecule-based conductors.

Peter Day gained his first degree and DPhil in inorganic chemistry from Oxford University, where he was subsequently Departmental Demonstrator, University Lecturer and Ad Hominem Professor of Solid State Chemistry, and a Fellow of St. John's College. From 1988–1991 he was Director of the Institut Laue-Langevin, Grenoble, the European neutron scattering centre and from 1991–1998, Director of the Royal Institution in London and its Davy-Faraday Research Laboratory, where he remains Fullerian Professor of



Peter Day

Chemistry. He was elected FRS in 1986 and, in addition to numerous awards from the Royal Society of Chemistry and the Royal Society, he holds honorary doctorates from the Universities of Newcastle and Kent, and Honorary Fellowships of St. John's and Wadham Colleges, Oxford, and University College London. His research interests have long centred on the synthesis and electronic properties of molecular organic and metal-organic solids. From 1998–2002 he was Scientific Advisory Editor of the Journal of Materials Chemistry.

in the family of compounds described below.

The ion-radical salts of TTF-type donors are good conductors because strong non-covalent S⋯S interactions enhance the inter-molecular D⋯D transfer integrals. We therefore used the same strategy to build up D⋯X interactions by synthesising salts in which X also contains S or Se. An obvious point of departure is the NCS ligand, bound to 3d-metal ions through N, with the S able to interact with the TTF. Indeed, salts such as (BEDT-TTF)₄[M(NCS)₆]₂·CH₂Cl₂ (M = Cr, Fe) do show numerous close cation-anion S⋯S contacts and the closely-knit layers of donor molecules characteristic of BEDT-TTF salts are substantially disrupted.⁷ On the other hand, however, they behave as almost perfect paramagnets, obeying the Curie-Weiss law down to 2 K (e.g. for M = Fe, the Weiss constant is -0.19 K). It appears that S⋯S interactions are not sufficient to induce significant D⋯X exchange.

Fortunately all is not lost, as there exist a large class of paramagnetic anions based on Reinecke's salt, first synthesised over 100 years ago.⁸ In these, two of the NCS ligands are replaced by aliphatic or aromatic amines B, yielding *cis*- or *trans*-[M(NCS)₄B₂]⁻. When B = NH₃ there is still no detectable D⋯X interaction (e.g. in (BEDT-TTF)₂[Cr(NCS)₄(NH₃)₂] the Weiss constant is less than 0.1 K⁹) but for B = isoquinoline and 1,10-phenanthroline (phen), long-range ferrimagnetic order is established between 6 and 9 K.¹⁰ A typical example is (BEDT-TTF)[Cr(NCS)₄(isoquinoline)₂]. The crystal structure (Fig. 1) contains many S⋯S contacts between D and X but, more importantly, π-π overlaps between D⁺ and the isoquinoline.¹¹ The magnetic susceptibility (Fig. 2) is typical of a ferrimagnet, with a minimum in χ_T indicating antiferromagnetic ic near-neighbour exchange between the D⁺ (S = 1/2) and X⁻ (S = 3/2) sub-lattices.¹⁰

However, the structurally simplest example is (TTF)[Cr(NCS)₄(phen)] (Fig. 3),¹² which has the further advantage that the larger quantities needed for detailed physical studies can be obtained by metathesis rather than electrochemical oxidation.¹³ Fig. 4 shows the AC susceptibility of this phase, indicating a T_c

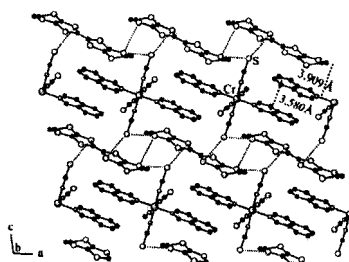


Fig. 1 Crystal structure of (BEDT-TTF)[Cr(NCS)₄(iso-quinoline)₂].¹¹

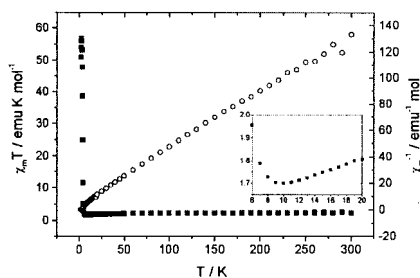


Fig. 2 Temperature dependence of magnetic susceptibility for (BEDT-TTF)[Cr(NCS)₄(iso-quinoline)₂].¹⁰ Open circle, right-hand scale; filled squares, left hand scale. Inset is an enlargement of the 6–20 K region.

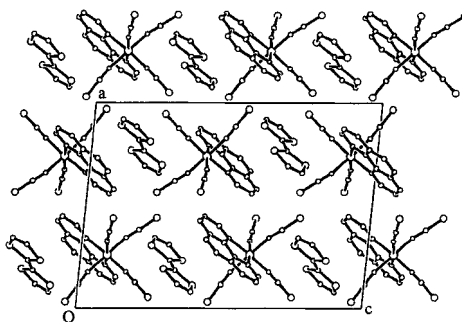


Fig. 3 Crystal structure of (TTF)[Cr(NCS)₄(phen)].¹²

of 8.3 K.¹³ Recently this class of ferrimagnets has been enlarged further by reports of analogous salts of tetramethyl-TTF¹⁴ and of non-TTF organo-sulfur donors.¹⁵

Finally, although the concept of a simple π-d ferrimagnet, based on an ion-radical salt is undoubtedly attractive, this family may be more complicated than

appears at first sight. For example, the first muon spin rotation measurements on such salts reveal, surprisingly, that in addition to the ordering transition at 8.3 K in (TTF)[Cr(NCS)₄(phen)], there is a further transition at 2 K,¹⁶ also evident in the heat capacity.¹⁷ Likewise the first electronic structure calculations on this class of salt suggest that the

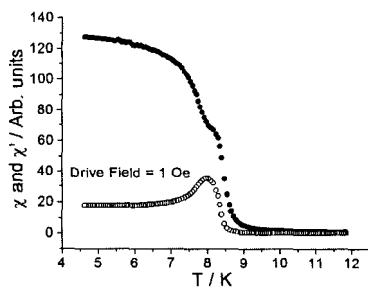


Fig. 4 Temperature dependence of AC susceptibility of per-deuterated (TTF)[Cr(NCS)₄(phen)] at 10 kHz.¹³ Full circles, in-phase; empty circles, out-of-phase signals.

S··S contacts contribute more than the π - π ones to the inter-molecular exchange, in contrast to the empirical finding that cation-anion S··S contacts alone are not enough to engender long-range ferromagnetic order at accessible temperatures.¹⁸ So there remains much more to learn about ion-radical salts as π -d ferrimagnets.

Acknowledgements

The work summarised here was supported by the UK Engineering and Physical Sciences Research Council and the European Commission (TMR Network on Molecular Magnetism and COST Action D14).

Scott S. Turner^a and Peter Day^{a,b}
^aChemistry Department, University of Exeter,
 Stocker Road, Exeter, EX4 4QD, UK.

E-mail: S.S.Turner@exeter.ac.uk
^bDavy-Faraday Research Laboratory, The
 Royal Institution, 21 Albemarle Street,
 London W1S 4BS, UK. E-mail: pday@ri.ac.uk

References

- 1 L. Néel, *Ann. Phys. (Paris)*, 1948, 1, 137.
- 2 See e.g. J. B. Goodenough, *Magnetism and the Chemical Bond*, Interscience, New York, 1963, *passim*.
- 3 See e.g. J. M. Williams, J. R. Ferraro, R. J. Thorn, K. D. Carlson, U. Geiser, H. H. Wang, A. M. Kini and M-H. Wangbo, *Organic Superconductors (including Fullerenes): Synthesis, Structure, Properties and Theory*, Prentice-Hall, New York, 1992.
- 4 T. Ishiguro, K. Yamaji and G. Saito, *Organic Superconductors*, Springer, Berlin, 1998; J. Singleton, *Rep. Prog. Phys.*, 2000, 63, 1111.
- 5 D. Jerome, A. Mazaud, M. Ribault and K. Bechgaard, *J. Phys. Lett.*, 1980, 41, L95.
- 6 H. Urayama, H. Yamochi, G. Saito, S. Sato, A. Kawamoto, J. Tanaka, T. Mori, Y. Maruyama and H. Inokuchi, *Chem. Lett.*, 1988, 463.
- 7 S. S. Turner, P. Day, T. Gelbrich and M. B. Hursthouse, *J. Solid State Chem.*, 2001, 159, 385; S. S. Turner, D. Le Pevelen, P. Day and C. K. Prout, *J. Solid State Chem.*, 2002, 168, 573.
- 8 O. T. Christensen, *J. Prakt. Chem.*, 1892, 45, 213, 356; *Handbuch Präparativen Anorganischen Chemie*, ed. G. Brauer, Ferdinand Enke Verlag, Stuttgart, 3rd edn., 1975-1981, vol. 3, p. 1516.
- 9 C. J. Kepert, M. Kurmoo and P. Day, *J. Chem. Soc., Dalton Trans.*, 1997, 607.
- 10 S. S. Turner, C. Michaut, P. Durot, P. Day, T. Gelbrich and M. B. Hursthouse, *J. Chem. Soc., Dalton Trans.*, 2000, 905.
- 11 F. Setifi, S. Golhen, L. Ouahab, S. S. Turner and P. Day, *Cryst. Evol. Commun.*, 2002, 4, 1.
- 12 S. S. Turner, D. Le Pevelen, P. Day and C. K. Prout, *J. Chem. Soc., Dalton Trans.*, 2000, 2739; D. Le Pevelen, S. S. Turner, P. Day and C. K. Prout, *Synth. Met.*, 2001, 120, 1842.
- 13 S. S. Turner, S. G. Carling, P. Day, C. J. Gomez-Garcia and E. Coronado, *J. Phys. IV*, 2004, 114, 585.
- 14 M. Mas-Torrent, S. S. Turner, K. Wurst, J. Vidal-Gancedo, X. Ribas, J. Veciana, P. Day and C. Rovira, *Inorg. Chem.*, 2003, 42, 7544.
- 15 F. Setifi, S. Golhen, L. Ouahab, A. Miyazaki, K. Okabe, T. Enoki, T. Toita and J. Yamada, *Inorg. Chem.*, 2002, 41, 3786; F. Setifi, S. Golhen, L. Ouahab, A. Miyazaki, T. Enoki and J. Yamada, *C. R. Chim.*, 2003, 6, 309.
- 16 P. Day, S. G. Carling, S. S. Turner, J. Bradley, D. Hautot and D. Visser, *ISIS Annual Report (Science Highlights)*, CLRC Rutherford Appleton Laboratory, Didcot, Oxfordshire, 2003, p. 8.
- 17 C. J. Gomez-Garcia, S. S. Turner, E. Coronado and P. Day, to be published.
- 18 T. Mori and M. Katsuhara, *J. Phys. Soc. Jpn.*, 2003, 72, 149.

TTF based charge transfer salts of $[M(NCS)_4(C_9H_7N)_2]^-$ where $M = Cr, Fe$ and $C_9H_7N =$ isoquinoline; observation of bulk ferrimagnetic order

Scott S. Turner,^{*,a} Cecile Michaut,^a Stephanie Durot,^a Peter Day,^{*,a} Thomas Gelbrich^b and Michael B. Hursthouse^b

^a Davy-Faraday Research Laboratory, Royal Institution of Great Britain, 21 Albemarle Street, London, UK W1X 4BS. E-mail: sst@ri.ac.uk, pday@ri.ac.uk

^b Department of Chemistry, University of Southampton, Southampton, UK SO17 1BJ

Received 22nd December 1999, Accepted 10th February 2000

Three new charge transfer salts of BEDT-TTF and TTF with the counter ions $[M(NCS)_4(C_9H_7N)_2]^-$ ($M = Cr, Fe$; $C_9H_7N =$ isoquinoline) are described. The materials are prepared by standard electrocrystallisation techniques. The nature of the anion is verified in the crystal structure of the salt $[C_9H_7N][Cr(NCS)_4(C_9H_7N)] \cdot C_{12}H_{24}O_6 \cdot H_2O$ which is used as the electrolyte when $M = Cr$. All of the charge transfer salts display long range ferrimagnetic order originating from the interaction between M ($S = 3/2$ or $S = 5/2$) and the donor ($S = 1/2$). The measured critical temperatures are 4.2 K (BEDT-TTF, $M = Cr$), 4.5 K (BEDT-TTF, $M = Fe$) and 8.9 K (TTF, $M = Cr$). Each of the compounds also shows a modest magnetic hysteresis of 338, 18 and 75 Oe for BEDT-TTF salts of $M = Cr, Fe$ and the TTF salt of Cr, respectively.

Introduction

Charge transfer salts of organic donors are characterised by having a wide range of conducting properties from insulating through semi-conducting to metallic and superconducting.¹ The transport properties can be correlated with the relative orientation of donors in the crystal which are arranged, in part, by the spatial organisation of the counter ions and other included molecules.²⁻⁴ Bis(ethylenedithio)tetrathiafulvalene, BEDT-TTF, has thus far been proved to be the most flexible organochalcogenide electron donor for such salts, being a component in a large number of highly conducting compounds.¹ Until relatively recently the focus of research has been concerned with the transport properties of salts although emphasis has now moved towards the possibility of preparing materials with mixed physical properties such as high conductivity and magnetism. The magnetic properties are typically introduced *via* anionic complexes which have paramagnetic centres distinct from any magnetic effects due to the radical donors,⁵ which are usually minor. The vast majority of systems of this type contain d-block metals and display simple paramagnetism together with varying transport properties. For example TTF based salts have been made of anions $[FeCl_4]^-$,⁶ $[Fe(CN)_6]^{3-}$,⁷ Reineckes anion, $[Cr(NCS)_4(NH_3)_2]^{3-}$ ⁸ and $[Cr(C_2O_4)_3]^{3-}$.⁹

Charge transfer salts with $[M^{III}(C_2O_4)_3]^{3-}$ include the first molecular superconductor containing paramagnetic metal ions, β'' -(BEDT-TTF)₄[(H₂O)Fe(C₂O₄)₃] $\cdot C_6H_5CN$.¹⁰ We have prepared and characterised many variations of this material by, for example, replacing Fe with other M(III) ions which controls the magnitude of paramagnetism.⁹ Many groups, including ours, have been engaged in trying to replace H₃O⁺ with M(n) which in principle could produce a material that exhibited simultaneous molecular long range magnetic ordering and molecular conductivity.¹¹ The sources of the magnetism and conductivity would be distinct in this case and the magnetic order would not be mediated by the radical donor. The aim of the work described here is to prepare TTF based salts which exhibit long range magnetic order arising in part from the radical donor.

This is with a view to making materials in which the donor participates both in the magnetism and conductivity.

Experimental

Two probe DC transport measurements were made on several crystals of the title compound and since they had high intrinsic resistance any contact resistance was assumed to be negligible. Gold wire electrodes (0.025 mm diameter) were attached directly to the crystals using Pt paint (Degussa) and measurements taken using an Oxford Instruments Mag Lab 2000 equipped with an EP probe. AC magnetisation measurements were also made using the Mag Lab 2000 at frequencies of 10 Hz–10 kHz and a drive field of 1 Oe. DC magnetisation experiments were made with a Quantum Design MPMS7 SQUID magnetometer using randomly orientated polycrystalline material encased in a gel capsule. Magnetisation was recorded from 2 to 300 K at 100 G and at 2 K between 0 and 7 T. The crystallographic study was performed at 150(2) K using an Enraf-Nonius Kappa CCD area detector with Mo-K α radiation (0.71073 Å). The structure was solved using DIRDIF-96¹² and refined by full matrix least squares on F^2 using SHELXL97.¹³ The absorption correction was achieved with SORTAV.¹⁴ Crystal parameters and collection data are listed in Table 1.

CCDC reference number 186/1855.

See <http://www.rsc.org/suppdata/dt/a9/a910259k/> for crystallographic files in .cif format.

Synthesis

Reineckes salt, $NH_4[Cr(NCS)_4(NH_3)_2] \cdot H_2O$ and isoquinoline (C_9H_7N) were purchased from Aldrich and used as received. 18-crown-6 (Aldrich) was dried over acetonitrile and CH_2Cl_2 was distilled over P_2O_5 immediately before use. $[N(C_4H_9)_4][Fe(SCN)_6]$ was prepared by a slight variation of the published method¹⁵ by using $[N(C_4H_9)_4]SCN$ rather than $[N(CH_3)_4]SCN$ to precipitate the product.

Table 1 Crystallographic data for II

Empirical formula	C ₄₃ H ₄₈ CrN ₇ O ₇ S ₄
Formula weight	955.12
<i>T</i> /K	150(2)
Radiation	0.71073 Å
Crystal system	Triclinic
Space group	<i>P</i> 1 (no. 2)
<i>a</i> /Å	8.2051(5)
<i>b</i> /Å	9.5548(7)
<i>c</i> /Å	16.1340(11)
<i>a</i> ^o	75.502(3)
<i>β</i> ^o	78.898(4)
<i>γ</i> ^o	74.485(4)
<i>V</i> /Å ³	1169.23(14)
<i>Z</i>	1
<i>μ</i> /mm ⁻¹	0.479
Reflections collected	12540
Independent reflections	4554 [<i>R</i> (int) = 0.0565]
<i>R</i> values (all data)	<i>R</i> 1 = 0.0653, <i>wR</i> 2 = 0.1062
Final <i>R</i> values [<i>I</i> > 2σ(<i>I</i>)]	<i>R</i> 1 = 0.0418, <i>wR</i> 2 = 0.0975

[C₉H₈N][Cr(NCS)₄(C₉H₇N)₂]-3H₂O. Isoquinoline (3.87 g, 30 mmol) and Reineckes salt (3.54 g, 10 mmol) were refluxed at 70 °C in 100 ml absolute ethanol for three hours. During this time all solids dissolved and the mixture became deep red. The clear solution was refluxed for a further twelve hours until the red product precipitated. After cooling the solid was isolated by filtration and washed with cold absolute ethanol. The solid was found to be sparingly soluble in common organic solvents and was not recrystallised. Yield 74% based on Cr. Found C 51.10, H 3.67, N 13.70, S 16.09, Cr 7.12. Calc. for C₃₁H₂₈N₇S₄O₃Cr, C 51.23, H 3.88, N 13.49, S 17.64, Cr 7.15%.

BEDT-TTF[Cr(NCS)₄(C₉H₇N)₂], I. The charge transfer salt was prepared by *in situ* oxidation of BEDT-TTF (10 mg), placed in the anode arm of an H-shaped electrochemical cell. The remainder of the cell was filled with a filtered solution of [C₉H₈N][Cr(NCS)₄(C₉H₇N)₂]-3H₂O (80 mg) and 18-crown-6 (100 mg) in CH₂Cl₂ (50 ml). 1 μA was applied across the cell for 1 week giving 3 mg of dark brown plates which grew on the anode. The crystals were found to be unsuitable for structure solution by X-ray single crystal diffraction due to excessive twinning. Found C 41.52, H 2.33, N 9.04, S 41.49, Cr 5.61, Cl 0.0. Calc. for C₃₂H₂₂N₆S₁₂Cr, C 41.45, H 2.39, N 9.06, S 41.49, Cr 5.61, Cl 0.0%.

A portion (2 ml) of the electrolyte solution was removed and the solvent allowed to slowly evaporate giving red prisms containing the anion which were suitable for X-ray single crystal structure determination. The crystals were identified from their structure as [C₉H₈N][Cr(NCS)₄(C₉H₇N)₂]-C₁₂H₂₄O₆·H₂O, II.

TTF[Cr(NCS)₄(C₉H₇N)₂], III. The TTF charge transfer salt was prepared using an identical method to that which gave the BEDT-TTF salt. 4 mg of a dark brown amorphous powder grew on the anode after two weeks. Found C 41.20, H 2.7, N 8.99, S 42.00, Cr 5.42. Calc. for C₃₂H₂₂S₁₂N₆Cr, C 41.45, H 2.39, N 9.06, S 41.49, Cr 5.50%.

[N(C₄H₉)₄][Fe(NCS)₄(C₉H₇N)₂]. [N(C₄H₉)₄][Fe(SCN)₆] (2 g, 1.7 mmol) and isoquinoline (0.684 g, 5.3 mmol) were refluxed in 50 ml absolute methanol for four hours over which time the solution changed colour from deep red to black. The clear solution was left at -10 °C for one week giving a black powder and light yellow solution. The product was isolated by filtration and washed with cold methanol followed by diethyl ether. Upon drying the powder proved to be very deep purple in colour. Yield 69% based on Fe. Found C 58.17, H 6.25, N 12.39, S 17.08, Fe 6.84. Calc. for C₃₉H₃₀N₈S₄Fe, C 57.84, H 6.39, N 12.43, S 16.26, Fe 7.07%.

BEDT-TTF[Fe(NCS)₄(C₉H₇N)₂], IV. A method identical to that used for the Cr derivative was used to synthesise this salt on

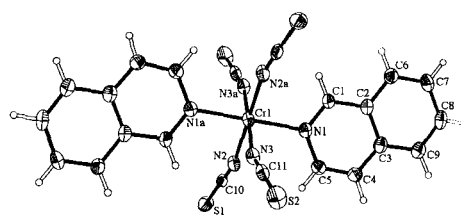


Fig. 1 ORTEP²² diagram of [Cr(NCS)₄(C₉H₇N)₂]⁻ in II showing 50% thermal ellipsoids and the atom numbering scheme.

replacing [C₉H₈N][Cr(NCS)₄(C₉H₇N)₂]-3H₂O with [N(C₄H₉)₄][Fe(NCS)₄(C₉H₇N)₂] as electrolyte. 3 mg of a dark brown microcrystalline powder grew on the anode after one week. Found C 40.96, H 2.78, N 9.22, S 40.67, Fe 6.30. Calc. for C₃₂H₂₂N₆S₁₂Fe, C 41.27, H 2.38, N 9.02, S 41.32, Fe 6.00%.

A similar route to the TTF derivative was attempted without success.

Results and discussion

Since crystals of I were unsuitable for X-ray structure determination, the structure of the anion found in I was confirmed by solving the structure of the salt employed as the electrolyte in the electrochemical cells. As anticipated the unit cell of II contains the isoquinolinium cation, [C₉H₈N]⁺, and [Cr(NCS)₄(C₉H₇N)₂]⁻, together with one molecule of H₂O and a molecule of 18-crown-6, which was added to aid solubility. A standard ORTEP diagram of the anion is given in Fig. 1 showing 50% thermal ellipsoids and the atom numbering scheme. The anion presents octahedral co-ordination about Cr with two *trans* co-ordinated C₉H₇N ligands. The metal atom is on an inversion centre with the Cr–N (of NCS) distances slightly shorter than those to N of isoquinoline (*i.e.* Cr1–N1 is 2.077(2) as compared to 1.984(2) and 1.991(2) for Cr1–N2 and Cr1–N3, respectively). Fig. 2 shows the crystal packing in II. The water molecule, which has been located in the cavity of the crown ether, is disordered equally over two positions related by an inversion centre and is hydrogen bonded to the macrocycle. The cation [C₉H₈N]⁺ is disordered in the same manner and is hydrogen bonded, through N–H, to the water molecule. During the refinement twenty-two restraints for chemically equivalent bond distances were used for the disordered cation.

The magnetic properties of I are characteristic of a bulk ferrimagnet exhibiting long range magnetic order below the critical temperature, *T*_c, of 4.2 K. The temperature dependencies of $\chi_m T$ and χ_m^{-1} in a field of 100 G are given in Fig. 3 where χ_m is the molar magnetic susceptibility and *T* the temperature measured. The value of $\chi_m T$ at 300 K is 2.26 emu K mol⁻¹ which is very close to the spin only value of 2.251 emu K mol⁻¹ for an uncorrelated spin system with an acceptor spin *S*_A = 3/2 (from Cr³⁺) and a donor spin *S*_D = 1/2 (from BEDT-TTF⁺), assuming *g* = 2 for both magnetic centres. This indicates that at this temperature short range order is low and there is minimal orbital contribution to the *g* factor. As the temperature is lowered the value of $\chi_m T$ decreases and there is a rounded minimum of 1.7 emu K mol⁻¹ at 10 K (inset Fig. 3). Below 10 K the value of $\chi_m T$ increases rapidly up to a maximum of 56.6 emu K mol⁻¹ at 2.7 K at which point the salt is saturated. Below the saturation point χ_m is roughly constant and so $\chi_m T$ decreases linearly with *T*. This behaviour confirms that I is a ferrimagnet.¹⁶ At high temperature $\chi_m T$ approaches the paramagnetic limit and as *T* is lowered the decrease in $\chi_m T$ corresponds to a short range order where local spins *S*_A and *S*_D are aligned antiparallel but have no correlation with neighbouring Cr–BEDT-TTF units. As *T* is lowered beyond the minimum the correlation length increases which leads to spontaneous

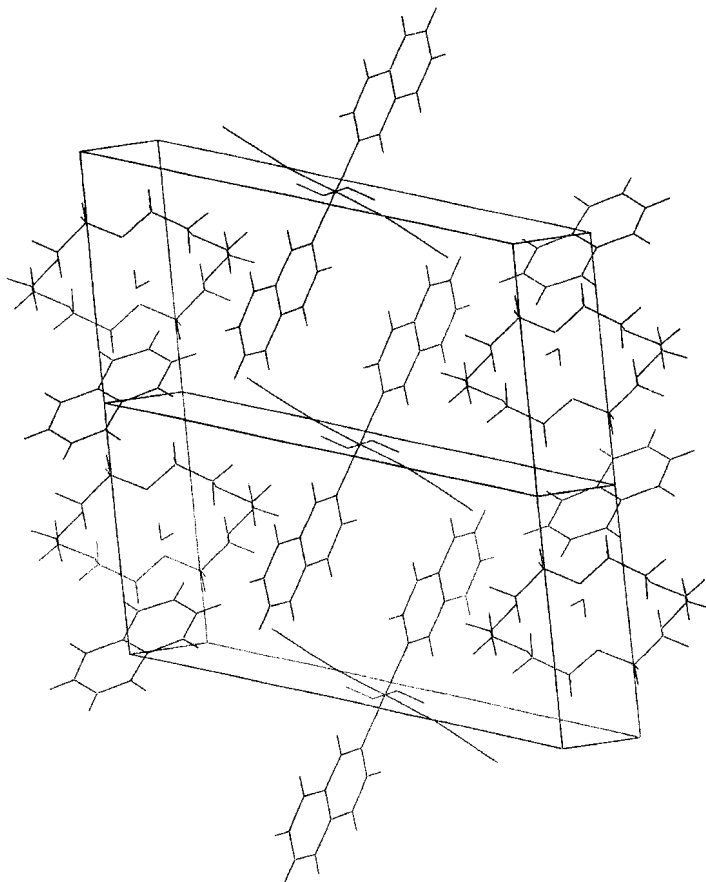


Fig. 2 Crystal packing in **II**. For clarity the disorder in $[\text{C}_9\text{H}_8\text{N}]^+$ and H_2O is not shown.

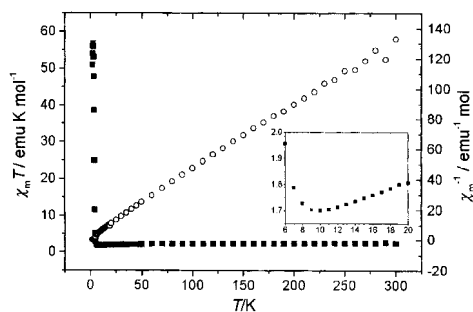


Fig. 3 $\chi_m T$ (filled squares) and χ_m^{-1} (open circles) versus T for **I**. The expanded view (inset) shows the minimum in $\chi_m T$ at 10 K.

magnetisation below T_c , due to the interaction of non-equivalent spins. Above 50 K the temperature dependence of χ_m^{-1} follows the Curie-Weiss law with a Weiss parameter, corresponding to the T -intercept of χ_m^{-1} , of -12.17 K. The negative sign indicates that antiferromagnetic interactions dominate. Ferrimagnetism was further confirmed by measuring the magnetisation as a function of field (Fig. 4) which reveals

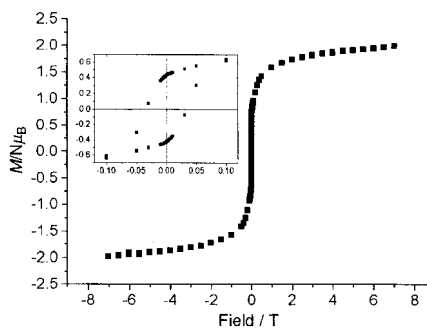


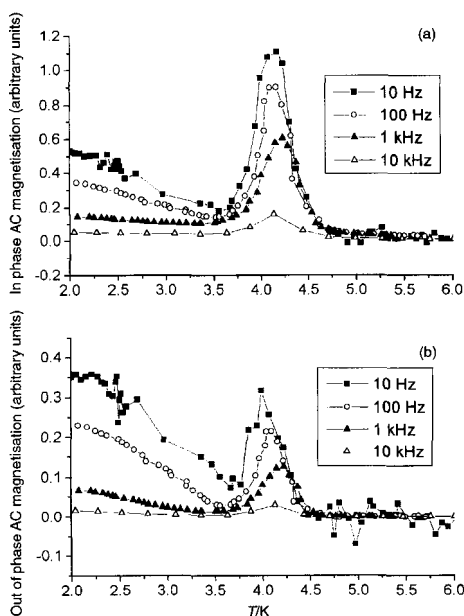
Fig. 4 Magnetisation versus field for **I**. Inset shows expanded view about 0 G.

saturation at $2 N\mu_B$ corresponding to all S_A spins aligned with the field direction and the S_D spins aligned in the opposite direction.

Approximately 90% of the saturation magnetisation is reached within a few hundred Oersted and on cycling the field a modest hysteresis (shown inset Fig. 4) is found (338 Oe). Fig. 5a and 5b show the in phase and out of phase AC magnetisation

Table 2 Magnetic parameters for I, III and IV

	I	III	IV
T_c/K	4.2	8.9	4.5
$\chi_m T$ (at 300 K)/emu K mol ⁻¹	2.26	2.18	4.75
Minimum $\chi_m T$ /emu K mol ⁻¹	1.7	0.99	3.97
Minimum T/K	9.9	16.9	14.8
Coercive field/Oe	338	75	18
Remnant $M/N\mu_B$	0.42	0.74	0.38
M_{sat} at 7 T/ $N\mu_B$	2.0	2.1	4.3

**Fig. 5** (a) In phase and (b) out of phase AC magnetisation versus T for I as a function of frequency at a drive field of 1 Oe.

as a function of frequency. There is no frequency dependence and T_c , taken at the curve peak, is estimated at 4.2 K. Two approaches were used to enhance T_c in I. First the number of unpaired electrons was increased by substituting Fe for Cr and secondly a smaller donor was used to increase the electron density. The corresponding curves for III and IV take the same form as that described above for I and the magnetic parameters for all three salts are summarised in Table 2. For the Fe containing salt, IV, the room temperature value of $\chi_m T$ of 4.747 emu K mol⁻¹ is close to the spin only value of 4.752 emu K mol⁻¹ for isolated $S_A = 5/2$ and $S_B = 1/2$ spins. By comparison magnetic data for the starting materials, $[N(C_4H_9)]_2[Fe(NCS)_4(C_9H_7N)_2]$ and $[C_9H_7N][Cr(NCS)_4(C_9H_7N)_2] \cdot 3H_2O$ show normal $S = 5/2$ and $S = 3/2$ paramagnetism.

The transport properties for each of the charge transfer salts were measured by both four and two probe conductivity methods on compressed pellets using Au wire electrodes attached by Pt paste (Degussa). At room temperature all of the salts gave resistance values too high to be measured, indicating I, III, and IV are extremely good insulators. The magnetic data indicates that the strongest exchange pathway is between donor and acceptor ions since the major interaction is between S_D and S_A , and the transport data suggests that the donor molecules are isolated from each other. Together with consideration of coulomb interactions, the most likely structure of the salts is therefore stacks of alternating donor and acceptor ions. This

structure type is common in other charge transfer molecular magnets such as $[M(C_5(CH_3)_2)_2]^+ [TCNQ]^-$ ($M = Cr, Mn$),¹⁷ $[Fe(C_5(CH_3)_2)_2]^+ [TCNE]^-$ and porphyrin based materials.¹⁹ Since other BEDT-TTF salts with Reinecke type anions, $[Cr(NCS)_4(amine)_2]^-$ with a large range of amines²⁰ do not show long range magnetic order, the properties described here are consistent with exchange mediated by the isoquinoline ligand. It is well known that isoquinoline derivatives can act as a radical stabiliser or radical trap through charge transfer²¹ so it is reasonable to assume the closest anion to cation distances in the donor-acceptor stacks are between the planar donor and planar isoquinoline ligand.

Conclusions

We have described the synthesis of three new charge transfer salts with stoichiometry $[donor][M(NCS)_4(C_9H_7N)_2]$ where $M = Cr$ and Fe for donor = BEDT-TTF and $M = Cr$ for donor = TTF. The salts were grown by standard electrochemical techniques and the configuration of the anion was confirmed from the crystal structure of the isoquinolinium salt. All three salts display bulk ferrimagnetism via antiferromagnetic exchange between the donor radical spin and the acceptor spin on the M ion. Small coercive fields were measured for each of the compounds, the largest of 338 Oe being found when $M = Cr$ and donor = BEDT-TTF. The highest T_c of 8.9 K was found for $M = Cr$ and donor = TTF. A combination of magnetic and transport data implies that the magnetic properties are mediated by π stacking of the donor and isoquinolinium ligand. Further work will concentrate on preparing new examples of this series in an effort to clarify the mechanism of the exchange, to increase T_c and to obtain single crystal structural information.

Acknowledgements

This work was supported by the UK Engineering and Physical Sciences Research Council and the European Commission Training and Mobility of Researchers Programme.

References

- J. M. Williams, J. R. Ferraro, R. J. Thom, K. D. Carlson, U. Gesser, H. H. Wang, A. M. Kini and M.-H. Whangbo, *Organic Superconductors (including Fullerenes) Synthesis, Structure, Properties and Theory*, Prentice-Hall, NY, 1992.
- H. Yamochi, K. Tokutaro, N. Matsukawa, G. Saito, M. Takehiko, M. Kusunoki and K. Sakaguchi, *J. Am. Chem. Soc.*, 1993, **115**, 11319.
- S. S. Turner, P. Day, D. E. Hibbs, K. M. A. Malik, M. B. Hursthouse, S. Teat, E. J. MacLean, L. Martin and S. A. French, *Inorg. Chem.*, 1999, **38**, 3543.
- L. Martin, S. S. Turner and P. Day, *Synth. Met.*, 1999, **102**, 1638; S. S. Turner, L. Martin, P. Day, K. M. A. Malik, S. J. Coles and M. B. Hursthouse, *Chem. Commun.*, 1999, 513.
- E. Coronado, J. R. Galan-Mascaros, C. Gimenez-Saiz and C. J. Gomez-Garcia, *Adv. Mater. Opt. Electron.*, 1998, **8**, 61.
- H. Kobayashi, T. Naito, A. Sato, K. Kawano, A. Kobayashi, H. Tanaka, T. Saito, M. Tokumoto, L. Brossard and P. Cassoux, *Mol. Cryst. Liq. Cryst. Sci. Technol., Sect. A*, 1996, **284**, 61.
- P. LeMagueres, L. Ouahab, N. Conan, D. J. Gomez-Garcia, P. Delhaes, J. Even and M. Bertault, *Solid State Commun.*, 1996, **97**, 27.
- C. J. Kepert, M. Kurmoo, M. R. Truter and P. Day, *J. Chem. Soc., Dalton Trans.*, 1997, 607.
- L. Martin, S. S. Turner, P. Day, F. E. Mabbs and E. J. L. McInnes, *Chem. Commun.*, 1997, 1367.
- M. Kurmoo, A. W. Graham, P. Day, S. J. Coles, M. B. Hursthouse, J. L. Caulfield, J. Singleton, F. L. Pratt, W. Hayes, L. Ducasse and P. Guionneau, *J. Am. Chem. Soc.*, 1995, **117**, 12209; A. W. Graham, M. Kurmoo and P. Day, *J. Chem. Soc., Chem. Commun.*, 1995, 2061.
- E. Coronado, J. R. Galan-Mascaros and C. J. Gomez-Garcia, *Synth. Met.*, 1999, **102**, 1459; M. Clement-Leon, E. Coronado, J. R. Galan-Mascaros, C. J. Gomez-Garcia, C. Rovira and V. N. Lauthkin, *Synth. Met.*, 1999, **103**, 2339.

- 12 P. T. Beurskens, G. Beurskens, W. P. Bosman, R. de Gelder, S. Garcia-Granda, R. O. Gould, R. Israël and J. M. M. Smits, DIRDIF-96, Crystallography Laboratory, University of Nijmegen, The Netherlands, 1996.
- 13 G. M. Sheldrick, SHELXL97, University of Göttingen, Germany, 1997.
- 14 R. H. Blessing, *Acta Crystallogr., Sect. A*, 1995, **51**, 33; R. H. Blessing, *J. Appl. Crystallogr.*, 1997, **30**, 421.
- 15 D. Forster and D. M. L. Goodgame, *J. Chem. Soc.*, 1965, 268.
- 16 O. Kahn, *Molecular Magnetism*, VCH, New York, 1993.
- 17 W. E. Broderick, J. A. Thompson, E. P. Day and B. M. Hoffman, *Science*, 1990, **249**, 401; W. E. Broderick and B. M. Hoffman, *J. Am. Chem. Soc.*, 1991, **113**, 6334.
- 18 J. S. Miller and A. J. Epstein, *J. Am. Chem. Soc.*, 1987, **109**, 3850;
- J. S. Miller, A. J. Epstein and W. M. Reiff, *Chem. Rev.*, 1988, **88**, 201.
- 19 D. K. Rittenberg, K. Sugiura, Y. Sakata, I. A. Guzei, A. L. Rheingold and J. S. Miller, *Chem. Eur. J.*, 1999, **5**, 1874; S. Mikami, K. Sugiura, J. S. Miller and Y. Sakata, *Chem. Lett.*, 1999, 413.
- 20 S. S. Turner, P. Day, S. Coles and M. B. Hursthouse, in preparation.
- 21 P. Tsai, S. Pou, R. Straus and G. M. Rosen, *J. Chem. Soc., Perkin Trans. 2*, 1999, 1759; A. E. A. M. Gaber, *Bull. Pol. Acad. Sci., Chem.*, 1998, **46**, 185; X. Q. Wang and R. Silverman, *J. Org. Chem.*, 1998, **63**, 7357.
- 22 C. K. Johnson, ORTEP, Report ORNL-5138, Oak Ridge National Laboratory, Oak Ridge, TN, 1976.

Paper a910259k

CHAPTER 6

This page intentionally left blank

Molecular Metals and Superconductors

Like ferromagnetism (Chaps. 4 and 5), superconductivity was not a word found in the molecular chemist's lexicon until at least the 1970s. As one of the most bizarre manifestations of collective electronic behaviour (quantum mechanics writ large, you might say), it had of course attracted the attention of solid-state practitioners, but exclusively those who dealt with continuous, i.e. non-molecular, lattices. Indeed, until TTF-TCNQ came along in 1973, even the phrase 'molecular metal' was a contradiction in terms. After all, a molecular crystal was by definition one in which the bonding between the atoms in the molecular unit was much stronger than between the units, scarcely a recipe for coherent inter-molecular electron transport. TTF-TCNQ changed all that, just as the one-dimensional metal Krogmann's Salt (see Chap. 2) had for coordination chemists in the late 1960s.

TTF-TCNQ (TTF=tetrathiafulvalene, first synthesised by Fred Wudl [1] and TCNQ=tetracyano-quinodimethane, first synthesised at DuPont [2]) is a charge transfer complex. The phrase implies combining two molecules, a donor (TTF) and an acceptor (TCNQ), the former having a low ionisation potential and hence transferring electronic charge to the acceptor (a molecule with a high electron affinity). In spite of the chemical formula of this famous compound being simple (just 1:1 donor-to-acceptor) the degree of transfer of electronic charge from one to the other is not so. Considerable experimentation [3] was needed to demonstrate that the charge distribution was roughly $\text{TTF}^{0.59+}\text{TCNQ}^{0.59-}$. It is worth noting that the word 'roughly' was used not because the estimates derived from Raman and NMR spectra were imprecise, but because the degree of charge transfer itself was not a rational fraction; it comes about through balancing the coulomb energy gained by ionising an electron from the donor and transferring it to the acceptor. As the balance is struck at an irrational charge (in the mathematical rather than scientific sense, of course), both TTF and TCNQ sublattices end up with partly filled frontier orbitals, and since these orbitals overlap, the metallic properties arised from partly filled conduction bands.

TTF-TCNQ created a great furore because its conductivity increased up to an exceptionally high level of ~ 60 K, at least in some crystals, almost to the same value as copper at the same temperature [4]. Unfortunately, it then underwent a phase transition that destroyed the conductivity but that did not inhibit 'superconducting fluctuations'. In fact, the world had to wait another seven years for the first

genuine superconductor to emerge, in which the Fermi surface was built from the $p\pi$ -orbitals of aromatic organic molecules. The molecule in question, tetramethyl-tetraselenofulvalene (TMTSF) came from the same chemical family as TTF, but the compound in question, $(\text{TMTSF})_2(\text{PF}_6)$ [5], shortly followed by $(\text{TMTSF})_2(\text{ClO}_4)$ [6], was not a charge transfer complex but a charge transfer salt. This may sound like an arcane distinction, but it is in fact quite fundamental.

Whereas both donors and acceptors had fractional charges in $(\text{TTF})(\text{TCNQ})$, the salts contain small inorganic anions whose charges are perforce integers, although the cation-anion ratio requires the mean donor charge to be +0.5. The donor molecules form plane-to-plane stacks, and again, it is the inter-molecular overlap between $p\pi$ -orbitals that produces the conduction band. The superconducting critical temperature was not high (1.4K), but to paraphrase Dr. Johnson's comment about the dog that walked on its hind legs, what was surprising was not so much that it was done well but the fact that it was done at all.

The advent of the so-called Bechgaard salts placed superconductivity firmly on the agenda of the synthetic chemists of two very different persuasions. On one hand, with the theoretical physicists telling them to reduce the on-site Coulomb repulsion to arrive at wider band metallic conductors, organic chemists set about extending the conjugation in the donor molecules. They also heeded the theorists who said the metallic state would be stabilised against lattice distortions (in particular, the so-called Peierls instability described in Chap. 2) by increasing the lattice dimensionality from one to two. The latter prescription was accomplished by building in more chalcogen atoms to enhance inter-molecular chalcogen-chalcogen contacts. Out of that activity came the molecule *bis*-ethylenedithio-tetrathiafulvalene (BEDT-TTF, sometimes called ET since it resembled TTF but with large ears). Most of our work on molecular metals and superconductors exploited that molecule.

Meanwhile, in another part of the chemical forest, inorganic chemists like myself were busy trying to extend the range and variety of anions forming this kind of charge transfer salt. We immediately came up against one of the marvels and frustrations of supramolecular chemistry, especially where collective electronic properties are concerned, namely small and apparently trivial changes in the chemistry that brought about very large changes in the bulk physical properties. For example, changing $(\text{TMTSF})_2(\text{ClO}_4)$ into $(\text{TMTSF})_2(\text{BF}_4)$, i.e. replacing one tetrahedral anion with another slightly smaller one, removed the superconductivity [7].

Given that the phenomenon of superconductivity was first discovered almost a century ago, and that optimising the properties of superconductors has formed an important part of materials science ever since, it is quite legitimate to ask why people should spend even more effort looking for molecular examples. For a chemist, the answer is clear, because they had never been made before, but in our utilitarian times, that would probably not satisfy a funding agency. A more persuasive answer

might be that all superconductors up to this time had been made and fabricated by high-temperature processes like sintering and arc-melting, whilst molecular solids are crystallised from solution at room temperature, so should they ever enter into production, they would be processed in a completely different, less energy-intensive way. In my opinion, an even better answer would be that molecular chemistry is inherently more flexible than metallurgy. For example, by substituting an ethyl- for a methyl-group, the molecules whose p-orbital overlaps constitute the solids Fermi surface may be modified profoundly. Best of all, there is the chance to build in properties quite incapable of existing in non-molecular lattices, analogous to the soluble magnet mentioned in Chap. 4. Properties never found in continuous-lattice solids are mesomorphism and chirality. When combined with metallic (or still better super-) conductivity, each would introduce completely new physical phenomena. To date, a series of other combinations of properties are not found co-existing previously in the same lattice, some of which are described in the following pages.

Approaching the synthesis of charge transfer salts as an inorganic chemist, it seems self-evident to play with the anions. If the Fermi surface is formed primarily through overlap between $p\pi$ frontier orbitals on the organo-chalcogen radical cations, then changing the size and shape alone of the anions is bound to impact on the cation packing, and hence the band structure through changes in the transfer integrals. A simple example of that was just given in the Bechgaard salts. Another example comes from the BEDT-TTF series where the first superconductor in that family was β'' -(BEDT-TTF)₂I₃ [8], but the Group 11 metals also form linear tri-atomic anions $[\text{MX}_2]^-$ with various halide ions X. We quickly showed that β'' -(BEDT-TTF)₂[AuI₂] (where β denotes one of the polymorphs rife among those salts) was also a superconductor, and that as the molecules were pushed together under hydro static pressure, T_c decreased [9]. This is to be expected if the mechanism for superconductivity is the conventional BCS, since increasing the inter-molecular transfer integrals broadens the conduction band. Using pseudo-halides (e.g. CN⁻, NCS⁻ etc.) in place of the halide X in $[\text{MX}_2]^-$ yielded a large number of iso-structural salts with slightly different unit-cell volumes; thus, we were exerting 'chemical' pressure. In that way, a direct correlation between T_c and electronic bandwidth and carrier effective mass was achieved, although it must be admitted that hydrostatic pressure is easier to control [10].

Better than just permitting small variations in the lattice spacing is the opportunity presented by inorganic chemistry to introduce new kinds of property into the conducting lattice. Principal among these is magnetism. To an inorganic chemist, the word 'magnetism' conjures up transition metals, so we chose copper (II) to begin the simplest example (one unpaired electron). The tetrahalogeno-cuprate(II) anions $[\text{CuX}_4]^{2-}$ are interesting species in their own right because they are usually distorted from regular tetrahedral by the operation of the Jahn-Teller effect, but the chloride and bromide examples behave in quite different ways when formed into charge trans-

fer salts with BEDT-TTF. Both form crystals in which the organic radical cations and inorganic anions are segregated into alternating layers, but in the $[\text{CuCl}_4]^{2-}$ salt, we find a flattened tetrahedral arrangement of halide ions around the copper [11], while in the bromide, the metal coordination is uniquely square planar [12].

The physical properties of the two compounds likewise make a striking contrast. The chloride salt is a metal down to 40 mK without becoming superconducting, but with the added bonus that it contains stoichiometric quantities of paramagnetic Cu^{II} embedded in the lattice [11]. Co-existing conduction-band and localised electrons are extremely rare in solids. On the other hand, the bromide starts out semi-metallic at room temperature, but an abrupt and still mysterious transition renders it insulating at low temperature [13]. At the same time, the charges on the radical cations disproportionate [14], i.e. they go from Class III to Class II in the Robin–Day classification of mixed-valence systems (see Chap. 3); albeit, here, the ‘valences’ (for which read molecular charges) are those of organic and not inorganic building blocks. Throughout, the paramagnetic Cu centres sit unmoved, even though there are at least in the chloride salt signs of local ferromagnetic exchange between pairs of $[\text{CuCl}_4]^{2-}$ that may inhibit superconductivity.

Making direct comparisons between magnetic and non-magnetic charge transfer salts with otherwise identical structures is not straightforward, but since the coordination chemistry of Fe^{III} and Ga^{III} is so similar, the salts $(\text{BEDT-TTF})_2[\text{MCl}_4]$ with $\text{M}=\text{Ga}$ or Fe provide such an opportunity. What we found [15] is a near-complete segregation between the organic and inorganic components of the lattice which (as is normal in this class of compounds) form alternate layers. Subsequently, a more teasing relationship was found in salts with the same anions but the selenium-substituted cation bis-ethylenedithio-tetraselenofulvalene (BETS) [16]. Briefly, the Ga salt is a superconductor but the Fe one becomes abruptly insulating at 10 K, the temperature at which long-range magnetic order sets in. Disentangling the effect of small lattice changes from the effect of the localised magnetic moment of the Fe was to prove a challenging problem, but since it was accomplished by Japanese and French colleagues, I leave it aside from this personal account.

Finding superconductors containing embedded magnetic centres is more than a private preoccupation of the chemists. Forty years ago the eminent Russian theoretical physicist Ginzburg proclaimed in the sweeping manner cultivated by theorists that the two potential ground states, ferromagnetic and superconducting, were mutually exclusive; you could have either separately but not both together. Naturally among synthetic chemists, that set off a search for compounds that might confirm or refute the hypothesis. The reasoning behind Ginzburg’s prediction can be stated quite simply: if superconductivity arises when charge is transported by pairs of electrons (Cooper pairs), instead of by electrons moving individually, a magnetic field, whether applied externally or generated internally as in a ferromagnet, will break the pairs apart. In the 1970s, superconducting sulphides (so-called Chevrel phases)

had been made with lanthanide ions [17], but it is well known that the 4f-shells in the latter are deeply shielded by comparison with the d-shells of transition-metals. Thus, there was a lot of interest when we found the first superconductors containing paramagnetic 3d-ions, in the form of BEDT-TTF charge transfer salts with *tris*-oxalato-metallate anions [18].

The series in question, with the general formula β'' -(BEDT-TTF)₄[AM(C₂O₄)₃].G, where A is a cation like H₃O⁺, NH₄⁺ etc; M is Ti, Cr, Fe, Al, Ga; and G is a guest molecule (usually the solvent from which the salt is crystallised), offer many points of interest to the aficionados of structure-property relations. The metal ion can have a spin of 1/2, 3/2, 5/2 or 0 and changing the guest molecule profoundly influences the superconductivity. Finally, the [M(C₂O₄)₃]³⁻ species is chiral, which raises the possibility, as yet unrealised in any compound, of a chiral superconductor.

To summarise the results very concisely, the magnitude of the magnetic moment on the 3d-ion only has a small effect on the superconducting properties, probably because the anions form layers segregated from the organic cations where the conduction electrons circulate. In contrast, without changing the overall structure much, the guest molecule has a major influence — instead of superconductivity when G=C₆H₅CN or C₆H₅NO₂, the ground state is resistive when G=C₅H₅N and CH₂Cl₂. Finally, the chiral anions lead to polymorphism because the two chiral enantiomers can be arranged in different ways in the racemic lattice. In fact, one polymorph is superconducting and the other is semiconducting! [19]

We continue to seek new combinations of properties through building up organic and inorganic components in more and more elaborate charge transfer salts. Many of them have layer structures in which the two components are segregated to form alternating ABAB... arrangements, with the properties emanating respectively from one or the other. Laying down multilayers by essentially physical means such as electron beam epitaxy, is of course at the heart of the micro-electronics industry, so being able to make multilayers through self-assembly is a highly prized objective. The latest advance is to make more complicated sequences such as ABCBA... On one hand, C can be the same organic donor as in layer A, but with a different packing or [20] it can also be a completely different molecule. The latter type is exemplified by the first molecular charge transfer salt combining metallic conductivity with high mobility of protons [21]. That combination could be interesting for fuel-cells. Clearly, there is no limit to the variety of chemical structures and properties that could be envisaged in these versatile crystals!

References

- [1] F. Wudl, G. M. Smith and E. J. Hufnagel, *J C S Chem Commun* 1453 (1970).
- [2] D. S. Acker, R. J. Harder, W. R. Hertler, W. Mahler, L. R. Melby, R. E. Benson and W. E. Mockel, *J Amer Chem Soc* **82**: 6408 (1960).

- [3] J. S. Chappel, A. N. Bloch, W. A. Bryden, M. Maxfield, T. O. Poehler and D. O. Cowan, *J Amer Chem Soc* **103**: 2442 (1981).
- [4] L. B. Coleman, M. J. Cohen, D. J. Sandman, F. G. Yamagishi, A. F. Garito and A. J. Heeger, *Sol State Commun* **12**: 1125 (1973).
- [5] D. Jerome, A. Mazaud, M. Ribault, and K. Bechgaard, *J Physique* **41**: L95 (1980).
- [6] K. Bechgaard, K. Carneiro, M. Olsen, F. S. Rasmussen and C. S. Jacobson, *Phys Rev Lett* **46**: 852 (1981).
- [7] K. Bechgaard, C. S. Jacobson, K. Mortensen, H. J. Pedersen and N. Thorup, *Sol State Commun* **33**: 1119 (1980).
- [8] E. Yagubskii, I. F. Shchegolev, V. N. Laukhin, P. A. Kononovitch, M. V. Karatsovnik, A. V. Zvarykina and L. I. Buravov, *Pis'ma Zh Eksp Teor Fiz* **39**: 12 (1984).
- [9] D. R. Talham, M. Kurmoo, D. S. Obertelli, I. D. Parker and R. H. Friend, *J Phys C: Sol State Phys* **19**: L383 (1986).
- [10] J. Caulfield, W. Lubczynski, F. L. Pratt, J. Singleton, D. Y. K. Ko, W. Hayes, M. Kurmoo and P. Day, *J Phys C: Cond Matt* **6**: 2911 (1994).
- [11] P. Day, M. Kurmoo, T. Mallah, L. Marsden, R. H. Friend, F. L. Pratt, W. Hayes, D. Chasseau, J. Gaultier, G. Bravic and L. Ducasse, *J Amer Chem Soc* **114**: 10722 (1992); **(Reprint 6.1)**.
- [12] P. Guionneau, G. Bravic, J. Gaultier, D. Chasseau, M. Kurmoo, D. Kanazawa and P. Day, *Acta Cryst C* **50**: 1894 (1994).
- [13] I. R. Marsden, M. L. Allen, R. H. Friend, M. Kurmoo, D. Kanazawa, P. Day, G. Bravic, D. Chasseau, L. Ducasse and W. Hayes, *Phys Rev B* **50**: 2118 (1994); **Reprint 6.2**.
- [14] P. Guionneau, J. Gaultier, D. Chasseau, G. Bravic, Y. Barrans, L. Ducasse, D. Kanazawa, P. Day and M. Kurmoo, *J. Physique I (France)* **6**: 1581 (1996).
- [15] M. Kurmoo, P. Day, P. Guionneau, G. Bravic, D. Chasseau, L. Ducasse, M. L. Allen, I. D. Marsden and R. H. Friend, *Inorg Chem* **35**: 4719 (1996); **Reprint 6.3**.
- [16] H. Kobayashi, H. Tomita, T. Naito, A. Kobayashi, F. Sakai, T. Watanabe and P. Cassoux, *J Amer Chem Soc* **118**: 368 (1996).
- [17] M. Ishikawa and O. Fischer, *Sol State Commun* **23**: 37 (1977).
- [18] M. Kurmoo, A. W. Graham, P. Day, S. J. Coles, M. B. Hursthouse, J. L. Caulfield, J. Singleton, F. L. Pratt, W. Hayes, L. Ducasse and P. Guionneau, *J Amer Chem Soc* **117**: 12209 (1995). **(Reprint 6.4)**
- [19] L. Martin, S. S. Turner, P. Day, P. Guionneau, J. A. K. Howard, D. E. Hibbs, M. E. Light, M. B. Hursthouse, M. Uruichi and K. Yakushi, *Inorg Chem* **40**: 1363 (2001). **(Reprint 6.5)**.
- [20] H. Akutsu, A. Akutsu-Sato, S. S. Turner and P. Day, *Chem Commun* **18** (2004).
- [21] A. Akutsu-Sato, H. Akutsu, S. S. Turner, P. Day, M. R. Probert, J. A. K. Howard, T. Akutagawa, S. Takeda and T. Nakamura, *Angew Chem Int Ed* **44**: 292 (2004). **(Reprint 6.6)**

Structure and Properties of Tris[bis(ethylenedithio)tetrathiafulvalenium]tetrachloro- copper(II) Hydrate, (BEDT-TTF)₃CuCl₄·H₂O: First Evidence for Coexistence of Localized and Conduction Electrons in a Metallic Charge-Transfer Salt

P. Day,^{*†} M. Kurmoo,[†] T. Mallah,[†] I. R. Marsden,[†] R. H. Friend,[‡] F. L. Pratt,[§]
 W. Hayes,[§] D. Chasseau,^{||} J. Gaultier,^{||} G. Bravic,^{||} and L. Ducasse[⊥]

Contribution from The Royal Institution of Great Britain, 21 Albemarle Street, London W1X 4BS, U.K., Cavendish Laboratory, Madingley Road, Cambridge CB3 0HE, U.K., Clarendon Laboratory, Parks Road, Oxford OX1 3PU, U.K., and Laboratoire de Cristallographie et de Physique Cristalline, UA144 CNRS, and Laboratoire de Physico-Chimie Théorique, URA CNRS 503, Université de Bordeaux I, 351 Cours de la Libération, 33405 Talence Cedex, France. Received April 22, 1992

Abstract: The synthesis and physical characterization of a complex of BEDT-TTF [bis(ethylenedithio)tetrathiafulvalenium] with Cu^{II}Cl₄²⁻ are reported. The structure of (BEDT-TTF)₃CuCl₄·H₂O (I) (crystal data: triclinic, space group *P*1, *a* = 16.634 Å, *b* = 16.225 Å, *c* = 8.980 Å, $\alpha = 90.72^\circ$, $\beta = 93.24^\circ$, $\gamma = 96.76^\circ$, *V* = 2402 Å³, *Z* = 2) consists of alternating layers of organic cations and inorganic anions. The organic layers contain three crystallographically independent molecules, each ²/₃+ and two distinct stacks alternating with each other. The anion is dimerized as [CuCl₄·H₂O]₂ with the Cu^{II} in a distorted tetrahedral geometry. I is metallic down to 200 mK with a conductivity anisotropy at 300 K of 7:1 (($\sigma \parallel a-c$):($\sigma \perp a-c$) = 140:20 S cm⁻¹) within the layers and an EPR spectrum characterized by two lines, one from each spin system (conduction and Cu²⁺ localized moments). The *g* value of the Cu resonance ($g_{\parallel} = 2.29$ and $g_{\perp} = 2.05$) decreases at a gradient of -4×10^{-5} K⁻¹ from 4 to 300 K, while that of the conduction electron ($g = 2.03$ – 2.05) is temperature independent. The EPR line width increases by 25% and 90% for the Cu and the conduction electrons, respectively, over the same temperature range. The spin susceptibility derived from the Cu resonance fits to a Curie-Weiss law ($\Theta = 1$ (1) K) or to a Bleaney-Bowers model for a dimer ($J \approx 4$ (1) K), and that of the free carriers shows a Pauli type temperature-independent behavior between 30 and 300 K. Below 30 K, the intensity of the free-carrier resonance falls to 30% of the room-temperature value. From the EPR, there is indication of weak interaction between the two spin systems. From the optical reflectivity data, the width of the conduction band is estimated to be 0.6 eV. A band-structure calculation indicates several zero-transfer integrals, and the Fermi surface has very anisotropic pockets of both electrons and holes, suggesting a semi-metal.

Superconductivity and long-range magnetic ordering are two different cooperatively ordered states whose coexistence in the same material leads to numerous interesting phenomena.¹ The search for coexisting superconductivity and magnetic order has been pursued most vigorously up to now among ternary compounds; 15 classes of such compounds have been discovered, in five of which both superconductivity and long-range magnetic order have been found with certainty, for example, among borides, (RE)T₂B₄ (RE = rare earth; T = Rh, Ir), chalcogenides, (RE)Mo₆X₈ (X = S, Se), silicides, (RE)₂T₃Si₃ (T = Fe, Co), stannides, (RE)T₂Sn₃ (T = Rh, Os), and phosphides, TiRuP. Most recently, high-*T*_c superconductors (for example, ErBa₂Cu₃O_{7-x}, *T*_c ~ 90 K) have been observed to order antiferromagnetically without destroying the superconducting state.² Most of the rare earth ternary compounds have ordered sublattices of magnetic RE ions and show superconductivity combined with long-range antiferromagnetic order. In those that order ferromagnetically, the appearance of long-range order is accompanied by the destruction of superconductivity, at the re-entrant temperature *T*_{c2}.

All the systems mentioned above contain continuous lattices, and the magnetic and conducting sublattices are independent of each other. To date, analogous systems are unknown among low-dimensional molecular conductors. However, the latter show several forms of magnetic order. For example, the organic conductor (TMTSF)₂PF₆ (TMTSF = tetramethyltetraselenafulvalenium) exhibits itinerant magnetism with a spin

density wave (SDW) at 10 K.³ The latter compound is metallic down to 10 K, but below this temperature, an energy gap opens at the Fermi surface due to the SDW. This transition is suppressed by pressure, and at 8 kbar, a superconducting ground state is established. On the other hand, when samples of (TMTSF)₂ClO₄ are slowly cooled at ambient pressure, a superconducting ground state is observed at ca. 1.5 K, while for rapidly cooled samples, a SDW state is observed in the temperature range 1 < *T* < 5.5 K and superconductivity occurs below 1 K. Coexistence of SDW and superconductivity has not been proven.

The TMTSF salts are quite one-dimensional in character. However, in the two-dimensional layered salts of BEDT-TTF, several competing states are also found.³ For example, superconducting, metallic, and semiconducting, as well as Pauli paramagnetic, 1D or 2D antiferromagnetic, SDW, and spin Peierls states have all been observed. Most recently, the metallic salt (BEDT-TTF)₂KHg(SCN)₄, which has an antiferromagnetic ground state below 10 K in low field,⁴ was inferred to have a ferromagnetic character in fields above 22 T.⁵

(1) See for example: (a) *Superconductivity in Magnetic and Exotic Materials*; Matsubara, T., Kotani, A., Eds.; Springer Series in Solid State Sciences; Springer: Berlin, 1984; Vol. 52, pp 1–211. (b) *Superconductivity in Ternary Compounds*; Maple, M. B., Fischer, O., Eds.; Topics in Current Physics; Springer: Berlin, 1982; Vol. 34, pp 1–292. (c) Bulaevskii, L. N.; Buzdin, A. I.; Kulin, M. L.; Panjukov, S. V. *Adv. Phys.* **1985**, *34*, 175–261.

(2) Hor, P. H.; Meng, R. L.; Wang, Y. Q. *Phys. Rev. Lett.* **1987**, *58*, 1891–1894.

(3) Proceedings of the International Conference on Synthetic Metals. *Synth. Met.* **1987**, *19*, 1989, 27–29; **1991**, 41–43.

(4) Sasaki, T.; Toyota, N.; Tokumoto, M.; Kinoshita, N.; Anzai, H. *Solid State Commun.* **1990**, *75*, 93–96, 97–100.

(5) Pratt, F. L.; Doporito, M.; Singleton, J.; Janssen, T. J. B. M.; Perenboom, J. A. A. J.; Kurmoo, M.; Hayes, W.; Day, P. *Physica B* **1992**, *177*, 333–338; *Phys. Rev. B* **1992**, *45*, 13904–13912.

^{*} Royal Institution.

[†] Cavendish Laboratory.

[‡] Clarendon Laboratory.

[§] Laboratoire de Cristallographie et de Physique Cristalline, Université de Bordeaux I.

[⊥] Laboratoire de Physico-Chimie Théorique, Université de Bordeaux I.

*(BEDT-TTF)₃CuCl₄·H₂O**J. Am. Chem. Soc., Vol. 114, No. 27, 1992 10723*

In the present paper, we adopt a novel approach to the study of interactions between free carriers and localized moments. Our aims are to tune the long-range magnetic order and to stabilize a superconducting state in a magnetically ordered molecular lattice.^{6,7} The approach is to develop charge-transfer salts having magnetic moments on the anions.

We chose to investigate BEDT-TTF salts containing CuCl₄²⁻ for two reasons: first, because a ferromagnetic ground state has been found in several Cu(II) salts with layered structures,⁸ as well as the more common antiferromagnetic ones, and, second, because the EPR of Cu d⁹ electrons is easily studied due to the dipole-dipole narrowing effects and the fact that it has one hole in an otherwise filled subshell.⁹ Incorporation of magnetic ions into organic conductors has been successfully achieved in a few cases. For example, in Cu(pc)I, (pc is phthalocyanine), a molecular metal with a one-dimensional array of local moments embedded in a Fermi sea of charge carriers,¹⁰ it has been shown by EPR and NMR that the principal magnetic interactions between Cu²⁺ moments arise from indirect exchange involving the conduction electrons.¹⁰

In this paper, we report the synthesis, the crystal and electronic structures, and the electrical-transport, magnetic, and optical properties of (BEDT-TTF)₃Cu¹¹Cl₄·H₂O (I). In this connection, we also review briefly the structures and properties of known BEDT-TTF salts containing magnetic anions, as well as compare the properties of the titled material with those having the same stoichiometry and approximately the same structure but containing nonmagnetic anions. Preliminary notes of the crystal structure and properties of I have been published.^{6,7}

Experimental Section

Synthesis. BEDT-TTF was obtained by the method of ref 11 and recrystallized twice from chloroform. [(CH₃)₄N]₂CuCl₄ was synthesized by metathesis of equivalent amounts of [(CH₃)₄N]Cl and CuCl₂·6H₂O in absolute ethanol and recrystallized from ethanol just before use. Elemental analyses confirmed the purity of the materials. The charge-transfer salts were obtained by electrocrystallization of BEDT-TTF (50 mg) in either benzonitrile or a mixture of acetonitrile (10%) and dichloromethane (90%) saturated with [(CH₃)₄N]₂CuCl₄. All solvents were distilled before use. A three-compartment cell with platinum electrodes was used. The current was kept constant at 2 μA for at least 10 days. Two types of crystals were obtained: hexagonal plates, I, and multifaceted needles, (BEDT-TTF)₂CuCl₄.

The quality of crystals can vary widely depending on the amount of water present in the electrochemical crystal-growing cell. In addition to the two salts just mentioned, several byproducts can be obtained due to

Table I. Crystal Data for I

formula	C ₃₀ H ₂₆ S ₂₄ OCuCl ₄
<i>a</i> /Å	16.634 (4)
<i>b</i> /Å	16.225 (9)
<i>c</i> /Å	8.980 (3)
α /deg	90.72 (3)
β /deg	93.24 (3)
γ /deg	96.76 (3)
<i>V</i> /Å ³	2402 (1)
<i>Z</i>	2
<i>T</i> /K	295
space group	P1̄
crystal size/mm ³	0.34 × 0.12 × 0.06
λ (Cu K α)/Å	1.54178
μ /cm ⁻¹	122.36
$\theta/2\theta$ scan, θ_{\max} /deg	71.5
scan width/deg	$\Delta\theta = 0.8 + 0.142 \tan \theta$
no. of data collected	9638
no. of unique data	9314
no. of unique data (<i>I</i> > 3 σ (<i>I</i>))	7266
no. of variables	541
<i>R</i>	0.050
<i>R_w</i>	0.053
(Δ/σ) _{max}	0.04

the fact that the CuCl₄²⁻ ion is unstable in the presence of water and reacts to yield eventually Cu(H₂O)₆²⁺ and Cl⁻. The Cu²⁺ will oxidize BEDT-TTF, as we have shown previously,^{12a} to give α' -(BEDT-TTF)₂Cu⁺Cl₂, a Mott-Hubbard semiconductor ($E_g = 0.3$ eV) with a one-dimensional antiferromagnetic chain ($J = 53$ K). In the presence of chloride ions and water molecules, we have demonstrated that three types of crystals,¹¹ (BEDT-TTF)₂Cl₂·2H₂O, (BEDT-TTF)₂Cl₂·4H₂O, and (BEDT-TTF)₂Cl₂·6H₂O, can be obtained. They are all highly conducting at room temperature, with a semimetallic character and a very broad minimum in resistivity at ca. 150 K. The charge stoichiometry of (BEDT-TTF)₂Cl₂·2H₂O and its crystal structure are quite analogous to those of I. The modes of packing of the BEDT-TTF molecules within a layer are almost identical in the two materials. Although the volumes differ by 4% (2300 Å³ for the chloride and 2402 Å³ for I), it is conceivable that a solid solution of the chloride and I might occur. This may account for the difference in conductivity behavior of different crystals (see below), though it will not affect EPR measurements greatly as this technique probes localized Cu²⁺ ions and the conduction electrons irrespective of the small lattice defects that may accompany slight doping.

X-ray Diffraction. A crystal of I (Table I) of dimensions 0.34 × 0.12 × 0.06 mm³ was mounted on a Siemens AED four-circle diffractometer using Ni-filtered Cu K α radiation ($\lambda = 1.54178$ Å). Intensities of 9314 reflections were collected using the $\theta/2\theta$ scan technique ($\theta_{\max} = 71.5^\circ$). Refined cell parameters were obtained from the setting angles of 11 reflections within $22 < \theta < 60^\circ$. Three intensity standard reflections (18, -1, 0; 5, -6, 0; 12, -7, 9) were monitored every 50 data collected. No significant variation was observed. The data were corrected for absorption, using a Gaussian integration procedure,¹⁴ and for Lorentz and polarization effects. A total of 7266 reflections with $I > 3\sigma(I_0)$ were considered as observed. The structure was solved by direct methods using SIR88.¹⁵ The positions of the heavy atoms (Cu, Cl, and S) were found, and the remainder were located by Fourier methods. The H atoms on the water molecules were observed from the difference maps, and those of the BEDT-TTF molecules were placed at idealized positions with fixed isotropic thermal parameters. Scattering factors, including terms for

(6) (a) Gudenko, A. V.; Ginodman, V. B.; Korotkov, V. E.; Koshelap, A. V.; Kushch, N. D.; Laukhin, V. N.; Rozenberg, L. P.; Khomenko, A. G.; Shibaeva, R. P.; Yagubskii, E. B. *The Physics and Chemistry of Organic Superconductors*; Saito, G., Kagoshima, S., Eds.; Springer Proceedings in Physics; Springer: Berlin, 1990; Vol. 51, pp 365-368. (b) After submission of the present paper for publication, a more extended report of the crystal structure of I appeared: Shibaeva, R. P.; Korotkov, V. E.; Rozenberg, L. P. *Sov. Phys.—Crystallogr. (Engl. Transl.)* **1991**, *36*, 820-824. The latter is in overall agreement with the structure reported here, though based on a smaller data set (5012 unique reflections with $I \geq 3\sigma(I)$) and a larger *R* factor (0.065).

(7) (a) Kurmoo, M.; Mallah, T.; Day, P.; Marsden, I.; Allan, M.; Friend, R. H.; Pratt, F. L.; Hayes, W.; Chasseau, D.; Gaultier, J.; Bravic, G. *The Physics and Chemistry of Organic Superconductors*; Saito, G., Kagoshima, S., Eds.; Springer Proceedings in Physics; Springer: Berlin, 1990; Vol. 51, pp 290-293. (b) Mallah, T.; Hollis, C.; Bott, S.; Day, P.; Kurmoo, M. *Synth. Met.* **1988**, *27*, A381-386. (c) Mallah, T.; Hollis, C.; Bott, S.; Kurmoo, M.; Day, P. *J. Chem. Soc., Dalton Trans.* **1990**, 859-865.

(8) See e.g.: Carlin, R. L. *Magnetochemistry*; Springer Verlag: Berlin, 1986; p 143.

(9) Abragam, A.; Bleaney, B. *Electron Paramagnetic Resonance of Transition Ions*; Clarendon Press: Oxford, U.K., 1970.

(10) (a) Ogawa, M. Y.; Martisen, J.; Palmer, S. M.; Stanton, J. L.; Tanaka, J.; Greene, R. L.; Hoffman, B. M.; Ibers, J. A. *J. Am. Chem. Soc.* **1987**, *109*, 1115-1121. (b) Ogawa, M. Y.; Hoffman, B. M.; Lee, S.; Yudkowsky, M.; Halperin, W. P. *Phys. Rev. Lett.* **1986**, *57*, 1177-1180. (c) Ogawa, M. Y.; Palmer, S. M.; Liou, K.; Quirion, G.; Thompson, J. A.; Poirier, M.; Hoffman, B. M. *Phys. Rev. B* **1989**, *39*, 10682-10692.

(11) (a) Larsen, J.; Lenoir, C. *Synthesis* **1988**, *2*, 134. (b) Wang, H. H.; Reed, P. E.; Williams, J. M. *Synth. Met.* **1986**, *14*, 165-172. (c) Geiser, W.; Wang, H. H.; Hammond, C. E.; Firestone, M. A.; Beno, M. A.; Carlson, K. D.; Numez, L.; Williams, J. M. *Acta Crystallogr.* **1987**, *C43*, 656.

(12) (a) Kurmoo, M.; Talham, D. R.; Day, P.; Howard, J. A. K.; Stringer, A. M.; Obertelli, D. S.; Friend, R. H. *Synth. Met.* **1988**, *22*, 415-418. (b) Bu, X.; Coppens, B.; Lederle, B.; Naughton, M. J. *Acta Crystallogr.* **1991**, *C47*, 2082-2085.

(13) (a) Kurmoo, M.; Rosseinsky, M. J.; Day, P.; Auban, P.; Kang, W.; Jerome, D.; Batail, P. *Synth. Met.* **1988**, *27*, A425-431. (b) Rosseinsky, M. J.; Kurmoo, M.; Talham, D. R.; Day, P.; Chasseau, D.; Watkin, D. J. *Chem. Soc., Chem. Commun.* **1988**, 88-90. (c) Mori, T.; Inokuchi, H. *Chem. Lett.* **1987**, 1657-1660. (d) Mori, T.; Inokuchi, H. *Solid State Commun.* **1987**, *64*, 335-337. (e) Obertelli, S. D.; Marsden, I. R.; Friend, R. H.; Kurmoo, M.; Rosseinsky, M. J.; Day, P.; Pratt, F. L.; Hayes, W. *The Physics and Chemistry of Organic Superconductors*; Saito, G., Kagoshima, S., Eds.; Springer Proceedings in Physics; Springer: Berlin, 1990; Vol. 51, pp 181-184. (f) Bravic, G.; Chasseau, D.; Gaultier, J.; Rosseinsky, M. J.; Kurmoo, M.; Day, P.; Filhol, A. *Synth. Met.* **1991**, *41-43*, 2035-2038.

(14) Coppens, P.; Leiserowitz, L.; Rabinovitch, D. *Acta Crystallogr.* **1965**, *18*, 1035-1038.

(15) Burla, M. C.; Camalli, M.; Cascarano, G.; Giacovazzo, C.; Polidori, G.; Spagna, R.; Viterbo, D. *J. Appl. Crystallogr.* **1989**, *22*, 389-393.

10724 *J. Am. Chem. Soc.*, Vol. 114, No. 27, 1992

Day et al.

Table II. Modes of Stacking Intermolecular S-S Distances (<3.9 Å) and Intermolecular Transfer Integrals (t) in **1**^a

mode	molecules	atoms	S-S/Å	t /meV
A Stacks				
A1	I ↔ I + a + b	S(12)-S(22)	3.76	2.47
A2	I ↔ I + a + b + c	shortest S-S	3.83	0
B Stacks				
B1	II ↔ III	S(42)-S(51)	3.88	28.9
		S(44)-S(61)	3.84	
		S(44)-S(62)	3.81	
B2	II ↔ III + c	S(31)-S(52)	3.78	28.9
		S(41)-S(62)	3.78	
AB1	I ↔ II	S(13)-S(32)	3.40	-36.8
		S(13)-S(34)	3.34	
		S(21)-S(44)	3.53	
		S(23)-S(44)	3.42	
AB2	I ↔ II	S(12)-S(32)	3.78	98.7
		S(14)-S(42)	3.72	
		S(22)-S(34)	3.80	
		S(24)-S(34)	3.75	
AB3	I ↔ III	S(14)-S(62)	3.60	-32.9
		S(14)-S(64)	3.55	
		S(22)-S(54)	3.41	
		S(24)-S(54)	3.38	
AB4	I ↔ III	S(11)-S(54)	3.70	100.5
		S(23)-S(62)	3.76	
		S(23)-S(64)	3.61	
BB1	II ↔ III	S(33)-S(61)	3.44	-42.4
		S(41)-S(53)	3.32	
		S(43)-S(53)	3.42	
BB2	II ↔ II	S(31)-S(51)	3.78	64.2
		S(33)-S(43)	3.71	
BB3	III ↔ III	S(53)-S(61)	3.70	98.7

^a Labeling of stacks and molecules is shown in Figure 3.

anomalous dispersion, were taken from ref 16. All non-H atoms were refined anisotropically using block-diagonal least-squares refinement based on F_o with weights of the form

$$\omega = \omega_o [1 + \omega_o (aF_o)^b]^{-1} \quad \omega_o = [\sigma(F_o)^2 / 2|F_o|]^{-2}$$

The values of a and b were adjusted to 0.03 and 1.8, respectively, to obtain a flat variance distribution with F_o . Convergence to $R = 0.050$ ($R_w = 0.053$) was obtained using 541 variable parameters. A difference Fourier map calculated after final refinement was essentially featureless with maximum electron densities of $\pm 0.3 \text{ e}\text{\AA}^{-3}$. Final values are $S = 1.15$ and $(\Delta/\sigma)_{\text{max}} = 0.04$.

Charge-Transport Measurements. Temperature dependence of conductivity and thermopower over the range 2–350 K was measured by use of an Oxford Instruments CF200 continuous-flow cryostat. Conductivity measurements were performed on single crystals by both ac and dc methods. Contact to the crystals was made by gold wires attached to pre-evaporated gold pads with silver paint (gold paint for thermopower measurements) or directly to the crystal surface with platinum paint, in either the four-in-a-line or the Montgomery configuration. Pressure dependence of the conductivity was measured using a hydrostatic method employing a mixture of pentane and isopentane as described earlier.¹⁷

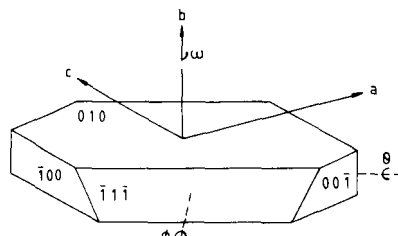
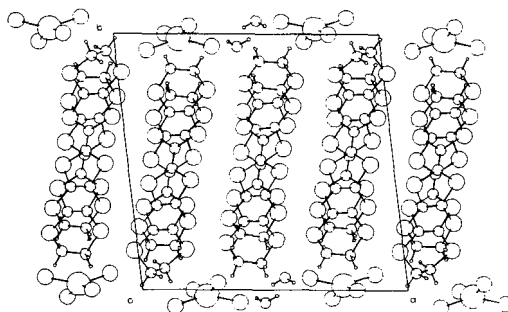
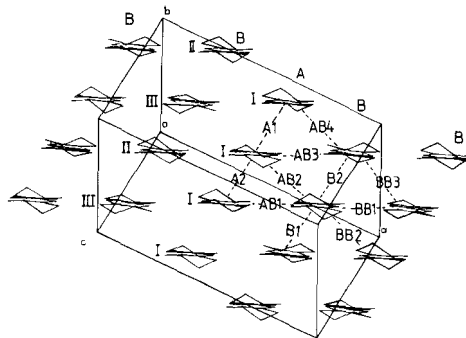
Electron Paramagnetic Resonance Measurements. Variable-temperature EPR spectra of single crystals were recorded using a Varian E9 X-band reflection spectrometer with a rectangular TE₁₀₂ microwave cavity and an Oxford Instruments CF200 cryostat and temperature controller. Angular dependence of the EPR spectra was measured by use of a homemade goniometer. The single crystals were mounted with silicone grease on a Spectrosil quartz rod, which had been previously checked for magnetic impurities. Data were recorded both on an analog chart recorder and in digitized form for further analyses. The field was measured by a Hall-effect probe and calibrated using a diphenylpicrylhydrazyl (DPPH, $g = 2.0037$) marker. To take account of the Dysonian line shape,^{18,19} each spectrum was fitted to the theoretical model for a flat-plate geometry sample. Several crystals were employed to check for sample dependence (and for other crystal phases). No variation was observed among different samples.

(16) *International Tables for X-ray Crystallography*; Kynoch Press: Birmingham, U.K., 1974; Vol. IV.

(17) Parker, I. D. Ph.D. Thesis, Cambridge University, 1988.

(18) Dyson, F. J. *J. Phys. Rev.* **1955**, *98*, 349–359.

(19) Feher, G.; Kip, A. F. *J. Phys. Rev.* **1955**, *98*, 337–348.

**Figure 1.** Crystal morphology of **1**, showing the labeling of the faces and the crystal orientation in the EPR rotation experiments.**Figure 2.** View of the unit cell of **1** along c .**Figure 3.** View of the 2D layer along the C=C bonds of the BEDT-TTF molecules in **1**, with the labeling of the transfer integrals employed in the band-structure calculation.

Optical Reflectivity Measurements. Two spectrometers were employed to record the reflectance spectra of the single crystals: a Perkin-Elmer 1710 (400–4300 cm^{-1}) and a Perkin-Elmer Lambda 9 (3000–50000 cm^{-1}). The incident beam was focused on the samples or the reference gold or aluminum mirror. Spectra were obtained for two crystals. Both KRS5 and calcite polarizers were employed. All measurements were performed at room temperature.

Results

Crystal Structure of (BEDT-TTF)₂CuCl₄·H₂O (1**).** The atomic positional and thermal parameters arising from the structure determination of (BEDT-TTF)₂CuCl₄·H₂O (**1**) are given in Table A, and the bond lengths and angles, in Table B of the supplementary material. The intermolecular S-S contacts less than 3.9 Å are given in Table II.

The crystal belongs to the triclinic system $P\bar{1}$, with $a = 16.634 \text{ \AA}$, $b = 16.225 \text{ \AA}$, $c = 8.980 \text{ \AA}$, $\alpha = 90.72^\circ$, $\beta = 93.24^\circ$, $\gamma = 96.76^\circ$, $V = 2402 \text{ \AA}^3$, and $Z = 2$. The crystal morphology and labeling of the crystal faces are shown in Figure 1, and the labeling scheme of the atoms is shown in Figure A of the supplementary

$(\text{BEDT-TTF})_3\text{CuCl}_4\cdot\text{H}_2\text{O}$

material. The crystal structure consists of stacks of the organic donor BEDT-TTF parallel to the *c*-axis, with short interstack S-S contacts leading to the formation of layers in the *ac*-plane (Figure 2). These layers are interleaved by the inorganic anions and the water of crystallization. There are three crystallographically independent BEDT-TTF molecules (labeled I, II, and III in Figure 3) and two different stacks (labeled A and B). Stack A contains only BEDT-TTF of type I, and stack B has an alternate arrangement of II and III. Within the *ac*-layer, the stacks form an ABBABBA array (Figure 3). The anions lie in planes parallel to the layers of the donor, within which pairs of CuCl_4 anions are connected by hydrogen bonds through the two water molecules to form discrete units.

Since Cu can occur in any of three oxidation states and in principle any combination of these might exist within the same crystal, it is important to establish the exact oxidation state of the Cu atom as this determines the band filling of the conducting layers, and hence the shape of the Fermi surface and the transport properties. As the first step, we can gain some insight into the mean Cu oxidation state from the bond lengths of BEDT-TTF. Within this series of charge-transfer salts, there is an established correlation between the bond lengths and the formal charge on the BEDT-TTF molecules. First, it is reasonable to assume that the close similarity between the bond lengths of the central C=C bond of the three independent BEDT-TTF molecules in I indicates that they all carry the same charge. The average value of 1.363 (5) Å lies in the range of $(\text{BEDT-TTF})^{1/2+}$ (1.35 Å,^{12a} 1.361 Å²⁰) and $(\text{BEDT-TTF})^{2/3+}$ (1.38 Å,^{13b} 1.37 Å²¹).

If the Cu atoms are divalent, then the latter is expected. For the former, the oxidation state of the Cu is required to be 2.5+, i.e. a mixed-valent material. Since the coordination geometries around all the Cu atoms in I are identical, such mixed valency would have to be class III type in the Robin-Day scheme.²² Mixed valency of class II type has been invoked for $(\text{BEDT-TTF})\text{CuCl}_2$,^{23a,b} and of class III type for $(\text{BEDT-TTF})_3\text{CuBr}_3$,^{23c-e} In both cases, the oxidation states of the Cu are 1+ and 2+; Cu^{III} halides are not known, apart from fluorides.²⁴

The CuCl_4 moieties lie with the pseudo-4-fold axes perpendicular to the plane of the organic layers (Figure 2). The Cu-Cl bond lengths within the molecular complexes average 2.25 Å with a Cl-Cu-Cl angle of 150°. This coordination geometry is the most common for Cu^{II} halides, which are Jahn-Teller distorted. The Cu-Cl bond length is consistent with Cu^{II} distances; e.g., among Cu^{II} chlorides one finds for $\text{Cu}^{\text{II}}\text{Cl}_2\cdot 2\text{H}_2\text{O}$ 2.290 Å,²⁵ for $[(\text{C}_6\text{H}_5)_2\text{NH}_2]_2\text{CuCl}_4$ 2.254 Å,²⁶ and for $(\text{R}_n\text{H}_{4-n})\text{N}]_2\text{CuCl}_4$ 2.252 Å,²⁷ while for Cu^{I} chlorides one finds for α' - $(\text{BEDT-TTF})_2\text{Cu}^{\text{I}}\text{Cl}_2$ 2.086 Å,^{12a} for β' - $(\text{BEDT-TTF})_2\text{Cu}^{\text{I}}\text{Cl}_2$ 2.098 Å,^{12b} and for $[(\text{C}_6\text{H}_5)_4\text{N}]\text{Cu}^{\text{I}}\text{Cl}_2$ 2.107 Å.²⁸ Thus, the C=C and Cu^{II} -Cl bond lengths, as well as the geometry of the anion, strongly suggest that the BEDT-TTF molecules are all $2/3+$. The two water molecules serve to bridge two CuCl_4 groups into a dimeric unit. The H—Cl

J. Am. Chem. Soc., Vol. 114, No. 27, 1992 10725

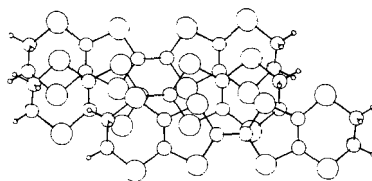


Figure 4. Mode of overlap of the BEDT-TTF molecules in I.

distances are 2.34 and 2.63 Å. The distance between the two Cu atoms ($\text{Cu1}\cdots\text{Cu2}$) of a pair in the unit cell is 8.761 (9) Å, and the nearest neighbor distances to those of adjacent unit cells are 8.98 (9) Å for $\text{Cu1}\cdots(\text{Cu1} + c)$, 8.576 (1) Å for $\text{Cu2}\cdots(\text{Cu1} + a)$, and 10.180 (1) Å for $\text{Cu2}\cdots(\text{Cu1} + a + c)$.

The bond lengths and angles of the three independent BEDT-TTF molecules are almost identical (see Table B of the supplementary material), except for the disorder of one of the $-\text{CH}_2\text{CH}_2-$ groups on molecule III. The thermal parameters of the latter carbon atoms are twice those of the others. The ethylene groups of the molecules I and II are all eclipsed. The two different modes of overlap of the BEDT-TTF molecules are the same in each of the two stacks (Figure 4). In addition, the molecules in both stacks form dimers, the mean interplanar distances defined by the four inner sulfur atoms in stack A being 3.58 and 3.74 Å and in stack B, 3.66 and 3.85 Å. Although at first sight these spacings appear to be quite different in the two stacks, in fact they are not because the mean planes defining the molecules are parallel in stack A but not in stack B; thus, the dihedral angle is 0° in stack A but 1.75° in stack B.

Band Structure of $(\text{BEDT-TTF})_3\text{CuCl}_4\cdot\text{H}_2\text{O}$ (I). In principle, estimation of the intermolecular transfer integrals allows one to calculate the electronic band structure. However, the choice of approximation to be used in calculating the band structures of organic conductors is not straightforward. The most widely used method in recent years employs the tight-binding approximation in the context of a semiempirical extended Huckel theory (EHT).²⁹⁻³¹ Beyond this simple approach, only two attempts have been made to use the self-consistent-field ab-initio method.³² However, the characteristics of the Fermi surface obtained by the EHT method generally agree well with the ones deduced experimentally from the Shubnikov-de Haas and de Haas-van Alphen oscillations in some representative salts of the β and κ phases of the BEDT-TTF salts.³³ For these reasons, the EHT approach has been retained in the calculation of the transfer integrals of I.

Within the EHT approach, in the metallic organic charge-transfer salts, the bands near the Fermi level are mainly built from the HOMO of the organic moiety.^{30c} As the donor is nearly planar, the HOMO is of π -character, the molecular orbital being formed from the p_z atomic orbitals of the carbon and chalcogenide atoms. The tight-binding approximation can be used because the transfer integrals decrease very quickly with increasing intermolecular distance, so the gross features of the band structure of the charge-transfer salts may be accounted for by determining

(20) Kurmoo, M.; Talham, D. R.; Day, P.; Parker, I. D.; Friend, R. H.; Stringer, A. M.; Howard, J. A. K. *Solid State Commun.* **1987**, *61*, 459-464.

(21) Kobayashi, H.; Kato, R.; Mori, T.; Kobayashi, A.; Sasaki, Y.; Saito, G.; Enoki, T.; Inokuchi, H. *Chem. Lett.* **1984**, 179-182.

(22) Robin, M. B.; Day, P. *Adv. Inorg. Chem. Radiochem.* **1967**, *10*, 248-403.

(23) (a) Tanaka, M.; Kawamoto, A.; Tanaka, J.; Sano, M.; Enoki, T.; Inokuchi, H. *Bull. Chem. Soc. Jpn.* **1987**, *60*, 2531-2534. (b) Kawamoto, A.; Tanaka, J.; Tanaka, M. *Acta Crystallogr.* **1987**, *C43*, 205-207. (c) Kurmoo, M.; Kanazawa, D.; Day, P. In *Mixed-Valency Systems: Application to Chemistry, Physics and Biology*; Prassides, K., Ed.; NATO ARW Series, C343; Kluwer: 1991; pp 419-424. (d) Mori, T.; Sakai, T.; Saito, G.; Inokuchi, H. *Chem. Lett.* **1987**, 927-930. (e) Kurmoo, M.; Kanazawa, D.; Day, P. *Synth. Met.* **1991**, *41-43*, 2123-2126.

(24) Wells, A. F. *Structural Inorganic Chemistry*, 4th ed.; Oxford University Press: Oxford, U.K., 1975; p 877.

(25) Engberg, A. *Acta Chem. Scand.* **1970**, *24*, 3510-3526.

(26) (a) Simonsen, S. H.; Harlow, R. L. *Am. Crystallogr. Assoc. Abstr. Ser.* **2** **1977**, 5, HN5. (b) Halvorson, K. E.; Patterson, C.; Willett, R. D. *Acta Crystallogr.* **1990**, *B46*, 508-519 and references therein.

(27) (a) Clay, R.; Murray-Rust, J.; Murray-Rust, P. *Acta Crystallogr.* **1975**, *B31*, 289-290. (b) Smith, D. W. *Coord. Chem. Rev.* **1976**, *21*, 93-158.

(28) Apslund, M.; Jagner, S.; Nilsson, M. *Acta Chem. Scand.* **1983**, *A37*, 57-62.

(29) Hoffmann, R. *J. Chem. Phys.* **1963**, *39*, 1397-1412.

(30) (a) Whangbo, M.-H.; Walsh, W. M.; Haddon, R. C.; Wudl, F. *Solid State Commun.* **1982**, *43*, 637-639. (b) Mori, T. Ph.D. Thesis, Tokyo University, 1985. (c) Grant, P. M. *J. Phys. Colloq.* **1983**, *44* (C3), 847-857.

(31) Ducasse, L.; Abderrabba, M.; Hoarau, J.; Pesquer, M.; Gallois, B.; Gaultier, J. *J. Phys. C: Solid State Phys.* **1986**, *19*, 3805-3820.

(32) (a) Kasowski, R. V.; Whangbo, M.-H. *Inorg. Chem.* **1990**, *29*, 360-362. (b) Kübler, J.; Weger, M.; Sommers, C. B. *Solid State Commun.* **1987**, *62*, 801-805.

(33) (a) Oshima, K.; Mori, T.; Inokuchi, H.; Urayama, H.; Yamochi, H.; Saito, G. *Phys. Rev.* **1988**, *B38*, 938-941. (b) Pratt, F. L.; Singleton, J.; Kurmoo, M.; Spermon, S. J. R. M.; Hayes, W.; Day, P. *The Physics and Chemistry of Organic Superconductors*; Saito, G., Kagoshima, S., Eds.; Springer Proceedings in Physics; Springer: Berlin, **1990**; Vol. 51, pp 200-203. (c) Kang, W.; Montambaux, G.; Cooper, J. R.; Jerome, R.; Lenoir, C. *Phys. Rev. Lett.* **1989**, *62*, 2559-2562. (d) Heidmann, C.-P.; Müller, H.; Biberacher, W.; Neumaier, K.; Probst, Ch.; Andres, K.; Jansen, A. G. M.; Joss, W. *Synth. Met.* **1991**, *41-43*, 2029-2032.

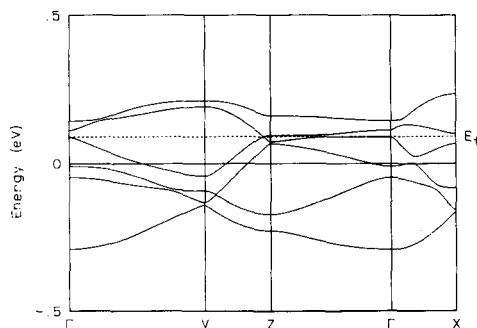


Figure 5. Calculated band structure of I.

the transfer integrals t between the HOMO of pairs of neighboring molecules evaluated using the dimer-splitting approximation³¹

$$t = \langle \text{HOMO}_1 | \mathcal{H} | \text{HOMO}_2 \rangle$$

where \mathcal{H} is the EHT effective Hamiltonian. The parameters used in the present work were set equal to those used in calculations on the Bechgaard salts using the same approximations. The transfer integrals are labeled in Figure 3, and the values are included in Table II.

The largest overlaps are found along the a direction (AB2, AB4, BB3 ~ 100 meV); they are negative for the a - c direction (AB1, AB3, BB1) (see Figure 3), which corresponds to the side-by-side arrangement of the dimers, with absolute values that represent between 30 and 40% of t_a . In contrast, they are small (20% of t_a) or zero in the stack along the c direction. These results may be compared to the overlap integrals calculated by Mori^{13d} for (BEDT-TTF)₃Cl₂·2H₂O, a material which exhibits the same charge stoichiometry and packing motifs. In the latter, the ratio of the negative to the positive overlaps is increased to 67%, and there are no zero interactions along the stacks. It is possible that the different ratios of negative to positive overlaps are model dependent. However, the intrastack transfer integrals should be more closely related to the structures: in particular, the three translationally inequivalent molecules in each unit cell belong to the same stack in the chloride salt but to neighboring stacks in the present case.

The calculated band structure of I is shown in Figure 5. The Fermi energy ($E_F = 90$ meV) is determined by assuming a $2/3+$ average charge per molecule, as discussed above. The four lower bands are almost completely filled so that the Fermi surface comprises very small pockets of electrons and holes. The results predict that I should be a semi-metal, but because of the approximations involved in the calculation, slight changes in the transfer integrals could lead either to a more conducting metal or to a semiconductor. It should be noted that the bands close to the Fermi level along the Γ -Z direction are extremely flat, so that minor modification of the structure and/or the stoichiometry would reinforce the semimetallic character.

Electrical-Transport Properties. The room-temperature conductivity of (BEDT-TTF)₃CuCl₄·H₂O shows an anisotropy of 7:1 within the layer; that is, $\sigma_{RT} \parallel a$ - c is 140 (20) S cm⁻¹ and $\sigma_{RT} \perp a$ - c is 20 (2) S cm⁻¹, with only minor variation between samples. Some crystals show metallic conductivity down to very low temperatures (200 mK in one case), while some show a minimum in resistivity below 50 K. All the crystals studied show a broad maximum in resistance above 200 K (Figure 6a). The ratio of the maximum resistance to that at room temperature is at most 2, and the resistance of the purely metallic crystals at 4 K to that at room temperature is a maximum of 100. Pressure measurements of the resistance up to 12 kbar were possible down to 2 K; in those temperature and pressure regions, no superconductivity was observed. Our results confirm those of Shibaeva et al.⁶

The thermopower of (BEDT-TTF)₃CuCl₄·H₂O along the a - c direction is shown in Figure 6b. It increases to a maximum of

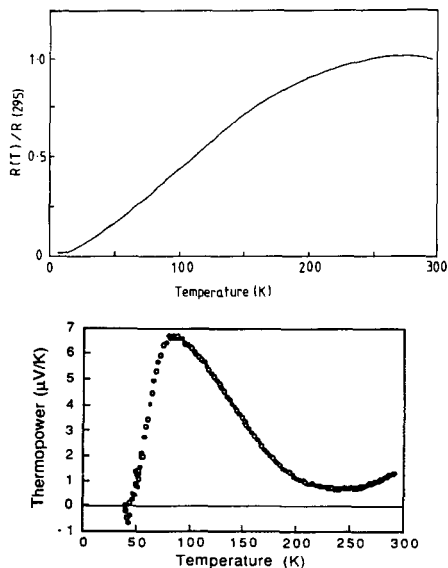


Figure 6. (a, Top) Temperature dependence of the resistivity of I at 3 kbar. (b, Bottom) Thermopower versus temperature for I.

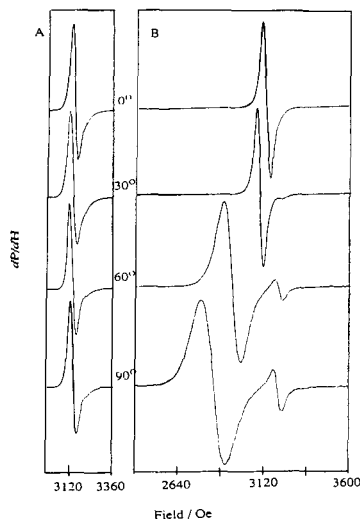


Figure 7. EPR spectra of I at 35 K showing the orientation dependence of the line shape and the overlap of the conduction and the Cu electron resonances: (A) ω rotation about b^* ; (B) θ rotation about a - c .

7 μ V/K at ~ 80 K and drops to ~ 1 μ V/K between 200 and 300 K. The small value of the thermopower is consistent with the metallic behavior. The temperature variation is probably the result of competition between electrons and holes as majority charge carriers.

Electron Paramagnetic Properties. The EPR spectra of (BEDT-TTF)₃CuCl₄·H₂O are characterized by two Lorentzian signals at $g \sim 2$ (Figure 7). The g value and line shape and width of the strong line depend on the orientation of the crystal with respect to the static magnetic field (H_0) and the microwave oscillating field (H_1), and for the weak signal, the dependence of these parameters can only be measured for a limited angular region

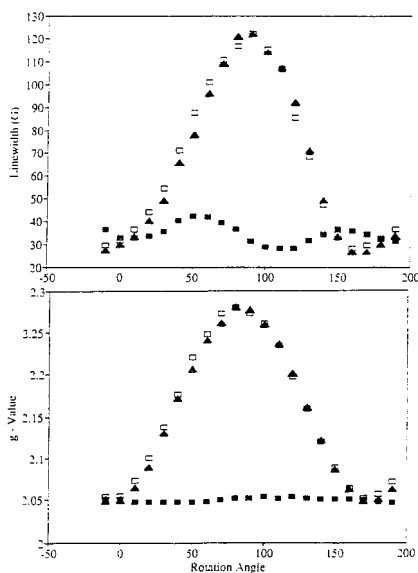
(BEDT-TTF)₂CuCl₄·H₂O

Figure 8. Angular dependence of the line width and *g* value of the Cu resonance of I at 35 K: triangle, θ rotation; empty square, ϕ rotation; filled square, ω rotation.

due to the strong overlap of the two signals. However, it is clear that the *g* value of the weak signal is less sensitive to the orientation of the crystal. The dependence of the EPR spectra on microwave power was measured in the range 0.1–100 mW at a modulation frequency of 100 kHz in order to check for saturation effects. The intensities of the lines were found to be linear in the square of the power at both 300 and 35 K, indicating no saturation effects. The line shape, that is, the asymmetry *A/B* (the ratio of the positive to the negative part of the first derivative of the power with respect to the field) of the Dysonian line,¹⁸ was found to be independent of the microwave power. This validates the application of Feher–Kip procedure for the line shape analysis for a flat-plate geometry sample.¹⁹ The following experiments were performed: (i) the angular dependence of the line width, *g* value, spin susceptibility, and microwave conductivity at room temperature and at 35 K, for the crystal orientation shown in Figure 1; (ii) temperature dependence of the above observables for four different orientations.

At room temperature, the lines are so wide that the two resonances cannot be separated, but at 35 K, they are sufficiently narrow to permit independent fitting of each. The *g* values and line widths are shown in Figure 8 and are compared with those of the mixed-valence (BEDT-TTF)₆[Cu^{II}Cl₂Br₂]₆[Cu^IBr₂] and (BEDT-TTF)₆[Cu^{II}Br₄][Cu^IBr₂] salts (Table III). The *g* value of the stronger line varies from 2.05 to 2.29 when the crystal is rotated about the pseudo-4-fold axis of the CuCl₄ ion with the static field perpendicular to this axis, while it remains constant at 2.05 for rotation along the 4-fold axis. These values are within the range for isolated Jahn-Teller distorted CuCl₄²⁻ ions in the solid state.^{27b} If we assume that the anions show axial symmetry, the calculated molecular *g* values are $g_{\parallel} = 2.28$ and $g_{\perp} = 2.05$ by fitting the observed *g* values to

$$g_{\text{obs}}^2 = g_{\parallel}^2 \cos^2(\theta + \pi/2) + g_{\perp}^2 \sin^2(\theta + \pi/2)$$

The line widths vary from 30 to 120 G according to $31.6[1 + 3 \cos^2(\theta + \pi/2)]$ for θ and ϕ rotation and $28 + 2[1 + 3 \cos^2(2\theta + \pi/2)]$ for ω rotation.

The *g* value of the weak line is almost constant (2.03–2.05) with the angle. The angular dependences of the *g* value and line width of the strong signal are both consistent with those of Cu^{II} salts.

J. Am. Chem. Soc., Vol. 114, No. 27, 1992 10727

Table III. *g* Values and EPR Line Widths of Copper Halide Salts of BEDT-TTF

compound	<i>g</i> value		<i>H</i> ₀₀ /G		θ /K
	min	max	min	max	
(BEDT-TTF) ₂ CuCl ₄ ·H ₂ O					
Cu electron	2.05	2.25	44	150	~+1
cond electron	2.03	2.04	40	60	
(BEDT-TTF) ₂ CuCl ₄					
Cu electron	2.05	2.30	25	66	~0
(BEDT-TTF) ₃ CuBr ₃ ^a					
>60 K	2.02	2.065	115	135	-107
<60 K	2.04	2.11	37	60	
(BEDT-TTF) ₃ CuClBr ₂ ^a					
>60 K	2.02	2.08	90	100	-61
<60 K	2.037	2.16	90	100	

^a Reference 23a,c. The signals from Cu electrons and conduction electrons in these two compounds are not separable at all angles and temperatures studied.

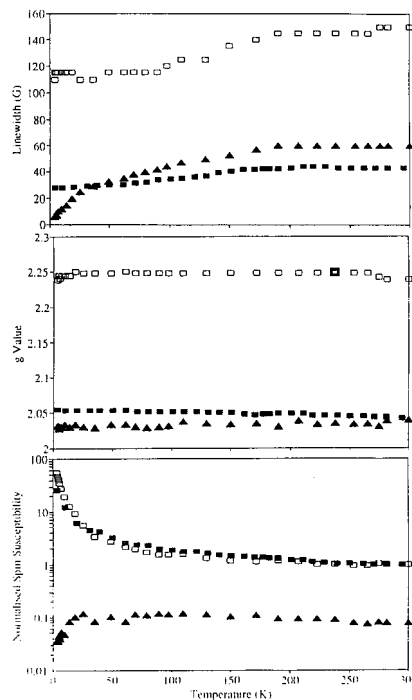


Figure 9. Temperature dependence of the normalized spin susceptibility, line width, and *g* value of the Cu ($H \parallel a-c$, empty square; $H \parallel b^*$, filled square) and conduction ($H \parallel a-c$, triangle) electron resonances of I.

Thus, we assign the intense line to the localized moments (i.e. Cu) and the weak one to BEDT-TTF conduction electrons. The angular dependence of the microwave conductivity is not precisely determined due to the irregular shape of the small crystals used. However, the derived conductivities parallel and perpendicular to the needle axis (*a-c*) of the crystals at 300 K (137/17 S cm⁻¹) are quite consistent with those measured at 15 Hz and dc (140/20 S cm⁻¹).

The temperature dependences of the line width, *g* value, and normalized spin susceptibility are shown in Figure 9. The line widths of both signals decrease as the temperature is lowered: that of Cu from 150 to 115 G for $H_0 \parallel a-c$ and from 40 to 28 G for $H_0 \parallel b^*$ and that of the conduction electrons from 60 to 5 G for $H_0 \parallel a-c$. The relative change of the line widths with temperature reinforces the conclusion that the strong and weak signals are the

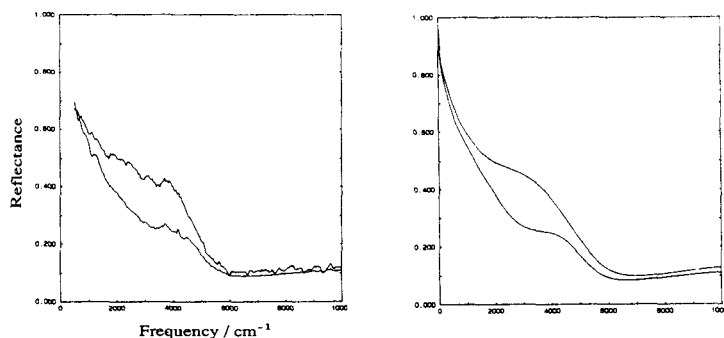


Figure 10. Reflectivity of 1 for $E \parallel a-c$ and $E \perp a-c$. The solid line is a Drude-Lorentz fit to the data.

Cu and the free-carrier resonances, respectively. For example, the line width of conduction electron resonance in the organic superconductor β -(BEDT-TTF)₂AuI₂³⁴ decreases from 16 to 2 G on lowering the temperature from 300 to 4 K; in the conductor β' -(BEDT-TTF)₂AuBr₂²⁰ it decreases from 60 to 0.3 G; and in the semiconductor β' -(BEDT-TTF)₂AuCl₂³⁵ it decreases from 7 to 1 G. The susceptibility derived from the Cu resonance was found to increase on lowering temperature, and that of the conduction electron is temperature independent in the range 30–300 K, while below 30 K, it falls monotonically to 30% of the room-temperature value. The g value of the conduction-electron resonance remains constant within experimental accuracy over the temperature range studied. That of the Cu resonance decreases at a rate of $4 \times 10^{-5} \text{ K}^{-1}$.

The temperature dependence of the microwave conductivity derived from analysis of the line shape of the spectra is orientation dependent. That along $a-c$ shows an increase of 5-fold on lowering the temperature from 300 to 4 K, whereas that perpendicular to the $a-c$ direction decreases by $\sim 10\%$ of the room-temperature value. The skin depth [$\delta_s = c/(2\pi\sigma\omega)^{1/2}$, where the microwave is propagating in the y direction, the oscillating electric field is along z , the oscillating magnetic field is along x , σ is the conductivity along z , and ω is the microwave frequency] is estimated to be 0.13 ($\parallel a-c$) and 0.05 mm ($\perp a-c$).^{18,19} This temperature-dependent anisotropy of the conductivity may be responsible for the sample dependence seen in resistive measurements (since contact alignment on such small crystals can be very difficult).

Optical Properties. The reflectivities of two crystals of 1 were measured in the spectral range 400–30 000 cm^{-1} . Careful examination of the polarization dependence of the reflectivity indicate that the principal axes of the optical constants lie parallel and perpendicular to the $a-c$ needle axis. Figure 10 shows the reflectance with the electric vector polarized parallel and perpendicular to this axis. No significant difference was observed between the two crystals. The reflectivity spectra are characterized by a peak at ca. 4000 cm^{-1} overlapping a Drude-like tail. Some very weak vibrational structures can also be observed.

The reflectivity was fitted in the region 400–20 000 cm^{-1} , using the Drude-Lorentz formula for the dielectric constant

$$\epsilon(\omega) = \epsilon_c - \omega_p^2/\omega(\omega + i\gamma) + \Omega_0^2/(\omega_0^2 - \omega^2 - i\omega\gamma_0)$$

where ϵ_c is the underlying core dielectric constant due to all higher energy processes, γ is the Drude relaxation rate, and ω_p is the unscreened plasma frequency. Ω_0 , ω_0 , and γ_0 are respectively the oscillator strength, the frequency, and the width of the Lorentzian oscillator. As the absolute reflectivity was difficult to measure

Table IV. Parameters of the Drude-Lorentz Fit to and Band Parameters from the Optical Reflectivity of 1

	$E \parallel a-c$	$E \perp a-c$
$\omega_p/10^3 \text{ cm}^{-1}$	9.4	8.9
$\gamma/10^3 \text{ cm}^{-1}$	2.71	3.38
ϵ_c	6.0	5.0
$\omega_0/10^3 \text{ cm}^{-1}$	2.93	4.24
$\gamma_0/10^3 \text{ cm}^{-1}$	3.52	2.48
$\Omega_0/10^3 \text{ cm}^{-1}$	8.9	5.3
m^*_{opt}/m_e	1.25	1.5
$4t/eV$	0.24	0.66
$d/\text{\AA}$	6.6	4.3
ρ	$2/3^+$	
$(1/V_m)/\text{\AA}^3$	600	

reliably, an additional scaling factor α was allowed for in fitting the reflectivity, i.e.

$$R(\omega) = \alpha(\epsilon(\omega)^{1/2} - 1)/(\epsilon(\omega)^{1/2} + 1)$$

The fit to the reflectivity is shown in Figure 10 using the fitting parameters listed in Table IV. In the same table are listed some effective band parameters derived from the Drude fit. For example, the optical effective mass is related to the plasma frequency by the relation

$$m^* = ne^2/(\epsilon_0\omega_p^2)$$

with n being the carrier density, while the transfer integral t is obtained from the tight-binding formula

$$4t = \pi\rho^2/(m^*d^2 \sin(\pi\rho/2))$$

where ρ is the number of carriers per molecule and d is the average intermolecular spacing.

Discussion

The electrical properties of 1 can usefully be compared with those of other BEDT-TTF salts having 3:2 charge stoichiometry, and in particular the chloride salt. For example, the electrical conductivity of 1 is 3–5 times less than that of (BEDT-TTF)₃Cl₂·2H₂O,¹³ in agreement with smaller transfer integrals (100 meV in 1 versus 160 meV in the latter^{13d}). The conductivity anisotropies are identical in the two salts, with the larger component along the side-by-side contacts of the BEDT-TTF molecules. In the former case, this result does not correspond to the larger calculated transfer integrals which are t_a .

A much more important discrepancy between theory and experiment is the prediction from the band-structure calculations^{13d} that both salts should be semi-metals, whereas at room temperature they both exhibit metallic conductivity. On the other hand, 1 is the only BEDT-TTF salt of 3:2 stoichiometry to remain metallic to very low temperatures at ambient pressure. In general, the 3:2 salts suffer a metal (or semi-metal) to insulator (or semiconductor) transition at low temperature. Some have sharp transitions [e.g. (BEDT-TTF)₃(ClO₄)₂]²¹ and others have broad

(34) Talham, D. R.; Kurmoo, M.; Day, P.; Obertelli, D. S.; Parker, I. D.; Friend, R. H. *J. Phys. C: Solid State Phys.* **1986**, *19*, L383–388.

(35) Kurmoo, M.; Talham, D. R.; Day, P. In *Lower Dimensional Systems and Molecular Devices*; Metzger, R. M.; Day, P., Papavassiliou, G., Eds.; NATO ASI Series B, Vol. 248; Plenum: New York, 1991; pp 169–173.

*(BEDT-TTF)₃CuCl₄·H₂O**J. Am. Chem. Soc., Vol. 114, No. 27, 1992 10729*

ones (e.g. (BEDT-TTF)₃Cl₂·2H₂O).¹³ We have demonstrated that the transition in the chloride salt is accompanied by a gradual trimerization of the BEDT-TTF molecules within the chain.^{13f} It is important to note that, in the latter, the three independent molecules belong to one stack while, for I, the corresponding molecules belong to two different stacks, so that trimerization in the same sense is not possible. The chloride is also the only example of a 3:2 salt in which the metal-insulator transition can be suppressed by pressure to stabilize a superconducting state.^{13a}

The interaction between the localized moments and the conduction electrons in I is manifested in two ways:³⁶

First, there is a shift in g value and broadening of the EPR line. The two conditions for strongly interacting systems are (i) the g value of the localized moments and that of the conduction electrons should be close to one another and (ii) the spin-lattice relaxation rate of the localized moments must be sufficiently small. Unfortunately, for such a molecular system, the g value as well as the line width is very dependent on the geometry adopted by the ions, and in the absence of data on the g values and spin-lattice relaxation rates of an isolated ion, no estimate can be made. The fact that we observe two signals for the two spin sublattices indicates that we are not in a "bottleneck" regime and the exchange interaction is small. Should exchange be present, the temperature dependence of the g value should scale the change in susceptibility by

$$g_{\text{obs}} = (g_c \chi_c + g_i \chi_i) / (\chi_c + \chi_i) \sim g_0 + bT$$

$$\chi_i = C / (T - \theta)$$

where e is for conduction electrons and i for localized moments. Our results fit a g_0 ($H_0 \parallel b^*$) value of 2.052 and b of $-4 \times 10^{-5} \text{ K}^{-1}$. The g value is distinctly larger than those found in β - or α' -phase BEDT-TTF salts (2.003–2.010),^{12,34} which strongly suggests that there is interaction between the two spin systems.

A second indication of interaction between localized and conduction electrons in the fall in χ_c from its Pauli limit as the χ_i increases at low temperature (Figure 9). Most striking of all, however, on plotting $(\chi - \chi_0)T$ versus T for the Cu resonance, one observes a gradual increase at low temperature, indicating short-range ferromagnetic interaction. Fits to the data for the Cu resonance using a simple Curie-Weiss law and a Bleaney-Bowers³⁷ model for a dimer give a positive ferromagnetic temperature factor of 1 (1) and 4 (1) K, respectively. However, detailed bulk susceptibility measurements at very low temperatures

will be needed to confirm the EPR data. Such measurements need a greater quantity of crystals, which have to be individually selected due to the polymorphism. It should be borne in mind that the Cu-Cu distances are at least 8.5 Å, so direct exchange interaction between the Cu atoms will be very small. On the other hand, the CuCl₄²⁻ groups are arranged in dimeric units bridged by H₂O molecules, which may provide an exchange pathway. Nor can we rule out the possibility of exchange between the Cu atoms via the free carriers of the conducting BEDT-TTF layers.

There may be several reasons for not observing superconductivity in I. Whether it is due to a small amount of chloride impurity or whether it is the effect of introducing a magnetic anion into the lattice is not known. Further work will be needed to decide this point.

Conclusion

The compound (BEDT-TTF)₃CuCl₄·H₂O described in this paper is the first example of a conducting charge-transfer salt of the BEDT-TTF series containing a magnetic anion to be fully characterized both structurally and electronically. The crystal structure consists of alternating layers of organic cations and inorganic anions, the former consisting of side-by-side stacks of BEDT-TTF, each bearing the same charge of ²/₃+, though with three crystallographically inequivalent molecules per unit cell. The CuCl₄²⁻ anions, with strongly flattened tetrahedral geometry, are linked together by pairs of H₂O molecules to form dimers. (BEDT-TTF)₃CuCl₄·H₂O provides the first instance in which spin resonance due to both localized and conduction electrons has been observed in the BEDT-TTF class of compounds. While it is metallic from room temperature down to 200 mK, there is no transition to a superconducting state. The EPR g values and line widths give evidence for a weak interaction between the spin systems of the organic and inorganic parts of the structure, and at low temperature, there is a small positive deviation of $\chi(\text{Cu})T$, suggesting weak short-range ferromagnetic spin correlations, probably of intradimer type. It remains to be seen whether the absence of superconductivity is the result of these correlations. We are continuing our efforts to synthesize other molecular charge-transfer salts designed to investigate the possible coexistence of superconductivity and magnetic order in a molecular lattice.

Acknowledgment. We thank the SERC (U.K.), CNRS (France), and NATO for partial support of this work.

Supplementary Material Available: Figures showing the labeling scheme of atoms and tables of atomic coordinates, bond lengths and angles, and thermal parameters (9 pages); a listing of calculated and observed structure factors (46 pages). Ordering information is given on any current masthead page.

(36) (a) Barnes, S. E. *Adv. Phys.* **1980**, *30*, 801–938. (b) Odermatt, R. *Helv. Phys. Acta* **1981**, *54*, 1–84.

(37) (a) Bleaney, B.; Bowers, K. D. *Proc. R. Soc. London, A* **1952**, *214*, 451–465. (b) Kato, M.; Muto, Y. *Coord. Chem. Rev.* **1988**, *92*, 45–83.

Crystal and electronic structures and electrical, magnetic, and optical properties of two copper tetrahalide salts of bis(ethylenedithio)-tetrathiafulvalene

I. R. Marsden, M. L. Allan, and R. H. Friend

Cavendish Laboratory, University of Cambridge, Madingley Road, Cambridge CB3 0HE, United Kingdom

M. Kurmoo, D. Kanazawa, and P. Day

The Royal Institution of Great Britain, 21 Albemarle Street, London W1X 4BS, United Kingdom

G. Bravic and D. Chasseau

Laboratoire de Cristallographie et Physique Cristalline, Université Bordeaux I, 351, Cours de la Libération, F-33405 Talence, France

L. Ducasse

Laboratoire de Physico-Chimie Théorique, Université Bordeaux I, 351, Cours de la Libération, F-33405 Talence, France

W. Hayes

Clarendon Laboratory, University of Oxford, Parks Road, Oxford OX1 3PU, United Kingdom

(Received 25 October 1993; revised manuscript received 4 April 1994)

We report the crystal and electronic band structures at 295 K and measurements of temperature-dependent magnetic susceptibility, electron paramagnetic resonance, optical reflectivity, conductivity, and thermopower for two copper tetrahalide salts of bis(ethylenedithio)-tetrathiafulvalene (BEDT-TTF), (BEDT-TTF)₃CuBr₄ and (BEDT-TTF)₃CuCl₂Br₂. The two salts are isostructural with layers of BEDT-TTF having charges of 0 and +*e* separated by layers of pseudo-square-planar tetrahalides of copper (II). At ambient pressure these salts show conductivities near 1 S cm⁻¹, and the magnetic properties indicate coupled localized spins present on both BEDT-TTF and the *d*⁹ copper layers. At 60 K, there is a discontinuous drop in susceptibility, a sharpening of the electron paramagnetic resonance linewidth, and an increase in *g* value that we attribute to the loss of the contribution from the BEDT-TTF sheets. This may be associated with a Jahn-Teller distortion of the planar copper complexes. Below the transition temperature the susceptibility can be fitted to a quadratic layer antiferromagnet with *J* = 15 K (CuBr₄) and 8 K (CuCl₂Br₂) and one spin per formula unit. Under pressure there is a very rapid increase in conductivity, to 500 S/cm at 24 kbar, the largest increase of conductivity under pressure in any molecular solid yet studied. There is a sharp transition from metal to insulator at temperatures rising to 111 K near 5 kbar, and falling to 80 K at 20 kbar. We consider that these salts are nearly metallic at ambient pressure, with strongly enhanced susceptibilities, but are brought to a fully metallic state under pressure as a result of increased intermolecular contacts.

I. INTRODUCTION

Organic charge transfer salts now provide a very wide range of model electronic materials, with properties ranging from metallic and superconducting behavior through to nonmetallic magnetically ordered materials. The charge transfer salts formed with bis(ethylenedithio)-tetrathiafulvalene (BEDT-TTF) have provided an important series of materials, particularly regarding superconducting properties,^{1,2} and examples have been prepared with a very wide range of anions. The most common structural motifs in such salts are sheets of BEDT-TTF donors, sometimes arranged as one-dimensional chains, separated by sheets of the anions. Intermolecular contacts within the BEDT-TTF sheets are responsible for the formation of delocalized carriers and the metallic behavior when found. The primary effect of the anion is to control the packing of the BEDT-TTF donors, and

systematic studies of structural changes brought about by selection of modified anions have produced the two families of superconducting salts; the β polytype 2:1 salts formed with linear anions^{3,4} and the κ polytype 2:1 salts formed with polymeric anions.⁵ However, other properties can be introduced by selection of the anion, and we and other groups⁶⁻¹⁴ have made salts with anions containing magnetic moments localized on transition-metal ions. The interaction of local magnetic moments on the anions with the delocalized conduction electrons in the organic sheets is of considerable interest, and it is for this reason that we have investigated the copper tetrahalide salts that form the subject of this paper. We note that there are at present relatively few coupled magnetic and/or superconductor materials; examples included erbium rhodium boride, ErRh₃B₄ and some of the Chevrel phases, e.g., HoMo₆S₈.¹⁵⁻¹⁷

Although our goal was to make superconducting salts

containing these paramagnetic anions, none has been isolated so far; in general they are semiconductors. In most cases the electron transport is confined to the BEDT-TTF layers while the magnetic properties are defined by the sum of two magnetic sublattices, the conduction electrons on the BEDT-TTF moiety and the unpaired spins on the anions. For example, in (BEDT-TTF)₃CuCl₄·H₂O, the only salt with a magnetic anion to show metallic behavior,⁸ we have demonstrated that there is a very weak interaction between the two kinds of spin, while for the semiconducting salt (BEDT-TTF)₂FeCl₄ and insulating salt (BEDT-TTF)FeBr₄,⁷ there is no measurable interaction. By contrast, in the present case, we present evidence for a strong interaction between the two sublattices in the BEDT-TTF series, as well as structural phase transitions of the anions from planar (*D*_{2d}) to distorted tetrahedral (*C*_{2v}) that modify the electronic structure and thus the electrical and magnetic properties.¹⁸

The CuBr₄²⁻ and CuCl₂Br₂²⁻ salts investigated here were selected because the CuCl₄²⁻ salt mentioned above had shown interesting metallic behavior. However, this new salt is very different structurally from the CuCl₄²⁻ salt, and their electronic properties are unrelated. Whereas the CuCl₄²⁻ anions are distorted from square planar, as is usually expected for Jahn-Teller *d*⁹ ion (the *trans* Cl-Cu-Cl angle being 150°), the anions in the new salts are, very unusually, undistorted pseudosquare planar at room temperature (though we have evidence that the Jahn-Teller distortion is present at low temperatures). It is to our knowledge the first complex of CuBr₄²⁻ found to be planar.^{19,20} It is interesting that the stoichiometry of all the salts is 3:1, which in terms of charge is 3:2 for comparison with the β and κ phases; and that for the CuCl₄²⁻ salt a water molecule is included to make up the size of the cavities formed between the BEDT-TTF layers.

The room temperature crystal structure of a CuBr₄²⁻ salt of BEDT-TTF has previously been determined by Mori *et al.*²¹ The crystal belongs to the monoclinic space group *P*2₁/*c* with the long needle axis parallel to the crystallographic *b* axis; two independent BEDT-TTF molecules were observed with different bond lengths, which Mori *et al.* assigned charges of 0 and $\frac{1}{2}e^+$, respectively. The model used for the structural refinement was based on a composition (BEDT-TTF)₂(BEDT-TTF^{3+/4+})₄Cu^IBr₂Cu^{II}Br₄ with equivalent Cu-Br distances for both oxidation states of the copper atom. The stacking of the donor molecules resembles that of the α polytype of the tri-iodide salt.²² However, some ambiguity remained in the estimation of both the charge separation and the bromine atom population in the crystal structure refinement and this was noted as the cause for the high *R* value. In addition, the above stoichiometry cannot account for the number of unpaired electrons per formula unit observed in the susceptibility measurements.^{18,13} In the present paper we resolve this problem by redetermining the crystal structure of the bromide salt and fully characterizing the structure of the newly synthesised isostructural mixed halide salt.

Taking advantage of new structural informations, we report the calculated electronic band structure and a full range of magnetic, transport, and optical measurements on single crystals of (BEDT-TTF)₃CuBr₄ and (BEDT-TTF)₃CuCl₂Br₂ both at ambient pressure and in the case of transport studies as a function of hydrostatic pressure up to 24 kbar. Some of the results have been reported in a preliminary publication.¹⁸

II. EXPERIMENT

BEDT-TTF was prepared by the method of Larsen and Lenoir²³ and recrystallized twice from chloroform before use. The tetra-alkyl ammonium salts of the anions were obtained by reacting CuBr₂ and (R₄N)X (X = Cl or Br) in absolute ethanol. The purity was checked by elemental analysis before use. The charge transfer salt was obtained by electrocrystallization of BEDT-TTF (20 mg) in a benzonitrile solution (50 ml) of [(C₂H₅)₄N]₂CuBr₄ or [(CH₃)₄N]₂CuBr₂Cl₂ (200 mg). A three-compartment cell with platinum wire electrodes was used, with a constant applied current of 1.2 μA for two weeks. The crystals were black shiny needles of dimension 4 × 1 × 0.2 mm³.

Several synthetic routes for the preparation of the CuBr₄²⁻ salt exist. Mori *et al.* obtained the CuBr₄ salt by electrocrystallisation of BEDT-TTF and Cu^IBr₂⁻ in 112-trichloroethane, and Susuki *et al.* by diffusion of BEDT-TTF and Cu^{II}Br₂ in benzonitrile or acetonitrile. While in the former the BEDT-TTF as well as the anion need to be oxidized to give the product, for the latter the CuBr₂ is used as the oxidant and the source of the anion.

We have used the most direct method; applying a potential low enough to oxidize only the organic molecules. When the anions and BEDT-TTF are mixed together in chlorinated solvents such as 112-trichloroethane, dichloromethane, or chloroform, we noted that all the BEDT-TTF is consumed within a short time to give black microcrystals without even passing a current. The salt (BEDT-TTF)₃Cu^{II}Br₄·Br₃ has been identified as one of the products from 12-dichloroethane;²⁴ it crystallizes in the orthorhombic group (*Pccn*). In benzonitrile, however, the reaction is slow, such that crystals of the titled compounds are formed on the electrode. In this paper all the measurements were conducted on single crystals harvested from the electrodes of several cells.

The band structure was calculated from transfer integrals obtained by the extended Hückel method. The highest occupied molecular orbitals (HOMO's) are generated from the dimer splitting method.²⁵

Electrical conductivity was measured using four-probe techniques, with high-pressure measurements performed in a clamp pressure cell with pentane-isopentane (1:1) mixture as the pressure transmitting medium.²⁶ Conductivity measurements were limited to the long axis (*b*) of the needle crystals. Contacts were made with silver paint on evaporated gold pads. Data were collected using both ac and dc techniques. Thermopower was measured using similar contacts with a temperature gradient of typically 1 K across the crystals, and corrected for the absolute thermopower of the gold contact wires.

Electron paramagnetic resonance spectra were mea-

sured on several single crystals as a function of angle and temperature. Crystals were mounted on a cut flat face of Spectrosil Quartz rod using a smear of silicone grease. The spectrometer is a Varian E9 operating at a microwave frequency of 9 GHz and 100 kHz field modulation. Variable temperature (4–300 K) were obtained by use of a continuous flow Oxford Instrument cryostat and an ITC-4 temperature controller. The field was calibrated with a diphenylpicrylhydrazol standard.

Static magnetic susceptibility measurements were made on two independent batches of randomly oriented crystals of ~2 mg each. Data were recorded for cooling and warming runs as well as for different applied magnetic fields on a Faraday balance employing a Cahn microbalance. Data were corrected for the core diamagnetism and a small amount of ferromagnetic impurities.

Optical reflectivity was measured on a Perkin Elmer 1710 spectrometer equipped with an IR plan microscope operating in the range 400–4300 cm^{-1} and a Perkin Elmer Lamda 9 (3000–50 000 cm^{-1}). The data were normalized to that of a gold mirror. A KRS5 and a calcite polarizer were employed for the mid- to near-infrared and visible regions, respectively.

III. RESULTS

A. Crystal structure

The compounds are isostructural belonging to the monoclinic system (Fig. 1), $P2_1/c$, $a = 17.001(3)$, $b = 10.140(2)$, $c = 14.178(3)$ Å, $\beta = 102.75(2)^\circ$, $V = 2383(1)$ Å³, $d_c = 2.14$ g/cm³ for (BEDT-TTF)₃CuBr₄, and $a = 16.895(3)$, $b = 10.108(4)$, $c = 14.150(4)$ Å, $\beta = 102.60(2)^\circ$, $V = 2358(1)$ Å³, $d_c = 2.04$ g/cm³ for (BEDT-TTF)₃CuBr₂Cl₂. The volume of the unit cell found by Mori *et al.*²¹ lies in between those of the CuBr₄

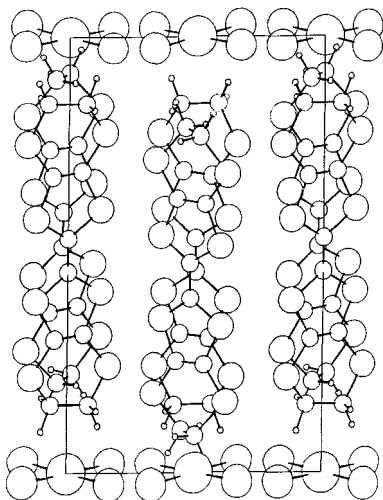


FIG. 1. View of the crystal structure of (BEDT-TTF)₃CuBr₄ along the c axis.

and CuBr₂Cl₂ salts suggesting that there might be some chlorine in their compound. If so, the chlorine must come from the solvent (*vide infra*), a synthetic problem that has been encountered previously.^{27,28}

The final refinement using the atomic coordinates of Mori *et al.*²¹ as the starting point for the two compounds results in lower values of the reliability R factor (0.034 and 0.036) and subsequently to smaller standard deviations on atomic coordinates. Here we have also refined the occupancy factor of the halogen atoms. The high precision of the present results allows us to assert that the occupancy factor of the bromine atoms is 100% for the (BEDT-TTF)₃CuBr₄ salt and that in the case of the CuCl₂Br₂ salt it is possible to differentiate the positions of the chlorine and the bromine atoms, with occupancy factors of 50%. This confirms, contrary to what was assumed by Mori *et al.* that the two copper atoms in the unit cell are in oxidation state two. As the copper atom lies on an inversion center, the CuBr₄²⁻ and CuBr₂Cl₂²⁻ anions are strictly planar. The Cu-Br distances are 2.407 and 2.421 Å in (BEDT-TTF)₃CuBr₄ and equal to 2.394 and 2.389 Å in CuBr₂Cl₂ while Cu-Cl distances are found to be 2.309 and 2.313 Å. Note that the average Cu^{II}-Cl is 2.24 Å and Cu^{II}-Br is 2.38 Å,²⁹ while Cu^I-Cl and Cu^I-Br are 2.107 and 2.226 Å, respectively.³⁰ Due to the two independent bond lengths, both anions have a D_{2d} symmetry.

Two crystallographically independent BEDT-TTF molecules (A and B) were observed in both compounds; the difference in the bond lengths and comparison with BEDT-TTF salts with well-defined charges strongly suggest that the charges of A and B are, respectively, 0 and $+e$. The two salts consist of layers of BEDT-TTF, stacked in a $ABBAB$ manner, separated by pseudosquare planar tetrahalides of copper (II) (Fig. 1). Complete details of the crystal structure are given elsewhere.^{31,32}

B. Electronic band structure

The transfer integrals and the calculated band structure of (BEDT-TTF)₃CuBr₄ are given in Fig. 2. They were found to be very different from those published by Mori *et al.*²¹ The energy dispersion is quite small along the c direction in relation to the transfer integrals shown. This small dispersion together with the average charge of $2/3e$ per BEDT-TTF molecule implies that the four lowest bands are completely filled. The calculated electronic structure corresponds to a semiconductor with a small gap of ~5 meV. This result might be expected from the previous discussion about the existence of two crystallographically independent molecules with different oxidation states.

Several other BEDT-TTF salts exhibit the same zigzag stacking as those under study, for example, the two forms of (BEDT-TTF)₂Ag(CN)₂,³³ θ -(BEDT-TTF)₂I₃,³⁴ α -(BEDT-TTF)₂I₃,²² and α -(BEDT-TTF)₂MHg(SCN)₄.³⁵ In particular, the θ phase and the Ag(CN)₂ salts have quite similar transfer integrals and Fermi surfaces. It appears that the Hg salt and the CuBr₄ salt bear some similarities together with striking differences. Within the stack, the

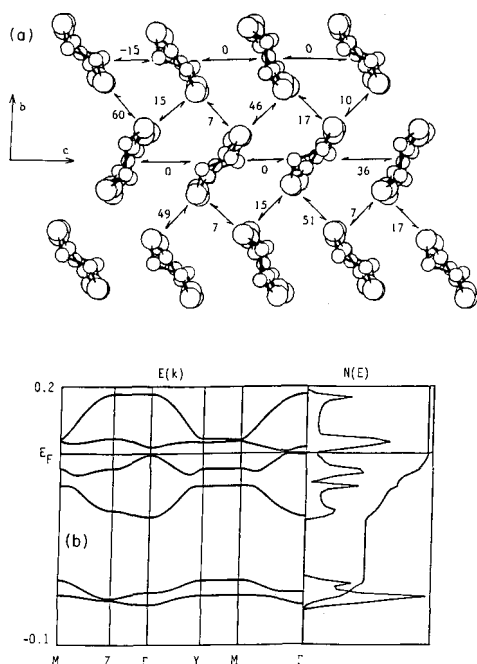


FIG. 2. (a) View of the structure along the central C=C bonds showing the calculated transfer integrals (meV). (b) Band structure and density of state calculated from the transfer integrals. Dispersion is shown within the plane of the BEDT-TTF sheets.

transfer integrals may be large with positive or negative values or even close to zero, depending on small differences in the shifts along the long molecular axis or along the short one; in $(\text{BEDT-TTF})_3\text{CuBr}_4$ they are close to zero while they are much larger in the Hg salt. The interstack interactions are also much stronger in the Hg salt than in the CuBr_4 salt. These results, together with the different molecular charges in CuBr_4 , lead to a band structure for a semiconductor while that for the Hg salt corresponds to a metal.

C. Transport properties

The room-temperature conductivities along the b axis of the two materials are very similar, being 0.7(1) S/cm, a low value for metallic organic conductors of the BEDT-TTF family, and a high value for the semiconductors. At ambient pressure the conductivity of both salts decreases steadily on cooling with no evidence of any sharp transitions, as shown in Fig. 3. However closer examination of the data shows a gradual change in the activation energy on lowering the temperature and two more slight changes in the activation energy at ca. 60 and 50 K.

Application of pressure to both compounds has a dramatic effect on the absolute value of the conductivity

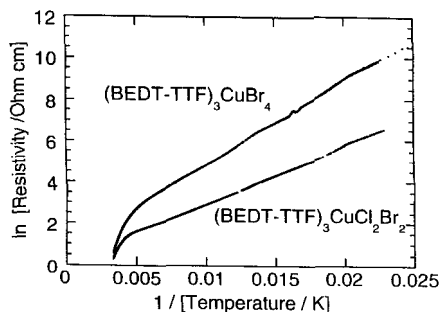


FIG. 3. Log_e (resistivity) measured along the b axis vs reciprocal temperature at ambient pressure.

as well as on the phase transitions, as shown in Ref. 18. In fact, these two materials show the largest change in conductivity on application of pressure of all known organic conducting solids. The conductivities of both increase almost linearly at a rate of 25 (S/cm)/kbar up to about 8 kbar finally attaining a plateau of approximately 500 times the ambient pressure value at 22 kbar. As we discuss later, we consider that at ambient pressure these salts are just on the insulating side of the Mott-Hubbard transition, and that pressure rapidly brings them into the metallic regime. This change in character is seen also in the temperature dependence of the conductivity, which increases with decreasing temperature above 7 kbar. The two salts show similar behavior. The temperature dependence of the conductivities along the needle axis (b) of the crystals of the CuBr_4^{2-} salt is shown at several pressures in Fig. 4, that for the $\text{CuCl}_2\text{Br}_2^{2-}$ salt is presented in Ref. 18. At low temperatures there is clear evidence for the presence of phase transitions that take both salts from the

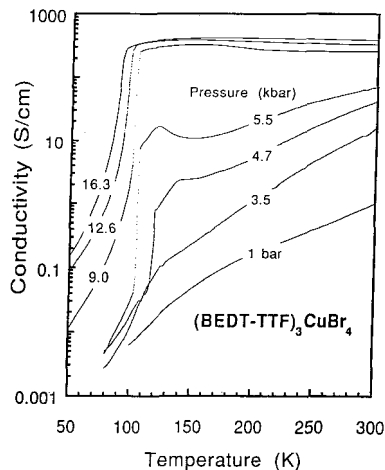


FIG. 4. Temperature dependence of the b -axis conductivity of $(\text{BEDT-TTF})_3\text{CuBr}_4$ at several pressures.

metallic to a readily observable semiconducting regime. The sharp transition to the low-temperature semiconductor phase is readily observable at pressures above about 3 kbar, where it occurs at around 80 K in both materials. The transition temperature rises to a little above 100 K near 6 kbar, and falls gradually to around 80 K by 20 kbar. We note that there is some structure in the temperature dependence of the conductivity just above the transitions, seen particularly clearly around 5 kbar, it is possible that they are associated with changes in pressure at the freezing point of the pressure medium, which is about 0.7 kbar for this pressure system.

The temperature dependence of the thermopower measured with the temperature gradient along the *b* axis has been shown in Ref. 18. Although the thermopower is very low near room temperature, it becomes large and negative on cooling, reaching values of -120 and -230 $\mu\text{V}/\text{K}$ near 170 K. These large values indicate that the materials are semiconductors, and the size of the thermopower being similar to that measured in some of the α' BEDT-TTF salts that behave as Mott-Hubbard insulators.³⁶ We note that the thermopower is larger in the bromide salt, as is the activation energy of the conductivity, see Fig. 3.

D. Optical properties

The polarized reflectivity spectra parallel and perpendicular to the needle axis (*b*) are shown in Fig. 5. The spectra are characterized by sharp vibrational structures on a strong electronic background centered around 2000 cm^{-1} . Many more intermolecular BEDT-TTF vibrational modes are observed than in those salts with one crystallographically independent molecule per unit cell, indicating that we are observing modes belonging to the two independent molecules of different electronic charge in the unit cell. For example, the C-S stretching mode,³⁷ $\nu_{49}(b_{2u})$ in the β , κ , and α' polytype, in which the BEDT-TTF molecules carry a charge of $\frac{1}{2}e^+$, is at 884 cm^{-1} ,³⁸ which for a charge of $\frac{2}{3}+$ is at 892 cm^{-1} (BEDT-TTF)₃[ReO₄]₂, and for $+e$, in (BEDT-TTF)Ag₄(CN)₅ and (BEDT-TTF)FeBr₄ it is observed at 900 cm^{-1} . Neutral BEDT-TTF has a band at 770 cm^{-1} .

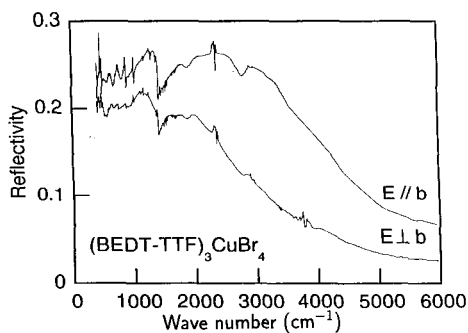


FIG. 5. Optical reflectivity in the midinfrared region for (BEDT-TTF)₃CuBr₄ at room temperature for $E // b$ and $E \perp b$.

Thus the peaks at 768 and 896 cm^{-1} can be assigned to vibrational modes of (BEDT-TTF)⁰ and (BEDT-TTF)⁺, respectively, while the broad band at ~ 2000 cm^{-1} arises from an intraband transition. Unfortunately the C=C region is more difficult to interpret; the shapes and frequencies of the bands vary with the electronic nature of the compound in question.

In the visible region the spectra are dominated by charge transfer (ligand to metal) and *d-d* transitions. The spectrum for $E // b$ (Fig. 6), has been studied down to 30 K. There is a gradual sharpening of the spectrum on lowering the temperature such that at 30 K, there are four features (6200, 8000, 17 500, and 20 000 cm^{-1}). Kramers-Krönig transformation of the data reveals a redshift of 200–300 cm^{-1} in the peak at 17 500 cm^{-1} from 300 to 30 K. A Jahn-Teller distortion of the CuBr₄²⁻ would result in a lowering of the energy of the *d-d* transition as has been observed for the CuCl₄²⁻.³⁹ These values are of the right order of magnitude for the observed increase in the *g* values.

E. Magnetic properties

1. Static susceptibility

The temperature dependence of the bulk magnetic susceptibilities of the two compounds, shown in Fig. 7, are very similar. At high temperatures the susceptibilities obey a Curie-Weiss law with $\theta \sim -110$ K (CuBr₄²⁻) and -59 K (CuCl₂Br₂²⁻). The susceptibility of the bromide salt decreases abruptly between 58–60 K, and shows a rounded maximum at ~ 30 K indicative of short-range antiferromagnetic order. The susceptibility of the mixed halide salt shows a similar abrupt decrease between 53 and 56 K and a maximum at ~ 10 K. At the abrupt transition, the susceptibilities of both salts fall by a similar amount (2.5×10^{-3} emu/mol formula unit). A change in the *g* values, of the magnitude reported below would give an increase in susceptibility of 2.7%, whereas the observed decrease is an order of magnitude larger.

Below 50 K the temperature dependence of the susceptibility of the bromide salt can be fitted by a model of a quadratic layer antiferromagnet (QLAF) with 0.95 spins per formula unit and $J = 15$ K.⁴⁰ This shows that below the transition there are two unpaired electrons per unit cell (note that $z = 2$) that interact two dimensionally, with a temperature-independent *J*. The susceptibility of the mixed-halide salt likewise fits the QLAF model between 15 and 55 K with 1.0 spins per formula unit and $J = 8$ K. The anisotropy of the *g* value at 30 K (Ref. 41) indicates that below the 60-K transition the spins are mainly localized on Cu^{II}. The antiferromagnetic interaction between the spins of the copper atoms is probably mediated by the electrons on the BEDT-TTF layers through a superexchange mechanism, which may be responsible for the observation of a single line in the electron paramagnetic resonance (EPR) spectra. The shortest Cu-Cu distance is ~ 8.7 Å and the halogen atoms on neighboring anions are at least ~ 4.3 Å apart. The *J* values of the two salts in this temperature range depend on the extent to which the copper atoms interact with the BEDT-TTF mole-

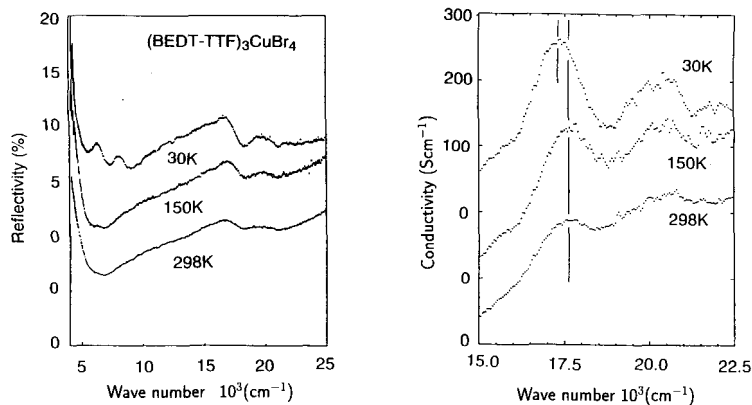


FIG. 6. Visible region optical reflectivity and conductivity for $(\text{BEDT-TTF})_3\text{CuBr}_4$ with $E\parallel b$.

cules. Clearly the interaction is stronger in the bromide ($\theta = -110$ and $J = 15$ K) than in the mixed halide salt ($\theta = -59$ and $J = 8$ K), in agreement with the fact that bromine is larger and more polarizable than chlorine. The similarity between the two salts is even more marked when an extrapolation of the low-temperature behavior is subtracted from the high-temperature data:¹⁸ the residual susceptibility of the two salts is almost identical.

2. EPR

The spin susceptibility, g -value, and peak-to-peak linewidth of the resonance line have been derived from the spectra as a function of temperature and angle to the applied field. At all temperatures and crystals' orientations the spectra of both materials are dominated by a single resonance line.^{41,42} The temperature-dependent data were recorded along three orthogonal axes, the crystallographic axis b and c and a^* . The angular dependences of the spectra of the two materials are similar while those of the spin susceptibility differ marginally at

low temperatures. In both cases, there is an abrupt change in linewidth, g value, and integrated area at ca. 60 K. The changes in the spectra for the bromide salt take place over a temperature range of ca. 10 K (Fig. 8). A loss of intensity of the wide peak and an increase for the narrow peak is observed on lowering the temperature through the transition. For the mixed halide the transition takes place over a wider temperature range.

The angular dependences of the g values at room temperature show uniaxial symmetry with the principal values $g_{\parallel} = 2.070$ and $g_{\perp} = 2.021$ for the CuBr_4^{2-} salt and $g_{\parallel} = 2.085$ and $g_{\perp} = 2.016$ for the $\text{CuCl}_2\text{Br}_2^{2-}$ salt. These values lie close to the mean of those of the square planar Cu ion and BEDT-TTF cation, for example, square planar CuBr_4^{2-} doped in PdBr_4^{2-} has g values⁴³ $g_{\parallel} = 2.143$ and $g_{\perp} = 2.044$ while for $(\text{BEDT-TTF})_2\text{I}_3$ the g values are $g_1 = 2.0011$, $g_2 = 2.0065$, and $g_3 = 2.0025$.⁴⁴ At ~ 30 K, below the phase transition, the g values $g_{\parallel} = 2.110$ and $g_{\perp} = 2.040$ for the CuBr_4^{2-} salt are close to those for the nonplanar ion in

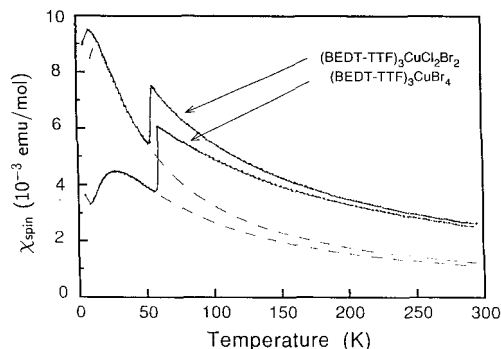


FIG. 7. Static magnetic susceptibility for randomly oriented samples of the copper tetrahalide salts. Broken lines are fits to the quadratic layer antiferromagnet model discussed in the text. Susceptibilities are shown in emu/mol formula unit.

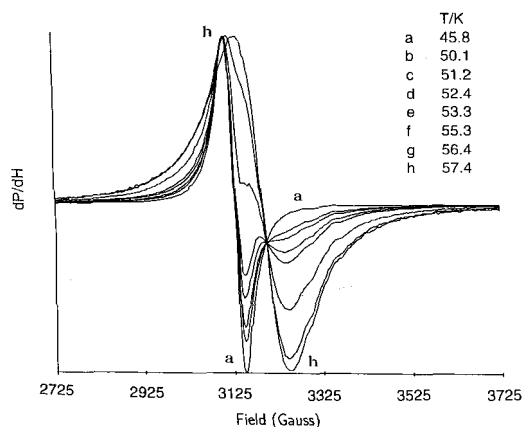


FIG. 8. EPR spectra of $(\text{BEDT-TTF})_3\text{CuBr}_4$ at various temperatures through the phase transition near 60 K, with the static field parallel to the b axis.

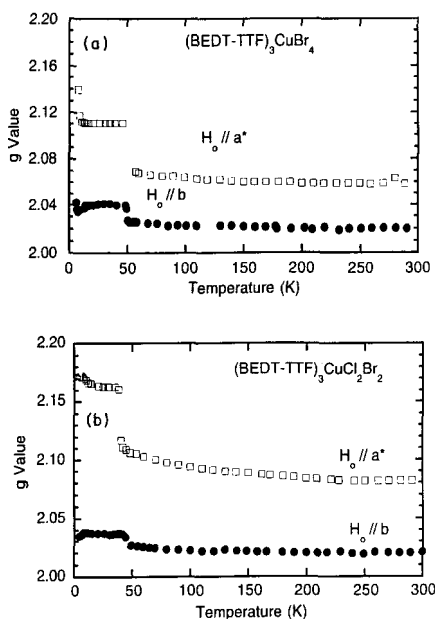


FIG. 9. Temperature dependence of the two g values of the copper tetrahalide salts.

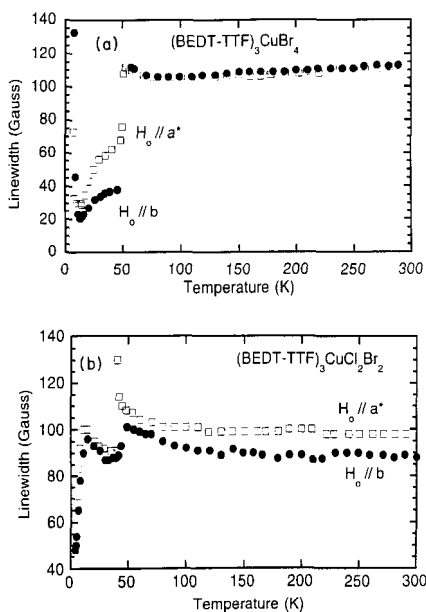


FIG. 10. Temperature dependence of the EPR linewidths measured parallel and perpendicular to the b axis.

$[\text{NH}_3(\text{CH}_2)_n\text{NH}_3][\text{CuBr}_4]$, $g_{\parallel}=2.097$ and $g_{\perp}=2.047$.⁴⁵

The angular dependences of the g values at room temperature show uniaxial symmetry with the principal values $g_{\parallel}=2.070$ and $g_{\perp}=2.021$ for the CuBr_4^{2-} salt and $g_{\parallel}=2.085$ and $g_{\perp}=2.016$ for the $\text{CuCl}_2\text{Br}_2^{2-}$ salt. These values lie close to the mean of those of the square planar Cu ion and BEDT-TTF cation, for example, square planar CuBr_4^{2-} doped in PdBr_4^{2-} has g values⁴³ $g_{\parallel}=2.143$ and $g_{\perp}=2.044$ while for $(\text{BEDT-TTF})_2\text{I}_3$ the g values are $g_1=2.0011$, $g_2=2.0065$, and $g_3=2.0025$.⁴⁴ At ~ 30 K, below the phase transition, the g values $g_{\parallel}=2.110$ and $g_{\perp}=2.040$ for the CuBr_4^{2-} salt are close to those for the nonplanar ion in $[\text{NH}_3(\text{CH}_2)_n\text{NH}_3][\text{CuBr}_4]$, $g_{\parallel}=2.097$ and $g_{\perp}=2.047$.⁴⁵

The temperature dependence of the g values of both salts is shown in Fig. 9: that of the bromide salt divides into three regions; one between 60 and 300 K, the second between 8 and 60 K, and the third below 8 K, while in the $\text{CuCl}_2\text{Br}_2^{2-}$ salt we find only the first two regions with a transition temperature of ~ 40 K. The angular dependence of the g values above and below the transition at ~ 50 K is similar except for the slightly larger values below the transition. The divergence of the g value and the linewidth (*vide supra*) of the CuBr_4^{2-} salt is indicative of a three-dimensional magnetic ordering.

The linewidths of the two materials (Fig. 10) behave differently; that of the CuBr_4^{2-} salt does not show any dispersion while the $\text{CuCl}_2\text{Br}_2^{2-}$ shows a weak dispersion with orientation at room temperature. Below the transition, the reverse is observed. In both cases, the linewidth is constant from 300 K to the transition temperature, though there is sign of softening of the lattice near the transition. Below the transition at ~ 50 K the two salts behave quite differently. For the CuBr_4^{2-} salt, the linewidth decreases on lowering temperature to a minimum at ~ 8 K, where there is a sudden divergence within a few degrees. The latter is associated with an increase of the g value. For the $\text{CuCl}_2\text{Br}_2^{2-}$ salt, the linewidth increases to maximum at ~ 15 K and a gradual lowering to low temperature.

IV. DISCUSSION

Our calculated transfer integrals and band structure on the CuBr_4 salt are very different from those of Mori *et al.*²¹ We find several zero transfer integrals [Fig. 2(a)] due to the large slip of the molecules with respect to one another along the short molecular axis, similar to that found for $(\text{BEDT-TTF})_3\text{CuCl}_4\cdot\text{H}_2\text{O}$.⁸ Note that the interstack transfer integral along the b axis is greater than those within the stacks. This is found to be the case in most of the BEDT-TTF salts, and results in higher conductivities perpendicular to the stacking axis. With the 3:2 stoichiometry, assuming divalent copper tetrahalide anions, the BEDT-TTF HOMO bands are two-thirds filled, and also with six BEDT-TTF molecules within the unit cell, which requires four of the six bands to be filled. In contrast, the calculation of Mori *et al.* leads to three degenerate bands with very small dispersion; the band filling assuming the correct stoichiometry would result in

a semiconductor on the border line being a metal. Our calculation leads to six well-dispersed bands. Whether this gives a semiconductor or semimetal depends on the band dispersions, and we find here that the Fermi energy lies between the fourth and fifth bands with a minimum semiconducting gap at the zone center of ~ 5 meV. We note that the bands are calculated to be narrow, with a full bandwidth of less than 0.3 eV, and expect to see effect due to Coulomb interactions, as indeed is observed.

The two salts whose properties we have described are particularly interesting members of the BEDT-TTF series of charge transfer salts because they lie on the border line between metallic and semiconducting behavior. The room-temperature conductivities of about 1 S/cm, are too low for metallic behavior [the κ -phase superconducting materials such as the $\text{Cu}(\text{NCS})_2^-$ salts has conductivities an order of magnitude larger], and yet are very high for a semiconductor. The magnetic properties are also unusual in that, as we discuss further below, the susceptibility associated with the "conduction electrons" on the BEDT-TTF stacks is apparently very high. We consider that the jump of 2.5×10^{-3} emu/mole formula unit in susceptibility at the low-temperature transition is due to the loss of the contribution from these electrons, and we note that this is an exceptionally large susceptibility for salt of such a type. To account for a contribution of this magnitude to the susceptibility one must assume that two spins per formula unit which are both fully localized, and which are weakly antiferromagnetically coupled. Comparison can be made with the α' polytype such as $(\text{BEDT-TTF})_2\text{Ag}(\text{CN})_2$, in which there is one localized spin per dimer of BEDT-TTF and which shows quasi-one-dimensional antiferromagnetic coupling; peak susceptibilities at temperatures (60 K) comparable to the exchange coupling energy are 1.7×10^{-3} emu/mol formula unit. Note that the conduction electron susceptibility in a related 3:2 salt that exhibits metallic (and superconducting behavior under pressure), $(\text{BEDT-TTF})_3\text{Cl}_2 \cdot 2\text{H}_2\text{O}$, is only 7×10^{-4} emu/mole formula unit.⁴⁶

These facts suggest strongly that these materials are just on the insulator side of the Mott-Hubbard transition. Semiconducting behavior is not due to a gap in the one-electron density of states, but arises because the holes on the BEDT-TTF stacks localize due to the strong Coulomb interaction. The 3:2 charge stoichiometry of these salts requires that two holes are accommodated per three BEDT-TTF sites. Comparison of the bond lengths within the BEDT-TTF molecule with those of well-defined charges shows clearly that two of the BEDT-TTF molecules are charged and that one is close to neutral.

The transport properties are therefore those of a "magnetic" semiconductor, with the activation energy for conductivity identified as $U_{\text{eff}}/2$, where U_{eff} is the on-site Coulomb energy (Hubbard energy) associated with the transfer of a charge to place two changes on a single site. This model has been applied to the case of α' polytypes by Parker *et al.*³⁶ The activation energies measured for the copper tetrahalide salts are relatively low in comparison with the α' polytype salts, indicating that the Coulomb localization is weak. The size of the thermo-

power is consistent with this model.³⁶

The magnetic properties of these two salts are unusual. We note that only a single EPR line is seen, though there is clear evidence that this has contributions from both the localized d^9 copper moments and the localized moments present on the BEDT-TTF sites. For example, the g values above the low-temperature transition are intermediate between those expected for the copper moment and as found for spins on BEDT-TTF sites. This indicates that there is a significant level of interaction between the two spin systems, in contrast to the other magnetic anion salts which we have studied.^{7,8} Below the phase transitions seen in both salts around 60 K the susceptibilities are well fitted by a quadratic layer antiferromagnetic ordering model, and values for the exchange interaction of 15 and 8 K are found for $(\text{BEDT-TTF})_3\text{CuBr}_4$ and $(\text{BEDT-TTF})_3\text{CuCl}_2\text{Br}_2$, respectively. These values provide some indication of the strength of the exchange interactions present in these materials.

The phase transitions at 58–60 and 53–56 K in $(\text{BEDT-TTF})_3\text{CuBr}_4$ and $(\text{BEDT-TTF})_3\text{CuCl}_2\text{Br}_2$, respectively, cause the loss of a significant fraction of the susceptibility, change the g values close to those expected for copper d^9 ions, and cause a large reduction in linewidth. Below the transition the susceptibilities and g values are fully consistent with the presence of one spin per copper. We consider therefore that the higher susceptibility above the transition must result from a large contribution from the BEDT-TTF sheets. We do not have information about the low-temperature structure at present. However, a Jahn-Teller distortion of the square-planar copper tetrahalide is expected for this d^9 ion, and we propose that it is this that drives the change in properties observed here. The shift in the $d-d$ optical transitions is consistent with this change in copper environment. The most likely explanation for the loss of susceptibility from the BEDT-TTF sites is that there is pairing of the two spins present on two out of the three BEDT-TTF sites along the stacks.

The behavior of these salts under pressure shows a remarkable change from semiconductor to metallic properties. The increase in conductivity by a factor of 500 in 20 kbar is the highest such increase that we are aware of in molecular conductors, and takes these salts well into the domain of fully metallic behavior. It is certainly not surprising to see some increase in conductivity on cooling when the room-temperature conductivity has reached 500 S/cm. Such a very large increase in conductivity is only likely to be found when pressure transforms the material from one domain of behavior (magnetic insulator) to another (metal). Of the few other examples of materials which show comparable increases in conductivity under pressure, $\text{Cs}_{0.83}\{(\text{Pd}[\text{C}_2\text{S}_2(\text{CN})_2])\} \cdot 0.5\text{H}_2\text{O}$ (Refs. 47 and 48) shows an increase by a factor of 250 at 20 kbar, and we note that this is also attributed to a transition from Mott-Hubbard insulator to metal.

The low-temperature transition to a semiconducting state under pressure is very abrupt and indicates the presence of a phase transition. We consider that the Jahn-Teller distortion proposed to account for the ambient pressure properties is unlikely to be suppressed rapidly

under pressure, hence it is very likely that this transition is present and responsible for the metal to insulator transition. The Jahn-Teller distortion lowers symmetry, and it is likely that this further reduces symmetry at the BEDT-TTF sites, possibly by setting up a superlattice. The band structure shown in Fig. 2(b) will be modified under pressure principally through the broadening of the bands, and we expect the Fermi energy to continue to lie close to the band that is calculated at ambient pressure.

V. CONCLUSIONS

The two salts (BEDT-TTF)₃CuBr₄ and (BEDT-TTF)₃CuCl₂Br₂ reveal a range of properties new to this class of low-dimensional conductors. Evidence for cou-

pling of the spin states of the copper and BEDT-TTF stacks is very clear, and we observe a crossover from magnetic insulator to metal under modest hydrostatic pressures. Further work, particularly on the low-temperature structure, is in progress.

ACKNOWLEDGMENTS

We thank the Science and Engineering Research Council, CNRS, NATO, and the British Council for partial support of this work. We thank Dr. F. L. Pratt for useful discussions and comments. Laboratoire de Cristallographie et Physique Cristalline and Laboratoire de Physico-Chimie Théorique are URAs numbers 144 and 503 of CNRS.

- ¹D. Jérôme, *Science* **252**, 1509 (1991).
- ²J. M. Williams, A. J. Schultz, U. Geiser, K. D. Carlson, A. M. Kini, H. H. Wang, W. K. Kwok, M. H. Whangbo, and J. E. Schirber, *Science* **252**, 1501 (1991).
- ³E. B. Yagubskii, I. F. Shchegolev, V. N. Laukhin, P. A. Kononovich, M. V. Kartsovnik, A. V. Zvarykhina, and L. I. Buranov, *Pis'ma Zh. Eksp. Teor. Fiz.* **39**, 12 (1984) [*JETP Lett.* **39**, 12 (1984)].
- ⁴S. S. P. Parkin, E. M. Engler, S. R. R., R. Lagier, V. Y. Lee, J. C. Scott, and R. L. Greene, *Phys. Rev. Lett.* **50**, 270 (1983).
- ⁵H. Urayama, H. Yamochi, G. Saito, K. Nozawa, T. Sugano, M. Kinoshita, S. Saito, K. Oshima, A. Kawamoto, and J. Tanaka, *Chem. Lett.* **1988**, 55.
- ⁶M. Kurmoo, T. Mallah, P. Day, I. Marsden, M. Allan, R. H. Friend, F. L. Pratt, W. Hayes, D. Chasseau, J. Gaultier, and G. Bravic, in *The Physics and Chemistry of Organic Superconductors*, edited by G. Saito and S. Kagoshima, Springer Proceedings in Physics Vol. 51 (Springer, Berlin, 1990), p. 290.
- ⁷T. Mallah, C. Hollis, S. Bott, K. Kurmoo, P. Day, M. Allan, and R. H. Friend, *J. Chem. Soc. Dalton Trans.* **1990**, 859.
- ⁸P. Day, M. Kurmoo, T. Mallah, I. R. Marsden, R. H. Friend, F. L. Pratt, W. Hayes, D. Chasseau, G. Bravic, and L. Ducasse, *J. Am. Chem. Soc.* **114**, 10722 (1992).
- ⁹M. Kurmoo, P. Day, M. Allan, and R. H. Friend, *Mol. Cryst. Liq. Cryst.* (to be published).
- ¹⁰A. V. Gudenko, V. B. Ginodman, V. E. Korotkov, A. V. Koshelap, N. D. Kushch, V. N. Laukhin, L. P. Rozenberg, A. G. Khomenko, R. P. Shibaeva, and E. B. Yagubskii, in *The Physics and Chemistry of Organic Superconductors* (Ref. 6), p. 365.
- ¹¹T. Mori, P. Wang, K. Imeada, T. Enoki, H. Inokuchi, F. Sakai, and G. Saito, *Synth. Met.* **27**, A451 (1989).
- ¹²T. Sugano, H. Takenouchi, D. Shiomi, and M. Kinoshita, *Synth. Met.* **55-57**, 2217 (1993).
- ¹³K. Susuki, J. Yamaura, N. Sugiyasu, T. Enoki, and G. Saito, *Synth. Met.* **55-57**, 2191 (1993).
- ¹⁴C. Bellitto, M. Bonamico, and G. Staulo, *Mol. Cryst. Liq. Cryst.* **232**, 155 (1993).
- ¹⁵Author, in *Superconductivity in Ternary Compounds*, edited by M. B. Maple and Ø. Fischer (Springer, Berlin, 1982), Vol. 34.
- ¹⁶Author, in *Superconductivity in Magnetic and Exotic Materials*, edited by T. Matsubara and A. Kotani (Springer, Berlin, 1984), Vol. 52.
- ¹⁷K. P. Sinha and S. L. Kakani, *Magnetic Superconductors* (Nova, New York, 1989).
- ¹⁸M. Kurmoo, D. Kanazawa, P. Day, I. R. Marsden, M. Allan, and R. H. Friend, *Synth. Met.* **55-57**, 2347 (1993).
- ¹⁹A. C. Massabni, O. R. Nascimento, K. Halvorson, and R. D. Willett, *Inorg. Chem.* **31**, 1779 (1992).
- ²⁰K. Waizumi, H. Masuda, H. Einaga, and N. Fukushima, *Chem. Lett.* **1993**, 1145.
- ²¹T. Mori, F. Sakai, G. Saito, and H. Inokuchi, *Chem. Lett.* **1987**, 927.
- ²²K. Bender, I. Hennig, D. Schweitzer, K. Dietz, H. Endres, and H. J. Keller, *Mol. Cryst. Liq. Cryst.* **108**, 359 (1984).
- ²³J. Larsen and C. Lenoir, *Synthesis* **2**, 134 (1988).
- ²⁴M. B. Inoue, Q. Fernando, and M. Inoue, *Synth. Met.* **41-43**, 2069 (1991).
- ²⁵L. Ducasse, A. Abderrabba, J. Hoarau, M. Pesquer, B. Gallois, and J. Gaultier, *J. Phys. C* **19**, 3085 (1986).
- ²⁶D. R. P. Guy and R. H. Friend, *J. Phys. E* **19**, 430 (1986).
- ²⁷M. J. Rosseinsky, M. Kurmoo, D. R. Talham, P. Day, D. Chasseau, and D. Watkin, *J. Chem. Soc.* **1988**, 88.
- ²⁸M. Kurmoo, M. J. Rosseinsky, P. Day, P. Auban, W. Kang, D. Jerome, and P. Batail, *Synth. Met.* **27**, A425 (1989).
- ²⁹K. E. Halvorson, C. Patterson, and R. D. Willett, *Acta Crystallogr. Sec. B* **46**, 508 (1990).
- ³⁰M. Apslund, S. Jagner, and M. Nilsson, *Acta Chem. Scand. A* **37**, 57 (1983).
- ³¹P. Guionneau, G. Bravic, J. Gaultier, D. Chasseau, M. Kurmoo, D. Kanazawa, and P. Day, *Acta Crystallogr. Sec. C* (to be published).
- ³²S. Hebrard, G. Bravic, J. Gaultier, D. Chasseau, M. Kurmoo, D. Kanazawa, and P. Day, *Acta Crystallogr. Sec. C* (to be published).
- ³³M. Kurmoo, P. Day, A. M. Stringer, J. A. K. Howard, L. Ducasse, F. L. Pratt, J. Singleton, and W. Hayes, *J. Mater. Chem.* (to be published).
- ³⁴H. Kobayashi, R. Kato, A. Kobayashi, Y. Nishio, K. Kajita, and W. Sasaki, *Chem. Lett.* **1986**, 833.
- ³⁵H. Mori, S. Tanaka, M. Oshima, T. Mori, Y. Murayama, and H. Inokuchi, *Bull. Chem. Soc. Jpn.* **63**, 2183 (1990).
- ³⁶I. D. Parker, R. H. Friend, M. Kurmoo, and P. Day, *J. Phys. Condens. Matter* **1**, 5681 (1989).
- ³⁷K. Kornelsen, J. Eldridge, H. H. Wang, and J. M. Williams, *Solid State Commun.* **74**, 501 (1990).
- ³⁸F. L. Pratt, W. Hayes, M. Kurmoo, and P. Day, *Synth. Met.* **27**, A 439 (1989).
- ³⁹M. R. Bond, T. J. Johnson, and R. D. Willett, *Can. J. Chem.* **66**, 963 (1988).
- ⁴⁰M. E. Lines, *J. Phys. Chem. Solids* **31**, 101 (1970).
- ⁴¹M. Kurmoo, D. Kanazawa, and P. Day, *Synth. Met.* **41-43**, 2123 (1991).

- ⁴²M. Kurmoo, D. Kanazawa, and P. Day, in *Mixed Valency Systems: Applications in Chemistry, Physics and Biology*, edited by K. Prassides (Kluwer, Dordrecht, 1990), p. 419.
- ⁴³C. Chow, K. Chang, and R. D. Willett, *J. Chem. Phys.* **59**, 2629 (1973).
- ⁴⁴T. Sugano, G. Saito, and M. Kinoshita, *Phys. Rev. B* **34**, 117 (1986).
- ⁴⁵T. M. Kite and J. E. Drunheller, *Magn. Res.* **54**, 253 (1983).
- ⁴⁶S. D. Obertelli, I. R. Marsden, R. H. Friend, M. Kurmoo, M. J. Rosseinsky, P. Day, F. L. Pratt, and W. Hayes, in *The Physics and Chemistry of Organic Superconductors* (Ref. 6), p. 181.
- ⁴⁷I. D. Parker, R. H. Friend, and A. E. Underhill, *Synth. Met.* **29**, F195 (1989).
- ⁴⁸I. D. Parker, R. H. Friend, P. Clemenson, and A. E. Underhill, *Nature* **324**, 547 (1986).

Crystal Structure and Magnetism of (BEDT-TTF)₂MCl₄ (BEDT-TTF = Bis(ethylenedithio)tetrathiafulvalene; M = Ga, Fe)

Mohamedally Kurmoo,^{*,†,‡} Peter Day,[†] Philippe Guionneau,[§] George Bravic,[§] Daniel Chasseau,[§] Laurent Ducasse,^{||} Margaret L. Allan,[⊥] Ian D. Marsden,[⊥] and Richard H. Friend[⊥]

The Royal Institution of Great Britain, 21 Albemarle Street, London W1X 4BS, U.K., Laboratoire de Cristallographie et de Physique Cristalline, CNRS, ERS 133, Université Bordeaux 1, 33405 Talence Cedex, France, Laboratoire de Physico-Chimie Théorique, CNRS, URA 503, Université Bordeaux 1, 33405 Talence Cedex, France, and Cavendish Laboratory, University of Cambridge, Madingley Road, Cambridge CB3 0HE, U.K.

Received February 21, 1996[Ⓢ]

The relation between crystal structure and bulk magnetic properties is investigated in the molecular charge transfer salts (BEDT-TF)₂MCl₄ (M = Ga, Fe). (BEDT-TTF)₂GaCl₄ crystallizes in the triclinic system. Its crystal structure consists of pairs of BEDT-TTF molecules arranged in layers with intermolecular S...S interactions. Band structure calculations predict semimetallic behavior contrary to the semiconductivity observed even under a pressure of 6 kbar ($\sigma(300\text{ K}, 1\text{ bar}) = 10^{-1}\text{ S cm}^{-1}$ and $E_A = 0.2\text{ eV}$). The static (Faraday and SQUID magnetometry) and spin (EPR) susceptibilities indicate low-dimensional Heisenberg antiferromagnetic behavior with the susceptibility tending to zero as the temperature approaches zero. The data are analyzed using several low-dimensional magnetic models and are best fitted to a model consisting of two different spin dimers ($\Delta_1 = 108\text{ K}$ and $\Delta_2 = 212\text{ K}$). The static magnetic susceptibility of (BEDT-TTF)₂FeCl₄ is modeled by a sum of Curie–Weiss ($S = 5/2$ for Fe(d⁵) and $\Theta = -4\text{ K}$), χ_{up} , and single dimer ($\Delta = 45\text{ K}$) parameters. The BEDT-TTF layers in these compounds thus behave as Mott–Hubbard-localized systems, and the interaction between the magnetic moment on the Fe with those on the organic layer is negligible.

Introduction

The transition from localized to delocalized ground states in inorganic and organic molecular systems has long been a subject of controversy.¹ In particular, for organic conductors the competition between several ground states is more delicate since it can be controlled by very slight differences in the crystal structures.^{2,3} Charge-transfer salts of the BEDT-TTF (BEDT-TTF = bis(ethylenedithio)tetrathiafulvalene) family, for example, embrace both localized and delocalized systems which display semiconducting, metallic, and superconducting electrical properties and Pauli paramagnetic, low-dimensional (1D and 2D) antiferromagnetic, and 3D-ordered (antiferromagnetic and weak ferromagnetic) ground states.⁴ Such a range of behaviors arises from the variety of crystal packing and electronic band structures. Thus, one of the dilemmas facing chemists trying to synthesize organic conductors and superconductors is that

they have exquisite control over the design of individual molecules but practically no control over designing molecular packing patterns in solid-state materials. We have been engaged in the past years in correlating the electrical and magnetic properties of BEDT-TTF charge-transfer salts with the crystal and electronic band structures with the aim of deriving synthetic guidelines.^{5–10} Our present conclusion is that despite notable advances in extending the range of packing motifs by tuning the size, shape, and the charge of the anions, there are still no general synthetic tools available for controlling the crystal structures.

Isostructural compounds have been obtained by choosing similar anions (e.g., I₃⁻, IBR₂⁻, AuI₂⁻).³ For example, several salts of the two superconducting phases (β and κ) have been synthesized and correlations between structures and supercon-

[†] The Royal Institute of Great Britain.

[‡] Present address: Institut de Physique et Chimie des Matériaux de Strasbourg, 23 rue de Loess, F-67037 Strasbourg Cedex, France.

[§] CRNS, ERS 1333.

^{||} CRNS, URA 503.

[⊥] University of Cambridge.

[Ⓢ] Abstract published in *Advance ACS Abstracts*, July 1, 1996.

- (1) (a) Mott, N. F. *Metal-Insulator Transitions*; 2nd ed.; Taylor Francis Publ.: London, 1990. (b) *Metal-Insulator Transition Revisited*; Edwards, P. P., Rao, C. N. R., Eds.; Taylor Francis Publ.: London, 1995.
- (2) (a) Ishiguro, T.; Yamaji, K. *Organic Superconductors*; Springer Verlag: Berlin, 1990. (b) *Organic Superconductivity*; Kresin, V. Z., Little, W., Eds.; Plenum: New York, 1990.
- (3) Williams, J. M.; Ferraro, J. R.; Thorn, R. J.; Carlson, K. D.; Geiser, U.; Wang, H. H.; Kini, A. M.; Whangbo, M.-H. *Organic Superconductors (including Fullerenes)*; Prentice Hall: Englewood Cliffs, NJ, 1992.
- (4) See for example: Proceedings of the International Conference on Synthetic Metals. *Synth. Met.* **1987**, *19*; **1989**, *27*; **1991**, *42*; **1993**, *56*; **1995**, *71*.

- (5) Day, P.; Kurmoo, M.; Mallah, T.; Marsden, I. R.; Friend, R. H.; Pratt, F. L.; Hayes, W.; Chasseau, D.; Gaultier, J.; Bravic, G.; Ducasse, L. *J. Am. Chem. Soc.* **1992**, *114*, 10722.
- (6) Marsden, I. R.; Allan, M. L.; Friend, R. H.; Kurmoo, M.; Kanazawa, D.; Day, P.; Chasseau, D.; Bravic, G.; Ducasse, L. *Phys. Rev.* **1994**, *B50*, 2118.
- (7) Kurmoo, M.; Day, P.; Stringer, A. M.; Howard, J. A. K.; Ducasse, L.; Pratt, F. L.; Singleton, J.; Hayes, W. *J. Mater. Chem.* **1993**, *3*, 1161.
- (8) Rosseinsky, M. J.; Kurmoo, M.; Day, P.; Marsden, I. R.; Friend, R. H.; Chasseau, D.; Gaultier, J.; Bravic, G.; Ducasse, L. *J. Mater. Chem.* **1993**, *3*, 801.
- (9) Bellitto, C.; Bonamico, M.; Fares, V.; Federici, F.; Righini, G.; Kurmoo, M.; Day, P. *Chem. Mater.* **1995**, *7*, 1475.
- (10) Kurmoo, M.; Graham, A. W.; Day, P.; Coles, S. J.; Hursthouse, M. B.; Caulfield, J. L.; Singleton, J.; Pratt, F. L.; Hayes, W.; Ducasse, L.; Guionneau, P. *J. Am. Chem. Soc.* **1995**, *117*, 12209.
- (11) (a) Yamochi, H.; Komatsu, T.; Matsukawa, N.; Saito, G.; Mori, T.; Kusunoki, M.; Sakaguchi, K. *J. Am. Chem. Soc.* **1993**, *115*, 11319. (b) Williams, J. M.; Schultz, A. J.; Wang, H. H.; Carlson, K. D.; Beno, M. A.; Emge, T. J.; Geiser, U.; Hawley, M. E.; Gray, K. E. *Physica* **1986**, *143B*, 346. (c) Saito, G.; Urayama, H.; Yamochi, H.; Oshima, K. *Synth. Met.* **1988**, *27*, A331.

ducting critical temperatures have been drawn.¹¹ Similar success was experienced for other phases with linear anions such as α and α' , which were found to have metal–semiconductor and semiconductor–semiconductor transitions, respectively. Similarly, it is possible to replace the donor BEDT-TTF in α -(BEDT-TTF)₂I₃ by BEDT-TSF and BEDT-STF (BEDT-TSF = bis(ethylenedithio)tetrathiafulvalene; BEDT-STF = bis(ethylenedithio)diselenadithiafulvalene).¹² We have employed such a strategy to study the interaction between localized moments on the anion and the electrons in the conduction band formed by the organic donor. Thus we have used GaCl₄⁻ as the nonmagnetic counterpart to the magnetic FeCl₄⁻. In both cases salts of a 2:1 stoichiometry with BEDT-TTF are obtained, which have similar structures and behave as semiconductors. Recently, Naito et al.¹³ have used the same two anions to crystallize isostructural salts with BEDS-TTF (BEDS-TTF = bis(ethylenediselenatetra)thiafulvalene), where the GaCl₄⁻ salt is a superconductor ($T_c \sim 8$ K) and the FeCl₄⁻ salt shows a metal–insulator transition at ca. 8 K. However, the BEDT-TTF salts are not isostructural with the BEDS-TTF salts.

We have reported the structure and properties of (BEDT-TTF)₂FeCl₄ previously and have given a brief note on the electrical and magnetic properties of (BEDT-TTF)₂GaCl₄.^{14,15} We describe here the full crystal structure determination and electronic band structure calculation, electrical properties at high pressure, and the magnetic properties of (BEDT-TTF)₂GaCl₄. We also re-examine the magnetic properties of (BEDT-TTF)₂FeCl₄ considering our present findings and correlate the results with the crystal structures.

Experimental Section

Synthesis. BEDT-TTF, prepared by the method of Larsen and Lenoir,¹⁶ was recrystallized twice from chloroform before use. [(CH₃)₄N]GaCl₄ was obtained as colorless needles by reacting [(CH₃)₄NCl] and GaCl₃ in degassed absolute ethanol under an inert atmosphere of argon. The purity was checked by chemical analysis. The charge-transfer salt was obtained by electrocrystallization of BEDT-TTF (20 mg) in CH₂Cl₂ (50 mL) containing [(CH₃)₄N]GaCl₄ (200 mg). A three-compartment cell equipped with platinum wire (0.5 mm) electrodes was used, with a constant applied current of 1–2 μ A for 2 weeks. The crystals of (BEDT-TTF)₂GaCl₄ were black shiny needles of maximum dimensions 4 \times 0.2 \times 0.1 mm³.

X-ray Crystal Structure. After the screening of many twinned crystals under the microscope and by Weissenberg photographs, a single crystal of dimension 0.46 \times 0.1 \times 0.06 mm³ was found to give sharp and single Bragg reflections and was thus selected for intensity data collection using a Nonius CAD-4 with graphite-monochromatized Cu K α ($\lambda = 1.5418$ Å) radiation. The unit cell parameters (Table 1) were obtained from accurately measured angles of 20 intense reflections with $13 < 2\theta < 51^\circ$. The space group was found unambiguously to be $P\bar{1}$. Intensities of 11 720 reflections were measured at room temperature and reduced to give 10 844 independent ones. Three reflections were monitored hourly, and a maximum variation of intensity or position of 0.05% was observed. Data were corrected for Lorentz and polarization. An empirical absorption correction based on ψ scans was applied.

The crystal structure was solved by direct methods using the package SIR88.¹⁷ The hydrogen atoms were placed in theoretical positions

Table 1. Crystallographic Data for (BEDT-TTF)₂GaCl₄

C ₂₀ H ₁₆ S ₁₆ GaCl ₄	$f_w = 980.9$
$a = 31.911(6)$ Å	space group = $P\bar{1}$ (No. 2)
$b = 16.580(4)$ Å	$T = 298$ K
$c = 6.645(2)$ Å	$\lambda = 1.5418$ Å
$\alpha = 98.15(2)^\circ$	$\rho_{\text{calcd}} = 1.878$ g cm ⁻³
$\beta = 85.60(2)^\circ$	$\mu = 127.23$ cm ⁻¹
$\gamma = 90.55(2)^\circ$	$R = 4.7\%$
$V = 3470$ Å ³	$R_w = 4.8\%$
$Z = 4$	

$$^a R = \sum |F_o| - F_c / \sum |F_o|. R_w = [\sum w(|F_o| - F_c)|^2 / \sum w|F_o|]^2. w = 1/[\sigma^2 + 0.005F^2].$$

(C–H = 1 Å) and refined isotropically in the last cycle. The carbon, sulfur, gallium, and chlorine atoms were refined anisotropically. The atomic positions and isotropic or anisotropic thermal factors were obtained by the least-squares method to a final $R = 0.047$ and $R_w = 0.048$, using 3295 reflections with $I \geq 3\sigma(I)$ for 835 parameters. Difference Fourier maps at the end of the refinement give residual electron density of less than ± 1 e/Å³. The considerable number of parameters with so few reflections results in high standard deviations. Attempts to refine with more reflections by taking all those larger than $2\sigma(I)$ results in a poorer reliability factor (7%) and similar accuracy in bond lengths and angles.

Transfer Integrals and Band Structure Calculation. The transfer integrals, band structure, and Fermi surface of (BEDT-TTF)₂GaCl₄ have been calculated within the semi-empirical extended Hückel theory¹⁸ using a double- ζ basis set and tight binding.¹⁹ We have checked that the results presented here are very close to the ones obtained using a single- ζ basis set.

Electrical Transport. Conductivity measurements were limited to the long axis (crystallographic c -axis) of the needle crystals. Data were collected by the four-probe method using both ac and dc techniques. No apparent difference was noted. Pressure experiments were performed in a clamp cell with a 1:1 mixture of pentane–isopentane as the pressure-transmitting fluid.²⁰ The contacts were made with 25 μ m gold wire onto pre-evaporated gold pads.

Electron Spin Resonance. Spectra were collected on several single crystals as a function of angle and temperature. Crystals were mounted on a cut flat face of Spectrosil quartz rods using a smear of silicone grease. The spectrometer was a Varian E9 with a cavity operating in a TE₁₀₂ mode at 9 GHz and 100 kHz field modulation. Variable temperatures (4–300 K) were effected by use of a continuous-flow Oxford Instruments cryostat and an ITC-4 temperature controller.

Static Magnetic Susceptibility. Data were recorded on cooling and warming two independent batches of randomly oriented crystals (6.55 and 7.16 mg) as well as for different applied magnetic fields on a homemade Faraday balance employing a Cahn microbalance. A third batch was measured on a MPMS-7 SQUID magnetometer in fields ranging from 10 G to 2 T. The data were corrected for the core diamagnetism estimated from the sums of Pascal constants amounting to -4.85×10^{-4} emu/formula unit.

Results

Crystal Structure. (BEDT-TTF)₂GaCl₄ crystallizes in the triclinic system $P\bar{1}$ (Table 1). The crystal habit is needlelike, parallel to the crystallographic c axis. The labeling scheme adopted is shown in Figure 1. The atomic coordinates and selected bond lengths and angles are given in Tables 2 and 3. The asymmetric unit contains four crystallographically independent BEDT-TTF molecules and two GaCl₄⁻ ions. With $Z = 2$ the unit cell (Figure 2) contains four formula units of (BEDT-TTF)₂GaCl₄.

The structure consists of stacks of nonplanar BEDT-TTF molecules along b separated by GaCl₄⁻ anions in the a direction.

- Inokuchi, M.; Tajima, H.; Kobayashi, A.; Ohta, T.; Kuroda, H.; Kato, R.; Naito, T.; Kobayashi, H. *Bull. Chem. Soc. Jpn.* **1995**, *68*, 547.
- (a) Naito, T. Ph.D. Thesis, Toho University, Japan, 1994. (b) Kobayashi, H.; Udagawa, T.; Tomita, H.; Bun, K.; Naito, T.; Kobayashi, A. *Chem. Lett.* **1993**, 1559. (c) Kobayashi, A.; Udagawa, T.; Tomita, H.; Naito, T.; Kobayashi, H. *Chem. Lett.* **1993**, 2179.
- Mallah, T.; Hollis, C.; Bott, S.; Kurmoo, M.; Day, P.; Allan, M.; Friend, R. H. *J. Chem. Soc., Dalton Trans.* **1990**, 859.
- Kurmoo, M.; Allan, M. L.; Friend, R. H.; Chasseau, D.; Bravic, G.; Day, P. *Synth. Met.* **1991**, *41*, 2127.
- Larsen, J.; Lenoir, C. *Synthesis* **1988**, 2, 134.
- Burla, M. C.; Camalli, M.; Cascarano, G.; Giacovazzo, C.; Polidori, G.; Spagna, R.; Viterbo, J. *J. Appl. Crystallogr.* **1989**, *22*, 389.

- (18) (a) Ducasse, L.; Abderrabba, A.; Hoarau, J.; Pesquer, M.; Gallois, B.; Gaultier, J. *J. Phys. C, Solid State Phys.* **1986**, *19*, 3805. (b) Hoffmann, R. *J. Chem. Phys.* **1963**, *39*, 1397.
- (19) Ducasse, L.; Fritsch, A. *Solid State Commun.* **1994**, *91*, 201.
- (20) Guy, D. R. P.; Friend, R. H. *J. Phys. E: Sci. Instrum.* **1986**, *19*, 430.

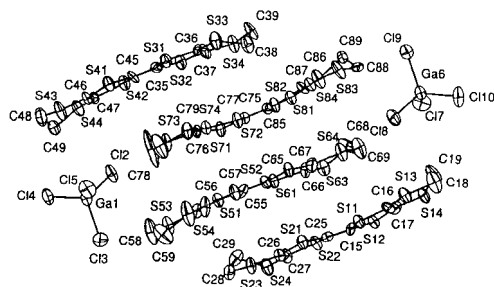


Figure 1. Labeling scheme adopted showing the thermal vibration ellipsoids.

The BEDT-TTF molecules in one stack form close S...S contacts with molecules in neighboring stacks along *c* to form layers. Molecules in each layer are parallel to one another.

The thermal parameters of the four independent BEDT-TTF molecules become progressively larger from the center of the molecules to the $\text{H}_2\text{C}-\text{CH}_2$ ends (Figure 1). The bond lengths and angles of the central TTF part of the molecules are thus more accurate than those in the outer parts. Some ethylene groups are disordered. The four crystallographically independent molecules belong to the same stack, and there are four different modes of overlap and average intermolecular distances between nearest neighbors (Figure 3). The average distance, calculated from the mean plane defined by the four inner sulfur atoms and the two central carbon atoms, between molecules I and IV is 3.35 Å, and the overlapping mode is bond-over-ring, which is quite favorable for large transfer integrals and thus high electrical conductivity. Between II and III, the distance is slightly longer, 3.41 Å, and the overlap is almost identical to the I/IV pair. The molecules in each dimer are parallel but translated along their long axes.

In contrast, the interplanar distances between I and II and between III and IV are much longer than the other two, 3.6 and 4.0 Å, respectively. The overlap between the latter pairs is also quite different; their long axes are twisted from one another by 34°. These irregular modes of overlap within the stacks lead to a strongly dimerized and alternate structure, with short intradimer and long interdimer separations. Each dimer is rotated with respect to its neighbors along the normal to the plane of the molecules. This structure resembles those reported for the $(\text{BEDT-TTF})_2\text{X}$ set, where X is FeCl_4^- ,¹⁴ InBr_4^- , InI_4^- , and GaI_4^- .²¹ The difference is that the latter compounds have only two independent molecules in the asymmetric unit and thus no alternation in interdimer distances. In the GaCl_4^- salt one of the molecules in the stack is translated along its long axis so that there are some short atomic contacts between molecules from adjacent layers. These molecules then interrupt the regular spacing of the anions. Thus, there is a pair of anions in the cavities formed by the ethylenic hydrogen atoms. In the FeCl_4^- and other MX_4^- salts there is no offset of the molecules in a layer, and we have a regular spatial distribution of anions with one anion per cavity.

The mode of overlap of the twisted molecules in $(\text{BEDT-TTF})_2\text{GaCl}_4$ is the same as that observed in $\alpha'-(\text{BEDT-TTF})_2\text{X}$, X = CuCl_2^- , $\text{Ag}(\text{CN})_2^-$, $\text{Au}(\text{CN})_2^-$, and AuBr_2^- ,²²⁻²⁵ except

that in this series all the molecules are twisted by 32° with respect to their neighbors. In $(\text{BEDT-TTF})_2\text{GaCl}_4$ several short interstack S...S distances between equivalent molecules translated along *c* (3.40–3.52 Å) were observed to be less than the sum of van der Waals radii (S...S = 3.6 Å).

The C=C bond lengths range from 1.31 to 1.37 Å, from which one may assign charges between 0 and 0.5+ by comparison with neutral BEDT-TTF (1.32 Å) and $\text{BEDT-TTF}^{1/2+}$ (1.36 Å),^{14,26} although the stoichiometry requires that the average charge per BEDT-TTF molecule be 0.5+. However it is possible that the lattice contains molecules of different charge but, because of the large number of structural parameters compared to the number of observable, the accuracy of the structure determination is too low to reach a conclusive judgement. Infrared reflectivity on a single crystal with the incident beam parallel and perpendicular to the needle axis shows in both cases a broad band centered at $\sim 1375\text{ cm}^{-1}$ with a width of $\sim 40\text{ cm}^{-1}$. This band can be assigned to the C=C mode of the BEDT-TTF molecules. Since there are three such bonds per molecules and eight molecules per cell in addition to the low site symmetry of the molecules, it is very difficult to assign exact charge distribution among the independent molecules.

The GaCl_4^- ions are almost tetrahedral with an average bond length of 2.164 Å. For each of the GaCl_4^- anions, one of the Ga-Cl bond length (average 2.185 Å) is longer than the other three. The two independent GaCl_4^- ions have similar environments but slightly different distances between the chlorine atoms and the thioethylene surrounding. Two short anion-cation distances (3.43 Å, Cl(20)...S(730); 3.481 Å, Cl(80)...S(640)) were observed between the sulfur atoms bonded to the disordered ethylene group (C-C distances of 1.31 and 1.40 Å).

Band Structure. The values of the intermolecular transfer integrals are indicated in Figure 4. The peculiar stacking of the BEDT-TTF molecules induces a strong alternation of the intrastack transfer integrals: the ratio of the intra- to interdimer integrals amounts to ~ 6 . The interstack integrals between the molecule I and its neighbors are very similar to the ones arising from molecule IV. On the other hand, the transfer integrals from molecule III are significantly larger than the ones from molecule II.

The corresponding band structure and Fermi surface are depicted in Figure 5. The highest occupied molecular orbital of the four independent molecules in the unit cell leads to four bands which are $3/4$ filled. The large gap between the two upper and the two lower bands is a direct consequence of the alternating intrastack transfer integrals. The existence of sizable interactions along *c*, roughly similar to the interdimer intrastack integrals, induces a dispersion along c^* . As a consequence, the Fermi level cuts the two upper bands, so that the Fermi surface has both electron sheets and hole orbits which indicates semimetallic character. It is interesting that the band structure and Fermi surface are similar to those calculated for the superconductor $(\text{BEDS-TTF})_2\text{GaCl}_4$ and yet it is a semiconductor.²⁷

- (21) (a) Beno, M. A.; Cox, D. D.; Williams, J. M.; Kwak, J. F. *Acta Crystallogr.* **1984**, C40, 1334. (b) Geiser, U.; Wang, H. H.; Schluter, J. A.; Hallenbeck, S. L.; Allen, T. J.; Chen, M. Y.; Kao, H. C. I.; Carlson, K. D.; Gerdorn, L. E.; Williams, J. M. *Acta Crystallogr.* **1988**, C44, 1544.
- (22) Kurmoo, M.; Talham, D. R.; Day, P.; Howard, J. A. K.; Stringer, A. M.; Obertelli, D. S.; Friend, R. H. *Synth. Met.* **1988**, 22, 415.

- (23) Guionneau, P.; Rahal, M.; Bravic, G.; Gaultier, J.; Mellado, J. M.; Chasseau, D.; Ducasse, L.; Kurmoo, M.; Day, P. *J. Mater. Chem.* **1995**, 5, 1639.
- (24) Beno, M. A.; Firestone, M. A.; Leung, P. C. W.; Sowa, L. M.; Wang, H. H.; Williams, J. M.; Whangbo M.-H. *Solid. State Commun.* **1986**, 57, 735.
- (25) Amberger, E.; Fuch, H.; Polborn, K. *Angew. Chem.* **1986**, 25, 729.
- (26) (a) Abboud, K. A.; Clevenger, M. B.; de Oliveira, G. F.; Talham, D. R. *J. Chem. Soc., Chem. Commun.* **1993**, 1560. (b) Chou, L.-K.; Quijada, M. A.; Clevenger, M. B.; de Oliveira, G. F.; Abboud, K. A.; Tanner, D. B.; Talham, D. R. *Chem. Mater.* **1995**, 7, 530.
- (27) Montgomery, L. K.; Burgen, T.; Huffman, J. C.; Ren, J.; Whangbo, M.-H. *Physica* **1994**, 219C, 490.

Table 2. Fractional Atomic Coordinates and B_{eq} Values (\AA^2) for $(\text{BEDT-TTF})_2\text{GaCl}_4$ at 298 K

	x/a	y/b	z/c	B_{eq}^a		x/a	y/b	z/c	B_{eq}^a
Ga(10)	0.01818(6)	0.2232(1)	0.6409(3)	3.6(1)	C(480)	0.0687(5)	-0.046(1)	0.709(3)	4.7(9)
Cl(20)	0.0763(1)	0.2379(3)	0.7907(7)	4.6(2)	C(490)	0.0693(5)	0.015(1)	0.891(3)	4.4(9)
Cl(30)	-0.0154(2)	0.3392(3)	0.6940(8)	4.7(2)	S(440)	0.1186(1)	0.0388(3)	0.9903(7)	3.8(2)
Cl(40)	-0.0210(1)	0.1342(3)	0.7707(8)	4.7(2)	C(470)	0.1499(4)	0.0438(9)	0.770(2)	2.4(6)
Cl(50)	0.0314(2)	0.1898(3)	0.3167(7)	5.3(2)	S(420)	0.1996(1)	0.0861(3)	0.8083(6)	3.1(2)
Ga(60)	0.50294(6)	0.7865(1)	0.2676(3)	3.8(1)	S(510)	0.1558(1)	0.5348(3)	0.5830(6)	3.1(2)
Cl(70)	0.4919(2)	0.8260(3)	0.5919(7)	5.3(2)	C(560)	0.1197(5)	0.4974(8)	0.408(2)	2.5(6)
Cl(80)	0.4436(1)	0.7654(3)	0.1331(7)	4.4(2)	S(530)	0.0724(1)	0.4635(3)	0.5070(7)	4.4(2)
Cl(90)	0.5378(1)	0.6710(3)	0.2198(8)	4.6(2)	C(580)	0.0477(6)	0.424(1)	0.279(3)	6.7(9)
Cl(100)	0.5384(2)	0.8767(3)	0.1265(8)	5.9(3)	C(590)	0.0567(6)	0.449(1)	0.090(3)	5.9(9)
S(110)	0.2805(1)	0.8985(3)	0.3093(6)	2.8(2)	S(540)	0.1071(2)	0.4610(4)	-0.0072(7)	6.3(3)
C(160)	0.3285(4)	0.9445(9)	0.355(2)	2.8(7)	C(570)	0.1336(5)	0.498(1)	0.212(2)	4.1(9)
S(130)	0.3613(1)	0.9494(3)	0.1353(7)	3.6(2)	S(520)	0.1833(1)	0.5368(3)	0.1533(6)	3.4(2)
C(180)	0.4082(6)	0.997(1)	0.232(3)	7.1(9)	C(550)	0.1930(5)	0.5649(8)	0.405(2)	2.2(6)
C(190)	0.4180(6)	0.988(1)	0.434(3)	5.4(9)	C(650)	0.2288(4)	0.6051(9)	0.464(2)	2.4(6)
S(140)	0.3806(1)	1.0205(3)	0.6418(7)	3.6(2)	S(610)	0.2387(1)	0.6351(3)	0.7153(6)	2.8(2)
C(170)	0.3355(5)	0.9715(8)	0.547(2)	2.7(6)	C(660)	0.2859(5)	0.6867(9)	0.660(2)	2.6(6)
S(120)	0.2958(1)	0.9565(3)	0.7358(6)	2.6(2)	S(630)	0.3080(1)	0.7361(3)	0.8776(7)	3.7(2)
C(150)	0.2625(4)	0.9065(8)	0.564(2)	1.9(6)	C(680)	0.3608(5)	0.742(1)	0.778(3)	5.3(9)
C(250)	0.2282(5)	0.8700(8)	0.626(2)	3.0(7)	C(690)	0.3696(6)	0.764(1)	0.585(3)	5.9(9)
S(210)	0.1954(1)	0.8143(3)	0.4502(6)	3.0(2)	S(640)	0.3465(1)	0.7185(3)	0.3642(7)	4.0(2)
C(260)	0.1550(4)	0.7938(9)	0.629(2)	2.6(7)	C(670)	0.2989(5)	0.6820(9)	0.470(3)	3.4(8)
S(230)	0.1122(1)	0.7404(3)	0.5301(7)	3.5(2)	S(620)	0.2691(1)	0.6269(3)	0.2866(6)	3.1(2)
C(280)	0.0815(5)	0.713(1)	0.756(3)	3.8(8)	S(710)	0.2451(1)	0.4009(3)	0.6672(6)	2.8(2)
C(290)	0.1056(6)	0.7099(9)	0.941(2)	3.4(8)	C(760)	0.2165(4)	0.3401(8)	0.479(2)	2.1(6)
S(240)	0.1274(1)	0.8074(3)	1.0371(7)	3.9(2)	S(730)	0.1717(1)	0.2954(3)	0.5840(7)	3.6(2)
C(270)	0.1612(5)	0.8213(9)	0.827(2)	3.1(7)	C(780)	0.1480(8)	0.260(2)	0.365(4)	13(2)
S(220)	0.2086(1)	0.8695(3)	0.8794(6)	2.7(2)	C(790)	0.1595(6)	0.266(1)	0.173(3)	6.6(9)
S(310)	0.2706(1)	0.1135(3)	0.2365(6)	2.7(2)	S(740)	0.2072(1)	0.2965(3)	0.0703(7)	3.6(2)
C(360)	0.3158(4)	0.1703(8)	0.284(2)	2.2(6)	C(770)	0.2308(4)	0.3443(8)	0.285(2)	2.8(7)
S(330)	0.3482(2)	0.1834(3)	0.0667(7)	4.4(2)	S(720)	0.2737(1)	0.4018(3)	0.2363(6)	2.8(2)
C(380)	0.3775(5)	0.271(1)	0.163(3)	4.5(9)	C(750)	0.2837(4)	0.4279(8)	0.494(2)	2.2(6)
C(390)	0.3976(4)	0.261(1)	0.357(3)	4.8(9)	C(850)	0.3195(4)	0.4661(8)	0.547(2)	2.2(6)
S(340)	0.3629(1)	0.2576(3)	0.5790(7)	4.1(2)	S(810)	0.3585(1)	0.4920(3)	0.3696(6)	2.8(2)
C(370)	0.3222(4)	0.199(1)	0.477(2)	3.5(7)	C(860)	0.3956(4)	0.5205(9)	0.551(2)	2.2(6)
S(320)	0.2840(1)	0.1731(3)	0.6616(6)	3.1(2)	S(830)	0.4437(1)	0.5527(3)	0.4423(7)	4.1(2)
C(350)	0.2526(4)	0.1172(9)	0.495(2)	2.8(7)	C(880)	0.4667(5)	0.6034(9)	0.669(3)	3.6(8)
C(450)	0.2166(4)	0.0832(9)	0.554(2)	2.2(6)	C(890)	0.4627(5)	0.5570(9)	0.845(3)	3.0(8)
S(410)	0.1827(1)	0.0299(3)	0.3862(6)	3.1(2)	S(840)	0.4108(1)	0.5497(3)	0.9563(7)	4.2(2)
C(460)	0.1418(4)	0.0168(9)	0.570(2)	2.7(6)	C(870)	0.3837(4)	0.5188(9)	0.745(2)	1.8(5)
S(430)	0.0966(1)	-0.0247(3)	0.4804(7)	4.5(2)	S(820)	0.3315(1)	0.4893(3)	0.8004(6)	3.1(2)

$$^a B_{eq} = \frac{1}{3} \sum_i \sum_j \beta_i \beta_j a_i a_j$$

Electrical Transport. Conductivity measurements on several crystals show semiconducting behavior with a room-temperature value of $10^{-1} \text{ S cm}^{-1}$ (Figure 6) and an activation energy of 0.2 eV. Applying pressure increases the conductivity slightly while the activation energy remains constant up to 6 kbar. The room-temperature conductivity and activation energy are comparable to those of $(\text{BEDT-TTF})_2\text{FeCl}_4$ and $(\text{BEDT-TTF})_2\text{InBr}_4$ but quite different from $(\text{BEDT-TTF})_2\text{GaCl}_4$. The latter has surprisingly lower conductivity but a smaller activation energy.

Magnetism. The magnetic properties have been studied on a single crystal by EPR and on polycrystalline samples by Faraday and SQUID magnetometry. The EPR results will be presented first, followed by the static susceptibility results.

Electron Paramagnetic Resonance. At every temperature and crystal orientation the spectrum consists of a single Lorentzian signal, consistent with the low conductivity of the sample. The temperature dependence of the g -value and line width of the resonance line along three almost orthogonal axes is shown in Figures 7 and 8. Between 30 and 300 K the g -values are temperature independent and the line widths decrease smoothly. Below 30 K there is a gradual lowering of the g -value and a sharpening of the line width along two orientations but a broadening along the third axis. This is accompanied by an increase of the intensity of the resonance line along all three axes. The anomalies below 30 K may be due to small amount of paramagnetic impurities (see static susceptibility data below).

Static Susceptibility. At room temperature the susceptibility of $(\text{BEDT-TTF})_2\text{GaCl}_4$ is $8 \times 10^{-4} \text{ emu/formula unit}$. It increases to a broad maximum of $1.3 \times 10^{-3} \text{ emu/formula unit}$ at 80 K and shows a small Curie contribution at low temperatures (Figure 9). By removal of the latter (which is equivalent to $\sim 0.8\% S = 1/2$ spins) the intrinsic susceptibility of the $(\text{BEDT-TTF})_2\text{GaCl}_4$ crystals can be seen to tend to a value of zero emu/formula unit as the temperature approaches zero. The magnitude of the Curie tail is sample dependent; the bigger the crystals the smaller the Curie contribution, thus suggesting that it may originate from ends effects. For convenience, as will be shown later, the susceptibility is best discussed per unit cell as the content of the cell is eight molecules with a total of four spins, that is, two pairs of spin dimers ($S = 1/2$).

Discussion

The anion GaCl_4^- is diamagnetic with an effective volume between that of ClO_4^- and InBr_4^- and close to that of FeCl_4^- . Thus it should be an ideal diamagnetic diluent to replace the paramagnetic ($S = 5/2$) FeCl_4^- in $(\text{BEDT-TTF})_2\text{FeCl}_4$ since it satisfies the requirements of size, shape, and charge. The structure of $(\text{BEDT-TTF})_2\text{GaCl}_4$ contains dimers of BEDT-TTF which give rise to alternating weak and strong interdimer and intradimer transfer integrals along the stacks of face to face cations. Nevertheless, the band structure calculated within the extended Hückel formalism from the observed crystal structure predicts a semimetallic rather than the observed semiconducting

(BEDT-TTF)₂GaCl₄

Inorganic Chemistry, Vol. 35, No. 16, 1996 4723

Table 3. Selected Bond Lengths (Å) and Angles (deg)

GaCl ₄ ⁻			
Ga(10)-Cl(20)	2.167(5)	Ga(60)-Cl(70)	2.164(6)
Ga(10)-Cl(30)	2.182(6)	Ga(60)-Cl(80)	2.160(5)
Ga(10)-Cl(40)	2.155(5)	Ga(60)-Cl(90)	2.195(6)
Ga(10)-Cl(50)	2.157(6)	Ga(60)-Cl(100)	2.144(6)
Cl(20)-Ga(10)-Cl(30)	108.7(2)	Cl(70)-Ga(60)-Cl(80)	109.7(2)
Cl(20)-Ga(10)-Cl(40)	109.8(2)	Cl(70)-Ga(60)-Cl(90)	108.9(2)
Cl(20)-Ga(10)-Cl(50)	110.1(2)	Cl(70)-Ga(60)-Cl(100)	110.2(2)
Cl(30)-Ga(10)-Cl(40)	108.0(2)	Cl(80)-Ga(60)-Cl(90)	108.1(2)
Cl(30)-Ga(10)-Cl(50)	108.4(2)	Cl(80)-Ga(60)-Cl(100)	110.1(2)
Cl(40)-Ga(10)-Cl(50)	111.7(2)	Cl(90)-Ga(60)-Cl(100)	109.8(2)
BEDT-TTF I			
C(150)-C(250)	1.31(2)	C(250)-S(210)	1.78(2)
C(150)-S(110)	1.73(2)	S(210)-C(260)	1.75(2)
S(110)-C(160)	1.73(2)	C(260)-C(270)	1.36(2)
C(160)-C(170)	1.33(2)	C(270)-S(220)	1.74(2)
C(170)-S(120)	1.75(2)	S(220)-C(250)	1.75(2)
S(120)-C(150)-S(110)	115.6(8)	S(220)-C(250)-S(210)	112.0(9)
C(150)-S(110)-C(160)	95.1(7)	C(250)-S(210)-C(260)	97.0(7)
S(110)-C(160)-C(170)	117(1)	S(210)-C(260)-C(270)	116(1)
C(160)-C(170)-S(120)	118(1)	C(260)-C(270)-S(220)	118(1)
C(170)-S(120)-C(150)	94.2(7)	C(270)-S(220)-C(250)	97.0(8)
BEDT-TTF II			
C(350)-C(450)	1.33(2)	C(450)-S(410)	1.76(1)
C(350)-S(310)	1.76(2)	S(410)-C(460)	1.75(2)
S(310)-C(360)	1.74(2)	C(460)-C(470)	1.38(2)
C(360)-C(370)	1.33(2)	C(470)-S(420)	1.75(2)
C(370)-S(320)	1.76(2)	S(420)-C(450)	1.73(2)
S(320)-C(350)-S(310)	114.1(9)	S(420)-C(450)-S(410)	113.7(8)
C(350)-S(310)-C(360)	95.2(7)	C(450)-S(410)-C(460)	96.7(7)
S(310)-C(360)-C(370)	118(1)	S(410)-C(460)-C(470)	116(1)
C(360)-C(370)-S(320)	116(1)	C(460)-C(470)-S(420)	116(1)
C(370)-S(320)-C(350)	96.7(8)	C(470)-S(420)-C(450)	97.0(7)
BEDT-TTF III			
C(550)-C(650)	1.37(2)	C(650)-S(610)	1.73(2)
C(550)-S(510)	1.73(2)	S(610)-C(660)	1.76(2)
S(510)-C(560)	1.75(2)	C(660)-C(670)	1.29(2)
C(560)-C(570)	1.34(2)	C(670)-S(620)	1.74(2)
C(570)-S(520)	1.74(2)	S(620)-C(650)	1.75(2)
S(520)-C(550)-S(510)	115.9(9)	S(620)-C(650)-S(610)	114.6(8)
C(550)-S(510)-C(560)	95.9(7)	C(650)-S(610)-C(660)	95.4(7)
S(510)-C(560)-C(570)	114(1)	S(610)-C(660)-C(670)	116(1)
C(560)-C(570)-S(520)	120(1)	C(660)-C(670)-S(620)	119(1)
C(570)-S(520)-C(550)	93.8(8)	C(670)-S(620)-C(650)	94.2(8)
BEDT-TTF IV			
C(750)-C(850)	1.35(2)	C(850)-S(810)	1.74(2)
C(750)-S(710)	1.72(2)	S(810)-C(860)	1.77(2)
S(710)-C(760)	1.79(2)	C(860)-C(870)	1.32(2)
C(760)-C(770)	1.35(2)	C(870)-S(820)	1.72(2)
C(770)-S(720)	1.70(2)	S(820)-C(850)	1.74(2)
S(720)-C(750)-S(710)	115.3(9)	S(820)-C(850)-S(810)	114.5(8)
C(750)-S(710)-C(760)	94.5(7)	C(850)-S(810)-C(860)	94.8(7)
S(710)-C(760)-C(770)	115(1)	S(810)-C(860)-C(870)	118(1)
C(760)-C(770)-S(720)	120(1)	C(860)-C(870)-S(820)	116(1)
C(770)-S(720)-C(750)	94.7(7)	C(870)-S(820)-C(850)	95.7(7)

behavior. Evidently the localized electron behavior of (BEDT-TTF)₂GaCl₄ cannot be accounted for by the one-electron approach which supposes that the insulating character is mainly driven by symmetry considerations and band filling. Thus, semiconducting character is predicted for $3/4$ filled bands and

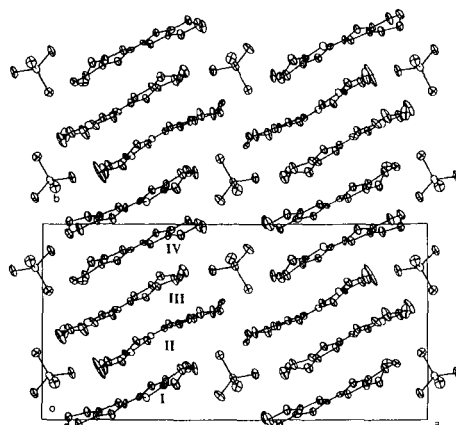
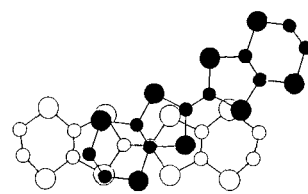
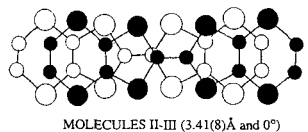


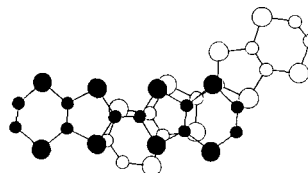
Figure 2. View of the unit cell along *c* showing the distortion of the molecules from planarity and the disorder of the ethylene groups.



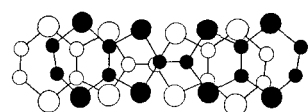
MOLECULES I-II (3.6(1)Å and 4°)



MOLECULES II-III (3.41(8)Å and 0°)



MOLECULES III-IV (4.0(2)Å and 4°)



MOLECULES I-IV (3.35(3)Å and 0°)

Figure 3. Modes of overlap between nearest-neighbor molecules.

is indeed found in (MDT-TTF)₄Pt(CN)₄·2H₂O,²⁸ whose unit cell likewise contains 4 molecules with an average charge of $1/2$ +. In this case the observed semiconducting state comes from a combination of a large ratio (~3) of the two intradimer transfer integrals, together with small transverse interactions which results in small band dispersions. However, there are other cases of BEDT-TTF salts where semiconducting behavior is found either at room temperature or at low temperature (e.g., BEDT-

(28) Mousdis, G. A.; Ducasse, L.; Fettouhi, M.; Ouahab, L.; Dupart, E.; Garrigou-Lagrange, C.; Amiell, J.; Canet, R.; Delhaes, P. *Synth. Met.* 1992, 48, 219.

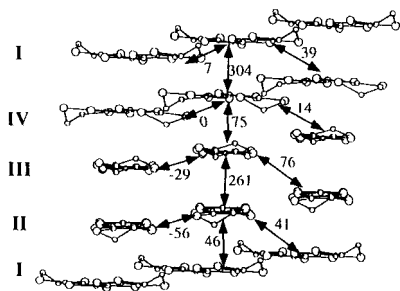


Figure 4. View of the layer along the central C=C bond of molecule II, showing the transfer integrals (meV) between neighboring molecules.

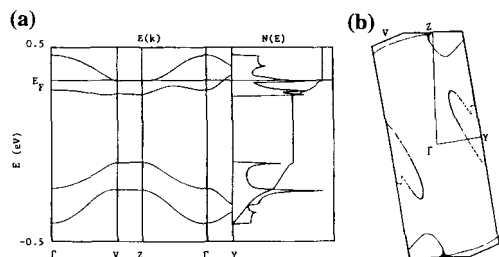


Figure 5. Band structure: (a) Energy dispersion and density of states; (b) Fermi surface.

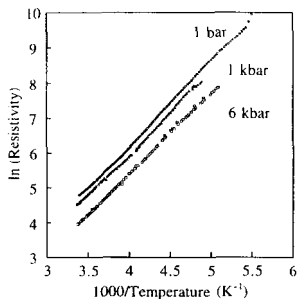


Figure 6. Temperature dependence of the electrical resistivity along *c* for three different applied pressures.

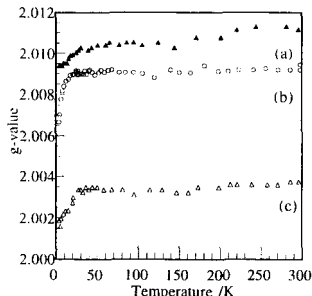


Figure 7. Temperature dependence of the *g*-values of the EPR signal along three orthogonal axes: (a) $H_0 \perp c$; (b) $H_0 \parallel c$; (c) $H_0 \parallel c$.

$\text{TTF})_4\text{Cl}_2 \cdot 6\text{H}_2\text{O}^8$) even though the band structure predicts a metallic or semimetallic character. In that case an alternative must be sought to explain the localized ground state. One such is a multi-electron valence bond approach to analyze the effect

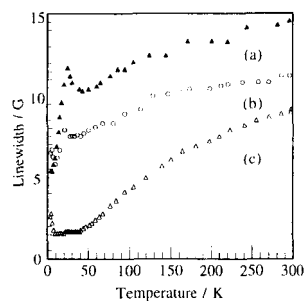


Figure 8. Temperature dependence of the peak-to-peak line widths of the EPR signal along three orthogonal axes: (a) $H_0 \perp c$; (b) $H_0 \parallel c$; (c) $H_0 \parallel c$.

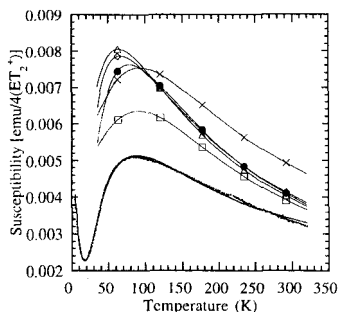


Figure 9. Temperature dependence of the magnetic susceptibility of $(\text{BEDT-TTF})_2\text{GaCl}_4$ (open circles) and the theoretical model, Bonner-Fisher ($J/k_B = 70$ K, open squares), 2D-quadratic layer antiferromagnet ($J/k_B = 50$ K, open triangles), alternate chain ($\alpha = 0.7$, $J/k_B = 70$ K, open diamonds), spin ladder (closed circles), $S = 1$ Haldane chain ($J/k_B = 70$ K, crosses), and two-dimer fits (solid line).

of the electronic correlations.²⁹ According to that model, a correlation-driven localization may occur in $3/4$ -filled 1D band systems, where there is strong dimerization along the molecular stacks. A correlation-driven localization may occur in systems where a stack dimerization is rather large. Some examples will illustrate the point.

In the α' series of BEDT-TTF salts, which are localized at room temperature (e.g., $(\text{BEDT-TTF})_2\text{AuBr}_2$ ³⁰) the ratio between the intra- and interdimer integral is about 3. Similarly, a ratio of 1.5 is found in $(\text{BEDT-TTF})_4\text{Cl}_2 \cdot 6\text{H}_2\text{O}$,⁸ which qualitatively explains the broad metal-semiconductor transition at low temperature, while in the $(\text{BEDT-TTF})_4\text{M}(\text{CN})_4$ ($M = \text{Ni}, \text{Pt}$) salts³¹ the corresponding ratio is reduced to 1.29, which again could explain the existence of a metallic phase at high temperature and the transition to a semiconductor at 150 K. Finally, in the $(\text{TMTTF})_2\text{X}$ series, the ratio is less than 1.5, again in agreement with the broad transition observed around 100–200 K.

The second and third of the examples just quoted share a common structural characteristic. Along the main stacking direction (perpendicular to the molecular plane), two modes of packing are found: one involves parallel BEDT-TTF molecules, while the second one invokes a twist angle of 34° . Just the same motif is found in $(\text{BEDT-TTF})_2\text{GaCl}_4$, where in this case

(29) Fritsch, A.; Ducasse, L. *J. Phys. (Fr.)* **1991**, *1*, 855.

(30) Chasseau, D.; Gaultier, J.; Bravic, G.; Ducasse, L.; Kurmoo, M.; Day, P. *Proc. R. Soc. London A* **1993**, *442*, 207.

(31) Ducasse, L.; Mousdis, G. A.; Fettouhi, M.; Ouahab, L.; Amiel, J.; Delhaes, P. *Synth. Met.* **1993**, *56*, 1995.

(BEDT-TTF)₂GaCl₄

the ratio of the intrastack integrals is 6. In comparison with the other examples, such a large ratio would be expected to lead to a localized regime already at room temperature.

The susceptibility of (BEDT-TTF)₂GaCl₄ is much higher than would be expected for a metallic system; the broad maximum indicates low-dimensional antiferromagnetic exchange while the fact that the susceptibility tends to zero at $T = 0$ K suggests a system with a magnetic gap. As already pointed out by several authors,^{3,32} it is probable that Coulomb repulsion is large and the spins are localized with one spin for each BEDT-TTF dimer, consistent with the semiconducting nature of the salt. Similar behavior is found in α' -(BEDT-TTF)₂X, X = CuCl₂, AuBr₂, and Ag(CN)₂.³² These salts are Mott–Hubbard insulators with poor π delocalization and large Coulomb repulsion between the conduction electrons. Their susceptibilities follow that of a 1-D $S = 1/2$ antiferromagnet with $J/k_B \sim 55$ K. In addition, the Ag(CN)₂ and AuBr₂ salts undergo a spin-Peierls transition below 7 K, emphasizing the 1-D nature of these salts.³³

The susceptibility of (BEDT-TTF)₂GaCl₄ is compared to the models for 1-D and 2-D antiferromagnets in Figure 9.^{34,35} The curves have been calibrated for 4 mol of $S = 1/2$ spins using the average experimental value of g (2.0078), and the value of the exchange interaction J/k_B (70 K for the 1D- and 50 K for the 2D-model) has been chosen to match the maximum in the measured susceptibility. It can be seen that the measured susceptibility at the maximum is only 70% to 80% of that predicted by the theoretical models and, furthermore, that both models have finite susceptibilities at $T = 0$ K and thus not appropriate to describe the magnetic properties of (BEDT-TTF)₂GaCl₄. To model the observed behavior more closely, various models were examined which predict a magnetic gap [Haldane ($S = 1$),³⁶ alternate chain,³⁷ singlet–triplet,³⁸ and spin ladder ($S = 1/2$)³⁹]. A better agreement between observed and calculated was obtained when we fitted the data to the following:

$$\chi_{\text{obs}} = n_s \chi_{\text{model}} + \chi_o + \chi_{\text{Curie}}$$

where n_s is the number of spins per unit cell and χ_o allows for any discrepancy from the estimated diamagnetic corrections and the temperature-independent paramagnetism that may arise from the system which contains low-lying excited states. The last term is the Curie contribution due to impurities and end effects.

To justify a Haldane system, one must first have a one-dimensional $S = 1$ chain. Since the molecules can have different charge, we consider the structure is made up of pairs of molecules carrying charge +1 each separated by chains of neutral dimers. Thus a $S = 1$ ground state requires that the triplet state be the most stable. Compounds containing (BEDT-TTF)₂²⁺ units are invariably diamagnetic; thus, the singlet state is more stable. For example, (BEDT-TTF)FeBr₄,¹⁴ (BEDT-

Inorganic Chemistry, Vol. 35, No. 16, 1996 4725

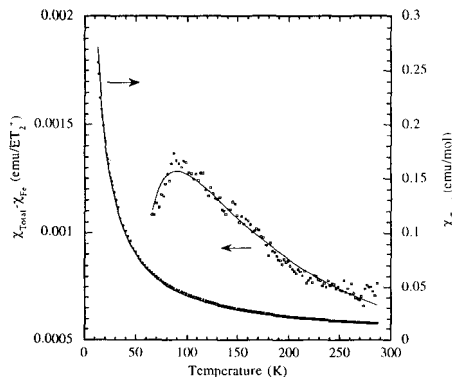


Figure 10. Temperature dependence of the observed magnetic susceptibility of (BEDT-TTF)₂GaCl₄ (open circles) and that of the BEDT-TTF contribution. The solid lines are the theoretical fits (see text).

TTF)₄[KFe(C₂O₄)₃]·C₆H₅CN,⁴⁰ and (BEDT-TTF)₃CuBr₄⁴¹ contain dimers of BEDT-TTF⁺ and all show no contribution to the susceptibility at low temperature. Nevertheless, the susceptibility of (BEDT-TTF)₂GaCl₄ does not fit the model of the Haldane chain and the magnitude of n_s is less than the number of spins in the unit cell. Figure 9 shows the theoretical curve for fixed $J/k_B = 70$ K, $n_s = 4$, and $\chi_o = \chi_{\text{Curie}} = 0$ in the temperature range 50 K ($T \geq J/2k_B$) to 320 K. Similar goodness of fit and n_s values were obtained for the alternate chain ($\alpha = 0.7–0.9$) and the spin ladder models. However, an acceptable value of n_s was obtained with a singlet–triplet model. The goodness of fit was improved when a model allowing for two gaps was employed, *i.e.*, two different spin dimers (Figure 9). The values of n_s and χ_o are 1.92 \times 2 and 0.0013 emu/unit cell (or 0.0003 emu/formula unit), respectively. The two singlet–triplet energy separations are 108 K (9.3 meV) and 212 K (18.3 meV).

In considering this conclusion about the ground state in (BEDT-TTF)₂GaCl₄, we have re-examined our earlier susceptibility data for (BEDT-TTF)₂FeCl₄. Previously we had interpreted the magnetic susceptibility as the sum of a Curie–Weiss term ($S = 5/2$ and $\Theta = -5$ K) and a temperature-independent term. Here we have fitted the low-temperature data and extracted a value of the Weiss constant for fixed values of $S = 5/2$ and $g = 2$ and then used the parameters ($S = 5/2$, $g = 2$, $\Theta = -4$ K) of the fit to calculate the difference between observed and calculated at all temperatures to obtain the contribution from the BEDT-TTF. The resulting difference was fitted to a singlet–triplet model. The simplest model of a dimer ($\Delta = 45$ K and $n_s = 1$) gives the best fit to the data between 50 and 300 K. Figure 10 shows the observed data and the fit to

$$\chi_{\text{obs}} = n_s \chi_{\text{dimer}} + \chi_o + \chi_{\text{Curie-Weiss}}$$

together with the susceptibility minus the contribution from the anion and the fit to the dimer model and a temperature-independent term.

The number of spins per formula unit for an expected localized system emphasizes the importance of Coulomb repulsion and low-dimensional spin correlation in this com-

- (32) (a) Obertelli, S. D.; Friend, R. H.; Talham, D. R.; Kurmoo, M.; Day, P. *J. Phys.: Condens. Matter* **1989**, *1*, 5671. (b) Parker, I. D.; Friend, R. H.; Kurmoo, M.; Day, P. *J. Phys.: Condens. Matter* **1989**, *1*, 5681.
 (33) Kurmoo, M.; Green, M. A.; Day, P.; Bellitto, C.; Staulo, G. *Synth. Met.* **1993**, *55–57*, 2380 and unpublished results.
 (34) (a) Bonner, J. C.; Fisher, M. E. *Phys. Rev.* **1964**, *A135*, 640. (b) Hall, J. W.; Marsh, W. E.; Weller, R. R.; Hatfield, W. E. *Inorg. Chem.* **1981**, *20*, 1033.
 (35) Lines, M. E. *J. Phys. Chem. Solids* **1970**, *31*, 101.
 (36) (a) Meyers, A.; Gleizes, A.; Giered, J. J.; Verdagner, M.; Kahn, O. *Inorg. Chem.* **1982**, *21*, 1729. (b) Sandvik, A. W.; Kurkjärvi, J. *Phys. Rev. B* **1991**, *43*, 5950.
 (37) Hatfield, W. E.; Estes, W. E.; Marsh, W. E.; Pickens, M. W.; ter Haar, L. W.; Weller, R. R. In *Linear Chain Compounds*; Miller, J. S., Ed.; Plenum Press: New York, 1983; Vol. 3, p 43.
 (38) Bleaney, B.; Bowers, K. D. *Proc. R. Soc. London* **1952**, *A214*, 451.
 (39) (a) Johnston, D. C.; Johnson, J. W.; Goshorn, D. P.; Jacobson, A. J. *Phys. Rev.* **1987**, *B35*, 219. (b) Barnes, T.; Riera, J. *Phys. Rev.* **1994**, *B50*, 6817.

- (40) Day, P.; Graham, A. W.; Kepert, C. J.; Kurmoo, M. *Synth. Met.* **1995**, *70*, 767.
 (41) (a) Guionneau, P.; Bravic, G.; Gaultier, J.; Chasseau, D.; Kurmoo, M.; Day, P. *Acta Crystallogr.* **1994**, *C50*, 1894. (b) Hebrard, S.; Bravic, G.; Gaultier, J.; Chasseau, D.; Kurmoo, M.; Day, P. *Acta Crystallogr.* **1994**, *C50*, 1892.

pound. Low-dimensional charge-transfer salts such as (BEDT-TTF)₂GaCl₄ are expected to behave as Heisenberg antiferromagnets, given the almost isotropic g values. In such solids there are two possible low-temperature instabilities that arise from the weak transverse coupling between the spin chains, the spin-Peierls (1-D) and SDW antiferromagnetic (3-D) instabilities. Below the spin-Peierls transition the spin chain dimerizes gradually to form a nonmagnetic singlet state at 0 K; thus, the susceptibility along any direction is exponential up to the transition temperature. The antiferromagnetic instability leads to a 3-D ordered spin lattice, in which, as the temperature tends to zero, the susceptibility tends to zero along the preferred spin direction, and to a constant value perpendicular to this direction. These two transitions can be differentiated clearly in both static susceptibility and EPR measurements. The average susceptibility tends to zero for a spin-Peierls and to a constant value for a 3-D antiferromagnet. The line width of the EPR signal is approximately constant in the spin-Peierls but diverges at the transition to a 3-D antiferromagnetic state, e.g., β' -(BEDT-TTF)₂AuCl₄⁴² and (BEDT-TTF)₂Ag₄CN₅.⁴³ The fall in the susceptibility of (BEDT-TTF)₂GaCl₄ at ~50 K may indicate such phase transitions, but the lack of any divergence in line width and g -value of the EPR resonance eliminates the possibility of a 3-D ordered antiferromagnetic state and the absence of a knee in the susceptibility and the poor fit to a uniform one-dimensional antiferromagnet suggest it is not a spin-Peierls transition. High-field magnetization will be needed to resolve these ambiguities.

The Hubbard model still applies to (BEDT-TTF)₂GaCl₄; since the BEDT-TTF molecules are dimerized the band structure is built up from the bonding and antibonding orbitals of a pair of BEDT-TTF molecules. The Coulomb repulsion energy, U (between electrons in the same molecular orbital), is large in this salt (usually $U \sim 1-1.4$ eV) so that these levels are only singly occupied, and there is an upper Hubbard level separated by an energy U from the lower levels. The Hubbard model predicts that the magnetic exchange energy is given by $J = 2t^2/U_{\text{eff}}$, where U_{eff} is the energy to put two spins on the same site. Since the repulsion energy between two electrons occupying the same orbital is larger than the energy difference between the bonding and antibonding levels ($=2t_1$), the lowest energy

state becomes the one with one electron occupying the bonding orbital and one the antibonding orbital. This requires an energy $2t_1$, so $U_{\text{eff}} = 2t_1$, an energy that is independent of the on-site interaction U . For a real system of dimers the interdimer transfer integral t_2 broadens the energy levels so that U_{eff} is reduced to $U_{\text{eff}} = 2(t_1 - t_2)$. The semiconducting energy gap is given by $E_g = U_{\text{eff}}/2 = (t_1 - t_2)$, since exciting an electron to the upper band, with energy U_{eff} , creates two charge carriers, an electron and a hole. For (BEDT-TTF)₂GaCl₄ the same considerations apply (although the charges on the BEDT-TTF molecules are holes and not electrons), so that the exchange interaction is given by $J = 2t_2^2/U_{\text{eff}} = t_2^2/E_g$. Using $J/k_B \sim 70$ K and $E_g = 0.4$ eV, the Hubbard model thus predicts a bandwidth $4t_2 \sim 0.3$ eV.

Conclusion

We have demonstrated that a good understanding of the electrical and magnetic properties of organic conductors with nonmagnetic anions is a prerequisite to the understanding of the interaction between moments from conduction electrons and those localized on anions. Magnetically, the organic cations in (BEDT-TTF)₂GaCl₄ and (BEDT-TTF)₂FeCl₄ behave as dimers, the former containing two dimers with different singlet-triplet energy separations and the latter with a single singlet-triplet gap. The difference between the two compounds can be traced to the crystal structures, since the unit cell in the former is double that of the latter. The observed susceptibility is the sum of contributions from the organic and inorganic moieties, and there is no measurable exchange between the two spin sublattices.

Acknowledgment. This work was supported by the EPSRC, British Council (Alliance Programme), and EU (Human Capital and Mobility Programme (Network on Molecular Superconductors)). This manuscript was written while on a visit, funded by a British Council-Monbuscho collaborative program, to the Japan Advanced Institute of Science and Technology at Hokuriku, Japan. M.K. thanks Professors T. Mitani and Y. Iwasa and Dr. H. Kitagawa for many discussions. We thank Dr. D. Watkin (Oxford University) for his help with the crystallography and Prof. Z. Soos for useful discussions.

Supporting Information Available: Tables giving a summary of crystallographic and refinement data, anisotropic displacement parameters, and bond lengths and angles (9 pages). Ordering information is given on any current masthead page.

IC951456Y

(42) (a) Coulon, C.; Laversanne, R.; Amiel, J.; Delhaes, P. *J. Phys. Condens. Matter* **1986**, *19*, L753.

(43) Geiser, U.; Wang, H. H.; Gerdorf, L. E.; Firestone, M. A.; Sowa, L. M.; Whangbo, M.-H.; Williams, J. M. *J. Am. Chem. Soc.* **1985**, *107*, 8305.

Superconducting and Semiconducting Magnetic Charge Transfer Salts: (BEDT-TTF)₄AFe(C₂O₄)₃·C₆H₅CN (A = H₂O, K, NH₄)

Mohamedally Kurmoo,[†] Anthony W. Graham,[†] Peter Day,^{*†} Simon J. Coles,[‡] Michael B. Hursthouse,[‡] Jason L. Caulfield,[‡] John Singleton,[‡] Francis L. Pratt,[§] William Hayes,[§] Laurent Ducasse,[‡] and Philippe Guionneau[†]

Contribution from the Davy Faraday Research Laboratory, Royal Institution of Great Britain, 21 Albemarle Street, London W1X 4BS, U.K., School of Chemistry and Applied Chemistry, University College of Wales, Cardiff CF1 3TB, U.K., Clarendon Laboratory, Parks Road, Oxford OX1 3PU, U.K., and Université Bordeaux I, 351 cours de la Libération, Talence 33405, France

Received July 17, 1995[⊗]

Abstract: Three new molecular charge transfer salts of bis(ethylenedithio)tetrathiafulvalene (BEDT-TTF), (BEDT-TTF)₄AFe(C₂O₄)₃·C₆H₅CN (A = H₂O, K, NH₄), have been prepared, and their crystal structures and physical properties determined. The structures of all three salts consist of successive layers of BEDT-TTF and layers of approximately hexagonal geometry containing alternating A and Fe(C₂O₄)₃³⁻, with C₆H₅CN lying within the hexagonal cavities. When A = K or NH₄ the BEDT-TTF layers consist of dimers (BEDT-TTF)₂²⁺ separated by isolated (BEDT-TTF)⁰, the charge difference being estimated from the C=C and C-S bond lengths. These salts are semiconductors ($\sigma \sim 10^{-4}$ S cm⁻¹, $E_A = 0.14$ eV), and their magnetic susceptibilities are dominated by the $S = 5/2$ Fe^{III}. The EPR spectra accordingly show only one sharp signal. When A = H₂O the BEDT-TTF adopt the β'' packing, and the salt is a superconductor (T_c 7.0(3) K). The magnetic susceptibility above the critical temperature is the sum of a Pauli component (2×10^{-3} emu mol⁻¹) and a Curie-Weiss term. Below the transition the susceptibility depends on the field penetration according to the London penetration depth, increasing with increasing field until the critical field. The Meissner effect is almost complete, indicating absence of pinning. The EPR spectra of the A = H₂O compound are characterized by two resonances, one of Dysonian shape due to the conduction electrons on the organic cations and the other of Lorentzian shape arising from the 3d electrons of Fe^{III}. Electronic band structure calculations suggest that the A = K compound is semiconducting ($E_g = 0.3$ eV) in good agreement with that result obtained from electrical measurement and the A = H₂O is metallic ($W = 1.1$ eV) with both electron and hole pockets in the Fermi surface. Optical reflectivity of the latter gives an electronic bandwidth of 1.0 eV, fully consistent with the band structure calculation.

Introduction

A challenge in synthesizing new molecular-based materials is to bring together in the same crystal lattice combinations of physical properties that are not normally found in chemically simpler continuous lattice compounds. A feature of the superconducting charge transfer salts based on the donor molecule bis(ethylenedithio)tetrathiafulvalene (BEDT-TTF) is the spatial segregation of the organic cations and inorganic anions into alternating layers, which has led us to cite them as examples of "organic-inorganic molecular composites"¹ or "chemically constructed multilayers".² Because of this separation into well-defined organic and inorganic components the BEDT-TTF charge transfer salts appear attractive synthetic targets for attempts to combine superconductivity in a molecular lattice with properties more characteristic of the inorganic solid state like cooperative magnetism. The electrons close to the Fermi surface are largely confined to frontier orbitals of the BEDT-TTF, while magnetic moments localized on the anions can be built in if the latter are transition metal complexes.

Establishing superconductivity in a crystal lattice containing localized magnetic moments is a desirable aim because superconductivity and magnetism have long been considered inimical

to one another: Cooper pairs are disrupted both by externally applied fields or by the internal fields generated in ferromagnets.³ Nevertheless a few examples exist of magnetic superconductors containing 4f elements (Ln) such as the Chevrel phases LnMo₆S₈,⁴ the borides LnRh₄B₄,⁵ and the cuprates LnBa₂Cu₃O₇.⁶ No corresponding stoichiometric phases containing 3d ions have been reported. Of the small number of BEDT-TTF salts containing 3d complex anions, several are semiconductors,⁷ but we reported one example, (BEDT-TTF)₂CuCl₄·H₂O, which remains metallic down to 400 mK though without becoming superconducting and in which magnetic resonance from the conduction electrons and the localized 3d electrons can be resolved.⁸

(3) See, e.g.: *Topics in Current Physics*; Fisher, Ø., Maple, M. B., Eds.; Springer Verlag: New York, 1983; Vols. 32, 34 passim.

(4) (a) Ishikawa, M.; Fischer, Ø. *Solid State Commun.* 1977, 23, 37. (b) Lynn, J. W.; Shirane, G.; Thomlinson, W.; Sheldon, R. N. *Phys. Rev. Lett.* 1981, 46, 368-371.

(5) (a) Fertig, W. A.; Johnston, D. C.; DeLong, L. E.; McCallum, R. W.; Maple, M. B.; Matthias, B. T. *Phys. Rev. Lett.* 1977, 38, 987-990. (b) Moncton, D. E.; McWhann, D. B.; Schmidt, P. H.; Shirane, G.; Thomlinson, W.; Maple, M. B.; MacKay, H. B.; Wolf, L. D.; Fisk, Z.; Johnston, D. C. *Phys. Rev. Lett.* 1980, 45, 2060-2063.

(6) Beauchamp, K. M.; Spalding, G. C.; Huber, W. H.; Goldman, A. M. *Phys. Rev. Lett.* 1994, 73, 2752-2755.

(7) (a) Mallah, T.; Hollis, C.; Bott, S.; Kurmoo, M.; Day, P. *J. Chem. Soc., Dalton Trans.* 1990, 859-865. (b) Marsden, I. R.; Allan, M. L.; Friend, R. H.; Kurmoo, M.; Kanazawa, D.; Day, P.; Bravic, G.; Chasseau, D.; Ducasse, L.; Hayes, W. *Phys. Rev. B* 1994, 50, 2118-2127.

(8) Day, P.; Kurmoo, M.; Mallah, T.; Marsden, I. R.; Allan, M. L.; Friend, R. H.; Pratt, F. L.; Hayes, W.; Chasseau, D.; Bravic, G.; Ducasse, L. *J. Am. Chem. Soc.* 1992, 114, 10722-10729.

[†] Royal Institution.

[‡] University College of Wales.

[§] Clarendon Laboratory.

[⊙] Université Bordeaux.

[⊗] Abstract published in *Advance ACS Abstracts*, December 1, 1995.

(1) Day, P. *Philos. Trans. R. Soc. London* 1985, A314, 145-158.

(2) Day, P. *Phys. Scr.* 1993, T49, 726-730.

12210 *J. Am. Chem. Soc.*, Vol. 117, No. 49, 1995Kurmoo *et al.*Table 1. Crystal Data and Structure Refinement Data for (BEDT-TTF)₄AFe(C₂O₄)₃·C₆H₅CN: (a) A = K, (b) A = NH₄, (c) A = H₂O

	(a)	(b)	(c)
empirical formula	C ₃₃ H ₃₇ FeKNO ₁₃ S ₁₂	C ₃₃ H ₄₁ FeN ₇ O ₁₂ S ₁₂	C ₃₃ H ₃₉ FeNO ₁₃ S ₁₂
formula weight	1999.70	1974.61	1979.78
temperature	120(2) K	120(2) K	120(2) K
wavelength	0.71069 Å	0.71069 Å	0.71069 Å
crystal system	orthorhombic	orthorhombic	monoclinic
space group	<i>Pbcn</i>	<i>Pbcn</i>	<i>C2/c</i>
unit cell dimensions	<i>a</i> = 10.33(2) Å <i>b</i> = 19.53(3) Å <i>c</i> = 35.94(2) Å	<i>a</i> = 10.370(5) Å <i>b</i> = 19.588(12) Å <i>c</i> = 35.790(8) Å	<i>a</i> = 10.233(12) Å <i>b</i> = 20.04(3) Å <i>c</i> = 34.97(2) Å β = 93.25(11) deg
volume	7252(15) Å ³	7270(6) Å ³	7157(13) Å ³
Z	4	4	4
density (calculated)	1.832 Mg/m ³	1.804 Mg/m ³	1.835 Mg/m ³
absorption coefficient	1.247 mm ⁻¹	1.187 mm ⁻¹	1.207 mm ⁻¹
<i>F</i> (000)	4056	4008	4016
crystal size	0.15 × 0.2 × 0.2 mm		0.2 × 0.2 × 0.07 mm
θ range for data collection	2.09–25.07°	2.08–25.07°	2.33–24.87°
index ranges	–10 ≤ <i>h</i> ≤ 11, –15 ≤ <i>k</i> ≤ 15, –39 ≤ <i>l</i> ≤ 23	–11 ≤ <i>h</i> ≤ 11, –22 ≤ <i>k</i> ≤ 22, –39 ≤ <i>l</i> ≤ 8	–8 ≤ <i>h</i> ≤ 11, –22 ≤ <i>k</i> ≤ 20, –39 ≤ <i>l</i> ≤ 83
reflexes collected	16763	14915	13774
independent reflns	4796 [<i>R</i> (int) = 0.0562]	5561 [<i>R</i> (int) = 0.0987]	5110 [<i>R</i> (int) = 0.1011]
refinement method	full-matrix least-squares on <i>F</i> ²	full-matrix least-squares on <i>F</i> ²	full-matrix least-squares on <i>F</i> ²
data; restraints; parameters	4786; 0; 462	5561; 0; 205	5094; 6; 454
goodness-of-fit on <i>F</i> ²	1.062	2.178	0.661
final <i>R</i> indices [<i>I</i> > 2σ(<i>I</i>)]	<i>R</i> ₁ = 0.0490, <i>wR</i> ₂ = 0.1280	<i>R</i> ₁ = 0.1557, <i>wR</i> ₂ = 0.3831	<i>R</i> ₁ = 0.0416, <i>wR</i> ₂ = 0.0760
<i>R</i> indices (all data)	<i>R</i> ₁ = 0.0596, <i>wR</i> ₂ = 0.1416	<i>R</i> ₁ = 0.1902, <i>wR</i> ₂ = 0.3935	<i>R</i> ₁ = 0.0982, <i>wR</i> ₂ = 0.0934
largest diff. peak and hole	0.702 and –1.185 e.Å ⁻³	2.371 and –1.516 e.Å ⁻³	0.651 and –0.439 e.Å ⁻³

Recently a number of instances have come to light of two-dimensional bimetallic layers containing uni- or dipositive cations and M^{III}(C₂O₄)₃³⁻ in which the oxalato-ion acts as bridging ligand, leading to infinite sheets of approximately hexagonal symmetry, separated by bulky organic cations.^{9,10} When the latter are electronically inactive the resulting compounds show interesting and unusual ferrimagnetic behavior.^{11,12} In parallel with our studies of their magnetic properties we have therefore begun to explore the synthesis of compounds containing anion lattices of similar type but interleaved with BEDT-TTF molecules. The present paper reports the synthesis and crystal structures of three such compounds, (BEDT-TTF)₄AFe(C₂O₄)₃·C₆H₅CN, (A = H₂O, K, NH₄) together with characterization of their physical properties. While the stoichiometric ratio of BEDT-TTF to Fe is the same in all three compounds, as is the basic topology of the anion layer, the presence or absence of a monovalent cation within the latter not only changes the electron count (and hence the band filling) in the organic layer but also drastically alters the packing motif of the BEDT-TTF. Thus, the compounds with A = K, NH₄ are semiconductors with the organic molecules present as (BEDT-TTF)₂²⁺ and (BEDT-TTF)⁰. In contrast the compound with A = H₂O has BEDT-TTF packed in the β'' arrangement¹³ and is the first example of a molecular superconductor containing magnetic ions. A preliminary account of part of this work has appeared.¹⁴

Experimental Section

Preparation. BEDT-TTF was synthesized following the method of Larsen and Lenoir¹⁵ and recrystallized from CHCl₃. A₃Fe(C₂O₄)₃·H₂O (A = K, NH₄) were prepared by literature methods¹⁶ and recrystallized from water. C₆H₅CN was dried over CaCl₂ and freshly distilled prior to use. 18-Crown-6-ether (Aldrich) was recrystallized from acetonitrile and dried in a desiccator over P₂O₅. To remove small traces of Fe(II)C₂O₄·¹/₂H₂O, the benzonitrile solution of the anion and the 18C6 was filtered before electrocrystallization.

Electrochemical crystal growth was carried out in conventional H-shaped cells with Pt electrodes in a constant temperature (295(2) K) over 20 days at a current of 1 μA. The cells were fixed inside sand-filled compartments on a concrete table to minimize vibration. Each cell contained 10 mg of BEDT-TTF and 100 mg of either K₃Fe-

(C₂O₄)₃·3H₂O or (NH₄)₃Fe(C₂O₄)₃·3H₂O together with 200 mg of 18-crown-6 in 50 mL of C₆H₅CN. Under dry conditions, for the K and NH₄ salts the crystals adhering to the anode were diamond shaped but upon addition of water to the cell with (NH₄)₃Fe(C₂O₄)₃·3H₂O two phases were obtained, with diamond and needle morphology. The phases were identified from their crystal structures (see below) and by their morphology.

Structure Determination. The crystal structures of the three compounds with A = H₂O, K, NH₄ were determined from single crystal X-ray diffraction data collected at 120 K at University College of Wales, Cardiff, UK. The four circle diffractometer is equipped with a Delft Instruments FAST TV area detector and utilizes graphite monochromated Mo Kα (0.71069 Å) radiation from a rotating anode generator.¹⁷ Temperature was controlled by an Oxford Cryostream system. Lattice parameters were initially derived from more than 50 reflections. Crystal data are tabulated in Table 1, with details of the refinements.

The structures were solved by direct methods using SHELXL 93¹⁸ and refined by full-matrix least squares on *F*² for data corrected for Lorentz and polarization factors and also for absorption. The non-hydrogen atoms were refined with anisotropic temperature factors while the hydrogen atoms were refined freely with individual *U*_{iso} values. The weighting scheme used was *w* = 1/*σ*²(*F*_o²). Scattering factors were taken from the ref 18. The final reliability factors are given in Table 1.

(9) Tamaki, H.; Zhong, Z. J.; Matsumoto, N.; Kida, S.; Koikawa, M.; Achiwa, N.; Hashimoto, Y.; Okawa, H. *J. Am. Chem. Soc.* 1992, 114, 6974–6979.

(10) (a) Descurtins, S.; Schmalte, H. W.; Oswald, H. R.; Linden, A.; Ensling, J.; Gütllich, P.; Hauser, A. *Inorg. Chim. Acta* 1994, 216, 65–72. (b) Farrell, R. P.; Hambley, T. W.; Lay, P. *Inorg. Chem.* 1995, 34, 757–758.

(11) Mathonière, C.; Carling, S. G.; Dou, Y.; Day, P. *J. Chem. Soc., Chem. Commun.* 1994, 1551–1552.

(12) Mathonière, C.; Nuttall, C. J.; Carling, S. G.; Day, P. *Inorg. Chem.* In press.

(13) Kurmoo, M.; Talham, D.; Day, P.; Parker, I. D.; Friend, R. H.; Stringer, A. M.; Howard, J. A. K. *Solid State Commun.* 1987, 61, 459–464.

(14) Graham, A. W.; Kurmoo, M.; Day, P. *J. Chem. Soc., Chem. Commun.* 1995, 2061–2062.

(15) Larsen, J.; Lenoir, C. *Synthesis* 1988, 2, 134.

(16) Bailar, J. C.; Jones, E. M. *Inorg. Synth.* 1939, 1, 35–39.

(17) Darr, J. A.; Drake, S. R.; Hursthouse, M. B.; Abdul Malik, K. M. *Inorg. Chem.* 1993, 32, 5704–5708.

(18) Sheldrick, G. M. SHELXL 93 Programme System. *J. Appl. Crystallogr.* In press.

$(\text{BEDT-TTF})_4\text{AFe}(\text{C}_2\text{O}_4)_3\text{C}_6\text{H}_5\text{CN}$ ($A = \text{H}_2\text{O}, \text{K}, \text{NH}_4$)

J. Am. Chem. Soc., Vol. 117, No. 49, 1995 12211

Electronic Band Structure. The electronic band structures of both the semiconducting $A = \text{K}$ and superconducting $A = \text{H}_2\text{O}$ compounds were calculated in the tight binding approximation within the Extended Hückel hamiltonian using the highest filled molecular orbitals (HOMO) of BEDT-TTF as basis functions. Transfer integrals were calculated using the dimer splitting model.¹⁹ For crystal structures containing several crystallographically independent molecules in the unit cell this approach allows us to determine the difference in the HOMO energies of the different molecules which are then taken into account in the band structure calculation. These differences may be crucial in evaluating the electronic gap in semiconducting salts when they become large compared to the bandwidth, as for example in $(\text{TMTSF})_2\text{ReO}_4$ below the anion ordering temperature.²⁰ In the present series, the two BEDT-TTF in the $A = \text{K}$ compound carry distinctly different charges and hence the respective HOMOs have different energies.

Electrical Conductivity. Two-probe dc and both four-probe ac (15–33 Hz) and dc resistance measurements were made on single crystals with current flow along different axes. Electrical contacts to the crystals were made with 25 μm gold wire and platinum paint. The crystals were held in an Oxford Instruments continuous flow helium cryostat, and temperature was monitored by a Rh-Fe sensor. Magnetoresistance measurements of the metallic salt were made in the same way but with the crystal holder placed within the superconducting solenoid of a Quantum Design MPMS 7 SQUID magnetometer. The temperature was swept from 2 to 7 K at different applied fields in the range 1–640 mT. The contacts were 4 in a line and the current applied was 10 μA . Contact resistances were $\sim 30 \Omega$ per pair and the nested/unnested voltage was > 100 .

Magnetic Susceptibility. Measurements were made on polycrystalline samples held in gelatine-capsules inside a plastic tube (drinking straw) using a Quantum Design MPMS 7 SQUID magnetometer. Magnetization data were taken in different applied fields on warming from 2 to 300 K. Correction was made to the measured susceptibility for core diamagnetism using Pascal constants. To detect a Meissner effect in the $A = \text{H}_2\text{O}$ compound the sample was cooled in zero field to 2 K prior to measuring the magnetization on warming to 10 K in a field of 5 G followed by cooling to 2 K in the same field. This procedure was followed for increasing field up to 410 G. To circumvent the remnant field of the superconducting solenoid the low field magnetization was measured as a function of applied field to locate the value of the applied field at which the magnetization was zero above the superconducting transition within the detection limit of the magnetometer.

Electron Spin Resonance. Electron spin resonance spectra of single crystals of the $A = \text{K}$ and $A = \text{H}_2\text{O}$ compounds as well as a polycrystalline sample of $\text{K}_3\text{Fe}(\text{C}_2\text{O}_4)_3 \cdot 3\text{H}_2\text{O}$ for comparison were measured at room temperature on a Varian E9 reflection spectrometer operating at 9.2 GHz. The crystals were oriented in a TE₁₀₂ cavity by means of a home made goniometer.

Optical Reflectivity. Spectra were recorded at room temperature on two instruments: a Perkin Elmer 1710 equipped with a Spectra Tech microscope and an evacuable Bruker 66VS employing a Specac reflection attachment. KRS5 was used as polarizer. All data were referenced to a gold mirror, and data from the Bruker spectrometer were then normalized to that of the absolute value obtained on the Perkin Elmer instrument. A flat needle crystal was glued onto two pieces of fine (100 μm) noninsulated copper wire and then suspended on a washer mount to minimize the effect of stray light. For measurements under the microscope the crystal was placed on a transparent KBr plate.

Results and Discussion

Crystal Structures. The crystal structures of all three compounds consist of alternating layers containing only BEDT-TTF and only $\text{AFe}(\text{C}_2\text{O}_4)_3 \cdot \text{C}_6\text{H}_5\text{CN}$. Whilst the molecular packing in the latter is quite similar in all three cases, the molecular packing arrangement within the BEDT-TTF layers

differs markedly from the other two when $A = \text{H}_2\text{O}$. We therefore describe the anion layers together but consider the BEDT-TTF layers separately. Crystals of the NH_4 salt were invariably twinned so the structure determination in that case is much less precise. However, it is sufficient to delineate the broad outlines of the structure. Selected bond lengths and angles relevant to the anion layers and the central tetrathiafulvalene moieties of the BEDT-TTF are listed in Tables 2 and 3. Numbering of the atoms is given in Figure 1.

When projected on to the mean plane of the A and Fe, the anion layers have a clear honeycomb arrangement, with alternate A and Fe forming an approximately hexagonal network (Figure 2). The Fe are octahedrally coordinated by three bidentate oxalate ions, giving rise to a trigonal component of the crystal field. The mean Fe–O bond lengths (2.011 Å) are identical in the K and H_2O compounds though the extent of the trigonal distortion is greater in the latter, as measured by the mean *trans* O–Fe–O angles (K, 170.6°; H_2O , 164.1°). In the discrete $\text{Fe}(\text{C}_2\text{O}_4)_3^{3-}$ as found in the NH_4 salt the corresponding figures are Fe–O 2.002 Å, *trans* O–Fe–O 163.5°.²¹ The O atoms of the oxalate which are not coordinated to Fe form cavities occupied either by K or H_2O . In the former case the coordination number of the K is seven, since the CN group of a benzonitrile molecule is oriented toward it with the N–K distance being 2.952 Å (Figure 2a). The benzonitrile molecules show twofold disorder with respect to the orientation of the CN group but occupy cavities in the $\text{KFe}(\text{C}_2\text{O}_4)_3$ lattice of approximately hexagonal shape. The mean plane of the benzonitrile coincides with that found by the K and Fe, and there can be little doubt that it performs an important “templating” role in stabilizing the lattice. The mean K–O bond length of 2.87 Å is close to that expected.

Turning to the superconducting phase, the underlying hexagonal network of Fe and A is retained. A crystallographic point crucial to rationalizing the electronic structure and properties concerns the nature and disposition of the atoms occupying the cavity analogous to the one that contains K or NH_4 in the semiconducting phases. Attempts to refine a structure based on occupation by N failed, while assumption that the atom occupying the cavity was O proved successful (Table 1). Furthermore, the electron count (and hence the Fermi energy) depends on whether the species in question is H_2O or H_3O^+ . The H atoms could not be located, but two pieces of evidence point strongly to the molecular species being H_2O . First, the site symmetry of the O is C_2 , and the distances to the six O on neighboring $\text{C}_2\text{O}_4^{2-}$ are 2.81 ($\times 2$), 2.93 ($\times 2$), 2.95 Å ($\times 2$), i.e., two distances are distinctly shorter than the other four. Second, the two closest oxalate O subtend an angle of 137.4° at the central O, quite compatible with a H-bonded H_2O . For example in $(\text{COOD})_2 \cdot 2\text{D}_2\text{O}$ the distances between the D_2O and CO groups are 2.84–2.90 Å and the O–D \cdots O angles are 156° and 168°.²²

In the $A = \text{H}_2\text{O}$ compound the included benzonitrile molecules are fully ordered, with the $-\text{CN}$ groups oriented toward Fe, so the hexagonal network of Fe and H_2O is elongated along one axis. There is an accompanying lowering of symmetry from orthorhombic to monoclinic ($\beta = 93.2^\circ$), although the unit cell parameters and volumes of the K and H_2O compounds are quite comparable (7252 and 7157 Å³ respectively). It appears that in the K-salt the lattice is loosely packed probably as a result of the hexagonal structure forced on the BEDT-TTF layer by the Fe oxalate sublattice. The difference of $\sim 100 \text{Å}^3$ is equivalent to an extra 4–5 atoms.

A final structural point about the anion layers concerns their chirality. The point symmetry of $\text{Fe}(\text{C}_2\text{O}_4)_3^{3-}$ is D_3 , and the

(19) Ducasse, L.; Abderrabba, A.; Hoarau, J.; Pesquer, M.; Gallois, B.; Gaultier, J. *J. Phys. C: Solid State Phys.* 1986, 19, 3805–3820.

(20) Ducasse, L.; Abderrabba, A.; Gallois, B.; Chasseau, D. *Synth. Met.* 1987, 19, 327–332.

Table 2. Selected Bond Lengths (Å) and Angles (deg) for (BEDT-TTF)₂AFe(C₂O₄)₃·C₆H₅CN (A = K, NH₄)

	K	NH ₄		K	NH ₄
Fe(1)–O(1)	1.998(4) 2×	1.997(10)	A(1)–O(5)	2.825(6)	2.91(2)
Fe(1)–O(3)	2.019(4) 2×	2.012(10)	A(1)–O(6)	2.878(5)	2.88(3)
Fe(1)–O(4)	2.017(4) 2×	1.999(11)			
O(1)–C(21)	1.279(8)	1.23(2)	O(4)–C(23)	1.292(7)	1.25(2)
O(2)–C(21)	1.219(8)	1.27(2)	O(5)–C(22)	1.210(7)	1.26(2)
O(3)–C(22)	1.293(7)	1.25(2)	O(6)–C(23)	1.230(7)	1.24(2)
C(22)–C(23)	1.544(8)	1.53(2)	C(21)–C(21)'	1.583(12)	1.52(4)

BEDT-TTF (1)			BEDT-TTF (2)		
S(3)–C(3)	1.754(5)	1.79(2)	S(11)–C(13)	1.773(5)	1.80(2)
S(3)–C(5)	1.730(5)	1.74(2)	S(11)–C(15)	1.755(5)	1.75(2)
S(4)–C(4)	1.745(5)	1.74(2)	S(12)–C(15)	1.760(6)	1.77(2)
S(4)–C(5)	1.735(5)	1.72(2)	S(12)–C(14)	1.756(5)	1.77(2)
S(4)–C(5)	1.735(5)	1.72(2)	S(12)–C(14)	1.756(5)	1.77(2)
S(5)–C(7)	1.753(5)	1.76(2)	S(13)–C(16)	1.767(6)	1.74(2)
S(5)–C(6)	1.731(6)	1.72(2)	S(13)–C(17)	1.756(5)	1.76(2)
S(6)–C(8)	1.741(5)	1.73(2)	S(14)–C(16)	1.769(5)	1.78(2)
S(6)–C(6)	1.727(5)	1.74(2)	S(14)–C(18)	1.757(5)	1.76(2)
C(3)–C(4)	1.350(7)	1.34(2)	C(13)–C(14)	1.338(7)	1.32(2)
C(5)–C(6)	1.381(7)	1.40(2)	C(15)–C(16)	1.342(8)	1.35(2)
C(7)–C(8)	1.357(8)	1.33(2)	C(17)–C(18)	1.340(8)	1.29(2)
C(9)–C(10)	1.513(9)	1.52(3)			
O(1)–Fe(1)–O(1)'	81.2(2)	81.1(6)	C(21)–O(2)–K(1)''	120.7(4)	
O(4)–Fe(1)–O(3)'	91.8(2) 2×	91.6(4)	C(21)–O(1)–Fe(1)	116.0(4)	113.4(11)
O(1)–Fe(1)–O(4)	96.4(2) 2×	96.7(4)	C(22)–O(5)–K(1)	122.4(4)	
O(4)–Fe(1)–O(4)'	170.3(2)	169.4(6)	C(22)–O(3)–Fe(1)	114.5(3)	113.4(10)
O(1)–Fe(1)–O(4)	91.0(2) 2×	91.3(4)	C(23)–O(6)–K(1)	119.9(4)	
O(4)–Fe(1)–O(3)	81.3(2) 2×	80.9(4)	C(23)–O(4)–Fe(1)	114.1(3)	114.3(10)
O(1)–Fe(1)–O(3)	94.8(2) 2×	94.7(4)	O(1)–Fe(1)–O(3)''	170.9(2)	170.8(4)
O(3)–Fe(1)–O(3)	90.3(2)	90.6(6)			

Table 3. Selected Bond Lengths (Å) and Angles (deg) for (BEDT-TTF)₂(H₂O)Fe(C₂O₄)₃·C₆H₅CN

Fe(1)–O(1)	2.008(3)	O(7)–O(3)	2.95
Fe(1)–O(2)	2.011(3)	O(7)–O(4)	2.81
Fe(1)–O(5)	2.016(3)	O(7)–O(6)	2.93
O(1)–C(21)	1.292(5)	O(4)–C(22)	1.235(5)
O(2)–C(22)	1.285(5)	O(5)–C(23)	1.268(5)
O(3)–C(21)	1.221(5)	O(6)–C(23)'	1.243(5)
C(21)–C(22)	1.549(6)	C(23)–C(23)	1.536(9)
S(3)–C(5)	1.744(4)	S(3)–C(3)	1.752(4)
S(4)–C(5)	1.749(4)	S(4)–C(4)	1.768(4)
S(5)–C(6)	1.739(5)	S(5)–C(7)	1.764(4)
S(6)–C(8)	1.732(4)	S(6)–C(6)	1.755(4)
S(12)–C(14)	1.739(4)	S(12)–C(15)	1.756(4)
S(11)–C(15)	1.741(4)	S(11)–C(13)	1.750(4)
S(14)–C(16)	1.732(5)	S(14)–C(18)	1.766(5)
S(13)–C(16)	1.746(4)	S(13)–C(17)	1.747(5)
C(3)–C(4)	1.343(5)	C(13)–C(14)	1.351(6)
C(5)–C(6)	1.345(6)	C(15)–C(16)	1.363(6)
C(7)–C(8)	1.369(6)	C(17)–C(18)	1.335(6)
O(1)–Fe(1)–O(1)'	159.2(2)	O(2)–Fe(1)–O(2)	104.0(2)
O(1)–Fe(1)–O(2)'	86.77(13)	O(2)–Fe(1)–O(5)	88.9(2)
O(1)–Fe(1)–O(2)	80.46(13)	O(2)–Fe(1)–O(5)'	166.59(12)
O(1)–Fe(1)–O(5)'	96.88(12)	O(5)–Fe(1)–O(5)	78.5(2)
O(1)–Fe(1)–O(5)	99.18(12)		

ion may exist in principle in Δ or Λ enantiomers. In the compounds reported in this paper, which were synthesized from racemic starting material, we find that alternate anion layers are composed exclusively either of Δ or Λ anions. It would be interesting to synthesize the corresponding salts with optically resolved anions. It is worth noting that an analogous sequence of Δ and Λ -containing layers is observed in the crystal structure of P(C₆H₅)₂MnCr(C₂O₄)₃ synthesized from racemic starting material.¹⁰

In contrast to the closely similar anion layers, the molecular arrangements in the BEDT-TTF layers are quite different in the K and NH₄ salts from that found in the H₂O one. In the former the asymmetric unit consists of two independent BEDT-

TTF, distinguished from one another in two ways. First, the terminal ethylene groups are staggered in one while being eclipsed in the other; second, the central C=C bond lengths differ markedly (1.340(8) and 1.381(7) Å). The latter difference signifies a difference in the charge states of the molecules. Comparison with corresponding bond lengths in other BEDT-TTF salts with established levels of oxidation²³ indicates charges of 0 and +1. The unipositive ions occur as face-to-face dimers, surrounded by monomeric neutral molecules (Figure 3a). Molecular planes of neighboring dimers along [011] are oriented nearly orthogonal to one another, as in the κ -phase structure of (BEDT-TTF)₂X,²⁴ but the planes of the dimers along [100] are parallel. Different charge states of BEDT-TTF have been found to coexist in the same lattice,²⁵ but the arrangement of (BEDT-TTF)₂²⁺ surrounded by (BEDT-TTF)⁰ has not been observed before. The distance between the mean plane of the molecules within the dimer (3.36 Å) is short, and the mode of overlap is not quite the "bond over ring" arrangement found in the κ -(BEDT-TTF)₂X phases.^{24,26} Overall the neutral molecules of the BEDT-TTF layer in the K and NH₄ salts describe an approximately hexagonal network, commensurate with that of the anion sublattice. The net effect is that the charged dimers are positioned in the neighborhood of the oxalate ions, leading to weak H-bonding between the terminal ethylene groups and oxalate O (2.51–3.05 Å). Short S...S distances are also observed between the molecules forming the dimers (3.46–

(21) Merrachi, E.-H.; Mentzen, B. F.; Chassigneux, F.; Boux, J. *Rev. Chim. Miner.* **1987**, *24*, 56–67.

(22) Wells, A. F. *Structural Inorganic Chemistry*, 4th ed.; Clarendon Press: Oxford, 1975; p 305.

(23) E.g.: Abdoud, K. A.; Clevenger, M. B.; de Oliveira, G. F.; Talham, D. R. *J. Chem. Soc., Chem. Commun.* **1993**, 1560–1562.

(24) E.g.: Yamochi, H.; Komatsu, T.; Matsukawa, N.; Saito, G.; Mori, T.; Kusunoki, M.; Sakaguchi, K. *J. Am. Chem. Soc.* **1993**, *115*, 11319–11327.

(25) Mori, T.; Inokuchi, H. *Bull. Chem. Soc. Jpn.* **1988**, *61*, 591–593.

(26) Kurmoo, M.; Pritchard, K. L.; Talham, D. R.; Day, P.; Stringer, A. M.; Howard, J. A. K. *Acta Crystallogr.* **1990**, *B46*, 348–354.

(BEDT-TTF)₄AFe(C₂O₄)₃C₆H₅CN (A = H₂O, K, NH₄)

J. Am. Chem. Soc., Vol. 117, No. 49, 1995 12213

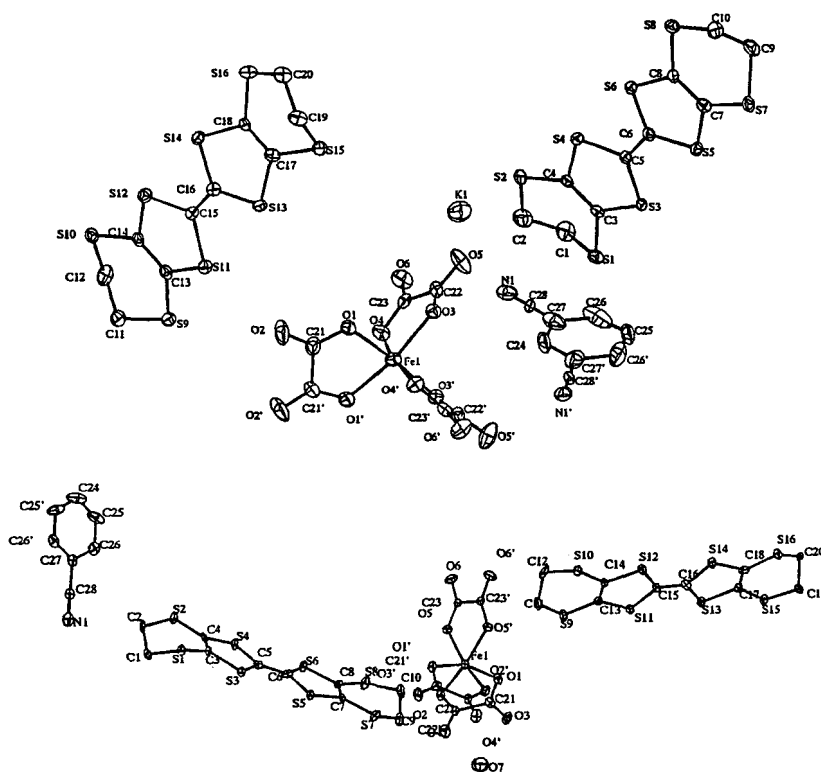


Figure 1. Atom numbering in (BEDT-TTF)₄AFe(C₂O₄)₃C₆H₅CN [A = K, NH₄ (a, top) and H₂O (b, bottom)] including thermal ellipsoids.

3.77 Å) and likewise between the charged and neutral molecules (3.19–4.45 Å). Further evidence for specific interaction between the terminal CH₂ groups of the BEDT-TTF and the anion layer comes from the translation of the Fe(C₂O₄)₃³⁻ complexes within the plane of the anion layer on passing from one layer to the next. The displacement of the Fe(C₂O₄)₃³⁻ matches with the tilt of the long axes of the intervening BEDT-TTF. Thus the contacts between H atoms and O are the same at both ends of the BEDT-TTF.

Packing of the BEDT-TTF molecules in the H₂O salt is quite different from that in the K and NH₄ salts: there are no discrete dimers (Figure 3b). Instead stacks are formed, with short S...S distances between them. Overall the packing closely resembles that of the β''-structure found in metallic (BEDT-TTF)₂AuBr₂¹³ and the pressure-induced superconductor (BEDT-TTF)₃Cl₂·2H₂O.²⁷ Finally, the planes of the BEDT-TTF molecules in adjacent layers are twisted with respect to one another, an unusual feature in BEDT-TTF salts, the only other example known being one phase of (BEDT-TTF)₂Ag(CN)₂.²⁸

Electronic Band Structure. The labeling of neighboring BEDT-TTF molecules in the A = K and A = H₂O compounds are shown in Figure 4 and the respective band structures, electronic densities of states, and Fermi surface in Figure 5. The transfer integrals are listed in Table 4. As far as the semiconducting K salt is concerned, the very large value of the intradimer transfer integral (563 meV) is immediately apparent, five times bigger than any of the others (Figure 3a). This large

value corresponds to a face-to-face (almost eclipsed) overlap of the two BEDT-TTF⁺ molecules. In fact the transfer integrals between the undimerized BEDT-TTF which carry zero charge are ten times smaller (45–58 meV), while between the dimer and single molecules, several are zero, and only one (A – II (B) – b) has a substantial value (110 meV). It is important to recall that the magnitude of the intermolecular transfer integral depends on the directional character of the intermolecular overlap between S orbitals, as much as the S...S distances. The other BEDT-TTF compounds containing well-defined dimeric units are the superconducting κ-phase salts,^{24,26} in which the intradimer transfer integrals lie within the range 200–300 meV, while all other integrals range between 50 and 150 meV. Moreover, the calculation shows that the difference in site energies between the crystallographically independent molecules, of the A = K salt (labeled A and B in Figure 4) amounts to 300 meV, while it is close to zero for the κ-(BEDT-TTF)₂Cu(NCS)₂ which contains two independent molecules of the same charge. However, in the present case this large difference and "dilution" of the dimers by individual BEDT-TTF serves to produce a closed shell semiconducting ground state, as indicated by the band structure shown in Figure 5a. The calculated band gap (0.3 eV) is in good agreement with that observed experimentally (0.28 eV). There exists certain similarity with the semiconducting salt κ-(MDT-TTF)₂Pt(CN)₄·H₂O²⁹ whose unit cell contains two orthogonal and independent dimers with different site energies and charges. One dimer exhibits an eclipsed geometry leading to a very large transfer integral, while the second intradimer integral is more than one-third smaller.

(27) Rosseinsky, M. J.; Kurmoo, M.; Talham, D. R.; Day, P.; Chasseau, D.; Watkin, D. *J. Chem. Soc., Chem. Commun.* 1988, 88–90.

(28) Kurmoo, M.; Day, P.; Stringer, A. M.; Howard, J. A. K.; Ducasse, L.; Pratt, F. L.; Singleton, J.; Hayes, W. *J. Mater. Chem.* 1993, 3, 1161–1170.

(29) Ducasse, L.; Mousdis, G.; Fettohi, M.; Ouahab, L.; Amiel, J.; Delhaes, P. *Synth. Met.* 1993, 56/1, 1995–2000.

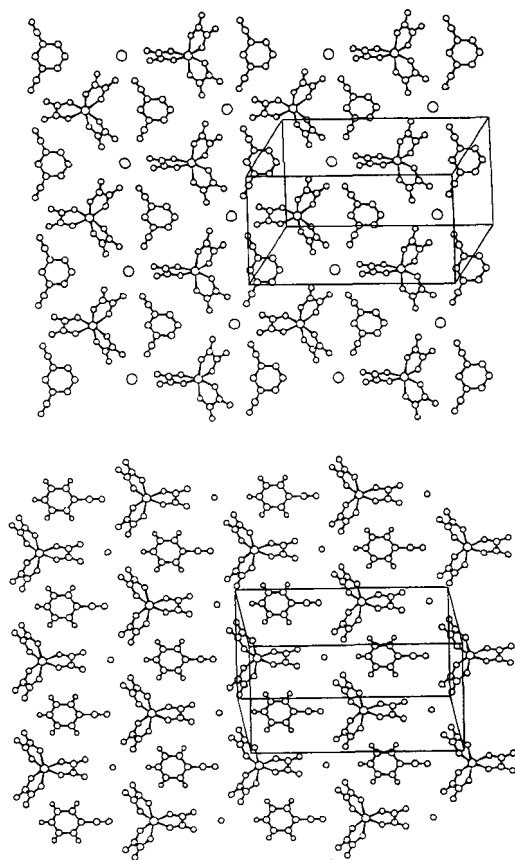


Figure 2. The anion and solvent layers in $(\text{BEDT-TTF})_4\text{AFe}(\text{C}_2\text{O}_4)_3 \cdot \text{C}_6\text{H}_5\text{CN}$: (a, top) $\text{A} = \text{K}$ and (b, bottom) $\text{A} = \text{H}_2\text{O}$.

As in the present case, several transfer integrals are close to zero. The following sections indicate that the physical properties of the $\text{A} = \text{K}$ salt agree with this prediction.

Turning to the $\text{A} = \text{H}_2\text{O}$ salt, we find the principal transfer integral values shown in Table 4. In contrast to the $\text{A} = \text{K}$ salt no one transfer integral dominates the others though the largest (188 and 156 meV) are between molecules in the [110] direction. This is therefore expected to be the most highly conducting direction. Transfer integrals orthogonal to that direction are only slightly smaller, however (111 meV), so conduction within the layers should not be very anisotropic. The average charge on each BEDT-TTF is $+3/4$, so the conduction band is $5/8$ filled. The energy band structure (Figure 5b) indicates that the Fermi level intersects bands in the MX and MY directions, leading to a prediction of metallic behavior. In fact the band structure predicts the existence of electron and hole pockets in the Fermi surface, as shown in Figure 5c. The physical measurements described in the following sections show that this material is indeed a metal, and the bandwidth derived from the optical data (1.0 eV) is in good agreement with the calculated one (1.1 eV).

Electrical Transport. The K and NH_4 salts are both semiconductors over the temperature range 130–300 K with the same activation energy (0.14 eV) along all three crystal axes, though with markedly anisotropic conductivity.³⁰ The conductivity in two orthogonal directions within the basal plane is quite similar (10^{-4} and $2 \times 10^{-4} \text{ S cm}^{-1}$ at 300 K), and orthogonal

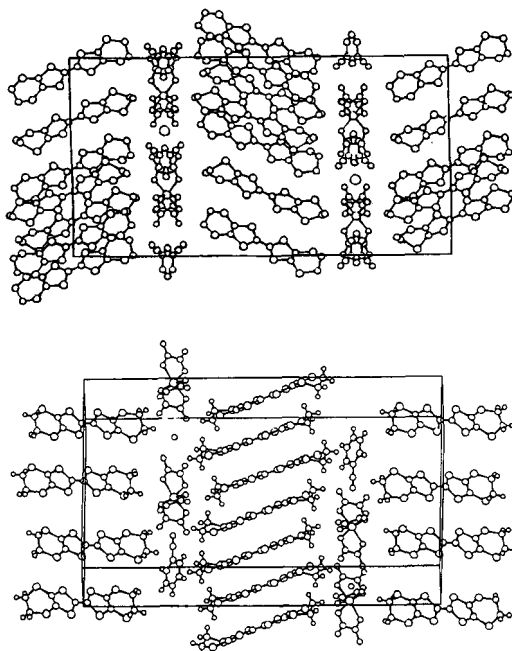


Figure 3. The layers of BEDT-TTF and anion layers in $(\text{BEDT-TTF})_4\text{AFe}(\text{C}_2\text{O}_4)_3 \cdot \text{C}_6\text{H}_5\text{CN}$: (a, top) $\text{A} = \text{K}$ and (b, bottom) $\text{A} = \text{H}_2\text{O}$.

to the plane is $8 \times 10^{-7} \text{ S cm}^{-1}$. In contrast the H_2O salt is a metal with resistivity of $\sim 10^{-2} \Omega \text{ cm}$ at 200 K, decreasing monotonically by a factor of about 8 down to just below 7 K, at which temperature it becomes superconducting (Figure 6). In some crystals there is a small upturn in the resistance just above T_c , but in others it continues to diminish with decreasing temperature to the point where it falls suddenly to zero. The transition is sharp (width about 0.2 K), and there is very little hysteresis on cooling and warming within the resolution of the temperature controller ($< 0.1 \text{ K}$). Application of a magnetic field parallel to the long axis of the needle crystals broadens the transition toward lower temperature in the manner seen in other quasi-two-dimensional BEDT-TTF salts³¹ so that the crystal remains resistive down to 2 K in fields above 0.7 T (Figure 7). With the applied field perpendicular to the needle axis the same effect is found at lower field (0.2 T) (Figure 8).

An important structural factor in the dimensionality of the conduction in the family of molecular charge transfer salts is the "thickness" of the anion layer separating the conducting planes of BEDT-TTF. A convenient measure of the thickness is the distance between the terminal C atoms of BEDT-TTF molecules on either side of the anion layer. Following that measure, a salt with a linear anion such as $\text{Cu}(\text{NCS})_2^-$ has an effective thickness of 5.32 \AA ,³² while ones with double anion layers like $[\text{KHg}(\text{SCN})_4]^-$ are distinctly thicker (7.42 \AA).³³ In the present compound the corresponding figure is 4.86 or 6.08

(30) Graham, A. W.; Kurmoo, M.; Day, P.; Coles, S. J.; Hursthouse, M. B.; Coomber, A. T.; Friend, R. H. *Mol. Cryst. Liq. Cryst.* In press.

(31) Ito, H.; Nogami, Y.; Ishiguro, T.; Komatsu, T.; Saito, G.; Hosoito, N. *Jpn. J. Appl. Phys.* **1992**, *7*, 419–425.

(32) Urayama, H.; Yamochi, H.; Saito, G.; Sato, S.; Kawamoto, A.; Tanaka, J.; Mori, T.; Maruyama, Y.; Inokuchi, H. *Chem. Lett.* **1988**, 463–466.

(33) Mori, H.; Tanaka, S.; Oshima, M.; Saito, G.; Mori, T.; Maruyama, Y.; Inokuchi, H. *Bull. Chem. Soc. Jpn.* **1990**, *63*, 2183–2190.

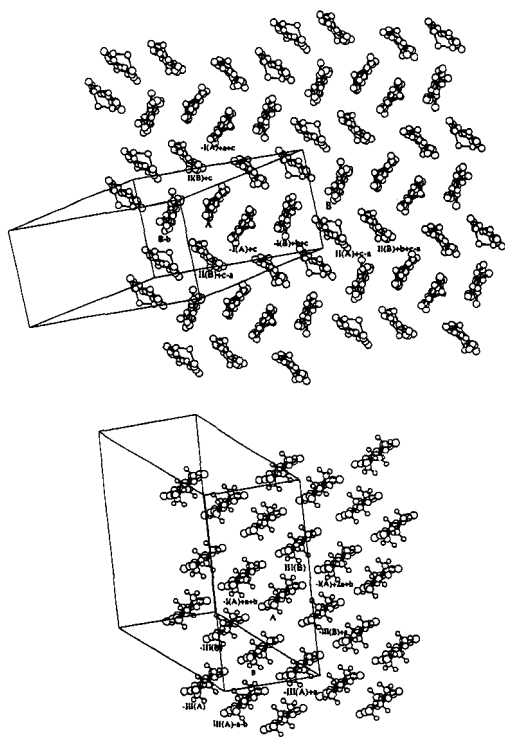
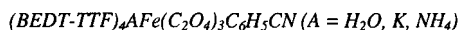


Figure 4. View of the BEDT-TTF layers along the C=C bonds including the labeling of neighboring BEDT-TTF molecules in $(\text{BEDT-TTF})_4\text{AFe}(\text{C}_2\text{O}_4)_3\text{C}_6\text{H}_5\text{CN}$: (a, top) $\text{A} = \text{K}$ and (b, bottom) $\text{A} = \text{H}_2\text{O}$.

Å depending on the BEDT-TTF molecule concerned. Evidently such a simple parameter cannot predict whether a given phase will be superconducting or not, or in case it is, what will be T_c , since the three cases quoted have T_c 10.4, 1.1, and 7.0 K, respectively. Nevertheless it is interesting that the present compound has such a relatively high T_c .

Magnetic Properties. The bulk susceptibilities of polycrystalline samples of $(\text{NH}_4)_3\text{Fe}(\text{C}_2\text{O}_4)_3 \cdot 3\text{H}_2\text{O}$ and $(\text{BEDT-TTF})_4\text{AFe}(\text{C}_2\text{O}_4)_3\text{C}_6\text{H}_5\text{CN}$ ($\text{A} = \text{K}, \text{H}_2\text{O}$) were measured in a variety of field and temperature protocols to determine the contribution of the conduction electrons and those localized on the Fe to the total magnetic response. $(\text{NH}_4)_3\text{Fe}(\text{C}_2\text{O}_4)_3 \cdot 3\text{H}_2\text{O}$ behaves as a Curie-Weiss paramagnet from 4–300 K with fitted $C = 4.38$ emu K mol⁻¹ and $\Theta = -1.29$ K. In the case of the semiconducting $\text{A} = \text{K}$ compound the susceptibility can be fitted to the Curie-Weiss law over the entire temperature range from 2 to 300 K. The least-square fitted value of the Curie constant $C = 4.44$ emu K mol⁻¹ and the Weiss constant = -0.25 K. On the assumption that $g = 2$, and there is no orbital contribution to the moment the value of C calculated for $S = 5/2$ is 4.375. Thus the Fe dominates the measured moment. In particular, there is effectively zero contribution from the BEDT-TTF, including those molecules whose bond lengths designate them as carrying a charge of +1. Hence the $(\text{BEDT-TTF})_2^{2+}$ dimers are spin-paired, while the remaining BEDT-TTF contribute nothing to the paramagnetic susceptibility, in agreement with the assignment of zero charge.

The susceptibility of the superconducting $\text{A} = \text{H}_2\text{O}$ salt obeys the Curie-Weiss law from 300 to about 1 K above T_c , though in contrast to the semiconducting $\text{A} = \text{K}$ salt, a temperature

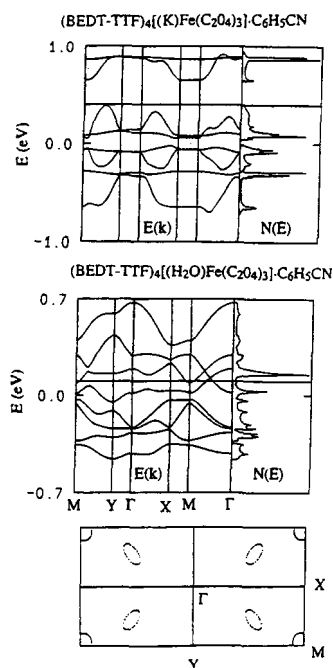


Figure 5. Band structures of $(\text{BEDT-TTF})_4\text{AFe}(\text{C}_2\text{O}_4)_3\text{C}_6\text{H}_5\text{CN}$: (a, top) $\text{A} = \text{K}$; (b, middle) $\text{A} = \text{H}_2\text{O}$; and (c, bottom) the calculated Fermi surface of $(\text{BEDT-TTF})_4(\text{H}_2\text{O})\text{Fe}(\text{C}_2\text{O}_4)_3\text{C}_6\text{H}_5\text{CN}$ showing electron and hole (shaded) pockets.

Table 4. Transfer Integrals (meV) of $(\text{BEDT-TTF})_4\text{AFe}(\text{C}_2\text{O}_4)_3\text{C}_6\text{H}_5\text{CN}$ ($\text{A} = \text{K}$ or H_2O)^a

		A = K			
A	-I (A) + c	+563	B	-I (B) + c + b	+45
A	-II (B) - b	-110	B	II(A) + c - a	0
A	-II (B) + c	0	B	II (A) + c	0
A	B - b	0	B	-II(A)	-106
A	II (B) + c - a	0	B	II (B) + c + b	+58
A	I + a + c	+11	B	II (B) + c - a + b	+58
-I (A)	II (B) + c - a	0	-II (B)	II (B) + c + b	+45
		A = H ₂ O			
A	B	+156	B	-III(B)	-46
A	III (B)	+188	B	III - a - b	187
A	-I (A) + a + b	-48	B	-III (A) + a	-110
A	-III (B) + a	-111	B	III (A)	-92
A	-I (A) + 2a + b	-109	B	-III (B) + a	-58
A	-III (B)	-92			

^a The labeling of the molecules relates to Figure 4.

independent paramagnetic term is present amounting to 20×10^{-4} emu mol⁻¹. This may be compared with metallic compounds having varying numbers of holes in the conduction band, viz. 4×10^{-4} emu mol⁻¹ for one hole in β - $(\text{BEDT-TTF})_2\text{AuI}_2$ ³⁴ and 7×10^{-4} emu mol⁻¹ for two holes in $(\text{BEDT-TTF})_3\text{Cl}_2 \cdot 2\text{H}_2\text{O}$.³⁵ The fitted Curie constant of 4.38 emu K mol⁻¹ is close to the value predicted for Fe^{3+} (${}^6\text{A}_1$), while the fitted Θ value (-0.2 K) signifies very weak antiferromagnetic exchange

(34) Talham, D. R.; Kurmoo, M.; Obertelli, D. S.; Parker, I. D.; Friend, R. H. *J. Phys. C: Solid State Phys.* 1986, 19, L383-L388.

(35) Obertelli, S. D.; Marsden, I. R.; Friend, R. H.; Kurmoo, M.; Rosseinsky, M. J.; Day, P.; Pratt, F. L.; Hayes, W. In *Physics and Chemistry of Organic Superconductors*; Saito, G., Kagoshima, S., Eds.; Springer Proceedings in Physics 51; Springer-Verlag: Berlin, 1990; pp 181-184.

(36) Caulfield, J.; Blundell, S. J.; Du Croc de Jongh, M. S. L.; Hendriks, P. T. J.; Singleton, J.; Doporo, M.; House, A.; Perenboom, J. A. A. J.; Hayes, W.; Kurmoo, M.; Day, P. *Phys. Rev. B* 1995, 51, 8325-8336.

12216 *J. Am. Chem. Soc.*, Vol. 117, No. 49, 1995

Kurmoo et al.

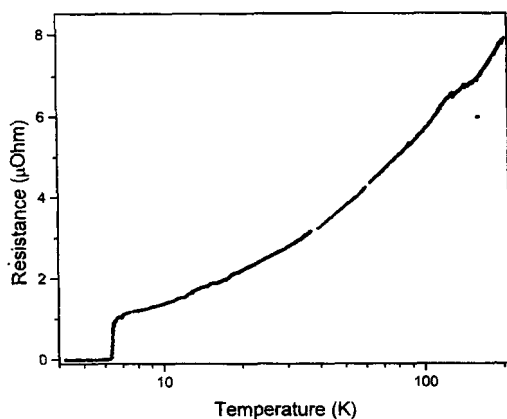


Figure 6. Temperature dependence of resistance of (BEDT-TTF)₄-(H₂O)Fe(C₂O₄)₃·C₆H₅CN from 5–200 K.

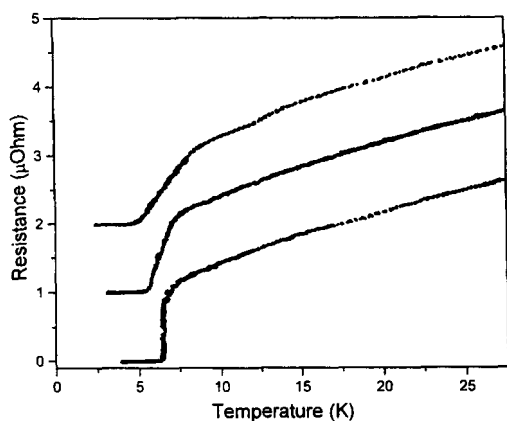


Figure 7. The superconducting transition in (BEDT-TTF)₄-(H₂O)Fe(C₂O₄)₃·C₆H₅CN as a function of magnetic field applied parallel to the needle axis: H = 0; 0.2 T; 0.6 T (bottom to top); the plots are displaced by 1 μohm).

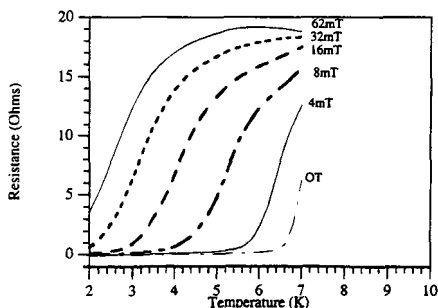


Figure 8. The superconducting transition as a function of magnetic field perpendicular to the needle axis from 0–62 mT.

between the Fe moments. As expected though, the temperature dependence of the susceptibility below 10 K is strongly dependent on the measurement field (Figure 9). When the sample is cooled to 2 K in zero field and then warmed in a measurement field of 0.5 mT, the susceptibility shows a distinct diamagnetic contribution expected in the superconducting temperature range, returning to Curie–Weiss behavior above

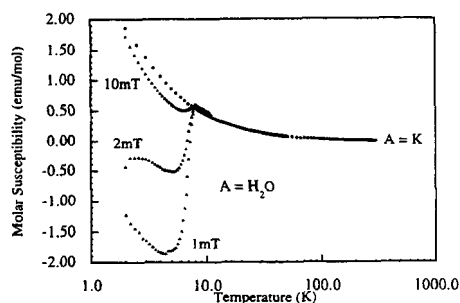


Figure 9. Temperature dependence of magnetic susceptibility of (BEDT-TTF)₄AFe(C₂O₄)₃·C₆H₅CN: A = K (dots) and A = H₂O (triangles).

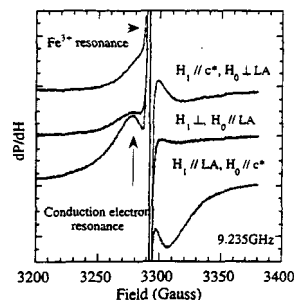


Figure 10. EPR spectra of (BEDT-TTF)₄(H₂O)Fe(C₂O₄)₃·C₆H₅CN at room temperature, at different crystal orientations.

10 K. On warming in increasingly large measurement fields the diamagnetic response diminishes, till it vanishes above 50 mT. At higher cooling or measurement fields (above 1 T) Curie–Weiss behavior persists down to 2 K, with a temperature independent contribution as at high temperature. Furthermore the onset of the diamagnetic contribution decreases from 8.0–(1) K (1 mT) to 7.2(2) K (40 mT). Finally the magnetization of both the H₂O and K compounds at high field can be fitted quite precisely to a Brillouin curve for $S = 5/2$, $g = 2$ with an extra contribution in the conductor for Pauli paramagnetism. To detect a Meissner effect the polycrystalline sample was cooled to 2 K in zero field, and the temperature dependence of the magnetization was measured in a field of 0.5 mT up to 20 K, followed by cooling in the same field. The Meissner effect is complete at 0.5 mT.

Further insight into the behavior of the magnetic electrons in both the semiconducting and superconducting compounds can be obtained from the EPR spectra of single crystals. The EPR spectrum of the semiconducting A = K compound consists of a single narrow resonance at $g = 2.002$ with peak to peak line width $H_{pp} = 1.6$ G independent of the crystal orientation. The line width and g -value are identical to those found in K₃Fe(C₂O₄)₃·3H₂O so the resonance is assigned to the Fe³⁺. As expected, because of the closed shell structure of the BEDT-TTF no other resonance signal is observed. On the other hand, the room temperature EPR spectrum of the A = H₂O compound consists of two resonances: an orientation independent narrow one ($H_{pp} = 1.5$ G) centered at 2.002, which can be assigned to the Fe³⁺ by analogy with the A = K compound, and a much broader resonance ($g = 2.002$ –2.012 and $H_{pp} = 23$ –35 G) which we assign to the conduction electrons (Figure 10). The former peak is Lorentzian in shape at all orientations of the crystal, while the conduction electron resonance becomes Dysonian at certain orientations. Considering the small size of

$(\text{BEDT-TTF})_4\text{AFe}(\text{C}_2\text{O}_4)_3\text{C}_6\text{H}_5\text{CN}$ ($A = \text{H}_2\text{O}, \text{K}, \text{NH}_4$)

the crystal this result points to a high conductivity, even at room temperature. Since the Dysonian line shape implies that the microwaves only penetrate the crystal to the skin depth, one would anticipate that all the resonances in the spectrum should have a similar line shape. It is therefore surprising that in the present case the Fe^{3+} resonance remains Lorentzian, while that of the conduction electrons is Dysonian. As a tentative explanation, we suggest that the fact that the conducting BEDT-TTF layers and the "insulating" anion layers are of comparable thickness may permit transmission of the microwaves through the latter, at the same time reducing it through the former. Further work is needed to clarify this point.

The condition to observe separate resonances due to the simultaneous presence of localized and conduction electrons in a lattice is that a large difference exists between the respective g -values and relaxation rates of the two spin systems. In the present case one of these conditions is clearly met, because the Fe^{3+} relaxation rate is high, producing a narrow signal. Furthermore, the loci of the two spin systems are certainly well separated spatially. Only in one other metallic charge transfer salt, $(\text{BEDT-TTF})_3\text{CuCl}_4 \cdot \text{H}_2\text{O}$, have separated resonances due to conduction and 3d electrons been observed,⁸ and there the angular dependence of the spectrum prevented direct comparison of the two line shapes. However in that compound, just as in the present example, the 3d ions are disposed in layers alternating with the BEDT-TTF sheets.

Optical Reflectivity. Figure 11 shows polarized spectra of the semiconducting ($A = \text{NH}_4$) and superconducting ($A = \text{H}_2\text{O}$) salts measured at room temperature. The spectrum of the semiconducting salt is less anisotropic than that of the metallic one and shows a broad electronic band which peaks near 2500 cm^{-1} (0.3 eV). This result should be compared with the electrical conductivity measurement which also indicates a gap of 0.28 eV. The spectrum of the semiconducting salt also contains several sharp vibrational bands below 1700 cm^{-1} which can be assigned to the oxalate C—O (1656 cm^{-1} terminal and 1280 cm^{-1} bridging) and C=C (1352 cm^{-1}) modes. When the electric vector is parallel to the layers, the spectrum of the metallic $A = \text{H}_2\text{O}$ salt is dominated by the electronic response with only weak vibrational structure superimposed, in contrast to the spectrum with electric vector perpendicular to the layers, which contains only vibrational bands. The Drude fit to the data observed in the parallel polarization is shown in Figure 11a. Analysis of the Drude edge was made using a one-dimensional model. The bandwidth is found to be 1.0 eV, in good agreement with that calculated for the band structure, and the optical mass (m^*) is 1.0 m_e . This mass and the large enhancement of the magnetic susceptibility again emphasize the substantial correlation between carriers at the Fermi level.

Conclusions

We have shown that the hexagonal layer motif $[\text{AM}^{\text{III}}(\text{C}_2\text{O}_4)_3]^{n-}$ containing bridging oxalate groups, which has been shown to form a wide variety of compounds with electronically inactive counter-cations having unusual cooperative magnetic properties⁹, can also stabilize lattices containing the organic π -donor BEDT-TTF. In the compounds whose

J. Am. Chem. Soc., Vol. 117, No. 49, 1995 12217

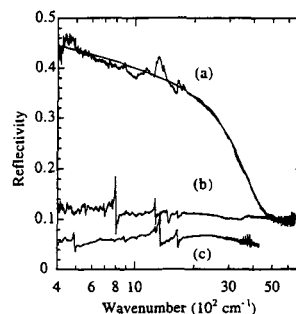


Figure 11. Room temperature polarized reflectivity spectra with the electric vector (a) parallel and (b) perpendicular to the layers of $(\text{BEDT-TTF})_4(\text{H}_2\text{O})\text{Fe}(\text{C}_2\text{O}_4)_3 \cdot \text{C}_6\text{H}_5\text{CN}$ and (c) parallel to the layers of $(\text{BEDT-TTF})_4(\text{NH}_4)\text{Fe}(\text{C}_2\text{O}_4)_3 \cdot \text{C}_6\text{H}_5\text{CN}$.

structures we describe here, $(\text{BEDT-TTF})_4\text{AFe}(\text{C}_2\text{O}_4)_3 \cdot \text{C}_6\text{H}_5\text{CN}$ ($A = \text{H}_2\text{O}, \text{K}, \text{NH}_4$), the lattice is stabilized by $\text{C}_6\text{H}_5\text{CN}$ molecules included in the hexagonal cavities. The oxalato-bridged network of A and M^{III} provides an elegant means of introducing transition metal ions carrying localized magnetic moments into the lattice of a molecular charge transfer salt. In the case of the $A = \text{H}_2\text{O}$ compound it has enabled us to prepare the first molecular superconductor containing localized magnetic moments within its structure, while the $A = \text{K}, \text{NH}_4$ compounds are semiconducting. The packing of the BEDT-TTF in the $A = \text{K}, \text{NH}_4$ phases is of a type not previously observed, with spin-paired $(\text{BEDT-TTF})_2^{2+}$ separated by closed shell $(\text{BEDT-TTF})^0$, while that in the superconductor is of β'' type. Both the superconducting $A = \text{H}_2\text{O}$ and semiconducting $A = \text{K}, \text{NH}_4$ phases contain high spin $3d^5 \text{Fe}^{\text{III}}$ with only very weak exchange interaction between them. Additional low temperature and high magnetic field experiments (e.g., of Schubnikov-de Haas oscillatory magnetoresistance³⁶) will be needed to delineate the Fermi surface in the superconductor. A further synthetic challenge will be to incorporate other transition metal ions at the A site to create a two-dimensional magnetically ordered array between the BEDT-TTF layers. Our efforts are continuing in this direction.

Acknowledgment. We thank the UK Engineering and Physical Science Research Council and the European Union (DG XII) for financial support. We thank Drs. S. G. Carling and P. A. Pattenden for discussions and technical help.

Supporting Information Available: Tables of fractional atomic coordinates, isotropic and anisotropic displacement parameters, and bond lengths and angles (8 pages); listing of observed and calculated structure factors (20 pages). This material is contained in many libraries on microfiche, immediately follows this article in the microfilm version of the journal, can be ordered from the ACS, and can be downloaded from the Internet; see any current masthead page for ordering information and Internet access instructions.

JA952346T

Crystal Chemistry and Physical Properties of Superconducting and Semiconducting Charge Transfer Salts of the Type (BEDT-TTF)₄[A^IM^{III}(C₂O₄)₃]·PhCN (A^I = H₃O, NH₄, K; M^{III} = Cr, Fe, Co, Al; BEDT-TTF = Bis(ethylenedithio)tetrathiafulvalene)

Lee Martin,[†] Scott S. Turner,^{*,†} Peter Day,^{*,†} Philippe Guionneau,[‡] Judith A. K. Howard,[§] Dai E. Hibbs,^{||} Mark E. Light,^{||} Michael B. Hursthouse,^{||} Mikio Uruichi,[⊥] and Kyuyo Yakushi[⊥]

Davy-Faraday Research Laboratory, The Royal Institution of Great Britain, 21 Albemarle Street, London, W1X 4BS, U.K., Laboratoire des Sciences Moléculaires, Institut de Chimie de la Matière Condensée de Bordeaux, 33608 Pessac Cedex, France, Department of Chemistry, University of Durham, South Road, Durham, DH1 3LE, U.K., Chemistry Department, University of Southampton, Highfield, Southampton, SO17 1BJ, U.K., and Institute of Molecular Sciences, Myodaichi, Okazaki, 444 Japan

Received October 31, 2000

Synthesis, structure determination by single-crystal X-ray diffraction, and physical properties are reported and compared for superconducting and semiconducting molecular charge-transfer salts with stoichiometry (BEDT-TTF)₄[A^IM^{III}(C₂O₄)₃]·PhCN, where A^I = H₃O, NH₄, K; M^{III} = Cr, Fe, Co, Al; BEDT-TTF = bis(ethylenedithio)tetrathiafulvalene. Attempts to substitute M^{III} with Ti, Ru, Rh, or Gd are also described. New compounds with M = Co and Al are prepared and detailed structural comparisons are made across the whole series. Compounds with A = H₃O⁺ and M = Cr, Fe are monoclinic (space group *C2/c*), at 150, 120 K *a* = 10.240(1) Å, 10.232(12) Å; *b* = 19.965(1) Å, 20.04(3) Å; *c* = 34.905(1) Å, 34.97(2) Å; β = 93.69(1)°, 93.25(11)°, respectively, both with *Z* = 4. These salts are metallic at room temperature, becoming superconducting at 5.5(5) or 8.5(5) K, respectively. A polymorph with A = H₃O⁺ and M = Cr is orthorhombic (*Pbcn*) with *a* = 10.371(2) Å, *b* = 19.518(3) Å, *c* = 35.646(3) Å, and *Z* = 4 at 150 K. When A = NH₄⁺, M = Fe, Co, Al, the compounds are also orthorhombic (*Pbcn*), with *a* = 10.370(5) Å, 10.340(1) Å, 10.318(7) Å; *b* = 19.588(12) Å, 19.502(1) Å, 19.460(4) Å; *c* = 35.790(8) Å, 35.768(1) Å, 35.808(8) Å at 150 K, respectively, with *Z* = 4. All of the *Pbcn* phases are semiconducting with activation energies between 0.15 and 0.22 eV. For those compounds which are thought to contain H₃O⁺, Raman spectroscopy or C=C and C–S bond lengths of the BEDT-TTF molecules confirm the presence of H₃O⁺ rather than H₂O. In the monoclinic compounds the BEDT-TTF molecules adopt a β'' packing motif while in the orthorhombic phases (BEDT-TTF)₂ dimers are surrounded by monomers. Raman spectra and bond length analysis for the latter confirm that each molecule of the dimer has a charge of +1 while the remaining donors are neutral. All of the compounds contain approximately hexagonal honeycomb layers of [AM(C₂O₄)₃] and PhCN, with the solvent occupying a cavity bounded by [M(C₂O₄)₃]³⁻ and A. In the monoclinic series each layer contains one enantiomeric conformation of the chiral [M(C₂O₄)₃]³⁻ anions with alternate layers having opposite chirality, whereas in the orthorhombic series the enantiomers form chains within each layer. Analysis of the supramolecular organization at the interface between the cation and anion layers shows that this difference is responsible for the two different BEDT-TTF packing motifs, as a consequence of weak H-bonding interactions between the terminal ethylene groups in the donor and the [M(C₂O₄)₃]³⁻ oxygen atoms.

Introduction

Since the 1957 report by Ginzburg,¹ which set out the conditions under which superconductivity could occur in magnetic materials, there have been numerous efforts by solid-state chemists to synthesize superconducting compounds containing arrays of magnetic ions. Among the earliest were the ternary borides such as ErRh₄B₄,² followed by the Chevrel phases, e.g., Pb_xSn_{1-x}Mo₆S₈³ and the borocarbides ErNi₂B₂C.⁴

Most recent is RuSr₂GdCu₂O₈,⁵ which becomes ferromagnetically ordered at a temperature (132 K) well above its superconducting *T*_c (40 K).⁶ Apart from the last example, all these systems involve exclusively 4f moments, so it is pertinent to search for highly conducting compounds containing magnetic 3d ions. A potentially fertile area is that of molecular-based charge-transfer salts, where the first superconducting example was reported as long ago as 1981.⁷ In such salts organochalcogenide donor molecules form the cations and may be combined with a wide variety of inorganic or organic anions.

* E-mail: sst@ri.ac.uk, pday@ri.ac.uk.

[†] Davy-Faraday Research Laboratory.

[‡] Institut de Chimie de la Matière Condensée de Bordeaux.

[§] University of Durham.

^{||} University of Southampton.

[⊥] Institute of Molecular Sciences.

(1) Ginzburg, V. L. *Sov. Phys. JETP* 1957, 4, 157.

(2) Fertig, W. A.; Johnston, D. C.; DeLong, L. E.; McCallum, R. W.; Maple, M. B.; Matthias, B. T. *Phys. Rev. Lett.* 1977, 38, 987.

(3) Ishikawa, M.; Fischer, Ø. *Solid State Commun.* 1977, 23, 37.

(4) Ng, T. K.; Varma, C. M. *Phys. Rev. Lett.* 1997, 78, 330.

(5) Bernhard, C.; Tallon, J. L.; Neidermayer, C.; Blasius, T.; Golnik, A.; Brucher, E.; Kremer, R. K.; Noakes, D. R.; Stronach, C. E.; Ansaldo, E. J. *Phys. Rev. B* 1999, 14099.

(6) Pringle, D. J.; Tallon, J. L.; Walker, B. G.; Trodahl, H. J. *Phys. Rev. B* 1999, R11679.

(7) Bechgaard, K.; Carriero, K.; Olsen, M.; Rasmussen, F.; Jacobsen, C. S. *Phys. Rev. Lett.* 1981, 46, 452.

Some years ago we embarked on a systematic examination of transition metal complexes as anions in charge-transfer salts⁸ and reported the first molecular superconductor which contained paramagnetic metal ions (and incidentally the first superconductor of any kind containing paramagnetic 3d ions).⁹ Subsequently one other molecular system has been reported,¹⁰ and its properties have been measured as a function of temperature, pressure, composition, and applied fields.¹¹

The paramagnetic molecular superconductor,⁹ initially formulated as β'' -(BEDT-TTF)₄[(H₂O)Fe(C₂O₄)₃]-PhCN (BEDT-TTF = bis(ethylenedithio)tetrathiafulvalene), consists of alternating layers of BEDT-TTF cations and layers containing the complex anions and solvent molecules. It is monoclinic (*C2/c*) but, in parallel, an orthorhombic phase (*Pbcn*) developed, in which the H₂O was replaced by K⁺ or NH₄⁺ while retaining the same overall arrangement of alternating cationic and anionic layers. However, the *Pbcn* derivatives are semiconducting, principally because the packing of the BEDT-TTF is different: in place of the β'' packing motif as found in numerous other superconducting BEDT-TTF charge-transfer salts is an arrangement that we called "pseudo κ ",⁹ consisting of neutral BEDT-TTF molecules surrounding a (BEDT-TTF⁺)₂ dimer. In both phases the [Fe(C₂O₄)₃]³⁻ anion, together with the H₂O, K⁺, or NH₄⁺, forms a planar hexagonal honeycomb network, reminiscent of that found in the extensive series of molecular-based bimetallic magnets with stoichiometry A^I[M^{II}M^{III}(C₂O₄)₃], where here A^I is an organic cation such as tetraalkyl- or tetraarylammonium or -phosphonium.^{12,13} An important issue arose as to why a similar arrangement of anions should lead to two such different arrangements of the BEDT-TTF cations. Furthermore, a crucial point of detail in relating the crystal and electronic structure of the superconducting phase to its physical properties concerns the mean charge on the BEDT-TTF. This charge is balanced by that of the anion layer, so the determining factor is whether the water molecule is present as H₂O or H₃O⁺. The earlier crystallographic work⁹ was inconclusive, but the water was assigned as H₂O on considering the O(H₂O)...O(oxalate) distances.

It is clearly of interest to explore other phases with the general formula (BEDT-TTF)₄[M(C₂O₄)₃]-solvent, where M is a transition or even nontransition metal ion, to see how the transport and magnetic parameters change with the magnitude of the magnetic moment, and any small systematic changes in

intra- and intermolecular distances. It is also important to clarify whether the monoclinic and orthorhombic compounds can be regarded as polymorphs with the same mean charge on the BEDT-TTF cations and, if so, to clarify the physical origin of the polymorphism. Here we report our efforts to prepare materials with other metal ions, the crystal structures of two new compounds with M = Co and Al, and their basic physical characterization by transport and magnetic susceptibility measurements. Additionally, we report Raman spectra of these and the earlier compounds, which show in every case that the (BEDT-TTF)₄ unit has a +2 charge, irrespective of the donor packing motif or the salt composition. A comparison of the supramolecular organization of the monoclinic and orthorhombic phases leads to an explanation for the different packing arrangements of the donor cations, based on different spatial distributions of the enantiomeric [M(C₂O₄)₃]³⁻ in the racemic lattices. Preliminary brief accounts of part of this work have appeared.^{14,15} It is interesting to note that recently a BEDT-TTF salt with a bimetallic layer anion [MnCr(C₂O₄)₃]⁻ was reported to be metallic down to 4 K and ferromagnetic below 5.5 K. However, only a partial structure was determined because of disorder in the anion layer, and furthermore the included solvent molecules were not located.¹⁶

Experimental Section

Synthesis of Starting Materials. Numerous tris(oxalato)metalate-(III) salts were synthesized by literature methods for use in the subsequent electrochemical crystal growth of BEDT-TTF charge-transfer salts. For the previously reported salts with M = Fe or Cr, see the published articles for details.^{9,14} The following starting materials were also prepared as indicated and recrystallized several times before use. (NH₄)₃[Ti(C₂O₄)₃]-10H₂O,¹⁷ K₃[Cr(C₂O₄)₃]-2H₂O,¹⁸ (NH₄)₃[Co(C₂O₄)₃]-3.5H₂O,¹⁸ (NH₄)₃[Ru(C₂O₄)₃]-1.5H₂O,¹⁹ K₃[Ru(C₂O₄)₃]-4.5H₂O,²⁰ (NH₄)₃[Rh(C₂O₄)₃]-4.5H₂O,^{21,22} Gd₃(C₂O₄)₃-10H₂O,²³ (NH₄)₃[Al(C₂O₄)₃]-3H₂O,¹⁸ K₃[Al(C₂O₄)₃]-3H₂O.¹⁸ The compositions were confirmed by elemental analysis, carried out by University College London Microanalytical Laboratory. BEDT-TTF (Aldrich) was recrystallized from CHCl₃, 18-crown-6 (Aldrich) was purified over MeCN, PhCN (Aldrich) was fractionally distilled over P₂O₅ immediately prior to use, and H₂O was also freshly distilled.

Synthesis of BEDT-TTF Charge-Transfer Salts. Crystal growth took place in H-shaped electrocrystallization cells (maximum volume 50 mL) with a Pt electrode in each arm separated by a glass frit in the "H" cross piece. The cathode was protected by a second frit to prevent contamination by reduction products. The cells were washed with aqua regia followed by distilled H₂O and dried thoroughly. The electrodes were cleaned with nitric acid, after which an ac current was passed through them in dilute H₂SO₄, and finally they were washed in distilled H₂O and thoroughly dried.

In each case 100 mg of the tris(oxalato)metalate salt and 200 mg of 18-crown-6 were dissolved in 50 mL of PhCN. For those compounds which finally contain H₃O⁺, the anion source was the ammonium salt, and two drops of water were added after rapid stirring. Ten milligrams of solid BEDT-TTF was placed in the anode side of the H-cell, and

- (8) Mallah, T.; Hollis, C.; Bott, S.; Kurmoo, M.; Day, P. *J. Chem. Soc., Dalton Trans.* **1990**, 859. Day, P.; Kurmoo, M.; Mallah, T.; Marsden, I. R.; Allan, M. L.; Friend, R. H.; Pratt, F. L.; Hayes, W.; Chasseau, D.; Bravic, G.; Ducasse, L. *J. Am. Chem. Soc.* **1992**, *114*, 10722. Marsden, I. R.; Allan, M. L.; Friend, R. H.; Kurmoo, M.; Kanazawa, D.; Day, P.; Bravic, G.; Chasseau, D.; Ducasse, L.; Hayes, W. *Phys. Rev. B* **1994**, *50*, 2118. Kurmoo, M.; Day, P.; Guionneau, P.; Gaultier, J.; Chasseau, D.; Ducasse, L.; Allan, M. L.; Marsden, I. R.; Bravic, G.; Friend, R. H. *Inorg. Chem.* **1996**, *35*, 4719. Kepert, C. J.; Kurmoo, M.; Day, P. *Inorg. Chem.* **1997**, *36*, 1128. Kepert, C. J.; Kurmoo, M.; Day, P. *J. Chem. Soc., Dalton Trans.* **1997**, 607. Kepert, C. J.; Kurmoo, M.; Day, P. *J. Mater. Chem.* **1997**, *7*, 221.
- (9) Kurmoo, M.; Graham, A. W.; Day, P.; Coles, S. J.; Hursthouse, M. B.; Caulfield, J. L.; Singleton, J.; Pratt, F. L.; Hayes, W.; Ducasse, L.; Guionneau, P. *J. Am. Chem. Soc.* **1995**, *117*, 12209.
- (10) Kobayashi, H.; Tomita, H.; Naito, T.; Kobayashi, A.; Sakai, F.; Watanabe, T.; Cassoux, P. *J. Am. Chem. Soc.* **1996**, *118*, 368.
- (11) Kobayashi, H.; Sato, A.; Arai, E.; Akutsu, H.; Kobayashi, A.; Cassoux, P. *J. Am. Chem. Soc.* **1997**, *119*, 12392. Sato, A.; Ojima, E.; Akutsu, H.; Kobayashi, H.; Kobayashi, A.; Cassoux, P. *Chem. Lett.* **1998**, 673. Kobayashi, H.; Akutsu, H.; Ojima, E.; Sato, A.; Tanaka, H.; Kobayashi, A.; Casoux, P. *Synth. Met.* **1999**, *103*, 1837.
- (12) Decurtins, S.; Schmalla, H. W.; Oswald, H. R.; Linden, A.; Enstling, J.; Gutlich, P.; Hauser, A. *Inorg. Chim. Acta* **1994**, *216*, 65.
- (13) Mathioniere, C.; Nuttall, C. J.; Carling, S. G.; Day, P. *Inorg. Chem.* **1996**, *35*, 1201.
- (14) Martin, L.; Turner, S. S.; Day, P.; Mabbs, F. E.; McInnes E. *J. Chem. Soc., Chem Commun.* **1997**, 1367.
- (15) Martin, L.; Turner, S. S.; Day, P.; Malik, K. M. A.; Coles, S. J.; Hursthouse, M. B. *J. Chem. Soc., Chem. Commun.* **1999**, 513.
- (16) Coronado, E.; Galan-Mascaros, J. R.; Gomez-Garcia, C. J.; Laukhin, V. *Nature* **2000**, *408*, 447.
- (17) Piper, T. S.; Carlin, R. L. *J. Chem. Phys.* **1961**, *35*, 1800.
- (18) Bachar, J. C.; Jones, E. M. *Inorg. Synth.* **1939**, *1*, 35.
- (19) Key, D. L.; Larkworthy, L. F.; Salmon, J. E. *J. Chem. Soc. A* **1971**, 371.
- (20) Kaziro, R.; Hambley, T. W.; Bunstead, R. A.; Beattie, J. K. *Inorg. Chim. Acta* **1989**, *164*, 85.
- (21) Werner, A.; Poupardin, J. *Ber. Dtsch. Chem. Ges.* **1914**, *47*, 1955.
- (22) Gillard, R. D.; Laurie, S. H.; Mitchell, R. J. *Chem. Soc. A* **1969**, 3006.
- (23) Wendlandt, W. W. *Ann. Chem.* **1958**, *30*, 58.

Properties of Charge Transfer Salts

the remainder of the cell was filled with the filtered PhCN mixture. At a temperature of 295(2) K a constant current of 1 μ A was applied across the cell and where crystals grew on the anode they did so over an average of 21 days.

Results of the crystal growth, with the named tris(oxalato)metalate complexes, were as follows. $(\text{NH}_4)_3[\text{Ti}(\text{C}_2\text{O}_4)_3] \cdot 10\text{H}_2\text{O}$: very thin black needles. $\text{K}_3[\text{Cr}(\text{C}_2\text{O}_4)_3] \cdot 3\text{H}_2\text{O}$: no crystals grew over 21 days. $(\text{NH}_4)_3[\text{Co}(\text{C}_2\text{O}_4)_3] \cdot 3.5\text{H}_2\text{O}$: black needle-shaped crystals which were of good enough quality for single-crystal X-ray structural determination and were found to be (BEDT-TTF) $_4$ [(NH₄)₃Co(C₂O₄)₃]·PhCN, **I**. $(\text{NH}_4)_3[\text{Ru}(\text{C}_2\text{O}_4)_3] \cdot 1.5\text{H}_2\text{O}$: no crystal growth occurred after 28 days. $\text{K}_3[\text{Ru}(\text{C}_2\text{O}_4)_3] \cdot 4.5\text{H}_2\text{O}$: no crystals grew over 21 days. $(\text{NH}_4)_3[\text{Rh}(\text{C}_2\text{O}_4)_3] \cdot 4.5\text{H}_2\text{O}$: a small amount of very small black needles grew over 14 days but formed as aggregates and were unsuitable for physical measurements. $\text{Gd}_2(\text{C}_2\text{O}_4)_3 \cdot 10\text{H}_2\text{O}$: large black plates. $(\text{NH}_4)_3[\text{Al}(\text{C}_2\text{O}_4)_3] \cdot 3\text{H}_2\text{O}$: a small quantity of square plates of very good quality which were suitable for single-crystal X-ray structural determination were found to be (BEDT-TTF) $_4$ [(NH₄)₃Al(C₂O₄)₃]·PhCN, **II**. $\text{K}_3[\text{Al}(\text{C}_2\text{O}_4)_3] \cdot 3\text{H}_2\text{O}$: no crystals grew over 21 days.

Enantiomerically Pure Starting Materials. Since tris(oxalato)metalate complexes are chiral, the opportunity exists in principle to make BEDT-TTF salts containing only a single enantiomer. For example with Λ - $(\text{NH}_4)_3[\text{Cr}(\text{C}_2\text{O}_4)_3] \cdot \text{H}_2\text{O}$ or Δ - $(\text{NH}_4)_3[\text{Cr}(\text{C}_2\text{O}_4)_3] \cdot \text{H}_2\text{O}$, prepared by literature methods,²⁴ no crystals grew in the first 12 days, followed by a period of rapid growth for 3 days which yielded a large quantity of black cubes.¹⁴ However, with Λ - $(\text{NH}_4)_3[\text{Rh}(\text{C}_2\text{O}_4)_3] \cdot \text{H}_2\text{O}$ or Δ - $\text{K}_3[\text{Cr}(\text{C}_2\text{O}_4)_3] \cdot \text{H}_2\text{O}$ no crystals had grown after 28 days.

Crystal Structure Determination. For M = Co, compound **I**, a black needle single crystal was mounted on a glass fiber and positioned on a Bruker smart CCD. The quality of the crystal was checked at room temperature from a cell parameter determination which gave an orthorhombic crystal system ($a = 10.407(1)$ Å, $b = 19.600(1)$ Å, $c = 36.162(1)$ Å). Then the sample was cooled (4 K min⁻¹) in order to reduce the strong thermal agitation which usually affects the BEDT-TTF/[M(C₂O₄)₃]^{m-} salts at room temperature.²⁵ The data collection was then run at 150(2) K with graphite-monochromated Mo K α radiation ($\lambda = 0.71069$ Å). The diffraction frames were integrated using the SAINT package²⁶ and corrected with SADABS.²⁷ The crystal structures were solved and refined with the SHELXTL-plus programs.²⁸ For M = Al single plate crystals, X-ray diffraction data were collected at 150-(2) K using an Enraf Nonius Kappa CCD area detector with Mo K α radiation and an Oxford Cryosystem N₂ open flow cryostat. The structure was solved by direct methods and refined anisotropically on F^2 by full-matrix least squares using SHELXL97.²⁹ All hydrogen atoms were placed in idealized positions and refined using a riding model.

Physical Measurements. Transport Measurements. Transport measurements of low-resistance and metallic samples were made by the four-probe dc method. Two probe measurements were used for samples with high intrinsic resistance where contact effects were assumed to be negligible. Gold wire electrodes were attached to the crystal using Pt paint, and the attached wires were connected to a standard eight-pin integrated circuit plug with Ag paint. Silver paint was not used for contacts to the sample due to the possible formation of AgS at the electrode-crystal interface. The eight-pin plugs were mounted in an Oxford instruments CF200 continuous-flow cryostat and connected to a Hewlett-Packard 3478A digital multimeter.

Magnetic Susceptibility. Magnetic susceptibility data were measured using a Quantum Design MPMS7 SQUID magnetometer. Measurements were made on polycrystalline samples in a gelatine capsule, and

Inorganic Chemistry, Vol. 40, No. 6, 2001 1365

the molar susceptibility was corrected for core diamagnetism estimated from Pascal's constants. For the superconducting compounds a strong field exclusion effect was observed when the samples were cooled in zero field to 2 K and a small field of 5 G was applied. Magnetization measurements were then made while heating the sample to 12 K, which was assumed to be above T_c . The Meissner-Ochsenfeld field expulsion effect is observed on keeping the field constant and then measuring the magnetic susceptibility while recooling. Each superconductor showed an increase in magnetization which indicated some flux penetration.

Infrared Spectroscopy. Polarized optical reflectivity of single crystals was recorded at ambient temperature from 800 to 4000 cm⁻¹ using a Perkin-Elmer 1710 spectrometer fitted with a Spectra Tech microscope and a KRSS polarizer. Measurements were made with the electric vector both parallel and perpendicular to the edge of the crystal. Ambient and low-temperature reflectivity was measured using a Spectra-Tech IR-plan microscope fitted in the sample chamber of an FT-IR Nicolet Magna 760 spectrometer. Spectra were collected between 600 and 4000 cm⁻¹ using an IR light source, MCT detector, KBr beam splitter, and wire grid polarizer with 4 cm⁻¹ resolution; between 3500 and 10000 cm⁻¹ using a white light source, MCT detector, quartz beam splitter, and NIR/VIS Glan-Thompson polarizer with 32 cm⁻¹ resolution; and between 9000 and 12000 cm⁻¹ using a white light source, Si detector, quartz beam splitter, and the same polarizer. Single crystals were fixed on a copper sample holder with silicon grease. The crystal face was adjusted to be nearly normal to the incident light using a small goniometer head attached to an Oxford Instruments CF1104S cryostat. The sample was covered by a radiation shield and vacuum shroud with a KBr window. To avoid the sample being contaminated at low temperature, the window of the radiation shield was only opened during measurement. The absolute reflectivity was obtained by comparison with the reflected light from a Au mirror placed close to the sample. At each temperature the reflectivity of this inner mirror was monitored with respect to a gold mirror outside the cryostat chamber. Spectra from 10000 to 32000 cm⁻¹ were measured using the same microscope, combined with a multichannel detection system (Atago Macs320) using a xenon lamp light source and Glan-Thompson polarizer.

Raman Spectroscopy. Raman spectra of single crystals were measured at room temperature with a Renishaw Raman Imaging microscope using a He-Ne laser ($\lambda = 632.6$ nm) with 10% filter. Samples were measured both parallel and perpendicular to the incident beam and were scanned from 100 to 4000 cm⁻¹ while longer scans were performed from 1150 to 1650 cm⁻¹ to observe the stretching frequencies of the C=C bonds in BEDT-TTF. Spectra were identical when measured both parallel and perpendicular to the incident beam (in the same plane of the crystal plates or needles) with only minor changes in peak shifts and intensity. Spectra of metallic salts showed considerably more noise and broader absorption than those of the semiconducting samples and of neutral BEDT-TTF.

Results and Discussion

Description of Crystal Structures. A common feature of charge-transfer salts, based on the donor molecule BEDT-TTF, is the spatial segregation of cations and anions into alternating layers, although occasionally "chess board" patterns can appear as with the [Ge(C₂O₄)₃]⁴⁻ salt.²⁵ The structures of all of the salts of BEDT-TTF and tris(oxalato)metalate(III) anions with PhCN consist of layers of BEDT-TTF molecules interleaved with anionic layers which contain [M^{III}(C₂O₄)₃]³⁻, PhCN, and cations A¹ = H₃O⁺, NH₄⁺ or K⁺. Figure 1 shows an example of the layered structure in one of these salts. Crystal data for the new compounds are presented in Table 1 along with comparative data for other compounds in this series; compounds **I** and **II** are the new salts, and **III-VI** are included for structural comparisons. The compound shorthand, **I-VI**, is used in the other tables; compound **VII** is that with M = Fe and A = K. As noted in the original work,⁹ two distinct phases have been found in this series with monoclinic ($C2/c$) and orthorhombic

(24) Kauffman, G. B.; Sugisaka, N.; Reid, I. K. *Inorg. Chem.* **1989**, *28*, 139.

(25) Martin, L.; Turner, S. S.; Day, P.; Guionneau, P.; Howard, J. A. K.; Uruchi, M.; Yakushi, K. *J. Mater. Chem.* **1999**, *9*, 2731.

(26) SAINT, version 4.050; Siemens Analytical X-ray Instruments: Madison, WI, 1995.

(27) Sheldrick, G. M. *SADABS, Empirical Absorption Program*; University of Göttingen: Göttingen, Germany, 1995.

(28) Sheldrick, G. M. *SHELXTL-Plus*, release 4.1; Siemens Analytical X-ray Instruments Inc.: Madison, WI, 1991.

(29) Sheldrick, G. M. *SHELXL97*; University of Göttingen: Göttingen, Germany, 1997.

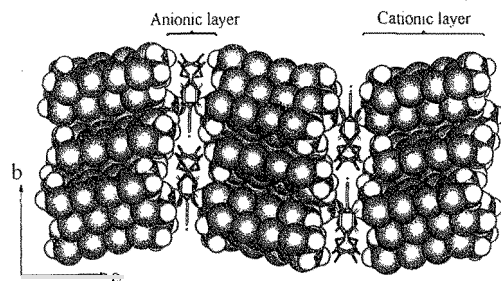


Figure 1. The layered structure in $(\text{BEDT-TTF})_4[\text{AM}(\text{C}_2\text{O}_4)_3]\cdot\text{PhCN}$ salts.

(*Pbcn*) space groups. Standard ORTEP³⁰ diagrams with the atom-numbering scheme and 50% thermal ellipsoids for compounds **I** and **II** with $M = \text{Co}$ and Al , respectively, both of which have the *Pbcn* structure, are shown in Figures 2 and 3.

Anion Layers. Within each anion layer, the A^1 and $[\text{M}^{\text{III}}(\text{C}_2\text{O}_4)_3]^{3-}$ groups adopt a "honeycomb" arrangement with a PhCN molecule occupying a hexagonal cavity (Figure 4, top). The PhCN is fully ordered in the monoclinic phases with the $\text{C}\equiv\text{N}$ bond directed toward the metal atom of the tris(oxalato) anion, while in the orthorhombic phases it exhibits 2-fold disorder over two static orientations with the $\text{C}\equiv\text{N}$ bonds directed toward A^1 . The solvent may play a "templating" role in stabilizing the lattice. The area of the cavity is $\approx 1 \text{ \AA}^2$ smaller in the orthorhombic series, because a longer metal to metal distance (c in Figure 4, top right) is needed to accommodate the $-\text{C}\equiv\text{N}$ groups on either side, while the cavity in the monoclinic phases is extended along the b axis (a in Figure 4, top left). The orthorhombic salt with $M = \text{Al}$ and $A = \text{NH}_4$ has a slightly smaller cavity than the corresponding Cr, Fe, and Co salts, having a longer $M^{\text{III}}-A^1$ distance (a in Figure 4, top right) yet shorter "b" and "c" distances. The metals are octahedrally coordinated to three bidentate $[\text{C}_2\text{O}_4]^{2-}$ ligands which confer D_3 point symmetry about the metal. The O atoms of the oxalato ion which are not coordinated to M bound a cavity which is occupied by A^1 (Figure 4, bottom). In the monoclinic phase the A^1 site is approximately octahedral, whereas in the orthorhombic one it also accommodates two $\text{C}\equiv\text{N}$ groups of the PhCN, rendering the site eight coordinate. Furthermore, in the orthorhombic phases the terminal O atoms are not disposed octahedrally because one of the three $[\text{M}(\text{C}_2\text{O}_4)_3]^{3-}$ around the A^1 cavity has chirality opposite to that of the other two (Figure 4, bottom right).

The mean $A^1-\text{O}(\text{oxalate})$ distances are close to those expected for H-bonded cations for $A^1 = \text{NH}_4$ or H_3O . In both monoclinic and orthorhombic phases, there are three crystallographically independent $[\text{C}_2\text{O}_4]^{2-}$ O atoms (O2, O4, and O6 in Figures 2 and 3) at short distances from the cation A. In the monoclinic structures, two of these distances are distinctly shorter than the third (Table 2), which led to the initial suggestion that A^1 might be H_2O rather than H_3O^+ .

Perhaps the most unusual aspect of these two series of compounds concerns the chirality of the anion layer. Since the $[\text{M}^{\text{III}}(\text{C}_2\text{O}_4)_3]^{3-}$ has D_3 point symmetry, it can exist in two enantiomeric forms, Δ and Λ . In the monoclinic phases, each anionic layer consists exclusively of a single enantiomer (Figure 4, left), with the next layer containing only the other enantiomer, to give a $\dots\Delta-\Lambda-\Delta-\Lambda-\Delta-\Lambda\dots$ repeating pattern (where $-$

represents segregation by a layer of donor molecules). By contrast, in the orthorhombic phases each anion layer contains a 1:1 ratio of Δ and Λ enantiomers arranged in alternating rows with a $\dots\Delta\Lambda-\Delta\Lambda-\Delta\Lambda-\Delta\Lambda\dots$ pattern (Figure 4, right). In both phases there is a C_2 rotation from one anion layer to the next.

In all compounds the planes of the PhCN solvent molecule are not parallel to the plane defined by the metal atoms in the anionic layer, although to a different extent. In monoclinic materials the solvent is slightly closer to one edge of the hexagonal cavity than in orthorhombic salts. As a result, the phenyl ring of the solvent lies close to the two oxalate ligands which form the base of the hexagonal cavity (see dashed line in Figure 4, top left). The planes of these two ligands make angles of $\approx 70^\circ$ to the plane of this cavity, and the phenyl ring is almost parallel to these ligands, thus minimizing the void space around the included solvent molecule. However, in the orthorhombic phases, the phenyl ring is closer to the center of the cavity.

Finally we examine the geometry of the $[\text{M}(\text{C}_2\text{O}_4)_3]^{3-}$ themselves. Figures 2 and 3 shows the atom-numbering scheme used for comparing the bond lengths and angles, a selection of which are listed in Table 3. First, it should be noted that the $M^{\text{III}}-\text{O}(\text{oxalate})$ bonds are significantly shorter in the orthorhombic salts with $A^1 = \text{NH}_4^+$ than in any of the other structures, while the $M^{\text{III}}-\text{O}(\text{oxalate})$ bond lengths in the Cr salts are slightly longer than those observed in the crystal structure of $(\text{NH}_4)_3[\text{Cr}(\text{C}_2\text{O}_4)_3]\cdot 3\text{H}_2\text{O}$ (1.96 \AA at 293 K²⁸). The inner O-C distances (not listed) are very similar and close to that expected (1.28 \AA at 293 K³¹). The O- M^{III} -O angles in most of the salts are less than the 85° found in the 293 K crystal structure of $(\text{NH}_4)_3[\text{Cr}(\text{C}_2\text{O}_4)_3]\cdot 3\text{H}_2\text{O}$, being slightly smaller in the monoclinic phases (78.5 – 82.7°) than the orthorhombic ones (80.9 – 86.2°).

BEDT-TTF Cation Layers. We find two quite different types of packing of the donor molecules. The monoclinic phases adopt a β'' packing motif, similar to the pressure-induced superconductor $(\text{BEDT-TTF})_2\text{Cl}_2\cdot 2\text{H}_2\text{O}$,³² while the orthorhombic phases have a novel "pseudo- κ " arrangement (Figure 5). In the β'' phases, the planes of the BEDT-TTF molecules in adjacent layers are twisted with respect to one another, a feature only observed previously in a phase of $(\text{BEDT-TTF})_2\text{Ag}(\text{CN})_2$.³³ The two crystallographically independent BEDT-TTF are rotated by 61.8° and 63.9° , respectively, measured between the planar central TTF portions of the donors, due to the steric influence imposed upon them by the anion layer. The BEDT-TTF molecules form regular stacks with numerous close $S\cdots S$ distances, those below and close to the van der Waals distance (3.6 \AA) being given in Table 4 and marked in Figure 5. The shortest $S\cdots S$ contacts are side-to-side interactions between neighboring stacks (Figure 5a), the shortest being between the S atoms of adjacent outer, six-membered rings. The two crystallographically independent BEDT-TTF molecules each have a twisted and eclipsed conformation. The terminal ethylene C-C bonds and C=C double bond lengths increase slightly

(30) Johnson, C. K. ORTEP. Report ORNL-5138; Oak Ridge National Laboratory: Oak Ridge, TN, 1976.

(31) Van Nierkerk, J. N.; Schoening, F. R. L. *Acta Crystallogr.* **1952**, *5*, 499.

(32) Rosseinsky, M. J.; Kurmoo, M.; Talham, D. R.; Day, P.; Chasseau, D.; Watkin, D.; *J. Chem. Soc., Chem. Commun.* **1983**, 88. Gaultier, J.; Gebrand-Brachetti, S.; Guionneau, P.; Kepert, C. J.; Chasseau, D.; Ducasse, L.; Burrows, Y.; Kurmoo, M.; Day, P. *J. Sol. State Chem.* **1999**, *145*, 496.

(33) Kurmoo, M.; Day, P.; Stringer, A. M.; Howard, J. A. K.; Ducasse, L.; Pratt, F. L.; Singleton, J.; Hayes, W. J. *Mater. Chem.* **1993**, *3*, 1161.

Table 1. Summary of Crystal Data for Selected Compounds with the Stoichiometry (BEDT-TTF)₄[A^{III}(C₂O₄)₃]·PhCN

	I	II	III	IV	V	VI
M ^{III}	Co	Al	Fe ^{II}	Cr ^{II}	Cr ^{II}	Fe ^{II}
A ^I	NH ₄	NH ₄	H ₂ O	H ₂ O	H ₂ O	NH ₄
chem formula	C ₅₃ H ₄₁ O ₁₂ S ₁₂ CoN ₂	C ₅₃ H ₄₁ O ₁₂ S ₁₂ AlN ₂	C ₅₃ H ₃₉ FeN ₂ O ₁₃ S ₁₂	C ₅₃ H ₃₇ O ₁₃ S ₁₂ CrN	C ₅₃ H ₃₉ O ₁₃ S ₁₂ CrN	C ₅₃ H ₄₁ FeN ₂ O ₁₂ S ₁₂
<i>a</i> /Å	10.340(10)	10.318(7)	10.232(12)	10.240(1)	10.371(2)	10.370(5)
<i>b</i> /Å	19.5016(2)	19.460(4)	20.04(3)	19.965(1)	19.518(3)	19.588(12)
<i>c</i> /Å	35.7684(5)	35.808(8)	34.97(2)	34.905(1)	35.646(2)	35.790(8)
β /deg	90.0	90.0	93.25(11)	93.69(1)	90.0	90.0
<i>V</i> /Å ³	7212.6(14)	7190(5)	7157(13)	7121.6(2)	7216(2)	7270(6)
<i>Z</i>	4	4	4	4	4	4
fw	1982.90	1950.96	1979.78	1973.76	1975.99	1974.61
crys syst	orthorhombic	orthorhombic	monoclinic	monoclinic	orthorhombic	orthorhombic
space group	<i>Pbcn</i>	<i>Pbcn</i>	<i>C2/c</i>	<i>C2/c</i>	<i>Pbcn</i>	<i>Pbcn</i>
<i>T</i> /K	150(2)	150(2)	120(2)	120(2)	150(2)	120(2)
λ /Å	0.71073 (Mo K α)	0.71073	0.71073	0.71073	0.71073	0.71073
ρ_{calc} /g cm ⁻³	1.825	1.798	1.835	1.809	2.137	1.804
μ /mm ⁻¹	1.226	1.019	1.207	1.141	1.146	1.187
<i>R</i> (<i>F</i> _o) ^a [<i>I</i> < 2 σ (<i>I</i>)]	<i>R</i> = 0.0742	<i>R</i> = 0.0437	<i>R</i> = 0.0416	<i>R</i> = 0.0394	<i>R</i> = 0.0655	<i>R</i> = 0.1557
<i>R</i> _w (<i>F</i> _o ²) ^d	<i>R</i> _w = 0.2046	<i>R</i> _w = 0.1058	<i>R</i> _w = 0.0760	<i>R</i> _w = 0.0907	<i>R</i> _w = 0.1033	<i>R</i> _w = 0.3831

^a Reference 9. ^b Reference 14. ^c $R = \sum(F_o - F_c)/\sum F_o$. ^d $R_w = \{\sum[w(F_o^2 - F_c^2)^2]/\sum[w(F_o^2)^2]\}^{1/2}$.

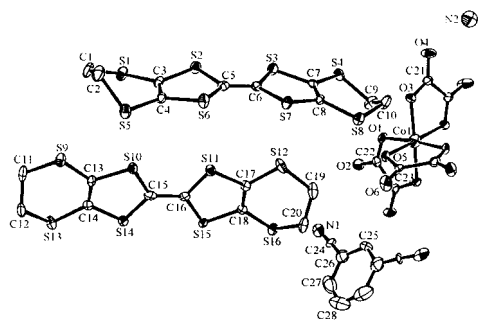


Figure 2. ORTEP³⁰ diagram with 50% thermal ellipsoids and the atom-numbering scheme for compound I, (BEDT-TTF)₄[(NH₄)Co(C₂O₄)₃]·PhCN.

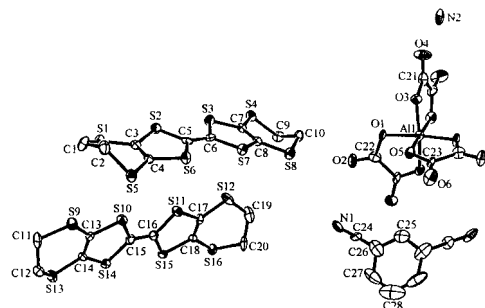


Figure 3. ORTEP³⁰ diagram with 50% thermal ellipsoids and the atom-numbering scheme for compound II, (BEDT-TTF)₄[(NH₄)Al(C₂O₄)₃]·PhCN.

upon cooling from 293 to 120 K, an effect that is usually associated with an increase in charge. In the orthorhombic phases there are again two crystallographically independent BEDT-TTF, each having the twisted and eclipsed conformation at both ends.

Adjacent donor layers are rotated by much greater angles than in the β'' salts at 83.2–85.5° and 85.8–87.8°. The layers consist of face-to-face dimers, each of which is surrounded by six further donors. Neighboring dimers are arranged orthogonal to each other as in the κ -phase salts, though the motif of (BEDT-

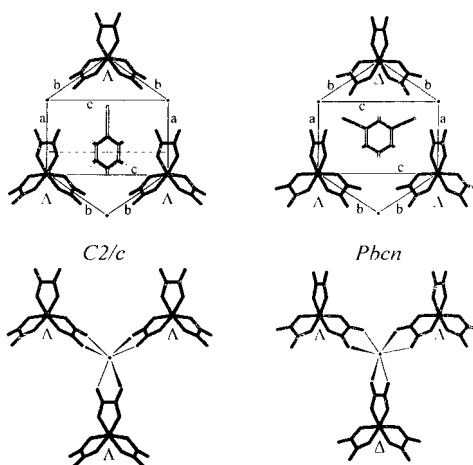


Figure 4. The anionic layer in (BEDT-TTF)₄[AM(C₂O₄)₃]·PhCN for the monoclinic *C2/c* (left) and orthorhombic *Pbcn* (right) structures.

Table 2. Distances (Å) from the Terminal O Atoms of [M(C₂O₄)₃]³⁻ to the Group A in the Title Compounds

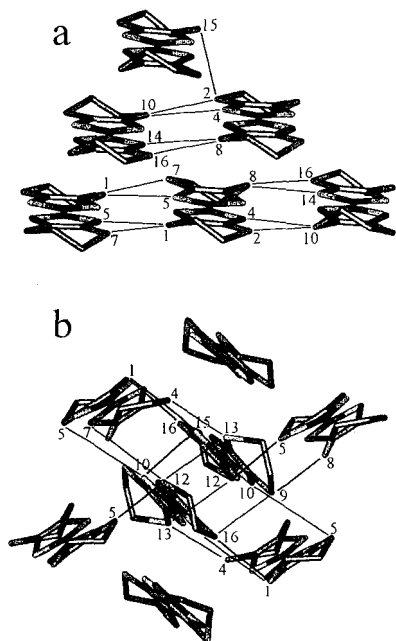
compd	<i>T</i> /K	O4–A	O6–A	O2–A
I	150(2)	2.947(10)	2.981(9)	3.001(9)
II	150(2)	2.977(9)	2.881(9)	2.918(8)
III	120(2)	2.917(5)	2.816(5)	2.952(5)
IV	120(2)	2.960(4)	2.809(4)	3.038(4)
IV	293(3)	3.011(7)	2.845(8)	3.058(7)
V	150(2)	2.891(11)	2.927(11)	2.901(12)
VI	120(2)	2.899(20)	2.919(20)	2.887(20)
VII	120(2)	2.866(8)	2.834(7)	2.885(7)

TTF)₂²⁺ surrounded by six BEDT-TTF⁰ is unique to this series. The closest S \cdots S contact distances occurring between the two molecules of the dimer are 3.43–3.45 Å, and the mode of overlap found in the dimer is not quite the “bond-over-ring” arrangement found in κ -(BEDT-TTF)₂X phases.³⁴ The shortest S \cdots S contacts between dimer and monomer are 3.38–3.42 Å, and the shortest distance between monomers is 3.65–3.67 Å. The S \cdots S contacts in the *Pbcn* structures are listed in Table

(34) Yamochi, H.; Kamatsu, T.; Matsukawa, N.; Saito, G.; Mori, T.; Kusunoki, M.; Sakaguchi, K. *J. Am. Chem. Soc.* **1993**, *115*, 11319.

Table 3. Selected Bond Lengths (Å) and Angles (deg) about M in the Title Compounds

compd	T/K	M–O3	M–O1	M–O5	O3–M–O3	O5–M–O1
I	150(2)	1.908(5)	1.908(5)	1.913(5)	85.8(3)	86.2(2)
II	150(2)	1.888(6)	1.908(5)	1.906(6)	84.2(4)	83.9(2)
III	120(2)	2.018(3)	2.007(3)	2.011(3)	78.5(2)	80.5(1)
IV	120(2)	1.984(2)	1.985(2)	1.966(2)	81.7(1)	82.7(1)
IV	293(3)	1.983(5)	1.976(4)	1.957(4)	81.2(3)	82.7(2)
V	150(2)	1.973(6)	1.982(6)	1.966(6)	81.5(4)	83.5(3)
VI	120(2)	1.995(10)	2.00(11)	2.012(12)	81.1(6)	80.9(4)
VII	120(2)	2.000(4)	2.021(4)	2.021(4)	80.9(2)	81.0(2)

**Figure 5.** Network of close S...S contacts between BEDT-TTF molecules in (a) monoclinic $C2/c$ structures with β'' packing and (b) orthorhombic $Pbcn$ structures.

4b, and a scheme of the contacts is shown in Figure 5. The donor layers are identical, within experimental error, in all the “pseudo- k ” structures. A full list of bond lengths, angles, and S...S contact distances for the previously unpublished salts with $M = Co$ and Al are available as Supporting Information in CIF format. The arrangement of the BEDT-TTF molecules is directed by the anion layer and is found to be sensitive to changes in the chirality of $[M(C_2O_4)_3]^{3-}$ and even the solvent molecule.³⁵

Anion Cation Interdependency. It has been suggested that weak H-bonding and/or steric interaction between the terminal ethylene groups of BEDT-TTF and the anion layer influences the packing arrangement of the donor layers and, thus, the transport properties of the salts. “Docking” of the donor terminal ethylene groups into cavities between the anions³⁴ is not a relevant consideration in the present case since there are no cavities of sufficient size when the hexagonal cavity is occupied by a solvent molecule. Consequently, the packing mode of the donor is primarily influenced by short atomic contacts, i.e., H-bonding between the BEDT-TTF terminal ethylene groups and the O atoms of $[M(C_2O_4)_3]^{3-}$. Indeed to preserve this

Table 4. S...S Intermolecular Distances (Å) in the Title Compounds: (a) $C2/c$ Phases and (b) $Pbcn$ Phases^a

	(a) $C2/c$ Structures				
	III	IV	IV		
T/K	120(2)	120(2)	293(3)		
S1–S5	3.49(1)	3.49(1)	3.56(1)		
S1–S7	3.37(1)	3.35(1)	3.40(1)		
S2–S10	3.47(1)	3.47(1)	3.57(1)		
S2–S15	3.60(1)	3.61(1)	3.65(1)		
S4–S10	3.44(1)	3.42(1)	3.51(1)		
S8–S14	3.33(1)	3.34(1)	3.37(1)		
S8–S16	3.30(1)	3.31(1)	3.35(1)		
	(b) $Pbcn$ Structures				
	I	II	V	VI	VII
T/K	150(2)	150(2)	150(2)	120(2)	120(2)
S16–S1	3.41(1)	3.38(1)	3.42(1)	3.41(3)	3.40(1)
S12–S13	3.58(1)	3.58(1)	3.58(1)	3.58(3)	3.59(1)
S12–S7	3.49(1)	3.48(1)	3.49(1)	3.49(3)	3.48(1)
S12–S5	3.51(1)	3.50(1)	3.52(1)	3.53(1)	3.52(1)
S15–S1	3.20(1)	3.19(1)	3.20(1)	3.21(3)	3.20(1)
S10–S15	3.45(1)	3.43(1)	3.45(1)	3.45(3)	3.45(1)
S14–S11	3.48(1)	3.46(1)	3.48(1)	3.48(3)	3.48(1)
S10–S5	3.43(1)	3.43(1)	3.41(1)	3.42(3)	3.43(1)
S13–S4	3.43(1)	3.42(1)	3.43(1)	3.46(3)	3.44(1)
S9–S8	3.49(1)	3.49(1)	3.51(1)	3.51(3)	3.51(1)

^a See Figure 5 for atom numbering.

interaction, the $[M(C_2O_4)_3]^{3-}$ units are translated parallel to the b axis (see Figure 1) on passing from one layer to the next to an extent that matches the tilt in the long axes of the intervening BEDT-TTF molecules. The fact that H(ethylene)...O(oxalate) contacts are identical at both ends of the donor molecules suggests very strongly that it is these contacts which stabilize the structure.

Because the spatial distribution of the Δ and Λ enantiomers is different in the two sets of compounds, the relative positions of the oxalato O atoms likewise differ. Hence the short atomic contacts with the donor molecules are altered, resulting in the two very different BEDT-TTF packing modes. Given that the distribution of the two $[M(C_2O_4)_3]^{3-}$ enantiomers determines the donor packing motif, it is pertinent to attempt the synthesis of a BEDT-TTF salt starting from a single enantiomer (see synthesis section). Since $[Fe(C_2O_4)_3]^{3-}$ racemizes rapidly, crystals were grown with Cr and Co complexes. When racemic $[M(C_2O_4)_3]^{3-}$ was used crystal growth started quickly whereas for the chiral pure materials no crystals grew over the first 12 days in the case of Cr. Presumably as the anion racemized in solution, crystals of the orthorhombic phase grew over the next few days. However, in contrast to the orthorhombic phases grown from racemic $(NH_4)_3[M(C_2O_4)_3] \cdot xH_2O$ which all contain NH_4^+ (Table 1), the orthorhombic crystals resulting from this in situ racemization process contain H_3O^+ . Clearly the nucleation and crystal growth of these phases is a very subtle process in which the packing mode of the two chiral enantiomers of $[M(C_2O_4)_3]^{3-}$ is a crucial factor.

(35) Turner, S. S.; Day, P.; Malik, K. M. A. Hursthouse, M. B. *Inorg. Chem.* 1999, 38, 3543.

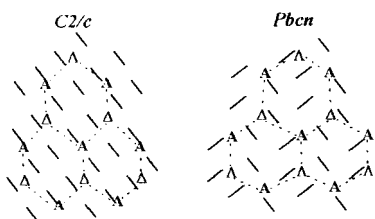


Figure 6. Schematic relationship between the BEDT-TTF donors viewed along their long axes (thick lines) and the anionic "honeycomb" layer (dashed lines) for monoclinic *C2/c* (left) and orthorhombic *Pbcn* (right) structures.

Figure 6 shows a schematic representation of the position of the BEDT-TTF molecules with respect to the anion hexagonal layer. In those structures determined at 120 K, the three shortest O(oxalate)...H(donor) distances are from terminal $[\text{C}_2\text{O}_4]^{2-}$ oxygen atoms. The $-\text{CH}_2\text{CH}_2-$ terminal group interacts with four sites in the anionic layer of the monoclinic structure: over the O adjacent to the phenyl ring of the PhCN, over the $\text{C}\equiv\text{N}$ group of PhCN, and above the M^{III} and in the space between PhCN and one of the $[\text{C}_2\text{O}_4]^{2-}$ units. In the orthorhombic salts the $-\text{CH}_2\text{CH}_2-$ groups also lie close to four sites in the anion layer: the two BEDT-TTF⁰ ethylene groups are below the PhCN, while those of the BEDT-TTF dimer lie close to the O of the $[\text{M}^{\text{III}}(\text{C}_2\text{O}_4)_3]^{1-}$. The close $\text{O}\cdots\text{H}$ contacts are similar in all the orthorhombic structures, the shortest being between 2.3 and 2.7 Å. In Figure 6 (left) it is evident that the donor molecules which are H-bonded to an anionic layer of single $[\text{M}(\text{C}_2\text{O}_4)_3]^{3-}$ enantiomers gives rise a well-ordered packing motif of identically orientated donors. In this case interaction with a pure Δ anionic layer gives a donor layer consisting of stacks propagating from bottom left to top right of Figure 6; interaction with a layer of the Λ enantiomer would give rise to an identical donor packing ranging from bottom right to top left. From Figure 6 (right), it can be seen that in the orthorhombic case those donor dimers which are close to Δ enantiomers of the oxalato anions have similar orientations to those in Figure 5 (left). Similarly those dimers in Figure 6 (right) which are close to Λ oxalato enantiomers have the same orientations to those in the monoclinic structure which interact with a purely Λ anionic layer.

The formal charge associated with each BEDT-TTF donor molecule is an important aid to understanding the physical properties of these salts. The presence of more than one crystallographically independent BEDT-TTF molecule is found in many charge-transfer salts, carrying with it the possibility of charge localization. We have used both bond length analysis and Raman spectroscopy to estimate the charges associated with the donor molecules.

Bond Length Analysis. Molecular orbital calculations on the BEDT-TTF molecule in various oxidation states indicate that it is the central region of the BEDT-TTF molecule which donates charge upon oxidation, and also undergoes the largest changes in bond lengths, which vary monotonically and approximately linearly with charge. The charges on the BEDT-TTF cations have been estimated from the length of the central $\text{C}=\text{C}$ bond³⁶ and, more recently, through a systematic search of the Cambridge Crystallographic Database to compare the formal charge from stoichiometry with the bond lengths in the central TTF portion of the molecule.³⁷ Increased oxidation

Table 5. The Charge, Q , Calculated from $\text{C}=\text{C}$ and $\text{C}-\text{S}$ Bond Distance for the Two Crystallographically Independent BEDT-TTF Molecules (a and b); the Semiconducting Activation Energies of the *Pbcn* Phases

compd	T/K	$Q(\text{BEDT-TTF}_a)$	$Q(\text{BEDT-TTF}_b)$	E_{sc}/eV
I	150(2)	+0.2	+1.0	0.225
II	150(2)	+0.1	+0.8	0.222
III	120(2)	+0.4	+0.5	n/a
IV	120(2)	+0.6	+0.7	n/a
IV	293(3)	+0.3	+0.4	n/a
V	150(2)	+0.0	+0.8	0.153
VI	120(2)	-0.1	+0.8	0.140
VII	120(2)	+0.1	+0.8	0.141

lengthens the $\text{C}=\text{C}$ bonds which are bonding with respect to the HOMO. There are also smaller changes to the bond lengths in the outer six-membered rings of the molecule, but structural disorder and increased thermal vibration impede the observation of any systematic variation.

Guionneau, Kepert, et al.³⁷ showed that the charge Q on a BEDT-TTF molecule can be estimated using an empirical relationship between Q and the BEDT-TTF $\text{C}-\text{S}$ and $\text{C}=\text{C}$ bond lengths. This relationship provides an estimate of the charge residing on a BEDT-TTF molecule with approximately twice the precision of the earlier correlations.³⁶ However, it should be noted that the assumption of a linear relationship relies upon single structures for salts containing BEDT-TTF⁰ and BEDT-TTF²⁺. Taking into account the standard deviations in bond lengths we estimate that this method is capable of obtaining charges to an error of 10%. From Table 5 it is clear that in all the salts with formulas β' -(BEDT-TTF)₄[AM(C₂O₄)₃]·PhCN the two crystallographically independent BEDT-TTF molecules have charges close to +0.5 (average +0.48). Thus A is always monovalent, indicating that the H₂O unit is in fact H₃O⁺. This conclusion is also consistent with the site symmetry of the H₂O site (*D*₃) with three H-bonds to the terminal O atoms of the neighboring $[\text{M}(\text{C}_2\text{O}_4)_3]^{3-}$. It also suggests the more commonly observed 3/4 filling of the four BEDT-TTF HOMO bands rather than 5/8 filling, which would be required if BEDT-TTF had +0.75 formal charge. The presence of H₃O⁺ in the "pseudo-*k*" salts is likewise supported since the two BEDT-TTF molecules have charges of approximately 0 and +1 (± 0.1). The BEDT-TTF⁺ form the face-to-face dimers which are surrounded by six neutral BEDT-TTF. Spin-pairing between the radical cations forming the dimers is confirmed by the magnetic susceptibility measurements, which contain no contribution from BEDT-TTF.

Raman Spectroscopy. Raman spectroscopy provides an additional means for determining the charges on BEDT-TTF molecules by monitoring the two symmetric Raman active $\text{C}=\text{C}$ stretching frequencies between 1400 and 1550 cm^{-1} (designated ν_3 and ν_4 ³⁸). Table 6 lists ν_3 and ν_4 for each of the salts and the calculated charge on each BEDT-TTF molecule according to the relations given by Wang et al.³⁸ Figure 7 shows examples of Raman spectra for the *Pbcn* (Figure 7a) and *C2/c* (Figure 7b) phases. Raman spectra of the β' -phase salts all contain very strong ν_4 peaks between 1466 and 1475 cm^{-1} , and a slightly weaker ν_3 peak between 1492 and 1498 cm^{-1} . The charge $Q(\nu_3)$ calculated from ν_3 is close to 0.5⁺ in all cases (Table 6), while those calculated from the ν_4 peaks are slightly lower (0.38⁺ to 0.48⁺). The *Pbcn* series all show intense ν_4 peaks in the region 1493–1496 cm^{-1} characteristic of BEDT-

(36) For example, see: Abboud, K. A.; Clevenger, M. B.; de Oliveira, G. F.; Talham, D. R. *J. Am. Chem. Soc.* **1993**, *115*, 1560.

(37) Guionneau, P.; Kepert, C. J.; Chasseau, D.; Truter, M. R.; Day, P. *Synth. Met.* **1997**, *86*, 1973.

(38) Wang, H. H.; Ferraro, J. R.; Williams, J. M.; Geiser, U.; Schleuter, J. A. *J. Chem. Soc., Chem. Commun.* **1994**, 1893.

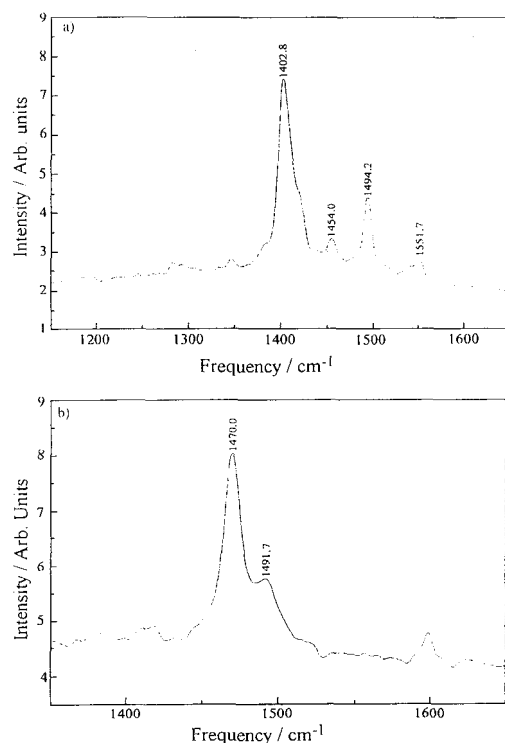


Figure 7. Raman spectra of (a) compound I with an orthorhombic *Pbcn* structure and (b) compound IV with a monoclinic *C2/c* structure.

Table 6. Raman Active Vibrational Frequencies (ν_3 and ν_4) for the C=C Bonds in BEDT-TTF and Calculated Charges

compd	ν_3	ν_4	$Q\nu_3$	$Q\nu_4$
I	1551.7	1494.2	-0.15	0.15
	1454.0	1402.8	0.99	1.19
II	1550.8	1493.2	-0.14	0.17
	1453.0	1403.7	1.00	1.18
III	1495 (sh)	1475.0	0.51	0.37
	1491.7	1470.0	0.55	0.43
IV	1552.6	1494.2	-0.16	0.15
	1454.0	1402.8	0.99	1.19
VI	1552.1	1494.6	-0.15	0.15
	1454.2	1420.0	0.99	1.00
BEDT-TTF ⁰	1552.6	(1510.8)	-0.16	0.15
		(1511.5)		

TTF⁰ and at 1403–1423 cm⁻¹ indicating BEDT-TTF⁺. In addition slightly weaker ν_3 peaks occur between 1549 and 1553 cm⁻¹ (BEDT-TTF⁰) and from 1454 to 1470 cm⁻¹ (BEDT-TTF⁺). The relations of Wang et al.³⁸ give charges very close to zero (± 0.025) for those molecules thought to be BEDT-TTF⁰, while for peaks assigned to BEDT-TTF⁺, the value of $Q(\nu_4)$ is slightly larger than that of $Q(\nu_3)$, but in all cases gives charges close to +1. In conclusion the Raman spectra confirm the charges estimated from the bond lengths, indicating that all salts contain a (BEDT-TTF)₄²⁺ moiety with molecule A being monovalent.

Infrared Reflection Spectroscopy. In the infrared reflection spectra of all the monoclinic and orthorhombic phases, peaks are observed in the regions 1264–1286 and 1307–1354 cm⁻¹

Table 7. Curie (*C*) and Weiss (*θ*) Magnetic Constants for the Title Compounds

compd	<i>C</i> (emu K mol ⁻¹)		<i>θ</i> /K
	obsd	caled spin-only	
I	n/a	0.00	n/a
II	2.84	3.001	+0.86
III	4.38	4.377	-1.29
IV		1.876	
2–150 K	1.96		-0.21
150–270 K	2.91		-61.5
V	1.73	1.876	+0.88
VI	4.37	4.377	+0.11
VII	4.44	4.377	-0.25

(O–C–O stretching vibration), 1364–1417 cm⁻¹ (O–C–O symmetric stretch), and 1636–1664 cm⁻¹ (O–C–O asymmetric stretch). Characteristic features of the spectra of the β''-phases are peaks at 872–884 cm⁻¹ while pseudo-κ phases have peaks at ca. 772, 924–971, 1010–1026, 1036–1076, 1082–1124, 1147–1776, and 1204–1240 cm⁻¹. Very sharp bands are observed in all pseudo-κ salts between 802 and 840, 1307 and 1354, 1364 and 1417, and 1636 and 1664 cm⁻¹.

In addition to sharp peaks due to localized molecular vibrations, the infrared reflectivities of the metallic β''-phases contain broad reflectivity edges at the plasma frequency. The reflectivity is only weakly dependent on whether the polarization is parallel and perpendicular to the axis of the needlelike crystals, both being measured in the same plane as the 2D BEDT-TTF conducting network. As expected, the reflected intensity increases slightly with decreasing temperature. The onset of high reflectivity defines the plasma frequency as 5000 ± 200 cm⁻¹. Finally, for the materials prepared with M = Ti or Gd, the infrared spectra did not show any peaks which could be assigned to the oxalate ligands and so no further physical properties were investigated.

Conductivity Measurements. The monoclinic phases show metal to superconducting transitions,^{9,14} but all the orthorhombic phases, including the new compounds, are semiconducting with resistivity increasing exponentially with decreasing temperature. The activation energies for the semiconductors are listed in Table 5. As shown above, the BEDT-TTF molecules in the orthorhombic series form dimers of BEDT-TTF⁺ surrounded by BEDT-TTF⁰. The neutral molecules have filled HOMOs, while the monopositive donors have half-filled HOMOs. The dimerization of the BEDT-TTF⁺ molecules leads to the formation of a full band and an empty band separated by an energy gap.

Magnetic Properties. All the compounds that contain paramagnetic 3d ions have moments close to that expected for spin only contributions. In addition, the superconducting salts show both flux exclusion and the Meissner–Oschenfeld flux expulsion effect when cooled in fields below 50 G. Table 7 lists the Curie and Weiss constants extracted from plots of inverse molar susceptibility versus temperature. All the Weiss constants are close to zero, indicating that there is very little interaction between paramagnetic centers. The plot of β''-(BEDT-TTF)₄[(H₃O)Cr(C₂O₄)₃]·PhCN shows a distinct change in slope at ~150 K, accompanied by a sharp drop in infrared reflectivity when the electric vector is perpendicular to the needle axis. Above 150 K the Curie constant is higher than anticipated for Cr³⁺ (*S* = 3/2), and the Weiss constant of -61.5 K suggests antiferromagnetic interaction between metal centers. However, the crystal structure of the (H₃O)Cr salt has been solved at both 120 and 293 K with no evidence for a structural phase transition.

Conclusions

We have compared the structural and physical characteristics of a number of charge-transfer salts with the general formula $(\text{BEDT-TTF})_x[\text{A}^I\text{M}^{\text{III}}(\text{C}_2\text{O}_4)_3] \cdot \text{PhCN}$ where $\text{A}^I = \text{NH}_4^+$, K^+ , or H_3O^+ and $\text{M}^{\text{III}} = \text{Cr}$, Fe , Co , or Al , the compounds with $\text{M} = \text{Co}$ and Al being new members of this series. Analysis of the C=C and C-S bond lengths and Raman spectra of the BEDT-TTF molecules shows that, in all the examples containing water, it is in the form of H_3O^+ and not H_2O . The compounds fall into two categories. Monoclinic phases with $\text{A}^I = \text{H}_3\text{O}$ and $\text{M}^{\text{III}} = \text{Cr}$ and Fe have β'' packing of the BEDT-TTF and are room temperature metals, becoming superconducting at 5.5 K (Cr) and 8.3 K (Fe). Since the magnetic moment of the 3d ion in the Fe ($S = 5/2$) compound is larger than in the Cr ($S = 3/2$), it is clear that the presence of a higher paramagnetic moment in the lattice does not inhibit the superconductivity. A second series of phases found for $\text{A}^I = \text{NH}_4$, K , H_3O and $\text{M}^{\text{III}} = \text{Cr}$, Fe , Co , Al are orthorhombic. The BEDT-TTF bond lengths and Raman spectra confirm the presence of two types of donor molecule: face to face dimers with a charge of +1 per molecule surrounded by molecules with charges close to zero. All the members of the orthorhombic series are semiconducting with low activation energies between 0.14 and 0.22 eV.

Both the monoclinic and orthorhombic phases consist of alternating layers of BEDT-TTF and the tris(oxalato)metalate-(III) anions. The anion layers always consist of approximately hexagonal arrays of A and M, bridged by the $[\text{C}_2\text{O}_4]^{2-}$ with PhCN occupying the hexagonal cavities. Both structures are achiral and contain equal proportions of the enantiomers of $[\text{M}(\text{C}_2\text{O}_4)_3]^{3-}$. However, in the monoclinic phase each layer contains one enantiomer with nearest neighbor layers having opposite chirality whereas each layer of the orthorhombic phase contains enantiomers arranged in alternate rows. As a conse-

quence, while the cavity occupied by A^I consists of an approximately octahedral array of O atoms, that of the orthorhombic phase has a more irregular shape, leaving space for the N atom of the PhCN to coordinate to A^I , bringing the coordination number to 7. Furthermore the array of O atoms which forms the interface with the BEDT-TTF layers differs greatly and, via H-bonding, promotes the different donor packing modes. In one case ($\text{A} = \text{H}_3\text{O}$; $\text{M} = \text{Cr}$) both orthorhombic and monoclinic phases have been found. Our belief is that this constitutes the first example in any compound where polymorphism arises from different spatial distributions of chiral enantiomers in a racemic crystal.

Clearly it will be of great interest to prepare BEDT-TTF salts analogous to the bimetallic tris(oxalato)metalate (II, III) molecular based magnets^{12,13} because there would be a good chance of combining metallic behavior or superconductivity with long-range magnetic order in a molecular lattice. Efforts are continuing along these themes.

Acknowledgment. This work has been supported by the UK Engineering and Physical Sciences Research Council and the European Commission Training and Mobility of Researchers Program. We are also grateful to the British Council and Monbusho exchange program (grant to L.M.) and to Dr. W. Hayes (Clarendon Laboratory, Oxford) for access to the infrared spectrometer.

Supporting Information Available: Tables of atomic positional parameters, anisotropic thermal parameters, interatomic contacts, and complete bond distances and angles for compounds **I** and **II** in CIF format. This material is available free of charge via the Internet at <http://pubs.acs.org>.

IC001193U

New superconducting charge-transfer salts (BEDT-TTF)₄[A·M(C₂O₄)₃]-C₆H₅NO₂ (A = H₃O or NH₄, M = Cr or Fe, BEDT-TTF = bis(ethylenedithio)tetrathiafulvalene)

Samina Rashid,^a Scott S. Turner,^a Peter Day,^{*,a} Judith A. K. Howard,^b Philippe Guionneau,^b Eric J. L. McInnes,^c Frank E. Mabbs,^c Robin J. H. Clark,^d Steven Firth^e and Tim Biggs^e

^aDavy-Faraday Research Laboratory, The Royal Institution of Great Britain, 21 Albemarle Street, London, UK W1X 4BS. E-mail: pday@ri.ac.uk

^bDepartment of Chemistry, University of Durham, Durham, UK DH1 3LE

^cChemistry Department, University of Manchester, Oxford Road, Manchester, UK M13 9PL

^dChristopher Ingold Laboratories, University College, 20 Gordon Street, London, UK WC1H 0AJ

^eClarendon Laboratory, Oxford, Oxford University, Parks Road, Oxford, UK OX1 3PU

Received 2nd February 2001, Accepted 13th June 2001

First published as an Advance Article on the web 9th July 2001

The syntheses, crystal structures, and physical properties of two new crystalline charge-transfer salts of BEDT-TTF, bis(ethylenedithio)tetrathiafulvalene, containing tris(oxalato)metallate(III) anions of 3d elements are reported. Electrochemical oxidation of BEDT-TTF in the presence of (NH₄)₃[Fe(C₂O₄)₃]-3H₂O or (NH₄)₃[Cr(C₂O₄)₃]-3H₂O in C₆H₅NO₂, yields crystals of β⁺-(BEDT-TTF)₄[A·Fe(C₂O₄)₃]-C₆H₅NO₂ [1] or β⁻-(BEDT-TTF)₄[A·Cr(C₂O₄)₃]-C₆H₅NO₂ [2] (A = H₃O⁺ or NH₄⁺). The crystal structure of [1] has been solved at 120 K in the monoclinic space group *C2/c*, and that of [2] in the same space group at 298 and 120 K. For [1], *a* = 10.273 Å, *b* = 19.949 Å, *c* = 35.030 Å, β = 92.97°, *V* = 7169.6(2) Å³, *Z* = 8. For [2], at 298 K: *a* = 10.304 Å, *b* = 20.091 Å, *c* = 35.251 Å, β = 92.70°, *V* = 7289.3(2) Å³, *Z* = 8, and at 120 K *a* = 10.283 Å, *b* = 19.917 Å, *c* = 34.939 Å, β = 93.30°, *V* = 7144.4(1) Å³, *Z* = 8. The crystal structures of both compounds consist of alternating layers of BEDT-TTF cations and layers containing [M(C₂O₄)₃]³⁻, H₃O⁺ or NH₄⁺, and PhNO₂. The BEDT-TTF molecules are arranged in the β⁺ packing motif and the tris(oxalato)metallate(III) ions form the well-known honeycomb motif found in many molecular based magnets. SQUID magnetometry, Raman spectroscopy and electron paramagnetic resonance (EPR) measurements were performed on crystals of [1]. SQUID magnetometry, single-crystal four-probe conductivity measurements, Raman spectroscopy, EPR and polarised infrared reflectance were performed on crystals of [2]. Both compounds have metal to superconducting transitions with *T*_c = 6.2 K for [1] and for [2], *T*_c = 5.8 K.

Introduction

Charge transfer salts of BEDT-TTF, bis(ethylenedithio)tetrathiafulvalene, have become a fruitful source of novel collective electronic ground states, including semiconductors,¹ spin-Peierls systems,² metals and superconductors.^{1,3,4} This variety stems from the way in which the supramolecular organisation of the donors is structured by the size, charge and arrangement of the inorganic anions. In this respect, salts with tris(oxalato)metallate(III) anions have been particularly interesting: they provided the first example of a molecular superconductor containing paramagnetic metal ions and the first superconductor of any kind to contain paramagnetic 3d ions.³ In addition, the structures and hence properties are extremely sensitive to changes to the solvent molecule included in the lattice. For example, the first BEDT-TTF tris(oxalato)metallate(III) superconductors, β⁺-(BEDT-TTF)₄[H₃O·M(C₂O₄)₃]-PhCN (M = Fe, Cr), with β⁺ packing mode of the donors, contain PhCN within the hexagonal cavities between the [M(C₂O₄)₃]³⁻. Surprisingly, however, on replacing the included PhCN by C₂H₅N, phases that exhibit metal-insulator transitions arise.⁵ To explore further how change in the solvent molecules included in the crystal modulates the physical properties of this class of compound, we have prepared the corresponding salts containing PhNO₂. They are found to be superconductors like the PhCN solvates, but with lower *T*_c's.

Experimental section

Synthesis and purification of starting materials

Crystals of (NH₄)₃[M(C₂O₄)₃]-3H₂O (M = Fe, Cr), were recrystallised twice from water.⁶ BEDT-TTF (Aldrich) was recrystallised from chloroform and 18-crown-6 ether (Aldrich) was purified over CH₃CN. Nitrobenzene (Aldrich) was washed with 2 M NaOH, then water, and then 2 M hydrochloric acid followed by water again and dried with MgSO₄. Prior to use, the solvent was also fractionally distilled under reduced pressure.

Electrocrystallisation

100 mg of (NH₄)₃[M(C₂O₄)₃]-3H₂O (M = Fe, Cr) was dissolved in 50 cm³ of nitrobenzene with the aid of 18-crown-6 ether (200 mg). BEDT-TTF (10 mg) was placed in the anode compartment of an H-shaped cell and the remainder was filled with the solution of the tris(oxalato)metallate salt. A constant current of 1 μA was passed across the cell. Small dark, flat needles of β⁺-(BEDT-TTF)₄[A·Fe(C₂O₄)₃]-PhNO₂ (A = H₃O⁺ or NH₄⁺, 6 mg), [1], suitable for X-ray diffraction, were harvested from the platinum anode after three weeks and small, dark-brown flat striated sheets of β⁺-(BEDT-TTF)₄[A·Cr(C₂O₄)₃]-PhNO₂ (A = H₃O⁺ or NH₄⁺, 7 mg), [2], suitable for X-ray diffraction, after two weeks.

Physical measurements

The magnetic susceptibilities of polycrystalline samples of [1] and [2], held in gelatine capsules inside a plastic tube, were measured using a Quantum Design MPMS7 SQUID magnetometer. The diamagnetism was estimated as $-911.8 \times 10^{-6} \text{ cm}^3 \text{ mol}^{-1}$ for [1] and $-912.8 \times 10^{-6} \text{ cm}^3 \text{ mol}^{-1}$ for [2] from Pascal's constants. Conductivity measurements were performed on an Oxford Instruments Maglab System 2000 in the temperature range 2–300 K, and applied fields from 0 to 7 T. Gold wires (0.0025 mm diam.) were attached to the crystals using Pt paint (Degussa), and the attached wires were connected to an eight-pin integrated circuit plug with Ag paint (RS components). This assembly was fixed onto an IC socket with a 6-way formed pin.

Single crystal X-ray diffraction data were collected using a Bruker Smart CCD diffractometer. The quality of the crystals was first checked at room temperature. In all cases, the strategy was to collect data at θ angle values lower than 28° with a completeness to this value of θ greater than 99.9%. The diffraction frames were integrated using the SAINT package⁷ and the intensities corrected for absorption with SADABS⁸ while the crystal structures were solved and refined with SHELXTL-Plus.⁹

For [2], separate data were collected at 298 and 120 K using the same crystal. In both cases, the full set of data was collected from four ω -scans (starting at $\omega = -26, -21, -23, -26^\circ$ respectively) at values $\phi = 0, 88, 180, 0^\circ$ with the detector at $2\theta = -29^\circ$ for the three first runs and $+29^\circ$ for the last one. At each of these runs, frames (606, 435, 606, 100 respectively) were collected at 0.3° intervals and at 10 seconds per frame. In view of the ambiguity for the monovalent ion it is referred to as A. However, some information concerning this ion is obtained from the infrared and Raman spectra (see below), and its monovalent nature is proven from the charge calculations and Raman reflectivity data. For [1], one data collection was run at 120 K using the same strategy as used previously but with the time exposure of 15 s per frame, the step of 0.2° between two frames, and hence 909, 653, 909, 100 frame collected. All hydrogen atoms for both compounds were placed in idealized positions and refined using the riding model.

Raman spectra of single crystals of [1] and [2] were measured at room temperature on a Renishaw Raman microscope System 1000 using a He–Ne laser (632.8 nm), a CCD detector, a slit width of 10 μm and 10% neutral density filter. Polarised infrared reflectance spectra of [2] were measured using a Bruker IFS 66v interferometer combined with a Nicolet infrared

microscope. Data were collected in the range from 800 to 10000 cm^{-1} using a glowbar, an MCT detector and a KBr beamsplitter in the mid-IR and a tungsten lamp, an InSb detector and a CaF₂ beamsplitter in the near-IR. In both ranges a BaF₂ polariser was used, the spectral resolution being 4 cm^{-1} . Absolute values of reflectance were obtained by comparison with that of a Au mirror placed in the position of the sample. The mismatch between the two ranges of measurement was less than 2%.

The EPR spectra of polycrystalline samples were recorded at X-band (9.5 GHz) and K-band (24 GHz) on a Bruker ESP300E spectrometer with either an ER4102ST, ER6706 or an ER5106 resonator. In the temperature range 290 to 4.2 K, cooling was via an Oxford Instruments ESR910 cryostat at X-band, and an ER4118CF cryostat at K-band. Zero-field crossing capabilities allowed sweeping through a range of fields from -40 to $+40 \text{ G}$ in order to study zero-field absorptions.

Results and discussion

Crystal structure

As anticipated, the structures of [1] and [2] are very closely similar to those of $\beta''\text{-(BEDT-TTF)}_4[\text{H}_3\text{O-Fe}(\text{C}_2\text{O}_4)_3]\cdot\text{PhCN}$ in which the BEDT-TTF cations and tris(oxalato)metallate(m) anions are arranged in alternating layers. Table 1 shows the crystallographic data for [1] at 120 K and [2] at 298 and 120 K respectively. Figs. 1 and 2 show the standard ORTEP diagrams of [1] and [2] respectively with the atom numbering scheme and 50% thermal ellipsoids. For the purposes of the ORTEP diagrams, the monovalent ion is set as H_3O^+ . However, it was difficult to establish crystallographically whether the ion was H_3O^+ or NH_4^+ since the *R* factors showed no significant differences when refined with each alternative (Table 2).

The anionic layers consist of chiral $[\text{M}(\text{C}_2\text{O}_4)_3]^{3-}$ and A^+ ions forming an approximately hexagonal network where successive layers contain either the Δ or Λ forms of the tris(oxalato)metallate(m) anion. The hexagonal cavity is occupied by the solvent molecule PhNO_2 , which sits in the cavity at a slight angle to the mean plane of the oxalate layer. The cationic layers are formed from BEDT-TTF ions alone which are packed in the β'' arrangement, forming conducting sheets in the *a* and *c* directions. CCDC reference number 157874–157876. See <http://www.rsc.org/suppdata/jm/b1/b101134k/> for crystallographic files in .cif format.

Table 1 Crystallographic data for [1] at 120(2) K and [2] at 298/120 K

Compound	[1]	[2]
<i>TK</i>	120(2)	298(2) 120(2)
Empirical formula	$\text{C}_{26}\text{H}_{20}\text{Fe}_{0.5}\text{N}_{0.5}\text{O}_{7.5}\text{S}_{16}$	$\text{C}_{26}\text{H}_{20}\text{Cr}_{0.5}\text{N}_{0.5}\text{O}_{7.5}\text{S}_{16}$
Molecular wt.	998.39	998.39
Crystal system	Monoclinic	Monoclinic
Space group	<i>C2/c</i>	<i>C2/c</i>
<i>a</i> / \AA	10.2732(2)	10.3039(2)
<i>b</i> / \AA	19.9494(3)	20.0908(3)
<i>c</i> / \AA	35.0304(6)	35.2508(4)
β /deg.	92.969(1)	92.701(1)
<i>V</i> / \AA^3	7169.6(2)	7289.3(2)
<i>Z</i>	8	8
μ/mm^{-1}	1.207	1.137
<i>T</i> min, max	0.814, 0.949	0.692, 0.849
Ref. measured	30838	34583
Independent ref.	8238	8365
<i>R</i> int(%)	3.5	6.4
Obs. refl. (<i>I</i> > 2 σ (<i>I</i>))	6799	4188
Refined parameters	462	460
<i>R</i>	0.038	0.065
<i>wR2</i> (<i>F</i> ²)	0.073	0.129
		0.088

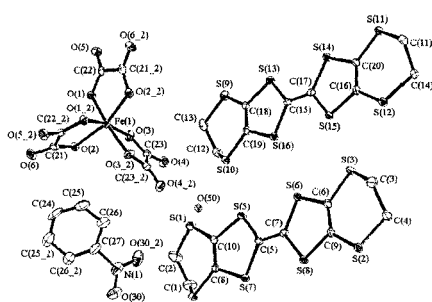


Fig. 1 ORTEP diagram of β'' -(BEDT-TTF)₄[A·Fe(C₂O₄)₃]·C₆H₅NO₂ (A = H₂O or NH₄) at 120(2) K.

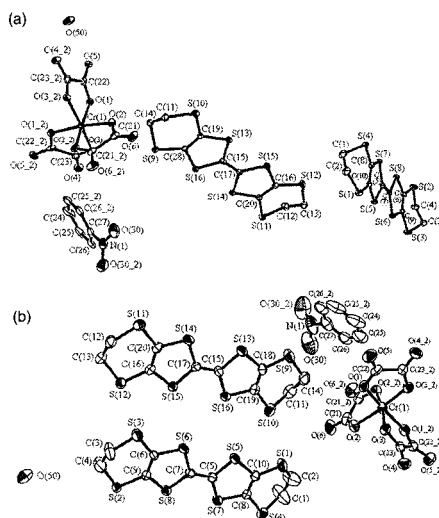


Fig. 2 ORTEP diagram of β'' -(BEDT-TTF)₄[A·Cr(C₂O₄)₃]·C₆H₅NO₂ (A = H₂O or NH₄) at (a) 120 K and (b) 298 K.

β'' -(BEDT-TTF)₄[A·Fe(C₂O₄)₃]·C₆H₅NO₂, [1] (A = H₃O⁺ or NH₄⁺)

The asymmetric unit of [1] at 120 K contains two crystallographically independent BEDT-TTF molecules. The charge on a BEDT-TTF molecule can be estimated with an accuracy close to 10% using the empirically determined relationship between C–C and C–S bond lengths in the central TTF portion of the molecule.¹⁰ Using this method the BEDT-TTF molecules have similar but not identical positive charges of $+0.6 \pm 0.1$

Table 2 R factors for structural refinements of [1] and [2] with A = H₃O⁺ or NH₄⁺

Compound	R		wR2	
	A = H ₃ O ⁺	A = NH ₄ ⁺	A = H ₃ O ⁺	A = NH ₄ ⁺
[1] at 120 K	0.0380	0.0378	0.0730	0.0724
[2] at 120 K	0.0469	0.0470	0.088	0.0902
[2] at 298 K	0.0652	0.0646	0.129	0.1265

Table 3 Selected bond lengths used to calculate the charge on the BEDT-TTF molecules in [1] at 120 K

BEDT-TTF _A		BEDT-TTF _B	
S16–C15	1.746(3)	S7–C5	1.740(3)
S15–C17	1.745(3)	S5–C5	1.741(3)
S14–C17	1.742(3)	S8–C7	1.734(3)
S14–C20	1.758(3)	S6–C7	1.740(3)
S13–C18	1.755(3)	S7–C8	1.752(3)
S16–C19	1.752(3)	S5–C10	1.755(3)
S15–C16	1.746(3)	S8–C9	1.757(3)
C19–C18	1.350(4)	S6–C6	1.745(3)
C20–C16	1.358(4)	C9–C6	1.355(4)
C17–C15	1.362(4)	C10–C8	1.352(4)
C15–S13	1.743(3)	C7–C5	1.369(3)

and $+0.5 \pm 0.1$ (Table 3) For both of the independent BEDT-TTF molecules the terminal CH₂–CH₂ groups display the twisted conformation in which one of the carbon atoms is above the central TTF plane and the other is below. The ends of the donor molecules are also eclipsed. There are four short S...S contacts between the BEDT-TTF molecules: S3...S12, 3.31(1) Å, S3...S15, 3.33(1) Å, S5...S10, 3.44(1) Å and S4...S2, between crystallographically identical molecules is 3.39(1) Å. These contacts are slightly longer than those found in the analogous PhCN compound, and indicate that [1] should have narrower conduction bands.

The PhNO₂ sits in the hexagonal cavity of the anionic layer at an angle of 31.0° to the mean plane of the layer. The CH₂–CH₂ groups of the BEDT-TTF molecules in the organic layer form H-bonds to the O atoms of the [C₂O₄]²⁻ ligands in the inorganic layer, allowing the BEDT-TTF CH₂–CH₂ groups to dock into the anion layer. When compared to the extent of H-bonding between the donor–acceptor layers in the analogous PhCN compound, it is apparent that those in [1] are longer. In fact the closest H...O contact in [1] is 2.88(2) Å, whereas in the PhCN derivative it is 2.44(1) Å.

β'' -(BEDT-TTF)₄[A·Cr(C₂O₄)₃]·C₆H₅NO₂, [2] (A = H₃O⁺ or NH₄⁺)

As with [1] there are two crystallographically independent BEDT-TTF molecules in the unit cell with calculated charges of $+0.7 \pm 0.1$ and $+0.6 \pm 0.1$, unchanged on change of temperature from 298 to 120 K (Table 4) In the molecule which contains atoms C15 and C17 the CH₂–CH₂ groups are twisted and eclipsed, as previously defined. However, at 298 K, the CH₂–CH₂ group on one side in the second molecule containing atoms C5 and C7 is twisted, though it retains the boat conformation at the other end. A “boat” conformation results where both CH₂–CH₂ carbon atoms are on the same side of the plane defined by the central TTF portion of the molecule. Torsion angles of the CH₂–CH₂ groups in the crystallographically independent donors, BEDT-TTF_A and BEDT-TTF_B are given in Table 5. The torsion angle is defined as the angle between a plane composed of three atoms (the S atom on the outer ring of BEDT-TTF and the two C atoms of the terminal ethylene group) and a fourth atom (the second S atom on the outer BEDT-TTF ring).

The torsion angles of the twisted conformations are each about 70° whereas that for the boat conformation is considerably smaller. A perfect boat conformation would result in a torsion angle of 0°. It is noteworthy that there is considerably more thermal disorder on the C atoms in the boat CH₂–CH₂ group, as can be seen clearly on C1 and C2 from the 50% thermal ellipsoids for the 298 K structure shown in Fig. 2. The H atoms which are attached to these C atoms are in close contact with the O atom of the PhNO₂, which may promote a weak H bonding interaction. Thus the H2A–O30 distance is 2.47(1) Å and the H2B–O30 distance is 2.94(1) Å. This arrangement, in which a quarter of the CH₂–CH₂ groups has

Table 4 Selected bond lengths used to calculate the charge on the BEDT-TTF molecules in [2] at 120(2) and 298(2) K

298 K		120 K	
BEDT-TTF_A			
S16-C15	1.724(6)	S13-C15	1.739(4)
S13-C15	1.732(6)	S16-C15	1.741(4)
S15-C17	1.741(6)	S15-C17	1.744(4)
S14-C17	1.743(5)	S14-C17	1.746(4)
S14-C20	1.749(6)	S15-C16	1.751(4)
S13-C18	1.752(6)	S14-C20	1.747(4)
S16-C19	1.746(6)	S13-C19	1.755(4)
S15-C16	1.740(6)	S16-C28	1.748(3)
C19-C18	1.346(8)	C21-C20	1.745(4)
C20-C16	1.360(8)	C20-C16	1.363(5)
C17-C15	1.379(7)	C28-C19	1.360(5)
BEDT-TTF_B			
S7-C5	1.740(5)	S6-C7	1.739(4)
S5-C5	1.735(6)	S8-C7	1.744(4)
S8-C7	1.733(6)	S5-C5	1.745(4)
S6-C7	1.730(6)	S7-C5	1.74(4)
S7-C8	1.751(6)	S6-C9	1.747(4)
S5-C5	1.735(6)	S8-C6	1.748(4)
S8-C9	1.739(6)	S5-C10	1.75(4)
S6-C6	1.742(5)	S4-C8	1.748(4)
C9-C6	1.342(7)	C5-C7	1.358(5)
C10-C8	1.335(7)	C9-C6	1.359(5)
C7-C5	1.373(7)	C8-C10	1.364(5)

a different conformation from the rest, has been found before in the closely related compound β'' -(BEDT-TTF)₄[H₃O-Cr(C₂O₄)₃]-C₅H₅N² which undergoes a metal-insulator transition at 116 K. The torsion angles for the latter compound are listed for comparison in Table 5. In the C₅H₅N compound, the conformation of the fourth CH₂-CH₂ group remains disordered and does not change with decreasing temperature. However, as can be seen in Table 5, the magnitude of the torsion angle for S1-C2-C1-S4 in [2] increases from -23 to -57° on lowering the temperature, indicating that the CH₂-CH₂ group becomes more twisted. This increase in ordering could be the reason for the formation of a superconducting state in [1] at a lower temperature, as distinct from the insulating state observed for the C₅H₅N compound.

The angle of the PhNO₂ plane (defined by three points on the phenyl ring) was measured with respect to the anion plane (defined by three terminal oxygen atoms on the tris(oxalato)metallate(III) anion pointing in the *c* direction). This angle is 32.0° at both 298 and 120 K. At 298 K the four shortest S...S distances are S3...S12, 3.34(2) Å, S3...S15, 3.38(1) Å, S5...S10, 3.51(1) Å and S2...S4, 3.42(1) Å, which at 120 K decrease to 3.31(1) Å, 3.34(1) Å, 3.43(1) Å, 3.39(1) Å, respectively. When compared to the analogous PhCN compound the S...S contacts are slightly the longer, suggesting smaller transfer integrals and narrower conduction bands.

The derivation of structure-property relationships requires a detailed analysis of the crystal structures. It is well known that for these compounds minor modifications to the structure can lead to drastic changes in the properties. Analysis is further complicated by the effect of incorporating functionalised

Table 5 Torsion angles on the CH₂-CH₂ groups of the crystallographically independent BEDT-TTF molecules in [1], [2] and in β'' -(BEDT-TTF)₄[H₃O-Fe(C₂O₄)₃]-C₅H₅N, [3]

Compound	BEDT-TTF _A		BEDT-TTF _B	
[1] at 120 K	S2-C4-C3-S3	-71.0	S12-C14-C11-S11	-69.8
	S4-C1-C2-S1	58.0	S10-C12-C13-S9	70.6
[2] at 120 K	S11-C12-C13-S12	68.9	S2-C4-C3-S3	71.0
	S9-C14-C11-S10	-70.2	S1-C2-C1-S4	-57.2
	S9-C14-C11-S10	-70.4	S1-C2-C1-S4	-22.9
[2] at 298 K	S11-C12-C13-S12	68.1	S2-C4-C3-S3	57.7
[3] at 150 K	-69.7 and 66.9		57.6 and 6.9	

anions that are not only different in size but have different localized magnetic moments. The solvent molecule, thought to have a templating effect in stabilizing the structure, is assumed to be inert and therefore exerts an effect by altering the solubility during electrocrystallisation or by determining the size of the hexagonal cavity.

In fact it is the anion that primarily determines the size of the solvent cavity, with the Fe salts having larger cavity volumes than the corresponding Cr ions. Consequently, the solvent molecule plane in the Fe salts is at a smaller angle to the mean plane of the metal tris(oxalato)metallate(III) anions.

The unit cell volumes of [1] and [2] indicate that their lattices are more loosely packed than those of the analogous PhCN compounds. The greatest difference between the two solvates is in the crystallographic angle β (0.7%), which essentially governs the size of the *bc* plane, the latter being parallel to the BEDT-TTF layer; this difference would therefore determine the extent of overlap of the *s* orbitals between the BEDT-TTF molecules. There is less overlap in the PhNO₂ compounds because the unit cell volume is larger and, as a result of this, they have longer S...S contacts, resulting in reduced conductivity and lower *T_c*'s. So far in this family of compounds, β'' -(BEDT-TTF)₄[H₃O-Fe(C₂O₄)₃]-PhCN has the highest *T_c* with the shortest S...S contacts of between 3.30 and 3.47 Å, and [2] with the lowest *T_c*, has close contacts of between 3.31(1) and 3.58(1) Å.

The most disordered atoms are those on the terminal CH₂-CH₂ groups of the BEDT-TTF molecules. They adopt different conformations, depending on how they interact with the anion layer. The PhNO₂ salts have weaker hydrogen-bonding interactions between the organic and inorganic layers. This "docking" interaction is probably one of the factors accounting for the lower *T_c*'s of the PhNO₂ compounds.

Physical properties

Magnetic susceptibility

To detect the Meissner-Oshenfield effect, samples were cooled in zero field and a field of 5 G was applied while measuring the magnetisation while warming to above *T_c*. The sample was then re-cooled and the magnetisation measured again in the same applied field. This procedure was repeated for increasing fields up to 80 G over the temperature range 2 to 14 K. The magnetic susceptibility was also measured at 10⁴ G from 2 to 300 K. For compound [1] the susceptibility obeys the Curie-Weiss law above 80 G and has a temperature-independent Pauli contribution of 1×10^{-5} cm³ mol⁻¹. The fitted Curie constant is 3.877 emu mol⁻¹ (4.375 is expected for high spin Fe³⁺)¹¹ and the Weiss constant is -0.16 K indicating very weak antiferromagnetic interaction between the Fe centres. On cooling the sample in zero applied field and measuring the magnetisation in an applied field of 5 G from 2 to 14 K, the response is diamagnetic below 6.2 K which indicates the onset of superconductivity at this temperature. Type II superconducting behavior was indicated, since the magnetic flux is able to penetrate the sample as the sample is re-cooled in the same applied field (Fig. 3).

Compound [2] is also a type II superconductor but has a lower *T_c* of 5.8 K. At fields above 80 G, superconductivity is completely suppressed, Fig. 4, and Curie-Weiss behaviour is observed with a Curie constant of 2.129 (1.87 is expected for Cr³⁺)¹¹ and a Weiss constant of -1.44 K indicating weak antiferromagnetic interaction between the Cr centres.

In view of the fact that both Curie constants for [1] and [2] were slightly different to those expected, the SQUID experiment was repeated on three separate preparations of each compound. This gave identical results as reported above. In the case of [1] this indicates some antiferromagnetic interactions. For [2] it seems that there must be a small contribution from

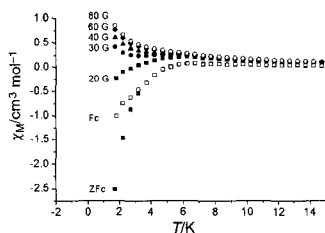


Fig. 3 Temperature dependence of magnetic susceptibility of [1] in fields from 0 to 80 G. Zero field cooled (ZFc), field cooled (Fc) plots show the superconducting T_c .

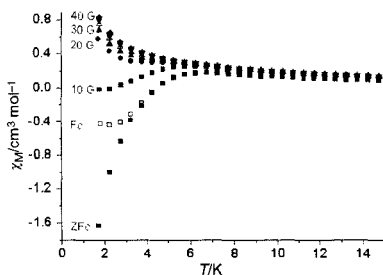


Fig. 4 Temperature dependence of magnetic susceptibility of [2] in fields from 0 to 40 G. Zero field cooled (ZFc), field cooled (Fc) plots show the superconducting T_c .

the spin on the BEDT-TTF radicals. It is not clear why these isostructural materials should show slightly different magnetic phenomena.

Electrical conductivity

Single crystals of [1] were not suitable for transport measurements due to excessive twinning and the small crystal size. Four probe dc conductivity measurements on single crystals of [2] confirm that the compound is superconducting with the onset of the superconducting transition at about 6 K reaching zero resistance at 3.2 K (Fig. 5). The crystals are flat thin rectangular sheets, limiting the measurement of conductivity to that parallel to the c axis only. Measurements were made from 31 to 2 K at 1 K steps. On applying a magnetic field the resistance increases as expected, and the superconducting state is completely destroyed at 1000 G. The critical field, H_{c2} , was determined by applying fields from 0 to 1000 G in 10 G

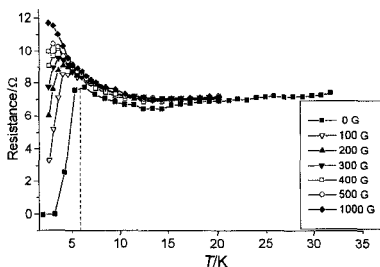


Fig. 5 Magnetoresistance measurements of [1] in fields from 0 to 1 T.

intervals and from 1000 to 2×10^4 G in 1000 G intervals at 2 K. The critical field at which the Cooper pairs are disrupted is 300 G, much higher than that obtained from SQUID measurements.

Raman spectroscopy

The two totally symmetrical C=C stretching frequencies of BEDT-TTF between 1400 and 1550 cm^{-1} (ν_3 and ν_4) have large electron-phonon coupling constants and so are very sensitive to the charge on the donor molecule. Wang *et al.*¹² showed for related complexes that there is an approximately linear relationship between the degree of charge-transfer and the shift in the wavenumbers of ν_3 and ν_4 . From the BEDT-TTF charges calculated for [1] from the C-C and C-S bond lengths, the expected Raman band wavenumbers would be 1492 cm^{-1} (ν_3) and 1459 cm^{-1} (ν_4). From the experimental spectrum the two bands attributed to totally symmetrical C=C stretching modes occur at $\nu_3 = 1495 \text{ cm}^{-1}$ and $\nu_4 = 1466 \text{ cm}^{-1}$, corresponding to an approximate charge of +0.51 and +0.48 on the two BEDT-TTF ions in [1]. This agrees with the conclusions drawn from the crystal structure (Fig. 6). The charge found on the BEDT-TTF also confirms that the A group is monopositive. The weak band at 1420 cm^{-1} is in the correct place expected for ν_4 of NH_4^+ even though this band would be typically broader. The Raman spectrum of [2] shows that $\nu_3 = 1494.6 \text{ cm}^{-1}$ and $\nu_4 = 1470.3 \text{ cm}^{-1}$ and corresponds to BEDT-TTF with a charge of +0.48, (Fig. 6). As with compound [1], since the formal charge on the anion is 3- the A group must be monopositive.

Electron paramagnetic resonance

As with other compounds in the same series, both [1] and [2] exhibit low field microwave absorption (LFMA) signals indicative of superconductivity¹³⁻¹⁶ (Figs. 7a and 7b). For [1] the LFMA is detected up to 18 K at the K-band frequency and for [2] the LFMA is observed below 10 K at X-band and K-band frequencies. Since these temperatures are above the T_c measured by susceptibility, the effect may be due to two-dimensional short-range superconducting fluctuations or surface effects.

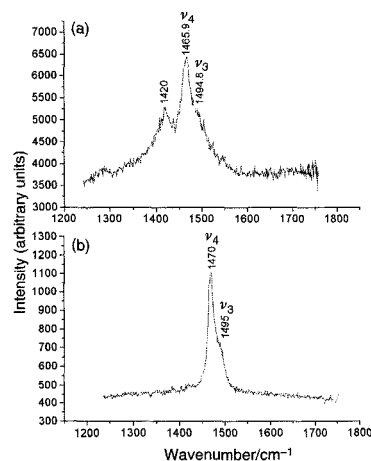


Fig. 6 Room temperature Raman spectra of [1] and [2] in the range 1200 to 1800 cm^{-1} .

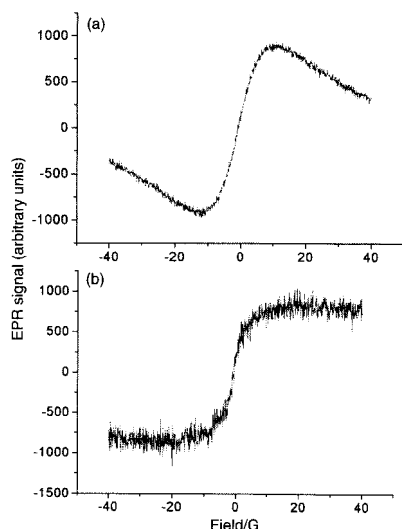


Fig. 7 Low field microwave absorption (LFMA) signals for [1], and [2]. Measured at 4.2 K with K-band EPR.

Polarised infrared reflectance

The polarised infrared reflectivity of single crystals of [2] at room temperature was measured both parallel and perpendicular to the long axis of the rectangular crystal (Fig. 8). The spectrum is of the form expected for a metal, with high reflectivities, and an approximate threefold difference in reflectance for polarisation of the incident electric vector 0 and 90° to the crystal *c* axis. This indicates that the band structure is highly anisotropic, as expected (the unpolarised spectra are the mean of the 90 and 0° measurements). The frequency dependence of the reflectivity could not be fitted to the simple Drude model, which suggests that a more complex conduction mechanism is in operation. Superimposed on the electronic contribution are peaks close to the vibrational transitions, which can be assigned to fundamentals of the $[\text{Cr}(\text{C}_2\text{O}_4)_3]^{2-}$ ion: e.g. the O–C–O asymmetric stretching vibration which occurs at 1655 cm^{-1} . It is noted that there is no strong band about 3050 cm^{-1} for the N–H stretch, which would be expected if [2] contained NH_4^+ . This, together with the Raman data, may indicate that compound [1] crystallises with $\text{A}=\text{NH}_4^+$ whereas [2] has $\text{A}=\text{H}_3\text{O}^+$, although more definitive evidence is required to be certain.

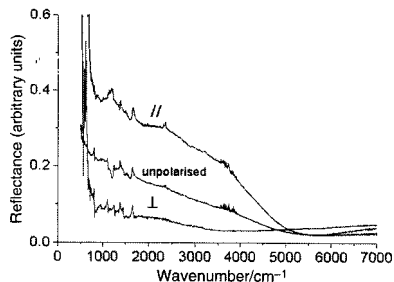


Fig. 8 Polarised infrared reflectance spectra of [2] measured parallel (//) and perpendicular (⊥) to the crystallographic *c* axis.

Conclusion

We have synthesised and characterised the crystal structures and physical properties of two new molecular charge transfer salts belonging to the general class $\beta''\text{-(BEDT-TTF)}_4[\text{A}\cdot\text{M}(\text{C}_2\text{O}_4)_3]\text{S}$, where S is an included solvent molecule. Like the compounds where $\text{S}=\text{PhCN}$, but in contrast to those where $\text{S}=\text{C}_6\text{H}_5\text{N}$, the new compounds with $\text{S}=\text{PhNO}_2$ are type II superconductors, though with T_c 's and H_c 's slightly lower than in the PhCN compounds that contain the same 3d metal ion M. Surprisingly, in view of correlations between increasing unit cell volume and higher T_c for other series of molecular superconductors such as $\beta''\text{-(BEDT-TTF)}_2\text{X}^{17,18}$ ($\text{X}=\text{I}_3, \text{AuI}_2$, etc.) and A_3C_{60} ¹⁹ ($\text{A}=\text{group 1 cation}$), the lower T_c of the PhNO₂ compounds are associated with slightly larger unit cell volumes. Thus at 120 K, for $\text{M}=\text{Fe}$, $\text{S}=\text{PhCN}$, $V=7157\text{ \AA}^3$ while for $\text{M}=\text{Fe}$, $\text{S}=\text{PhNO}_2$, $V=7169\text{ \AA}^3$. However, given the very small differences of less than 0.2% in unit cell volumes caution is needed in interpreting these results. Furthermore, intermolecular S...S distances are, on the whole, slightly larger in the PhNO₂ compounds than the PhCN ones, suggesting narrower bands and, on a simple BCS view, higher T_c . However, probably a more significant determinant of the collective properties of this series of compounds is the disorder of the terminal $\text{CH}_2\text{-CH}_2$ groups of the BEDT-TTF, which is determined by the volume and the H-bonding capabilities of the solvent molecule. It is clear that the lower T_c of the PhNO₂ salts is not correlated with one single structural parameter. More salts in this series with different included solvent molecules will need to be examined to identify the critical structural parameters and to classify the supramolecular chemistry of such complex lattices.

Acknowledgements

The UK Engineering and Physical Sciences Research Council and the University of London Intercollegiate Research Service have supported this work. Philippe Guionneau thanks the European Commission for the award of a Marie Curie Research Fellowship.

References

- 1 M. Kurmoo, A. W. Graham, P. Day, S. J. Coles, M. B. Hursthouse, J. L. Caulfield, J. Singleton, F. L. Pratt, W. Hayes, L. Ducasse and P. Guionneau, *J. Am. Chem. Soc.*, 1995, 117, 12209.
- 2 P. Guionneau, J. Gaultier, M. Rahal, G. Bravic, J. M. Mellado, D. Chasseau, L. Ducasse, M. Kurmoo and P. Day, *J. Mater. Chem.*, 1995, 5, 1639.
- 3 A. W. Graham, M. Kurmoo and P. Day, *J. Chem. Soc., Chem. Commun.*, 1995, 20, 2061.
- 4 L. Martin, S. S. Turner, P. Day, F. E. Mabbs and E. J. L. McInnes, *Chem. Commun.*, 1997, 1367.
- 5 S. S. Turner, P. Day, K. M. A. Malik, M. B. Hursthouse, S. J. Teat, E. J. MacLean, L. Martin and S. A. French, *Inorg. Chem.*, 1999, 38, 3543.
- 6 J. C. Bailar and E. M. Jones, *Inorg. Synth.*, 1939, 1, 1993.
- 7 SAINT Version 4.050, Siemens Analytical X-ray Instruments, Madison, USA, 1995.
- 8 SADABS Empirical Absorption Program, G. M. Sheldrick University of Göttingen, Germany.
- 9 SHELXTL-Plus, G. M. Sheldrick, Release 4.1 edn., Siemens Analytical X-ray Instruments Inc., Madison, Wisconsin, USA, 1991.
- 10 P. Guionneau, C. J. Kepert, G. Bravic, D. Chasseau, M. R. Truter, M. Kurmoo and P. Day, *Synth. Met.*, 1997, 86, 1973.
- 11 R. L. Carlin, *Magnetochemistry*, Springer Verlag, Weinheim, 1986.
- 12 H. H. Wang, J. R. Ferraro, J. M. Williams, U. Geiser and J. A. Schlueter, *J. Chem. Soc., Chem. Commun.*, 1994, 16, 1893.
- 13 D. Achkir, M. Poirier, C. Bourbonnais, G. Quiron, C. Lenoir, P. Batail and D. Jerome, *Phys. Rev. B*, 1993, 47, 11595.
- 14 A. Dulcic, R. H. Crepeau and J. H. Freed, *Phys. Rev. B*, 1989, 39, 4249.
- 15 F. J. Owens, *Phys. C (Amsterdam)*, 1991, 178, 456.

-
- 16 M. J. Rosseinsky, A. P. Ramirez, S. H. Glarum, D. W. Murphy, A. F. Haddon, T. T. M. Palstra, A. R. Kortan, S. M. Zahurak and A. V. Makhija, *Phys. Rev. Lett.*, 1991, **66**, 2830.
- 17 V. F. Kaminskii, T. G. Prokhorova, R. P. Shibaeva and E. B. Yagubskii, *JETP Lett. Engl. Transl.*, 1984, **39**, 17.
- 18 H. H. Wang, M. A. Beno, U. Geiser, M. A. Firestone, K. S. Webb, L. Nunez, G. W. Crabtree, K. D. Carlson, J. M. Williams, L. J. Azevedo, J. F. Kwak and J. E. Schirber, *Inorg. Chem.*, 1985, **24**, 2465.
- 19 M. Baenitz, M. Heinze, K. Luders, H. Werner and R. Schlogl, *Solid State Commun.*, 1994, **91**, 337.

Conducting Materials
The First Proton-Conducting Metallic Ion-Radical Salts**

Akane Akutsu-Sato, Hiroki Akutsu, Scott S. Turner, Peter Day,* Michael R. Probert, Judith A. K. Howard, Tomoyuki Akutagawa, Sadamu Takeda, Takayoshi Nakamura, and Takehiko Mori

Metallic materials that also conduct protons are being sought because of their potential as components in solid-state electrochemical devices, such as batteries and fuel cells.^[1] To date, the search has concentrated mainly on purely inorganic materials, and in particular continuous lattice oxides. In fact, there is a clear lack of candidates among electronically conducting organic molecular crystals, despite the existence of proton-conducting polymers, such as perfluorinated Nafion. Recently a 2,2'-[2,5-cyclohexadiene-1,4-diylidene]-bis(propanedinitrile) (TCNQ) charge transfer complex of benzimidazolyl-benzimidazole was shown to exhibit coupled protonic and electronic conductivity, and a TCNQ complex of 1,4-diazabicyclo[2.2.2]octane also exhibited proton transfer.^[2] Herein we report what we believe to be the first molecular ion-radical salts that are metallic conductors at room temperature, and also show a high proton conductivity. We provide evidence that the mobility of both protons and electrons is

[*] Dr. A. Akutsu-Sato, Dr. H. Akutsu, Dr. S. S. Turner, Prof. P. Day
Davy-Faraday Research Laboratory (DFRL)
Royal Institution of Great Britain
21 Albemarle Street, London, W1S 4BS (United Kingdom)
Fax: (+44) 20-7629-3569
E-mail: pday@ri.ac.uk

Dr. S. S. Turner
School of Biological and Chemical Sciences
Department of Chemistry, University of Exeter
Exeter, EX4 4QD (United Kingdom)

M. R. Probert, Prof. J. A. K. Howard
Department of Chemistry, University of Durham
South Road, Durham, DH1 3LE (United Kingdom)

Dr. H. Akutsu
Graduate School of Material Science
University of Hyogo, Hyogo, 678-1297 (Japan)

Dr. A. Akutsu-Sato, Prof. T. Mori
Department of Organic and Polymeric Materials
Tokyo Institute of Technology
O-okayama, Meguro-ku, Tokyo, 113-0033 (Japan)

Prof. T. Akutagawa, Prof. T. Nakamura
Research Institute for Electronic Science
Hokkaido University, Sapporo, 060-0812 (Japan)

Prof. S. Takeda
Division of Chemistry, Graduate School of Science
Hokkaido University, Sapporo, 060-0812 (Japan)

[**] This work was supported by the Engineering and Physical Sciences Research Council, EPSRC, (UK), and Monbukagakusho (Japanese Ministry for Education, Culture, Sports, Science and Technology). H.A. and A.A.-S. wish to thank the Japanese Society for the Promotion of Science (JSPS) for postdoctoral fellowships at the DFRL. JAKH thanks the EPSRC for a Senior Research Fellowship.

high in these lattices because of a unique crystal structure consisting of layers of organic donor molecules interleaved with arrays of stacked crown ether molecules. The crown ether molecules form "pipes" filled with water molecules. The crystal structure, resolved from X-ray data recorded at 30 K,^[9] gives strong indication of a hydrogen-bonding network, which gives rise to the protonic conductivity.

The series of cation-radical salts $(\text{BEDT-TTF})_4[(\text{Cat})\text{M}(\text{C}_2\text{O}_4)_3]\text{G}$, where BEDT-TTF = bis(ethylenedithio)tetrathiafulvalene, has proven to be an exceptionally fruitful source of different collective electronic ground states, promoted by the ease with which the monocation Cat, 3d metal M^{3+} , and neutral guest molecule G can be varied. Thus we found the first examples of paramagnetic superconductors (Cat = H_3O^+ ; M = Cr, Fe; G = PhCN, PhNO_2)^[4] and the first case of polymorphism, in the whole realm of solid-state chemistry, that arose from different spatial distributions of chiral antiomers $[\text{M}(\text{C}_2\text{O}_4)_3]^{3-}$ in a racemic lattice.^[5] By inserting asymmetrically substituted aromatic G molecules in cavities within the anion sublattice, it has also been possible to synthesize unique conducting salts containing a superlattice of two different packing types (α and β') of the BEDT-TTF cations.^[6] The present salts also contain superlattices of cation layers but, instead of being made up from two different arrangements of the BEDT-TTF molecules, they consist of BEDT-TTF and crown ether molecules that incorporate both H_2O and H_3O^+ or NH_4^+ ions.

β' -(BEDT-TTF)₄[(Cat)M^{III}(C₂O₄)₃]₂(Cat)₂[(18]crown-6 ether)₅·5H₂O, where M^{III} is Cr or Ga (**1** and **2**, respectively) and Cat is H_3O^+ or NH_4^+ , were synthesized by electrochemical crystallization. Both **1** and **2** crystallized in the triclinic space group (*P*¹). From single-crystal X-ray diffraction data recorded at 150 K,^[7] the structure of the Cr salt has been resolved, with all Cat molecules assigned to H_3O^+ . X-ray data recorded at 30 K on the Ga salt established the molecular structure, but in addition enabled many of the protons to be resolved.^[8] The crystal structure consists of successive layers

BEDT-TTF with a β' packing motif (layer A), Δ -[(Cat)M(C₂O₄)₃] (layer B), (Cat/H₂O)·[18]crown-6 (layer C), and Λ -[(Cat)M(C₂O₄)₃] (layer D) arranged in the sequence ...ABCD... (Figure 1). Within experimental error the C–C and C–S bond lengths of the crystallographically inequivalent BEDT-TTF are equal and from the correlation between bond length and charge in BEDT-TTF salts,^[9] these identify a mean charge on each cation of +0.5, as seen in the β' phase paramagnetic superconductors.

Considering the stoichiometry of **1** and **2** and the known charges of the molecular species, overall charge neutrality requires four monocations (Cat), which could be H_3O^+ or NH_4^+ . The 30 K structure refinement of **2** confirms the Cat molecules, embedded in the anionic oxalate layers, are all well ordered NH_4^+ ions. In this case there is a marginal improvement in the residual factors for occupancy by nitrogen as compared to oxygen. The remaining cations are predicted to be located in the channels formed by the stack of crown ether molecules. The water molecules found in the channels, refined with a fixed 50% occupancy, form zigzag hydrogen-bonded chains that align with the axis of the crown ether stacks. Additional electron density is located, off the stack axis

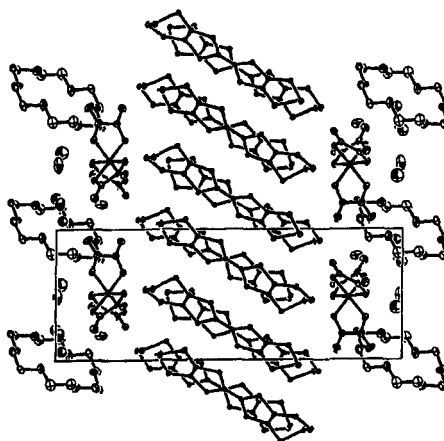


Figure 1. The crystal structure of **2** at 30 K, showing the sequence of BEDT-TTF, [(Cat)Ga(C₂O₄)₃], and crown ether layers. Protons have been removed for clarity.

between adjacent crown ether molecules. Refinements were carried out to try to distinguish between the preferred occupancy of these sites as oxygen or as nitrogen atoms, but these refinements were inconclusive. Despite the very low-temperature diffraction data, there is not sufficient information therein to identify individual atomic sites for occupancy by nitrogen or oxygen in these channel regions. Figure 2 shows the zigzag hydrogen-bonded network within the crown ether stacks, with these atoms assigned as oxygen.

Four-probe DC electrical conductivity measurements on single crystals of **1** and **2** with current flow parallel to the layers reveals high electronic conductivities at room temperature (300 Scm^{-1} for **1** and 200 Scm^{-1} and **2**) with temperature dependence characteristic of a metal. However, in each case the resistance shows an upturn at lower temperature, which occurs at 190 K for **1** and 240 K and **2** (Figure 3). These metal–semiconductor transitions contrast with the behavior of other BEDT-TTF salts of tris(oxalato)metallates, which have metal–superconducting transitions.^[4]

Measurements of proton conductivity of **1** and **2** from 260–297 K made on pellet samples, show specific conductivities varying from 10^{-6} to 10^{-3}Scm^{-1} over this temperature range (Figure 4a). For each compound the conductivity is activated, as anticipated, but does not follow a simple Arrhenius Law. Instead the measured activation energies change slightly for **1** from 1.06–1.59 eV and for **2** from 1.01–1.92 eV with the lower activation energy at higher temperatures and a gradual change across approximately 280 K. For a similar measurement on Nafion 117 (Figure 4a) there is a constant activation energy of 0.27 eV. A slight discontinuity in protonic conductivity at about 280 K can be seen clearly in Figure 4a for **1** and to a lesser extent for **2**. Typical complex impedance plots are shown for **1** in Figure 4b. The relatively high values of the room-temperature specific conductivity are comparable to those found in polymeric electrolytes of the polyethylene oxide type.^[10] The mechanism of the proton

Communications

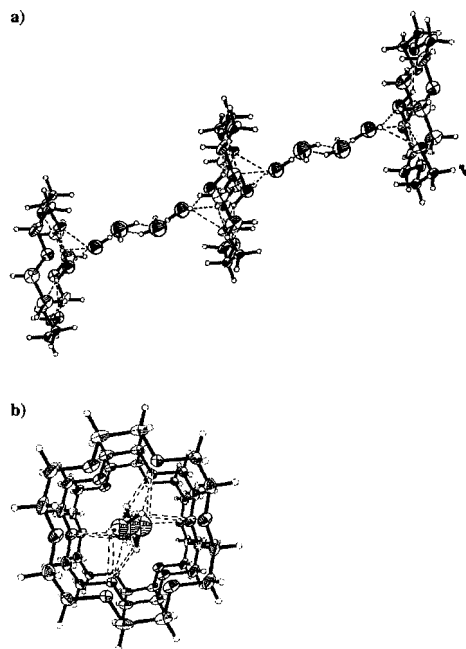


Figure 2. Hydrogen-bonding (broken lines) of water molecules within the crown ether stacks of **2** a) perpendicular and b) parallel to the stacks. O black ellipsoids, H small gray circles, C gray ellipsoids.

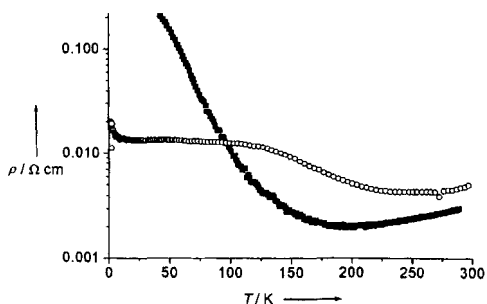


Figure 3. Four-probe single-crystal electronic conductivity of **1** (■) and **2** (○).

conductivity is not known. However, it has been established that significant proton conductivity can be mediated by a diffusion mechanism involving $\text{NH}_4^+/\text{H}_2\text{O}$ or $\text{NH}_4^+/\text{H}_3\text{O}^+$ species. The former has been found in $(\text{NH}_4)_4[\text{Fe}(\text{CN})_6] \cdot 1.5\text{H}_2\text{O}$ and the latter in the polytungstate $(\text{NH}_4)_{10}[\text{W}_{12}\text{O}_{41}] \cdot 5\text{H}_2\text{O}$,^[13] albeit with smaller absolute conductivities than the compounds presented herein.

Solid-state NMR spectra were studied as a function of the temperature in the diamagnetic salt **2**, under magic-angle spinning (MAS) and static conditions. At room temperature, the high-resolution ^1H spectrum of a fully protonated sample

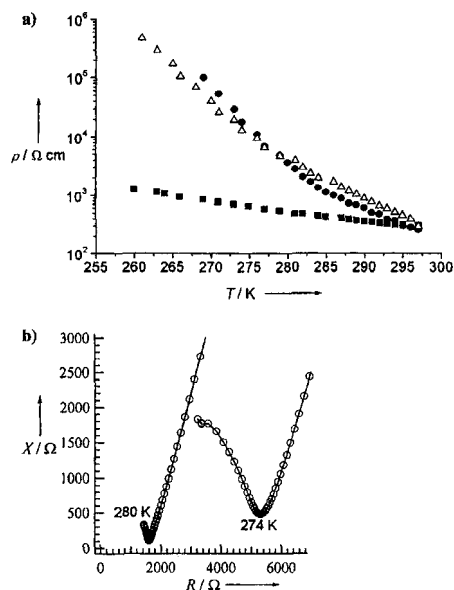


Figure 4. a) Proton conductivity of **1** (Δ, ●), and Nafion 117 (■) from 260–297 K with logarithmic y axis; b) typical complex impedance plots for **1** at 274 and 280 K.

consisted of three resonance signals A ($\delta = 7.7$ ppm), B ($\delta = 4.3$ ppm), and C ($\delta = 4.8$ ppm) with intensity ratio 1:0.3: >2 and widths of 1.6, 0.6, and 7.4 ppm, respectively. Signal A can be assigned to H_2O , H_3O^+ (and/or NH_4^+) since it corresponds to a signal, found in the ^2H NMR spectrum, which appears when a sample is prepared with D_2O . A separate experiment indicates that the chemical shift of ND_4 is $\delta = 7.4$ ppm, similar to the shift of signal A. It is difficult to distinguish between deuterated water and this species since the details of hydrogen bonding, not known from crystallography, could affect the chemical shifts. Signal C is assigned to the $-\text{CH}_2-$ group of BEDT-TTF and the [18]crown-6 ether. The assignment of signal C is supported by its behavior at low temperature; in the wide-line ^1H NMR spectrum at 130 K it splits into a doublet with a separation of approximately 30 kHz, which is typical for the nuclear dipole interaction between the two protons in a $-\text{CH}_2-$ group. Furthermore, the signal is absent in the ^2H NMR spectrum of the sample when exchanged with D_2O . Signal B, which is much weaker and narrower than the other two, is tentatively assigned to water molecules adsorbed on the surface of the crystallites. The increasing line width of signal C in the wide-line ^1H NMR spectrum of the fully protonated sample (Figure 5) clearly indicates freezing of the thermal fluctuations of the $-\text{CH}_2-$ on lowering the temperature. In contrast, the width of signal A, remains relatively constant and small (11 kHz) between 130 and 250 K before decreasing further between 250 and 300 K. The ^2H NMR spectrum of the D_2O sample further confirms an almost isotropic and rapid rotation of those molecules producing signal A, at least down to 195 K.

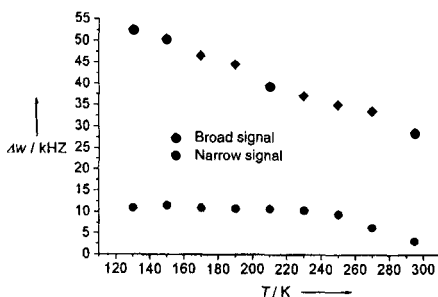


Figure 5. Temperature dependence of the spectral width (Δw) of the wide-line ^1H NMR spectra of a fully ^1H substituted sample of **2**. The spectral width of BEDT-TTF and [18]crown-6- CH_2^- groups (\bullet) and of H_2O (\circ) including the weak signal (signal B, see text) are shown.

In summary, we have identified the first molecular ion-radical salts that are both protonic and metallic conductors. The high values of both the ionic and electronic conductivities at room temperature are especially noteworthy and are attributed to the presence of discrete conducting layers in the crystal consisting of either organosulfur molecules or of crown ether stacks containing disordered H_2O , H_3O^+ , and/or NH_4^+ . This discovery expands the search for other mixed ionic-electronic conductors among the large and versatile family of TTF and BEDT-TTF ion-radical salts.

Experimental Section

The BEDT-TTF salts were prepared by in situ oxidation of BEDT-TTF (12 mg) in an H-shaped electrochemical cell in the presence of a racemic solution of $(\text{NH}_4)_x[\text{M}(\text{C}_2\text{O}_4)_x]$ ($\text{M} = \text{Cr}, \text{Ga}$; 120 mg), [18]crown-6-ether (250 mg) and four drops of distilled H_2O in a mixture of freshly distilled CH_3CN (10 mL) and CH_2Cl_2 (10 mL). A constant current of 1 μA was applied across the cell and thin dark brown elongated plates of the product grew on the Pt anode in 2–3 days. Elemental analysis calcd (%) for $(\text{BEDT-TTF})_x[(\text{NH}_4)_x\text{M}(\text{C}_2\text{O}_4)_x] \cdot [(\text{NH}_4)_x(\text{[18]crown-6})] \cdot 5\text{H}_2\text{O}$: **1** C 29.58, H 3.18, N 2.16; found: C 29.48, H 2.91, N 1.70; **2** C 29.30, H 2.77, N 2.14; found: C 29.47, H 2.82, N 2.17.

Single-crystal DC conductivity were made using four contacts (15 μm diameter Au wires attached to the crystals with Au paste) and an Oxford Instruments Maglab 2000 cryostat with EP probe.

Temperature-dependent protonic conductivity was measured by the AC impedance method in the frequency range $100\text{--}5 \times 10^6$ Hz using an HP4194A impedance analyzer. The sample, prepared as a compressed pellet with a diameter of 3 mm, was enclosed by a Teflon ring to avoid short circuit, this pellet was then sandwiched by proton-conducting Nafion 117 (Aldrich). The sample was clamped by metal electrodes, and was inserted into a Daikin PS24SS cryogenic refrigerating system. The conductivity was measured in vacuo ($< 10^{-3}$ torr).

Solid-state high-resolution ^1H and ^2H NMR spectra were measured by a magic-angle spinning technique with spinning speed of 25 (^1H NMR) and 7 kHz (^2H NMR) using a Bruker DSX 300 spectrometer. Echo pulse sequence synchronized with spinning speed was used for ensuring the phase of all spinning side-band signals. The thermometers of the NMR probes were calibrated by standard samples. Wide-line ^1H NMR spectrum under static conditions was measured by the solid echo pulse sequence $\pi/2\text{--}\tau\text{--}\pi/2$; the $\pi/2$ pulse width and τ were 1.5 μs and 15 μs , respectively.

Received: August 17, 2004

Keywords: conducting materials · electron transport · ion channels · proton transport

- [1] For example see W. R. M. Kinnon in *Solid State Electrochemistry* (Ed.: P. G. Bruce), Cambridge University, 1994, pp. 163–178.
- [2] a) T. Akutagawa, T. Hasegawa, T. Nakamura, T. Inabe, G. Saito, *Chem. Eur. J.* **2002**, *8*, 4402–4411; b) T. Akutagawa, S. Takeda, T. Hasegawa, T. Nakamura, *J. Am. Chem. Soc.* **2004**, *126*, 291–294.
- [3] A. E. Goeta, L. K. Thompson, C. L. Sheppard, S. S. Tandon, C. W. Lehmann, J. Cosier, C. Webster, J. A. K. Howard, *Acta Cryst.* **1999**, *C5*, 1243–1246.
- [4] a) M. Kurmoo, A. W. Graham, P. Day, S. J. Coles, M. B. Hursthouse, J. L. Caulfield, J. Singleton, F. L. Pratt, W. Hayes, L. Ducasse, P. Guionneau, *J. Am. Chem. Soc.* **1995**, *117*, 12209–12217; b) S. Rashid, S. S. Turner, P. Day, J. A. K. Howard, P. Guionneau, E. J. L. McInnes, F. E. Mabbs, R. J. H. Clark, S. Firth, T. Biggs, *J. Mater. Chem.* **2001**, *11*, 2095–2101.
- [5] a) L. Martin, S. S. Turner, P. Day, K. M. A. Malik, S. J. Coles, M. B. Hursthouse, *Chem. Commun.* **1999**, 513–514; b) L. Martin, S. S. Turner, P. Day, P. Guionneau, J. A. K. Howard, K. M. A. Malik, M. B. Hursthouse, M. Uruichi, K. Yakushi, *Inorg. Chem.* **2001**, *40*, 1363–1371.
- [6] H. Akutsu, A. Akutsu-Sato, S. S. Turner, P. Day, E. Canadell, S. Firth, R. J. H. Clark, J. Yamada, S. Nakatsujii, *Chem. Commun.* **2004**, *1*, 18–19.
- [7] S. Rashid, S. S. Turner, P. Day, M. E. Light, M. B. Hursthouse, S. Firth, R. J. H. Clark, *Chem. Commun.* **2001**, 1462–1463.
- [8] Crystallographic data for **2**: $\text{C}_{64}\text{H}_{70}\text{Ga}_2\text{N}_2\text{O}_7\text{S}_{23}$, $M_r = 2633.65$, dark red crystal, crystal size = $0.3 \times 0.25 \times 0.02$ mm³, triclinic, $P\bar{1}$, $a = 10.2070(3)$, $b = 11.2012(3)$, $c = 24.2433(6)$ Å, $\alpha = 88.4170(10)$, $\beta = 24.2433(6)$, $\gamma = 63.4470(10)^\circ$, $V = 2478.15(12)$ Å³, $Z = 1$, $\rho_{\text{calcd}} = 1.766$ g cm⁻³, $\mu = 1.302$ mm⁻¹, graphite monochromated $\text{MoK}\alpha$ radiation ($\lambda = 0.71073$ Å), $T = 30(2)$ K, 10910 independent reflections of which 9167 with $F_o > 4\sigma(F_o)$ were included in the refinement, $R_{\text{int}} = 0.026$, max residual density = 0.859 e Å⁻³, $R_1 = 0.0357$, $wR_2 = 0.0794$. Data were collected through ω -scans, at 30 K, using an Oxford Cryosystems HELIX³ on a Bruker SMART 1K diffractometer. A numerical absorption correction was applied using SADABS.^[11] The structure was solved by direct methods and refined using full-matrix least-squares methods (SHELX97),^[12] with all fully occupied atoms having position and thermal-displacement parameters refined. Hydrogen atoms were placed by Fourier and geometric methods, and refined as riding atoms. Multiple refinements were attempted to definitively determine the cations between adjacent crown ether molecules. The final model was chosen as it gave the best residual Fourier map. CCDC-234609 (**2**) contains the supplementary crystallographic data for this paper. These data can be obtained free of charge via www.ccdc.cam.ac.uk/conts/retrieving.html (or from the Cambridge Crystallographic Data Centre, 12 Union Road, Cambridge CB2 1EZ, UK; fax: (+44) 1223-336-033; or deposit@ccdc.cam.ac.uk).
- [9] a) P. Guionneau, C. J. Kepert, D. Chasseau, M. R. Truter, P. Day, *Synth. Met.* **1997**, *86*, 1973–1974; b) P. Guionneau, PhD thesis, Université de Bordeaux I (France), 1996.
- [10] M. F. Daniel, B. Desbat, J. C. Lassegues, *Solid State Ionics* **1988**, *28–30*, 632.
- [11] G. M. Sheldrick, *SADABS* Empirical absorption correction program, University of Göttingen, Göttingen, 1997.
- [12] *SHELXTL* version 5.1, Bruker Analytical X-ray instruments, Madison, Wisconsin, U.S.A., 1999.
- [13] *Proton Conductors, Solids, Membranes and Gels: Materials and Devices* (Ed.: P. Colomban), CUP, Cambridge, 1992, p. 25.



Magnetic molecular semiconductors and superconductors: BEDT-TTF tris-oxalato-metallate(III) salts

P. Day, M. Kurmoo^a

The Royal Institution of Great Britain, 21 Albemarle Street, London W1X 4BS, UK

Abstract

Making new compounds that combine different physical properties in the same crystal lattice is a significant goal for chemists working on synthetic metals. As part of our ongoing programme to synthesise molecular conductors containing embedded magnetic moments we have investigated charge transfer salts of BEDT-TTF with tris-oxalatometallate (III) ions $M(C_2O_4)_3^{3-}$ ($M = Cr, Fe$). The series $(BEDT-TTF)_x[AM(C_2O_4)_3]_y(C_6H_5CN)_z$ is especially rich and interesting since it contains semiconductors ($A = K, NH_4; M = Cr, Fe$) and the first molecular superconductor containing paramagnetic ions ($A = H_2O; M = Fe; x = 4, y = z = 1$). The steric and charge factors determining the geometry of cation and anion layers in these compounds are surveyed, as well as the relation between the crystal structures and physical properties.

Keywords: Magnetic measurements, Organic superconductors

1. Introduction

One of the challenges in synthesising new molecular-based materials is to bring together combinations of physical properties not normally found in chemically simpler continuous lattice compounds. A feature of the superconducting charge transfer salts based on the donor molecule bis(ethylenedithio)-tetrathiafulvalene (BEDT-TTF) is the spatial segregation of the organic cations and inorganic anions into alternating layers, which led us some time ago to cite them as examples of 'organic-inorganic molecular composites'[1] or 'chemically constructed multilayers'[2]. Because of this separation into well-defined organic and inorganic components BEDT-TTF charge transfer salts are suitable synthetic targets for attempts to combine superconductivity in a molecular lattice with properties more characteristic of the inorganic solid state like co-operative magnetism. The electrons close to the Fermi surface are the HOMO's of BEDT-TTF so magnetic moments can be built in by using transition metal complexes as the anions.

Establishing superconductivity in a crystal lattice containing localised magnetic moments is important because superconductivity and magnetism have long been considered to exclude one another: Cooper pairs are

disrupted both by externally applied fields and by the internal fields generated in ferromagnets[3]. The small number of examples currently known are all continuous lattice compounds containing 4f elements (Ln) such as the Chevrel phases $LnMo_6S_8$ [4], the borides $LnRh_4B_4$ [5] and the cuprates $LnBa_2Cu_3O_7$ [6]. No corresponding stoichiometric phases containing 3d ions have been reported. Of the small number of BEDT-TTF salts containing 3d complex anions, several are semiconductors[7] but one example, $(BEDT-TTF)_3CuCl_4 \cdot H_2O$, remains metallic down to 400 mK though without becoming superconducting, and magnetic resonance from the conduction electrons and the localised 3d electrons is observed[8].

In the last few years a fascinating new class of molecular-based magnets has been investigated, consisting of two-dimensional bimetallic layers containing uni- or dipositive cations and $M^{III}(C_2O_4)_3^{3-}$ in which the oxalato-ion acts as a bridging ligand, leading to infinite sheets of approximately hexagonal symmetry, separated by bulky organic cations[9, 10, 11, 12]. We are therefore synthesising compounds containing similar anion lattices, but interleaved with BEDT-TTF molecules. The present paper presents an overview of the present state of our work with $M^{III} = Fe$ and Cr . Three such compounds, $(BEDT-TTF)_4AFe(C_2O_4)_3 \cdot C_6H_5CN$, ($A = H_2O, K, NH_4$) have been

^a Present address: IPCMS-GMI, 23 rue Loess, BP 20/CR, 67037 Strasbourg cedex, France

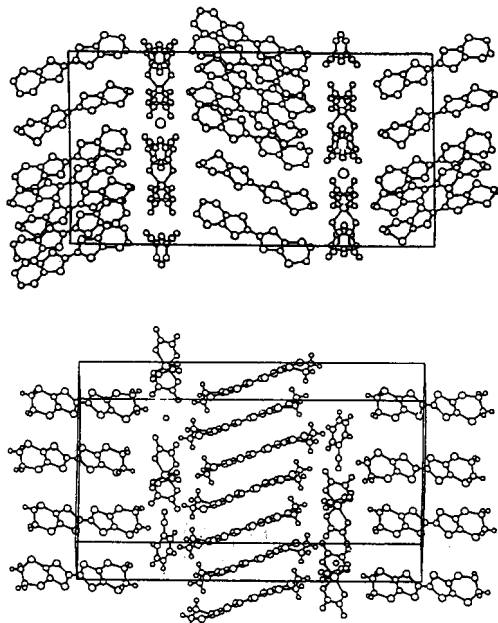


Figure 1 The layers of BEDT-TTF and anion layers in $(\text{BEDT-TTF})_x\text{AFe}(\text{C}_2\text{O}_4)_3\cdot\text{C}_6\text{H}_5\text{CN}$: (a, top) $\text{A} = \text{K}$ and (b, bottom) $\text{A} = \text{H}_2\text{O}$.

fully characterised structurally and physically. While the stoichiometric ratio of BEDT-TTF to Fe is the same in all three compounds, as is the basic topology of the anion layer, the presence or absence of a monocation within the latter not only changes the electron count (and hence the band filling) in the organic layer, but drastically alters the packing motif of the BEDT-TTF. Thus, the compounds with $\text{A} = \text{K}$, NH_4 are semiconductors containing $(\text{BEDT-TTF})_2^{2+}$ and $(\text{BEDT-TTF})^0$. In contrast the compound with $\text{A} = \text{H}_2\text{O}$ has BEDT-TTF packed in the β'' arrangement[13] and is the first example of a molecular superconductor containing magnetic ions[14, 15]. Unit cell parameters and physical properties of a number of Cr phases have also been determined, and we comment on the 'docking' between cation and anion layers in all these phases.

2. Crystal Structures

The crystal structures of the three Fe-compounds consist of alternating layers containing only BEDT-TTF and only $\text{AFe}(\text{C}_2\text{O}_4)_3\cdot\text{C}_6\text{H}_5\text{CN}$ (Fig. 1). Whilst the molecular packing in the latter is quite similar in all three cases the molecular packing arrangement within the BEDT-TTF layers differs markedly from the other two when $\text{A} = \text{H}_2\text{O}$.

The anion layers have a clear honeycomb arrangement, with alternate A and Fe forming an approximately hexagonal network (Fig. 2). The Fe are octahedrally coordinated by three bidentate oxalate ions, giving rise to a trigonal component of the crystal field. The O atoms of the oxalate which are not co-ordinated to Fe form cavities occupied either by K or H_2O . In the former case the coordination number of the K is seven, since the CN group of a benzonitrile molecule is oriented towards it. The benzonitrile molecules occupy cavities in the $\text{KFe}(\text{C}_2\text{O}_4)_3$ lattice of approximately hexagonal shape with their mean planes coinciding with the plane formed by the K and Fe and there is no doubt that it plays an important 'templating' role in stabilising the lattice.

In the superconducting phase, the hexagonal network of Fe and A is retained, though the site symmetry of the O is reduced to C_2 with distances to the six O on neighbouring $\text{C}_2\text{O}_4^{2-}$ being 2.81 (x2), 2.93 (x2), 2.95 Å (x2). The fact that two distances are distinctly shorter than the other four strongly suggests that the molecule is H_2O and not H_3O^+ .

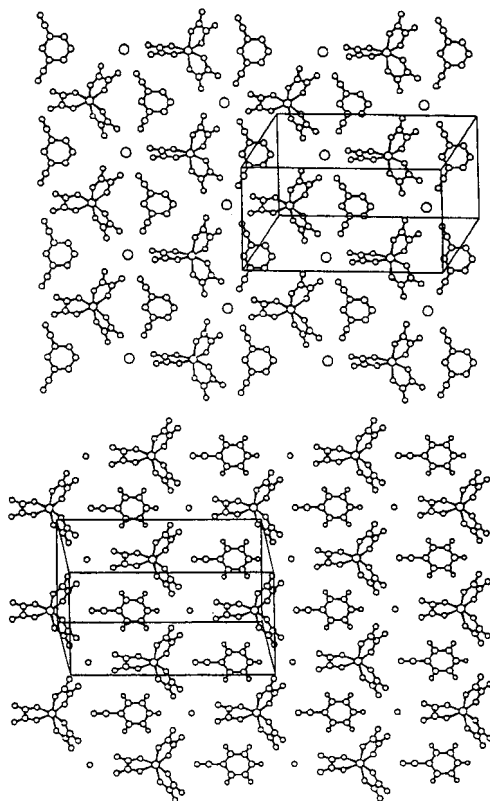


Figure 2 The anion and solvent layers in $(\text{BEDT-TTF})_x\text{AFe}(\text{C}_2\text{O}_4)_3\cdot\text{C}_6\text{H}_5\text{CN}$: (a, top) $\text{A} = \text{K}$ and (b, bottom) $\text{A} = \text{H}_2\text{O}$.

In the $A = \text{H}_2\text{O}$ compound the $-\text{CN}$ groups of the $\text{C}_6\text{H}_5\text{CN}$ are oriented towards Fe, so the hexagonal network of Fe and H_2O is elongated along one axis, with lowering of symmetry from orthorhombic to monoclinic ($\beta = 93.2^\circ$).

An interesting structural point about the anion layers concerns their chirality. The point symmetry of $\text{Fe}(\text{C}_2\text{O}_4)_3^{3-}$ is D_3 and the ion may exist in Δ or Λ enantiomers. In compounds synthesised from racemic starting material, alternate anion layers are composed exclusively either of Δ or Λ anions. We are attempting to synthesise the corresponding salts with optically resolved anions and thus generate what would be the first chiral superconductor.

The molecular arrangements in the BEDT-TTF layers are quite different in the K and NH_4 salts from the H_2O one. In the former the central $\text{C}=\text{C}$ bond lengths of the two independent molecules differ markedly (1.340(8) and 1.381(7) Å), signifying charges of 0 and +1. The latter form face to face dimers, surrounded by monomeric neutral molecules (Fig. 3(a)). Molecular planes of neighbouring dimers along [011] are oriented nearly orthogonal to one another, as in the κ -phase structure of $(\text{BEDT-TTF})_2\text{X}$ [16], but the arrangement of $(\text{BEDT-TTF})_2^{2+}$ surrounded by $(\text{BEDT-TTF})^0$ has not been observed before. Overall the neutral BEDT-TTF describe an approximately hexagonal network in the K and NH_4 salts commensurate with the anion sublattice. Thus the charged dimers are closest to the oxalate ions, leading to weak H-bonding between the terminal ethylene groups and oxalate O (2.51 - 3.05 Å). The intradimer S...S distances (3.46 - 3.77 Å) and between the charged and neutral molecules (3.19 - 4.45 Å), are short. Further evidence for specific interaction between the terminal CH_2 groups of the BEDT-TTF and the anion layer comes from the translation of the $\text{Fe}(\text{C}_2\text{O}_4)_3^{3-}$ complexes within the plane of the anion layer on passing from one layer to the next. The displacement of the $\text{Fe}(\text{C}_2\text{O}_4)_3^{3-}$ matches with the tilt of the long axes of the intervening BEDT-TTF. Thus the contacts between H atoms and O are the same at both ends of the BEDT-TTF.

In the H_2O salt packing of the BEDT-TTF molecules is quite different, without discrete dimers (Fig. 3(b)). Overall the packing closely resembles the β'' -structure found in metallic $(\text{BEDT-TTF})_2\text{AuBr}_2$ [13] and the pressure-induced superconductor $(\text{BEDT-TTF})_3\text{Cl}_2 \cdot 2\text{H}_2\text{O}$ [17]. Finally, the planes of the BEDT-TTF molecules in adjacent layers are twisted with respect to one another, an unusual feature in BEDT-TTF salts, the only other example known being one phase of $(\text{BEDT-TTF})_2\text{Ag}(\text{CN})_2$ [18].

Turning to the Cr compounds, we have crystallised several new phases but it has not been possible up to now to determine full three dimensional structures because of twinning. Nevertheless the values of the lattice parameters allow us to make useful comparisons with the Fe salts. In the phase that we have characterised structurally and electrically in greatest detail the volume of the cell is smaller than the Fe salts, and the absence of potassium was confirmed by X-ray fluorescence. The compound has one lattice parameter in common (c-axis $\sim 35\text{Å}$) with the Fe series which corresponds to two BEDT-TTF layers per cell. The c-axis of the Cr compound is longer, so that either the BEDT-TTF is more perpendicular to the anion layer than in

the Fe compounds or the anion is a monomer and sits in cavities created by the ethylene groups. The lattice parameter $b = 4.229\text{Å}$ implies that the layers are one

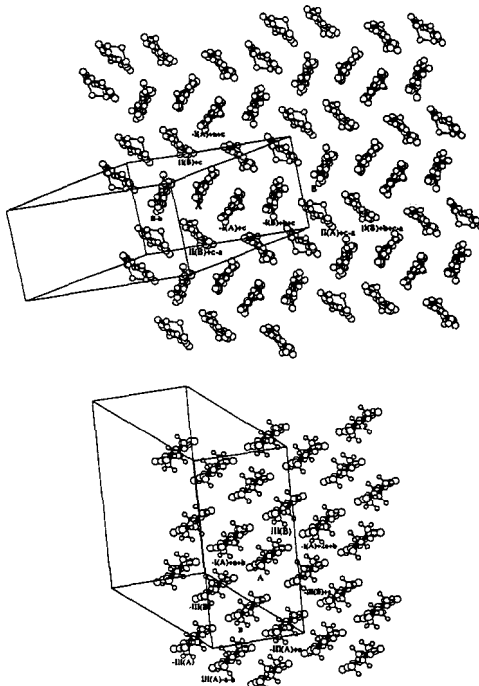


Figure 3 View of the BEDT-TTF layers along the $\text{C}=\text{C}$ bonds including the labeling of neighboring BEDT-TTF molecules in $(\text{BEDT-TTF})_4\text{Fe}(\text{C}_2\text{O}_4)_3 \cdot \text{C}_6\text{H}_5\text{CN}$: (a, top) $A = \text{K}$ and (b, bottom) $A = \text{H}_2\text{O}$.

molecule thick along the stacking axis while $a = 11.106\text{Å}$ corresponds to two BEDT-TTF with short side-by-side S...S distances. The a and b parameters are close to those found in numerous α and θ phases[19-21], especially those with a 4-5 Å lattice parameter. Recently, we correlated the dihedral angles between the BEDT-TTF molecules in adjacent stacks and the electrical conductivity[18]. In the present case the ratio of the crystallographic axes defining the conducting plane divided by the number of molecules in that direction for the α , θ or η -phases suggests a dihedral angle of $\sim 45^\circ$ which, applying the same correlation as before would predict that the Cr salt is a semiconductor (see below).

3. Electrical transport

The K and NH_4 salts containing Fe are both semiconductors over the temperature range 130-300 K with the same activation energy (0.14 eV) along all three crystal axes, though with markedly anisotropic conductivity[15]. In contrast the H_2O salt is a metal with resistivity of $\sim 10^{-2}\Omega\text{cm}$ at 200 K, decreasing monotonically by a factor of about 8

1448

P. Day, M. Kurmoo / Synthetic Metals 85 (1997) 1445-1450

down to 8.3 K, at which temperature it becomes superconducting (Fig. 4). The transition is sharp (width about 0.2 K) and application of a magnetic field parallel to the long axis of the needle crystals broadens it towards lower temperature in the way seen in other quasi-two-dimensional BEDT-TTF salts[22] so that the crystal is resistive down to 2 K in fields above 0.7 T (Fig. 4 (inset)). With the applied field perpendicular to the needle axis the same effect occurs at lower field (0.2 T) (Fig. 4 (inset)).

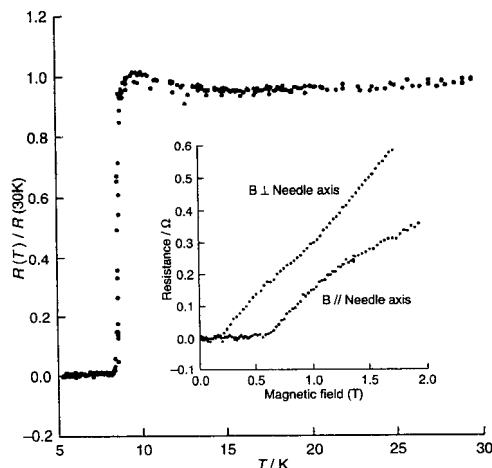


Fig. 4 Temperature dependence of the resistivity of a single crystal of β'' -(bedt-ttf)₄((H₂O)Fe(C₂O₄)₃)·PhCN. The inset shows the magnetoresistance at 2 K for field parallel and perpendicular to the needle axis.

The room temperature conductivities of several crystals of the Cr salt range from 1 to 10 Scm⁻¹, i.e. intermediate between that of (BEDT-TTF)₄[KFe(C₂O₄)₃].C₆H₅CN (10⁻⁴ Scm⁻¹) and (BEDT-TTF)₄[(H₂O)Fe(C₂O₄)₃].C₆H₅CN (10² Scm⁻¹)[15]. The activation energy (0.09 eV) is also smaller than for (BEDT-TTF)₄[KFe(C₂O₄)₃].C₆H₅CN. The room temperature conductivity and the activation energy are similar to those found for the α -phase compounds with magnetic anions, (BEDT-TTF)₃CuBr₄[23] and (BEDT-TTF)₈PMo₁₂O₄₀·(CH₃CN·H₂O)₂[24].

4. Magnetic Properties

Dealing first with the Fe series, in the case of the semiconducting A = K compound the susceptibility obeys the Curie-Weiss law over the entire temperature range from 2 to 300 K, and the least-square fitted value of the Curie constant ($C = 4.44$ emu K mol⁻¹) and the Weiss constant (-0.25 K) indicate that the Fe dominates the measured moment. Hence the (BEDT-TTF)₂²⁺ dimers are spin-paired while the neutral BEDT-TTF do not contribute to the paramagnetic susceptibility.

The susceptibility of the superconducting A = H₂O salt obeys the Curie-Weiss law from 300 to about 1 K above T_c , though a temperature independent paramagnetic term is

present amounting to 20. 10⁻⁴ emu mol⁻¹. When the sample is cooled to 2 K in zero field and then warmed in a measurement field of 0.5 mT the susceptibility shows a diamagnetic contribution in the superconducting temperature range, returning to Curie-Weiss behaviour above 10 K (Fig. 5). In larger measurement fields the diamagnetic response diminishes, till it vanishes above 50 mT, in which case Curie-Weiss behaviour persists down to 2 K, with a temperature independent contribution as a high temperature. The Meissner effect is complete at 0.5 mT (Fig. 6).

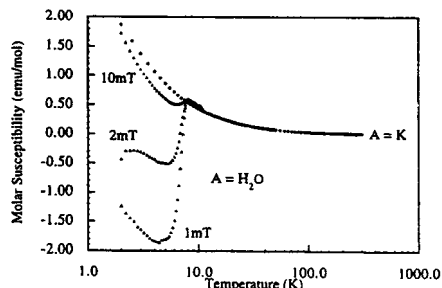


Figure 5 Temperature dependence of magnetic susceptibility of (BEDT-TTF)₄AFe(C₂O₄)₃·C₆H₅CN: A = K (dots) and A = H₂O (triangles).

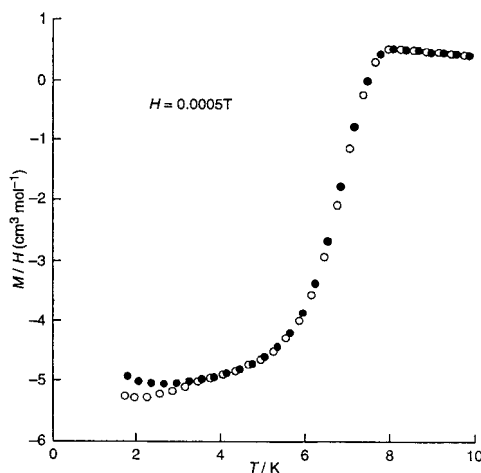


Fig 6 Temperature dependence of the magnetization. Filled circles are zero-field cooled data and open circles are field cooled data.

The e.p.r. spectrum of the semiconducting A = K compound consists of a single narrow resonance whose linewidth and g-value are identical to those found in K₃Fe(C₂O₄)₃·3H₂O. On the other hand the room temperature EPR spectrum of the A = H₂O compound consists of two resonances: an orientation independent

narrow one assigned to the Fe^{3+} by analogy with the $A = \text{K}$ compound, and a much broader one ($g = 2.002 - 2.012$ and $H_{pp} = 23 - 35 \text{ G}$) assigned to the conduction electrons. The former peak is Lorentzian in shape at all orientations of the crystal while the conduction electron resonance becomes Dysonian at certain orientations.

The fact that we observe separate resonances due to localised and conduction electrons reveals a large difference between the g -values and relaxation rates of the two spin systems. In the present case the Fe^{3+} relaxation rate is high, producing a narrow signal, whilst the two spin systems are certainly well separated spatially. In the only other metallic charge transfer salt, $(\text{BEDT-TTF})_3\text{CuCl}_4 \cdot \text{H}_2\text{O}$, with separated resonances due to conduction and 3d electrons[8], the angular dependence of the spectrum prevented direct comparison of the two lineshapes.

The e.p.r. spectrum of the Cr salt is characterised by a single Lorentzian line centred near $g = 2$ independent of temperature and orientation. The observed g -value is lower than those for BEDT-TTF radical salts[25] containing non-magnetic anions (2.003 - 2.011). The reported g -value for Cr(III) is 1.98 when in a cubic and 1.984 in trigonal symmetry with very little anisotropy[26].

The linewidth of the resonance, which is Lorentzian, is almost isotropic in the bc plane. It decreases gradually to a minimum at $\sim 75\text{K}$ before diverging rapidly at low temperature to 5 times that at 300 K. The value of 4.5 mT at room temperature is comparable to many BEDT-TTF salts. However, it is narrower than expected for chromium oxalate complexes, which have very wide resonances ($>100 \text{ mT}$) at room temperature. It is possible that the linewidth is narrowed by exchange between the two spin systems of BEDT-TTF and Cr^{III} . Furthermore, the lack of hyperfine structure from ^{53}Cr (9.55%) may also be due to exchange between the moment on the organic molecules and that on the metal.

The spin susceptibility derived from the intensity of the resonance is shown in Fig. 7. The temperature dependence is very smooth suggesting there is no structural, electronic or magnetic transition. However, it does not follow the Curie-Weiss law since the observed ratio $\chi(4 \text{ K})/\chi(300 \text{ K}) \sim 10$ is much smaller than expected (75), again suggesting considerable interaction between the moments.

As far as the bulk magnetic susceptibility of the Cr salt is concerned, its magnitude at 120 K is that expected for one $S = 3/2$ magnetic ion. It increases at lower temperature according to the Curie-Weiss law with $\theta = -2.0(2) \text{ K}$ and $C = 1.70 \text{ emu K mol}^{-1}$, close to the value ($1.84 \text{ emu K mol}^{-1}$ for $g = 1.98$) expected for Cr (d^3 , $S = 3/2$), so that there is no contribution from the BEDT-TTF.

5. Conclusions

The hexagonal layer motif $[\text{AM}^{\text{III}}(\text{C}_2\text{O}_4)_3]^{n-}$, with bridging oxalate groups, which forms a wide variety of compounds with electronically inactive counter-cations having unusual co-operative magnetic properties[9], can also stabilise lattices containing the organic π -donor BEDT-TTF. In the

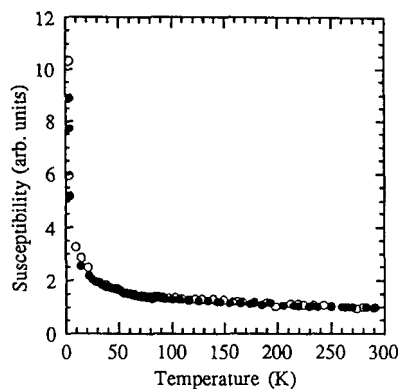


Figure 7 Temperature dependence of the spin susceptibility for the applied field parallel (filled circles) and the perpendicular (open circles) to the crystal plate.

compounds described here, $(\text{BEDT-TTF})_4\text{AFe}(\text{C}_2\text{O}_4)_3 \cdot \text{C}_6\text{H}_5\text{CN}$ ($A = \text{H}_2\text{O}, \text{K}, \text{NH}_4$), and the $\text{M}^{\text{III}} = \text{Cr}$ compound of unknown structure, the lattice is stabilised by $\text{C}_6\text{H}_5\text{CN}$ molecules included in the hexagonal cavities. The oxalato-bridged network of A and M^{III} provides an elegant way to introduce transition metal ions with localised magnetic moments into the lattice of a molecular charge transfer salt. In the $A = \text{H}_2\text{O}$ compound we have prepared the first molecular superconductor containing localised magnetic moments in the lattice, while the $A = \text{K}, \text{NH}_4$ compounds are semiconducting. The packing of the BEDT-TTF in the $A = \text{K}, \text{NH}_4$ phases is of a type not previously observed, with spin-paired $(\text{BEDT-TTF})_2^{2+}$ separated by closed shell $(\text{BEDT-TTF})^0$, while that in the superconductor is of β'' type. Both the superconducting $A = \text{H}_2\text{O}$ and semiconducting $A = \text{K}, \text{NH}_4$ phases contain high spin $3d^5 \text{ Fe}^{\text{III}}$ with only very weak exchange interaction between them. Additional low temperature and high magnetic field experiments (e.g. of Schubnikov-de Haas oscillatory magnetoresistance[27]) will be needed to delineate the Fermi surface in the superconductor. A further synthetic challenge will be to incorporate other transition metal ions at the A site to create a two-dimensional magnetically ordered array between the BEDT-TTF layers. Our efforts are continuing in this direction.

6. Acknowledgements

We acknowledge the UK Engineering and Physical Science Research Council, the British Council, Monbusho and the European Union (DG XII) for financial support. We thank our many collaborators referenced below for discussions and technical help.

References

- [1] P. Day, *Phil. Trans. Roy. Soc.*, A314 (1985) 145.
- [2] P. Day, *Phys. Scripta*, T49 (1993), 726.
- [3] See, e.g. Ø. Fisher and M.B. Maple (eds.), *Topics in Current Physics*, Springer Verlag, New York, 1984.
- [4] (a) M. Ishikawa and Ø. Fischer, *Sol. St. Commun.*, 23 (1977) 37.
(b) J.W. Lynn, G. Shirane, W. Thomlinson and R.N. Sheldon, *Phys. Rev. Lett.*, 46 (1981) 368.
- [5] (a) W.A. Fertig, D.C. Johnston, L.E. DeLong, R.W. McCallum, M.B. Maple and B.T. Matthias, *Phys. Rev. Lett.*, 38 (1977) 987.
(b) D.E. Moncton, D.B. McWhat, P.H. Schmidt, G. Shirane, W. Thomlinson, M.B. Maple, H.B. MacKay, L.D. Woolf, Z. Fisk and D.C. Johnston, *Phys. Rev. Lett.*, 45 (1980) 2060.
- [6] K.M. Beauchamp, G.C. Spalding, W.H. Huber and A.M. Goldman, *Phys. Rev. Lett.*, 73 (1994) 2752.
- [7] (a) T. Mallah, C. Hollis, S. Bott, M. Kurmoo and P. Day, *J.C.S., Dalton Trans.* (1990) 859.
(b) I.R. Marsden, M.L. Allan, R.H. Friend, M. Kurmoo, D. Kanazawa, P. Day, G. Bravic, D. Chasseau, L. Ducasse and W. Hayes, *Phys. Rev. B.*, 50 (1994) 2118.
- [8] P. Day, M. Kurmoo, T. Mallah, I.R. Marsden, M.L. Allan, R.H. Friend, F.L. Pratt, W. Hayes, D. Chasseau, G. Bravic and L. Ducasse, *J. Am. Chem. Soc.*, 114 (1992) 10722.
- [9] H. Tamaki, Z.J. Zhong, N. Matsumoto, S. Kida, M. Koikawa, N. Achiwa, Y. Hashimoto and H. Okawa, *J. Am. Chem. Soc.*, 114 (1992) 6974.
- [10] (a) S. Descurtins, H.W. Schmalle, H.R. Oswald, A. Linden, J. Ensling, P. Gülich and A. Hanser, *Inorg. Chim. Acta*, 216 (1994), 65.
(b) R.P. Farrell, T.W. Hambley and P. Lay, *Inorg. Chem.*, 34 (1995) 757.
- [11] C. Mathonière, S.G. Carling, Y. Dou and P. Day, *J.C.S. Chem. Commun.* (1994), 1551.
- [12] C. Mathonière, C.J. Nuttall, S.G. Carling and P. Day, *Inorg. Chem.* 35 (1996) 1201.
- [13] M. Kurmoo, D. Talham, P. Day, I.E. Parker, R.H. Friend, A.M. Stringer and J.A.K. Howard, *Sol. St. Commun.*, 61 (1987), 459.
- [14] A.W. Graham, M. Kurmoo and P. Day, *J.C.S. Chem. Commun.* (1995), 2061.
- [15] M. Kurmoo, A.W. Graham, P. Day, S.J. Coles, M. B. Hursthouse, J.M. Caulfield, J. Singleton, L. Ducasse and P. Guionneau, *J. Am. Chem. Soc.*, 117 (1995) 12209.
- [16] M. Kurmoo, K. Pritchard, D. Talham, P. Day, A.M. Stringer and J.A.K. Howard, *Acta. Cryst.*, B46 (1990), 348.
- [17] M. Kurmoo, M.J. Rosseinsky, P. Day, P. Autan, W. Kang, D. Jerome and P. Batail, *Synth. Met.*, 27 (1988) 425.
- [18] M. Kurmoo, P. Day, A.M. Stringer, J.A.K. Howard, L. Ducasse, F.L. Pratt, J. Singleton and W. Hayes, *J. Mater. Chem.*, 3 (1993) 1161.
- [19] H. Mori, S. Tanaka, M. Oshima, G. Saito, T. Mori, Y. Murayama and H. Inokuchi, *Bull. Chem. Soc. Jpn.*, 63 (1990) 2183.
- [20] H. Kobayashi, R. Kato, A. Kobayashi, Y. Nishio, K. Kajita and W. Sasaki, *Chem. Lett.* (1986) 833.
- [21] P. Day, T. Mitani, H. Kitagawa, H. Shinoda, D. Yoshida, P. Guionneau, Y. Barrans, D. Chasseau and L. Ducasse, *Bull. Chem. Soc. Jpn.*, 69 (1996) 1233.
- [22] K. Murata, Y. Honda, H. Anzai, M. Tokumoto, K. Takahashi, N. Kinoshita, T. Ishiguro, N. Toyota, T. Susaki and Y. Muto, *Synth. Met.*, 27 (1988) A341.
- [23] I.R. Marsden, M.L. Allan, R.H. Friend, M. Kurmoo, D. Kanazawa, P. Day, G. Bravic, D. Chasseau, L. Ducasse and W. Hayes, *Phys. Rev. B.*, 50 (1994) 2118.
- [24] C. Bellitto, M. Bonamico, V. Fares, F. Federici, G. Riglini, M. Kurmoo and P. Day, *Chem. of Mater.*, 7 (1995) 1475.
- [25] T. Sugano, G. Saito and M. Kinoshita, *Phys. Rev. B.*, 35 (1987) 6554.
- [26] G.E. Pake, *Paramagnetic Resonance*, W.A. Benjamin, New York, 1962.
- [27] S.J. Blundell, A.A. House, J. Singleton, P.A. Pattenden, M. Kurmoo, F.L. Pratt, W. Hayes, A.W. Graham, P. Day and J.A.A.J. Perenboom, *This proceeding*.



DETERMINING THE CHARGE DISTRIBUTION IN BEDT-TTF SALTS

P. Guionneau ^a, C.J. Kepert ^{b,c}, G. Bravic ^a, D. Chasseau ^a, M.R. Truter ^d, M. Kurmoo ^b, P. Day ^b

^aLaboratoire de Cristallographie, Université Bordeaux I, 351 cours de la Libération, 33405 Talence Cedex, France

^bThe Royal Institution of Great Britain, 21 Albemarle Street, London W1X 4BS, U.K.

^cInorganic Chemistry Laboratory, South Parks Road, Oxford, OX1 3QR, U.K.

^dChristopher Ingold Laboratories, University College London, 20 Gordon Street, London W1CH 0AS, U.K.

Abstract

The intramolecular bond lengths of the donor BEDT-TTF (bis(ethylenedithio)tetrathiafulvalene, also ET) are sensitive to the charge carried by the molecule. By considering a large number of ET salts, we have developed a method for determining experimentally the charges of the ET molecules. The standard deviation in charge is only 0.1 for high quality structures.

Keywords: Organic conductors, Crystal structures

1-Introduction

One of the more interesting characteristics of ET salts is that they form with a wide range of stoichiometries and symmetries, and thus have a variety of asymmetric units [1]. In salts where there is more than one crystallographically-independent ET molecule, energy differences between the ET HOMO's may have important consequences to the discrete intermolecular interactions and band structure. An evaluation of the degree of ionicity is therefore vital to the understanding of physical properties of such salts.

From the many crystallographic studies performed on ET salts it is well known that the intramolecular ET bond lengths vary systematically with the charge carried. Primarily, the variation of the central C=C bond length has been used to estimate the ET charge, although this has been shown to have limited accuracy due to moderate natural deviations [2]. Here we present a relevant method for charge estimation based on the four most central intramolecular ET bond lengths.

2-The method

The chemically-equivalent central C-S and C=C bond lengths may be averaged to give values a, b, c and d (Fig. 1). Oxidation of the ET molecule lengthens a and d (which are bonding with respect to the ET HOMO) and shortens b and c (antibonding). Systematic variations in the outer region of the molecule are much smaller, and are commonly swamped by disorder.

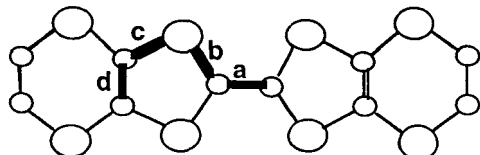


Fig. 1: Labelling of the C-S and C=C averaged central bond lengths in ET salts.

In searching for empirical relationships between the intramolecular geometry and charge, we selected salts with

unambiguous charges on the ET (charges found were 0+, 1/2+, 2/3+, 1+ and 2+). Structures with R-factors greater than 8% or bond length e.s.d.'s greater than 0.010 Å were not considered. The structure of neutral ET was redetermined, since the published structure [3] did not satisfy our quality criteria.

Of many parameters considered, the one found to give the maximum distinction between and the minimum deviation within each charge state is defined as follows:

$$\delta = (b+c) - (a+d)$$

The parameter δ was subsequently tested on salts containing inequivalent ET molecules by summing the calculated charges and comparing with the stoichiometric values.

3-Results

The structure of neutral ET has been accurately redetermined ($R=4\%$ with $(\sigma)<0.004$ Å) [4] and leads to different bond lengths from those determined by Kobayashi *et al.*. Notably, the difference between the central C=C distances exceeds the estimated errors.

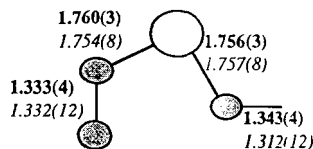


Fig. 2: Averaged intramolecular bond lengths (Å) of neutral ET; our results are in bold, those of Kobayashi [3] are in italics.

The calculation of δ for salts with one independent ET molecule gives distinct values for each charge state (Table 1). By considering the spread in these values for the 1/2+ and 1+ charge states we obtain a standard deviation on δ of 0.012.

1974

P. Guionneau et al. / Synthetic Metals 86 (1997) 1973-1974

Charge	0	1/2+	2/3+	1+	2+
δ (Å)	0.842	0.797	0.763	0.715	0.581
dispersion		0.012		0.012	
X: Number of Salts used	1	18	1	9	1

Table 1: Averaged value of δ for number of charges calculated from the bond lengths of X salts; the dispersion of the results is given.

The variation of δ with the charge carried, Q, appears nearly linear, the equation of variation being:

$$Q = 6.347 - 7.463\delta$$

A similar calculation performed on other molecular donors (TTF, TMTSF) does not give the same relation [4,5].

The relation was tested on a large number of ET salts, a selection of which are presented in Table 2. Figure 3 is a plot of the values of the summed calculated charge versus the charge defined by the stoichiometry. The standard deviation in charge is approximately 0.1 per ET cation, in agreement with that expected from the natural deviations in δ .

Salt	Ref.	Qcalc	ΣQ_{calc}	Charge
ET ₂ Gal ₄	[6]	A: 0.50 B: 0.50	1.00	1
β -ET ₄ Pt(CN) ₄	[7]	A: 0.62 B: 0.33	0.95	1
ET ₄ Mo ₆ Cl ₈ Br ₆ .2THF	[2]	A: 0.08 B: 0.82	0.90	1
α -ET ₂ Ag(CN) ₂	[8]	A: 0.51 B: 0.40	0.91	1
ET ₄ Cu(C ₂ O ₄) ₂	[9]	A: 0.53 B: 0.50	1.03	1
ET ₂ FeCl ₄	[10]	A: 0.56 B: 0.43	0.99	1
κ -ET ₂ Ag(CN) ₂ .H ₂ O	[11]	A: 0.53 B: 0.53	1.06	1
ET ₄ PtCl ₆ .C ₆ H ₅ CN	[12]	A: 0.00 B: 0.98 C: 0.07 D: 0.87	1.92	2
α -ET ₄ Pt(CN) ₄	[7]	2A: 0.54 B: 0.66 C: 0.33	2.07	2
ET ₃ CuCl ₄ .H ₂ O	[13]	A: 0.70 B: 0.54 C: 0.78	2.02	2
ET ₂ TiHg(SeCN) ₄	[14]	2A: 0.89 B: 0.22 C: 0.08	2.08	2
ET ₃ (MnCl ₄) ₂	[15]	2A: 0.90 B: 1.87	3.67	4

Table 2: Example of calculation; values of the charge for each independent entity (Qcalc), the calculated sum (ΣQ_{calc}) and the real charge (Charge).

4-Examples of applications

Table 2 shows that in many salts there is a high degree of ionicity within the ET layer. The method of charge estimation developed here directly provides the independent molecular contributions to the conduction and valence bands. We have

studied the temperature-dependence of the degree of ionicity within 5 salts: in ET₃Cl₂.3H₂O [16], ET₄Cl₂.6H₂O [4,16], α -ET₂AuBr₂ and α -ET₂Ag(CN)₂ [17] the degree of ionicity increases with cooling through metal-insulator transitions, whereas in ET₃CuBr₄ the charge surprisingly becomes delocalised with cooling through an electronic transition at 60 K [4,18].

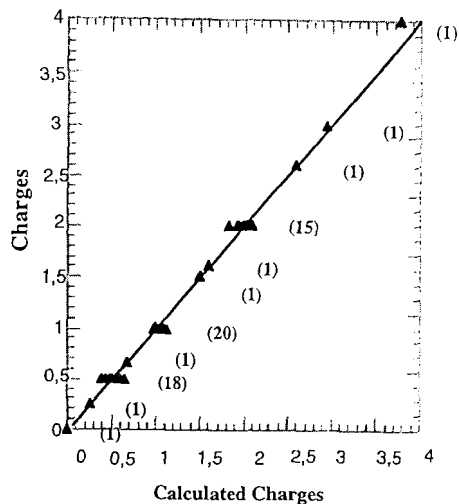


Fig. 3: Values of the calculated charges versus the stoichiometric charge. The number of salts tested is reported.

5-Conclusions

We present here a reliable method for evaluating experimentally the charge carried by the ET cation. The estimated accuracy of this technique is 0.1 for high quality structures.

References

- [1] J.M. Williams et al., *Organic Superconductors*, ed. Prentice hall: Englewood Cliffs (1992).
- [2] C.J. Kepert, PhD, *University of London, U.K.* (1996).
- [3] H. Kobayashi et al., *Chem. Lett.*, (1984) 183.
- [4] P. Guionneau, PhD. *Université Bordeaux I, France* (1996).
- [5] S. Flandrois et al., *Acta Cryst.*, **B33** (1977) 2744.
- [6] U. Geiser et al., *Acta Cryst.*, **C44** (1988) 1544.
- [7] M. Fettohui et al., *Acta Cryst.*, **B49** (1993) 685.
- [8] M. Kurmoo et al., *J. Mater. Chem.*, **3** (1993) 1161.
- [9] X. Bu et al., *Acta Cryst.*, **47** (1991) 279.
- [10] T. Mallah et al., *J. Chem. Soc. Dalton.*, (1990) 859.
- [11] M. Kurmoo et al., *Acta Cryst.*, **B46** (1990) 348.
- [12] V.E. Korotkov et al., **37** (1992) 1437.
- [13] P. Day et al., *J. Am. Chem. Soc.*, **114** (1992) 10722.
- [14] R.P. Shibaeva et al., *Kristolografya*, **39**(1) (1994) 825.
- [15] T. Mori et al., *Bull. Chem. Soc. Jpn.*, **61** (1988) 591.
- [16] S. Hébrard et al. to be published in *Acta Cryst B*.
- [17] P. Guionneau et al., *J. Mater. Chem.*, **5**(10) (1995) 1639.
- [18] P. Guionneau et al., *J. Phys. France I*, in the press (1996).

Acknowledgements: This work was supported by The European Union (HCM network).

Crystal Structures and Physical Properties of Bis(ethylenedithio)-tetrathiafulvalene Charge-transfer Salts with FeX_4^- ($X = \text{Cl}$ or Br) Anions†

Talal Mallah, Claire Hollis, Simon Bott, Mohamedally Kurmoo, and Peter Day*
Inorganic Chemistry Laboratory, Oxford University, South Parks Road, Oxford OX1 3QR
 Margaret Allan and Richard H. Friend
Cavendish Laboratory, Madingley Road, Cambridge CB3 0HE

Two new charge-transfer salts $[\text{bettf}]_2[\text{FeCl}_4]$ (1) and $[\text{bettf}][\text{FeBr}_4]$ (2) have been prepared and crystallised electrochemically [bettf = bis(ethylenedithio)tetrathiafulvalene]. The crystal structures of both salts have been refined in the $P\bar{1}$ space group, the unit-cell parameters being: (1), $a = 6.626(2)$, $b = 15.025(2)$, $c = 17.805(2)$, $\alpha = 82.80(2)$, $\beta = 89.53(2)$, $\gamma = 88.15(2)$, $Z = 2$, $R = 0.044$; (2), $a = 8.634(2)$, $b = 10.980(2)$, $c = 11.773(2)$, Å , $\alpha = 91.91(2)$, $\beta = 102.84(2)$, $\gamma = 93.73(2)$, $Z = 2$, $R = 0.054$. The structure of (1) consists of stacks of dimerised bettf molecules with short $\text{S} \cdots \text{S}$ contacts, forming layers separated by sheets of FeCl_4^- . In (2) there are no stacks of bettf molecules: the structure consists of discrete dimers separated by FeBr_4^- . Compound (1) shows semi-conducting behaviour from 160 to 300 K with $\varepsilon_a = 0.21$ eV and $\sigma \approx 10^{-2}$ S cm^{-1} at 300 K while (2) is a quasi-insulator at room temperature with $\sigma \approx 10^{-6}$ S cm^{-1} . The magnetic susceptibility of both salts from 5 to 300 K is dominated by the $S = \frac{5}{2}$ Fe^{3+} with small Weiss constants [$-6(1)$ for (1) and $-5(1)$ K for (2)].

The last few years have seen the synthesis of numerous charge-transfer salts of the S-heterocyclic molecule bis(ethylenedithio)tetrathiafulvalene (bettf), following the discovery of superconductivity, first under pressure in $[\text{bettf}]_2[\text{ReO}_4]$ (T_c 2 K, $P \approx 4.5$ kbar)¹ and later at ambient pressure in β - $[\text{bettf}]_2[\text{I}_3]$ (T_c 1.4 K).² These efforts culminated recently in the preparation of κ - $[\text{bettf}]_2[\text{Cu}(\text{NCS})_2]$ with the highest superconducting critical temperatures yet found in a molecular solid (10.4 K).³ One aspect of the potential flexibility of structures in this class of compound that has not received much attention so far⁴ is the incorporation of anions carrying a magnetic moment, although the interplay of magnetism and superconductivity is a recurring theme in the theory of classical superconductors. For this reason, as part of our extended programme on the relationship between structure and physical properties in bettf salts, we have synthesised compounds containing transition elements within the anions. In this paper we report the preparation, crystal structures, conductivity, and magnetic susceptibility of bettf salts of FeX_4^- ($X = \text{Cl}$ or Br). Comparisons can be made between these compounds and those containing non-magnetic anions such as Ga_4^{5-} and InBr_4^- .⁶

Experimental

Synthesis and Crystal Growth.—The compound bettf was prepared by the literature method.⁷ Tetraethylammonium salts of the anions FeX_4^- ($X = \text{Cl}$ or Br) were prepared by treating the metal halide with ammonium halides in ethanolic solution. The resulting precipitates were recrystallised from hot ethanol. All products had satisfactory elemental analyses. Electrocrystallisation was carried out in a three-compartment H-shaped cell consisting of an anode separated from the cathode cell by two porous frits, which minimise the influence of unwanted side reactions of reduced species generated at the cathode. All solvents used [CH_2Cl_2 , CH_3CN , and tetrahydrofuran (thf); h.p. l.c. Grade] were dried by passing through an alumina column prior to use. The use of CH_2Cl_2 alone as a solvent in the electrocrystallisation of the FeCl_4^- salt led to the formation of two crystal phases while a CH_2Cl_2 — CH_3CN (2:1) solvent

mixture resulted in only one phase. A single phase was obtained in the electrocrystallisation of the FeBr_4^- salt in neat CH_2Cl_2 . The concentration of tetrahalogenoferrate(III) was 1–2 mmol dm^{-3} in both cases. The platinum electrodes were soaked in *aqua regia*, rinsed in deionised water, then acetone, and dried at 120 °C. The cells were cleaned by the same sequence of solvents.

Crystal growth was carried out under galvanostatic conditions. Current levels greater than 10 μA resulted in very rapid crystal growth and produced microcrystals or powder, whereas for low current levels ($< 1 \mu\text{A}$), side reactions and diffusion from the electrode competed with nucleation at the electrode and led to poor-quality crystals and low yields. The optimum current was determined by initially setting it to a low value and then increasing it by 1 μA every 24 h until crystal growth began at the anode, after which a constant current was maintained until all the bettf had been used. The crystals of $[\text{bettf}]_2[\text{FeCl}_4]$ (1) were long, thin, black needles and those of $[\text{bettf}][\text{FeBr}_4]$ (2) were black and rod-shaped. Both had a metallic lustre.

Determination of the Crystal Structures.—Data were collected on crystals whose quality had been checked by Laue photographs using an Enraf-Nonius CAD4 automatic diffractometer. Rotation photographs confirmed that the crystals were suitable for data collection. The crystals were indexed and orientation matrices calculated using 24 reflections from a search routine. Reflections were collected by ω —2 θ scans over a 2 θ range 0–52° for (1) and 0–52° for (2) (scan widths 1.0 + 0.35 $\tan\theta$ and 0.9 + 0.5 $\tan\theta$ respectively) using graphite-monochromated Mo-K_α radiation, of which 2 744 were considered unique and observed [$F \geq 3\sigma(F)$], $R(\text{merge}) = 0.047$, for (1) and 2 168 [$R(\text{merge}) = 0.039$] for (2). These were corrected for Lorentz and polarisation effects and an

* Present address: Institut Laue-Langevin, 156X, 38042 Grenoble, France.

† Tetrathiafulvalene = 2-(1',3'-dithiol-2'-ylidene)-1,3-dithirole.

Non-S.I. units employed: bar = 10^5 Pa, eV $\approx 1.6 \times 10^{-19}$ J.

Supplementary data available: see Instructions for Authors, *J. Chem. Soc., Dalton Trans.*, 1990, Issue 1, pp. xix—xxii.

Table 1. Positional parameters for [bettf]₂[FeCl₄] (fractional co-ordinates × 10⁴)

Atom	X/a	Y/b	Z/c	Atom	X/a	Y/b	Z/c
Fe	234(2)	2 487(1)	5 017.6(8)	C(1)	5 850(19)	7 761(12)	2 764(7)
Cl(1)	-1 678(5)	1 888(3)	5 929(2)	C(2)	7 742(18)	7 854(13)	2 567(7)
Cl(2)	2 290(5)	1 466(2)	4 650(2)	C(3)	6 652(13)	8 271(6)	1 102(5)
Cl(3)	-1 662(5)	3 070(3)	4 081(2)	C(4)	4 713(12)	8 336(6)	1 307(5)
Cl(4)	2 061(6)	3 519(2)	5 415(2)	C(5)	4 769(13)	8 891(6)	-115(5)
S(1)	3 677(4)	8 103(2)	2 218(1)	C(6)	4 225(13)	9 150(6)	-849(5)
S(2)	8 750(4)	7 909(2)	1 655(2)	C(7)	4 283(13)	9 551(6)	-2 297(5)
S(3)	7 237(4)	8 639(2)	155(1)	C(8)	2 323(14)	9 546(6)	-2 105(5)
S(4)	2 985(4)	8 745(2)	609(1)	C(9)	1 241(19)	9 775(12)	-3 596(7)
S(5)	6 019(3)	9 314(2)	-1 565(1)	C(10)	3 174(19)	9 438(12)	-3 741(7)
S(6)	1 746(4)	9 313(2)	-1 144(1)	C(11)	6 300(18)	4 643(11)	6 159(6)
S(7)	231(4)	9 762(2)	-2 690(2)	C(12)	8 335(18)	4 832(10)	6 369(7)
S(8)	5 278(4)	9 707(2)	-3 210(1)	C(13)	7 168(14)	4 347(7)	7 824(5)
S(9)	4 238(4)	4 962(2)	6 767(2)	C(14)	5 258(14)	4 595(6)	7 662(5)
S(10)	9 238(5)	4 284(3)	7 225(2)	C(15)	5 268(13)	4 123(6)	9 095(5)
S(11)	7 713(4)	4 004(2)	8 780(1)	C(16)	4 716(13)	3 893(6)	9 832(5)
S(12)	3 520(4)	4 538(2)	8 404(1)	C(17)	4 723(14)	3 163(6)	11 257(5)
S(13)	6 469(4)	3 485(2)	10 518(1)	C(18)	2 797(14)	3 531(7)	11 094(5)
S(14)	2 233(4)	3 959(2)	10 151(1)	C(19)	1 641(18)	2 680(9)	12 439(7)
S(15)	709(4)	3 472(3)	11 697(2)	C(20)	3 607(17)	2 880(9)	12 755(6)
S(16)	5 769(4)	2 890(2)	12 133(1)				

empirical absorption correction was applied [minimum and maximum corrections: 1.00 and 1.15 for (1) and 1.2 and 1.4 for (2)]. The space group was *P* $\bar{1}$ in each case, which, combined with the values of the density, molecular weight, and unit-cell volumes, indicated two formula units per unit cell in each compound.

Crystal data. C₂₀H₁₆Cl₄FeS₁₆, (1), *M*_r = 967, triclinic, space group *P* $\bar{1}$, *a* = 6.626(2), *b* = 15.025(2) Å, *c* = 17.805(2) Å, α = 82.80(2), β = 89.53(2), γ = 88.15(2)°, *U* = 1 757.5 Å³, *Z* = 2, *D*_c = 1.834 g cm⁻³, Mo-*K* α radiation (λ = 0.710 69 Å), 4 530 independent reflections, *R* = 0.044.

C₁₀H₈Br₄FeS₈, (2), *M*_r = 760, triclinic, space group *P* $\bar{1}$, *a* = 8.634(2), *b* = 10.980(2), *c* = 11.773(2) Å, α = 91.91(2), β = 102.84(2), γ = 93.73(2)°, *U* = 1 084.5 Å³, *Z* = 2, *D*_c = 2.33 g cm⁻³, Mo-*K* α radiation (λ = 0.710 69 Å), 5 986 independent reflections, *R* = 0.054.

The structures were solved by routine direct and Fourier methods using the SHELXS program.⁸ It was possible to assign the Fe, Cl, and S in compound (1) but only 18 C. The remaining two carbon atoms were found from a difference map. Full-matrix least-squares refinement of the non-hydrogen atoms converged at *R* 0.130. Inclusion of anisotropic thermal parameters for Fe, Cl, and S resulted in an *R* value of 0.060. Further inclusion of anisotropic thermal parameters for the carbons gave *R* 0.048. The hydrogen atoms were generated geometrically but not refined. Following further refinements the model converged at *R* = 0.044, *R'* = 0.050.

In the case of compound (2) it was immediately possible to assign all non-hydrogen atoms which were refined by the full-matrix least-squares method. Initially only the positional and isotropic thermal parameters of the Fe, Br, and S atoms were refined, while later refinements included the parameters relating to the C atoms, to give *R* 0.140. After including anisotropic thermal parameters for all atoms, a difference map readily revealed the positions of some of the hydrogen atoms and the rest were generated geometrically. The latter were included in the list but not refined. Following further refinements and the application of the Chebyshev weighting scheme⁹ the model converged at *R* = 0.054, *R'* = 0.062.

Additional material available from the Cambridge Crystallographic Data Centre comprises thermal parameters.

Electrical Conductivity.—Conductivities of single crystals

were measured from 160 to 300 K by the two-probe d.c. method using silver paint as electrical contact.

Magnetic Susceptibility.—The temperature dependence of the magnetic susceptibility of samples consisting of randomly oriented microcrystals was measured by the Faraday method from 5 to 300 K. In each case the samples came from a single batch, checked for homogeneity by microscopic examination of the crystal morphology. The crystals used for the structure determinations were selected from the same batches. Honda-Owen¹⁰ corrections were made for small fractions of ferromagnetic impurities [fitted as 270 p.p.m. of iron for (1) and 25 p.p.m. for (2)]. Diamagnetic corrections of 301 × 10⁻⁶ for (1) and 341 × 10⁻⁶ e.m.u. mol⁻¹ for (2) were also applied to the data (e.m.u. = S.I. × 10⁶/4 π).

Results

Crystal Structures.—[bettf]₂[FeCl₄] (1). Positional parameters of the final solution of the structure of compound (1) are shown in Table 1, bond lengths and angles in Table 2, and intermolecular distances less than 4.0 Å in Table 3. The asymmetric unit contains two independent bettf molecules, labelled X and Y, and one FeCl₄⁻ anion.

The structure of [bettf]₂[FeCl₄] consists of dimerised stacks of bettf molecules separated by sheets of tetrahedral FeCl₄⁻ anions (Figure 1). The anions are situated in an 'anion cavity' formed by the ethylene groups of the bettf molecules. Within the stacks, the bettf molecules are normal to the *b*-direction and are parallel with respect to each other (Figure 2). The intrastack packing-mode alternates between the *a* and *c* modes, as defined by Williams.¹¹ The molecules are arranged in the sequence ... X Y Y X X Y Y X ... (Figure 1). Adjacent molecules of the same type (XX' and YY') have a mode of intrastack packing [Figure 3(a)], i.e. the molecules stack uniformly on top of each other but with a slight displacement between neighbours along the long in-plane molecular axis. On the other hand, adjacent molecules of different type (XY' and YX') have the *c* mode of stacking [Figure 3(b)] in which the long in-plane molecular axes along a column are rotated relative to one another. This arrangement of the bettf molecules also leads to a slight dimerisation within the stacks; the related bettf molecules X and

Table 2. Bond lengths (Å) and angles (°) for [bettf]₂[FeCl₄]

Cation 1				Cation 2			
S(1)–C(1)	1.77(1)	S(1)–C(4)	1.755(9)	S(9)–C(11)	1.83(1)	S(9)–C(14)	1.753(9)
S(2)–C(2)	1.74(1)	S(2)–C(3)	1.743(9)	S(10)–C(12)	1.74(1)	S(10)–C(13)	1.738(9)
S(3)–C(3)	1.751(9)	S(3)–C(5)	1.725(9)	S(11)–C(13)	1.751(9)	S(11)–C(15)	1.721(9)
S(4)–C(4)	1.739(9)	S(4)–C(5)	1.740(9)	S(12)–C(14)	1.741(9)	S(12)–C(15)	1.741(9)
S(5)–C(6)	1.735(8)	S(5)–C(7)	1.741(9)	S(13)–C(16)	1.734(9)	S(13)–C(17)	1.745(9)
S(6)–C(6)	1.729(9)	S(6)–C(8)	1.745(9)	S(14)–C(16)	1.740(9)	S(14)–C(18)	1.76(1)
S(7)–C(8)	1.738(9)	S(7)–C(9)	1.74(1)	S(15)–C(18)	1.74(1)	S(15)–C(19)	1.76(1)
S(8)–C(7)	1.741(9)	S(8)–C(10)	1.78(1)	S(16)–C(17)	1.75(1)	S(16)–C(20)	1.80(1)
C(1)–C(2)	1.31(2)	C(3)–C(4)	1.34(1)	C(11)–C(12)	1.45(2)	C(13)–C(14)	1.33(1)
C(5)–C(6)	1.36(1)	C(7)–C(8)	1.34(1)	C(15)–C(16)	1.36(1)	C(17)–C(18)	1.33(1)
C(10)–C(9)	1.40(2)			C(19)–C(20)	1.48(2)		
C(4)–S(1)–C(1)	101.7(5)	C(3)–S(2)–C(2)	101.7(5)	C(14)–S(9)–C(11)	100.5(5)	C(13)–S(10)–C(12)	102.7(5)
C(5)–S(3)–C(3)	95.1(4)	C(5)–S(4)–C(4)	95.0(4)	C(15)–S(11)–C(13)	95.5(4)	C(17)–S(13)–C(16)	95.6(4)
C(7)–S(5)–C(6)	95.5(4)	C(8)–S(6)–C(6)	95.4(4)	C(18)–S(14)–C(16)	95.0(4)	C(19)–S(15)–C(18)	100.0(5)
C(9)–S(7)–C(8)	103.5(5)	C(10)–S(8)–C(7)	100.7(5)	C(20)–S(16)–C(17)	102.3(5)	C(12)–C(11)–S(9)	117.5(9)
C(2)–C(1)–S(1)	128.0(10)	C(1)–C(2)–S(2)	127.0(10)	C(11)–C(12)–S(10)	117.1(9)	S(11)–C(13)–S(10)	113.8(5)
S(3)–C(3)–S(2)	113.9(5)	C(4)–C(3)–S(2)	129.2(7)	C(14)–C(13)–S(10)	129.8(7)	C(14)–C(13)–S(11)	116.4(7)
C(4)–C(3)–S(3)	116.9(7)	S(4)–C(4)–S(1)	114.7(5)	S(12)–C(14)–S(9)	114.7(5)	C(13)–C(14)–S(9)	127.3(7)
C(3)–C(4)–S(1)	127.8(7)	S(4)–C(5)–S(3)	115.4(5)	S(2)–C(15)–S(11)	115.4(5)	C(16)–C(15)–S(11)	122.7(7)
C(6)–C(5)–S(3)	122.8(7)	C(6)–C(5)–S(4)	121.7(7)	C(16)–C(15)–S(12)	121.9(7)	S(14)–C(16)–S(13)	115.1(5)
S(6)–C(6)–S(5)	115.1(5)	C(5)–C(6)–S(5)	121.4(7)	C(15)–C(16)–S(14)	123.3(7)	S(16)–C(17)–S(13)	114.5(5)
C(5)–C(6)–S(6)	123.5(7)	S(8)–C(7)–S(5)	116.3(5)	C(18)–C(17)–S(13)	117.3(7)	C(18)–C(17)–S(16)	128.2(7)
C(8)–C(7)–S(5)	117.0(7)	C(8)–C(7)–S(8)	126.6(7)	S(15)–C(18)–S(14)	114.0(6)	C(17)–C(18)–S(14)	117.1(7)
S(7)–C(8)–S(6)	114.5(5)	C(7)–C(8)–S(6)	117.0(7)	C(20)–C(19)–S(15)	115.7(9)	C(19)–C(20)–S(16)	117.2(8)
C(7)–C(8)–S(7)	128.5(7)	C(9)–C(10)–S(8)	120.6(11)				
C(10)–C(9)–S(7)	123.5(10)						
Anion							
Fe–Cl(1)	2.174(3)	Fe–Cl(2)	2.177(3)	Cl(2)–Fe–Cl(1)	109.7(1)	Cl(3)–Fe–Cl(1)	109.0(1)
Fe–Cl(3)	2.174(3)	Fe–Cl(4)	2.186(4)	Cl(3)–Fe–Cl(2)	110.1(2)	Cl(4)–Fe–Cl(2)	110.1(2)
				Cl(4)–Fe–Cl(1)	107.7(2)	Cl(4)–Fe–Cl(2)	110.2(2)

X' (or Y and Y') are closer to each other (≈ 3.60 Å) than the two independent ones X and Y (3.81 Å).

The shortest distances between bettf molecules in compound (1) are observed between the stacks in the *a*-direction [e.g. S(1)⋯S(2) 3.455, S(6)⋯S(8) 3.423; S(5)⋯S(7) 3.457, S(15)⋯S(16) 3.472, and S(13)⋯S(15) 3.519 Å]. These distances are shorter than the sum of the van der Waals radii of two sulphur atoms ($d = 3.60$ Å), thus suggesting the possibility of a quasi-one-dimensional interaction along the *a* direction.

[bettf][FeBr₄] (2). Final positional parameters for compound (2) are shown in Table 4, bond lengths and angles in Table 5, and intermolecular distances less than 4.0 Å in Table 6. The asymmetric unit contains one bettf molecule and one FeBr₄⁻ anion (Figure 4). Compound (2) is the third 1:1 bettf charge-transfer salt observed to date, the others being [bettf][ReO₄]-0.5 thf and [bettf][IO₄]-0.5 thf.

The main feature of the structure of [bettf][FeBr₄] is the absence of stacks and planes of closely spaced bettf, in marked contrast to most bettf compounds. Intradimer overlap is of the *a* type, but there are no S⋯S distances within each dimer shorter than the combined van der Waals radii of two sulphur atoms (3.60 Å), the shortest being 3.72 Å, which indicates the absence of any intradimer interaction. The only short S⋯S distances (<3.50 Å) are between two bettf molecules in different pairs, as shown in Figures 2 and 3, but there is no continuous network of short S⋯S contacts through the lattice.

The FeBr₄⁻ anions form a three-dimensional lattice separated by pairs of bettf molecules (Figure 5). One FeBr₄⁻ ion has short intermolecular distances to two bettf molecules but this is isolated from any other short interactions so that no long-range interaction between bettf molecules through the FeBr₄⁻ anions is possible, which correlates with the insulating behaviour of this compound.

Electrical Conductivity.—From 160 to 300 K the conductivity of compound (1) follows a simple semiconducting activation law, with an activation energy $\epsilon_a = 0.21$ eV and a specific conductivity of 10^{-2} S cm⁻¹ at 300 K. There was no evidence for any discontinuities in the conductivity or changes of activation energy over this temperature range, such as have been found in some other semiconducting bettf salts like α -[bettf]₂[AuBr₂]¹³ and [bettf]₂[CF₃SO₃]¹⁴. Below 160 K the resistance of the crystals became too high to measure. Compound (2) has a much lower conductivity than (1) (10^{-6} S cm⁻¹ at 300 K) so that its temperature dependence could not be measured to determine an activation energy.

Magnetic Susceptibility.—After applying the corrections for diamagnetism and ferromagnetic impurities, the excess molar susceptibilities of the two compounds were fitted to the Curie-Weiss law $\chi = \chi_0 + C/(T - \theta)$. Excellent fits were obtained over the whole temperature range from 5 to 300 K. The values of the parameters were as follows: (1), C 4.7(3), χ_0 0(5) $\times 10^{-4}$ e.m.u. mol⁻¹, $\theta = -6(1)$ K; (2), C 4.4(1), χ_0 0(8) $\times 10^{-4}$ e.m.u. mol⁻¹, $\theta = -5(1)$ K. From the values of C one can estimate the magnetic moment per molecule as 6.1(1) μ_B for (1) and 5.9(1) μ_B for (2). These moments are close to that expected for an $S = \frac{3}{2}$ ion with an orbital singlet ground state (5.92 μ_B) as required for high-spin $3d^5$ Fe³⁺, and show that the magnetic properties are dominated by the anions. In particular, the quality of the fits of the susceptibility to a simple Curie-Weiss temperature dependence from 5 to 300 K suggests that there is no detectable contribution from interacting moments on the cations.

Discussion

Structurally and electronically, the most striking feature of the

862

J. CHEM. SOC. DALTON TRANS. 1990

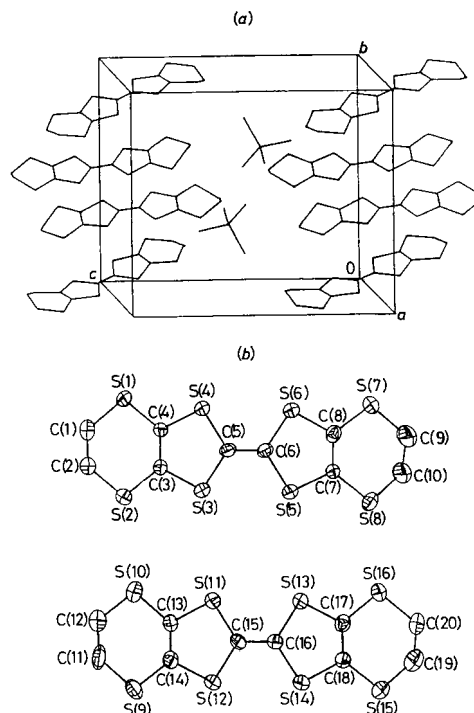
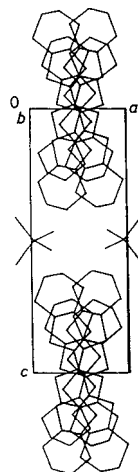
Table 3. Intermolecular S...S distances in $[\text{bettf}]_2[\text{FeCl}_4]$ less than 4 Å

Cation 1-cation 1			
$x - 1, y, z$			
S(1)...S(2)	3.455	S(6)...S(8)	3.423
$1 - x, 2 - y, -z$			
S(1)...S(5)	3.920		
S(3)...S(4)	3.992	S(3)...S(6)	3.813
$1 + x, y, z$			
S(2)...S(4)	3.533	S(3)...S(4)	3.912
S(3)...S(6)	3.846	S(5)...S(6)	3.874
S(5)...S(7)	3.457		
Cation-cation 2			
$1 - x, 1 - y, 1 - z$			
S(1)...S(11)	3.957	S(5)...S(16)	3.809
$2 - x, 1 - y, 1 - z$			
S(2)...S(10)	3.837	S(2)...S(11)	3.800
Cation 2-cation 2			
$x - 1, y, z$			
S(9)...S(10)	3.556	S(15)...S(16)	3.472
$1 - x, 1 - y, 2 - z$			
S(9)...S(16)	3.979	S(11)...S(15)	3.953
S(11)...S(14)	3.803	S(12)...S(13)	3.734
S(12)...S(16)	3.906	S(13)...S(14)	3.995
$1 + x, y, z$			
S(11)...S(12)	3.990	S(11)...S(14)	3.873
S(13)...S(15)	3.519		
Anion-cation 1			
$-x, 1 - y, 1 - z$		$1 - x, 1 - y, -z$	
Cl(1)...S(1)	3.546	Cl(2)...S(8)	3.627
$x, y - 1, 1 - z$			
Cl(1)...S(7)	3.958		
Anion-cation 2			
$x - 1, y, z - 1$			
Cl(3)...S(16)	3.919		
$x - 1, y, z$		$-x, 1 - y, 1 - z$	
Cl(4)...S(10)	3.987	Cl(3)...S(9)	3.540

Table 4. Positional parameters for $[\text{bettf}][\text{FeBr}_4]$ (fractional coordinates $\times 10^4$)

Atom	X/a	Y/b	Z/c
Fe	4 307(3)	1 967(2)	7 247(2)
Br(1)	4 014(2)	1 829(2)	9 160(1)
Br(2)	6 250(2)	700(1)	6 958(2)
Br(3)	1 903(2)	1 345(2)	5 966(1)
Br(4)	5 098(3)	3 959(1)	6 887(2)
S(1)	-1 555(4)	1 063(3)	536(3)
S(2)	1 683(4)	2 323(3)	2 729(3)
S(3)	-474(4)	2 957(3)	-877(3)
S(4)	2 218(4)	3 967(3)	932(3)
S(5)	3 196(4)	5 849(3)	-896(3)
S(6)	491(5)	4 808(3)	-2 675(3)
S(7)	4 268(5)	7 661(3)	-2 416(3)
S(8)	1 014(16)	6 399(3)	-4 518(3)
C(1)	-351(18)	316(11)	1 722(12)
C(2)	200(16)	1 112(12)	2 826(11)
C(3)	1 104(16)	2 737(11)	1 319(10)
C(4)	-159(15)	2 281(10)	456(10)
C(5)	1 096(15)	4 033(10)	-463(10)
C(6)	1 544(15)	4 816(10)	-1 248(10)
C(7)	2 910(16)	6 479(9)	-2 239(10)
C(8)	1 622(15)	5 995(10)	-3 097(10)
C(9)	4 105(21)	7 468(14)	-3 972(13)
C(10)	2 521(25)	7 509(16)	-4 700(15)

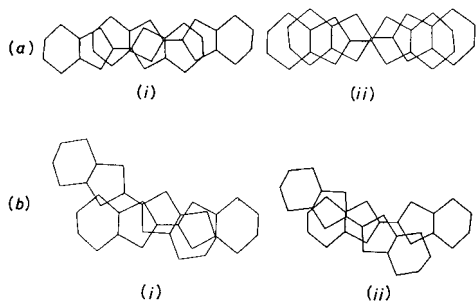
two FeX_4^- salts of bettf is that they have different chemical stoichiometries, and hence band fillings. The structure of (1) is closely related to those of $[\text{bettf}]_2[\text{InBr}_4]$,⁶ α - $[\text{bettf}]_2[\text{PF}_6]$,¹⁵

**Figure 1.** (a) The XXYYXX stacking sequence of bettf molecules in $[\text{bettf}]_2[\text{FeCl}_4]$. (b) Atom numbering of the independent bettf**Figure 2.** A projection of the unit cell of $[\text{bettf}]_2[\text{FeCl}_4]$ along the *b* axis

β - $[\text{bettf}]_2[\text{PF}_6]$,¹⁶ and $[\text{bettf}]_2[\text{AsF}_6]$.¹⁷ In the case of $[\text{bettf}]_2[\text{InBr}_4]$ the intrastack distances ($X \cdots X'$ 3.43, $X \cdots Y$ 3.87, and $Y \cdots Y'$ 3.47 Å) are shorter than those found in $[\text{bettf}]_2[\text{FeCl}_4]$, indicating a greater degree of intrastack dimerisation, whilst the interstack distances are greater

Table 5. Bond lengths (Å) and angles (°) for [bettff]₂[FeBr₄]

Cation		Cation–anion	
S(1)–C(1)	1.802(14)	1–x, y, 1–z	
S(2)–C(2)	1.810(13)	S(1)···S(5)	3.806
S(3)–C(4)	1.733(11)	S(2)···S(8)	3.772
S(4)–C(3)	1.739(13)	S(3)···S(4)	3.783
S(5)–C(6)	1.729(13)	S(4)···S(6)	3.724
S(6)–C(6)	1.723(12)	1–x, 1–y, –z	
S(7)–C(7)	1.741(13)	S(2)···S(7)	3.595
S(8)–C(8)	1.720(12)	S(4)···S(5)	3.961
C(1)–C(2)	1.508(19)	–x, 1–y, –1–z	
C(5)–C(6)	1.383(15)	S(6)···S(8)	3.454
C(9)–C(10)	1.448(24)		
		Cation–anion	
		1+x, y, 1+x	
C(1)–S(1)–C(4)	97.57(63)	Br(1)···S(1)	3.965
C(4)–S(3)–C(5)	98.84(58)	x, y, 1+z	
C(6)–S(5)–C(7)	95.86(62)	Br(1)···S(4)	3.722
C(7)–S(7)–C(9)	99.53(69)	1–x, –y, 1–z	
S(1)–C(1)–C(2)	114.00(85)	Br(2)···S(2)	3.861
S(2)–C(3)–S(4)	115.73(77)	–x, –y, 1–z	
S(4)–C(3)–C(4)	114.57(84)	Br(1)···S(1)	3.776
S(3)–C(5)–S(4)	116.15(62)	1–x, 1–y, 1–z	
S(4)–C(5)–C(6)	121.76(93)	Br(1)···S(5)	3.625
S(5)–C(6)–C(5)	123.37(93)	Br(4)···S(4)	3.664
S(5)–C(7)–S(7)	117.43(78)	1–x, 1–y, –z	
S(7)–C(7)–C(8)	125.25(87)	Br(2)···S(7)	3.820
S(6)–C(8)–C(7)	115.04(85)	x, y, z	
S(7)–C(9)–C(10)	115.93(120)	Br(3)···S(2)	3.961
		–x, 1–y, –z	
		Br(3)···S(8)	3.817
		Cation–anion	
		1+x, y, 1+x	
		Br(1)···S(1)	3.965
		x, y, 1+z	
		Br(1)···S(4)	3.722
		1–x, –y, 1–z	
		Br(2)···S(2)	3.861
		–x, –y, 1–z	
		Br(1)···S(1)	3.776
		1–x, 1–y, 1–z	
		Br(1)···S(5)	3.625
		Br(4)···S(4)	3.664
		1–x, 1–y, –z	
		Br(2)···S(7)	3.820
		x, y, z	
		Br(3)···S(2)	3.961
		–x, 1–y, –z	
		Br(3)···S(8)	3.817

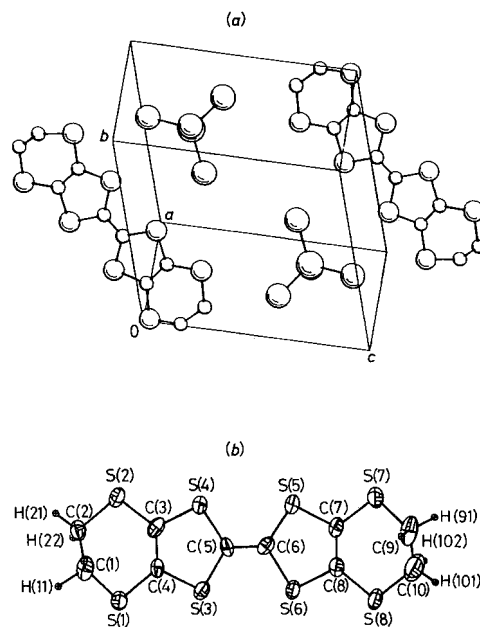
**Figure 3.** Modes of stacking in [bettff]₂[FeCl₄]. (a) Between molecules of the same type: (i) X and X', (ii) Y and Y'. (b) Between molecules of different types: (i) X and Y', (ii) Y and X'

($d > 3.55$ Å). This is probably due to the greater size of the InBr_4^- anion. However, the structure of salts containing octahedral anions, α - and β -[bettff]₂[PF₆] and [bettff]₂[AsF₆], exhibit interstack side-by-side contact distances nearly identical to those found in [bettff]₂[FeCl₄].

As is the case for [bettff]₂[FeCl₄], no short contact distances between sulphur atoms are observed in the PF₆ and AsF₆ compounds along the molecular stacking direction and so their conduction properties are highly one-dimensional. For example, conductivity measurements on β -[bettff]₂[PF₆] have shown that the ratio of the conductivities along the direction of side-by-side contacts to that along the molecular stacking

Table 6. Intermolecular distances (Å) in [bettff]₂[FeBr₄]

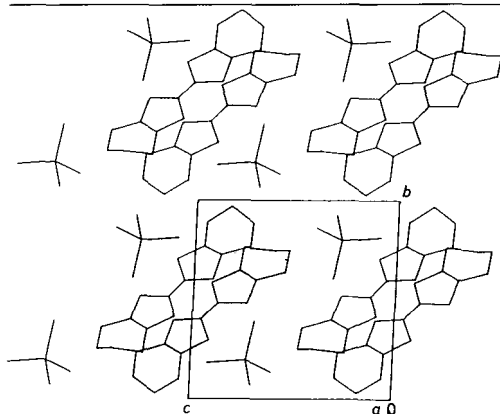
Cation–cation		Cation–anion	
–x, 1–y, –z		1+x, y, 1+x	
S(1)···S(5)	3.806	Br(1)···S(1)	3.965
S(2)···S(8)	3.772	x, y, 1+z	
S(3)···S(4)	3.783	Br(1)···S(4)	3.722
S(4)···S(6)	3.724	1–x, –y, 1–z	
1–x, 1–y, –z		Br(2)···S(2)	3.861
S(2)···S(7)	3.595	–x, –y, 1–z	
S(4)···S(5)	3.961	Br(1)···S(1)	3.776
–x, 1–y, –1–z		1–x, 1–y, 1–z	
S(6)···S(8)	3.454	Br(1)···S(5)	3.625
		Br(4)···S(4)	3.664
		1–x, 1–y, –z	
		Br(2)···S(7)	3.820
		x, y, z	
		Br(3)···S(2)	3.961
		–x, 1–y, –z	
		Br(3)···S(8)	3.817

**Figure 4.** (a) The unit cell of [bettff]₂[FeBr₄]. (b) Atom numbering of bettff

direction is 200:1.^{15,16} Our single-crystal conductivity measurements show that [bettff]₂[FeCl₄] is also semi-conducting, like the PF₆ and AsF₆ salts, with an activation energy of

Table 7. Volume of unit cell (V_{cell}) and anion (V_{anion}) in $[\text{bettf}]_2\text{X}$ salts with tetrahedral anions X

Salt	$V_{\text{cell}}/\text{\AA}^3$	$V_{\text{anion}}/\text{\AA}^3$	Ref.
$[\text{bettf}]_2[\text{ReO}_4]$	1 565	157	18
$[\text{bettf}]_2[\text{BrO}_4]$	1 589	136	18
$[\text{bettf}]_2[\text{FeCl}_4]$	1 758	272	This work
$[\text{bettf}]_2[\text{InBr}_4]$	1 820	370	6
$[\text{bettf}]_2[\text{AsF}_6]$	3 274	111	17

**Figure 5.** Projection of the unit cell of $[\text{bettf}][\text{FeBr}_4]$ along a , showing the presence of dimers

0.21 eV, but because of the needle-like crystal habit we have no information on the anisotropy.

There are several possible origins for the tendency towards a side-by-side packing arrangement of the bettf in these three compounds: (i) as the atoms of the ethylene groups are not on the molecular plane, intermolecular steric repulsions make the more normal face-to-face overlap unstable; (ii) in π -donor molecules with chalcogen atoms, face-to-face overlap may not in fact be necessary for significant intermolecular interaction since a mixing of the p_x and d_x orbitals can be expected. A side-by-side arrangement is not suitable for p_x - p_x interaction but it is not unfavourable for d_x - d_x interaction.

The structure of compound (1) contrasts with the structures of bettf salts with tetrahedral oxyanions such as $[\text{bettf}]_2[\text{ReO}_4]$ and $[\text{bettf}]_2[\text{BrO}_4]$,¹⁸ which have a zigzag arrangement of bettf molecules along the a direction that allows the formation of a 'corrugated sheet' network with intermolecular separations less than 3.60 Å. The two-dimensional nature of the latter structure is reflected in the conductivities of the ReO_4 and BrO_4 salts. Thus, $[\text{bettf}]_2[\text{ReO}_4]$ is metallic at room temperature and is a superconductor at 2 K under a pressure of 5 kbar.¹

The unit cell and anion volumes of some related bettf salts of tetrahedral anions are listed in Table 7. The volumes of the anions were estimated as those of spheres with radii equal to the observed M-X bond length of MX_n^- plus the radius of X. The large volumes of FeCl_4^- and InBr_4^- lead to a bigger unit cell and therefore to a greater intermolecular separation between the bettf.

Molecular orbital calculations¹⁹ have shown that increasing the positive charge on the bettf molecule results in an increase in the distance between the two carbon atoms in the centre of the molecule and a decrease in the C-S bond lengths. Both of the crystallographically independent bettf molecules in $[\text{bettf}]_2[\text{FeCl}_4]$ have a C=C bond length of 1.36 Å, indicating that they

Table 8. Some bond lengths (Å) within the bettf molecules in salts of different stoichiometry (d_1 is the central C=C double bond; d_2 the C-S bond nearest the molecular centre, d_3 the other C-S bond, and d_4 the outer C=C bond)

Compound	Charge	d_1	d_2	d_3	d_4
bettf	0	1.32	1.76	1.75	1.33
β - $[\text{bettf}]_2\text{I}_3$	$+\frac{1}{2}$	1.35	1.74	1.76	1.34
$[\text{bettf}]_2[\text{FeCl}_4]$:					
Cation 1	$+\frac{1}{2}$	1.360	1.732	1.744	1.340
Cation 2	$+\frac{1}{2}$	1.360	1.734	1.749	1.330
γ - $[\text{bettf}]_3[\text{ClO}_4]_2$	$+\frac{2}{3}$	1.37	1.73	1.74	1.34
$[\text{bettf}][\text{ReO}_4] \cdot 0.5 \text{ tff}$	+1	1.38	1.72	1.73	1.37
$[\text{bettf}][\text{FeBr}_4]$	+1	1.38	1.72	1.73	1.38

are essentially identical and that the formal charge on each is $+\frac{1}{2}$. The intramolecular bond lengths of the bettf in some other $[\text{bettf}]_n\text{X}_m$ charge-transfer salts are shown in Table 8, from which the bond lengths of those compounds, in which the molecules carry a formal positive charge of $+\frac{1}{2}$, can be seen to be very similar to the corresponding bond lengths in $[\text{bettf}]_2[\text{FeCl}_4]$.

Given that the formal charge per bettf molecule is $+\frac{1}{2}$, a contribution to the susceptibility from unpaired spins on the cations would be expected. For example, $[\text{bettf}]_2[\text{GaCl}_4]$ has a temperature-dependent excess molar susceptibility with a broad maximum near 90 K of $\chi_{\text{max}} = 1.6 \times 10^{-3}$ e.m.u. mol⁻¹, which can be fitted over the temperature range 70–300 K by either a one-dimensional (Bonner-Fisher) or quadratic layer antiferromagnetic model²⁰ to yield values of the exchange parameter J of respectively 66.5(5) and 89.6(1) K. These values of χ_{max} and J are of similar magnitude to those found for the semiconducting α - $[\text{bettf}]_2\text{X}$ with X = AuBr₂, Ag(CN)₂, or CuCl₂²¹, where the absolute value of the susceptibility was in good agreement with that expected for localised moments corresponding to $S = \frac{1}{2}$ per pair of bettf. Unfortunately, in the FeCl_4^- salt, the susceptibility is dominated by the anion so that, for example, $\chi = 4.76 \times 10^{-2}$ e.m.u. mol⁻¹ at 90 K, about 30 times larger than χ_{max} for the GaCl_4^- salt. Thus the magnetic properties of the cation sublattice are obscured by those of the anions. Nevertheless, it remains of interest that the Weiss constant is small (-6K), indicating only weak antiferromagnetic interaction between the anions.

In $[\text{bettf}][\text{FeBr}_4]$, on the other hand, the bettf molecules are fully oxidised, each having a formal positive charge of +1. Extended-Hückel calculations¹⁹ have characterised the highest occupied molecular orbital of bettf as bonding with respect to the C=C bonds, and antibonding with respect to the C-S bonds. Thus, loss of an electron from this molecular orbital diminishes the bonding character of the C=C bond (which results in a lengthening of the bond) and the antibonding character of the C-S bond (resulting in a shortening of the C-S bonds). That this is indeed the case can be seen in Table 8. It is likely that the absence of stacks of cations in the structure is a result of Coulomb repulsion between the relatively large charges. That, and the stoichiometry, lead to an insulating ground state.

As far as the magnetic properties of $[\text{bettf}][\text{FeBr}_4]$ are concerned, one might anticipate a moment equivalent to $S = \frac{1}{2}$ per bettf molecule in addition to $S = \frac{3}{2}$ per FeBr_4^- . That the susceptibility obeys the Curie-Weiss law from 5 to 300 K with a moment equivalent to 5.9 μ_B per formula unit suggests that, as in the FeCl_4^- salt, the Fe^{3+} dominates the contribution of the bettf. It is worth noting that a similar conclusion was reached in two earlier studies of charge-transfer salts containing high-spin anions, $[\text{tff}][\text{MnCl}_4]_{0.25}$ ²² and $[\text{bettf}]_3[\text{MnCl}_4]_2$.²³ Crystallographic evidence suggests that the latter contains one third its cations in the form of bettf⁺, as in $[\text{bettf}][\text{FeBr}_4]$.

Acknowledgements

We acknowledge the S.E.R.C. for partial support of this work, and thank Dr. D. Watkin for helpful discussions.

References

- 1 S. S. S. Parkin, E. M. Engler, R. R. Schumaker, R. Lagier, V. Y. Lee, J. C. Scott, and R. L. Greene, *Phys. Rev. Lett.*, 1983, **50**, 270.
- 2 E. B. Yagubskii, I. F. Shchegolov, V. N. Laukhin, P. A. Kononovich, M. V. Kartsovnik, A. V. Zvarykina, and L. I. Buravov, *Zh. Eksp. Teor. Fiz., Pis'ma Red.*, 1984, **39**, 12.
- 3 H. Urayama, H. Yamochi, G. Saito, K. Nozawa, T. Sugano, M. Kinoshita, S. Sato, K. Oshima, A. Kawamoto, and J. Tanaka, *Chem. Lett.*, 1988, 55.
- 4 T. Mori and H. Inokuchi, *Synth. Met.*, 1988, **27**, A451; *Bull. Chem. Soc. Jpn.*, 1988, **61**, 591.
- 5 U. Geiser, H. H. Wang, J. A. Schlueter, S. L. Hallenbeck, T. J. Allen, M. Y. Chen, H.-C. Ivy Kao, K. D. Carlson, L. E. Gerdorn, and J. M. Williams, *Acta Crystallogr., Sect. C*, 1988, **44**, 1544.
- 6 M. A. Beno, D. D. Cox, J. M. Williams, and J. F. Kwak, *Acta Crystallogr., Sect. C*, 1984, **40**, 1334.
- 7 H. H. Wang, P. E. Reed, and J. M. Williams, *Synth. Met.*, 1986, **14**, 165; M. Mizuno, A. F. Garito, and M. P. Cava, *J. Chem. Soc., Chem. Commun.*, 1978, 18.
- 8 G. M. Sheldrick, SHELXS 86, User Guide, University of Göttingen, 1986.
- 9 E. Prince, 'Mathematical Techniques in Crystallography,' Springer, New York, 1982.
- 10 K. Honda, *Ann. Phys. (Leipzig)*, 1910, **32**, 1048; M. Owen, *ibid.*, 1912, **37**, 657.
- 11 J. M. Williams, H. H. Wang, T. J. Emge, U. Geiser, M. A. Beno, P. C. W. Leung, K. D. Carlson, R. J. Thorn, A. J. Schultz, and M. Whangbo, *Prog. Inorg. Chem.*, 1987, **35**, 51.
- 12 H. Kobayashi, A. Kobayashi, Y. Sasaki, G. Saito, and H. Inokuchi, *Chem. Lett.*, 1984, 183.
- 13 I. D. Parker, R. H. Friend, M. Kurmoo, and P. Day, *Synth. Met.*, 1988, **27**, 455; *J. Phys. Condensed Matter*, 1989, **1**, 5681.
- 14 D. Chasseau, D. Watkin, M. J. Rosseinsky, M. Kurmoo, D. R. Talham, and P. Day, *Synth. Met.*, 1988, **24**, 117.
- 15 H. Kobayashi, R. Kato, T. Mori, A. Kobayashi, Y. Sasaki, G. Saito, and H. Inokuchi, *Chem. Lett.*, 1983, 759.
- 16 H. Kobayashi, T. Mori, R. Kato, A. Kobayashi, Y. Sasaki, G. Saito, and H. Inokuchi, *Chem. Lett.*, 1983, 581.
- 17 P. C. W. Leung, M. A. Beno, G. S. Blackman, B. R. Coughlin, C. A. Miderski, W. Joss, G. W. Crabtree, and J. M. Williams, *Acta Crystallogr., Sect. C*, 1984, **40**, 1331.
- 18 J. M. Williams, M. A. Beno, H. H. Wang, P. E. Reed, L. J. Azevedo, and J. E. Schirber, *Inorg. Chem.*, 1984, **23**, 1790.
- 19 T. Mori, A. Kobayashi, Y. Sasaki, H. Kobayashi, G. Saito, and H. Inokuchi, *Bull. Chem. Soc. Jpn.*, 1984, **57**, 627.
- 20 J. C. Bonner and M. E. Fisher, *Phys. Rev. A*, 1964, **135**, 640; M. E. Lines, *J. Phys. Chem. Solids*, 1970, **31**, 101.
- 21 D. Obertelli, R. H. Friend, D. R. Talham, M. Kurmoo, and P. Day, *Synth. Met.*, 1988, **27**, A375; *J. Phys. Condensed Matter*, 1989, **1**, 5671.
- 22 M. Lequan, R. M. Lequan, C. Hauw, J. Gaultier, G. Maceno, and P. Delhaes, *Synth. Met.*, 1987, **19**, 409.
- 23 T. Mori, P. Wang, K. Imaeda, T. Enoki, H. Inokuchi, F. Sakai, and G. Saito, *Synth. Met.*, 1988, **27**, A451.

Received 21st March 1989; Paper 9/01222B

Epilogue — but not Ending

The stories told in these pages through text and the original articles have a common theme of trying to understand how electrons move from one place to another, when atoms or molecules are brought together. Much of it therefore comes under the general heading of ‘charge transfer’ between neighbouring atoms in Chap. 1, metal atoms with differing oxidation states in Chap. 3, electron exchange in Chaps. 4 and 5, and molecules in Chap. 6. Another important theme, stemming from chemistry rather than physics, is to identify and construct the entities most suitable for studying the phenomena in question. A convincing case can be made that chemistry is possibly the only truly creative science; it does not accept the world around us as it is, and then attempt to explain it the way astronomy or biology is, but actually creates its own new objects to study that which never existed previously.

From time to time, the chemists get more than they bargained for (e.g. the ferromagnet in Chap. 4 that changes colour, or high temperature superconductors). As the properties at the centre of attention are the ones called ‘emergent’, they are properties belonging to the ensemble and not the ingredients alone. To put it colloquially (but not inaccurately), the whole really is greater than the sum of its parts. Nanoscience and even nanotechnology, in the sense of applying nano-scale properties, has been flourishing long before these buzzwords came along. It is founded in chemistry but it is more than chemistry; physics and materials science play a role in it as well.

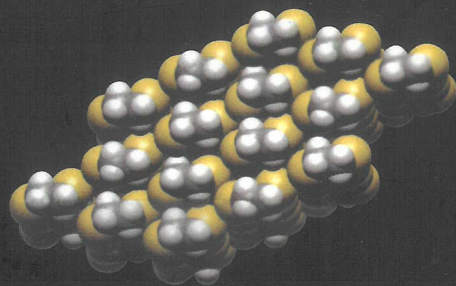
In these circumstances, the direction taken by time’s arrow points firmly towards increasingly complex molecular architectures, leading to increasingly complex physical behaviour, or more often, combinations of behaviour. The latter have been called ‘multi-functional materials’ [1]. For example, the molecular metallic conductor that also transports protons described in Chap. 6 [2] has these twin attributes because the aromatic radical cations and metal-organic coordination complex anions organise themselves in separate layers, one of which sustains the electron transport, while the other transports the protons. Such co-existence of properties is fascinating, but synergy between them would be even more so. Synergy between conduction electrons and localised magnetic moments centred on 3d-shells has been widely sought in metals and superconductors, but proves elusive in practice, i.e. effects observed are obstinately small. Photomagnetism, as first seen in the halochromates [3], and in a different guise in the Prussian Blue analogues [4], is a spectacular instance of such a synergy, and there are others waiting to be found without doubt.

Behind all this hovers the prospect of technology and the fruits, societal and financial, of exploitation. Properties that can be switched by light, temperature or magnetic fields just might (if many other criteria are satisfied) end up in a device, but at least equally appealing is the chance of finding some completely new phenomenon. There is no physical law that says we have explained all the options open to many-body ground-states in condensed matter. Surprises like high temperature superconductivity may still await us and materials chemistry is as powerful a tool as any for seeking them. The show goes on.

References

- [1] E. Coronado and P. Day, *Chem Rev* **104**: 5419 (2004).
- [2] A. Akutsu-Sato, H. Akutsu, S. S. Turner, P. Day, M. R. Probert, J. A. K. Howard, T. Akutagawa, S. Takeda and T. Nakamura, *Angew Chem Int Ed* **44**: 292 (2004).
- [3] C. Bellitto and P. Day, *J Chem Soc Chem Commun* 511 (1978).
- [4] S. Ohkoshi, A. Fujishima and K. Hashimoto, *J Amer Chem Soc* **120**: 5349 (1998).

This page intentionally left blank



MOLECULES INTO MATERIALS

Case Studies in Materials Chemistry —
Mixed Valency, Magnetism and Superconductivity

The last decade has seen the emergence and explosive growth of a new field of condensed matter science: materials chemistry. Transcending the traditional boundaries of organic, inorganic and physical chemistry, this new approach aims to create new molecular and lattice ensembles with unusual physical properties. One of its pioneers, the author has worked on structure-property relations in the inorganic and metal-organic solid state for over 40 years. His seminal work on mixed-valency compounds and inorganic charge transfer spectra in the 1960s set the scene for this new type of chemistry, and his discovery of transparent metal-organic ferromagnets in the 1970s laid the ground rules for much current work on molecular magnets. He has also published extensively on molecular metals and superconductors, especially on charge transfer salts combining conductivity with magnetism. This indispensable volume brings together for the first time a selection of his articles on all these topics, grouped according to theme. Each group is prefaced by a brief introduction for the general reader, putting the articles into their context in the evolution of the subject and describing the intellectual circumstances in which each project was conceived and executed.

World Scientific
www.worldscientific.com
6247 hc

ISBN-13 978-981-270-038-4
ISBN-10 981-270-038-2



9 789812 700384